INTERNATIONAL JOURNAL OF MODERN ENGINEERING RESEARCH (IJMER)

ISSN : 2249-6645

Volume 3 - Issue 5

Web : www.ijmer.com

Email : ijmer.editor@gmail.com

International Journal of Modern Engineering Research (IJMER)

Editorial Board

Evaluation Of Factors Affecting Sliding Wear Behaviour Of Al-Flyash Metal Matrix Composites By Using Design Of Experiments

K.N.P. Prasad[1], M. Ramachandra[2]

[1] *Associate Professor, Dept of Industrial Engineering & Management, BMSCE, Bangalore, India*
[2] *Professor, Dept of Mechanical Engineering, BMSCE, Bangalore, India*

ABSTRACT: *The ability to produce near net shape components is made possible by means of squeeze casting process. Squeeze casting is a hybrid metal forming process which combines the features of both casting and forging in a single operation. The primary objective of this paper is to study the influence of the process parameters on wear resistance in squeeze casting of LM6 Al-flyash composite using Taguchi method. The parameters studied include percentage wt. of flyash, squeeze pressure, and squeeze time. In Taguchi method, a four level orthogonal array has been used to determine the S/N ratio. In this investigation, composites have been produced by incorporating flyash as a reinforcement material and eutectic Al–Si alloy as a matrix. Stir casting route has been adopted to disperse fly ash (from 5% to 12.5%wt.) in the Al–Si alloy matrix which is followed by applying the squeeze pressure of 30, 60, 90 and 120 bar for a varying squeeze time. The Pin-on-disc test was conducted on the specimen prepared out of these castings to determine the sliding wear behavior of the composite. The results of experimental investigation on wear resistance of flyash reinforced aluminium metal matrix composite shows that the inclusion of the flyash by weight percentage and the squeeze pressure are the recognized parameters to cause appreciable improvement in the wear resistance of the squeeze cast components*.

Keywords : *Al-flyash mmc, S/N ratio, wear.*

I. INTRODUCTION

Aluminium metal matrix composites are finding extensive applications in automobile and aerospace applications because of their superior mechanical and tribological properties. The increasing demand for lighter weight and fuel efficient materials is the major factor which is motivating the researchers for the development of more advanced metal matrix composite materials (1-5). Metal matrix composites containing hard or ceramic particulates offer superior operating performance. Aluminium based discontinuously reinforced metal matrix composites have attracted lot of the attention of the researchers because of their improved strength, high modulus and increased wear resistance when compared to conventional aluminium alloys (6,7,8).

The metal matrix composites are produced by several processes. The most economical one being the gravity die casting process. However, the main hindrance in the process is the presence of casting defects such as voids, cracks, shrinkage and porosity. It is reported that an improved method over the gravity die casting is squeeze casting process (**9**). It is a casting process in which metal is solidified under the direct action of external pressure. It is a combination of both gravity die casting and closed die forging. Squeeze casting process has several advantages such as, no feeder or risers are required. Therefore there is no wastage of the material. Parts are produced with no gas porosity or shrinkage porosity and castings produced by squeeze casting are found to have better mechanical properties and wear resistance (10,11,12).

Over the past two decades, squeeze casting process is found to be an important and proven process to produce near net shape high quality engineering products which are very much used in the automotive industry because of their superior quality and enhanced mechanical properties over those produced by conventional castings process (13,14).

One of the selection criteria for the discontinuously reinforced aluminium metal matrix composite is wear resistance. The wear resistance of the composite materials depends upon lot of factors apart from process parameters such as load, speed, temp., hardness and other conditions (15). The wear performance of the particulate reinforced aluminium metal matrix composites depends upon the type of reinforcement used, ranging from very hard ceramics particulates such as SiC, Al_2O_3, B_4C to soft materials such as graphite (16). Another important factor on which the wear of the composite material depends upon is the method of production of the composites.

Most of the available literature on the wear of the Aluminium metal matrix composites provide information about the different types of reinforcements used in different volume % and the production of the aluminium metal matrix composites by various methods (17,18). However limited information is available regarding the processing of the aluminium composite by squeeze casting with flyash as the reinforcement, and the analysis of their wear behavior using statistical method.

There has been increasing interest in developing composites containing low density and low cost reinforcements. In this regard flyash is one such least expensive, low density reinforcement which is available in huge quantities as a solid waste due to the combustion of coal in thermal power plants (19,20). Therefore by the incorporation of flyash as reinforcement in aluminium alloy many purposes can be achieved such as the cost of aluminium metal matrix composites and the weight of the products can be reduced, and by using the flyash as reinforcement to an extent, the environmental hazards can be prevented. Also some researchers have reported that the incorporation of flyash has resulted in enhanced mechanical properties and wear resistance in aluminium flyash metal matrix composites produced by liquid metallurgy routes (21-26). It is with this intent that the present investigation is carried out to study the wear behavior of the aluminium flyash composites produced by squeeze casting method using Taguchi method.

II. TAGUCHI TECHNIQUE

The design of experiments (DOE) approach using Taguchi technique has been used prominently by many researchers to study the effect of process parameters in different context. Taguchi technique is a powerful tool for the design of high quality systems (27,28). The Taguchi approach to experimentation provides an orderly way to acquire data and to analyze the effects of process and material parameters over some specific response. This method combines experimental and analytical concepts to determine the parameters with the strongest influence on the resulting response for a considerable improvement in the overall performance (29,30). The plan of experiments is generated in Taguchi method by the use of standard orthogonal arrays. DOE is not a single step process it is a series of steps which must be followed in a certain sequence for the experiment to yield an improved understanding of product or process performance. This design of experiments process is made up of three main phases, namely, the planning phase, the conducting phase and analysis or interpretation phase. The planning phase is the most important phase one must give a maximum importance to this phase. The data collected from all the experiments in the second phase are analyzed to determine the effect of various design parameters. This method makes use of fractional factorial approach and this may be accomplished with the aid of orthogonal arrays. The experimental results are then analyzed by using signal-to-noise ratio to determine the parameters that has the maximum influence on the sliding wear behavior of the composites produced.

III. EXPERIMENTAL PROCEDURE

3.1 Materials Used:

Aluminium casting alloy that conforms to British Standards 1490 LM6 has been used as the matrix material in the present investigation. The chemical composition of the aluminium alloy is as shown in the Table.1. The aluminium alloy was reinforced with 5 wt%, 7.5 wt%, 10 wt%, and 12.5 wt% flyash to synthesize the composite through liquid metallurgy route followed by squeeze casting. The flyash which is used as a reinforcing material was tested in the laboratory and the test results are as given the Table.2.

Chemical Composition	**Cu**	**Mg**	**Zn**	**Fe**	**Mn**	**Si**	**Al**
Wt. %	0.002	0.065	0.021	0.32	0.62	12.2	Balance

Table 1: Chemical composition of the LM6 aluminium alloy

Sio_2	**Tio_2**	**Al_2O_3**	**Fe_2O_3**	**CaO**	**MgO**	**Na_2O**	**K_2O**	**L.O.I**	**SO_3**
63.96%	0.5%	25.5%	6.07%	1.97%	0.81%	0.54%	0.45%	0.15%	<0.1%

Table 2: Chemical composition of the flyash

Density of Fly ash = 1.31 g/cc. Type of Flyash: F Class (CaO < 20%) Source: RTPS Raichur, INDIA

3.2 Processing:

The composites were produced by liquid metallurgy route which was followed by squeeze casting. Firstly the matrix material was superheated to 800^{o}C in the Electric resistance furnace. It was the de-gassed by using Hexacholroethane tablets. By using a mechanical stirrer with a rotational speed of 600 rpm the vortex was created. At this stage the preheated flyash was slowly introduced into the slurry and a small quantity of magnesium was also added into the molten metal to enhance the wettability of the reinforcements with molten metal. The stirring of the slurry was carried out for nearly five minutes to promote wetting and uniform dispersion of the reinforcement. After that a metered quantity of mixture was poured into the preheated steel die of D4 grade mounted on the 20 tonne Hydraulic press and was squeezed through the punch by the application of pressure. The squeezed casting was allowed to cool down to the room temperature in the die itself and was later ejected out from the die. The test specimen for conducting hardness, wear testing and for microstructure were machined from as-cast samples.

3.3 Production of castings based on Orthogonal Array :

Dr. Taguchi has developed a method based on "Orthogonal array" of experiments which gives reduced number of experiments to be conducted without any significant loss of accuracy. Thus the Design of Experiments with Taguchi Method reduces time, cost, resources involved in the experiment.

Orthogonal Arrays (OA) provide a set of well balanced (minimum) experiments and Dr. Taguchi's Signal-to-Noise ratios (S/N), which are log functions of desired output, serve as objective functions for determining the significant effect on the performance characteristics (wear, hardness, productivity etc).

In this work the independent factors such as flyash % wt, Squeeze Pressure, and Squeeze time are considered at four levels of each and are shown in Table 3.

Factors	**Level 1**	**Level 2**	**Level 3**	**Level 4**
Flyash (wt. %)	5	7.5	10	12.5
Squeeze Pressure (bar)	30	60	90	120
Squeeze time (min)	5	10	15	20

Table 3: The factors and the levels chosen for Squeeze casting of the composites

In this investigation three factors and four levels for each factor is used and the Orthogonal Array corresponding to L'16 is selected for the production of the castings.

3.4 Conduct of experiments according to the Orthogonal array table:

The casting of the composites based on the factors and their level selected were produced by squeeze casting method as per the Orthogonal Array table shown in the Table 4.

Specimen	**Flyash**		**Squeeze pressure (bar)**		**Squeeze time (min)**	
	Levels	**% wt. Flyash**	**Levels**	**Sq. Pr.(bar)**	**Levels**	**Sq. time (min)**
C1	1	5	1	30	1	5
C2	1	5	2	60	2	10
C3	1	5	3	90	3	15
C4	1	5	4	120	4	20
C5	2	7.5	1	30	2	10
C6	2	7.5	2	60	1	5
C7	2	7.5	3	90	4	20
C8	2	7.5	4	120	3	15
C9	3	10	1	30	3	15
C10	3	10	2	60	4	20
C11	3	10	3	90	1	5
C12	3	10	4	120	2	10
C13	4	12.5	1	30	4	20
C14	4	12.5	2	60	3	15
C15	4	12.5	3	90	2	10
C16	4	12.5	4	120	1	5

Table 4: Orthogonal Array table for the three factor and four levels

3.5 Macro and Microstructural Analysis

Macrostructural study was conducted on the as processed and machined composite castings in order to investigate distribution of flyash particles retained in the MMC. Castings were plain turned on lathe to remove 5mm of material to reveal the particle distribution on macroscopic scale.

Microstructural characterization studies were conducted on reinforced samples. This is accomplished by using Nikon metallurgical microscope. The composite samples were metallographically polished prior to examination.

3.6 Hardness Test

One of the important properties which effects wear resistance of any metal or alloy is hardness. The hardness measurements were carried out on Al-flyash particulate composite specimens by using Brinell hardness tester in order to investigate the influence of flyash particles on the matrix alloy hardness. The applied load was 500 Kgs and an indenter of 10 mm diameter steel ball was used. The specimens were prepared and polished on different grits of emery paper. The test was carried out at four different locations to controvert the possible effect of indenter resting on the harder particles and the average of all the four readings was taken.

3.7 Sliding Wear Test

The wear test was performed using computerized pin-on-disc wear testing machine to evaluate the dry sliding wear behavior of the composite specimen. The computerized pin-on-disc wear tester, shown in Figure 1 & 2, with data acquisition system is used for recording the wear rate. The specimen of Φ6 mm and 30 mm long prepared with different percentage of flyash, Squeeze Pressure and Squeeze time was subjected to the wear test.

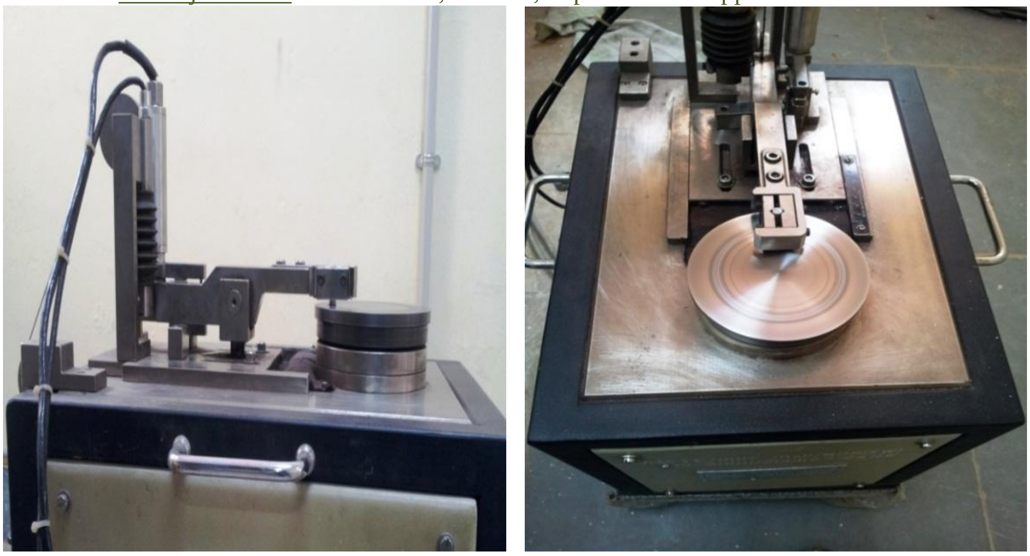

Fig 1 & 2: Computerized Pin-on-disc Wear tester

The load, speed and the track radius was set before the experiment was started. All the specimens were tested under a particular load of 9.81N, speed 500 rpm and track radius of 40mm. The experiment was carried-out for one hour on each specimen. The machine was started and the corresponding wear was recorded by the system. The experimental results were transformed into signal-to-noise (S/N) ratios. S/N ratio is defined as the ratio of the mean of the signal to the standard deviation of the noise. The S/N ratio indicates the degree of the predictable performance of a product or process in the presence of noise factors. The S/N ratio for wear rate using 'smaller the better' characteristic, which can be calculated as logarithmic transformation of the loss function, is given as: $S/N = -10 \log [1/n (\Sigma y^2)]$ where y is the observed data (wear rate) and n is the number of trials. The above S/N ratio transformation is suitable for minimization of wear rate.

IV. RESULTS AND DISCUSSION

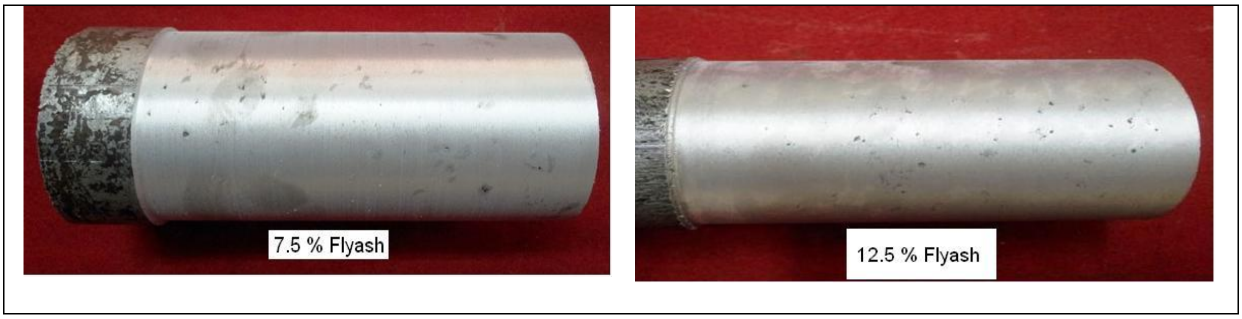

Figure 3 & 4: Marcograph of the squeeze cast specimen.

4.1 Macro and microstructural characterization

Macrostructural studies revealed reasonably uniform distribution of flyash particles with small percentages of segregation of particles. The distribution of flyash particles is influenced by the tendency of particles to float due to density differences and interactions with the solidifying metal. Photo macrograph, fig.3 & 4, shows the distribution of flyash particles (7.5% and 12.5% wt percentage) in squeeze cast ingot. The concentration of flyash particles was found to be more at the top than at the bottom of the castings which is due to the lesser density of the flyash particles.

The optical micrograph of 5%, 7.5%, 10% and 12.5% wt. Al-flyash composites is shown in Fig. 5. The micrographs show that there is a good interfacial bonding between flyash particles and Al matrix. Good interfacial bonding is attributed to heating of flyash particulates prior to dispersion and addition of magnesium in small quantities during stirring which improved wettability of flyash particles.

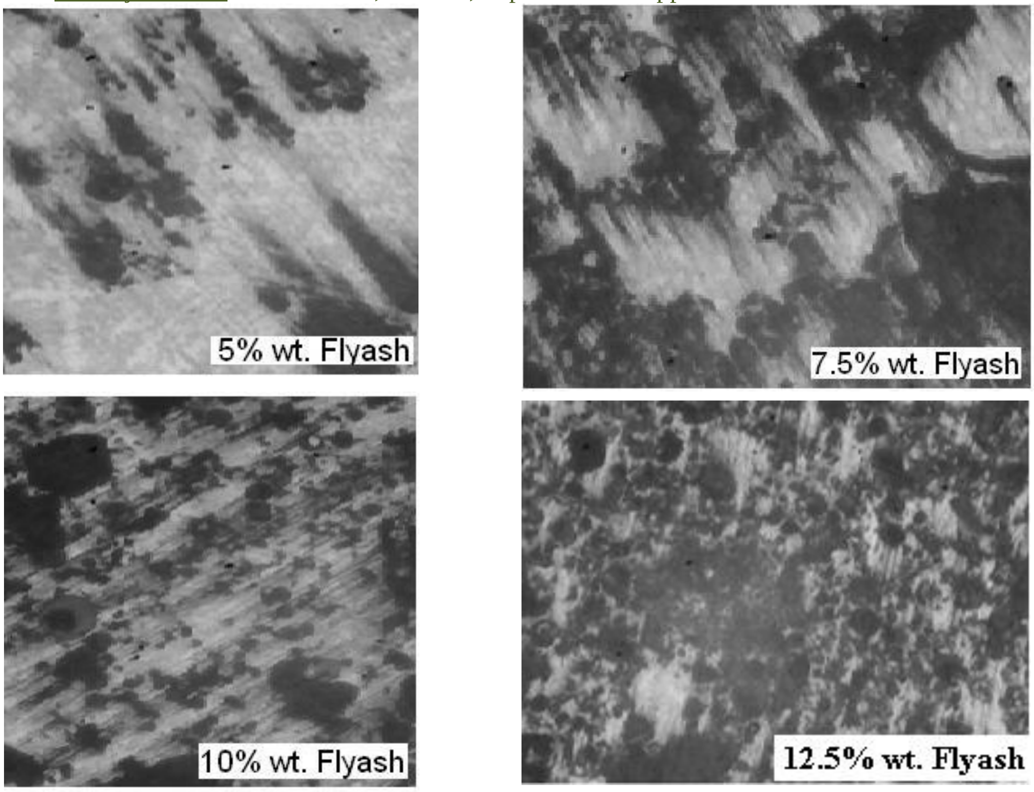

Figure 5: Optical micrograph of Al-flyash composites.

4.2 Hardness

The results of the hardness test for the various combinations of flyash wt.%, squeeze pressure and squeeze time are shown in the Table 5. It is observed from the graph 1 & 2 that hardness increases with increase in weight percentage of Flyash particles and the squeeze pressure on the matrix alloy of the squeeze cast composites. Increased hardness with increased weight percentage of flyash particles and the squeeze pressure can be attributed to the following reasons:

i) The flyash particles whose hardness is higher than the aluminium matrix material generally enhances the hardness of the composite material.
ii) Good interfacial bonding between matrix alloy and particle reinforcement.
iii) Increase in squeeze pressure increases the compaction of the matrix alloy.

Table 5: Readings of the Hardness test conducted on the composites

Specimen	L	Fly ash (Wt.%)	L	Squeeze pr. in (kg/cm^2)	L	Squeeze time (min)	T1	T2	T3	T4	Avg BHN
C1	1	5	1	30	1	5	55	60	53	56	56
C2	1	5	2	60	2	10	59	59	56	56	57
C3	1	5	3	90	3	15	58	59	60	59	59
C4	1	5	4	120	4	20	60	61	59	62	61
C5	2	7.5	1	30	2	10	62	62	63	63	62
C6	2	7.5	2	60	1	5	64	65	65	66	65
C7	2	7.5	3	90	4	20	69	69	68	69	69
C8	2	7.5	4	120	3	15	73	73	77	65	72
C9	3	10	1	30	3	15	64	64	63	66	64
C10	3	10	2	60	4	20	65	67	64	67	66
C11	3	10	3	90	1	5	68	69	69	69	69
C12	3	10	4	120	2	10	73	73	72	73	73
C13	4	12.5	1	30	4	20	65	65	65	66	65
C14	4	12.5	2	60	3	15	67	67	68	67	67
C15	4	12.5	3	90	2	10	69	71	73	70	71
C16	4	12.5	4	120	1	5	79	77	75	73	76

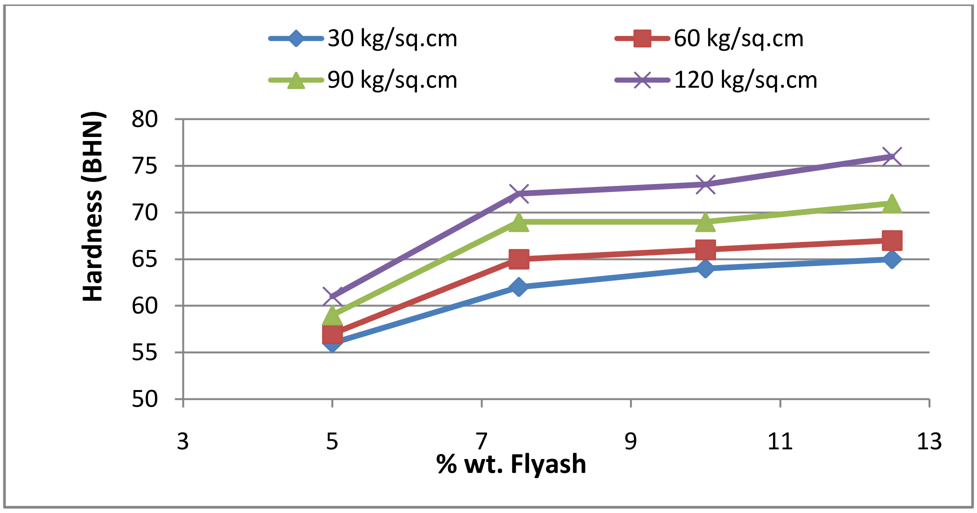

Graph 1: Graph of Hardness Vs %wt. Flyash

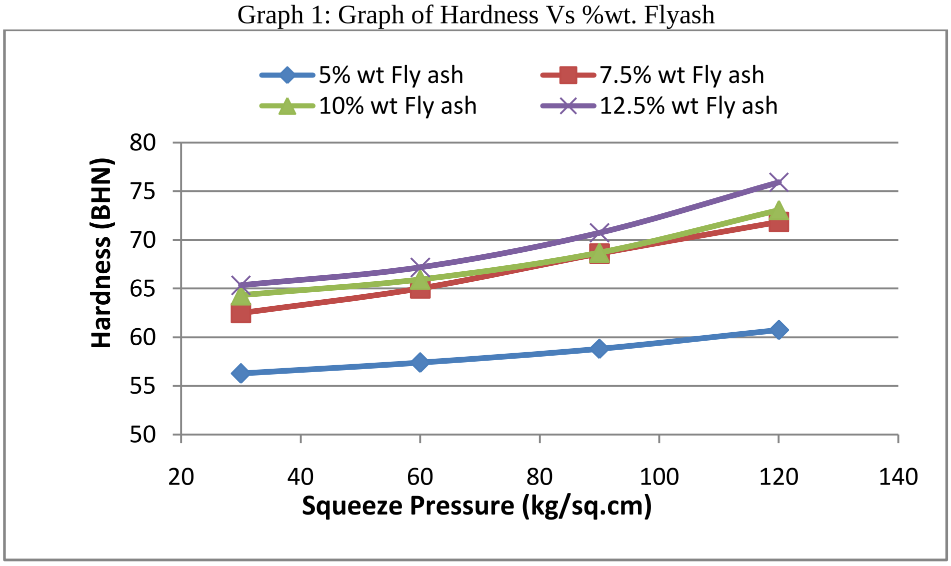

Graph 2: Graph of Hardness Vs Squeeze Pressure

4.3 Sliding Wear Test

The composites produced as per orthogonal array and their wear rate results obtained for various combinations of factors are shown in Table 6. The experimental values were transformed into S/N ratios and the calculated S/N ratio for each experiment is shown in Table 7.

Specimen	**% wt. Flyash**	**Sq. Pr. (bar)**	**Sq. time (min)**	**T1 in µm**	**T2 in µm**	**T3 in µm**	**T4 in µm**	**Ave. Wear (µm)**
C1	5	30	5	632	705	318	230	471
C2	5	60	10	640	636	434	400	528
C3	5	90	15	276	410	262	276	306
C4	5	120	20	409	437	380	524	438
C5	7.5	30	10	565	435	330	262	398
C6	7.5	60	5	402	507	385	333	407
C7	7.5	90	20	821	403	464	364	513
C8	7.5	120	15	517	560	483	440	500
C9	10	30	15	330	704	213	413	415
C10	10	60	20	425	387	330	291	358
C11	10	90	5	605	477	219	421	431
C12	10	120	10	495	709	580	372	539
C13	12.5	30	20	813	709	604	565	673
C14	12.5	60	15	821	609	528	388	587
C15	12.5	90	10	705	282	610	389	497
C16	12.5	120	5	490	508	463	554	504

Table 6: Pin on disc wear test results

Specimen	**SN Ratio**	**Spe. No**	**Ave. of SN Ratio for fly ash**	**Spe. No**	**Ave. of SN Ratio for Sq. Pr**	**Spe. No**	**Ave. of SN Ratio for Sq. time**
C1	-54.19	C1	-52.8978	C1	-54.0754	C1	-53.4144
C2	-54.63	C2		C5		C6	
C3	-49.88	C3		C9		C11	
C4	-52.88	C4		C13		C16	
C5	-52.34	C5	-53.3399	C2	-53.4402	C2	-54.0552
C6	-52.29	C6		C6		C5	
C7	-54.71	C7		C10		C12	
C8	-54.01	C8		C14		C15	
C9	-53.12	C9	-53.0638	C3	-53.0245	C3	-53.1695
C10	-51.17	C10		C7		C8	
C11	-53.11	C11		C11		C9	
C12	-54.85	C12		C15		C14	
C13	-56.65	C13	-55.1918	C4	-53.9532	C4	-53.8542
C14	-55.67	C14		C8		C7	
C15	-54.39	C15		C12		C10	
C16	-54.06	C16		C16		C13	
	MAX-MIN		2.2940		1.0509		0.8857
	RANK		I		II		III

Table 7: SN ratio values for flyash, squeeze pressure and squeeze time

The average wear of each trials are taken and SN ratios for all the experiments are calculated by using the SN ratio formula.

4.4 S/N Ratio Analysis

The influence of parameters such as % wt. fly ash content, squeeze pressure and squeeze time on wear rate has been evaluated using S/N ratio response analysis. The SN ratio for fly ash, squeeze pressure and squeeze time was calculated using $SN_i = -10 \log\left(\sum_{u=1}^{N_i} \frac{y_u^2}{N_i}\right)$ where, i=experiment number, u=trial number and N_i=number of trials for experiment number i. The control parameter with the strongest influence was determined by taking the difference between the maximum and minimum values of mean SN ratio of a particular parameter, SN max-min $_F$ = maximum-minimum. Higher the difference between the mean of S/N ratios, the more influential is the control parameter. The S/N ratio response analysis, presented in Table 7 shows that among all the factors, % wt. fly ash content was found to have highest difference than the other two parameters. Therefore, it can be construed that % wt. fly ash is the most influential and significant parameter followed by squeeze pressure and squeeze time respectively in controlling the wear rate of the composite material.

V. CONCLUSIONS

From the present investigation the following conclusions are drawn.

1. The squeeze casting process was successfully carried out in producing Al-flyash composites containing upto 12.5 wt. % flyash as reinforcement.
2. From the macrostructure analysis it was evident that presence of porosity in the composites produced by squeeze casting method was almost eliminated.
3. The S/N ratio analysis results show that the % wt of flyash has the strongest effect among the other parameters on the sliding wear resistance of the Al-flyash composite.
4. The order of influence of the controllable factors on the wear resistance of the composite is as follows: % wt. fly ash content, squeeze pressure and squeeze time respectively.

REFERENCES

1. M K Surappa, Aluminium matrix composites: Challenges and Opportunities, *Sadhana* Vol. 28, Parts 1&2, February / April 2003, pp. 319–334
2. S. Anoop, S. Natarajan, S.P. Kumaresh Babu, Analysis of factors influencing dry sliding wear behavior of Al/SiCp–
3. brake pad tribosystem, *Materials and Design* 30 (2009) 3831–3838
4. D. Milosavljević, G. Jovičić, Properties of Metal Matrix Composites for Automotive Applications , *Tribology in industry*, Volume 24, No. 3&4, 2002.
5. Ray Erikson, Syntactic Metals: A Survey of Current Technology, *5th Aerospace Materials, Processes and Environmental Technology Conference*, Von Braun Center, Huntsville, Alabama, September 16—18, 2002.
6. M.R.Ghomashchi, A.Vikhrov, Squeeze casting: an overview, *Journal of Materials Processing Technology 101*(2000) 1-9
7. A. Daoud, M.T. Abou El-Khair, and A.N. Abdel-Azim, Effect of Al_2O_3 Particles on the Microstructure and Sliding Wear of 7075 Al Alloy Manufactured by Squeeze Casting Method, *Journal of Materials Engineering and Performance* (2004) 13:135-143
8. Bekir Sadık Unlu, Investigation of tribological and mechanical properties Al2O3–SiC reinforced Al composites manufactured by casting or P/M method, *Materials and Design 29* (2008) 2002–2008.
9. Varuzan Kevorkijan, Development of Al MMC composites for automotive Industry , *Yugoslav Association of Metallurgical Engineers*, June 26-27 2002
10. J. Bienia, M. Walczak, B. Surowska, J. Sobczaka, Microstructure And Corrosion Behaviour Of Aluminum Fly Ash Composites, *Journal of Optoelectronics and Advanced Materials*, Vol. 5, No. 2, June 2003, p. 493 - 502
11. L.J. Yang, The effect of casting temperature on the properties of squeeze cast aluminium and zinc alloys, *Journal of Materials Processing Technology 140* (2003) 391–396
12. T.M. Yue, Squeeze casting of high-strength aluminium wrought alloy AA7010, *Journal of Materials Processing Technology 6* & (1997) 179-185
13. D.J. Britnell, K. Neailey, Macrosegregation in thin walled castings produced via the direct squeeze casting process, *Journal of Materials Processing Technology 138* (2003) 306–310
14. T.M. Yue, G.A. Chadwick , Squeeze Casting of Light alloys and their Composites, *Journal of Material Processing Technology 58* (1996) 302-307
15. C.S. Goh, K.S. Soh , P.H. Oon , B.W. Chua, Effect of squeeze casting parameters on the mechanical properties of AZ91–Ca Mg alloys, *Materials and Design 31* (2010) S50–S53
16. S. Venkat Prasad, R. Subramanian, N. Radhika, L. Arun, N. Praveen, Influence of Parameters on the Dry Sliding Wear Behaviour of Aluminium/Fly ash/Graphite Hybrid Metal Matrix Composites, *European Journal of Scientific Research* Vol.53 No.2 (2011), pp.280-290
17. S.V. Prasad, and R. Asthana, Aluminum metal–matrix composites for automotive applications: tribological considerations, *Tribology Letters*, Vol. 17, No. 3, October 2004
18. D.B. Miracle, Metal matrix composites – From science to technological significance, *Composites Science and Technology 65* (2005) 2526–2540
19. Pradeep K. Rohatgi, Metal-matrix Composites, *Defence Science Journal*, Vol 43, No 4, October 1993, pp 323-349
20. T.P.D. Rajan, R.M. Pillai, B.C. Pai, K.G. Satyanarayana, P.K. Rohatgi, Fabrication and characterisation of Al–7Si–0.35Mg/fly ash metal matrix composites processed by different stir casting routes, *Composites Science and Technology 67* (2007) 3369–3377.
21. P.K. Rohatgi, D. Weiss, and Nikhil Gupta, Applications of Fly Ash in Synthesizing Low-Cost MMCs for Automotive and Other applications , *Low-Cost Composites in Vehicle Manufacture* an Overview.
22. Sudarshan, M.K. Surappa, Dry sliding wear of fly ash particle reinforced A356 Al composites, *Wear 265* (2008) 349–360
23. K.V. Mahendra, K. Radhakrishna, Fabrication of Al–4.5% Cu alloy with fly ash metal matrix composites and its characterization 23), *Materials Science-Poland*, Vol. 25, No. 1, 2007,
24. M. Ramachandra, K. Radhakrishna, Effect of reinforcement of flyash on sliding wear, slurry erosive wear and corrosive behavior of aluminium matrix composite, *Wear 262* (2007) 1450–1462
25. Pradeep. K. Rohatgi, Pressure infiltration technique for the synthesis of A356 Al/Fly ash composites: Microstructure and Tribological performance Grigorious Itskos, *World of Coal ash (WOCA) Conference*: May 9-12, 2011
26. J. Babu Rao, D. Venkata Rao and N.R.M.R. Bhargava, Development of light weight ALFA composites, *International Journal of Engineering, Science and Technology* Vol. 2, No. 11, 2010, pp. 50-59 www.ijest-ng.com

27. T.P.D. Rajan, R.M. Pillai, B.C. Pai, K.G. Satyanarayana, P.K. Rohatgi, Fabrication and characterisation of Al–7Si–0.35Mg/fly ash metal matrix composites processed by different stir casting routes, *Composites Science and Technology 67* (2007) 3369–3377
28. S. Basavarajappa and G. Chandramohan, Dry Sliding Wear Behavior of Metal Matrix Composites: A Statistical Approach, *JMEPEG (2006)* 15:656-660
29. S. Basavarajappa, G. Chandramohan, J . Paulo Davim, Application of Taguchi techniques to study dry sliding wear behaviour of metal matrix composites, Materials and Design 28 (2007) 1393–1398
30. H. Siddhi Jailani & A. Rajadurai & B. Mohan & A. Senthil Kumar & T. Sornakumar, Multi-response optimisation of sintering parameters of Al–Si alloy/fly ash composite using Taguchi method and grey relational analysis, *Int J Adv Manuf Technol (2009)* 45:362–369.
31. P. Vijian, V.P. Arunachalam, Optimization of squeeze cast parameters of LM6 aluminium alloy for surface roughness using Taguchi method, *Journal of Materials Processing Technology 180* (2006) 161–166

Experimental Investigations of Exhaust Emissions of four Stroke SI Engine by using direct injection of LPG and its analysis

Mr. Hitesh B. Bisen[1], Mr. Y. R. Suple[2]
[1]*M.Tech. Student K.I.T.S. college of engineering, Ramtek, Email:*
[2]*Asst. Prof. Mechanical Department K.I.T.S. College of Engineering, Ramtek*

ABSTRACT: *Gaseous fuels such as liquefied petroleum gas (LPG) and liquefied natural gas (LNG) have been widely used in commercial vehicles. In this project the main aim is to evaluate the exhaust emission by running the conventional engine on Liquefied Petroleum Gas (LPG) as an alternative fuel for four-stroke spark ignition engine. The primary objective of the study is to determine the performance and the exhaust emissions of the engine using LPG as a fuel. The engine used in the study is originally single cylinder; four-stroke spark ignition engine with certain modifications is to make to permit the experiments to run on LPG fuel. During the running, the engine was coupled to a ropeway dynamometer to measure several engine performance parameters and a 5-gas analyzer is to be inserted into the engine exhaust tailpipe for measuring the exhaust emissions. Experimental investigations have been carried out to emissions of single cylinder four-stroke spark ignition engine at full throttling position of engine and different load conditions is used to different fuels (Gasoline and LPG). Exhausts are the five gasses measured by the latest technology exhaust analysers are: HC, CO, CO2, O2 and NOx.*

Keyword: *Exhaust, Emission, Four-stroke SI Engine, LPG, Injector, Analyser etc.*

I. INTRODUCTION

Traffic exhaust emissions are significant sources of air pollution in the world and may threaten human health and cause global warming effect. Therefore, governments are compelled to minimize motor-vehicle pollution problems with more stringent emission standards for reducing pollution-related chemicals and improving air quality. In most Asian countries, motorcycles contribute to air pollution more than other vehicles. Previous research shows that three-way catalytic converter used in spark ignition (SI) engines could reduce most exhaust pollution, such as HC, CO and NOx, towards achieving exhaust standards. However, converters are expensive to apply in motorcycles and would not reduce carbon dioxide (CO2), a major cause of global warming effect. It may be more acceptable, especially cost wise, to address the problem in the design and manufacture of motorcycles. Exhaust pollution from a motorcycle gasoline engine contains nitrogen oxides (NOx), carbon monoxide (CO) and unburned hydrocarbon emissions (HC). HC emissions are the results of incomplete combustion and could be used to evaluate the combustion inefficiency. NOx emissions are affected by the air/fuel ratio, the burned gas fraction of the in-cylinder unburned mixture, and spark timing. Increasing the burned-gas fraction and decreasing spark timing could reduce NOx emission levels. These solutions, however, would reduce combustion rate and engine torque. Controlling the air/fuel ratio could have a greater effect on NOx emission and could reduce NOx levels up to 98% at an air/fuel ratio of 23.5. However, it is difficult to achieve so high an air/fuel ratio in a conventional gasoline engine. Carbon monoxide (CO) emission of gasoline engine depends heavily on the air/fuel ratio. While a lean combustion decreases the amount of CO in exhaust gas, a spark-ignition engine is often operated closely to stoichiometric mixture, making CO emissions considerably difficult to reduce without an exhaust treatment like a catalytic converter. Nevertheless, a conventional motorcycle gasoline engine could reduce overall exhaust pollution if it could operate with high air/ fuel ratio.

In a previous paper, introduced a new design system for gasoline fuel engines, called semi-direct injection (SDI) system for application in motorcycle engines. By increasing swirl ratio to 3.8 and injecting fuel when the intake valve is opened, the SDI system can make a stratified mixture and extend the air/fuel ratio lean limit to 24. CO is tremendously decreased by 92.9% and a relatively low combustion temperature in lean burn decreases NOx by 32%. Furthermore, brake specific fuel consumption (BSFC) decreases to 11% compared with an original gasoline engine at low- and part load. As a result, SDI engine produces lower CO2, as well. From this result, we can affirm that SDI system in motorcycle engine can help to improve air quality and reduce greenhouse gas. To become a viable product, the SDI system should reduce CO2, as well as exhaust pollution. This could be achieved with a method that allows switching between stratified mixture at low load, and a homogeneous mixture at full load. This cannot be done in the current design. The SDI engine could have better results with CO2 and exhaust emission if there were an increase in the stratification of mixture.. Liquefied petroleum gas (LPG) in gaseous phase could be an alternative fuel for an SDI system. Previous research has observed that the brake mean effective pressure (BMEP) of gasoline is higher than LPG, while LPG fuel consumption and emission, which includes CO, HC and CO2, are lower than gasoline.

II. LPG AS AN ALTERNATIVE FUEL FOR IC ENGINE

The gaseous nature of the fuel/air mixture in an LPG vehicle's combustion chambers eliminates the cold-start problems associated with liquid fuels. LPG defuses in air fuel mixing at lower inlet temperature than is possible with either gasoline or diesel. This leads to easier starting, more reliable idling, smoother acceleration and more complete and efficient burning with less unburned hydrocarbons present in the exhaust. In contrast to gasoline engines, which produce high emission levels while running cold, LPG engine emissions remain similar whether the engine is cold or hot. Also, because LPG enters an engine's combustion chambers as a vapour, it does not strip oil from cylinder walls or dilute the oil when the engine is cold. This helps to have a longer service life and reduced maintenance costs of engine. Also helping in this regard is the fuel's high hydrogen-to-carbon ratio (C3H8), which enables propane-powered vehicles to have less carbon build-up than gasoline and diesel-powered vehicles. LPG delivers roughly the same power, acceleration, and cruising speed characteristics as gasoline. Its high octane rating means engine's power output and fuel efficiency can be increased beyond what would be possible with a gasoline engine without causing *Destructive Knocking.* Such fine-tuning can help compensate for the fuel's lower energy density. The higher ignition temperature of gas compared with petroleum based fuel leads to reduced auto ignition delays, less hazardous than any other petroleum based fuel and expected to produce less CO, NOx emissions and may cause less ozone formation than gasoline and diesel engines.

Properties/fuels	**Gasoline**	**LPG**
Chemical structure	C7H17/C4 to C12	C3H8
Energy density	109,000-125,000	84,000
Octane number	86-94	105+
Lower heating value (MJ/Kg)	43.44	46.60
High heating value (MJ/Kg)	46.53	50.15
Stoichiometric air/fuel ratio	14.7	15.5
Density at 15˚C ,kg/m3	737	1.85/505
Auto ignition temperature o K	531	724
Specific Gravity 60° F/60°	0.72-0.78	0.85

Experimental Setup and Test Procedure:

Experiments were conducted on a Bajaj saffier type, four stroke, single cylinder, air-cooled petrol engine test rig. Figure 1.0 shows the schematic experimental set up. Rope brake dynamometer was used for loading the engine, five gas analyzer tested exhaust emission contain CO, CO2, NO_x, O2 and HC.

The fuel flow rate was measured on the volumetric basis using a burette and stopwatch also. The engine was Operated at a rated constant speed of 300, 400, 500, 600 r/min. The emission characteristic was measured by using five gas analyzer. The tests were conducted with neat petrol and LPG. Petrol injected in the combustion chamber through carburettor and LPG Direct injected in the combustion chamber through injector. LPG fuel Injector mechanically operated on/off.

It consists of following components:-

1. Fuel tank, 2. Engine, 3. Rope brake drum type dynamometer, 4. Five gas analyzer, 5. Injector
6. Flash Black arrestor, 7. LPG regulating valve

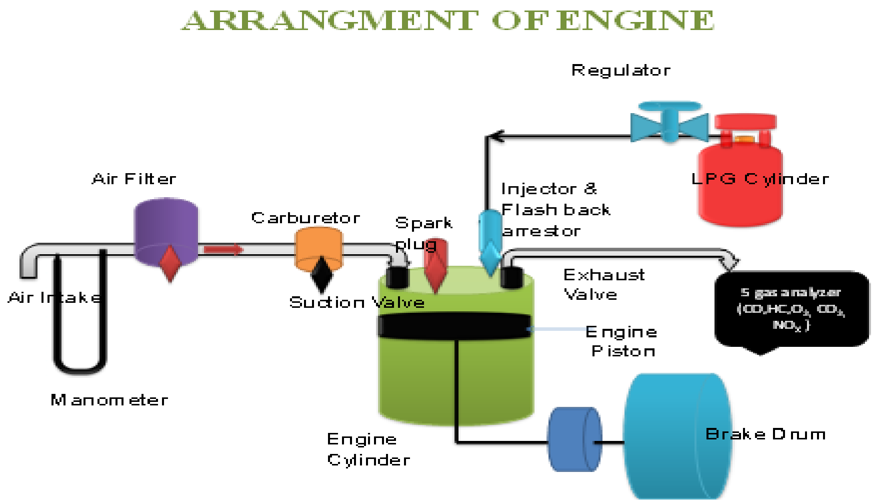

Schematic view of experimental setup

III. ENGINE SPECIFICATIONS

Bajaj saffire.
Type- Single Cylinder 4-Stroke SI engine, Rated Power- 5.4 KW, Rated RPM- 5800, Stroke- 56.9 mm
Bore- 50 mm, Displacement - 92.2 cc

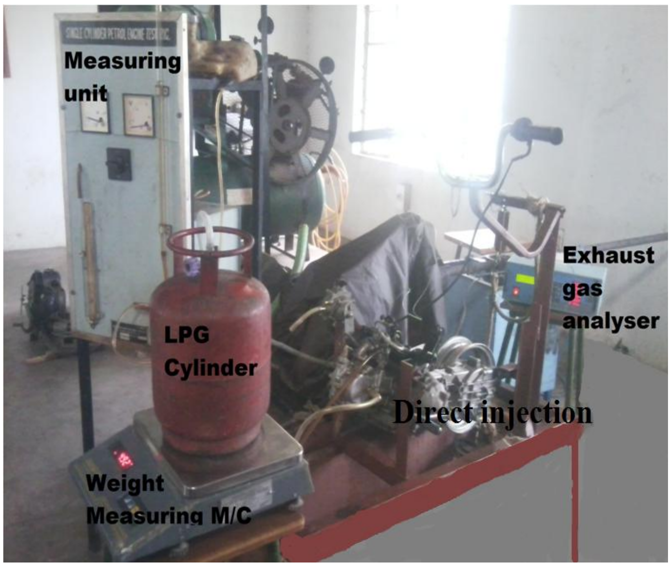

IV. RESULTS AND DISCUSSION

Effect of Exhaust Pollution of the % CO

% CO EMISSION VS LOAD

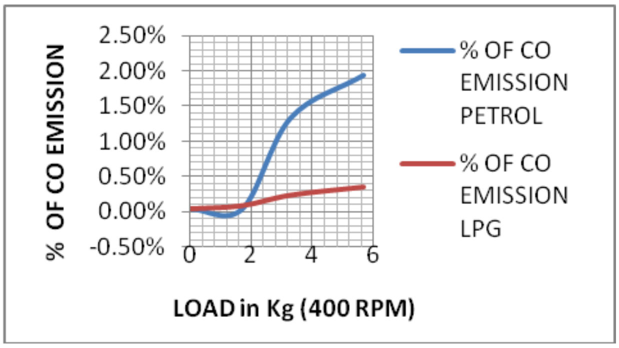

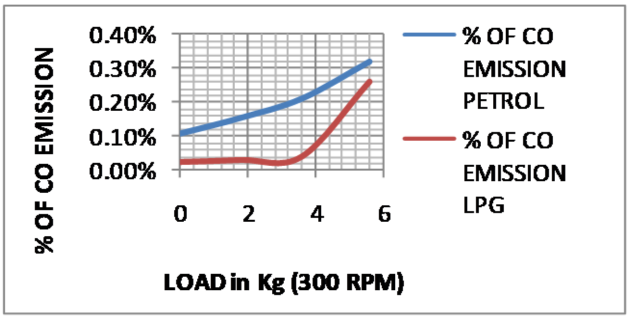

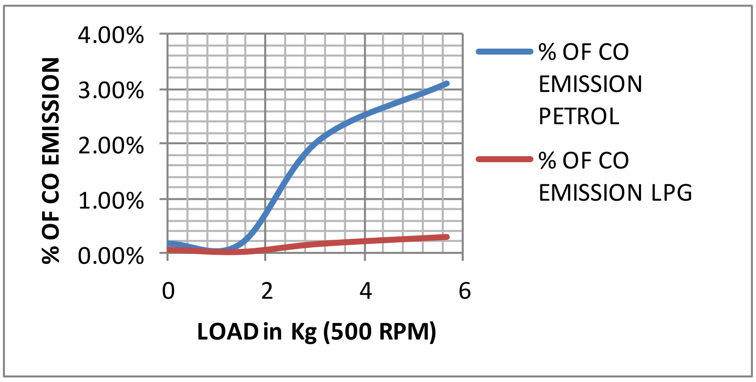

With rich fuel-air mixture, there is insufficient Oxygen to burn fully all the carbon in the fuel to CO_2 also CO high temperature produces. Maximum is generated when an engine runs rich fuel ratio. Poor mixing, local rich regions and incomplete Combustion will also be the source for CO emission. In this experiment Load engine will be increases so increases fuel-air mixture rich, amount oxygen is less so emission of CO will increases. CO emission produced by DI engine is even lower than original petrol engine. The value of CO concentration increases steadily with increases load.

Effect of Exhaust Pollution of the HC in PPM

HC EMISSION VS LOAD

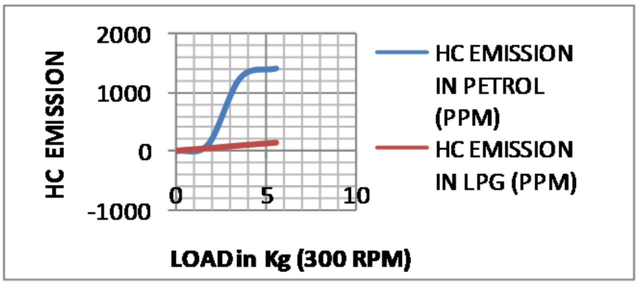

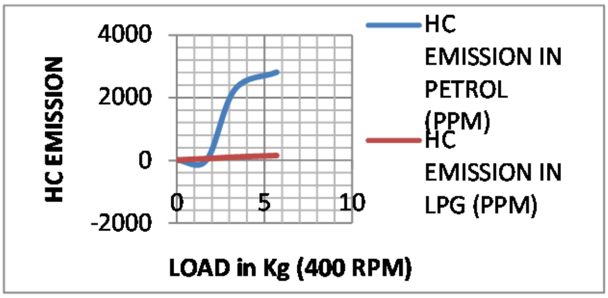

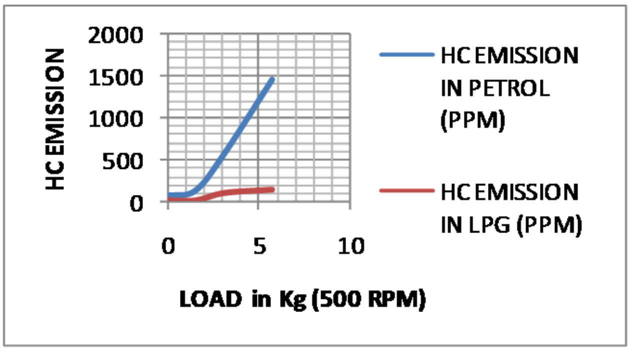

Petrol is in liquid from and LPG is in gaseous state so in combustion chamber quench layer containing Unburned and partially burned fuel-air mixture is left at the wall more in petrol. It is evident that it is a strong function of air –fuel ratio. With a fuel –rich mixture there is not enough oxygen to react with all the carbon, resulting in high level of HC and CO in the exhaust products. If air-fuel ratio is too lean poorer combustion occurs, against resulting in HC emission. Piston blowby gases and fuel evaporation

And release to the atmosphere through vent in the fuel tank and carburetor after engine shut- down, are also sources of unburned hydrocarbon. A quench layer containing unburned and partially burned fuel-air mixture is left at the wall when the flame is extinguished as it approaches the wall. Any engine oil left in a thin film on the cylinder wall, piston and perhaps on the cylinder head. In this experiment LPG injected in combustion chamber direct . HC emissions with varying engine speed for LPG and gasoline were illustrated in Fig. Load goes on increases with constant speed, emission of HC increases but in petrol HC emission rate is high than LPG. Load goes on increases, so increases combustion temperature and increases rich condition the fuel that the time oxygen quantity will be a less. That the reason HC is increases. As comparing between gasoline (C_7H_{18}) and LPG (C_3H_8) contain of hydrogen is less in LPG, so emission of HC is also less than gasoline.

Effect of Exhaust Pollution of the NO_x in PPM

NO_x **VS LOAD**

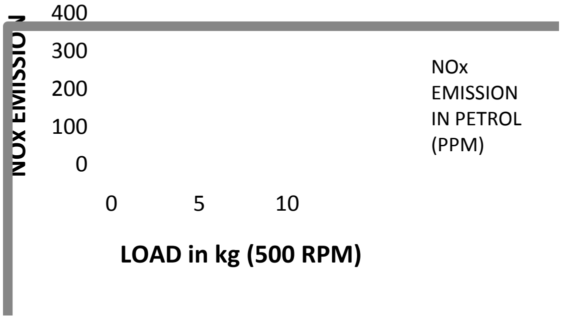

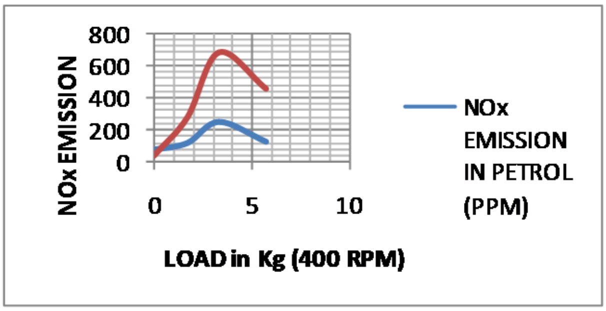

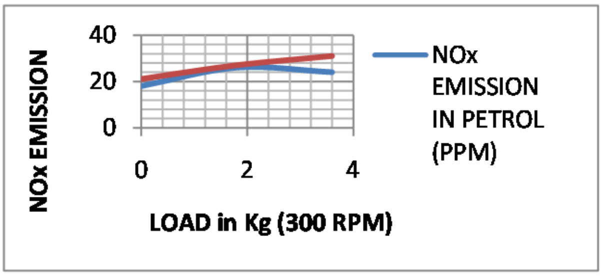

Higher the burned temperature, the higher the rate of formation of NOx, Most of the NO with a small amount of NO_2. Maximum NOx emission occurs in stoichiometric fuel-air ratio at slightly lean condition Excess of oxygen react with the nitrogen. In this experiment NOx in DI engine is always higher than original engine. The results regarding NOx also indicate that NOx emission from LPG is higher than petrol. Combustion temperature is high in LPG systems, so NOx emission is high in LPG because CV of LPG higher than petrol.

Effect of Exhaust Pollution of the % CO_2

% CO_2 EMISSION VS LOAD

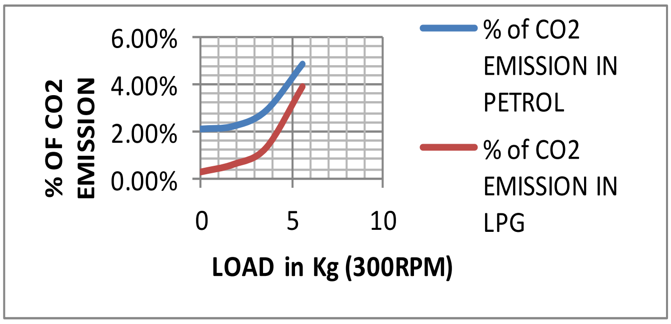

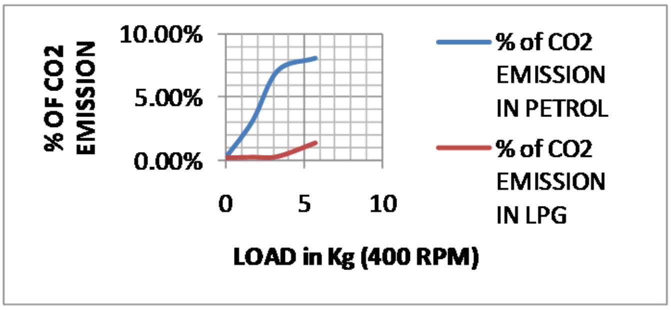

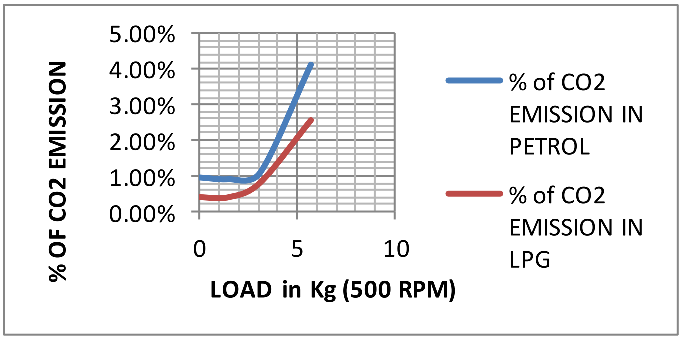

LPG gas has low carbon and high octane no. fuel Produces lower CO_2 than petrol. With rich fuel -air mixture, there are insufficient Oxygen to burn fully all the carbon in the fuel to CO_2 also CO High temperature produces. Maximum is generated when an engine runs rich fuel ratio. In this experiment LPG direct injected in combustion chamber and petrol mix with air injected through carburetor in combustion Chamber.

Conclude that LPG direct injected system CO_2 emission is higher than gasoline. Because of carbon contain in gasoline is high than LPG.

V. CONCLUSIONS

In this exhaust emission test five types of emission are to be tested. These emissions are CO, CO_2, HC, O_2, and NO_x. These are five types of emission are test will be perform on four stroke SI engine. Test will be performs on petrol and LPG.

Engine emitted CO emission in various speed, LPG system has been CO emission emitted less than petrol system. The CO emission is reducing in LPG then Gasoline for same load and rpm In Direct injection. Engine speed and load increases, so increasing percentage of CO in petrol system. As compare to gasoline HC is low in LPG direct injection as load increase HC increases. In HC emission also more in petrol system. Engine speed and load increases, so increasing percentage of HC in petrol system. HC emitted percentage is high in petrol system because hydrogen and carbon contain in petrol (C_8H_{18}) is high and low calorific value than LPG. Also petrol is in the liquid state and LPG is in gaseous state. The CO_2 emission of LPG is also lower than Gasoline for same load and rpm In Direct injection. In CO_2 emission in petrol system is always be more than LPG. Because of carbon contain is less and calorific value is more so LPG is emitted CO_2 less than petrol. Engine speed and load increases. NO_x is slightly increases in LPG In Direct injection. In The results regarding NOx also indicate that NOx emission from LPG is higher than petrol. Combustion temperature is high in LPG system NOx emission is high in LPG because CV of LPG higher than petrol. In NOx emission also more in LPG system.

REFERENCES

[1] Yuh-Yih Wu, Bo-Chiuan Chen, Anh-Trung Tran(*Emissions and Performances Improvement of Semi-Direct Injection Spark Ignition Engine Fuelled by LPG)*Journal Aerosol and quality Research , ISSN:1680-8584, Taiwan Association for Aerosol Research .

[2] Seshaiah N. **(***Efficiency and exhaust gas analysis of variable compression ratio spark ignition engine fuelled with alternative fuels)* International journal of volume 1, Issue 5, 2010 pp.861-870.

[3] Meghare D, Kannake D. R., S. S. Sontakke (*Experimental investigations on LPG as alternative Fuel for two wheeler)* International Journal of Engineering and Innovative Technology (IJEIT) Volume 2, Issue 1, July 2012 ISSN: 2277-3754

[4] Albela H.Pundkar, S.M. Lawankar, Dr. Sameer Deshmukh(*Performance and Emissions of LPG Fueled Internal Combustion Engine)*International Journal of Scientific & Engineering Research Volume 3, Issue 3, March -2012 1 ISSN 2229-5518 IJSER © 2012 http://www.ijser.org

[5] Syed Yousufuddin, *(Performance and Emission Characteristics of LPG-Fuelled Variable Compression Ratio SI Engine)*Turkish J. Eng. Env. Sci.32 (2008) , 7 – 12.@TUBITAK

[6] Tasic, Ppgorevc, Brajilih *(Gasoline and LPG Exhaust Emission comparison)* Advances in production engineering and management 6(2011)2,87-94 ISSN 1854-6250.

[7] Mayank Jha, Archana Singh, R.K Tyagi and M K Verma (*Comparative Study of Exhaust Emission of Commonly Used Fuel in an Internal Combustion Engine)*JECET; December 2012 –February 2013; Vol.2, No.1, 52-56.

[8] Ganeshan V.‘‘internal combustion engine ” third edition Published By the Tata McGraw-Hill Publishing company Limited, 7 West Patel Nagar New Delhi 110008. Pp185-234,313-355.371-407

[9] www.cryton.co.za on dt.26.06.2012

[10] www.freepatentsonline.com on dt.26.06.2012

[11] aaqr.org/Articleslnpress/AAQR-11-09-OA-0142-Prof.pdf on dt. 13.07.2012

[12] www.tsme.org/tsme-icome01/paper/AEC/AEC004. pdf on dt. 13.07.2012

A Special Type Of Differential Polynomial And Its Comparative Growth Properties

Sanjib Kumar Datta[1], Ritam Biswas[2]
[1]Department of Mathematics, University of Kalyani, Kalyani, Dist.- Nadia, PIN- 741235, West Bengal, India.
[2]Murshidabad College of Engineering and Technology, Banjetia, Berhampore, P. O.-Cossimbazar Raj, PIN-742102, West Bengal, India

Abstract: *Some new results depending upon the comparative growth rates of composite entire and meromorphic function and a special type of differential polynomial as considered by Bhooshnurmath and Prasad[3] and generated by one of the factors of the composition are obtained in this paper.*
AMS Subject Classification (2010) : *30D30, 30D35.*

Keywords and phrases: *Order (lower order), hyper order (hyper lower order), growth rate, entire function, meromorphic function and special type of differential polynomial.*

I. INTRODUCTION, DEFINITIONS AND NOTATIONS.

Let $\mathbb{C}$ be the set of all finite complex numbers. Also let f be a meromorphic function and g be an entire function defined on $\mathbb{C}$. In the sequel we use the following two notations:

$$(i)\ \log^{[k]}x = \log(\log^{[k-1]}x) \quad for\ k = 1,2,3,\ldots;\ \log^{[0]}x = x$$

and

$$(ii)\ \exp^{[k]}x = \exp\left(exp^{[k-1]}x\right)\ for\ k = 1,2,3,\ldots;\ \exp^{[0]}x = x.$$

The following definitions are frequently used in this paper:

Definition 1 *The order ρ_f and lower order λ_f of a meromorphic function f are defined as*

$$\rho_f = \limsup_{r\to\infty} \frac{\log T(r,f)}{\log r}$$

and

$$\lambda_f = \liminf_{r\to\infty} \frac{\log T(r,f)}{\log r}.$$

If f is entire, one can easily verify that

$$\rho_f = \limsup_{r\to\infty} \frac{\log^{[2]} M(r,f)}{\log r}$$

and

$$\lambda_f = \liminf_{r\to\infty} \frac{\log^{[2]} M(r,f)}{\log r}.$$

Definition 2 *The hyper order $\overline{\rho}_f$ and hyper lower order $\overline{\lambda}_f$ of a meromorphic function f are defined as follows*

$$\overline{\rho}_f = \limsup_{r\to\infty} \frac{\log^{[2]} T(r,f)}{\log r}$$

and

$$\overline{\lambda}_f = \liminf_{r\to\infty} \frac{\log^{[2]} T(r,f)}{\log r}.$$

If f is entire, then

$$\overline{\rho}_f = \limsup_{r\to\infty} \frac{\log^{[3]} M(r,f)}{\log r}$$

and

$$\overline{\lambda}_f = \liminf_{r\to\infty} \frac{\log^{[3]} M(r,f)}{\log r}.$$

Definition 3 *The type σ_f of a meromorphic function f is defined as follows*

$$\sigma_f = \limsup_{r\to\infty} \frac{T(r,f)}{r^{\rho_f}}, 0 < \rho_f < \infty.$$

When f is entire, then

$$\sigma_f = \limsup_{r\to\infty} \frac{\log M(r,f)}{r^{\rho_f}}, 0 < \rho_f < \infty.$$

Definition 4 *A function $\lambda_f(r)$ is called a lower proximate order of a meromorphic function f of finite lower order λ_f if*

(i) $\lambda_f(r)$ *is non-negative and continuous for* $r \geq r_0$, *say*

(ii) $\lambda_f(r)$ *is differentiable for* $r \geq r_0$ *except possibly at isolated points at which* $\lambda_f'(r+0)$ *and* $\lambda_f'(r-0)$ *exists,*

(iii)

$$\lim_{r\to\infty} \lambda_f(r) = \lambda_f,$$

(iv)

$$\lim_{r\to\infty} r\lambda_f'(r)\log r = 0$$

and

(v)

$$\liminf_{r\to\infty} \frac{T(r,f)}{r^{\lambda_f(r)}} = 1.$$

Definition 5 *Let 'a' be a complex number, finite or infinite. The Nevanlinna's deficiency and Valiron deficiency of 'a' with respect to a meromorphic function f are defined as*

$$\delta(a;f) = 1 - \limsup_{r\to\infty} \frac{N(r,a;f)}{T(r,f)} = \liminf_{r\to\infty} \frac{m(r,a;f)}{T(r,f)}$$

and

$$\Delta(a;f) = 1 - \liminf_{r\to\infty} \frac{N(r,a;f)}{T(r,f)} = \limsup_{r\to\infty} \frac{m(r,a;f)}{T(r,f)}.$$

Let f be a non-constant meromorphic function defined in the open complex plane $\mathbb{C}$. Also let $n_{0j}, n_{1j},\ldots, n_{kj}$ $(k \geq 1)$ be non-negative integers such that for each j, $\sum_{i=0}^{k} n_{ij} \geq 1$. We call

$$M_j[f] = A_j(f)^{n_{0j}}(f^{(1)})^{n_{1j}} \ldots (f^{(k)})^{n_{kj}}$$

where $T(r,A_j) = S(r,f)$, to be a differential monomial generated by f. The numbers

$$\gamma_{M_j} = \sum_{i=0}^{k} n_{ij}$$

and

$$\Gamma_{M_j} = \sum_{i=0}^{k} (i+1)n_{ij}$$

are called the degree and weight of $M_j[f]$ {cf. [4]} respectively. The expression

$$P[f] = \sum_{j=1}^{s} M_j[f]$$

is called a differential polynomial generated by f. The numbers

$$\gamma_P = \max_{1\leq j\leq s} \gamma_{M_j}$$

and

$$\Gamma_P = \max_{1\leq j\leq s} \Gamma_{M_j}$$

are respectively called the degree and weight of $P[f]$ {cf. [4]}. Also we call the numbers

$$\underline{\gamma_P} = \min_{1\leq j\leq s} \gamma_{M_j}$$

and k (the order of the highest derivative of f) the lower degree and the order of $P[f]$ respectively. If $\underline{\gamma_P} = \gamma_P$, $P[f]$ is called a homogeneous differential polynomial.

Bhooshnurmath and Prasad [3] considered a special type of differential polynomial of the form $F = f^n Q[f]$ where $Q[f]$ is a differential polynomial in f and n = 0, 1, 2,…. In this paper we intend to prove some improved results depending upon the comparative growth properties of the composition of entire and meromorphic functions and a special type of differential polynomial as mentioned above and generated by one of the factors of the composition. We do not explain the standard notations and definitions in the theory of entire and meromorphic functions because those are available in [9] and [5].

II. LEMMAS.

In this section we present some lemmas which will be needed in the sequel.

Lemma 1 *[1] If f is meromorphic and g is entire then for all sufficiently large values of r,*

$$T(r,f_o g) \leq \{1+o(1)\}\frac{T(r,g)}{\log M(r,g)} T(M(r,g),f).$$

Lemma 2 *[2] Let f be meromorphic and g be entire and suppose that $0 < \mu < \rho_g \leq \infty$. Then for a sequence of values of r tending to infinity,*

$$T(r,f_o g) \geq T(\exp(r^\mu),f).$$

Lemma 3 *[3] Let $F = f^n Q[f]$ where Q[f] is a differential polynomial in f. If $n \geq 1$ then $\rho_F = \rho_f$ and $\lambda_F = \lambda_f$.*

Lemma 4 *Let $F = f^n Q[f]$ where Q[f] is a differential polynomial in f. If $n \geq 1$ then*

$$\lim_{r\to\infty} \frac{T(r,\ F)}{T(r,f)} = 1.$$

The proof of Lemma 4 directly follows from Lemma 3.

In the line of Lemma 3 we may prove the following lemma:

Lemma 5 *Let $F = f^n Q[f]$ where Q[f] is a differential polynomial in f. If n ≥ 1 then $\overline{\rho}_F = \overline{\rho}_f$ and $\overline{\lambda}_F = \overline{\lambda}_f$.*

Lemma 6 *For a meromorphic function f of finite lower order, lower proximate order exists.*

The lemma can be proved in the line of Theorem 1 [7] and so the proof is omitted.

Lemma 7 *Let f be a meromorphic function of finite lower order λ_f. Then for $\delta(> 0)$ the function $r^{\lambda_f + \delta - \lambda_f(r)}$ is an increasing function of r.*

Proof. Since

$$\frac{d}{dr} r^{\lambda_f + \delta - \lambda_f(r)} = \{\lambda_f + \delta - \lambda_f(r) - r\lambda_f' \log r\} r^{\lambda_f + \delta - \lambda_f(r) - 1} > 0$$

for sufficiently large values of r, the lemma follows.

Lemma 8 *[6] Let f be an entire function of finite lower order. If there exists entire functions a_i (i= 1, 2, 3,…, n; n ≤ ∞) satisfying $T(r, a_i) = o\{T(r, f)\}$ and*

$$\sum_{i=1}^{n} \delta(a_i, f) = 1,$$

then

$$\lim_{r\to\infty} \frac{T(r, f)}{\log M(r, f)} = \frac{1}{\pi}.$$

III. THEOREMS.

In this section we present the main results of the paper.

Theorem 1 *Let f be a meromorphic function and g be an entire function satisfying*
(i) λ_f, λ_g are both finite and
(ii) for $n \geq 1, G = g^n Q[g]$. Then

$$\liminf_{r\to\infty} \frac{\log T(r, f_o g)}{T(r, G)} \leq 3.\rho_f.2^{\lambda_g}.$$

Proof. If $\rho_f = \infty$, the result is obvious. So we suppose that $\rho_f < \infty$. Since $T(r, g) \leq \log^+ M(r, g)$, in view of Lemma 1 we get for all sufficiently large values of r that

$$T(r, f_o g) \leq \{1 + o(1)\} T(M(r, g), f)$$

i.e.,

$$\log T(r, f_o g) \leq \log\{1 + o(1)\} + \log T(M(r, g), f)$$

i.e.,

$$\log T(r, f_o g) \leq o(1) + (\rho_f + \varepsilon) \log M(r, g)$$

i.e.,

$$\liminf_{r\to\infty} \frac{\log T(r, f_o g)}{T(r, g)} \leq (\rho_f + \varepsilon) \liminf_{r\to\infty} \frac{\log M(r, g)}{T(r, g)}.$$

Since $\varepsilon(> 0)$ is arbitrary, it follows that

$$\liminf_{r\to\infty} \frac{\log T(r, f_o g)}{T(r, g)} \leq \rho_f . \liminf_{r\to\infty} \frac{\log M(r, g)}{T(r, g)}. \quad (1)$$

As by condition (v) of Definition 4

$$\liminf_{r\to\infty} \frac{T(r, g)}{r^{\lambda_g(r)}} = 1,$$

so for given $\varepsilon(0 < \varepsilon < 1)$ we get for a sequence of values of r tending to infinity that

$$T(r, g) \leq (1 + \varepsilon) r^{\lambda_g(r)} \quad (2)$$

and for all sufficiently large values of r,

$$T(r, g) > (1 - \varepsilon) r^{\lambda_g(r)} \quad (3)$$

Since

$$\log M(r, g) \leq 3T(2r, g)$$

{cf. [5]}, we have by (2), for a sequence of values of r tending to infinity,

$$\log M(r, g) \leq 3T(2r, g) \leq 3(1 + \varepsilon)(2r)^{\lambda_g(2r)}. \quad (4)$$

Combining (3) and (4), we obtain for a sequence of values of r tending to infinity that

$$\frac{\log M(r, g)}{T(r, g)} \leq \frac{3(1 + \varepsilon)}{(1 - \varepsilon)} . \frac{(2r)^{\lambda_g(2r)}}{r^{\lambda_g(r)}}.$$

Now for any $\delta(> 0)$, for a sequence of values of r tending to infinity we obtain that

$$\frac{\log M(r, g)}{T(r, g)} \leq \frac{3(1 + \varepsilon)}{(1 - \varepsilon)} . \frac{(2r)^{\lambda_g + \delta}}{(2r)^{\lambda_g + \delta - \lambda_g(2r)}} . \frac{1}{r^{\lambda_g(r)}}$$

i.e.,

$$\frac{\log M(r,g)}{T(r,g)} \leq \frac{3(1+\varepsilon)}{(1-\varepsilon)}.2^{\lambda_g+\delta} \qquad (5)$$

because $r^{\lambda_g+\delta-\lambda_g(r)}$ is an increasing function of r by Lemma 7. Since $\varepsilon(>0)$ and $\delta(>0)$ are arbitrary, it follows from (5) that

$$\liminf_{r\to\infty} \frac{\log M(r,g)}{T(r,g)} \leq 3.2^{\lambda_g}. \qquad (6)$$

Thus from (1) and (6) we obtain that

$$\liminf_{r\to\infty} \frac{\log T(r,f_o g)}{T(r,g)} \leq 3.\rho_f.2^{\lambda_g}. \qquad (7)$$

Now in view of (7) and Lemma 3, we get that

$$\liminf_{r\to\infty} \frac{\log T(r,f_o g)}{T(r,G)} = \liminf_{r\to\infty} \frac{\log T(r,f_o g)}{T(r,g)}.\lim_{r\to\infty}\frac{T(r,g)}{T(r,G)}$$
$$\leq 3.\rho_f.2^{\lambda_g}.$$

This proves the theorem.

Theorem 2 *Let f be meromorphic and g be entire such that $\rho_f < \infty, \lambda_g < \infty$ and for $n \geq 1, G = g^n Q[g]$. Then*

$$\liminf_{r\to\infty} \frac{\log^{[2]} T(r,f_o g)}{\log T(r,G)} \leq 1.$$

Proof. Since

$$T(r,g) \leq \log^+ M(r,g),$$

in view of Lemma 1, we get for all sufficiently large values of r that

$$\log T(r,f_o g) \leq \log T(M(r,g),f) + \log\{1+o(1)\}$$

i.e.,

$$\log T(r,f_o g) \leq (\rho_f+\varepsilon)\log M(r,g) + o(1)$$

i.e.,

$$\log^{[2]} T(r,f_o g) \leq \log^{[2]} M(r,g) + O(1). \qquad (8)$$

It is well known that for any entire function g,

$$\log M(r,g) \leq 3T(2r,g) \qquad \{cf.[5]\}.$$

Then for $0<\varepsilon<1$ and $\delta(>0)$, for a sequence of values of r tending to infinity it follows from (5) that

$$\log^{[2]} M(r,g) \leq \log T(r,g) + O(1). \qquad (9)$$

Now combining (8) and (9), we obtain for a sequence of values of r tending to infinity that

$$\log^{[2]} T(r,f_o g) \leq \log T(r,g) + O(1)$$

i.e.,

$$\frac{\log^{[2]} T(r,f_o g)}{\log T(r,g)} \leq 1. \qquad (10)$$

As by Lemma 4,

$$\lim_{r\to\infty}\frac{\log T(r,g)}{\log T(r,G)}$$

exists and is equal to 1, then from (10) we get that

$$\liminf_{r\to\infty} \frac{\log^{[2]} T(r,f_o g)}{\log T(r,G)} = \liminf_{r\to\infty} \frac{\log^{[2]} T(r,f_o g)}{\log T(r,g)}.\lim_{r\to\infty}\frac{\log T(r,g)}{\log T(r,G)}$$
$$\leq 1.1 = 1.$$

Thus the theorem is established.

Remark 1 The *condition $\rho_f < \infty$ is essential in Theorem 2 which is evident from the following example.*

Example 1 *Let $f = \exp^{[2]} z$ and $g = \exp z$. Then $f_o g = \exp^{[3]} z$ and for $n \geq 1, G = g^n Q[g]$. Taking $n=1, A_j = 1, n_{0j} = 1$ and $n_{1j} = \cdots = n_{kj} = 0$; we see that $G = \exp(2z)$. Now we have*

$$\rho_f = \limsup_{r\to\infty} \frac{\log^{[2]} M(r,f)}{\log r} = \limsup_{r\to\infty} \frac{\log^{[2]}(\exp^{[2]} r)}{\log r} = \infty$$

and

$$\lambda_g = \liminf_{r\to\infty} \frac{\log^{[2]} M(r,g)}{\log r} = \liminf_{r\to\infty} \frac{\log^{[2]}(\exp r)}{\log r} = 1.$$

Again from the inequality

$$T(r,f) \leq \log^+ M(r,f) \leq 3T(2r,f)$$

{cf. p.18, [5]} we obtain that

$$T(r,G) \leq \log M(r,G) = \log(\exp 2r)$$

i.e.,

$$\log T(r,G) \leq \log r + O(1)$$

and

$$T(r, f_o g) \geq \frac{1}{3} \log M\left(\frac{r}{2}, f_o g\right) = \frac{1}{3} \exp^{[2]}\left(\frac{r}{2}\right)$$

i.e.,

$$\log^{[2]} T(r, f_o g) \geq \frac{r}{2} + O(1).$$

Combining the above two inequalities, we have

$$\frac{\log^{[2]} T(r, f_o g)}{\log T(r,G)} \geq \frac{\frac{r}{2} + O(1)}{\log r + O(1)}.$$

Therefore

$$\liminf_{r\to\infty} \frac{\log^{[2]} T(r, f_o g)}{\log T(r,G)} = \infty,$$

which is contrary to Theorem 2.

Theorem 3 *Let f and g be any two entire functions such that $\rho_g < \lambda_f \leq \rho_f < \infty$ and for $n \geq 1, F = f^n Q[f]$ and $G = g^n Q[g]$. Also there exist entire functions a_i ($i = 1, 2,\dots, n$; $n \leq \infty$) with*

$$(i) T(r, a_i) = o\{T(r,g)\} \text{ as } r \to \infty \text{ for } i = 1, 2, \dots, n$$

and

$$(ii) \sum_{i=1}^{n} \delta(a_i; g) = 1.$$

Then

$$\lim_{r\to\infty} \frac{\{\log T(r, f_o g)\}^2}{T(r,F)T(r,G)} = 0.$$

Proof. In view of the inequality

$$T(r,g) \leq \log^+ M(r,g)$$

and Lemma 1, we obtain for all sufficiently large values of r that

$$T(r, f_o g) \leq \{1 + o(1)\} T(M(r,g), f)$$

i.e.,

$$\log T(r, f_o g) \leq \log\{1 + o(1)\} + \log T(M(r,g), f)$$

i.e.,

$$\log T(r, f_o g) \leq o(1) + \left(\rho_f + \varepsilon\right) \log M(r,g)$$

i.e.,

$$\log T(r, f_o g) \leq o(1) + \left(\rho_f + \varepsilon\right) r^{(\rho_g + \varepsilon)}. \tag{11}$$

Again in view of Lemma 3, we get for all sufficiently large values of r that

$$\log T(r,F) > (\lambda_F - \varepsilon) \log r$$

i.e.,

$$\log T(r,F) > \left(\lambda_f - \varepsilon\right) \log r$$

i.e.,

$$T(r,F) > r^{\lambda_f - \varepsilon}. \tag{12}$$

Now combining (11) and (12), it follows for all sufficiently large values of r that

$$\frac{\log T(r, f_o g)}{T(r,F)} \leq \frac{o(1) + (\rho_f + \varepsilon) r^{(\rho_g + \varepsilon)}}{r^{\lambda_f - \varepsilon}}. \tag{13}$$

Since $\rho_g < \lambda_f$, we can choose $\varepsilon (> 0)$ in such a way that

$$\rho_g + \varepsilon < \lambda_f - \varepsilon. \tag{14}$$

So in view of (13) and (14), it follows that

$$\lim_{r\to\infty} \frac{\log T(r, f_o g)}{T(r,F)} = 0. \tag{15}$$

Again from Lemma 4 and Lemma 8, we get for all sufficiently large values of r that

$$\frac{\log T(r, f_o g)}{T(r,G)} \leq \frac{o(1) + \left(\rho_f + \varepsilon\right) \log M(r,g)}{T(r,G)}$$

i.e.,

$$\limsup_{r\to\infty} \frac{\log T(r, f_o g)}{T(r,G)} \leq (\rho_f + \varepsilon) \limsup_{r\to\infty} \frac{\log M(r,g)}{T(r,G)}$$

i.e.,

$$\limsup_{r\to\infty} \frac{\log T(r, f_o g)}{T(r,G)} \leq (\rho_f + \varepsilon) \limsup_{r\to\infty} \frac{\log M(r,g)}{T(r,g)} . \lim_{r\to\infty} \frac{T(r,g)}{T(r,G)}$$

i.e.,

$$\limsup_{r\to\infty} \frac{\log T(r, f_o g)}{T(r,G)} \leq (\rho_f + \varepsilon). \pi.$$

Since $\varepsilon(> 0)$ is arbitrary, it follows from above that

$$\limsup_{r\to\infty} \frac{\log T(r, f_o g)}{T(r,G)} \leq \rho_f . \pi. \qquad (16)$$

Combining (15) and (16), we obtain that

$$\limsup_{r\to\infty} \frac{\{\log T(r, f_o g)\}^2}{T(r,F) T(r,G)}$$

$$= \lim_{r\to\infty} \frac{\log T(r, f_o g)}{T(r,F)} . \limsup_{r\to\infty} \frac{\log T(r, f_o g)}{T(r,G)}$$

$$\leq 0. \pi. \rho_f = 0,$$

i.e.,

$$\lim_{r\to\infty} \frac{\{\log T(r, f_o g)\}^2}{T(r,F) T(r,G)} = 0.$$

This proves the theorem.

Theorem 4 *Let f and g be any two entire functions satisfying the following conditions:* (i) $\lambda_f > 0$ (ii) $\overline{\rho}_f < \infty$ (iii) $0 < \lambda_g \leq \rho_g$ *and also let for* $n \geq 1, F = f^n Q[f]$. *Then*

$$\limsup_{r\to\infty} \frac{\log^{[2]} T(r, f_o g)}{\log^{[2]} T(r,F)} \geq \max\{\frac{\lambda_g}{\overline{\lambda}_f}, \frac{\rho_g}{\overline{\rho}_f}\}.$$

Proof. We know that for $r > 0$ {cf. [8]} and for all sufficiently large values of r,

$$T(r, f_o g) \geq \frac{1}{3} \log M \left\{\frac{1}{8} M\left(\frac{r}{4}, g\right) + o(1), f\right\}. \qquad (17)$$

Since λ_f and λ_g are the lower orders of f and g respectively then for given $\varepsilon(> 0)$ and for all sufficiently large values of r we obtain that

$$\log M(r,f) > r^{\lambda_f - \varepsilon}$$

and

$$\log M(r,g) > r^{\lambda_g - \varepsilon}$$

where $0 < \varepsilon < \min\{\lambda_f, \lambda_g\}$. So from (17) we have for all sufficiently large values of r,

$$T(r, f_o g) \geq \frac{1}{3} \left\{\frac{1}{8} M\left(\frac{r}{4}, g\right) + o(1)\right\}^{\lambda_f - \varepsilon}$$

i.e.,

$$T(r, f_o g) \geq \frac{1}{3} \{\frac{1}{9} M(\frac{r}{4}, g)\}^{\lambda_f - \varepsilon}$$

i.e.,

$$\log T(r, f_o g) \geq O(1) + (\lambda_f - \varepsilon) \log M(\frac{r}{4}, g)$$

i.e.,

$$\log T(r, f_o g) \geq O(1) + (\lambda_f - \varepsilon) (\frac{r}{4})^{\lambda_g - \varepsilon}$$

i.e.,

$$\log^{[2]} T(r, f_o g) \geq O(1) + (\lambda_g - \varepsilon) \log r. \qquad (18)$$

Again in view of Lemma 1, we get for a sequence of values r tending to infinity that

$$\log^{[2]} T(r,F) \leq (\overline{\lambda}_F + \varepsilon) \log r$$

i.e.,

$$\log^{[2]} T(r,F) \leq (\overline{\lambda}_f + \varepsilon) \log r. \qquad (19)$$

Combining (18) and (19), it follows for a sequence of values of r tending to infinity that

$$\frac{\log^{[2]} T(r, f_o g)}{\log^{[2]} T(r,F)} \geq \frac{O(1) + (\lambda_g - \varepsilon) \log r}{(\overline{\lambda}_f + \varepsilon) \log r}.$$

Since $\varepsilon(> 0)$ is arbitrary, we obtain that

$$\limsup_{r\to\infty} \frac{\log^{[2]} T(r, f_o g)}{\log^{[2]} T(r,F)} \geq \frac{\lambda_g}{\overline{\lambda}_f}. \qquad (20)$$

Again from (17), we get for a sequence of values of r tending to infinity that

$$\log T(r, f_o g) \geq O(1) + (\lambda_f - \varepsilon)(\frac{r}{4})^{\rho_g - \varepsilon}$$

i.e.,

$$\log^{[2]} T(r, f_o g) \geq O(1) + \left(\rho_g - \varepsilon\right) \log r. \quad (21)$$

Also in view of Lemma 5, for all sufficiently large values of r we have

$$\log^{[2]} T(r, F) \leq \left(\overline{\rho}_F + \varepsilon\right) \log r$$

i.e.,

$$\log^{[2]} T(r, F) \leq \left(\overline{\rho}_f + \varepsilon\right) \log r. \quad (22)$$

Now from (21) and (22), it follows for a sequence of values of r tending to infinity that

$$\frac{\log^{[2]} T(r, f_o g)}{\log^{[2]} T(r, F)} \geq \frac{O(1) + \left(\rho_g - \varepsilon\right) \log r}{\left(\overline{\rho}_f + \varepsilon\right) \log r}.$$

As $\varepsilon (0 < \varepsilon < \rho_g)$ is arbitrary, we obtain from above that

$$\limsup_{r \to \infty} \frac{\log^{[2]} T(r, f_o g)}{\log^{[2]} T(r, F)} \geq \frac{\rho_g}{\overline{\rho}_f}. \quad (23)$$

Therefore from (20) and (23), we get that

$$\limsup_{r \to \infty} \frac{\log^{[2]} T(r, f_o g)}{\log^{[2]} T(r, F)} \geq \max\{\frac{\lambda_g}{\overline{\lambda}_f}, \frac{\rho_g}{\overline{\rho}_f}\}.$$

Thus the theorem is established.

Theorem 5 *Let f be meromorphic and g be entire such that (i) $0 < \overline{\lambda}_f < \overline{\rho}_f$, (ii) $\rho_g < \infty$, (iii) $\rho_f < \infty$ and (iv) for $n \geq 1$, $F = f^n Q[f]$. Then*

$$\liminf_{r \to \infty} \frac{\log^{[2]} T(r, f_o g)}{\log^{[2]} T(r, F)} \leq \min\{\frac{\lambda_g}{\overline{\lambda}_f}, \frac{\rho_g}{\overline{\rho}_f}\}.$$

Proof. In view of Lemma 1 and the inequality

$$T(r, g) \leq \log^+ M(r, g),$$

we obtain for all sufficiently large values of r that

$$\log T(r, f_o g) \leq o(1) + \left(\rho_f + \varepsilon\right) \log M(r, g). \quad (24)$$

Also for a sequence of values of r tending to infinity,

$$\log M(r, g) \leq r^{\lambda_g + \varepsilon}. \quad (25)$$

Combining (24) and (25), it follows for a sequence of values of r tending to infinity that

$$\log T(r, f_o g) \leq o(1) + (\rho_f + \varepsilon) r^{\lambda_g + \varepsilon}$$

i.e.,

$$\log T(r, f_o g) \leq r^{\lambda_g + \varepsilon} \{o(1) + (\rho_f + \varepsilon)\}$$

i.e.,

$$\log^{[2]} T(r, f_o g) \leq O(1) + \left(\lambda_g + \varepsilon\right) \log r. \quad (26)$$

Again in view of Lemma 5, we obtain for all sufficiently large values of r that

$$\log^{[2]} T(r, F) > \left(\overline{\lambda}_F - \varepsilon\right) \log r$$

i.e.,

$$\log^{[2]} T(r, F) > \left(\overline{\lambda}_f - \varepsilon\right) \log r. \quad (27)$$

Now from (26) and (27), we get for a sequence of values of r tending to infinity that

$$\frac{\log^{[2]} T(r, f_o g)}{\log^{[2]} T(r, F)} \leq \frac{O(1) + \left(\lambda_g + \varepsilon\right) \log r}{\left(\overline{\lambda}_f - \varepsilon\right) \log r}.$$

As $\varepsilon (> 0)$ is arbitrary, it follows that

$$\liminf_{r \to \infty} \frac{\log^{[2]} T(r, f_o g)}{\log^{[2]} T(r, F)} \leq \frac{\lambda_g}{\overline{\lambda}_f}. \quad (28)$$

In view of Lemma 1, we obtain for all sufficiently large values of r that

$$\log^{[2]} T(r, f_o g) \leq O(1) + \left(\rho_g + \varepsilon\right) \log r. \quad (29)$$

Also by Remark 1, it follows for a sequence of values of r tending to infinity that

$$\log^{[2]} T(r, F) > \left(\overline{\rho}_F - \varepsilon\right) \log r$$

i.e.,

$$\log^{[2]} T(r, F) > \left(\overline{\rho}_f - \varepsilon\right) \log r. \quad (30)$$

Combining (29) and (30), we get for a sequence of values of r tending to infinity that

$$\frac{\log^{[2]}T(r,f_o g)}{\log^{[2]}T(r,F)} \le \frac{O(1)+(\rho_g+\varepsilon)\log r}{(\overline{\rho}_f-\varepsilon)\log r}.$$

Since $\varepsilon(>0)$ is arbitrary, it follows from above that

$$\liminf_{r\to\infty}\frac{\log^{[2]}T(r,f_o g)}{\log^{[2]}T(r,F)} \le \frac{\rho_g}{\overline{\rho}_f}. \tag{31}$$

Now from (28) and (31), we get that

$$\liminf_{r\to\infty}\frac{\log^{[2]}T(r,f_o g)}{\log^{[2]}T(r,F)} \le \min\{\frac{\lambda_g}{\overline{\lambda}_f},\frac{\rho_g}{\overline{\rho}_f}\}.$$

This proves the theorem.
The following theorem is a natural consequence of Theorem 4 and Theorem 5:

Theorem 6 *Let f and g be any two entire functions such that*
$(i)\ 0<\overline{\lambda}_f<\overline{\rho}_f<\infty, (ii)\ 0<\lambda_f\le\rho_f<\infty, (iii)\ 0<\lambda_g\le\rho_g<\infty$ and
$(iv) for\ n\ge 1, F=f^nQ[f]$. Then

$$\liminf_{r\to\infty}\frac{\log^{[2]}T(r,f_o g)}{\log^{[2]}T(r,F)} \le \min\{\frac{\lambda_g}{\overline{\lambda}_f},\frac{\rho_g}{\overline{\rho}_f}\} \le \max\{\frac{\lambda_g}{\overline{\lambda}_f},\frac{\rho_g}{\overline{\rho}_f}\} \le \limsup_{r\to\infty}\frac{\log^{[2]}T(r,f_o g)}{\log^{[2]}T(r,F)}.$$

Theorem 7 *Let f be meromorphic and g be entire satisfying $0<\lambda_f\le\rho_f<\infty,\rho_g>0$ and also let for $n\ge 1$, $F=f^nQ[f]$. Then*

$$\limsup_{r\to\infty}\frac{\log^{[2]}T(\exp(r^{\rho_g}),f_o g)}{\log^{[2]}T(\exp(r^{\mu}),F)} = \infty,$$

where $0<\mu<\rho_g$.
Proof. Let $0<\mu^{'}<\rho_g$. Then in view of Lemma 2, we get for a sequence of values of r tending to infinity that

$$\log T(r,f_o g) \ge \log T(\exp(r^{\mu}),f)$$

i.e.,

$$\log T(r,f_o g) \ge (\lambda_f-\varepsilon)\log\{\exp(r^{\mu^{'}})\}$$

i.e.,

$$\log T(r,f_o g) \ge (\lambda_f-\varepsilon)r^{\mu^{'}}$$

i.e.,

$$\log^{[2]}T(r,f_o g) \ge O(1)+\mu^{'}\log r. \tag{32}$$

Again in view of Lemma 3, we have for all sufficiently large values of r,

$$\log T(\exp(r^{\mu}),F) \le (\rho_F+\varepsilon)\log\{\exp(r^{\mu})\}$$

i.e.,

$$\log T(\exp(r^{\mu}),F) \le (\rho_f+\varepsilon)r^{\mu}$$

i.e.,

$$\log T(\exp(r^{\mu}),F) \le O(1)+\mu\log r. \tag{33}$$

Now combining (32) and (33), we obtain for a sequence of values of r tending to infinity that

$$\frac{\log^{[2]}T(\exp(r^{\rho_g}),f_o g)}{\log^{[2]}T(\exp(r^{\mu}),F)} \ge \frac{O(1)+\mu^{'}r^{\rho_g}}{O(1)+\mu\log r}$$

from which the theorem follows.

Remark 2 *The condition $\rho_g>0$ is necessary in Theorem 7 as we see in the following example.*

Example 2 *Let $f=\exp z, g=z$ and $\mu=1(>0)$. Then $f_o g=\exp z$ and for $n\ge 1, F=f^nQ[f]$. Taking $n=1, A_j=1, n_{0j}=1$ and $n_{1j}=\cdots=n_{kj}=0$; we see that $F=\exp 2z$. Then*

$$\rho_f = \limsup_{r\to\infty}\frac{\log^{[2]}M(r,f)}{\log r} = 1,$$

$$\lambda_f = \liminf_{r\to\infty}\frac{\log^{[2]}M(r,f)}{\log r} = 1$$

and

$$\rho_g = \limsup_{r\to\infty}\frac{\log^{[2]}M(r,g)}{\log r} = 0.$$

Also we get that

$$T(r,f) = \frac{r}{\pi}.$$

Therefore

$$T(\exp(r^{\rho_g}), f_o g) = \frac{e}{\pi}$$

and

$$T(\exp(r^{\mu}), F) = \frac{2\exp r}{\pi}.$$

So from the above two expressions we obtain that

$$\frac{\log^{[2]} T(\exp(r^{\rho_g}), f_o g)}{\log^{[2]} T(\exp(r^{\mu}), F)} = \frac{O(1)}{\log r + O(1)}$$

i.e.,

$$\limsup_{r\to\infty} \frac{\log^{[2]} T(\exp(r^{\rho_g}), f_o g)}{\log^{[2]} T(\exp(r^{\mu}), F)} = 0,$$

which contradicts Theorem 7.

REFERENCES

[1] Bergweiler, W.: *On the Nevanlinna Characteristic of a composite function*, Complex Variables, Vol. 10 (1988), pp. 225-236.
[2] Bergweiler, W.: *On the growth rate of composite meromorphic functions*, Complex Variables, Vol. 14 (1990), pp. 187-196.
[3] Bhooshnurmath, S. S. and Prasad, K. S. L. N.: *The value distribution of some differential polynomials*, Bull. Cal. Math. Soc., Vol. 101, No. 1 (2009), pp. 55- 62.
[4] Doeringer, W.: *Exceptional values of differential polynomials*, Pacific J. Math., Vol. 98, No. 1 (1982), pp. 55-62.
[5] Hayman, W. K.: *Meromorphic functions*, The Clarendon Press, Oxford, 1964.
[6] Lin, Q. and Dai, C.: *On a conjecture of Shah concerning small functions*, Kexue Tongbao (English Ed.), Vol. 31, No. 4 (1986), pp. 220-224.
[7] Lahiri, I.: *Generalised proximate order of meromorphic functions*, Mat. Vensik, Vol. 41 (1989), pp. 9-16.
[8] Niino, K. and Yang, C. C.: *Some growth relationships on factors of two composite entire functions*, Factorization Theory of Meromorphic Functions and Related Topics, Marcel Dekker, Inc. (New York and Basel), (1982), pp. 95- 99.
[9] Valiron, G.: *Lectures on the general theory of integral functions*, Chelsea Publishing Company, 1949.

International Journal of Modern Engineering Research (IJMER)
www.ijmer.com Vol. 3, Issue. 5, Sep - Oct. 2013 pp-2615-2625 ISSN: 2249-6645

Scope of Improving Energy Utilization in Coal Based Co-Generation on Thermal Power Plant -Review

Sarang J. Gulhane[1], Prof. Amit Kumar Thakur[2], A. P. Pathre[3]

[1]*Department of Mechanical Engineering, Sagar Institute of Science and Technology Bhopal, India*
[2]*Department of Mechanical Engineering, Sagar Institute of Science and Technology Bhopal, India*
[3]*Department of Mechanical Engineering, Raisoni College of Engineering and Management, Amravati, India*

ABSTRACT: *Effective energy utilization and its management for minimizing irreversibility has made human to look for efficient energy consumption & conversion. Based on several research activity and local power plant experience some key observation has made and is presented in this paper The aim of this paper is to be find out amount and source of irreversibility's generated in boiler of 35 TPH boiler in 6 MW captive power plant so that any process in the system that having largest energy destruction can be identified that help designer to re design the system components.*

Keyword: *First law of thermodynamic, Second law of thermodynamic, Irreversibility.*

I. Introduction

Energy consumption is the most important problem in the today's era. In the present scenario per capita energy consumption determines the level of development of the nation. With the increased awareness that the world's energy resources are limited has caused many countries to reassess their energy policies and take measures for eliminating the waste. It has also ignited the interest in the scientists and researchers to take a close look at the energy conversion devices and to develop new techniques for better utilization of the available resources.

The First Law deals with the amounts of energy of various forms transferred between the system and its surroundings and with the changes in the energy stored in the system. It treats work and heat interactions as equivalent forms of energy in transit and offers no indication about the possibility of a spontaneous process proceeding in a certain direction. The first law places no restriction on the direction of a process, but satisfying the first law does not ensure that the process can actually occur. This inadequacy of the first law to identify whether a process can take place is remedied by introducing another general principle, the second law of thermodynamics

The exergy method of analysis is based on the Second law of thermodynamics and the concept of irreversible production of entropy. The fundamentals of the exergy method were laid down by Carnot in 1824 and Clausius in 1865. The energy-related engineering systems are designed and their performance is evaluated primarily by using the energy balance deduced from the First law of thermodynamics. Engineers and scientists have been traditionally applying the First law of thermodynamics to calculate the enthalpy balances for more than a century to quantify the loss of efficiency in a process due to the loss of energy. The exergy concept has gained considerable interest in the thermodynamic analysis of thermal processes and plant systems since it has been seen that the First law analysis has been insufficient from an energy performance stand point. Keeping in view the facts stated above, it can be expected that performing an analysis based on the same definition of performance criteria will be meaningful for performance comparisons, assessments and improvement for thermal power plants. Additionally, considering both the energetic and exergetic performance criteria together can guide the ways of efficient and effective usage of fuel resources by taking into account the quality and quantity of the energy used in the generation of electric power in thermal power plants. The purpose of this study presented here is to carry out energetic and exergetic performance analyses, at the design conditions, for the existing coal and gas-fired thermal power plants in order to identify the needed improvement. For performing this aim, we summarized thermodynamic models for the considered power plants on the basis of mass, energy and exergy balance equations. The thermodynamic model simulation results are compared. In the direction of the comprehensive analysis results, the requirements for performance improvement are evaluated.

II. Energy and EXERGY Analysis Of Coal Fired Cogeneration Power Plant With Condensate Extraction Turbine

In general coal based thermal plant works on Rankin cycle. Several advancement has made in recent thermal power plant to increase the energy output per unite mass of fuel burnt like reheating, regeneration etc. The design of any power plant is based on location, avaibility of fuel and it effectiveness. Since thermal power plant works on fossile fuel, it has made great interest to research to look for more efficient utilization of this fuel due to it's stock limitation under earth. Which results into no. of analysis based on energy losses and irreversibility, various attempts where made to over come this loss as and hence reheat cycle, regenerative cycle are the some fruitful outcome that came out for improvement.

2.1. Description of Coal fired power plant:

Several observed processes are considered for the analysis of a cumulative coal fixed thermal like lowering condenser pressure, superheating the to high temperatures, increasing the boiler pressure, reheat regenerative Rankin cycle is used.

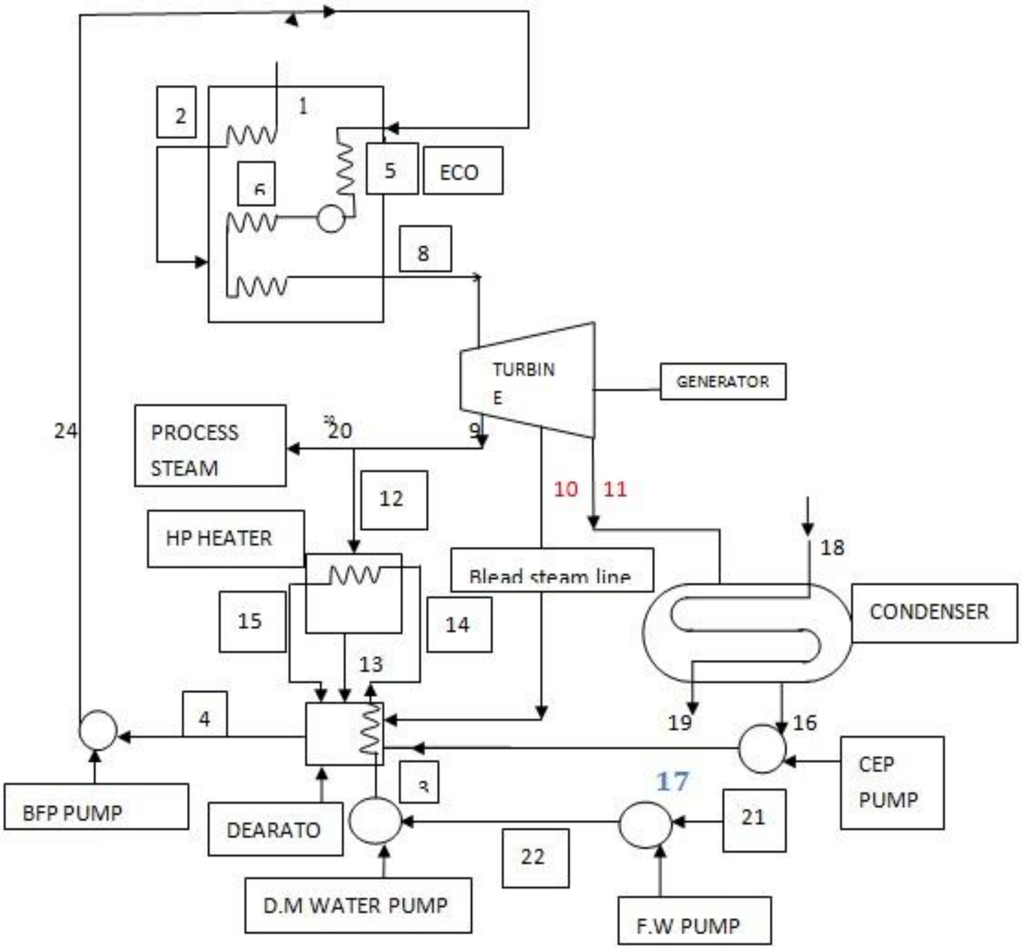

Fig. 1. Flow diagram of cogeneration thermal power plant with condensate extraction turbine

Fig.1 describes the detail part of cogeneration coal based with condensate extraction turbine consists of Boiler (B), Condensate extraction turbine with there stages (T) Pump (P), Decretory (D), a generator (S) , condense (c) high pressure feed water heater (HPH). The thermodynamic models of power plant are based on fundamental mass and energy balances. Using the energy and mass balance equation for each component in the power plant model, it is possible to compute energy and energy contents in terms of turbine power outputs, pump power consumptions boiler heat requirements, energy and exergy flows at each node of the plants, component first and second low efficiencies, component irreversibility in the plant etc.

2.2. Energy Analysis

In an open flow system there are three types of energy transfer across the control surface like work transfer, heat transfer, and energy associated with mass transfer and / or flow. The first law of thermodynamics or energy balance for the steady flow process of an open system is given by

$$\sum Q_k + m\left(hi + \frac{ci^2}{2} + g.z_i\right) = m\left(ho + \frac{co^2}{2} + g.z_o\right) + w$$

$$ή = \frac{desired\ output\ energy}{input\ energy\ supplied}$$

The energy balance for boiler and its component

2.2.1. Energy balance for combustion of boiler

The energy balance for boiler form energy equation can be given as,

$0 = Q_k - m_w(h_8 - h_{24})$-energy loss - $m_a(h_2 - h_1)$

Where m_w is mass flow rate of water , m_a is a mass flow rate of air

Energy loss = $Q_K - m_w(h_8 - h_{24}) - m_a(h_2 - h_1)$Type equation here.

The first law efficiency is given by

$$ή= \frac{desired\ output\ energy}{input\ energy\ supplied}$$

$$= \frac{\text{Energy input – Energy loss}}{\text{Energy input}}$$

=1-(enegy loss)/(energy input)

$$= 1- \frac{Q_k - m_k(h_8-h_{24}) - m_a(h_2-h_1)}{Q_k - m_a(((h_2-h_1)}$$

ή= $(m_w\ (h_8 - h_{24}))/(Q_k - m_a((h_2 - h_1))$ this is efficiency of boiler

since air is heated in a preheated in boiler which would otherwise would have absorb the heat from boiler

2.2.2.Eenergy balance for turbine

From energy balance equation,

$W_T = m_8(h_8 - h_9) + (m_8 - m_9)(h_9 - h_{10}) + (m_8 - m_9 - m_{10})(h_{10} - h_{11})$-energy loss

Energy loss= ή $= 1 - \frac{energy\ loss}{energy\ input}$

$$=1- \frac{m_8(h_8-h_9)+(m_8-m_9)(h_9-h_{10})+(m_8-m_9-m_{10})(h_{10}-h_{11})-WT}{m_8(h_8-h_9)+(m_8-m_9)(h_9-h_{10})+(m_8-m_9-m_{10})(h_{10}-h_{11})}$$

$$= \frac{WT}{m_8(h_8-h_9)+(m_8-m_9)(h_9-h_{10})+(m_8-m_9-m_{10})(h_{10}-h_{11})}$$

2.2.3. Energy balance for condenser

From energy balance equations,

$0=m_{11}(h_{11}-h_{16})-\ Q_k-$ energy loss

$0= m_{11}(h_{11}-h_{16})-\ mcw(h_{19}-h_{18})$- energy loss

Energy loss= $m_{11}(h_{11}-h_{16})-\ mcw(h_{19}-h_{18})$

Efficiency of condenser is given by

$$ή= 1 - \frac{energy\ loss}{energy\ input}$$

$$=1 - \frac{m_{11}(h_{11}-h_{16}) - mcw(h_{19}-h_{18})}{m_{11}(h_{11}-h_{16})}$$

$$= \frac{mcw(h_{19}-h_{18})}{m_{11}(h_{11}-h_{16})}$$

2.2.4.Pump system

(a) Condensate extraction pump ie CEP pump

$W_{cp}=m_{16}(h_{17}-h_{16})$-Energy loss

Energy loss=$W_{cp}+ m_{16}(h_{17}-h_{16})$

$$ή =1 - \frac{energy\ loss}{energy\ input}$$

$$=1- \frac{Wcp+ m_{16}(h_{17}-h_{16})}{wcp}$$

$$\eta_{condenser} = \frac{m_{16}(h_{17}-h_{16})}{wcp}$$

(b) Efficiency of DM water pump

Energy loss $=m_{21}(h_{22}-h_{21})+Wfw_p$

$$ή = \frac{m_{21}(h_{22}-h_{21})}{Wfwp}$$

(c)Boiler feed pump

Energy loss $=m_4(h_{24}-h_4)+Wb_pf$

$$ή = \frac{m_4(h_{24}-h_4)+_{14})}{Wb_pf}$$

2.2.5. Energy flow equation for high pressure feed water heater

From fig and steady state energy equation is given by

$0=m_{12}(h_{12}-h_{13})-m_{14}(h_{15}-h_{14})$-energy loss

$$ή\ hph = 1 - \frac{energy\ loss}{energy\ input}$$

$$=1 - \frac{m_{12}(h_{12}-h_{13})-m_{14}(h_{15}-h_{14})}{m_{12}(h_{12}-h_{13})}$$

$$= \frac{m_{14}(h_{15}-h_{14})}{m_{12}(h_{12}-h_{13})}$$

2.2.6. Dearetor sub system

It is well insulated system consider adiabatic one to which hot steam 13 ton from h.p heater and hot feed water from 15 enter into mix together forming mixture as well as D.M is heated from atmospheric condition to some higher level and left to dearator ,the energy supplied is sum of energies of hot steam and water and losing energy to cold water

The energy flow equation for dearetor is given by

$0=m_{13}.h_{13}+m_{15}h_{15}-m_3(h_{13}-h_3)+m_{10}.h_{10}+m_{17}.h_{17}.-m_4.h_4-h_{20}.m_{20}$-energy loss

Energy loss= $m_{13}.h_{13}+m_{15}h_{15}-m_3(h_{13}-h_3)+m_{10}.h_{10}+m_{17}h_{17}..-m_4.h_4-h_{20}.m_{20}$

But $m_3=m_{14}=m_{15}$

$$ή = 1- \frac{m_{13}.h_{13}+m_{15}h_{15}-m_3(h_{13}-h_3)+m_{10}.h_{10}+m_{17}.-m_4.h_4-h_{20}.m_{20}}{m_{13}.h_{13}+m_{15}h_{15}-m_3(h_{13}-h_3)+m_{10}.h_{10}+m_{17}h_{17}}$$

$$ή = \frac{m_{15}\ (h_{13}-h_3)+m\ _4.h_4+h_{20}.m_{20}}{m_{13}.h_{13}+m_{15}h_{15}+m_{10}.h_{10}+m_{17}h_{17}}$$

above is the efficiency of dearator

2.2.7. Energy balance for process steam application

The steam supplied to the process is consider as a lost steam from cycle even though it is utilized for some application providing money

Energy utilized in the process $= m_{20}.h_{20}$

Scop energy analysis for particular application not consider in this article.

2.3. Exergy Analysis of Condensate Extraction turbine

Exergy is a generic term for a group of concepts that define the maximum possible work potential of a system, a stream of matter and/or heat interaction, the state of the (conceptual) environment being used as the datum state. In an open flow system there are three types of energy transfer across the control surface namely working transfer, heat transfer, and energy associated with mass transfer and/or flow. The work transfer is equivalent to the maximum work which can be obtained from that form of energy. The exergy of heat transfer Q from the control surface at temperature T is determined from maximum rate of conversion of thermal energy to work Wmax is given by. kinetic, potential and physical exergy. The kinetic and potential energy are almost equivalent to exergy. The physical specific exergy and depends on initial state of matter and environmental state. Energy analysis is based on the first law of thermodynamics, which is related to the conservation of mass and degradation of the quality of energy along with the entropy generation in the analysis design and improvement of energy systems. Exergy analysis is useful method, to complement but not to replace energy analysis. The exergy flow for steady flow process of an open system is given by.

$$Wmax=\Psi\varrho=\varrho\left(1-\frac{To}{T}\right)$$

$$\sum\left(1-\frac{To}{Tk}\right)+\sum \left[m\Psi i = \Psi w + \Sigma m\Psi o + I_{destroyed}\right.$$

Where

$$\Psi=m^{o}[h^{\circ}\_ho^{\circ}]\_To(s-so)$$

And

$$h^{\circ}=h+\frac{c^{2}}{2}+gZ$$

Where ψ_i and ψ_o are exergy associated will mass inflow and outflows are respectively, is useful work done on/by system I destroyed is irreversibility of process and h^0 is the enthalpy as summation of enthalpy, KE and PE. The other notations C is the bulk velocity of the working fluid, Z is the altitude of the Steam above the sea level, g is the specific gravitational force. The irreversibility may be due to various losses occurring like to overcome Friction may be surface and steam or between adjacent layers of steam.Exergy analysis is an effective means to pinpoint losses due to irreversibility in a real situation.The second law efficiency is defined as

$$\acute{\eta}=\frac{actual\ thermal\ efficience}{maximu\ m\ possible\ reversible\ thermal}$$

$$=\frac{exergy\ output}{exergy\ input}$$

To analyze the possible realistic performance, a detailed exergy analysis of coal fired cogeneration thermal power plant with condensate extraction turbine has between carried out by ignoring the KE & PE change. For steady State flow the exeran balance for a thermal system is given below.

$$\Psi\omega=\sum_{k=1}^{n}\left(1-\frac{To}{Tk}\right)Q_{k}+\sum \left[m\Psi i - m\Psi o]k - Togen\right]$$

$\Psi\omega$=exergy summation supplied through heat transfer

$\sum\left(1-\frac{To}{Tk}\right)Q_k$= exergy summation supplied through heat transfer

$m\Psi i - m\Psi o$= change in exergy summation of working fluid

Where,

Q=heat transfer
M=mass flow rate
Ψ=exergy flow rate per unit mass
Sgen=entropy generation rate
T_0=ambient temp
T_k=temp of source

Component wise exergy balance of the coal fire co generating thermal power plant with condensate extraction turbine

2.3.1. Exergy balance for boiler combustion the exergy balance for the combustion

Exergy balance equation for combustion can be written as,

$$0=\sum_{k=1}^{n}(m\Psi)f+\dot{a}-m\Psi p)-ToSgen$$

m_f = sum of mass of coal
m_g=mass of product after combustion which give

$$(m\Psi)_{(f+a)} - (m\Psi p) = ToSgen$$

second law efficiency is given by

$$ή = \frac{exergy\ output}{exergy\ input}$$

$$= 1 - \frac{exergy\ loss}{exergy\ input}$$

$$= 1 - \frac{T0.Sgen}{(m\Psi)f+a} = \frac{(m\Psi)p}{m\Psi)f+a}$$

2.3.2. Exergy balance for high pressure turbine is given by

For high pressure turbine form fig ure and steady state ewqaution,

$$0=m_8(\psi_8- \psi_9)+(m_8-m_9)(\psi_9- \psi_{10})+(m_8-m_9-m_{10})(\psi_{10}- \psi_{11})-T_0.Sgen$$

$$T_0.Sgen= m_8(\psi_8- \psi_9)+(m_8-m_9)(\psi_9- \psi_{10})+(m_8-m_9-m_{10})(\psi_{10}- \psi_{11})- W_T$$

And entropy generation rate is

$$Sgen= m_8(s_8- s_9)+(m_8-m_9)(s_9- s_{10})+(m_8-m_9-m_{10})(s_{10}- s_{11})$$

Iirreversibility=exergy loss

$$I_{destroyed} = T_0.Sgen=T_0(m_8(s_8- s_9)+(m_8-m_9)(s_9- s_{10})+(m_8-m_9-m_{10})(s_{10}- s_{11})$$

The second law efficiency is given by

$$ή=1 - \frac{I_{destroyed}}{exergy\ input}$$

$$=1- \frac{T0.Sgen}{T_0.Sgen+W_T}$$

$$=1- \frac{m_8(\psi_8-\psi_9)-(m_8-m_9)(\psi_9-\psi_{10})+(m_8-m_9-m_{10})(\psi_{10}-\psi_{11})-W_T}{m_8(\psi_8-\psi_9)-(m_8-m_9)(\psi_9-\psi_{10})+(m_8-m_9-m_{10})(\psi_{10}-\psi_{11})-T_0.Sgen+T_0.Sgen}$$

$$= \frac{WT}{m_8(s_8-s_9)+(m_8-m_9)(s_9-s_{10})+(m_8-m_9-m_{10})(s_{10}-s_{11})}$$

2.3.3. Exergy balance for condenser is given by

From fig and steady flow energy equation,

$$0=m_{11}(\psi_{11}-\psi_{16})-m_{cw}(\psi_{19}-\psi_{18})-T_0.Sgen$$

$$T_0.Sgen= m_{11}(\psi_{11}-\psi_{16})-mcw(\psi_{19}-\psi_{18})$$

Also,

Irreversibility=exergy loss

$$I_{destroyed}= T_0.Sgen$$

$$ή =1 - \frac{I_{destroyed}}{exergy\ input}$$

$$=1- \frac{T0.Sgen}{m_{11}(\psi_{11}-\psi_{16})}$$

$$=1 - (m_{11}(\psi_{11}-\psi_{16}) - mc_w(\psi_{19}-\psi_{18}))/(m_{11}(\psi_{11}-\psi_{16}))$$

$$ή_{condenser} = \frac{mc_W(\psi_{19}-\psi_{18})}{m_{11}(\psi_{11}-\psi_{16})}$$

2.3.4. Pump system

(a)Condenser pump

$$-Wc_p = m_{16}((\psi_{17} - \psi_{16}) - T_0 . Sgen)$$

:.

$$I_{destroyed} = T_0 . Sgen$$
$$= m_{16}((\psi_{17} - \psi_{16}) + Wcp$$

$$ή = 1 - \frac{m_{16}((\psi_{17} - \psi_{16}) + Wcp}{Wc_p}$$

$$= \frac{m_{16}((\psi_{17} - \psi_{16})}{Wc_p}$$

(b)DM water feed pump

$$I_{destroyed} = T_0 . Sgen = m_{21}(\psi_{22} - \psi_{21}) + Wcp$$

$$ή = \frac{m_{21}(\psi_{22} - \psi_{21})}{Wc_p}$$

(c)Boiler feed pump

$$T_0 . Sgen = m_4(\psi_{24} - \psi_4) + Wbfp$$

$$ή = \frac{m_4(\psi_{24} - \psi_4)}{Wbfp}$$

2.3.5. Exergy flow equation for high pressure feed water heater

Exrgy equation for high pressure feed water can be given as,

$$0 = m_{12}(\psi_{12} - \psi_{12}) - m_{14}(\psi_{15} - \psi_{14}) - T_0 . Sgen$$

$$I_{destroyed} = T_0 . Sgen = m_{12}(\psi_{12} - \psi_{12}) - m_{14}(\psi_{15} - \psi_{14})$$

$$ή_{hph} = 1 - \frac{I_{destroyed}}{exergy\ input}$$

$$= \frac{m_{14}(\psi_{15} - \psi_{14})}{m_{12}(\psi_{12} - \psi_{12})}$$

2.3.6. Dearetor sub system

The exergy equation from fig can be given as

$$ή = 1 - \frac{I_{destroyed}}{exergy\ input}$$

$$= \frac{m_{13}(\psi_{13} - \psi_3) + m_4\psi_4 + m_{20}.\psi_{20}}{m_{13}\psi_{13} + m_{13}\psi_{13} + m_{20}\psi_{20} + m_{17}\psi_{17}}$$

III. Discussion On Results Of Different EXERGY - Energy Study Of Co-Generation Power Plant

S. C. Kamate et.al. investigated cogeneration power plant in sugar industries for exergy analysis, with back pressure turbine the exergy and energy efficiency is found better over condensate extraction turbine plant with boiler as least efficient component and turbine is the most efficient component of the plant. Kotas [2] has been explained in this work the concept of exergy used to define criteria of performance of thermal plant. [3] Yongping yan studied comprehensive base analysis state of art USE CP plant the boiler has a largest energy destruction . [4] P Regulagada el al studied energy analysis of thermal power plant with measured boiler and turbine losses in 32 MW coal fired boiler he determine power plant energy efficiency 30.21 %for gross generation output as well as exergy efficiency is 25.38 % for gross generator output, the max energy destruction is found to be in the boiler .Ganapathy ***el al.*** [5] studied with an exergy analysis performed on an operating 50 MWe unit of lignite fired steam power plant at Thermal Power Station-I, Ncyveli Lignite Corporation Limited, Neyveli. Tamil Nadu, India. The distribution of the exergy losses in several plant components during the real time plant running conditions has been assessed to locate the process irreversibility. The comparison between the energy losses and the exergy losses of the individual components of the plant shows that the maximum energy losses of 39% occur in the condenser, whereas the maximum exergy losses of 42.73% occur in the combustor.[6] selcuk atas studied comparative energetic and exergetic performance analysis for coal fired nine thermal power plant performance under control govt of turkey he use low quality of coal and boiler was conventional reheat . Kamate and Gangavati [7] studied exergy analysis of a heat-matched bagasse -based cogeneration plant of a typical 2500 tpd sugar factory, using backpressure and extraction condensing steam turbine is presented. In the analysis, exergy methods in addition to the more conventional energy anal) ses are employed to evaluate overall and component efficiencies and to identify and assess the thermodynamic losses. Boiler is the least efficient component and turbine is the most efficient component of the plant. The results show that, at optimal steam inlet conditions of 61 bar and 475 C. the backpressure steam turbine cogeneration plant perform with energy and exergy efficiency of 0.863 and 0.307 and condensing steam turbine plant perform with energy and exergy efficiency of 0.682 and 0.260.Arif hepbasli [8]thermodynamic analysis of a building using exergy analysis method heated by convection boiler in a heating centre ,a convectional boiler in a heating centre and fan coil unit are consider in this analysis tatal exergy input rate is to be 694.5kw while largest exergy loss rate is obtained to be 333kw .exergetic effiency of convectional boiler and fan coil unit are also found to be 13.4% and 37.6%.for future work exergetic analysis is preferred for both the exergetic and economical analysis. as per his experiment installation of well insulated building material support low exergy heating system.

Datta etal [9] was presented work on exergy analysis of a coal-based thermal power plant is done using the design data from a 210 MW thermal power plant under operation in India. The exergy efficiency is calculated using the operating data from the plant at different conditions, viz. at different loads, different condenser pressures, with and without regenerative heaters and with different settings of the turbine governing. The load variation is studied with the data at 100. 75. 60 and 40% of full load. Effects of two different condenser pressures, ***i.e.*** 76 and 89 mmllg (abs.). are studied. It is observed that the major source of irreversibility in the power cycle is the boiler, which contributes to exergy destruction of the order of 60%. Part load operation increases the irreversibility in the cycle and the effect is more pronounced with the reduction of the load. Increase in the condenser back pressure decreases the exergy efficiency. Successive withdrawal of the high pressure heaters shows a gradual increment in the exergy efficiency for the control volume excluding the boiler.M.K Gupta [10] the energy and exergy analysis has been carried out of conceptually proposed direct steam generation solar thermal power plant having only one feed heater the exergy loss are found in condenser followed by collector field ,it shows that main source of energy destruction that was found in collector field,the results of exergy analysis of direct steam generation point out that collector and receiver required improvement for reduced exergy loss the material of collector plays an important role and reduced exergy loss in the receiver inlet temp should be optimum he maximum efficiencies equal to 16.13% be achieved by using two feed water heater without dry pump, it is found that if we use three water heater maximum efficiencies improves was 16.60 and for higher efficiency three feed water heater is use , Aljundi [11] was presented in this study, the energy and exergy analysis of Al-Hus-sein power plant in Jordan is presented. The primary ob-jectives of this paper are to analyze the system components separately and to identify and quantify the sites having largest energy and exergy losses. In addition, the effect of varying the reference environment state on this analysis will also be presented. Energy losses mainly occurred in the condenser where 134 MW is lost to the environment while only 13 MW was lost from the boiler system. The percentage ratio of the exergy destruction to the total exergy destruction was found to be maximum in the boiler system (77%) followed by the turbine (13%), and then the forced draft fan condenser (9%). In addition, the calculated thermal efficiency based on the lower heating value of fuel was 26% while the exergy efficiency of the power cycle was 25%. For a moderate change in the reference environment state temperature, no drastic change was noticed in the performance of major components. Anit patel [12] the energy and exergy analysis of boiler plant Indian coal as fuel ,it seems that energy analysis found all inefficiency to losse is 23.46% ,the first law efficiency of the boiler is 76.64% and second law efficiency is 37% there is large amount of energy degradation ,this degradation of energy reduce exergy of second law efficiency and increase entropy generation, so stack loss are very less it is found major loss are in boiler so increase the efficiency of boiler by 1% for that reduced the temp of flue gas by 22 degree so preheat combustion of a air with a waste heat improvement oxygen control .R Saidur[13] in this paper the useful concept of energy and exergy utilization is analyzed and applied to the boiler system in this paper he was calculate the energy and exergy efficiency 72.46%and 24.89%,according to his concept major contributor of energy destruction is combustors. Dai ***el al.*** [14] was done exergy analysis for each cogeneration system is examined, and a parameter optimization for each cogeneration system is achieved by means of genetic algorithm to reach the maximum exergy efficiency. The cement production is an energy intensive industry with energy typically accounting for 50-60% of the production costs. In order to recover waste heat from the preheated exhaust and clinker cooler exhaust gases in cement plant, single Hash steam cycle, dual-pressure steam cycle, organic Rankine cycle (ORC) and the Kalina cycle are used for cogeneration in cement plant. The optimum performances for different cogeneration systems are compared under the same condition. The results show that the exergy losses in turbine, condenser, and heat recovery vapor generator are relatively large. R jyothu naik et [15]al studied exergy analysis of 120MW of coal base thermal power plant, in this paper he investigate exergy value at all location ,it observed that exergetic efficiency of overall plant is 39.75% and over all thermal effiency is 37% ,now difference of 2.75%is destruction of available energy observed. the exergy analysis of boiler ,turbine is calculated and losses in exergy is calculate ,it can be seem that maximum energy destruction is found in boiler with the value of 89.37% of total exergy destruction. the Rosen [16] reported results were of energy- and exergy-based comparisons of coal-fired and nuclear electrical generating stations. A version of a process-simulation computer code, previously enhanced by the author for exergy analysis, is used. Overall energy and exergy efficiencies, respectively, are 37% and 36% for the coal-fired process, and 30% and 30% for the nuclear process. The losses in both plants exhibit many common characteristics. Energy losses associated with emissions '(mainly with spent cooling water) account for all of the energy losses, while emission-related exergy losses account for approximately 10% of the exergy losses. The remaining exergy losses are associated with internal consumptions. M.k Pal [17] st udied exergy and energy analysis of a coal fired thetmal power plant he calculate the exergy and energy loss. In this paper energy and exergy analysis of reheat and regeration rankine cycle is being carried out ,the energy analysis is done with the help of first law effiency and exergy analysis is done with second law effiency the exergy loss or irreversibilities are maximum at the boiler i.e 61% of total input while maximum exergy loss in low pressure turbine .Dincer and Rosen [18] present effects on the results of energy and exergy analyses of variations in dead-state properties, and involves two main tasks: 1) examination of the sensitivities of energy and exergy values to the choice of the dead-state properties and 2) analysis of the sensitivities of the results of energy and exergy analyses of complex systems to the choice of dead-state properties. A case study of a coal-fired electrical generating station is considered to illustrate the actual influences. The results indicate that the sensitivities of energy and exergy values and the results of energy and exergy analyses to reasonable variations in dead-state properties are sufficiently small. Alpesh mehata el al[19] studied in thermodynamic analysis of gandhinagar thermal power station of 210 MW in this paper seem that boiler efficiency is highest 86.84% and heat losses are only 13.16% out of all boiler losses maximum heat loss occur in the 5.29% in flue gas .Turbine efficiency is very low that is 43.59% and power plant overall efficiency is 37.01%.the effectiveness of HP heater is working good condition 0.85. Erdem ***el al.*** [20] analyzes comparatively the performance of nine thermal power plants under control governmental bodies in Turkey, from energetic and exergetic viewpoint. The considered power plants are mostly conventional reheat steam power plant fed by low quality coal. Firstly, thermodynamic models of the plants are developed based on first and second law of thermodynamics. Secondly, some energetic simulation results of the developed models are compared with the design values of the power plants in order to demonstrate the reliability. Thirdly, design point performance analyses based on energetic and exergetic performance criteria such as thermal efficiency, exergy efficiency, exergy loss, exergetic performance coefficient are performed for all considered plants in order to make comprehensive evaluations, Amir vosough el al [21]improvement of power plant effiency with varying condenser pressure ,the analysis shows that condenser pressure is valuable parameter for power putout.the maximum energy loss found to in condenser where as 60.86 %of input energy was lost to the environment the major loss was found in the boiler is 86.21%of the fuel exergy input to the cycle was destroyed.the percent exergy destruction in the condenser and other components was 13.22%,The calculated thermal and exergy effiency of the ower cycle was found to be 38.89% ,45.85%.

Isam H Aljundi [22] studied energy and exergy analysis of steam power plant in jordan the primary objective of this paper was analysise the system component separately and identify the exergy losses .according to him mainly energy losses are found in condenser where 134MW is lost to the environment while In boiler 13 mw energy lost ,the percentage ratio of exergy destruction to the total exergy destruction was found to be maximum in the boiler system 77%followed by turbine 13% and force draft fan in the condenser 9% the main conclusion of this paper boiler is major source of irreversibility in the boiler . Vidal ***el al.*** [23] analysis exergy method was applied in order to evaluate the new combined cycle proposed by Goswami. using Ilasan-Goswami-Vijayaraghavan parameters. This new combined cycle was proposed to produce both power and cooling simultaneously with only one heat source and using ammonia-water mixture as the working fluid. At the irreversible process two cases were considered, changing the environmental temperature. However, in order to know the performance ol" the new cycle at different conditions of operation, the second irreversible case was analyzed varying the rectification temperatures, the isentropic efficiency of the turbine and the return temperature of the chilled water. Exergy effectiveness values of 53% and 51% were obtained for the irreversible cycles; with heat input requirements at temperatures of 125 and 150*C. Solar collectors or waste heat are suggested as heat sources to operate the cycle.

Arai ***el al.*** [24] presents an exergy analysis on combustion and energy conversion processes, which is based on the above-mentioned concept of exergy and energy supported by temperature level. When we discuss high temperature air combustion in furnace, this process shows a hig**her** performance than that of the ambient air combustion. beacause it will reduced the coal combustion and increase the effiency of the boiler.

3.2. Captive and Combined Cycle Thermal Power Plants

Khaliq and Kaushik [27| presented thermodynamic methodology for the performance evaluation of combustion gas turbine cogeneration system with reheat i.e steam at low stage of turbine again heated in the boiler with the help of reheater and then again use in the turbine inorder to reduced the moisture. The energetic and exergetic efficiencies have been defined. The effects of process steam pressure and pinch point temperature used in the design of heat recover) steam generator, and reheat on energetic and exergetic efficiencies have been investigated. The power to heat ratio and second-law efficiency increases significantly with increase in process steam pressure, but the first-law efficiency decreases with the same. Results also show that inclusion of reheat provides significant improvement in electrical power output, process heat production, fuel-utilization (energetic) efficiency and second-law (exergetic) efficiency.

3.3. Gas Turbine Based Thermal Power Plants

Khaliq and Kaushik [28] were presented theoretical second-law approach for the thermodynamic analysis of the reheat combined Brayton/ Rankine power cycle. Expressions involving the variables for specific power-output, thermal efficiency, exergy destruction in components of the combined cycle, second-law efficiency of each process of the gas-turbine cycle, and second law efficiency of the steam power cycle have been derived. It is found that the exergy destruction in the combustion chamber represents over 50% of the total exergy destruction in the overall cycle. The combined cycle efficiency and its power output were maximized at an intermediate pressure-ratio, and increased sharply up to two reheat-stages and more slowly thereafter. Chen and Tyagi [29] were presented parametric study of an irreversible cycle model of a regenerative-intercooled-reheat Brayton heat engine along with a detailed. The power output and the efficiency are optimized with respect to the cycle temperatures for a typical set of operating conditions. It is found that there arc optimal values of the turbine outlet temperature, inter cooling, reheat and cycle pressure ratios at which the cycle attains the maximum power output and efficiency. But the optimal values of these parameters corresponding to the maximum power output are different from those corresponding to the maximum efficiency for the same set of operating condition. Kaushik and Tyagi [30]

IV. Conclusion

Exergy analysis of cogeneration power plant. Proves useful tool for analyzing various losses occurring in different parts of power plant and possibility for improvement in it. Exergy analysis in different power concluded the maximum losses in boiler which we already tried to minimum by adopting different accessories. Further this plant can be improved by adopting methodology used in big thermal power plant irreversibility generally due to temp, loss to atm and heat lost to exhaust gas which is impossible to remove but can be minimized to optimum naw. The minimum exergy loss occur in turbine generally due to insulation it, which works life adiabatic section with minimum losses. Condensers are important part of condenser which is necessary to create the back pressure and increase the efficiency of power plant. This heat rejected by steam or hot water is the reused by circulating cold feed water to hot water which could other wire be rejected to atmosphere. The demand of power per day per hr. various with situation and the leads to fluctuation of load on to power plant. According to different wading condition the exergy and energy analysis can be the scope of study for optimizing the different values of parameter to act best Performa with varying. This also can be studied with change in operating parameter and then its effect on load which difficult to carry out practical but with aid of new computational it may be possible to work with some ready data calculation.

Acknowledgements

The author wish to thank Raymond India Limited, Yavatmal, for granting the permission to carry out work and their kind support during work.

References

[1] A. Yunus and A. Michael, "Thermodynamics an Engineering Approach," Tata McGraw Hill, New Delhi, 2007.
[2] T. J. Kotas, "Exergy Criteria of Performance for Thermal Plant: Second of Two Papers on Exergy Techniques in Thermal Plant Analysis," International Journal of Heat and Fluid Flow, Vol. 2, No. 4, 1980, pp. 147-163.
[3] yongping yang "comprehensive exergy based evaluation and parametric study of a coal fired ultra super critical power plant
[4] P Regulagadda "energy analysis of a thermal power plant with measured boiler and turbine losses" applied thermal engineering vol 30-[2010]970-976
[5] T. Ganapathy, N. Alagumurthi, R. P. Gakkhar and K. Murugesan, "Exergy Analysis of Operating Lignite Fired Thermal Power Plant," *Journal of Engineering Science and Technology Review*, Vol. 2, No. 1, 2009, pp. 123-130.
[6] Seluk Atas "comparative energetic and exergetic performance analysis for coal fired thermal power plant in turkey" vol 48(2009)2179-2186
[7] S. C. Kamate and P. B. Gangavati, "Exergy Analysis of Cogeneration Power Plants in Sugar Industries," *Applied Thermal Engineering*, Vol. 29, No. 5-6, 2009, pp. 1187-1194.
[8]. Arif hepbasil "Thermodynamic analysis of a building using exergy analysis method"
[9] A. Datta, S. Sengupta and S. Duttagupta, "Exergy Analysis of a Coal-Based 210 mw Thermal Power Plant," *International Journal of Energy Research*, Vol. 31, No. 1, 2007, pp. 14-28.
[10]. M.K Gupta "exergy analysis and investigation for various feed water heater of direct steam generation solar thermal power plant
[11]. I. H. Aljundi, "Energy and Exergy Analysis of a Steam Power Plant in Jordan," *Applied Thrmal Engineering*, Vol. 29, No. 2-3, 2009, pp. 324-328**.**
[12.] Ankit patel "energy and exergy analysis of boiler with different fuels like Indian coal ,imported coal and L.H.H.S oil vol 8 oct 2012
[13]. R saidur "energy and exergy economic analysis of industrial boiler" Vol 38(2010)2188-2197
[14.] I. Dincer and M. A. Rosen, "Effect of Varying Dead-State Properties on Energy and Exergy Analyses of Thermal Systems," *International Journal of Thermal Sciences*, Vol. 43, No. 3, 2004, pp. 121-133..
[15] R Jyothu naik "exergy analysis of 120MWcoal based thermal power plant ''vol 2 4 apil 2013 issn 2278-0181
[16.] M. A. Rosen, "Energy- and Exergy-Based Comparison of Coal-Fired and Nuclear Steam Power Plants," *Exergy*, Vol. 1, No. 3, 2001, pp. 180-192.
[17.] M.k pal "energy and exergy analysis of boiler and turbine of a coal fired thermal power plant ''vol 2 Issue 6 jun 2013
[18.] I. Dincer and M. A. Rosen, "Effect of Varying Dead-State Properties on Energy and Exergy Analyses of Thermal Systems," *International Journal of Thermal Sciences*, Vol. 43, No. 3, 2004, pp. 121-133.
[19.] Alpesh mehata "thermodynamic analysis of gandhinagar thermal power station''vol 3 oct –dec 2010
[20.] H. Erdem, A. V. Akkaya., A. Dagdas, S. H. Sevilgen, B. Sahin, I. Tek, C. Gungor and S. Atas, "Comparative Energetic and Exergctic Performance Analyses for Coal-Fired Thermal Power Plants in Turkey." *International Journal of Thermal Sciences*, Vol. 48, No. 11, 2009, pp. 2179-2186.
[21]. Amir vosough "improvement power plant efficiency with condenser pressure vol 2 No 3 june 2011
[22.] i . H. Aljundi, "Energy and Exergy Analysis of a Steam Power Plant in Jordan," *Applied Thrmal Engineering*, Vol. 29, No. 2-3, 2009, pp. 324-***328.***
[23.] A. Vidal, R. Best, R. Rivero and J. Cervantes. "Analysis of a Combined Power and Refrigeration Cycle by the Exergy Method," *Energy*, Vol. 31, No. 15, 2006, pp. 3401-3414,
[24]. N. Arai, H. Taniguchi. K. Mouri and T. Nakahara. "Exergy Analysis on Combustion and Energy Conversion Processes," *Energy*, Vol. 30, No. 2-4. 2005. pp. 111-117.
[25.] Nestor Garcia herando "energy and exergy analysis of an absorption power cycle"vol 55(2013)69-77
[26.]. Dincer and M. A. Rosen, "Exergy Analysis of Waste Emissions," International Journal of Energy Reserch, Vol. 23. No. 13, 1999. pp. 1153-1163.
[27]. A. Khaliq and S. C. Kaushik, "Thermodynamic Performance Evaluation of Combustion Gas Turbine Cogeneration System w ith Reheat." Applied Thermal Engineering, Vol. 24. No. 13. 2004, pp. 1785-1795.
[28.] G. M. Chen, S. K. Tyagi, Q. Wang and S. C. Kaushik. A New Thcrmoeconomic Approach and Parametric Study of an Irreversible Regenerative Brayton Refrigeration Cycle," International Journal of Refrigeration, Vol. 29. No. 7, 2006. pp. 1167-1174.

[29.] S. C. Kaushik, S. K. Tyagi and M. K. Singhal. "Parametric Study of an Irreversible Regenerative Brayton Cycle with Isothermal Heat Addition," Energy- Conversion & Management, Vol. 44. No. 12. 2003, pp. 2013-2025.

[30.] S M. Zubair and M A. Habib. "Second-Law-Based Thermodynamic Analysis of Regenerative-Reheat Rankine-Cycle Power Plants." Energy. Vol. 17, No. 3, 1992, pp. 295-301.

[31]. M. Yilmaz, O. N. Sara and S. Karsli, "Performance Evaluation Criteria for Heat Exchangers Based on Second Law Analysis," Exergy, Vol. 1, No. 4, 2001, pp. 278-294.

[32] P. K. Nag. "Power Plant Engineering."

International Journal of Modern Engineering Research (IJMER)
www.ijmer.com Vol. 3, Issue. 5, Sep - Oct. 2013 pp-2626-2630 ISSN: 2249-6645

An efficient model for design of 64-bit High Speed Parallel Prefix VLSI adder

M. Mahaboob Basha[1], Dr. K. Venkata Ramanaiah[2], Dr. P. Ramana Reddy[3], B. Lokeshwar Reddy[4]

[1]*Assoc.Professor, ECE, AVR & SVR College of Eng. Technology, Nandyal, JNTUA, A.P.State*
[2]*Assoc. Professor & Head, Dept. of ECE, YSR Engg.College,Yogi Vemana University, Kadapa, A.P.State, India*
[3]*Assoc.Professor, Department of ECE, JNTUA, Anantapur, A.P.State, India*
[4]*PG Student, AVR & SVR College of Eng. Technology, Nandyal, JNTUA, A.P.State*

Abstract: *To make addition operations more efficient parallel prefix addition is a better method. In this paper 64-bit parallel prefix addition has been implemented with the help of cells like black cell and grey cell operations for carry generation and propagation. This process gives high speed computations with high fan-out and makes carry operations easier. Xilinx 14.1 vivado tool has been used for the simulation of proposed 64-bit adder. The comparison can be made with the help various range of inputs and the proposed parallel prefix adder has produced high speed computation and also efficient in terms of number of transistors and their topology and number of nodes.*

Keywords: *parallel prefix adder; dot operators and logic cells; high speed adder; 64- bit addition.*

I. INTRODUCTION

Parallel addition is the most important computation in many processors like microprocessors, DSPs, mobile devices and other high speed applications. The main theme of the parallel prefix adder is to reduce logic complexity and delay. However, improving the performance of Design constraint with other factors like area and power. Basing on the implementation of adder like Carry Look Ahead adder, the parallel prefix computation has been developed [1] by targeting high performance computations. Parallel prefix adder's terminology is equivalent to Carry Look Ahead addition, but the transistor topology is different. Parallel prefix adders have unique style of carry generation and carry propagation. The main theme of the parallel prefix addition is to accelerate the n-bit addition process in VLSI technology. Parallel prefix adders are desired in high speed arithmetic circuits and they are popular since twenty years. Parallel prefix addition involves in three steps. First, computation of carry generation and carry propagation signals by using number of input bits. Second, calculating all the carry signals in parallel i.e. prefix computation. Third, evaluating total sum of the given inputs. The entire mechanism consists of XOR gates, AND gates and OR gates. Black and grey cells plays key role in the generation and propagation of carry to a particular stage. Black cells consists one OR gate and two AND gates, whereas grey cell consists one AND gate and one OR gate. In some parallel prefix adders there will be another module as white cell, which is a replica of general half adder circuit.

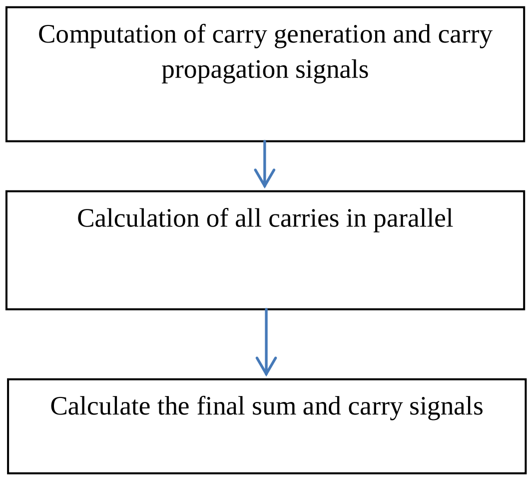

Figure 1: parallel prefix adder mechanism

II. EXISTED PARALLEL PREFIX ADDERS

Design of prefix addition network specifies the model of parallel prefix adder. The parallel prefix adder given by Kogg Stone gives low fan-out and high logic depth which leads to a complex network of prefix addition and also contains more number of interconnections. Brent Kung adder design gives minimal number of calculating nodes, but the design itself has maximum logic depth. The area will be reduced due to number of nodes but complexity will be high due to high logic depth. Han-Carlson adder design is the combination of both Brent Kung and Kogg Stone adders, which gives balance between nodal count and logic depth. Knowles also presented an adder design, which gives low logic depth and improved fan-out. There is another adder which combines the benefits of prefix addition and Carry save adder i.e. sparse tree binary adder. Sklansky developed a topology which leads to low depth in the interconnecting nodes. Ladner and Fischer proposed a general design to construct a parallel prefix network with high depth when compared with Sklansky topology but achieved maximum fan-out for the critical path. Integer linear programming is also another method for parallel prefix computation. Mathew Ziegler and Mircea Stan proposed an adder for parallel prefix computation for minimizing delay and area known as best logarithmic adder for fan-out of two. There are some more adders designed by Haiku Zhu, Chung-Kuan and Ronald Graham, can produce minimal depth for n-bit adder. The proposing adder is about 64-bit adder with parallel prefix computation which is closely related to Ladner and Fischer adder.

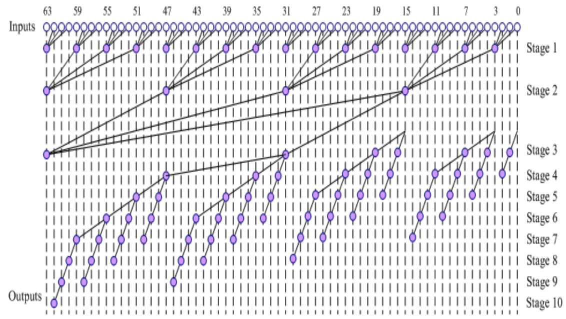

Fig2: existed 64-bit parallel prefix adder

III. PROPOSEDHIGH SPEED 64-BITPARALLEL PREFIX ADDER

The proposed high speed 64-bit parallel prefix adder is shown fig 2. Main theme of the design is to eliminate huge delays in overall for carry calculations. So the logic depth of the proposed design is optimal.The 64-bit parallel prefix adder has seven stages of computations. Design of parallel prefix adder can be implemented with the help of CMOS logic, but CMOS logic constructs only inverting functions so that cascading odd cells and even cells alternatively gives the result of eliminating inverters between those two cells. Two inputs of each stage will be given to XOR gate and AND gate such that it looks like a half adder circuit. In the first stage we calculate all 64-bit inputs with the help of half adders such that the results will be propagated towards next stages. Subsequent stages follows the same procedure so as the number of half adders will be reduced stage by stage. Each half adder consist one AND gate, which requires five transistors and XOR gate requires thirteen transistors so that each half adder requires 65 transistors. The topology of the design must be simple to reduce the logic depth, because each input again requires one buffer for impedance matching. So we are going to use cells like black, grey and white cells for the reduction of number of transistors. White cell is a half adder and black cell consists one OR gate and two AND gates and grey cell consists of one OR gate and one AND gate. By all means we reduced transistor count, which also leads to low power and low area specifications.In the proposed 64-bit parallel prefix adder logic cells has been preferred, depending upon the stage we use number of logic cells. The final stage of the design gives the sum signal as one output and carry signal as other output. The stages at both ends can be operated with high speed because of simple topology in the network. Amid, all of this the performance depends on the intermediate stages. We also compared Brent Kung and Ladner Fischer adders for n-bit at various values of n, like propagation delay andnetwork complexity. The proposed adder is as shown in Fig(3), which can overcome various problems in existed adders like shown in Fig(2).

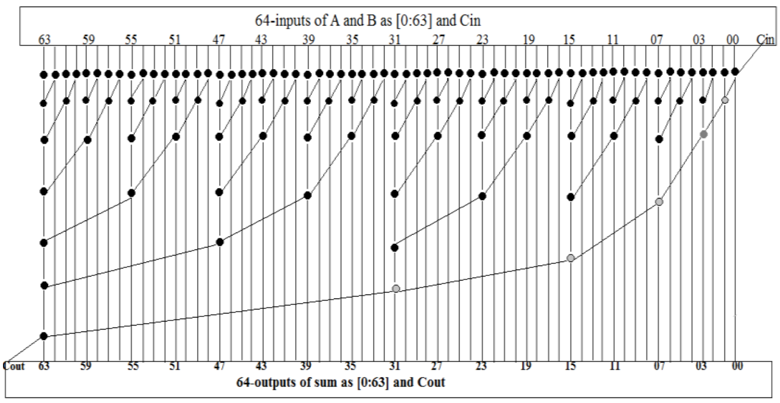

Fig3: proposed 64-bit parallel prefix adder

IV. CELLS LOGIC DIAGRAMS

A. BLACK CELL

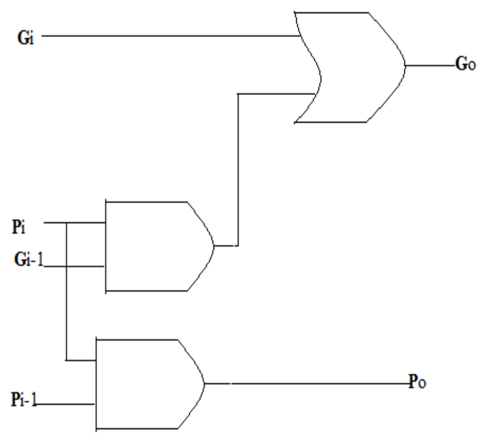

Fig4: Black Cell Logic Diagram

The Boolean equations (1) for the above logic diagram of black cell are

(1) Go = Gi +Pi.Pi-1; Po = Pi.Pi-1

B.GREY CELL

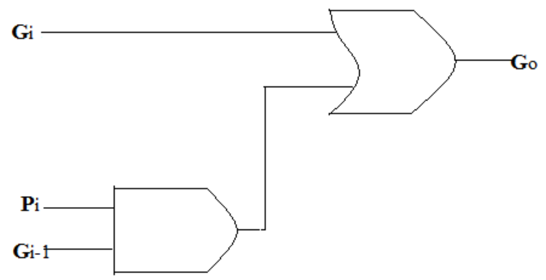

Fig5: Logic Diagram of Grey Cell

The Boolean equation (2) of the above logic diagram of grey cell is

(2) Go = Gi+Pi.Pi-1

The two cells shown in the figures (4) and (5) are for the purpose of reducing number of transistors such that the logic will become simple and the number of transistors be also reduced. Black cell gives two outputs one for normal sum and the other is for propagation of carry.

C. WHITE CELL

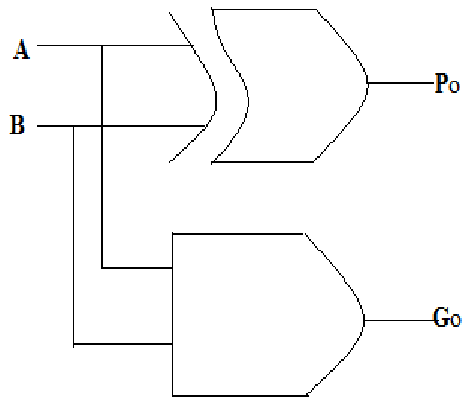

Fig6: Logic Diagram of White Cell

The Boolean equation (3) of the above logic diagram of white cell is

(3) $Po = A \oplus B = A\bar{B} + \bar{A}B$; $Go = AB$

The simulation results shown in Fig (7) gives complete idea about the design of proposed 64-bit parallel prefix adder and also gives the values like propagation delay and logic depth. The values shown in the table are obtained from the code and simulation results. We also compared those results with the existed adders like Brent Kung, Kogg Stone and etc. so that the comparison describes the efficiency of the proposed 64-bit parallel prefix adder. Chart of the simulated results is a pictorial representation of the design's comparison is also shown. Transistor count also reduced such that the logic depth and propagation delay reduced as followed in the charts.

V. SIMULATION RESULTS

A. Proposed 64-bit parallel prefix adder

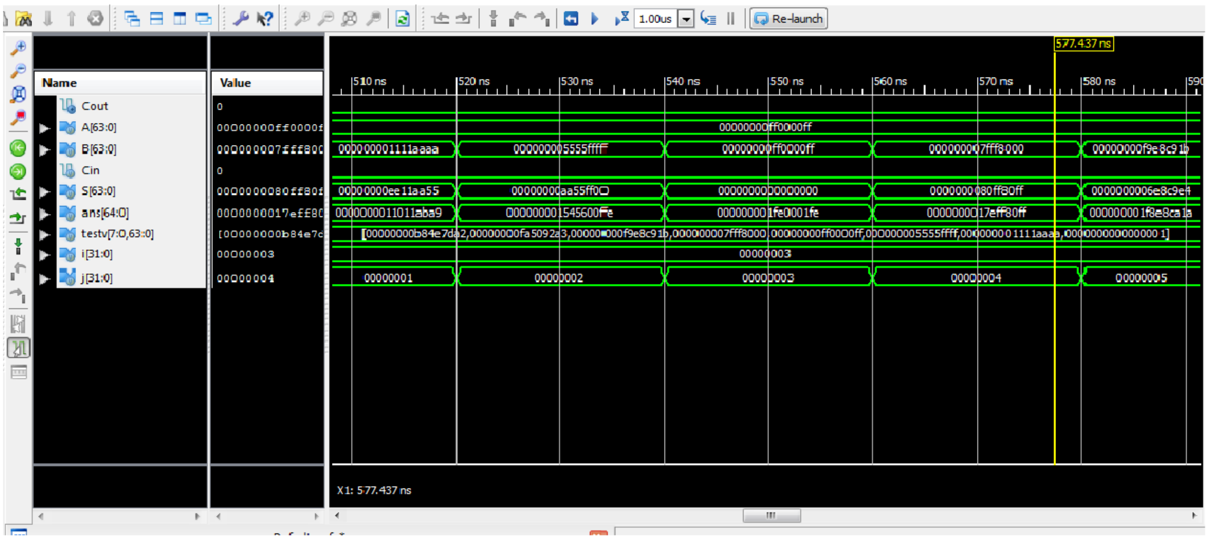

Fig7: simulation result of proposed 64-bit parallel prefix adder

B. Comparison table with output results

Parameter	Existed adders	Proposed adder	Comparison
Delay in ns	**>1280(B.K)**	**1280**	**Reduced**
Logic depth	**High(B.K)**	**low**	**Reduced**
Transistor count	**>2500**	**1880**	**Reduced**

C. Comparison chart in pictorial representation

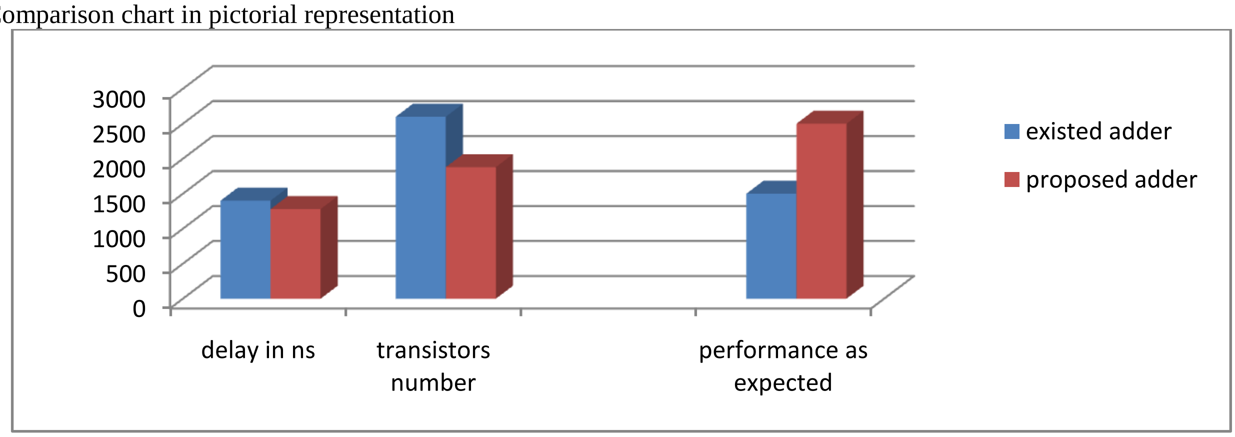

VI. CONCLUSION

The parallel prefix adders design is an efficient method of all conventional adders. Proposed 64-bit high speed parallel prefix adder has achieved the low propagation delay by overcoming the problems in previous adders like 16-bit, 32-bit Brent Kung and Ladner and Fischer designs. The performance has been compared at various input ranges by keeping trade-off between propagation time and logic depth, and also achieved high fan-out. The proposed 64-bit high speed parallel prefix VLSI adder made the computation in seven numbers of stages and also generated sixty three outputs with the help of 845 nodes. We have used Xilinx 14.1 vivado version tool for the purpose of simulating the Verilog code. The simulation result of proposed 64-bit parallel prefix adder has proved the efficiency of the design. This design is a conventional one for the purpose of arithmetic and logic calculations at wide and complex range of inputs. The proposed design is also preferable for multipliers and for various data computations.

REFERENCES

[1] S.Knowles' "A family of adders"' Proceedings of the 15th IEEE Symposium on Computer Arithmetic. Vail' Colarado' pp.277-281' June 2001.
[2] David Harris' "A Taxonomy of parallel prefix networks"' Proceedings of the 37th Asilomar Conference on Signals' Systems and Computers Pacific Grove' California' pp.2213-2217' November 2003.
[3] Andrew Beaumont-Smith’ and Cheng-Chew Lim’ "Parallel Prefix Adder Design"' Department of Electrical and Electronic Engineering' the University of Adelaide' 2001.
[4] P.Ramanathan' P.T.Vanathi' "Novel Power Delay Optimized 32-bit Parallel Prefix Adder for High Speed Computing"' International Journal of Recent Trends in Engineering' Vol 2' No. 6' November 2009.
[5] R. Zimmermann' Binary Adder Architectures for Cell-Based VLSI and their Synthesis' ETH Dissertation 12480' Swiss Federal Institute of Technology' 1997.
[6] R.P Brent and H.T Kung ‘A regular layout for parallel adders’ IEEE Trans., C-31(3):260-264, March 82
[7] R. Ladner and M. Fischer' "Parallel prefix computation"' Journal of ACM. La Jolla' CA' vol.27' no.4' pp. 831-838' October 1980.
[8] J. Sklansky' "Conditional sum addition logic"' IRE Transactions on Electronic computers. New York' vol. EC-9' pp. 226-231' June 1960.
[9] P.Kogge and H.Stone' "A parallel algorithm for the efficient solution of a general class of recurrence relations"' IEEE Transactions on Computers' vol. C-22' no.8' pp.786-793' August 1973.
[10] P.Ramanathan' P.T.Vanathi' "A Novel Logarithmic Prefix Adder with Minimized Power Delay Product"' Journal of Scientific & Industrial Research' Vol. 69' January 2010' pp. 17-20.
[11] T. Han and D. Carlson' "Fast area efficient VLSI adders"' Proceedings of the Eighth Symposium on Computer Arithmetic. Como' Italy' pp.49-56' September 1987. (Pubitemid 17613979) .

International Journal of Modern Engineering Research (IJMER)
www.ijmer.com Vol. 3, Issue. 5, Sep - Oct. 2013 pp-2631-2639 ISSN: 2249-6645

A High Performance PWM Voltage Source Inverter Used for VAR Compensation and Utility Grid Stability Improvement

Azeddine Draou[1]
Department of Electrical and Electronics, College of Engineering/ University of Hail, Saudi Arabia

ABSTRACT: *A high performance advanced static VAR compensator (ASVC) which uses a Pulse Width Modulation (PWM) voltage source inverter is presented and analyzed in this paper. A fast control approach of the ASVC system has been implemented for applications that require leading or lagging power compensation. The proposed control strategy is based on an explicit control of the reactive power, implicit of the voltage amplitude of the capacitor of the dc side and is more flexible. The analysis of the simulation results, inserted in this paper, reveal the technical feasibility of using such an ASVC to improve the stability of the infinite bus system and allow us to conclude that the use of the inverter as compensator of reactive power brings better performances than classical ones.*

Keywords: *VAR Compensation. PWM inverter, ASVC, Control, Utility Grid, Stability*

I. INTRODUCTION

The requirement to design and operate power systems with highest degree of efficiency, security, and reliability have been central focus for the power system designer, ever since the interconnected networks came into existence. To satisfy these requirements, various advances in technology of AC power transmission have taken place in the context of effective control of reactive power and its compensation [1].

In the past, synchronous condensers, mechanically switched capacitors and inductors, and saturated reactors have been applied to control the system voltage in this manner[1,2]. Since the late 1960s, thyristor controlled reactor (TCR) devices together with fixed capacitor or thyristor switched capacitor have been used to inject or absorb reactive power[3,4]. The controllable series compensator such as the thyristor controlled series compensation (TCSC) has been developed to change the apparent impedance of a line by either inductive or capacitive compensation, facilitating active power transfer control. It suffers from the disadvantages that it generates low order harmonic components into the power system. Recently, voltage source converter has been developed to operate as static VAR compensators [5-7]. Such compensators are dynamic reactive power compensation devices which use a voltage source inverter transforming a DC component to AC through a capacitor seen here as a power storage device. They have also the advantage of reduced size and weight, precise control and very fast response. The advanced static VAR compensator i.e. known as ASVC may resemble the operation of synchronous condensers but in a static manner. The converter supplies reactive power to the network by increasing the synthesized inverter output voltage. And similarly, it absorbs VARs from the network by reducing the output voltage below the network voltage, i.e., no large power components such as capacitor banks or reactors are used. Only a small capacitor is employed to provide the required reference voltage level to the inverter. The possibility of PWM voltage source converters with high switching frequency for reactive power compensation is also reported [8,9]. In this paper, the operating principles of the advanced static VAR compensator (ASVC) which is developed in this work is based on the technique of the exact equivalence with the conventional rotating synchronous compensator. The ASVC system has been modeled using the d-q transform. Computer simulation results are provided and discussed to validate the performance of the proposed model.

II. REACTIVE POWER PHENOMENA

2.1 Reactive Power in Electrical Systems

In order to enhance the quality of the power and energy in the grid transmission system we have to control the reactive power by usually compensating individual or group of loads. Moreover, the voltage and frequency must be constant everywhere and display a pure sine wave and a near unity power factor, and must be independent of the size and kind of the consumer loads. This can only be achieved by inserting reactive power compensators and may lead to a better power factor correction; improvement of the voltage regulation; and a good load balancing [14-15].

2.2 Classical Solutions for Compensating the Reactive Power

Classical reactive power compensators are an essential part of the power system in order to minimize transmission losses, maximize power transmission capability, and maintain the supply voltage. In the following, a brief description of some of these classical compensators is given:

- Synchronous compensator: the cost of such system is high and encumbering [16].
- Bank of capacitors are generally designed for compensating parameters that vary slowly, usually fractioned so to adjust the reactive power to be compensated.
- The thyristor-Switched capacitor type of compensator consists of switching on and off capacitors by using static switches. It may be slow since equating the supply-capacitors voltages will lead to a delay in the action.
- Thyristor controlled reactor is constituted of an inductance supplied through an AC-AC converter made of two thyristors in anti-parallel. In general TCR is associated with batteries so that it can absorb or supply reactive power.

- Figure 1 shows the typical method of static VAR compensation. The leading reactive current necessary for VAR compensation is actually supplied by connecting capacitor banks across the AC lines. A capacitor bank connected in this way is called a thyristor switched capacitor (TSC).

2.3 Proposed Advanced Static VAR Compensator

After introducing classical methods for compensating the reactive power, we propose a new concept of the advanced static var compensation [10] based on the exact equivalence with the classical rotating synchronous compensator. This type of compensator uses a source voltage type inverter with a capacitor in the DC side used as energy storage element. The dynamic behavior of the system in open loop will be the key of the synthesis of such an approach of control, and it will be shown that this control approach is more efficient for industry applications [11-13]. The major ASVC system component is a three phase PWM forced commutated voltage source inverter as shown in Figure 2. The ac terminals of the inverter are connected to the ac mains through a first order low pass filter. Its function is to minimize the damping of current harmonics on utility lines. The dc side of the converter system is connected to a dc capacitor, which carries the input ripple current of the inverter and is the main reactive energy storage element. The dc supply provides a constant dc voltage and the real power necessary to cover the losses of the system. Figure 3 shows a simplified equivalent circuit of the ASVC. In this representation, the series inductance L_s accounts for the leakage of the transformer and R_s represents the active losses of the inverter and transformer. C is the capacitor on the dc side. The inverter is assumed to be loss less. V_{oa} and V_{sa} are the amplitude of the fundamental of the output voltage of the converter and phase voltage of the supply, respectively. The operating principles of the ASVC can be explained by using its phasor diagram . When the amplitude of the inverter output voltage V_{oa} is smaller than the supply voltage V_{sa}, the reactive power is absorbed by the ASVC. Otherwise, the ASVC generate the reactive power when the amplitude of the supply voltage is larger than the output voltage of the inverter.

III. BEHAVIOR ANALYSIS OF THE ASVC SYSTEM

To achieve an easier modeling of the system, the original circuit is subdivided in several basic sub-circuits as shown in Figure 3. Detailed analysis are given in [18]. Collecting all parts of the system, while introducing the model of the dc part in the system, the complete mathematical model of the ASVC in d-q axis will be as follows:

$$\frac{d}{dt}\begin{bmatrix} i_q \\ i_d \\ v_{dc} \end{bmatrix} = \begin{bmatrix} -\frac{R_s}{L_s} & -\omega & 0 \\ \omega & -\frac{R_s}{L_s} & -\frac{m}{L_s} \\ 0 & \frac{m}{C} & 0 \end{bmatrix} \begin{bmatrix} i_q \\ i_d \\ v_{dc} \end{bmatrix} + \frac{V_s}{L_s}\begin{bmatrix} -\sin\alpha \\ \cos\alpha \\ 0 \end{bmatrix} \qquad (1)$$

From equation system (1), we can extricate the expressions for i_d, i_q, v_{dc}

Expressions of real and reactive power are given by:

$$p_c(p) = v_{sq} i_q + v_{sd} i_d = -V_s(i_q \sin\alpha - i_d \cos\alpha) \qquad (2)$$

$$q_c(p) = v_{sq} i_d - v_{sd} i_q = -V_s(i_d \sin\alpha + i_q \cos\alpha) \qquad (3)$$

3.1 The ASVC behavior in steady state

Equations governing the steady state behavior of the ASVC can be obtained by equating the term of derivatives in the mathematical model given by equations (1) to zero, which comes to similarly having to short-circuit inductors and to open the capacitor. We note that the active and reactive power depend only on the square of the supply voltage and the resistor of coupling of the ASVC to the ac mains, and independent of the other parameters of the circuits (L_s and C).

In addition, the dc side voltage depends on α, the modulation index, and the resistor and inductor of the coupling, but independent of the value of the dc capacitor. While the system parameters are given by: Supply: $V_s = 220\ V$, $f = 50\ H_Z$, $R_s = 1\Omega$, $L_s = 5\ mH$ DC side : $C = 50\mu F$, $m = 1.12/\sqrt{3}$

By varying the angle α in an interval of *-30° to +30°* which is the linear zone for sine and cosine, we obtain the following responses.

Figure 4 shows that i_q, i_d and v_{dc} values for different values of α, where we can note that the real current i_d is always zero, on the other hand the reactive current i_q and the dc voltage v_{dc} are linear according to α .

3.2 The ASVC behavior in transient state:

Taking as an initial condition for the DC side voltage, the maximum voltage of the supply, a series of dynamic responses of the system to step changes of $\pm 10°$ of the angle α have been established [16]:

Figure 5 shows the response of the reactive current i_q to a step change of $\alpha = -10°$, which after a short transient state attains a stable value of 38 *A* supplied to the network.

Figure 6 shows the response of the active current i_d, $\alpha = -10°$ which after the voltage v_{dc} reaches its stable value, it goes to zero, because its action on the transient state is only for charging and discharging the DC side capacitor.

3.3 Programmed PWM generation pattern

Two methods of PWM generating pattern were thoroughly investigated and the method which offers better voltage utilization and lower switching frequencies thus less stress on switching devices and reduction of the switching losses was used in the paper. The set of non linear equations might be solved by the method of Newton Raphson. The expressions of the slopes are :

$$m_p = 5.0391 e^{-0.07125M}$$

$$m_n = -6.4384 e^{-0.05672M}$$

Hence, we give the approximations of the angles of initial commutation as a function of the modulation index as :

$$\alpha_K = m_p IM + c_K \quad K = 1, 2, 4, \ldots etc.$$

$$\alpha_K = m_n IM + c_K \quad K = 3, 5, 7, \ldots etc.$$

with :

$$\text{for } MI = 0 \quad c_1 = 0 \quad c_2 = \frac{120}{(M+1)}$$

$$c_K = c_{K+1} = \frac{(K+1)60}{M+1}$$

$$c_{M-2} = \frac{(M-1)60}{M+1} \qquad 3 \le K \le M-2, K \text{ odd}$$

$$\text{et } c_{M-1} = 60 \qquad c_M = \frac{(M+3)60}{M+1}$$

For our case, we took *M=11*, that is to eliminate the harmonics having the following order :
5, *7*, *11*, *13*, *17*, *19*, *23*, *25*, *27*, and *29*.
Hence, Figure 7 shows the trajectories of the angle of commutations for modulation index varying between *0* to *1.15*.
Figure 8 shows the switching pattern, and the corresponding line to neutral output inverter voltage.
The switching angles of the programmed PWM pattern are obtained by the resolution of a set of nonlinear equations as shown in [8], [9].
A programmed PWM switching pattern which allows the elimination of selected number of harmonics [1] is continuously applied to the six controlled switches. This method is used because it offers better voltage utilization and lower switching frequencies thus less stress on switching devices and reduction of the switching losses (increase of the efficiency of the converter).
The parameters of the programmed PWM pattern used in this paper are given by: MI (modulation index) = 1.12

3.4 Controller design [18]

The controller design of the ASVC is based on the linearized model of the system under some assumptions such as disturbance α_Δ being small, the second-order terms are dropped, and the quiescent operating α_0 is near zero. Thus the PI controller is conceived so that the ASVC has a desired dynamic performance. The PI transfer function is:
The closed loop transfer function of PI associated to the transfer function of the ASVC is given by:

$$[F_{PI}.G]_{BF}(p) = \frac{F_{PI}.G}{1 + F_{PI}.G} \qquad (4)$$

The parameters of the PI controller can be shown to be:

$$K_p = K = 7.5\,10^{-6}$$

$$K_I = \frac{K}{T_i} = 2.5\,10^{-3}$$

IV. CONTROL STRATEGY AND PERFORMANCE ANALYSIS OF THE PROPOSED ASVC

3.1 Proposed control block diagram

Figure 9 shows the main control circuit of the system, it represents the different blocks constituting the control system. The source voltage and the ASVC's currents are transformed in the d-q axis for calculating the reactive power generated by the system which is compared to the reference, the vector PLL detect the phase angle of the supply which is added to the control variable α (output of the PI controller). This sum adjusts the reading frequency of the counter connected to the EPROM where switching pattern is stored.

3.2 Simulation results of the ASVC acting alone

To verify analytical key results and the validity of the proposed control scheme [16], the aforementioned ASVC structure was tested on Pentium personal computer. Computer simulation was carried out using Mat lab, with the system parameters given by: Supply: $V_s = 220\ V$, $f = 50\ H_Z$, $R_s = 1\Omega$, $L_s = 5\ mH$; Dc side : $C = 500\ \mu F$; PI controller : $K_P = 7.5\ 10^{-6}$, $K_I = 2.5\ 10^{-3}$

Testing of the ASVC system shown in Figure 9 was performed for dynamic response. The amplitude of the reference was adjusted to cause the system to swing from leading to lagging mode.

Figure 10 shows the simulated reactive power response to a reference change from *10 kVar* lagging to *10 kVar* leading.

Performance evaluation of the subject model has also been tested for current and voltage responses to step changes.

Figure11 shows the simulated current and voltage waveforms to a step reference change from *10 kVar* lagging to *10 kVar* leading, this figure confirms that the compensator time response is fast (about *10 ms*).

3.3 Application of the advanced static VAR compensator for the improvement of stability of a turbo alternator

Recent developments in the solid state VAR compensators have opened a very optimistic door towards achieving a very efficient control of reactive power. This stems from the fact that the voltage is maintained constant within a specified level, to improve the dynamic stability of the power system and its power factor as well as correcting the phase unbalance.

In this section, we will study the case when disturbances occur at the studied machine without affecting the behaviour of the other machines that is (speed and E.M.F are constants). This means that the voltage and frequency of the network can be considered constants. The turbo-alternator is then connected to a distribution network called 'infinite'.

3.3.1 Proposed control strategy of the network-ASVC

Based on Figure12 we can establish various equations [19], hence our model will be made up of ten differential equations, seven for the alternator and three for the ASVC. For the initialisation of the system, we take for the machine the same conditions given in [16], and for the ASVC the following initial conditions:

$$v_{dC} = \frac{\sqrt{2}\,v}{m}$$

$$i_{dC} = 0$$

$$i_{qC} = 0$$

Figure 12 shows the main principles of the proposed control of the ASVC, the reactive power demanded is always compensated partly by the capacitive reactive power generated by the ASVC, this method of compensation help ease the alternator and increase the security boundary for the heating of the rotor circuit. The reactive power demanded being inductive must be compensated by a capacitive reactive power generated by the ASVC. A PI regulator controls this compensation, which synthesize the control variable α which is added to the angle δ that is necessary for synchronizing with the voltages of the bus bar considered. This sum being α_c is applied to the ASVC to generate the necessary reactive power; the control variable α being limited by two upper and lower levels will allow preserving the stability of the compensator. If we suppose that the reference is always the voltage of the bus bar connected to the ASVC, the transfer function relating the reactive power to the control angle α is given by [17]. As for the PI regulator, it is designed similarly as given in section 29.3.5 with the same constant of time of integration, but the voltage level will change. Hence by using the root locus method, the parameters of the regulator are given as follows:

$$K_p = 2.3\,10^{-9}$$

$$\mathrm{K_I} = 7.7\,10^{-7}$$

3.3.2 Simulation results

To further demonstrate the usefulness of the proposed ASVC, we used it with a turbo alternator to analyze the performance of its stability. A series of simulation tests have been carried out and will be give below. To analyze the performance of the stability of the turbo-alternator with ASVC, a series of simulation tests have been carried out, by taking the compensator parameters as follows: AC side : $R_s = 1\Omega$, $L_s = 5$ mH; DC side : C = 500 μF.

Figure13 represents the variation of the load angle of the turbo alternator group with and without compensation after clearing the fault of *0.08 s*, we notice that the response with the compensation is more damped and the load angle is smaller than that of the turbo alternator without compensation.

Figure14 represents the variation of the voltage of the first bus bar with and without compensation, the voltage of the system compensated is higher than that without compensation, this is due to the decrease in reactive power in the lines by the ASVC which generates a capacitive reactive current which annuls a part of the inductive reactive current absorbed by the line.

Figure15 shows the variation of the load angle of the turbo-alternator with and without compensation after the clearing of the fault of *0.3 s*, which is the critical time for clearing the fault for the alternator without compensation. We notice that the introduction of the ASVC has allowed to improve this clearing time and to increase the level of stability of the system.

V. CONCLUSION

A new model of advanced static VAR compensator has been developed. A fast control approach of the ASVC system has been implemented for applications that require leading or lagging power compensation.

The proposed control strategy is based on an explicit control of the reactive power, implicit of the voltage amplitude of the

capacitor of the dc side and is more flexible.
The simulation results show that this control strategy has good dynamic performances for generating or consuming of the reactive power.
In this paper a new approach to improve the stability of a turboalternator using a static VAR compensator has been presented. The proposed system has been analyzed and a fast current controller been implemented for reactive power applications. The mathematical model derived and the transient simulated results obtained are included to confirm the applicability of the proposed control scheme.

REFERENCES

1. H. S. Patel, and R. G. Hoft, "Generalized Technique of Harmonic Elimination and Voltage Control in Thyristor Inverters: Part I-Harmonic Elimination", IEEE Trans. on Ind. Appl. Vol. IA-9, pp. 310-317, May / June 1973.
2. S. R. Bowes, R. R. Clements, "Computer aided design of PWM inverter systems", IEE. Proc., Vol. 129, Pt. B, N°1, January 1982.
3. H. Akagi, Y. Kanazawa, A. Nabae, "Generalized Theory of The Instantaneous Reactive Power in Three - Phase Circuits" IPEC, Tokyo'83, pp1375-1386.
4. H. Akagi, Y. Kanazawa, A. Nabae, " Instantaneous Reactive Power Compensators Comprising Switching Devices Without Energy Storage Components " IEEE Trans On Ind. Appl. Vol. IA-20, N° 3, May/June 1984.
5. H. W. Van der Broeck, H.-CH. Skudelny, G. Stanke, "Analysis and Realization of a Pulse Width Modulator Based on Voltage Space Vectors", Proc. of IAS'86, 1986, pp. 244-251
6. P. N. Enjeti, J. F. Lindsay, " Solving Nonlinear Equations of Harmonic Elimination PWM in Power Control ", IEEE Trans. Ind. Appl. Electronics Letters Vol. 32, No 12, 4th June 1987.
7. L. Moran, P. D. Ziogas, and G. Joos, "Analysis and design of a Synchronous Solid-state Var Compensator", IEEE Trans. on Ind. Appl. Vol. IA-25, No 4, July / Aug. 1989, pp.598-608.
8. P. N. Enjeti, P.D. Ziogas, and J. F. Lindsay, " Programmed PWM Techniques to Eliminate Harmonics: A Critical Evaluaton", IEEE Trans. Ind. Appl. Vol. 26, No 2, March / april 1990.
9. G. Joos, L. Moran, and P. D. Ziogas, "Performance Analysis of a PWM Inverter VAR Compensator", IEEE Trans. on Power Electronics, Vol. 6, No 3, July 1991, pp. 380-391.
10. L. Gyugi, "Unified Power-Flow Control Concept for Flexible AC Transmission Systems", IEE. Proced. C, Vol. 139, N°4, July 1992.
11. D. R. Trainer, S. B. Tennakoon, R. E. Morrison, " Analysis of GTO-based Static VAR Compensators " IEE Proc.-Electr. Power Appl., Vol. 141, No 6, November 1994.
12. J.B. Ekanayake ., N.Jenkins. , N.B. Cooper. : 'Experimental investigation of an advanced static Var compensator'. IEE Proc.-Gener. Transm. Distrib., Vol. 142,No.2, March 1995.
13. A. R. Bakhshai, G. Joos, H. Jin, '' Space Vector Pattern Generators for Multi-Module Low Switching Frequency High Power Var Compensators'', Proc. of PESC'97, 1997, pp.344-350.
14. H. Akagi, Fellow, IEEE, "The State-of -the -Art of Power Electronics in Japan",IEEE,Trans.Power.Electr. Vol.13, No. 2. 1998
15. G.C.Cho, G.H.Jung, N.S. Choi, and G.H. Cho, Member, IEEE, Analysis and Controller Design of Static Var Compensator Using Three-Level GTO Inverter, *IEEE Trans. Power Electron*. Vol.11, no. 1, jan 1996, 111-111.
16. T. J. E. Miller, " Reactive Power Control in Electric Systems ", John Wiley and Sons, Inc. 1982.
17. M. H. Rashid, *Power Electronics: Circuits, Devices, and Applications* (Prentice Hall, Englewood Cliffs, Inc. 1994).
18. A. Tahri, M. Benghanem and A. Draou, ''A Non-linear Control and Modelling of an Advanced Static Var Compensator'', International Conference on Electronics, ICEL'98, 5-7 October 1998, U.S.T.Oran, Algeria, pp 209-213.
19. A. Draou, M. Benghanem, A. Tahri, and L. Kotni, 'A New Approach to Modelling Advanced Static Var Compensator', Conf. Rec IEEE/CESA Vol.3, No.7, pp.573-578, Hammamet, Tunisia, April 1998.

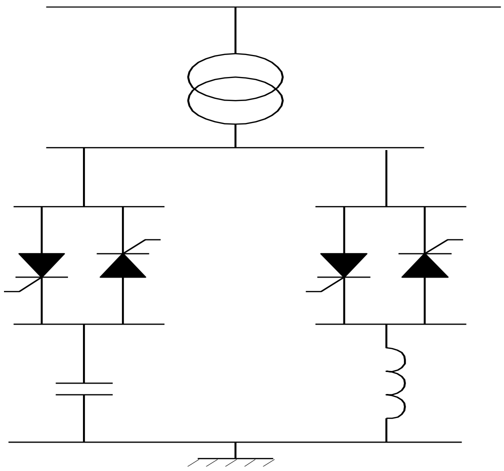

Fig.1 Static VAR compensation using TSC and TC

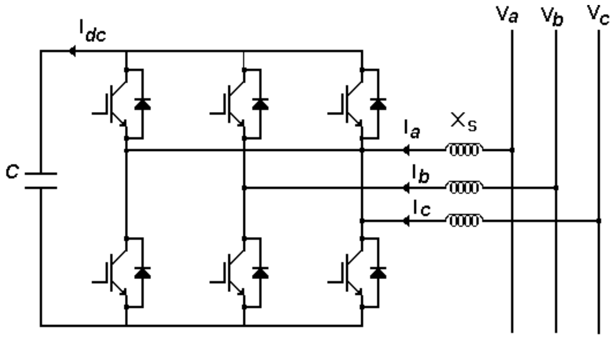

Fig.7 Main circuit of ASVC

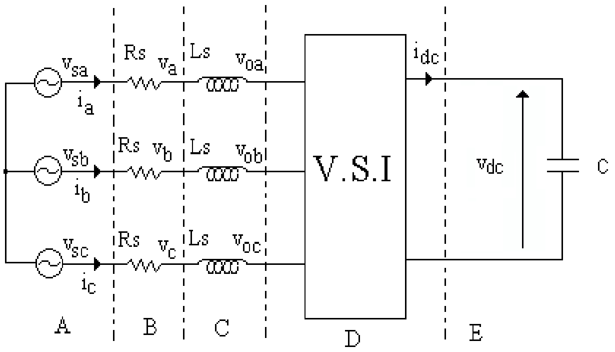

Fig.3 Equivalent circuit

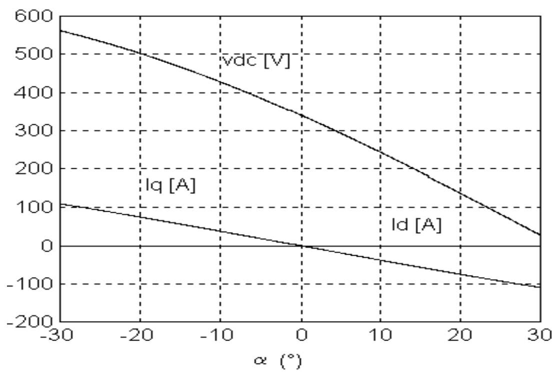

Fig.4 Steady state values

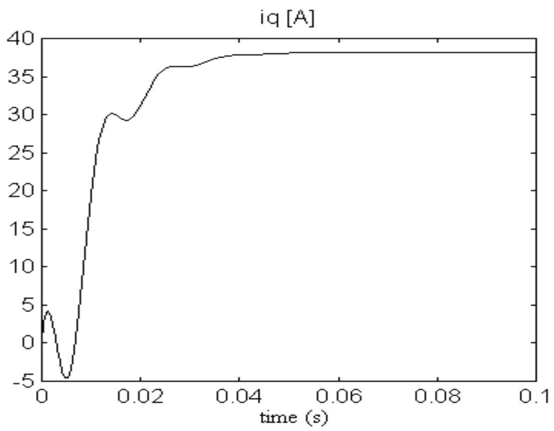

Fig.5 Transient reactive current response

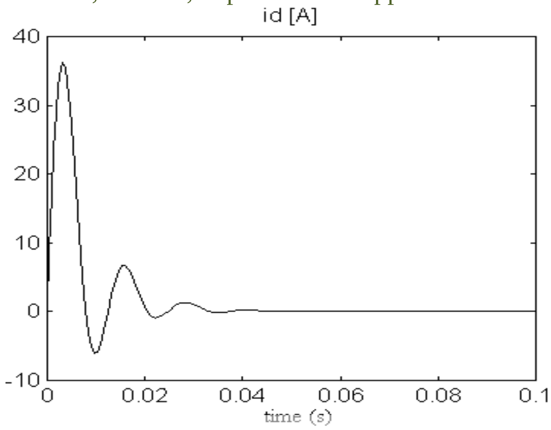

Fig.6 Active current response to change of □

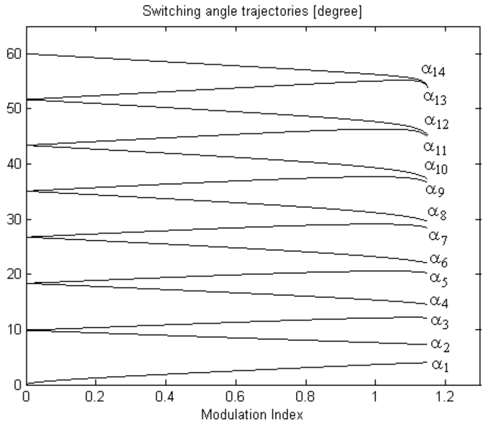

Fig.7 Switching angle trajectories for eliminating 13harmonics

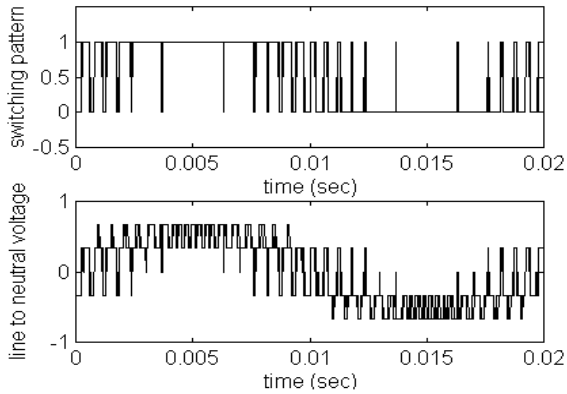

Fig. 8 Switching pattern and line to neutral

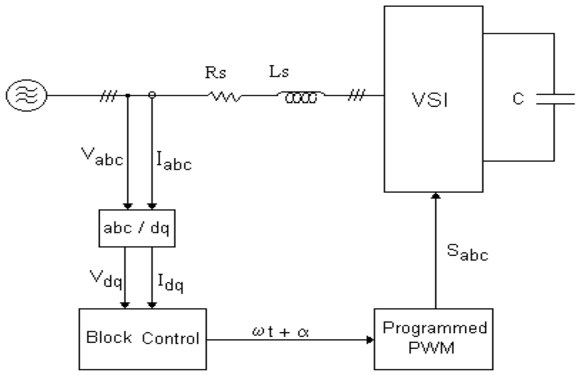

Fig.9 Main and control circuit of the proposed system.

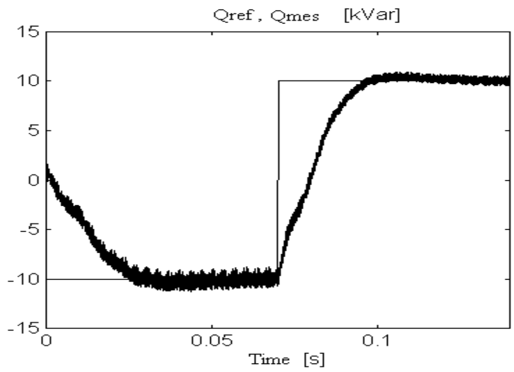

Fig.10 Simulated reactive power response

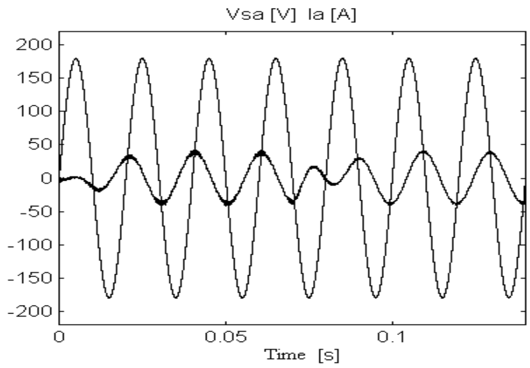

Fig. 11 Simulated current and voltage waveforms

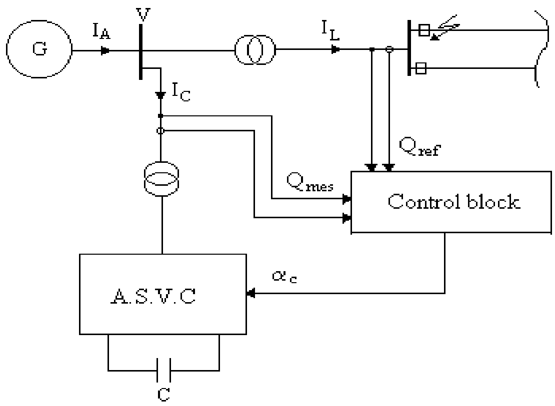

Fig.12 Main circuit configuration of the proposed system

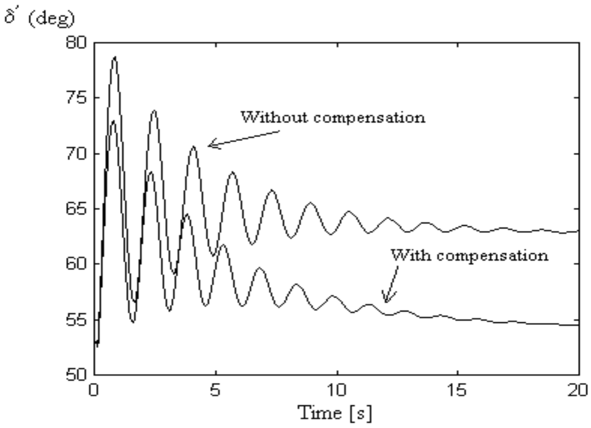

Fig.13 Load angle variation

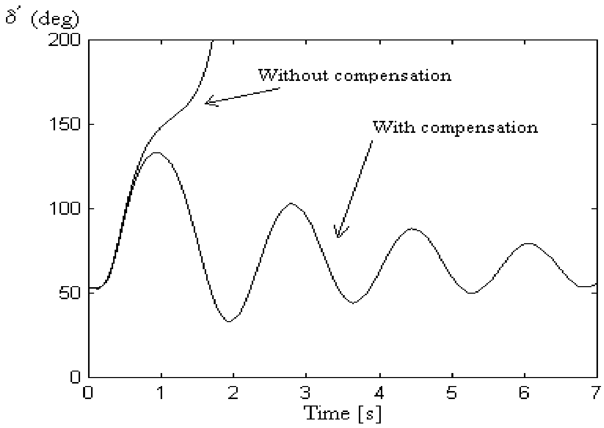

Fig. 14 Variation of the voltage of the first busbar

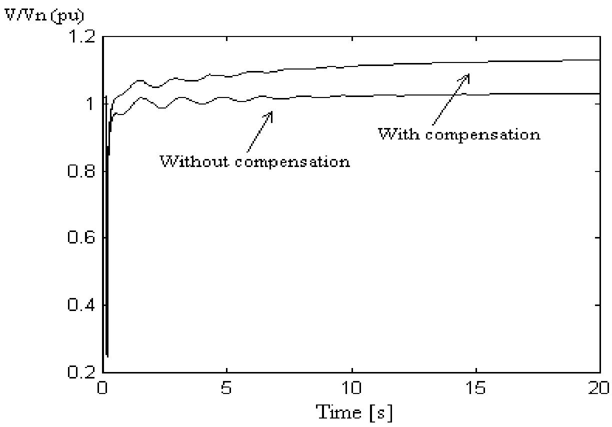

Fig. 15 Variation of the load angle of the turboalternator

International Journal of Modern Engineering Research (IJMER)
www.ijmer.com Vol. 3, Issue. 5, Sep - Oct. 2013 pp-2640-2645 ISSN: 2249-6645

Optimized CAM Design

S. Haroon Rasheed[1], M. Anand Vijay Kamalnath[2]
Department of ECE, AVR & SVR E C T, Nandyal, India

Abstract: *Content-addressable memories (CAMs) are hardware search engines that are faster than algorithmic approaches for searching applications. CAMs consist of conventional semiconductor memory (usually SRAM) with added comparison circuitry that performs search operation to complete in a unique clock cycle. In case of sophisticated and high end applications we need large sized CAM which utilizes large amount of power but this has to be avoided. This paper proposes an idea for improving power, area and performance of the system of recently proposed high Performance Hybrid-Type CAM Designs. For this we replace the basic 9T CAM cell with a 4T CAM cell. The simulation results show the success of the method.*

Key words: *Basic 9T CAM cell, 4T CAM cell, NOR-Type Array, NAND-Type Array, Hybrid CAM Design.*

I. INTRODUCTION

Content Addressable Memory is used to access the memory through the data rather than the address which is used in the case of normal RAM's. The output of the CAM will be the location where the associated content is stored. In CAM with parallel comparison feature the power consumption is lesser than the normal CAM. In case of CAM, the input data and the stored data are being compared, if both matches then the match line are used to indicate it. Due to its low power and fast matching capability it is mainly used in advanced applications like Strong ARM processors, ATM switches, etc.

In this paper we are designing a Hybrid Type CAM[7] design so that it should have low power and high performance. Normally basic CAM cell consists of 9 transistors to write, read and match the data. It consists of both store unit and match unit. The main drawback of this basic CAM cell is that it occupies more area, needs more power and has large delay. So we need to explore modifications to it so that area, power and performance can be improved. So we are designing 4 transistor CAM cell[8] such that these can be effectively used in many applications.

In the design CAM different techniques have been proposed to reduce the power consumption and improve the performance of the CAM cell. A CAM cell design with XOR and XNOR blocks were designed [2], with different combinations of pmos and nmos transistors, depending upon the type of application. But the main drawback of the proposed design are usage of more number of transistors and more power consumption. A two stage CAM cell design is proposed [3], to reduce power consumption where a control circuitry consisting of an inverter is used between the two stages. Performance of this CAM cell design is degraded in this design and there exists the disadvantage of short circuit power dissipation. A static pseudo nmos CAM has been designed[4] which requires an extra pmos transistor for every CAM cell which use in it, so it is very bad idea to for each and every pmos for each stages. Other method has been designed which requires separate cmos parallel CAM for searching the data[5] which requires lot of area to implement it and also extra precharge device[6] to implement CAM. To overcome the disadvantages of the previous designs a Hybrid-Type CAM design[7] is proposed to improve the power, area and performance of the CAM cell. This consists of both the NOR-type CAM design for the high performance and NAND-type CAM design for Low-Power, as constraints.

II. BASIC CONTENT ADDRESSABLE MEMORY

Basic CAM cell consists of both store unit for storing the data and compare unit for comparing the data. We store the data using two cross-

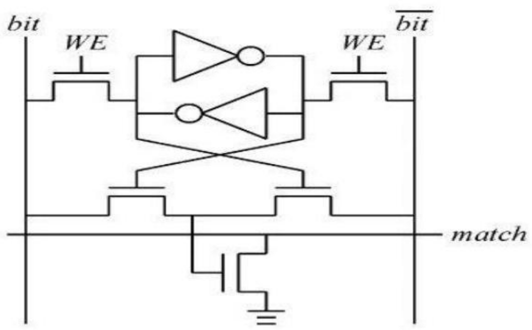

Fig 1: Basic XOR CAM cell

coupled inverters and is implemented with 6T SRAM cell. The compare unit is designed using pass transistors. The fast pull down transistor is used to discharge the data so that it indicates whether the data is matched. Depending on different applications the compare unit can be designed with XOR type or XNOR type blocks. The main operation of CAM cell can be described as: when the cross- coupled inverters store the data '1' and then the bit and nbit(bit bar/bitc) line has the data '1' and '0' respectively. Now one of the two pull down transistors will be ON state and the other will be OFF state so that there won't be any transistor path to discharge the match line and hence it remains in High-impedance state. Now if the bit and nbit line has the data ‘0’ and ‘1’ respectively, then in the compare unit one of the pull down transistor will be in ON state so that the fast pull down transistor moves to ON state. This discharges the match line indicating that the data have been matched.

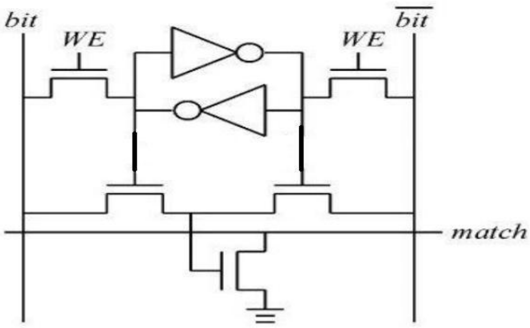

Fig 2: Basic XNOR CAM cell

III. MODIFIED CAM CELL (4T CELL)

This modified 4T CAM cell design consists of 4 nmos transistors and the cells are arranged such that the two transistors (tc1 and tco) are used to store the data and the remaining two transistors (tw1 and tw0) are used to write the data[8]. The gates of tc1(‘a’) and tco(‘b’) are used as storage capacitance elements so that it can be used to store the data as shown in fig 3. When the transistors tw1 and tw0 are in ON state the data can be transferred to the nodes a and b and then these can be read using transistors tc1 and tc0.

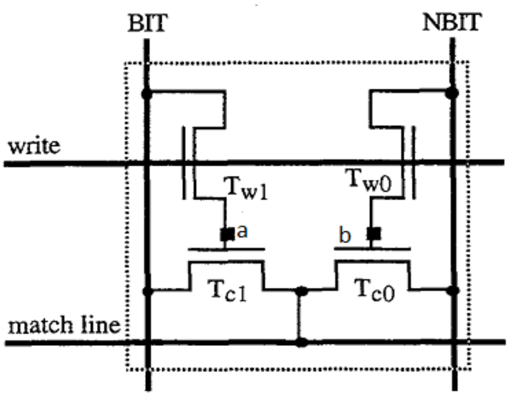

Fig 3:4T XOR CAM cell

Normally matching operation can be done using match line that is connected to the output of the XOR type transistors which are arranged using transistors tc1 and tc0. If the match line output is at logic ‘1’ that indicates that the ‘data stored’ and the ‘input data’ are matched. If the match line output is at logic ‘0’, it indicates that there is no match and then the match line gets discharged. Basically in this operation, first the match line has to be charged to logic ‘1’ by using precharge transistor and then the matching operation can be done. Even in case of mismatch, the match line needs to be discharged, which can be done by using read transistor that is arranged between match line and ground. Fig 4. Shows the 4T XNOR CAMCell.

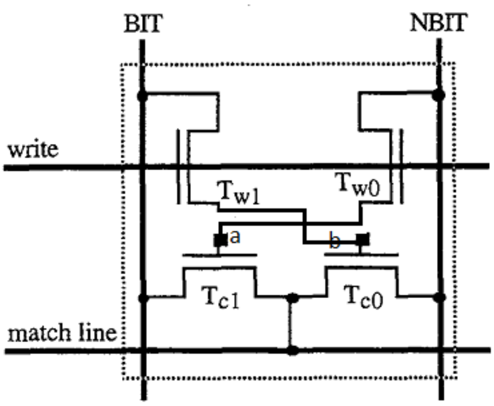

Fig 4: 4T XNOR CAM cell

IV. NOR-TYPE CAM ARRAY

In NOR-type CAM cell design, XOR-type CAM cell is used for better performance of the system. Here the pull-down transistors are arranged in NOR fashion so that it can discharge very fast and hence the performance improves. In case of pre-charge, the Match-line is precharged to HIGH.

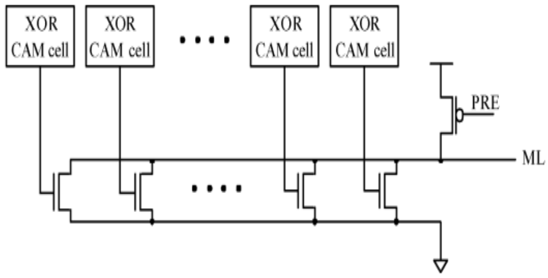

Fig 5: NOR type CAM Array

In the Evaluation phase, if the input data is matched with the stored data then the match line remains HIGH and if all the cells are mismatched then the Match-line will discharge through the pull-down transistors. Thus the NOR-type CAM cell provides better performance. But the drawback in this design is increase in Drain-Capacitance due to more number of transistors. This drawback, increases Power consumption. Hence, it is only useful in case of High performance.

V. NAND-TYPE CAM ARRAY

Unlike the NOR-type CAM cell, NAND-type CAM cell is used to reduce the power consumption of the system. In this the NAND-type CAM, cell is arranged using XNOR type and the transistors are arranged in NAND fashion.

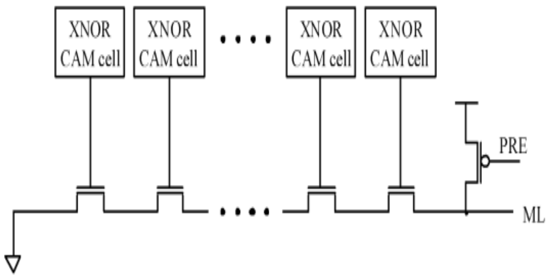

Fig 6: NAND CAM Array

Since the drain capacitance is less, the power consumption of the system is also less. In searching the data, initially the match line is precharged to HIGH, in the pre-charge phase and the match line discharges to ground in the evaluation phase, only when all the CAM cells are matched with the stored data. In case of mismatch the match line remains HIGH as in that of the pre-charge phase. Thus the power consumption of the system can be improved. But the drawback with this design is the time taken to discharge the match line is more, as it has long pull-down path. Hence, this NAND-type design is performance inefficient/slow.

VI. HYBRID-TYPE CAM DESIGN

Hybrid-type CAM design consists of both NOR-type Array with XOR CAM cell for performance advantage and NAND-type Array with XNOR CAM cell for power advantage. Mainly we divide the complete circuit into 3 parts namely, SEG1, SEG2 and CONTROL circuitry. In the SEG 1, we design the circuit using XNOR type and then arrange the pull-down transistors using NAND-type. In the SEG 2, we design the circuit using XOR type and the pull-down transistors are arranged in NOR type design as shown in fig.7.

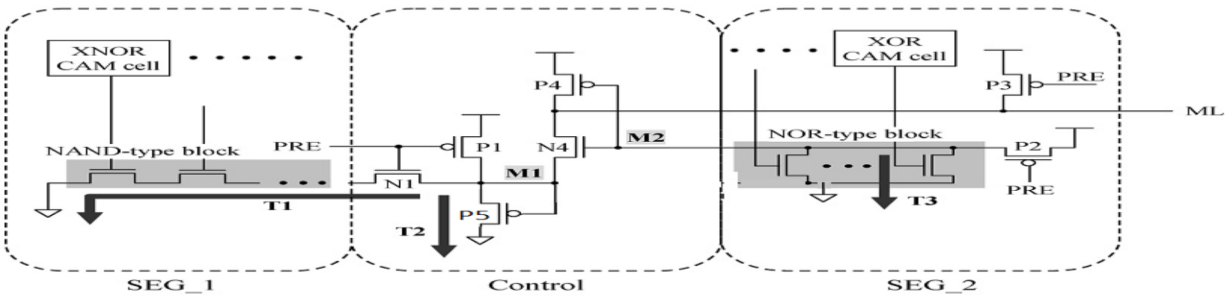

Fig 7: HYBRID CAM Structure [Ref 7]

SEARCH OPERATION OF CAM CELL

In case of searching a data, the input data is compared with that of stored data. The circuit operates in two different phases namely Pre-charge phase and Evaluation Phase. In Pre-charge phase the Match-line is kept in HIGH state and in the Evaluation Phase the state of Match-line depends upon the data matched.

1. PRE-CHARGE PHASE

The control signal PRE is kept LOW so that the circuit starts to Pre-charge. Thus when the PRE signal is kept LOW the match line that is connected to one of the pmos transistor **P3** is made to be in HIGH state. In this circuit we have 3 discharge paths namely **T1,T2 and T3** that are connected to three transistors **N1, P5 and NOR block** respectively. As both the nodes **M1** and **M2** are HIGH, there are no discharge paths for the Match-line in this phase. As there is no chance of discharging the data, the Match-line doesn't require much power. This design is very efficient in Power saving.

2. MATCH-EVALUATION PHASE

In this phase the control signal PRE is made HIGH to start the matching process of the design. The data to be searched is given to the bit lines of the CAM cell. When we search the data we come across 4 different cases but the exact matching occurs only when both the segments are matched. The voltages of each node are shown in Table.1. The detailed explanation of this matching process is given below.

Case1: In this case, SEG1 is mismatched and SEG2 is mismatched or matched. As the SEG1 is mismatched there exists no discharge path because there may be at least one transistor that is OFF. So the node voltage M1 remains HIGH and hence, there won't be any discharge path. Thus in this case the matching process doesn't depend on the SEG2. As there is no discharge path the Match-line still remains in the HIGH state.

Case2: In this case, SEG1 is matched and SEG2 is mismatched. As the SEG1 is matched all the transistors that are connected in the NAND fashion are in ON state, so that there exists a discharge path through the path T1. And thus, the node M1 remains LOW and the two pull-down transistor **P5** gets ON and so, there exists a path T2 to discharge. Now as the SEG 2 is mismatched there exists at least one path to discharge through N3 so that the node M2 remains LOW. Hence in this case, there won't be any path to discharge the match-line.

	SEG 1	SEG 2	Path			Key Node			Result
			T1	T2	T3	M1	M2	ML	
Case 1	Mismatch	Mismatch	X	X	X	H	H	H	Mismatch
	Mismatch	Match	X	X	X	H	H	H	Mismatch
Case 2	Match	Mismatch	0	0	0	L	L	H	Mismatch
Case 3	Match	Match	0	0	X	L	H	L	Match

Table 1: Node Voltages of each node of HYBRID CAM Cell.

Case3: In this case, both the segments are matched. Thus, as the SEG1 is matched, the node M1 gets LOW value as there exists a discharge path. Now in case of SEG2, as it is matched all the transistors are turned OFF and the path T3 to ground is disconnected. Now the node M2 is at HIGH state making the transistor N4 to turn ON. Now there exists a path for Match-line to discharge the data, through the paths T1 or T2. As the path T2 is the fastest path to discharge the data, the Match-line discharges through the transistor P5. Thus it indicates that the data have been matched properly. In this design as we have two pull-down paths to discharge the match-line. It discharges through path T2 as path T1 has transistors connected which takes long time to discharge. Thus, this design provides better performance.

VII. EXPERIMENTAL RESULTS

0.18um technology is used to implement the design. The below Figure 8 shows all the three cases of both SEG 1 and SEG 2 that have been used to search the data .

	Power	Area(um^2)
9T	314.17pw(XOR) 316.55pw(XNOR)	65.81
4T	100.92pw(XOR) 100.829pw(XNOR)	34.04

Table 2: Comparison between 9T and 4T

Thus, 9T CAM cell is compared with 4T CAM cell and the power of the CAM cell have been reduced by 3 times as shown in Table 2.

The NOR type and NAND CAM Arrays are also compared on the basis of power and performance as shown in Tables 3 and 4.

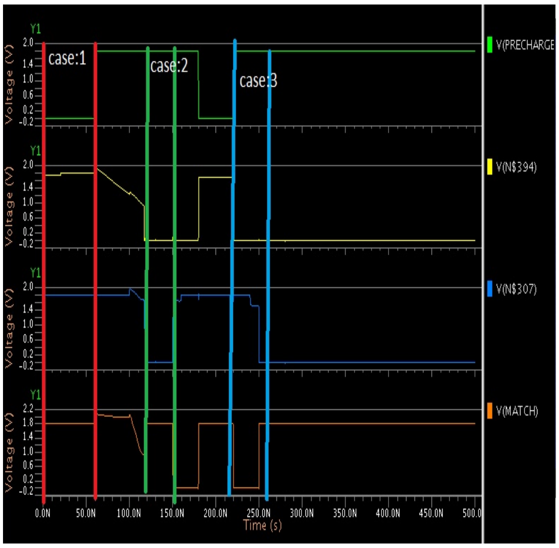

Fig 8. Simulation results of HYBRID CAM

	Power	Delay
9T	397.2uw	88.86ns
4T	19.60nw	60.9ns

Table 3: NOR Type CAM Array

	Power	Delay
9T	70.10nw	109.9ns
4T	840.25pw	69.39ns

Table 4: NAND Type CAM Array

Thus, by combining NAND type CAM Array for power efficiency and NOR type CAM Array for performance efficiency, the HYBRID DYNAMIC CAM design have been designed and it is observed that the design has low power consumption and increased performance. The total power consumption of HYBRID CAM design is shown in Table 5.

	Power	Delay
9T	38.57uw	58.12ns
4T	548.34pw	23.48ns

Table 5: HYBRID CAM Design

Thus by observing the results we can say that by replacing 9T CAM cell with 4T CAM cell the power consumption of the system has been improved and also its performance is also improved drastically. The above Figure 8 shows the simulation results of HYBRID CAM cell, done using MENTOR GRAPHICS and all the three different cases of CAM cell for matching the data is shown.

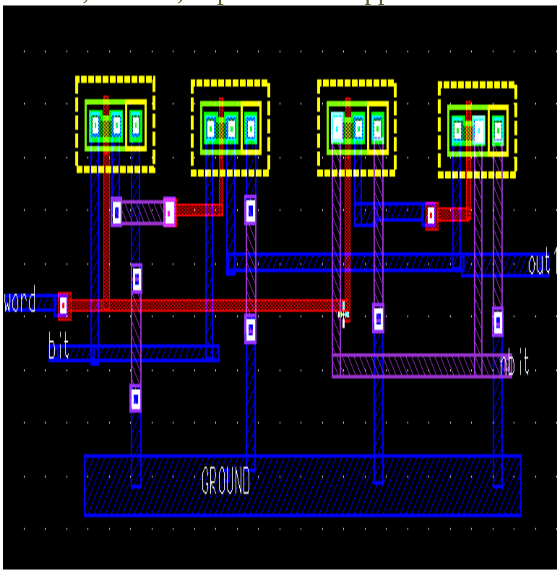

Fig 9: 4T CAM Cell layout in 0.18 um standard CMOS Technology.

VIII. CONCLUSION

Thus, a HYBRID CAM Structure has been designed for Low Power and High Performance using NOR and NAND type CAM Array and area of the complete system has been reduced by replacing 9T basic CAM cell with 4T CAM cell with a fast pull down path to accelerate the search operation.

REFERENCES

[1]. K. Pagiamtzis and A. Sheikholeslami, "Content-addressable memory(CAM) circuits and architectures: A tutorial and survey," *IEEE J. Solid-State Circuits, vol. 41, no. 3, pp. 712–727, Mar. 2006.*

[2]. Content Addressable Memory for Low Power and High Performance Applications by Ataur R. Patwary, Bibiche M. Geuskens, Shih-Lien L. Lu, Solid-State Circuits, no.8, April 2008.

[3]. An Improved Comparison Circuit for Low Power Pre-computation-Based Content-Addressable Memory designs by Yu-Ting Pai, Chia-Han Lee, and Shanq-Jang Ruan, IEEE. Solid-State Circuits, vol. 97,no. 9, June. 2009.

[4]. Design of Low-Power Content Addressable Memory Cell by KUO-HSING CHENG, CHIA-HUNG WEI, JIANN-CHYI RAU, Solid-State Circuits.

[5]. H.Miyatake, M.Tanaka and Y.Mori," A Design for high speed low power CMOS fully parallel Content Addressable Memory macros", IEEE J.Solid-StateCircuits,vol.38,no.11,pp.1958–1966, Nov 2003.

[6]. C.A.ZukowskiandS.Y.Wang," Use of selective precharge for low power content addressable memories", in Proc.Int.Symp.Circuits and Syst.,1997,pp.1788–1791.

[7]. Yen-Jen Chang and Yuan –Hong Liao,"Hybrid-Type CAM design for both power and performance efficiency", in VLSI systems, Vol 16,No:8,Aug 2008.

[8]. Jose G.Delgado –Frias, Andy Yu and Jabulani Nyathi, "A Dynamic Content Addressable Memory Cell", in VLSI Synstems, Vol 99, No:1, Sep 1999.

www.ijmer.com Vol. 3, Issue. 5, Sep - Oct. 2013 pp-2646-2655 ISSN: 2249-6645

Development of Algorithm for Voice Operated Switch for Digital Audio Control Systems

Gokula Krishnan[1], Ram Singh[2], Satyanarayana[3]
[1](M.Tech, DSCE, ECE Department, SNIST, Hyderabad, INDIA)
[2](Scientist 'E', RCMA, DRDO, Hyderabad, INDIA)
[3](Assistant professor, ECE Department, SNIST, Hyderabad, INDIA)

ABSTRACT: *VOS (voice Operated Switch) is a switch that operates when sound over a certain threshold is detected. It is usually used to turn on a transmitter or recorder when someone speaks and turn it off when they stop speaking. It is used instead of a push-to-talk button on transmitters or to save storage space on recording devices. Unlike push-to-talk (PTT) operation, VOS is automatic. The user can keep his hands free while talking. But VOS also has some significant disadvantages that explain why PTT is still common. The Present VOS technology works based on the comparison of the energy estimate in speech band and the noise band. The bandwidth of speech band is from 300Hz to 3.3 KHz and for noise band it is from 3.3 KHz to 6.6 KHz. The major disadvantage with this technique is false operation of VOS due to noise interference or heavy breathing or a side conversation. Hence, a DSP based algorithm is proposed to be developed for DACS (Digital Audio Control System) to improve the performance and the noise suppression.*

Keywords: *Envelope dynamics, Noise estimation, Speech pause detection, SNR (Signal to Noise ratio), VAD (Voice activity detection).*

I. INTRODUCTION

Now a day's speech recognition is becoming more and more popular technology in the society. The innovative technologies in mobile telecommunication, robust speech recognition and digital hearing aids are a strongly dynamic force in the development of real-time noise reduction algorithms. The number of publications on single-microphone noise reduction algorithms indicates an unbroken interest in this research field over the past two or three decades. A decisive point for these kind of algorithms is the synchronized estimate of the object speech spectrum and the interfering noise spectrum in particular. Cockpit voice recorder in aircraft records many cockpit voices, such as speaker voices, noises and background sounds. In these communications, the speech signal which is transmitted is corrupted by additive acoustical noises. These noises may be from non-stationary source and hence there may be situations where only noise segment or non-speech segment is present, hence it is necessary to update the noise spectrum estimate as often as possible to sustain an effective noise reduction. This can be done, whenever target speech is absent, which means that the input signal consists of only noise. Computational and memory requirements should be as low as possible since these algorithms may be ported on a digital circuit.

Speech detection is a process where speech segments be reliably separated from non-speech and activates VOS when only speech segments are detected. The required characteristics of an ideal endpoint detector are: reliability, robustness, accuracy, adaptation, implicitly, real-time processing and know a priori knowledge of the noise.

Earlier, the VOS technology works based on the comparison of the energy estimate in speech band and the noise band. We calculate the signal to noise ratio for both the bands i.e. speech band and noise band and based on a threshold the operation of VOS will take place. The major disadvantage with this technique is false operation of VOS due to noise interference or heavy breathing or a side conversation or any other background noise such as helicopter noise or babble noise etc. The techniques used in this algorithm are discussed in the later sections.

Hence VAD (Voice activity detector) algorithms are developed and employed to make voice operated switch work efficiently and this also increases the switching speed of the voice operated switch.

VAD techniques are designed using various methods. Most of them use heuristically chose statistical properties of speech parameters like: energy, pitch, entropy etc. Therefore, the performances of different VAD are different and varying according to the level and type of signal-to-noise ratio (SNR). As a result, the performances of different speech based systems are significantly sensitive to the employed VAD technique. Therefore, VAD algorithm should be carefully chosen while designing a speech based system.

Several VAD algorithms have been standardized for specific applications. The most commonly mentioned includes ITU-T Recommendation G.729 Annex B [1] and ETSI AMR Option 2 VAD [2], which aim to design simple features that can be implemented in embedded applications efficiently, such as audio recording and transmission on mobile phones. In these systems, speech are often recorded with close-talk microphones, which ensures the sound level of speech is always much higher than background noise. Back then, VAD algorithms often dealt with only little or no noise corruption in speech coding applications and with separate recording utterances in speech recognition systems. Up to recently, advances in various speech applications require the detection of human speech in a continuous real-time fashion, and is often corrupted by a wide variety classes of noise. Algorithms for VAD had grown accordingly over the years. Most of the speech activity detectors are based on either time domain or frequency domain approach. Sangwan, Chiranth [3] have compared various VAD algorithms. The core of any VAD proposed consists of two parts: a 'feature extraction' and a 'speech/ non-speech decision mechanism.

It is necessary to update the noise spectrum estimate as often as possible to sustain an effective noise reduction. Different algorithms have been proposed which continuously update the noise estimate and hence avoid the need for explicit speech pause detection. Martin [4] uses the minimum of the sub-band signal power within a time window of about 1S as an estimate of the noise power in the respective sub-band. Paul proposed a continuous noise estimation scheme similar to Martin's which is computationally more efficient. This scheme was, however, not systematically tested.

Hirsch and Ehrlicher proposed an algorithm [5] which is based on the observation that the most commonly occurring spectral magnitude value in clean speech. Hence, having noisy speech their algorithm measures the distribution density function of the spectral magnitude and density determines the maxima which are then used as an estimate of the respective noise magnitude. These kind of algorithms which avoid speech pause detection for noise estimation are supposed to cope better with non-stationary (i.e., fluctuating) noise, since they are generally faster in their adaptation to changing noise levels even during speech activity. On the other hand, the continuous update of the noise estimate (Independently in the sub-bands) is susceptible to erroneously capture speech energy. This, however, leads inevitably to speech deterioration in a subsequent noise reduction process. Fischer and Stahl proposed a spectral subtraction noise reduction algorithm with a continuous noise spectrum up- dating scheme. They found that the corruption of the noise estimate by speech is too large to be further considered and conclude that voice activity detection plays an important role and cannot be fully omitted, Recently Nemer et al. proposed to use the kurtosis (fourth-order statistics) of the noisy signal to continuously estimate speech and noise energies. The examples presented used noisy speech signals with positive signal-to-noise ratios (SNRs) and yield promising results, but further research is required to extend these results to negative SNR s and different classes of noise, respectively. Dendrinos and Bakamidis [6] presented an algorithm for determining the starting and ending points of speech segments in colored-noise environments through singular value decomposition based on some thresholds which have been determined experimentally. Good performance was proved for SNRs higher than 0 db. However, the complexity of the algorithm makes a real-time implementation difficult.

Weiwu Jiang, Wai Kit Lo [7] presented a novel VAD algorithm using MVSS (Maximum Values of Sub-band SNR) as a decision feature. Here the given the spectrum of a speech utterance transformed by DFT, it first divides the whole spectrum into several sub-bands. Secondly, sub-band SNRs are estimated and maximum values of sub-band SNR (MVSS) are extracted as detection features. The background noise estimation and final VAD decision are made by comparing feature value with an estimated threshold. During initialization, the estimated noise spectrum and threshold are calculated by assuming that speech always follows an initial period of noise.

As the basic requirement to develop or modify an algorithm is to identify the noise i.e. the noisy speech sample is processed by voice operated switch to allow the presence of audio in case of speech and mute when only noise is present.
Based on the above algorithms a modified algorithm is presented and compared with the conventional energy based algorithm.

This paper is organized as it starts with a review of the conventional energy based algorithm and proposed algorithm. Next section reports the expected results of the algorithms under various background noise conditions. Finally, conclusions are presented.

II. ALGORITHMS

The algorithms that were implemented for voice operated switch are discussed in this chapter. In all the mentioned algorithms the plain speech is mixed with various noises like white noise, pink noise, brown noise, helicopter noise etc. with 0db, 3db, 5db, 10db, 15db SNR levels (Signal to Noise Ratio). It will be called as noisy speech from now, which are used in the experiments.

2.1 Conventional energy based algorithm

This algorithm works based on the comparison of the energy estimate of the noisy speech. In general the bandwidth of the speech band is from 300Hz to 3.3 KHz and for noise band it is from 3.3 KHz to 6.6 KHz. Therefore using the filters the noisy speech is divided into two bands, that is the speech band and the noise band by assuming the cut off frequency of 3000 Hz. The Butterworth filter was preferred over other filters based on the parameters suitable to the algorithm.

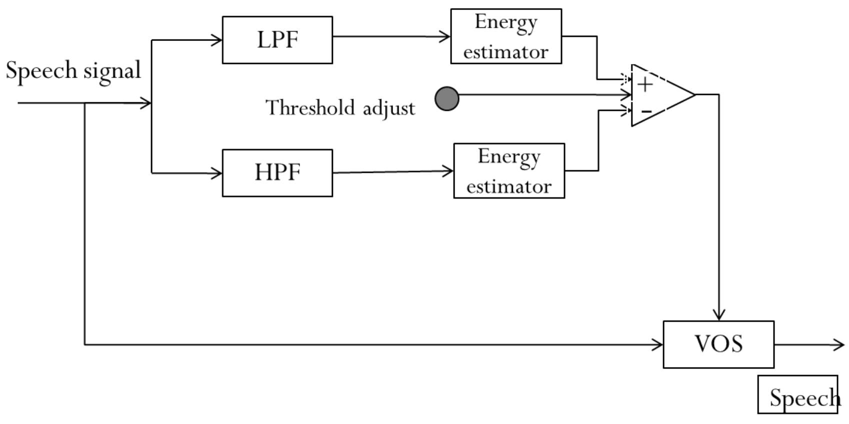

Fig1: Conventional energy based algorithm block diagram

The energies of both the speech band and noise band are calculated by considering a window or frame length of 160 samples. Later the Signal to Noise Ratio of the each frame is determined. The threshold is calculated based on the previous experiments.

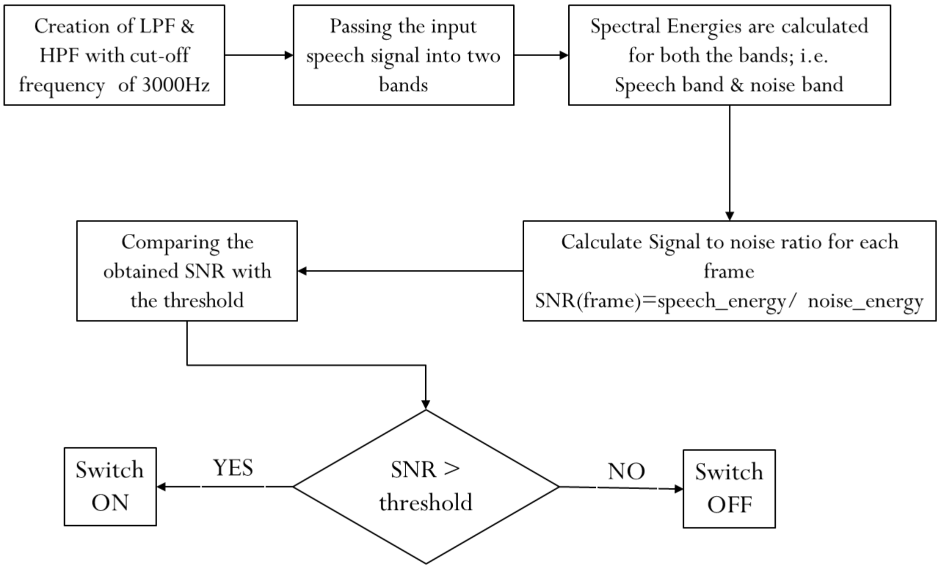

Fig2 : Conventional energy based algorithm - flowchart

The operation of the Voice operated switch is based on the obtained SNR when compared with the assumed threshold. i.e., when the SNR is greater than threshold then switch gets activated (VOS=1). When the SNR is less than threshold then the switch deactivates (VOS=0). The noisy speech sample is processed by voice operated switch to allow the presence of audio in case of speech (VOS=1) and mute when only noise (VOS=0) is present. The simulation and results are shown in the next section.

The performance of the conventional energy based algorithm was not as anticipated and the result was not satisfactory, will be discussed in further section.

2.2 Power envelope based algorithm

An algorithm is proposed which detects speech pauses by adaptively tracking minima and maxima in a noisy signal's power envelope both for the broadband signal and for the high-pass and low-pass filtered signal.

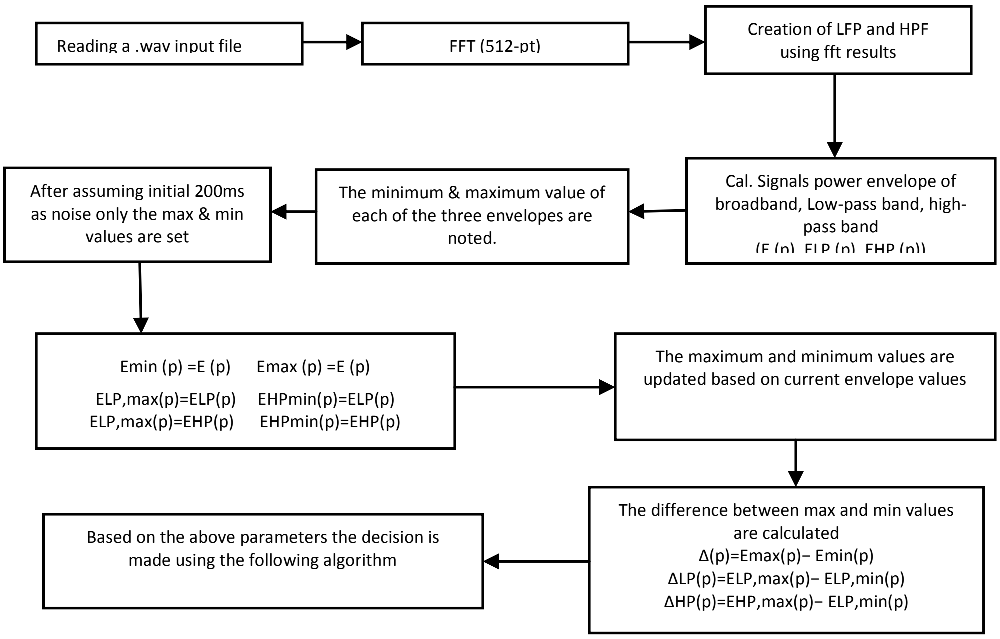

Fig3: Power envelope based algorithm- Flowchart

The speech pause detection algorithm calculates the signal's temporal power envelope E (p) by summing up the squares of the spectral components of the input signal in each short-time frame

: $E(p) = \sum_k |X\ (p, \omega k)|^2$……………. (1)

Here, X (p, ωk) denotes the spectral component of the noisy input signal at frequency ωk at time frame. In addition a low-pass band envelope and a high-pass band envelope are calculated:

: $E_{LP}(p) = \sum_l |X\ (p, \omega k)|^2$……… (2)

: $E_{HP}(p) = \sum_m |X\ (p, \omega k)|^2$…….. (3)

Where "l" runs over all spectral components up to the cut-off frequency, and "m" runs over the remaining spectral components. In order to slightly smooth the envelopes, E(p), $E_{LP}(pp)$and $E_{HP}(pp)$are averaged over a few frames by a recursive low-pass filter of first order with a release time constant ȚE no smoothing is per- formed in case of an increase in energy (i.e., attack time zero) to avoid smearing over onsets. The algorithm tracks the minimum and maximum value of each envelope and uses these for the speech pause decision as described by the following scheme.

I. After an assumed 200 ms initial phase of noise only the minimum and maximum values are set as follows:

:$E_{min}(p) \equiv E_p(p)$ $E_{max}(p) \equiv E_p(p)$

:$E_{LP,min}(p) \equiv E_{LP}(p)$ $E_{LP,max}(pp) \equiv E_{LP}(p)$

:$E_{HP,min}(p) \equiv E_{HP}(p)$ $E_{HP,max}(p) \equiv E_{HP}(p)$……. (4)

This guarantees that the minimum envelope values correspond roughly with the noise energy at the beginning.

II. The minimum and maximum values are updated for each of the three envelopes in the following manner.

a) If the current envelope value is larger than the maximum value for the corresponding envelope, then the maximum value is set to the current value. Otherwise, the maximum value slowly decays. This is done by a recursive low-pass filter of first order with a release time constant τ_{decay}, which takes as input the current envelope value.

b) If the current envelope value is smaller than the minimum value for the corresponding envelope, then the minimum value is set to the current value. Otherwise, the minimum value is slowly raised. This is done by a recursive low-pass filter of first order with attack time constant τ_{rise}, which takes as input the current envelope value.

III. The differences between the maximum and the minimum values are calculated for each envelope

$\Delta(p) = E_{max}(p) - E_{min}(p)$

$\Delta_{LP}(p) = E_{Lp,max}(p) - E_{Lp,min}(p)$

$\Delta_{HP}(p) = E_{Hp,max}(p) - E_{Hp,min}(p)$…… (5)

IV. Three different criteria are introduced of which only one has to be true for making the decision that target speech is not present in the actual frame: a) the speech pause decision can be made because of a low signal dynamics in both the low-pass and the high-pass band(Syn speech pause); b) the decision can be based on the low-pass band information (LP Speech Pause); and c) it can be made upon the high-band information (HP Speech Pause). These decision criteria are derived as follows:

a) If ΔLP is smaller than some threshold ή and ΔHP (p) < ή then it is assumed that only noise is present due to the very small dynamic range of the signal (Dyn Speech Pause).

b) If a) is not true, it is checked whether ΔLP is bigger than (otherwise the dynamic range in the low-pass band is very small and it should not receive too much attention no LP Speech Pause). Now, if the difference between the current $E_{Lp}(p)$ and $E_{Lp,min}(p)$ of the low-pass band envelope is smaller than some fraction pc of ΔLP (which means that the actual envelope is near its minimum), a closer look at the high-pass band is necessary to support speech pause detection.

Case 1) ΔHP of the high-pass band is smaller than threshold in this case no additional information can be obtained from the high-pass band because of its small dynamic range. Now, if at least E (p) (the signal's envelope) lies in the lower half of its dynamic range [i.e., in the lower half between $E_{min}(p)$and $E_{max}(p)$ the current frame can be assumed to be a speech pause because of the closeness of the low-pass band energy to its minimum value (LP speech pause) otherwise, however, there is not enough support for a speech pause decision (No LP Speech Pause).

Case 2) ΔHP is bigger than two times the threshold ή .In this case, there is enough dynamic range to pay attention to the high-pass band. Thus, it is demanded that the difference between the current $E_{Hp}(p)$and $E_{Hp,min}(p)$of the high-pass envelope is smaller than two times the fraction pc of ΔHP to support the small envelope value in the low-pass band. Then a noise-only frame is assumed (LP Speech Pause). This demand is not as strict as that for the low-pass band, to account for the case that the disturbing noise has a rather high-frequency characteristic. But if this condition is not fulfilled, speech may be present in the actual frame (no LP Speech Pause).

Case 3) ΔHP Is smaller than two times the threshold ή , but bigger than. In this case, which is not as clear as Case 2, it is only demanded that EHP(p) (the high-pass Envelope) lies in the lower half of its dynamic range to support the small envelope value in the low-pass band Then it is assumed that target speech is absent (LP Speech Pause). However if this condition is not fulfilled, speech may be present in the actual frame (no LP Speech pause).

c) Condition b) accounts for the case that the disturbing noise has a rather high frequency characteristic, hence the speech pause detection should mainly be made upon the information in the low-pass band. To account also for the case that it has be checked but now with reverse roles of the low-pass and the high–pass bands to determine whether target speech is absent (HP Speech Pause).

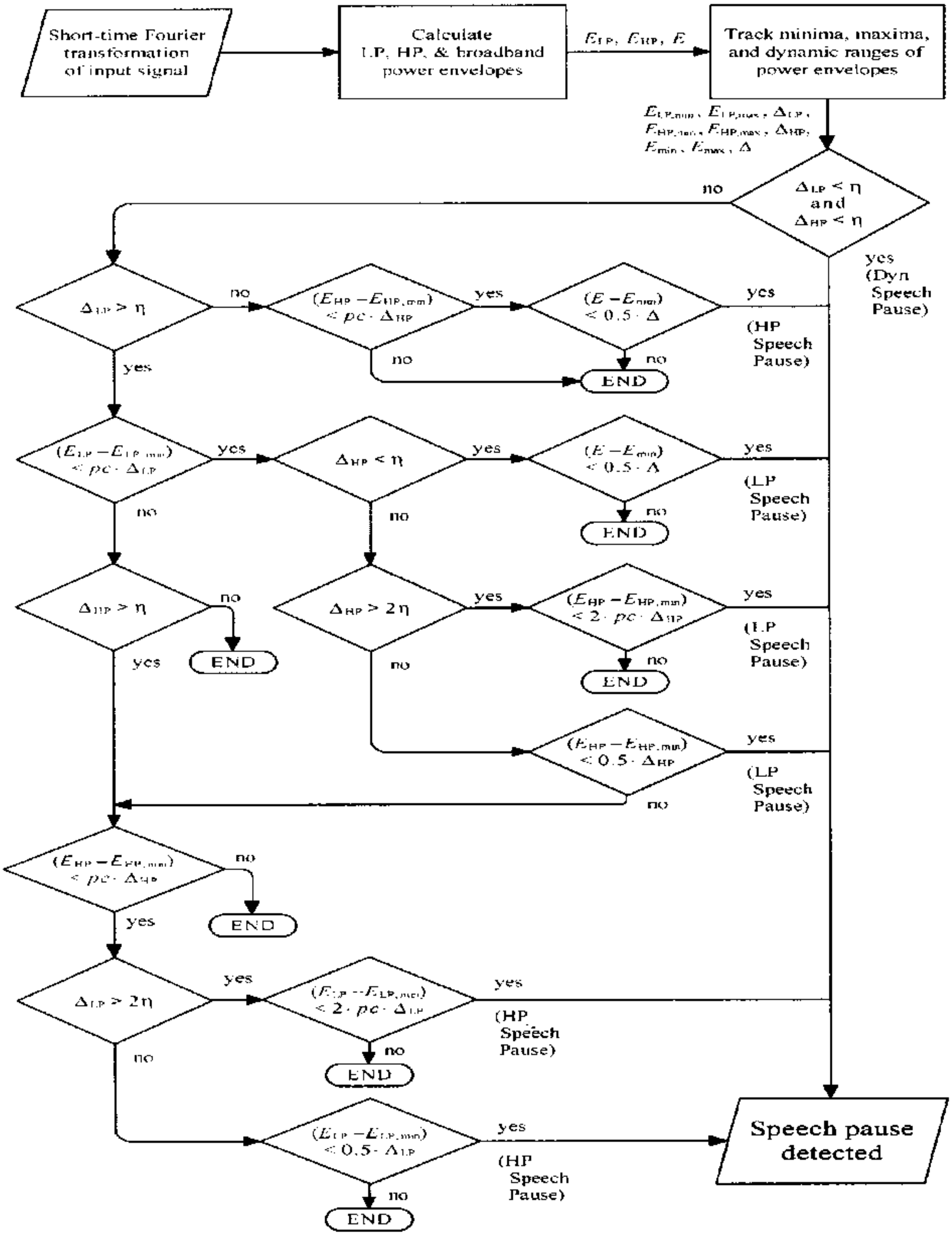

Fig 4: Flowchart of the proposed speech pause detection algorithm operating on a single time frame

Fig above gives a flowchart of the proposed power envelope detection algorithm. The flowchart is not fully symmetrical with respect to LP and HP speech pause detection since several redundant tests are omitted.

Due to its flexible design this novel approach for speech pause detection can easily be adjusted to obtain a rather low false- alarm rate by adapting the main parameters ή and *pc*. Generally, a Low-false-alarms rate is desirable to reduce speech distortions in the subsequent noise reduction process. However, this also results in a reduced hit rate.

During the development of the algorithm noisy signals generated from various different noise types and speech signals at several SNRs were used for performance verification. Finally, the following values were chosen for the free parameters: The input signal was digitized with a sampling Frequency of 8000 Hz and partitioned in Hamming-windowed segments of length 20 ms with 50% overlap. These segments were padded with zeros and a 512-point FFT was performed. This framework is compatible with most single-microphone noise reduction algorithms which can thus easily be integrated. Such short segments are motivated by the fact that then the same signal analysis and synthesis as necessary for a real-time noise reduction environment can be used. The cut-off frequency between low-pass and high-pass band was set to 2 kHz, motivated by the fact that excluding speech frequencies above 1.9 kHz has a roughly similar effect on speech intelligibility as excluding those below this value. With these settings a good approximation to the actual dynamic range of the signal and of its “placement” in the level area under a variety of conditions was achieved. However, systematic variations of these parameters were not investigated. The threshold was set to 5 dB and the fraction was set to 0.1.

III. SIMULATION RESULTS

In this section the procedure to carry out experiments is discussed and comparison between the proposed algorithm and conventional energy based algorithm is discussed

3.1 Procedure

The plain speech is recorded at a sampling rate of 8000Hz and is mixed with various noises like white noise, pink noise, brown noise, helicopter noise etc. with 0db, 3db, 5db, 10db, 15db SNR levels. The algorithms are implemented and simulated in MATLAB and simulation results are discussed below.

3.2 Simulation results

3.2.1 Conventional energy based algorithm results

The following are the results of conventional energy based algorithm for voice operated switch

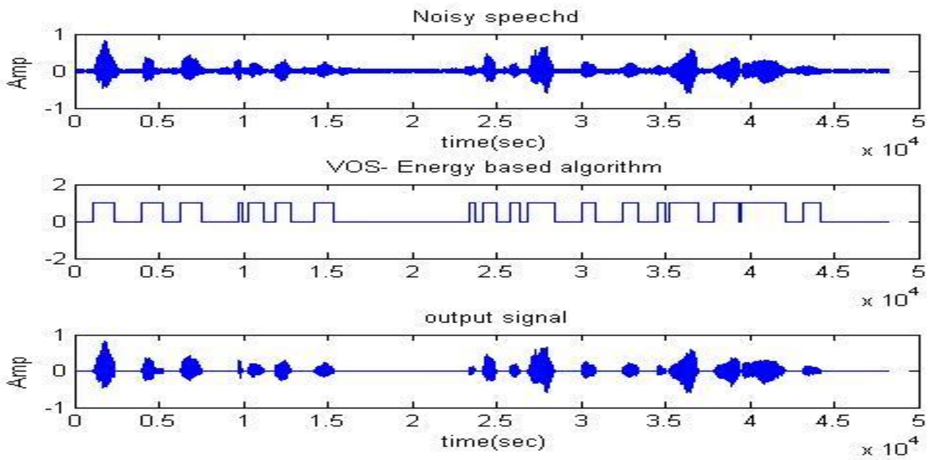

Fig 5: Plot of (a) 10dB white noise mixed speech signal (b) Switch on/off for energy based algorithm(c) output

Fig 5 shows the results of voice operated switch when plain speech is mixed with 10 dB white noise and the output of conventional energy based algorithm.

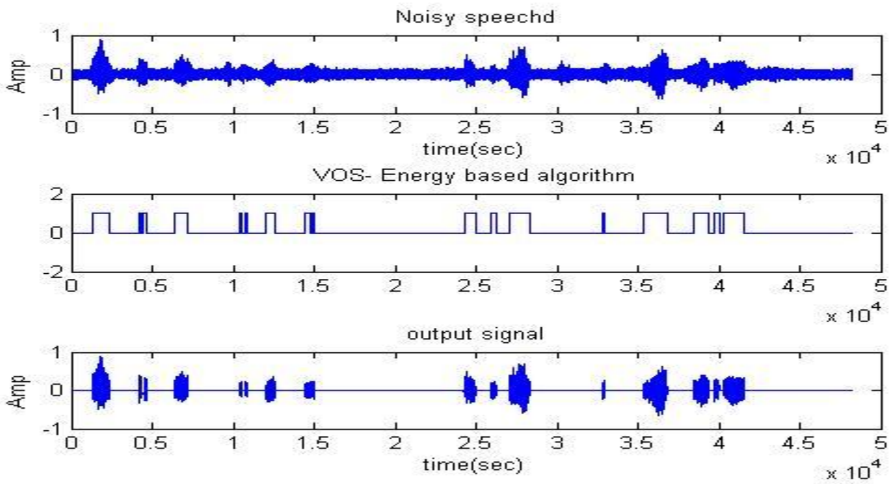

Fig 6: Plot of (a) 5dB white noise mixed speech signal (b) Switch on/off for energy based algorithm(c) output

Fig 6 shows the results of voice operated switch when plain speech is mixed with 5 dB white noise and the output of conventional energy based algorithm.

Fig 7 shows the results of voice operated switch when plain speech is mixed with 10 dB pink noise and the output of conventional energy based algorithm.

Fig 8 shows the results of voice operated switch when plain speech is mixed with 5 dB helicopter noise and the output of conventional energy based algorithm.

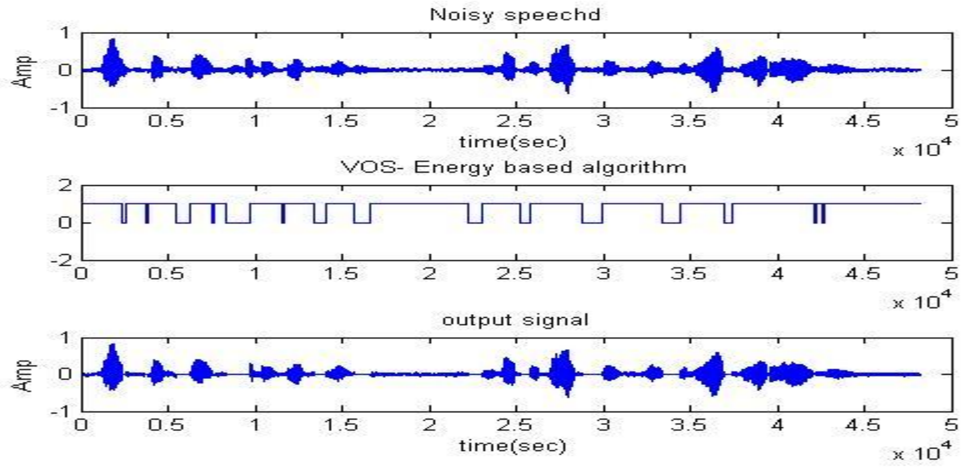

Fig 7: Plot of (a) 10dB pink noise mixed speech signal (b) Switch on/off for energy based algorithm(c) output

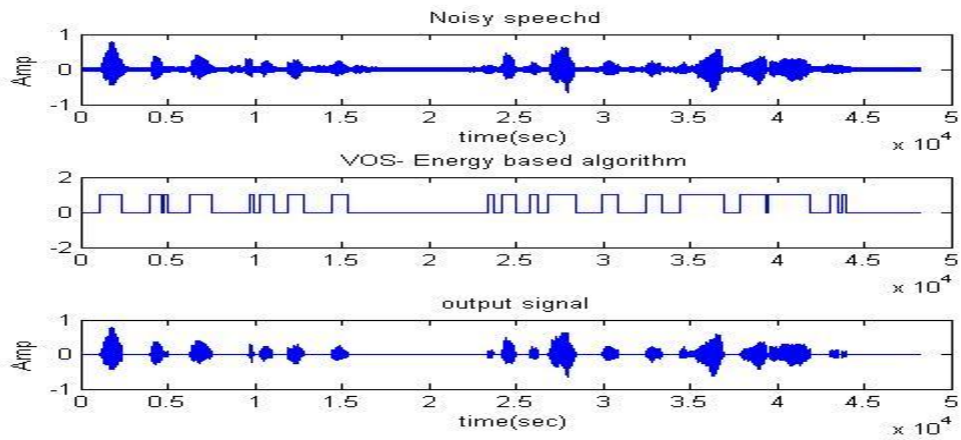

Fig 8: Plot of (a) 5dB helicopter noise mixed speech signal (b) Switch on/off for energy based algorithm(c) output

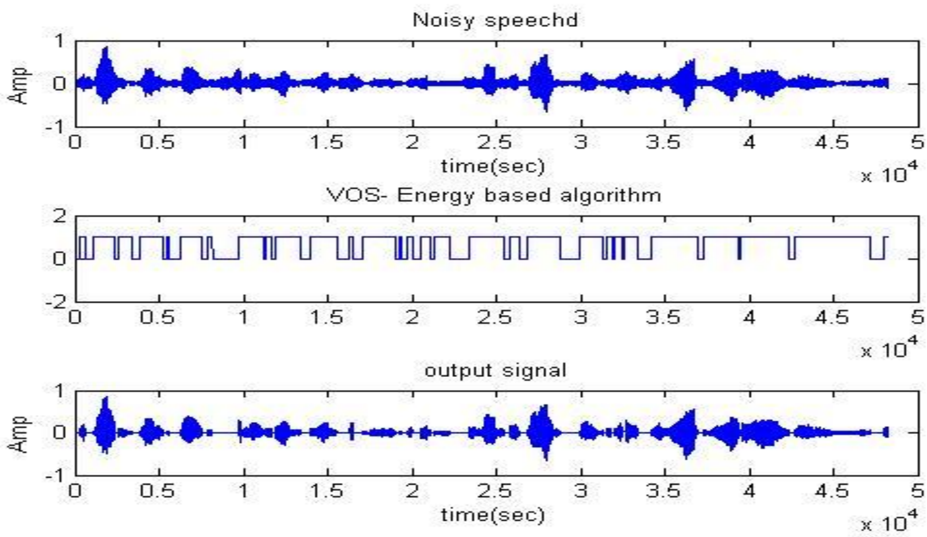

Fig 9: Plot of (a) 10dB babble noise mixed speech signal (b) Switch on/off for energy based algorithm(c) output

Fig 9 shows the results of voice operated switch when plain speech is mixed with 10 dB babble noise and the output of conventional energy based algorithm.

3.2.2 Power envelope based algorithm results

The following are the results of power envelope based algorithm for voice operated switch

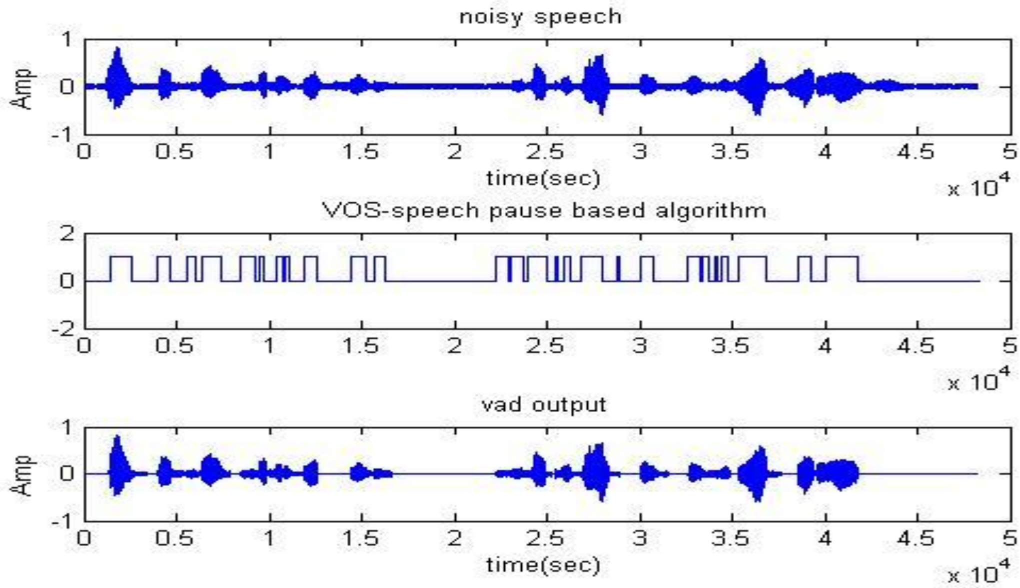

Fig 10: Plot of (a) 10dB white noise mixed speech signal (b) Switch on/off for power envelope based algorithm(c) output

Fig 10 shows the results of voice operated switch when plain speech is mixed with 10 dB white noise and the output of power envelope based algorithm

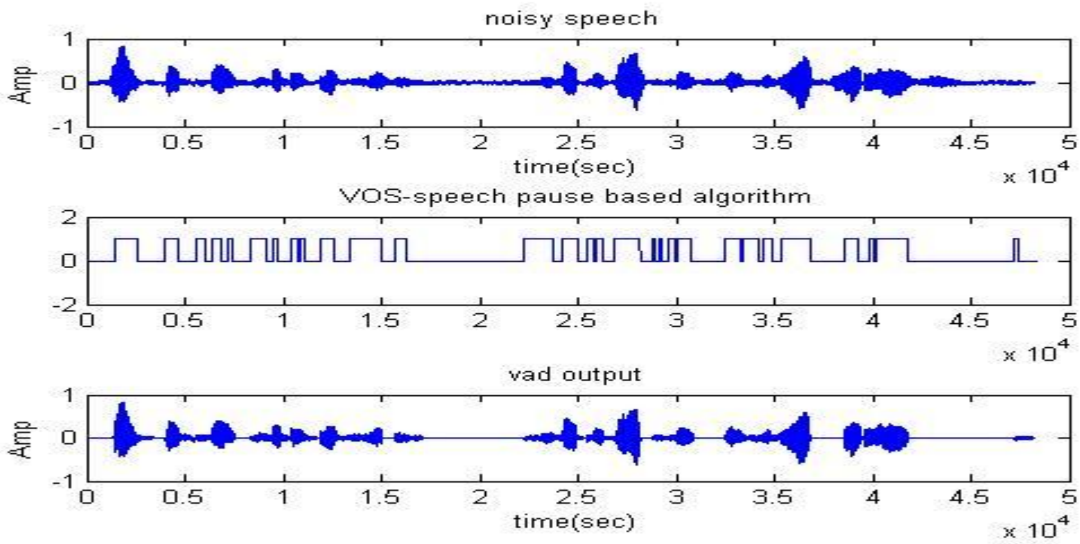

Fig 11: Plot of (a) 10dB pink noise mixed speech signal (b) Switch on/off for power envelope based algorithm(c) output

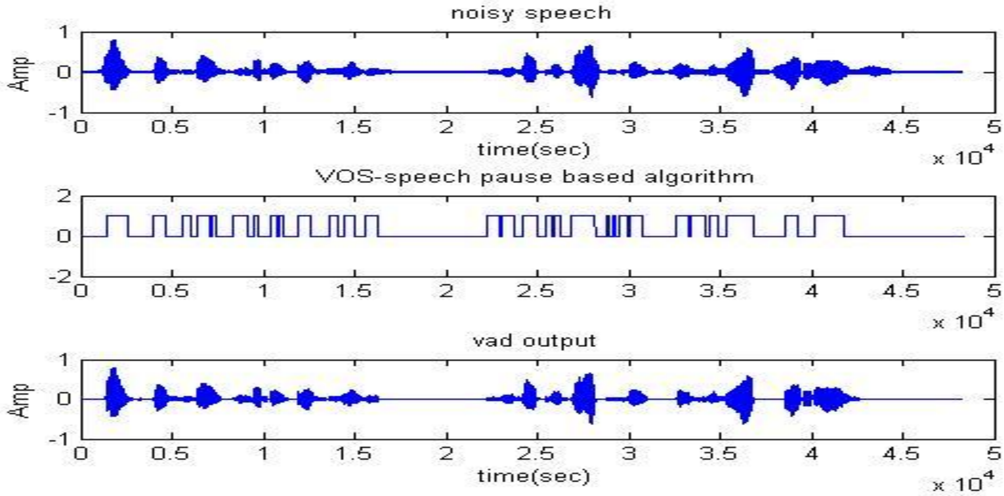

Fig 12: Plot of (a) 10dB helicopter noise mixed speech signal (b) Switch on/off for power envelope based algorithm(c) output

Fig 11 shows the results of voice operated switch when plain speech is mixed with 10 dB pink noise and the output of power envelope based algorithm

Fig 12 shows the results of voice operated switch when plain speech is mixed with 10 dB helicopter noise and the output of power envelope based algorithm

Fig 13 shows the results of voice operated switch when plain speech is mixed with 5 dB helicopter noise and the output of power envelope based algorithm

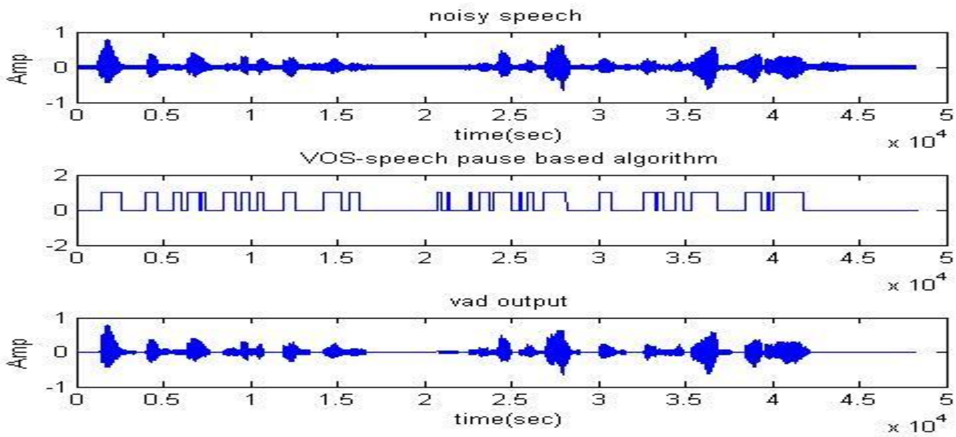

Fig 13: Plot of (a) 5dB helicopter noise mixed speech signal (b) Switch on/off for power envelope based algorithm(c) output

There were other simulation results considered and only few of them. In energy based algorithm the switch activates at few places even when only noise is present. The major disadvantage because of this algorithm is it doesn't perform well due to noise interference or heavy breathing or a side conversation etc.

IV. CONCLUSION

The present VOS technology works based on the conventional energy based algorithm, which works well for white noise at 10dB, 15dB etc., but results are not promising for helicopter, pink and babble noise. The pilot or co-pilot has to adjust the threshold (SNR) level which is inside the audio control system (as shown in the figure1) to hear a clear speech signal. Using the proposed algorithm, the pilot doesn't need to change the threshold control every time (unlike conventional energy based algorithm) to hear the speech signal clearly i.e. the speech is transmitted when speech is detected (VOS=1), it is muted when noise is present (VOS=0).

From the simulation results and observation it is clearly seen that the power envelope detection based algorithm gives better and efficient performance when compared with the conventional energy based algorithm. Many research are however to be analyzed on basis to modify the algorithm to improve the performance on different noise levels. The proposed power envelope detection algorithm maintains a low and approximately constant false-alarm rate over a wide range of SNRs. The hit rate decreases only slightly at poorer SNRs.

The efficient voice operated switches can be father used for commercial and defense purpose which leads to save battery life and helpful to save storage spaces on recording devices.

ACKNOWLEDGEMENT

I am grateful to my guides Mr. Ram Singh, Scientist 'E', and Mr. Satyanarayana, Assistant professor for constantly encouraging me, for their inspiration and innovative ideas, valuable suggestions and guidance without which I would not have achieved our goal.

REFERNCES

[1] Benyassine, E. Shlomot, H.-Y. Su, and E. Yuen, "A robust low complexity voice activity detection algorithm for speech communication systems," in *Speech Coding For Telecommunications Proceeding, 1997, 1997 IEEE Workshop on, p. 97, 1997.*

[2] ETSI, "Universal mobile telecommunication systems mandatory speech codec speech processing functions, AMR speech codec; voice activity detector *(3GPP TS 26.094 version 4.0.0 release 4)," 2001.*

[3] Sangwan, Chiranth M. C, R. Shah, V. Gaurav, R. Venkatesha Prasad, "Voice Activity Detection for VoIPTime and Frequency domain Solutions", *TENTH ANNUAL IEEE symposium on multimedia communications and signal processing, bangalore, nov 2001, pp 20-24.*

[4] R. Martin, "An efficient algorithm to estimate the instantaneous SNR of speech signals," *in Proc. EUROSPEECH'93, vol. 1, 1993.*

[5] H. G. Hirsch and C. Ehrlicher, "Noise estimation techniques for robust speech recognition," *in Proc. IEEE Int. Conf. Acoustics, Speech, Signal Processing 1995, vol. 1, 1995, pp. 153–156.*

[6] M. Dendrinos and S. Bakamidis, "Voice activity detection in colorednoise environment through singular value decomposition," *in Proc. 5th Int. Conf. Signal Processing Applications and Technology.Waltham, MA: DSP Associates, 1994, vol. 1, pp. 137–141.*

[7] Weiwu Jiang, Wai Kit Lo and Helen Meng," A New Voice Activity Detection Method Using Maximized Sub-band SNR",*978-1-4244-5857-8/10/$26.00©2010, ieee,icalip2010*

[8] "Digital Processing of Speech Signals" by L. R. Rabiner and R. W. Schafer, *Prentice Hall Publication, 1978*

[9] "Discrete-time speech signal processing" by Thomas F. Quatieri

Comparative Losses and Economic Feasibility of the Improved Onion Storage with Low Cost of Onion Storage Structure

[1]Seema T. Borole, [2]Rajesh Burbade, [3]Anil Shinde
[123]K K Wagh college of Agricultural engg & Tech. Nashik-422003,

Abstract: *Onion produced in Kharif and Late Kharif season is not suitable for storage while onion produced in summer season can be stored upto 5-6 months and it can be brought in the during market rainy season i.e., from June to Oct. There are certain problems which arise during conventional storage of onion viz. loss in weight, sprouting and rotting of bulb. There are three types onion storage structure developed by NHRDF and domestic onion storage structure located at Kalwan. The construction cost per sq.ft. of this structure ie.Traditional onion storage structure, Dindigul onion storage structure, Improved low cost onion storage structure developed by NHRDF, and Low cost onion storage structure (Kalwan) are Calculated. The quantity of onions were stored in different onion storage structure during the last week of May is about 1000kg .There are some losses such as weight losses ,rotting losses and sprouting losses were found to be in storage.This losses were found high in storage structure developed by NHRDF as compared to domestic onion storage structure (Kalwan).The Cost per sq.ft (Rs) and per kg storage cost against construction cost (Rs) of domestic onion storage structure is less as compare to onion storage structures in NHRDF.*

Keywords: *NHRDF- National Horticultural Research Development Foundation*

I. INTRODUCTION

Onion is a term used for many plants in the genus Alliums. They are known by the common name "onion" but, used without qualifiers; it usually refers to Alliums cepa. Alliums cepa is also known as the "garden onion" or "bulb" onion. It is grown underground by the plant as a vertical shoot that is used for food storage, leading to the possibility of confusion with a tuber, which it is not. Onions, one of the oldest vegetables, are found in a large number of recipes and preparations spanning almost the totality of the world's cultures. They are now available in fresh, frozen, canned, pickled, powdered, chopped, and dehydrated forms. Onions can be used, usually chopped or sliced, in almost every type of food including cooked foods and fresh salads and as a spicy garnish. They are rarely eaten on their own but usually act as accompaniment to the main course. Depending on the variety, an onion can be sharp, spicy, tangy and pungent or mild and sweet.

There is an annual production of approximately 58-60 lakh mt of onions in the country. Out of this about 26-28%, approximately 16 lakh mt onions are produced in Maharashtra. Last year 8.26 lakh mt onions have been exported from the country, out of which 5.40 lakh mt has been produced in Maharashtra. For this purpose continuous export quota and stable onion prices in domestic market are necessary.

II. MATERIALS AND METHODS

2.1 Storage Structure

Material used for construction of onion storage structure

1. Cement

Cement is used for purpose of construction work; it is also used to bind the stone, sand, bricks etc.

2. Concrete

It is carefully mixture of cement, fine aggregates, sand and water. It is used for construction of storage structure.

3. Bamboos

It is flexible, very strong, durable and abundantly. So it is used for construction of storage structure.

4. Leaves of sugarcane and coconut

It is one of the wastes material and available easily in the field. So it is used for roofing purpose. Coconut leaves are strong yet flexible .The leaves are actually fronds composed of numerous leaflets, which have a flat and a thin midrib.

5. Gunny cloth

Gunny cloth is used at inner lining of roof to check the leakage of rain water. The gunny cloth also reduces the temperature inside the storage structure.

6. Iron angle

Iron angle is used support to side wall. It provides stability to the structure and increases the life of the structure It also provides rigid support to the side wall of the onion storage structure.

2.2 Cost estimation of onion storage Structure developed by NHRDF

2.2.1 Traditional onion storage structure:-Size=20`*15`, Life -8 years

Figure 1: Traditional onion storage structure

Table I: Traditional onion storage structure materials

Material	Size(ft)	Quantity	Rate(Rs.)	Total(Rs)
Bamboo	6	240	6	1440
Wooden block	15	8	100	800
Wooden strip	6	240	6	1440
Iron angle	10	4	150	600
Shelter material	-	80	15	1200
Cement	-	2(bags)	150	300
Labour	-	9(person)	100	900

Total Cost:-Rs.6680
Cost per sq.ft:- Total cost/size of structure/life
= 6680/300/8 = Rs.2.78
Per kg storage cost against construction cost: - x/1000=6680/1000 = Rs 6.68

2.2.2 Dindigul onion storage structure:-Size=20`*15`, Life-8years

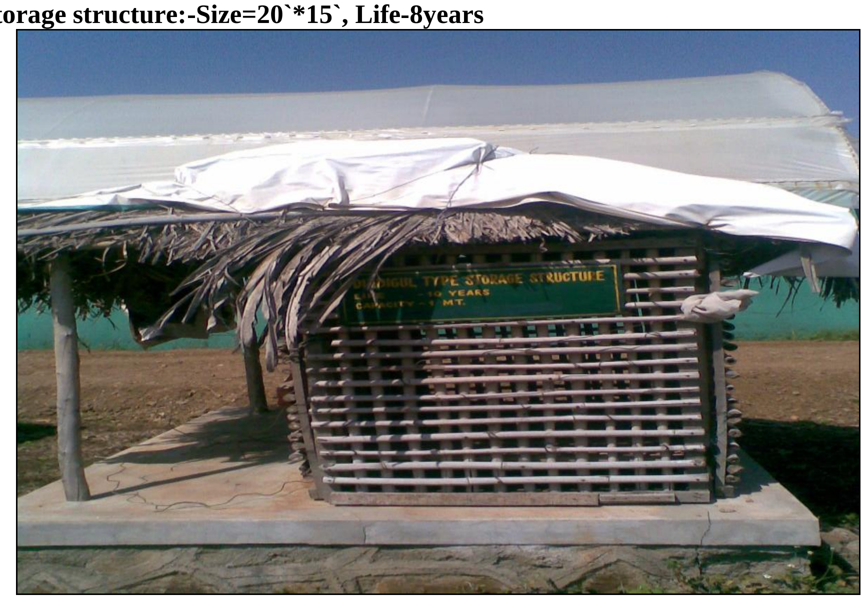

Figure 2: Dindigul onion storage structure

Table II: Dindigul onion storage structure material

Material	Size(ft)	Quantity	Rate(Rs.)	Total(Rs)
Bamboo	6 8 12 20	32 72 36 5	6 8 12 20	1300
Wooden block	1)20 2)15	8 2	100 80	960
Wooden strip	1)6 2)8 3)12	4 4 4	6 8 12	104
Polythene	-	1 kg	110	110
Cement	-	3(bags)	150	450
Labour	-	9(person)	100	900

Total Cost:-Rs.3824
Cost per sq.ft:- 3824/300/8 =Rs.1.59
Per kg storage cost against construction cost:- 3824/1000 =Rs.3.824

2.2.3 Improved low cost onion storage structure developed by NHRDF:-Size=20`*15`, Life-8 years

Figure 3: Improved low cost onion storage structure developed by NHRDF

Table III: Improved low cost onion storage structure material developed by NHRDF

Material	Size(ft)	Quantity	Rate(Rs.)	Total(Rs)
Bamboo	1) 6 2) 8 3) 10	54 84 8	6 8 10	1076
Wooden strip	1) 6 2) 8	6 6	6 8	84
Shelter material	-	28	15	420
Cement	-	4(bags)	150	600
Labour	-	9(person)	100	900

Total Cost:-Rs 3080
Cost per sq.ft:- =3080/300/8 = Rs. 1.28
Per kg storage cost against construction cost: - x /1000 =Rs 3.080

2.2.4 Low cost onion storage structure (Kalwan):-Size=20`*15`, Life-4years

Figure 4: Low cost onion storage structure (Kalwan)

Table IV: Low cost onion storage structure material (Kalwan)

Material	Size(ft)	Quantity	Rate(Rs.)	Total(Rs)
Bamboo	8	40	8	320
Wooden block	1) 6 2) 12 3) 20	6 3 3	30 60 100	660
Polythene	-	3kg	110	330
Labour	-	5(person)	100	500
Tur waste	-	-	-	nil
Sugarcane trash	-	-	-	nil

These structures have life span 4 years. After 4 years this structure is reconstructed and its cost of construction is Rs.1000 this is due to reuse of bamboo and wooden block. Thus total cost =Rs.1810+Rs.1000=Rs.2810
Cost per sq.ft.=2810/300/(4+4)= Rs.1.17
Per kg storage cost against construction cost: - x/1000 =Rs.2810/1000 = Rs 2.81

2.3 METHODS

1. Unmarketable
In this bulb which is less than 20mm in size are excluded. Also the bulbs which are rotten, decayed are not considered. If we considered 100kgs of onion bulbs around 5% are unmarketable.

2. Spoilage
This losses is depends upon temperature variation .As the temperature increases spoilage loss increases .They are around 2-3%

3. Double splitted
These losses are due to temperature variation during the bulb development period these splitted bulb are strictly avoided .These losses are around 2.57%

4. Off Coloured bulbs
Generally the kharif onion is dark red colour and rabbi onion is light red in colour. According to the onion which is not resembling to this colour should be avoided.

5. Bolting losses
These losses depends upon temperature variation .As the temperature increases spoilage increases .They are around 1.29%

6 Mis shaped
The bulbs which are nearly round are considered .The bulb which are flat, globular are avoided .These losses are around 1.5%.

7. Other losses
Other losses are microbial decay losses, damage in transport are negligible.

2.4 LOSSES

Traditional onion storage structure

Quantity of onion stored in Traditional onion storage structure developed by NHRDF during last week of May is about 1000kg and then after 4-5 month the quantity of onion obtained is about 777.54kg.Thus the weight losses calculated as 222.46 kg. According to weight losses Rotting losses and Sprouting losses were calculated as 13.34 kg and 8.898 kg respectively. There are some sub losses such as unmarketable; Spoilage, Double splitted, bolting and mis shaped which were calculated as 38.87 kg, 23.32 kg, 19.98 kg, 10.03 kg and 11.66 kg respectively.

Dindigul type onion storage structure

Quantity of onion stored in Dindigul type onion storage structure during last week of May is about 1000kg and then after 4-5 month the quantity of onion obtained is about 658.62 kg.Thus the weight losses calculated as 341.38 kg.According to weight losses Rotting losses and Sprouting losses were calculated as 20.48 kg and 13.65 kg respectively. There are some sub losses such as unmarketable; Spoilage, Double splitted, bolting and mis shaped which were calculated as 32.93 kg, 19.75 kg, 16.92 kg, 8.49 kg and 9.87kg respectively.

Improved low cost onion storage structure developed by NHRDF

Quantity of onion stored in Improved low cost onion storage structure developed by NHRDF during last week of May is about 1000kg and then after 4-5 month the quantity of onion obtained is about 560 kg.Thus the weight losses calculated as 440 kg.According to weight losses Rotting losses and Sprouting losses were calculated as 26.4 kg and 17.6 kg respectively. There are some sub losses such as unmarketable; Spoilage, Double splitted, bolting and mis shaped which were calculated as 28 kg, 16.80 kg, 14.39 kg, 7.22 kg and 8.40 kg respectively.

Low cost domestic onion storage structure

Quantity of onion stored in Low cost domestic onion storage structure during last week of May is about 1000kg and then after 4-5 month the quantity of onion obtained is about 800 kg.Thus the weight losses calculated as 200 kg.According to weight losses Rotting losses and Sprouting losses were calculated as 12 kg and 08 kg respectively. There are some sub losses such as unmarketable; Spoilage, Double splitted, bolting and mis shaped which were calculated as 40 kg, 24 kg, 20.56 kg, 10.32 kg and 12 kg respectively.

III. RESULT AND DISCUSSION

Table V: Comparison of storage cost against construction cost (Rs) of different Onion Storage structure

Name of onion storage structure	Cost per sq.ft(Rs)	Per kg storage cost against construction cost(Rs)
Traditional onion storage structure	2.79	6.68
Dindigul type onion storage structure	1.59	3.824
Improved low cost onion storage structure developed by NHRDF	1.28	3.080
Low cost domestic onion storage structure	1.17	2.81

Table VI: Comparison between losses of different Onion Storage Structure

Sr.No.	Particulars	Traditional onion storage structure	Dindigul type onion storage structure	Improved low cost onion storage structure developed by NHRDF	Low cost domestic onion storage structure
1.	Weight losses	222.46 kg	341.38 kg	440kg	200kg
2.	Rotting losses	13.34 kg	20.48 kg	26.4 kg	12 kg
3.	Sprouting losses	8.898 kg	13.65kg	17.6kg	8kg

IV. CONCLUSION

Based on the results of experiment conducted on onion storage structures in NHRDF and domestic onion storage structure (Kalwan), losses were found to be highest in storage structures in NHRDF is 222.46kg for Weight losses. The construction cost per sq.ft. of this structure ie.Traditional onion storage structure, Dindigul onion storage structure, Improved low cost onion storage structure developed by NHRDF, and Low cost onion storage structure (Kalwan) are Rs.2.79 ,1.59,1.28 and

1.03 respectively The quantity of onions were stored in different onion But these losses may be varies according to climate, and location.

Result and discussion reveals that the domestic onion storage structure is proved to be best. The losses are very less, quality and quantity of produce is maintained. The Cost per sq.ft (Rs) and per kg storage cost against construction cost (Rs) of domestic onion storage structure is less as compare to onion storage structures in NHRDF. The low cost domestic onion storage structure may be beneficial to small growers. This may profitable to those growers who are growing onion at two or three year's interval due to shortage of irrigation water and inclusion of rotation of crops.

REFERENCES

[1] Bhonde S.R., Srivastava K.J., Singh D.K., and Pandey J.P .N (20020: Studies on nutritional and chemical composition.
[2] Bhonde S.R.(1998) Storage of onion and salient features of post harvest technology, NHRDF News letter
[3] Brice B.D.Shukla, R.K.Gupta "Development and evaluation of concentric-type storage structure for onions".
[4] Brice, J.L. Currah, A. Malins, R. Bancroft.1997. Onion storage in the tropics : A practical guide to methods of storage and their selection. Chatam,UK: Natural resources institute.
[5] Chauhan K.P.S, Singh S.P and Chougule A.B(2002):Studies on the effect of windrow curing, neck cut and shade curing on export quality of onion bulbs during storage;NHRDF,news letter,XV(4);5-7.
[6] Dr.Kirti Singh studied on "current status of India and future prospects"
[7] Pandey U.B. (2000) problems in post harvest handling of onion and current status of research work done by AADF in field of post harvest technology.
[8] Susan MacKinnon ;studies on bulb storage and removal of any thick or diseased onions.

International Journal of Modern Engineering Research (IJMER)
www.ijmer.com Vol. 3, Issue. 5, Sep - Oct. 2013 pp-2662-2666 ISSN: 2249-6645

Numerical Investigation of the Perfomance of Convergent Divergent Nozzle

Kunal Pansari[1], S. A. K. Jilani[2]
Department of Mehanical Engineering Chhattisgarh Swami Vivekananda University Raipur (C.G.), India

ABSTRACT: *The main objective of the work is to analyse the performance and flow characteristics of convergent divergent nozzle and also to compare the numerical values of the two methods i.e "HIT & TRIAL METHOD" AND "ANALYTICAL METHOD". In this paper we have determine the location and strength of normal shock wave in the divergent portion of the nozzle under varying operating conditions and with different nozzle geometry.*

KEYWORD: *Mach number, Sub-sonic, Super-sonic, Sonic, Compressible flow, Throat.*

I. INTRODUCTION

A nozzle is a relatively simple device, just a specially shaped tube through which hot gases flow. However, the mathematics, which describes the operation of the nozzle, takes some careful thought. Nozzles come in a variety of shapes and sizes. Simple turbojets, and turboprops, often have a fixed geometry convergent nozzle as shown on the left of the figure. Turbofan engines often employ a co-annular nozzle. The core flow exits the centre nozzle while the fan flow exits the annular nozzle. Mixing of the two flows provides some thrust enhancement and these nozzles also tend to be quieter than convergent nozzles. Afterburning turbojets and turbofans require a variable geometry convergent-divergent - CD nozzle. In this nozzle, the flow first converges down to the minimum area or throat, then is expanded through the divergent section to the exit at the right. The variable geometry causes these nozzles to be heavier than a fixed geometry nozzle, but variable geometry provides efficient engine operation over a wider airflow range than a simple fixed nozzle. Rocket engines also use nozzles to accelerate hot exhaust to produce thrust. Rocket engines usually have a fixed geometry CD nozzle with a much larger divergent section than is required for a gas turbine.

1.1 SHOCKS IN NOZZLE

A shock wave (also called shock front or simply "shock") is a type of propagating disturbance. Like an ordinary wave, it carries energy and can propagate through a medium (solid, liquid or gas) or in some cases in the absence of a material medium, through a field such as the electromagnetic field. Shock waves are characterized by an abrupt, nearly discontinuous change in the characteristics of the medium. Across a shock there is always an extremely rapid rise in pressure, temperature and density of the flow. In supersonic flows, expansion is achieved through an expansion fan. A shock wave travels through most media at a higher speed than an ordinary wave. Unlike solutions (another kind of nonlinear wave), the energy of a shock wave dissipates relatively quickly with distance. Also, the accompanying expansion wave approaches and eventually merges with the shock wave, partially cancelling it out. Thus the sonic boom associated with the passage of a supersonic aircraft is the sound wave resulting from the degradation and merging of the shock wave and the expansion wave produced by the aircraft. When a shock wave passes through matter, the total energy is preserved but the energy which can be extracted as work decreases and entropy increases. This, for example, creates additional drag force on aircraft with shocks. Shock waves can be

- Normal: at 90° (perpendicular) to the shock medium's flow directions.
- Oblique: at an angle to the direction of flow.
- Bow: Occurs upstream of the front (bow) of a blunt object when the upstream velocity exceeds Mach 1.

Shock waves form when the speed of a gas changes by more than the speed of sound. At the region where this occurs sound waves travelling against the flow reach a point where they cannot travel any further upstream and the pressure progressively builds in that region, and a high pressure shock wave rapidly forms. Shock waves are not conventional sound waves; a shock wave takes the form of a very sharp change in the gas properties on the order of a few mean free paths (roughly micro-meters at atmospheric conditions) in thickness. Shock waves in air are heard as a loud "crack" or "snap" noise. Over longer distances a shock wave can change from a nonlinear wave into a linear wave, degenerating into a conventional sound wave as it heats the air and loses energy. The sound wave is heard as the familiar "thud" or "thump" of a sonic boom, commonly created by the supersonic flight of aircraft.

II. METHODOLOGY

2.1 ANALYTICAL APPROACH

To determine shock location and shock strength in convergent divergent nozzle.

STEP 1: Find the pressure ratio that will produce a shock in the divergent portion of the nozzle.

STEP 2: Determine exit Mach number (M_e)

$$M_e^2 = \frac{-1}{\gamma-1} + \sqrt{\left(\frac{1}{\gamma-1}\right)^2 + \left(\frac{2}{\gamma-1}\right)\left(\frac{2}{\gamma+1}\right)^{\frac{\gamma+1}{\gamma-1}}\left(\frac{P_{01}}{P_e}\right)^2\left(\frac{A_t}{A_e}\right)^2}$$

STEP 3: Use M_e to determine P_e/P_{02}

$$\frac{P_{02}}{P_e} = \left(1+\frac{\gamma-1}{2}M_e^2\right)^{\frac{\gamma}{\gamma-1}}$$

STEP 4: Since $M_e<1$, $P_e=P_b$

$$\frac{P_{02}}{P_{01}} = \frac{P_b}{P_{01}} * \frac{P_{02}}{P_e}$$

STEP 5: Determine M_1, by using the value of P_{02}/P_{01}

$$\frac{P_{02}}{P_{01}} = \left[\frac{\frac{\gamma+1}{2}M_1^2}{1+\frac{\gamma-1}{2}M_1^2}\right]^{\frac{\gamma}{\gamma-1}}\left[\frac{1}{\frac{2\gamma}{\gamma+1}M_1^2 - \frac{\gamma-1}{\gamma+1}}\right]^{\frac{1}{\gamma-1}}$$

STEP 6: Determine Shock Location A_s/A_t

$$\frac{A_s}{A_t} = \frac{1}{M_1}\left[\left(\frac{2}{\gamma+1}\right)\left(1+\frac{\gamma-1}{2}M_1^2\right)\right]^{\frac{\gamma+1}{2(\gamma-1)}}$$

STEP 7: Determine Shock Strength

$$\frac{P_y - P_x}{P_x} = \left[\frac{2\gamma}{\gamma+1}\left(M_1^2-1\right)\right]$$

STEP 8: Determine Temperature Ratio across the shock

$$\frac{T_2}{T_1} = \frac{\left(1+\frac{\gamma-1}{2}M_1^2\right)\left(\frac{2\gamma}{\gamma-1}M_1^2-1\right)}{\left(\frac{(\gamma+1)^2}{2(\gamma-1)}\right)M_1^2}$$

STEP 9: Determine Pressure Ratio across the shock

$$\frac{P_2}{P_1} = \frac{2\gamma M_1^2}{\gamma+1} - \frac{\gamma-1}{\gamma+1}$$

STEP 10: Determine density ratio across the shock

$$\frac{\rho_2}{\rho_1} = \frac{(\gamma+1)M_1^2}{(\gamma-1)M_1^2+2}$$

2.2 HIT AND TRIAL APPROACH

To determine the shock location and shock strength in convergent divergent nozzle

Let us consider a convergent divergent nozzle with inlet and outlet section specified in the diagram as 1 and 5 respectively. In the diagram section 2 represent the throat while the section 3 and 4 represent the flow condition before and after the shock.

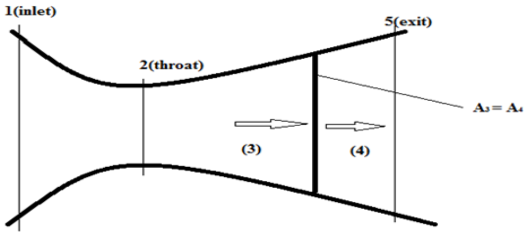

Fig.2.2.1 Convergent divergent nozzle

Let,

A_e/A_t=exit area/throat area=1.53

Inlet condition P_0=1atm.

Now let us determine the various flow characteristics for this case.

STEP 1:

If we assume chocked flow at the throat then from the IFT for A_e/A_t we have two solutions

1) For FIRST critical point(fully isentropic subsonic flow)
   From IFT at (A_e/A_t)=1.53,we have
   (P_e/P_o)=.886
   M_e=.42

For THIRD critical point(fully isentropic supersonic flow)
   From IFT at (A_e/A_t)=1.53,we have
   (P_e/P_o)=.154
   M_e=1.88

Now as we know that normal shock takes place in the divergent portion of the nozzle i.e in the supersonic flow. Therefore for supersonic flow conditions we have

M_e=1.88 and

$P_e/P_o(P_3/P_{03})$=.154

STEP 2:

Now from the normal shock table for M_e=1.88, we have

M_e(aftershock)=.599

P_y/P_x(after shock)=3.957

And the operating pressure ratio will be

$P_{rec}/P_0=P_4/P_{01}=P_4/P_3*P_3/P_{03}*P_{03}/P_{01}$

P_4/P_{01}=3.957*.154*1

P_4/P_{01}=.609378

Thus for our C-D nozzle with A_e/A_t=1.53,any operating pressure ratio between .886 and .609378 will cause a normal shock to be located some where in the divergent portion of the nozzle.

STEP 3:

Now let us find shock location at the operating pressure ratio of 0.75

Let us assume shock wave is located at A_s/A_t=1.204

Note-this value is selected because it is one of the numbers in IFT. by selecting this value we don't need to interpolate.

Key equation:

$P_e=P_e/P_{02}*P_{02}/P_{01}*P_{01}$

From IFT, corresponding to A_s/A_t=1.204, we have

M_1=1.54

From NST corresponding to M_1=1.54, we have

M_2=.687 and P_{02}/P_{01}=.917

From IFT corresponding to M_2=.687,we have

A_s/A^*=1.1018

$A_e/A^*=A_e/A_t*A_t/A_s*A_s/A^*$

=1.53*1/1.204*1.1018

=1.4

From IFT corresponding to A_e/A^*=1.4, we have

M_e=0.47

P_{02}/P_e=1/.859=1.163

P_e=1/1.163*.917*1
P_e=.788 atm.
But it is given that P_e=.75 atma . , hence we to move the shock a bit downstream.
STEP 4:
Let us assume shock wave is located at A_s/A_t=1.301
We have M_1=1.66,from NST corresponding to M_1=1.66, we have
M_2=.6512 and P_{02}/P_{01}=.872
From IFT corresponding to M_2=.6512, we have A_s/A^*=1.1356
$A_e/A^*=A_e/A_t*A_t/A_s*A_s/A^*$
=1.53*1/1.301*1.1356
=1.335
From IFT corresponding to A_e/A^*=1.335,we have
M_e=0.5
P_{02}/P_e=1/.843=1.1862
P_e=1/1.1862*.872*1
P_e=.735atm
Again the pressure ratio does not exactly match our given exit pressure. Now we can interpolate between the two assumed values. So
A_s/A_t=1.301-(1.301-1.204)*(.75-.735)/(.788-.735)
A_s/A_t=1.274
STEP 5:
Let us assume that shock wave is located at A_s/A_t=1.274
From IFT corresponding to A_s/A_t=1.274, we have M_1=1.63
From NST corresponding to M_1=1.63,we have M_2=.6595 and P_{02}/P_{01}=.8838
From IFT corresponding to M_2=.6595,we have A_s/A^*=1.1265
$A_e/A^*=A_e/A_t*A_t/A_s*A_s/A^*$
=1.53*1/1.274*1.1265
=1.353
From IFT corresponding to A_e/A_*=1.353, we have
M_e=0.49 and P_{02}/P_e=1/.848=1.178
P_e=1/1.178*.8838*1
=.750atm
Thus the properties obtained for a C-D nozzle of area ratio A_e/A_t=1.53 at operating pressure ratio of 0.75 are
M_1=1.63
P_{02}/P_{01}=.8838
M_e=0.49
P_{02}/P_e=1.178
P_e=0.75
A_s/A_t=1.274

III. RESULTS AND DISCUSSIONS

TABLE.1 FOR AREA RATIO 2.035

	Pe/Po						
Properties across shock		0.90	0.84	0.78	0.69	0.6	0.5
	M_e	.312923	.334810	.359950	.405523	.464070	.552165
	P_{o2}/P_e	1.070239	1.080692	1.093671	1.119925	1.159045	1.230187
	P_{02}/P_{01}	.963215	.907781	.853063	.772748	.695427	.615094
	M_1	1.380000	1.566000	1.707000	1.889000	2.055000	2.229000
	$(P_y-P_x)/P_x$	1.055133	1.694415	2.232824	2.996374	3.760196	4.629848
	T_2/T_1	1.241814	1.364657	1.463361	1.599362	1.732700	1.882576
	P_2/P_1	2.055133	2.694415	3.232824	3.996374	4.760196	5.629848
	ρ_2/ρ_1	1.654945	1.974427	2.209177	2.498731	2.747271	2.990502
	A_s/A_t	1.104193	1.223588	1.344237	1.541706	1.767480	2.057396

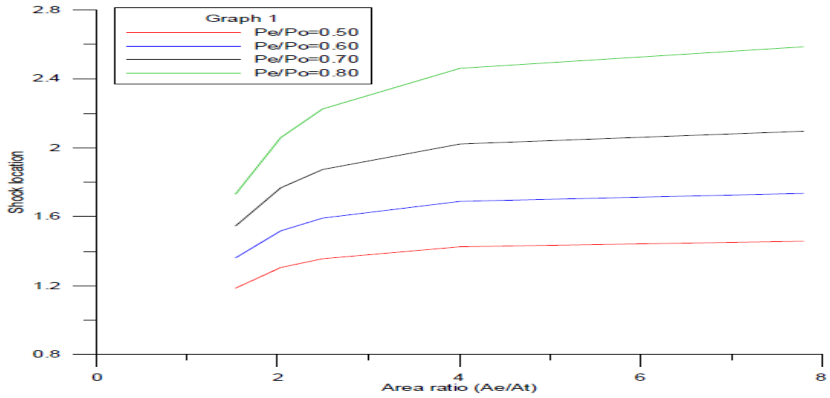

Fig.3.1variation of shock location with area ratio

TABLE 2.Comparison between analytical and hit & trial method

Properties	Analytical method	Hit and trial method
Exit mach number(M_e)	.3812	.38
Stagnation pressure ratio(P_{02}/P_{01})	.6632	.6628
Inlet mach number(M_1)	2.1240	2.12
Temperature ratio(T_2/T_1)	1.7908	1.787
Pressure ratio(P_2/P_1)	5.0966	5.077
Shock location(A_s/A_t)	1.8755	1.869
Shock strength(P_y-P_x)/P_x	4.096	4.077

The above values have been calculated for properties across Normal shock waves, where working fluid consider here is air with specific heat ratio γ=1.4 for a nozzle geometry of area ratio of 2.494 and the operating pressure ratio of 0.60 which has been chosen arbitrarily in between the critical pressure ratios to compare the result obtained by both the methods i.e. "Analytical method" and "Hit& trial method".

IV. CONCLUSIONS

1) Shock strength increases significantly by increasing (M_1),whereas shock location do not vary much with (M_1).
2) For constant operating pressure ratio, shock strength shows significant variation for smaller area ratio(A_e/A_t).
3) For a constant area ratio (A_e/A_t), shock location varies significantly for higher pressure ratios as compared to lower pressure ratios.
4) Shock location moves towards exit, by decreasing (P_e/P_o).

REFERENCES

[1] Goodenough, G. A. *Principles of Thermodynamics,* 3rd edition. New York, NY: Henry Holt and Company; 1911, 1920, 1931.
[2] Shapiro, A. H. *The Dynamics and Thermodynamics of Compressible Flow,* volumes 1 and 2. New York, NY: *The Ronald Press; 1954.*
[3] M.h.m. Noh , a.h.a. Hamid, r. Atan and h. Rashid,**"** NUMERICAL INVESTIGATION OF CHOCKED CONVERGING-DIVERGING NOZZLES FOR THRUSTER APPLICATION**",** *IIUM Engineering Journal, Special Issue, Mechanical Engineering, 2011*
[4] Hunter, C.A., "EXPERIMENTAL, THEORETICAL, AND COMPUTATIONAL INVESTIGATION OF SEPARATED NOZZLE FLOWS," *AIAA Paper 1998-3107, 1998*
[5] K.M. Pandey, *Member IACSIT* and A.P. Singh," CFD ANALYSIS OF CONICAL NOZZLE FOR MACH 3 AT VARIOUS ANGLES OF DIVERGENCE WITH FLUENTSOFTWARE", International Journal of Chemical Engineering and Applications, *Vol. 1,No. 2, August 2010, ISSN: 2010-0221*
[6] Ishibashi, M.; Takamoto, M. Discharge Coefficient of Super Accurate Critical Nozzle at Pressurized Condition,Proceedings of 4th International Symposium on Fluid Flow Measurement. *Denver, CO.: June 1999.*
[7] M. Leyko , S.Moreau , F.Nicoud , T.Poinsot," NUMERICAL AND ANALYTICAL MODELLING OF ENTROPY NOISE IN A SUPERSONIC NOZZLE WITH A SHOCK", *Journal of Sound and Vibration 330 (2011) 3944–3958*

International Journal of Modern Engineering Research (IJMER)
www.ijmer.com Vol. 3, Issue. 5, Sep - Oct. 2013 pp-2667-2673 ISSN: 2249-6645

Fast Data Collection with Interference and Life Time in Tree Based Wireless Sensor Networks

I. Shalini[1], B. Vamsee Mohan[2], T. Bharath Manohar[3], B. Susrutha[4]

[1, 4,] *M.Tech 2ndyr, Dept of CSE, PBRVITS (Affiliated to JNTU Anantapur), Kavali,Nellore.Andhra Pradesh.India.*
[2] *Assoc. Prof., Dept of CSE, PBRVITS (Affiliated to JNTU Anantapur), Kavali, Nellore. Andhra Pradesh. India.*
[3]*Asst.Professor, Dept of CSE, CMR College of Engineering &Technology,*
(Affiliated to JNTU Hyderabad)Hyderabad.Andhra Pradesh.India.

ABSTRACT: *We investigate the following fundamental question - how fast can information be collected from a wireless sensor network organized as tree? To address this, we explore and evaluate a number of different techniques using realistic simulation models under the many-to-one communication paradigm known as converge cast. We first consider time scheduling on a single frequency channel with the aim of minimizing the number of time slots required (schedule length) to complete a converge cast. Next, we combine scheduling with transmission power control to mitigate the effects of interference, and show that while power control helps in reducing the schedule length under a single frequency, scheduling transmissions using multiple frequencies is more efficient. We give lower bounds on the schedule length when interference is completely eliminated, and propose algorithms that achieve these bounds. We also evaluate the performance of various channel assignment methods and find empirically that for moderate size networks of about 100 nodes, the use of multi-frequency scheduling can suffice to eliminate most of the interference. Then, the data collection rate no longer remains limited by interference but by the topology of the routing tree. To this end, we construct degree-constrained spanning trees and capacitated minimal spanning trees, and show significant improvement in scheduling performance over different deployment densities. Lastly, we evaluate the impact of different interference and channel models on the schedule length.*

Keywords: *Convergecast, TDMA scheduling, multiple channels, power-control, routing trees.*

I. INTRODUCTION

CONVERGECAST, namely the collection of data from a set of sensors toward a common sink over a treebased routing topology, is a fundamental operation in wireless sensor networks (WSN) [1]. In many applications, it is crucial to provide a guarantee on the delivery time as well as increase the rate of such data collection. For instance, in safety and mission-critical applications where sensor nodes are deployed to detect oil/gas leak or structural damage, the actuators and controllers need to receive data from all the sensors within a specific deadline [2], failure of which might lead to unpredictable and catastrophic events. This falls under the category of one-shot data collection. On the other hand, applications such as permafrost monitoring [3] require periodic and fast data delivery over long periods of time, which falls under the category of continuous data collection.

In this paper, we consider such applications and focus on the following fundamental question: "*How fast can data be streamed from a set of sensors to a sink over a treebased topology?*" We study two types of data collection: (i) *aggregated convergecast* where packets are aggregated at each hop, and (ii) *raw-data convergecast* where packets are individually relayed toward the sink. Aggregated con-vergecast is applicable when a strong spatial correlation exists in the data, or the goal is to collect summarized information such as the maximum sensor reading. Rawdata convergecast, on the other hand, is applicable when every sensor reading is equally important, or the correlation is minimal. We study aggregated convergecast in the context of continuous data collection, and rawdata convergecast for one-shot data collection. These two types correspond to two extreme cases of data collection. In an earlier work [4], the problem of applying different aggregation factors, i.e., data compression factors, was studied, and the latency of data collection was shown to be within the performance bounds of the two extreme cases of no data compression (raw-data convergecast) and full data compression (aggregated convergecast). For periodic traffic, it is well known that contentionfree medium access control (MAC) protocols such as TDMA (Time Division Multiple Access) are better fit for fast data collection, since they can eliminate collisions and retransmissions and provide guarantee on the completion time as opposed to contention-based protocols However, the problem of constructing conflictfree (interference-free) TDMA schedules even under the simple graph-based interference model has been proved to be NP-complete. In this work, we consider a TDMA framework and design polynomial-time heuristics to minimize the schedule length for both types of convergecast. We also find lower bounds on the achievable schedule lengths and compare the performance of ourheuristics with these bounds.

II. MOTIVATION

Existing System:

Existing work had the objective of minimizing the completion time of converge casts. However, none of the previous work discussed the effect of multi-channel scheduling together with the comparisons of different channel assignment techniques and the impact of routing trees and none considered the problems of aggregated and raw converge cast, which represent two extreme cases of data collection.

Proposed System:

Fast data collection with the goal to minimize the schedule length for aggregated converge cast has been studied by us in, and also by others in, we experimentally investigated the impact of transmission power control and multiple frequency channels on the schedule length Our present work is different from the above in that we evaluate transmission power control under realistic settings and compute lower bounds on the schedule length for tree networks with algorithms to achieve these bounds. We also compare the efficiency of different channel assignment methods and interference models, and propose schemes for constructing specific routing tree topologies that enhance the data collection rate for both aggregated and raw-data converge cast.

We start by identifying the primary limiting factors of fast data collection, which are: (i) *interference* in the wireless medium, (ii) *half-duplex* transceivers on the sen- sor nodes, and (iii) *topology* of the network. Then, we explore a number of different techniques that provide a hierarchy of successive improvements, the simplest among which is an interference-aware, minimum-length, TDMA scheduling that enables spatial reuse. To achieve further improvement, we combine transmission power control with scheduling, and use multiple frequency channels to enable more concurrent transmissions. We show that once multiple frequencies are employed along with spatial-reuse TDMA, the data collection rate often no longer remains limited by interference but by the topology of the network. Thus, in the final step, we construct network topologies with specific properties that help in further enhancing the rate. Our primary conclusion is that, combining these different techniques can provide an order of magnitude improvement for aggregated convergecast, and a factor of two improvement for raw-data convergecast, compared to single-channel TDMA scheduling on minimum-hop routing trees. Although the techniques of transmission power control and multi-channel scheduling have been well studied for eliminating interference in general wireless networks, their performances for bounding the completion of data collection in WSNs have not been explored in detail in the previous studies. The fundamental novelty of our approach lies in the extensive exploration of the efficiency of transmission power control and multichannel communication on achieving fast convergecast operations in WSNs. Besides, we evaluate the impact of routing trees on fast data collection and to the best of our knowledge this has not been the topic of previous studies. As we will discuss in Section 2, some of the existing work had the objective of minimizing the completion time of convergecasts. However, none of the previous work discussed the effect of multi-channel scheduling together with the comparisons of different channel assignment techniques and the impact of routing trees and none considered the problems of aggregated and raw convergecast, which represent two extreme cases of data collection, together. As the new concepts in this paper, we introduce polynomial-time heuristics for TDMA scheduling for both types of data collection, i.e., Algorithms 1 and 2, and prove that they do achieve the lower bound of data collection time once interference is eliminated. Besides, we elaborate on the performance of our previous work, a receiver-based channel assignment method, and compare its efficiency with other channel assignment methods and introduce heuristics for constructing optimal routing trees to further enhance data collection rate. The following lists our key findings and contributions:

Bounds on Convergecast Scheduling:

We show that if all interfering links are eliminated, the schedule length for aggregated convergecast is lower bounded by the maximum node degree in the routing tree, and for raw-data convergecast by $\max(2nk - 1, N)$, where nk is the maximum number of nodes on any branch in the tree, and N is the number of source nodes. We then introduce optimal time slot assignment schemes under this scenario which achieve these lower bounds.

Evaluation of Power Control under Realistic Setting:

It was shown recently [5] that under the idealized setting of unlimited power and continuous range, transmission power control can provide an unbounded improvement in the asymptotic capacity of aggregated convergecast. In this work, we evaluate the behavior of an optimal power control algorithm [6] under realistic settings considering the limited discrete power levels available in today's radios. We find that for moderate size networks of 100 nodes power control can reduce the schedule length by $15 - 20\%$.

Evaluation of Channel Assignment Methods:

Using extensive simulations, we show that scheduling transmissions on different frequency channels is more effective in mitigating interference as compared to transmission power control. We evaluate the performance of three different channel assignment methods: (i) *Joint Frequency and Time Slot Scheduling* (JFTSS), (ii) *Receiver-Based Channel Assignment* (RBCA) [7], and (iii) *Tree-Based Channel Assignment (TMCP)* [8]. These methods consider the channel assignment problem at different levels: the link level, node level, or cluster level. We show that for aggregated convergecast, TMCP performs better than JFTSS and RBCA on minimum-hop routing trees, while performs worse on degree-constrained trees. For raw-data convergecast, RBCA and JFTSS perform better than TMCP, since the latter suffers from interference inside the branches due to concurrent transmissions on the same channel.

Impact of Routing Trees:

We investigate the effect of network topology on the schedule length, and show that for aggregated convergecast the performance can be improved by up to 10 times on degreeconstrained trees using multiple frequencies as compared to that on minimum-hop trees using a single frequency. For raw-data convergecast, multi-channel scheduling on capacitated minimal spanning trees can reduce the schedule length by 50%.

Impact of Channel Models and Interference:

Under the setting of multiple frequencies, one simplifying assumption often made is that the frequencies are orthogonal to each other. We evaluate this assumption and show that the schedules generated may not always eliminate interference, thus causing considerable packet losses. We also evaluate and compare the two most commonly used interference models.

III. LITERATURE SURVEY

Fast data collection with the goal to minimize the schedule length for aggregated convergecast has been studied by us in and also by others.In we experimentally investigated the impact of transmission power control and multiple frequency channels on the schedule length, while the theoretical aspects were discussed where we proposed constant factor and logarithmic approximation algorithms on geometric networks (disk graphs). Raw-data convergecast has been studied where a distributed time slot assignment scheme is proposed by Gandham *et al.* to minimize the TDMA schedule length for a single channel. The problem of joint scheduling and transmission power control is studied by Moscibroda for constant and uniform traffic demands. Our present work is different from the above in that we evaluate transmission power control under realistic settings and compute lower bounds on the schedule length for tree networks with algorithms to achieve these bounds. We also compare the efficiency of different channel assignment methods and interference models, and propose schemes for constructing specific routing tree topologies that enhance the data collection rate for both aggregated and raw-data convergecast. The use of orthogonal codes to eliminate interference has been studied by Annamalai *et al.* [10], where nodes are assigned time slots from the bottom of the tree to the top such that a parent node does not transmit before it receives all the packets from its children.

This problem and the one addressed by Chen *et al.* [11] are for one-shot raw-data convergecast. In this work, since we construct degree-constrained routing topologies to enhance the data collection rate, it may not always lead to schedules that have low latency, because the number of hops in a tree goes up as its degree goes down. Therefore, if minimizing latency is also a requirement, then further optimization, such as constructing bounded-degree, bounded-diameter trees, is needed. A study along this line with the objective to minimize the maximum latency is presented by Pan and Tseng [15], where they assign a beacon period to each node in a Zigbee network during which it can receive data from all its children. For raw-data convergecast, Song *et al.* [12] presented a time-optimal, energy-efficient, packet scheduling algorithm with periodic traffic from all the nodes to the sink. Once interference is eliminated, their algorithm achieves the bound that we present here, however, they briefly mention a 3-coloring channel assignment scheme, and it is not clear whether the channels are frequencies, codes, or any other method to eliminate interference.

Moreover, they assume a simple interference model where each node has a circular transmission range and cumulative interference from concurrent multiple senders is avoided. Different from their work, we consider multiple *frequencies* and evaluate the performance of three different channel assignment methods together with evaluating the effects of transmission power control using realistic interference and channel models, i.e., physical interference model and overlapping channels and considering the impact of routing topologies. Song *et al.* [12] extended their work and proposed a TDMA based MAC protocol for high data rate WSNs in [16]. TreeMAC considers the differences in load at different levels of a routing tree and assigns time slots according to the depth, i.e. the hop count, of the nodes on the routing tree, such that nodes closer to the sink are assigned more slots than their children in order to mitigate congestion. However, TreeMAC operates on a single channel and achieves 1/3 of the maximum throughput similar to the bounds presented by Gandham *et al.* [1] since the sink can receive every 3 time slots. The problem of minimizing the schedule length for raw-data convergecast on single channel is shown to be NP-complete on general graphs by Choi *et al.* [13]. Maximizing the throughput of convergecast by finding a shortest-length, conflict-free schedule is studied by Lai *et al.* [14], where a greedy graph coloring strategy assigns time slots to the senders and prevent interference. They also discussed the impact of routing trees on the schedule length and proposed a routing scheme called *disjoint strips* to transmit data over different shortest paths.

However, since the sink remains as the bottleneck, sending data over different paths does not reduce the schedule length. As we will show in this paper, the improvement due to the routing structure comes from using capacitated minimal spanning trees for raw-data convergecast, where the number of nodes in a subtree is no more than half the total number of nodes in the remaining subtrees. The use of multiple frequencies has been studied extensively in both cellular and ad hoc networks, however, in the domain of WSN, there exist a few studies that utilize multiple channels To this end, we evaluate the efficiency of three particular schemes that treat the channel assignment at different levels.

IV. SYSTEM ANALYSIS & DESIGN

Algorithms used:
1. BFSTIMESLOTASSIGNMENT.
2. LOCAL-TIMESLOTASSIGNMENT
Algorithm 1 BFS-TIMESLOTASSIGNMENT
1. Input: T = (V, ET)
2. While ET _= φ do
3. e ← next edge from ET in BFS order
4. Assign minimum time slot t to edge e respecting adjacency and interfering constraints
5. ET ← ET \ {e}
6. end while

Algorithm 2 LOCAL-TIMESLOTASSIGNMENT
1. node.buffer = full
2. if {node is sink} then
3. Among the eligible top-subtrees, choose the one with the largest number of total (remaining) packets, say top-subtree i
4. Schedule link (root(i), s) respecting interfering constraint
5. else
6. if {node.buffer == empty} then
7. Choose a random child c of node whose buffer is full
8. Schedule link (c, node) respecting interfering constraint
9. c.buffer = empty
10. node.buffer = full
11. end if
12. end if

Architecture

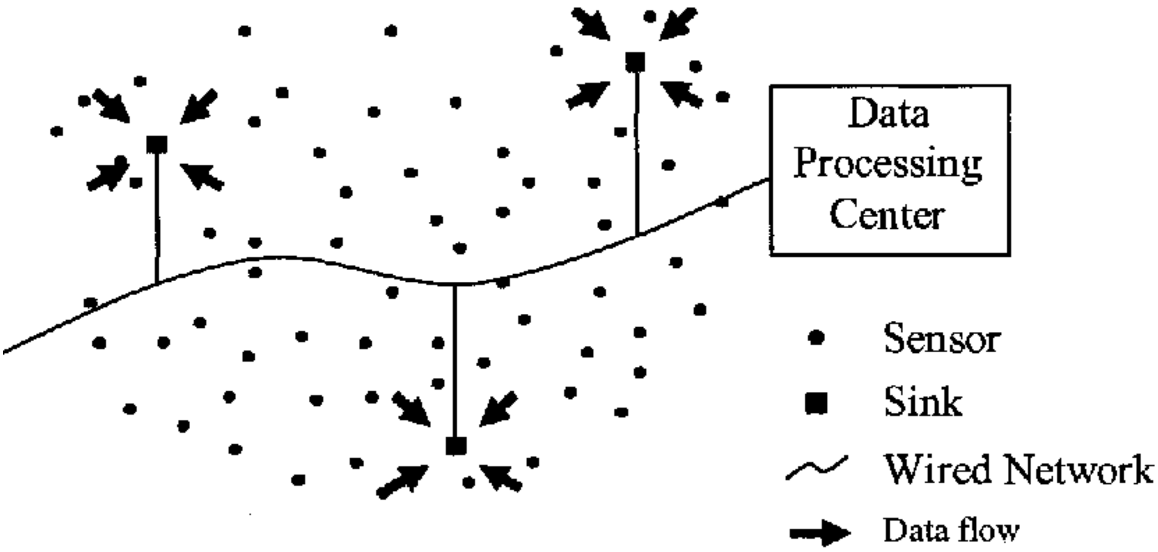

Modules:

1. Periodic Aggregated Converge cast.
2. Transmission Power Control
3. Aggregated Data Collection
4. Raw Data Collection
5. Tree-Based Multi-Channel Protocol (TMCP)

1. Periodic Aggregated Converge cast.

Data aggregation is a commonly used technique in WSN that can eliminate redundancy and minimize the number of transmissions, thus saving energy and improving network lifetime. Aggregation can be performed in many ways, such as by suppressing duplicate messages; using data compression and packet merging techniques; or taking advantage of the correlation in the sensor readings.

We consider continuous monitoring applications where perfect aggregation is possible, i.e., each node is capable of aggregating all the packets received from its children as well as that generated by itself into a single packet before transmitting to its parent. The size of aggregated data transmitted by each node is constant and does not depend on the size of the raw sensor readings.

2. Transmission Power Control

We evaluate the impact of transmission power control, multiple channels, and routing trees on the scheduling performance for both aggregated and raw-data converge cast.. Although the techniques of transmission power control and multi-channel scheduling have been well studied for eliminating interference in general wireless networks, their performances for bounding the completion of data collection in WSNs have not been explored in detail in the previous studies. The fundamental novelty of our approach lies in the extensive exploration of the efficiency of transmission power control and multichannel communication on achieving fast converge cast operations in WSNs.

3. Aggregated Data Collection

We augment their scheme with a new set of rules and grow the tree hop by hop outwards from the sink. We assume that the nodes know their minimum-hop counts to sink.

4. Raw Data Collection

The data collection rate often no longer remains limited by interference but by the topology of the network. Thus, in the final step, we construct network topologies with specific properties that help in further enhancing the rate. Our primary conclusion is that, combining these different techniques can provide an order of magnitude improvement for aggregated converge cast, and a factor of two improvement for raw-data converge cast, compared to single-channel TDMA scheduling on minimum-hop routing trees.

5. Tree-Based Multi-Channel Protocol (TMCP)

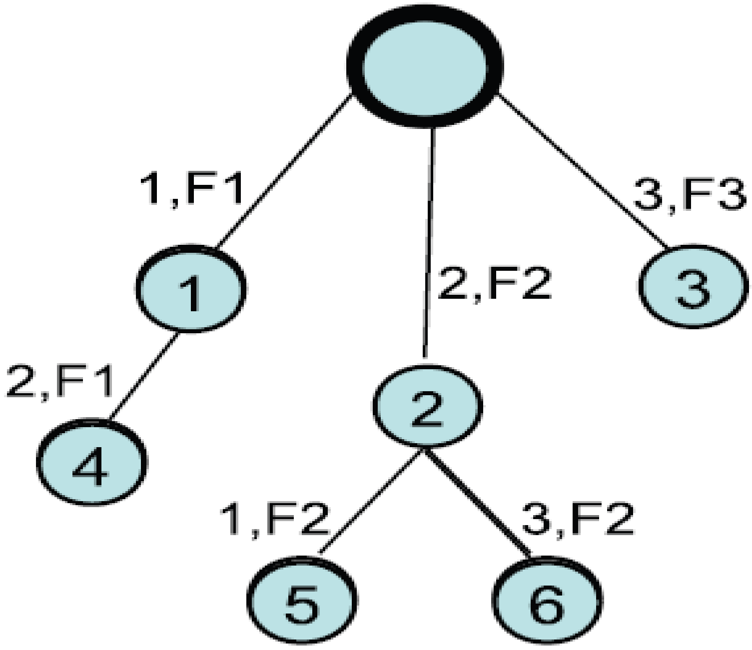

Fig: Schedule generated with TMCP

TMCP is a greedy, tree-based, multi-channel protocol for data collection applications. It partitions the network into multiple sub trees and minimizes the intra tree interference by assigning different channels to the nodes residing on different branches starting from the top to the bottom of the tree. Figure shows the same tree given in Fig. which is scheduled according to TMCP for aggregated data collection. Here, the nodes on the leftmost branch is assigned frequency F1, second branch is assigned frequency F2 and the last branch is assigned frequency F3 and after the channel assignments, time slots are assigned to the nodes with the BFS Time Slot Assignment algorithm.

Advantage

Advantage of TMCP is that it is designed to support converge cast traffic and does not require channel switching. However, contention inside the branches is not resolved since all the nodes on the same branch communicate on the same channel

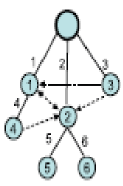

(a)

	Frame 1						Frame 2					
	S1	S2	S3	S4	S5	S6	S1	S2	S3	S4	S5	S6
s	1	2	3	-	-	-	{1,4}	{2,5,6}	3	-	-	-
1	-	-	-	4	-	-	-	-	-	4	-	-
2	-	-	-	-	5	6	-	-	-	-	5	6

(b)

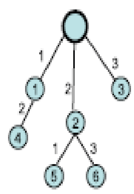

(c)

Fig. Aggregated convergecast and pipelining: (a) Schedule length of 6 in the presence of interfering links. (b) Node ids from which (aggregated) packets are received by their corresponding parents in each time slot over different frames. (c) Schedule length of 3 using BFS-TIMESLOTASSIGNMENT when all the interfering links are eliminated.

V. RESULTS

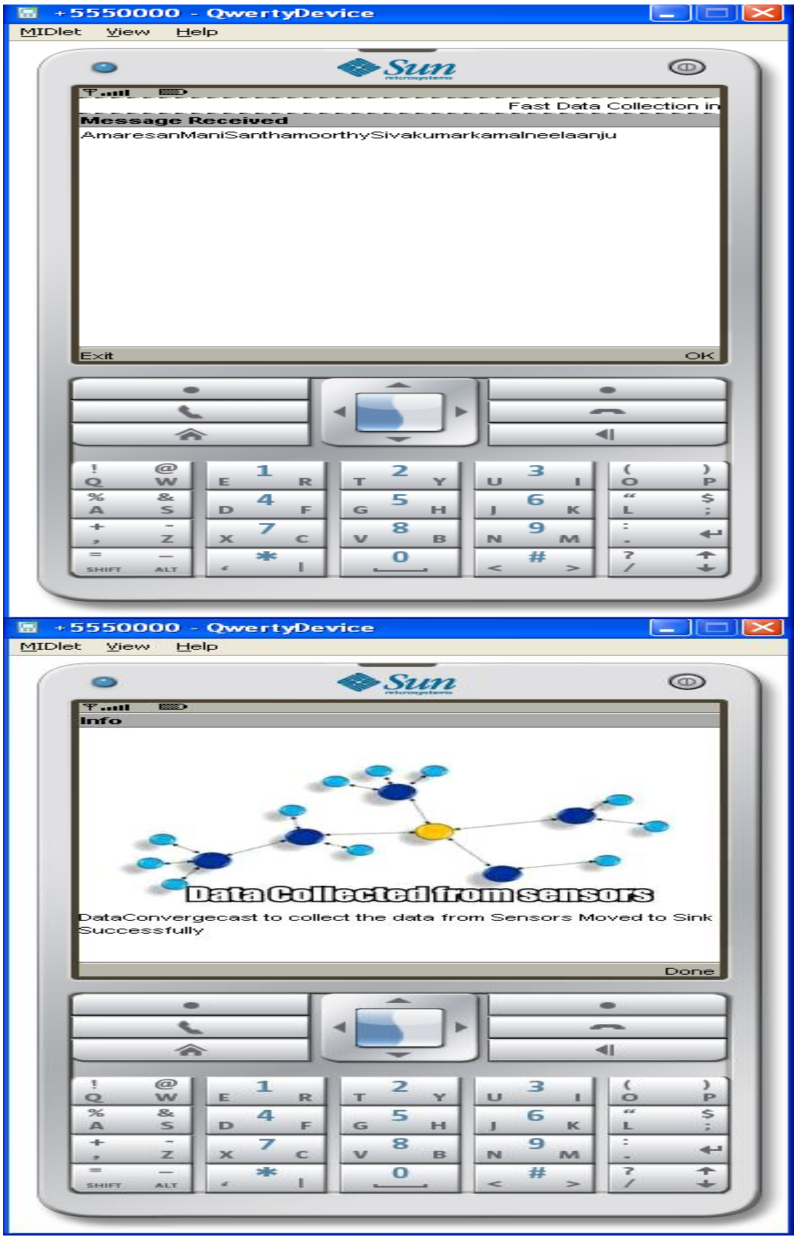

Fig: Showing Results Algorithm Implemented Screen

VI. CONCLUSION

In this paper, we studied fast converge cast in WSN where nodes communicate using a TDMA protocol to minimize the schedule length. We addressed the fundamental limitations due to interference and half-duplex transceivers on the nodes and explored techniques to overcome the same. We found that while transmission power control helps in reducing the schedule length, multiple channels are more effective. We also observed that node-based (RBCA) and link-based (JFTSS) channel assignment schemes are more efficient in terms of eliminating interference as compared to assigning different channels on different branches of the tree (TMCP). Once interference is completely eliminated, we proved that with half-duplex radios the achievable schedule length is lower-bounded by the maximum degree in the routing tree for aggregated converge cast, and by max $(2nk - 1, N)$ for raw-data converge cast. Using optimal converge cast scheduling algorithms, we showed that the lower bounds are achievable once a suitable routing scheme is used. Through extensive simulations, we demonstrated up to an order of magnitude reduction in the schedule length for aggregated, and a 50% reduction for raw-data converge cast. In future, we will explore scenarios with variable amounts of data and implement and evaluate the combination of the schemes considered.

ACKNOWLEDGMENT

I would like to express my sincere thanks to my Guide and my Co-Authors for their consistence support and valuable suggestions.

REFERENCES

[1] S. Gandham, Y. Zhang, and Q. Huang, "Distributed time optimal scheduling for converge cast in wireless sensor networks," Computer Networks, vol. 52, no. 3, pp. 610–629, 2008.
[2] K. K. Chintalapudi and L. Venkatraman, "On the design of mac protocols for low-latency hard real-time discrete control applications over 802.15.4 hardware," in IPSN '08, pp. 356–367.
[3] I. Talzi, A. Hasler, S. Gruber, and C. Tschudin, "Permasense: investigating permafrost with a wsn in the swiss alps," in EmNets '07, Cork, Ireland, pp. 8–12.
[4] S. Upadhyayula and S. Gupta, "Spanning tree based algorithms for low latency and energy efficient data aggregation enhanced convergecast (dac) in wireless sensor networks," Ad Hoc Networks, vol. 5, no. 5, pp. 626–648, 2007.
[5] O. D. Incel and B. Krishnamachari, "Enhancing the data collection rate of tree-based aggregation in wireless sensor networks," in SECON '08, San Francisco, CA, USA, pp. 569–577.
[6] Y. Wu, J. Stankovic, T. He, and S. Lin, "Realistic and efficient multi-channel communications in wireless sensor networks," in INFOCOM '08, pp. 1193–1201.
[7] A. Ghosh, O. D. Incel, V. A. Kumar, and B. Krishnamachari, "Multi-channel scheduling algorithms for fast aggregated convergecast in sensor networks," in MASS '09, Macau, China.
[8] V. Annamalai, S. Gupta, and L. Schwiebert, "On tree-based convergecasting in wireless sensor networks," in WCNC '03, vol. 3, pp. 1942–1947.
[9] X. Chen, X. Hu, and J. Zhu, "Minimum data aggregation time problem in wireless sensor networks," in MSN '05, pp. 133–142.
[10] H. Choi, J. Wang, and E. Hughes, "Scheduling for information gathering on sensor network," Wireless Networks (Online), 2007.
[11] M. Pan and Y. Tseng, "Quick convergecast in zigbee beaconenabled tree-based wireless sensor networks," Computer Communications, vol. 31, no. 5, pp. 999–1011, 2008.

Effect of Radiation on Mixed Convection Flow of a Non-Newtonian Nan fluid over a Non-Linearly Stretching Sheet with Heat Source/Sink

S. Vijaya Lakshmi[1], M. Suryanarayana Reddy[2]
[1]Research Scholar, JNTU Anantapur, Anantapuram, A.P, India.
[2]*Department of mathematics, JNTUA College of engineering, Pulivendula-516 390.A.P, India*

ABSTRACT: *A boundary layer analysis is presented for the effect of radiation on mixed convection flow of a non-Newtonian nanofluid in a nonlinearly stretching sheet with heat source/sink. The micropolar model is chosen for the non-Newtonian fluid since the spinning motion of the nanoparticles as they move along the streamwise direction can be best described by the micropolar fluid model. Numerical results for friction factor, surface heat transfer rate and mass transfer rate have been presented for parametric variations of the micropolar material parameters, Brownian motion parameter* N_B*, thermophoresis parameter* N_T*, radiation parameter R, heat source/sink parameter Q and Schmidt number Sc. The dependency of the friction factor, surface heat transfer rate and mass transfer rate on these parameters has been discussed.*

KEYWORDS: *Mixed Convection, Stretching Sheet, Non-Newtonian Flow, Nanofluid, Radiation, Heat source/sink.*

I. INTRODUCTION

Study of non-Newtonian fluids over a stretching surface achieved great attention due to its large number of application. In fact, the effects of non-Newtonian behavior can be determined due to its elasticity, but sometimes rheological properties of fluid are identified by their constitutive equations. In view of rheological parameters, the constitutive equations in the non-Newtonian fluids are morecomplex and thus give rise the equations which are complicated than the Navier–Stokes equations. Many of the fluids used in the oil industry and simulate reservoirs are significantly non-Newtonian. In different degree, they display shear-dependent of viscosity, thixotropy and elasticity (Pearson and Tardy [1]; Ellahi and Afza [2]; Ellahi [3]). Gorla and Kumari [4] studied the mixed convection flow of a non-newtonian nanofluid over a non-linearly stretching sheet.

Nanoparticles range in diameter between 1 and 100 nm. Nanofluids commonly contain up to a 5% volume fraction of nanoparticlesto ensure effective heat transfer enhancements. One of the main objectives of using nanofluids is to achieve the best thermal properties with the least possible (<1%) volume fraction of nanoparticles in the base fluid. The term nanofluid was first proposed by Choi [5] to indicate engineered colloids composed of nanoparticles dispersed in a base fluid. The characteristic feature of nanofluids is thermal conductivity enhancement; a phenomenon observed by Masuda et al. [6].There are many studies on the mechanism behind the enhanced heat transfer characteristics using nanofluids. Eldabe et al. [7] analyzed the effects of magnetic field and heat generation on viscous flow and heat transfer over a nonlinearly stretching surface in a nanofluid.

Micropolar fluids are subset of the micromorphic fluid theory introduced in a pioneering paper by Eringen[8]. Micropolar fluids are those fluids consisting of randomly oriented particles suspended in a viscous medium, which can undergo a rotation that can affect the hydrodynamics of the flow, making it a distinctly non-Newtonian fluid. They constitute an important branch of non-Newtonian fluid dynamics where microrotation effects as well as microinertia are exhibited. Eringen's theory has provided a good model for studying a number of complicated fluids, such as colloidal fluids, polymeric fluids and blood.

In the context of space technology and in processes involving high temperatures, the effects of radiation are of vital importance. Studies of free convection flow along a vertical cylinder or horizontal cylinder are important in the field of geothermal power generation and drilling operations where the free stream and buoyancy induced fluid velocities are of roughly the same order of magnitude. Many researchers such as Arpaci [9], Cess [10], Cheng and Ozisik [11], Raptis [12], Hossain and Takhar [13, 14] have investigated the interaction of thermal radiation and free convection for different geometries, by considering the flow to be steady. Oahimire et al.[15] studied the analytical solution to mhd micropolar fluid flow past a vertical plate in a slip-flow regime in the presence of thermal diffusion and thermal radiation. El-Arabawy [16] studied the effect of suction/injection on a micropolar fluid past a continuously moving plate in the presence of radiation. Ogulu [17] studied the oscillating plate-temperature flow of a polar fluid past a vertical porous plate in the presence of couple stresses and radiation. Rahman and Sattar [18] studied transient convective heat transfer flow of a micropolar fluid past a continuously moving vertical porous plate with time dependent suction in the presence of radiation. Mat et al. [19] studied the radiation effect on marangoni convection boundary layer flow of a nanofluid.

The heat source/sink effects in thermal convection, are significant where there may exist a high temperature differences between the surface (e.g. space craft body) and the ambient fluid. Heat Generation is also important in the context of exothermic or endothermic chemical reaction. Sparrow and Cess [20] provided one of the earliest studies using a similarity approach for stagnation point flow with heat source/sink which vary in time. Pop and Soundalgekar [21] studied unsteady free convection flow past an infinite plate with constant suction and heat source. Rahman and Sattar [22] studied magnetohydrodynamic convective flow of a micropolar fluid past a vertical porous plate in the presence of heat

generation/absorption. Lin et al. [23] studied the marangoni convection flow and heat transfer in pseudoplastic non-newtonian nanofluids with radiation effects and heat generation or absorption effects.
The present work has been undertaken in order to analyze the two mixed convection boundary layer flow of a non-Newtonian nanofluid on a non-linearly stretching sheet in the presence of radiation and heat source/sink. The micropolar model is chosen for the non- Newtonian fluid since the spinning motion of the nanoparticles as they move along the streamwise direction can be best described by the micropolar fluid model. The effects of Brownian motion and thermophoresis are included for the nanofluid. The governing boundary layer equations have been transformed to a two-point boundary value problem in similarity variables and the resultant problem is solved numerically using the fourth order Runga-Kutta method along with shooting technique. The effects of various governing parameters on the fluid velocity, temperature, concentration, and Nusselt number are shown in figures and analyzed in detail.

II. MATHEMATICL ANALYSIS

Consider a steady, mixed convection boundary layer flow of a micropolar nanofluid over a non-linearly stretching sheet. The velocity components in x and y directions are u and v respectively. At the surface, the temperature T and the nano particle fraction take values T_w and C_w, respectively. The ambient values, attained as the radial distance r tends to infinity, of T and C are denoted by T_∞ and C_∞, respectively. The governing equations within boundary layer approximation may be written as:

Continuity equation

$$\frac{\partial u}{\partial x}+\frac{\partial v}{\partial y}=0 \tag{2.1}$$

Momentum equation

$$u\frac{\partial u}{\partial x}+v\frac{\partial u}{\partial y}=\left(\frac{\upsilon+\kappa}{\rho}\right)\frac{\partial^2 u}{\partial y^2}+\frac{\kappa}{\rho}\frac{\partial N}{\partial y}+g\beta_T(T-T_\infty)+g\beta_c(C-C_\infty) \tag{2.2}$$

Angular Momentum equation

$$\rho j\left(u\frac{\partial N}{\partial x}+v\frac{\partial N}{\partial y}\right)=\gamma\frac{\partial^2 N}{\partial y^2}-\kappa\left(2N+\frac{\partial u}{\partial y}\right) \tag{2.3}$$

Energy equation

$$u\frac{\partial T}{\partial x}+v\frac{\partial T}{\partial y}=\alpha_m\frac{\partial^2 T}{\partial y^2}-\frac{\alpha_m}{k}\frac{\partial q_r}{\partial y}+\tau\left(D_B\frac{\partial C}{\partial y}\frac{\partial T}{\partial y}+\left(\frac{D_T}{T_\infty}\right)\left(\frac{\partial T}{\partial y}\right)^2\right)+\frac{Q_0}{(\rho c)_f}(T-T_\infty) \tag{2.4}$$

Species equation

$$u\frac{\partial C}{\partial x}+v\frac{\partial C}{\partial y}=D_B\frac{\partial^2 C}{\partial y^2}+\frac{D_T}{T_\infty}\frac{\partial^2 T}{\partial y^2} \tag{2.5}$$

The boundary conditions may be written as:

$$u=u_W=cx^n, v=0, N=-m\frac{\partial u}{\partial y}, T=T_W, C=C_W \quad \text{at} \quad y=0 \tag{2.6}$$

$$u\to 0, N\to 0, T\to T_\infty, C\to C_\infty \text{ as } y\to\infty \tag{2.7}$$

In the above equations, *N* is the component of microrotation vector normal to the *xy*-plane; U_∞ the free stream velocity, D_B is the Brownian diffusion coefficient, D_T is the Thermophoretic diffusion coefficient, α_m is the thermal diffusivity, q_r is the heat flux, Q_0 is the heat generation or absorption coefficient such that $Q_0 > 0$ corresponds to heat generation while $Q_0 < 0$ corresponds to heat absorption, g is the acceleration due to gravity, ρ_f is the material density of the base fluid, ρ_p is the material density of nanoparticles, $(\rho c)_f$ and $(\rho c)_p$ are the heat capacity of the base fluid and the effective heat capacity of the nano particle material, respectively and $\mu, \kappa, \rho, j, \gamma$ and α_m are respectively the dynamic viscosity, vortex viscosity (or the microrotation viscosity), fluid density, microinertia density, spin gradient viscosity and thermal diffusivity. We follow the work of many authors by assuming that $\gamma=(\mu+\kappa/2)j=\mu(1+K/2)j$ where $K=\kappa/\mu$ is the material parameter. This assumption is invoked to allow the field of equations to predict the correct behavior in the limiting case when the microstructure effects become negligible and the total spin *N* reduces to the angular velocity (see Ahmadi14 or Yücel15).

The radiative heat flux q_r is described by Roseland approximation such that

$$q_r=-\frac{4\sigma^*}{3k'}\frac{\partial T^4}{\partial y} \tag{2.8}$$

where σ^* *and* k' are the Stefan-Boltzmann constant and the mean absorption coefficient, respectively. Following Chamkha [20], we assume that the temperature differences within the flow are sufficiently small so that they T^4 can be expressed as a linear function after using Taylor series to expand T^4 about the free stream temperature T_∞ and neglecting higher-order terms. This result is the following approximation:

$$T^4 \approx 4T_\infty^3 T - 3T_\infty^4 \tag{2.9}$$

In view of equations (2.8) and (2.9), equation (2.4) reduces to

$$u\frac{\partial T}{\partial x} + v\frac{\partial T}{\partial y} = \alpha_m\left(1+\frac{16\sigma^* T_\infty^3}{3kk'}\right)\frac{\partial^2 T}{\partial y^2} + \tau\left(D_B\frac{\partial C}{\partial y}\frac{\partial T}{\partial y}+\left(\frac{D_T}{T_\infty}\right)\left(\frac{\partial T}{\partial y}\right)\right)^2 + \frac{Q_0}{(\rho c)_f}(T-T_\infty) \tag{2.10}$$

Proceeding with the analysis, we de.ne the following transformations:

$$\psi = \sqrt{\frac{2\upsilon}{c(n+1)}}\,\frac{1}{x^{(n+1)/2}}\,cx^n f(\eta),\ \eta = \sqrt{\frac{c(n+1)}{2\upsilon}}\,x^{(n-1)/2}y$$

$$N = cx^n\sqrt{\frac{c(n+1)}{2\upsilon}}\,x^{(n-1)/2}g(\eta), \theta(\eta) = \frac{T-T_\infty}{T_w-T_\infty}, \phi(\eta) = \frac{C-C_\infty}{C_w-C_\infty} \tag{2.11}$$

The mass conservation equation (2.1) is satisfied by the Cauchy-Riemann Equations

$$u = \frac{\partial\psi}{\partial y} \text{ and } v = -\frac{\partial\psi}{\partial x}. \tag{2.12}$$

The Darcian velocity components:

$$u = cx^n f'(\eta), v = -\frac{\eta\upsilon}{y}\left[f(\eta)+\frac{(n-1)}{(n+1)}\eta f'(\eta)\right], \alpha_m = \frac{k_m}{(\rho c)_f}, \tau = \frac{(\rho c)_p}{(\rho c)_f}, Gr_x = \frac{g_c\beta(T_w-T_\infty)x^3}{\upsilon^2}$$

$$\mathrm{Re}_x = \frac{u_w x}{\upsilon} = \frac{cx^{n+1}}{\upsilon}, N_B = \frac{(\rho c)_p D_B(C_w-C_\infty)}{(\rho c)_f\,\alpha_m}, \lambda = \frac{Gr_x}{\mathrm{Re}_x^2}, N_T = \frac{(\rho c)_p D_T(T_w-T_\infty)}{(\rho c)_f\,\alpha_m T_\infty} \tag{2.13}$$

$$R = \frac{4\sigma^* T_\infty^3}{kk'}, Q = \frac{Q_1 x}{u_w(\rho c)_f(T_w-T_\infty)}, \mathrm{Pr} = \frac{\upsilon}{\alpha_m}, Sc = \frac{\upsilon}{D_B}, S = \frac{\beta^*(C_w-C_\infty)}{\beta(T_w-T_\infty)}$$

In view of the Equation (2.11), (2.12) and (2.13) , and the equations (2.2), (2.3), (2.5) and (2.10) reduce to the following non-dimensional form

$$(1+K)f''' + ff'' - \frac{2n}{n+1}f'^2 + Kg' + \frac{2}{n+1}\lambda(\theta+S\phi) = 0 \tag{2.14}$$

$$(1+K/2)g'' + fg' - \frac{3n-1}{n+1}f'g - \frac{2K}{n+1}(2g+f'') = 0 \tag{2.15}$$

$$\left(1+\frac{4}{3}R\right)\frac{1}{\mathrm{Pr}}\theta'' + \frac{1}{\mathrm{Pr}}N_B\theta'\phi' + \frac{1}{\mathrm{Pr}}N_T(\theta')^2 + \frac{2}{n+1}Q\theta + f\theta' = 0 \tag{2.16}$$

$$\frac{1}{Sc}\phi'' + \frac{1}{Sc}\frac{N_T}{N_B}\theta'' + f\phi' = 0 \tag{2.17}$$

Also the boundary conditions in (2.5) reduces to

$$f(0) = 0, f'(0) = 1, g(0) = -mf''(0), \theta(0) = \phi(0) = 1$$

$$f'(\infty) \to 0, g(\infty) \to 0, \theta(\infty) \to 0, \phi(\infty) \to 0 \tag{2.18}$$

The wall shear stress is given by

$$\tau_w = (\mu+k)\left(\frac{\partial u}{\partial y}\right)_{y=0} + kN_{y=0} \tag{2.19}$$

Friction factor is given by

$$C_{fx} = \frac{\tau_w}{(\rho u_w^2/2)} = 2\,\mathrm{Re}_x^{-1/2}\left(\frac{n+1}{2}\right)^{1/2}\left[(1+K)f''(0)+Kg(0)\right] \tag{2.20}$$

The wall couple stress is given by

$$M_w = \gamma\left(\frac{\partial N}{\partial y}\right)_{y=0} = \left(\frac{\gamma u_w^2}{\upsilon x}\right)\left(\frac{n+1}{2}\right)g'(0) \tag{2.21}$$

The dimensionless wall couple stress may be written as

$$M_w\left(\frac{\upsilon x}{\gamma u_w^2}\right) = \left(\frac{n+1}{2}\right)g'(0) \tag{2.22}$$

Heat transfer rate is given by

$$Nu_x = \frac{xq_w}{k_m(T_w - T_\infty)} = -\mathrm{Re}_x^{1/2}\left(\frac{n+1}{2}\right)^{1/2}\theta'(0) \tag{2.23}$$

Local Sherwood number is given by

$$Sh_x = \frac{xm_w}{D_B(C_w - C_\infty)} = -\mathrm{Re}_x^{1/2}\left(\frac{n+1}{2}\right)^{1/2}\phi'(0) \tag{2.24}$$

III. SOLUTION OF THE PROBLEM

The set of coupled non-linear governing boundary layer Equations (2.14) - (2.17) together with the boundary conditions (2.18) are solved numerically by using Runge-Kutta fourth order technique along with shooting method. First of all, higher order non-linear differential Equations (2.14) - (2.17) are converted into simultaneous linear differential equations of first order and they are further transformed into initial value problem by applying the shooting technique (Jain et al. [25]). The resultant initial value problem is solved by employing Runge-Kutta fourth order technique. The step size $\Delta\eta = 0.05$ is used to obtain the numerical solution with five decimal place accuracy as the criterion of convergence. From the process of numerical computation, the skin-friction coefficient, the wall couple stress, the Nusselt number and the Sherwood number, which are respectively proportional to $f''(0), g'(0), -\theta'(0)$ and $-\phi'(0)$, are also sorted out and their numerical values are presented in a tabular form.

IV. RESULTS AND DISCUSSIONS

The governing equations (2.14) - (2.17) subject to the boundary conditions (2.18) are integrated as described in section 3. In order to get a clear insight of the physical problem, the velocity, temperature and concentration have been discussed by assigning numerical values to the governing parameters encountered in the problem.

In order to assess the accuracy of the results, we compared our results for $R=Q=N_T=N_B=0$ with literature data from Gorla and Kumari [4] in Table I and found that they are in excellent agreement. This suggests that the present results are accurate. Tables' II–X present data for friction factor, heat and mass transfer rates for parametric values of variables governing the problem. Thermophoresis parameter, N_T appears in the thermal and concentration boundary layer equations. As we note, it is coupled with temperature function and plays a strong role in determining the diffusion of heat and nanoparticle concentration in the boundary layer. Table II shows that as the thermophoresis parameter increases, friction factor increase, where as the heat and mass transfer rates decrease. N_B is the Brownian motion parameter. Brownian motion decelerates the flow in the nanofluid boundary layer. Brownian diffusion promotes heat conduction. The nanoparticles increase the surface area for heat transfer. Nanofluid is a two phase fluid where the nanoparticles move randomly and increase the energy exchange rates. Brownian motion reduces nanoparticle diffusion. Table III shows that as the Brownian motion parameter N_B increases, mass transfer rate increase, whereas the friction factor and heat transfer rate decrease. Table IV shows that as the power law exponent n increases, heat transfer rate increases whereas friction factor and mass transfer rate decrease. Table V shows that as the parameter S increases, friction factor, heat and mass transfer rates increases. Table VI shows that as the vortex viscosity parameter K increases, the friction factor, and the heat and mass transfer rates increases. Table VII shows that friction factor, heat and mass transfer rates increases with the buoyancy parameter λ. Table VIII shows that as the Schmidt number increases, the friction factor and mass transfer rates increase. Table IX shows that as the constant m increases, the wall friction, heat and mass transfer rates decreases. The value m=0 represents concentrated particle flows in which the particle density is sufficiently great that microelements close to the wall are unable to rotate. This condition is also called as the strong interaction. When m = 0.5 the particle rotation is equal to fluid viscosity at the boundary for one particle suspension. When m = 1, we have flows which are representative to turbulent boundary layers. Table X shows that as the radiation and heat source/sink parameters increases, the friction factor and mass transfer rate increase, where as heat transfer rate decreases.

Figures 1(a)-1(d) and 2(a)-2(d) show the effect of the thermophoresis number, N_T as well as the Brownian motion parameter, N_B on velocity, angular velocity, temperature and concentration profiles. As N_T increases, velocity, angular velocity, temperature and concentration within the boundary layer increase. As N_B increases, temperature increases whereas the velocity, angular velocity and concentration decrease within the boundary layer. Figure 3(a)-3(d) shows that as the exponent n increases, velocity decreases whereas the angular velocity, temperature and concentration increase. The effects of the parameter S on the boundary layer profiles are opposite to the effects of n as seen from Figure 4(a)-4(d). Figures 5(a)-5(d) and 6(a)-6(d) show that as the vortex viscosity parameter K increases, the velocity and angular velocity increases whereas the temperature and concentration within the boundary layer decrease. As the mixed convection parameter λ increases, the velocity increases whereas the angular velocity, temperature and concentration within the boundary layer decrease. Figure 7(a)-7(d) shows that as the Prandtl number Pr increases, velocity and temperature decreases whereas the angular velocity and concentration increase. As the Schmidt number increases, the velocity and concentration boundary layer thickness decreases whereas angular velocity and temperature increase. This is seen from Figure 8(a)-8(d). As the constant m increases, the velocity decreases whereas the angular velocity, temperatures and concentration increases. This is seen from Figure 9(a)-9(d). Figures 10(a)-10(d) and 11(a)-11(d) shows that as the radiation parameter R and heat source/sink parameter Q increases, angular velocity decreases whereas velocity, temperature and concentration increase.

Table I: Numerical values of $(1+K/2)f''(0)$ and $-\theta'(0)$ at the sheet for different values of *K and n* when $\lambda=1.0, S=N_T=N_B=R=Q=0.0, m=0.5$ and *Pr=0.72*, Comparison of the present results with that of Gorla and Kumari [4]

K	n	Present results		Gorla and Kumari [4]	
		$(1+K/2)f''(0)$	$-\theta'(0)$	$(1+K/2)f''(0)$	$-\theta'(0)$
0.0	0.50	-0.129346	0.586095	-0.129016	0.584934
0.0	0.75	-0.312889	0.568677	-0.311993	0.567454
0.0	1.00	-0.444373	0.555571	-0.443205	0.554359
0.0	1.50	-0.621160	0.536891	-0.619938	0.535696
0.0	3.00	-0.874189	0.507159	-0.873003	0.505097
1.0	0.50	-0.293989	0.593002	-0.292302	0.592127
1.0	0.75	-0.497473	0.577915	-0.495675	0.577132
1.0	1.00	-0.643706	0.566632	-0.641769	0.565834
1.0	1.50	-0.840768	0.550693	-0.838697	0.549797
1.0	3.00	-1.123040	0.525838	-1.121011	0.524109

Table II: Numerical values of $f''(0), g'(0), -\theta'(0)$ and $-\phi'(0)$ at the sheet for different values of N_T when $K=S=\lambda=1, N_B=0.3, m=0.5, Q=0.2, n=2, \Pr=10$ and Sc=10.

N_T	$f''(0)$	$g'(0)$	$-\theta'(0)$	$-\phi'(0)$
0.1	-0.664881	-0.243793	1.065830	2.26034
0.2	-0.655741	-0.239314	1.045970	2.16199
0.3	-0.646809	-0.234939	1.026430	2.07338
0.4	-0.638081	-0.230668	1.007200	1.99418
0.5	-0.629554	-0.226498	0.988283	1.92407

Table III: Numerical values of $f''(0), g'(0), -\theta'(0)$ and $-\phi'(0)$ at the sheet for different values of N_B when $K=S=\lambda=1, N_T=0.3, m=0.5, Q=0.2, n=2, \Pr=10$ and Sc=10.

N_B	$f''(0)$	$g'(0)$	$-\theta'(0)$	$-\phi'(0)$
0.1	-0.599733	-0.211426	1.111610	1.30727
0.2	-0.635423	-0.229303	1.065070	1.88328
0.3	-0.646809	-0.234939	1.026430	2.07338
0.4	-0.652032	-0.237504	0.990473	2.16771
0.5	-0.654779	-0.238841	0.956098	2.22387

Table IV: Numerical values of $f''(0), g'(0), -\theta'(0)$ and $-\phi'(0)$ at the sheet for different values of *n* when $K=S=R=\lambda=1, N_T=N_B=0.3, m=0.5, Q=0.2, \Pr=10$ and Sc=10.

n	$f''(0)$	$g'(0)$	$-\theta'(0)$	$-\phi'(0)$
0.5	-0.197829	0.172956	1.00874	2.20583
1.0	-0.430952	-0.0263596	1.06582	2.10284
1.5	-0.563788	-0.15134	1.10126	2.04072
2.0	-0.649813	-0.23634	1.12576	1.99916
3.0	-0.754761	-0.344031	1.15695	1.94704
5.0	-0.857058	-0.452846	1.18866	1.89471

Table V: Numerical values of $f''(0), g'(0), -\theta'(0)$ and $-\phi'(0)$ at the sheet for different values of *S* when $K=\lambda=R=1, N_T=N_B=0.3, m=0.5, Q=0.2, n=2, \Pr=10$ and Sc=10.

S	$f''(0)$	$g'(0)$	$-\theta'(0)$	$-\phi'(0)$
0.5	-0.705108	-0.267333	1.11713	1.99127
0.6	-0.694000	-0.261128	1.11888	1.99287
0.7	-0.682917	-0.254928	1.12062	1.99445
0.8	-0.671858	-0.248728	1.12234	1.99603
0.9	-0.660824	-0.242532	1.12406	1.99760
1.0	-0.649813	-0.230340	1.12576	1.99916

Table VI: Numerical values of $f''(0), g'(0), -\theta'(0)$ and $-\phi'(0)$ at the sheet for different values of K when $S=\lambda=R=1, N_T=N_B=0.3, m=0.5, Q=0.2, n=2, \Pr=10$ and Sc=10.

K	$f''(0)$	$g'(0)$	$-\theta'(0)$	$-\phi'(0)$
0.0	-0.708256	-0.368713	0.99671	2.05477
0.5	-0.678646	-0.284347	1.01363	2.06507
1.0	-0.646809	-0.234939	1.02043	2.07338
2.0	-0.593866	-0.176569	1.04481	2.08581
3.0	-0.554020	-0.142405	1.05753	2.09470

Table VII: Numerical values of $f''(0), g'(0), -\theta'(0)$ and $-\phi'(0)$ at the sheet for different values of λ when $K=S=R=1, N_T=N_B=0.3, m=0.5, Q=0.2, n=2, \Pr=10$ and Sc=10.

λ	$f''(0)$	$g'(0)$	$-\theta'(0)$	$-\phi'(0)$
0.0	-0.902584	-0.3743770	0.976165	2.03765
0.5	-0.772424	-0.3042750	1.002770	2.05617
1.0	-0.646809	-0.2349390	1.026430	2.07338
1.5	-0.524913	-0.1662230	1.047850	2.08950
2.0	-0.406157	-0.0980246	1.087500	2.10473

Table VIII: Numerical values of $f''(0), g'(0), -\theta'(0)$ and $-\phi'(0)$ at the sheet for different values of λ when $K=S=R=1, N_T=N_B=0.3, m=0.5, Q=0.2, n=2, \Pr=10$ and Sc=10.

Sc	$f''(0)$	$g'(0)$	$-\theta'(0)$	$-\phi'(0)$
1	-0.444950	-0.144039	1.27846	-0.185624
10	-0.649813	-0.236340	1.12596	1.999160
20	-0.683747	-0.254022	1.10025	3.160030
50	-0.714107	-0.270606	1.08001	5.353600
100	-0.729246	-0.279186	1.07134	7.757390

Table IX: Numerical values of $f''(0), g'(0), -\theta'(0)$ and $-\phi'(0)$ at the sheet for different values of *m* when $K=S=\lambda=R=1, N_T=N_B=0.3, Q=0.2, n=2, \Pr=10$ and Sc=10.

m	$f''(0)$	$g'(0)$	$-\theta'(0)$	$-\phi'(0)$
0.0	-0.556371	0.175433	1.14406	2.01556
0.5	-0.649813	-0.23634	1.12576	1.99916
1.0	-0.781214	-0.805276	1.09812	1.97507

Table X: Numerical values of $f''(0), g'(0), -\theta'(0)$ and $-\phi'(0)$ at the sheet for different values of *R* and *Q* when $K=S=\lambda=1, N_T=N_B=0.3, m=0.5, n=2, \Pr=10$ and Sc=10.

R	Q	$f''(0)$	$g'(0)$	$-\theta'(0)$	$-\phi'(0)$
0	0.2	-0.677021	-0.248789	1.420510	1.885870
1	0.2	-0.646809	-0.234939	1.026430	2.073380
2	0.2	-0.624100	-0.225284	0.825949	2.165100
3	0.2	-0.605761	-0.217902	0.701209	2.219370
1	-0.5	-0.664790	-0.243369	1.701410	1.556840
1	0.0	-0.655018	-0.238772	1.308890	1.308890
1	0.5	-0.639733	-0.231650	0.807817	2.234470

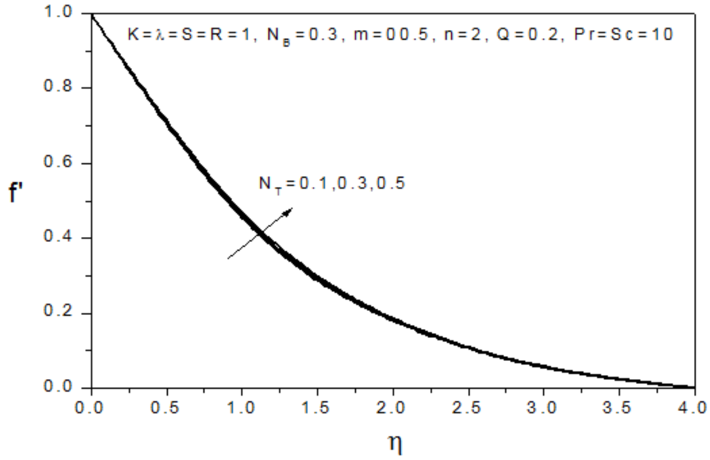

Fig.1(a) Velocity profiles for different values of N_T

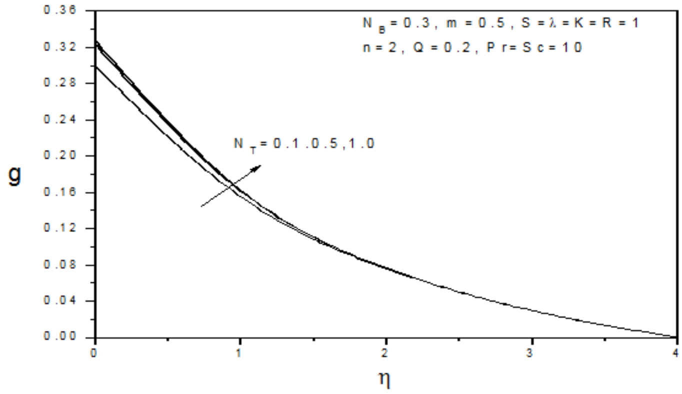

Fig.1 (b) Angular velocity profiles for different values of N_T

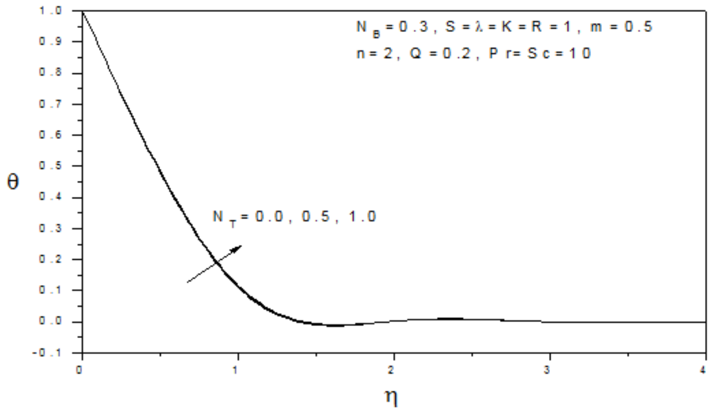

Fig.1(c) Temperature profiles for different values of N_T

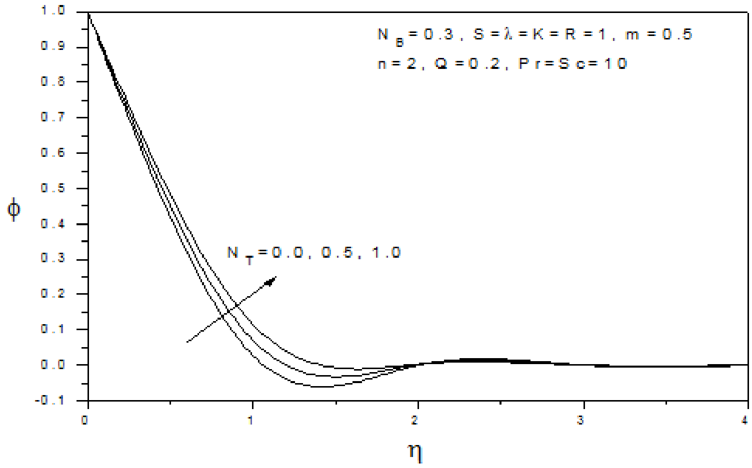

Fig.1(d) Concentration profiles for different values of N_T

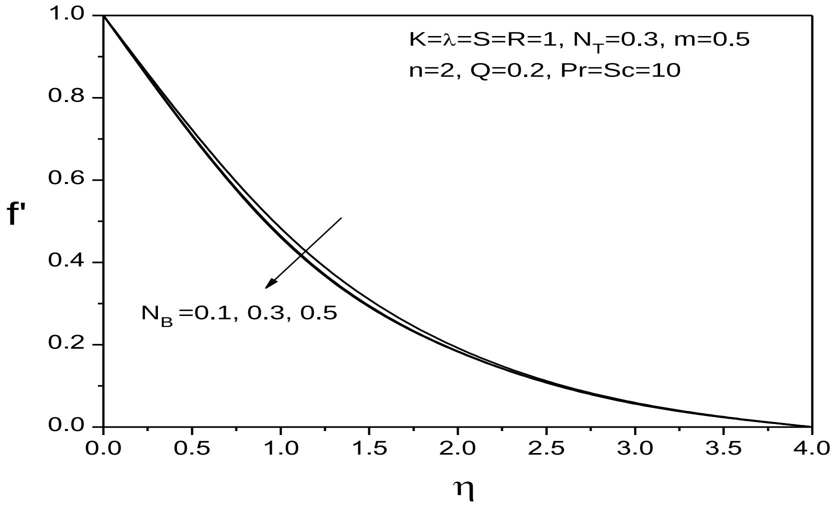

Fig.2(a) Velocity profiles for different values of N_B

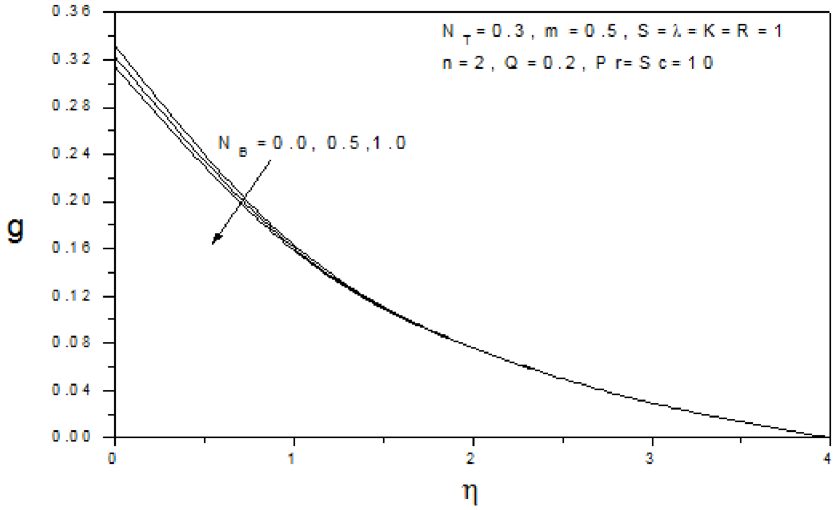

Fig.2 (b) Angular velocity profiles for different values of N_B

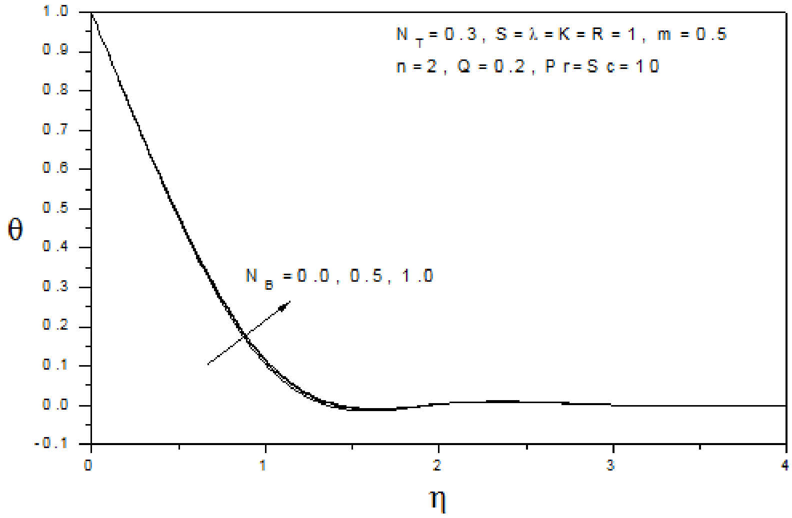

Fig.2(c) Temperature profiles for different values of N_B

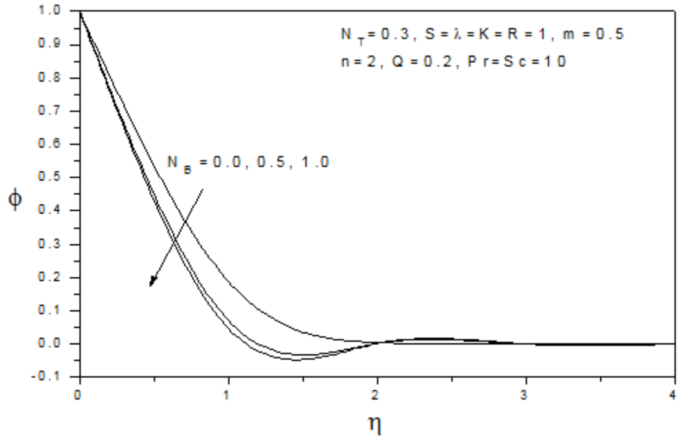

Fig.2 (d) Concentration profiles for different values of N_B

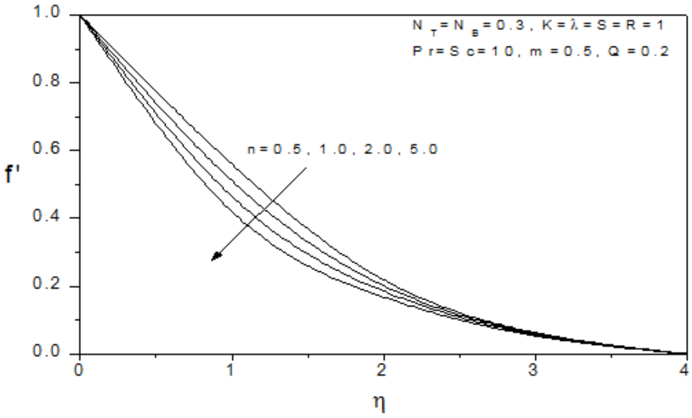

Fig.3 (a) Velocity profiles for different values of *n*

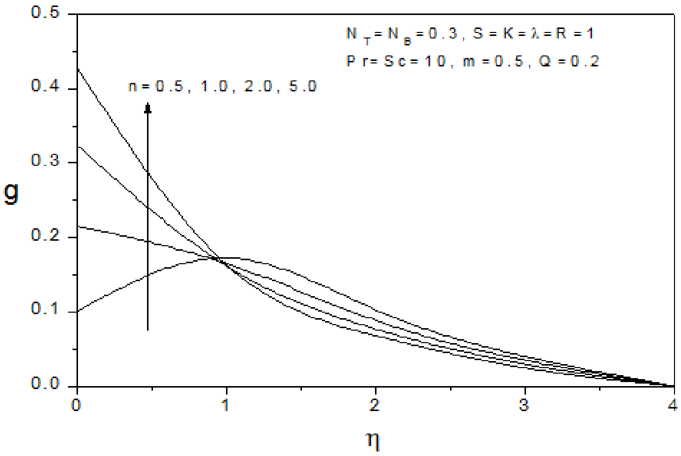

Fig.3 (b) Angular velocity profiles for different values of *n*

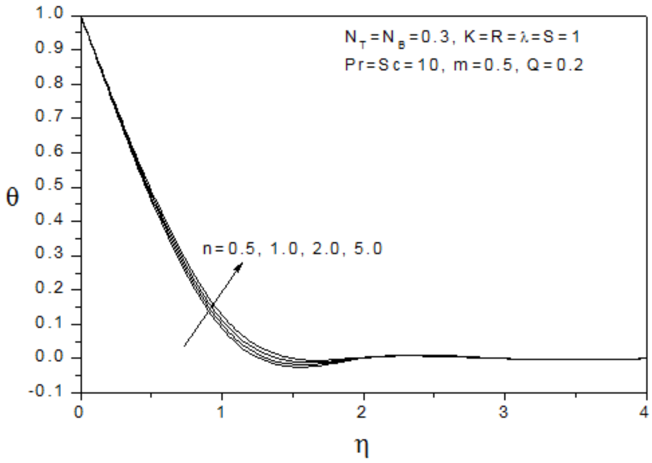

Fig.3(c) Temperature profiles for different values of *n*

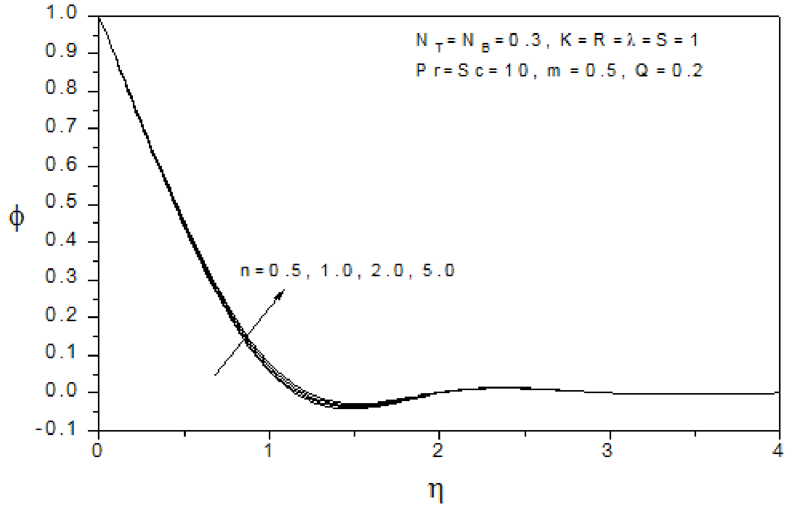

Fig.3 (d) Concentration profiles for different values of *n*

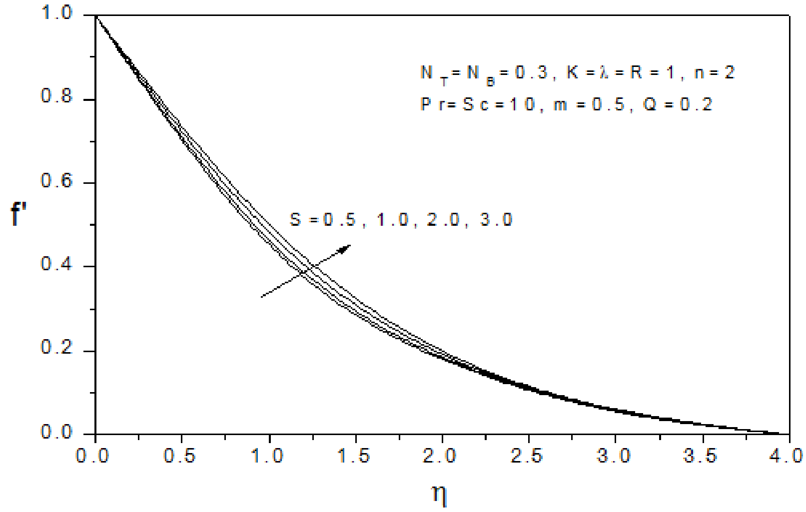

Fig.4 (a) Velocity profiles for different values of *S*

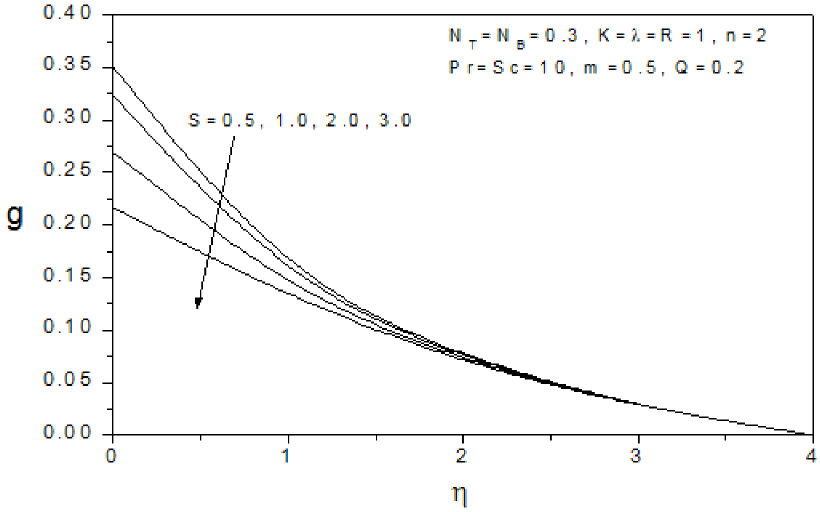

Fig.4 (b) Angular velocity profiles for different values of *S*

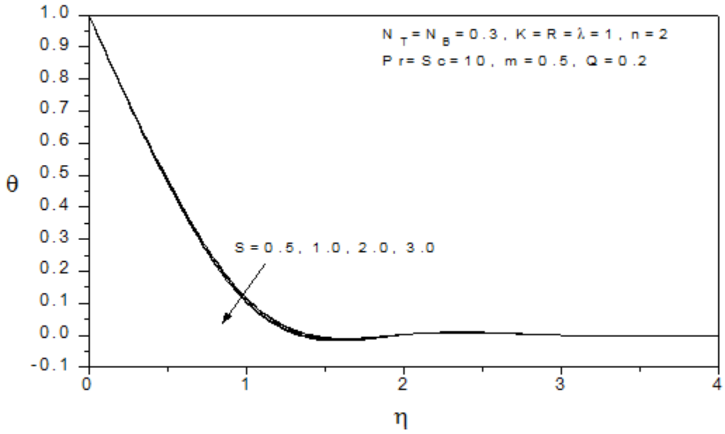

Fig.4 (c) Temperature profiles for different values of *S*

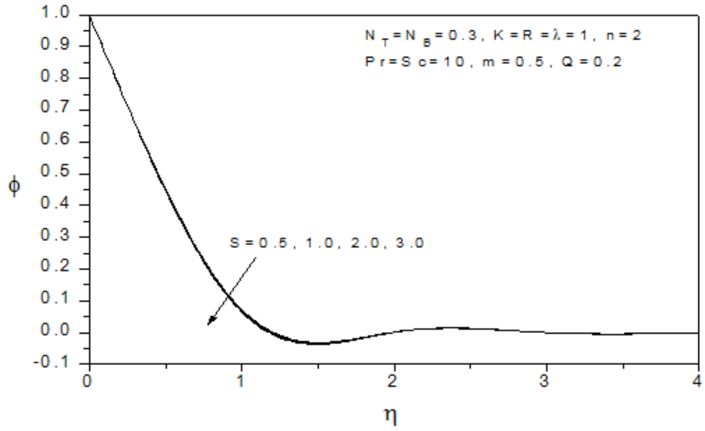

Fig.4 (d) Concentration profiles for different values of *S*

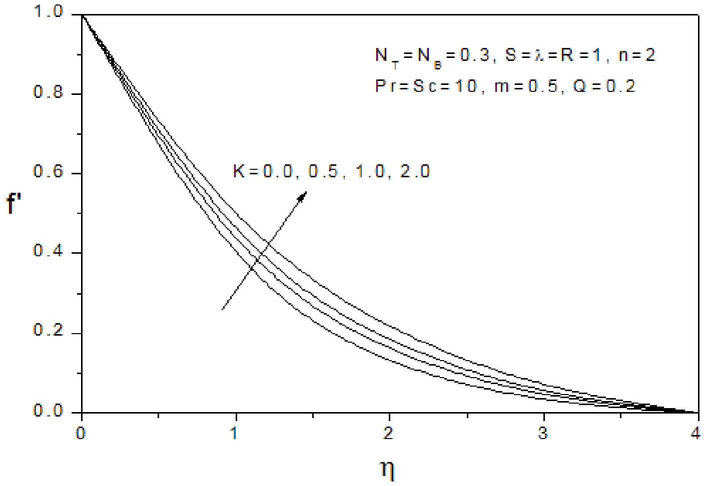

Fig.5 (a) Velocity profiles for different values of *K*

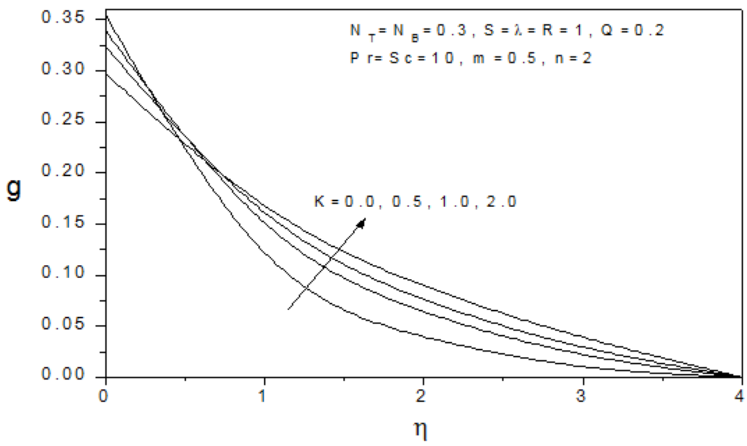

Fig.5 (b) Angular velocity profiles for different values of *K*

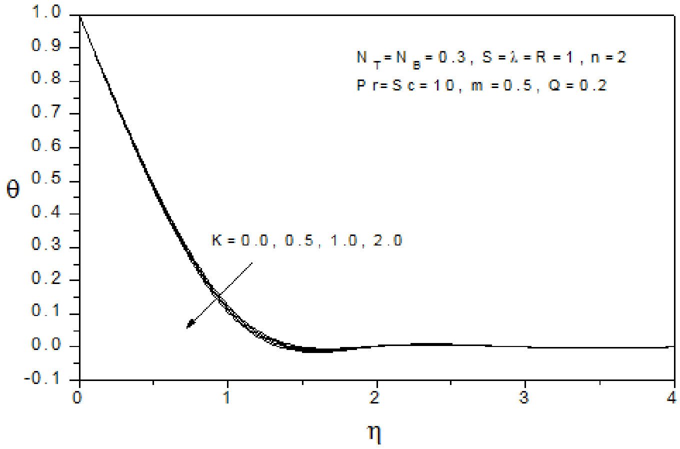

Fig.5 (c) Temperature profiles for different values of *K*

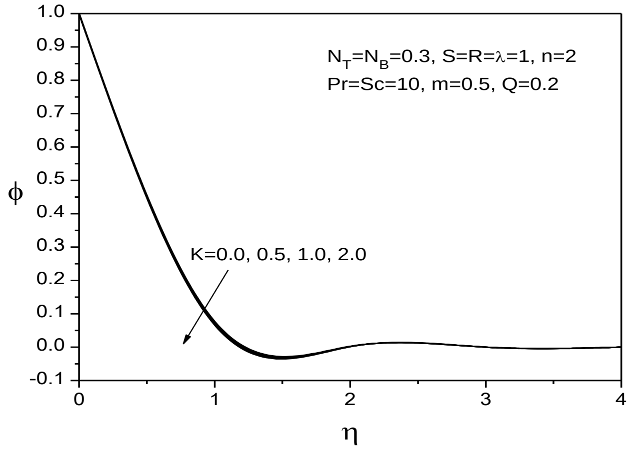

Fig.5(d) Concentration profiles for different values of *K*

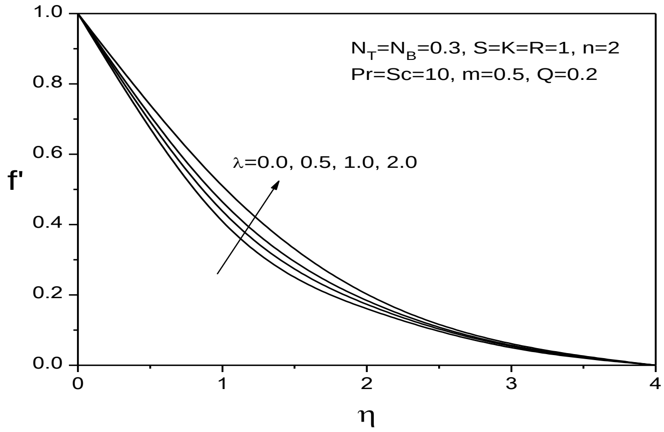

Fig.6 (a) Velocity profiles for different values of λ

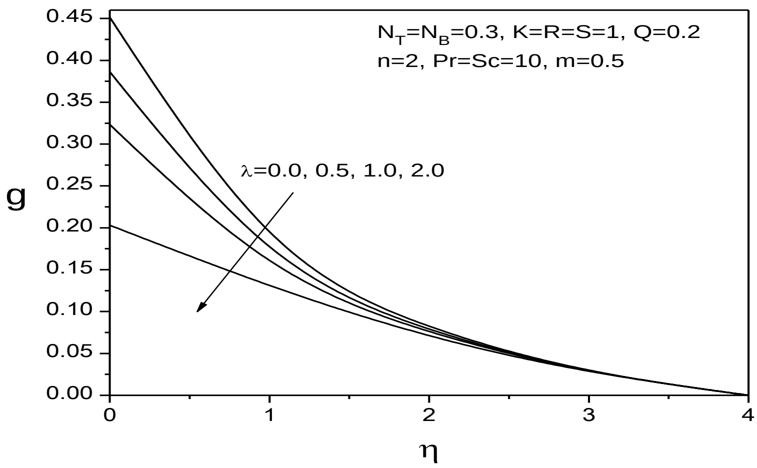

Fig.6(b) Angular velocity profiles for different values of λ

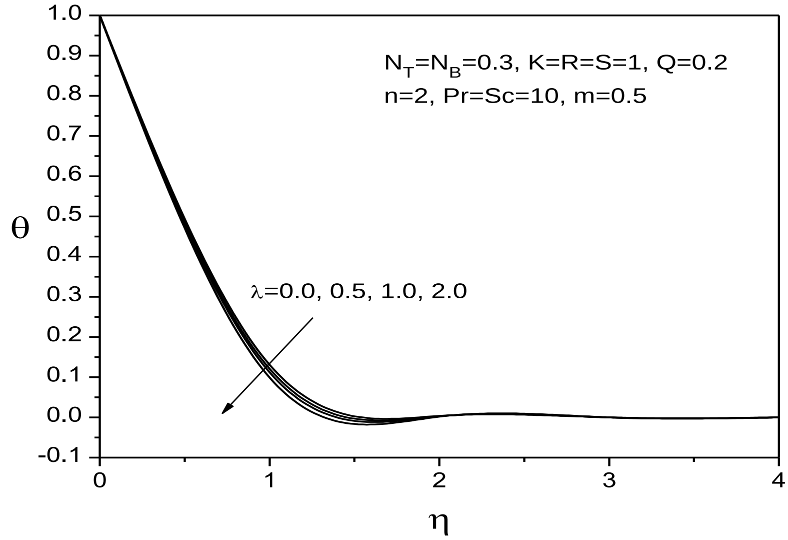

Fig.6(c) Temperature profiles for different values of λ

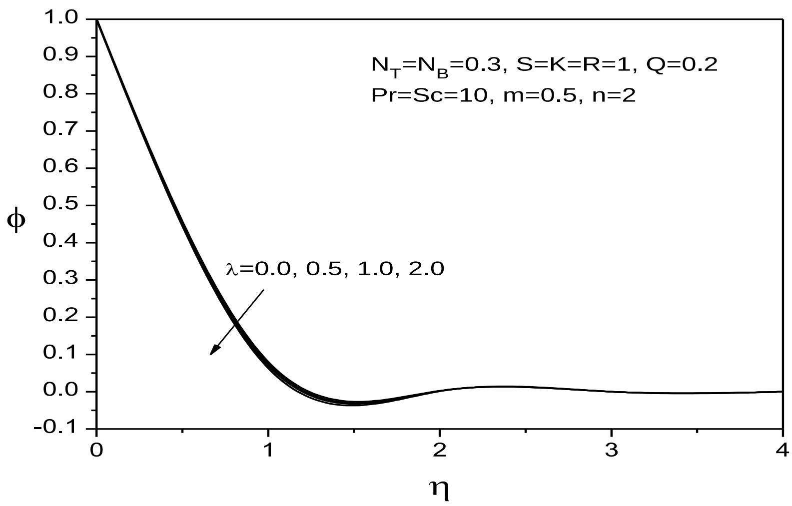

Fig.6(d) Concentration profiles for different values of λ

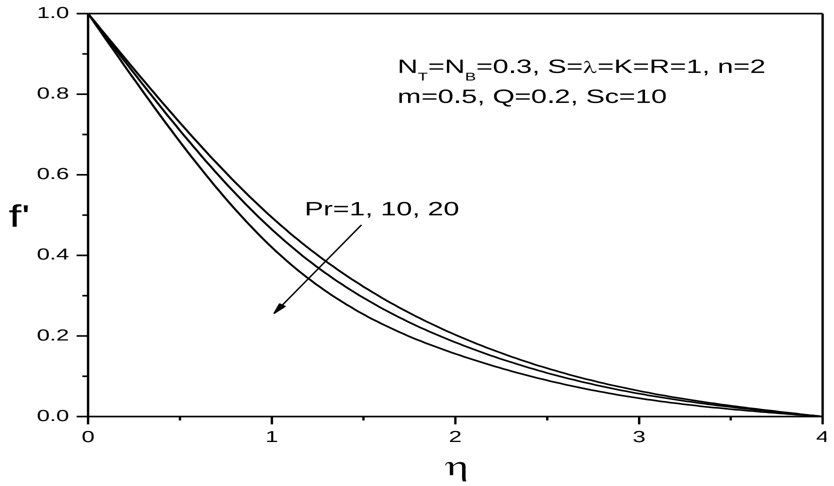

Fig.7(a) Velocity profiles for different values of *Pr*

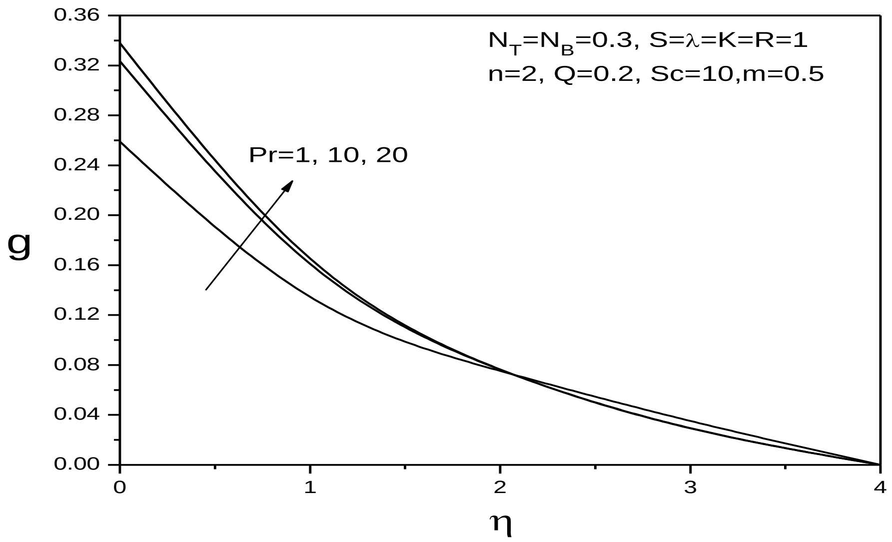

Fig.7(b) Angular velocity profiles for different values of *Pr*

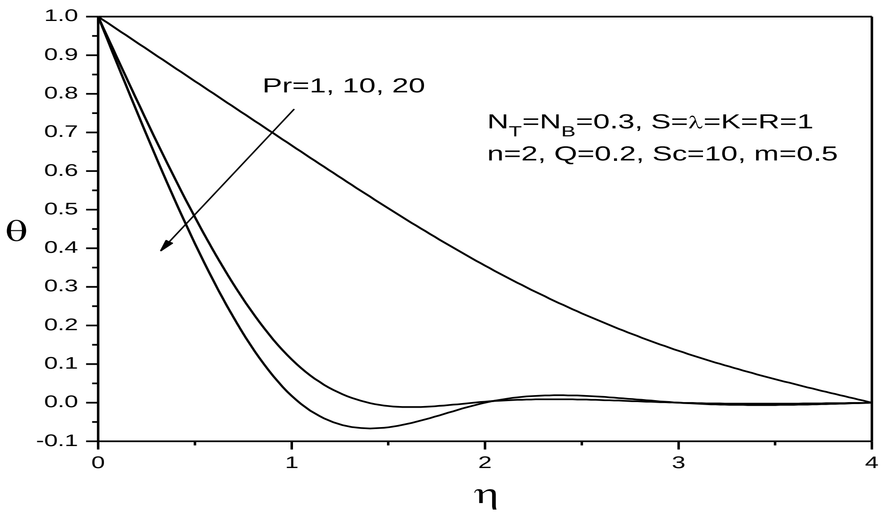

Fig.7(c) Temperature profiles for different values of *Pr*

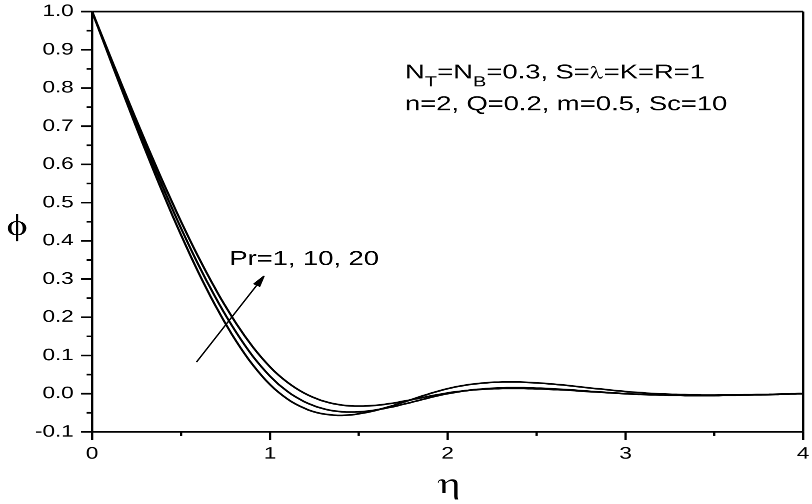

Fig.7(d) Concentration profiles for different values of *Pr*

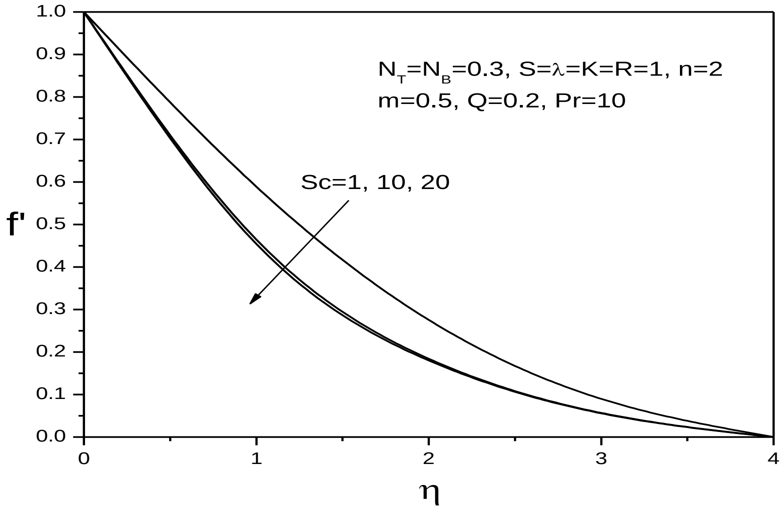

Fig.8(a) Velocity profiles for different values of *Sc*

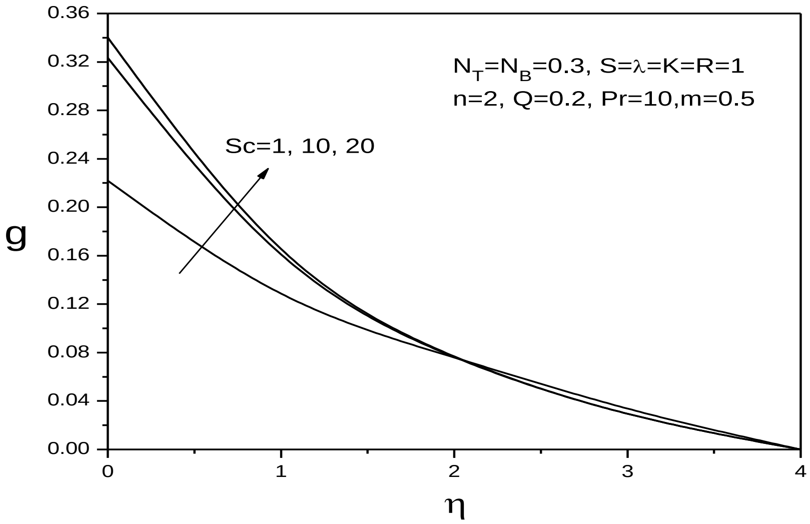

Fig.8(b) Angular velocity profiles for different values of *Sc*

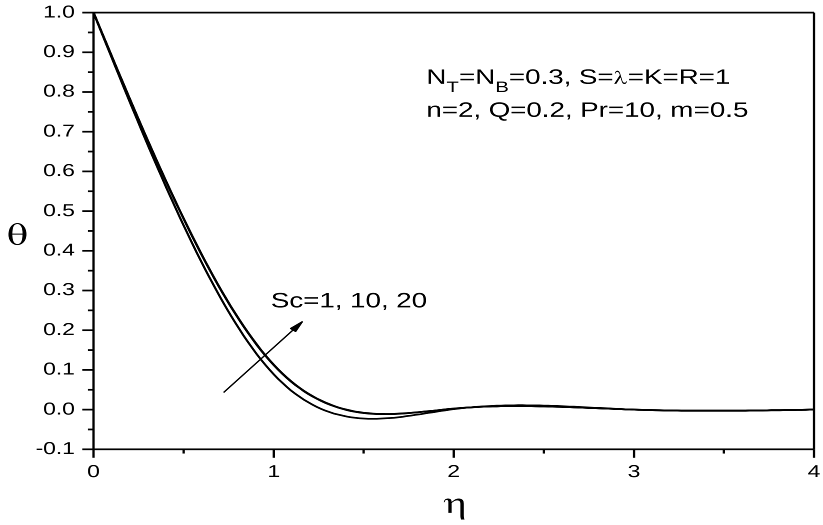

Fig.8(c) Temperature profiles for different values of *Sc*

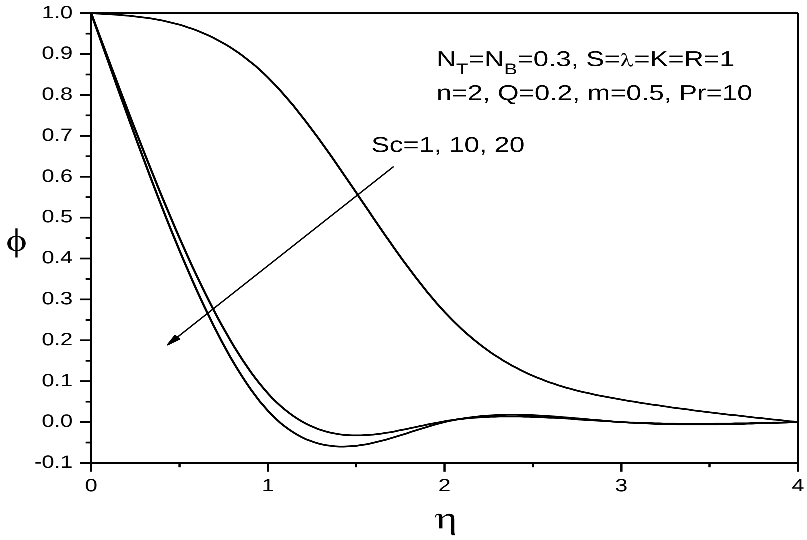

Fig.8(d) Concentration profiles for different values of *Sc*

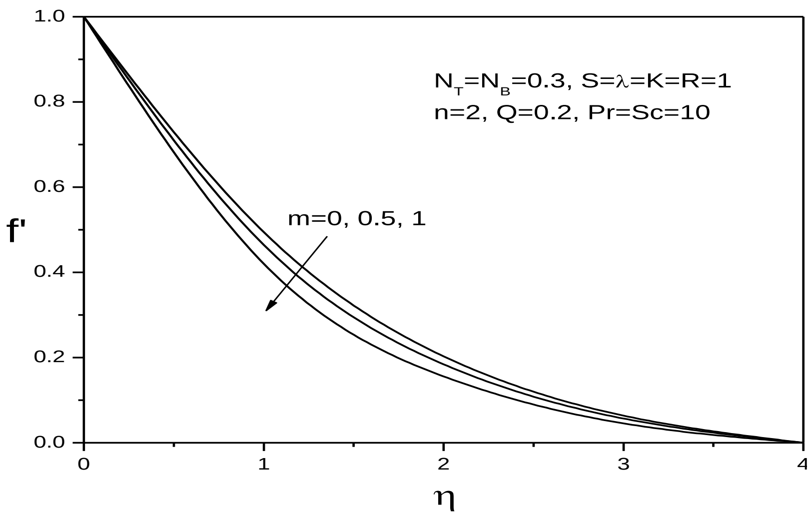

Fig.9(a) Velocity profiles for different values of *m*

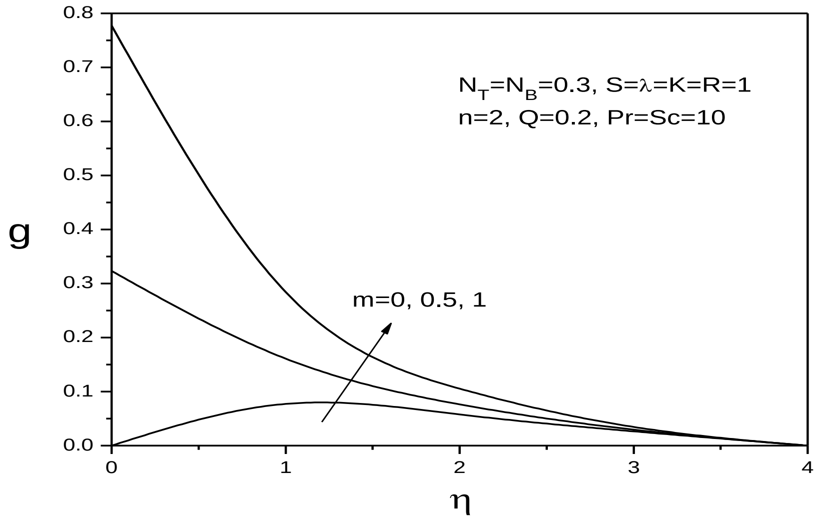

Fig.9(b) Angular velocity profiles for different values of *m*

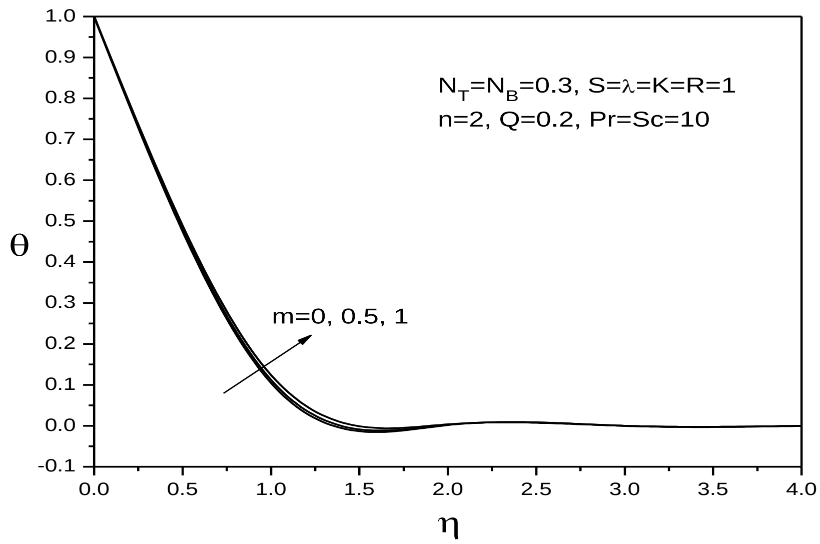

Fig.9(c) Temperature profiles for different values of *m*

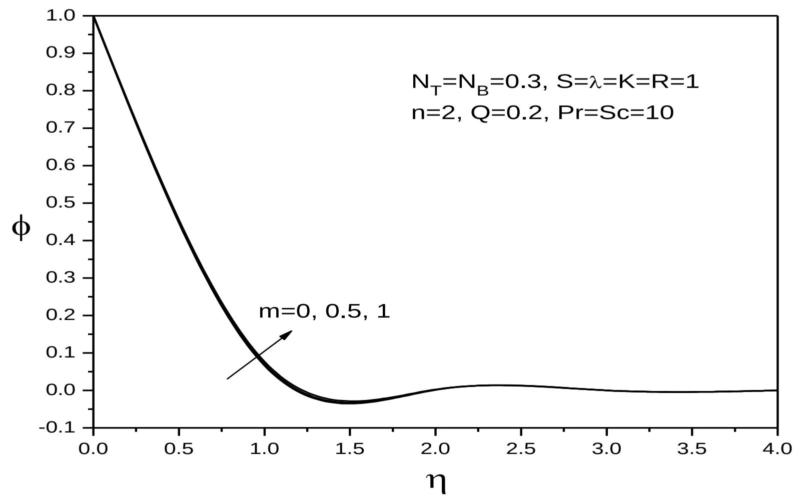

Fig.9(d) Concentration profiles for different values of *m*

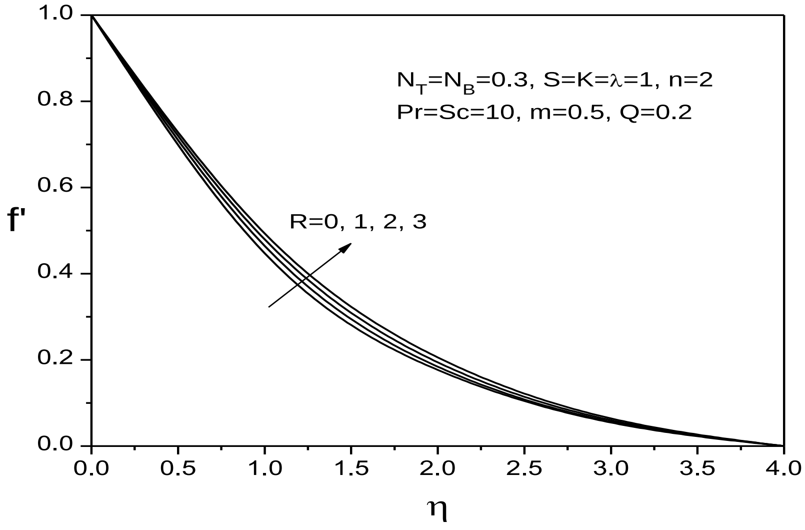

Fig.10(a) Velocity profiles for different values of *R*

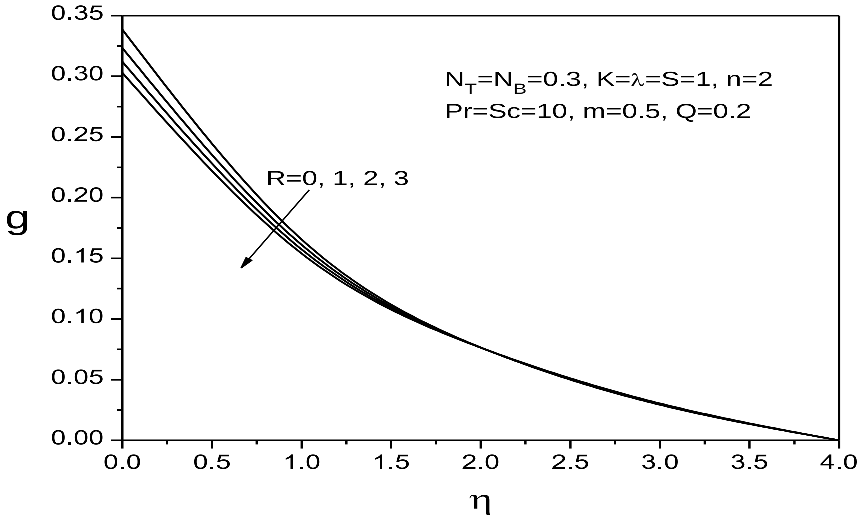

Fig.10(b) Angular velocity profiles for different values of *R*

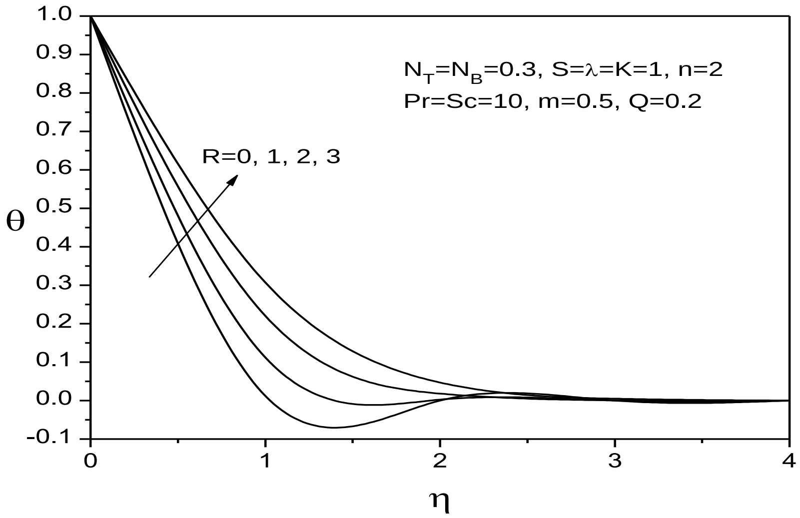

Fig.10(c) Temperature profiles for different values of *R*

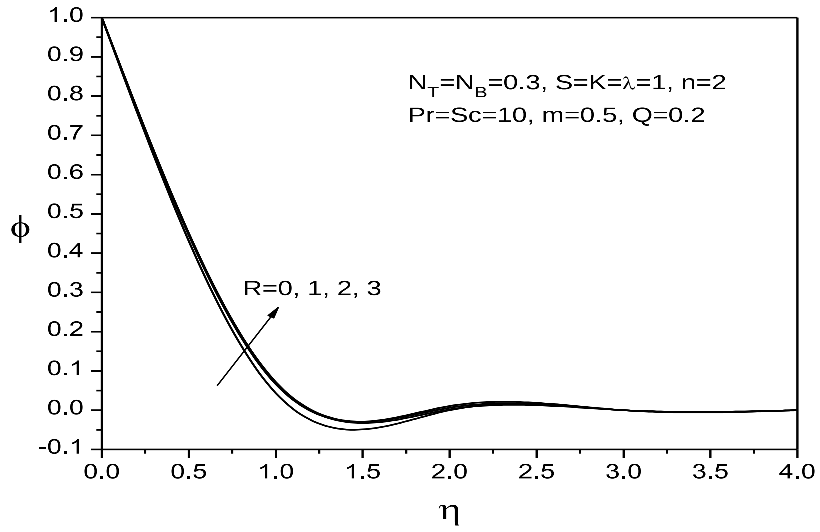

Fig.10(d) Concentration profiles for different values of *R*

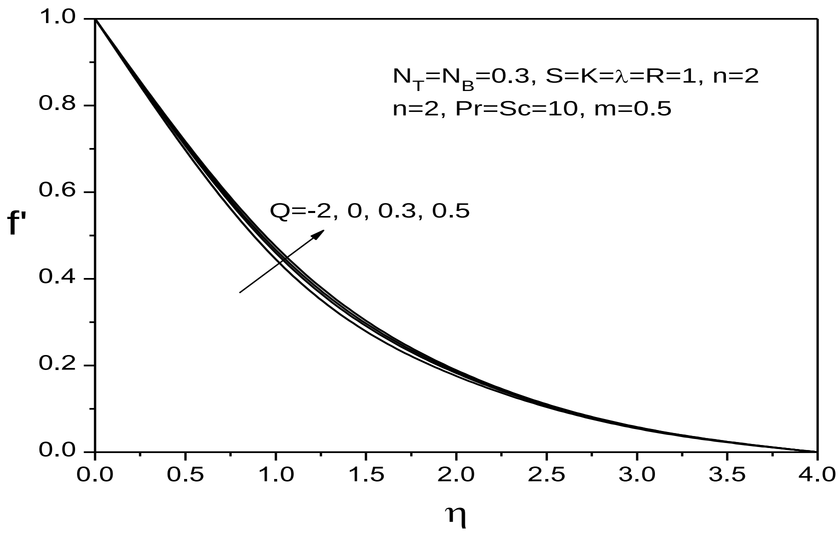

Fig.11(a) Velocity profiles for different values of *Q*

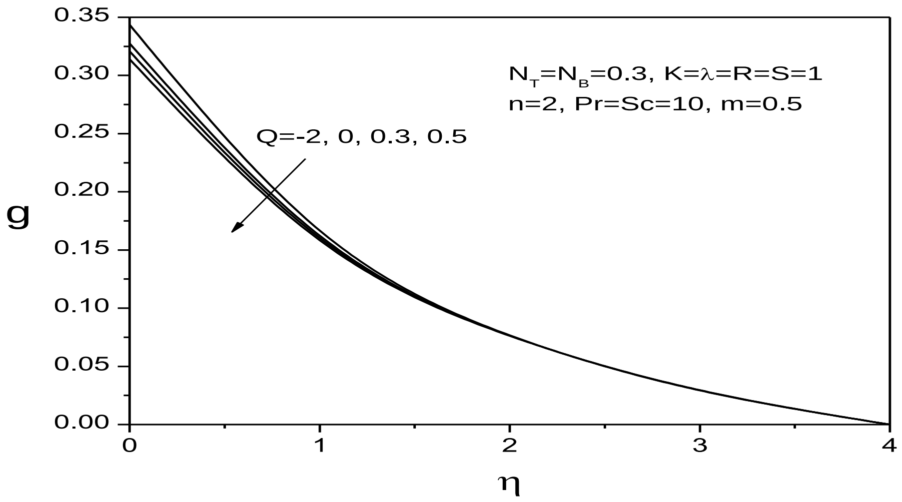

Fig.11 (b) Angular velocity profiles for different values of *Q*

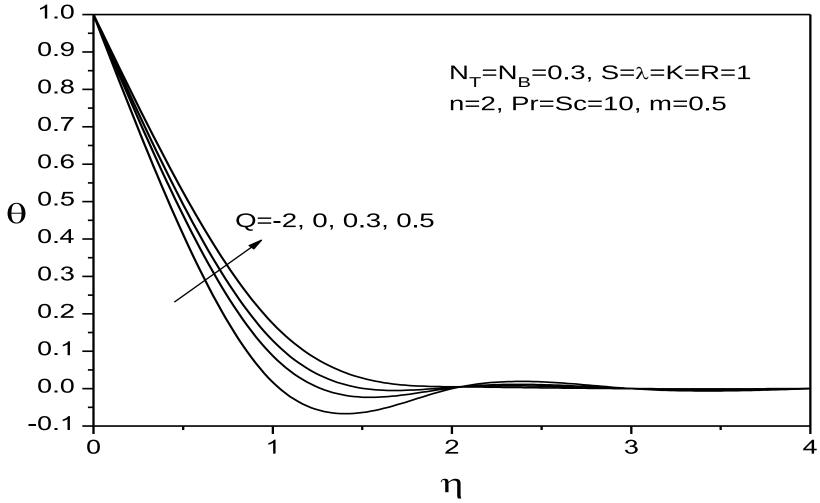

Fig.11(c) Temperature profiles for different values of *Q*

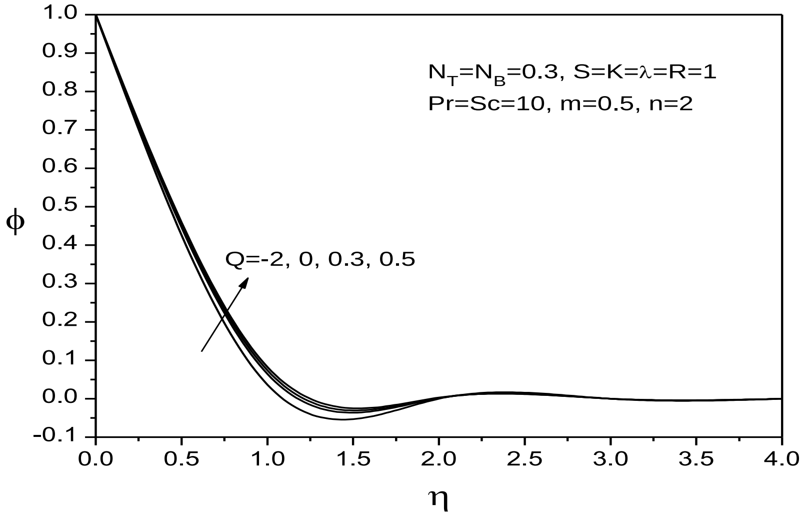

Fig.11 (d) Concentration profiles for different values of *Q*

V. CONCLUSIONS

In this paper, we have presented a boundary layer analysis for the mixed convection flow of a non-Newtonian nanofluid on a non-linearly stretching sheet by taking radiation and heat source/sink into account. The micropolar model is chosen for the non-Newtonian fluid since the spinning motion of the nanoparticles as they move along the streamwise direction can be best described by the micropolar fluid model. The governing boundary layer equations have been transformed to a two-point boundary value problem in similarity variables and the resultant problem is solved numerically using the fourth order Runga-Kutta method along with shooting technique. The particular solutions reported in this paper were validated by comparing with solutions existing in the previously published paper. Our results show a good agreement with the existing work in the literature. The results are summarized as follows

1. The thermophoresis parameter increases, friction factor increase, where as the heat and mass transfer rates decreases.
2. Brownian motion reduces nanoparticle diffusion.
3. The radiation and heat source/sink increases the friction factor and mass transfer rate and reduces the heat transfer rate.
4. The radiation and heat source/sink reduces the angular velocity, and increase the velocity, temperature and concentration.

REFERENCES

[1] Pearson, J. R. A., Tardy, P. M. J, (2002), Models for flow of non-Newtonian and complex fluids through porous media, J Non Newton Fluid Mech, Vol.102, pp.447–473.

[2] Ellahi R, Afza, S, (2009), Effects of variable viscosity in a third grade fluid with porous medium: an analytic solution, Commun Nonlinear Sci Numer Simul., Vol.14(5), pp.2056–2072.

[3] Ellahi, R, (2009), Effects of the slip boundary condition on non- Newtonian flows in a channel, Commun Nonlinear Sci Numer Simul., Vol.144, pp.1377–1384.

[4] Rama Subba Reddy Gorla and Mahesh Kumari, (2012), Mixed Convection Flow of a Non-Newtonian Nanofluid Over a Non-Linearly Stretching Sheet, Journal of Nanofluids, Vol. 1, pp. 186–195.

[5] Choi, S., Enhancing thermal conductivity of fluids with nanoparticles, in: D.A. Siginer, H.P.

[6] Masuda, H., Ebata, A,Teramae, K., Hishinuma, N., (1993), Alteration of thermal conductivity and viscosity of liquid by dispersing ultra-fine particles, NetsuBussei (Japan), Vol.7, No.4, pp.227–233.

[7] Eldabe, N. T., Elbashbeshy, E. M. A., Elsaid, E. M.,(2013), Effects of Magnetic Field and Heat Generation on Viscous Flow and Heat Transfer over a Nonlinearly Stretching Surface in a Nanofluid, International Journal of Applied Mathematics, ISSN:2051-5227, Vol.28, Issue.1

[8] Erigen, A. C., (1966), Theory of micropolar fluids, J. math. Mech., Vol. 16, pp.1-18.

[9] Arpaci, V.S., (1968), Effects of thermal radiation on the laminar free convection from a heated vertical plate, Int. J. Heat Mass Transfer, Vol.11, pp.871-881.

[10] Cess, R.D., (1966), Interaction of thermal radiation with free convection heat transfer, Int. J. Heat Mass transfer, Vol.9, pp.1269-1277.

[11] Cheng, E.H and Ozisik, M.N., (1972), Radiation with free convection in an absorbing emitting and scattering medium, Int. J. Heat Mass Transfer, Vol.15, pp.1243-1252.

[12] Raptis, A., (1998), Radiation and free convection flow through a porous medium, Int. Comm. Heat Mass Transfer, Vol.25(2), pp.289-295.

[13] Hossain, M.A. and Takhar, H.S., (1996), Radiation effects on mixed convection along a vertical plate with uniform surface temperature, Heat Mass Transfer, Vol.31, pp.243-248.

[14] Hossain, M.A. and Takhar, H.S., (1999), Thermal radiation effects on the natural convection flow over an isothermal horizontal plate, Heat Mass Transfer, Vol.35, pp.321-326.

[15] Oahimire, J. I., Olajuwon, B.I., Waheed, M. A., and Abiala, I. O., (2013), Analytical solution to mhd micropolar fluid flow past a vertical plate in a slip- flow regime in the presence of thermal diffusion and thermal radiation, Journal of the Nigerian Mathematical Society, Vol. 32, pp. 33-60.

[16] El-Arabawy, H.A.M., (2003), Effect of suction/injection on the flow of a micropolar fluid past a continuously moving plate in the presence of radiation, *Int. J. Heat Mass Transfer*, Vol.46, pp. 1471–1477.

[17] Ogulu, A., (2005), On the oscillating plate-temperature flow of a polar fluid past a vertical porous plate in the presence of couple stresses and radiation, *Int. comm. Heat Mass Transfer*, Vol.32, pp. 1231–1243.

[18] Rahman, M. M. and Sattar, M. A., (2006), Magneto hydrodynamic convective flow of a micropolar fluid past a continuously moving vertical porous plate in the presence of heat generation/absorption, *ASME J. H. Transfer*, Vol.128, pp. 142–152.

[19] Nor Azian Aini Mat, Norihan M Arifin, Roslinda Nazar and Fudziah Ismail, (2012), Radiation effect on Marangoni convection boundary layer flow of a nanofluid, Mathematical Sciences, 6:21.

[20] Sparrow, E.M. and Cess, R.D., (1961), Temperature-dependent heat sources or sinks in a stagnation point flow, Applied Scientific Research, Vol.A10, pp.185-189.

[21] Pop, I. and Soundalgekar, V.M., (1962), Viscous dissipation effects on unsteady free convection flow past an infinite plate with constant suction and heat source, Int. J. Heat Mass Transfer, Vol.17, pp.85-92.

[22] Rahman, M. M. and Sattar, M. A., (2007), Transient convective flow of micropolar fluid past a continuously moving vertical porous plate in the presence of radiation, *Int. J. App. Mech. Engi.*, Vol.12(2), pp. 497–51.

[23] Yanhai Lin, Liancun Zheng and Xinxin Zhang, (2012), Marangoni Convection Flow and Heat Transfer in Pseudoplastic Non-Newtonian Nanofluids with Radiation Effectsand Heat Generation or Absorption Effects, numerical analysis and applied mathematics, AIP Con.Proc., 1479, pp.50-53.

[24] Chamkha, A.J., (2000), Thermal radiation and buoyancy effects on hydromagnetic flow over an accelerating permeable surface with heat source or sink, Int.J.Heat Mass Transfer, Vol.38, pp.1699-1712.

[25] Jain, M.K., Iyengar, S.R.K. and Jain, R.K., (1985), Numerical Methods for Scientific and Engineering Computation, Wiley Eastern Ltd., New Delhi, India.

International Journal of Modern Engineering Research (IJMER)
www.ijmer.com Vol. 3, Issue. 5, Sep - Oct. 2013 pp-2695-2697 ISSN: 2249-6645

A Novel Framework for Securing Medical Records in Cloud Computing

Md. Irfan[1], Sayeed Yasin[2]

[1]*M. Tech, Nimra College of Engineering & Technology, Vijayawada, A.P., India.*
[2]*Asst. Professor, Dept.of CSE, Nimra College of Engineering & Technology, Vijayawada, A.P., India.*

ABSTRACT: *The patient health records are maintained in a data server under the cloud computing environment. A novel framework of secure sharing of personal health records (PHRs) under distributed environment in the cloud computing has been proposed in this paper .Public and personal access models are designed with privacy and security enabled mechanism. This framework addresses the unique challenges brought by multiple medical records owners and users, in that the complexity of key management is greatly reduced while guaranteeing the privacy compared with previous works. The attribute-based encryption (ABE) model is enhanced to support distributed ABE operations with MA-ABE. The system is improved to support the dynamic policy management model. Thus, PHRs are maintained with security and privacy. It is a server choice based security model and possess the central key management with attribute authorities.*

Keywords: *Cloud computing, Data privacy, Encryption, PHR.*

I. INTRODUCTION

Cloud computing is an emerging computing technology where applications and all the services are provided through Internet. It is a model for enabling on-demand network access to various pool resources. Cloud computing can be considered as a computing framework with greater flexibility and availability at lower cost [1]. Because of these characteristics, cloud environment has been receiving a great nowadays. Cloud computing environment services benefit from economies of scale achieved through versatile use of resources, specialization, and other efficiencies. The Internet has grown into a world of its own, and its large space now offers capabilities that could support Physicians in their duties in numerous ways. Nowadays software functions have moved from the individual user's local hardware to a central server that operates from a remote location. In recent years, is an emerging trend and medical records is a patient-centric model of health information exchange and management. A health record is an electronic record of an individual user's health information by which the individual controls access to the information and may have the ability to manage, track, and participate in her own health care.

Generally, medical record service allows a user to create, manage, and control her personal health data in one place through the web, which has made the storage, retrieval, and sharing of the medical information more efficient. The general principles of the security rule include that a covered entity must maintain both "reasonable and appropriate" administrative, technical, and physical safeguards to protect Electronic Personal Health Information, e-PHI [2], which include requirements to ensure integrity, confidentiality and availability of information; anticipation and protection against possible vulnerabilities to the privacy of the information or against inappropriate use; and compliance by the entity's workforce. Generally information is recorded on secured systems, hard drives, backups, flash drives, shared folders, professional networks etc. As health care professionals, physicians know that ensuring the accuracy of secret information involves more technical approaches, to avoid the security pitfalls. Privacy laws that speak to the protection of patients secrecy are complex and often difficult to understand in the context of an ever-growing cloud-based technology[3]. Due to the high cost of building and maintaining specialized data centers, many medical record services are outsourced to or provided by third-party service providers, for example, Samedi, Microsoft HealthVault and Medicine Brain. While it is exciting to have convenient medical record services for everyone, there are many security and privacy risks which could impede its wide adoption[4].

II. RELATED WORK

For access control of the outsourced data, partially trusted servers are often assumed. With cryptographic methods, the aim is trying to enforce who has (read) access to which parts of a patient's PHR documents in a fine-grained way. Symmetric key methods are a class of algorithms for cryptography that use the same cryptographic keys for both encryption of plaintext and decryption of ciphertext. The keys may be identical to each other or there may be a simple transformation to go between the two keys. The keys, in practice, represent a shared secret key between two or more parties that can be used to maintain a private information link. In [5], the authors proposed a solution for securing outsourced data on semi-trusted servers based on symmetric key derivation methods, which can achieve fine-grained access control. Unfortunately, the complexities of file creation and user grant or revocation operations are linear to the number of authorized users, which is less scalable.

Public key cryptosystems(PKC) based solutions were proposed due to its ability to separate write and read privileges. To realize fine-grained access control, the traditional public key encryption (PKE) based methods proposed by the authors in [6] in their work "Patient controlled encryption: ensuring privacy of electronic medical records, they purpose the solution scenario and shows how both public and symmetric based encryption used. The disadvantage of their solution is either incurs high key management overhead, or require encrypting multiple copies of a file using different users' keys.

A number of works used ABE to realize fine-grained access control for the outsourced data, especially, there has been an increasing interest in applying ABE to secure electronic healthcare records (EHRs). In [7], the authors proposed an attribute-based infrastructure for EHR systems, where each patient's EHR files are encrypted using a broadcast variant of Cipher Text-ABE (CP-ABE). However, the encrypted text length grows linearly with the number of unrevoked users. In [8], the authors applied ciphertext policy ABE (CP-ABE) to manage the sharing of PHRs, and introduced the concept of social/professional domains but they do not use multi-authority ABE . In [9], the authors investigated using ABE to generate self-protecting EMRs, which can either be stored on cloud servers or mobile phones so that EMR could be accessed when the health provider is offline.

III. PROPOSED WORK

A. Patient Centric Framework

The main aim of our framework (Figure 1) is to provide secure patient-centric medical record access and efficient key management at the same time. The key idea is to divide the system into several security domains (namely, public domains (PUDs) and personal domains (PSDs)) according to the different users' data access requirements. The PUDs consist of users who make access based on their professional roles, such as nurses, doctors and medical researchers. In practice, a PUD can be mapped to an independent sector in the society, such as the government, health care or insurance sector. For each PSD, its users are personally associated with the data owner (such as family members or close friends), and they make accesses to medical records based on access rights assigned by the owner. In both types of the security domains, we utilize ABE to realize cryptographically enforced, patient-centric PHR access.

Each data owner or patient is a trusted authority of her own PSD, who uses a KP-ABE system to manage the secret keys and access rights of users in her PSD. In our framework, there are multiple owners, multiple SDs, multiple AAs, and multiple users. In addition, two ABE systems are involved: for each PSD the YWRL's revocable KP-ABE scheme is adopted; for each PUD, our proposed revocable MA-ABE scheme is used.

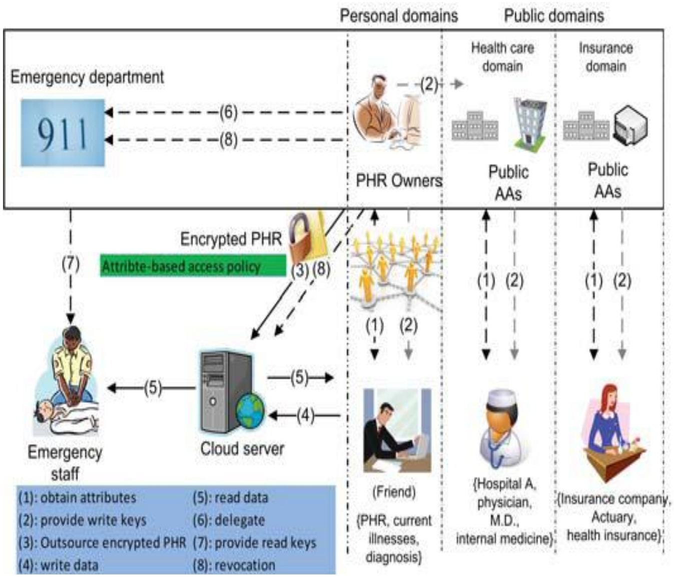

Figure 1: Proposed Framework

B. System setup and Key Distribution

The system first defines a common universe of data attributes shared by every domain, such as "basic profile", "medical history", "allergies", and "prescriptions". An emergency attribute is also defined for the break glass access. There are two ways for distributing shared secret keys. First, when first using the health record service, a PHR owner can specify the access privilege of a data reader in her PSD, and let her application generate and distribute corresponding key to the latter, in a way resembling invitations in GoogleDoc. Second, a reader in domain could obtain the secret key by sending a request (indicating which types of files she wants to access) to the record owner via HSN, and the owner will grant her a subset of requested data types. In addition, the data attributes can be organized in a hierarchical manner for efficient policy generation as shown in figure 2. When the user is granted all the file types under a category, his/ her access privilege will be represented by that category instead.

In practice, there exist multiple Attribute authorities (AAs) each governing a different subset of role attributes. For instance, hospital staffs shall have a different authorities from pharmacy specialists. This is reflected by (1) in Figure 1. In addition, the authorities distribute write keys that permit contributors in their PUD to write to some patients' PHR ((2)).

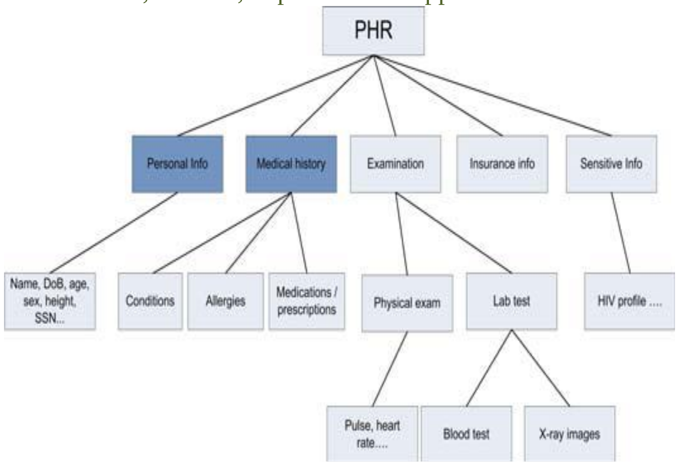

Figure 2: The attribute hierarchy of files

C. PHR Encryption and Access

The owners upload ABE-encrypted record files to the server ((3)). Each owner's record file is encrypted both under a certain fine- grained and role-based access policy for users from the PUD to access, and under a selected set of data attributes that allows access from users in the PSD. The data contributors will be granted write access to someone's records, if they present proper write keys ((4)). The data readers download record files from the server, and they can decrypt the files only if they have suitable attributebased keys ((5)).

D. Break Glass

When an emergency occurs, the regular access policies may no longer be applicable. To handle this situation, a method called break- glass access is needed to access the victim's PHR. In our framework, each owner's records access right is also delegated to an emergency department (ED, (6)). To prevent from abuse of break- glass option, the emergency staff needs to contact the department to verify her identity and the emergency situation, and obtain temporary read keys ((7)).

E. User Revocation

Here we consider revocation of a data reader or his attributes or access privileges. There are several possible cases: 1) revocation of one or more role attributes of a public domain user; 2) revocation of a public domain user which is equivalent to revoking that entire user's attributes. These operations are done by the attribute authority that the user belongs to, where the actual computations can be delegated to the server to improve efficiency ((8)). 3) Revocation of a personal domain user's access privileges; 4) revocation of a personal domain user.

IV. CONCLUSIONS

The personal health record (PHR) systems needs security against attackers and hackers. Scalable and Secure sharing includes basic securities to protect the confidential information from unauthorized access and loss. This paper proposed the new approach for existing PHR system for providing more security and privacy using attribute based encryption which plays an important role because these are unique and not easily hackable. We are reducing key management problem and also we enhance the privacy guarantee.

REFERENCES

[1] Cong Wang and Kui Ren, Jin Li, "Toward Publicly Auditable Secure Cloud Data Storage Services", IEEE Network ,pp. 19-24, July/August 2010.
[2] M. Li, S. Yu, K. Ren, and W. Lou, "Securing personal health records in cloud computing: Patient-centric and fine-grained data access control in multi-owner settings," in SecureComm'10, Sept. 2010, pp. 89–106.
[3] Zhiguo Wan, Jun‟ e Liu, and Robert H. Deng, "HASBE: A Hierarchical Attribute-Based Solution for Flexible and Scalable Access Control in Cloud Computing", IEEE Transactions on Information Forensics and Security, Vol. 7, No. 2, Pp. 743-754, April 2012.
[4] A. Vetro, H. Sun, P. DaGraca, and T. Poon, "Minimum drift architectures for three-layer scalable DTV decoding," IEEE Trans. Consumer Electron., vol. 44, no. 3, pp. 527-536, Aug. 1998.
[5] S. D. C. di Vimercati, S. Foresti, S. Jajodia, S. Paraboschi, and P. Samarati, "Over-encryption: management of access control evolution on outsourced data," in VLDB '07, 2007, pp. 123–134.
[6] J. Benaloh, M. Chase, E. Horvitz, and K. Lauter, "Patient controlled encryption: ensuring privacy of electronic medical records," in CCSW '09, 2009, pp. 103–114.
[7] S. Narayan, M. Gagn´e, and R. Safavi-Naini, "Privacy preserving ehr system using attribute-based infrastructure," ser. CCSW '10, 2010, pp. 47–52.
[8] L. Ibraimi, M. Petkovic, S. Nikova, P. Hartel, and W. Jonker, "Ciphertext-policy attribute-based threshold decryption with flexible delegation and revocation of user attributes," 2009.
[9] A. Akinyele, C.U. Lehmann, M.D. Green, M.W. Pagano, Z.N.J. Peterson, and A.D. Rubin. Self-protecting electronic medical records using attribute-based encryption on mobile device. Technical report, Cryptology ePrint Archive, Report 2010/565, 2010.

An Optimal Cooperative Provable Data Possession Scheme for Distributed Cloud Storage

Shaik Faizulla[1], G. Sreedevi[2]
[1]M. Tech, Nimra College of Engineering & Technology, Vijayawada, A.P., India.
[2]Assoc. Professor, Dept.of CSE, Nimra College of Engineering & Technology, Vijayawada, A.P., India.

ABSTRACT: *In recent years, cloud storage services has become a faster growth and makes large profits by providing the services to the customer for their needs on the internet and data sharing. Cloud environment provides the services at low cost, scalable position independent platform for the storage of client's data. Though it provides good services, cloud environment is based on the open architecture and with interfaces. It has capabilities to incorporate with multiple internal or external services together to provide the ability to exchange data's and use information so that we call such a distributed cloud environments as a multi- cloud or hybrid cloud. Provable data possession (PDP) is a technique for ensuring the integrity of data in cloud environment. Provable data possession is such a probabilistic proof technique for a storage provider to prove the integrity and ownership of the clients' data without downloading data. We present an optimal cooperative PDP (CPDP) scheme based on homomorphic verifiable response and hash index hierarchy.*

Keywords: *Cloud storage, Hash index, Hybrid cloud, PDP.*

I. INTRODUCTION

Cloud computing environment is made on the basis of exposed designs and boundaries, it has the proficiency to integrate numerous interior or exterior cloud computing services together to offer great interoperability and such a dispersed cloud environment is known as a multi-Cloud [1]. By means of virtual infrastructure management a distributed permits clients to effortlessly access their resources distantly over boundaries. Cloud storage package has developed into a quicker profit progression point by providing low-cost, accessible, position self-determining stage for the customers' records. It would fetch irreversible sufferers to the clients if a hybrid cloud storage platform is susceptible to safety attacks. The secured data in an enterprise may be illegitimately opened over a remote edge delivered by a distributed cloud and documentations may be mislaid with when they are deposited into an undefined storage group external to the enterprise [2] [3].

Several implements and skills were present for hybrid cloud which aid cloud providers to build a distributed cloud storage platform for handling customers' statistics [4]. The proof checking without moving makes it particularly significant for very large- size files and folders to check whether these data have been interfered with or deleted without transferring the latest version of data. As a consequence, it is able to substitute outdated hash and signature functions in the storage outsourcing. It is necessary for cloud computing providers to offer safety practices for handling their storage facilities. Provable data possession (PDP) or proofs of retrievability is a probabilistic proof system for a storage provider to demonstrate the integrity and ownership of clients' data without transferring data [5].

II. RELATED WORK

In [6], the authors proposed the first proof-of-retrievability schemes with full proofs of security. Their first scheme, built from BLS signatures and secure in the random oracle model has the shortest query as well as response of any proof-of-retrievability with public verifiability. Their second scheme, which builds elegantly on the pseudorandom functions (PRFs) and is secure in the standard model, has shortest response of any proof-of-retrievability scheme with private verifiability but a longer query. In [4], the authors constructed a highly efficient and provably secure PDP technique based entirely on symmetric key cryptography. Also, our data possession technique allows outsourcing of dynamic data, it efficiently supports operations, such as block modification, append and deletion. In [2], the authors introduced a model for provable data possession (PDP) that allows a client that has stored data at an untrusted server to verify that the server possesses the original data without retrieving it. The model generates probabilistic proofs of data possession by sampling random sets of blocks from the server, which significantly reduces I/O costs.

In [3], the authors constructed a dynamic provable data possession (DPDP), which extends the PDP model to support provable updates on the stored data. DPDP solution is based on a new variant of the authenticated dictionaries which use rank information to organize dictionary entries. Thus we can support efficient authenticated operations on the files at block level, such as authenticated insert and delete. They proved the security of their constructions using some standard assumptions. In [7], the authors proposed an innovative authentication scheme for mobile devices. While creating the password, the user chooses a theme of snapshots in thumbnail size and the sequence of those snapshots is fixed as a password. In [8], passface is an approach proposed by the Real User Corporation in which the user is allowed to choose four images of human faces from the face database as their password. During the verification step, the user is provided with a grid of nine faces, one already chosen during the registration and eight decoy faces. The user identifies the selected face and then clicks anywhere over it.

III. PROPOSED WORK

A. Verification Framework for Multi- Cloud

In the proposed work, we consider a data storage service involving three different entities: Granted clients, who have a large amount of data to be stored in multi-clouds and have the permissions to access and manipulate the stored data; Cloud service providers (CSPs), who work together for providing data storage services and have enough storage space sand computation resources; and Trusted third parties (TTPs),who are trusted to store the verification parameters and offer the query services for these parameters. Figure 1 shows the architecture.

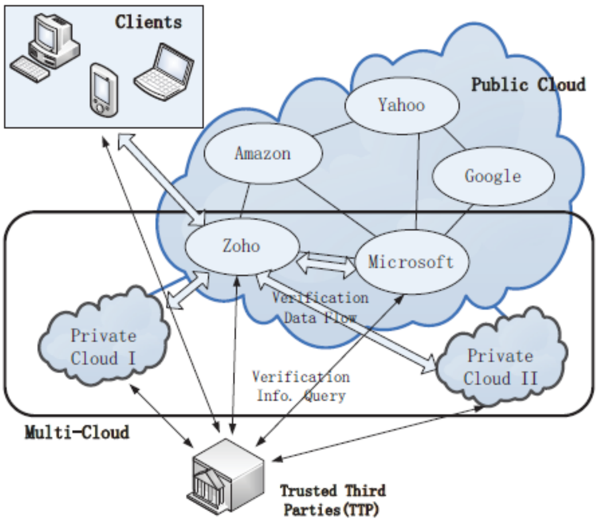

Figure 1: Verification architecture for data integrity

In this architecture, we consider the existence of many CSPs to collaboratively store and maintain the client‟ s data. Moreover, a cooperative PDP is used to verify the integrity and availability of the stored data in CSPs. The verification process is described as follows: Firstly, the client (data owner) uses the shared secret key to pre-process the file, which consists of a collection of n blocks. It generates a set of public verification information that is stored in TTP and then transmits the file and some verification tags to CSPs, and may delete its local copy. Later by using a verification protocol for cooperative PDP, the clients can issue a challenge for one CSP to check the integrity and the availability of outsourced data in terms of public verification information stored in TTP.

B. Cooperative PDP

Based on zero knowledge proof system and interactive proof system, the integrity of data stored in a multi cloud is maintained. A CPDP is a collection of two algorithms (Key Gen, Tag Gen) and the interactive proof system Proof.

- **Key Gen:** It takes a security parameter as an input and then returns a secret key as output.
- **Tag Gen:** It takes a shared secret key, file and set of cloud storage providers as input and returns triples.
- **Proof:** It is a protocol of proof of provable data possession between the CSP's and verifier.

Let H = { Hk } be a family of hash functions where Hk : $\{0,1\}^n \rightarrow \{0,1\}^k$ index, where k ε K. This algorithm has a benefit in breaking the collision resistance of hash H. In Collision-Resistance H, a hash family H(t, ε) collision resistant if no t-Time adversary has advantage atleast ε in breaking collision of H. First the KeyGen algorithm is run in this scheme to obtain the private or the public key for users. Then TagGen is generated by the clients for the cloud outsourced data.

C. Homomorphic Verifiable Response

A homomorphism is a map function f : p → q between two groups such that f(g1 $\oplus$ g2) = f(g1) $\otimes$ f(g2) for all g1, g2 ∈ p, where $\oplus$ denotes the operation in p and $\otimes$ denotes the operation in q. This notation was used to define a Homomorphic Verifiable Tags (HVTs) as : Given two values σ_i and σ_j for two message mi and mj , anyone can combine them into a value σ' corresponding to the sum of the message mi+mj . When provable data possession is considered as a challenge response protocol, we also extend this notation to introduce the concept of a Homomorphic Verifiable Responses (HVRs), which is used to integrate multiple responses from the various CSPs in cooperative PDP scheme, as follows:

A response is called homomorphic verifiable response in data possession protocol, if given two responses θi and θj for two challenges Qi and Qj from two CSPs, there exists an efficient algorithm to combine them into a response θ corresponding to the sum of the challenges Qi uQj.

D. Fragment Structure of CPDP

We propose a fragment structure of our data possession scheme based on the above-mentioned model as shown in Figure 2, which has following characters: 1) a file is split into n × s sectors and each block (s sectors) corresponds to a tag, so that the storage of the signature tags can be reduced with the order of s; 2) the verifier can check the integrity of a file by random sampling approach, which is a matter of the utmost importance for large or huge files; and 3) this structure relies on the homomorphic properties to aggregate the data and tags into a constant size response, which minimizes network communication overheads. The above structure, considered as a common representation for some of the existing schemes, can be converted to MAC-based, ECC or RSA schemes. By using BLS signatures and random oracle model, it is easy to design a practical data possession scheme with the shortest homomorphic verifiable responses for public verifiability. This structure also creates some favorable conditions for the architecture of CSPs.

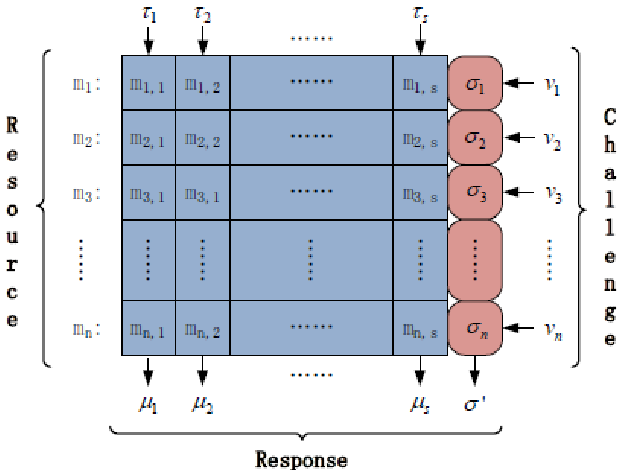

Figure 2: The fragment structure of CPDP model

E. Hash Index Hierarchy

A representative architecture for data storage in distributed is illustrated as follows: this architecture is a hierarchical structure H on 3 layers to represent the relationships among all blocks for stored resources. Three layers are as follows:

- **First-Layer (Express Layer):** It offers an abstract representation of the stored resources;
- **Second-Layer (Service Layer):** It immediately offers and manages cloud storage services;
- **Third-Layer (Storage Layer):** It practicably realizes data storage on many physical devices

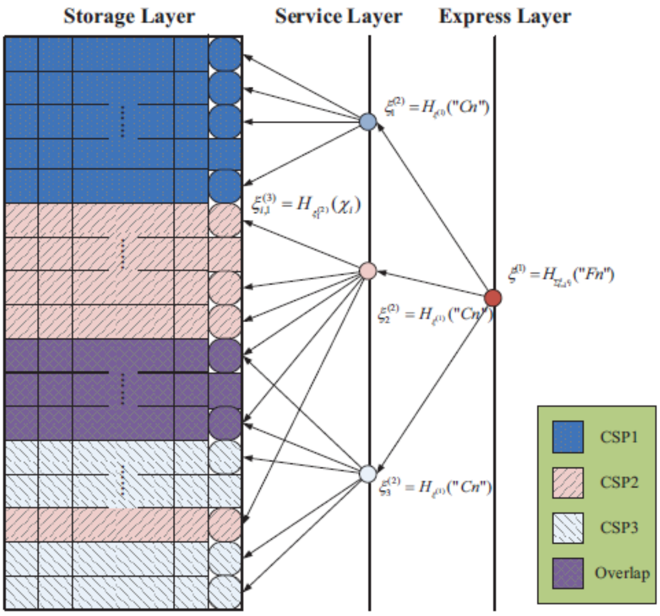

Figure 3: Index-hash hierarchy of CPDP model

Figure 3 shows index hash hierarchy of our model. This kind of architecture is a nature representation of the file storage. We make use of this simple hierarchy to organize many CSP services, which involve private clouds or public clouds, by shading the differences between these clouds. In this architecture, the resources in Express Layer are split and stored into

3 CSPs in Service Layer. Each CSP fragments and stores the assigned data into the cloud storage servers in Storage Layer. We follow the logical order of the data blocks to organize the cloud Storage Layer. Moreover, this proposed architecture could provide some special functions for data storage and management.

IV. CONCLUSION

In this paper, we proposed the scheme of optimal cooperative provable data possession and its distributed cloud storage to support the qualities of the services provides. In this work, we consider and maintains the existence of multiple cloud service providers to the cooperatively stores and it's also maintain the clients data in safe and security. We presented the scheme based on homomorphic verifiable response and hash index hierarchy. The security of our scheme is based on the multi- prover zero-knowledge proof performance optimization mechanisms for our scheme. In particularly, increasing the efficiency for our proposed scheme and minimize the system, which can satisfy completeness, knowledge soundness, and zero-knowledge properties.

REFERENCES

[1] B. Sotomayor, R. S. Montero, I. M. Llorente, and I. T. Foster, "Virtual infrastructure management in private and hybrid clouds," IEEE Internet Computing, vol. 13, no. 5, pp. 14–22, 2009.
[2] G. Ateniese, R. C. Burns, R. Curtmola, J. Herring, L. Kissner, Z. N. J. Peterson, and D. X. Song, "Provable data possession at untrusted stores," in ACM Conference on Computer and Communications Security, P. Ning, S. D. C. di Vimercati, and P. F. Syverson, Eds. ACM, 2007, pp. 598–609.
[3] C.C.Erway, A.Ku¨pc¸u¨, C.Papamanthou, and R.Tamassia, "Dynamic provable data possession," in ACM Conference on Computer and Communications Security, E. Al-Shaer, S. Jha, and A. D. Keromytis, Eds. ACM, 2009, pp. 213–222.
[4] G. Ateniese, R. D. Pietro, L. V. Mancini, and G. Tsudik, "Scal- able and efficient provable data possession," in Proceedings of the 4th international conference on Security and privacy in communication netowrks, SecureComm, 2008, pp. 1–10.
[5] H. Shacham and B. Waters, "Compact proofs of retrievabil- ity," in ASIACRYPT, ser. Lecture Notes in Computer Science, J. Pieprzyk, Ed., vol. 5350. Springer, 2008, pp. 90–107.
[6] H. Shacham and B. Waters, "Compact Proofs of Retrievability," Proc. 14th Int‟ l Conf. Theory and Application of Cryptology and Information Security: Advances in Cryptology (ASIACRYPT ‟ 08), pp. 90-107, 2008.
[7] W. Jansen, "Authenticating Mobile Device User through Image Selection," in Data Security, 2004.
[8] Real User Corporation: Passfaces. www.passfaces.com

Experimental Study of the Fatigue Strength of Glass fiber epoxy and Chapstan E-Glass epoxy laminates

D. Pitchaiah[1], K. Lalithababu[2], Ch. Ramesh Babu[3]

[1](Department, Mechanical Engineering, Sri Mittapalli College Engineering, A.P. INDIA)
[2](Department, Mechanical Engineering, Sri Mittapalli College Engineering, A.P. INDIA)
[3](Department, Mechanical Engineering, Sri Mittapalli College Engineering, A.P. INDIA)

ABSTRACT: *The present project work is aimed at establishing certain mechanical properties while designing fiber reinforced components for engineering applications. This experiment played an important role in estimation of stiffness of the laminate which in turn helps the user of the testing to evaluate the stiffness of the laminate for further mathematical purposes. The evaluating elastic properties and estimating the flexural stiffness of the composite beam and from the analytical evaluation of flexural stiffness has been matched with the theoretical calculations. This loss in stiffness of composite laminate is due to inherent defects generally occurs during welding and curing of the reinforced component.*

This reduction in stiffness can further be improved by advanced manufacturing process such as compressor moulding and auto clave moulding and the results obtained from the analytical testing are used to calibrate the load transducers. The load transducer shows a linear response to the load from this is clearly evident that the testing could be able to generate the useful data for evaluating the fatigue failure behavior of the composites. This data acquisition load generates the digital of time verses voltage by converting this data into time verses voltage with suitable multiplying factors. The data acquisition system from standard manufacturer of model pci-207 which exactly meets requirements. A continuous plot of time verses load could be obtained. We can say that the required data can be generated as per expectations, which could be utilized to establish the fatigue failure behavior any kind of composite laminate. (1)

Keywords: *Fiber reinforced composite material Fatigue, Mechanical Properties, Tensile Test, and CATIA.*

I. INTRODUCTION

The laminated composite materials usage is increasing in all sorts of engineering applications due to high specific strength and stiffness. Fiber reinforced composite materials are selected for weight critical applications and these materials have good rating as per the fatigue failure is concerned. Present work is aimed to analyze the behavior of each laminate under the flexural fatigue test rig. Therefore here different types of composite materials are selected for test specimens. For this load transducer, the accuracy level required in transducer body is an important task. As selection of a transducer and work for its consistency is important consideration. Therefore a sensitive, consistently strong transducer to meet the axial tension-compression fatigue loading is required. (2)To provide dynamic sensibility to the transducer, foil type resistance strain gauges are used. The geometric shape of the load transducer is an important factor to be considered, to impart sufficient strain to the strain gauge, which in turn generates a noticeable signal with noticeable amplitude in the form of a voltage signal. The dynamic nature of loading could be read in the form of a signal is possible only with the iso-elastic type of strain gauges. In order to get the information after which it fails software is created which produces the waves depicting the response of the transducer to the loads applied on it. The present project work mainly is focusing on development of manufacturing process and establishing critical test procedures for the polymer reinforced composite materials to be used in certain engineering applications.

II. FATIGUE

The flexural fatigue failure in laminated composite materials is a very common failure mode in most of the FRP components. As reinforced polymers used in weight critical applications, often over designed to compensate fatigue failure lead to the increase in weight which in turn hampers the objective of designer. In this connection the investigation on flexural fatigue failure behaviour of laminate to be used in the component is very important. As standard equipment and test procedures are not available.(3)

2 .1 Fatigue

When a material is subjected to repeated stresses or loads, it fails below the yield stress. Such type of failure of a material is known as fatigue.

2.1.1 Characteristics of Fatigue

- In metals and alloys, the process starts with dislocation movement, eventually forming persistent slip bands that nucleate short cracks.
- Fatigue is a stochastic process, often showing considerable scatter even in controlled environments.
- The greater the applied stress range, the shorter the life.
- Fatigue life scatter tends to increase for longer fatigue lives.
- Damage is cumulative. Materials do not recover when rested.

- Fatigue life is influenced by a variety of factors, such as temperature, surface finish microstructure, presence of oxidizing or inert chemicals, residual stresses, contact, etc.

2.2 Flexural Fatigue

When a material is subjected to variable bending stresses or loads, it fails below the yield stress.

2.3 Fatigue Test Applications

Fatigue testing helps determine how a material or product design will perform under anticipated service conditions. Many fatigue tests repeat the application of loads by controlling stress that is repeated for millions of cycles. In many engineering applications, products or materials experience vibration or oscillatory forces so it's important to predict and prove fatigue life, or cycles to failure under loading conditions.

There are as many specialized fatigue testing protocols or test methods as there are products designed for fatigue applications. A few are supported as industry standard test methods but most designs are unique so machines are configured to match their needs. Metals and metal substitutes such as advanced composites are commonly used for fatigue resistant designs, so standards are more available. Low Cycle Fatigue (LCF) or strain controlled tests, High Cycle Fatigue (HCF) or load controlled tests, and even Random Spectrum tests are now common. Medical implants for orthopedic and intravascular use are also widely tested to FDA requirements.(4)

2.4 Mechanism of Fatigue Failure in Laminated Composites

"Composites are a combination of a reinforcement fiber in a polymer resin matrix, where the reinforcement has an aspect ratio that enables the transfer of load between fiber, and the fibers are chemically bonded to the resin matrix. This precise definition accounts for the attributes of composites as an engineering material and differentiates them from a lot of combined materials having a lesser degree of synergy between the individual components.

Cyclic deformation process in fiber-reinforced materials differs widely from those in homogenous isotropic materials. For example, crack nucleation plays a significant role in the latter; in the former, cracks and failure zones are often formed in the very first few cycles. In fact, there are often voids and defects in the material even before cycling begins. Secondly, fiber reinforced materials are characterized by a high degree of anisotropy; the ratio of longitudinal to transverse moduli varies from about 5 for glass fiber-polymers to about 25 for graphite or boron fiber-polymers. The stress field around a flaw in such a highly anisotropic medium is significantly different from one in isotropic material consequently, while homogeneous isotropic materials usually fail in fatigue by the nucleation of a crack which propagates in single mode, composite materials generally exhibit a variety of failure modes including matrix crazing or micro cracking, individual fiber failures resulting from statistically distributed flaw strengths, debonding, delamation, void growth etc. In addition, several of these failure modes are generally present at any given time prior to failure.

Further, failure mechanisms in the fiber are different from those in the matrix. It is well established, for example, the glass by itself does not exhibit dynamic fatigue failure but fails in ''static '' fatigue as a result of thermally activated stress corrosion reactions of water vapor at surface flaws. When glass fiber are enclosed in a polymer matrix, and subjected to cyclic loading, it is not clear whether there would be reactions at the entire glass polymer interface due to moisture absorption through the polymer layer, or whether matrix micro cracks, alone (resulting from cyclic failure), would provide a conduit for preferential attack by water vapor over a localized area on the fibers at the crack front leading to further crack growth and eventual fatigue failure of the composite.(5) From this description it is clearly evident that the fatigue life of composite laminate is influenced by many factors. The degree of significance of the above mentioned factors cannot be established with confidence. This present work is aimed at establishing a suitable test procedure for the fatigue life characteristics with a low cost test rig to meet the real time design requirements. The features of the test rig are explained in following script.

As the test proceeds for so many number of load cycles (is of order 10^6 cycles) the generated from dynamic transducer cannot record manually. Then the signal conditioning system coupled with analog to digital conversion electronic circuit and the data logging software incorporated in the test rig. This logged data can be analyzed to establish the failure behavior and fatigue life characteristics of the composite laminates. This method of testing can be utilized for fatigue applications.

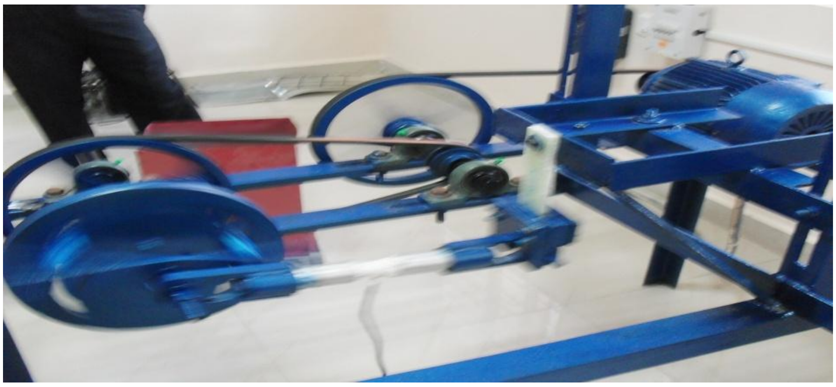

Fig. 2.1 Schematic Diagram of Fatigue Test Rig

The Bending fatigue test rig is capable of simulating bending fatigue load of 0 to 1000N on the test coupon at a frequency of 94 cycles per minute. The king pin is assembled to the dovetail mechanism which could be fixed at desired eccentricity. That provides desired bending force on the specimen.(6)

2.5.1 Important Components of Test Rig

i) Load cell
ii) Specimen holding beam
iii) Dovetail assembly
iv) Induction motor
v) Adjustable columns(Sliding)
vi) Electronic circuit(Signal Conditioning System)
vii) Data acquisition software
viii) Connector from the electronic circuit to the computer.
Printer(7)

2.5.2 Working Principle of Test Rig

The schematic diagram of test rig as shown in Fig. 3.2. is self explanatory. The hinge eccentricity from the center of the crank is directly proportional to the deflection of the composite specimen. And this deflection resisting force is experienced by the linkage which is equipped with strain measurement. (8)

The strain gauge bonded to the linkage (load cell) elongates and contracts along with the load cell which in turn imbalances the balanced bridge circuit connected to the strain gauge.

The output voltage of the bridge circuit is directly proportional to the deflection load of the composite specimen. As crank rotates with the constant rpm of 94 the strain measuring system develops voltage proportional to the degree of deflection. The voltage waveform is a pure sine wave. The cyclic load applied to the composite specimen generates a fatigue crack at the fixed end A from the Fig. 2.2.

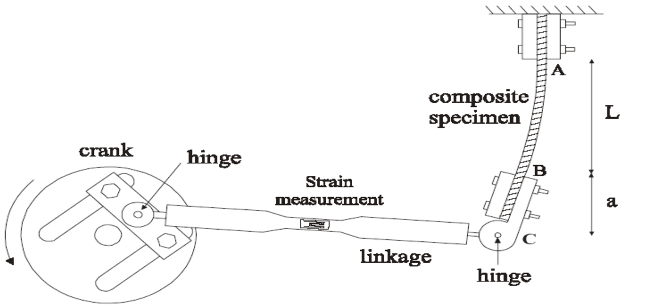

Fig.2.2 Schematic line diagram of Hinge Eccentricity, Load Cell and Specimen Holding Arrangement

Which in turn reduces the stiffness of the composite specimen and that is been clearly reflected on the voltage output from the strain measuring bridge circuit. The amplitude of wave form decreases as the damage progresses in the due course as the cyclic loading proceeds from 0 cycles to n number of cycles. This diminishing wave form reveals the health of the laminate as the time progresses. The recording of data in digital form could lead to analyze the fatigue damage pattern accurately. (9)

3.5.3 Specifications of the Test Rig

Bending load capacity --- 0 to 1000N
Frequency --- 1.57 to 10 RPS
Specimen specifications --- 200x40x6 mm
Eccentricity --- 0 to 200 mm

III. LOAD CELL

Introduction: Load cell is a very important component which senses load and delivers a voltage analog signal, which is proportional to the intensity of load. This consists of a metallic body designed to meet the requirements of the working load range, generally it is made of aluminum alloy. The foil type strain gages are fixed to the body of the load cell. When the body of the load cell is subjected to load, the strain induced is transmitted to the strain gage. Dynamic load sensor (LOAD CELL) is important component of the test rig.(10)

3.1 Selection of a Transducer

The selection of the correct load transducer is followed by the following steps:

1. Material selection.
2. Proposing geometric models.
   - High sensitive type
   - Medium sensitive type

3.1.1 Material Selection

The material selection is based on the elastic property that is young's modulus. This should be capable of providing sufficient elastic strain for a given load application range. As per the present load application range of 0-1000 N the material selected for this application is an aluminum alloy of Young's modulus 70 GPA.

a. High Sensitive Type Load Cells

Ring type load cell: The ring type load cell body is made of Aluminum. This is proposed in view of simulating more strain in the segments of hollow cylindrical segments, when the body is subjected to tensile and compressive stress. The ring type load cell is furnished in Fig. 4.1. The ring portion of the load cell body is first part of the body to undergo strain by virtue of changing its shape, which is a perfect circular to oval shape. (11)When the load cell is subjected to tensile load, the inner portion of the body is subjected to tensile strain and the outer portion is subjected to compressive strain. This is proposed in the view of gaining strong signal from the bridge circuit.

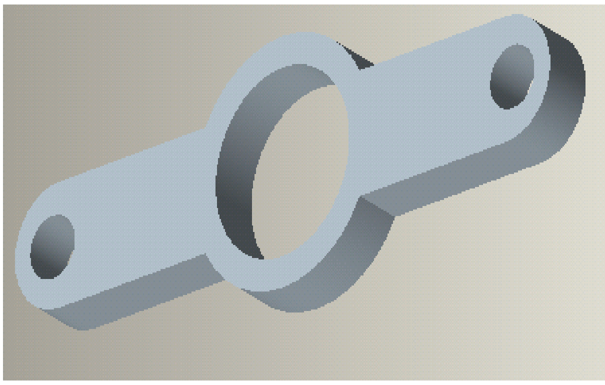

Fig. 3.1 Ring Type Load Cell

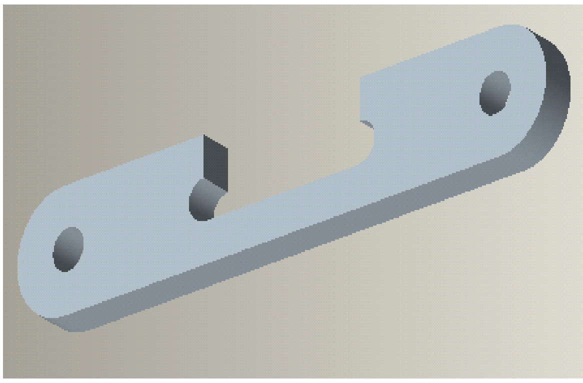

Fig. 3.2 C-Type Load Cell

"C" type load cell: The C type load cell is supposed to be strained in the thinner portion of the body.

b. Medium Sensitive Type Load Cells

H-Type Load Cell: "H" type of load cell body is proposed to meet the dynamic loading situation of the flexural fatigue test rig.

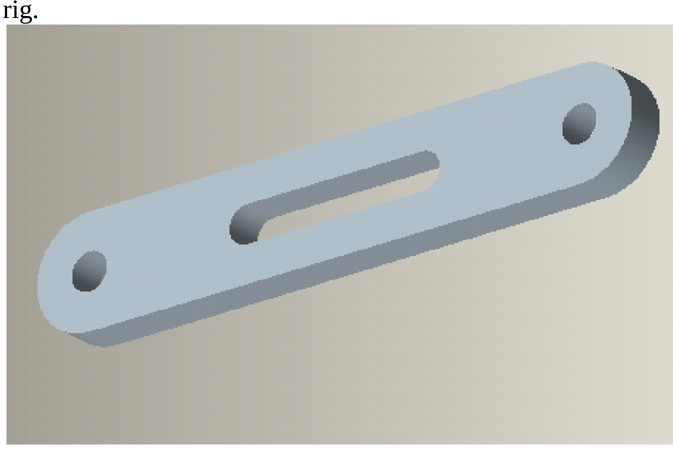

Fig. 3.3 H-Type Load Cell

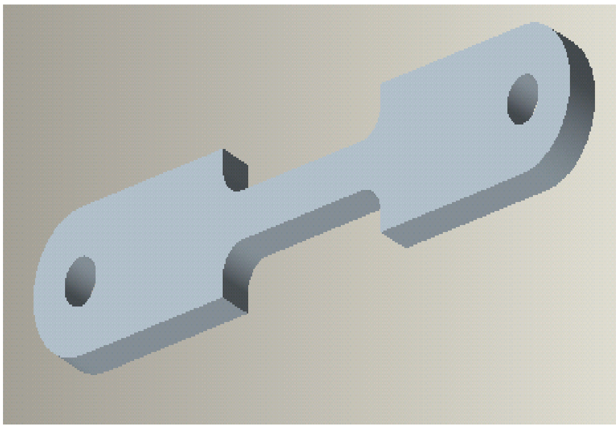

Fig. 3.4 I-Type Load Cell

"I" Type Load Cell:"I" type load cell having the thinnest gauge portion among the proposed load cell body models.

Pillar Type Load Cell: Among the load cell bodies proposed are observed carefully, and then the cylindrical gauge portion is proposed in view of achieving same strain on the gage bonding area of the load cell body.

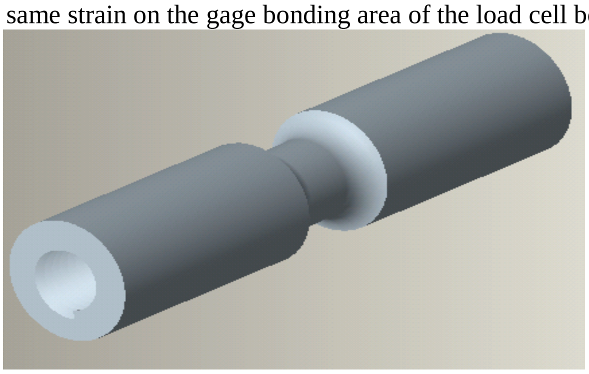

Fig. 3.5 Pillar Type Load Cell

IV. ELECTRONIC CIRCUIT

4. Introduction: The electronic circuits are also very important a component of system and this are capable of amplifying the analog signal coming from the load cell and digitizes it to have provision of storing the data accurately to analyzing the data regarding stiffness degradation behavior of the specimen.

4.1 Electronic Circuit for Signal Conditioning and Data Logging Systems

Dynamic load sensing is a mechanism, which senses the fluctuating loads with respect to time. A load cell (strain gage type) is a transducer, which senses the varying loads and changes its dimensions proportional to stress. The strain gage is incorporated in the bridge circuit and change in its resistance due to strain will unbalance the bridge. This unbalance voltage is amplified by the instrumentation amplifier. (12)

A real time application of dynamic load sensing which convert the analog voltage from instrumentation amplifier to digital voltage by an ADC. This digital voltage is fed to computer via USB port. The sensing element which is an electrical type load cell senses the strain. The strain gage is glued to the load cell. The resistance of the load cell is 350 ohms resistors. This bridge is excited by the 10volts DC supply. Under no load condition i.e., when strain gage is not strained the bridge is under balanced condition. When load is applied on the load cell, the dimensions of strain gage gets changed thereby its resistance is varied. The amount of strain applied on the load cell proportionally changes the resistance of the strain gage. This change in resistance causes the bridge to unbalance. (13)This unbalanced voltage is proportional to the load applied on the specimen.

In the first stage of amplification the gain has been limited to only 100 even though the capability of AD620AN is having a gain of 1000. This decision has been taken by carefully observing characteristics of the instrumentation amplifier to avoid unnecessary interference. The typical circuit to the signal conditioning system is shown in following Fig. 5.1.

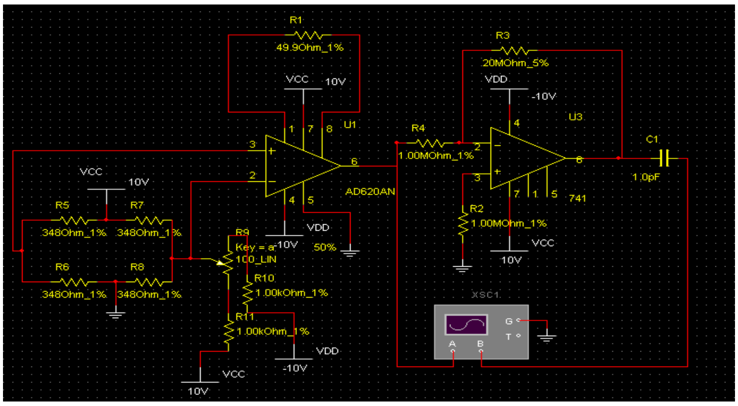

Fig. 4.1 Signal Conditioning

V. EXPERIMENTATION

5. Introduction to Flexural Fatigue Experimentation

The present experimentation is aimed to understand the flexural fatigue behavior under high cycle fatigue conditions of Glass Fiber Epoxy, Chapsten E-Glass Epoxy and Glass Fiber Polyester Epoxy laminates. Before getting into the experimentation work, the evaluation of mechanical properties of glass fiber epoxy laminates is very important.

A laminates of 200mm length, 40mm width and 6mm thickness were prepared. And from this laminates tensile tests were conducted for calculating the starting load on specimens for conducting fatigue test.

5.1 Loading Criteria for Flexural Fatigue Analysis of Glass Fiber Epoxy Laminates

For simulating high cycle flexural fatigue on test coupons, the calculations were made to estimate the bending loads considered to simulate stresses of the order of 50% of maximum tensile strength. To estimate the bending load, tensile tests were carried out on laminates. The tensile test results of specimens of Glass fiber epoxy, Chapsten E-glass epoxy and Glass fiber polyester epoxy are furnished in table No. 6.1.

And the corresponding bending loads to be applied are calculated with reference to the beam bending equation.

$$M/I = F/Y$$

The specimen is fixed to fatigue testing rig in cantilever mode, then the Maximum bending moment M = WL where W is the bending load applied on the specimen. The distance from the neutral axis to the surface of specimen is Y, which is equal to half the thickness of the specimen.

$$Y = t/2$$

Moment of Inertia of the specimen $I = bh^3/12$ and

Bending stresses induced in the specimen

$$F = 1/2(\text{Ultimate Tensile strength of the specimen})$$

From the above theory, bending load for each specimen is obtained.

a) Metallic Mould

The mould is made of MS material. To prevent the leakage of resin, four dams were fixed through nuts and bolts on a 10 mm thick MS plate which is machined by facing operation on lathe machine. The mould cavity area is 300X300 mm^2.

The mould with above specifications as shown in the figure 6.1. The required pressure is applied through pressure plate by tightening the nuts and bolts, the arrangement of which is shown in figure 6.2.

Fig. 5.1 Representation of Mould

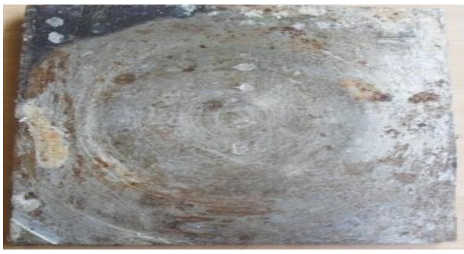

Fig. 5.2 Representation of Pressure Plate

b) Pressure Plate

20 mm thick MS pressure plate with flat turned surface finish ensuring perfect flatness is used in order to prevent crippling and flexing due to compressive forces produced due to the top cover plate.

With the above mentioned precautions a laminate, of good quality can be made as shown in figure 6.3. From this laminate the test coupons are cut with required specifications which have already been discussed.

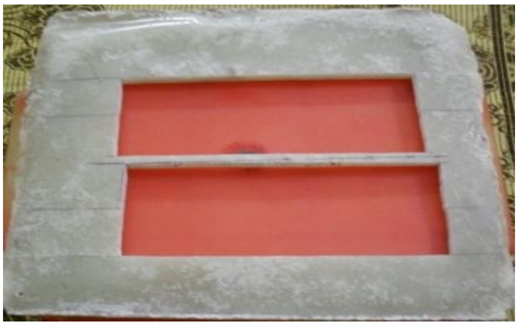

Fig 5.3 Laminate Moulded from the Metallic Mould by Compression Moulding Technique

5.2 Tensile Tests

Tensile tests are performed on the specimens and the tabulated values are furnished in table 6.1. The specifications of the test specimen are 200mm length, 6mm thickness and 40mm width. Following figures related to tensile tests conducted on various specimens. The figure represents the tensile test in progress. The figures to furnish below are specimens subjected to tensile test.

Specimens	Max Tensile strength(MPa)
Glass fiber epoxy	358
Chapsten E-glass epoxy	207
Glass fiber polyester epoxy	74.5

Table 5.1 Tensile Test Results

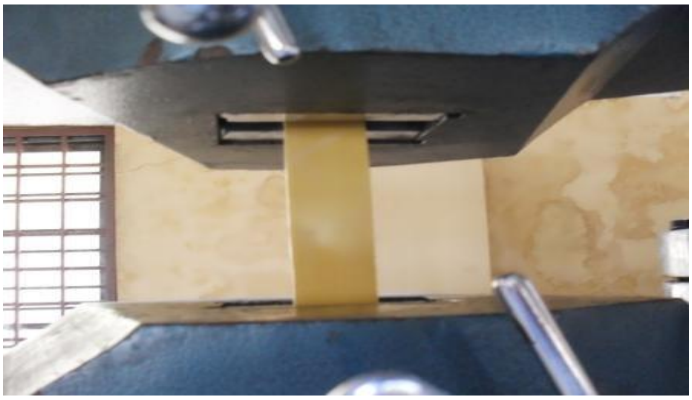

Fig. 5.4 Tensile Test in Process

Fig. 5.5 Tensile Test Specimens of Glass Fiber Epoxy, Chapsten E-Glass Epoxy and Glass Fiber Polyester Epoxy



Fig. 5.6 Glass Fiber Epoxy Specimen after Tensile Test Fig. 5.7 Chapsten E-Glass Epoxy Specimen after Tensile Test
Fig. 5.8 Glass Fiber Polyester Epoxy Specimen after Tensile Test

VI. RESULTS AND DISCUSSIONS

6. Introduction

The present project work is aimed at establishing certain mechanical properties while designing fiber reinforced components for engineering applications. This experiment played an important role in estimation of stiffness of the laminate which in turn helps the user of the testing to evaluate the stiffness of the laminate for further mathematical purposes. The evaluating elastic properties and estimating the flexural stiffness of the composite beam and from the analytical evaluation of flexural stiffness has been matched with the theoretical calculations. This loss in stiffness of composite laminate is due to inherent defects generally occurs during welding and curing of the reinforced component.

This reduction in stiffness can further be improved by advanced manufacturing process such as compressor moulding and auto clave moulding and the results obtained from the analytical testing are used to calibrate the load transducers. The load transducer shows a linear response to the load from this is clearly evident that the testing could be able to generate the useful data for evaluating the fatigue failure behavior of the composites. This data acquisition load generates the digital of time verses voltage by converting this data into time verses voltage with suitable multiplying factors. The data acquisition system from standard manufacturer of model pci-207 which exactly meets requirements.

A continuous plot of time verses load could be obtained. We can say that the required data can be generated as per expectations, which could be utilized to establish the fatigue failure behavior any kind of composite laminate.

6.1 Flexural Fatigue Failure Behaviour of Glass Fiber Epoxy Laminate

Flexural fatigue failure behavior of laminates exhibits stiffness decay with respect to number cycles of load application. In this work ORIGIN LAB curve fitting tool is used to plot the data, number of cycles verses instantaneous maximum bending load within the cycle. The total scheme of experimentation is conducted at constant amplitude of bending. This phenomenon of bending load for yielding constant deflection is also known as stiffness. The test specimen used is shown in Fig. 7.1.

Fig. 6.1 Glass Fiber Epoxy Test Specimen

From the data logging system, the converted data is load applied on the specimen and number of cycles is given in the table 7.1. This data is used in plotting stiffness degradation curves.

Table 6.1 Stiffness Degradation Data of Glass Fiber Epoxy laminate

Number of Cycles	LOAD in NEWTONS	5096.22 5532.68	168.473 168.306	14894.6 15305.93	116.910 114.223
0	320.006	4981.61	164.48	15769.08	113.781
100.48	311.663	6055.49	163.633	16552.51	113.09
219.8	291.354	6305.12	163.08	17397.17	113.046
345.4	281.055	6355.36	162.17	18012.61	111.728
405.06	278.333	6466.83	160.97	18552.7	108.632
538.51	278.356	6531.2	160.5	19196.4	104.075
591.89	270.37	6590.86	157.48	19915.45	100.07
676.67	267.555	6626.97	157.167	21078.82	95.11
797.56	267.553	6653.66	154.957	22000.41	88.041
904.32	264.895	6686.63	152.7	22564.04	87.966
943.57	262.481	6714.89	152.586	23242.28	84.687
1029.92	242.97	6749.43	152.16	23831.03	83.902
1146.1	234.243	6772.98	150.94	24287.9	77.38
1890.28	226.802	6821.65	150.982	24689.82	73.771
2138.34	225.75	7380.57	149333	25170.24	70.9
2474.32	223.974	7567.4	148.687	25481.1	68.147
2701.97	221.938	7892.4	145.935	25865.75	67.971
2739.65	219.28	8262.91	145.701	25906.57	65.935
2797.74	206.40	8700.94	142.19	26602.08	65.77
2824.43	202.321	9132.7	140.777	27245.78	65.16
2964.16	198.327	9679.05	137.973	28164.23	63.473
3058.36	195.506	9964.8	137.25	29088.96	62.413
3110.17	193.661	10489.17	133.216	29665.15	62.03
3303.28	185.08	11366.8	132.632	30506.67	60.127
3496.39	182.853	11999.51	130.713		
4114.97	179.851	12767.24	126.624		
4491.77	177.786	13547.53	125.163		

The data obtained from the experiments is plotted in plotted in Fig. 7.2. Results obtained reveal that the nature of behavior of the material is revealing exponential decay in its mechanical properties due to fatigue. This type of plotting is normally known as “Stiffness Degradation Curve plotting”. From the figure it is clear that the bending load is dropped from 320N to 60.127N and attained pivoting state where further reduction in stiffness is not noticed. Pivoting state is noticed at 25,000cycles.

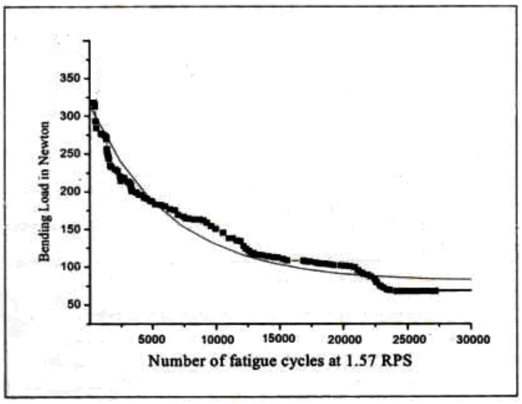

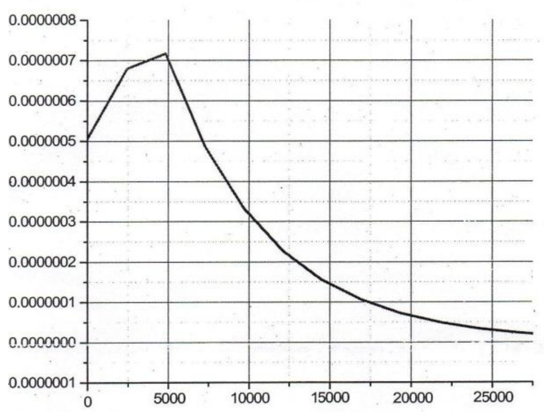

Fig. 6.2 Stiffness Degradation behaviour of Glass Fiber Epoxy laminate Number of Fatigue Cycles at 1.57 RPS for Glass Fiber Epoxy Laminate

Fig. 6.3 Second order differential curve of Glass Fiber Epoxy laminate derived from Fig.

7.2 Flexural Fatigue Failure Behaviour of Chapsten E-Glass Epoxy Laminate

The test specimen used is shown in Fig. 7.4.

Fig. 6.4 Chapsten E-Glass Epoxy Test Specimen

The Flexural fatigue analysis data obtained from the experiment for Chapsten E-glass epoxy laminate is given in table 7.2. And the stiffness degradation is plotted in Fig.7.5. From this figure it is observed that the bending load dropped from 318.764N to 27.416N. Compared to Glass fiber epoxy specimen stiffness degradation curve, it is observed that there is smooth reduction in stiffness. The stiffness at the pivoting state is 27.416N as per the experiment. The stiffness of the specimen at the pivoting state is 8.6% of the virgin specimen.

Table 7.2 Stiffness Degradation Data of Chapsten E-Glass Epoxy laminate

Number of Cycles	LOAD in NEWTONS
0	318.764
65.94	203.285
202.53	122.103
244.92	120.388
281.03	119.051
310.86	115.772
438.03	110.53
477.28	108.383
507.11	107.142
582.47	105.698
610.73	104.392
723.77	102.612
761.45	101.331
1339.21	98.353
1734.85	97.95
2391.11	97.62
2634.46	97.21
3367.65	96.73
4461.94	94.842
7353.88	79.787
7523.44	74.421
7656.89	71.113
8247.21	68.1
8597.32	65.6
8685.24	54.7
8859.51	47.73
8913.43	46.77
8962.47	45.356
9014.62	44.756
9452.74	43.9
9924.73	42.235
10732.22	41.766
11219.35	40.565
11763.48	39.96
12132.83	38.91
12764.03	38.565
13217.72	38.223
13741.35	37.881
14264.98	37.54
14788.61	37.2
18454.02	34.801
18977.65	34.46
19501.28	34.12
20024.91	33.775
20548.54	33.433
21072.17	33.091
21595.8	32.75
22119.43	32.406
22643.06	32.064
23166.69	31.722
23690.32	31.38
24213.95	31.04
24755.32	30.7
25296.69	30.354
25838.06	30.112
26379.43	29.67
26290.8	29.33
27462.17	28.985
28003.54	28.643
28544.91	28.3
29086.28	27.96

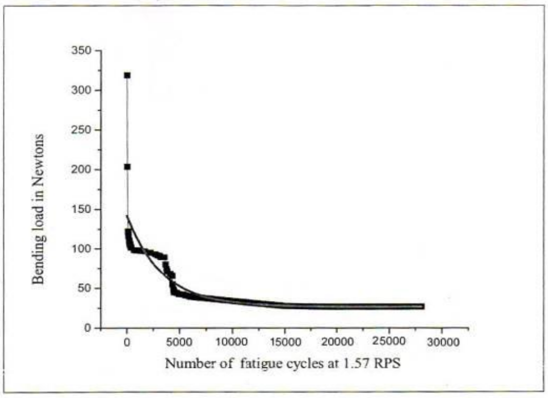

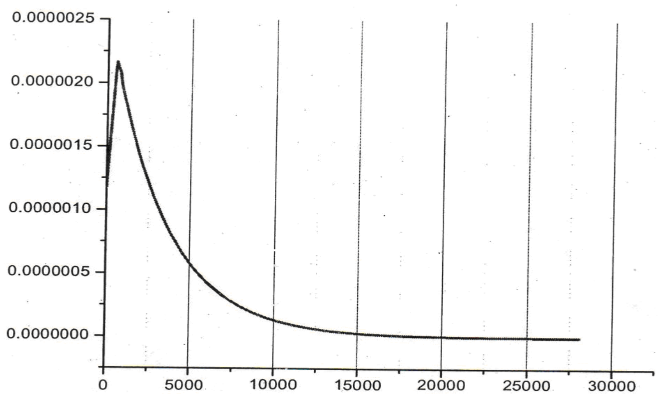

Fig. 6.5 Stiffness Degradation behaviour of Chapsten E-Glass Epoxy laminate Number of Fatigue Cycles at 1.57 RPS for Chapsten E-Glass Epoxy Laminate.

Fig. 6.6 second order differential curve of Chapsten E-Glass Epoxy laminate derived from Fig. 6.5.

The experiments carried out in the laminates of Glass Fiber Epoxy, Chapsten E-Glass Epoxy and Glass Fiber Polyester Epoxy clearly exhibited a variation in the residual load bearing capacity after pivoting state. The graphical representation in Fig. 6.7. The stiffness degradation process of each specimen under goes basically in three stages, in the first stage the stiffness reduction rate is very fast this is due to the top and bottom layers of the laminates are subjected to maximum strain which leads to the failure being the glass reinforcement is pure elastic in nature. In the second stage as the stress levels on the subsequent layers reduces as the distance from the neutral layer is continuously decreasing. In the third stage of the failure already broken fibers provides a cushioning effect and resist the free bending of the specimen hence the stiffness degradation tends to towards zero.

The results clearly establishes that the Glass Fiber Polyester Epoxy, exhibited very slow stiffness reduction rate when compared to the other specimens and the residual bending load bearing(residual stiffness) is also maximum i.e. 58.617N and the Stiffness retention after pivoting state is 73.26%. Hence it can be recommends that the Glass Fiber Polyester Epoxy material is best for fatigue critical applications.

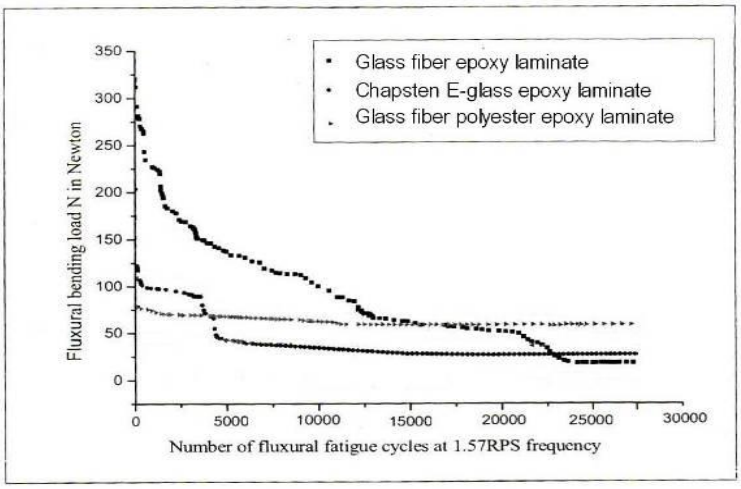

Fig. 6.7 Consolidated Flexural Fatigue Test Results of Glass Fiber Epoxy, Chapsten E-Glass Epoxy and Glass Fiber Polyester Epoxy laminates.

VII. CONCLUSION

From the experimental investigation:

1. Flexural fatigue failure behavior of Glass Fiber Polyester Epoxy laminate composite exhibited better results.
2. The results clearly establish that the Glass Fiber Polyester Epoxy laminate exhibited very slow stiffness reduction rate when compared to the other specimens.
3. The residual bending load (residual stiffness) is also maximum i.e. 58N and the Stiffness retention after pivoting state is 72.5% of the virgin specimen.
4. Hence it can be recommended that the Glass Fiber Polyester Epoxy laminate is good for flexural fatigue critical applications such as wind turbine blades, Air craft wing and auto motive leaf spring constructions.

REFERENCES

[1] Fatigue Calculations Over An Estimated Fatigue Limit A. Quesada, C. Álvarez-Caldas E. Olmeda J. L. San-Román June18-21, 2007
[2] Plastics Part Design: Low Cycle Fatigue Strength Of Glass-Fiber Reinforced Polyethylene Terephthalate (PET) BASF Corporation
[3] High-cycle Fatigue Strength of a Pultruded Composite Material C. Colombo, M.Guagliano, L. Vergani
[4] Formulation for Time-temperature Dependent Fatigue Strength of CFRP Laminates Yasushi Miyano, Junji Noda and Masayuki Nakada
[5] Mechanical Properties Of Composite Material Using Natural Rubber With Epoxy Resin Dr. Hani Aziz Ameen 9/3/2008
[6] Fatigue Strength Assessment Of A Short Fibre-Reinforced Plastic Based On The Energy Dissipation G. Meneghetti*, M. Quaresimin**, M. De Monte**
[7] Experimentally Investigation Effect Of Geometrical Cross- Section On Fatigue Strength Of Aluminum Alloy (6063) Ghazi S. Al-Marahleh and Khaleel Abushgair Received: July 19, 2010
[8] Fatigue and Ultrasonic Testing of Epoxy-Glass Composites M. Rojek, J. Stabik*, S. Sokół
[9] Mechanical Measurements by Thomas G.Beckwith, Roy D. Marangoni, John H. Lienhard Fifth edition an imprint of Addison Wesley Longman, Inc First ISE reprint 1999
[10] The Pressure and Strain Handbook, Vol.29, Omega Engineering.
[11] Fundamentals of Machine Component Design, 3rd Edition, Robert C. Juvinall Kurt M. Marshek.
[12] Mechanics of Materials, Fourth Edition, R.C. Hibbeler.
[13] http://efunda.com/designstandards/sensors/strain_gages/strain_gage_selection.cf
[14] http://www.vishay.com/brands/measurements_group/guide/guide.
[15] http://www.madgetech.com/pdf_File/bridge110_app_note.pdf

Improving Mechanical Properties of AL 7075 alloy by Equal Channel Angular Extrusion process

Mohan Reddy[1], Santhosh Kumar M[1], Venkata Ajay Kumar G[2]

1(Department of Mechanical Engineering,KSRM College of Engineering / JNT University, Annatapur, India)
2 (Department of Mechanical Engineering,Sri Venkateswara Institute of Science and Technology / JNT University, Annatapur, India)

ABSTRACT: *The influence of the microstructure and the tensile properties is investigated in specimens of ultrafine-grained materials processed by equal channel angular extrusion (ECAE) through route A, to refine grain size of 7075 AL alloy this was attempted at room temperature. Sub-grains/cells increases and the width of boundaries decrease while the cell/sub-grain size remains approximately constant as the number of passes increases. Yield stress and ultimate tensile stress reach a maximum after four passes. This study shows that severe plastic deformation has potential to significantly improve the mechanical properties of Al alloys. Static annealing experiments demonstrated that the extensive grain growth occurs at can be achieved after the age hardened treatment before that solution heat treatment at 480°C for 1 hour followed by age hardening at 177°C for 8 hours. Microstructure evolution during repetitive equal-channel angular extrusion (ECAE) of Al 7075 alloy with Φ=120◦ die and the outer arc ψ=50◦ was evaluated by optical microscopy.*

Keywords: *Aluminum alloy, Equal channel angular extrusion, Mechanical Properties, Microstructure analysis, Severe plastic deformation*

I. INTRODUCTION

Nanostructured (NC) and ultrafine grained (UFG) materials, defined, respectively, as polycrystalline materials with a grain size below ~100 nm and ~1µm, have been extensively studied over the past two decades because of their enhanced properties [1–3]. Generally, these materials exhibit a high strength but only limited ductility [4]. Recently, different approaches have been considered in an attempt to overcome this limitation [4, 5]. The grain size produced by conventional methods is greater than 1µm.The deformation mechanism of UFG metals is often considered to be governed not only by the activity of lattice dislocations, but also by mechanisms such as grain rotation and grain boundary sliding, especially in equiaxed microstructures [6]. There are also some methods for producing ultrafine-grained structure even to the size of nanometer, such as gas condensation and high-energy ball milling. These methods are difficult to produce in bulk form, which then limits the application in industries. Many researchers have shown that sub-micrometer grained (SMG) materials can be obtained after ECAP deformation. Although SMG materials can be produced by ECAP, the deformation mechanism and microstructure evolution in ECAP is still not clear. The SMG structure formed by SPD is characterized by mixture of both high angle boundaries (HABs) and low angle boundaries (LABs) (Bay et al. 1992a). The boundaries formed by SPD have been described as non-equilibrium boundaries. Which are associated with high internal stresses (Furukawa et at 1996a). The SMG structure of aluminum alloy formed by SPD has been suggested as a result of extended recovery (Humphrevs et al. 1995). In general, the microstructure developed by SPD is not well-defined ultrafine-grained structure for it doesn't consist of grains enclosed by HABs. Thus further annealing is required to construct a microstructure consists of fine grains enclosed by HABs. The present study deals with ECAE were used to deform the material and obtain ultrafine-grained structure. One important goal of this research is to advance our understanding of the deformation mechanism in ECAE, and to identify the key parameters that affect the microstructure evolution. The material is extruded up to two passes by route A. The detailed microscopic characterization was carried out to obtain comprehensive and quantitative information about the structure developed by various ECAP processes to achieve the goal.

II. EXPERIMENTAL MATERIAL AND PROCEDURES

2.1 Experimental Material

All the experiments were conducted using AL 7075 alloy. The material was produced in the form of ingot with a diameter of 14.9mm and a length of 50mm. The ECAE process uses a die, material for extrusion and plunger attached to the universal testing machine for the extrusion process.

2.2 Methodology

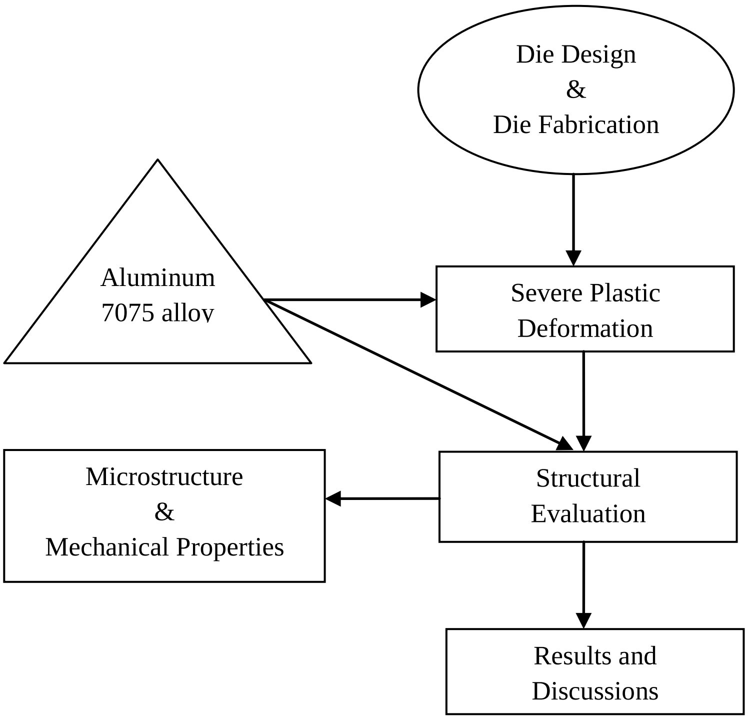

Fig. 1 Methodology

2.3 ECAE Die

The ECAE die contains two channels, equal in cross-section, intersecting at an angle near the center of the die. The test sample is machined to fit within these channels and it is pressed through the die using a plunger. Die material was mild steel and the plunger was EN8 steel (normalized condition), the normalizing of EN8 steel was carried out by heating above the upper-critical-temperature line followed by cooling in still air to room temperature. The purpose of normalizing is to produce harder and stronger steel than annealing, so that for some applications normalizing may be a final heat treatment. Normalizing may also be used to improve mach inability, modify and refine cast dendritic structures, and refine the grain and homogenize the microstructure in order to improve the response in hardening operations. The geometry of this die provides that the material is deformed by simple shear at ideal, frictionless, conditions. The cross section of the specimen remains about equal before and after a processing step, thus it is possible to subject one specimen several times to ECAP in order to reach highest degrees of plastic deformation.

Fig. 2.1 ECAE Die

A circular cross section of the channel provides the possibility of a materials processing at different routes that are distinguished by their different combinations of sample rotation around the channel axes between consecutive processing steps. Here route A is used for the extrusion of the material and four billets are prepared for four experiments i.e., basic material, one pass, two and three passes. The die angle 120° was used in this study. The outer arc (Ψ) of the 120° die is 50°. The dimension of the channel cross section in ECAE die is 120x120mm. According to equation (1), the strain per pass of the 120° die is 0.67. In considering both Φ and ψ, the equivalent strain of ECAE can be calculated by (Iahashi et al. 1996).

$$\epsilon_N = N \frac{\{2\cot(\Phi/2+\psi/2)+\psi\operatorname{cosec}(\Phi/2+\psi/2)\}}{\sqrt{3}} \quad \text{------ (1)}$$

III. EXPERIMENTAL RESULTS

3.1 Microstructural Characteristics

Al 7075 was solution treated at 480°C for 1 hour and then followed by water quenching.

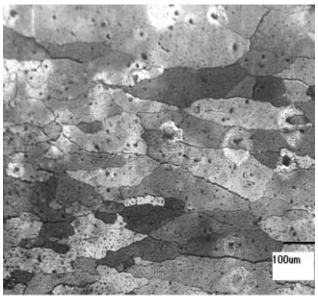

Fig 3.1.a

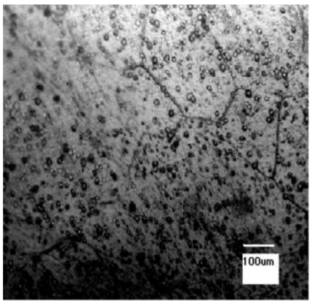

Fig 3.1.b

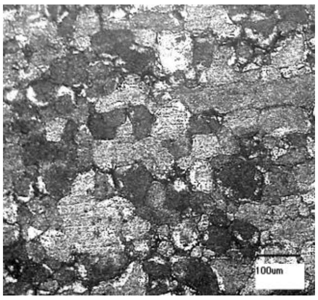

Fig 3.1.c

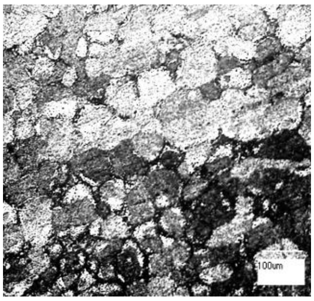

Fig 3.1.d

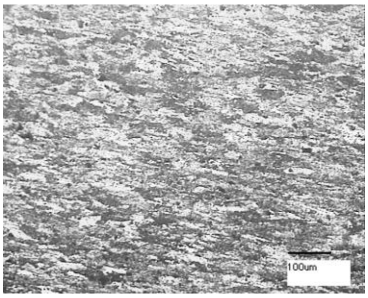

Fig 3.1.e

Fig 3.1a, optical micrograph of Al 7075, 100X, Keller's reagent. After solution heat treated at 480°C for 1 hour quenched with water, fusion voids, (black area) and agglomeration of insoluble phases (dark gray). Fig 3.1b, Al 7075 was solution heat treated at 480°C, and then artificial aging at 177°C for 8 hours, optical micrograph of Al 7075, 400X, solution treated at 480°C quenched to the water, eutectic melting temperature was exceeded during solution heat treatment, fine voids (black areas), and Keller's reagent. Al 7075 solution treated at 480°C for 1 hour and then aged at 177°C for 8 hours, which was processed through ECAP route A. Fig 3.1c, optical micrograph of Al 7075 extruded, solution heat treated, and artificially aged, fine particles of MgZn2 (dark), 100X, ECAP 1st pass, Keller's reagent. Fig 3.1d, optical micrograph of Al 7075 under ECAP processing, particles are insoluble (Fe, Mn) Al_6 (dark gray), 100X, ECAP 2nd pass Keller's reagent. Fig 3.1e, optical micrograph of Al 7075, under route A for ECAP processing 3rd pass, the fine particles of $MgZn_2$ (dark), the insoluble particles of $FeAl_3$ (light gray) 100X, ECAP 3rd pass Keller's reagent.

3.2 Tensile properties

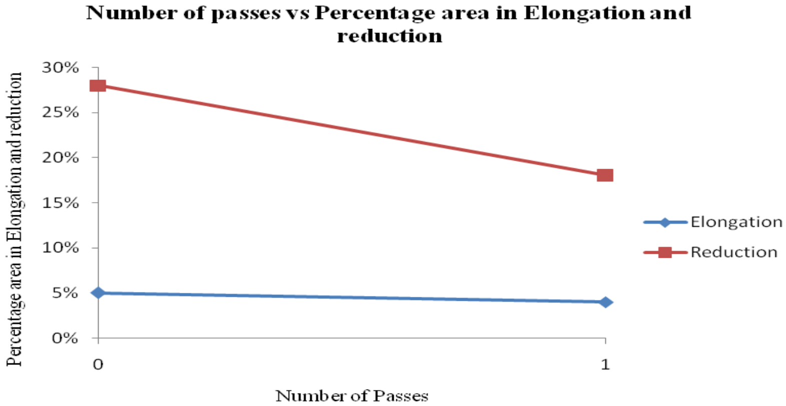

Fig. 3.2 Number of Passes Vs Percentage area in Elongation and reduction

For the Al 7075 alloy as received condition Elongation to failure occurs at 5% and it decrease to 4% after single pass, the area of reduction of 7075 alloy as received condition 28% and it reduced to 18% after single pass. It shows that percentage of area of reduction decreases drastically, while we increasing number of ECAP passes. The ultimate tensile strenth increases from 329 MPa as received condition for ultrafine grained Al 7075 alloy, it reaches about 487 MPa after single pass.

3.3 Hardness test

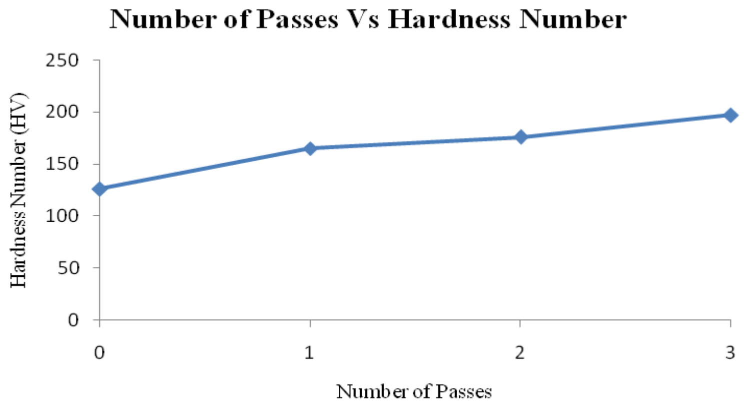

Fig 3.3 Number of passes vs Hardness number

The Al 7075 alloy hardness is tremendously increased while we increasing the number of ECAE passes, Al 7075 alloy has achieved high hardness after the third pass is about 197 HV.

IV. CONCLUSION

It was found two passes of ECAE are required for the formation of ultra fine grained structure in Al 7075 alloy. The resulting microstructure has been widely investigated by optical microscopy, putting in evidence the grain structure and precipitates distribution differences originated by the process. Tensile tests show the increase of strength from one pass to another pass of the material. Hardness is also increased by increasing the number of passes due to the fine grain structure; this survey gives clear prediction that tremendous increase of hardness has achieved compare to base metal.

REFERENCES

Journal Papers:

[1] Segal V. M., Reznikov V. I., Drobyshevskiy A. E., Kopylov V. I.,Plastic working of metals by simple shear, *Russian Metallurgy (Metally), 1, 1981, 99-105.*

[2] Iwanishi Y, Horita Z, Nemoto M, Langdon T, *Acta Mater., 46, 1998, 3317.*

[3] Aida T., Matsuki K., Horita Z. and Langdon T. G, Estimating the equivalent strain in equal-channel angular pressing. *Scripta Mater.,2001, 44, 575.*

[4] Valiev RZ, Alexandrov IV, Zhu YT, Lowe TC. J *Mater Res 2002; 17, 5.*

[5] Wang YM, Ma E., *Acta Mater 2004; 52, 1699.*

Theses:

[6] Dalla Torre FH, *Microstructure and deformation mechanism of nanocrystalline Ni synthesized by three different methods*.doctoral diss., Switzerland; 2003

International Journal of Modern Engineering Research (IJMER)
www.ijmer.com Vol. 3, Issue. 5, Sep - Oct. 2013 pp-2717-2725 ISSN: 2249-6645

Finite Element Analysis of Obround Pressure Vessels

Manish M. Utagikar[1], Prof. S.B. Naik[2]

[1]*M.E. Student, Dept. of Mechanical Engg, Walchand Institute of Technology, Solapur, India*
[2]*Professor, Dept. of Mechanical Engg, Walchand Institute of Technology, Solapur, India*

ABSTRACT: *This paper presents the work carried out for determination of stresses in an open ended pressure vessel of obround shape. In some situations, due to the limited space available, exit pipes are made of elliptical or obround shape. In this study, the stresses in the obround pressure vessel are determined using finite element method. The material of the vessel is aluminum alloy. Internal pressure is applied to the vessel. Software 'ANSYS' is used for modeling & analysis purpose. Considering the symmetry about both axes, only quarter model is prepared. Firstly analysis of circular pressure vessel is done. The results of the circular vessel are validated by analytical solution. Then using the same type of element & mesh density, analysis of obround pressure vessel is done. During the study, different parameters were varied & their effect on the stresses was observed.*

Keywords: *Obround Pressure Vessel, Finite element analysis, ANSYS*

I. INTRODUCTION TO PRESSURE VESSELS

Pressure vessels are a commonly used device in engineering. Cylindrical or spherical pressure vessels (e.g., hydraulic cylinders, gun barrels, pipes, boilers and tanks) are commonly used in industry to carry both liquids and gases under pressure. When the pressure vessel is exposed to this pressure, the material comprising the vessel is subjected to pressure loading, and hence stresses, from all directions. The normal stresses resulting from this pressure are functions of the radius of the element under consideration, the shape of the pressure vessel (i.e., circular, obround or elliptical) as well as the applied pressure.

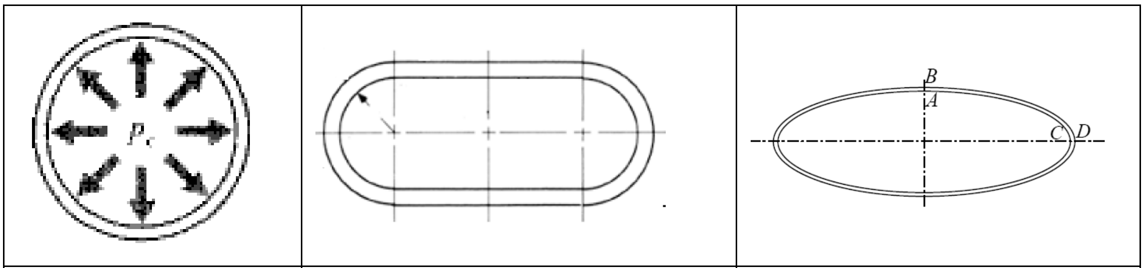

Circular Pressure Vessel	Obround Pressure Vessel	Elliptical Pressure Vessel

Figure.1 Types of Pressure Vessels

II. PROBLEM DEFINITION:

Analysis of a circular pressure vessel will be done for a certain pressure. Hoop stresses will be determined for this geometry. Analytical solution of the same will be determined. Comparison of the results will be done. To maintain the flow rate, the area of flow is kept same & shape is changed to obround & the stress analysis is done for this vessel. Following data will be used for the analysis work.

Inner Diameter (D) = 200 mm, Thickness of vessel (t) = 2.5 mm
Pressure applied (P) = 0.1 MPa
Material Properties: Material selected is Aluminum alloy used in aircraft.

Table.1 Material Properties

Young's Modulus	1.03458 e5 MPa
Poisson's Ratio	0.33

III. ANALYTICAL SOLUTION

Analytical solution is determined for circular pressure vessel using Formula,
Hoop Stress = (P x R) / t = (0.1 x 100) / 2.5 = 4 MPa

IV. FINITE ELEMENT ANALYSIS

Circular Pressure Vessel: Taking the advantage of symmetry about both the axes, a quarter model is prepared & the analysis is done using Finite Element Method based software ANSYS.

Meshing: For meshing quadrilateral elements with midside nodes are used. The details of this element are as below.

PLANE82: It is a higher order version of the 2-D, four-node element PLANE42. It provides more accurate results for mixed (quadrilateral-triangular) automatic meshes and can tolerate irregular shapes without as much loss of accuracy. The 8-node elements have compatible displacement shapes and are well suited to model curved boundaries.

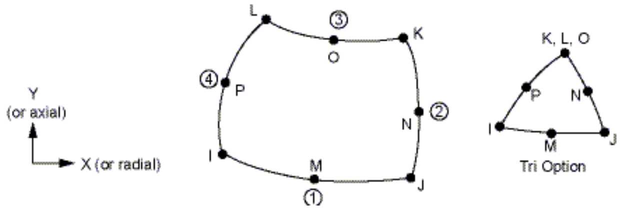

Figure.2 Structure of PLANE82 element

The 8-node element is defined by eight nodes having two degrees of freedom at each node: translations in the nodal x and y directions. The element may be used as a plane element or as an axi-symmetric element. The element has plasticity, creep, swelling, stress stiffening, large deflection, and large strain capabilities.

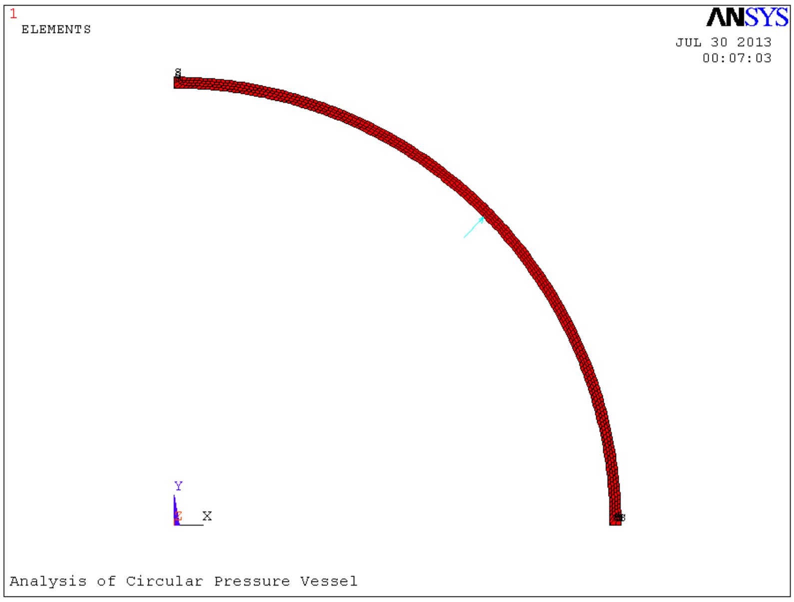

Figure.3 Circular Pressure vessel with load condition & boundary condition

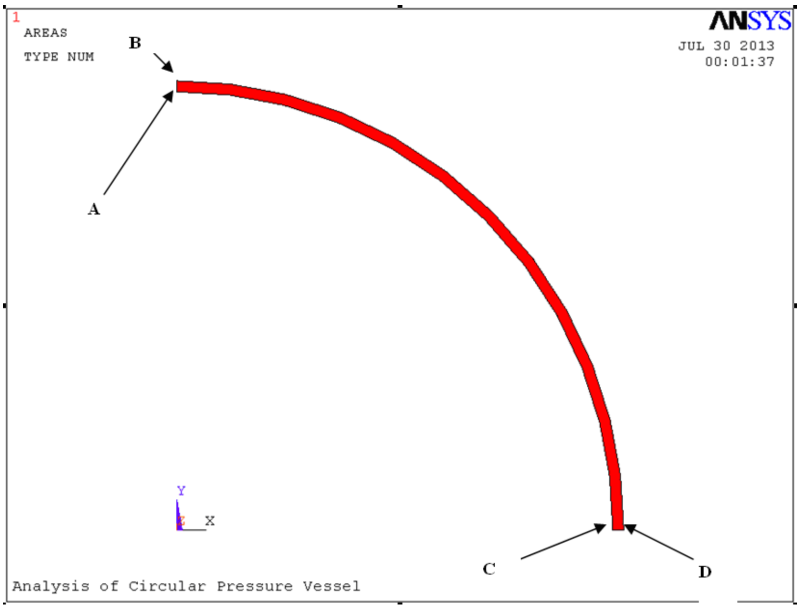

Figure.4 Location of Points A, B, C & D

The various points of interest are as shown in the above figure.

Obround Pressure Vessel: For the obround vessel radius of curved part is taken equal to 50mm.

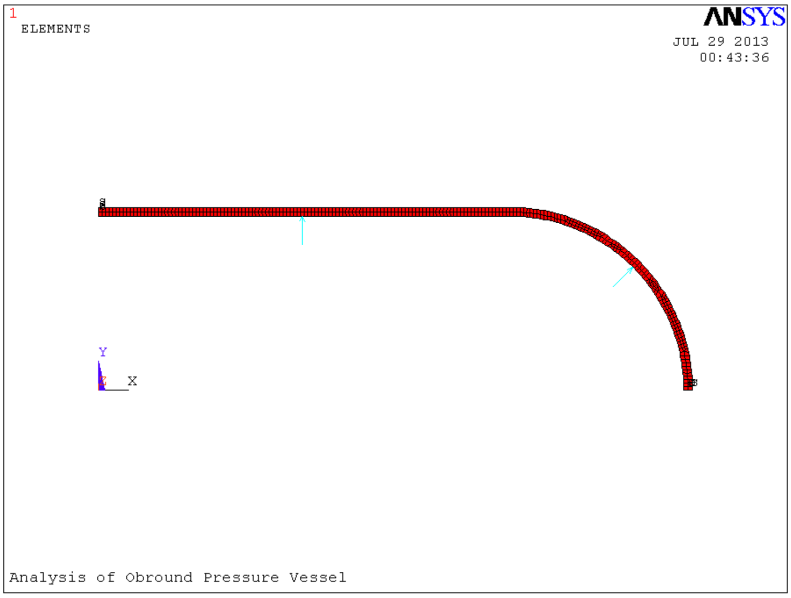

Figure.5 Meshed model of obround pressure vessel with boundary condition & Load Conditions

V. RESULTS & DISCUSSIONS

Circular Pressure Vessel:

Initially for circular pressure vessel, trials are taken to see the effect of mesh density. It is seen that using edge length of 1.25 mm for small edges & edge length of 1 mm for curved edges, we get more accuracy. Hence the same is finalized for further analysis. Following table gives the details of the results obtained with the above mesh density.

Table.2 Values of Principal Stresses

Stress at A (MPa)	Stress at B (MPa)	Stress at C (MPa)	Stress at D (MPa)
4.0504	3.9506	4.0504	3.9506

Fig.6 indicates the deformed shape along with un-deformed shape of the circular pressure vessel. I can be seen that the maximum deformation is only 0.003947 mm. Fig.7 indicates the values of principal stresses in this circular pressure vessel.

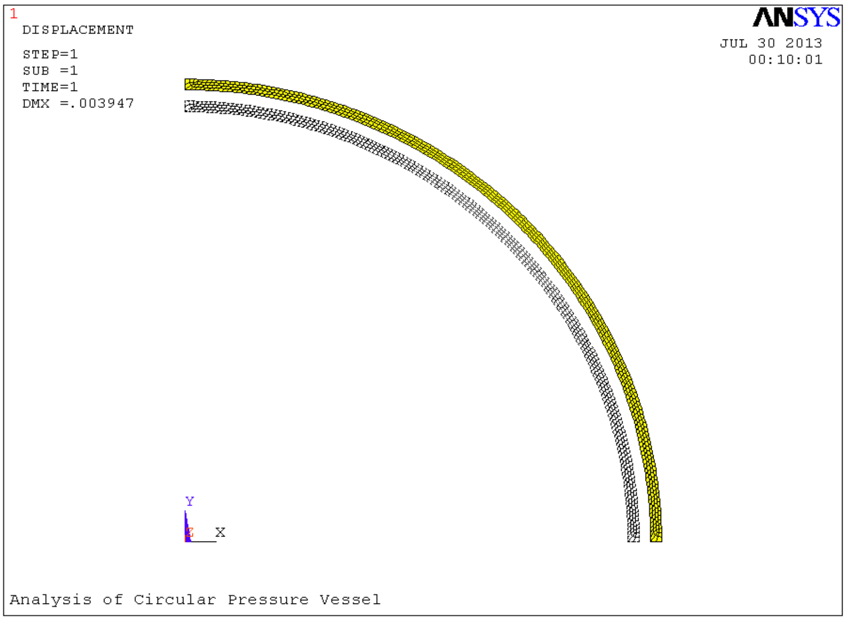

Figure.6 Deformed shape along with undeformed shape (Circular Pressure Vessel)

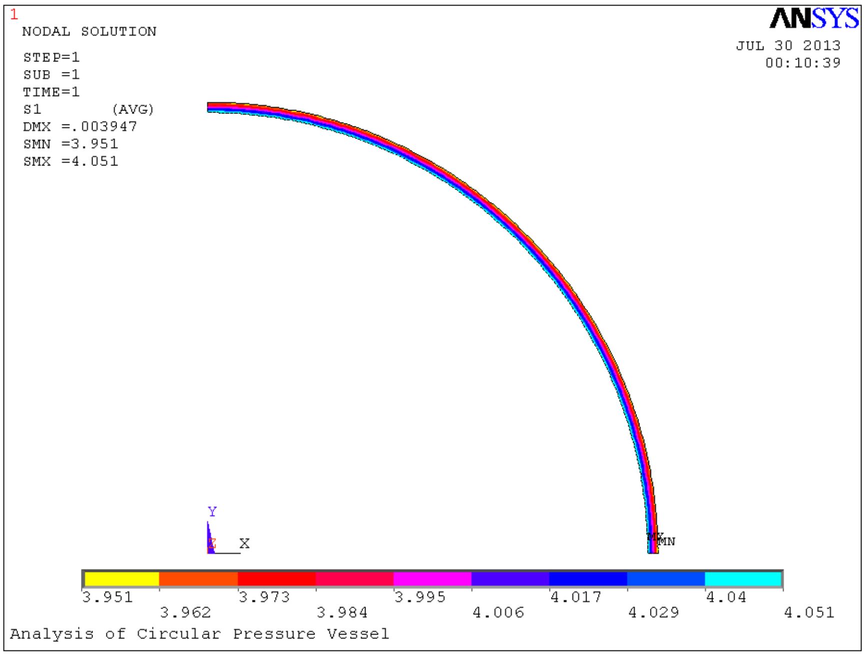

Figure.7 Principal stresses (Circular Pressure Vessel)

Stresses at A, B, C & D points: The output of nodal solution is listed & observation of the stresses at A, B, C & D points is done. The values obtained are as below.

Table.3 Principal Stresses at A, B, C & D for Circular Pressure Vessel

Node Position	Point	Node Number	Stress (ANSYS)	Hoop Stress (Analytical)
			MPa	MPa
Inner - Upper Side	A	326	4.0506	4
Outer - Upper Side	B	2	3.9506	
Inner - Lower Side	C	330	4.0506	
Outer - Lower Side	D	1	3.9506	

Obround Pressure Vessel:

Following figure indicates the deformed & un-deformed shape of the obround pressure vessel with radius of curved portion as 50 mm.

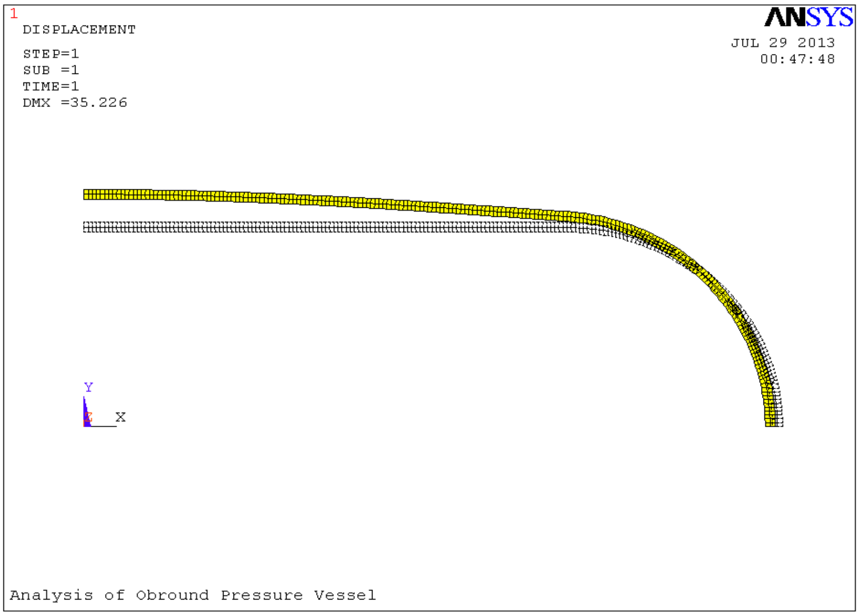

Figure.8 Deformed shape & Un-deformed shape of obround pressure vessel

Fig.9 shows the first principal stresses & fig.11 gives Third Principal Stress. Fig.10 & fig.12 shows the exaggerated views of the areas of high stresses.

The maximum stress values are given in Table.4.

Table.4 Principal Stresses at A, B, C & D for Obround Pressure Vessel

Stress at A (in MPa)	**Stress at B (in MPa)**	**Stress at C (in MPa)**	**Stress at D (in MPa)**
-550	554	708.77	-678.45

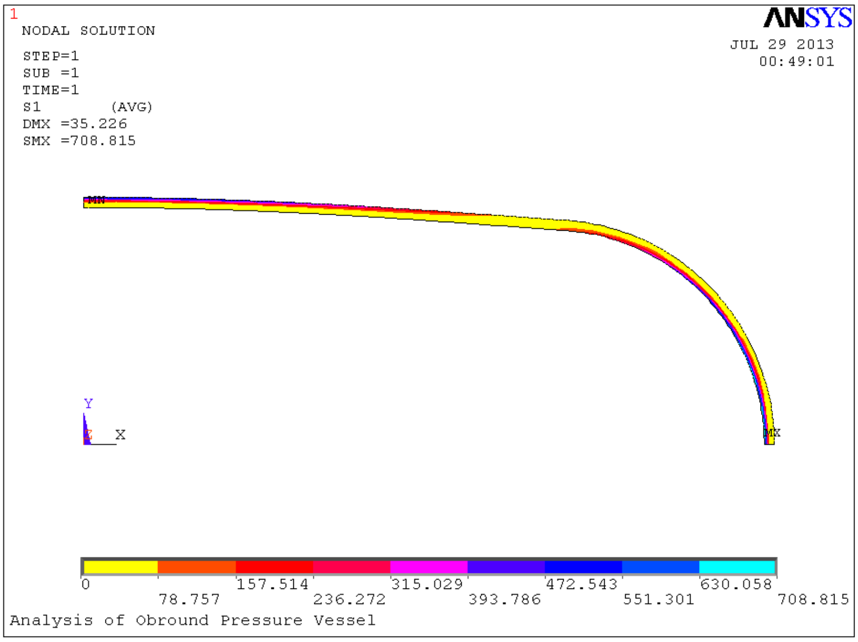

Figure.9 First Principal Stresses (Obround Pressure Vessel)

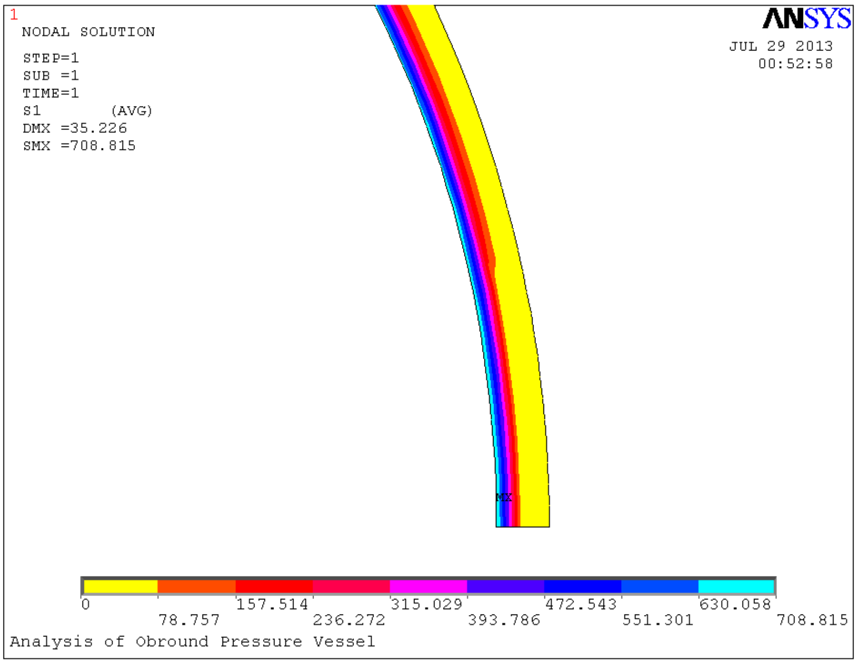

Figure.10 Exaggerated view of area near to point C & D (First Principal Stresses)

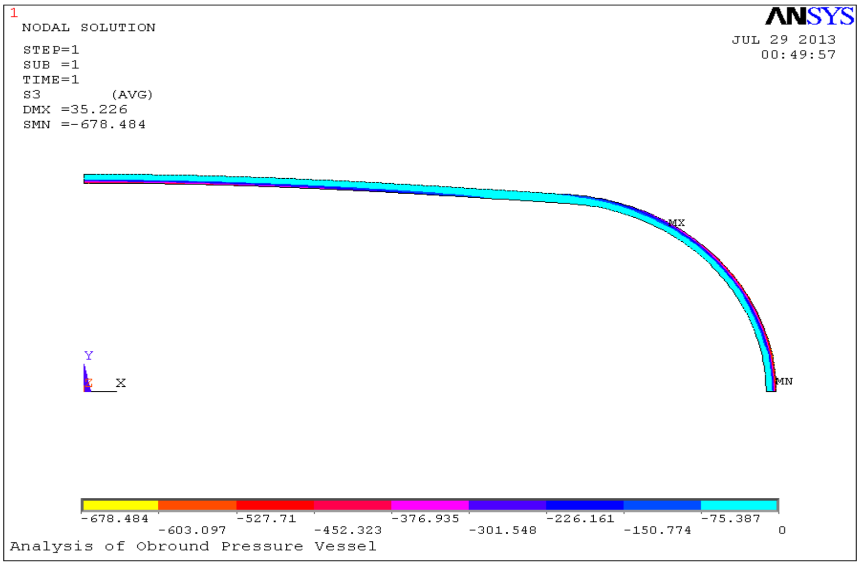

Figure.11 Third Principal Stress (Obround Pressure Vessel)

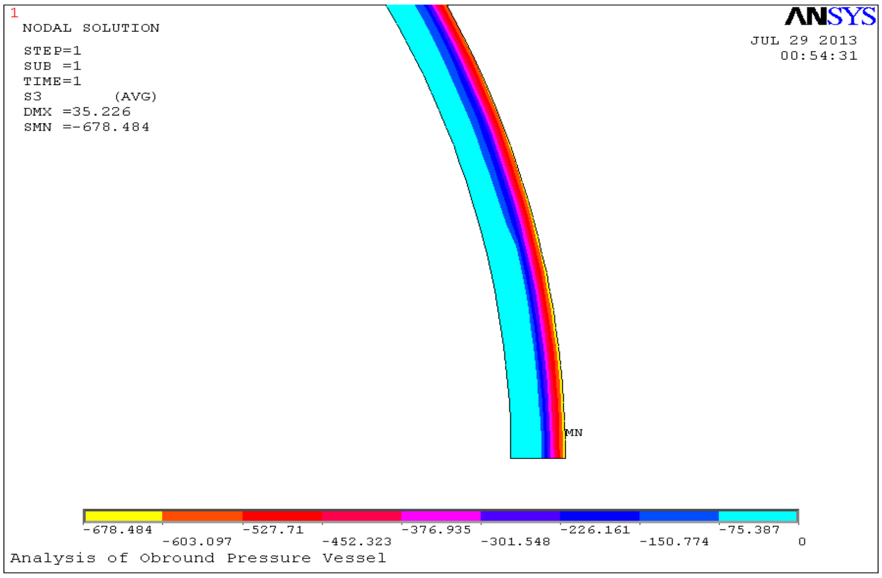

Figure.12 Exaggerated view of area near to point C & D (Third Principal Stress)

From the above study, it is seen that values of hoop stresses are very much higher than that of the circular pressure vessel. Also the maximum deformation is 35.226 mm which also is very much higher than that of circular pressure vessel.

Following table (Table.5) gives the details of the values of stresses at A, B, C & D points for values of radii of curved portion.

Table.5 Results of Hoop Stresses in Obround Pressure Vessel

Sr. No.	R	Stress at A	Stress at B	Stress at C	Stress at D
1	25	-1785.9	1787.9	3207.5	-3033
2	30	-1294.9	1297.3	2197.3	-2090
3	35	-995.07	997.87	1586.1	-1514
4	40	-796.35	799.55	1186.6	-1135
5	45	-655.64	659.24	909.85	-871.04
6	50	-550	554	708.77	-678.45
7	60	-397.46	402.26	439.6	-419.32
8	70	-283.43	289.35	269.28	-254.51
9	80	-185.35	191.8	152.58	-141.09
10	90	-91.346	98.546	67.891	-58.501
11	95	-43.97	51.621	33.812	-25.186

The following graph indicates the variation of stresses with references to the radius of curved portion.

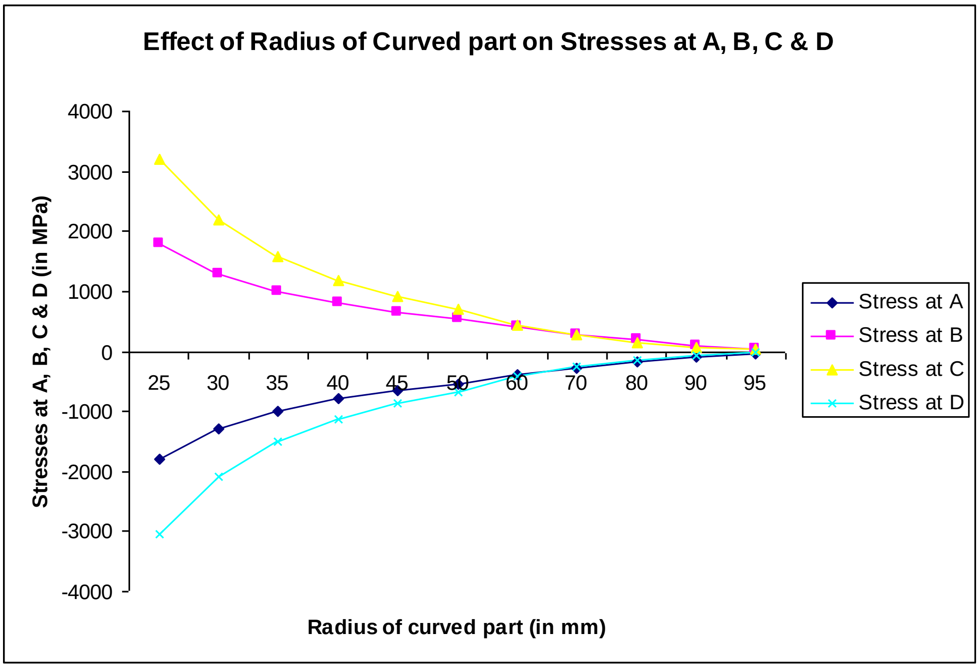

Figure.13 Radius of Curved part Vs Hoop Stresses at A, B, C & D

From all the above figures, it can be said that as radius of curved portion of obround pressure vessel goes on increasing, the hoop stresses go on reducing. The reduction is as per the curves indicated above.

Effect of thickness of Obround Pressure Vessel on the values of the Hoop Stress:

The effect of thickness on the values of the stresses is also observed. Following table indicates the values of the hoop stresses at different thickness of the pressure vessels. The analysis is done for the obround pressure vessel with radius = 50 mm for curved portion.

Table.6 Stresses at different thicknesses of Pressure Vessel

Sr. No.	**Thickness**	**Stress at A**	**Stress at B**	**Stress at C**	**Stress at D**
	mm	MPa	MPa	MPa	MPa
1	2.5	-550	554	708.77	-678.45
2	3	-382.84	386.17	496.51	-468.69
3	3.5	-281.92	284.78	367.1	-343.28
4	4	-216.34	218.84	283.21	-261.72
5	4.5	-171.33	173.55	225.21	-206.14
6	5	-139.1	141.1	183.58	-166.45
7	5.5	-115.22	117.04	152.82	-137.04
8	6	-97.036	98.706	129.23	-114.79

Following are the graphs showing relation between the thickness of pressure vessel & hoop stresses.

From the graph (fig.14) it is seen that as the thickness of vessel goes on increasing, stresses go on reducing.

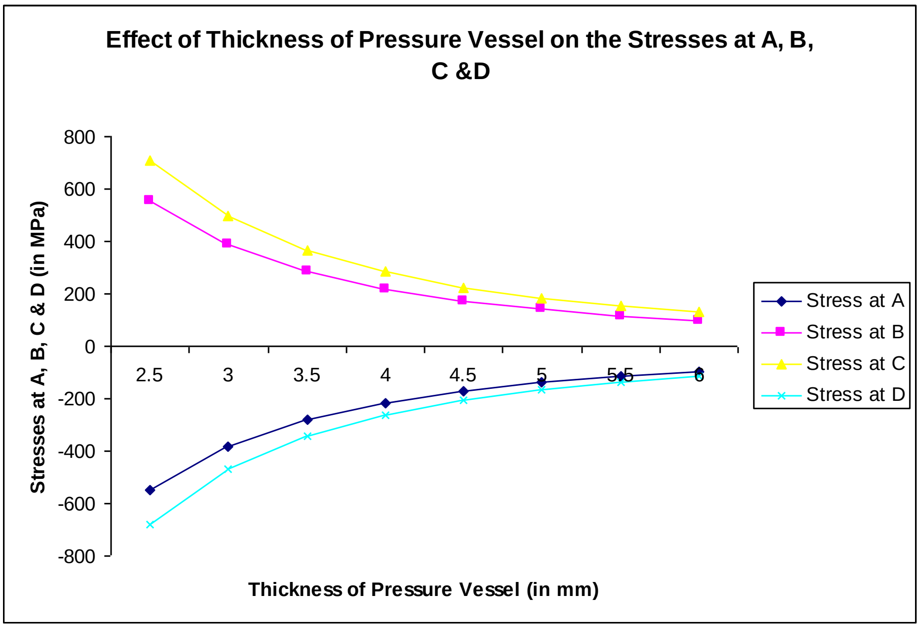

Figure.14 Thickness of Pressure Vessel Vs Stresses at point A, B, C & D

Effect of pressure on the on the values of Hoop Stress Obround Pressure Vessel:

For R= 50 mm & Thickness = 2.5 mm, Pressure variation is done & its effect on the values of the stresses are studied.

Table.7 Stresses at Different Values of Pressure inside the Pressure Vessel

Sr. No.	Pressure MPa	Stress at A MPa	Stress at B MPa	Stress at C MPa	Stress at D MPa
1	0.05	-275	277	354.39	-339.22
2	0.075	-412.5	415.5	531.58	-508.84
3	0.1	-550	554	708.77	-678.45
4	0.125	-687.5	692.5	885.97	-848.06
5	0.150	-825	831	1063.2	-1017.7
6	0.175	-962.5	969.5	1240.4	-1187.3
7	0.2	-1100	1108	1417.5	-1356.9

Following fig.15 indicates the relation between the pressure applied & the hoop stresses at points A, B, C & D.

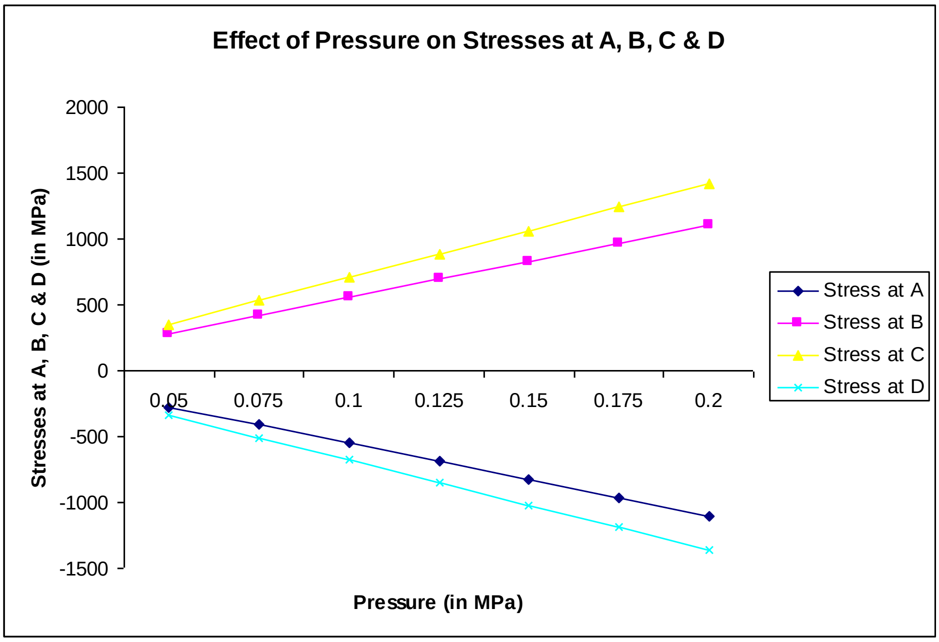

Figure.15 Pressure applied Vs Stress at point A, B, C & D

From the above figures, it is seen that the hoop stress is directly proportional to the pressure applied inside the vessel.

VI. CONCLUSIONS

- The hoop stresses in the obround pressure vessel are very much higher as compared to the stresses in circular pressure vessels.
- Deformation in the obround pressure vessel is also very much higher as compared to the deformation in circular pressure vessels.
- As radius of curved portion of obround pressure vessel goes on increasing, the hoop stresses go on reducing.
- As the thickness of vessel goes on increasing, stresses go on reducing.
- Hoop stress is directly proportional to the pressure applied inside the vessel.

ACKNOWLEDGEMENT

We are thankful to Principal, Management & Head –Mechanical Engg. Walchand Institute of Technology, Solapur, for their support during this work.

REFERENCES

[1] David Heckman, "Finite Element Analysis of Pressure Vessels", *University of California, Davis, Summer 1998*
[2] Jimit Vyas And Mahavir Solanki, "Design And Analysis of Pressure Vessel", Thesis, *U. V. Patel College of Engineering.*
[3] Jonathan C Wang, "Stress Analysis of an Elliptical Pressure Vessel Under Internal Pressure", *M.S. Seminar, Hartford CT, 2005*
[4] David Roylance, "Pressure Vessels", *Department of Materials Science and Engineering, Massachusetts Institute of Technology, Cambridge, 2001*
[5] D. Dewayne Howell, "Open End Cylindrical Pressure Vessel Development", *Society for The Advancement of Material And Process Engineering, Colorado. 2004*
[6] Reddy J.N. , *An Introduction to Finite Element Method*, (Tata McGraw-Hill Publication, Fifth Edition)
[7] Tirupati Chandrupatla, Ashok Belegundu, *Introduction to Finite Elements in Engineering*, (Prentice Hall India, 2007)
[8] V.B. Bhandari, *Design of Machine Elements*, (Tata McGraw Hill Publishing Co. Ltd, New Delhi, 2005)
[9] Joseph Edward Shigley, *Mechanical Engineering Design*, (McGraw Hill, 2009)

Cooperative Schedule Data Possession for Integrity Verification in Multi-Cloud Storage

O. Rahamathunisa Begam[1], T. Manjula[2], T. Bharath Manohar[3], B. Susrutha[4]

[1, 4,] M. Tech 2ndyr, Dept of CSE, PBRVITS (Affiliated to JNTU Anantapur), Kavali, Nellore. Andhra Pradesh. India.
[2] Assoc. Prof., Dept of CSE, PBRVITS (Affiliated to JNTU Anantapur), Kavali, Nellore. Andhra Pradesh. India.
[3]Asst.Professor, Dept of CSE, CMR College of Engineering &Technology,
(Affiliated to JNTU Hyderabad)Hyderabad.Andhra Pradesh.India.

ABSTRACT: *Provable data possession (PDP) is a technique for ensuring the integrity of data in storage outsourcing. In this paper, we address the construction of an efficient PDP scheme for distributed cloud storage to support the scalability of service and data migration, in which we consider the existence of multiple cloud service providers to cooperatively store and maintain the clients' data. We present a cooperative PDP (CPDP) scheme based on homomorphic verifiable response and hash index hierarchy. We prove the security of our scheme based on multi-prover zero-knowledge proof system, which can satisfy completeness, knowledge soundness, and zero-knowledge properties. In addition, we articulate performance optimization mechanisms for our scheme, and in particular present an efficient method for selecting optimal parameter values to minimize the computation costs of clients and storage service providers. Our experiments show that our solution introduces lower computation and communication overheads in comparison with non-cooperative approaches.*

Keywords: *Storage Security, Provable Data Possession, Interactive Protocol, Zero-knowledge, Multiple Cloud, Cooperative.*

I. INTRODUCTION

In recent years, cloud storage service has become a faster profit growth point by providing a comparably low-cost, scalable, position-independent platform for clients' data. Since cloud computing environment is constructed based on open architectures and interfaces, it has the capability to incorporate multiple internal and/or external cloud services together to provide high interoperability. We call such a distributed cloud environment as a *multi-Cloud* (or *hybrid cloud*). Often, by using virtual infrastructure management (VIM) , a multi-cloud allows clients to easily access his/her resources remotely through interfaces such as Web services provided by Amazon EC2. There exist various tools and technologies for multicloud, such as Platform VM Orchestrator, VMware vSphere, and Ovirt. These tools help cloud providers construct a distributed cloud storage platform (DCSP) for managing clients' data. However, if such an important platform is vulnerable to security attacks, it would bring irretrievable losses to the clients.

For example, the confidential data in an enterprise may be illegally accessed through a remote interface provided by a multi-cloud, or relevant data and archives may be lost or tampered with when they are stored into an uncertain storage pool outside the enterprise. Therefore, it is indispensable for cloud service providers (CSPs) to provide security techniques for managing their storage services. Provable data possession (PDP) (or proofs of retrievability (POR) is such a probabilistic proof technique for a storage provider to prove the integrity and ownership of clients' data without downloading data. The proof-checking without downloading makes it especially important for large-size files and folders (typically including many clients' files) to check whether these data have been tampered with or deleted without downloading the latest version ofdata. Thus, it is able to replace traditional hash and signature functions in storage outsourcing. Various PDP schemes have been recently proposed, such as Scalable PDP and Dynamic PDP. However,these schemes mainly focus on PDP issues at untrusted servers in a *single* cloud storage provider and are not suitable for a multi-cloud environment.

II. MOTIVATION

Existing System

There exist various tools and technologies for multi cloud, such as Platform VM Orchestrator, VMware, vSphere,and Ovirt. These tools help cloud providers construct a distributed cloud storage platform for managing clients' data. However, if such an important platform is vulnerable to security attacks, it would bring irretrievable losses to the clients. For example, the confidential data in an enterprise may be illegally accessed through a remote interface provided by a multi-cloud, or relevant data and archives may be lost or tampered with when they are stored into an • uncertain storage pool outside the enterprise. Therefore, it is indispensable for cloud service providers to provide security techniques for managing their storage services.

Proposed System

To check the availability and integrity of outsourced data in cloud storages, researchers have proposed two basic approaches called Provable Data Possession and Proofs of Retrievability.Ateniese et al. first proposed the PDP model for ensuring possession of files on untrusted storages and provided an RSA-based scheme for a static case that achieves the communication cost. They also proposed a publicly verifiable version, which allows anyone, not just the owner, to challenge the server for data possession..They proposed a lightweight PDP scheme based on cryptographic hash function and symmetric key encryption, but the servers can deceive the owners by using previous metadata or responses due to the lack of randomness in the challenges. The numbers of updates and challenges are limited and fixed in advance and users cannot perform block insertions anywhere.

DEFINITION OF COOPERATIVE PDP

In order to prove the integrity of data stored in a multi-cloud environment, we define a framework for CPDP based on interactive proof system (IPS) and multi prove zero-knowledge proof system (MPZKPS).

HASH INDEX HIERARCHY FOR CPDP

To support distributed cloud storage, we illustrate a representative architecture used in our cooperative PDP scheme. Our architecture has a hierarchy structure which resembles a natural representation of file storage. This hierarchical structure consists of three layers to represent relationships among all blocks for stored resources. They are described as follows:

(1) Express Layer: offers an abstract representation of the stored resources;
(2) Service Layer: offers and manages cloud storage services; and
(3) Storage Layer: realizes data storage on many physical devices.

We make use of this simple hierarchy to organize data blocks from multiple CSP services into a large size file by shading their differences among these cloud storage systems. For example the Resource in Express Layer are split and stored into three CSPs, that are indicated by different colors, in Service Layer. In turn, each CSP fragments and stores the assigned data into the storage servers in Storage Layer. We also make use of colors to distinguish different CSPs. Moreover, we follow the logical order of the data blocks to organize the Storage Layer. This architecture also provides special functions for data storage and management, e.g., there may exist overlaps among data blocks (as shown in dashed boxes) and discontinuous blocks but these functions may increase the complexity of storage management.

III. LITERATURE SURVEY

Literature survey is the most important step in software development process. Before developing the tool it is necessary to determine the time factor, economy n company strength. Once these things are satisfied, ten next steps are to determine which operating system and language can be used for developing the tool. Once the programmers start building the tool the programmers need lot of external support. This support can be obtained from senior programmers, from book or from websites. Before building the system the above consideration r taken into account for developing the proposed system.

IV. SYSTEM ANALYSIS & DESIGN

Implementation is the stage of the project when the theoretical design is turned out into a working system. Thus it can be considered to be the most critical stage in achieving a successful new system and in giving the user, confidence that the new system will work and be effective.

The implementation stage involves careful planning, investigation of the existing system and it’s constraints on implementation, designing of methods to achieve changeover and evaluation of changeover methods.

Modules:

Multi cloud storage

Distributed computing is used to refer to any large collaboration in which many individual personal computer owners allow some of their computer's processing time to be put at the service of a large problem. In our system the each cloud admin consist of data blocks . the cloud user upload the data into multi cloud. cloud computing environment is constructed based on open architectures and interfaces, it has the capability to incorporate multiple internal and/or external cloud services together to provide high interoperability. We call such a distributed cloud environment as a *multi-Cloud* .A multi-cloud allows clients to easily access his/her resources remotely through interfaces.

Cooperative PDP

cooperative PDP (CPDP) schemes adopting zero-knowledge property and three-layered index hierarchy, respectively. In particular efficient method for selecting the optimal number of sectors in each block to minimize the computation costs of clients and storage service providers. cooperative PDP (CPDP) scheme without compromising data privacy based on modern cryptographic techniques.

Data Integrity

Data Integrity is very important in database operations in particular and Data warehousing and Business intelligence in general. Because Data Integrity ensured that data is of high quality, correct, consistent and accessible.

Third Party Auditor

Trusted Third Party (TTP) who is trusted to store verification parameters and offe rpublic query services for these parameters. In our system the Trusted Third Party, view the user data blocks and uploaded to the distributed cloud. In distributed cloud environment each cloud has user data blocks. If any odification tried by cloud owner a alert is send to the Trusted Third Party.

Cloud User

The Cloud User who have a large amount of data to be stored in multiple clouds and have the permissions to access and manipulate stored data.the User's Data is converted into data blocks . the data blocks is uploaded to the cloud. The TPA view the data blocks and Uploaded in multi cloud. The user can update the uploaded data. If the user wants to download their files, the data's in multi cloud is integrated and downloaded.

SYSTEM DESIGN

Admin:

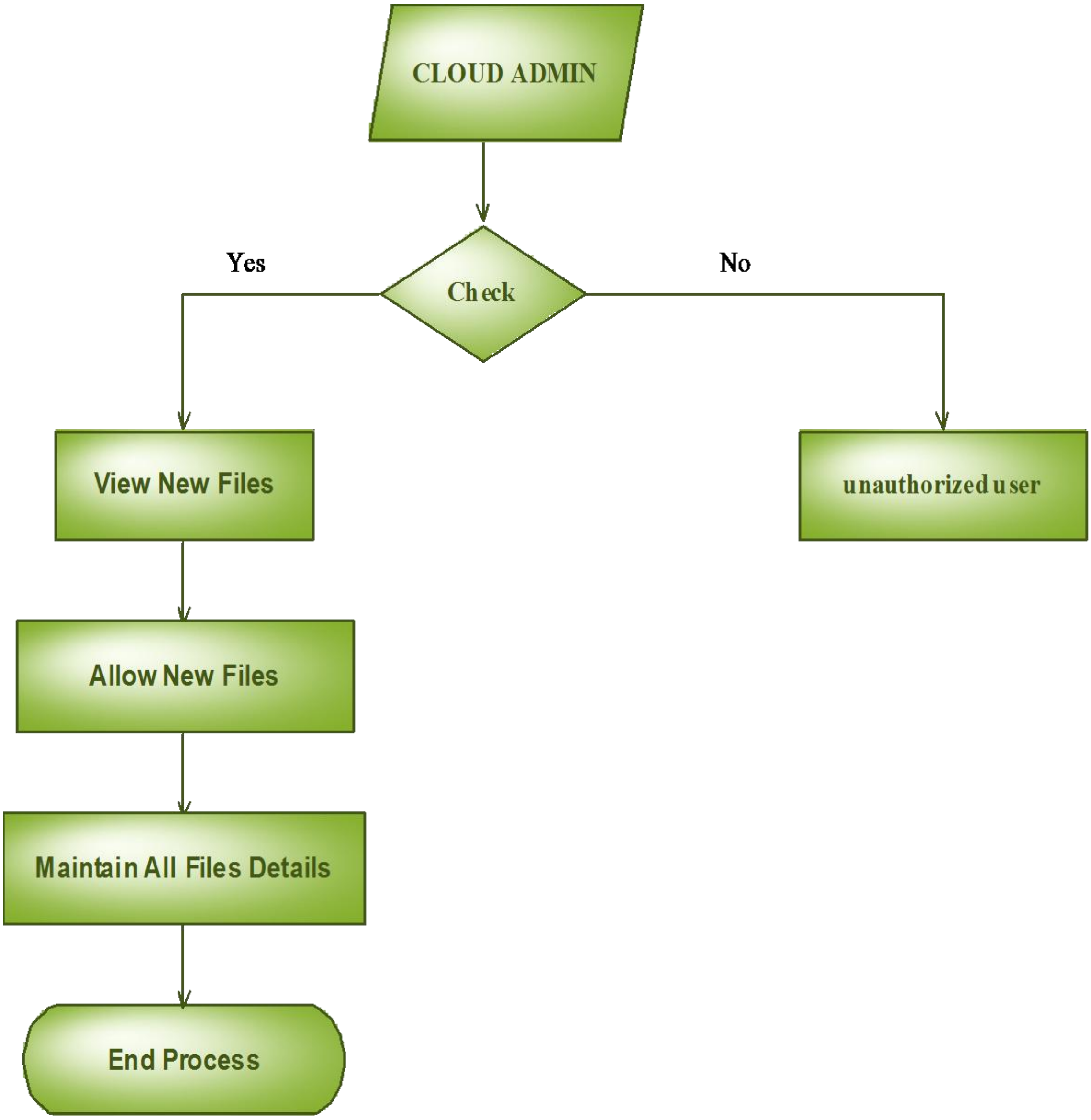

User:

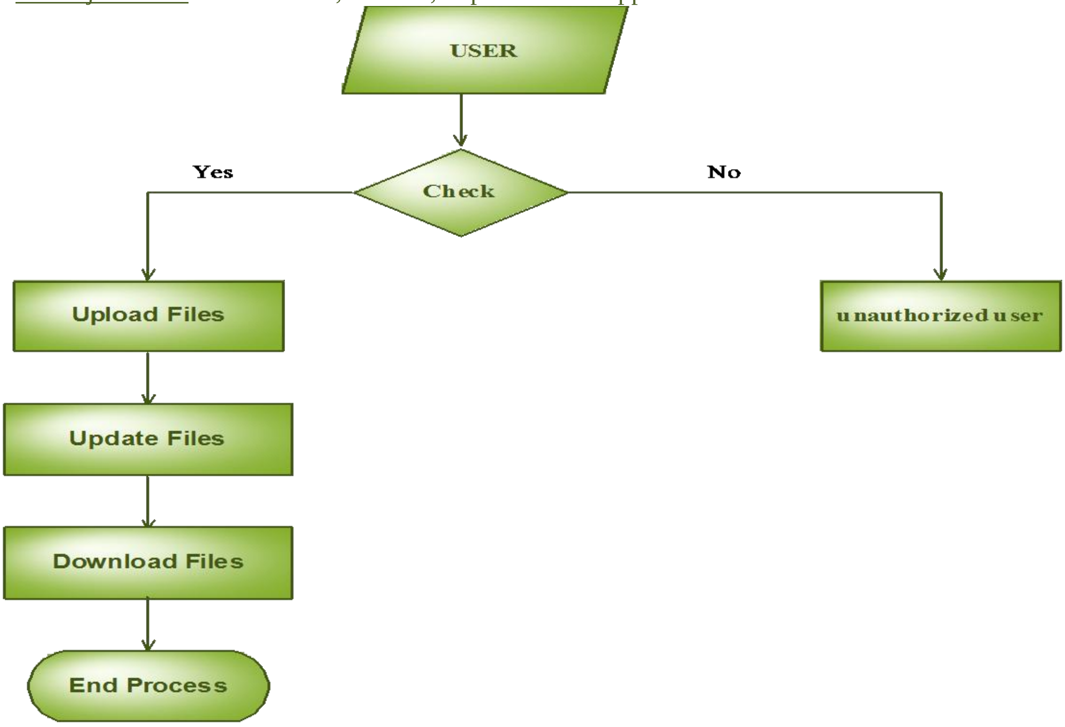

TPA(Third Party Auditor):

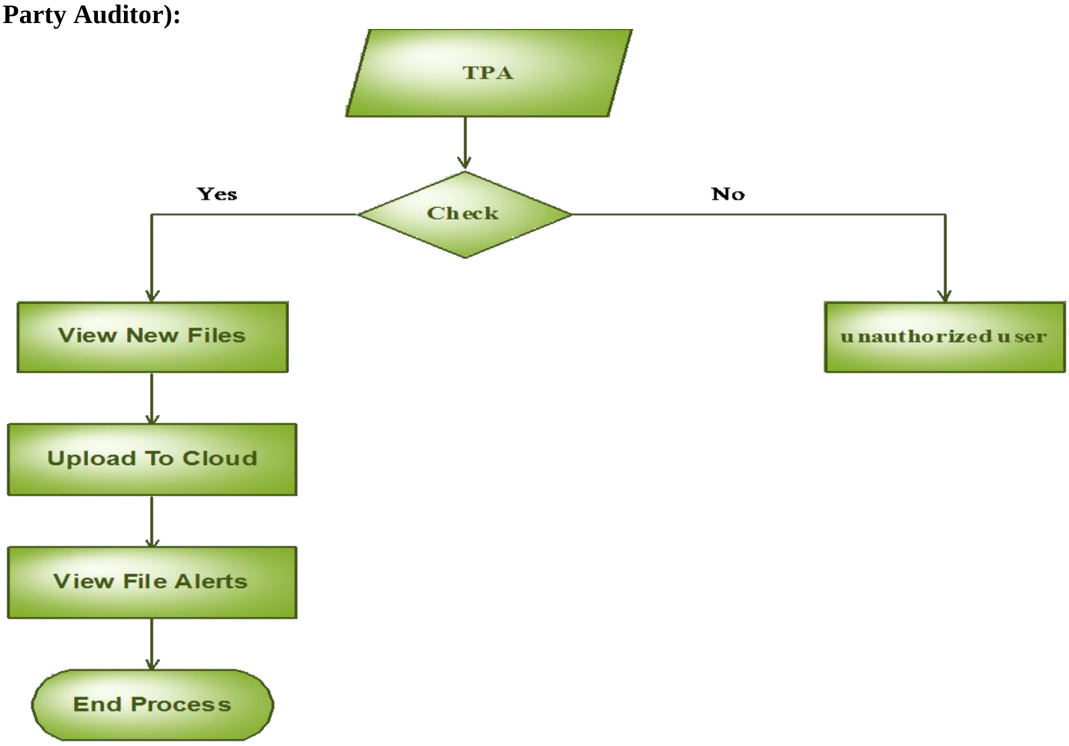

User Case Diagram:

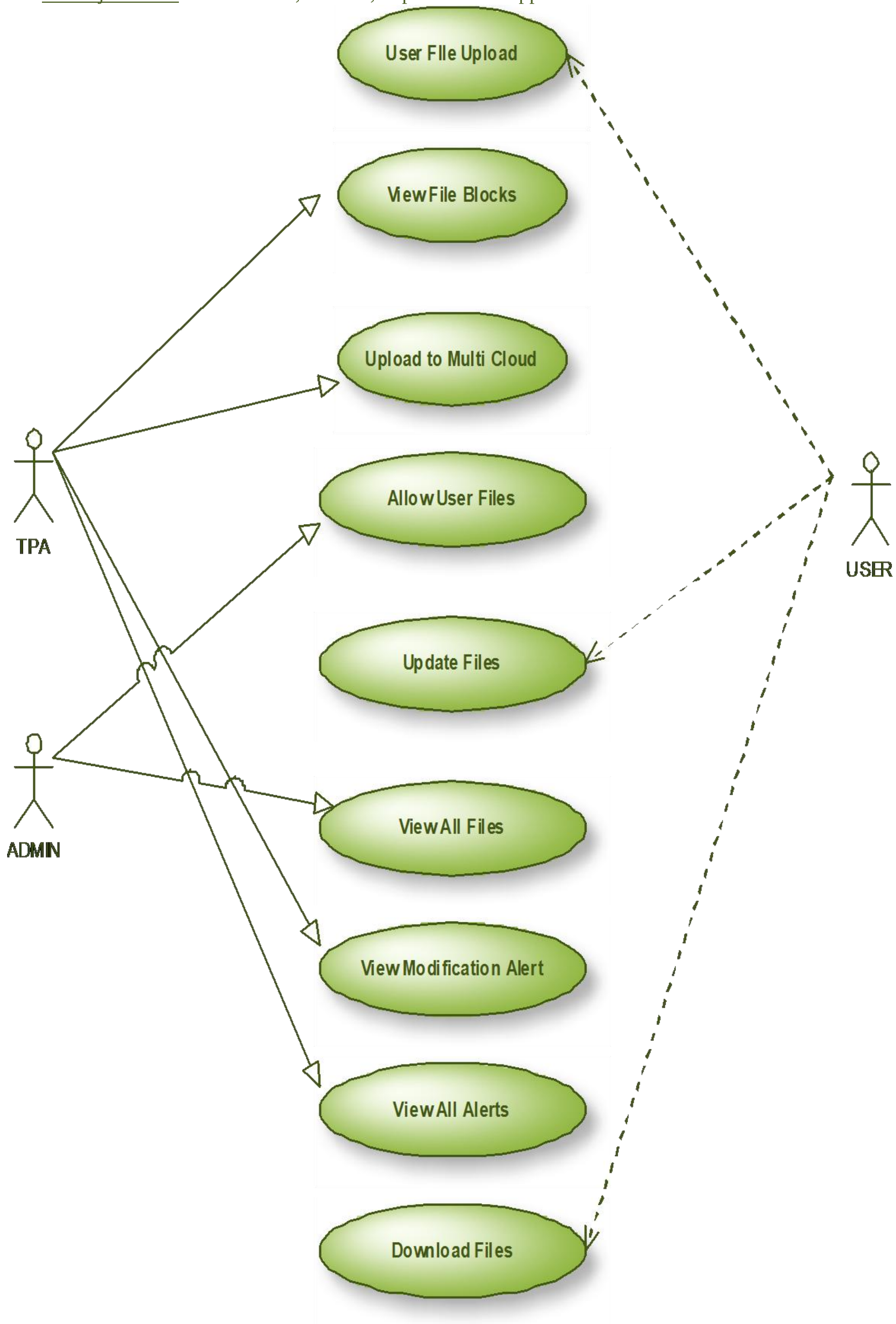

Class Diagram:

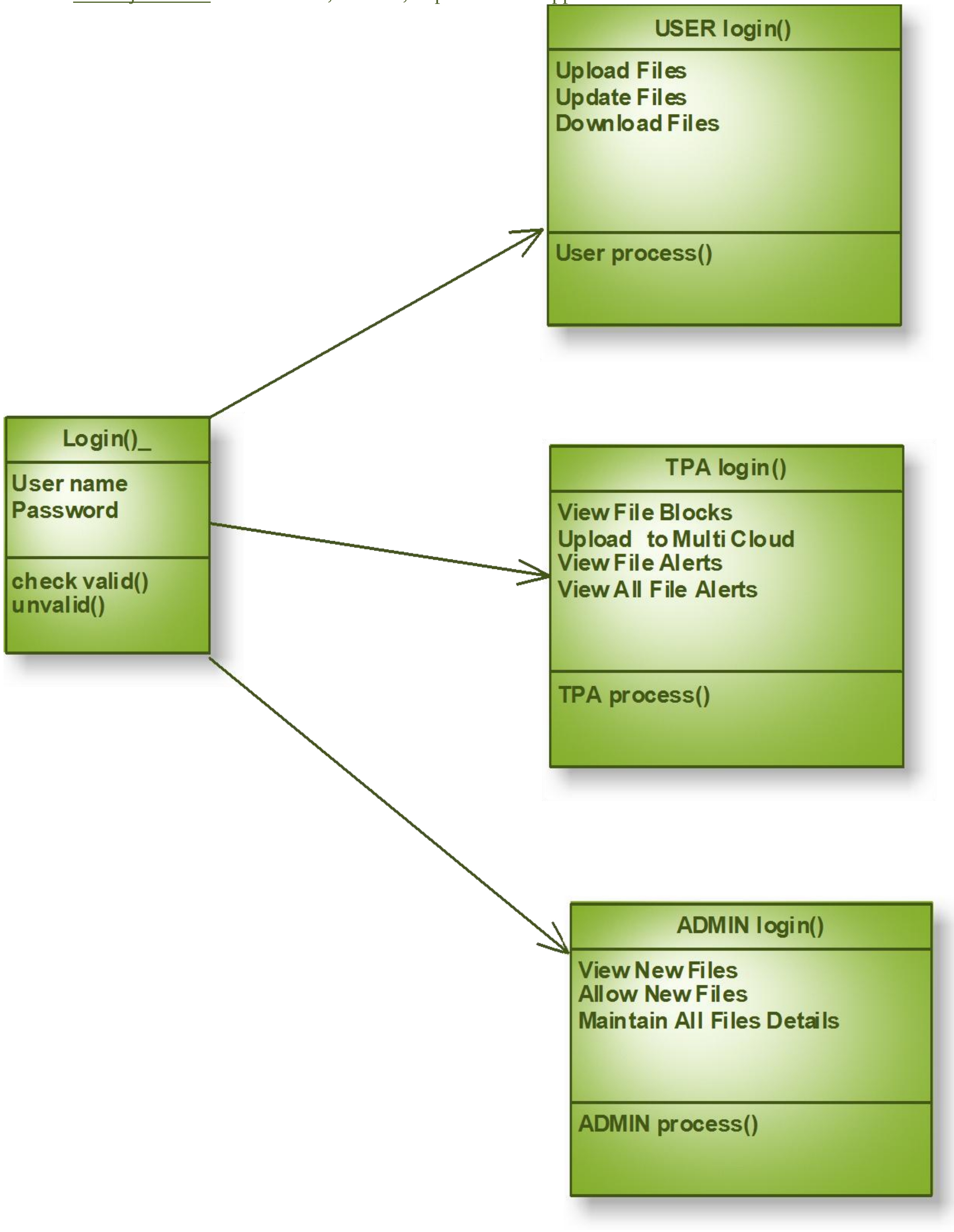

Activity Diagram:

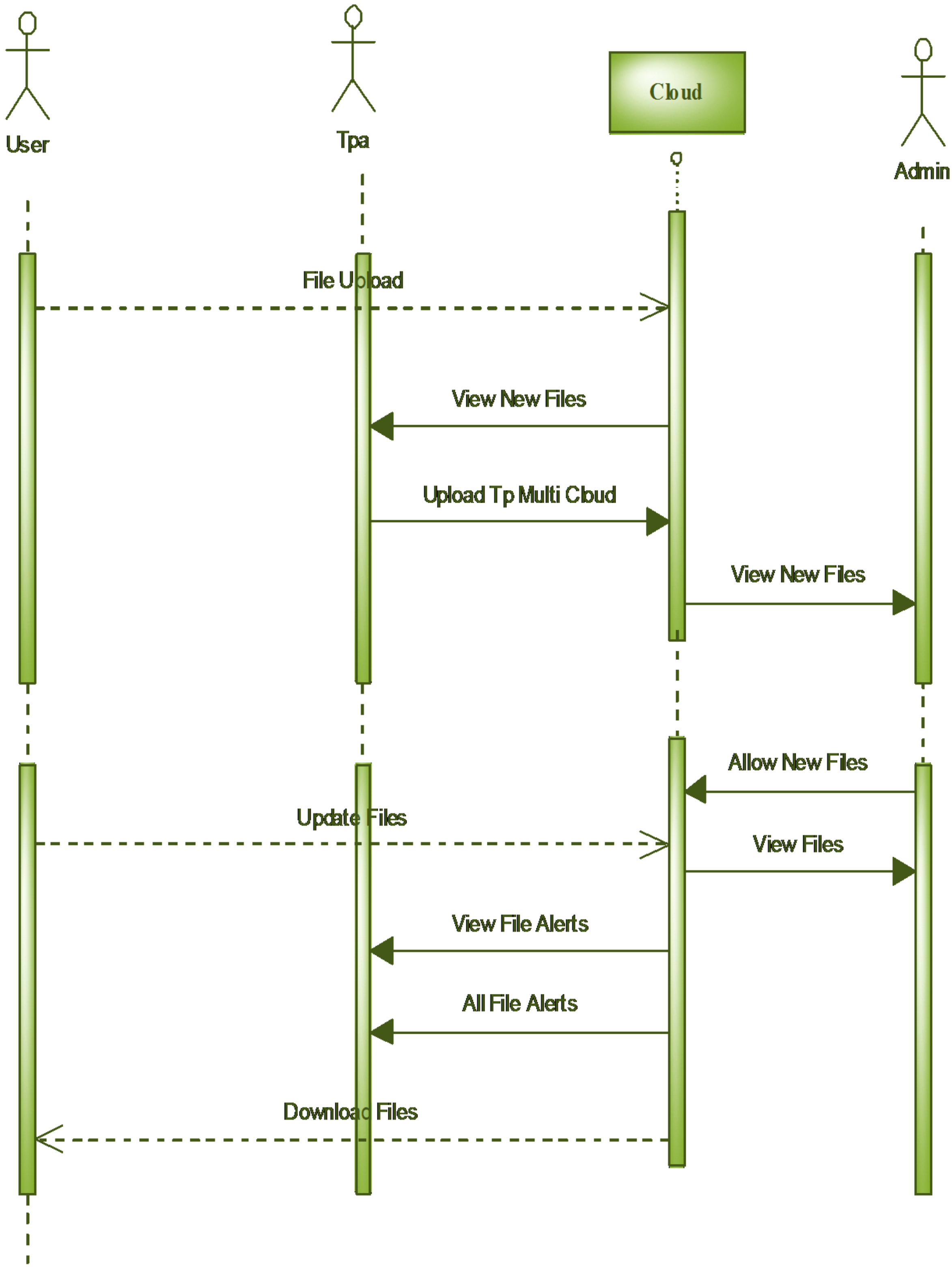
User
Tpa
Cloud
Admin
File Upload
View New Files
Upload Tp Multi Cloud
View New Files
Allow New Files
Update Files
View Files
View File Alerts
All File Alerts
Download Files

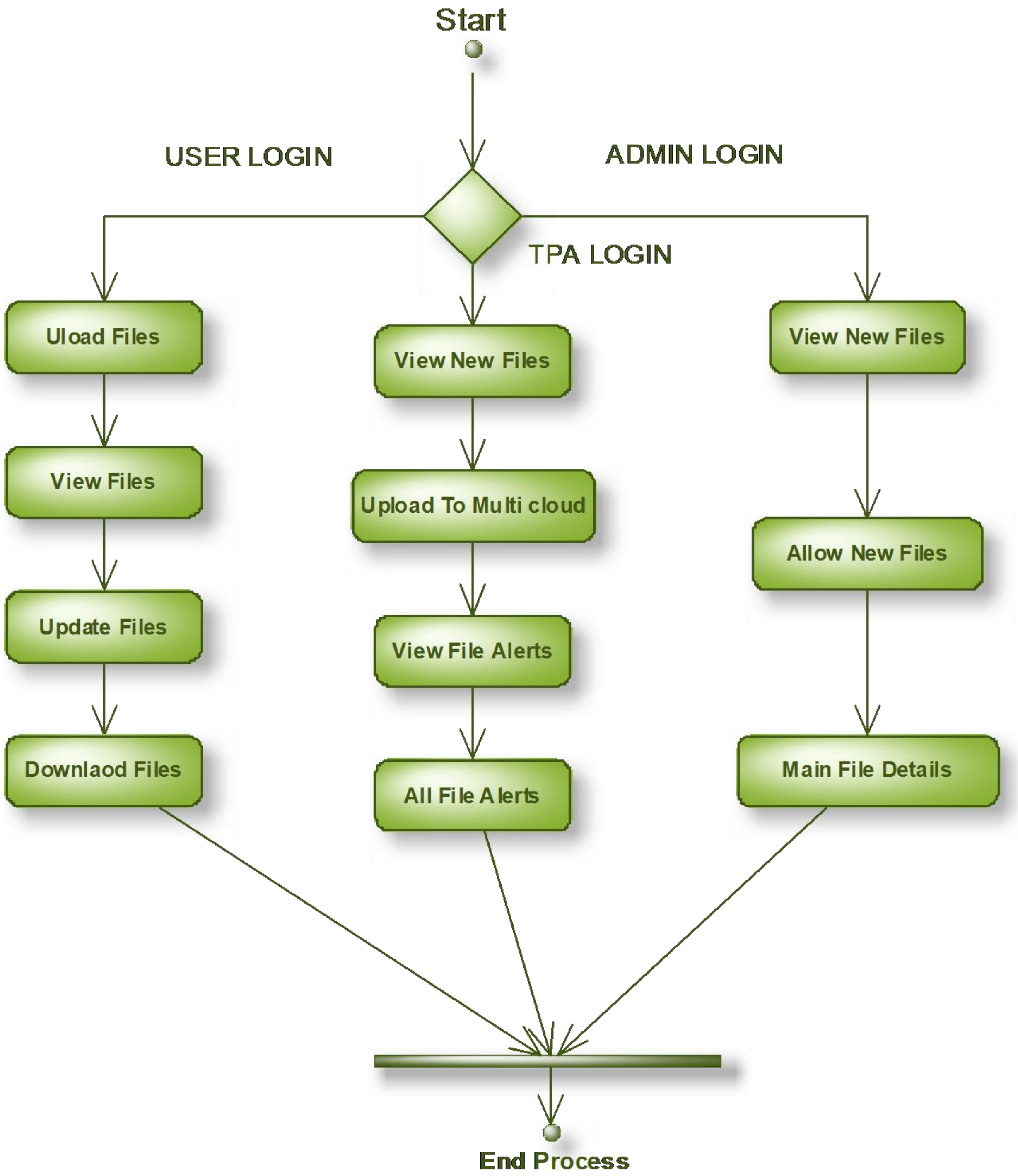

Sequence Diagram:

V. RESULTS

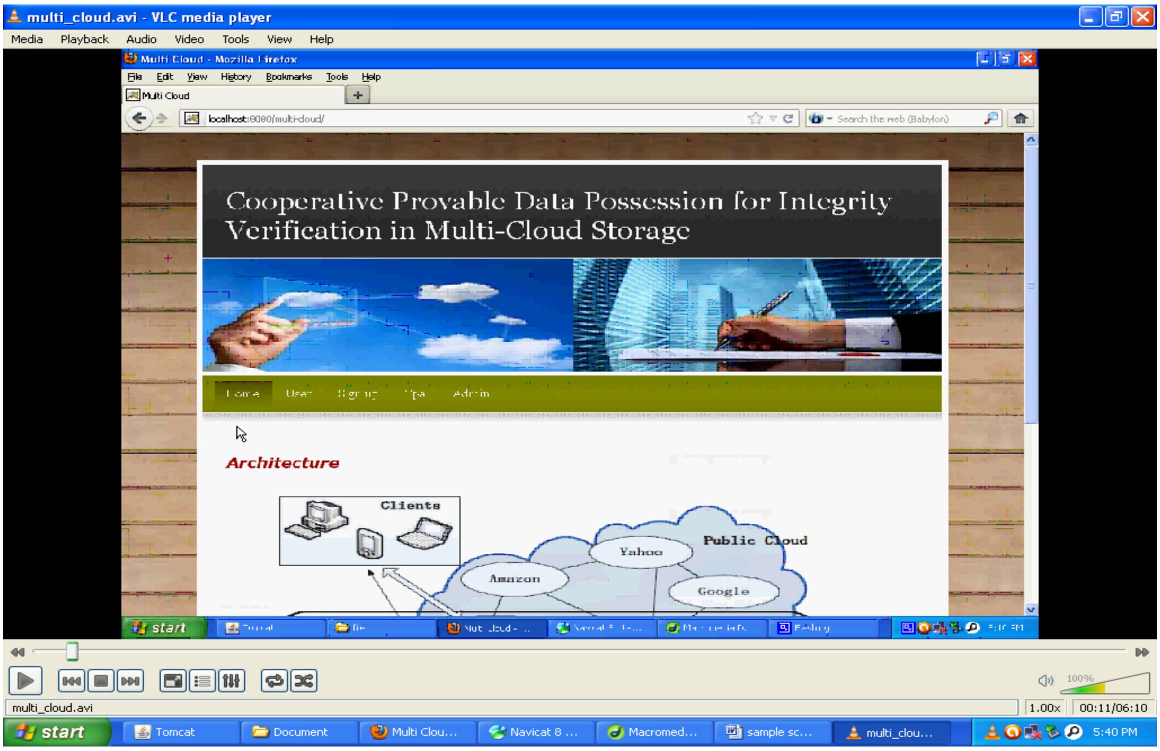
multi_cloud.avi - VLC media player
Cooperative Provable Data Possession for Integrity Verification in Multi-Cloud Storage
Architecture
Clients
Public Cloud
Yahoo
Amazon
Google

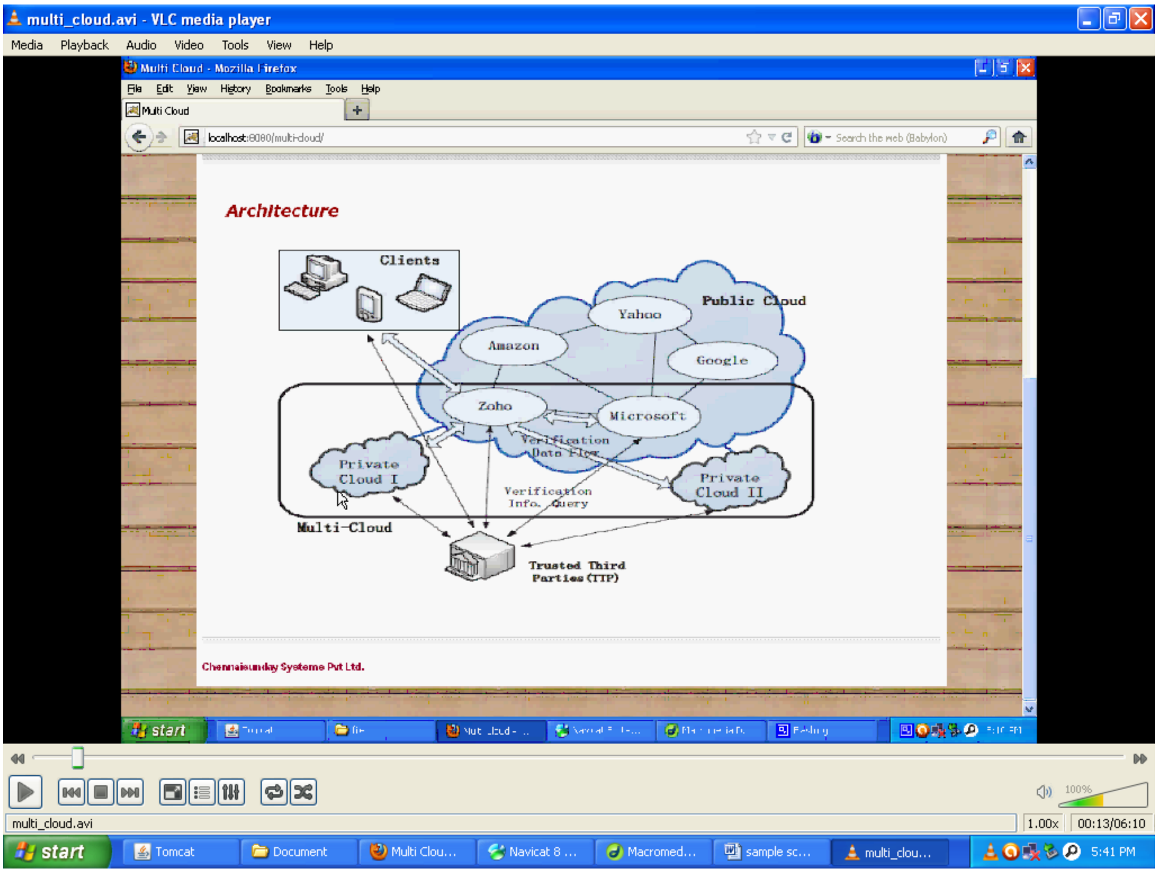
multi_cloud.avi - VLC media player
Architecture
Clients
Public Cloud
Yahoo
Amazon
Google
Zoho
Microsoft
Verification Data Flow
Private Cloud I
Private Cloud II
Verification Info.
Query
Multi-Cloud
Trusted Third Parties (TTP)

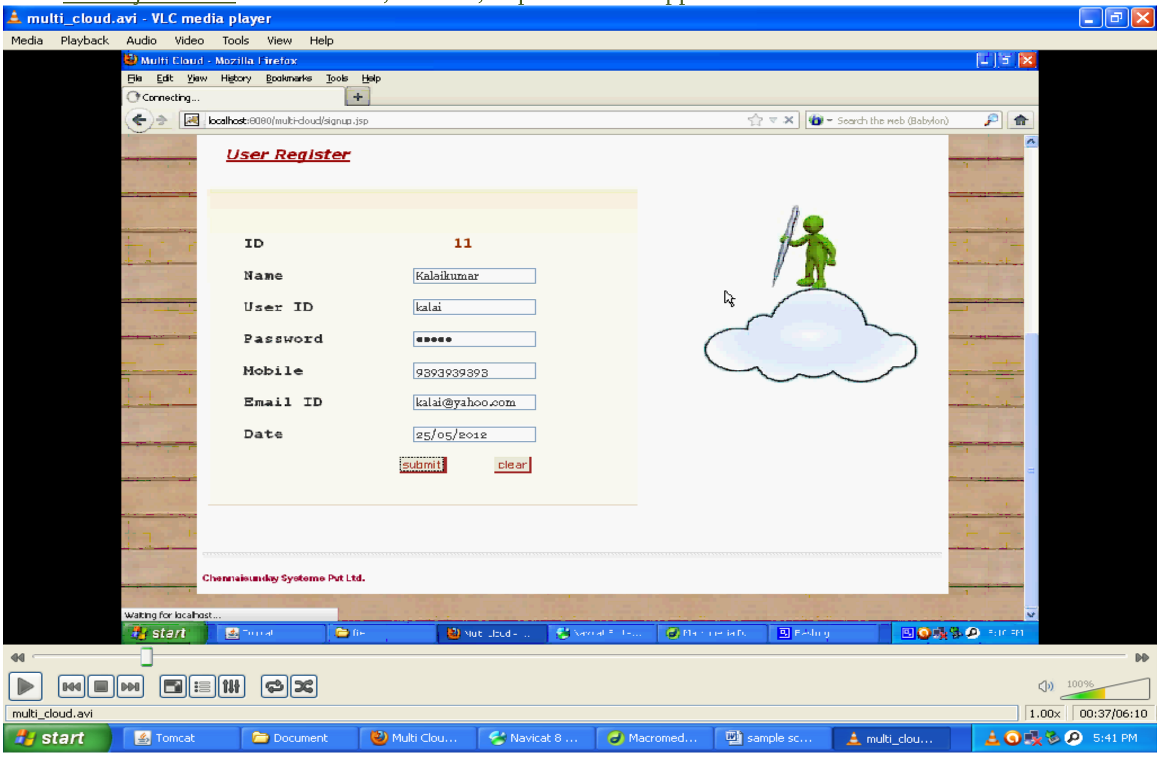
multi_cloud.avi - VLC media player
Multi Cloud - Mozilla Firefox
localhost:8080/multi-cloud/signup.jsp
User Register
ID
11
Name
Kalaikumar
User ID
kalai
Password
Mobile
9393939393
Email ID
kalai@yahoo.com
Date
25/05/2012
submit
clear
Chennaisunday Systems Pvt Ltd.
multi_cloud.avi
00:37/06:10
5:41 PM

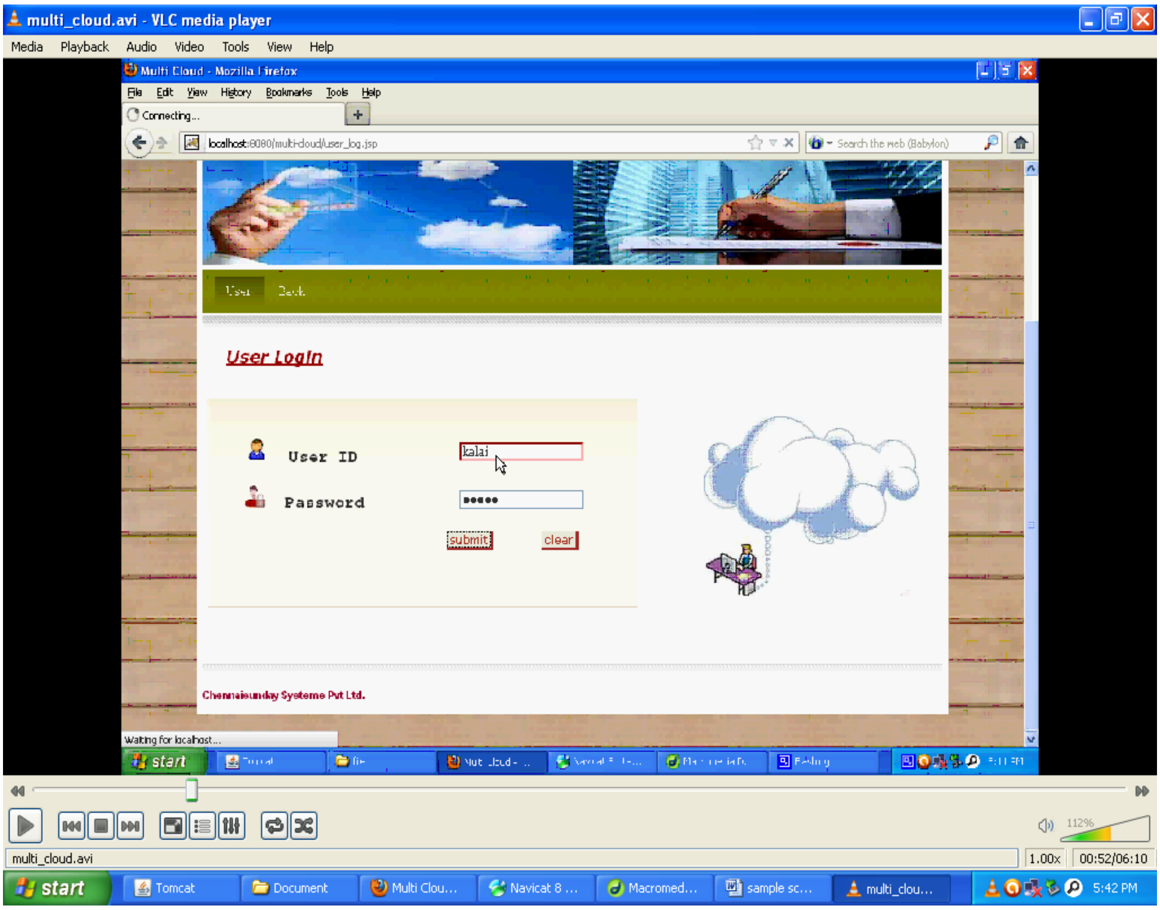
multi_cloud.avi - VLC media player
Multi Cloud - Mozilla Firefox
localhost:8080/multi-cloud/user_log.jsp
User Login
User ID
kalai
Password
submit
clear
Chennaisunday Systems Pvt Ltd.
multi_cloud.avi
00:52/06:10
5:42 PM

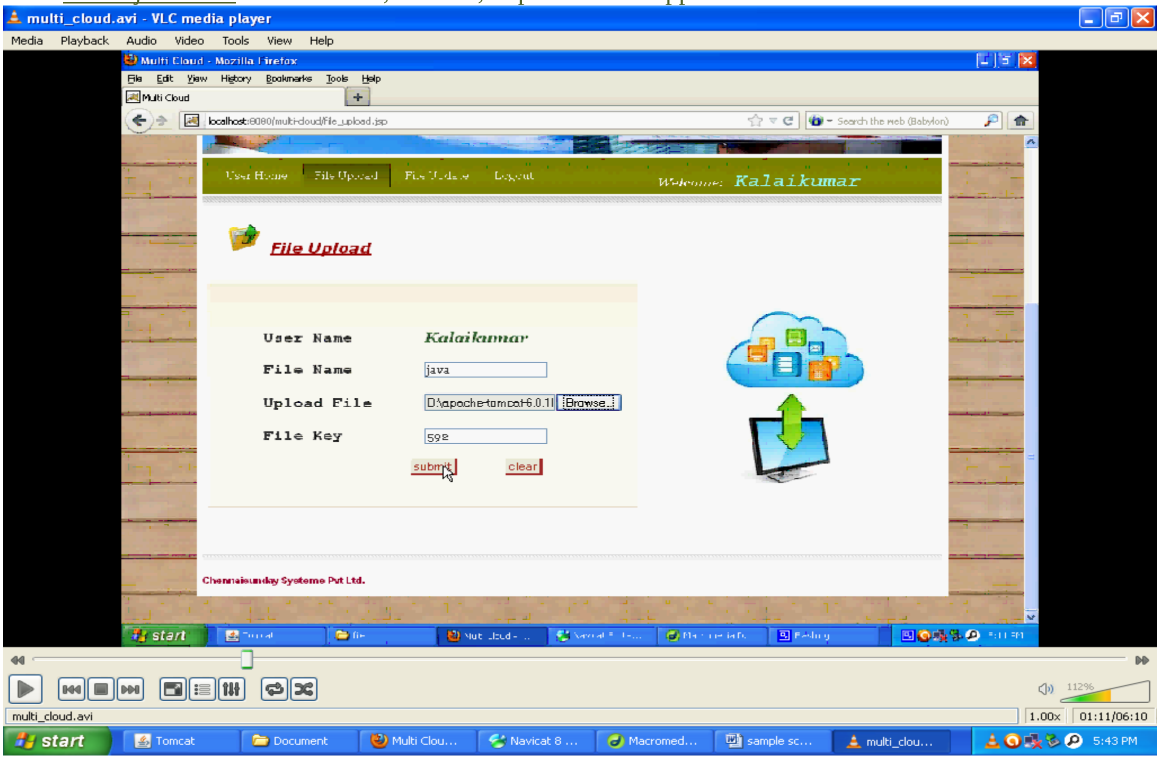
multi_cloud.avi - VLC media player
Multi Cloud - Mozilla Firefox
File Upload
User Name
Kalaikumar
File Name
java
Upload File
Browse...
File Key
592
submit
clear
Chennaisunday Systems Pvt Ltd.

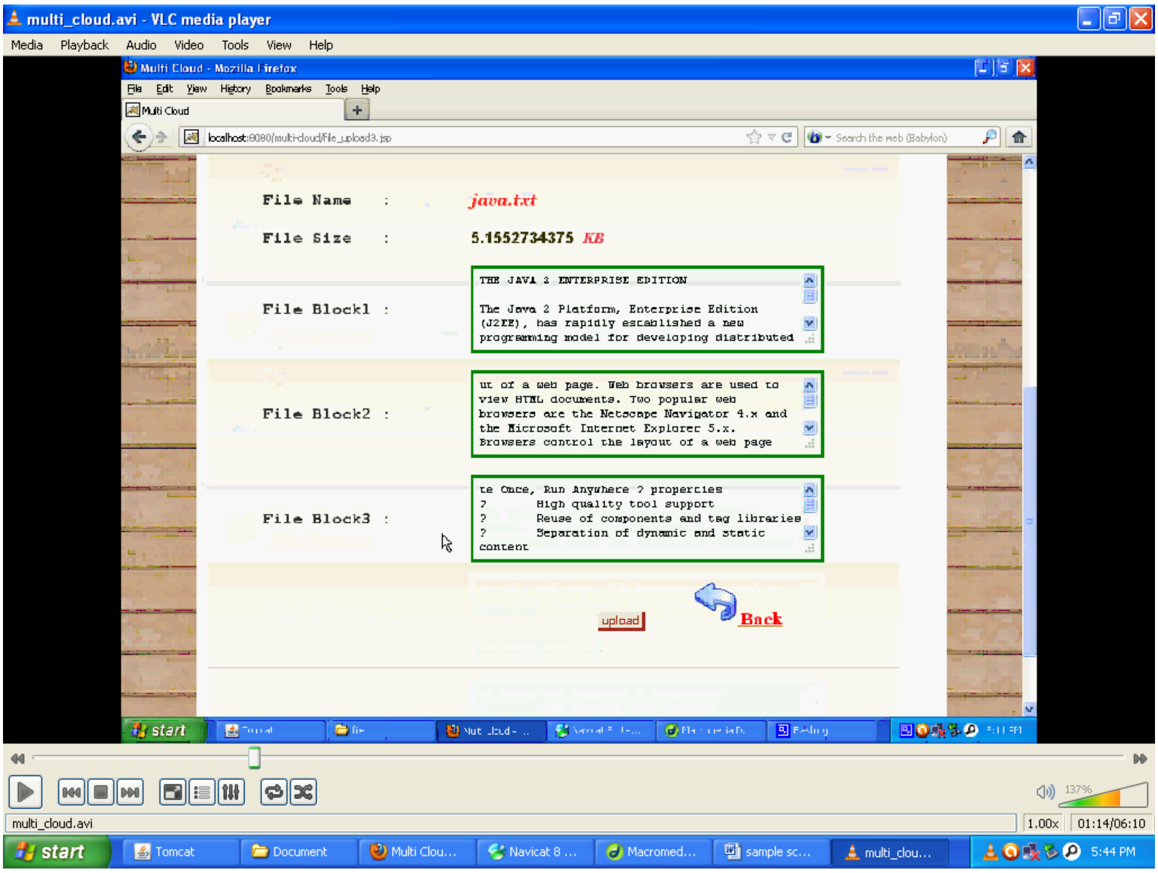
multi_cloud.avi - VLC media player
Multi Cloud - Mozilla Firefox
File Name :
java.txt
File Size :
5.1552734375 KB
File Block1 :
THE JAVA 2 ENTERPRISE EDITION
The Java 2 Platform, Enterprise Edition (J2EE), has rapidly established a new programming model for developing distributed
File Block2 :
ut of a web page. Web browsers are used to view HTML documents. Two popular web browsers are the Netscape Navigator 4.x and the Microsoft Internet Explorer 5.x. Browsers control the layout of a web page
File Block3 :
te Once, Run Anywhere ? properties
? High quality tool support
? Reuse of components and tag libraries
? Separation of dynamic and static content
upload
Back

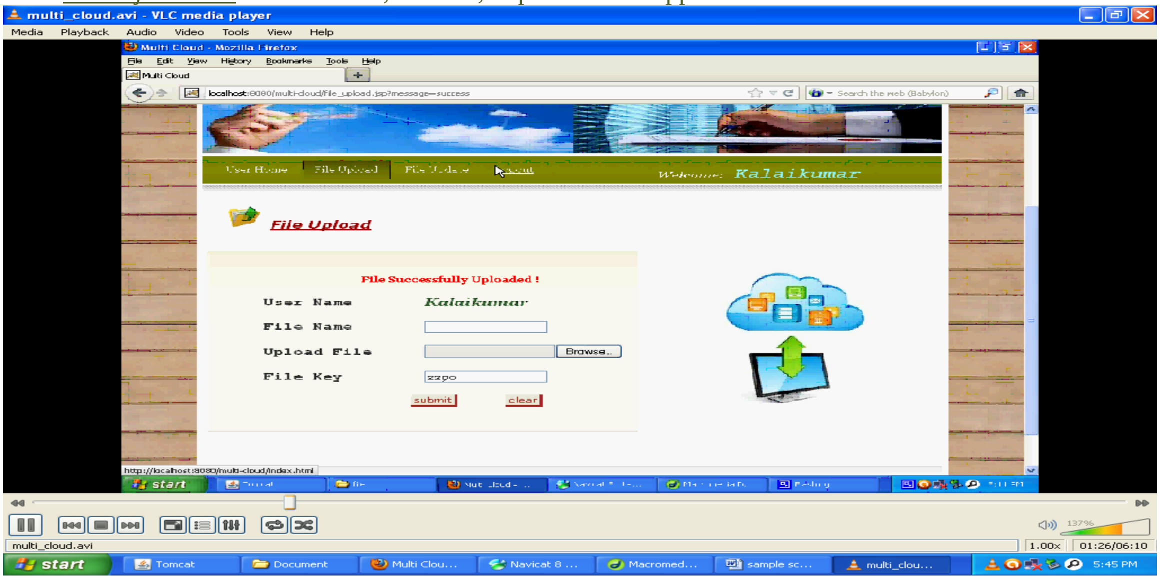
multi_cloud.avi - VLC media player
Multi Cloud - Mozilla Firefox
File Upload
File Successfully Uploaded !
User Name
Kalaikumar
File Name
Upload File
Browse...
File Key
submit
clear
Welcome: Kalaikumar

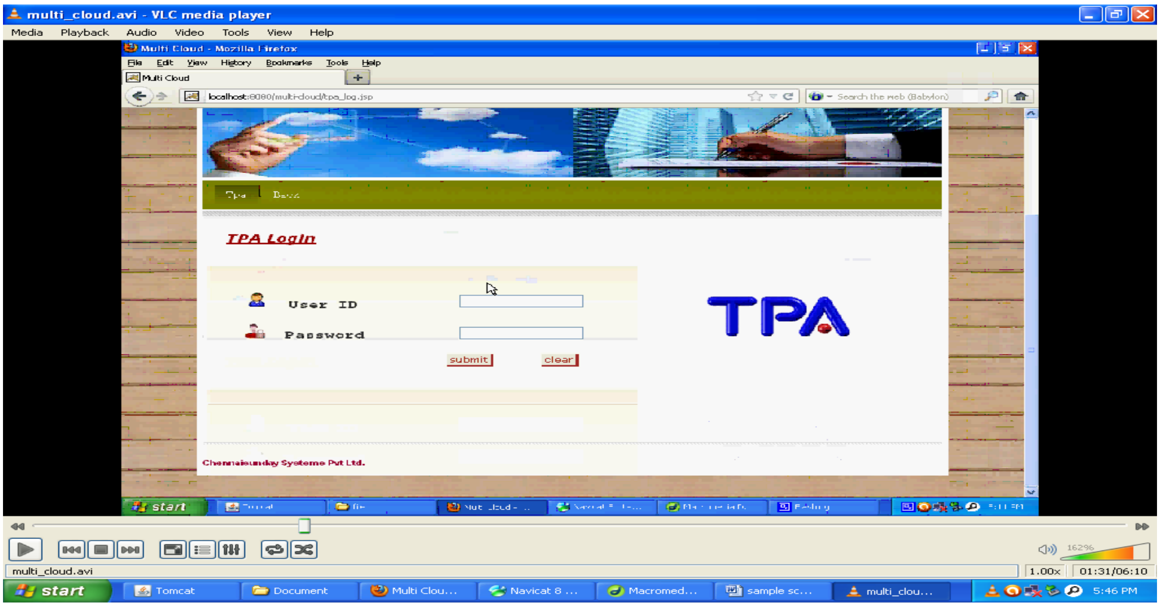
multi_cloud.avi - VLC media player
Multi Cloud - Mozilla Firefox
TPA Login
User ID
Password
submit
clear
TPA


multi_cloud.avi - VLC media player
Multi Cloud - Mozilla Firefox
Welcome: TPA
TPA ALL FILES
All Files
User ID
Name
Date
File ID
File Name
File Size
Status
9
Balaji
25/05/2012
8
java.txt
5.193359375 KB
uploaded
10
Satheshkumar
25/05/2012
9
sample.txt
2.0185546875 KB
uploaded
10
Satheshkumar
25/05/2012
10
sample.txt
0.9453125 KB
uploaded
11
Kalaikumar
25/05/2012
8
java.txt
5.1552734375 KB
uploaded

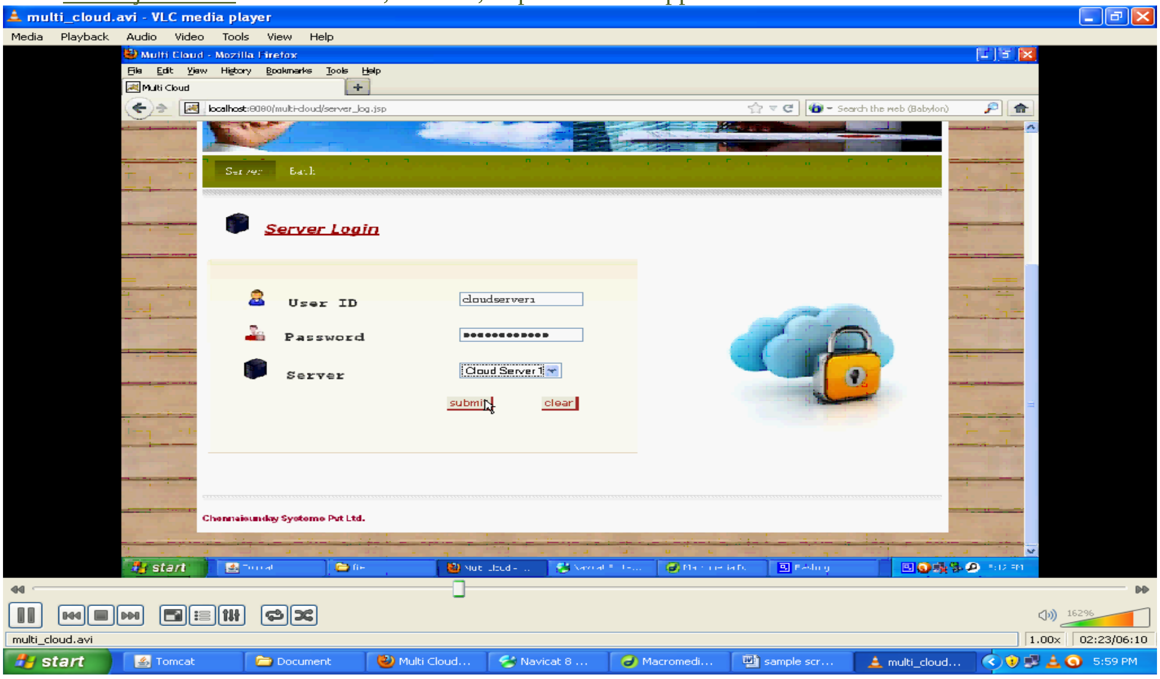
multi_cloud.avi - VLC media player
Multi Cloud - Mozilla Firefox
Server Login
User ID
cloudserver1
Password
Server
Cloud Server 1
submit
clear
Chennaisunday Systems Pvt Ltd.
02:23/06:10


multi_cloud.avi - VLC media player
Verification in Multi-Cloud Storage
Welcome: CLOUD1
Cloud Server Home
New Files
User ID
Name
Date
File ID
File Name
File Size
Status
Kalaikumar
java.txt
allow
02:25/06:10

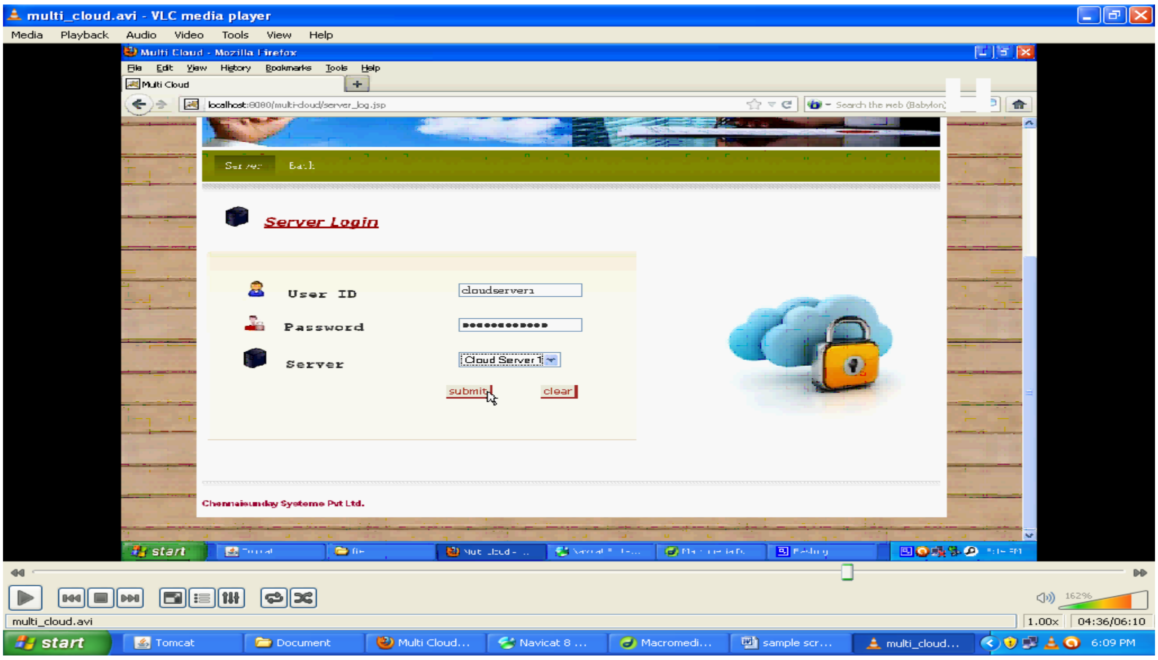
multi_cloud.avi - VLC media player
Multi Cloud - Mozilla Firefox
Server Login
User ID
cloudserver1
Password
Server
Cloud Server 1
submit
clear
Chennaisunday Systems Pvt Ltd.
04:36/06:10

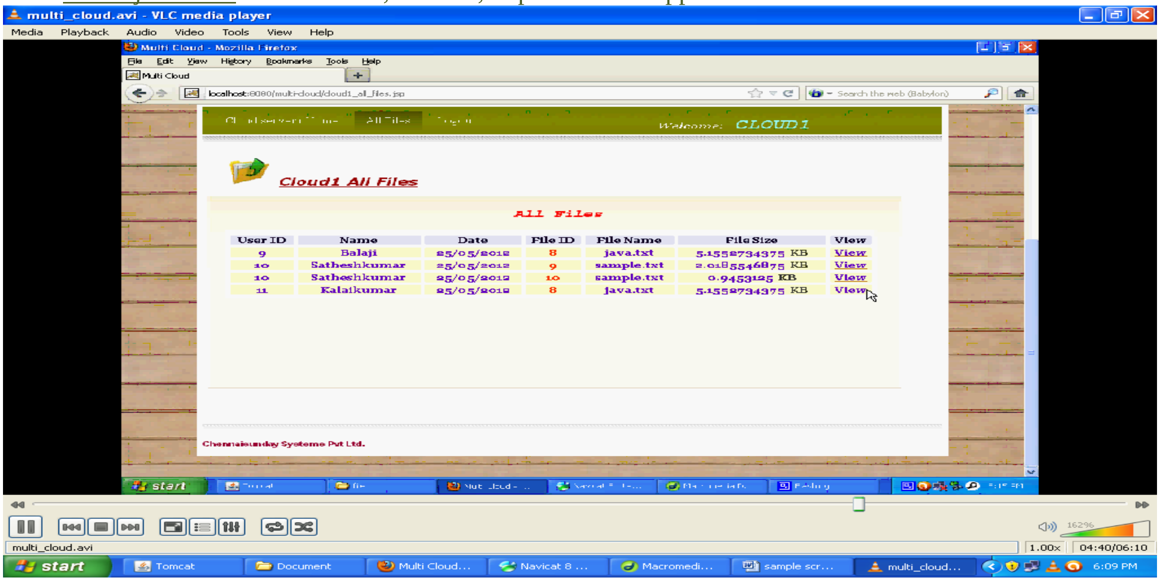
multi_cloud.avi - VLC media player
Cloud1 All Files
All Files
User ID Name Date File ID File Name File Size View
9 Balaji 25/05/2012 8 java.txt 5.1552734375 KB View
10 Satheshkumar 25/05/2012 9 sample.txt 2.0185546875 KB View
10 Satheshkumar 25/05/2012 10 sample.txt 0.9453125 KB View
11 Kalaikumar 25/05/2012 8 java.txt 5.1552734375 KB View
Chennaisunday Systems Pvt Ltd.

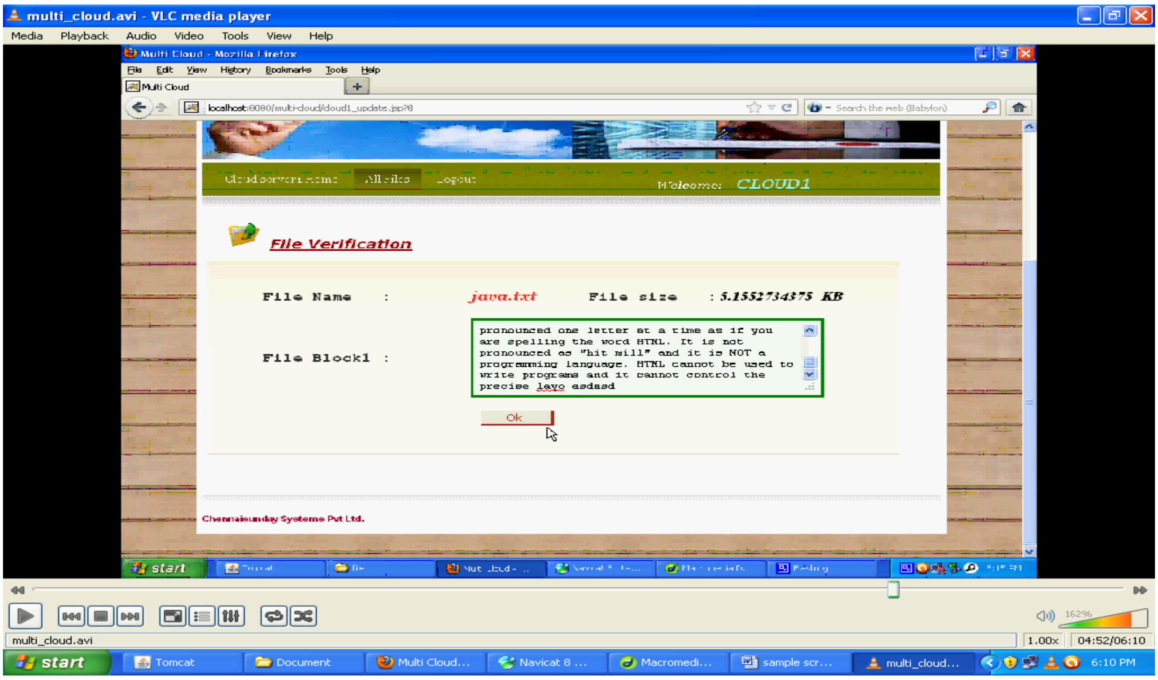
multi_cloud.avi - VLC media player
Welcome: CLOUD1
File Verification
File Name : java.txt File size : 5.1552734375 KB
File Block1 :
pronounced one letter at a time as if you are spelling the word HTML. It is not pronounced as "hit mill" and it is NOT a programming language. HTML cannot be used to write programs and it cannot control the precise layo asdasd
Ok
Chennaisunday Systems Pvt Ltd.

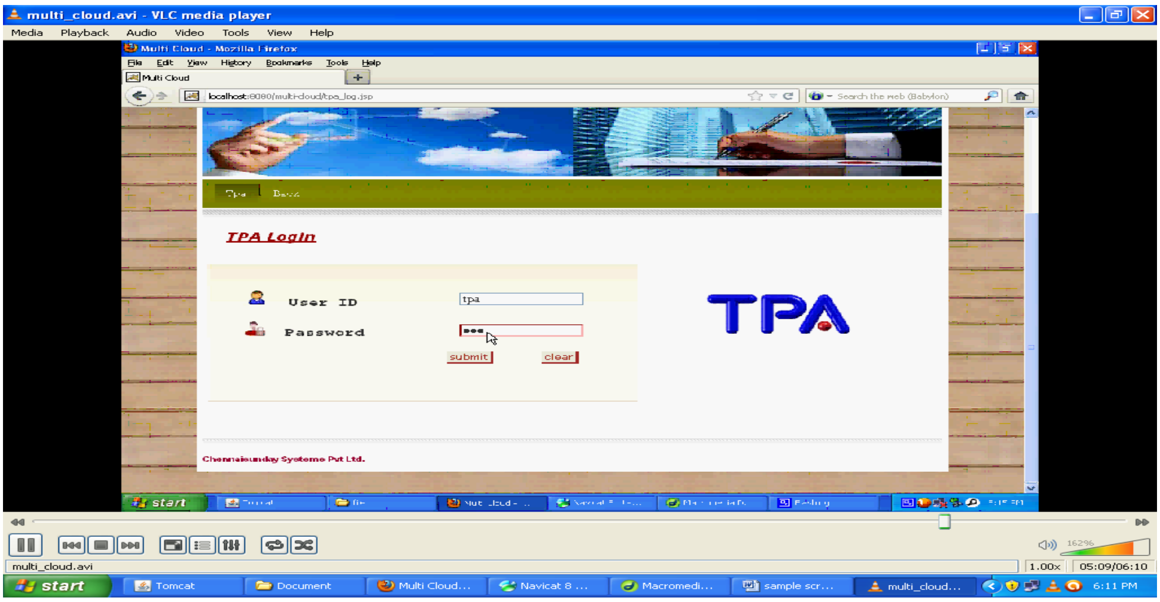
multi_cloud.avi - VLC media player
TPA Login
User ID
Password
submit
clear
TPA
Chennaisunday Systems Pvt Ltd.

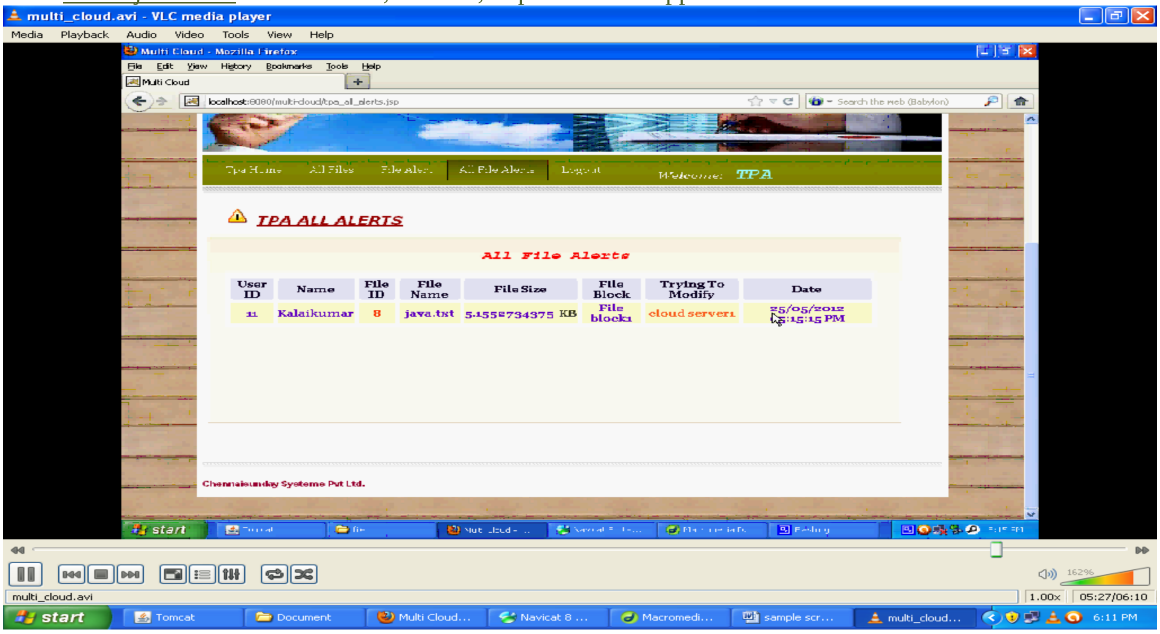

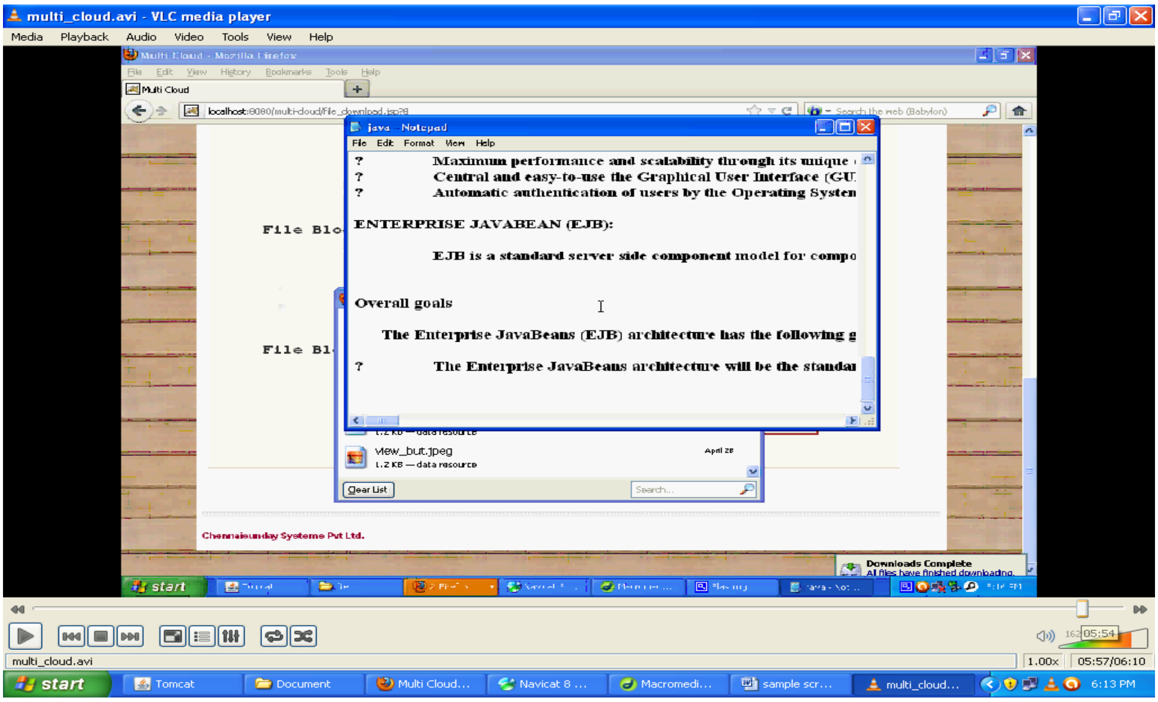

VI. CONCLUSION

We presented the construction of an efficient PDP scheme for distributed cloud storage. Based on homomorphic verifiable response and hash index hierarchy, we have proposed a cooperative PDP scheme to support dynamic scalability on multiple storage servers. We also showed that our scheme provided all security properties required by zero knowledge interactive proof system, so that it can resist various attacks even if it is deployed as a public audit service in clouds. Further more. we optimized the probabilistic query and periodic verification to improve the audit performance. Our experiments clearly demonstrated that our approaches only introduce a small amount of computation and communication overheads. Therefore, our solution can be treated as a new candidate for data integrity verification in outsourcing data storage systems. As part of future work, we would extend our work to explore more effective CPDP constructions. Finally, it is still a challenging problem for the generation of tags with the length irrelevant to the size of data blocks. We would explore such a issue to provide the support of variable-length block verification.

ACKNOWLEDGMENT

I would like to express my sincere thanks to my Guide and my Co-Authors for their consistence support and valuable suggestions.

REFERENCES

[1] B. Sotomayor, R. S. Montero, I. M. Llorente, and I. T. Foster, Virtual infrastructure management in private and hybrid clouds," IEEE Internet Computing, vol. 13, no. 5, pp. 14–22,2009.

[2] G. Ateniese, R. C. Burns, R. Curtmola, J. Herring, L. Kissner, Z. N. J. Peterson, and D. X. Song, "Provable data possession at untrusted stores," in ACM Conference on Computer and Communications Security, P. Ning, S. D. C. di Vimercati, and P. F. Syverson, Eds. ACM, 2007, pp. 598–609.

[3] A. Juels and B. S. K. Jr., "Pors: proofs of retrievability for large files," in ACMConference on Computer and Communications Security, P. Ning, S. D. C. di Vimercati, and P. F. Syverson, Eds. ACM, 2007, pp. 584–597.

[4] G. Ateniese, R. D. Pietro, L. V. Mancini, and G. Tsudik, "Scalable and efficient provable data possession," in Proceedings of the 4th international conference on Security and privacy in communication netowrks, SecureComm, 2008, pp. 1–10.

[5] C. C. Erway, A. K¨upc¸ ¨u, C. Papamanthou, and R. Tamassia, "Dynamic provable data possession," in ACM Conference on Computer and Communications Security, E. Al-Shaer, S. Jha, and A. D. Keromytis, Eds. ACM, 2009, pp. 213–222.

[6] H. Shacham and B. Waters, "Compact proofs of retrievability," in ASIACRYPT, ser. Lecture Notes in Computer Science, J. Pieprzyk, Ed., vol. 5350. Springer, 2008, pp. 90–107.

[7] Q. Wang, C.Wang, J. Li, K. Ren, and W. Lou, "Enabling public verifiability and data dynamics for storage security in cloud computing," in ESORICS, ser. Lecture Notes in Computer Science, M. Backes and P. Ning, Eds., vol. 5789. Springer, 2009, pp. 355–370.

[8] Y. Zhu, H. Wang, Z. Hu, G.-J. Ahn, H. Hu, and S. S. Yau, "Dynamic audit services for integrity verification of outsourced storages in clouds," in SAC, W. C. Chu, W. E. Wong, M. J. Palakal, and C.-C. Hung, Eds. ACM, 2011, pp. 1550–1557.

[9] K. D. Bowers, A. Juels, and A. Oprea, "Hail: a high-availability and integrity layer for cloud storage," in ACM Conference on Computer and Communications Security, E. Al-Shaer, S. Jha, and A. D. Keromytis, Eds. ACM, 2009, pp. 187–198.

[10] Y. Dodis, S. P. Vadhan, and D. Wichs, "Proofs of retrievability via hardness amplification," in TCC, ser. Lecture Notes in Computer Science, O. Reingold, Ed., vol. 5444. Springer, 2009, pp. 109–127.

[11] L. Fortnow, J. Rompel, and M. Sipser, "On the power of multiprover interactive protocols," in Theoretical Computer Science, 1988, pp. 156–161.

[12] Y. Zhu, H. Hu, G.-J. Ahn, Y. Han, and S. Chen, "Collaborative integrity verification in hybrid clouds," in IEEE Conference on the 7th International Conference on Collaborative Computing: Networking, Applications and Worksharing, CollaborateCom, Orlando, Florida, USA, October 15-18, 2011, pp. 197–206.

[13] M. Armbrust, A. Fox, R. Griffith, A. D. Joseph, R. H. Katz, A. Konwinski, G. Lee, D. A. Patterson, A. Rabkin, I. Stoica, and M. Zaharia, "Above the clouds: A berkeley view of cloud computing," EECS Department, University of California, Berkeley, Tech. Rep., Feb 2009.

[14] D. Boneh and M. Franklin, "Identity-based encryption from the weil pairing," in Advances in Cryptology (CRYPTO'2001), vol. 2139 of LNCS, 2001, pp. 213–229.

[15] O. Goldreich, Foundations of Cryptography: Basic Tools. Cambridge University Press, 2001.

(MCKIBBEN'S MUSCLE) Robots Make Our Work Lighter, But We Have Made the Robots Lighter.

Shripad Shashikant Chopade[1], Sagar Pradip Kauthalkar[2], Chaitanya Bhalchandra Bhandari[3]

Shripad Shashikant Chopade, M Tech (Machine Design & Robotics), Research Scholar, India
Sagar Pradip Kauthalkar, M Tech (Machine Design & Robotics), Research Scholar, India
Chaitanya Bhalchandra Bhandari, Research Scholar, India

ABSTRACT: *Industrial robots, which are heavy moving bodies, show high risk of damage when working and also sessions in dense environment of other robots. This initiated the allure for lighter robot constructions using soft arms. This paper reports on the design of a biorobotic actuator. Data from several vertebrate species (rat, frog, cat, and human) are used to evaluate the performance of a McKibben pneumatic actuator. Soft arms create powerful, compact, compliance and light robotic arms and consist of pneumatic actuators like McKibben muscles. Currently there are some trajectory problems in McKibben muscles, which restrict its application. This paper presents solutions to certain problems in the McKibben muscles by the use of Electro Active Polymers (EAP). The main attractive characteristic of EAP is their operational similarity to biological muscles, particularly their resilience and ability to induce large actuation strains.*

Electro Active Polymers (EAP) as sensors, which simplify a robotic finger, models by acting like an actuator (sensor cum actuator). Ion-exchange Polymer Metal Composite (IPMC), one of the EAPs, has been selected by us ahead of its alternatives like shaper memory alloys and electro active ceramics and the reason for its selection is also discussed in this paper.

We devise a unique model to eliminate trajectory errors by placing EAP stripes in robots' joints, which can also be applied to current (heavy) robots actuated by motors. This paper would obliterate all the difficulties currently present in McKibben muscles system, which currently restricts its application. Adroit use of the solutions provided in this paper would abet researchers to produce highly efficient artificial muscles system. We give the idea of an artificial muscle system which consume "less energy & oxygen" than a natural one. Therefore we discuss the world's most energy efficient robot with our innovative idea.

Keywords: *Actuator, Analyzer, Electro Active Polymers (EAP), Fingers, Gripper, Robotic Hand, Sensors etc….*

I. INTRODUCTION TO MCKIBBEN MUSCLES

Industrial robots are very heavy and highly rigid because of their mechanical structure and motorization. These kinds of robots in the dense environment of other robots may hit and damage each other due to technical errors or during the training sessions. This initiated the idea of developing lighter robot constructions. Replacing heavy motor driving units, which constitute much weight of a robot with lighter McKibben muscles, will serve the purpose. The McKibben Artificial Muscle is a pneumatic actuator, which exhibits many of properties found in real muscle. American physician Joseph L. McKibben first developed this muscle in 1950's. It was originally intended to actuate artificial limbs for amputee's spring-like characteristics, physical flexibility and lightweight. Its main advantage is the very high force to weight ratio, making it ideal for mobile robots.

II. CONSTRUCTION

The device consists of an expandable internal bladder (a rubber elastics tube) surrounded by helically weaved braided shell made of nylon cloth which are attached to either sides like tendon-like structures. A McKibben Artificial Muscle can generate an isometric force of about 200 N when pressurized to 5 bars and held to a length of 14 cm. This actuator is relatively small.

Fig.1

WORKING:

When the internal bladder is pressurized, expands in a balloon-like manner against the braided shell. The braided shell acts to constrain the expansion in order to maintain a cylindrical shape.

Fig.2

As the volume of the internal bladder increases due to increase in pressure, the actuator shortens and produces tension if coupled to a mechanical load. This basic principle is the conversion of the radial stress on the rubber tube into axial stress and during relaxation of the muscle the reverse happens. A thin rubber bladder is used to transmit the entire pressure acting on it to the unstreachable outside shell. One end of the muscles is sealed where loads can be attached and the other end is for the air from the regulator as shown in figure 3.

By using a finite element model approach, we can estimate the interior stresses and strains of the McKibben actuator.

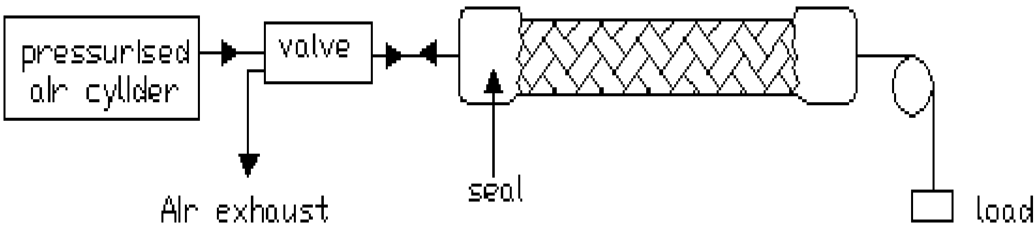

Fig.3

Performance Characteristics: The force generated by a McKibben Artificial Muscle is dependent on the weave characteristics of the braided shell, the material properties of the elastic tube, the actuation pressure, and the muscle's length.

Artificial versus Biological Muscle: The force-length properties of the McKibben actuator are reasonably close to biological muscle. However, the force-velocity properties are not. We have designed a hydraulic damper to operate in parallel with the McKibben actuator to produce the desired results.

Energy requirement: the energy requirement of a McKibben artificial robot is the least among all the robots. It is even less than that used up by the human muscle.

III. MCKIBBEN MUSCLES AS ACTUATOR

A PHYSIOLOGICAL MODEL

Two McKibben muscles put into antagonism define a rotoid actuator based on the physiological model of the biceps-triceps systems of human beings. The two muscles are the agonist and the antagonist and are connected by means of a chain and driving sprocket as shown in the figure 3.

The force difference between the two generates a Torque. An initial tension must be maintained against the passive tension found in human physiology. When the pressures are increased and decreased to P1 and P2 respectively, an angular deflection of θ is produced. The equation for the torque produced was deduced as:

$$T=k1\ (P1-P2)-K2\ (P1+P2)\ \theta$$

Where, k1 and K2 are constants. This equation is much similar and gives a near value to the one deduced by N.Hogan having the system of biceps-triceps as the basis.

$$T= Tmax\ (Ub-Ut)-k\ (Ub-Ut)\ \theta$$

Where Tmax, k are constants and Ub, Ut are normalized nervous control of biceps and triceps.

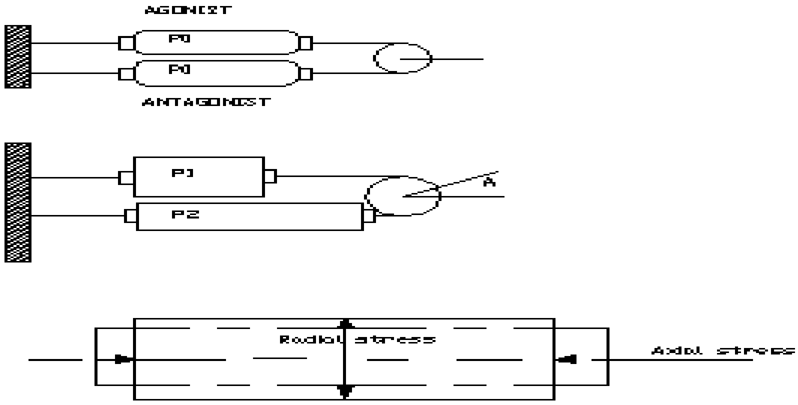

Fig.4

Advantages of the McKibben Artificial Muscle

- High force to weight ratio Size availability
- Flexible
- Powerful
- Damped
- Effective
- Lightweight
- Low-cost
- Smooth.

Electro active Polymer Artificial Muscles:

Electro active polymers (EAP) are being developed to enable effective, miniature, inexpensive and light robotic applications like surface wipers etc. The EAP material that is commonly used is known as IPMC (Ion- exchange polymer metal composite), which is dealt later. The EAP strip can be made as grippers and strings, which can grab and lift loads, among many other potential uses. These strips and strings have the potential to greatly simplify robotic spacecraft tasks.

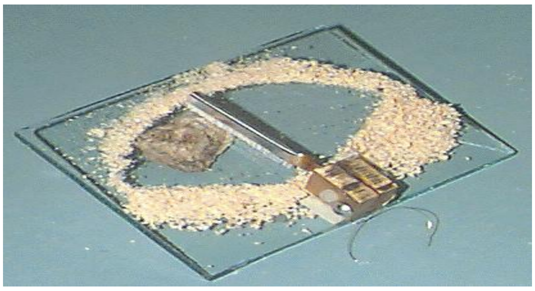

Fig. 5

When an electric charge follows through the ribbon, charged particles in the polymer get pushed or pulled on the ribbon's two sides, depending on the polarity. The net result: the ribbon bends. Four such ribbons can be made to lift a load. They can operate under cryogenic conditions like -140 degree Celsius. When the power supply is turned off, the cylinder relaxes, enabling it to lift or drop loads.

IV. INFLUENCE OF ELECTRIC FIELD (i.e. BENDING OF THE STRIP)

The bending can occur due to differential contraction and expansion of outer most remote regions of a strip if an electric field is imposed across its thickness as shown in figure. IPMC strips generally bend towards the anode and if the voltage signal is reversed they also reverse their direction of bending. Conversely by bending the material, shifting of mobile charges become possible due to imposed stresses. When a rectangular strip of the composite sensor is placed between two electrodes and is bent, a stress gradient is built on the outer fibers relative to the neutral axis (NA). The mobile ions therefore will shift toward the favored region where opposite charges are available. The deficit in one charge and excess in the other can be translated into a voltage gradient that is easily sensed by a low power amplifier. Since these muscles can also be cut as small as one desires, they present a tremendous potential to micro-electro-mechanical systems (MEMS) sensing and actuation applications.

V. ADVANTAGES OF EAP

- Can be manufactured and cut in any size and shape.
- Have good force to weight characteristics in the presence of low applied voltages.
- Work well in both humid and dry environments.

- Work well in cryogenic conditions and at low pressures.
- Unique characteristics of low density as well as high toughness, large actuation strain and inherent damping vibrations.
- Show low impedance.

VI. IPMC

Construction:

The IPMC are composed of a per fluorinated ion exchange membrane which consist of a polymer matrix that is coated on the outer surface with platinum in most cases (silver and copper have also been used).This coating aids in the distribution of the voltage over surface. These are made into sheets that can be cut into different shapes and sizes as needed.

Working:

Strips of these composites can undergo large bending and flapping displacement if an electric field is imposed across the thickness. A circuit is connected to surface to produce voltage difference, causing bending. Thus, in this sense they are large motion actuators. Conversely by bending the composite strip, either quasi-statically or dynamically, a voltage is produced across the thickness of the strip. Thus, they are also large motion sensors.

When the applied signal frequency is varied, so does the displacement up to a point where large deformations are observed at a critical frequency called resonant frequency. At resonant frequency maximum deformation is observed and beyond this frequency the actuator response is diminished. Lower frequencies (down to 0.1 or 0.01 Hz) lead to higher displacement (approaching 25 mm) for a 0.5cm X 2cm X 0.2mm thick strip and failed for other frequency values under similar conditions. IPMC films have shown remarkable displacement under relatively low voltage, using very low power. A film-pair weighing 0.2-g was configured as an actuator and using 5V and 20mW successfully induced more than 11% contraction displacement. Since the IPMC films are made of a relatively strong material with a large displacement capability, we investigated their application to emulate fingers. The gripper we suggested may be supported using graphite/epoxy composite rod to emulate a lightweight robotic arm.

Advantages of IPMC

- Light
- Compact
- Driven by low power & voltage
- Large strain capability

VII. MCKIBBEN MUSCLES AND EAP SENSORS

INTELLIGENT ROBOTS:

Developing intelligent robots requires the combination of strong muscles (actuators) and acute sensors, as well as the understanding of the biological model. Using effective EAP materials as artificial muscles, one can develop biologically inspired robots and locomotives that possibly can walk, fly, hop, dig, swim and/or dive. Natural muscles are driven by a complex mechanism and are capable of lifting large loads at short (millisecond) response times.. Since muscle is fundamental to animal life and changes little between species, we can regard it as a highly optimized system. The mobility of insects is under extensive study.

Development of EAP actuators is expected to enable insect-like robots that can be launched into hidden areas of structures to perform inspection and various maintenance tasks. In future years, EAP may emulate the capabilities of biological creatures with integrated multidisciplinary capabilities to launch space missions with innovative plots. Some biological functions that may be adapted include soft-landing like cats, traversing distances by hopping like a grasshopper and digging and operating cooperatively as ants.

VIII. DEVELOPMENT OF EAP FOR SPACE APPLICATIONS

Since 1995, under the author's lead, planetary applications using EAP have been explored while improving the understanding, practicality and robustness of these materials. EAP materials are being sought as a substitute to conventional actuators, and possibly eliminating the need for motors, gears, bearings, screws, etc. Generally, space applications are the most demanding in terms of operating conditions, robustness and durability offering an enormous challenge and great potential for these materials.

A comparison between IPMCs and other types of actuators is given below:

PROPERTIES	Ionic polymer –Metal Composites (IPMC)	Shape Memory Alloys (SMA)	Electro Active Ceramics (EAC)
Actuation Displacement	>10%	<8% short fatigue life	0.1-0.3%
Force (Mpa)	10-30	About 700	30-40

Reaction speed	Micro sec to second	Sec to min	Micro sec to sec
Density	1.25 g/cc	5-6g/cc	6-8g/cc
Drive voltage	4-7 V	NA	50-800V
Fracture Toughness	Resilient, elastic	Elastic	Fragile

Table 1

IX. SUGGESTIONS

EAP AS SENSORS:

This paper suggests placing of EAP strips (IPMC) at each joint of the robot with each and fixed to each arm as shown in diagram. Relative angular deflections of the arms bend the strip (mechanical deformation), which generates current. During robot's training session the current signals from each joint is converted (using transducer) into data signals for a PC-platform data acquisition system which stores the data as a base. During the robot's regular work, the signal from each joint is analyzed for every microsecond and compared with the stored database. Any variation would develop error signals, which are processed for correction signals by the system. These signals are then used to control the piezo-electric or high-speed matrix pneumatic valve which regulates the air flow to muscles.

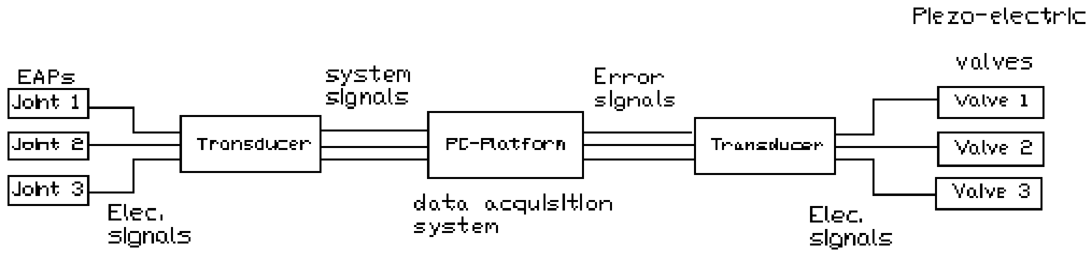

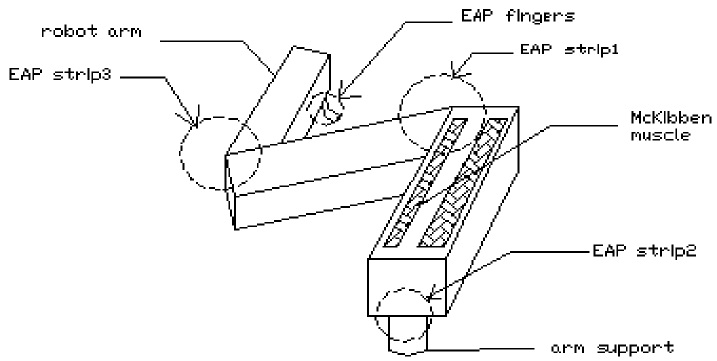

Fig.6 Inserting EAP stripes 1, 2, 3 in the robot arm

X. EAP FINGERS

This paper suggests two or more EAP (IPMC) strips supported by an epoxy/graphic composite holder can act as robotic fingers (lifters and grippers).When the stripes are actuated by passing current, the fingers bend outwards to allow the object in.

The fingers are then de-energized by reducing the voltage. During the training session, the maximum and minimum voltages required for opening and closing respectively is stored in the database. When the object having less/more dimension (than the standard) is gripped, the additional bend produced in the strips would generate current which is sensed and processed for dimensional inaccuracy and the object is rejected. The error signals can also be possessed for correction signals, which control the manufacturing machines.

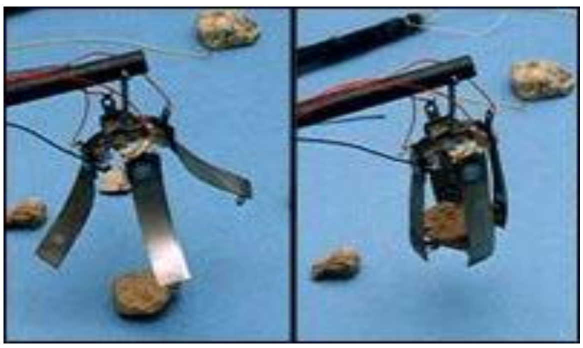

Fig. 7

XI. EAP AS DAMAGE ANALYSER

Since the equation for the stress on an EAP stripe is available, the force with which a robot arm hits any obstacle can be analyzed. Having known the geometry and material properties of the arm, the analysis will infer the replacement or extension of life span of that arm without getting into the depth study of the damage caused which takes time and money. The stress acting on the metal composite can be calculated using the following equation.

$$s = k\ (C0, Ci)\ E^2$$

Where k (C0, Ci) is an electromechanical coefficient and E is the local electric field.

XII. DESIGN OF INTELLIGENT ROBOTIC HAND:

Fig. 8 An EAP actuated hand with fingers

The robotic hand muscles are made up of McKibben muscles while the fingers are supported with EAP strips which can act as sensors as well as actuators and can be used for lifting loads as shown in the diagram 8.

XIII. DESIGN OF MUSCLES FOR HUMAN BEINGS-BIONIC MEN

The McKibben muscles along with the EAP strips can be used to replace damaged muscles for handicaps. Years from now, the McKibben muscles could also conceivably replace damaged human

Fig. 9

These Biorobotic muscles:
- ✓ Reduce the metabolic cost of locomotion.
- ✓ Reduce the level of perceived effort.
- ✓ Improve gait symmetry as measured by kinematics and kinetic techniques.
- ✓ Consume less oxygen and energy than even a natural system.

XIV. CONCLUSION

Electro active polymers are changing the paradigm about the complexity of robots. In the future, we see the potential to emulate the resilience and fracture tolerance of biological muscles, enabling us to builds simple robots that dig and operate cooperatively like ants, soft-land like cats or traverse long distances like a grass hopper. The observed remarkable vibrational characteristics of IPMC composite artificial muscles clearly point to the potential of these muscles for biomimetic applications such as swimming robotic structures, wing flapping flying machines, slithering snakes, heart and circulation assist devices, peristaltic pumps etc..It has recently been established that the tweaking of the chemical composition of IPMC the force capability of these muscles can be greatly improved. IPMCs are the artificial muscles that give space robots animal-like flexibility and manipulation ability based on a simple, light-weight strip of highly flexible plastic that bends and functions similarly to human fingers when electrical voltage is applied to it. Two EAP actuators are used as miniature wipers to clear dust off the viewing windows of optical and infrared science instruments. Studies made by robotics specialists and neurophysiologists suggest that McKibben artificial muscles can be used to develop Biorobotic arms for handicaps. Years from now, the McKibben muscles could also conceivably replace damaged human muscles, leading to partially “bionic men” and “bionic women” of the future.

REFERENCES

[1] Bar-Cohen Y., T. Xue and S.-S., Lih, "*Polymer Piezoelectric Transducers for Ultrasonic NDE,*"
[2] Alexander R. M., “*Elastic Mechanisms in Animal Movement*”, The Cambridge University Press: Cambridge, 1988.

International Journal of Modern Engineering Research (IJMER)
www.ijmer.com Vol. 3, Issue. 5, Sep - Oct. 2013 pp-2749-2753 ISSN: 2249-6645

Three Element Beam forming Algorithm with Reduced Interference Effect in Signal Direction

V. Manjula, M. Tech, K.Suresh Reddy, M.Tech, (Ph.D)
[1]Deparment of ECE, G. P. R Engg. College, Kurnool
[2]Head of the department ECE Dept., G.P.R Engg College, Kurnool

ABSTRACT: *The beam forming algorithm simulated in this project is motivated by analyzing a low-cost radar system that provides wide spatial coverage and very rapid target detection as well as tracking.Desigining towards these goals, a reasonable and mostly generic receiver would employ a three-antenna receiver. Because the minimum number of sensing elements needed to determine two dimensional angles is three the system cost has been mostly minimized.*
In this project 1 consider the problem of using our low cost system to detect and estimate the direction of arrival (DOA) of a desired signal in the presence of a dominant interference signal.

Unlike most direction of arrival (DOA) estimation algorithms, the proposed algorithm does not use grid search. Instead the estimates result from a closed-form solution, a great advantage in time-sensitive applications. Additionally, we carry out numerical simulations and results will be analyzed to demonstrate that our algorithm is capable of achieving more reliable DOA estimates than those found with the well-known multiple signal classification algorithm. Finally, a complete radar signal processing example will be presented.

MATLAB/GNU OCTAVE simulation tool will be used for simulation. The simulation results, applications, merits and demerits of proposed approach will be analyzed and will be documented.

Keywords: *Three antenna receiver, direction of arrival*

I. INTRODUCTION

A conventional technique of processing temporal sensor array measurements for signal estimation ,interference suppression, or source direction and spectrum estimation is beam forming [1-3].It has been exploited in numerous applications (e.g.,radar,sonar,wireless communications, speech processing, medical imaging, radio astronomy).
The beam forming algorithm presented in this paper is motivated by analyzing low –cost radar system that provides wide spatial coverage and very rapid target detection as well as tracking. Designing towards these goals, reasonable and mostly generic receiver would employ a three antenna receiver. because the minimum number of sensing elements needed to determine two dimensional angles is three, the system cost has been mostly minimised..we now consider the problem of using our low cost system to detect and estimate the direction of arrival of a desired signal in the presence of dominant interfering signal.

The rest of the paper is organized as follows. In section1,first,we give a full description of our algorithm ,starting with the system model and continuing with a tabular list of algorithm steps .Next we proceed with the system model and continuing with a tabular list of algorithm steps .Next ,we proceed with a detailed description on our methodology for interference cancellation ,target detection ,and phase angle estimation. Afterwards, we analytically identify the spatial scenarios of a jammer and target in which the proposed technique will reliably estimate a target's DOA. Next, in section 3 the stastical performance of the algorithm is explained through a collection of simulations..Finally; section5 contains the conclusions of this work.

II. SYSTEM MODEL

Three antennas in an arbitrary geometry make up our receiver structure. The received signal at the *i*th element at time n,is denoted by $x_i(n)$ and is formed from the coherent condition of the target signal $t_i(n)$,the jammer signal $u_i(n)$,and the noice $v_i(n)$.Therefore

$$x_i(n) = t_i(n) + u_i(n) + v_i(n) \quad i=1,2,3. \qquad (1)$$

Assuming point sources and equal gains for the three receivers, the target and interfering signal at each sensor will be phased replicas [10].We also assume sensor will be phased replicas [10].We also assume narrow band signals, which means that relative phases of the received signal s will be constant across the entire band.the target signals are modelled as

$$t_2(n) = t_1(n)e^{j\theta}$$
$$t_3(n) = t_1(n)e^{j\delta} \qquad (2)$$

Where

$$t_1(n) = \alpha(n)e^{j\phi(n)} \qquad (3)$$

And the interfering signals are

$$u_2(n) = u_1(n)e^{j\epsilon}$$
$$u_3(n) = u_1(n)e^{j\eta} \qquad (4)$$

Where

$$u_1(n) = \beta(n)e^{j\lambda(n)} \qquad (5)$$

The variables $\alpha(n)$ and $\phi(n)$ respectively denote the amplitude and the time varying phase of the target at antenna 1,while θ and δ denote the relative phase angles at antenna 2 and 3.In a similar manner ,the parameters $\beta(n)$,$\lambda(n), \epsilon,$ and η denote the amplitude ,time varying phase ,and electrical phase angles of the jamming signal .The noise ,$v_i(n)$ is a white zero –mean complex random variable with variance σ^2 and is uncorrelated with $v_m(n)$ for $i \neq m.$ All greek letter variables represent real numbers.

We now give an overview of our algorithm which does not fit either of the paradigms introduced above, i.e. we do not scan a narrow beam nor do we use a parametric method to estimate the steering vectors of all present source signals.Throughout the rest of this paper, we refer to the desired signal as the target signal because this approach has been motivated from the signal processing needs of a radar system.we have also choosen to use a noise jammer for the interference source because of the ease at which one can be simulated, but application need not be limited to this case.the algorithm steps are enumerated in table I.Like [11] instead of using beam forming is used to null a jamming signal. Nulling the jammer enables a reduced –complexity mathematical technique for estimating target signal parameters. Unlike [11], we employ phase interferometery and require one less receiver channel. Adapting a beam based solely on information about an processing techniques that attempt to reduce computational complexity.

Table1

Algorithm overview
Step 1: Find beam forming weights that minimize the jammer's power.
Step 2: Apply threshold detection to the Beam former outputs of each range - Doppler bin of interest.
Step 2a: If a target is detected, record its range and Doppler and proceed to step 3.
Step 2b: If no target is detected, start over with the next coherent processing interval.
Step 3: Estimate relative phase information for each detected target.
Step 4: Calculate DOAs from the phase information.

III. METHODOLOGY DESCRIPTION-STEPS

I. Interference Cancellation

If a weighted sum of the received signals is formed, it is possible to choose non-zero, equal magnitude weights that completely cancel, or null the jammer signals. The importance of the weights being non-zero is obvious because we still desire to detect the target.A L shaped is assumed with 3 antennas located at (0,5) ,(0,0) and (5,0) . A jammer signal is assumed to be located to predefined coordinates. The jammer signal is a cosine wave with random noise added to it. The goal is to null of the three antennas due to the jammer signal. We calculate each of the antenna's net output due to the jammer signal by taking relative delays (time taken for the signal to reach the antenna) into consideration. The phase weights of each of 3 antennas are calculated using the below formulas

Antennas(1,2) = X1 + X2 * e^(jwt)
Antennas(1,3) = X1 + X3 * e^(jwt)

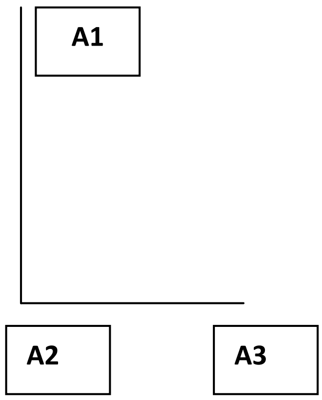

The phase weights are calculated by varying the value of pi from -180 to 180 in steps of 0.0001.We find minimum value value occurs and consider the pi value to be the corresponding phase weight value.After obtaining the phase weight values, we multiply the respective phase weight with the antenna output the compare the results.

II. Target Detection and Range estimation

We assume the target coordinates and calculate the Radar signal for 3 pulses. We then observe the output when the radar emits the signal, how it is reflected from the receiver and how it is received back by the transmitter. The total output will be the sum of the radar signal due to target and the jammer signal. A threshold value is computed based on the assumed noise power. The complete antenna output is compared with this threshold value. If a match is found, the corresponding index is noted and the round trip time and the range of the target are both calculated. If no match is found the entire process is repeated with another set of radar pulse signals.

III. Angle of arrival (AOA)

The Angle of arrival is calculated building the look up table for sample delays between antenna outputs to DOA of signal.The angles are measured considering the line joining antenna 2 and 3 as initial line where the location of antenna 2 is the origin.All angles are measured in anti clock wise direction.For example if the target is on the line joing the 1 and 2 antennas then it will be reported as 90 degrees. We first calculate maximum delays corresponding to Antenna pairs(1,2) and (2,3).Taking a loop from min to max value we calculate all the angles possible to the antenna pairs (1,2) and (2,3) by using the below formulae

Theta (1,2,1) = (180/ π) * sind(dd12/d12)
dd12: Additional distance travelled by the signal
d12: Distance between Antennas 1 and 2 Theta(1,2,2) = - Theta(1,2,1)
Theta(2,3,1) = (180/ π) * cosd(dd23/d23)
dd23: Additional distance travelled by the signal d23 : Distance between Antennas 1 and 2 Theta(2,3,2) = - Theta(2,3,1)
After building the look up table we now calculate cross correlation between Antenna 1 and 2 outputs, Antenna 2 and 3 outputs. The maximum peak from the cross correlation outputs is found for the 2 antenna pairs. Based on the maximum peak index the corresponding angles from the look up table are extracted for the Antenna pairs (1, 2) and (2,3).Therefore 4 angles are obtained A and B for the first antenna pair, C and D for the second antenna pair. The angle of arrival is then found by taking the differences of the angles (A,C), (A,D), (B,C) and (B,D). Wherever the least difference is obtained, angle of arrival is found by averaging the 2 angles where the minimum difference was obtained. For

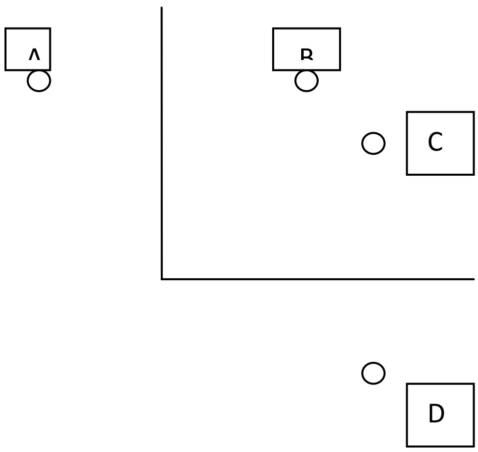

Ex:
Angles due to Antenna pair (1,2) is A,B
Angles due to Antenna pair (2,3) is C,D
Taking all the differences, minimum difference is obtained from B and C.
Therefore angle of arrival = (B+C)/2.

IV. SIMULATION RESULTS

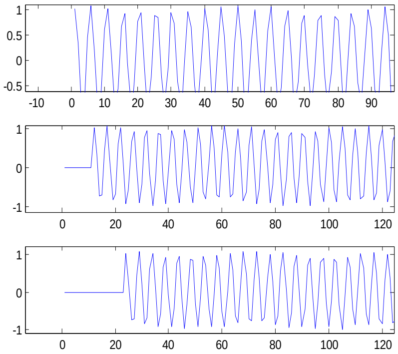

Fig.1.Data generation

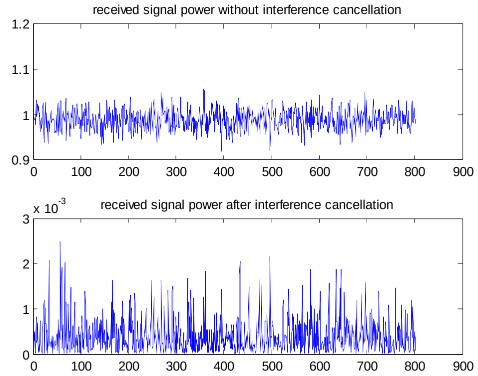

Fig.2. Interference cancellation

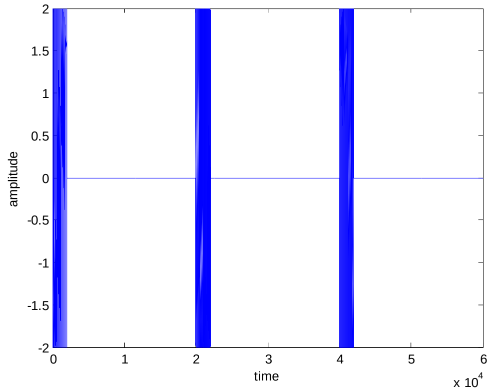

Fig.3. Radar Signal Generation

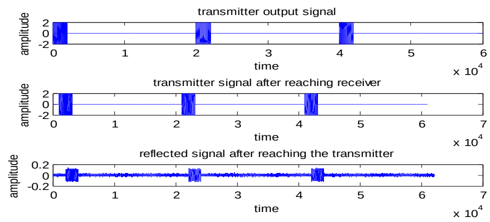

Fig.4. Phase Angle Estimation

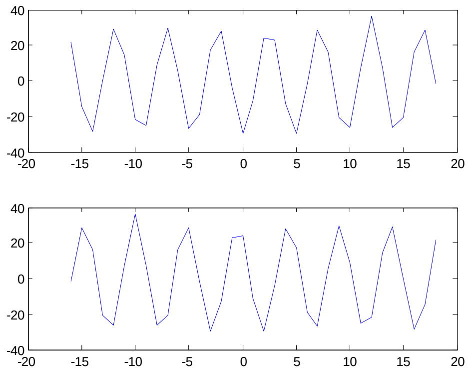

Fig. 5. Obtaining Angle of Arrival of Desired Signal

V. CONCLUSION

While in the presence of a dominant interference source, our proposed algorithm yields unbiased target DOA estimates from a low-cost, three-element receiver. We also mathematically identified the spatial scenarios where those estimates will have low variances. Unlike most DOA estimation methods, our estimates are found from closed-form expressions. In contrast to MUSIC, our algorithm performs well even when the number of target-containing snapshots available is small. This property makes it attractive for use in post-Doppler processing where it is common for a target signal to straddle only a few range-Doppler bins. Te DOAs of multiple targets can be estimated from one CPI as long as those target signals are resolvable in range or Doppler.

REFERENCES

[1] Krim,H.Viberg,M. Two decades of array signal processing researh:The parametric approach. IEEE signal processing Magazine,13(July 1996),67-94.
[2] Van veen, B.D.andBuckley,K.M. Beamforming:A Versatile approach to spatial filtering. IEEE signal processing Magazine,5(Apr 1988),4-24.
[3] Van Trees, H. L.Optimal Array Processing (Detection, Estimation, andModulation Theory, Part IV).New York: Wiley-Interscience, 2002.
[4] Capon, J.High resolution frequency-wavenumber spectrumanalysis. Proceedings of the IEEE, **57**, 8 (Aug. 1969), 1408—1418.
[5] Schmidt, R. O. Multiple emitter location and signal parameter estimation. IEEE Transactions on Antennas Propagation, **AP-34**, 3 (Mar. 1986), 276—280.

Numerical Analysis of Rotating Mixing of Fluids in Container Induced by Contra Rotating Stirrers

[1]Rafique A. Memon, [2]Mahera E. Baloch, [3]M. Anwer Solangi, [4]Ahsanullah Baloch

[1]*Lecturer in Mathematics, Government Degree College Gambat District, KhairpurMirs Sindh Pakistan.*
[2]*Institute of Computer System Engineering, TechnicalUniversity of Duisburg, Germany.*
[3]*Department Basic Sciences and Related Studies, Mehran University of Engg. & Tech. Jamshoro.*
[4]*Professor and Chairperson, Department of Computer Science, Isra University Hyderabad.*

ABSTRACT: *In this paper the numerical predictions are studied for contra–rotating mixing flow within a cylindrical container. The behaviour compared against previously simulated numerical results and found with good agreement. Two-dimensional incompressible complex flow of Newtonian fluid is relevant to the food industry. The numerical method adopted is a finite element semi-implicit time-stepping Taylor-Galerkin/pressure-correction multi stepping scheme, posed in a cylindrical coordinate system. The flow replicates the behaviour of actual industrial dough mixing.*

Key words: *Finite Element Method, Mixing Flows, Newtonian Fluids, Contra Rotating Stirrer, Power Law Model*

I. INTRODUCTION

This study is focusing on optimization of the mixer design to reduce the power consumption and improves the amount of work done on the dough mixing [1]. This problem is generally related with mixing industry such as in the field of chemical process applications, powder mixing processes [2], granular mixing, mixing of paper pulp in paper industry, particularly with mixing of dough in a food processing industry and many other industrial processes [3–4]. In many mixing processes the complicating factors are the use of the complex fluids which exhibits very complicated behaviour and the use of stirrer with agitators. Infact, the agitators may be operated in the transitional regime, the different rotational directions of motion of stirrers and velocities.

The geometry is considered in this study consists of a cylindrical container, fitted with a pair of contra rotating stirrers fixed with lid eccentrically [6]. For industrial mixers, the dough partially fills the geometry, is driven around a bowl by stirring rods [6]. The stability, accuracy and convergence of a numerical method are significant issues for the robustness of the numerical algorithm [7–8], when applied to a challenging system of fundamental governing system of equations.

Great consideration of researcher and mathematicians in the field of computational fluid dynamics has been focused on finite element method (FEM) due to its flexibility to adjust the complex computational domain and its accuracy. The success of the finite element method in solving a wide range of nonlinear problems in virtually every phase of science and engineering has been phenomenal. In previous studies a stream function and vorticity formulation is used, here, in the present study the primitive variables formulation is employed [5, 9-10].

Two–dimensional Navier–Stokes equations in cylindrical coordinates consider in this study. The consideration is given a time marching semi implicit Taylor–Galerkin/Pressure–Correction (TGPC) multi stages scheme adopted [13, 14]. The flow is modelled as incompressible via so called TGPC finite element scheme as introduced by the pioneers of this algorithm [5].The effects of inertia, impact of rotational velocity for Newtonian fluids are clearly marked. The predicted solutions are displayed through contours plots and isobars, these are plotted from non–dimensional minimum value (marked by oval shape) to maximum value (marked by square shape), over a range. The Reynolds numbers are Re = 8.0, Re = 0.8 and Re = 0.08 corresponding to zero shear viscosities μ = 1.05 Pas, μ = 10.5 Pas and μ = 105.0 Pas respectively, a range of material properties is covered from those for model fluids, to model dough, to actual dough respectively [11–12].

II. PROBLEM SPECIFICATION

Stirring is one of the most important operations in process technology [15]. The case of cylindrical container with a pair of contra rotating stirrers fixed at the top of the container by a lid eccentrically is considered. Three cases of velocity of rotating stirrers are analysed i.e., half, same and double (v_θ= 0.5, 1.0 and 2.0) rotational velocity. The outer cylindrical container is rotates in counter clockwise and stirrers in clockwise direction. In industries, outer container is fixed physically and stirrers rotate around its own centres as well as around the centre of container. Due to mathematical complexities in the problem and to preserve the originality of physical problem instead of the rotation of stirrers around centre of vessel, the rotation of container is considered.

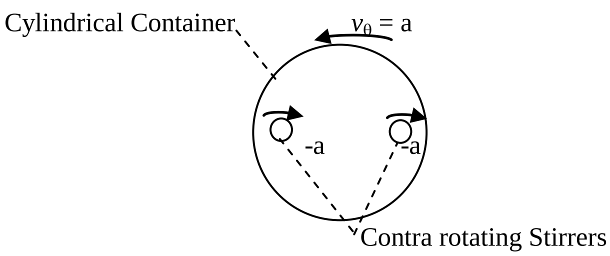

Figure 01:Two dimensional computational domain of eccentric rotating container.

Eccentric rotating cylindrical flow domain of interest involved is shown in figure 01. For the analysis of computational domain, the discretisation adopts triangular finite elements. For the simulation, a two-dimensional cylindrical coordinate frame of reference is taken over the domain.

III. GOVERNING SYSTEM OF EQUATIONS AND NUMERICAL SCHEME

Incompressible Newtonian rotating flowis considered in this research work. In the absence of body force, the system of equations can be represented through the conservation of mass and the conservation of momentum transport equations as$\nabla \cdot \mathbf{u} = 0$ and $\rho \frac{\partial \boldsymbol{u}}{\partial t} = \nabla . \boldsymbol{\sigma} - \rho \boldsymbol{u} . \nabla \boldsymbol{u}$ respectively over the spatial domain Ω.

The details of numerical scheme adopted here, reader is referred to [12, 12]. For well–posed problem it is necessary to define initial and boundary conditions. Simulations starts from rest and on both container and stirrers follow moving wall conditions ($v_r = 0$ and $v_{\theta} = a$).A pressure datum is specified as zero on outer rotating vessel wall [6].For the time marching process, the pre described level of tolerance for which the steady state convergence is achieved to be of the order of $10^{-6}$and Δt is fixed as 10^{-2}. The mesh density is highly affected to the accuracy of the numerical predictions. The study on mesh independency was conducted earlier [6], where mesh M2 is realised for optimal solution of various flow characteristics, also adopted in this study[4].In experiment, dough mixing the rotational velocity of outer cylinder is taken 75 rpm, which relate to Reynolds number equal to 0.08.

IV. NUMERICAL RESULTS AND DISCUSSIONS

Predicted solutions are analysed through contours of flow structure to demonstrate the effects of inertia (Re = 0.08, 0.8 and 8.0) with respect to rotational velocities (half, same and double) on stirrers against the velocity of outer container. These numerical results illustrate typical solution contours of streamlines (shown in figure–02) and pressure (shown in figure–03) for Newtonian fluids. At half speed of stirrers; six vortices formed throughout the geometry and minimum value of recirculation is noticed at container wall which is zero and maximum value in upper and lower regions at Re = 8.0 i.e., 2.62734.As inertia increases; centre of vortices moved counter clockwise away from horizontal line at half speed. At the same speed, all six vortices are formed but a noticeable new feature is emerges, that is the vortices twist clockwise direction when inertial level is increased and maximum values are noted at centre of vortices formed in upper and lower and nip of stirrers in narrow gap and minimum value at centre of vortices formed on the vertical axis line. Similar fashion of recirculation regions is observed at the double speed of the stirrers. The magnitude and smooth shape is noticed in formation, but as the speed of the stirrers increased from half to double speed, the gap between vortices reduces and central vortices appears together.

In the case of contra rotating stirrers, the fluid gets condensed on the entry to the constricted region within stirrers and container and hence the maximum pressure arises. When the fluid exit from the gap, the flow expands, here the minimum value of pressure is noticed due to release of energy. The pressure differential at all comparable parameter values for contra rotating instances influence relate across the geometry at Re = 0.08 and at Re = 0. 8, symmetric pressure isobars appear with equal magnitude in non–dimensional positive and negative extrema on both the sides of the stirrers in the narrow gap at half and same speed and there is replicated pattern about each stirrer with respect to upstream and downstream (pre and post nip gap) flow. When the inertia reaches at 8.0 in the case of double speed of stirrers, change in the position of positive maxima is noticed i.e., 6.93863at the container wall before the fluid entering in the narrow gap and similar fashion is analysed at same speed.

Initially, the graph of work-done and power consumption is high to drive the flow in the container. Afterwards, graph of power consumption decreases rapidly and reaches at steady state some level asymptotic solution for contra rotating stirrers at the low speed but for high speed, this passion is steadily decreases. Whilst, work-done increases in same fashion up to steady state. Numerical results are tabulated in Table–01.

V. CONCLUSION

We have successfully demonstrated the use of a numerical flow solver for Newtonian fluids as a predictive tool for dough kneading. We have been able to provide physically realistic simulations for these complex rotating flows. Contra rotating stirrer solutions display certain aspects of symmetry. The streamlines and pressure isobars are localized in extrema in the neighbourhood of the stirrers. Maxima rate-of-work done noticed at the narrowest part of the nip-gap between stirrers and container. However, the power consumption is higher for this contra rotating case. Increase of container rotation speed, raises inertia, twists vortex patterns. The reverse scenario to the container rotating demonstrates the actual industrial situation.

REFERENCES

[1.] Baloch A., Solangi M. A., Memon G. M., "Simulation of Rotational Flows in Cylindrical Vessel with Rotating Single Stirrer", PUJM, 40, 83–96, 2008.
[2.] Baloch, A. and Webster, M. F., "Distributed parallel computation for complex rotational flows of non–Newtonian fluids", Tech. Rep. CSR–6, 2001, Department of Computer University of Wales Swansea, UK, Int. J. Num. Meth. Fluids, 2002.
[3.] Baloch, A., and Webster, M. F., "Distributed Parallel Computation for Complex Rotating Flows of Non–Newtonian Fluids", Int. J. Num. Meth. Fluids, 43, 1301–1328, 2003.
[4.] Baloch, A., Grant, P. W. and Webster, M. F., "Parallel Computation of Two–Dimensional Rotational Flows of the Viscoelastic Fluids in Cylindrical Vessel", Int. J. Comp. Aided Eng. and Software, Eng. Comp., 19(7), 820–853, 2002.

[5.] Baloch. A, "Numerical Simulation of complex flows of non–Newtonian fluids", PhD Thesis, University of Wales, Swansea, 1994.
[6.] Binding, D. M., Couch, M. A., Sujatha, K. S., Webster, M. F., "Experimental and numerical simulation of dough kneading in filled geometries", J. Foods Eng., 57, 1–13, 2002.
[7.] Bochkarev S. A. , Matveenko V. P., "Numerical Analysis of Stability of a Stationary or Rotating Circular Cylindrical Shell Containing Axially Flowing and Rotating Fluid", International Journal of Mechanical Sciences, 68, 258-269, 2013.
[8.] Bochkarev S. A. , Matveenko V. P., "Stability of Rotating Circular Cylindrical Shell Subject to an Axial and Rotational Fluid Flow", VestnikSamGU, 9, 84–97, 2012.
[9.] Connelly, R. K. and Kokini, L. J., "Mixing simulation of a viscous Newtonian liquid in a twin sigma blade mixer", Fluid Mechanics and Transport Phenomena, Sydney, 2006.
[10.] Ding, D. and Webster, M.F., "Three–dimensional numerical simulation of dough kneading", XIII Int. Cong. on Rheol., British Society of Rheology, Cambridge, UK, 2, 318–320, 2000.
[11.] Memon, R. A., Baloch, A. and Solangi, M. A., "Simulation of Rotational Flows in Cylindrical Vessel with Double Rotating Stirrers (PART-A)", PUJM, 43, 47–67, 2011.
[12.] Memon, R. A., Solangi, M. A. and Baloch, A. "Stress Analysis of Mixing of Non-Newtonian Flows in Cylindrical Vessel Induced by Co-Rotating Stirrers", MURJ of ET, 32(2), 283–286, 2013.
[13.] Solangi, M. A., Baloch A. and Memon, R. A., "Influence of Blood Inertia on Vortex Enhancement in the Wake of Plaque Deposited Arties", MURJ of ET, 30(2), 213–224, 2011.
[14.] Solangi, M. A., Memon, R. A. And Baloch A., "Prediction of Pressure and Velocity Profile in Steady Flow through Axi-Symmetric Plaque Deposited Arties", MURJ of ET, 31(4), 723–732, 2012.
[15.] Zlokarnik, M., "Stirring: Theory & Practical", Wiley–VCH, Weinheim, 2001.

Table:Streamlines and Pressure of Newtonian fluids for contra rotating stirrers; inertial levels 0.08, 0.8 and 8.0; speed of stirrers is 0.5, 1 and 2.

Variables	Speed of Stirrer	Re = 0.08		Re = 0.8		Re = 8.0	
		Minima	Maxima	Minima	Maxima	Minima	Maxima
Streamlines	Half	0	2.66273	0	2.66225	0	2.62743
	Same	-0.93386	2.02191	-0.9386	2.01946	-1.49938	1.81904
	Double	-5.019	1.58694	-5.0849	1.58592	-7.41413	1.71834
Pressure	Half	-5.26616	5.24019	-5.38462	5.14477	-6.71983	4.5179
	Same	-7.18218	7.13253	-7.40446	6.92244	-10.0362	4.98229
	Double	-11.0943	10.9296	-11.8754	10.2863	-24.6213	6.93863

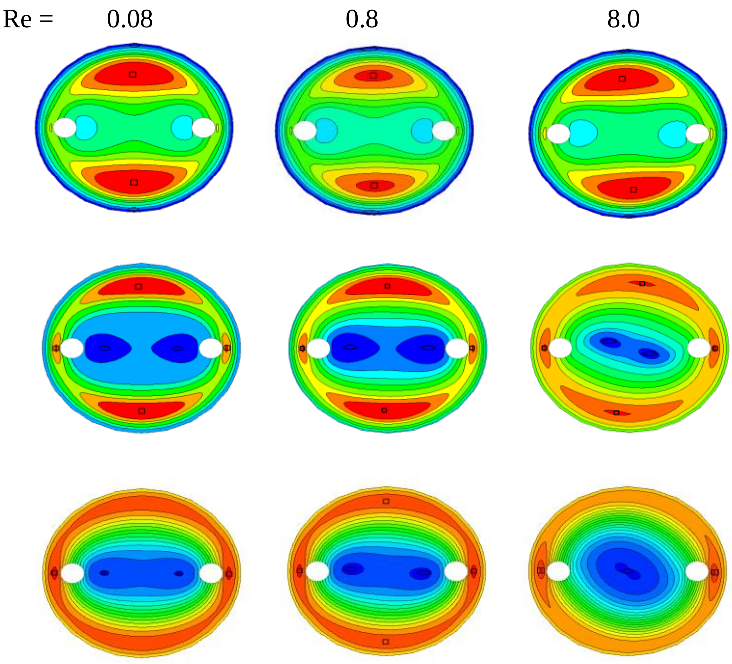

Figure 02: Flow structure patterns for contra rotating stirrers; at inertial levels 0.08, 0.8 and 8.0 (from left to right); speed of stirrers is 0.5, 1 and 2 (from top to bottom)

Re = 0.08 0.8 8.0

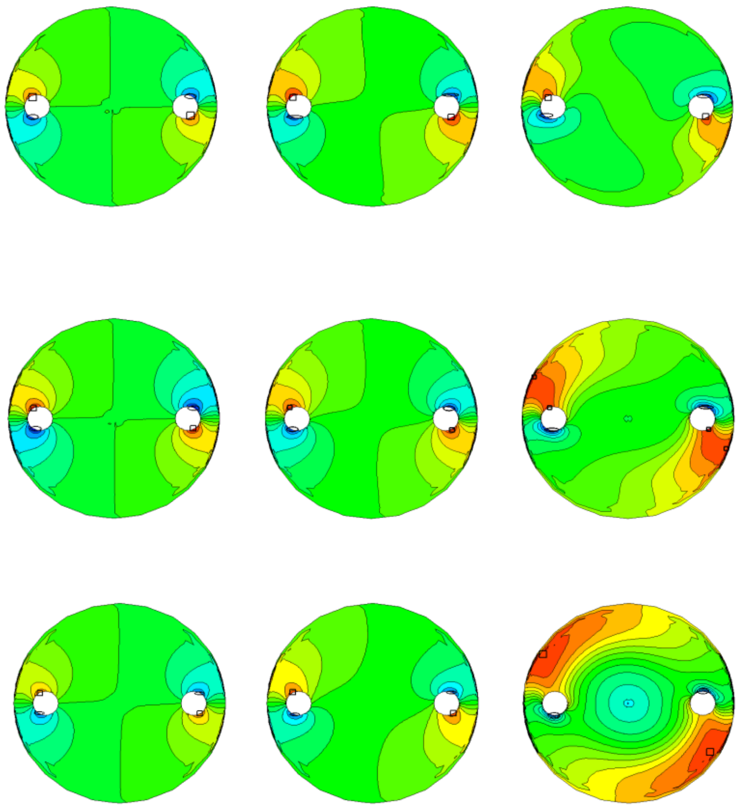

Figure 03: Pressure isobars for contra rotating stirrers; inertial levels 0.08, 0.8 and 8.0 (from left to right); speed of stirrers is 0.5, 1 and 2 (from top to bottom)

Performance Evaluation of Nine Level Modified CHB Multilevel Inverter for Various PWM Strategies

P. Satheesh Kumar[1], Dr. S. P. Natarajan[2], Dr. Alamelu Nachiappan [3], Dr. B. Shanthi[4]

*(Associate professor, Department of Electrical and Electronics Engineering, Mailam Engineering College, Mailam, Tamilnadu-604304, India,)

**(Professor & Head, Department of Instrumentation Engineering, Annamalai University, Annamalai Nagar, Tamilnadu-608002, India,)

*** (Professor, Department of Electrical and Electronics Engineering, Pondicherry Engineering College, Pondicherry- 605014, India,)

**** (Professor, Centralized Instrumentation and Service Laboratory, Annamalai University, Annamalai Nagar, Tamilnadu-608002, India,)

ABSTRACT: *In this paper nine level Modified Cascaded H-Bridge Multilevel Inverter (CHB-MLI) is analyzed for the various multi-carrier Pulse Width Modulation strategies. For the same nine level inverter output this particular topology has reduced count of switches, on comparing with the conventional Cascaded H Bridge Multilevel Inverter. For a single phase, nine level inverter output this topology requires one H-bridge and a multi conversion cell. Four equal voltage sources with four controlled switches and four diodes comprise a multi conversion cell. Instead of sixteen controlled switches as in conventional method, this topology requires only eight switches to obtain nine level output. The reduction of switches lowers switching losses, cost and total harmonic distortions. Performance parameters have been analyzed for the nine level CHB-MLI.*

Keywords: *Alternate phase opposition disposition, Modified Cascaded Multilevel Inverter H-bridge Inverter, Phase disposition, Phase opposition disposition, Phase shift Pulse width Modulation, Sinusoidal Pulse Width Modulation.*

I. INTRODUCTION

Multilevel inverter (MLI) has wide range of high-power applications and feeds demands in industries in recent years. The aptness of MLI attracts the hot researchers in the direction of renewable energy sources for its numerous benefits. As renewable energy sources such as photovoltaic, wind and fuel cells can be easily interfaced to a multilevel inverter system of high power applications, MLI still gains further credit to its field. MLI can operate at high switching frequencies while producing lower order harmonic components.

A multilevel inverter is a power-electronic system that generates a desired output voltage by synthesizing several levels of dc input voltages. The main advantages of multilevel inverters are lower cost, higher performance, less electromagnetic interference, and lower harmonic content [1].The most common multilevel inverter topologies are the diode-clamped, flying-capacitor, and cascaded H-bridge inverters with separate dc voltage sources [2]. The diode clamped multilevel inverter topology, restricts the use of it to the high power range of operation. Moreover flying capacitor based multilevel inverter also exhibits a disadvantage including more number of capacitors [3].

In recent years, the cascaded H-bridge inverters have wide applications. The merit includes modularity and the ability to operate at higher voltage levels and as the number of levels increases, the quality of the output signal will be improved. In addition inverter output voltage waveform will be closer to a sinusoidal waveform [4]. Moreover, high voltages can be managed at the dc and ac sides of the inverter, while each unit endures only a part of the total dc voltage. Needs of high number of semiconductor switches, involvement of separate DC source for each of H-bridge, voltage balancing issues are the notable drawbacks of cascaded H bridge inverter.

On comparing with the usual Cascaded H-Bridge multilevel inverters, for the same nine level output, this Modified cascaded multilevel inverter topology, the number of switches used reduced from 16 switches to 8 switches. Therefore for this reason, this Modified cascaded multilevel inverter has some value of importance. Hence this paper focuses on applying various multi carrier based PWM techniques to this Modified cascaded H Bridge multilevel inverter to analyze and compare the various parameters like THD & V_{rms}.

II. MODIFIED CASCADED MULTILEVEL INVERTER TOPOLOGY DESCRIPTION

The general structure of the Modified cascaded multilevel inverter is shown in Figure 1. This inverter consists of an H Bridge and multi conversion cell which consists of four separate voltage sources (V_{dc1}, V_{dc2}, V_{dc3} and V_{dc4}), four switches and four diodes. Each source connected in cascade with other sources through a circuit consists of one active switch and one diode that can make the output voltage source only in positive polarity with several levels. Only one H-bridge is connected with multi conversion cell to acquire both positive and negative polarity.

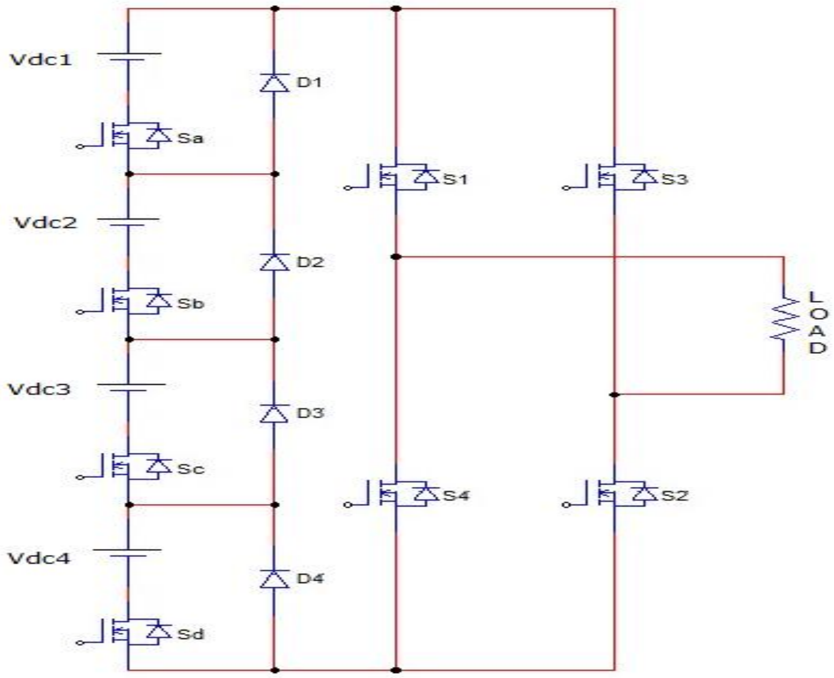

Figure 1: 9-Level Modified-Cascaded multilevel inverter

By turning on controlled switches S1 (S2, S3 and S4 turn off) the output voltage $+1V_{dc}$ (first level) is produced across the load. Similarly turning on of switches S1, S2 (S3 & S4 turn off) $+2V_{dc}$ (second level) output is produced across the load. Similarly $+3V_{dc}$ levels can be achieved by turning on S1, S2, S3 switches (S4 turn off) and $+4V_{dc}$ levels can be achieved by turning on S1, S2, S3 & S4 as shown in below Table 1.

S. No	Multi conversion Cell		H-Bridge		Voltage levels
	On switches	Off switches	On switches	Off switches	
1	S1, S2, S3, S4	D1,D2,D3,D4	Q1,Q2	Q3,Q4	$+4V_{dc}$
2	S1, S2, S3, D4	S4,D1,D2,D3	Q1,Q2	Q3,Q4	$+3V_{dc}$
3	S1, S2, D3, D4	S3, S4,D1,D2	Q1,Q2	Q3,Q4	$+2V_{dc}$
4	S1, D2, D3,D4	S2, S3, S4,D1	Q1,Q2	Q3,Q4	$+1V_{dc}$
5	D1, D2, D3,D4	S1, S2, S3,S4	Q1,Q2	Q3,Q4	0
6	S1, D2, D3,D4	S2, S3, S4,D1	Q3,Q4	Q1,Q2	$-1V_{dc}$
7	S1, S2, D3,D4	S3, S4,D1,D2	Q3,Q4	Q1,Q2	$-2V_{dc}$
8	S1, S2, S3, D4	S4,D1,D2,D3	Q3,Q4	Q1,Q2	$-3V_{dc}$
9	S1, S2, S3, S4	D1,D2,D3,D4	Q3,Q4	Q1,Q2	$-4V_{dc}$

Table: 1 Switching Patterns for 9 levels MC-MLI

From the above table, it is observed that for each voltage level, among the paralleled switches only one switch is switched ON. The input DC voltage is converted into a stepped DC voltage, by the multi conversion cell, which is further processed by the H Bridge and outputted as a stepped or approximately sinusoidal AC waveform. In the H Bridge, during the positive cycle, only the switches Q1 and Q3 are switched on. And during the negative half cycle, only the switches Q2 and Q4 are switched on.

The S number of DC sources or stages and the associated number output level can be calculated by using the equation as follows,

$N_{level} = 2S+1$ …………………………………………………….. (1)

For an example, if S=3, the output wave form will have seven levels (±3Vdc, ±2Vdc, ±1Vdc and 0). Similarly voltage on each stage can be calculated by using the equation as given,

$A_i = 1\ V_{dc}$ (1, 2, 3,) ……………………………………………….. (2)

The main advantage of proposed modified cascaded multilevel inverter is seven levels with only use of seven switches. For an example, if S=3, the output wave form will have seven levels (±3V_{dc}, ±2V_{dc}, ±1V_{dc} and 0). The number switches used in this topology is given by the equation as follows

$N_{Switch} = 2S+ 4$ ……………………………………….……….. (3)

III. MULTIPLE CARRIER PULSE WIDTH MODULATION TECHNIQUES

In this PWM technique, more than one carrier wave which be either triangular or saw tooth wave form can be used. This paper focuses on various strategies.utilising more than one triangular wave as carrier and the reference wave is sinusoidal. Though there are many carrier wave arrangements, in this paper, the following four arrangements have been carried out. THD and V_{rms} values for these four strategies for various modulation indexes are compared.

1. Phase disposition PWM strategy.
2. Phase Opposition Disposition PWM strategy.
3. Alternate Phase Opposition Disposition PWM strategy
4. Phase Shift PWM strategy.

In these Multicarrier PWM schemes, several triangular carrier waves are compared with the single Sinusoidal reference wave. The number of carriers required to produce N level output is (m-1) where m is the number of carrier waveforms. The single sinusoidal reference waveform has peak to peak amplitude of A_m and a frequency f_m. The multiple triangular carrier waves are having same peak to peak amplitude A_c and same frequency f_c. The single sinusoidal reference signal is continuously compared with all the carrier waveforms. A pulse is generated, whenever the single sinusoidal reference signal is greater than the carrier signal. The frequency ratio m_f is as follows: f_c / f_m

3.1. Phase Disposition PWM strategy (PDPWM)

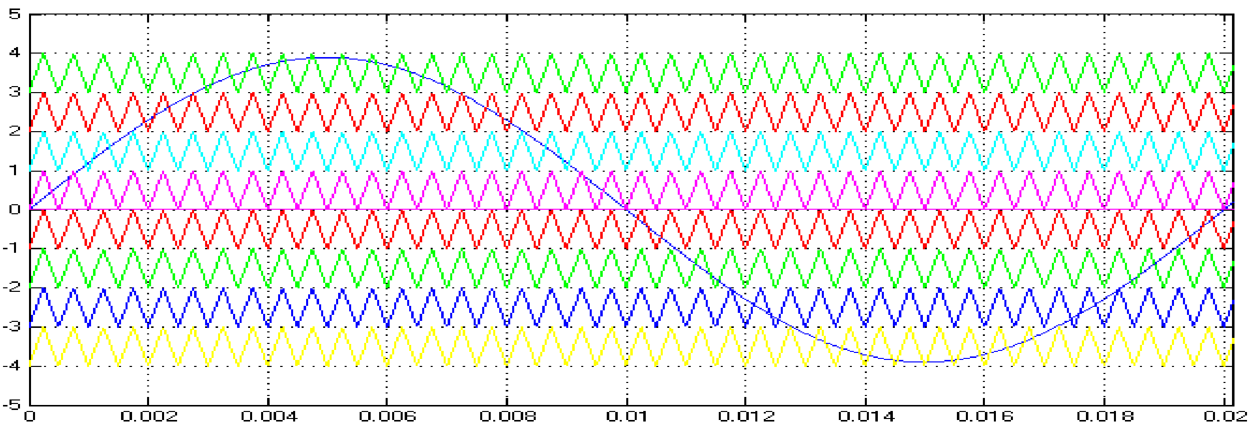

Figure 2: Carrier arrangement for Phase Disposition PWM strategy

The above fig. 2 shows, Phase Disposition PWM strategy (PDPWM), where (m-1) carrier signal with the same frequency f_c and same amplitude A_c are positioned such that the bands they occupy are contiguous. The reference wave form is single sinusoidal. During the continuous comparison, if the reference wave form is more than a carrier waveform, then the active switching device corresponding to that carrier is switched on. Otherwise, that concerned device is switched off.

The below fig: 3 shows Complete Gate signal for 9-level MC-MLI using Phase Disposition PWM strategy
Amplitude of modulation index for PDPWM is

$m_a = 2A_m / (m-1) A_c$ ……………………. (5)

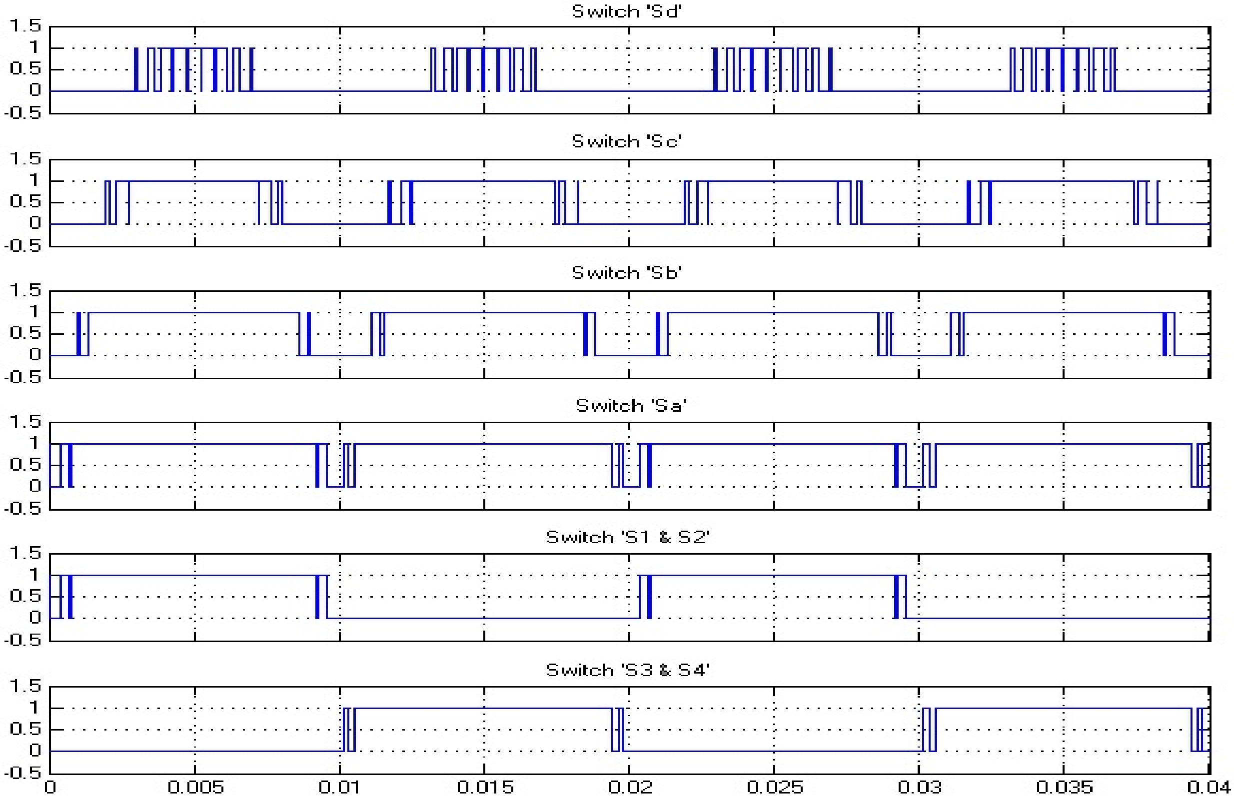

Figure 3 – Complete Gate signal for 9-level MC-MLI using Phase Disposition PWM strategy

3.2. Phase Opposition Disposition PWM strategy (PODPWM)

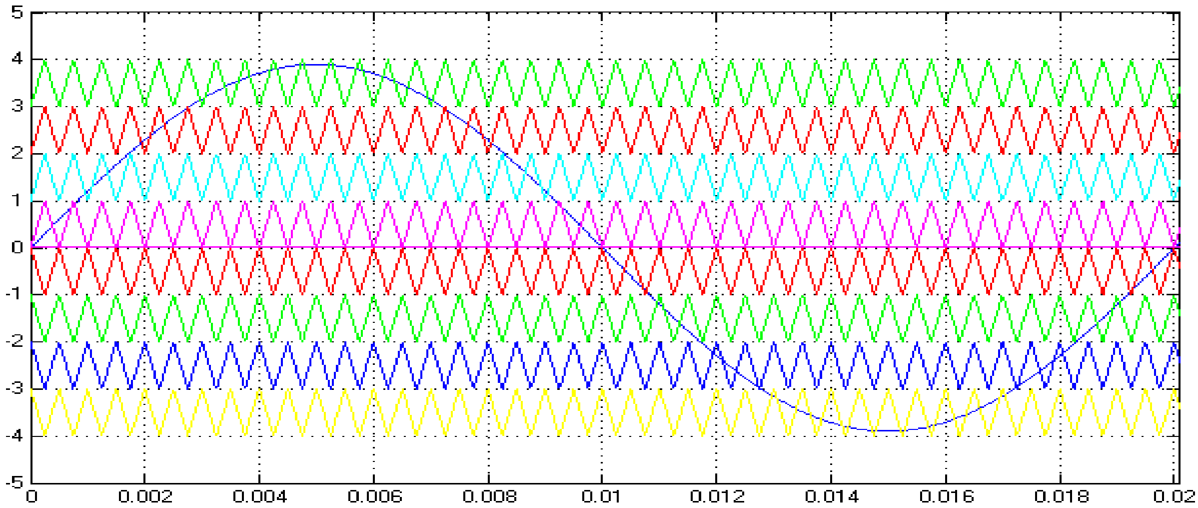

Figure 4: Carrier arrangement for Phase Opposition Disposition PWM strategy

POD PWM strategy is shown in fig.4, where the carrier waveforms, above the zero reference are in phase. The carrier waveforms below are also in phase, but are 180 degrees phase shifted from those above zero. The reference wave form is single sinusoidal. During the continuous comparison, if the reference wave form is more than a carrier waveform, then the active switching device corresponding to that carrier is switched on. Otherwise, that concerned device is switched off. The below fig: 5 shows Complete Gate signal for 9-level MC-MLI using Phase Opposition Disposition PWM strategy.

Amplitude of modulation index for PODPWM is

$$m_a = 2A_m / (m-1)^* A_c \quad \ldots\ldots\ldots\ldots\ldots\ldots \quad (6)$$

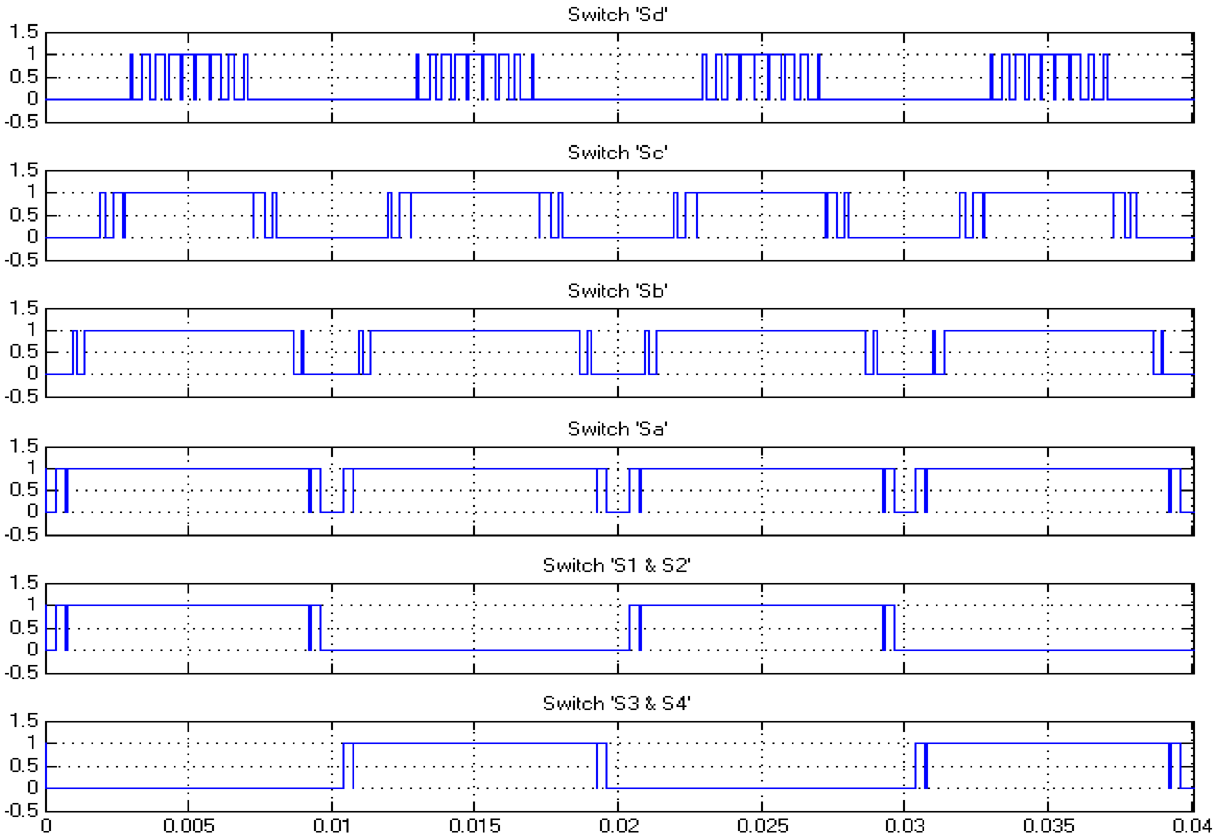

Figure 5: Complete Gate signal for 9-level MC-MLI using Phase Opposition Disposition PWM strategy

3.3. Alternate Phase Opposition Disposition PWM strategy (APODWM)

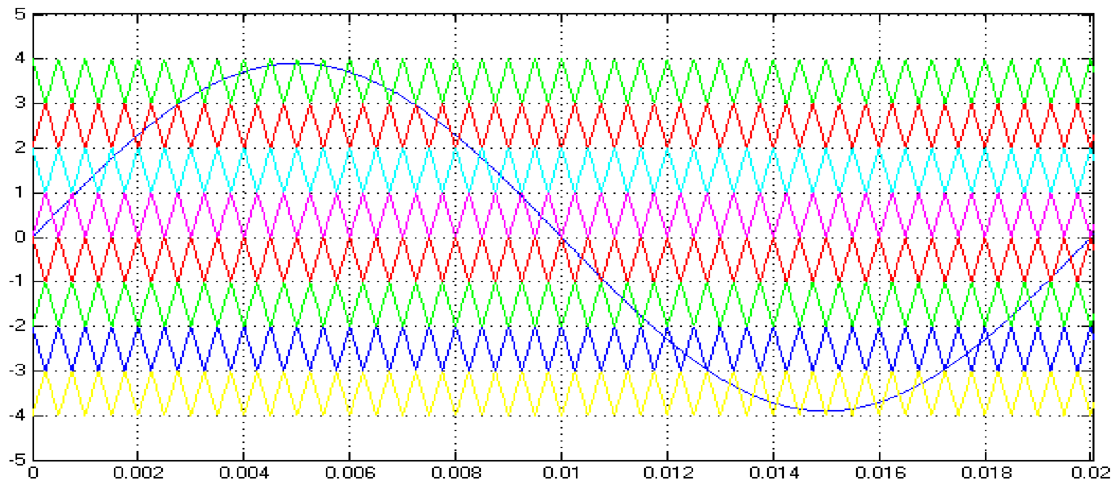

Figure 6: Carrier arrangement for Alternate Phase Opposition Disposition PWM strategy

The above fig. 6 shows APOD strategy where the multiple carriers having same amplitude are phase displaced from each other by 180 degrees alternately. During the continuous comparison, if the reference wave form is more than a carrier waveform, then the active switching device corresponding to that carrier is switched on. Otherwise, that concerned device is switched off. The below fig: 7 shows Complete Gate signal for 9-level MC-MLI using Alternate Phase Opposition Disposition PWM strategy.

Amplitude of modulation index for PODPWM is

$$m_{a} = 2A_m / (m-1)^* A_c \text{ ....(7)}$$

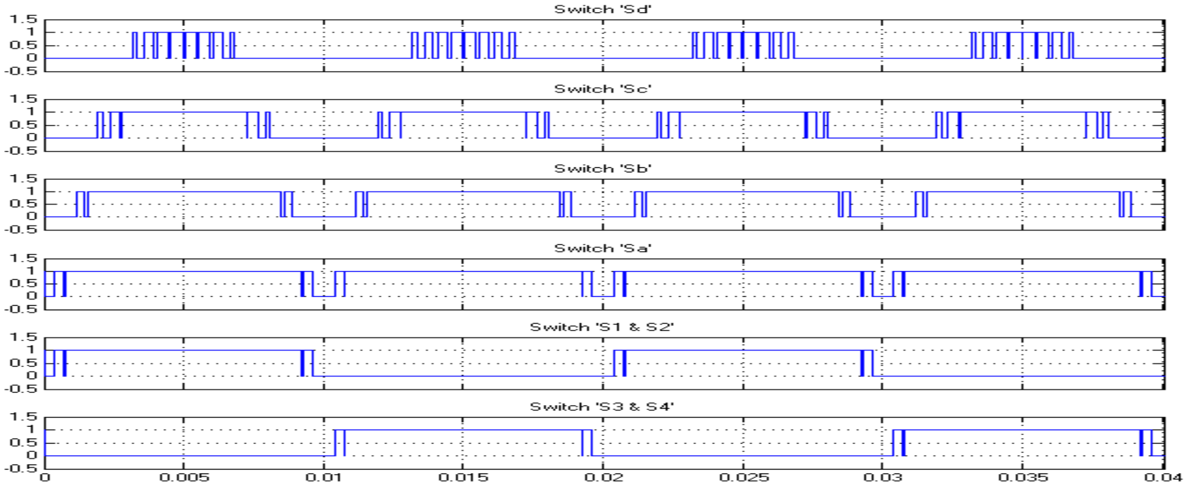

Figure 7: Complete Gate signal for 9-level MC-MLI using Alternate Phase Opposition Disposition PWM strategy

3.4. Phase shift PWM strategy (PSPWM)

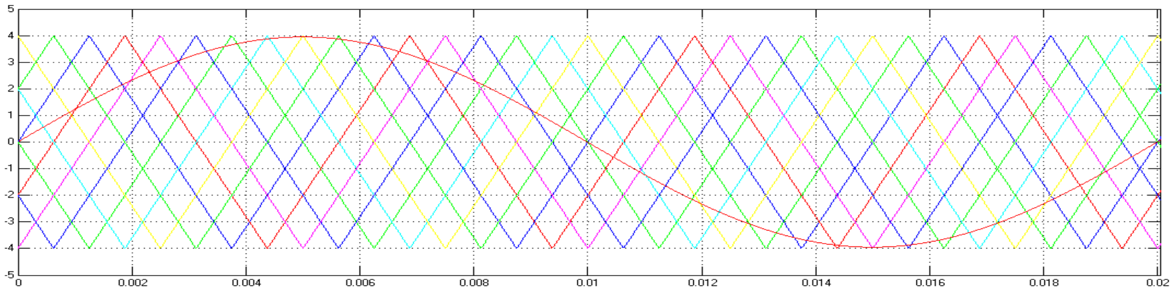

Figure 8: Carrier arrangement for Phase shift PWM strategy

The above fig. 8 shows PSPWM strategy where the multiple carriers having the same amplitude and frequency which are shifted to one another by certain degrees decided by the No. of levels. Thus for nine level output, 8 triangular carrier waves which are phase shifted by 45 degrees is utilized .The reference waveform is single sinusoidal (i) for odd m_f the waveforms have odd symmetry resulting in even and odd harmonics and (ii) for even m_f , PSPWM waves have quarter wave symmetry resulting in odd harmonics only. Amplitude of modulation index for PSPWM is

$$m_a = A_m / (A_c /2). \qquad (4)$$

The below fig.9 shows complete gate signal for 9-level MC-MLI using Phase shift PWM strategy

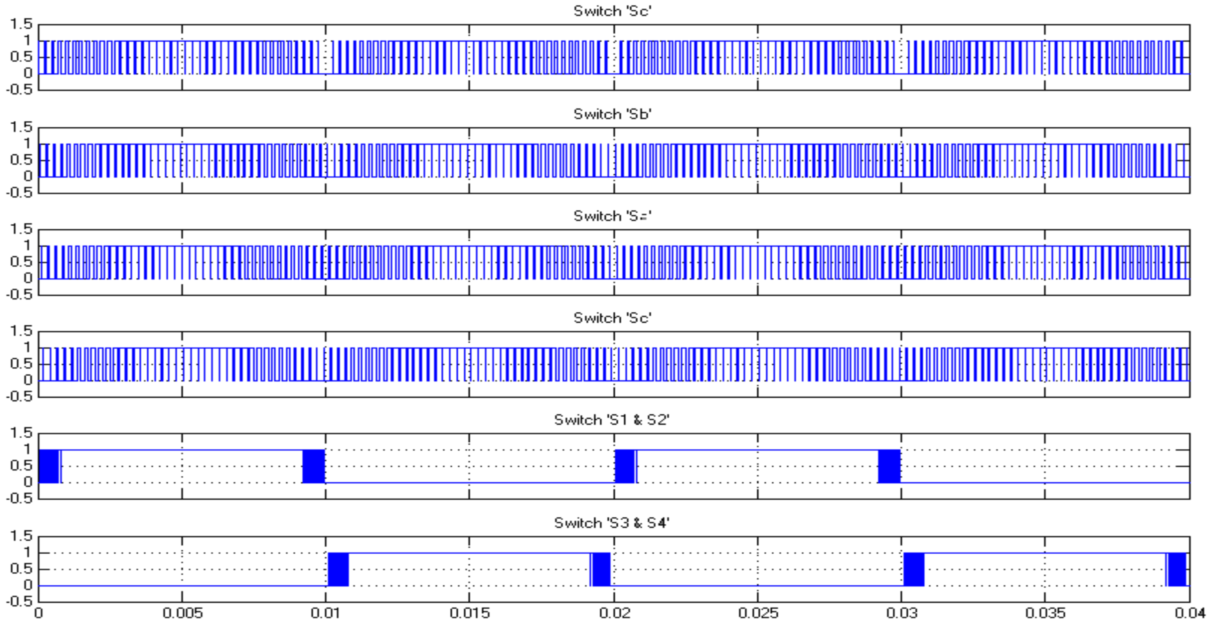

Figure: 9 – Complete Gate signal for 9-level MC-MLI using Phase shift PWM strategy

IV. SIMULATION RESULTS

The fig. 6 shown below is the simulink model of the 9 –level Modified cascaded H Bridge Multilevel inverter using power system block set. The following parameter values are used for simulation: V_1 =100v, V_2 =100v, V_3 = 100v, V_4= 100v f_c =2000 Hz and fm=50Hz .Gating signals for Phase shifted carrier wave arrangement and three different, level shifted carrier wave arrangements are simulated for 9 levels MC MLI. Simulations are done for various values of m_a and the corresponding THD% are observed using FFT block and listed in Table 2 The $V_{r\,ms}$ (fundamental) of the output voltage for various values of m_a and the corresponding Voltages are listed in Table3.

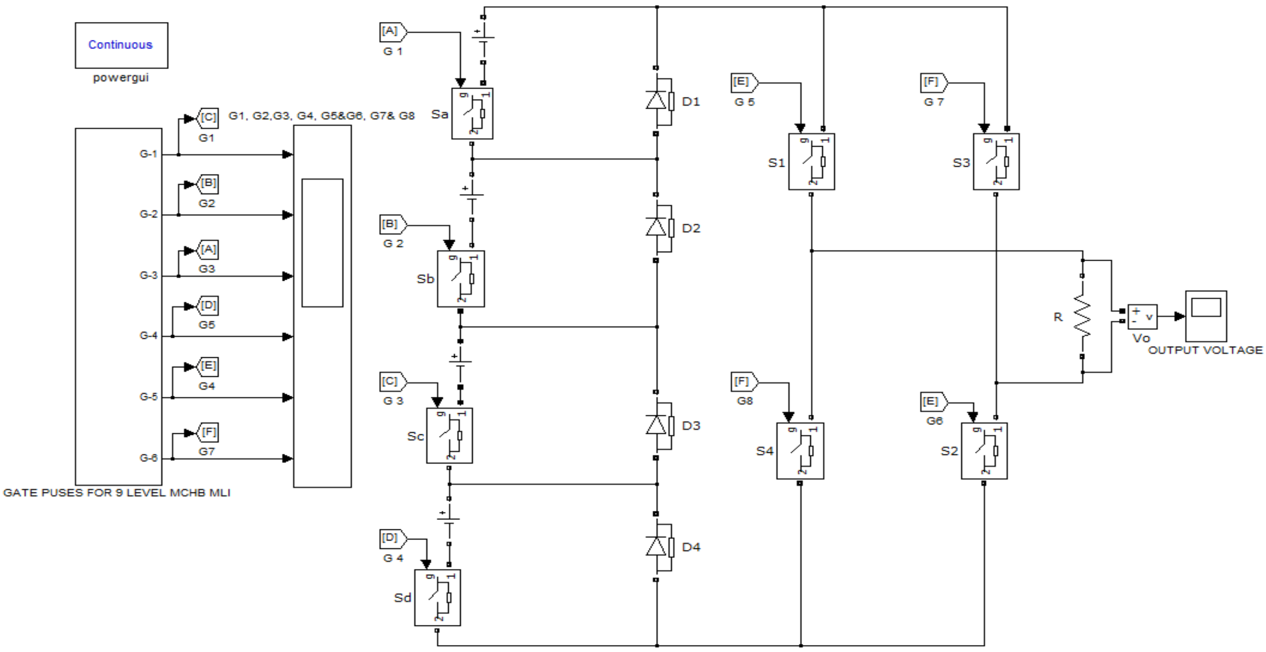

Figure 8: Simulink Model of the 9 level - Modified Cascaded Multilevel Inverter-MC-MLI

Table 2: THD comparison

M_a	PD PWM	POD PWM	APOD PWM	PS PWM
1	13.63	13.48	14.04	13.66
0.9	16.74	16.72	16.89	16.65
0.8	17.1	16.85	17.02	17.14

Table 3: V_{rms} comparison

M_a	PD PWM	POD PWM	APOD PWM	PS PWM
1	399	397.8	397	399
0.9	358.6	356.6	356.7	358.7
0.8	318.4	316.5	316.8	318.3

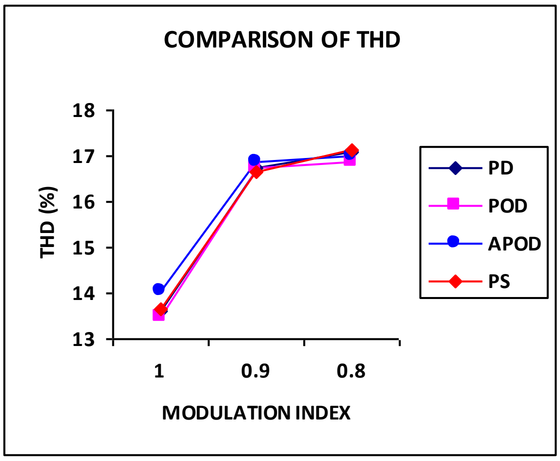

Figure 9 Comparison of THD

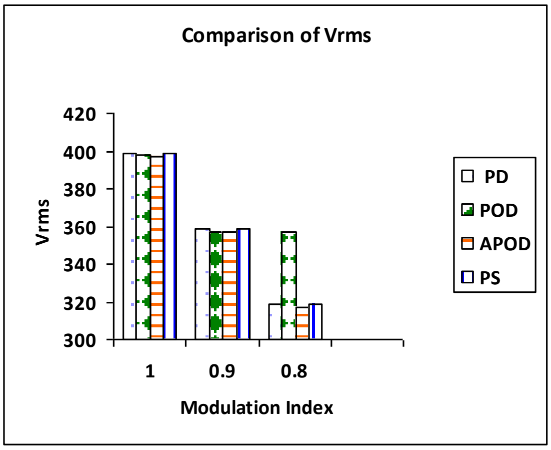

Figure 10 Comparison of V_{rms}

The Simulated 9-level Output Voltage waveform of MC-MLI using PDPWM Strategy is shown in fig. 11 and Fig. 12 shows the FFT plot of 9-level MC-MLI Using PDPWM using PDPWM Strategy. The Simulated 9-level Output Voltage waveform of MC-MLI using PODPWM Strategy is shown in fig 13 and Fig: 14 shows the FFT plot of 9-level MC-MLI using PDPWM Using PODPWM Strategy. The Simulated 9-level Output Voltage waveform of MC-MLI using APODPWM Strategy is shown in fig 15 and Figure: 16 shows the FFT plot of 9-level MC-MLI Using APDPWM using PODPWM Strategy. The Simulated 9-level Output Voltage waveform of MC-MLI using PSPWM Strategy is shown in fig 17 and Fig: 18 shows the FFT plot of 9-level MC-MLI Using PDPWM using PSPWM Strategy.

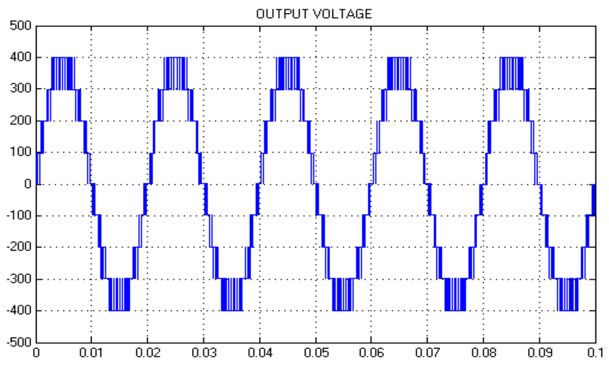

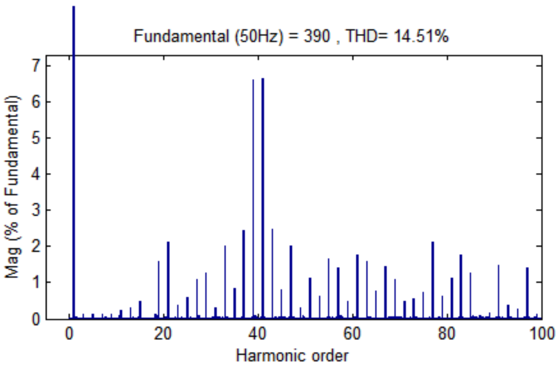

Figure 11: Simulated 9-level Output Voltage waveform of MC-MLI Using PDPWM Strategy

Figure 12: FFT plot of 9-level Output Voltage waveform MC-MLI Using PDPWM Strategy

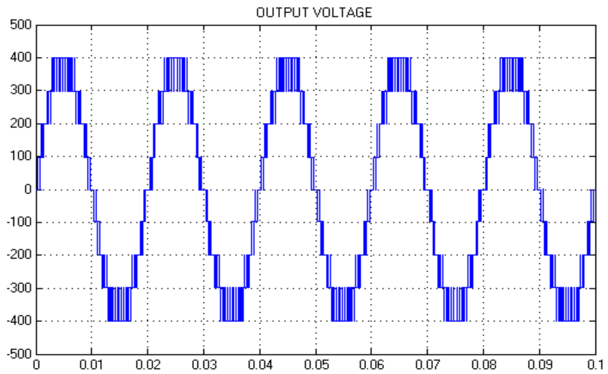

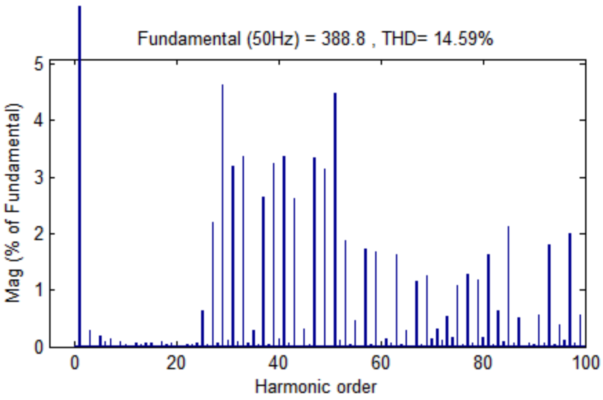

Figure 13: Simulated 9-level Output Voltage waveform of MC-MLI Using PODPWM Strategy

Figure 14: FFT plot of 9-level MC-MLI Using PODPWM Strategy

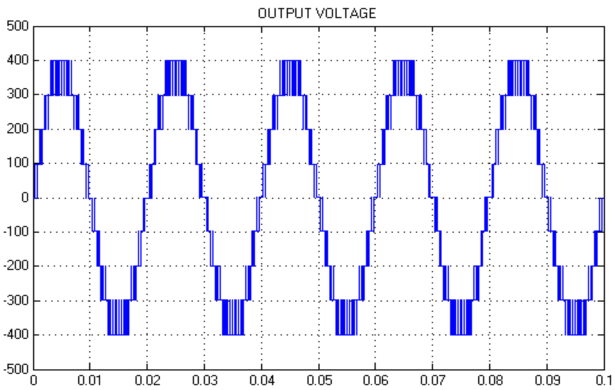

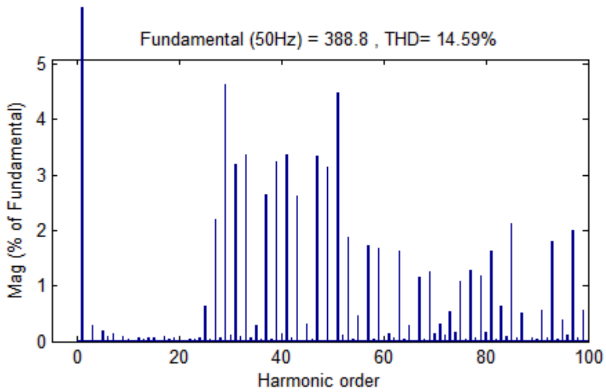

Figure 15: Simulated 9-level Output Voltage waveform of MC-MLI Using APODPWM Strategy

Figure 16: FFT plot of 9-level MC-MLI Using APODPWM Strategy

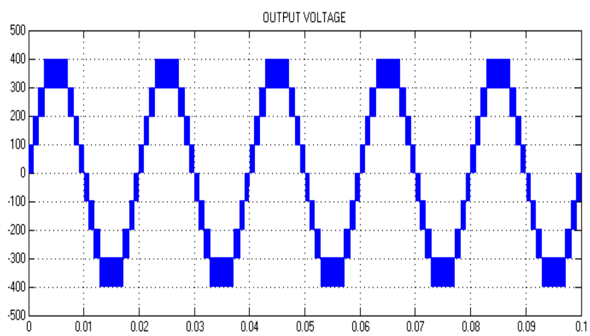

Figure 17: Simulated 9-level Output Voltage waveform of MC-MLI Using PSPWM Strategy

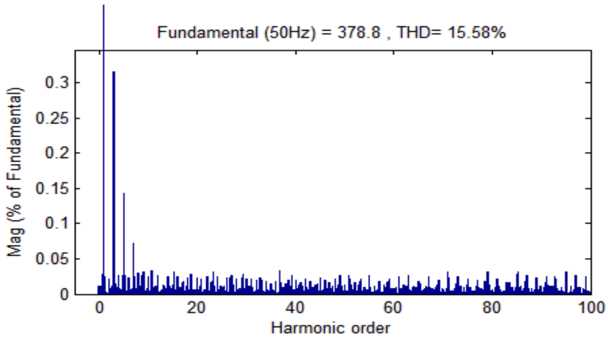

Figure 18: FFT plot of 9-level MC-MLI Using PSPWM Strategy

V. CONCLUSION

Single phase nine levels Modified cascaded multilevel inverter has been analyzed for various multi carrier sinusoidal Pulse Width Modulation strategies. This topology has the credit of having only eight switches with four diodes, instead of 18 switches in the conventional plants, which support reduction in switching losses, cost and circuit complexity.

Performance factors like %THD and V_{RMS} have been measured, and analyzed for Phase shifted carrier wave arrangement and three different, level shifted carrier wave arrangements both applied to the Single phase nine levels Modified cascaded multilevel inverter. The values have been measured for various modulation indexes. It is found that the PDPWM strategy provides appreciable %THD and acceptable V_{RMS}. In addition, it is also observed that it has less number of dominant harmonics than the other strategies.

REFERENCES

[1] L. G. Franquelo, J. Rodriguez, J. I. Leon, S. Kouro, R. Portillo, and M. A. M. Prats, "The age of multilevel converters arrives," *IEEE Ind.Electron. Mag., vol. 2, no. 2, pp. 28–39, Jun. 2008.*

[2] Z.Du, L.m.Tolbert, J.N.Chiasson, and B.Opineci, "A cascaded multilevel inverter using a single dc power source", in *Proc. IEEE APEC, pp.426-430, 2006.*

[3] Fang Zheng Peng "A Generalized Multilevel Inverter Topology with Self Voltage Balancing", *IEEE Trans. Ind .Appl., Vol.37, No.2, March/April 2001.*

[4] J. I. Leon, R. Portillo, S. Vazquez, J. J. Padilla, L. G. Franquelo, and J.M. Carrasco, "Simple unified approach to develop a time-domain modulation strategy for single-phase multilevel converters," *IEEE Trans.Ind. Electron., vol. 55, no. 9, pp. 3239–3248, Sep. 2008.*

[5] Y. Li and B. Wu, "A novel dc voltage detection technique in the chb inverter-based statcom," *IEEE Trans. Power Del., vol. 23, no. 3, pp.1613–1619, Jul. 2008.*

[6] J. Rodriguez, J. Lai, and F. Peng, "Multilevel inverters: A survey of topologies, controls and applications," *IEEE Trans. Ind. Electron, vol.49, no. 4, pp. 724–738, Aug. 2002.*

[7] Ebrahim Babaei "A Cascaded Multilevel converter Topology With Reduced Number of Switches*", IEEE Trans. Power Electron vol.23,no.6, Nov 2008.*

[8] Rokan Ali Ahmed, S. Mekhilef, Hew Wooi Ping, ''New multilevel inverter topology with reduced number of switches'',*Proceedings of the 14th International Middle East Power Systems Conference (MEPCON'10), Cairo University, Egypt, December 19-21, 2010, Paper ID 236.*

Lexical Pattern- Based Approach for Extracting Name Aliases

Mohammad Khasim[1], Sayeed Yasin[2]
[1]M. Tech, Nimra College of Engineering & Technology, Vijayawada, A.P., India.
[2]Asst. Professor, Dept.of CSE, Nimra College of Engineering & Technology, Vijayawada, A.P., India.

ABSTRACT: Searching for information about people in the web is one of the most common activities of many internet users. Around 30% of search engine queries include person names. Retrieving information about people from web search engines can become difficult when a person has nick names or name aliases. We will not be able to retrieve all the information about a cricket player, if we only use his real name. For example we can't retrieve all the information regarding the cricketer sachin tendulkar by using his real name only. So we need his nick names too. Identification of entities on the web is difficult mainly for two fundamental reasons: The first one is that different entities can share the same name (i.e., lexical ambiguity) and the second one is that a single entity can be designated by multiple names (i.e., referential ambiguity). In this paper, we propose a lexical pattern-based approach to extract aliases of a given name using snippets returned by a web search engine. The lexical patterns are generated automatically using a set of real world nick names or name alias data. The proposed work does not assume any language specific preprocessing such as part of speech tagging or dependency parsing, etc., which can be both inaccurate and computationally costly in web scale data processing.

Keywords: *Alias, Anchor text, Lexical analysis, Pattern.*

I. INTRODUCTION

Finding a relevant, information of a particular entity on the web is very important task as it is helpful in the information retrieval process. Retrieving information of a person simply by using his/her name is quite insufficient if the person has nick names [1]. Now- a- days celebrities are known by two or more name in the web. Entities may be a person, a location, an organization, a festival name, etc. Identification of entities on the web is difficult for two basic reasons- The first one is that different entities may share the same name (Lexical ambiguity) and the second one is that one entity is known by different names (Referential ambiguity). The name dis- ambiguation problem differs fundamentally from that of alias extraction because in name dis- ambiguation the objective is to identify the different entities that are referred by the same ambiguous name; in alias extraction, we are only interested in extracting all references to a single entity from the web. For example: "Diwali" is also known as Deepavali as a one word alias or Festival of Lights as a three word alias. The cricketer, Sachin Tendulkar is also known as Master blaster or little master. Similarly, entities are also referenced by profession, drama, etc.

Identifying aliases of a name is important in various tasks such as information retrieval, relation extraction and sentiment analysis and name disambiguation. In information retrieval, to improve recall of the web search on a person name, a search engine can automatically expand the query using aliases of the name. In this paper, we propose an alias identification method that is based on two main things such as links extraction and association measures used. For link extraction we used extract link and also consider the second level depth of the web pages [2]. We propose lexical pattern extraction algorithm to retrieve pattern with the help of name alias datasets. This lexical pattern is useful for the candidate alias extraction and which are independent of languages.

II. RELATED WORK

Alias identification is closely related to the problem of cross document co- reference resolution in which the objective is to determine whether two mentions of a name in different documents refer to the same entity. In [3], the authors proposed a cross document co- reference resolution algorithm by first performing within document co- reference resolution for each individual document to extract co- reference chains, and then, clustering the co- reference chains under a vector space model to identify all mentions of a name in the document set. However, the vastly numerous documents on the web render it impractical to perform within document co- reference resolution to each document separately, and then, cluster the documents to find aliases.

In personal name dis- ambiguation the goal is to dis- ambiguate various people that share the same name (namesakes) [4][5]. Given an ambiguous name, most name dis- ambiguation algorithms have modeled the problem as one of document clustering in which all documents that discuss a particular individual of the given ambiguous name are grouped into a single cluster. The web people search task (WePS) provided an evaluation data set and compared various name dis- ambiguation systems. However, the name dis- ambiguation problem differs fundamentally from that of alias extraction because in name dis- ambiguation the objective is to identify the different entities that are referred by the same ambiguous name; in alias extraction, we are interested in extracting all the aliases to a single name from the web.

III. PROPOSED WORK

The proposed method is outlined in Figure 1 and comprises two main components: pattern extraction, and alias extraction and ranking. Using a seed list of name- alias pairs, we first extract lexical patterns that are frequently used to convey information related to aliases on the web. The extracted patterns are then used to find the candidate aliases for a given name.

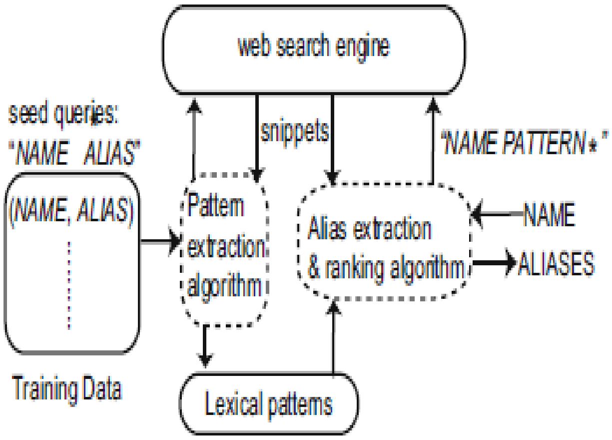

Figure 1: Proposed method

A. Lexical pattern extraction

For lexical pattern extraction input is given as name- alias pair. This list gives frequently occurred lexical patterns between the name and aliases. To retrieve the patterns query is given as input to the web search engine. The query is in the form of “name * alias”. The wild operator “*” is used to perform NEAR query. Algorithm 1 is used to capture the various ways in which information about aliases of names is expressed on the web.

Algorithm 1: ExtractPatterns(S)
comment: S is a set of (NAME, ALIAS) pairs
P ← null
for each (NAME,ALIAS) ∈ S
do
D ← GetSnippets(“NAME * ALIAS”)
for each snippet d ∈ D
do P ← P + CreatePattern(d)
return (P)

B. Candidate Alias Extraction

Once the set of lexical pattern is extracted, then the patterns are used to extract the candidate aliases for a given name as in Algorithm 2. If an entity name, name and a set “P” of lexical patterns is given as input, the Extract_Candidates function returns a list of candidate aliases for the name. Given name is associated with each pattern “p” in the set of patterns P and produce queries of the form: “NAME p *”. Thus we get a list of the candidate aliases.

Algorithm 2: ExtractCandidates(NAME,P)
comment: P is the set of patterns
C ← null
for each pattern p ∈ P
do D ← GetSnippets(“NAME p * ”)
for each snippet d ∈ D
do C ← C + GetNgrams(d,NAME, p)
return (C)

C. Ranking of Candidates

Considering the noise in web snippets, the candidates extracted by the shallow lexical patterns might include some invalid aliases. From among these candidates, we must identify those which are most likely to be correct aliases of the given name. We model this problem of alias recognition as one of the ranking candidates with respect to a given name such that the candidates, who are most likely to be correct aliases are scores to measure the association between a name and a candidate alias using three different approaches: lexical pattern frequency, word co-occurrences in anchor texts , and hub discounting.

D. Lexical Pattern Frequency

Using lexical pattern extraction algorithm retrieves a list of patterns with the help of a web search engine. We can use pattern frequency as one of the approach to calculate the weight of the aliases. If the personal name under consideration and a candidate name alias occur in many lexical patterns, then it can be considered as a good alias for the personal name. Consequently, we rank a set of candidate aliases in the descending order of the number of different lexical patterns in which they appear with a given name. The lexical pattern frequency of an alias is analogous to the document frequency (DF) popularly used in information retrieval process.

E. Co- Occurrences in Anchor Texts

Anchor texts have been used extensively in information retrieval process and have been used in various tasks such as synonym extraction, query translation in cross language information retrieval, and ranking and classification of the web pages. Anchor texts are particularly attractive because they not only contain concise texts but also provide links that can be considered as expressing a citation. We revisit anchor texts to measure the association between a name and its aliases on the Internet. Anchor texts pointing to a url provide useful semantic clues related to the resource represented by that url. For example, if the majority of inbound anchor texts of an url contain a personal name, it is likely that the remainder of the inbound anchor texts contain information about aliases of the name. Here, we use the term inbound anchor texts to refer the set of the anchor texts pointing to the same url. For example, consider the picture of Sachin Tendulkar shown in Figure 2. Figure 2 shows a picture of Sachin Tendulkar being linked to by four different anchor texts. According to our definition of co-occurrence, Sachin Tendulkar and Tendlya are considered as co-occurring.

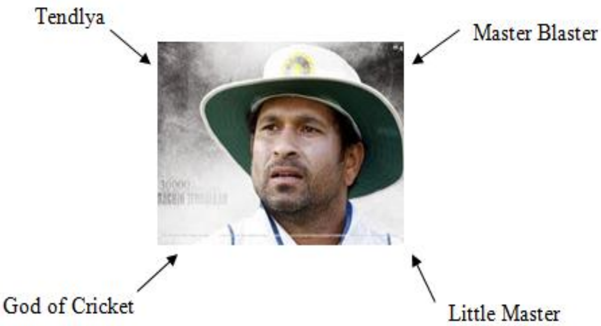

Figure 2: Picture of Sachin with different aliases

F. Hub Discounting

If the majority of the link contain person name in anchor text, then the confidence of that page as a source of information regarding the person whom we are interested in extracting aliases increases. We use this intuition to compute the simple discounting measure for co-occurrences in hubs as follows,

$$\alpha(h, n) = \frac{t}{d}$$

Where "t" is total number of inbound anchor text of "*h"* that contain real name n and d is total number of inbound anchor text of *h*.

IV. CONCLUSION

In this paper we proposed a lexical pattern-based approach to extract aliases of a given person name. We use a set of names and their aliases as the training data to extract lexical patterns that describe numerous ways in which information related to aliases of a name is presented on the web. An individual is typically referred by numerous nick names or name aliases on the web. Accurate identification of aliases of a given person name is useful in various web related tasks such as sentiment analysis, information retrieval, personal name disambiguation, and relation extraction. We propose a method to extract aliases of a given person name from the web. Given a person name, the proposed work first extracts a set of candidate aliases. Second, we rank the extracted candidates according to the likelihood of the candidate being a correct alias of the given name.

REFERENCES

[1] Danushka Bollegala, Yutaka Matsuo, and Mitsuru Ishizuka, Member, IEEE 2011 Automatic Discovery of Personal Name Aliases from the Web In IEEE Transaction on knowledge and data engineering, vol. 23, no. 6.
[2] D. Kavitha 2011 A Survey on Assorted Approaches to Graph Data Mining In International Journal of Computer Applications (0975 – 8887) Volume 14– No.1.
[3] M. Berland and E. Charniak, "Finding Parts in Very Large Corpora," Proc. Ann. Meeting of the Assoc. for Computational Linguistics (ACL '99), pp. 57-64, 1999.
[4] G. Mann and D. Yarowsky, "Unsupervised Personal Name Disambiguation," Proc. Conf. Computational Natural Language Learning (CoNLL '03), pp. 33-40, 2003.
[5] R. Bekkerman and A. McCallum, "Disambiguating Web Appearances of People in a Social Network," Proc. Int'l World Wide Web Conf. (WWW '05), pp. 463-470, 2005.

International Journal of Modern Engineering Research (IJMER)
www.ijmer.com Vol. 3, Issue. 5, Sep - Oct. 2013 pp-2770-2772 ISSN: 2249-6645

Layered Approach & HMM for Network Based Intrusion Dection

Archana patil, A. T. Bhole

***ABSTRACT**: In this, we are using two techniques together as signature based and anomaly based called as Hybrid technique. Anomaly detection, where the strategy is to suspect of what is considered an unusual activity for the subject (users, processes, etc.) and carry on further investigation. This approach is particularly effective against novel (i.e. previously unknown) attacks. Signature based detection systems detects previously known attack in a timely and efficient way. The main issue of this approach is that in order to detect an intrusion this must to be previously detected. This Hybrid technique gives better result than signature based and anomaly based technique. Also we are using here layered approach to get result faster ,because in layered approach we have different four layers as prob,U2R,R2L,DOS and we assigned different features to different layer so that if any layer find attack at that layer that attack will fix ,that attack should not go further .Main aim of this paper is to increase accuracy and efficiency .*

***Index Terms:** Intrusion detection, Layered Approach, Hidden Markov Model, network security, decision trees, naive Bayes.*

I. INTRODUCTION

Intrusion detection is defined as ``the problem of identifying individuals who are using a computer system without authorization (i.e., `crackers') and those who have legitimate access to the system but are abusing their privileges (i.e., the `insider threat')".Also we can say that the identification of attempts to use a computer system without authorization or to abuse existing privileges. According to Heady et al. where an intrusion is defined as ``any set of actions that attempt to compromise the integrity, confidentiality, or availability of a resource", disregarding the success or failure of those actions.[12] The definition of an intrusion detection system does not include preventing the intrusion from occurring, only detecting it and reporting it to an operator.[12]

There are two types of intrusion detection depending on way their components are distributed

1. A centralized intrusion detection system is one where the analysis of the data is performed in a fixed number of locations, independent of how many hosts are being monitored. We do not consider the location of the data collection components, only the location of the analysis components.

Eg: IDES, IDIOT .

2. A distributed intrusion detection system is one where the analysis of the data is performed in a number of locations proportional to the number of hosts that are being monitored. Again, we only consider the locations and number of the data analysis components, not the data collection components .

Eg: DIDS, GrIDS.

Also Intrusion detection is divided into :

1. Anomaly detection, where the strategy is to suspect of what is considered an unusual activity for the subject (users, processes, etc.) and carry on further investigation. This approach is particularly effective against novel (i.e. previously unknown) attacks. Its main drawback is the high rate of false positives, because any legitimate but new activity can rise an alert.

2. Signature detection, where the strategy is to look for some special activity (signature) of previously known attacks. Signature based detection systems detects previously known attack in a timely and efficient way. The main issue of this approach is that in order to detect an intrusion this must to be previously detected.

Previously there is only one technique is used at a time but In this we are using both as signature based and anomaly based combine called as hybrid based technique .That is we are developing hybrid system using HMM based layered approach for NIDS. We also integrate the Layered Approach with the HMMs to gain the benefits of computational efficiency and high accuracy of detection in a single system. By using this we get fast result because we are using layered approach .Layered approach means we have different four layers as PROBE , DOS , U2R ,R2L and for every layer different different features are assigned and whenever we got some malicious attack that attack must be detected at that moment ,that attack should not go further. Due to this technique speed of our operation increase.

A hidden Markov model(HMM) is a statistical generative model in which the system being modelled is assumed to be a Markov process with unobserved state. An HMM can be considered as the simplest dynamic Bayesian network. An HMM is like a finite state machine in which not only transitions are probabilistic but also output. An HMM is a doubly stochastic process with an underlying stochastic process that is not observable, and can only be observed through another set of stochastic processes that produce the sequence of observed symbols . HMM is a useful tool to model sequence information. This model can be thought of as a graph with N nodes called 'state' and edges representing transitions between those states. Each state node contains initial state distribution and observation probabilities at which a given symbol is to be observed. An edge maintains a transition probability with which a state transition from one state to another state is made.

II. RESEARCH ELABORATION

Layered Approach

The goal of using a layered model is to reduce computationand the overall time required to detect anomalous events. The time required to detect an intrusive event is significant and can be reduced by eliminating the communication overhead among different layers. This can be achieved by making thelayers autonomous and self-sufficient to block an attack without the need of a central decision-maker. Every layer in the LIDS framework is trained separately and then deployed sequentially. We define four layers that correspond to the four attack groups mentioned in the data set. They are Probe layer, DoS layer, R2L layer, and U2R layer. Each layer is then separately trained with a small set of relevant features. Feature selection is significant for Layered Approach and discussed in the next section. In order to make the layers independent, some features may be present in more than one layer. The layers essentially act as filters that block any anomalous connection.We have four different attacks probe attack,dos attack, u2r attack,r2l attack corresponding to four different layers.As Probe layer, R2L layer,U2R layer,DOS layer.

Probe Layer : The probe attacks are aimed at acquiring information about the target network from a source that is often external to thenetwork.

DoS Layer : The DoS attacks are meant to force the target to stop the service(s) that is (are) provided by flooding it with illegitimate requests.

R2L Layer : R2L attacks are one of the most difficult to detect as they involve the network level and the host level features.

U2R Layer:The U2R attacks involve the semantic details that are very difficult to capture at an early stage.

Decision tree

Decision tree builds classification or regression models in the form of a tree structure.

Dataset is a collection of data, usually presented in a tabular form. It breaks down a dataset into smaller and smaller subsets while at the same time an associated decision tree is incrementally developed.A decision tree is composed of three basic elements:

1. A decision node specifying a test attributes.
2. An edge or a branch corresponding to the one of the possible attribute values which means one of the test attribute outcomes.
3. A leaf which is also named an answer node contains the class to which the object belongs.

Naive Bayesian

The Naive Bayesian classifier is based on Bayes' theorem with independence assumptions between predictors. A Naive Bayesian model is easy to build, with no complicated iterative parameter estimation which makes it particularly useful for very large datasets. Despite its simplicity, the Naive Bayesian classifier often does surprisingly well and is widely used because it often outperforms more sophisticated classification methods. [6]

A naive Bayes classifier assumes that the presence (or absence) of a particular feature of a class is unrelated to the presence (or absence) of any other feature, given the class variable.

III. RESULT

Table I : Comparision Between Difference Techniques

Technique	Detection Rate in percentage	Time Required
Layered Approach	98.71740059854639	Less than 1 sec.
Hidden Markov Process	95.05439161966156	12 sec
Decision Tree	95.0544	2 sec
Navie Bayes	93.5133	4sec

From this , layered approach gives very high detection rate and time required for detecting attack is also less.

IV. CONCLUSION

In this ,we can detect intrusion detection fast and accurately .Layered HMMs can be very effective in detecting the Probe, the U2R, and the R2L attacks as well as the DoS attacks. However, if we consider all the 41 features given in the data set, we find that the time required to train and test the model is high. To address this, we performed experiments with our integrated system by implementing a four-layer system. The four layers correspond to Probe, DoS, R2L, and U2R. For each layer, we then selected a set of features that is sufficient to detect attacks at that particular layer. Feature selection for each layer enhances the performance of the entire system. By using layered approach we get high accuracy () and also time required for it is also less() than other two techniques HMM and WEKA (decision tree and navie bayes).

ACKNOWLEDGMENTS

The authors sincerely thank the anonymous reviewers whose comments have greatly helped clarify and improve this paper.

REFERENCES

[1] Kapil Kumar Gupta, Baikunth Nath, "Layered Approach Using ConditionalRandom Fields for Intrusion Detection" *IEEE Transaction On Dependable and Secure Computing*, Vol. 7, No. 1, January –March 2010.

[2] T. Abraham "IDDM: Intrusion Detection Using Data Mining Techniques" *International Journal of Network Security & Its Applications (IJNSA)*, Vol. 2, No. 2. 2008

[3] N.B. Amor, S. Benferhat, and Z. Elouedi, “Naive Bayes vs. Decision Trees in Intrusion Detection Systems”, *Proc. ACM Symp.Applied Computing* , 2004.
[4] K.K. Gupta, B. Nath, and R. Kotagiri, “Conditional Random Fields for Intrusion Detection,” *Proc. 21st Int'l Conf. Advanced Information Networking and Applications Workshops*, 2007.
[5] Yusufovna, S.F. “Integrating Intrusion Detection System and Data Mining” *IEEE Computer Society Washington* , Oct. 2008 , 978-0-7695-3427-5.
[6] Christopher Kruegel Darren Mutz William Robertson Fredrik Valeu ” Bayesian Event Classification for Intrusion Detection” *Reliable Software Group University of California, Santa Barbara*
[7] “Understanding Intrusion Detection Systems *’’ SANS Institute InfoSec Reading Room.*
[8] Ozalp Babaoglu “IDS:Intrusion Detection Systems”, *Babaoglu* 2006.
[9] Y. Du, H. Wang, and Y. Pang “A Hidden Markov Models-Based Anomaly Intrusion Detection Method”, *Intellegent Control and Automation* 2004.
[10] L. Portnoy, E. Eskin, and S. Stolfo, “Intrusion Detection with Unlabeled Data Using Clustering,” *Proc. ACM Workshop Data Mining Applied to Security* (DMSA), 2001
[11] Y.-S. Wu, B. Foo, Y. Mei, and S. Bagchi, “Collaborative Intrusion Detection System (CIDS): A Framework for Accurate and Efficient IDS,” *Proc. 19th Ann. Computer Security Applications Conf.* , 234-244, 2003.
[12] Autonomous Agents for Intrusion Detection, http://www.cerias.purdue.edu/research/aafid/, 2010.
[13] Probabilistic Agent Based Intrusion Detection, http://www.cse.sc.edu/research/isl/agentIDS.shtml, 2010.
[14] Shaik Akbar Dr.K.Nageswara Rao Dr.J.A.Chandulal “Intrusion Detection System Methodologies Based on Data Analysis” International Journal of Computer Applications , August 2010
[15] Wei Wang, Xiaohong Guan, Xiangliang Zhang, Liwei Yang “Profiling program behavior for anomaly intrusion detection based on the transition and frequency property of computer audit data” Center for Networked Systems and Information Security (CNSIS) and State Key Laboratory for Manufacturing Systems Engineering (SKLMSE), Xi’an Jiaotong University, Xi’an 710049, China,2006.
[16] Sam Drazin and Matt Montag “Decision Tree Analysis using Weka”, *University of Miami.*

International Journal of Modern Engineering Research (IJMER)
www.ijmer.com Vol. 3, Issue. 5, Sep - Oct. 2013 pp-2773-2785 ISSN: 2249-6645

Optimizing Bunsen burner Performance Using CFD Analysis

Aruna Devadiga[1], Prof. Dr. T. Nageswara Rao[2]
[1]M. Tech Student, Oxford College of Engineering, Bangalore – 560068, Karnataka
[2] Professors, Department Of Mechanical Engineering, Oxford College of Engineering, Bangalore– 560068, Karnataka

ABSTRACT: *Industry relies on heat from the burners in all combustion systems. Optimizing burner performance is critical to complying with stringent emissions requirements and to improve industrial productivity. Even small improvements in burner energy efficiency and performance can have significant impacts in a continuous operation, more so if the improvements can be used in other combustion systems and across industries. While tremendous advances have been made in understanding the fundamentals of combustion, the remaining challenges are complex. To make improvements, it is critical to understand the dynamics of the fuel fluid flow and the flame and its characteristics. Computational Fluid Dynamics offers a numerical modelling methodology that helps in this regard. In the existing work, valid computational models are used for the study of different modes of combustion and also to study the mixing of fuel and air inside the burner mixing chamber to obtain the optimum Air to Fuel ratio. Liquefied petroleum gas (LPG) which has a composition of Propane and Butane in the ratio 60:40 by volume, is used as the fuel. Bunsen burner is used for the experiments. The present work has attempted to establish the validity of the Computational results by conducting appropriate experiments. The first series of simulations were done for proper mixing of fuel-air in the mixing chamber of burner. These were done for different mass flow rates of the fuel. Variation in the mass flow rates resulted in variation of the flame lengths, flame velocity, and temperature profiles across the flame. The second stage included the modelling and meshing of the combustion zone (assumed to be cylindrical in shape) with different number of grid points to check the accuracy of the mesh and also to see the variation in the results obtained from solver. The results obtained from the mixing chamber are the values which are input to the combustion chamber. These results are in the ratio of air to fuel mixture, mass flow rate of the mixture, velocity, mass fractions of oxygen, propane and butane separately. The combustion zone results were analysed for variations in temperature, mass fractions of propane, butane, oxygen, carbon dioxide, carbon monoxide, at different heights. Pressure and velocity variations were also studied for different mass flow rates. The experimental part consisted of measuring the temperature profile of the flame obtained from the burner at different mass flow rates. Prior to this, the calibration of the rota meter was also done. The rota meter was used to obtain different flow rates of the fuel. With the experiments, combustion phenomena like flame lift, blow off and flash back can be observed and the corresponding flow rate can be input to the computations to study these phenomena using CFD. CFD provides more scope for study and analyses of the results than the experiments. The experimental results are compared with those of computational results and they are in close proximity to the CFD results. The deviation of the experimental results from the CFD obtained results are due to non ideal working conditions during the experiments. The results obtained from computations provide an estimate of Equivalence ratio, reactant and product concentrations in the flame, temperature, turbulence, inlet and outlet velocity of fuel-air mixture etc. These studies cannot be conducted experimentally and hence computational results are used to establish the validity and also for in depth study of the dynamics of Combustion.*

I. INTRODUCTION

Combustion is the most important process in engineering, which involves turbulent fluid flow, heat transfer, chemical reactions, radioactive heat transfer and other complicated physical and chemical phenomena. Typical engineering applications include internal combustion engines, power station combustors, boilers furnaces etc. It is important to study the different modes of combustion taking place in these instruments, chemical kinetics involved, temperature and flame velocity, mass flow rate of the fuel etc to improvise the working of these equipments and maximising the efficiency.

The different modes of Combustion are premixed combustion, diffusion combustion and mixed mode combustion. In premixed combustion air and fuel are premixed to the required stoichiometry before burning. In the diffusion mode, a diffusion flame may be defined as a non-premixed, quasisteady, nearly isobaric flame in which most of the reaction occurs in a narrow zone that can be approximated as a surface. In the mixed mode combustion there is partial premixing of flames as well as diffusion also occurs. Such flames occur in many practical applications like in industrial burners, gas-fired domestic burners, rocket burners and also gas turbine combustors. Although flows in combustors usually are turbulent, analyses of flame stabilization are often based on equations of laminar flow. This may not be as bad as it seems because in the regions of the flow where stabilization occurs, distributed reactions may be dominant, since reaction sheets may not have had time to develop; an approximation to the turbulent flow might then be obtained from the laminar solutions by replacing laminar diffusivities by turbulent diffusivities in the results.

The important combustion phenomena which have received considerable attention in the recent years are Flame lift-off mechanisms, lift-off height, lift-off velocity and blow off velocity. Study of these phenomena helps to fix the operating range or operating limits of a burner. We are studying these phenomena using different flames using a Bunsen burner at different mass flow rates of the fuel and simulating the data using time accurate, higher order numerical methods with detailed transport and chemistry models using ANSYS ICEM CFD software. Combustion modelling is done using ANSYS ICEM CFD software. This software uses Reynolds Average Navier Stokes Equations (RANS) to solve the continuity equations of mass, momentum and energy. Numerical flow simulation, or more common Computational Fluid Dynamics

(CFD), relies on solving conservation or transport equations for mass, momentum, energy and participating species. If the flow is turbulent, model equations for specific turbulent quantities have to be solved in addition. Since even with today's super computers resolving turbulent length scales directly results in tremendous effort, Reynolds averaged equations are applied to include the physics of turbulence. To discretize and solve the governing flow equations Finite Volume method is employed by the majority of commercial CFD codes.

II. METHODOLOGY

Methodology involves experimental analysis and CFD analysis. The complexity of combustion modelling was the challenging module of this entire work. In turbulent combustion one distinguishes between premixed, non-premixed and partially premixed combustion. The problem was initiated by taking the case of a most simple burner which is used in most engineering applications, the Bunsen burner. Prior to the combustion analysis, proper mixing of the fuel and air was analysed in the mixing chamber of the Bunsen burner by using the software ANSYS ICEM CFD and CFX solver. Selection of the appropriate turbulence model for the mixing of fuel in the mixing chamber is crucial. This was a direct consequence of the Air/Fuel ratio at the outlet of the burner, and hence played a crucial role in the formulation of the combustion phenomena occurring in the combustion zone. The nature of turbulent flow is irregular with rapid fluctuations in velocity, temperature, pressure, density and composition. This fluctuating nature makes turbulent flow highly diffusive resulting in enhanced transport of momentum, mass and energy. The Eddy Dissipation Model was selected in the CFX solver which is best suited for solving turbulent conditions as it uses the Reynolds Average Navier Stokes model to solve the equations. The results obtained from the solver are analysed with respect to variation of different properties like temperature, pressure, velocity, mass fractions. The same are compared at different number of grids to optimise the number of grid points. For the experiments, Liquefied Petroleum Gas (LPG) is used as the fuel and the ratio of mass fractions of propane: butane taken is 0.53: 0.47. The kinetics of LPG combustion is established and the validation of these results is done by measuring the temperature profile of the flame of the Bunsen burner. The CFD analysis is especially used to establish the flow dynamics in the burner and also to explain the different variations of properties inside the flame.

III. EXPERIMENTAL ANALYSIS OF FLAME TEMPARATURE AT GIVEN FUEL FLOW RATE

Liquid petroleum gas (LPG) is used as the fuel for Bunsen burner. The LPG composition has 60% propane and 40% butane by volume. The flow is controlled by a precision regulator and is measured using a rota meter. The flow rate must be kept constant for one full set of readings of the flame temperature. The rota meter least count is 10ml/min. The maximum flow rate that can be measured by this rota meter which is used for the experiments is 400ml/min. The scope of the experiment is to ensure that the assumptions in the computational and mathematical modelling are valid and not irrational. The aim of the experiment was to obtain the temperature profile in the flame, and match the experimental results to the computational results obtained. By doing this, the combustion model used, and chemical kinetics can be justified.

The aim is to measure the temperature of the flame along the length of the flame in both x and y axes. A travelling microscope is modified to traverse along x and y axes. It consists of a longitudinal and latitudinal slot with markings on it like a vernier scale. The connecting frame moves in the slots and this movement is caused by operating two motors with the help of battery or power box. The power box is used to supply constant voltage of 3.5 volts. This helps the thermocouple to traverse at constant speed. A fine thermocouple (Platinum-Platinum Rhodium-13%) is attached to the arm of the instrument which traverses along the x and y axes of the flame and measures the temperature. The thermocouple is connected to a power box which helps to maintain a constant velocity of traverse by keeping the voltage constant. With the help of a data acquisition, the temperature measured by the thermocouple is recorded in a computer. The software is preloaded in the computer and the time for which the temperature is to be recorded is set for 100ms which means for every 100 milliseconds the temperature data is recorded. The flow is controlled by a precision regulator and is measured using a rota meter. The flow rate must be kept constant for one full set of readings of the flame temperature. When a steady flame is achieved the flame is scanned at different heights. Care should be taken to keep the flame steady. Also, the fuel flow rate should be closely monitored, since any change in the flow rate can directly affect the flame height, and hence the kind of flame attained. Keeping in mind all these factors, steady readings were recorded and plotted.

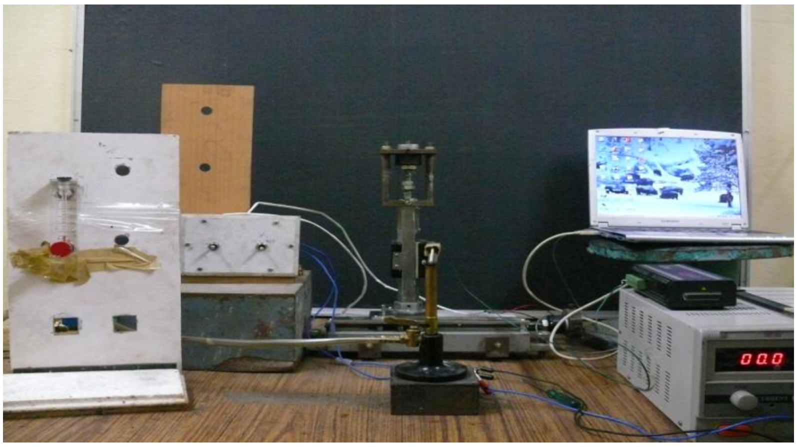

Figure 3.1 Experimental setup for recording Flame Temperature

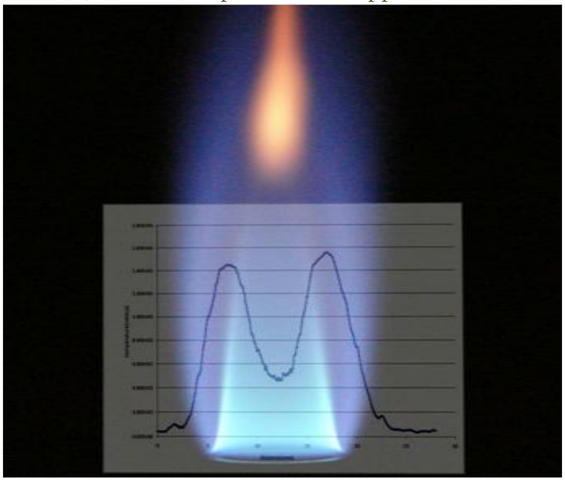

Figure 3.2 Temperature profiles at fuel mass flow rate 100ml/min

The figure 3.2 shows the temperature profile being overlapped on the flame. The temperature was recorded at 100ml/min flow rate at 2cm above the burner rim. The flame is axisymmetric and hence the temperature graph is also axisymmetric. At the burner ends it can be observed that the temperature is less due to heat transfer to the cold walls of the burner. The highest temperature is recorded at the edge of the inner cone, as the mixture gets adequate amount of oxygen for the complete combustion of fuel-air mixture. At the centre of the flame there is drastic dip in temperature. This is because the rich mixture from the mixing chamber which comes out like a jet lacks sufficient oxygen for combustion. Hence there is incomplete combustion in this region leading to formation of carbon monoxide.

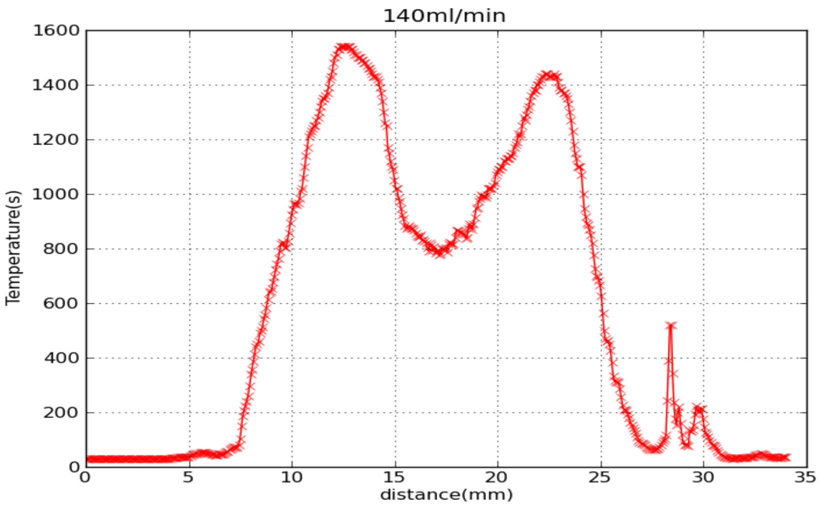

Figure 3.3 Bunsen Flame Temperature profile at flow rate of 140ml/min

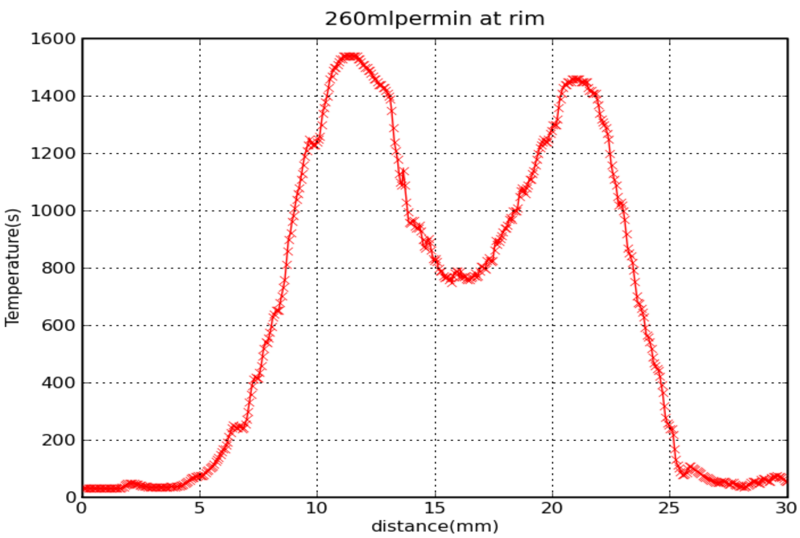

Figure 3.4 Bunsen Flame Temperature profile at flow rate of 260ml/min

IV. CFD ANALYSIS OF FLAME TEMPARATURE AT A GIVEN FUEL FLOW RATE

For CFD analysis of the Bunsen burner mixing chamber and the Combustion Zone, the details of the conditions specified for each of these domains are specified here. The modelling and meshing of geometries are done using the ANSYS ICEM CFD software and is imported to the CFX solver for pre processing and post processing. The Computational modelling is done for the burner mixing chamber and then for the combustion zone. The modelling and meshing techniques are used. The pre-processor consists of modelling and meshing of the geometry. The Burner mixing chamber is modelled using ANSYS ICEM CFD and the meshing is done using structured meshing technique. The length of the mixing chamber is taken to be equal to 100mm. The outlet rim diameter is equal to 10mm. The fuel inlet diameter is set to be equal to 1mm. Axisymmetric case is considered for the modelling of mixing chamber. Once the geometric modelling is done, mesh or grids should be generated for the model. This involves dividing the whole geometry into number of equally spaced volumes or cells. This process is termed as discritization. This discritization should be done in such a way that the continuity of the process variables from one cell to another should be maintained throughout the whole geometry. Structured meshing techniques are used for mesh generation, as structured meshing gives better results than unstructured meshing.

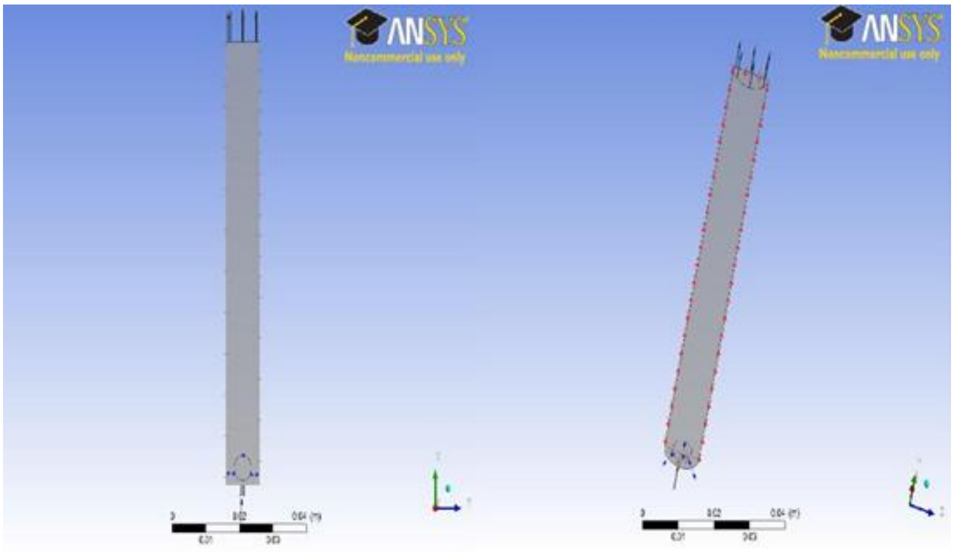

Figure 4.1 Bunsen burner mixing chamber geometric modelling (axisymmetric) showing air and fuel inlet, outlet in ANSYS CFX

Boundary Conditions are specified in the CFX solver as follows

Default Domain: a. Fluid = Liquefied Petroleum Gas(LPG) b. Reference Pressure = 1atm c. Turbulence Model = k-ε Model d. Temperature = 300K e. Constraint Component = N2	**Fuel Inlet:** a. Boundary Type = Inlet b. Mass Fraction C3H8 =.53 c. Mass Fraction C4H10 =.48 d. Relative Pressure = 0.0001 bar
Air Inlet: a. Boundary Type = Opening b. Mass Fraction C3H8 =0 c. Mass Fraction C4H10 =0 d. Mass Fraction O2 =.232 e. Flow Direction = Normal to Boundary Condition	**Outlet:** a. Boundary Type = Outlet b. Mass and Momentum = Average Static Pressure c. Relative Pressure = 0 bar
Solver Criteria: a. Advection Scheme: High Resolution b. Maximum Iterations: 10000 c. Residual Target: 1e-7	

V. BURNER MIXING CHAMBER RESULTS

The post processing results of the Mixing Chamber give variation of propane, butane, oxygen, outlet mixture mass flow rate, air to fuel ratio, velocity of the fuel air mixture at the outlet etc.

Fuel flow Rate (g/s)	C3H8 mass fraction	C4H10 mass fraction	Mass flow rate at outlet	Velocity of fuel at outlet (m/s)	Oxygen mass fraction	Velocity of air at Air-inlet (m/s)	Velocity of Fuel at fuel-inlet (m/s)
140	.115867	.10275	8.21214e-5	1.61207	.181619	2.4321	19.356
220	.115095	.102066	9.92093e-5	1.94883	.181811	3.20962	26.9487
260	.114877	.101872	11.5964e-5	2.27898	.181712	3.845	31.4304

Table 5.1 CFX solver Post processing results of the Burner mixing chamber at different mass flow rates.

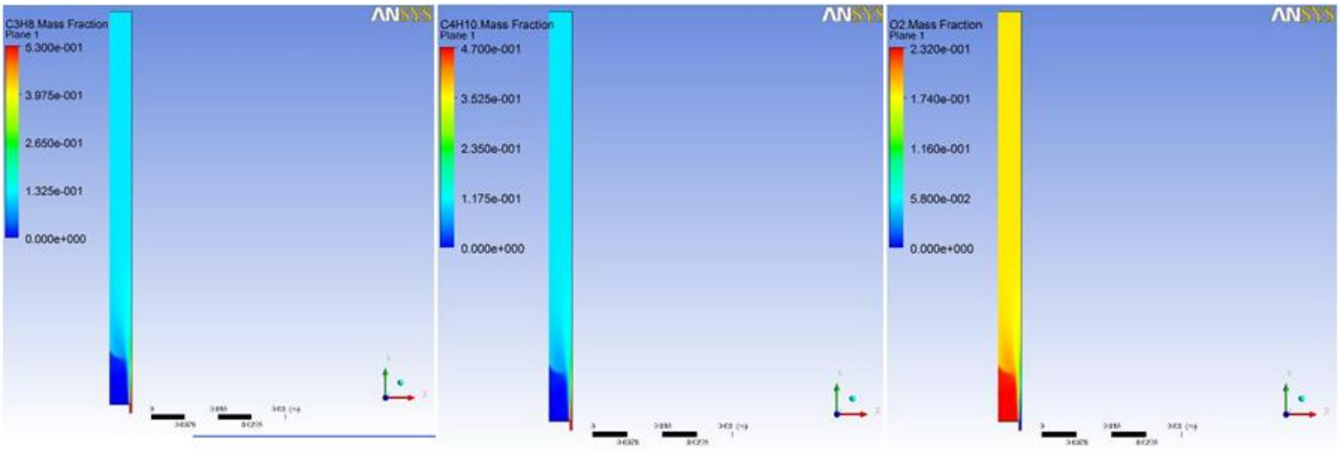

Figure 5.1 Mass fraction variation of propane, butane and oxygen (from top left, clockwise) separately in the burner mixing chamber as obtained from ANSYS CFX solver.

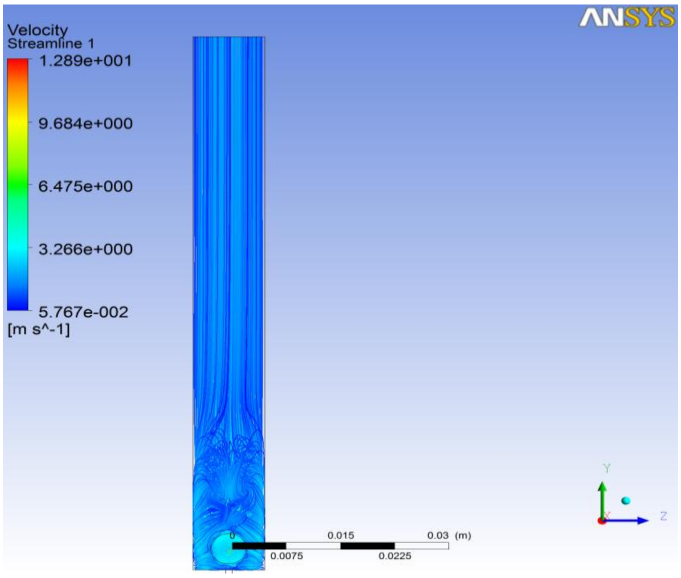

Figure 5.2 Air-Fuel mixtures velocity streamlines showing the velocity profile inside the burner mixing chamber

VI. MODELLING AND ANALYSIS OF THE COMBUSTION ZONE

The combustion zone modelling was done using ANSYS ICEM CFD. A section of the cylindrical combustion zone was modelled with angle of 45 degrees in between as shown in the figure. The vertical length of the combustion chamber is 200mm and the horizontal length is 50mm. The meshing was done using structured meshing technique. The results obtained from the mixing chamber are given as input conditions to the combustion chamber. The parameters selected for the input file to the combustion zone are velocity, mass fraction and mass flow rates. A dense grid is assigned carefully in and around the central fuel jet where large gradients are expected. To avoid singularity at centre in axisymmetric case of 45 degrees, a quarter O gird is used near the fuel jet. Mesh quality has been checked for grid skewness to ensure good convergence. The quality of the grid obtained is 65% and total number of nodes generated is 5, 00,000. Grid independent studies are also made for comparing and validating the results.

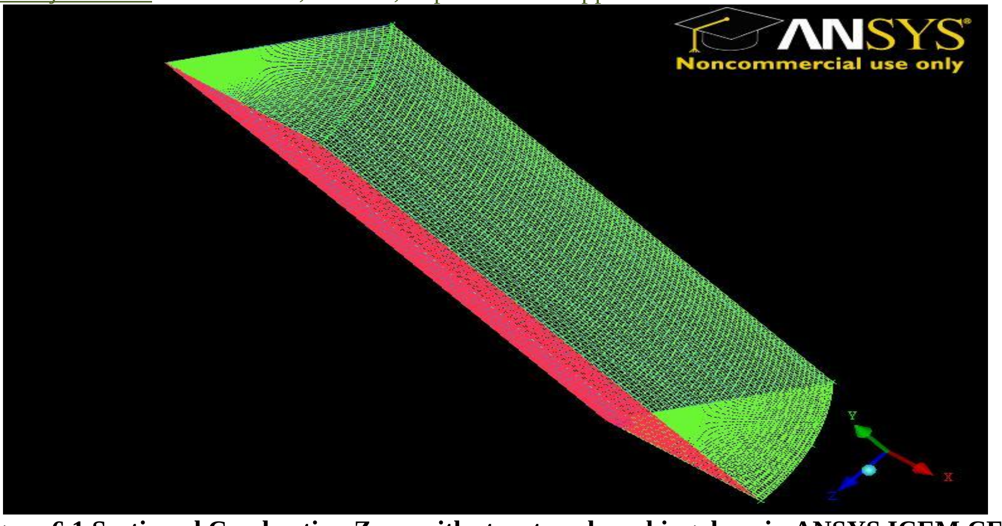

Figure 6.1 Sectioned Combustion Zone with structured meshing done in ANSYS ICEM CFD

Boundary Conditions for Combustion Zone:

The boundary conditions vary for different mass flow rates and are obtained from the result files (.res format). A situation is raised wherein a heat source needs to be modelled to initiate combustion. This heat source should not add to the heat generated by the flame and also this heat source should exist in a defined volume and for specified time duration. This is done by modelling a step function for the temperature near the inlet domain to be 900 K for time duration of 0.1s.

```
Step Function –CEL Code:
LIBRARY:
 CEL:
   EXPRESSIONS:
Temp Func = 300[K]+600[K]*step(0.005-z/1[m])*step(0.005-y/1[m])*step(0.1- t/1[s])
   END
 END
```

This serves as the ignition source for the combustible mixture at the outlet of the Bunsen burner.

The Boundary Conditions are:

Default Domain: a. Fluid = LPG b. Heat transfer Model = Thermal Energy c. Reference pressure = 1 atm d. Turbulence Model = k-ε model e. Combustion Model = eddy dissipation Model	**Material Creation:** a. Material created = LPG mixture b. Mixture properties = Reacting Mixture c. Material Group = Gas Phase Combustion d. Additional Material List = CO, CO2, H2O, N2, O2 **e.** Reaction List = Butane Air WD2, Propane Air WD2
Inlet Conditions: a. Boundary Type = Inlet b. Flow regime = Subsonic c. Fuel flow speed = Velocity corresponding to different flow rates d. C3H8 Mass Fraction = n.a e. C4H10 Mass Fraction = n.a f. O2 Mass Fraction = n.a	**Outlet Conditions:** a. Flow regime = subsonic b. O2 Mass Fraction = 0.232 **Solver Criteria:** a. Advection Scheme: High Resolution b. Maximum Iterations: 30000 c. Residual Target: 1e-7
Symmetry Conditions applied to the remaining parts of the domain for symmetry calculations along the domain, as explained above.	

A second order accurate scheme is used for spatial discritization with physical advection terms. A time step of 1xe-7 is used with 30000 iterations and the solutions is aid to be converged. The boundary conditions are specified for the combustion zone at different mass flow rates. For each mass flow rate, the mass fractions of butane, propane, oxygen and inlet mass flow rate of the fuel-air mixture, velocity (which are the outlet results of burner mixing Chamber) change.

VII. ANALYSIS OF COMBUSTION ZONE AT DIFFERENT MASS FLOW RATES

In this section, the post processing results obtained for combustion Zone at different flow rates are analysed. The variation of different properties like mass fractions, temperature, pressure, velocity and their effect on the flame can be studied.

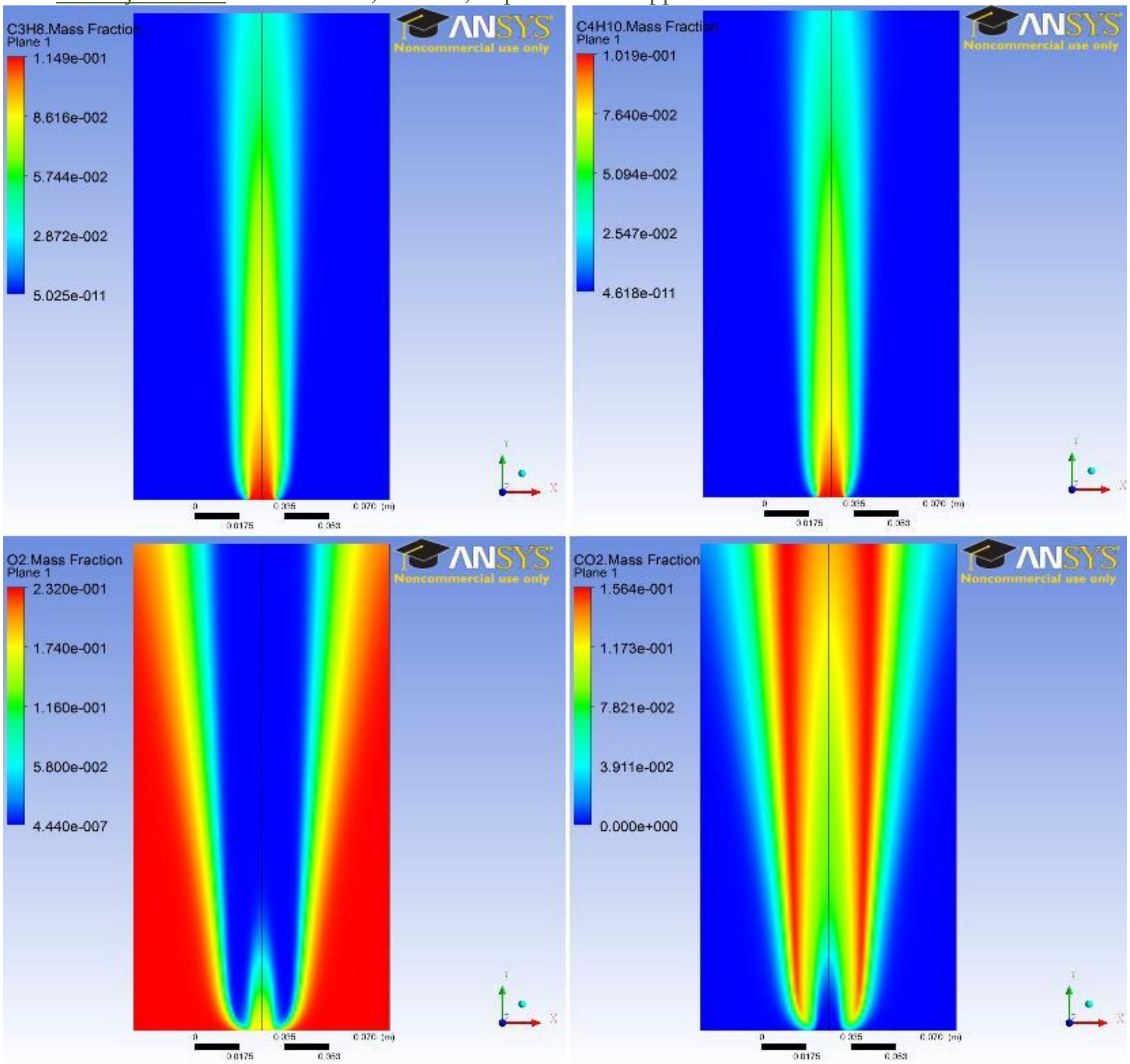

Figure 7.1 Variation of C3H8, C4H10, O2, CO2 in the Combustion Chamber at flow rate of 260ml/min

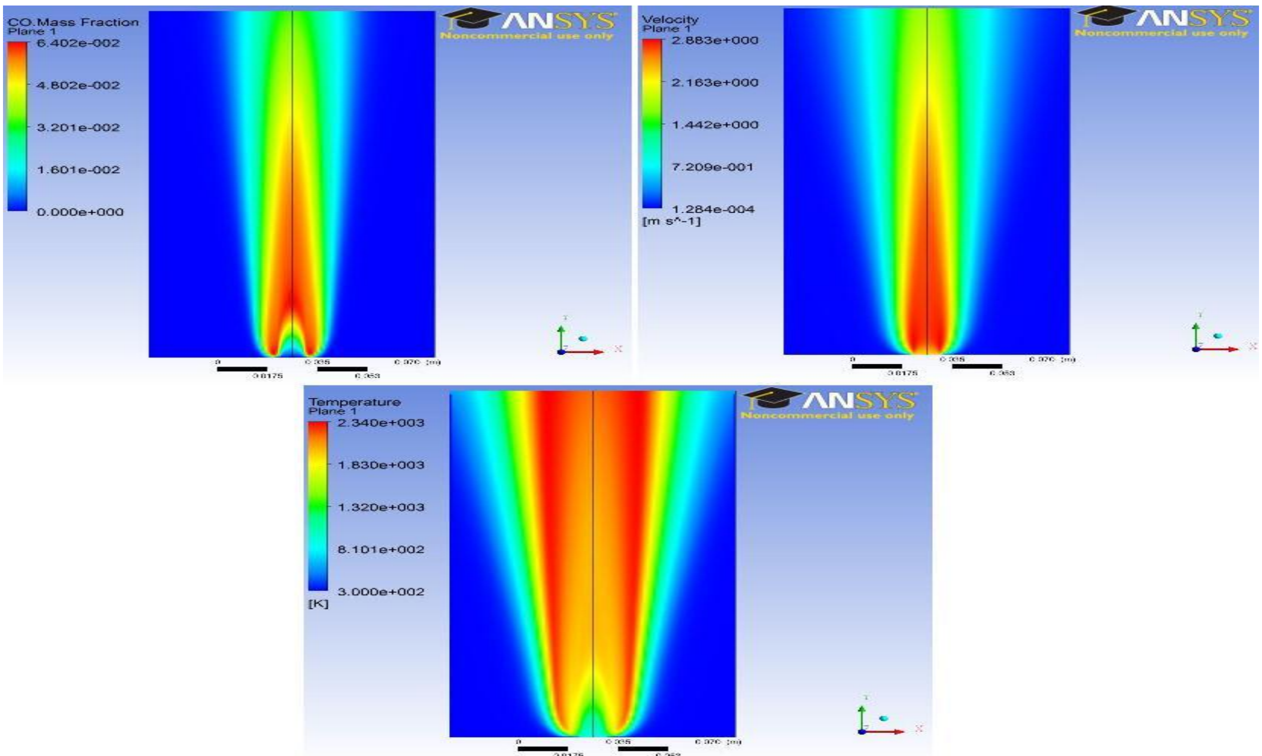

Figure 7.2 Variation of CO, Velocity, Temperature in the Combustion Chamber for flow rate of 260ml/min

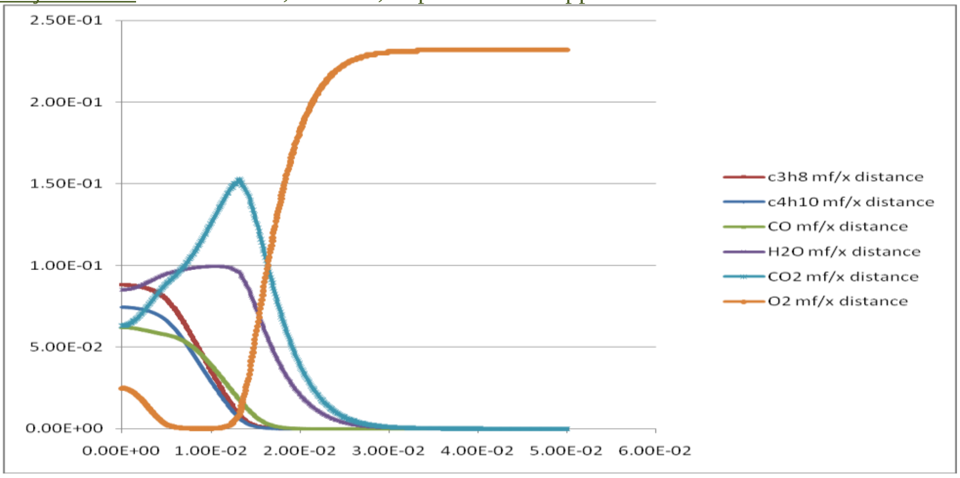

Figure 7.3 Variation of Mass Fractions of reactants and products inside the combustion zone for flow rate of 260ml/min

As it can be seen from the figure 7.3, the propane and butane mass fractions are decreasing from the centre and the consumption of oxygen rapidly increases between 10mm to 20mm from the centre and is the highest beyond 20mm as the availability of ambient oxygen is more. The CO2 composition increases first which shows that complete combustion occurs. Beyond 15mm from the centre the CO2 composition decreases which indicates that though there is oxygen available there is scarcity of the fuel beyond this point. This is also indicated by the rapid decrease in compositions of propane and butane beyond this point. There is presence of carbon monoxide only within 10mm from the centre which indicates that duel to rich fuel- air mixture in that area incomplete combustion has occurred leading to formation of carbon monoxide.

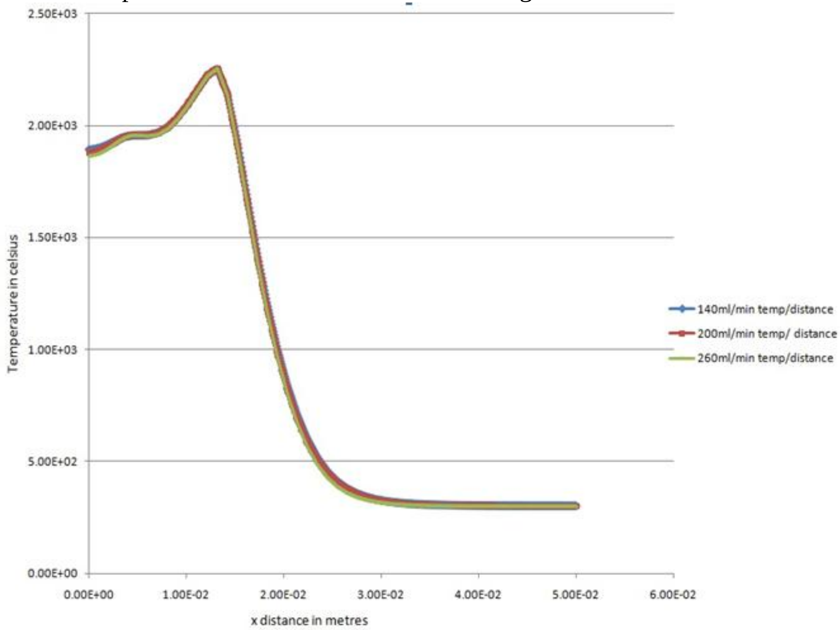

Figure 7.4 Temperature profiles in combustion zone at different flow rates read from CFX solver

In the figure 7.4, the temperature profiles of flames at all the flow rates are same, which indicates that the profiles of the flame at any flow rate which is similar as obtained in CFX solver. Comparing the profiles to the CO2 profile in the figure 7.3, it can be observed that the trend of the graphs is the same. This CO2 concentration indicates that there is complete oxidation taking place of the reactants, which results in increase in heat release rate. Hence, it can be said that temperature varies with the variation of CO2.

VIII. RESULTS AND DISCUSSIONS

Here, comparisons between the experimental and computational results are made and studied. Comparisons are made for different properties like mass fractions, temperature, etc and these are validated. The validations are also done by comparing with results of other research papers which have also established similar results.

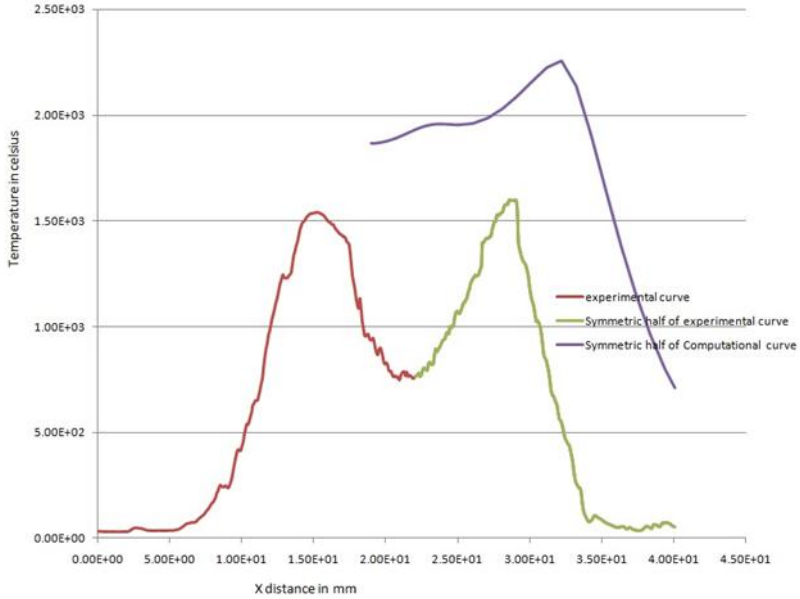

Figure 8.1 Comparison of experimental and computational temperature profiles at 260ml/min

The experimental curve is a axisymmetric curve which is obtained from the thermocouple traverse along the wholly length of the flame. But in the computational results it is not possible to obtain a axisymmetric curve as the measurement is made along the line extending from the centre of the combustion chamber to wall of the combustion chamber. This discrepancy in the measured temperature is attributed to uncertainties in the measurements and the model (e.g. related to the chemical mechanism and the thermo physical and transport properties). The high-temperature region appears to be slightly narrower in the laboratory flame due to burner edge effects. This will be corroborated by the species concentration measurements. The hotter regions do not necessarily correspond to regions of high chemical activity, because the heat released in the reaction zones is transported both upstream (by diffusion) and downstream to other portions of the flame. In both the measurements and predictions, the region with the highest temperatures lies between the inner premixed and the central non premixed reaction zone. The basic structure of the flame can be assumed to consist of distinct layers that include 1) an inner layer (PF) in which hydro carbon fuel and O_2 consumption occur and 2) an oxidation layer (NF) (surrounded by a preheat zone downstream of PF and a post flame zone downstream of NF). All of the hydrocarbon chemistry can be assumed to occur in the inner layer where fuel and radical consumption occurs to form CO and H_2. In the oxidation layer, the CO and H_2 formed in the inner layer are oxidized to form CO_2 and H_2O. The CO-oxidation layer is generally thicker than the H_2-oxidation layer, and the overall thickness of the oxidation layer itself is, in general, greater than that of the inner layer. Furthermore, the heat release is primarily due to the exothermic reactions occurring in the oxidation layer. A major exothermic reaction in the oxidation layer .NF/$CO + OH = CO_2 + H$ occurs on a relatively slower. Time scale than either the initiation reactions in the inner layer (PF), e.g., $CH_4 + H = CH_3 + H_2$, (in case methane is used) or the other major oxidation reaction in the NF, namely, $H_2 + OH = H_2O + H$. Thermocouple losses can also be accounted for the variation in temperature measurement. These are discussed in brief here. The thermocouple has become one of the most used instruments to measure this quantity. Although the devices are inexpensive, convenient and easy to use, there can be significant errors associated in temperature measurements when used in fire environments. If these errors are acknowledged and sensors are designed and used judiciously, the temperature measurement can be estimated with much greater accuracy. Most errors associated with the use of thermocouples are due to the fact that the temperature of the sensor may not be the temperature of the surrounding medium. Energy can be transferred to and from the bead of the thermocouple by radiation, convection and conduction. Unfortunately, when placed in the high intensity environments characteristic of fires, thermocouples can produce sensed temperatures significantly different than the actual temperature of the medium of interest. These errors can be attributed to variations in the rate of energy transfer to and from the TC bead, temperature variations along the lead wires, and catalytic reactions between the metals comprising the bead at the surrounding gases.

Radiant heat transfer from the temperature sensor to its surroundings can be a large source of error. The law governing radiation from an emitter is the Stefan-Boltzman law defined as: $q_{rad} = \varepsilon\sigma T^4$ where ε is the emissivity of the object and σ is the Stefan-Boltzman constant (~ 5.669×10^{-8} $W m^{-2} K^{-4}$). Since radiation is proportional to T^4, it is obvious that at high temperatures a thermocouple bead could be radiating much more energy that it is receiving. This is especially true when the surrounding environment is at a much lower temperature and not emitting radiation to the bead, which is common in fire environments. To compound the problem, a large radiant energy source is present as well. When the flame is in close proximity to the sensor it radiates energy that may increase the temperature of the bead significantly over that of the gas surrounding the sensor. The thermal radiation losses from the hot flame to the cold walls of the burner amount to maximum heat loss.

Energy is transferred to the surface of the bead from the gas flowing around it by convection. This mode of heat transfer is more efficient when the fluid has a high velocity and is the basis for aspirated thermocouples. The relative contributions of radiant and convective energy transfer to the thermocouple measurement vary with the application.

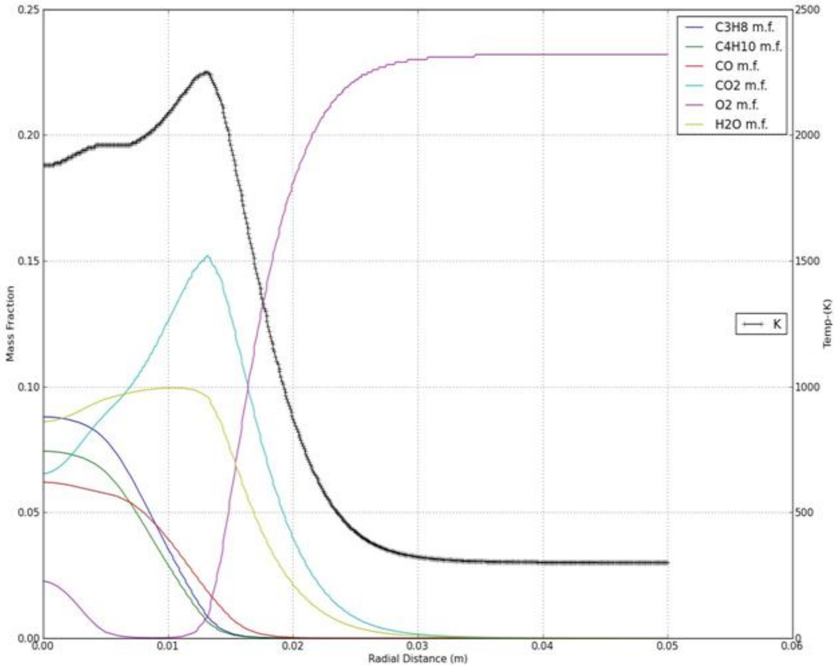

Figure 8.2 Comparisons of Mass Fraction profiles with temperature profile at 260ml/min along x-axis of the flame as obtained from CFX solver.

In the above figure 8.2, it can be seen that the trend of temperature variation and CO2 mass fraction variation are similar. This observation suggests that when complete oxidation takes place, the reactants are converted into CO2 and H2O and the heat energy release peaks at this point. This results in temperature peak at the same point. Another observation made from the figure 8.2 is that the oxygen is at the lowest point when the temperature and CO2 are at their peak values. This suggests that all the available oxygen was consumed for the complete oxidation of the reactants.

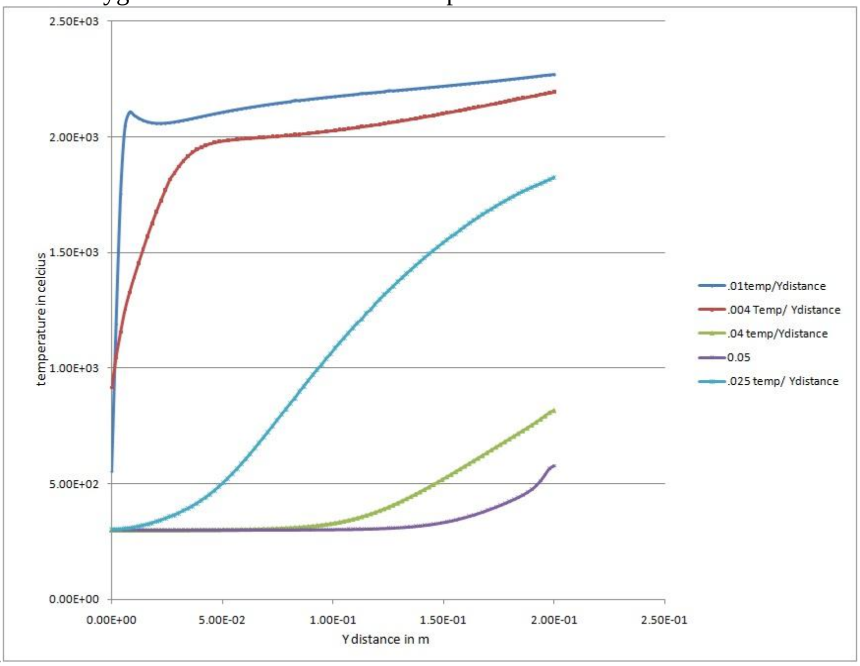

.

Figure 8.3 Variations of Temperature at different points in the flame along Y axis from centre of combustion zone at 260ml/min

From the figure 8.3, the temperature shows increasing trend at .004 m and .01 m from the centre and goes on decreasing then on for .025m, .04m and .05m. The part of the flame up to .01m is called the inner layer in which oxidation process occurs. Due to chemical reactions taking place in this region, there is heat release occurring which results in increase in temperature. The part of the flame up to .004 m is called the inner layer where all of the hydrocarbon chemistry can be assumed to occur where fuel and radical consumption occurs to form CO and H2. In the oxidation layer, which starts from a little beyond .04m and stretches up to .01m, the CO and H2 formed in the inner layer are oxidized to form CO2 and H2O. It can be seen in the later part that CO formation is more at x= .004 m than at x= .01m from the centre along y. This explains presence of CO2 in this region at .01m compared to other regions as shown figure 8.5

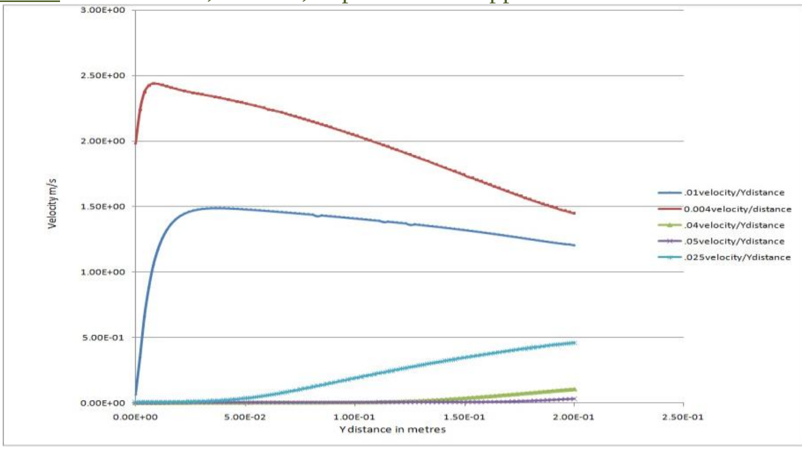

Figure 8.4 Variations of Velocity at different points in the flame along Y axis at 260ml/min

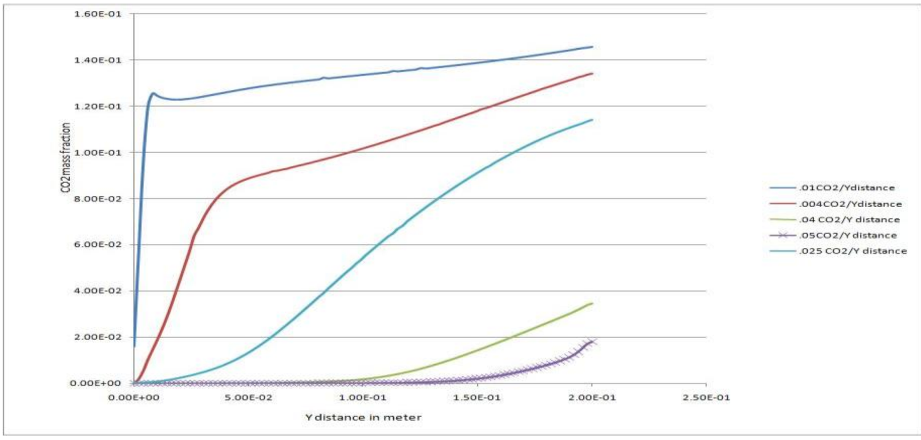

Figure 8.5 Variations of CO2 mass fraction at different points in the flame along Y axis at 260ml/min

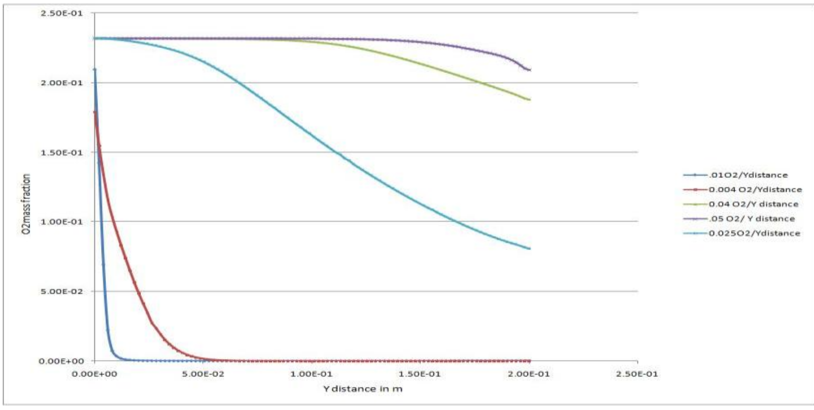

Figure 8.6 Variations of O2 mass fraction at different points in the flame along Y axis

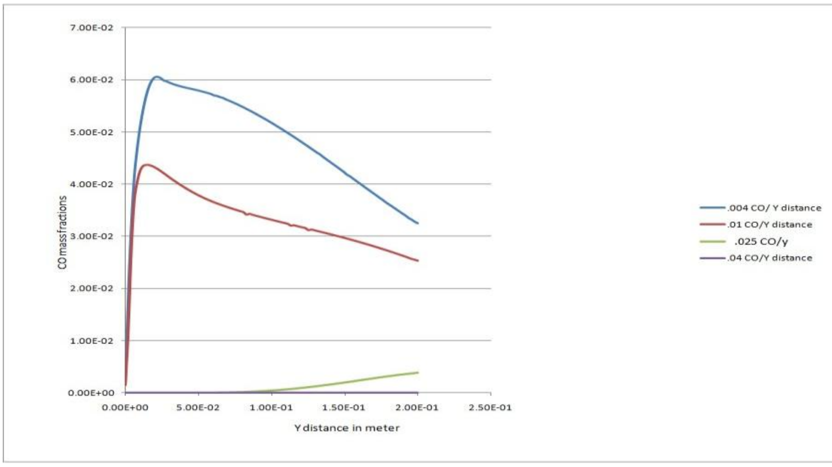

Figure 8.7 Variations of CO mass fraction at different points along Y axis

Comparing the figures 8.5 and 8.6, it is seen that as O2 decreases, CO2 increases. At x = .025m distance and beyond that, it is seen that there is excess O2 available from the ambient atmosphere, but is not consumed due to scarcity of fuel in this region. The chemical reactions do not occur in this region due to the presence of lean mixture, and even if they do occur they are incomplete. As seen from the figure 8.5, the concentration of carbon oxide is high at x=.004m as this region of the flame comprises of the inner layer where complete oxidation does not take place. At x=.01m distance, which comprises of the oxidation layer where conversion of CO is converted to CO2. Hence, as shown in figure 8.5, the concentration of CO2 is high at x= .01 than at x= .004m.

IX. CONCLUSIONS

The products obtained in the combustion process, adiabatic flame temperature, flame length, degree of diffusion flame, are all a direct function of the stoichiometry. The • flame structure is obtained in the form of instantaneous snapshots of the flow at various times. In the fuel-rich annular ring, the same initiation process is dominated by premixed combustion close to the nozzle exit. As oxygen is depleted inside the annular ring, the excess fuel emerging from the fuel-rich premixed zone is transported outward (by convection and diffusion), and non premixed flames are established on both sides of the annular ring. The two high-temperature product regions later merge into a single surface in the plume. Subsequently, the buoyant acceleration of hot gases outside the diffusion flame surface causes shear layer rollup, leading to the formation of toroidal vortex rings, which then interact with the flame/plume surface. The basic structure of the flame can be assumed to consist of distinct layers include 1) An inner layer in which methane and O2 consumption occur and 2) An oxidation layer (surrounded by a preheat zone downstream of inner layer and a post flame zone downstream of oxidation layer). All of the hydrocarbon chemistry can be assumed to occur in the inner layer where fuel and radical consumption occurs to form CO and H2. In the oxidation layer, the CO and H2 formed in the inner layer are oxidized to form CO2 and H2O. The CO-oxidation layer is generally thicker than the H2-oxidation layer, and the overall thickness of the oxidation layer itself is, in general, greater than that of the inner layer. Furthermore, the heat release is primarily due to the exothermic reactions occurring in the oxidation layer. A major exothermic reaction is in the oxidation layer. CO + OH =CO2 + H occurs on a relatively slower timescale than either the initiation reactions in the inner layer. e.g., CH4 + H =CH3 + H2, or the other major oxidation reaction in the oxidation layer, namely, H2 + OH =H2O + H. Partially premixed flames are hybrid flames containing multiple reaction zones. These flames are of fundamental importance to the phenomena of non premixed flame stabilization and liftoff, spray combustion, and localized extinction zone is established in between these two wings ~in the region where excess fuel and oxidizer from the rich and lean premixed reaction zones, respectively, mix in stoichiometric proportion. The overall flame structure is determined by the interactions between these three reaction regions, and can be controlled by changing the various reactant velocities and equivalence ratios. A fundamental difference between a partially premixed flame and an equivalent premixed or non premixed flame pertains to the existence of multiple synergistically coupled reaction zones. The structure of partially premixed flames is determined by the interactions that arise among these zones due to the synergy between the thermo chemistry and the heat and mass transport. For example, in a methane–air triple flame the inner rich premixed reaction zone provides CO and H2 , which serve as ''intermediate fuels,'' and excess methane to the non premixed zone, whereas the latter supplies heat and radical species ~H and OH! to both the inner and outer zones. The outer zone in turn provides excess O2 and oxygen atoms to the non premixed reaction zone. The interactions between the various reaction zones occur due to the advection and diffusion of both heat and mass. The experimental measurement values of temperature and Computational predictions are in agreement, though the highest temperature recorded in computational predictions is 2200 Celsius where as experimental values show highest temperature to be 1600 Celsius. Discrepancy in the measured temperature is attributed to uncertainties in the measurements and the model (e.g., related to the chemical mechanism and the thermo physical and transport properties). The various graphs obtained from the computational post processing results show variations of concentrations of reactants and products in the flame at different points and also temperature and velocity fluctuations which are in excellent agreement to various theories and concepts established in the combustion. In the CFD analysis, the highest temperature recorded is the adiabatic flame temperature for LPG. The radiation losses are not taken into account here. But in experiments, the major losses occur due to heat losses from the flame to the cold walls of the burner. The high-temperature region appears to be slightly narrower in the laboratory flame due to burner edge effects. This will be corroborated by the species concentration measurements. In both the measurements and predictions, the region with the highest temperatures lies between the inner premixed and the central non premixed reaction zone.

X. FUTURE WORK

Primary recommendation to the existing work would be to introduce detailed chemistry into the solver and solve for more species in the combustion zone. Introduction of detailed chemical kinetics would affect the temperature profile to an extent and also the computational flame established. The quality of the mesh for the mixing chamber could be improved by introducing additional hexahedron elements at the air inlets and fuel inlets to capture viscous layers flow phenomenon in detailed. Some modifications need to be introduced in conducting the experiments. Different types of fuel could be used and the flames obtained, temperature data could be analysed. Attempts should be made to calculate the mass flow rate or the velocity of air entering the burner. The further step would be to carry out the experiments of flame analysis at different air-to-fuel ratios. The temperature data obtained for flame at different equivalence ratios would take us step ahead in reaching our goal of setting up of the operating limits.

REFERENCES

[1]. J. Warnatz, U. Maas, R. W. Dibble, 'Combustion-Physical and chemical fundamentals', 4th edition, 2000, Springer.com.

[2]. Suresh K. Aggarwal and Ishwar K. Puri, 'Flame Structure Interactions and State Relationships in an Unsteady Partially Premixed Flame', University of Illinois at Chicago, Chicago, Illinois 60607-7022

[3]. Riccardo Azzoni, Stefano Ratti, Ishwar K. Puri, and Suresh K. Aggarwal, 'Gravity effects on triple flames: Flame structure and flow instability', University of Illinois at Chicago, Department of Mechanical Engineering (M/C 251),842 W. Taylor St. RM 2039 ERF, Chicago, Illinois 60607-7022.

[4]. Andrew J. Lock, Alejandro M. Briones, Xiao Qin, Suresh K. Aggarwal, Ishwar K. Puri, Uday Hegde, 'Liftoff characteristics of partially premixed flames under normal and microgravity conditions',Combustion and Flame 143 (2005) 159–173, www.elsevier.com/locate/combustflame.

[5]. SANDIP GHOSAL and LUC VERVISCH, 'Stability Diagram for Lift-Off and Blowout of a Round Jet Laminar Diffusion Flame', Northwestern University, Mechanical Engineering, Evanston, IL 60208-311 USA,INSA de Rouen and CNRS-Coria UMR 6614, France.

[6]. F.A. Williams, Combustion Theory, second ed., The Benjamin Publishing, 1985.

[7]. D.B. Spalding, 'A theory of inflammability limits and flame quenching', Proc. Roy. Soc. London. A 240 (1957) 83.

[8]. J. Adler, 'One-dimensional laminar flame propagation with distributed heat losses: thin-flame theory', Combust. Flame 7 (1963) 39.

[9]. Y.B. Zeldovich, F.L. Barenblatt, V.B. Librovich, G.M. Makhviladze, 'The Mathematical Theory of Combustion and Explosion', Nauka ed. Moscow, 1980.

[10]. B. J. Lee, S. H. Chung, 'Stabilization of Lifted Tribrachial Flames in a Laminar Nonpremixed Jet', Department of Mechanical Engineering, Seoul National University, Seou1151-742, Korea.

[11]. N. K. Aluri & S. Muppala & F. Dinkelacker, 'Large-Eddy Simulation of Lean Premixed Turbulent Flames of Three Different Combustion Configurations using a Novel Reaction Closure', Springer Science Business Media B.V. 2007

[12]. Andrew J. Lock , Alejandro M. Briones , Xiao Qin , Suresh K. Aggarwal, Ishwar K. Puri , Uday Hegde, 'Liftoff and Extinction characteristics of Fuel and Air-stream- diluted-Methane-air flames ', Combustion and Flame 143 (2005) 159–173, www.elsevier.com/locate/combustflame.

A ZVS Interleaved Boost AC/DC Converter Using Super Capacitor Power for Hybrid Electrical Vehicles

G. Rambabu[1], G. Jyothi[2]
*(PG Scholar, Department of EEE, TKR College of Engineering &Technology, Hyderabad, AP, INDIA)
**(Department of EEE, TKR College of engineering, Hyderabad, AP, INDIA)

ABSTRACT: *This paper presents the supercapacitor power management method for the Hybrid Electricals Vehicles.A simple zero-voltage switching(ZVS) interleaved boost power factor correction(PFC) AC/DC converter is used to charge the traction battery of an Hybrid Electrical Vehicle. The auxiliary circuit provides limited current to charge and discharge the MOSFETs output capacitors during turn-On times at zero voltages. The circuit maintains ZVS for the universal input voltage (85 to 265 Vrms), and having the very wide range of duty ratios (0.07 to 1). The proposed tropology consist of super capacitor, which connected across the hybrid electrical vehicle. The main objective of this paper is to study the management of the energy provided by supercapacitor by using multi full bridge converter tropology, which is having maximum voltage of 270v. The output of the full bridge converter is connected to the hybrid electrical vehicle. The supercapacitor output is connected to the load through planar Transformer, it provides peak voltages at starting of Electrical Vehicle.The experimental and simulation results are presented.*

Keywords: *AC/DC converter, Interleaved boost converter, Zero voltage switching, power factor correction, supercapacitor, boost converter, full bridge converter.*

I. INTRODUCTION

In the last few years the pollution problems and the increase of the cost of fossil energy (oil,gas) have become planetary problems. The car manufacturers started to react to the urban pollution problems in nineties by commercializing the electric vehicle. But the battery weight and cost problems were not solved. The batteries must provide energy and peaks power during the transient states. These conditions are severe for the batteries. To decrease these severe conditions, the super capacitors and batteries associate with a good power management present a promising solution.

In the electric traction system, Electric Vehicle (EV) power conditioning systems usually utilize a high-energy battery pack to store energy. This is typically charged from a utility ac outlet. The energy conversion during the battery charging is performed by an ac/dc converter. The need of Ac to Dc conversion is, while the Electrical Vehicle (EV) is moving it is not possible to connect the moving electrical vehicle to AC utility mains. The energy is supplied by the storage Energy batteries which is stores the energy in the form of DC. Thuts why we have to perform the AC/DC conversion. The conduction losses caused by the auxiliary circuit are minimized based on the operating condition. A control circuit is proposed to control the ZVS interleaved boost PFC converter.

At starting of Electric vehicles it draws more current. Then the electric vehicles are operating in unstable operating condition. To get the stable operation the superapacitor power is used in the ZVS interleaved boost converter of an Electrical vehicle.

II. ANALYSIS OF THE ZVS INTERLEAVED BOOST PFC CONVERTER:

The Fig. 1 shows the power circuit of the ZVS interleaved boost PFC converter. In this converter, two boost converters operate with 180◦ phase shift in order to reduce the input current ripple of the converter. This 180◦ phase shift can be used to provide reactive current for realizing ZVS for power MOSFETs. This auxiliary circuit consists of a HF inductor and a dc-blocking capacitor. Since there may be a slight difference between the duty ratios of the two phases, this dc-blocking capacitor is necessary to eliminate any dc current arising from the mismatch of the duty ratios of the main switches in the practical circuit.

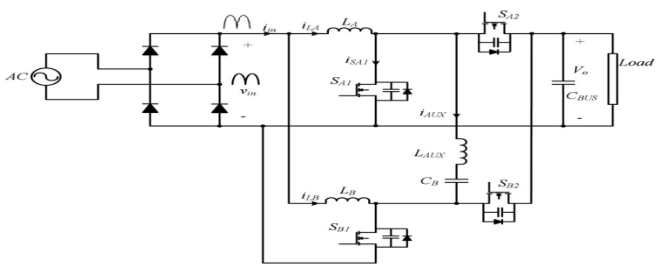

Fig.1. ZVS Interleaved boostconverter

The converter operates for two types of Duty ratios, those are D > 0.5 and D < 0.5.,and analysis of wave forms are explained by modes of operation Mode

1. Mode *1*($t0 < t < t1$) 2. Mode *II* ($t1 < t < t2$) 3. Mode *III* ($t2 < t < t3$) 4. Mode *IV* ($t3 < t < t4$)
5. Mode *V* ($t4 < t < t5$) 6 Mode *VI* ($t5 < t < t6$): 7. Mode *VII* ($t6 < t < t7$) 8 Mode *VIII* ($t7 < t < t8$):

III. CONTROL SYSTEM FOR THE ZVS INTERLEAVED BOOST PFC

The peak value of the auxiliary circuit current should be adjusted based on the load condition in order to optimize the circulating current between the two phases of the interleaved boost converter**.** Therefore, in order to optimize the circulating current, the envelope should be just enough to overcome the valley current of the boost inductor in the half cycle. There are two main difficulties related to the optimization of the circulating current in the proposed converter. The first problem is the operation with duty ratios lesser than 0.5 and the second issue is optimizing the circulating current for different load conditions. Fig. 2 shows the block diagram of the proposed control system. The proposed control system includes an external voltage loop, internal current loop, and a switching frequency control loop.Therefore, afrequency loop is added to the control system to optimize the circulating current of the auxiliary circuit based on the load and duty ratio of the converter. Such load-adaptive switching frequency variation has been proved to increase efficiency in ZVS converters.

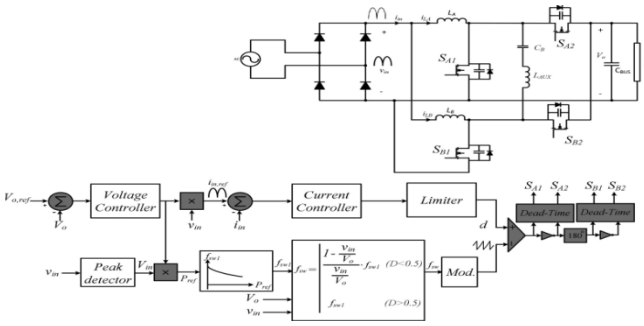

Fig:2. block diagram for the control system of ZVS interleaved boost PFC

Fig. 3 shows the typical switching frequency variation at heavier and lighter loads. At heavy loads, the frequency is lower to provide more reactive current in the auxiliary circuit to overcome higher values of *Iv* and charge and discharge the output capacitors. Whereas at light loads, the frequency is higher to reduce the auxiliary circuit current in order to avoid any extra circulating current between the two phases.

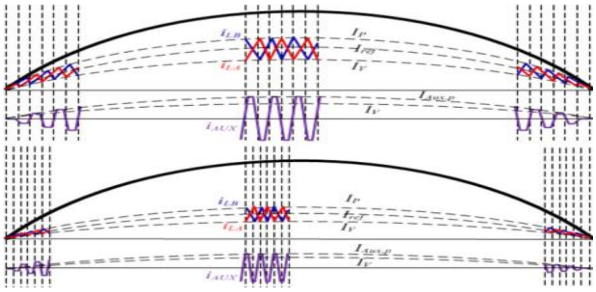

Fig: 3 Change in frequency for different loads

The variation of the frequency with respect to the converter output power is shown in fig.4. Owing to the change of frequency, the circulating current is optimized for a very wide range of operation. Since the converter is used to charge the traction battery, there is actually a need for very wide range of operating conditions and the converter has to work at very light loads for a long period of time also. Thus, this optimization is imperative in this particular application.

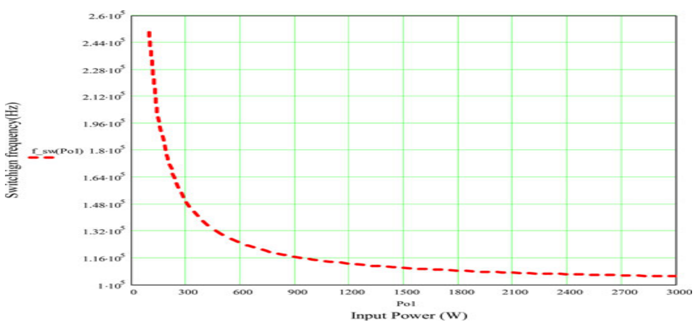

Fig: 4 switching frequencyfor variation versus load

There are two main points related to the control system. Those are (1) the frequency loop is completely decoupled from the duty cycle loop. Fig.5. illustrates the fact that by changing the frequency of the saw-tooth counter, the duty cycle does not change (i.e., D1 = D2). (2) the frequency change does not tamper the operating modes of the converter in terms of operating under CCM of the input inductors. Since the frequency is higher for light loads, the control system helps the converter to work in CCM for wider range of loads. In addition, for higher input voltage, frequency decreases at the peak value of the input current. Therefore, reducing the frequency does not bring the converter into discontinuous conduction mode.

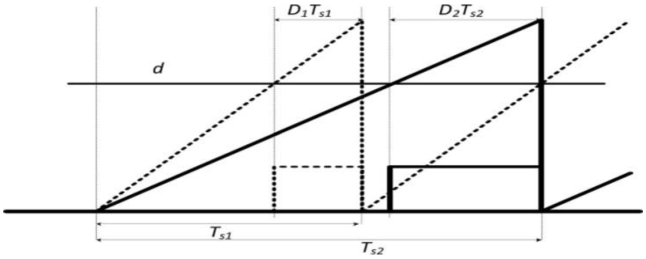

Fig: 5. PWM pulses for different frequencies

IV. SUPERCAPACITOR POWER MANAGEMENT FOR ZVS PFC

Supercapacito rare storage devices which enable to supply the peaks of power to hybrid vehicle during the transient states. During the steady states, batteries will provide the energy requested. This methodology enables to decrease the weight and increases the lifespan of the batteries. The multi boost and multi full bridge converters will be investigated because of the high power.

For range problems, traction batteries used until now cannot satisfy the energy needed for future vehicles. To ensure a good power management in hybrid vehicle, the multi boost and multi full bridge converters topologies and their control are developed. Two topologies proposed for the power management in ECCE Hybrid Vehicle are presented in Fig.6.

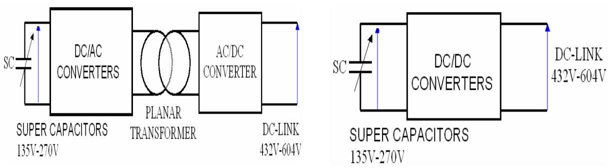

Fig(a): First solution Fig:(b): second solution
Fig:6 converter tropoiogies for ECCE hybrid vehicles

V. DESIGN OF THE CONVERTER CIRCUIT

Wiring in power electronic design is a general problem for electrical energy system and the voltage inverters do not escape to this problem. The switch action of semiconductors causes instantaneous fluctuations of the current and any stray inductance in the commutation cell will produce high voltage variations. Semiconductors, when switching off, leads to high voltage transitions which is necessary to control within tolerable limits. The energy stored in parasitic inductances, during switching on, is generally dissipated by this semiconductor.

In the case of the single-phase inverter, each cell includes two switches and a decoupling capacitor placed at the cell boundaries, which presents a double role. It enables to create an instantaneous voltage source very close to the inverter. The capacitor associated to an inductor enables to filter the harmonic components of the currents which are generated by the inverter. Parasitic inductances staying in the mesh include the capacitor inductance, the internal inductance of semiconductors and the electric connection inductances.

A good choice of the components with an optimal wiring enables to parasitic inductances. Using the semiconductors modules solves the connection problems between components. All these efforts can become insufficient, if residual inductances remain too high or if the inverter type is the low voltages and strong currents for which the voltage variations are much important. In both cases, the use of the chopping devices is necessary. These devices must be placed very close to the component to avoid any previous problem. The parameters used for experimental tests are presented in Table 2 and the principle of such circuits is given in Fig.7.

Table: parameters for full bridge topologie

Symbol	Value	Name
R1= R2=R3 = R4	10Ω	Chopping circuits resistances
C1=C2=C3=C4	220µF	Chopping circuits capacitors
λ	25µH	Battery current smoothing inductance
m	3	Planar transformer turns ratio
Vbus1	60V-43V	DC-link voltage
C	6800 µF	Super capacitors voltage smoothing capacitor
L1	50µH	Super capacitors currents smoothing inductance

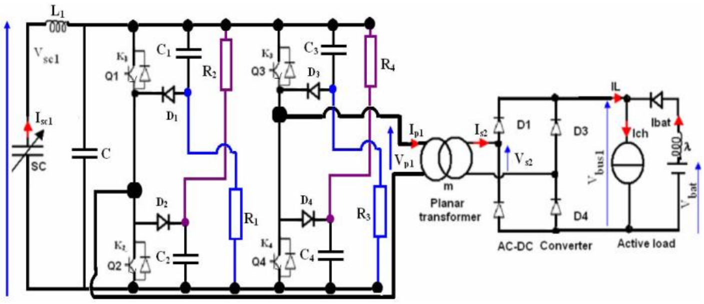

Fig: 7 Full bridge converter with chopping devices

During switching off of the semiconductors, the corresponding current stored in wiring inductances circulates in the following meshes C1, D1 ; C2 , D2; C3, D3 and C4 , D4 which limits the voltages applied to the switches. When electrical energy is fully transferred in C1, C2, C3 and C4 capacitors, the current becomes null and the meshes become closed. The C1, C2, C3 and C4 capacitors are used only for transient energy tank and it is necessary to recycle this switching energy while controlling the voltage at the semiconductors boundary. This function is ensured by R1, R2, R3 and R4 resistances. R1, R2, R3 and R4 resistances are identical and C1, C2, C3 and C4 capacitors are also identical.

In this the supercapacitor power is converted from DC to AC and connect to the planar transformer. The output of the planar transformer is again converted from AC to DC by using the diode converter. These DC output power is connected across the load of the ZVS Interleaved boost converter. The out put of supercapacitor is used at the starting of the Electrical vehicles, because ElectricalVehicles are draw more power at the starting. These extra power is provided by the SuperCapacitor.

VI. ZVS INTERLEAVED BOOST AC/DC CONVERTER WITH SUPERCAPACITOR

The following fig.6.6. shows the ZVS interleaved boost AC/DC converter with supercapacitor. In this the supercapacitor power is converted from DC to AC and connect to the planar transformer, which is having the turns ratio m=3. The output of the planar transformer is again converted from AC to DC by using the diode Rectifier. These DC output power is connected across the load of the ZVS Interleaved boost converter. At the starting the Electrical vehicles are draw more current. Then the System is working with unstable operation. These extra Current is provided by the Supercapacitor to maintain the system with stable operation.

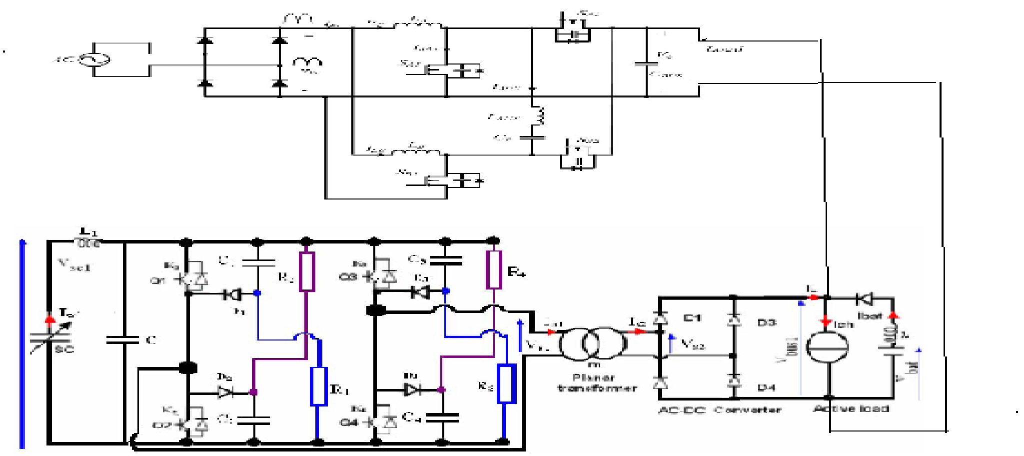

Fig.6.6. ZVS interleaved boost AC/DC converter with supercapacitor

VII. SIMULATION RESULTS

The boost converters experimental test is carried out in the following conditions: During the super capacitors discharge, the batteries current reference (Ibatref) is fixed at 13A so that, the super capacitors modules provide hybrid vehicle power request during the transient states. For these tests, the hybrid vehicle request (Ich) was fixed at 53A. The experimental and simulations results of the modules voltage are compared in Fig.8 (a) and Fig.8 (b). The (Isc1) and (Isc2) experimental currents are not identical Fig.9 (a), Fig.9 (b) because the super capacitors dispersion and the power electronic circuits (boost converters) inequality. The first boost converter ensures 50% and the second ensures also 50% of the DC-link current (IL).

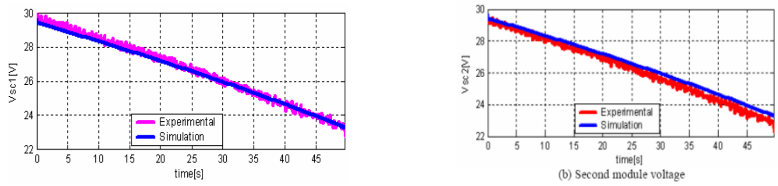

(a) First module voltage (b) second module voltage
Fig: 8 supercapacitor modules experimental and simu lation voltage results

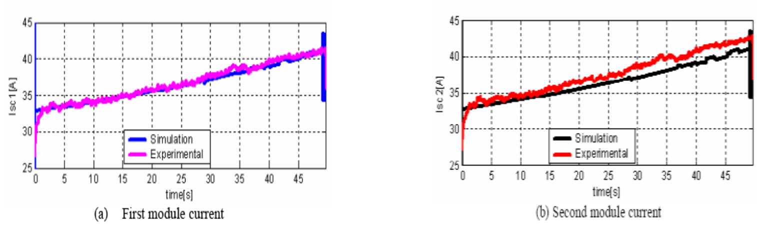

Fig: 9 supercapacitor modules experimental and simulation current results

Actully the voltage across the terminal of a Electrical Vehicle which is connected to Interleaved boost AC/DC converter is high at starting position of Electrical vehicle. So the system operating with unstability. At starting point the super capacitor gives that extra high voltage, So that the system maintains the stability. The output simulation results are shown in fig:10 and fig:11.

The following fig.10. shows the dc motor torque and armature current. In dc motor the torque and armature currents are in proportional. From the figure we observe that armature current waveform follows the torque waveform.

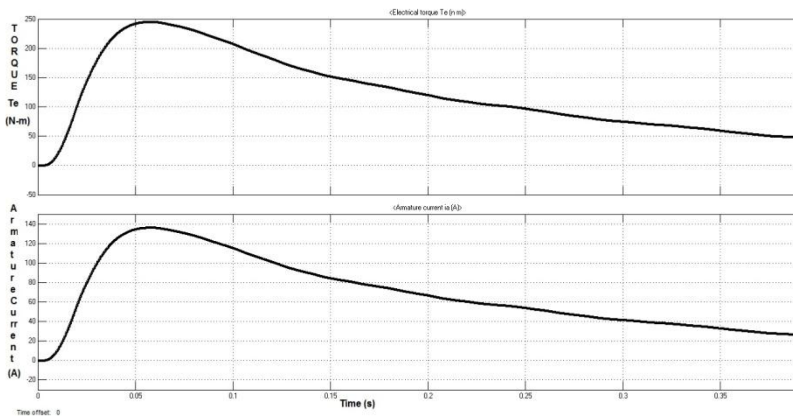

Fig: 10. output viltage of Diode bridge rectifier

The following fig.11 shows load terminal voltage and current waveforms. At starting of hybrid vehivles it draws more current as shown in figure.

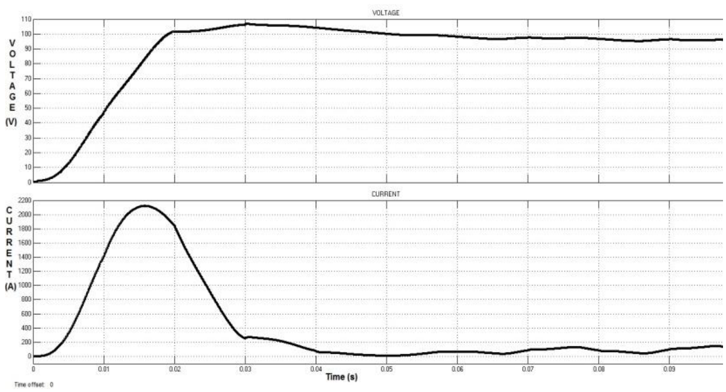

Fig:11. output voltage and currents at load terminal by using supsrcapacitor

VIII. CONCLUSION

The super capacitor power management of a ElectricalVehicle is explained by using multi boost and multi full bridge converters through a planer Transformer. An Interleaved boost PFC provides soft switching for the power MOSFETs, through an auxiliary circuit. The auxiliary circuit provides reactive current during the transition times of MOSFETs to charge and discharge the output capacitors of the MOSFETs. At the starting of Electricalvehicle it draws more voltage and current. This causes unstable operation. The Supercapacitor provides this extra current, and maintain the stability. For reasons of simplicity and cost,the multi boost converter is the most interesting topology regarding the multi full bridge converter topology. It enables a good power managemet in Hybridvehicle.

REFERENCES

[1] J.M Timmermans, P.Zadora, J. Cheng, Y. Van Mielo, and Ph.Lataire. Modelling and design of super capacitors as peak power unit for hybrid electric vehicles. Vehicle Power and Propulsion, IEEE Conference, 7-9 September, page 8pp, 2005.

[2] Huang jen Chiu, Hsiu Ming Li-Wei Lin, and Ming-Hsiang Tseng. A multiple- input dc/dc converter for renewable energy systems. ICIT2005, IEEE, 14-17 December, pages 1304–1308, 2005.

[3] M.B. Camara, H. Gualous, F. Gustin, and A. Berthon. Control strategy of hybrid sources for transport applications using Supercapacitors and batteries. IPEMC2006, 13-16 August, Shanghai, P.R.CHINA, 1:1–5, 2006.

[4] T. Nussbaumer, K. Raggl, and J. W. Kolar, "Design Guidelines for interleaved single-phase boost PFC circuits," *IEEE Trans. Ind. Electron.*, vol. 56, no. 7, pp. 2559–2573, Jul. 2009.

[5] T. Nussbaumer, M. Baumann, and J. W. Kolar, "Comparative evaluation of modulation methods of a three-phase buck + boost PWM rectifier. Part II: Experimental verification," *Power Electron., IET*, vol. 1, no. 2, pp. 268–274, Jun. 2008.

[6] T. Nussbaumer and J. W. Kolar, "Comparison of 3-phase wide output voltage range PWM rectifiers," *IEEE Trans. Ind. Electron.*, vol. 54, no. 6, pp. 3422–3425, Dec. 2007.

[7] R. Giral, L. Martinez-Salamero, and S. Singer, "Interleaved converters operation based on CMC," *IEEE Trans. Power Electron.*, vol. 14, no. 4, pp. 643–652, Jul. 1999.

Biographies:

Gudide Rambabu received the B.Tech Degree in EEE from KAKATIYA UNIVERSITY- Warangal, in 2008. He is currently pursuing M.Tech in TKR College of Engineering.

G. Jyothi She is currently working as an associate-Professor in the deparment of EEE in TKR college of Engineering, Hyderabad

Experimental Investigation of Performance & Emission Characteristics of Diesel Engine Working On Diesel and NOME with Ethanol and Triacetin Blends

Vivek pathak[1], Prof. Amitesh Paul[2]

[1] Department of Mechanical Engineering Sri Satya Sai Institute of Technology Sehore,Madhya Pradesh, India,
[2] Head of Department Department of Mechanical Engineering,Sri Satya Sai Institute of Technology Sehore,Madhya Pradesh,

ABSTRACT: *This research presents effect of triacetin and ethanol as additive to biodiesel (Neem oil methyl ester) on the performance and emission characteristics of a diesel engine at different loads and constant engine speed. Compared with biodiesel, slightly lower brake specific energy consumption for triacetin and ethanol bended fuels was observed. At higher engine loads CO,HC and smoke emission were found significantly lower with all blends[BD-1(5% triacetin,95% biodiesel), BD-2(10% triacetin,90% biodiesel) , BE-1(5% ethanol, 95% biodiesels) and BE-2 (10% ethanol ,90% biodiesel)] compared to Biodiesel , but NOx emission were found higher. The triacetin is also antiknock agent and has maximum oxygen content about 53.3%. by this reason combustion of fuel can be improve.*

Keywords: *Biodiesel, Triacetin , Emission , Ethanol , Neem oil Methyl ester.*

I. INTRODUCTION

Conventional energy sources such as oil, coal and natural gas have limited reserves that are expected not to lost for an extended period. World primary demand is projected to increase by 1.5% per year between 2007 to 2030, from just over 12,000 million tons of oil equivalent to 6800 million tones-as overall increase of 40%. As world reserves of fossil fuels and raw material are limited, it has stimulated active research interest in non petroleum and non polluting fuels.[1-8]. Diesel engines are the major source of power generation and transportation hence diesel is being used extensively, but due to the gradual impact of environmental pollution there is an urgent need for suitable alternate fuels for use in diesel engine without any modification.[5-9]There are different kinds of vegetable oils and biodiesel have been tested in diesel engines its reducing characteristic for green house gas emissions. Its help on reducing a country's reliance on crude oil imports its supportive characteristic on agriculture by providing a new market for domestic crops, its effective lubricating property that eliminates the need of any lubricate additive and its wide acceptance by vehicle manufacturers can be listed as the most important advantages of biodiesel fuel[2-12]. There are more than 350 oil bearing crops identified, among which only Jatropha, pongamia, sunflower, Soyabean, cottonseed, rapeseed, palm oil and peanut oil are considered as potential alternative fuels for diesel engines [3,4,5,7,9]. vegetable oil and their derivates as fuels are non-toxic biodegradable environment friendly and can be made from renewable resources[4,7,9,10,11,18,20,24] Transesterification can lower high viscosity of vegetable oils[4,5]. Biodiesel in diesel engine can reduce HC CO and smoke emission but NOx emission may increase [9,10,11]. Some studies have shown that biodiesel can decrease NOx emission but CO HC and smoke emission may increase. Poor flow of biodiesel is a barrier in using of neat biodiesel in cold weather. The present study aims to investigate the use of neem oil blend with diesel as an alternate fuel for compression ignition engine Triacetin and Ethanol (T&E) might improve cold flows and viscosity properties. This research presents effect of Triacetin and Ethanol as additive to biodiesel [neem oil methyl ester (NOME)] on the performance and emission characteristics of a diesel engine at different loads and constant engine speed [14,15,21].

II. MATERIALS AND METHODS

Biodiesel is the ester of vegetable oils produced through a process called Transesterification. Transesterification is a chemical reaction which occurs between triglyceride and methyl alcohol in the presence of potassium hydroxide (KOH). It consists of a sequence of three consecutive reactions where triglycerides are converted to diglycerides. diglycerides are converted to monoglycerides followed by the conversion of monoglycerides to glycerol. In each step an ester is produced and thus three ester molecules are produced from one molecule of triglyceride. Neem oil used in the present investigation was taken from JNKV Jabalpur, Madhya Pradesh, India and filtered by cheesecloth to remove solid particles. The moisture content was removed by heating the oil in an oven up to 110°C for one hour now the oil is taken in a round bottom flask and heated around 50-60°C on a hot plate having magnetic stirrer arrangement, then methanol and potassium hydroxide are added to the oil. The mixture was stirred continuously. Alcohol to vegetable oil molar ratio is one of the important factors that affect the conversion efficiency of the process for the transesterification process 3 mol of alcohol are required for each mole of the oil. However, in practice the molar ratio should be higher than this theoretical ratio in order to drive the reaction towards early completion. After the completion of reaction, the products are allowed to separate into two layers, the lower layer contains glycerol and the top layer contains ester which is separated and purified using water. Water is sprayed over the ester and stirred gently and allowed to settle in the separating funnel, the lower layer is discarded and upper layer (purified biodiesel) is separated.

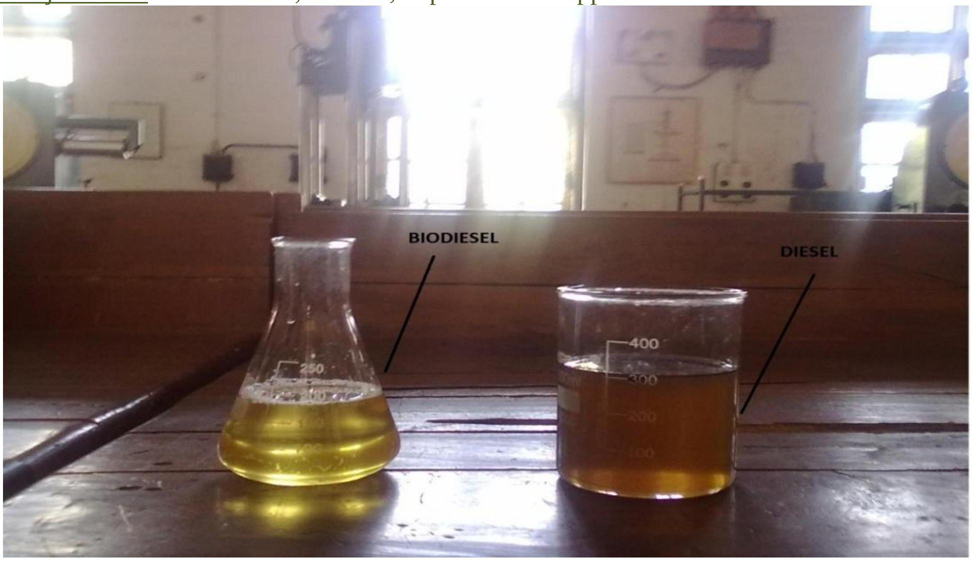

FIGURE 1

Biodiesel (methyl esters of neem oil) have several outstanding advantages among other new-renewable and clean engine fuel alternatives. The only drawback is it viscosity and incomplete combustion fuel. This can be improve by adding triacetin and ethanol. Triacetin is also anti-knock additive. The properties of diesel and biodiesel with additives (biodiesel with triacetin & biodiesel with ethanol) used in present investigation were compared with diesel fuel in Table.1

Table 1

Different Fuels	Calorific value (kj/kg)	Specific gravity (gm/cm^3)	Cetane number	Kinetic Viscosity at 40C	Flash Point ^{o} C
Diesel	42000	0.823	48	3.9	56
NOME	41000	0.867	51	4.5	165
Ethanol	27000	0.789	5-8	1.2	13.5
BD-1	40800	0.847	-	3.32	147
BD-2	40580	0.838	-	3.20	128
BE-1	40280	0.854	-	4.2	153
BE-2	39500	0.847	-	3.89	139

III. EXPERIMENTAL SETUP AND PROCEDURE

Table 2: Specification of Engine

Items	Specification
Model	Kirloskar Av1
No of cylinder	1
Bore	8cm
HP	5
Stroke	11cm
Compression ratio	16.5:1
Speed	1500 rpm

Table 3 Specification of dc machine

Items	Specification
Model	Samson D.C machine
Volt	150V
Power	4.6 KW
Current	40 Amp
Speed	1500 rpm

Table 4 Specification of exhaust gas analyzer

Measuring Quality	Measuring Range
CO	0-10%vol
HC	0-20000ppm

IV. EXPERIMENTAL SET-UP LINE DIAGRAM

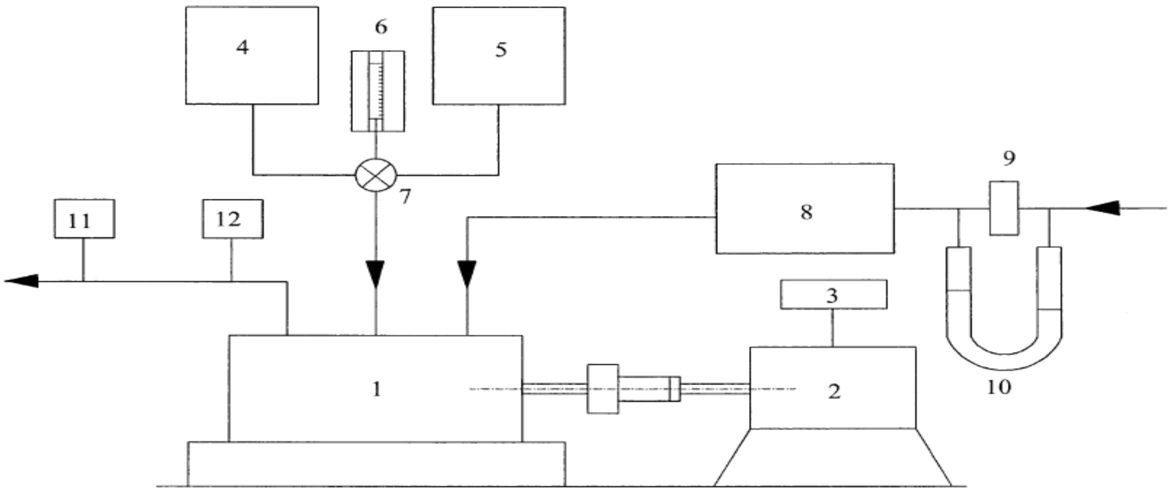

Schematics diagram of experimental setup (1) Engine; (2) Electrical load bank; (3) voltmeter, ammeter; (4) Diesel fuel tank; (5) Biodiesel fuel tank ;(6) Burette;(7) Two way valve;(8) Air box; (9) Orifice plate; (10) U tube manometer;(11) Smoke meter; (12) EGA

FIGURE 2

V. RESULTS AND DISCUSSION

Specific gravity and kinematic viscosity of biodiesel is higher than that of other fuel, but it can be reduced by additives. Latent heat of ethanol (850kj/kg) is higher than that of other fuels. Calorific value of biodiesel, T , E are lower by 4.6% 37.9% and 16.6% respectively as compared to diesel. Oxygen contents are higher by 53.3% and 34.8% respectively. The CO emission for different fuels are as shown in fig. 3. It is very clear indicated from the results that with the blending of triacetin and ethanol gives better result than the neat diesel oil or NOME. Only BE-1 gives high percentage because of less combustion of fuel in combustion chamber then BT-1 BT-2 BE-2. For the triacetin blends CO emission is very good. Because in the presence of higher oxygen fuel burns properly and give better performance. From the figure.4, we can say that the emission of HC is very lower than the other fuels used in this investigation. BT-1 , BT-2 and NOME gives less emission due to proper combustion. The Exhaust gas temperature is very close to neat diesel and within the imit. It can be considered is safe range as indicated in figure 5. All the bends give better characteristics of smoke density then the neat diesel except NOME.

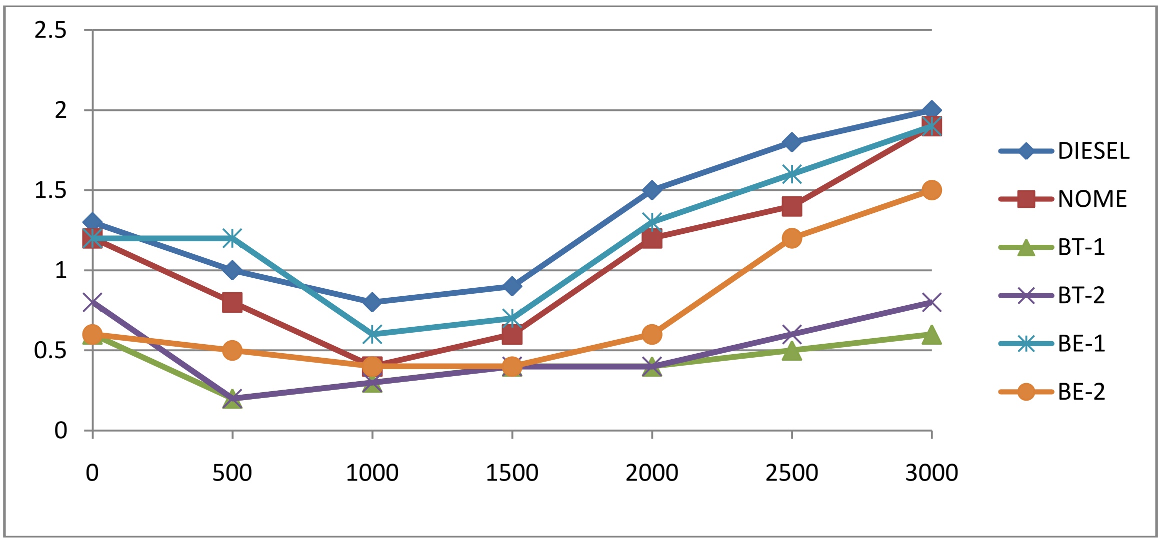

FIGURE 3(Percentage of Carbon mono oxide (CO%))

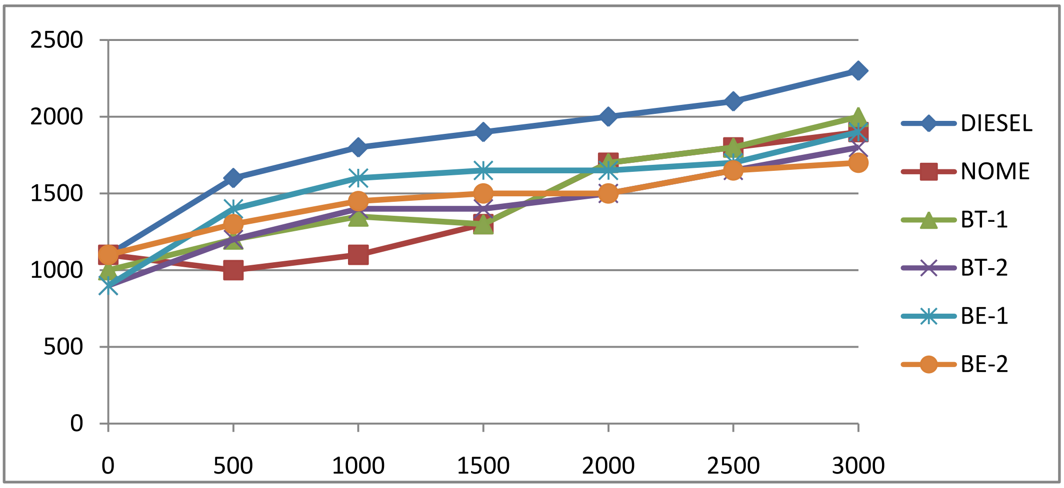

FIGURE 4 (Hydro Carbon particles (HC) in ppm)

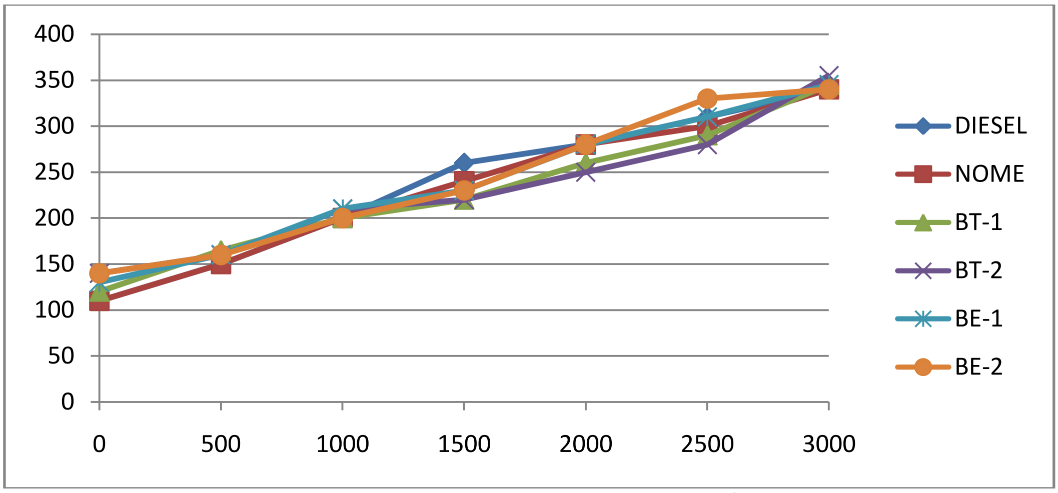

FIGURE 5 (Exhaust Gas temperature ^{o}C)

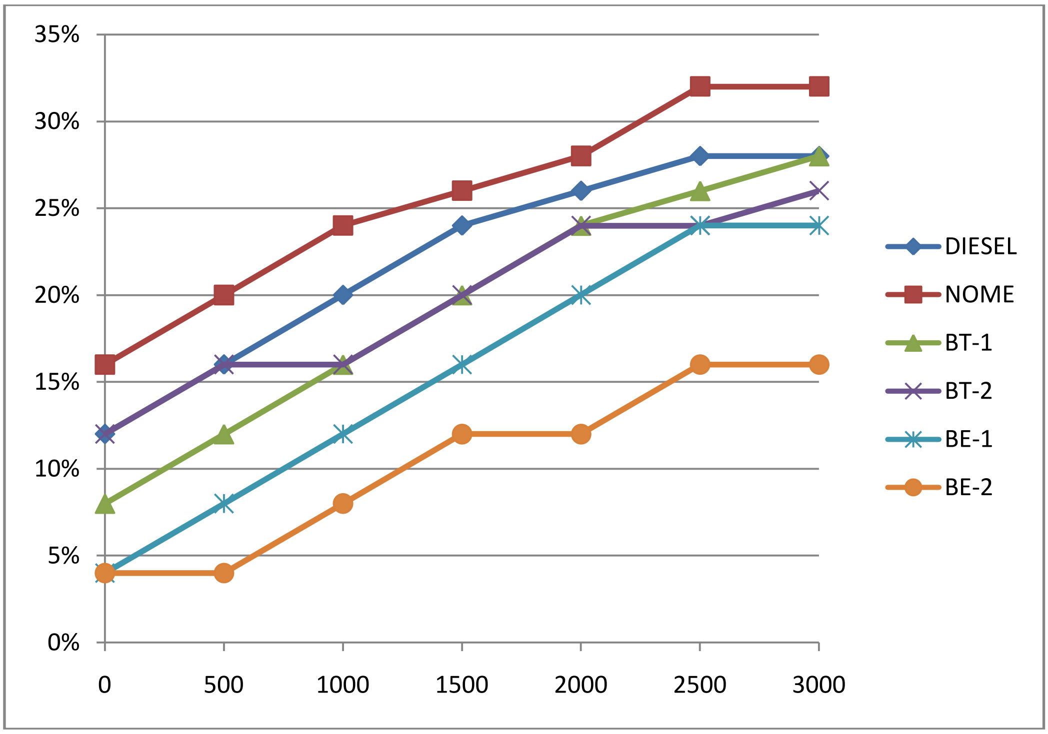

FIGURE 6(Percentage of Smoke Density)

VI. CONCLUSION

Biodiesel NOME and its blends can be better option for any diesel engine for better performance without any modification in engine and also environmental friendly. The emission of CO and HC can be decrease to a large extent, as output come from this investigation. Because of the higher percentage of oxygen, combustion can be improved and also reduce the knocking problem. The major output from this investigation is increase the NOME and its blends characteristics by adding additives. The major problem like knocking viscosity and lower performance characteristics can be improved and with less emission. From the above results we can say that , NOME and its bends will be better alternatives for diesel engines because of mass production of neem in india , production cost of biodiesel is cheap and give better characteristic of emission

REFERENCES

[1] C D Rakopoulos D C Rakopoulos D T Hountalas. Performance and emission of bus engine using blends of diesel fuel with bio diesel of sunflower and cotton seed oil derived from feedstock.
[2] C D Rakopoulos D T Hountalas] Comparative performance and emission study of direct injection diesel engine using blends o diesel fuel with vegetable oils or biodiesel of various orgin.
[3] Deepak Agarwal et.al. Performance and emissions characteristics of Jatropha oil (preheated and blend) in a direct injection compression ignition engine (2007).
[4] Deepak Agarwal et.al. Experimental investigation of control of NOx Emissions in biodiesel-fueled compression ignition engine (2006).
[5] Devendra Vashist et.al. A comparative study of castor and jatropha oil source and its methyl ester test on the diesel engine (2011).
[6] Dinesh Dabhi K., 2 Khiraiya Krunal B.*, 3Nityam P. OzaA Review of Neem Biodiesel As Fuel for CI Engine..
[7] Huseyin Aydin et.al. Effect of ethanol blending with biodiesel on engine performance and exhaust emissions in a CI engine. (2010).
[8] Joseph B. Gonsalves An Assessment of the Bio fuels Industry in India United Nations Conference on Trade and Development.(2006).
[9] Joshua Garba Abduljalal. Comparative study of biodiesel from kernel oil of jatropha curses and Azadirachta india in zaria nageria
[10] K.Dilip Kumar1 P.Ravindra Kumar2 Experimental Investigation of Cotton Seed Oil and Neem Methyl Esters as Biodiesel On Ci Engine.
[11] K. Suresh Kumar et.al. Performance and exhaust emission characteristics of a CI engine fueled with Pongamia pinnata methyl ester (PPME) and its blends with diesel (2008).
[12] K.V.Radha, G.ManikandanNovel Production Of Biofuels From Neem Oil.
[13] Lovekush Prasad1, Dr. Alka Agrawal2 Experimental Investigation of Performance of Diesel Engine Working On Diesel and Neem Oil Blends.
[14] M Pugazhvadvu S. Rajagopan. Investigation on a diesel engine fuelled with biodiesel blends and diethyl ether as an additive.
[15] Nandkishore D Rao B.Sudheer premkumar M. Yohan. Performance and emission characterstics of straight vegetable oil ethanol emission in a compression ignition engine.
[16] Nishant Tyagi1, Ambuj Sharma2Experimental Investigation Of Neem Methyl Esters As Biodiesel on C.I Engine.
[17] N.Janardan Rao M R Shasrty Dr P N Reddy.] Comparetive analysis of performance and emission of an engine with palm oil biodiesel blends with diesel.
[18] N.R. Banapurmath et.al. A comparative study of castor and jatropha oil source and its methyl ester test on the diesel engine. (2008).
[19] Nithyananda B. S, Anand A, Dr. G. V. Naveen Prakash Performance Study on Diesel Engine Using Different Blends of Neem Biodiesel.
[20] P.K Deven N.V. Mahalaxmi. Performance emission and combustion charcterstic of poon oil and its diesel blends in a D I Diesek Engine
[21] P. Venkateshwer Rao B.V. Appa Rao and D. Radhakrishna.] Experimental analysis of DI engine performance with blends fuels of Oxygenated additives and COME biodiesel.
[22] Ramning Amol M., Dhote Priya S. and Ganvir V.NProduction of Neem Oil Methyl Ester (NOME) from Oscillatory Baffled Reactor
[23] Revansiddappa Byakod1, Prasanna Phatate1, Vinodkumar Kamble1, Sharath Babu1, M. C Navindgi2 Comparative Analysis of Performance and Emission Charactristics of Neem Oil Using 3 And 4 Holes Injection Nozzle on DI Diesel Engine.
[24] Y. Azoumah et.al. Exergy efficiency applied for the performance optimization of a direct injection compression ignition (CI) engine using biofuels (2009).

International Journal of Modern Engineering Research (IJMER)
www.ijmer.com Vol. 3, Issue. 5, Sep - Oct. 2013 pp-2797-2803 ISSN: 2249-6645

Modelling the Effect of Industrial Effluents on Water Quality: "A Case Study of River Challawa in Nigeria"

T. A. Adedokun, Agunwamba, J. C.
Department of Civil Engineering, Bayero University, Kano, NIGERIA, +2348033281667
Department of Civil Engineering, University of Nigeria, Nsukka, NIGERIA, +2348035644561

ABSTRACT: *The physicochemical characteristics associated with industrial effluents from the Challawa and Sharada Industrial Estate in Kumbotso Local Government Area of Kano State ad the effect on water quality of a 10.6 km stretch downstream of River Challawa were investigated. The test period covered both wet and dry seasons, with laboratory analysis of field samples and study area. The results obtained indicated that the DO values varied from 0 mg/l to 3.5 mg/l, BOD_5 value ranged from 193 mg/l to 1025 mg/l along the river channel. The reaeration coefficient k_2 of River Challawa varied from 0.013 to 0.140. The 0.013 to 0.140. The coefficient of correlation between k_2 predicted with derived models were 0.229, 0.295, 0.994, 0.842, 0.676, 0.855 and 0.473. An improved technique using the reaeration coefficient values at each section and incorporating the fall velocity gave a profile closer to the measured oxygen deficit values than the conventional approach. The coefficients of correlation for the two approaches are 0.9572 and 0.4558 respectively. The comparison of k_2 observed and predicted k_2 O'Conner and Dobbins, Ugbebor and Agunwamba, Churchill and Buckingham, and Agunwamba indicated standard errors of 1.5156, 2.3376, 04216, 1.3891, 0.0488, 0.3854 and 1.7721 respectively. Test result also gave a purification factor of 0.40, indicating the stream was polluted and has poor assimilatory capacity. There is need for proper monitoring and impact control measures for River Challawa.*

I. INTRODUCTION

The direct discharge of effluents from industries into rivers and the streams in an arbitrary manner without predetermining the impact of such discharges on animal and plant life is a growing third world environmental problem. Most of the wastewaters are extremely hazardous mixtures containing inorganic and organic components (Fu, et al 1994). The industrial operation consists of converting raw hide or skin into leather which can be used in the manufacture of a wide range of products. Consequently, the tanning industry is a potentially pollution-intensive industry.

Chemical impurities mostly comprise of (i). inorganic salt cations such as Fe^{2+}, Zn^{2+}, Cu^{2+}, Ca^{2+}, Na^{+}, anions such as SO_4^{2-}, NO_3^{-}, PO_4^{3-} and (ii) inorganic parameters such as Dissolved Oxygen(DO), Total Dissolved Solids (TDS) (Bosni et al 2000). When industrial waste and domestic sewage are discharged into the receiving water bodies without treatment, it leads to increased water pollution, loss of aquatic life and an uptake of polluted water by plants and animals which eventually affect the human body through consumption resulting in health related problems and a degradation of a sustainable environment.

Effluents generated by the industries are the major sources of pollution and since most of the human and animal population especially in developing countries do not have access to portable water and in most cases use raw river water for drinking purposes, the quality of life is seriously hampered. Studies on heavy metals in industrial effluents (either in free form or adsorbed in suspended solids) have been found to be carcinogenic (Tamburlini et al, 2002) and other chemicals equally present are poisonous depending on the dose and exposure duration (Kupechella and Hyland (1989)). These chemicals are not only poisonous to humans but are found to be toxic to aquatic life (WHO, 2002) and may result in food contamination (Novick 1999).

Study Area

The study was carried out from three different areas: on (i) Challawa River with eight sampling stations, (ii) Waste discharges from effluents in the Sharada Industrial Estate such as the Unique Leather Finishing and others discharging into the Salanta river and flowing through Sabuwar Gandu, Kumbotso and entering the Challawa river at Tamburawa. There were a total number of five sampling points here (iii) The third sampling point was from the industries in the Challawa Industrial Estate, made up of Mario-Jones industrial effluent, God's Little industrial effluent, Maimuda industrial effluent, Clobus industrial effluent and Fata industrial effluent and the confluence of the waste discharges from the Challawa Industrial Estate which finally discharged directly into the Challawa River at Yandanko. There were five sampling points at the Challawa Industrial Estate. There were eighteen (18 No) sampling points in all. Other industries in the areas include the textile industries and bottling company.

Detailed reconnaissance survey of the study area was carried out to ascertain the sampling points. The survey was made by locating the industrial industries in the estates and following the flow through to the points of discharge on Challawa River. Figure 1 shows a schematic view of the study area. A detailed survey of all the points of wastewater discharge into Challawa river were noted and sampling stations designated 1 to 18 were established as explained earlier

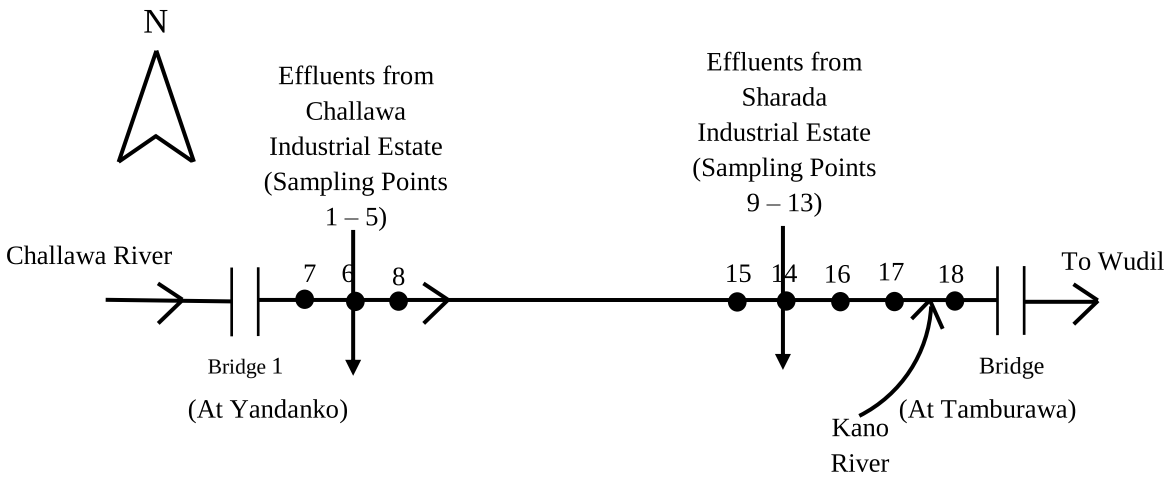

Fig. 1: A schematic outline of Challawa River, effluent discharges, sampling points and confluence with Kano River

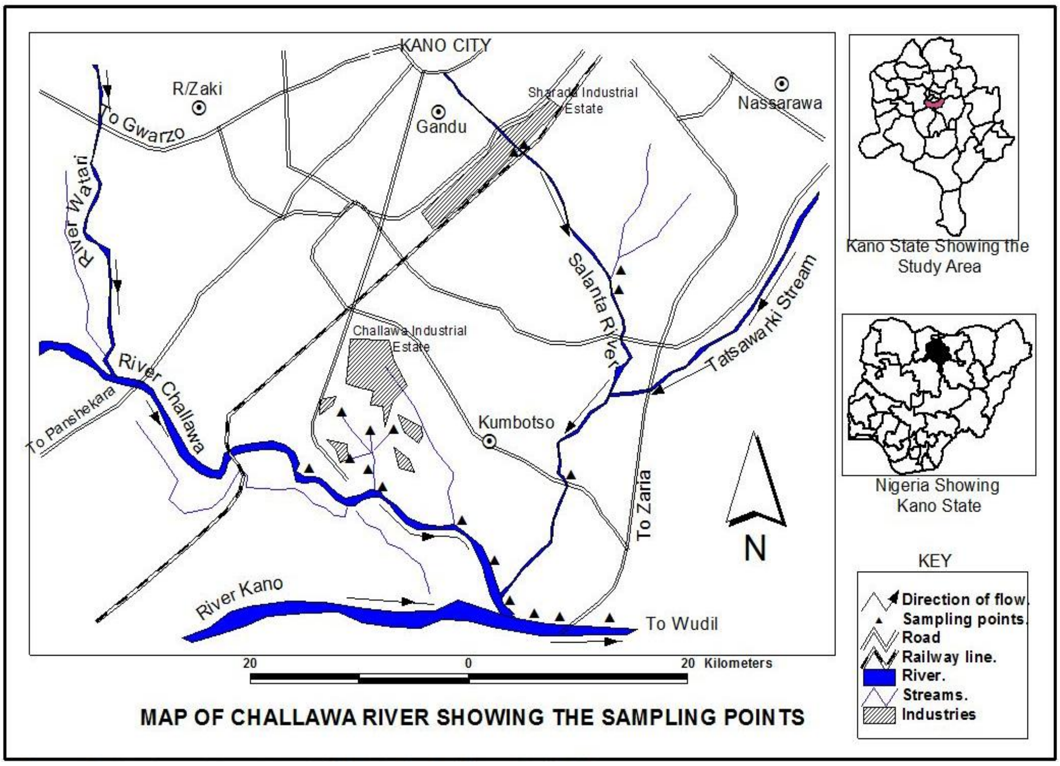

Fig. 2: Map of Challawa River showing the Sampling Points

Scope of Study

The study is composed of three (3) major aspects:

The first aspects is the reconnaissance survey and field work for the gathering of in-situ information on Dissolved Oxygen, the acquisition of raw wastewater effluent sample for BOD, COD, TDS analysis as well as information on other hydrodynamic factors such as stream velocity, depth and width. The sampled reach was limited to 10.644km from the upstream at Yandanko to the downstream at Tamburawa.

The second aspect was the laboratory analysis of the industrial effluents for physical, chemical and bacteriological characteristics.

The final aspect was the development of the k_2 model establishing the relationship between the parameters and developing the Oxygen sag curve for the area investigated based on the data collected. Data recording and handling were carried out with the aid of Microsoft Excel, SPSS and Regression analysis.

Limitations

The research work is limited to the Challawa River and the major sources of pollutants (industrial effluents) into the River. Many researches have been done on the mechanism of reaeration and factors affecting reaeration such as temperature, river geometry and hydrodynamics (Mcbride 1982, Agunwamba, 2001), assessment of assimilatory capacity of streams, and models of reaeration (Dobbins, 1964; Cohen & O'Connell 1976, Campolo et al, 2002). From field observation Nemerow (1987) reviewed series of equations and recommended those of Isaac (1967) and Streeter- Phelps (1925). Generally, it is agreed that Streeter- Phelps equation is not a (true) representative of stream self purification model as it suffers a number of limitations. Apart from questions of stream geometry and flow regime, it ignores a number of mechanisms where BOD and DO concentrations are raised or lowered (Leton, 2007). Some authors have included other parameters in the formulation of their models (Thomas and Mueller 1987, Leton, 2007).

Equations for Determination of Coefficient of Reaeration, k_2

Many attempts have been made to relate empirically the reaeration rate constant to key stream parameters. (Ademoroti, 1998). The most commonly used is O'Connor and Dobbins (1958) which states that

$$k_2 = \frac{3.9V^{1/2}}{H^{3/2}} \quad (1)$$

where k_2 = reaeration coefficient at 20°C (day^{-1})
V = average stream velocity (m/s)
H = average stream depth (m)

To adjust the temperature to stream temperature, the following equation is applied.

$$k_2 = k_{20}\theta^{T-20} \quad (2)$$

where θ is the measured temperature. Appropriate value of θ is recommended by early researchers, i.e.

θ = 1.135 for T ranging from 4° – 20°C
θ = 1.056 for T ranging from 20° – 30°C

O' Connor and Dobbins (1958) also produced a model for the determination of reaeration constant of any medium slope to be:

$$k_2 = 46.2679\,\frac{U^{2.696}}{H^{3.902}} \quad (3)$$

Churchill et al (1962) also produced a model for the determination of reaeration constant of any medium slope to be

$$k_2 = 1.923\,\frac{U^{1.325}}{H^{2.006}} \quad (4)$$

Churchill et al (1962) later improved the equation by considering temperature as a factor which influences reaeration constant as follows.

$$k_2 = 5.06(1.024)^{T-20}\,\frac{U^{0.919}}{H^{1.673}} \quad (5)$$

Gualtieri and Gualtieri (1999) show*ed that

$$k_2 = 3.93\,\frac{U^{0.5}}{H^{1/5}} \quad (6)$$

Agunwamba et al (2009) analyzed the polluted status of Amadi Creek and its management, considering the effect of hydraulic radius in place of the depth of the river at different location, and obtained.

$$k_2 = 11.635\,\frac{U^{1.0954}}{R^{0.016}} \quad (7)$$

Ademoroti (1988) confirmed in his work that reaeration rate constants (k_2) depend on the condition of the river. A fast moving shallow stream will have a higher reaeration rate constant than a sluggish stream of stagnant pond or lake.

II. CALIBRATION AND VERIFICATION OF THE RE-AERATION MODEL

Before the calibration was performed, the relationship between k_2 and velocity and water depth were explored. The parameter k_2 was found to increase as the velocity increases but reduces with decrease in water depth. The plot of k_2 versus velocity is shown in the figure below. Hence, a model of the type $k_2 = aV^b/H^C$ was assumed. Calibration of the model showed that it fitted the data well with a= 0.289, b=1.5464 and c= 1.5467. Verification of the model with a separate set of data gave a coefficient of correlation 0.8815.

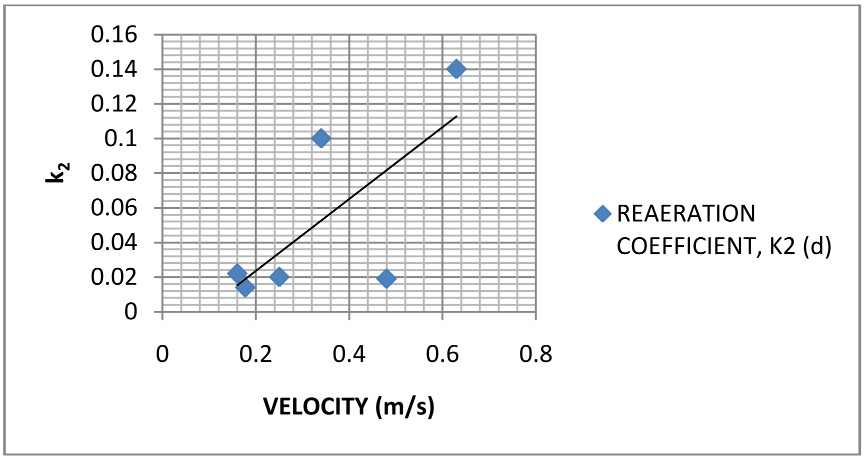

Fig. 3: k_2 versus velocity

Prediction of k_2 using six of the existing models and comparison with the model of this study based on data are shown in Fig 4 with the following corresponding coefficient of correlation: 0.229, 0.295, 0.794, 0.842, 0.0.676, 0.855, and

0.473. The corresponding standard errors of estimate are 1.5156, 2.3376, 0.4216, 1.3891, 0.0488, 0.3854, and 1.7721. Even though this study did not yield the highest coefficient of correlation the standard error of estimate was the least.

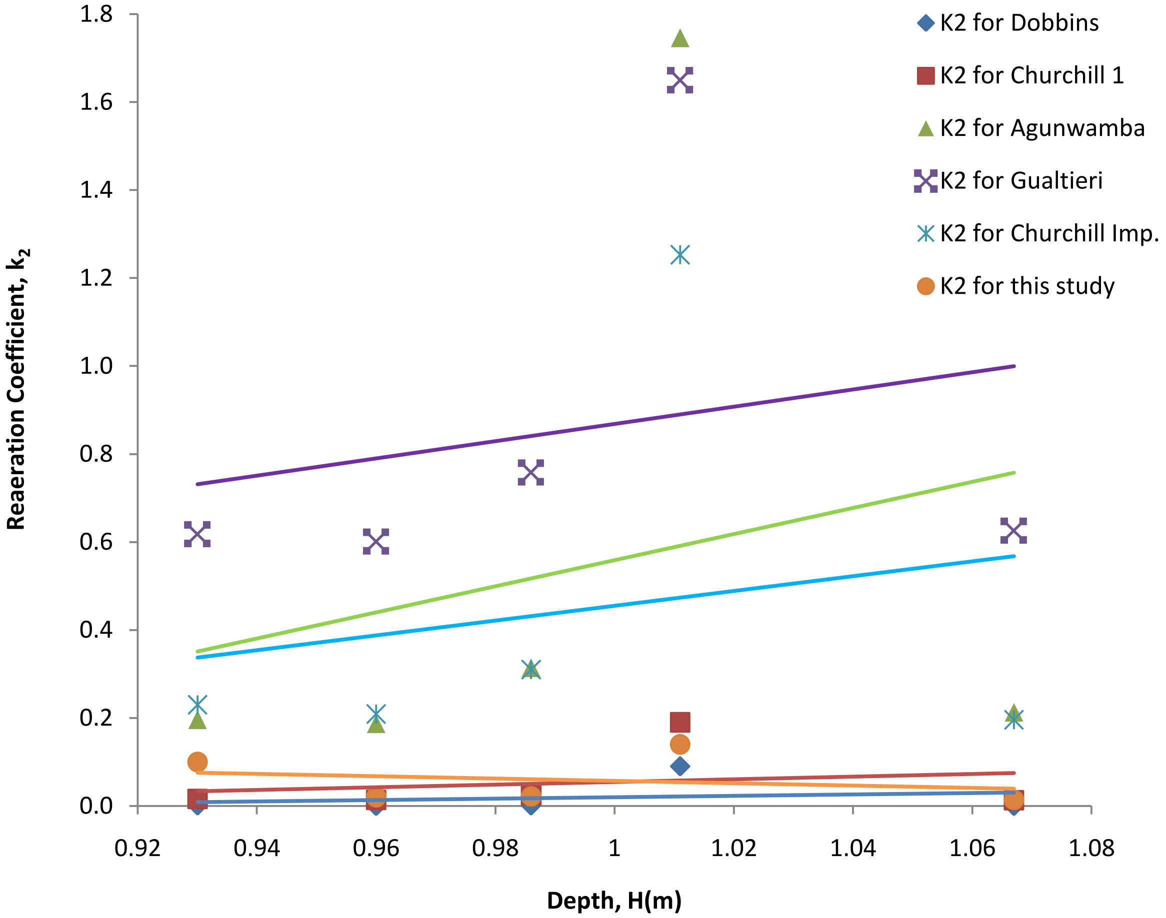

Fig. 4: Model Comparisons for Reaeration Coefficients

III. PREDICTION OF CHALLAWA RIVER OXYGEN SAG

The second modification is based on the fact that the re-aeration coefficient varies along the river reach as has been presented by previous researchers. Hence, computation of the oxygen sag equation based on an average value of k_2 is bound to result in inaccurate prediction.

Solution of the Conventional Oxygen Sag Equation

$$\frac{dD}{dt} = k_1 L - k_2 D \quad (8)$$

$$\frac{dL}{dt} = -kL \quad (9)$$

Where $L(0) = L_0$; $D(0) = D_0$ (10)

Using Laplace Transformation of (ft) defined by Lf(t) = $\int f(t)e^{-st}\,dt$ (Agunwamba, 2007)

Where $\sigma + i\omega = sD(s) - D(0) = \frac{k_1 L_0}{s+k_1} - k_2 D(s)$ (11)

Where $L = L_0 exp(-kt)$ (12)

Substituting the initial conditions in (8), we obtain

$$(sD(s) – D_0)[s + k_1] + k_2D(s)[s + k_1] = k_1L_0 \quad (13)$$

After rearranging, it is shown that:

$$[s^2+s(k_1 + k_2) + k_1k_2]D(s) = sD_0 + k_1D_0 + k_1L_0 \quad (14)$$

From where:

$$D(s) = \frac{sD_0 + k_1 D_0 + k_1 L_0}{s^2 + s(k_1 + k_2) + k_1 k_2} \quad (15)$$

If equation (15) is resolved into partial fraction, the equation below is obtained:

$$D(s) = \frac{A}{S+k_2} + \frac{B}{S+k_1} \quad (16)$$

With $A = \frac{-D_0 k_2 + k_1 D_0 + k_1 L_0}{k_1 - k_2}$ (17)

$$B = \frac{k_1 L_0}{k_2 - k_1} \quad (18)$$

Integrating (16) around the appropriate Greenwich contour, C using the formula

$$2\pi iF(t) = \int_c e^{st}F(s)ds \quad (19)$$

It is clearly shown that:

$$D(t) = L^{-1}[D(s)] = \frac{k_1 L_0}{(k_2-k_1)(e^{-k_1 t} - e^{-k_2 t})} + D_0 e^{-k_2 t} \quad (20)$$

Improved Oxygen Sag Equation

The conventional oxygen sag equation expressed in equations (1) and (2) are modified by incorporating the settling of the industrial waste which occurs along the River reaches. Equation (1) and (20), following the above analysis, may be expanded to include the rate of removal of BOD by benthal decomposition. The resulting relations are:

$$\frac{dD}{dt} = k_1 L_0 e^{-(k_2+V_s)t} - k_2 D \quad (21)$$

and

$$D = \frac{k_1 L_0}{[k_2-(k_1+V_s)]} + D_0 e^{(-k_2 t)} = e^{-(k_1+V_s)t} - e^{(-k_2 t)} + D_0 e^{(-k_2 t)} \quad (22)$$

Again, equations (1) and (2) are expressed as:

$$\frac{dD}{dt} = k_1 L - k_2(t) D \quad (23)$$

$$\frac{dL}{dt} = -KL \quad (24)$$

Since $L = L_o \exp(-k_1 t)$

$$\frac{dD}{dt} = k_1 L - k_2(t) D$$

$$\frac{dD}{dt} = k_1 L_o \exp(-k_1 t) - k_2(t) D \quad (25)$$

Obtaining explicit solution of equation (25), subject to the usual initial conditions, is possible only if the exact function $k_2(t)$ is determined. But $k_2(t)$ is a random variable since it is a function of the depth, flow and wind velocity at each section as well as temperature. In fact, the presence of k_2 makes equation (25) a stochastic equation. Hence, for simplicity, we resort to numerical solution.

The finite difference template of equation (21) can be expressed as

$$\frac{D_{i+1} - D_i}{\Delta t} = k_1 L_o \exp[(-k_2 + V_s)t] - \frac{(k_{2i+1}+k_{2i})}{2} \cdot \frac{(D_{i+1}-D_i)}{2} \quad (26)$$

Re-arranging, we have:

$$D_{i+1}\left[1 + \frac{\Delta t}{4}(k_{2i+1} + k_{2i})\right] = D_i + \Delta t \cdot k_1 L_o \exp[(-k_2 + V_s)t] + \frac{\Delta t}{4} \cdot D_i (k_{2i+1} + k_{2i})$$

$$\therefore\ D_{i+1} = \frac{D_i + \Delta t \cdot k_1 L_o \exp[(-k_2+V_s)t] + \frac{\Delta t}{4} \cdot D_i (k_{2i+1}+k_{2i})}{\left[1+\frac{\Delta t}{4}(k_{2i+1}+k_{2i})\right]} \quad (27)$$

For unit consistency, Δt values attached to k_1 have to be expressed in minutes

Table 1: Data requirement for computation of oxygen sag

Section	**Part**	**k_2**	**C_s**	**Temperature (T°C)**	**Dissolved Oxygen (C)**	**$D_u = C_s - C$**
Yandanko	Upstream	0.022	7.4	30.8	2.30	5.10
	Point Source	0.140	7.4	31.0	0	7.40
	Downstream	0.020	7.5	30.3	1.53	5.47
	Further Downstream	0.100	7.5	30.0	2.00	5.50
Tamburawa	Upstream	0.014	7.7	29.4	2.36	5.34
	Intermediate point	0.025	7.7	29.8	3.10	4.60
	Point source	0.013	7.7	29.8	1.07	6.63
	Downstream	0.019	7.7	29.4	1.85	5.80
	Further Downstream (G)	0.018	7.7	29.4	2.40	5.30

By substituting the values of Δt, Di, K_{2i}, K_{2i+1} and other parameters in equation (B7), D_{i+1} was obtained.

e.g. if t = 0, then Δt = 0, the value of deficit dissolved oxygen recorded against row 1, column 5 was obtained (Table 4.19).

$$D_{i+1} = \frac{7.4 + 0 - 0}{1} = 7.4\ mg/l$$

$K_1 = 0.251\ d^{-1}$; $V_s = 0.157$cm/min →

Deposition coefficient, V_s / h

Table 2: Oxygen Sag Calculation with Variable k_2

Section	Part	Δt (day)	Δt (min)	k_{2i}	k_{2i+1}	$\frac{(k_{2i+1}+k_{2i})\Delta t}{4}$	$e^{(-(k_1+V_s))}$	D_i	D_{i+1}
Yandanko	Upstream	0	26.52	0.140	0.020	0.259	0.974	7.40	7.40
	Point Source	0.018	25.92	0.020	0.020	0.259	0.965	7.40	6.32
	Downstream	0.037	27.36	0.018	0.018	0.2599	0.929	6.32	5.30
Tamburawa	Upstream	0.27	14.4	0.014	0.014	0.115	0.947	5.30	5.14
	Point Source	0.147	28.8	0.013	0.013	0.194	0.745	5.14	5.93
	Downstream	0.157	14.4	0.013	0.013	0.187	0.730	4.94	6.07

$V_s = 0.157\text{cm/min}$

$= \frac{0.157 \times 60 \times 24}{1.22}\ d^{-1}$

$= 1.853 d^{-1}$

$K_1 + V_S = 2.104\ d^{-1}$

Table 3: Measured versus Predicted Oxygen Sag

Section	Part along Challawa River	Distance (km)	Measured oxygen deficit (Cs – C)	Computed oxygen Deficit (mg/l) Conventional	With v_s and variable k_2
Yandanko	Upstream	0	7.4	5.60	7.4
	Point Source	1	5.47	1.21	6.32
	Downstream	2	5.50	0.75	5.30
Tamburawa	Upstream	8.015	5.34	4.92	5.14
	Point Source	8.565	4.60	5.76	5.93
	Downstream	9.610	6.63	1.38	6.07
	Further Downstream	10.644	5.30	11.68	5.45

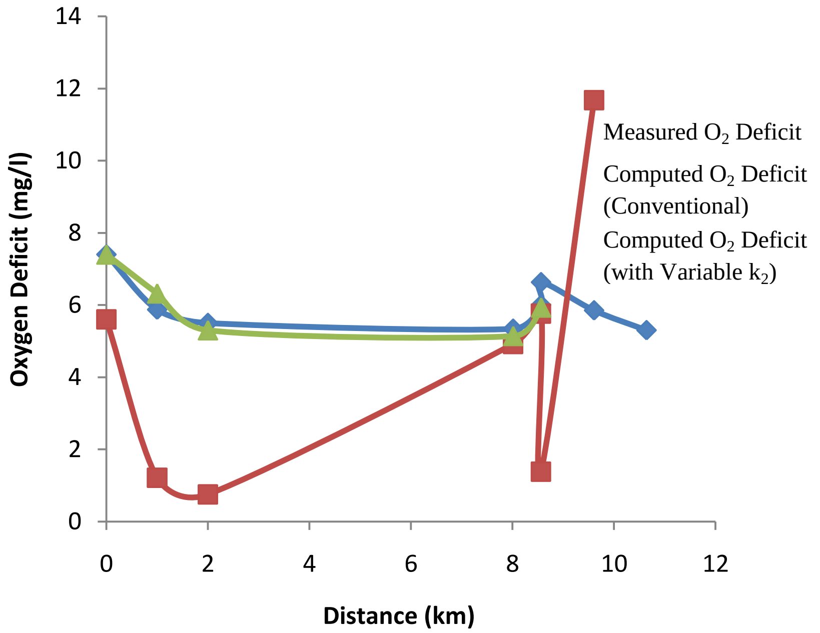

Fig. 5: Oxygen Deficit against Distance (combined graphs)

IV. CONCLUSION

Based on this study, the following conclusions were made

1. The concentrations of pollutants in industrial wastewaters in Challawa River are very high.
2. The industries should leverage on the ameliorating dilution effect in the wet season for discharging the wastewater into the rivers and storage pits in the dry season. However, considering the large concentration of pollutants, effective reduction of BOD is required to comply with Federal Ministry of Environment (FMEnv) standard.
3. The new re-aeration equation for River Challawa has been determined. This equation was found better than the existing six other equations.
4. An improved numerical approach for determination of the oxygen sag predicted the oxygen sag better than the conventional approach.

V. RECOMMENDATIONS

The recommendations arising from this work are as follows:

1. The industrial industries should treat their waste to avoid further pollution of River Challawa with its negative effects on public and environmental health
2. The BOD in River Challawa can be predicted using the relationship obtained from the study to reduce cost and time, especially for monitoring purposes.
3. The model proposed can be preferred to the existing models so far developed for use in the semi-arid areas.
4. Determination of the oxygen sag equation should be based on the spatial values rather than one time average value of the re-aeration coefficient.

REFERENCES

[1.] Ademoroti, C.M.A. (1988) Environmental Management: Case Studies in industrial wastewater treatment in Sada, P.O. and Odemerho, F.O.(Eds): Environmental issues and management in national development. Evans Brothers Publishers Ltd., Nigeria.
[2.] Agunwamba, J.C. (2001) Waste Engineering and Management Tools, Immaculate Publications Ltd., Enugu State, Nigeria
[3.] Agunwamba, J.C. (2007) Engineering Mathematical Analysis, De-Adroit Innovation, Enugu, pp 503-504
[4.] Bosni, M., Buljan, J. and Daniels, R.P.(2000) Regional programme for pollution control in the Tanning industry US/RAS/92/120 in South-East Asia pp1-14
[5.] Campolo, M., Andreussi, P. and Soldati, A. (2002) Water Quality Control in the River Arno: Water Research 36, pp 2673-2680
[6.] Churchill, M.A, Elmore, H.L and Buckingham, R.A (1962): The prediction of stream reaeration rates Journal of Sanitary Eng. Division ASCE 88 (SA4) pp 1-46
[7.] Cohen, J.B. & O'Connel, R.L. (1976) The analog computer as an aid to stream purification computation J. Wat. Pollut. Control Feder 35, 951-961.
[8.] Dobbins, W.E. (1964) BOD and Oxygen relationships in streams. Journal of Sanitation Eng.Div. ASCE1964; 90 (SA3):53-78.
[9.] Fu, L.J., Stares, R.E. and Stahy, R.G. Jr (1994) Assessing acute toxicities of pre and post treatment industrial wastewaters with *Hydra attenata.* A comparative study of acute toxicity with the *Fatheadminnows, Phimephales, Promelas*, Environ. Toxicol. Chem.,13:563-569
[10.] Gualtieri, C. and Gualterie, P. (1999) Statistical analysis of reparation rate in streams. International Agricultural Engineering conference (ICAE) 99, Pechino,China December 14117
[11.] Leton, T. G (2007): "Water and waste water Engineering, Pearl Publishers, Port Harcourt
[12.] McBride, G.B.(1982) Nomographs for rapid solutions for the Streeter-Phelps equations J. Water Pollut. Control Feder 54, 378-384.
[13.] Novick, R.(1999) Overview and the Health in Europe in the 1990s, World Health Organisation, Europe Regional Office, Copenhagen, EUR/ICP/EH/CO 02 02 05/6 pp.20
[14.] O'Connor, D.J.and Dobbins, W.E. (1958) Mechanism of Re-aeration in Natural Streams, Transaction of the American Society of Civil Engineers Vol 123, pp 641-666
[15.] Streeter, H.W. and Phelps, E.B. (1925) A study of the pollution and natural purification of the Ohio River,iii Factors concerned in the phenomena of oxidation and reaeration. US Public Health Bulletin 1925; 146:75
[16.] Tamburlini, G., Ehrenstein, O.V. and Bertollini, R. (2002) Children's Health and Environment: A Review of Evidence, In Environmental Issues, Report No 129, WHO/ European Environmental Agency, WHO Geneva, pp 223.
[17.] Thomas, R.V. and Mueller, J.A. (1987): Principles of water quality modelling and control. NY. Harper Collins.
[18.] WHO (2000): WHO Air Quality Guidelines, 2nd Edition, World Health Organization, Europe Regional Office, Copenhagen.

International Journal of Modern Engineering Research (IJMER)
www.ijmer.com Vol. 3, Issue. 5, Sep - Oct. 2013 pp-2804-2807 ISSN: 2249-6645

A Novel Background Subtraction Algorithm for Dynamic Texture Scenes

Rehana Begum[1], G. Minni[2]

[1]*M. Tech, Nimra College of Engineering & Technology, Vijayawada, A.P., India.*
[2]*Asst. Professor, Dept. of CSE, Nimra College of Engineering & Technology, Vijayawada, A.P., India*

ABSTRACT: *Background subtraction process is often one of the first tasks in machine vision applications, making it a critical part of the system. The output of background subtraction process is an input to a higher-level process that can be, for example, the tracking of an identified object. The performance of background subtraction process depends mainly on the background modeling technique used to model the scene background. Especially natural images put many challenging demands on background modeling since they are usually dynamic in nature including illumination changes, swaying vegetation, rippling water, flickering monitors etc. A robust background subtraction algorithm should also handle situations where new stationary objects are introduced to or old ones removed from the scene. This paper presents a novel background subtraction algorithm for dynamic texture scenes using fuzzy color histogram. The rationale behind the model is that color variations generated by background motions are greatly attenuated in a fuzzy manner.*

Keywords**:** *Fuzzy color histogram, Subtraction, Texture.*

I. INTRODUCTION

Natural scenes are often composed of several entities, from which usually only a small portion are relevant to tasks such as area surveillance, object recognition, event detection, or path planning. In fact the ability to separate various informative regions from the background clutter is an essential requirement to perform these assignments successfully. Biological systems have developed to be remarkably effective
in focusing their visual attention to relevant targets, as opposed to the computer vision where background subtraction(Figure 1) is still an unsolved problem.

Commonly background subtraction has been approached by the detecting moving objects against a static background [1][2]. While effective in certain scenes, this approach has severe problems when the scenes are dynamic nature or the camera is not static. These situations have been addressed by trying to compensate for the camera movements [3] [4], and by continuously updating the background subtraction model. However accurate camera movement estimation is not an easy problem and rapid background subtraction updating is often technically difficult, if not impossible. Furthermore these methods are not applicable at all if we have a single image instead of video frames, or if the objects of interest are not moving against the background. In this paper, we propose a simple and robust method for background subtraction in dynamic texture scenes. The rationale behind the model is that color variations generated by background motions are greatly attenuated in a fuzzy manner.

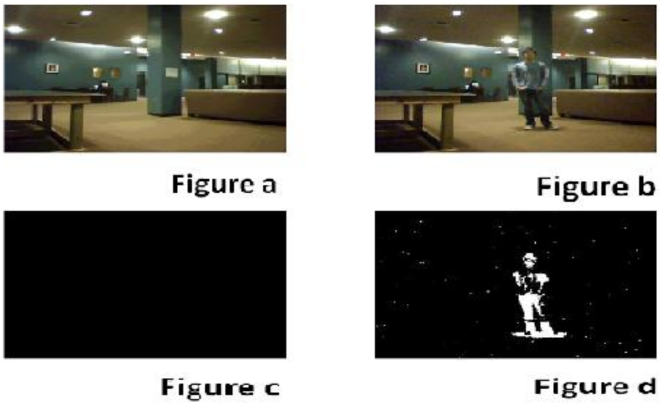

Figure 1: Background subtraction

II. EXISTING WORK

A large number of background subtraction methods [5][6] that have been proposed, but the task remains challenging due to many factors, such as illumination variation, moving object's shadow, addition or removal of stationary objects and scene motion. Pixel-wise methods such as temporal difference and the median filtering, assume that the observation sequence of each pixel is independent to each other and background scene is static. A very popular technique in [7] is to model each pixel in a video frame with a single Gaussian distribution. Many authors have proposed improvements and extensions [8] for using more than one Gaussian distribution per pixel to model very complex non-static backgrounds. Although the above background subtraction methods have different modeling schemes, most of them use standard color or intensity information, which limit their application in the dynamic environment. In [9], the authors detected people by fusing color and edge information, which is an illumination invariant feature. Edge information uniquely is not sufficient, because some part of the background might be uniform.

In [10], the authors concluded that the performance depends largely on the ideal combination of the used information, background model, and classification and combination strategies. In the different existing methods, the features commonly used to handle critical situations are color, edge, stereo, motion and texture [11]. The combination of several measuring features can strengthen the pixels classification as foreground or background. In [12], the authors have used Sugeno integral to aggregate color and texture features. In [12], Choquet integral seems to be more suitable than Sugeno integral, since the scale is continuum in the foreground detection.

III. PROPOSED WORK

A. Fuzzy Membership Based Local Histogram Features

Detection of specific dynamic textures (DTs), such as smoke or fire, is one of the most frequent surveillance applications of temporal dynamic texture analysis. In these applications, the detection is usually based on specific features (frequency, color, etc.) of the phenomena to be detected. A different task is detection of any dynamic texture in a video frame. The idea of using Fuzzy color histogram (FCH) in a local manner to obtain the reliable background model in dynamic texture scenes is motivated by the observation that the background motions do not make severe alterations of the scene structure even though they are widely distributed or occur abruptly in the spatiotemporal domain, and color variations yielded by such irrelevant motions can thus be efficiently attenuated by considering the local statistics defined in a fuzzy manner, i.e., regarding the effect of each pixel value to all the color attributes rather than only one matched color in the local region. In a probability view point, the conventional color histogram (CCH) can be regarded as the probability density function. Thus, the probability for pixels in the image to belong to the ith color bin w_i can be defined as follows:

$$h_i = \sum_{j=1}^{N} P(\omega_i \mid \mathbf{x}_j) P(\mathbf{x}_j) = \frac{1}{N} \sum_{j=1}^{N} P(\omega_i \mid \mathbf{x}_j)$$

where N denotes the total number of pixels.

The fuzzy c- means (FCM) algorithm finds a minimum of a heuristic global cost function defined as follows:

$$J = \sum_{i=1}^{c} \sum_{j=1}^{m} [P(\omega_i \mid \mathbf{x}_j)]^b ||\mathbf{x}_j - \mathbf{v}_i||^2$$

where x and v values denote the feature vector (e.g., values of each color channel) and the cluster center, respectively. Value b is a constant to control the degree of blending of the different clusters.
For the robust background subtraction process in dynamic texture scenes, we finally define the local FCH feature vector at the jth pixel position of the kth video frame as follows:

$$\mathbf{F}_j(k) = (f_{j,1}^k, f_{j,2}^k, \ldots, f_{j,c}^k), \quad f_{j,i}^k = \sum_{q \in W_j^k} u_{iq}$$

where w_j^k denotes the set of neighboring pixels centered at the position j. u_{iq} denotes the membership value, indicating the belongingness of the color feature computed at the pixel position q to the color bin i.

B. Background Subtraction With Local FCH Features

In this section, we describe the algorithm of background subtraction based on our local FCH features. To classify a given pixel into either background or moving objects in the current frame, we first compare the observed FCH vector with the model FCH vector renewed by the online update as expressed in:

$$B_j(k) = \begin{cases} 1, & \text{if } S(\mathbf{F}_j(k), \widehat{\mathbf{F}}_j(k)) > \tau \\ 0, & \text{otherwise,} \end{cases}$$

where $B_j(k) = 1$ denotes that the th pixel in the th video frame is determined as the background whereas the corresponding pixel belongs to moving objects if $B_j(k) = 0$.

The similarity measure S(.,.), which adopts normalized histogram intersection for simple computation, is defined as follows:

$$S(\mathbf{F}_j(k), \widehat{\mathbf{F}}_j(k)) = \frac{\sum_{i=1}^{c} \min\left[f_{j,i}^k, \widehat{f}_{j,i}^k\right]}{\max\left[\sum_{i=1}^{c} f_{j,i}^k, \sum_{i=1}^{c} \widehat{f}_{j,i}^k\right]}$$

Where $\hat{F}_j(k)$ denotes the background model of the jth pixel position in the kth video frame.

In order to maintain the reliable background model in dynamic texture scenes, we need to update it at each pixel position in an online manner as follows:

$$\widehat{\mathbf{F}}_j(k) = (1-\alpha)\cdot\widehat{\mathbf{F}}_j(k-1) + \alpha\cdot\mathbf{F}_j(k), \quad k \geq 1$$

Where $\hat{F}_j(0) = F_j(0)$.

The main steps of the proposed method is summarized in Algorithm 1.

Algorithm 1: Background subtraction using local FCH features
Step 1: Construct a membership matrix using fuzzy –means Clustering.
Step 2: Quantize RGB colors of each pixel at the th video frame into one of m histogram bins (e.g., rth bin where r=1,2,…..m).
Step 3: Find the membership value u_{ir} at each pixel position i-1,2,….,c.
Step 4: Compute local FCH features at each pixel position of the kth video frame.
Step 5: Classify each pixel into background or not based on $B_j(k)$.
Step 6: Update the background model using $\hat{F}_j(k)$.
Step 7: Go back to Step 2 until the input is terminated (k=k+1)
.
C. Extraction of Foreground Object

After successfully developing the background subtraction model, a local thresholding based background subtraction is used to find the foreground objects. A constant value C is considered that helps in computing the local lower threshold (TL) and the local upper threshold (TU). These local thresholds help in successful detection of the objects suppressing shadows if any. The steps of the algorithm are outlined in Algorithm 2.

Algorithm 2: Background Subtraction for a frame f
Step 1: for i ← 1 to height of frame do
Step 2: for j ← 1 to width of frame do
Step 3: Threshold T(i, j) = [M(i, j) + N(i, j)] / C
Step 4: TL(i, j) = M(i, j) − T(i, j)
Step 5: TU(i, j) = N(i, j) + T(i, j)
Step 6: if TL(i, j) ≤ f(i, j) ≤ TU(i, j) then
Step 7: Sf (i, j) = 0 //Background pixel
Step 8: else
Step 9: Sf (i, j) = 1 //Foreground pixel
Step 10: end if
Step 11: end for
Step 12: end for

IV. CONCLUSIONS

One of the most important aspects of an intelligent vision surveillance system is background subtraction method, which is used as a preprocessing step for object detection and tracking in vision systems. In this paper, we present a simple and robust method for background subtraction for dynamic texture scenes. The proposed work does not require estimation of any parameters (i.e., nonparametric). This is fairly desirable for achieving the robust background subtraction in a wide range of scenes with the spatiotemporal dynamics. Specifically, the work propose to derive the local features from the fuzzy color histogram (FCH). Then, the background subtraction model is reliably constructed by computing the similarity between local FCH features with an online update procedure.

REFERENCES

[1] Y. Sheikh and M. Shah. Bayesian modeling of dynamic scenes for object detection. IEEE Transactions on Pattern Analysis and Machine Intelligence, 27(11):1778–1792, 2005.
[2] A. Elgammal, D. Harwood, and L. Davis. Non-parametric model for background subtraction. In In Proc. European Conference of Computer Vision (ECCV), pages 751–757, 2000.
[3] A. Murray and D. Basu. Motion tracking with active camera. IEEE Transactions on Pattern Analysis and Machine Intelligence, 16(5):449–459, 1994.
[4] Y. Ren, C. Chua, and Y. Ho. Motion detection with nonstationary background. Machine Vision and Applications, 13(5- 6):332–343, 2003.
[5] M. Heikkila and M. Pietikainen, "A Texture-Based Method for Modeling the Background and Detecting Moving Objects," IEEE Trans. PAMI, vol. 28, no. 4, pp. 657-662, 2006.
[6] K. Kim, T.H. Chalidabhongse, D. Harwood and L. Davis, "Real-time foreground-background segmentation using codebook model," Elsevier Real-Time Imaging, vol. 11, pp. 172-185, 2005.
[7] B. Klare and S. Sarkar, "Background subtraction in varying illuminations using an ensemble based on an enlarged feature set," IEEE Conf. CVPR Workshops, pp. 66 – 73, 2009.
[8] P. KaewTraKulPong and R. Bowden, "An Improved Adaptive Background Mixture Model for Real-time Tracking with Shadow Detection," Proc. 2nd European Workshop on Advanced Video Based Surveillance Systems, 2001.
[9] S. Jabri, Z. Duric, H. Wechsler, and A. Rosenfeld, "Detection and Location of People in Video Images Using Adaptive Fusion of Color and Edge Information," Proc. IEEE Int'l Conf. Pattern Recognition, vol. 4, pp. 627-630, 2000.
[10] M. Karaman, L. Goldmann, D. Yu and T. Sikora, "Comparison of Static Background Segmentation Methods," Proc. SPIE, vol. 5960, pp. 2140-2151, 2005.
[11] F. El Baf, T. Bouwmans and B. Vachon, "Foreground Detection Using the Choquet Integral," IEEE Ninth Int'l WIAMIS, pp. 187-190, 2008.
[12] H. Zhang, D. Xu, "Fusing color and texture features for background model," Third Int'l Conference on Fuzzy Systems and Knowledge Discovery, vol. 4223, pp. 887– 893, 2006.

An Access Control Model for Collaborative Management of Shared Data in OSNS

Ch. Aruna[1], G. Minni[2]
[1]M.Tech, Nimra College of Engineering & Technology, Vijayawada, A.P., India.
[2]Asst. Professor, Dept.of CSE, Nimra College of Engineering & Technology, Vijayawada, A.P., India.

ABSTRACT: *Online social networks (OSNs) have attracted a large amount of users to regularly connect, interact and share information with each other for various purposes. Users share a tremendous amount of content with other users in social networks using various services. The recent growth of social network sites such as Twitter, Facebook and MySpace has created many interesting and challenging security and privacy problems. In OSNs, users manage their profile, interact with other users, and selforganize into different communities. Users profiles usually include information such as the user's name, address, birthdate, contact information, emails, education, interests, photos, music, videos, blogs and many other attributes The explosive growth of private or sensitive user data that are readily available in OSNs has raised an urgent expectation for effective access control that can protect these data from unauthorized users in OSNs. This paper presents an access control model for the protection of shared data associated with multiple users in online social networks.*

Keywords: *Access control, MController, OSN, Privacy.*

I. INTRODUCTION

Online social networks (OSNs) serve a number of purposes, but three primary roles stand out as common across all sites. First, OSNs are used to maintain and strengthen existing social ties, or make new social connections. The sites allow users to "articulate and make visible their online social networks", thereby "communicating with people who are already a part of their extended social network" [1]. Second, OSNs are used by each member to upload her own content. Note that the content shared often varies from site to site, and sometimes is only the user's profile itself. Third, OSNs are used to find new, interesting content by filtering, recommending, and organizing the content uploaded by users.

Full participation in OSNs requires users to register a (pseudo) identity with the network, though some sites do allow browsing public data without explicit sign-on. Users may volunteer information about themselves, for example their birthday, place of residence, interests, etc., all of which constitutes the user's profile. The online social network itself is composed of links between users. Some sites allow users to link to any other user, without consent from the link recipient, while other sites follow a two-phase procedure that only allows a link to be established when both parties agree. Certain sites, such as Flickr, have social networks with directed links- meaning a link from A to B does not imply the presence of a reverse link, whereas others, such as Orkut, have social networks with undirected links. Most sites also enable users to create special interest groups, which are akin to Usenet [2] newsgroups. Users can post messages to groups (visible to all group members) and even upload shared content to that group. Certain groups are moderated, and admission to the group is controlled by a single group administrator, while other groups are open for any member to join. All sites today require explicit group declaration by the users; users must manually create groups, appoint administrators (if necessary), and declare which groups they are a member of.

Once an identity is built, users of content sharing sites can upload content onto their account. Many such online sites enable users to mark content as public (visible to anyone) or private (visible only to their immediate "friends"), and to tag content with labels. Many sites, such as YouTube, allow users to upload an unlimited amount of video content, while other sites, such as Flickr, require that users either pay a subscription fee or be subject to an upload limit. All of the content uploaded by a given user is listed in their user's profile, allowing other users to browse through the social network to discover new content. Typically, the content is automatically indexed, and, if publicly available, made accessible though a textual search. An example is Flickr's photo search, which allows the users to locate photos by searching based on tags and comments.

II. RELATED WORK

Several studies have examined the interface design to support user awareness of the privacy risks and algorithms for relationship-based access-control scheme. In [3], the authors presented a social-networking-based access-control scheme for online information sharing by considering identities as key pairs and identifying the social relationship based on social attestations. Under this approach, a simple access-control list is employed to manage user access. A more sophisticated mechanism to manage access controls in [4], is rule- based and follows complex policies that are expressed as constraints on the type, depth, and trust level of existing relationships. This control methods is further extended by making access-control decisions completely decentralized and collaborative [5].

In [6], the authors introduced a conceptually-similar but more comprehensive trust-based access control model. This model allows the specification of access rules for online resources, where legitimate users are denoted in terms of the relationship type, depth, and trust level between users in OSNs. In [7], the authors proposed an access control model that formalizes and generalizes the access control mechanism implemented in Facebook, admitting arbitrary policy vocabularies that are based on theoretical graph properties. In [8], the authors described relationship-based access control as one of new security paradigms that addresses unique requirements of Web 2.0. In [9], the authors provided a solution for collective privacy management in OSNs. Their work considered access control policies of a data content that is co-owned by multiple users in an OSN, such that each co-owner may separately specify her/his own privacy preference for the shared content.

III. MULTIPARTY ACCESS CONTROL MODEL FOR OSNS

A. Multi party Access Control Model

A social network can be represented by a relationship network, a set of user groups and a collection of user data (Figure 1). The relationship network of a social network is a directed labeled graph, where each node denotes a user and each edge represents a relationship between two users. The label associated with each edge represents the type of the relationship. Edge direction denotes that the initial node of an edge establishes the relationship and the terminal node of the edge accepts that relationship. The number and type of supported relationships rely on the specific social network and its purposes. Social network should allow multiple controllers, who are associated with the shared data, to specify access control policies. In addition to the owner of data, other controllers, including the stakeholder, contributor and disseminator of data, need to regulate the access of the shared data as well.

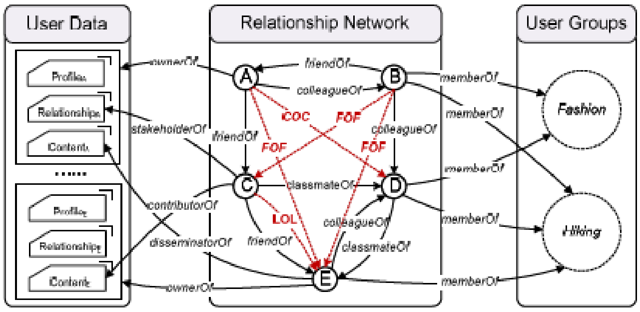

Figure 1: An Example of Multiparty Social Network Representation

B. MPAC Policy specification

To enable a collaborative authorization management of data sharing in OSNs, it is essential for multiparty access control policies to be in place to regulate access over shared data, representing authorization requirements from multiple associated users. Our policy specification scheme is built upon the proposed MPAC model.

Accessor Specification: Accessors are a set of users who are granted to access the shared data. Accessors can be represented with a set of user names, a set of relationship names or a set of group names in OSNs.

Data Specification: In OSNs, user data is composed of three types of information, user profile, user relationship and user content. To facilitate effective privacy conflict resolution for multiparty access control, we introduce sensitivity levels for data specification, which are assigned by the controllers to the shared data items. A user's judgment of the sensitivity level of the data is not binary (private/public), but multi-dimensional with varying degrees of sensitivity.

Access Control Policy: To summarize the above-mentioned policy elements, we introduce the definition of a multiparty access control policy as follows:

A multiparty access control policy is a 5-tuple P =< controller; ctype; accessor; data; effect >, where

- controller $\in$ U is a user who can regulate the access
- of data;
- ctype $\in$ CT is the type of the controller;
- accessor is a set of users to whom the authorization
- is granted, representing with an access specification.
- data is represented with a data specification and
- effect $\in$ {permit; deny} is the authorization effect of the policy.

C. Multiparty Policy Evaluation

Two steps are performed to evaluate an access request over multi- party access control policies. The first one checks the access request against the policy specified by each controller and yields a decision for the controller. The accessor element in a policy decides whether that policy is applicable to a request. If the user who sends the request belongs to the user set derived from the accessor of the policy, the policy is applicable and the evaluation process returns a response with the decision (either permit or deny) indicated by the effect element in the policy. Otherwise, the response yields deny decision if the policy is not applicable to that request. In the second one, decisions from all controllers responding to the access request are aggregated to make a final decision for the access request. Figure 2 illustrates the evaluation process of multi- party access control policies.

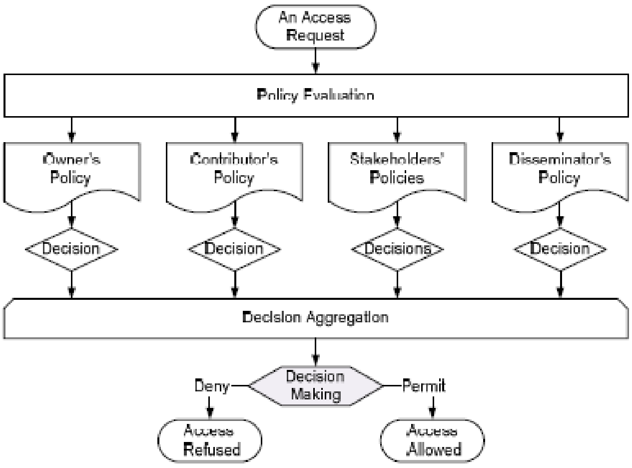

Figure 2: Multiparty Policy Evaluation Process

IV. IMPLEMENTATION OF MCONTROLLER

In our proposed work, we present an application called "MController" for supporting collaborative management of shared data. It enables multiple associated users to specify their access control policies and privacy preferences to co-control a shared data item. Consider the social network "Facebook". Facebook server accepts inputs from the users, and then forwards them to the application server. The application server is responsible for the input processing and the collaborative management of the shared data. Information related to the user data such as friend lists, user identifiers, user groups, and user contents are stored in the MySQL database. Once the user installs MController in his/her Facebook space, MController can access user's basic information and contents. In particular, MController can retrieve and list all the uploaded photos, which are owned or uploaded by the user, or where the user was tagged. Then, the user can select any photo to specify his/hery preference. If the user is not the owner of the selected photo, then he/she only edit the privacy setting and sensitivity setting of the photo. Otherwise, if the user is an owner of the photo, then he/she can further configure the conflict resolution mechanism for the shared photo.

The core component of MController is the decision making module, which processes access requests and then returns responses (either permit or deny) for the requests. Figure 3 depicts the system architecture of the decision making module in MController. To evaluate an access request, the control policies of each controller of the targeted content are enforced first to generate a decision for the Mcontroller. Then, the decisions of all of the controllers are aggregated to yield a final decision as the response to that request. During the process of decision making, policy conflicts are resolved when evaluating the controllers' policies by adopting a strategy chain pre-defined by the controllers.

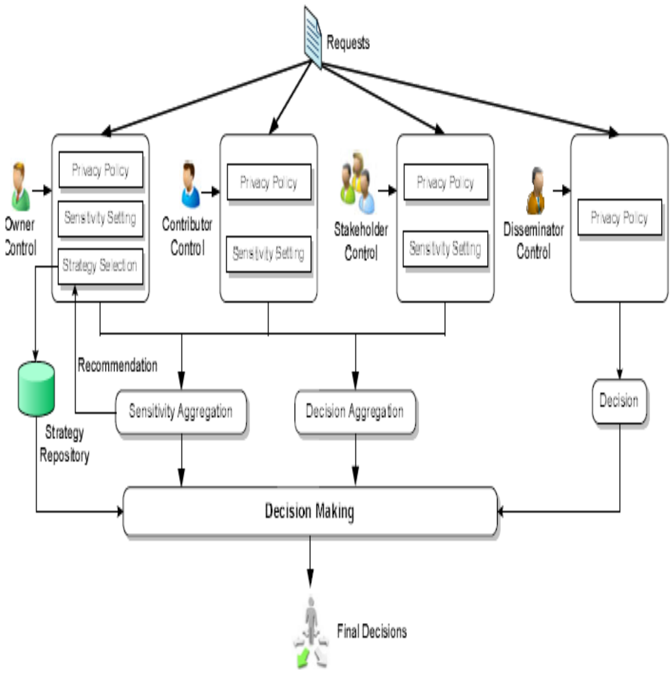

Figure 3: System Architecture of Decision Making in MController

In addition, multi- party privacy conflicts are also resolved based on the configured conflict resolution method when aggregating the decisions of controllers. If the owner of the content chooses the automatic conflict resolution, then the aggregated sensitivity value is utilized as a threshold for making a decision. Otherwise, multi- party privacy conflicts are resolved by applying the strategy selected by the owner, and the aggregated sensitivity score is considered as the recommendation for that strategy selection. Regarding access requests to the disseminated contents, the final decision is made by combining the disseminator's decision and the original controllers' decision through a deny-overrides combination mechanism.

V. SYSTEM USABILITY AND PERFORMANCE EVALUATION

A. Participants and Procedure

MController is a functional proof-of-concept implementation of collaborative privacy management. To measure the practicality and usability of our mechanism, we conducted a survey study (n=35) to explore the factors surrounding users' desires for privacy and discover how we might improve those implemented in MController. Specifically, we were interested in users' perspectives on the current Facebook privacy system and their desires for more control over photos they do not own. Users were given the opportunity to share our application and play with their friends. While this is not a random sampling, recruiting using the natural dissemination features of Facebook arguably gives an accurate profile of the ecosystem. Before Using MController. Prior to using MController, users were asked a few questions about their usage of Facebook to determine the user's perceived usability of the current Facebook privacy controls. Since we were interested in the maximum average perception of Facebook, we looked at the upper bound of the confidence interval. An average user asserts at most 25% positively about the likability and control of Facebook's privacy management mechanism, and at most 44% on Facebook's simplicity as shown in Table 1. This demonstrates an average negative opinion of the Facebook's privacy controls that users currently must use.

TABLE 1
Usability Evaluation for Facebook and MController Privacy Controls

Metric	Facebook		MController	
	Average	Upper bound on 95% confidence interval	Average	Lower bound on 95% confidence interval
Linkability	0.20	0.25	0.83	0.80
Simplicity	0.38	0.44	0.72	0.64
Control	0.20	0.25	0.83	0.80

After Using MController, users were then asked to perform a few tasks in MController. Since we were interested in the average minimum opinion of MController, we looked at the lower bound of the confidence interval. An average user asserts at least 80% positively about the likability and control, and at least 67% positively on MController's simplicity as shown in Table 1. This demonstrates an average positive opinion of the controls and ideas presented to users in MController.

B. Performance Evaluation

To evaluate the performance of the policy evaluation mechanism in MController, we changed the number of the controllers of a shared photo from 1 to 20, and assigned each controller with the average number of friends, 130, which is claimed by Facebook statistics. Also, we considered two cases for our evaluation. In the first case, each controller allows "friends" to access the shared photo. In the second case, controllers specify "friends of friends" as the accessors instead of "friends". In our experiments, we performed 1,000 independent trials and measured the performance of each trial. Since the system performance depends on other There are O(n) MySQL calls and data fetching operations and O(1) for additional operations. Moreover, we could observe there was no significant overhead when we run MController in Facebook.

VI. CONCLUSION

Although social networks attempt to improve security and privacy, they have not achieved the complete or ideal access control mechanisms that users actually demand. In current social networks, individual users can choose different preferences, causing privacy conflicts in shared information that multiple users co- own. In this paper, we have proposed an optimal solution for collaborative management of shared data in OSNs. A multi- party access control model was formulated, along with a multi- party policy specification scheme and corresponding policy evaluation method. In addition, we have introduced an approach for representing and reasoning about our proposed method. A proof-of-concept implementation of our solution called "MController" has been discussed as well, followed by the usability study and system evaluation of our proposed method.

REFERENCES

[1] Danah boyd and Nicole B. Ellison. Social network sites: Definition, history, and scholarship. Journal of Computer-Mediated Communication, 13(1), 2007.

[2] Bryan Pfaffenberger. The USENET Book: Finding, Using, and Surviving News- groups on the Internet. Addison Wesley, New York, NY, USA, 2004.

[3] Kiran K. Gollu, Stefan Saroiu, & Alec Wolman. (2007, October). A Social Networking-Based Access Control Scheme for Personal Content Proc. 21st ACM Symposium on Operating Systems Principles (SOSP '07), Stevenson,Washington. (WIP)

[4] Carminati, B., Ferrari, E., & Perego, A. (2006, October). Rule-based access control for social networks. Paper presented at the On the Move to Meaningful Internet SystemsWorkshops.

[5] Carminati, B., & Ferrari, E. (2008, October). Privacy-aware collaborative access control in Web-based social networks. Paper presented at the 22nd annual IFIPWorking Group 11.3Working Conference on Data and Applications Security, London, UK.

[6] B. Carminati, E. Ferrari, and A. Perego. Rule-based access control for social networks. In On the Move to Meaningful Internet Systems 2006: OTM 2006 Workshops, pages 1734–1744. Springer, 2006.

[7] P. Fong, M. Anwar, and Z. Zhao. A privacy preservation model for facebook-style social network systems. In Proceedings of the 14th European conference on Research in computer security, pages 303–320. Springer-Verlag, 2009.

[8] E. Carrie. Access Control Requirements for Web 2.0 Security and Privacy. In Proc. of Workshop on Web 2.0 Security & Privacy (W2SP). Citeseer, 2007.

[9] A. Squicciarini, M. Shehab, and F. Paci. Collective privacy management in social networks. In Proceedings of the 18th international conference on World wide web, pages 521–530. ACM, 2009.

An Efficient System for Traffic Control in Networks Using Virtual Routing Topologies

S. Viswanatha Raju[1], Sayeed Yasin[2]
[1]M. Tech, Nimra College of Engineering & Technology, Vijayawada, A.P., India.
[2]Asst. Professor, Dept. of CSE, Nimra College of Engineering & Technology, Vijayawada, A.P., India.

ABSTRACT: *Traffic Engineering (TE) is an important aspect of contemporary network management. Offline traffic engineering approaches aim to optimize network resources in a static manner, but require accurate estimation of traffic matrices in order to produce optimized network configurations for long-term operation. In order to avoid network congestion and subsequent service disruptions, handling traffic dynamics is one of the key tasks performed by many contemporary network management systems. In this paper, we introduce AMPLE (Adaptive Multi-toPoLogy traffic Engineering), a holistic system based on virtualized IGP routing topologies for dynamic traffic engineering. The fundamental idea behind this approach follows the strategy of offline provisioning of multiple diverse paths in the routing plane and online spreading of the traffic load for dynamic load balancing in the forwarding plane.*

Keywords: *AMPLE, OLWO, Routing, Topology.*

I. INTRODUCTION

Today's traffic engineering practices mainly depend on off-line settings that use traffic demand estimates to derive network configurations. However, because of their static nature, these practices do not take network and traffic dynamics into account and can lead to sub optimal overall performance. To cope with unexpected traffic variations and network dynamics, approaches that can dynamically adapt routing configurations and the traffic distribution are required [1]. Here, Offline link weight optimization(OLWO) component takes the physical network topology as input and tries to produce maximum routing path diversity across multiple virtual routing topologies for long term operation through the optimized setting of the link weights. Once the optimized link weight configuration has been enforced onto the network, the Adaptive Traffic Control (ATC) component performs very short timescale traffic splitting ratio adjustment for adaptive load balancing across diverse IGP paths in the engineered VRTs, according to the up-to-date monitored traffic conditions [2]. In AODV technique, when a source node generates a packet for particular destination node, it broadcasts the route request packet which is identified by the combination of source sequence number and broadcast ID [3].

An intermediate node only processes a route request if it has not received a previous copy of that request. When an active route link breaks, a route error packet is sent by the upstream node of the broken link to the source node. Upon receipt of an error, the source node initiates a new route discovery process if it still has packets to send to destination node [4]. To deal with this back routing process, the proposed system uses AOMDV (Ad hoc On-Demand Multipath Distance Vector) technique [5].

II. EXISTING WORK

In Existing System, IGP-based TE mechanisms are only confined to offline operation and hence cannot cope efficiently with the significant traffic dynamics. There are well known reasons for this limitation: IGP-based TE only allows for the static traffic delivery through native IGP paths, without flexible traffic splitting for dynamic load balancing. In addition, changing IGP link weights in reaction to emerging network congestion may cause routing re-convergence problems that potentially disrupt the ongoing traffic sessions. In effect, it has been recently argued that dynamic or online route re-computation is to be considered harmful even in the case of network failures, let alone for dealing with traffic dynamics [6].

The existing system does not achieve better performance in minimizing the MLU. Even if multiple traffic matrices with various pattern characteristics are considered in link weight optimization, unexpected traffic spikes may still introduce poor TE performance. AMPLE encompasses two distinct tasks- The first one is offline network dimensioning through link weight optimization for achieving maximum intra-domain path diversity across multiple MT-IGP routing topologies and the second one is adaptive traffic splitting ratio adjustment across these routing topologies for achieving dynamic load balancing in case of unexpected traffic dynamics [7] but these everything done only in MT-IGP. Figure 1 shows the AMPLE system.

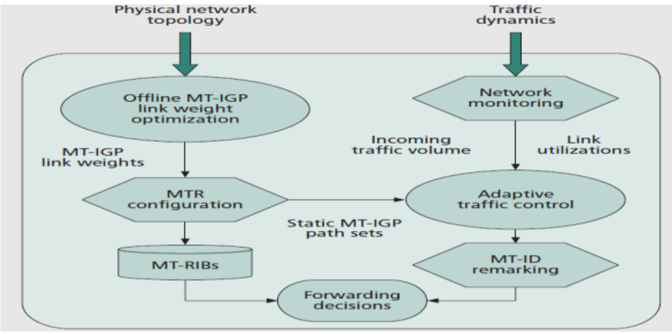

Figure 1: AMPLE System Overview

III. PROPOSED WORK

The proposed system consists of two complementary components: offline link weight optimization that takes as input the physical network topology and tries to produce maximum routing path diversity across multiple virtual routing topologies for long term operation through the optimized setting of the link weights. Based on these diverse paths, adaptive traffic control performs intelligent traffic splitting across the individual routing topologies in reaction to the monitored network dynamics at short timescale. According to our evaluation with real network topologies and various traffic traces, the proposed system is able to cope almost optimally with unpredicted traffic dynamics and, as such, it constitutes a new proposal for achieving better quality of service and overall network performance in the IP networks.

A. Virtual Traffic Allocation

In virtual traffic allocation, the diverse MT-BGP paths according to the link weights computed by OLWO. Monitored network and traffic data such as incoming traffic volume and the link utilizations. At each short time interval, ATC computes a new traffic splitting ratio across various individual VRTs for re-assigning traffic in an optimal way to the diverse BGP paths between each S-D pair. This functionality is handled by a centralized traffic engineering manager who has complete knowledge of the network topology and periodically gathers the up-to-date monitored traffic conditions of the operating network. These new splitting ratios are then configured by the traffic engineering manager to individual source PoP nodes, who use this configuration for remarking the multi-topology identifiers (MTIDs) of their locally originated traffic accordingly.

B. Offline Link Weight Optimization(OLWO)

OLWO is used to determine the definition of "path diversity" between PoPs for traffic engineering. Let's consider the following 2 scenarios of MT-BGP link weight configuration. In the first case, highly diverse paths are available for some Pop-level S-D pairs, while for some other pairs the individual paths are completely overlapping with each other across all VRTs. In the second case, none of the S-D pairs have any disjoint paths, but none of them are completely overlapping either. Obviously, in the first case if any "critical" link that is shared by all paths becomes congested, then its load cannot be alleviated through adjusting traffic splitting ratios at the associated sources, as their traffic will inevitably travel through this link no matter which VRT is used. Hence, our strategy targets the second scenario by achieving "balanced" path diversity across all the S-D pairs.

The ultimate objective of OLWO is to provision offline maximum intra-domain path diversity in the routing plane allowing the ATC component to adjust at very short timescale the traffic assignment across individual VRTs in the forwarding plane. While OLWO focuses on static routing configuration in a long timescale, the ATC enable short timescale control in response to the behaviour of network traffic. At each short-time interval, ATC computes a new traffic splitting ratio across the individual virtual routing technique (VRTs) for reassigning traffic in an optimal way between each source and destination (S-D) pair.

C. Adaptive Traffic Control

In ATC (figure 2), Measure the incoming traffic volume and the network load for the current interval as compute new traffic splitting ratios at each individual PoP source nodes based on the splitting ratio configuration in the previous interval, according to the newly measured traffic demand and the network load for the dynamic load balancing. An efficient algorithm for adaptive adjustment of the traffic splitting ratio at individual PoP source nodes. These parameters are used in the adaptive traffic algorithm. The algorithm consists of the folllowing steps. We define an iteration counter "*x*" which is set to zero initially.

ATC Parameters:

- t(u,v) – traffic between PoP node u and v.
- ϕ u,v(r) – traffic splitting ratio of t(u,v) at u on routing topology r, $0.0 \leq \phi$ u,v(r)≤ 1.0.

Step-1: Identify the most utilized link "lmax" in the network. This can be helpful for updated in the traffic engineering information base.
Step-2: For the set of PoP S-D pairs traffic flows that are routed through "lmax" in at least one but not all the routing topologies, Full Degree of Involvement is equal to zero, consider each at a time and compute its new traffic splitting ratio among the routing topologies until the first feasible one is identified. A feasible traffic flow means that, with the new splitting ratios, the utilization of "lmax" can be reduced without introducing new hot spots with utilization higher than the original value.
Step-3: If such a feasible network traffic flow is found, accept the corresponding new splitting ratio adjustment. Increment the counter k by one and go to Step-1 if the maximum "X" iterations have not been reached (i.e. $x \leq X$). If no feasible traffic flow exists or x = X, the algorithm stops and final result values for the computed traffic splitting ratios.

D. Network Monitoring

Monitoring agent gathers data on the locally originated traffic volume from all the access routers (ARs) attached to the customers at the PoP. In a periodic fashion (e.g. hourly),the central traffic engineering manager polls individual monitoring agents within each PoP and collects their locally monitored traffic volume and link utilizations. Traffic engineering information base (TIB) is needed by the traffic engineering manager to maintain necessary network state based on which new traffic splitting ratios are computed.

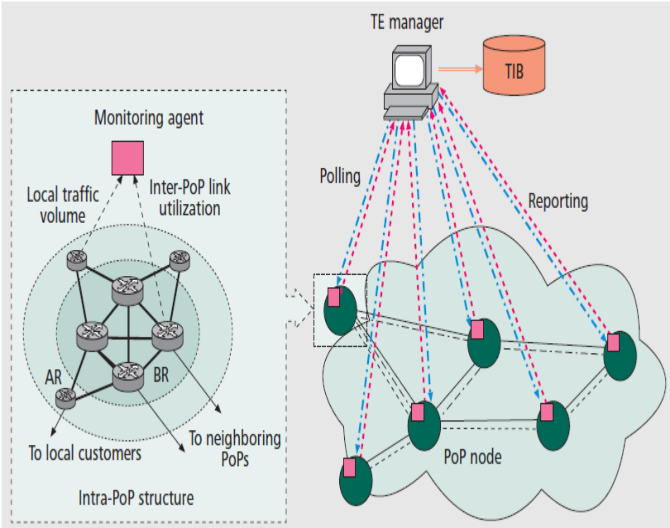

Figure 2: Network monitoring and ATC

IV. CONCLUSION

The traffic engineering system works as follows: First, optimized MT-IGP link weights are configured on top of the underlying MT-IGP platform and remain static until the next offline ofline link weight optimization(OLWO) cycle. During this period, ATC(adaptive traffic control) adaptively re-balancing the load according to the traffic dynamics in very short time scales. The traffic engineering manager updating the traffic volume between each S-D pair in the SDPL and link utilization information stored in the LL of the TIB. The alternate path is chosen for the packet Transfer based on the obtained link utilization information from the source to destination ends.

REFERENCES

[1] N.Wang, D.Tuncer and M.Charalambides “Towards Decentralized and Adaptive Network Resource Management” 2010.
[2] Ivan Gojmerac1, Thomas Ziegler and Peter Reichl “Adaptive Multipath Routing for Dynamic Traffic Engineering”, IEEE GLOBECOM 2007.
[3] C.E. Perkins and E.M. Royer, “Ad-Hoc On-Demand Distance Vector Routing”, IEEE Workshop, Feb. 1999.
[4] Raju J, Garcia-Luna-Aceves J “A new approach to on-demand loop-free multipath routing”, Conference on Computer Communications and Networks ,1999.
[5] Priya Sethuraman and N. Kannan “A Revised Optimal Network Service Based Load Balancing Technique for Traffic Engineering”, EuroJournals Publishing, 2012.
[6] Ning Wang, Kin Hon Ho, George Pavlou, AMPLE: “An Adaptive Traffic Engineering System Based on Virtual Routing Topologies”. IEEE communications Magazine March 2012.
[7] N. Wang, K-H. Ho and G. Pavlou, “Adaptive Multi-topology IGP Based Traffic Engineering with Near-Optimal Performance “, Proc. IFIP Networking 2008.

A Novel Method for Data Cleaning and User- Session Identification for Web Mining

Vijay Kumar Padala[1], Sayeed Yasin[2], Durga Bhavani Alanka[3]
[1]M.Tech, Nimra College of Engineering & Technology, Vijayawada, A.P., India.
[2]Asst. Professor, Dept.of CSE, Nimra College of Engineering & Technology, Vijayawada, A.P., India.
[3]Assoc. Professor, Dept. of CSE, Usharama College of Engineering, A.P., India.

ABSTRACT: *The World Wide Web(WWW) is serving as a huge widely distributed global information service center for technical information, news, advertisement, e-commerce and other information service. This makes information retrieval process very difficult. Most users may not have good knowledge of the structure of the information network, and may easily get bored by taking many access hops and losing their patience when waiting for the information. These challenges will have been solved efficiently by using Web mining, which is the application of data mining technologies. Web mining employs the technique of data mining process into the documents on the WWW. The overall process of web mining includes extraction of information from the WWW through the conventional practices of the data mining and putting the same into the website features. The task of web mining is to discover and extract interesting knowledge/patterns from Web is classified into three types as Web Structure Mining that focuses on hyperlink structure, Web Contents Mining that focuses on page contents as well as Web Usage Mining that focuses on Web logs. In this paper, we are concerned about Web Usage Mining (WUM), also called as Web log mining. We propose algorithms for cleaning a web log file, user and session identification.*

Keywords: *Log file, Session, Web Mining, WWW.*

I. INTRODUCTION

Web mining [1] that discovers and extracts interesting knowledge or patterns from Web is classified into three types as Web Structure Mining that focuses on hyperlink structure, Web Contents Mining that focuses on page contents as well as Web Usage Mining that focuses on Web logs. In this paper, we are concerned about Web Usage Mining (WUM), also called as Web log mining. In the web usage mining process, the techniques of data mining process are applied so as to discover the trends and the patterns in the browsing nature of the visitors of the website. There is an extraction of the navigation patterns as the browsing patterns could be traced and the structure of the websites can be designed accordingly. When it is talked about the browsing nature of the users, it deals with frequent access of the web site or the duration of using the web site. This information can be extracted from using a log file. Only these log files record the session information about the web pages [2]. The figure 1 shows the step wise procedure for web usage mining process.

Log files are files that list the actions that have been occurred on web sites. Such log files reside in the web server. Computers that deliver the web pages are called as “web servers”. The Web server stores all of the files necessary to display the Web pages on the user’s computer. All the individual web pages combines together to form the completeness of the Web site. Images or graphic files and any scripts that make dynamic elements of the site function. The browser requests the data from a Web server, and using HTTP, the server delivers the data back to the browser that had requested the web page. The browser in turn converts (formats) the files into a user viewable page. This gets displayed in the browser itself. In the same way the server can send the files to many user computers at the same time, allowing multiple clients to view the same page simultaneously.

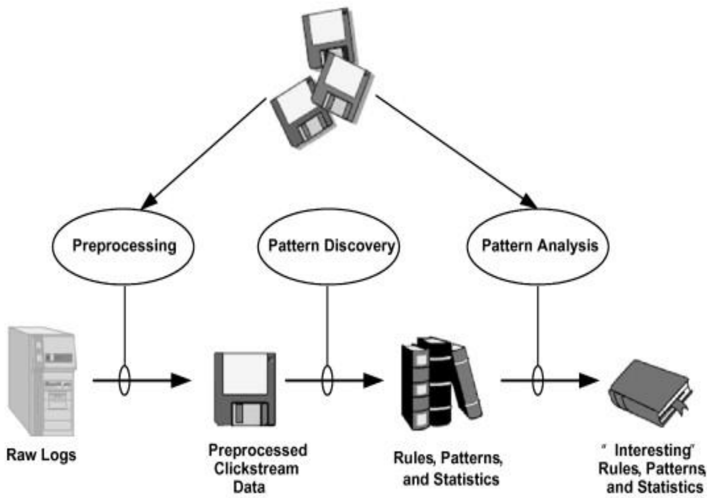

Figure 1: Web usage Mining Process

II. RELATED WORK

Data cleaning is a relatively new research field. The process is computationally expensive on very large data sets and thus it was almost impossible to do with using old technology. The new faster computers allow performing the data cleaning process in acceptable time on large amounts of data. There are many issues in the data cleaning area that researchers are attempting to tackle. They consist of dealing with missing data, erroneous data, determining record usability, etc. Some related research addresses these issues of data quality [3][4]. In [5], the authors introduced a new framework to separate human user and search engine access intelligently with less time span. And also Data Cleaning, User Identification, Session identification are designed correctly. The framework reduces the error rate and also improves significant learning performance of the algorithm.

In [6], the authors introduced a new data preprocessing technique to prune noisy data, irrelevant data, reduce data size and to apply pattern discovery techniques. This paper mainly focuses on data extraction and the data cleaning algorithms. Data cleaning algorithm eliminates unnecessary or inconsistent items in the analyzed data. In. [7], the authors described that the quality of data is an important issue in data mining, and 80 percent of mining efforts spend to improve the quality of data. The data quality depends on accuracy, consistency, completeness, timelines, believability, interpretability and accessibility. In [8], the authors presented a complete preprocessing technique such as data cleaning algorithm, filtering algorithm, user and session identification is performed. They proposed a new hierarchical session identification algorithm that generates the hierarchy of sessions. In [9], the authors classify data quality problems that can be addressed by data cleaning routines and provides an overview of the main solution approaches. In [10], the authors consider the cleansing of data errors in structure and content as an important aspect for data warehouse integration. In [11], the authors suggested that the quality of data is often defined as “fitness for use”, i.e., the ability of a data collection to meet user requirements. The assessment of data quality dimensions should consider the degree to which data satisfy the user’s needs.

III. PROPOSED WORK

A. Cleaning a Web Log File

Data ware house is the only viable solution that can bring that dream into reality. The enhancement of future endeavors to make decisions depends on the availability of correct information that is based on the quality of data underlying. The quality data can only be produced by cleaning data prior to loading into the data ware house since the data collected from different sources will be dirty. Once the data have been cleaned it will produce accurate results when the data mining query is applied to it. So correctness of the data is essential for well-formed and reliable decision making.

Data preprocessing is an important steps to filter and organize only appropriate information before applying any web mining procedure. Preprocessing reduce log file size and also increase quality of available data. The purpose of data preprocessing is to improve data quality and increase data mining accuracy. Preprocessing consists of: data cleansing, user identification, session identification. In this paper the main task is to clean the raw web log files and insert the processed data into a relational database. In this step remove noisy as well as unnecessary data. Remove log entry nodes contain file extension like jpg, gif means remove request such as multimedia files, image, page style file.

Data Cleaning Algorithm
Input: Web Server Log File
Output: Log Database
Step1: Read LogRecord from Web Server Log File
Step2: If((LogRecord.url-stem(gif,jpegjpg,cssjs)) AND
(LogRecord.mehod=’GET’) AND
(LogRecord.Sc-status<>(301,404,500)AND
(LogRecord.Useragent<>Crawler,Spider,Robot))
then Insert LogRecord in to LogDatabase.
End of If condition.
Step 3: Repeat the above two steps until eof (Web Server
Log File)
Step 4: Sop the process.

B. User Identification

The user identification step identify individual user by using their IP address. If there is new IP address, there is new user. If IP address is same but browser version or operating system is different then it represents a different user. The outcome of this algorithm1 is Unique Users Database gives information about total number of individual users, users IP address, browser used and user agent.

User Identification Algorithm
Input: Log Database
Output: Unique Users Database

Step1: Initialize
IPList=0; UsersList=0; BrowserList=0;
OSList=0; No-of-users=0;

Step2: Read Record from LogDatabase
Step3: If Record.IP address in not in IPList
then add new Record.IPaddress in to IPList
add Record.Browser in to BrowserList
add Record.OS in to OSList
increment count of No-of-users
insert new user in to UserList.
Else
If Record.IP address is present in IPList OR
Record.Browser not in BrowserList OR
Record.OS not in OSList
then
increment count of No-of-users
insert as new user in to UserList.
End of If
End of If
Step 5: Repeat the above steps 2 to 3
until eof (Log Database)
Step 6: Stop the process.

C. Session Identification

Each user spends total time in each web page of a web site. Session means time duration spent in web pages of the web site. A referrer-based method is used for identifying the sessions. If IP address, browsers and operating systems are same, then the referrer information should be taken. The cs_referer is checked, and a new user session is identified if the URL in the Refer URI – field is a large interval usually more than 30 minutes between the accessing time of this record.

Session Identification Algorithm
Input: Log Database
Output: Session Database

Step1: Initialize
SessionList=0
UserList=0
No-of-Sessions=0
Step2: Read LogRecord from Log Database
Step3: If (LogRecord.Refer='-') OR
LogRecord.time-taken>30min OR
LogRecord.UserID not in UserList)
then
Increment No-of-Sessions
Get Url address of corresponding Session and
Insert in to SessionList
End of If
Step4: Repeat the above steps 2 and 3 till eof (Log
Database)
Step5: End of process.

IV. CONCLUSION

Data preprocessing is an important steps to filter and organize only appropriate information before applying any web mining procedure. Preprocessing reduce log file size and also increase quality of available data. The purpose of data preprocessing is to improve data quality and increase data mining accuracy. Preprocessing consists of: data cleansing, user identification, session identification. In this paper main task is to clean the raw web log files and insert the processed data into a relational database. By cleaning the data, we can create a new database according to our application which includes the information about user identification, session identification. In some web sites the user identification is made by getting the user's profile and allows them to access the web site by using a user name and password. In this kind of access the user is being identified uniquely so that the revisit of the user can also be identified quickly. Next session identification. Session is the time duration spent in the web page of a web site. This done by using the time stamp details of the web pages of a site. The total time used by each of the user of each web page. This can also be done by noting down the user identification number those who have visited the web page and had traversed through the links of the web page.

REFERENCES

[1] R. Kosala, H. Blockeel. "Web Mining Research: A Survey," In SIGKDD Explorations, ACM press, 2(1): 2000, pp.1-15.
[2] R. Cooley, B. Mobasher, and J. Srivastava,(1999) "Data Preparation for Mining World Wide Web Browsing Patterns," KNOWLEDGE AND INFORMATION SYSTEMS, vol. 1.
[3] Ballou, D., Tayi, K.,"Methodology for Allocating Resources for Data Quality Enhancement", CACM, pp. 320-329, 1989.
[4] Redman, T.,"Data Quality for the Information Age", Artech House, 1996.
[5] Maheswara Rao.V.V.R, Valli Kumari.V,"An Enhanced Pre- Processing Research Framework for Web Log Data Using a Learning Algorithm", Computer Science and Information Technology, pp. 01–15, 2011.
[6] Aye.T.T,"Web Log Cleaning for Mining of Web Usage Patterns", International Conference on computer Researchand Development, IEEE, pp. 490-494, 2011.
[7] Marquardt.C, K. Becker, D. Ruiz,"A Preprocessing Tool for Web usage mining in the Distance Education Domain", InProceedings of the International Database Engineering and Application Symposium (IDEAS' 04), pp.78-87, 2004.
[8] Tasawar Hussain, Sohail Asghar and Nayyer Masood, "Hierarchical Sessionization at Preprocessing Level ofWUM Based on Swarm Intelligence", IEEE Conference on Emerging Technologies, pp.21-26, 2010.
[9] E. Rahm, H. Hai Do,"Data Cleaning: Problems and Current Approaches", University of Leipzig, Germany, [Online] Available: http://wwwiti.cs.uni-magdeburg.de/iti_db/lehre/ dw/paper/data_cleaning.pdf
[10] Raman, V.; Hellerstein, J.M.: Potter's Wheel: An Interactive Framework for Data Cleaning. Working Paper, 1999. http:// www.cs.berkeley.edu/~rshankar/papers/pwheel.pdf.
[11] Cinzia Cappiello, Chiara Francalanci, Barbara Pernici. "A Self-monitoring System to Satisfy Data Quality Requirements", OTM Conferences, pp. 1535-1552, 2005.

International Journal of Modern Engineering Research (IJMER)
www.ijmer.com Vol. 3, Issue. 5, Sep - Oct. 2013 pp-2820-2822 ISSN: 2249-6645

A Novel Information Accountability Framework for Cloud Computing

M. Vijaya Lakshmi[1], Syed Sadat Ali[2]

[1]M. Tech, Nimra College of Engineering & Technology, Vijayawada, A.P., India.

[2]Assoc. Professor & Head, Dept. of CSE, Nimra College of Engineering & Technology, Vijayawada, A.P., India.

ABSTRACT: *Cloud computing is an emerging paradigm in the computer industry where the computing is moved to a cloud of computer systems. The cloud computing core concept is, simply, that the vast computing resources that we need will reside somewhere out there in the cloud of computer systems and we will connect to them and use them as and when needed. The difficulty of how to provide proper security as well as privacy protection for cloud computing is very important, and as yet not solved. In this paper we propose a novel approach, namely Cloud Information Accountability (CIA) framework, based on the notion of information accountability. Unlike privacy protection technologies which are built on the hide-it-or-lose-it perspective, the information accountability focuses on keeping the data usage transparent and trackable. The design of the CIA framework presents substantial challenges, including uniquely identifying CSPs, adapting to a highly decentralized infrastructure, ensuring the reliability of the log, etc. Our basic approach toward addressing these issues is to leverage and extend the programmable capability of the JAR (Java ARchives) files to automatically log the usage of the users' data by any entity in the cloud. Users will send their data along with any policies such as access control policies and logging policies that they want to enforce, that is enclosed in JAR files, to cloud service providers.*

Keywords: *Cloud, CSP, Log file, JAR.*

I. INTRODUCTION

Cloud computing [1] technology is flexible, highly scalable and gives us technology enables services that can be easily consumed over the Internet on as-needed basis. The convenience and efficiency of this approach, however comes with security and privacy risks [2]. Privacy is a key business risk and compliance issue, as it sits at the intersection of the social norms [3]. The advantages of cloud computing is its ability to scale rapidly, share services in a dynamic environment and store data remotely (unknown places). Hence these can become disadvantages in maintaining both privacy and protection to their data to sustain confidence in potential customers. For example, the data processed on the clouds are often outsourced, leading to a number of issues related to accountability, including handling of personal information. Data represents an extremely important asset for any organization, and many users will face serious consequences if its confidential data is disclosed to their business competitors or the public. Thus, cloud users in the first place want to make sure that their data are kept secret to outsiders, including the cloud provider and their potential competitors. This is the first data security requirement for cloud environment.

Data confidentiality is not the only security requirement for cloud. Flexible and fine grained access control is also strongly desired in the service oriented cloud computing model. A health care information system on a cloud environment is required to restrict access of protected medical records to eligible doctors and a customer relation management system running on a cloud may allow access of customer information to high level executives of the company only [4]. To solve the security issues in cloud environment; other user cannot read the respective users data without having access. Data owners should not bother about their data, and should not get fear about damage of their data by hackers; there is need of security mechanism which will track usage of data in the cloud. Accountability is necessary for monitoring data usage, in this all actions of the users like sending of file are cryptographically linked to the server, that performs them and server maintain secured record of all the actions of past and the server can use the past records to know the correctness of action. It also provides reliable information about the usage of data and it observes all the records, so it helps in make trust, relationship and reputation. So accountability is for verification of authentication as well as authorization.

II. RELATED WORK

Cloud environment has raised a range of important privacy and security issues [5][6]. Such issues are due to the fact that, in the cloud environment, users' data and applications reside—at least for a certain amount of time—on the cloud cluster which is owned and maintained by the third party. In [7], the authors present a layered architecture for addressing the end-to-end trust management and accountability problem in many federated systems. They mainly consider trust relationships for accountability, along with both authentication and anomaly detection. Researchers have investigated the accountability mostly as a provable property through various cryptographic mechanisms, particularly in the context of electronic commerce [8]. In [9], the authors propose the usage of policies attached to the data and present logic for the accountability data in distributed settings.

In [10], the authors proposed the Proof Carrying authentication (PCA) framework. The PCA includes a high order logic language that allows the quantification over predicates, and focuses on access control for the web services. While related to ours to the extent that it helps maintaining safe, high performance, mobile code, the PCA's goal is highly different from our research work, as it focuses on validating code, rather than monitoring the content. In [11], the authors proposed an approach for strongly coupling content with access control with the help of Identity-Based Encryption (IBE).

III. PROPOSED WORK

The design of our framework presents substantial challenges, including uniquely identifying CSPs, ensuring the reliability of the log, adapting to a highly decentralized infrastructure, etc. Our basic approach toward addressing these issues is to leverage and extend the programmable capability of JAR (Java ARchives) files to automatically log the usage of the users' data by any entity in the cloud environment. Users will send their data along with any policies such as access control policies and logging policies that they want to enforce, that enclosed in JAR files, to cloud service providers. Any access to the data will trigger an automated and authenticated logging mechanism local to the JAR files. As shown in Figure 1, our proposed JAR file consists of one outer JAR enclosing one or more inner JARs. The main responsibility of the outer JAR is to handle authentication process of entities which want to access the data stored in the JAR file. In our context, the data owners may not know the exact CSPs that are going to handle the information. Hence, authentication is specified according to the servers' functionality (which we assume to be known through a lookup service), rather than the server's URL or identification. Log records are generated by using the logger component. Logging occurs at any access to the data in the JAR file, and new log entries are appended sequentially, in order of creation. Each record ri is encrypted individually and then appended to the log file.

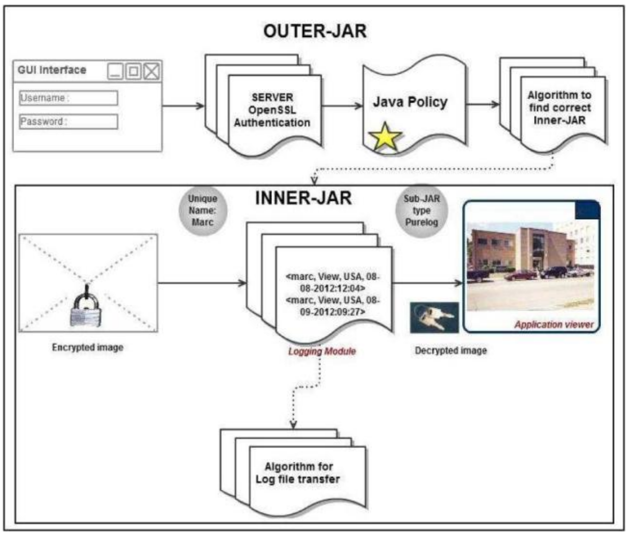

Figure 1: The Structure of the JAR File

Now we propose a new method based on the concept of information accountability. In contrast to the privacy safety is based on the concept of "hide-it-or-lose-it". This information accountability mainly focus on keep the data usage in transparent as well as track able manner. The proposed framework provides end to end accountability in a high dynamically distributed manner. The new innovation in this framework is ability of maintaining lightweight and powerful accountability models, also it integrates the access control methods, usage control and authentication polices.

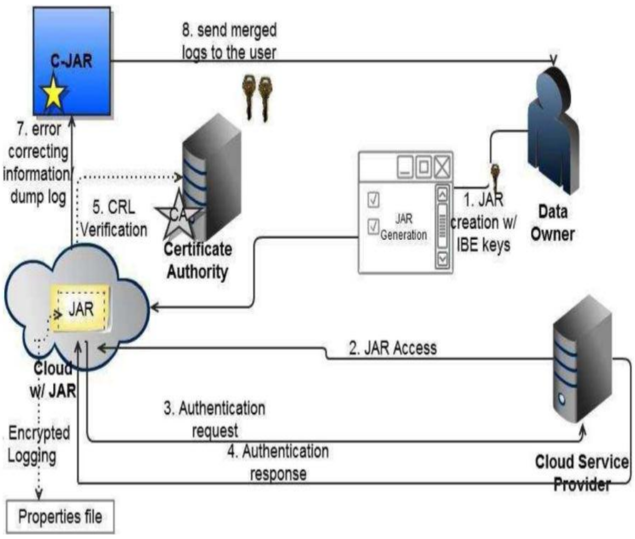

Figure 2: Information Accountability Framework

By means of this, data owners can track not only whether or not the service level agreements are being pleased, but also impose the access and usage control rules based on user needs. Also develop two distinct modes for auditing purpose, they are called as push and pull mode. In push mode, the logs are sporadically pushed to the data owner by using the log harmonizer while in the pull mode refers to another approach whereby the user (or another authorized party) can retrieve the logs as our needed. The overall proposed framework, which combines data, logger, users and log harmonizer, is shown in the figure 2. Initially, each user creates both private and public keys using Identity-Based Encryption. The user will create a logger component which is a JAR file using this secret key, to store its data elements. The JAR file includes a set of simple access control policies specifying whether and how the cloud servers and possibly the other data stakeholders are authorized to access the content itself. Then, user sends the JAR files to the cloud service provider that he/she subscribes to. To authenticate the CSP to the JAR file, it uses Open SSL(Secure Socket Layer) based certificates, wherein a trusted certificate authority certifies the CSP. In the event that the access is requested by the users, this employs SAML-based authentication, where in a trusted identity provider issues certificates verifying the user's identity based on his user identity. Once the authentication was successful then the service provider will be allowed to access the data enclosed in the JAR file.

IV. CONCLUSION

Cloud computing is receiving a great deal of attention, both in publications and among users, from individuals at home, office to the government. The cloud removes the need for you to be in the same physical location as the hardware that stores your information. A major feature of the cloud services is that user's data are usually processed remotely in unknown systems that users do not own or operate. Data handling in the cloud goes through a complex and dynamic hierarchical service chain which does not exist in various traditional environments. This can be addressed by a novel method, namely Cloud Information Accountability (CIA) framework. In this every access to the data are correctly and automatically logged. Log files should be sent back to their data owners periodically, which are used to inform them of the current usage of their data. More importantly, log files should be retrievable any time by their owners when needed regardless the location where the files are actually stored.

REFERENCES

[1] Jens, F. (September 2008). Defining cloud services and cloud computing. http://blogs.idc.com/ie/?p=190
[2] S.Pearson, "Taking Account of Privacy when Designing Cloud Computing Services".
[3] S. Pearson and A. Charlesworth, "Accountability as a Way Forward for Privacy Protection in the Cloud, " Proc First Int'l conf. Cloud Computing, 2009.
[4] ZhiguoWan, Jun'e Liu,Robert H. Deng, "HASBE: A Hierarchical Attribute-Based Solution for flexible and Scalable Access Control in Cloud Computing".
[5] P.T. Jaeger, J. Lin, and J.M. Grimes, "Cloud Computing and Information Policy: Computing in a Policy Cloud?," J. Information Technology and Politics, vol. 5, no. 3, pp. 269-283, 2009.
[6] T. Mather, S. Kumaraswamy, and S. Latif, Cloud Security and Privacy: An Enterprise Perspective on Risks and Compliance (Theory in Practice), first ed. O' Reilly, 2009.
[7] B. Chun and A.C. Bavier, "Decentralized Trust Management and Accountability in Federated Systems," Proc. Ann. Hawaii Int'l Conf. System Sciences (HICSS), 2004.
[8] B. Crispo and G. Ruffo, "Reasoning about Accountability within Delegation," Proc. Third Int'l Conf. Information and Comm. Security (ICICS), pp. 251-260, 2001.
[9] R. Corin, S. Etalle, J.I. den Hartog, G. Lenzini, and I. Staicu, "A Logic for Auditing Accountability in Decentralized Systems," Proc. IFIP TC1 WG1.7 Workshop Formal Aspects in Security and Trust, pp. 187-201, 2005.
[10] X. Feng, Z. Ni, Z. Shao, and Y. Guo, "An Open Framework for Foundational Proof-Carrying Code," Proc. ACM SIGPLAN Int'l Workshop Types in Languages Design and Implementation, pp. 67-78, 2007.
[11] M.C. Mont, S. Pearson, and P. Bramhall, "Towards Accountable Management of Identity and Privacy: Sticky Policies and Enforceable Tracing Services," Proc. Int'l Workshop Database and Expert Systems Applications (DEXA), pp. 377-382, 2003.

International Journal of Modern Engineering Research (IJMER)
www.ijmer.com Vol. 3, Issue. 5, Sep - Oct. 2013 pp-2823-2826 ISSN: 2249-6645

A Novel Clustering Method for Similarity Measuring in Text Documents

Preethi Priyanka Thella[1], G. Sridevi[2]
[1]M.Tech, Nimra College of Engineering & Technology, Vijayawada, A.P., India.
[2]Assoc.Professor, Dept.of CSE, Nimra College of Engineering & Technology, Vijayawada, A.P., India.

ABSTRACT: *Clustering is the process of grouping data into subsets in such a manner that identical instances are collected together, while different instances belong to different groups. The instances are thereby arranged into an efficient depiction that characterizes the populace that is being sampled. A general move towards the clustering process is to treat it as an optimization process. A best partition is found by optimizing an exacting function of similarity, or distance, among data. Basically, there is a hidden assumption that the true inherent structure of data could be correctly describe by using the similarity formula defined and fixed in the clustering decisive factor. In this paper, we introduce clustering with multi- view points based on different similarity measures. The multi- view point approach to learning is one in which we have 'views' of the data (sometimes in a rather abstract sense) and the goal is to use the relationship between these views to alleviate the difficulty of a learning problem of interest.*

Keywords: *Clustering, Text mining, Similarity measure, View point.*

I. INTRODUCTION

Clustering[1] or cluster analysis is the task of grouping a set of objects in such a way that objects in the same group (called cluster) are more similar (in some sense or another) to each other than to those in other groups (clusters). It is a main task of explorative data mining techniques, and a common technique for statistical data analysis used in many fields, including machine learning, pattern recognition, image analysis, information retrieval, and bioinformatics. Cluster analysis itself is not one specific algorithm or procedure, but the general task to be solved. It can be achieved by using various algorithms that differ significantly in their notion of what constitutes a cluster and how to efficiently find them. Popular notions of clusters include groups with low distances among the cluster members, intervals or particular statistical distributions, dense areas of the data space. Clustering can therefore be formulated as a Multi- objective optimization process.

The appropriate clustering algorithm and parameter settings, including values such as the distance function to use, a density threshold or the number of expected clusters, depend on the individual data set and intended use of the results. Clustering as such is not an automatic task, but an iterative process of Knowledge discovery or interactive multi- objective optimization that involves trial and failure. It will often be necessary to modify parameters and preprocessing until the result achieves the desired properties. Cluster analysis can be considered the most important unsupervised learning problem; so, as every other problem of this kind, it deals with finding a structure in a collection of unlabeled data. A loose definition of clustering process could be "the process of organizing objects into groups whose members are similar in some way". A cluster is therefore a collection of objects or items which are "similar" between them and are "dissimilar" to the objects belonging to other clusters. Figure 1 shows clustering process.

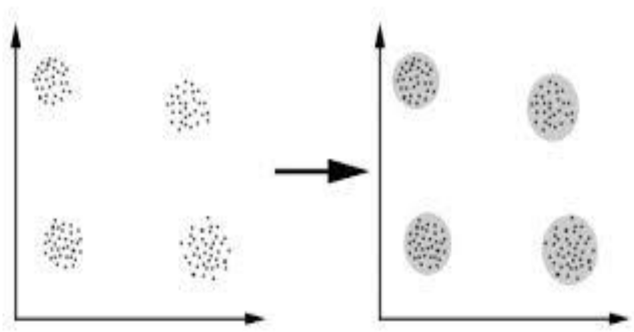

Figure 1: Clustering Process

In this case we easily identify the four clusters into which the data can be divided; the similarity criterion is distance: two or more objects belong to the same cluster if they are "close" according to a given distance (in this case geometrical distance). This is called as distance based clustering. Another kind of clustering is called conceptual clustering: two or more objects belong to the same cluster if this one defines a concept common to all that objects. In other words, objects are grouped according to their fit to descriptive concepts, not according to the simple similarity measures. The multi-view point approach to learning is one in which we have 'views' of the data (sometimes in a rather abstract sense) and the goal is to use the relationship between these views to alleviate the difficulty of a learning problem of interest.

II. RELATED WORK

Text clustering is required in the real world applications such as web search engines. It comes under text mining process. It is meant for grouping text documents into various clusters. These clusters are used by various applications in the real world, for example, search engines. A text document is treated as an object a word in the document is referred as a term. A vector is built to represent each text document. The total number of terms in the text document is represented by m. Some kind of weighting schemes like Term Frequency – Inverse Document Frequency (TF-IDF) is used to represent document vectors. There are many approaches for text document clustering. They include probabilistic based methods [2], nonnegative matrix factorization [3] and information theoretic co-clustering [4]. These approaches are not using a particular measure for finding similarity among text documents. In this paper, we make use of multi- view point similarity measure for finding the similarity. As found it literature, a measure widely used in text document clustering is ED (Euclidian Distance).

$$\text{Dist}\ (d_i, d_j) = ||d_i - d_j||$$

K-Means algorithm is most widely used clustering algorithm due to its ease of use and simplicity. Euclidian distance is the measure used in K-Means algorithm to measure the distance between objects to make them into clusters. In this case the cluster centroid is computed as follows:

$$\text{Min} \sum_{r=1}^{k} \sum_{d_i \in S_r} ||d_i - C_r||^2$$

Another similarity measure being used for text document mining is cosine similarity measure. It is best useful in hi-dimensional documents [5]. This measure is also being used in Spherical K-Means which is a variant of K-Means algorithm. The difference between the two flavors of K-Means algorithm that use cosine similarity measure and ED measure respectively is that the former focuses on vector directions while the latter focuses on vector magnitudes. Graph partitioning is yet another approach which is very popular. It considers the text document corpus as graph and uses min-max cut algorithm which represents centriod as follows:

$$\text{Min} \sum_{r=1}^{k} \frac{D_r^t\, D}{||Dr||^2}$$

There is a software package called CLUTO [6] which is meant for document clustering. It makes use of the graph partitioning approach. Based on the nearest neighbor graph it builds, it text documents are clustered. It is based on the Jacquard coefficient which is computed as follows:

$$Sim_{eJacc}\ (u_i, u_j) = \frac{ui\ uj}{||ui||2 + ||uj||2 - uti\ uj}$$

Jacquard coefficients use both magnitude and direction which is not the case with Euclidian distance and cosine similarity. However, it is similarity to cosine similarity when the documents are represented as unit vectors. In [7] there is comparison between the two techniques namely Jacquard and Pearson correlation. It also concludes that both of them are best used in clustering process of web documents. For tsxt document clustering other approaches can be used which are phrase based and concept based. In phrase based approach is found while in [8] tree similarity based approach is found. The common procedure used by both of them is “Hierarchical agglomerative Clustering”. The drawback of these approaches is that their computational cost is too high. For clustering XML documents also there are some measures. One such measure is called “Structural Similarity” which differs from text document clustering. This paper focuses on a new multi-view point based similarity measure for text clustering.

III. PROPOSED WORK

In proposed work, our approach in finding similarity between documents or objects while performing clustering is multi-view based similarity. It makes use of more than one point of reference as opposed to existing algorithms used for text document clustering. As per our approach the similarity between two documents is calculated as follows:

$$\underset{d_i, d_j \in S_r}{sim(d_i, d_j)} = \frac{1}{n - n_r} \sum_{d_h \in S \setminus S_r} sim(d_i - d_h, d_j - d_h)$$

Consider two point “di” and “dj” in the cluster Sr. The similarity between those two points is viewed from a point “dh” which is outside the cluster. Such similarity is equal to the product of the cosine angle between those points with respect to Euclidean distance between the points. An assumption on which this definition is based on is “dh” is not the same cluster as “di” and “dj”. When distances are very small, then the chances are higher that the “dh” is in the same cluster. Though various viewpoints are useful in increasing the accuracy of the similarity measure there is a possibility of having that give negative result. However the possibility of such a drawback can be ignored provided plenty of documents to be clustered.

Now we have to carry out the validity test for the cosine similarity and multi view based similarity as follows. For each type of the similarity measure, a similarity matrix called A = {aij}n×n is created. For CS, this is very simple, as aij = dti dj . The algorithm for building Multi view Similarity (MVS) matrix is described in Algorithm 1.

ALGORITHM 1: BUILDMVSMATRIX(*A*)

Step 1: for r ← 1 : c do

Step 2: DS \Sr ← $\sum_{d_i \notin S_r} d_i$

Step 3: nS \Sr←|S \ Sr|

Step 4: end for

Step 5: for i ← 1 : n do

Step 6: r ← class of di

Step 7: for j ← 1 : n do

Step 8: if dj ∈ Sr then

Step 9: $$a_{ij} \leftarrow d_i^t d_j - d_i^t \frac{D_{S\setminus S_r}}{n_{S\setminus S_r}} - d_j^t \frac{D_{S\setminus S_r}}{n_{S\setminus S_r}} + 1$$

Step 10: else

Step 11: $$a_{ij} \leftarrow d_i^t d_j - d_i^t \frac{D_{S\setminus S_r} - d_j}{n_{S\setminus S_r} - 1} - d_j^t \frac{D_{S\setminus S_r} - d_j}{n_{S\setminus S_r} - 1} + 1$$

Step 12: end if

Step 13: end for

Step 14: end for

Step 15: return A = {aij}n×n

First, the outer composite with respect to each class is determined. Then, for each row **a**i of "A", i = 1, . . . , n, if the pair of text documents di and dj, j = 1, . . . , n are in the same class, aij is calculated as in line 9. Otherwise, dj is assumed to be in di's class, and aij is calculated as shown in line 11.

After matrix "A" is formed, the code in Algorithm 2 is used to get its validity score:

ALGORITHM 2: GETVALIDITY(*validity,A, percentage*)

Step 1: for r ← 1 : c do

Step 2: qr ← floor(percentage × nr)

Step 3: if qr = 0 then

Step 4: qr ← 1

Step 5: end if

Step 6: end for

Step 7: for i ← 1 : n do

Step 8: {aiv[1], . . . , aiv[n] } ←Sort {ai1, . . . , ain}

Step 9: s.t. aiv[1] ≥ aiv[2] ≥ . . . ≥ aiv[n]

{v[1], . . . , v[n]} ← permute {1, . . . , n}

Step 10: r ← class of di

Step 11: $$validity(d_i) \leftarrow \frac{|\{d_{v[1]}, \ldots, d_{v[q_r]}\} \cap S_r|}{q_r}$$

Step 12: end for

Step 13: $$validity \leftarrow \frac{\sum_{i\leftarrow 1}^{n} validity(d_i)}{n}$$

Step 14: return validity

For each document "di" corresponding to row "**a**i" of matrix A, we select "qr" documents closest to point "di". The value of "qr" is chosen relatively as the percentage of the size of the class r that contains "di", where percentage ∈ (0, 1]. Then, validity with respect to "di" is calculated by the fraction of these "qr" documents having the same class label with "di", as shown in line 11. The final validity is determined by averaging the over all the rows of matrix A, as shown in line 13. It is clear that the validity score is bounded within values 0 and 1. The higher validity score a similarity measure has, the more suitable it should be useful for the clustering process.

IV. INCREMENTAL CLUSTERING ALGORITHM

The main goal of this algorithm is to perform text document clustering by optimizing I_R and I_V as shown below:

$$I_R = \sum_{r=1}^{k} \frac{1}{n_r^{1-\alpha}} \left[\frac{n+n_r}{n-n_r} \|D_r\|^2 - \left(\frac{n+n_r}{n-n_r} - 1 \right) D_r^t D \right]$$

$$I_V = \sum_{r=1}^{k} \left[\frac{n+\|D_r\|}{n-n_r} \|D_r\| - \left(\frac{n+\|D_r\|}{n-n_r} - 1 \right) \frac{D_r^t D}{\|D_r\|} \right]$$

With this general form, the incremental optimization algorithm, which has two major steps Initialization and Refinement, is shown in Algorithm 3 and Algorithm 4.

ALGORITHM 3: INITIALIZATION
Step 1: Select k seeds s1, . . . , sk randomly
Step 2: $cluster[d_i] \leftarrow p = \arg\max_r \{s_r^t d_i\}, \forall i = 1, \ldots, n$
Step 3: $D_r \leftarrow \sum_{d_i \in S_r} d_i, \; n_r \leftarrow |S_r|, \forall r = 1, \ldots, k$
Step 4: end

ALGORITHM 4: REFINEMENT
Step 1: repeat
Step 2: {v[1 : n]} ← random permutation of {1, . . ., n}
Step 3: for j ← 1 : n do
Step 4: i ← v[j]
Step 5: p ← cluster[di]
Step 6: $\Delta I_p \leftarrow I(n_p - 1, D_p - d_i) - I(n_p, D_p)$
Step 7: $q \leftarrow \arg\max_{r, r \neq p} \{I(n_r + 1, D_r + d_i) - I(n_r, D_r)\}$
Step 8: $\Delta I_q \leftarrow I(n_q + 1, D_q + d_i) - I(n_q, D_q)$
Step 9: if $\Delta I_p + \Delta I_q > 0$ then
Step 10: Move di to cluster q: cluster[di] ← q
Step 11: Update Dp, np,Dq, nq
Step 12: end if
Step 13: end for
Step 14: until No move for all n documents
Step 15: end

At Initialization, “k” arbitrary documents are selected to be the seeds from which initial partitions are formed. Refinement is a process that consists of a number of iterations. During each iteration, the “n” text documents are visited one by one in a totally random order. Each text document is checked if its move to another cluster results in improvement of the objective function. If yes, then the text document is moved to the cluster that leads to the highest improvement. If no clusters are better than the current cluster, the text document is not moved. The clustering process terminates when iteration completes without any text documents being moved to new clusters.

V. CONCLUSION

In the view point of data engineering, a cluster is a group of objects with similar nature. The grouping mechanism is called as clustering process. The similar text documents are grouped together in a cluster, if their cosine similarity measure is less than a specified threshold. In this paper we mainly focuses on view points and we introduce a novel multi-viewpoint based similarity measure for text mining. The nature of similarity measure plays a very important role in the success or failure of the clustering method. From the proposed similarity measure, we then formulate new clustering criterion functions and introduce their respective clustering algorithms, which are fast and scalable like k-means algorithm, but are also capable of providing high quality and consistent performance.

REFERENCES

[1] I. Guyon, U. von Luxburg, and R. C. Williamson, “Clustering: Science or Art?” , || NIPS’09 Workshop on Clustering Theory, 2009.
[2] Leo Wanner (2004). “Introduction to Clustering Techniques”. Available online at: http://www.iula.upf.edu/materials/040701wanner.pdf [viewed: 16 August 2012]
[3] D. Ienco, R. G. Pensa, and R. Meo, “Context-based distance learning for categorical data clustering,” in Proc. of the 8th Int. Symp. IDA, 2009, pp. 83–94.
[4] I. Guyon, U. von Luxburg, and R. C. Williamson, “Clustering: Science or Art?” NIPS’09 Workshop on Clustering Theory, 2009.
[5] C. D. Manning, P. Raghavan, and H. Sch ¨ utze, An Introduction to Information Retrieval. Press, Cambridge U., 2009.
[6] X. Wu, V. Kumar, J. Ross Quinlan, J. Ghosh, Q. Yang, H. Motoda, G. J. McLachlan, A. Ng, B. Liu, P. S. Yu, Z.-H. Zhou, M. Steinbach, D. J. Hand, and D. Steinberg, “Top 10 algorithms in data mining,” Knowl.Inf. Syst., vol. 14, no. 1, pp. 1–37, 2007.
[7] W. Xu, X. Liu, and Y. Gong, “Document clustering based on nonnegative matrix factorization,” in SIGIR, 2003, pp. 267–273.
[8] S. Zhong, “Efficient online spherical K-means clustering,” in IEEE IJCNN, 2005, pp. 3180–3185.

International Journal of Modern Engineering Research (IJMER)
www.ijmer.com Vol. 3, Issue. 5, Sep - Oct. 2013 pp-2827-2830 ISSN: 2249-6645

A Novel Method for Preventing Selective Jamming Attacks in Wireless Networks

Ashrafunnisa[1], G. Sridevi[2]
[1]M. Tech, Nimra College of Engineering & Technology, Vijayawada, A.P., India.
[2]Assoc. Professor, Dept.of CSE, Nimra College of Engineering & Technology, Vijayawada, A.P., India.

ABSTRACT: *Wireless networks are susceptible to numerous security vulnerabilities due to the open nature of the wireless medium. Anyone with a transceiver can eavesdrop on ongoing transmissions, block the transmission of legitimate ones or inject spurious messages. One of the fundamental ways for degrading the overall network performance is by jamming wireless transmissions. In this paper, we deal with the problem of selective jamming under an internal threat model. Here the eavesdropper who is aware of network secrets and the implementation details of all the layers of network protocols in the network stack. The attacker uses his/her internal knowledge for launching selective jamming attacks in which high importance messages are targeted. Hence we propose a novel method for preventing selective jamming attacks in wireless networks.*

Keywords: *All- or- nothing transform, Jamming, SHCS.*

I. INTRODUCTION

Wireless networks are prone to diverse set of attacks due to the nature of its shared medium. Well-designed network architectures may address several security threats [1][2][3]. However, wireless networks are even sensitive to number of security attacks. From the existing security attacks to be resolved, we kept our centre of interest on Selective Jamming (Figure 1) which is the recent headway on the bad side of technology. We do have various traditional jamming attacks like random jamming, constant jamming, deceptive jamming etc [4][5]. To have any of these attacks, the attacker has to spend more vigor but the impact on the network degradation is less. Moreover, there are wide varieties of techniques to prevent such several traditional jamming strategies in [6].

But, in Selective Jamming, the attacker will expend fewer resources and can create drastic bad consequences. Taking this as ground principle, we can assign a tagline for the selective jamming as “less effort, more impact” method. The attacker who does the selective jamming will target on specific sender node (SN) and receiver node (RN) and thereby corrupt only the significant packets (e.g. Route REQ / REPLY, ACK) that travel between them. Selective jammer (SJ) node will use packet classification methods [7] to know whether the packet is significant or not. To achieve this selective jamming attack, the jamming node should be an internal part of network which makes it to know all the networks secrets in an easier way. Finally, all these things make attacker to perform selective jamming with less energy consumption.

In this paper, we deal with the problem of selective jamming under an internal threat model. Here the adversary who is aware of network secrets and the implementation details of all the layers of network protocols in the network stack. The attacker uses his/her internal knowledge for launching selective jamming attacks in which high importance messages are targeted. For example, a jammer can target TCP acknowledgments in a TCP session or target route request or reply messages at the routing layer.

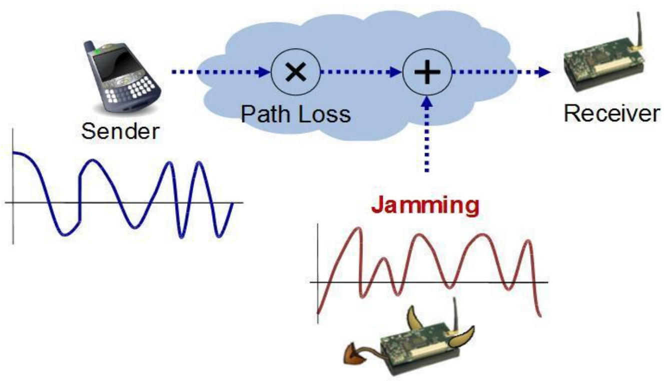

Figure 1: Jamming in wireless network

II. RELATED WORK

Selective jamming problem has been addressed under various threat models. The impact of external selective jammers targeting various control packets at the MAC layer is studied in the paper [8] by author Thuente. Selective jamming attack is based on protocol semantics, where they considered several packet identifiers for enciphered packets such as packet size, signal sensing and timing information of different protocols. Unification of packet characteristics like minimum length and the inter packet timing was used in order to prevent selectivity. In [9], the authors attempts to make use of protocols at

www.ijmer.com Vol. 3, Issue. 5, Sep - Oct. 2013 pp-2827-2830 ISSN: 2249-6645

various layers to get three advantages- targeted jamming, jamming gain, and reduced probability of detection. In targeted jamming attack, it may jam particular nodes, flows or links. Here the adversary may be interested in specific parts of the network and attacking those regions can lead to further jamming gains, where as in reduced probability of detection, the sufferer network may not be aware of jamming attack counter measures.

Selective jamming attacks have been experimentally implemented using the software defined radio engines [10]. USRP2-based jamming platform called RFReact was implemented in [10] that enables selective and reactive jamming. We develop 3 schemes that prevent jamming attacks: they are Strong Hiding Commitment Scheme, Cryptographic Puzzle Hiding Scheme and All or Nothing Transformation.

III. PROPOSED WORK

A. Problem Statement

Lets consider Figure 2 where A(alice) and B(bob) are communicating through a wireless network and "j" is jamming node whenever alice sending some packets m to bob. Node "j" will classify m and get first few bytes then adversary "j" corrupt them beyond the recovery and add them when received by Bob. The main objective is to prevent attackers who are going to do selective jamming attacks on our network.

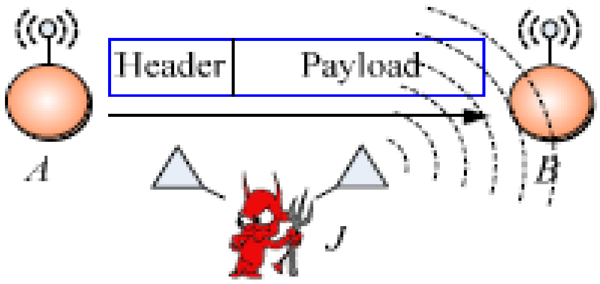

Figure 2: Realization of a selective jamming attack

Figure 3 shows the generic format for a wireless Physical header contains information regarding the length of frame and transmission rate in MAC protocol, source, destination field, MAC header is followed by frame body that contains IP datagram.

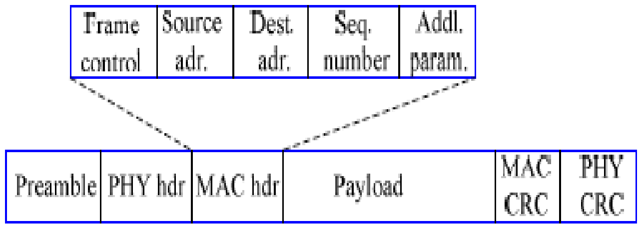

Figure 3: A generic frame format for a wireless network

B. Strong Hiding Commitment Scheme (SHCS)

Strong Hiding Commitment Scheme (SHCS) which is based on asymmetric cryptography. Our main goal is to satisfy the strong hiding property by keeping the computation overhead to a minimum. A commitment scheme allows an entity "S", to commit to a chosen value, to another entity "V" while keeping that value hidden to others. Commitment scheme must satisfy the following two properties:

- **Binding:** Deliver the committed value to the receiver end, here the sender cannot alter the value once it is committed
- **Hiding:** The receiver cannot see the message until he gets the secret key, after receiving the key receiver verifies that it is indeed the message to which the sender is committed.

Here the role of the committer is implicated by the sender or transmitting node, whereas role of the verifier is implicated by any receiver including the attacker. Consider that sender S has a packet "m" for the transmission for receiver R. First, before transmission S constructs the following:

(C,d) = commit (m)

C= Ek (π1(m)) and d=k

Where "Ek" the commitment function is an asymmetric encryption algorithm (eg. DSA or RSA [11]), "π1" is a publicly known permutation and k is a randomly selected key. At the receiver end, upon receiving d the receiver R computes m = π1(Dk (C)), where "π1" is the inverse permutation of π1 and also it verifies the signature which is attached to the packets.

C. Cryptographic Puzzle Hiding scheme

A sender “S” has a packet “m” for transmission. The sender selects a random secret key “k” , of a desired length. S generates a puzzle (key, time), where puzzle() denotes the puzzle generator function, and “tp” denotes the time period required for the solution of the puzzle. Parameter is measured in units of time, and it is directly dependent on the assumed computational capability of the attacker, denoted by N and measured in computational operations per second. After generating the puzzle “P”, the sender broadcasts (C, P). At the receiver side, any receiver R solves the received puzzle to recover secret key and then computes. Cryptographic Puzzle includes two types of methods.

- Time-lock Puzzles
- Puzzles based on hashing

Time lock Puzzles is based on the iterative application of the precisely controlled number of modulo operations. Time-lock puzzles have several attractive features such as the fine granularity in controlling “tp” and the sequential nature of the computation. Moreover, the Puzzle generation requires significantly less computation compared to the puzzle solving. Computationally limited receivers can incur significant delay and the energy consumption when dealing with modulo arithmetic. In this case, the hiding scheme can be implemented from cryptographic puzzles which employ computationally efficient cryptographic primitives. Client puzzles proposed in, use one way hash functions with partially disclosed inputs to force the puzzle solvers search through a space of a precisely controlled size. In our context, the sender picks a random secret key k with k = k1||k2. The lengths of k1 and k2 are s1, and s2, respectively. He then calculates C = Ek(π1(m)) and transmits (C, k1, h(k)) in this particular order. To obtain key k, any receiver has to perform On average 2s2−1 hash operations (assuming perfect hash functions). Because the puzzle cannot be solved before hash function h (k) has been received, the adversary cannot classify m before the completion of m’s transmission.

D. Hiding based on All-Or-Nothing Transformation

In this scheme, the packets are pre-processed by an AONT before transmission but remain unencrypted. The jammer cannot perform the packet classification until all the pseudo-messages corresponding to the original packet have been received and the inverse transformation has been applied. Packet “m” is partitioned to a set of “x” input blocks m = {m1, m2, m3….}, which serve as an input to an The set of pseudo messages m = {m1, m2, m3,…..} is transmitted over the wireless link. Recently Rivest motivated by different security concerns arising in the context of the block ciphers, introduced an intriguing primitive called the “All-Or-Nothing Transform (AONT)”. All- or- Nothing transform is an efficiently computable transformation “T” on strings such that

- For any string “x”, given *all* of T(x), one can efficiently recover “x”
- There exists some threshold value such that any polynomial time adversery that learns all but bits of T(x) obtains no information about “X” (in a computational sense).

Figure 4 shows the proposed AONT- based packet hiding method. The Sender transmits the secret message, which is divided into blocks of fixed size. These blocks are given as input to AONT system. Then AONT system encrypts these message blocks with a shared secret key and then sends to the receiver. Now the receiver decrypts the received blocks with the same key, thus retrieves the original data.

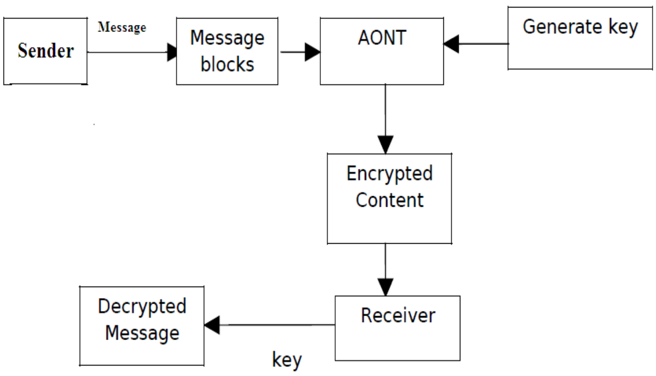

Figure 4: AONT- based packet hiding method

IV. CONCLUSION

There are various categories in wireless networks like sensor network, Ad hoc, WLAN networks. Jamming creates a very bad impact on any of these wireless networks. Specifically, if Selective Jamming is done, the impact is even more serious. Selective jamming is treated as an internal threat model, so it would be difficult to detect it for a normal sender node or receiver node. Here, we have proposed a solution to identify the exact node that is performing selective jamming attack, by initially checking the existence of selective jammer between specific sender and receiver node. Finally, we have given three novel methods to prevent selective jamming by ensuring privacy of the transmitted message.

REFERENCES

[1] B. Potter. Wireless security's future. IEEE Security Privacy Magazine, 1(4):68-72, 2003.
[2] Y. Hu, A. Perrig, and D. Johnson. Ariadne: A secure On-demand routing protocol for ad hoc networks. In 8th ACM International Conference on Mobile Computing andNetworking, pages 12{23, September 2002.
[3] Y. Hu, A. Perrig, and D. Johnson. Packet leashes: a defense against wormhole attacks in wireless networks. In Proceedings of IEEE Infocom 2003, pages 1976-1986, 2003.
[4] Wenyuan Xu, Wade Trappe, Yanyong Zhang andTimothy Wood, The Feasibility of launching andDetecting Jamming Attacks in Wireless Networks, MobiHoc‟ 05, May 25–27, 2005.
[5] K. Pelechrinis, M. Iliofotou, and S. V. Krishnamurthy. Denial of service attacks in wireless networks: The case of jammers. IEEE Communications Surveys & Tutorials, PP(99):1–13, second quarter 2011.
[6] K. Fazel and S. Kaiser, Multi-Carrier and Spread SpectrumSystems.Wiley, 2003.
[7] Alejandro Proano and Loukas Lazos,Packet-Hiding Methods for Preventing SeleJamming Attacks, IEEE Transactions 2012 on dependable and secure computing, vlo.9, N0.1, 2012
[8] D.Thuente and M.Acharya. Intelligent jamming in wireless networks with applications to 802.11b and other networks. In proceedings of the IEEE Military Communications Conference MILCOM, 2006.
[9] T. X. Brown, J. E. James, and A. Sethi. jamming and sensing of encrypted wireless adhoc networks.In proceedings of MobiHoc, pages 120-130 ,2006
[10] M. Wilhelm, I. Martinovic, J. Schmitt and V. Lenders. Reactive jamming in wireless networks: How realistic is the threat? In proceedings of Wi Sec, 2011.

Effect of SC5D Additive on the Performance and Emission Characteristics of CI Engine

[1]Samarjeet Bagri, [2]Dr. Alok Chaube
[1, 2]Department of Mechanical Engineering, Jabalpur Engineering College, Jabalpur M.P. INDIA

ABSTRACT: *In this experimental work polymer based additive are mixed in different proportions with diesel fuel. Their emissions and performance results are compared with base fuel diesel. By mixing of this additive, it is observed that cetane index number is increased from 46.22 as of base fuel to 47.63, 49.40, 51.91, 54.91 and 60.66 respectively. The tests conducted at full load and varying speed conditions. The results show that HC, CO& NO_X emissions are reduced by 35%, 30% & 4% respectively. Brake power is increased 6% whereas brake specific fuel consumption and smoke density are decreased by 23% and 35%. Here we also observed that, when cetane index number is increases from 54.91 to 60.66 the engine performance and emission characteristics are not effective.*

Keywords: *Engine performance, Emission, Fuel properties, SC5D additive, Diesel engine.*

I. INTRODUCTION

Today improvement of fuel quality is major challenge to reduce engine emission to protect environment. The additives play effective role to counter this problem without engine modification. The diesel engine provides better fuel economy and high power output compared with the gasoline engine. Z.H. Huang [a *]et al. [1], studied the combustion characteristics and heat release for different proportions of mixing DMM (Dimethoxy methane) in diesel fuel and found satisfactory results on emission reduction. Ruijun Zhu[a,b] et al. [2], Studied regulated and unregulated emissions from diesel engine blended fuel with diethyl adipate, showed using this additive cleaner combustion is achieved. Xiangang Wang[a] et al. [3], investigated the blends of diesel-ethanol, diesel-biodiesel and diesel-DGM (diethylene glycol dimethyl ether) or named as diglyme and found that using ethanol blended fuels HC, CO, NO_X and NO_2 emissions are increases but DGM blended fuels reduces HC,CO NO_X and NO_2 emission. PM emission is also reduces by using DGM as compare to diesel. By using biodiesel blended fuels noted that the HC, CO, NO_X, and NO_2 emissions, lies between ethanol and DGM blended fuels. Ruijun Zhu [a] et al. [4], studied the combustion and emission characteristics of CI engine by using DMM blends and got satisfactory reduction of HC, CO, NO_X, smoke and PM emission. W.M. Yang[*] et al. [5], Has used nano-organic additives and investigated that when engine speed increases the HC, CO and NO_X emissions reduces. Wang Ying[a,*]et al.[6], Mixing oxygenated DME (dimethyl ether) in diesel fuel and studied the engine performance and emission characteristics of CI engine. He observed that by mixing DME in diesel fuel, the cetane number increase as compare to pure diesel. The result showed that engine performance increases and emission characteristics reduce. F.K. Forson et al. [7], Investigated the engine performance of diesel engine by using jatropha oil blends. Here it is noted that pure jotropha, pure diesel and jatropha plus diesel oil given same results under different operating conditions, but mixing of jatropha oil in diesel fuel the exhaust gas temperature is reduced. Yakup Icingur et al. [8], Investigated the engine performance and emission characteristics of diesel engine by using different fuel cetane numbers. He observed that using different cetane numbers of fuel NO_X, SO_2, emission are reduces at different speed.
Here the previous study shows that additive play effective role in increasing mechanical efficiency and reduction emission.

II. OBJECTIVE

The objective of present study to carry at experimental analysis, to evaluate effect of SC5D additive on diesel engine. The SC5D additive compare to other additives cost wise very cheap as well as quality like mileage, performance, power, reliability and going to turn your simple diesel to SUPER DIESEL. The additive manufactured by sumafine chemicals ltd pune. The company tested diesel cetane index and smoke density in CIRT PUNE with SC5D additive and compare these results with pure diesel. Here it is noted that by adding this additive, the cetane index increases and smoke density reduces. But we used this additive in different proportion of diesel and calculate engine performance as well as emission characteristics and their results compare with pure diesel.

The physical and chemical properties of SC5D additive as follows:-

Appearance: Liquid, Color: Radish yellow liquid, Odor: Aromatic, Starts to Boil: 180^{0}c (1.03mbar) Method DIN 51751, Flash Point: Approx 30^{0}c, Ignition Temperature: Approx 210^{0}c Lower Explosion Limit: 0.9% (v), Upper Explosion Limit: 7% (v) method 51649, Vapor Pressure: Approx 3.9 mbar method 51649, Vapor Pressure: Approx 3.9 mbar (20^{0}c) method DIN 51754, Density: (29^{0}c) 0.795, Solubility in Water: Insoluble (20^{0}c), Solubility /Qualitative: Soluble in hydrocarbons.

EXPERIMENTAL SETUP AND FUEL PROPERTIES:-

The experimental work is conducted on single cylinder, water cooled, two stroke, direct injection, Textool Diesel Engine. A rope brake dynamometer is used to load the engine at maximum load of 50kg and maximum spring balance reading is 20kg which is attached to the dynamometer. Experiments were performed under full load and varying speed conditions. The schematic diagram of engine test bed is shown in fig.1. Speed of the engine shaft is measured by hand held tachometer. Flow rate was measured on the volume basis using a burette and stopwatch. The fuel from the tank is sent to the engine through a graduated burette using a two way valve. When the valve is set at position 1 the fuel is sent to the engine directly and in position 2 the fuel contained in the burette is sent to the engine. For the measurement of the fuel flow rate of the engine the valve is set at position 2 and the time for a definite quantity of the fuel flow is noted. An AVL exhaust gas analyzer and smoke meter are used to measure exhaust emission and smoke density respectively. Here fuel cetane index no. 46.22, 47.63, 49.40, 51.91, 54.91 and 60.66 respectively are tested. Increase in cetane number effect the combustion process and to short the ignition delay. The cetane number is increased by the paraffinic hydrocarbon in the fuel. The properties of fuel such as viscosity, volatility flash point is also affects the proper combustion process. Viscosity affects atomization and vaporization of the fuel and the volatility ensures good mixing of fuel to air [6].

Table 1
Fuel properties of pure diesel and mixing with additive used for experimental analysis.

S. no.	Fuel type	Density (@15^{0}C kg/m^3)	Degree of API gravity	Aniline point (^{0}C)	Flash point (^{0}C)	Cetane Index
1.	D_0 (Pure diesel)	835.13	36.80	52	56	46.22
2.	D_1 (1000:1)ml.	834.76	36.87	54	57	47.63
3.	D_2 (1500:2)	833.15	37.20	56	59	49.40
4.	D_3 (2000:3)	832.2	37.40	59	61	51.68
5.	D_4 (2500:5)	830.3	37.77	63	64	54.91
6.	D_5 (3000:7)	816.13	40.71	65	65	60.66

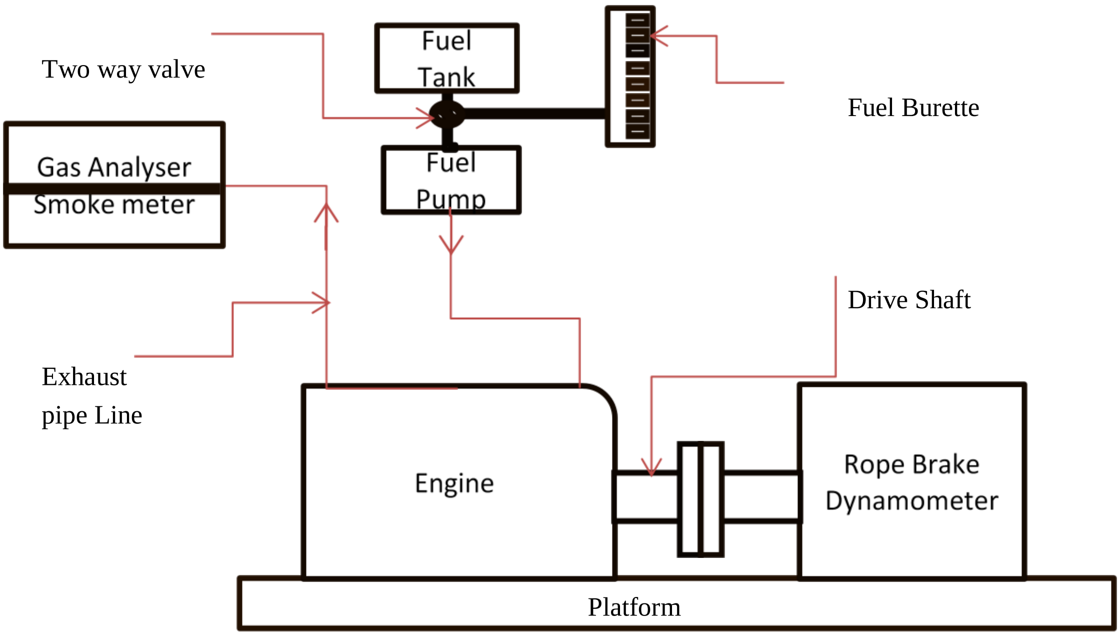

Fig1. Schematic block diagram of experimental setup.

EXPERIMENAL PROCEDURE:

The engine tests were conducted at different engine speed and full load conditions. After stable operating conditions were experiments are achieved, the engines were subjected to same load condition. The engine was stabilized before taking all measurements at constant static injection timing. An attempt was made to conduct all experiments without significant fluctuations to prevent possible discrepancies in engine operation during the tests and mainly, to avoid variations in engine loading. The experimental procedure consisted of the following three steps:

1. Initially engine tests using the base reference diesel fuel were conducted at full load condition to determine engine performance and emission characteristics of the engine base line operations.
2. The previous procedure was repeated at the same operating conditions with the engine fueled consecutively with fuels of different additives.
3. Taking the mean value by repeating the measurements at each operating conditions.

III. RESULTS AND DISCUSSION

The performance and emission characteristics of diesel fuel with additive and pure diesel are tested and compared at different speeds and full load condition. The results are shown in fig. 2-7. The brake power (BP) increases and brake specific fuel consumption (BSFC) reduces with respect to cetane index. We noted that the cetane index no. is increases from 46.22 to 54.91, brake power increases and brake specific fuel consumption reduces linearly in all speeds, 300, 500 and 700 rpm. The maximum reduction is obtained at 700 rpm. If the cetane index no. increases from 54.91 to 60.66 the results are not effective as shown in fig 2 and 3. Fig. 4-5 shows the effect of cetane index on HC and CO emission. It can be seen that the cetane index no. increases from 46.22 to 54.91 the HC and CO emission reduces at all engine speed. Here we also noted that the HC and CO reduces maximum at 700 rpm. The variation shows that the additive mix diesel as compare to pure diesel is very effective to improve the engine performance and decrease the emissions. The cetane index no. increase from 54.91 to 60.66, the results are not effective. Fig. 6 and 7 shows the effect of cetane index on NO_X emission and smoke density at engine speed, 300, 500 and 700 rpm. Here we noted that when engine speed is increases the NO_X emission and smoke density reduces with respect to cetane index. The maximum reduction of NO_X is obtained at 500 rpm and smoke density at 700 rpm. The results are not effective when cetane index no. increases from 54.91 to 60.66. Here we observed that by adding additive the combustion process is completed very smoothly and shorter the ignition delays. We compare all additive mix diesel and pure diesel results. Here we noted that the additive mix diesel is most beneficial to environmental protection as compare to pure diesel. The observation of different test results are plotted as following:-

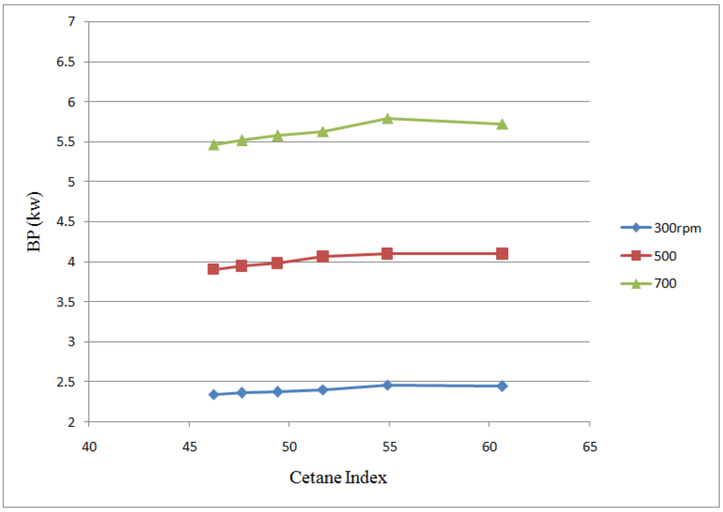

Fig.2. Effects of Cetane Index on BP (at full load)

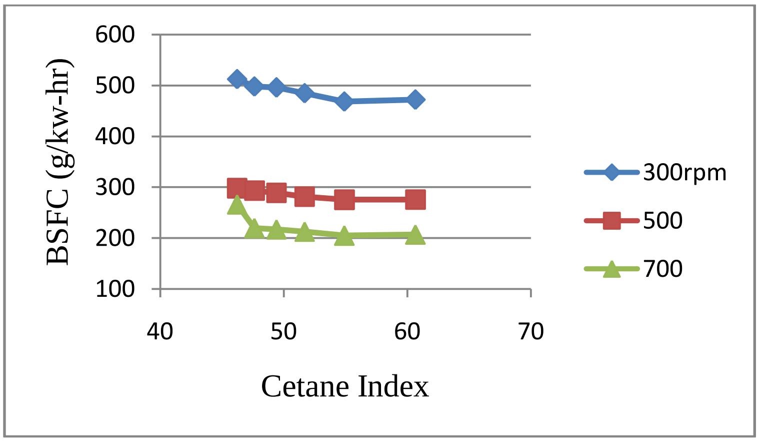

Fig.3. Effects of Cetane Index on BSFC (at full load)

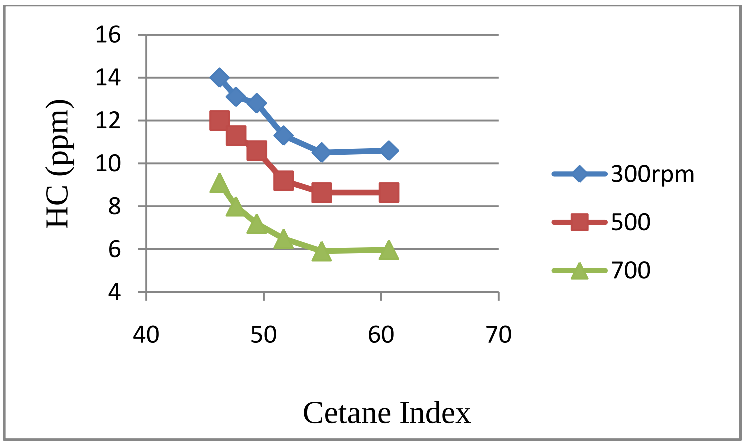

Fig.4.Effects of Cetane Index on HC emission (at full load)

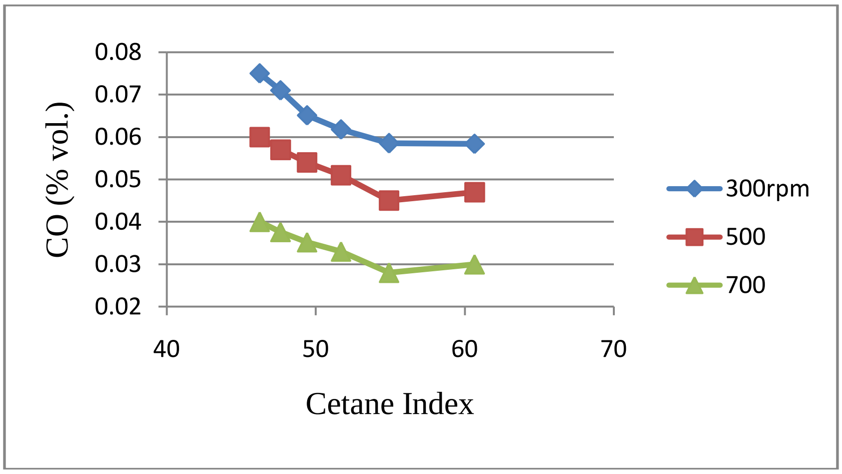

Fig.5.Effects of Cetane Index on CO emission (at full load)

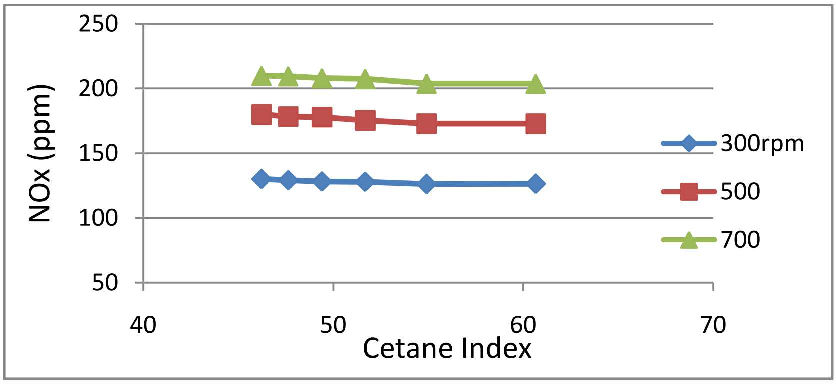

Fig.6.Effects Cetane Index on NO_X emission (at full load)

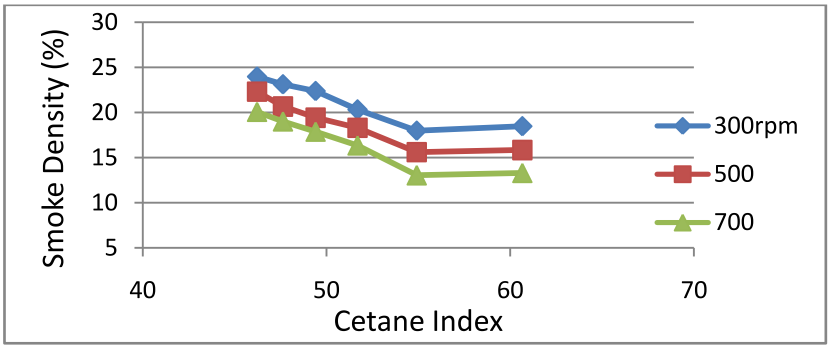

Fig.7.Effects of Cetane Index on Smoke Density (at full load)

IV. CONCLUSION

The experimental investigation of engine performance and emission characteristics is conducted in direct- injection single cylinder water-cooled two-stroke textool diesel engine and test results shows the following conclusions:

1. Test results show that when increasing cetane index number 46.22 to 54.91 the engine performance and emission is reduces at varying speed and full load condition.
2. By using additive HC, CO% &NO_X emission reduces 35%, 30% & 4% respectively as compare to pure diesel.
3. The smoke density is decreased by 35 %.
4. The brake power increases 6% and brake specific fuel consumption is reduces 23%.
5. When cetane index number is increases from 54.91 to 60.66 the results are not effective.

ACKNOWLEDGEMENT

Authors acknowledge the immense help received from the scholars whose articles are cited and included in reference of this manuscript. The authors are also grateful to authors/editors/publishers of all those articles, journals and books from where the literature for this article has been reviewed and discussed.

REFERENCES

[1] Z.H. Huang [a,*], Y. Ren[a], D.M. Jiang [b], L.X. Liu [b], K. Zeng [b], B. Liu [b], X.B. Wang [b]. Combustion and emission characteristics of a compression ignition engine fuelled with Diesel–dimethoxy methane blends. Energy Conversion and Management 47 (2006) 1402–1415.

[2] Ruijun Zhu [a, b], C.S. Cheung [b,*], Zuohua Huang [a], Xibin Wang [a]. Regulated and unregulated emissions from a diesel engine fueled with diesel fuel blended with diethyl adipate. Atmospheric Environment 45 (2011) 2174-2181.

[3] Xiangang Wang [a], C.S. Cheung [b], Yage Di [a, b], Zuohua Huang [a,*]. Diesel engine gaseous and particle emissions fueled with diesel–oxygenate blends. Fuel 94 (2012) 317–323.

[4] Ruijun Zhu [a], Haiyan Miao [b,*], Xibin Wang [a], Zuohua Huang [a]. Effects of fuel constituents and injection timing on combustion and emission characteristics of a compression-ignition engine fueled with diesel-DMM blends Proceedings of the Combustion Institute 34 (2013) 3013–3020.

[5] W.M. Yang[*], H. An, S.K. Chou, S. Vedharaji, R. Vallinagam, M. Balaji, F.E.A. Mohammad, K.J.E. Chua. Emulsion fuel with novel nano-organic additives for diesel engine application. Fuel xxx (2012) xxx–xxx.

[6] Wang Ying [a,*], Zhou Longbao [a], Wang Hewu[a, b]. Diesel emission improvements by the use of oxygenated DME /diesel blends fuel. http:/www.paper.edu.cn

[7] F.K. Forson[*], E.K. Oduro, E. Hammond-Donkoh. Performance of jatropha oil blends in a diesel engine. Renewable Energy 29 (2004) 1135–1145.

[8] Yakup Icingur *, Duran Altiparmak. Effect of fuel cetane number and injection pressure on a DI Diesel engine performance and emissions Energy Conversion and Management 44 (2003) 389–397.

Efficient Energy Management System with Solar Energy

P. Nagalaxmi[1], M. Veda Chary[2]
[1]II Year M. Tech (Embedded Systems), [2]Associate Professor
Dept of ECE, CMR College of Engineering and Technology, Hyderabad, AP-India

ABSTRACT: *As decaying of fossil fuels and scarcity of electricity generating resources, an alternate methods for generating electricity are highlighted and these methods uses renewable sources like solar power, wind power, tidal energy and so on. Many research companies concentrate on the elemental technologies to generate the power but the energy generated from these resources is not sufficient as the growth of power demands and need efficient and intelligent distribution system to distribute the energy. The intelligent energy distribution management system is developed and the results of managing the distribution of energy which is generated from renewable resources are used effectively as presented and discussed.*

Keywords: *Efficient energy distribution system, power monitoring device, renewable source, solar panel, Zigbee.*

I. INTRODUCTION

An increasing Global warming, currently occurring on this 4.6 billion years old earth, is a very critical issue to be addressed by the modern society that has been enjoying economical growth by consumption of fossil energies Since the Industrial Revolution in Great Britain, much carbon dioxide (CO2) has been emitted as a result of the combustion of petroleum and coal. In the past 200 years, the carbon dioxide concentration in the atmosphere has increased by as much as 25%. Now the entire earth is, so to speak, situ three of the most prominent issues facing the world today are escalating climate change, energy security and meeting the increasing global demand for electrical energy generated from renewable sources.

The renewable energy is growing technology for meeting the demands of energy consumption to solve the problems of fossil fuels and at the same time reduce the pollution in the atmosphere. In case of fossil fuels once it is used that can't regenerated means it is converted into electricity and is used by consumers. Where as in case of renewable sources the energy generated is unlimited. Hence the importance of renewable energy is becoming a great technology and today the world seeing to develop these technologies.

Now a day many companies are seeing that to increase the efforts on development of renewable sources by constructing smart grids having sustainable growth and connecting those smart grids to the commercial electricity grids. The renewable energy sources are of different forms like solar, wind, tidal ect. But the problems with this technology are that the energy generated from renewable sources may vary with time and climatic conditions, means these generate indefinite amount of energy but hard expect the constant generation [1].

In this paper, introduced an efficient energy distribution system to distribute the energy generated from the renewable sources [2]. In order to meet the current problems the energy generated from the renewable sources to maintain it constant, it was connected to a battery and inverter. In this research we have implemented a prototype system for the ideas. The preliminary tests show that this approach is promising for real applications. A case study on the basis of the California residential-sector shows that at 10% penetration levels for households with a 4-kW solar PV panel with a 0.5-kW.h battery, the daily systems cost savings per household could be over $5 a day in August[3].

In section II related work in renewable source technologies were discussed. Proposed efficient distribution system is mentioned in section III. Implementation of the system is then presented in section IV. Experiment results are placed in section V. Finally a brief conclusion and future work are given in section VI.

II. RELATEDWORK

Renewable sources are also called Echo friendly technologies are very important due to their pollution free energy generation and having sustainable growth. There are many sources of energy that are renewable and considered to be environmentally friendly and harmless natural processes [4]. These sources of energy provide an alternate 'cleaner' source of energy, helping to negate the effects of certain forms of pollution. All of these power generation techniques can be described as renewable since they are not depleting any resource to create the energy. While there are many large-scale renewable energy projects and production, renewable technologies are also suited to small off-grid applications, sometimes in rural and remote areas, where energy is often crucial in human development.

But the disadvantage with the renewable sources is that their power generation varies with climatic condition and hourly based. To store this unsteady generated energy from renewable sources required a huge, efficient battery and inverter [5], and these are necessary to connect to the power grid. In case of solar power systems variation in the power generation is largely depends on weather and season. Hence every renewable energy system requires storage systems. However the storage systems also have some limitations in the point of installation and return of investment. So to avoid this, in this paper we propose a management system that effectively distributes the energy generated from renewable sources and maximize the efficiency.

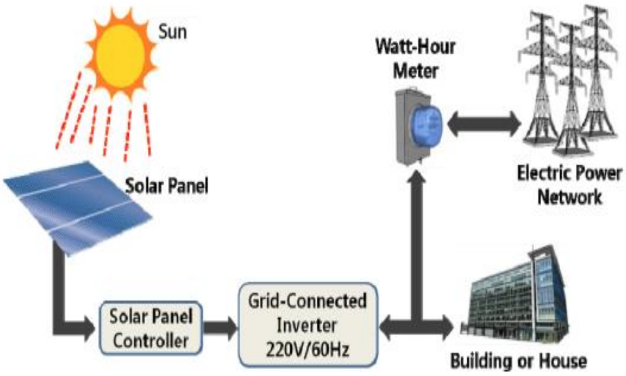

Fig.1.Structure of general renewable energy system

In this paper, we propose an efficient distribution management system, the combination of elemental technologies of renewable sources with commercial electricity maximize the efficiency.

III. INTELLIGENT SYSTEM

Intelligent energy distribution system is the most important in order to determine how effectively the power generated from renewable sources are distributed. The system decides when to use the energy stored in the battery, that is whenever the power generated from the commercial electricity grid is very low then the switching action takes place, switches to the solar grid. If the energy generated from the solar panel is sufficient then power supplied as usual as the commercial grid otherwise controlling action takes place. The energy stored in the battery is always compared with the preset levels and if it is low then it communicates with control room to take necessary steps. According to the energy levels in the stored battery the controlling of devices takes place.

If the energy level is below the first preset level then the power that goes to the least priority devices are automatically shut off and the high priority devices are run and if the energy is below that then the next priority devices are shut off and allows to run only the highest priority devices giving a signal to take the necessary actions.

The power monitoring device has three power sockets to measure the power consumption of devices and Zigbee network module, that can transmit the status of the battery and receives the control signals to control the power through the devices. Fig.2 shows the basic block diagram for intelligent and efficient distribution system consisting of microcontroller unit, relay control unit; Zigbee communication; user interface, power sensing unit (energy meter) and power supply exist in the system. The energy meter measure the power consumption, consisting of a CT sensor converted to a current value which can handled in the MCU. The renewable energy management system manages the generated power and battery charging conditions in the solar power generator. The power management methods are of two types, efficiency oriented and user oriented. In the efficient method the generated power and the battery charging conditions are transmitted to the smart power management system and it is compared with the power consumption data stored in the MCU. But the problem with this technique is that it finds only the optimal time to use the charging battery for decreasing power consumption and electric charges.

In this paper we proposed a user oriented method to run the devices by setting the priorities and run the device having highest priority for a long time compared to the devices having least priority, which increases the efficiency in the point of user. The block diagram in fig.2 having three sockets is nothing but three loads. The intelligent system efficiently distributes the power generated from the solar panel to these prioritized loads depending upon the status of the battery.

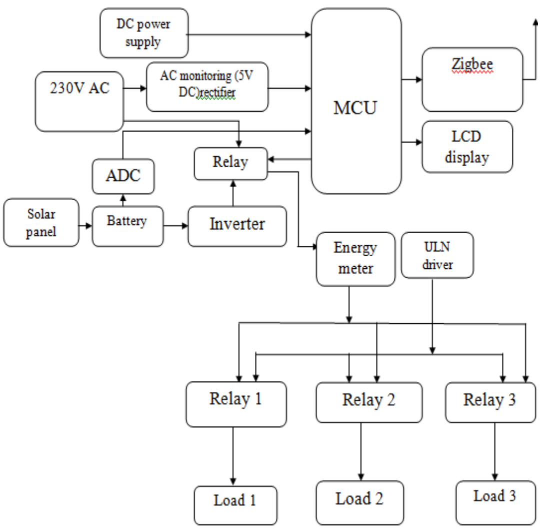

Fig.2 Hardware architecture of intelligent distribution system

IV. IMPLEMENTATION

In the previous section we describe the efficient intelligent energy distribution system. Now we can see how to implement this system, when the electricity generated from the thermal plants is enough then it is connected to the connected to the energy meter through the power grid network, otherwise when the this electricity is not available then the energy generated from the solar panel is connected to the energy meter trough the grid inverter and distributed to the devices according to the prioritization which increases the efficiency of the solar power. Always the power requires is compared with the stored value
in the battery and generates the control signals according to conditions specified.

As the consumption of power increases, the energy stored in the battery decreases causes that no longer the devices operate with the solar energy. In order to increase the efficiency of the solar system it is required to distribute the energy intelligently, sends a control signal from the control room to turn off the least priority devices and keep on monitoring the battery status. If the battery value reaches the threshold value which is set for safe operation runs only the highest priority device making all remaining devices turn off.

Fig.3 shows the efficient distribution system that distributes the power generated from the solar panel. To make the switching action between commercial electricity and solar power a relay is placed. To monitor the electricity from power grid network, 5v input is given to the MCU whenever the monitor pin reads 0V then relay connects the solar system to the energy meter and it displayed on the LCD display and on the PC in control room. Zigbee provides the communication between the control station and distribution system. The control commands are given remotely to control power going to the devices depending on the battery status.


Figure 3: Efficient Distribution System

The algorithm is as follows:

Step1: Initialization of devices.
Step2: Initially both AC and Inverter sections are in ON condition.
Step3: Devices are run with AC power
Step4: In microcontroller one pin is programmed to monitor the AC power, when it is goes off, the relay is connected to the inverter.
Step5: Now the solar energy is connected to the meter
Step6: In micro controller the stored energy is always compared with presetting levels
Step7: If the stored energy is greater than the power Consumption then the least priority device is automatically turn off.
Step8: Otherwise highest priority load will run by turning off other loads.
Step9: Whenever the AC power is available then the relay connects it to the energy meter.
Step10: Stop the process.

V. EXPERIMENT RESULTS

The results shows that, when the power from both power plant and solar system are present then the efficient distribution system connects the energy meter to power line generated from power plant and runs all the devices. Otherwise the remote control station sends the command signal to connect the solar system to the energy meter and compares the battery status continuously to run the prioritized devices.

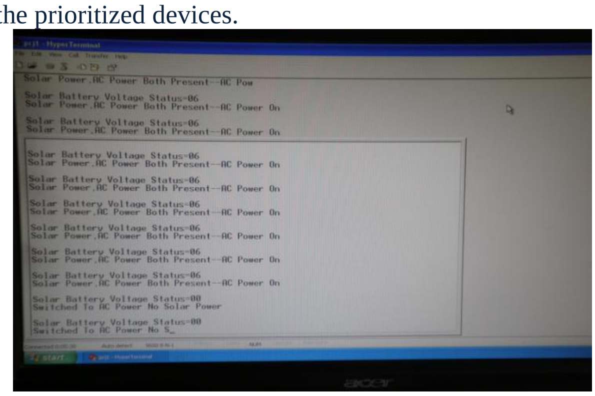

Figure 4: Controlling from remote station

Control station that is remotely located, communicates with the efficient system through the Zigbee and it displays the results like on PC like, when AC power and Solar power present AC power ON, Otherwise AC power off and solar power present and also display the voltage in the inverter. According to the battery status it operates the loads given in the following table in this for demo purpose three loads are considered.

Battery status	**Loads condition**
Between 12V-10V	Three loads are run
Between 10V-08V	Load -3 turn off(least priority device)
Between 08V-06V	Load-1 only ON(highest priority),turns off reaming devices
Below 6V	Along with running the highest priority device gives an alert signal

Table 1: Load Distribution

VI. CONCLUSION

In this paper we proposed a system to distribute the power generated from renewable sources efficiently. By increasing the capacity of solar panel and efficiency of the battery it is possible to construct a solar grid parallel to the commercial grid which solves the problems of electricity in future and it can be distributed effectively to the rural and urban areas which solves the problems of electricity. But the problem with this system is that to require huge inverter to store the largely variable solar energy and its maintenance. This can be overcome by constructing solar grids parallel to the existed grids by the government.

REFERENCES

[1] M.M.Amin and O.A. Mohammed,” development of high performance Grid connected wind energy conversion systems for optimum utilization of variable speed wind Turbines” *Sustainable energy. IEEE transaction on, vol 2, pp 235-245, 2011*

[2] M.B .Nisssen” high performance development of distribution generation”. *Potentials, IEEE, vol 28, pp 25-31, 2009.*

[3] Huang, S., Xiao, J., Pekny, J., Reklaitis, G., and Liu, A. (2012). ”Quantifying System-Level Benefits from Distributed Solar and Energy Storage.” J. Energy Eng., 138(2), 33–42.

[4] J. Lee, B. Han and K.Chol, “High efficiency grid tied power conducting system for fuel cell power generation,” *power electronics and ECE asia (ICPE&ECCE),2011 IEEE 8th international conference on 2011,pp,1492-1497.*

[5] A.O. Converse, “Seasonal energy storage in a renewable energy system “*proceedings of IEEE, vol.100, pp.401-409, 2012.*

Bibliography:

P. Nagalaxmi, received her B. Tech degree in Electronics & Communication Engineering from JNTU, Hyderabad, currently pursuing M. Tech in Embedded systems from JNTU Hyderabad

M. Veda Chary received his M. Tech degree in Electronics & Communication Engineering from JNTU, Hyderabad, currently working as an Associate Professor, ECE in CMR College of Engineering & Technology, Hyderabad.

International Journal of Modern Engineering Research (IJMER)
www.ijmer.com Vol. 3, Issue. 5, Sep - Oct. 2013 pp-2840-2847 ISSN: 2249-6645

SISO MMSE-PIC detector in MIMO-OFDM systems

A. Bensaad[1], Z. Bensaad[2], B. Soudini[3], A. Beloufa[4]
[1234]*Applied Materials Laboratory, Centre de Recherches (ex-CFTE), University of Sidi Bel Abbès, 22000 Sidi Bel Abbès, Algeria*

ABSTRACT: *MIMO-OFDM with bit-interleaved coded modulation (BICM) is an attractive technique for wireless communications over frequency selective fading channels which has gained significant interests as a promising candidate for the 4th Generation wireless communication. The SISO MMSE-PIC based detector is proposed in this paper. The SISO MMSE-PIC detector exchanges soft information with SISO channel decoder through iterative process. For reduction complexity, the Max Log MAP approximations decoder is exploited for iterative BICM decoding of MIMO-OFDM under perfect channel knowledge. Simulation results in the IEEE 802.11 channel model show that the SISO MMSE-PIC iterative detector decoder leads to a clear improvement of the performance than the SISO ZF-PIC based detector with saturation at 4th iterations. For a large number of iterations, the performance improvement is not significant which could be investigated for practical reduction complexity considerations. Furthermore, for a* 10^{-2} *bit error rate BER target, the gain in the performance of the SISO MMSE-PIC is approximately about 3dB when the number of antennas is twice. The performance of the SISO MMSE-PIC under different modulation schemes for MIMO-OFDM systems shows that with lower modulation size, the method can perform better and decreases when the channel delay spreads is increased.*

Keywords: *BICM, IEEE 802.11, MIMO iterative detection and decoding, MIMO-OFDM, SISO MMSE-PIC,.*

I. INTRODUCTION

The Multi-input multi-output orthogonal frequency-division multiplexing frequency-division multiplexing (MIMO-OFDM) has gained significant interests as a promising candidate for the 4th Generation (4G) wireless communication. It combines the capacity and diversity gain of MIMO systems with the equalization simplicity of Orthogonal Frequency Division Multiplexing (OFDM) modulation. A higher capacity with high bandwidth efficiency can be achieved over broadband multipath fading wireless channels [1, 2]. The use of multiple antennas at both the transmitter and receiver, which is usually referred to as MIMO communication, can yield large improvements in spectral efficiency and diversity compared to single systems, when using advanced signal processing and coding techniques. OFDM is a multicarrier transmission technique, which divides the available spectrum into many carriers; each one being modulated by a low data rate stream has been recently established for several systems such as American IEEE802.11, the European equivalent HiperLan/2, digital video and audio broadcasting.

MIMO-OFDM with bit-interleaved coded modulation (BICM) is a promising technique for wireless communications over frequency selective fading channels [3, 4]. Müller-Weinfurtner has demonstrated that for the multiple-input multiple-output (MIMO) system, BICM shows excellent performance in fast-fading channel when maximum likelihood (ML) detection is used [5]. However, as the complexity of ML detection is large, a low complexity solution based on Zero Forcing (ZF) and Minimum Mean Squared Error (MMSE) detection have been proposed. The BICM is incorporated in many modern wireless communication standards, such as IEEE 802.11n, IEEE 802.16m and 3rd Generation Partnership Project long term evolution (3GPP LTE) [6,7,8]. It was shown that the full potential of MIMO wireless systems can, in practice, only be achieved through iterative MIMO decoding [9].

In iterative MIMO detection and decoding method, a posteriori probability (APP) MIMO algorithm is the optimal way to calculate the probabilistic soft information of the inner coded bits expressed with Log-Likelihood Ratio (LLR) values [10]. The probabilistic soft information is then further processed in the outer channel decoder based on an optimal (Soft In Soft out) BCJR (MAP) algorithm and fed back to the inner detector [11]. The reliability information is exchanged between the two stages separated by a deinterleaver and an interleaver. However, the computational complexity of the optimum MIMO detection algorithm scales exponentially in the number of spatial streams. Various efficient MIMO-BICM soft detector algorithms providing approximate LLRs have been proposed. Existing approaches use the list extension of the Fincke-Phost Sphere Decoding (LFPSD) algorithm as well as algorithms based on Zero-Forcing (ZF) or Minimum Mean Squared Error (MMSE) equalization [12, 13, 14, 15]. The Jacobian logarithm and the so-called log-MAP algorithm reduces the complexity of the original symbol-by-symbol MAP algorithm [11]. A less complex max-log-MAP approximation can also be applied with rather small performance loss compared to the log-MAP [16]. A posteriori probability (APP) detection, optimal but exponentially complex, is usually replaced with Parallel Interference Cancellation (PIC) and Minimum Mean Square Error (MMSE) filtering. MMSE based “soft” successive interference cancellation [17], list sphere detection [18], and list sequential detection [19] are all known achieve performance close to the capacity limit of the MIMO channel while avoiding the prohibitive complexity of a full APP detector.

In this paper, we propose a combination of Parallel Interference Cancellation (PIC) detection with maximum a posteriori (MAP) decoding denoted by SISO MMSE PIC algorithm for MIMO-OFDM systems. The PIC technique applies a linear detector to obtain an initial estimate of the transmitted data layer based on the a priori LLRs obtained from the SISO

channel decoder. Each layer is then nulled with the estimate from other layers. The Interference Plus residual Noise (NPI) term is then equalized using a MMSE filter, followed by computation of per-stream a posteriori LLRs.
The remaining of the paper is organized as follows. In section II, the MIMO-OFDM system model is described. In section III, linear detection schemes, iterative detection and decoding and SISO MMSE Parallel Interference Cancelation (PIC) methods are introduced. Section IV is devoted to simulations and performance evaluation. Finally, Section V concludes the paper.

II. MIMO-OFDM SYSTEM MODEL

A MIMO-OFDM system model based on a bit-interleaved coded modulation (BICM) transmission strategy is depicted in Fig. 1. We consider a multiple antenna system with N_T transmit and N_R receive antennas ($N_R > N_T$). At the transmitter, a stream of information bits $\boldsymbol{d}$ is first encoded by an outer channel code with rare R and interleaved by a quasi-random interleaver. The resulting stream of coded and interleaved bits $\mathbf{b}$ is then de-multiplexed into N_T sub-streams $\mathbf{b} = [b_1(k), \dots, b_{N_T}(k)]^T$ and mapped to a sequence of N_T dimensional symbol vectors $\boldsymbol{s}(k)$. The entries of $\boldsymbol{s}(k)$ are drawn from a complex QAM (or MPSK) constellation Ω, where $|\Omega\,| = 2^Q$ and Q is the number of bits per symbol. The length of each symbol vector $\boldsymbol{s}(k) = [s_1(k), \dots, s_{N_T}(k)]^T$ is $N_T\,Q$, where $s_i(k)$ = Map $(b_{i,q}(k))$ is the q^{th} bit of the i^{th} entry of the symbol vector which takes its value from the QAM alphabet set $\Omega = \left[a_1, \dots, a_{2^Q}\right]$ and the bits $b_{i,q}$ are chosen from the set $\{+1, -1\}$ ($i = 1, \dots, N_T$ and $q = 1, \dots, Q$). Then, the modulated signals are passed through an IFFT operation and transmitted via N_T antennas.
The frequency-selective MIMO channel can be decomposed into parallel frequency at MIMO channels. For a MIMO-OFDM system with N_c subcarriers, the received signal for each subcarrier k can be written as:

$$\boldsymbol{r}(k) = \boldsymbol{H}(k)\boldsymbol{s}(k) + \boldsymbol{\eta}(k) \quad \text{for } 1 \le k \le N_c \tag{1}$$

Where $\boldsymbol{H}(k)$ is the $(N_R \times N_T)$ frequency domain channel matrix which is assumed to be perfectly known at the receiver, $\boldsymbol{r}(k)$ is the $(N_R \times 1)$ received signal vector and $\boldsymbol{\eta}(k)$ is a $(N_R \times 1)$ noise vector whose elements are zero mean independent identically distributed (i.i.d) circular symmetric complex Gaussian random variables with variance N_0 observed at the N_R receive antennas.
The channel coefficients of $\boldsymbol{H}(k)$ for each sub-carrier k are given by the discrete Fourier transform of the channel impulse responses $h_l^{i,j}(k)$ as:

$$\boldsymbol{H}^{i,j}(k) = \sum_{l=0}^{L-1} h_l^{i,j}(k) e^{-j2\pi kl/N_c} \tag{2}$$

The maximum multipath delay length is equal to L and the length of the Cyclic Prefix N_{cp} is assumed to be long enough to eliminate the inter-symbol interference. In the receiver, the symbols are transformed into frequency domain with the FFT. The soft detector provides soft output LLRs for the decoder.

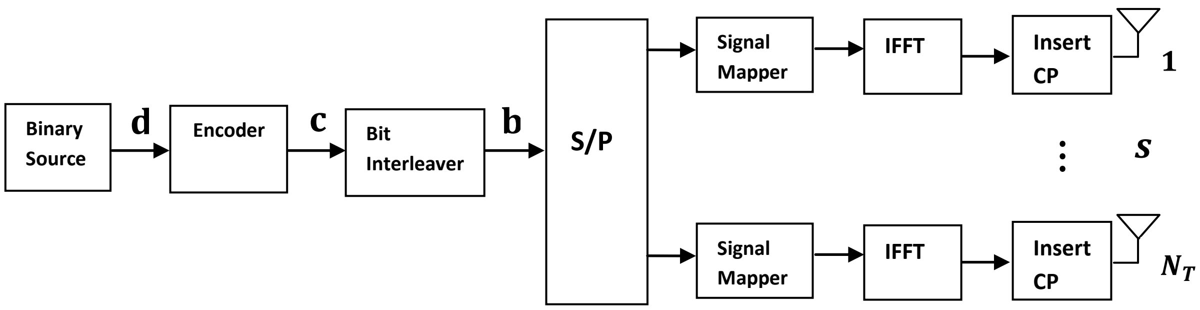

Fig. 1. Block diagram of MIMO OFDM transmission

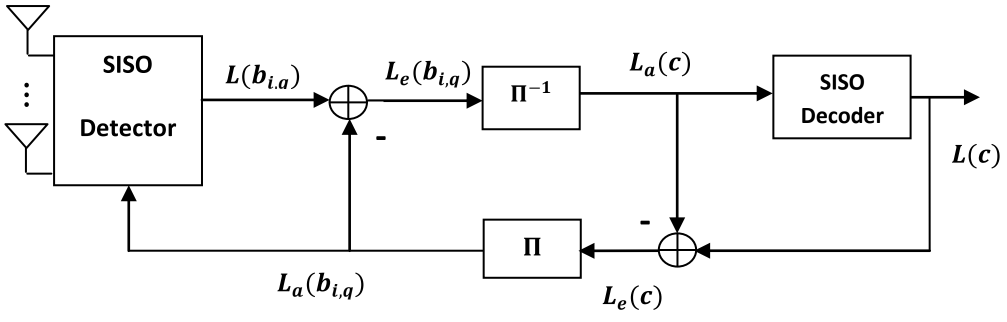

Fig. 2. MIMO iterative receiver scheme

III. LINEAR DETECTION SCHEME

In linear detection such as Zero forcing (ZF) and Minimum Mean Squared Error (MMSE), the receiver symbol vector $\boldsymbol{r}$ is multiplied with a linear filter:

1. **ZF:** $\tilde{\boldsymbol{s}} = \boldsymbol{G}_{ZF}\boldsymbol{r} = (\boldsymbol{H}^H\boldsymbol{H})^{-1}\boldsymbol{H}^H\,\boldsymbol{r} = \boldsymbol{s} + \tilde{\eta}_{ZF}$ (3)
2. **MMSE:** $\tilde{\boldsymbol{s}} = \boldsymbol{G}_{MMSE}\boldsymbol{r} = \left(\boldsymbol{H}^H\boldsymbol{H} + \frac{N_T}{\rho}\boldsymbol{I}_{N_T}\right)^{-1}\boldsymbol{H}^H\,\boldsymbol{r} = \boldsymbol{s} + \tilde{\eta}_{MMSE}$ (4)

Where ρ is the Signal to Noise Ratio (SNR).

III.1. Iterative detection and decoding

In Iterative MIMO decoding, the SISO detector has to generate reliability information, or "soft output", for each of the coded bits $b_{i,q}(k)$ in the symbol vector $\boldsymbol{S}(k)$. Fig. 2 depicts the iterative receiver structure based on the turbo-processing principle [9]. At each iteration, the soft output detector updates and delivers to the channel decoder the extrinsic information for each coded bit. The detector calculates a posteriori soft output values $L(b_{i,q})$ using the a priori information $L_a(b_{i,q})$. The contribution of the a priori information is subtracted from $L(b_{i,q})$ to obtain the extrinsic information $L_e(b_{i,q})$ as:

$$L_e\left(b_{i,q}\right) = L\left(b_{i,q}\right) - L_a\left(b_{i,q}\right) \tag{5}$$

The soft input soft output (SISO) decoder uses the de-interleaved $L_e(b_{i,q})$ as a priori information $L_a(c)$ to produce the a posteriori values $L(c)$. The extrinsic information $L_e(c)$ is again obtained by subtracting the a priori values from the a posteriori values. The interleaved $L_e(c)$ can then be used as a priori information for the detector. This iterative process continues until convergence is achieved.

The a posteriori LLR for each coded bit can be written as:

$$L(b_{i,q}) = \frac{P[b_{i,q}=+1|\hat{Y}]}{P[b_{i,q}=-1|\hat{Y}]} \tag{6}$$

III.2. SISO MMSE Parallel Interference Cancellation (PIC) detector

In Parallel Interference Cancellation (PIC) detector, a single layer is detected and the corresponding contribution to the received vector is subtracted; the other layers that have not been detected yet are equalized using a ZF or MMSE equalizer. The i^{th} interference-canceled received vector is given by:

$$\widehat{\boldsymbol{Y}}_i = \boldsymbol{Y} - \sum_{j=1, j\neq i}^{N_T} \boldsymbol{h}_j\,\hat{s}_j = \boldsymbol{h}_i s_i + \widetilde{w}_i \tag{7}$$

Where $\widetilde{w}_i$ is the Interference terms plus the residual Noise (NPI).

First, the SISO MMSE-PIC algorithm compute estimates $\hat{s}_i$ of the transmitted symbols s_i using a linear filter whose coefficients are given by the a priori LLRs $L_a(b_{i,q})$ obtained from the SISO channel decoder. These estimates are used to cancel interference in the received vector. The soft symbols estimates $\hat{s}_i$ are calculated as [20, 21, 22]:

$$\hat{s}_i = \mathbb{E}[s_i] = \sum_{a\in\Omega} P[s_i = a].a \quad \text{for } i = 1, \dots, N_T \tag{8}$$

Where the a-priori probability of the symbol can be easily derived due to the independence of the bits $b_{i,q}$:

$$P[s_i = a] = \prod_{q=1}^{Q} P\left[b_{i,q} = [a]_q\right] \tag{9}$$

$$= \frac{1}{2^Q}\prod_{q=1}^{Q}\left(1 + \tilde{b}_{i,q}\tanh\left(\frac{L_a(b_{i,q})}{2}\right)\right) \tag{10}$$

Where the a priori LLR's $L_a\left(b_{i,q}\right)$ are given by:

$$L_a(b_{i,q}) = \frac{P[b_{i,q}=+1]}{P[b_{i,q}=-1]} \tag{11}$$

With,

$$P[b_{i,q} = \mp 1] = \frac{\exp\left(\mp\frac{1}{2}L_a\left(b_{i,q}\right)\right)}{\exp\left(\frac{1}{2}L_a\left(b_{i,q}\right)\right) + \exp\left(-\frac{1}{2}L_a\left(b_{i,q}\right)\right)} \tag{12}$$

$[.]_q$: denotes to the q^{th} bit associated with the symbol a and $\tilde{b}_{i,q} \in \{+1, -1\}$. The reliability of each soft symbol $\hat{s}_i$ is characterized by its variance:

$$\mathrm{Var}[s_i] = \mathbb{E}[|s_i - \hat{s}_i|^2] = \left(\sum_{a\in\Omega} P[s_i = a].|a|^2\right) - |\hat{s}_i|^2 \tag{13}$$

Next, In order to further suppress the terms plus the residual noise (NPI), a linear MMSE filter $\boldsymbol{G}_i$ is applied to $\widehat{\boldsymbol{Y}}_i$, to obtain:

$$\tilde{y}_i = \boldsymbol{G}_i^H \widehat{\boldsymbol{Y}}_i = \boldsymbol{G}_i^H \boldsymbol{h_i} s_i + \boldsymbol{G}_i^H \widetilde{w}_i = \tilde{\beta}_i s_i + \tilde{\eta}_i \tag{14}$$

Where the MMSE filter vectors $\boldsymbol{G}_i^H$ is chosen to minimize the mean squared error between the transmitted symbols at the i^{th} antenna and the filter vector $\widehat{\boldsymbol{Y}}_{\boldsymbol{i}}$ as:

$$\boldsymbol{G}_{i,MMSE}^H = \underset{G_{MMSE}^H \in \mathbb{C}^{N_T}}{\arg\ min}\ \mathbb{E}\left[\left\|\boldsymbol{G}_{MMSE}^H \widehat{\boldsymbol{Y}}_i - s_i\right\|^2\right] \tag{15}$$

The solution to this problem is derived in [20] and the MMSE filter vectors is expressed as:

$$\boldsymbol{G}_{i,MMSE}^H = \sigma_s^2 (\boldsymbol{H} e_i)^H (\boldsymbol{H} \Lambda_i \boldsymbol{H}^H + N_0 \boldsymbol{I})^{-1} \tag{16}$$

Where $\Lambda_i = \mathrm{cov}(s_i, s_i)$ is a $(N_T \times N_T)$ diagonal matrix having its elements the variance of the symbol s_i , e_i is a $(N_T \times 1)$ vector with all elements equal to 0 except the i^{th} element is equal to 1 and $\sigma_s^2 = \mathbb{E}[|s_i|^2]$ is the symbol energy.
It is shown in [20, 21] that the distribution of the Interference terms plus the residual Noise (NPI) at the output of a linear MMSE detector is well approximated by a Gaussian distribution. Finally, the resulting LLR's of coded bits $L(b_{i,q})$ are calculated according to the formula:

$$L(b_{i,q}) \approx \log \frac{\sum_{a \in \chi_{i,q}^{+1}} exp\left(\frac{-|\tilde{y}_i - \tilde{\beta}_i a|^2}{\tilde{\sigma}_i^2} - P[s_i = a]\right)}{\sum_{a \in \chi_{i,q}^{-1}} exp\left(\frac{-|\tilde{y}_i - \tilde{\beta}_i a|^2}{\tilde{\sigma}_i^2} - P[s_i = a]\right)} \tag{17}$$

Where $\chi_{i,q}^{-1}$ and $\chi_{i,q}^{+1}$ denotes the subset of symbol vectors that have the q^{th} bit in the label of the i^{th} symbol equal to -1 and +1, respectively. $\tilde{\beta}_i$ is the bias introduced by the equalizer and $\tilde{\sigma}_i^2$represents the total variance of the interference terms plus the residual noise, such that:

$$\tilde{\sigma}_i^2 = Var[y_i] = \boldsymbol{G}_i^H \left(\sum_{j \neq i} \sigma_j^2 \boldsymbol{h}_j \boldsymbol{h}_j^H + N_0 \boldsymbol{I}_{N_R}\right) \boldsymbol{G}_i \tag{18}$$

The complexity of the previous relation can be reduced by using the Logarithm Jacobian defined by:

$$\log(\exp(-x) + \exp(-y)) = -\min(x, y) + \log\big(1 + exp(-|x - y|)\big) \tag{19}$$

This can be approximated by:

$$\log(\exp(-x) + \exp(-y)) = min(x, y) \tag{20}$$

The resulting intrinsic LLRs are then computed as:

$$L(b_{i,q}) \approx \min_{a \in \chi_{i,q}^{-1}} \left\{\frac{-|\tilde{y}_i - \tilde{\beta}_i a|^2}{\tilde{\sigma}_i^2} - \sum_{q=1}^{Q} \frac{\tilde{b}_{i,q} L_a(b_{i,q})}{2}\right\} - \min_{a \in \chi_{i,q}^{+1}} \left\{\frac{-|\tilde{y}_i - \tilde{\beta}_i a|^2}{\tilde{\sigma}_i^2} - \sum_{q=1}^{Q} \frac{\tilde{b}_{i,q} L_a(b_{i,q})}{2}\right\} \tag{21}$$

Then, the extrinsic a posteriori LLRs of the SISO MMSE-PIC can be obtained by using the equation:

$$L_e(b_{i,q}) = L(b_{i,q}) - L_a(b_{i,q}) \tag{22}$$

IV. SIMULATION RESULTS

Consider a 4x4 BICM MIMO-OFDM system based on MMSE-PIC detector. Our simulations are based on the following system parameters. The frame size is 1000 information bits. The convolutional encoder of rate 1/2 is used with generator polynomials g0=133_8 and g1=171_8 . The coded bits are then interleaved by a pseudo-random permutation. The number of subcarriers is N=64 and the modulation is M-QAM. The outer decoder of the receiver used is an optimal (soft-in soft-out) BCJR (MAP) decoder. Perfect CSI at the receiver is assumed.

Fig. 3 shows the performance of iterative MIMO-OFDM decoding using the SISO MMSE –PIC based detector for various number of iterations. The IEEE 802.11 channel model with RMS delay spread of $25ns$ is used. As we can conclude, the iterative detector decoder leads to a clear improvement of the performance with saturation at 4th iterations. For a large number of iterations ($>$ four), the performance improvement is not significant which could be investigated for practical reduction complexity considerations. The gain in performance attains more than 6dB for 10^{-2} bit error rate BER with four iterations. Similar performance was observed with all modulation schemes. In Fig. 4, the BER versus SNR performance of the MMSE-PIC method is plotted for QPSK modulation. Fig. 5 quantitatively illustrates the performance improvement of MMSE detection compared with ZF method, in terms of SNR gain.

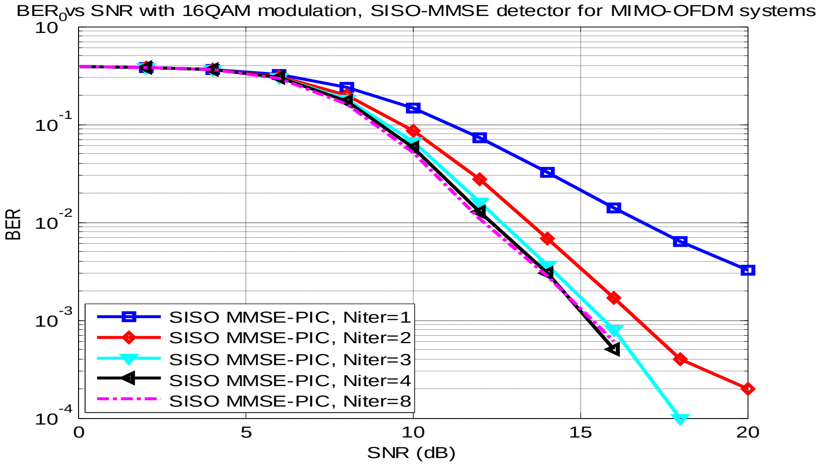

Fig. 3. BER vs. SNR performance of MIMO-OFDM systems based SISO MMSE-PIC detector with 16QAM modulation scheme and various iterations. The BCJR decoder is used.

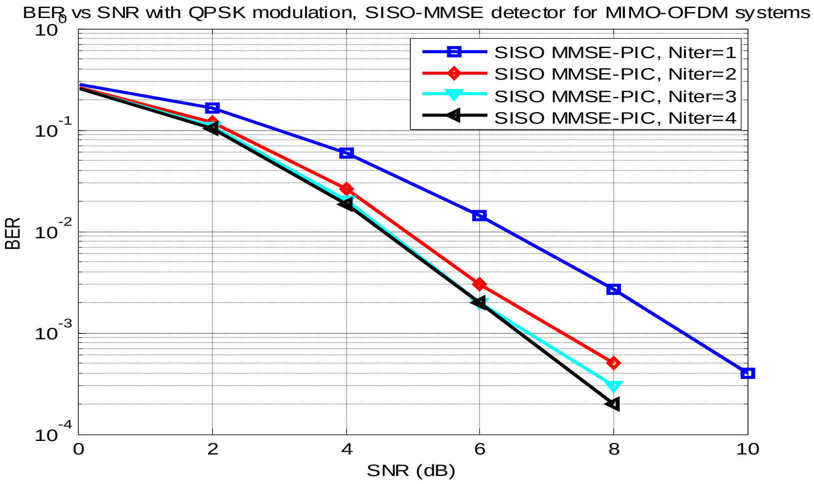

Fig. 4. BER vs. SNR performance of MIMO-OFDM systems based SISO MMSE-PIC detector with QPSK modulation scheme and 4x4 number of antennas.

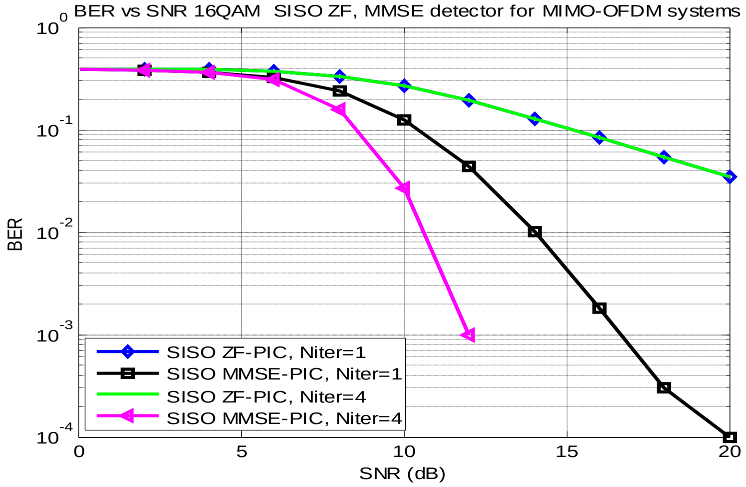

Fig. 5. BER vs. SNR performance comparison of MIMO-OFDM systems based ZF and SISO MMSE-PIC detectors with 16QAM modulation scheme and various iterations. The BCJR decoder is used.

Fig. 6 shows the performance of the proposed method compared with different number of coding rate (1/2, 2/3, 3/4). The performance improvement is obtained with the lowest coding rate and is enhanced with the number of iterations.

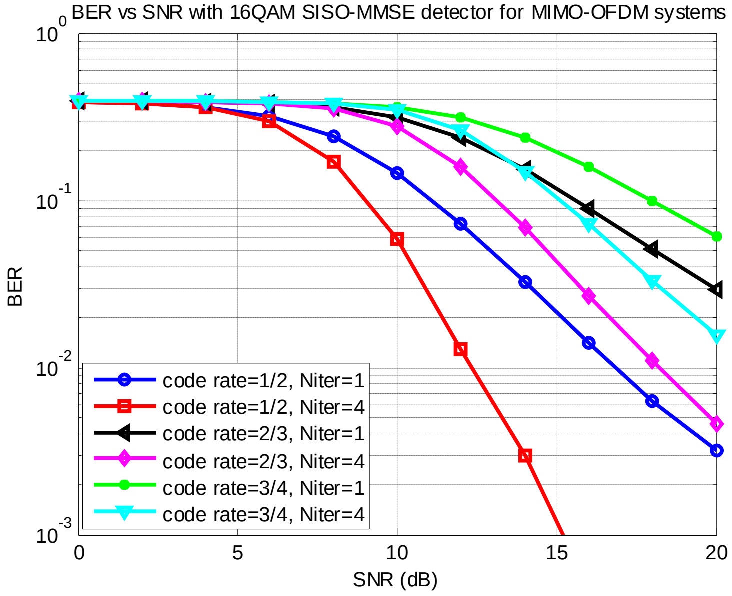

Fig. 6. BER vs. SNR performance of MIMO-OFDM systems based SISO MMSE-PIC detector with 16QAM modulation scheme and various coding rate ½, 2/3 and 3/4.

In Fig. 7, the performance of the SISO MMSE-PIC under different modulation schemes for MIMO-OFDM systems is considered. We can conclude that with lower modulation size, the method can perform better. For QPSK and 16QAM or 64QAM, the improvement is approximately 8dB for 10^{-2} bit error rate BER target.

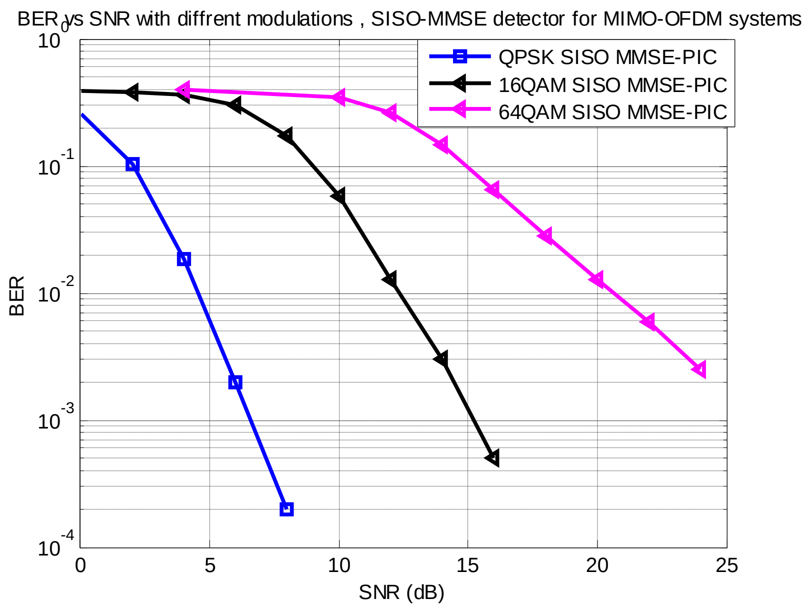

Fig. 7. BER vs. SNR performance of MIMO-OFDM systems based SISO MMSE-PIC detector with QPSK, 16QAM and 64QAM modulation

Fig. 8 show the BER versus SNR performance for a $N_T = N_R = 2$ and $N_T = N_R = 4$ MIMO-OFDM system, respectively, with QPSK data 16QAM modulation schemes. The number of iterations is set to four. For a 10^{-2} bit error rate BER target, the gain in the performance of the SISO MMSE-PIC is approximately about 3dB when the number of antennas is twice.

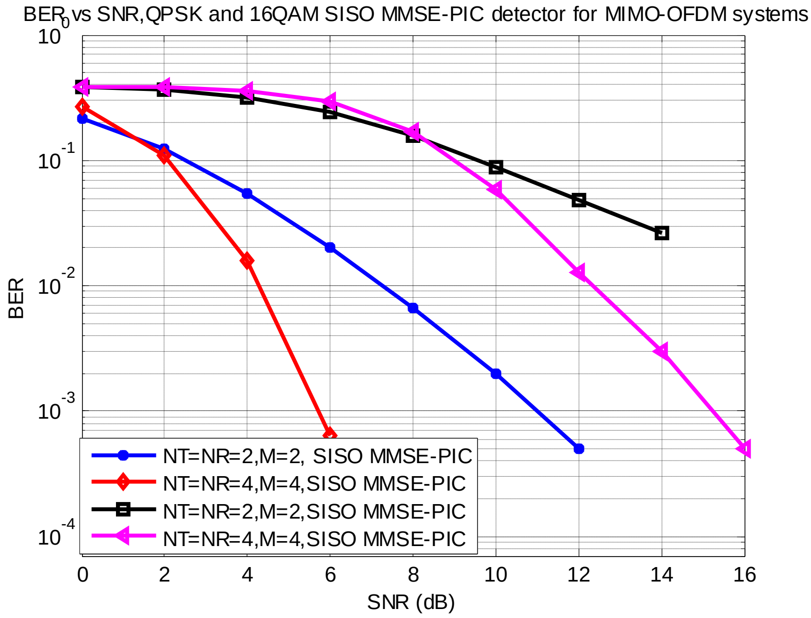

Fig. 8. BER vs. SNR performance of MIMO-OFDM systems based SISO MMSE-PIC detector for $N_T = N_R = 2$ and $N_T = N_R = 4$ number of

In Fig. 9, two indoor channel models with RMS delay spreads of 25ns and 50ns values corresponding to the IEEE 802.11 channel model are used. As expected, the later model decreases the performance of the MIMO-OFDM.

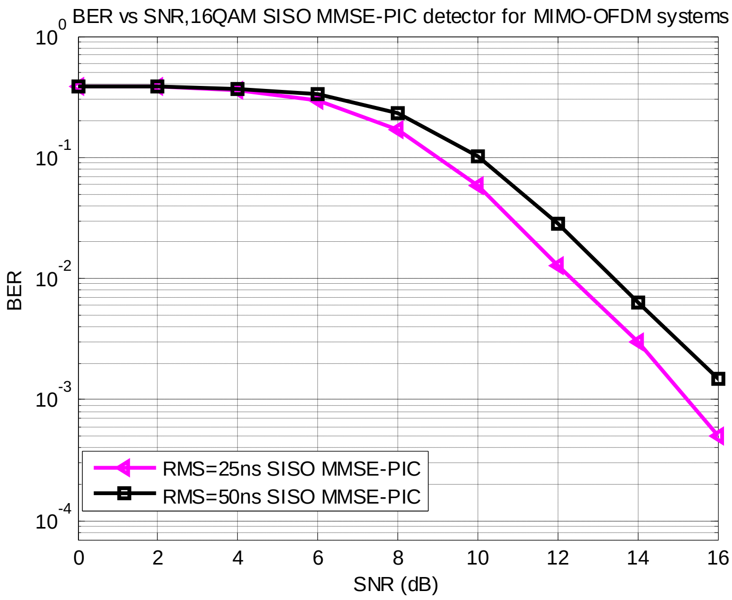

Fig. 9. BER vs. SNR performance of MIMO-OFDM systems based SISO MMSE-PIC detector for two RMS delay spreads 25ns and 50ns.

V. CONCLUSION

A MIMO-OFDM system model based on a bit-interleaved coded modulation (BICM) transmission strategy is presented in this paper. Simulations in the IEEE 802.11 channel model have shown that attractive performance is reached using SISO MMSE-PIC based detector in iterative manner with the BCJR decoder. The BICM decoder requires log likelihood ratios (LLRs) whose exact computation is extremely costly. In our simulations, the complexity is reduced by using the Max Log MAP approximations without a significant loss in the performance.

REFERENCES

[1] K. Lee and D. Williams, A space frequency transmitter diversity technique for OFDM systems, *Proc. IEEE GLOBECOM*, 2000, pp. 1473-1477

[2] Suto, K. and Ohtsuki, ”Performance evaluation of space-time frequency block codes over frequency selective fading channels,” *IEEE 56th Vehicular Technology Conference*, 2002. VTC 2002 -Fall. 2002, Vol.3, pp.1466 - 1470, 24-28 Sept. 2002.

[3] G. Caire, G. Taricco, and E. Biglieri, “Bit-interleaved coded modulation,” *IEEE Trans. Inf. Theory*, vol. 44, pp. 927–945, May 1998.

[4] R. Visoz, A. O. Berthet, and J. J. Boutros, Reduced-complexity iterative decoding and channel estimation for space time BICM over frequency selective wireless channels, *Proc. IEEE PIMRC-02*, Lisbon, Portugal, Sept. 2002, pp. 1017–1022.

[5] S. H. Müller-Weinfurtner, “Coding apporaches for multiple antenna transmission in fast fading and OFDM,” *IEEE Trans. Signal Process.*, vol. 50, no. 10, pp. 2442–2450, Oct. 2002.

[6] 802.11n, Enhancements for Higher Throughput. IEEE 802.11 WG. IEEE 802.11n/ D1.0, Draft Amendment, 2006.

[7] 802.16m, Draft IEEE 802.16m Evaluation Methodology. IEEE 802.16m -7/037r1, 2007.

[8] LTE, Requirements for Evolved UTRA (E-UTRA) and Evolved UTRAN (E-UTRAN). 3GPP TR 25.913 v.7.3.0, 2006.

[9] B. M. Hochwald and S. ten Brink, “Achieving near-capacity on a multiple-antenna channel,” *IEEE Trans. Comm*., vol. 51, no. 3, pp. 389–399, Mar. 2003.

[10] Hagenauer J, Offer E & Papke L (1996) Iterative decoding of binary block and convolutional codes. *IEEE Transactions on Information Theory 42(2):* 429–445.

[11] Bahl LR, Cocke J, Jelinek F & Raviv J (1974) Optimal decoding of linear codes for minimizing symbol error rate. *IEEE Transactions on Information Theory 20(2):* 284–287.

[12] B. M. Hochwald and S. ten Brink, Achieving near-capacity on a multiple-antenna channel, *IEEE Trans. Inf. Theory*, vol. 51, pp. 389– 399, March 2003.

[13] K.-B. Song and S. A. Mujtaba, A low complexity space-frequency BICM MIMO-OFDM system for next-generation WLANs, in *Proc. IEEE Globecom 2003*, (San Francisco, CA), pp. 1059–1063, Dec. 2003.

[14] M. Butler and I. Collings, A zero-forcing approximate log-likelihood receiver for MIMO bit-interleaved coded modulation, *IEEE Commun. Letters*, vol. 8, pp. 105–107, Feb. 2004.

[15] D. Seethaler, G. Matz, and F. Hlawatsch, An efficient MMSE-based demodulator for MIMO bit-interleaved coded modulation, *Proc. IEEE Globecom 2004*, vol. IV, (Dallas, Texas), pp. 2455–2459, Dec. 2004.

[16] Robertson P, Villebrun E & Hoeher P (1995), A comparison of optimal and sub-optimal MAP decoding algorithms operating in the log domain, *Proc. IEEE Int. Conf. Commun*. pp. 1009–1013.

[17] W. J. Choi, K. W. Cheong, and J. M. Cioffi, Iterative Soft Interference Cancellation for Multiple Antenna Systems, *Proceedings of the IEEE Wireless Communications and Networking Conference (WCNC’00)*, no. 1, 2000, pp. 304–309.

[18] B. M. Hochwald and S. ten Brink, Achieving Near-Capacity on a Multiple-Antenna Channel, *IEEE Transactions on Communications*, vol. 51, no. 3, pp. 389–399, Mar. 2003.

[19] S. Baero, J. Hagenauer, and M. Witzke, Iterative Detection of MIMO Transmission using a List-Sequential (LISS) Detector, *International Conference on Communications (ICC)*, Anchorage, USA, May 2003.

[20] Melanie Witzke, Stephan Baro, Frank Schreckenbach, Joachim Hagenauer, Iterative Detection of MIMO Signals with Linear Detectors,

[21] H.V. Poor and S. Verdu, Probability of error in MMSE multiuser detection, IEEE Transactions on Information Theory, vol.43, no.3, pp.858-871, May 1997

[22] M. Tüchler, A. C. Singer, and R. Kötter, Minimum mean squared error equalization using a priori information, *IEEE Trans. on Sig. Proc.*, vol. 50, no. 3, pp. 673–683, Mar. 2002.

[23] Liu Zhan-li, Zhao Chun-ming, Wang Jing Meng, Qing-min, Turbo Per-tone Equalization for MIMO OFDM Systems, *Journal of Electronics & Information Technology*, Vol.29 No.1, Jan. 2007.

Fitting Probability Distribution Functions To Discharge Variability Of Kaduna River

Haruna Garba[1], Abubakar Ismail[2] and Usman Tsoho[1]
[1] *Department of Civil Engineering, Nigerian Defence Academy,*
Department of Water Resources and Environmental Engineering, Ahmadu Bello University Zaria Email:

ABSTRACT: *In reliability based design of flood protection structures, frequency analysis aimed at determining the occurrence frequency or return periods is an indispensable tool. A frequency analysis was performed by fitting probability distribution functions of Normal, Log Normal Log pearson type III and Gumbel to the discharge variability of Kaduna River at Kaduna South Water Works. The Kolmongonov- Smirnov (K-S) goodness-of-fit test was used to check whether the mean annual discharge variability of the river basin is consistent with a regional GEV distribution for the site. From the measure of discrepancy, it was observed that at selected level of significance of α=1%, α=5% and α=10%, all the four theoretical distributions functions were acceptable.*

Keywords: *Discharge, Flood, Frequency distribution, Probability distribution function, Statistical analysis*

I. INTRODUCTION

Hydrologist must plan for extreme events. Dams must be built high enough to constrain or limit extreme floods, while bridges must be built high enough to remain above high water mark. The problem of how to plan for extreme events considering that they are so rare and that there is no comprehensive data is therefore a challenge to hydrologist. In [1] the information and data recorded in the past is normally applied to obtain statistical parameters that can be used to forecast events that may occur in the future. Although in [2] it has been recognized that many annual flood series are too short to allow for a reliable estimation of extreme events because of difficulties in the identification of the appropriate statistical distribution for describing the data and to the estimation of parameters of the selected distribution. Probability distribution therefore is a statistical tool most widely used in flood prediction and estimation. Hydrological variables such as rainfall, temperature, discharges etc are statistical quantities that can be estimated from a given probability of occurrence. [3] observed that the study of river hydrology is important in the overall understanding of river systems, which is a key component for river engineering and restoration of water resources planning and for river ecosystem studies. [3] Further opined that understanding the hydrology and geomorphology of river systems is important in conserving their natural beauty, habitat and resources. River hydrology influences the temporal and spatial distribution of discharge including water availability within a region. The monitoring of river discharge according to [2] is ideally suited to detect and monitor changes resulting from climate change. [4] Observed that floods from rainfall may appear several times within one year in Kaduna metropolis. [4] Further adduced that urbanization and structural development into traditional flood prone areas of Kaduna River modifies the channel shape, reduces the width of flood prone areas relative to bank full width at every point along Kaduna River channel and modifies the flood prone containment characteristics of the channel. In determination of probability distribution of maximum discharges on river basins of observed floods, [5] adopted the hypothesis of mutual independence of floods events in the computation of the annual probability of maximum seasonal discharges to take into account all suitable define floods. Flood frequency analysis is used to predict design floods for sites along a river. The technique involved using observed annual peak flow discharge data to calculate statistical information such as mean values, standard deviations, skewness and recurrence intervals. The statistical data are then used to construct frequency distributions which are graphs and tables that tell the likelihood of various discharges as a function of recurrence interval or exceedence probability. If a flood of a particular size occurs on average ones every Tr years, then Tr is called the return period and the probability P of such an event in any year is given by equation (1).

$$P = \frac{1}{Tr} \qquad (1)$$

Then the probability that there will be no such flood on a particular year is $(1-\mathrm{P})$ and the probability that there will be no such flood over the next n years is given by equation (2).

$$P = (1 - P)^{n} \qquad (2)$$

By adopting the hypothesis of mutual interdependence of floods events, it becomes possible in computation of annual probability of maximum seasonal discharge to take into account all suitable defined flows given by equation (3).

$$P = P_2\left[1-(1-P^1)\lambda^1\right] \qquad (3)$$

Where P is the probability referred to the year, P^1 is the probability referred to all floods while P_2 and λ^1 are the transformation parameters.

Flood frequency analysis according to [6] is a statistical analysis of floods, their magnitude and frequency. According to [6], to derive the risk of occurrence of any flood event, the frequency distribution which can best describe the past characteristics of the magnitude and possibility of such flood must be known and this requires determination of the most appropriate flood frequency model which can be fitted to the available historical data or record. Flood frequency distribution can take on many forms according to the equations used to carry out the statistical analysis. [7] observed that in many areas of civil engineering the questions often arises which probability should be used to model the load and resistance, instead of choosing one probability distribution.[7] further observed that it is possible to consider various probability distributions and to attached weight to these distributions according to how good the fits are. A probability distribution for the which the standard deviation of its prediction is large should be given less weight relative to those distributions that exhibit less scatter. A probability distribution is a continues mathematical expression that determines the probability of a particular event. Four of the common forms of probability distribution selected for this study are Normal, Log Normal, Log Pearson type 111 and Gumbel max distributions. In this study, observed maximum discharges of Kaduna River were used as the basis for fitting probability distribution to the design discharges.

II. MATERIALS AND METHODS

2.1 The Study Area

Kaduna River (fig 1) is the main tributary of Niger River in central Nigeria. It rises on the Jos plateau south west of Jos town in a North West direction to the north east of Kaduna town. It then adopts a south westerly and southerly course before completing its flow to the Niger River at Mureji. Most of its course passes through open savanna woodlands but its lower section cut several gorges including the granite ravine at Shiroro above its entrance into the extensive Niger flood plains.

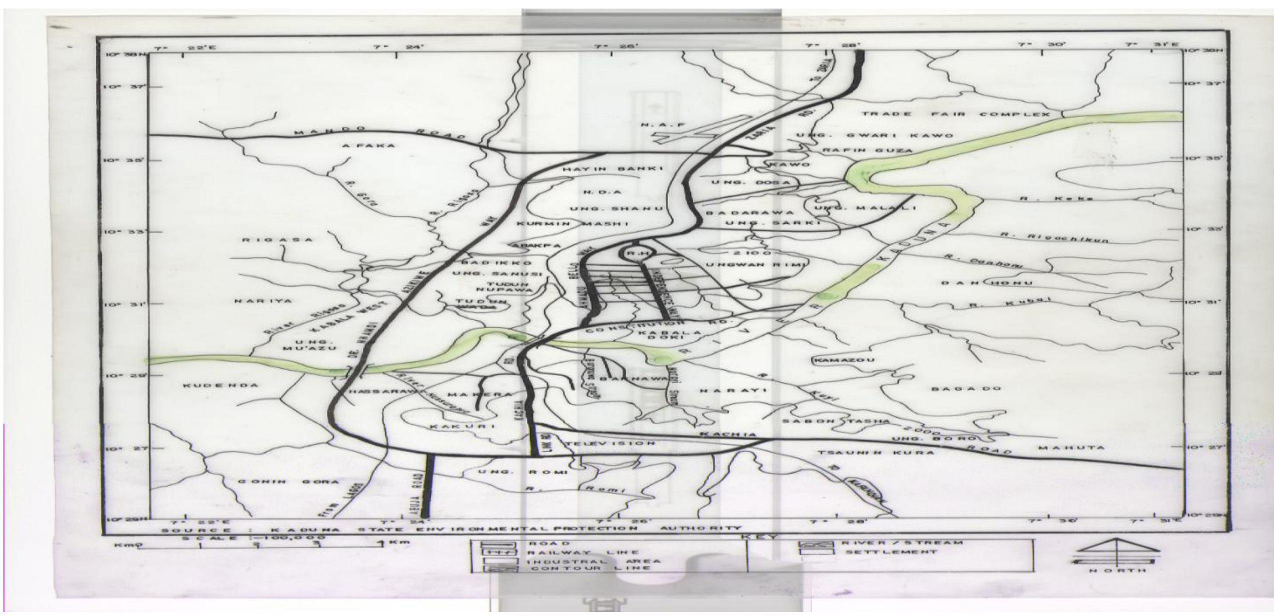

Fig 1 drainage map of Kaduna River

2.2. Data Used

In the study, the peak annual mean discharge data of Kaduna River for 11 years (2000-2010) were obtained from Kaduna State Water Board. To check the consistency of the data, a mass curve analysis was carried, to estimate missing record arising from human error, instrumental defect and improper citing.

2.3 The Flood Frequency Model

Hydrognomon is an open sources software tool used for the processing of hydrological data. Data are usually imported through standard text files, spread sheets or by typing. The available processing techniques for the tool includes time step aggregation and regularization, interpolation, regression analysis and infilling of missing values, consistency test, data filtering, graphical and tabular visualization of time series. Hydrognomon support several time step from the finest minutes scales up to decades. The programme also include common hydrological application such as evapotranspiration modeling, stage discharge analysis, homogeneity test, areal integration of point data series, processing of hydrometric data as well as lumped hydrological modeling with automatic calibration facilities (fig 2)

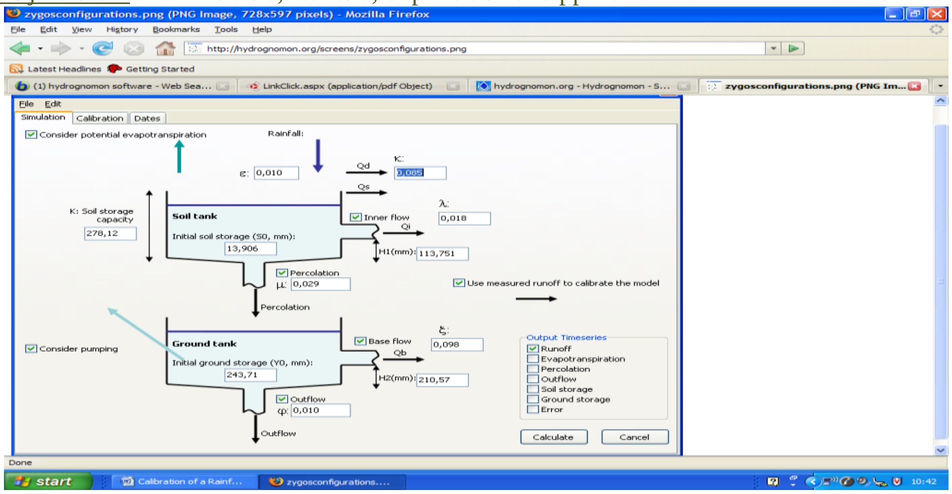

Figure 2 structure of the simulation module

2.4 The Procedure

Prior to the model application, the hydrognomon model was calibrated by [8] with historical data to obtained parameters to be used in studying the behaviors of Kaduna River. In order to assess the annual mean discharges with different return periods, or the occurrence frequencies of the return periods of extreme river floods reference was made flood frequency to predict the design floods at Kaduna South Water Works along Kaduna River as shown in fig 3. The hydrognomon probability distribution module was used to predict the likely values of discharges to expect along Kaduna River at various recurrence interval. For determining the most suitable statistical distribution that has the best fitting with the predicted values, the phytia statistical module was applied to the four theoretical distribution functions. The method of selecting the distribution and fitting values is the Kolmongonov- Smirnov (K-S) test.

2.5 Extrapolation of Point Measures to Watershed

The point measure of rainfall depth and intensity from a gauge is of value for estimating volume and runoff for large areas. For this, (a) the depth and intensity measured at a point must be considered as constant over an area, or (b) two or more point measures must be averaged .Intensity and Watershed Discharge. The calculated runoff considering the volume of water shed was obtained using the formula in equation (4).

$$Q = ICA. \qquad (4)$$

Where;Q is the Calculated runoff. I is the gauged water levels .C is a factor; the ratio maximum guage level at a point to the mean guage levels of Kaduna river. A is the drainage area of Kaduna river(18277.28km²).

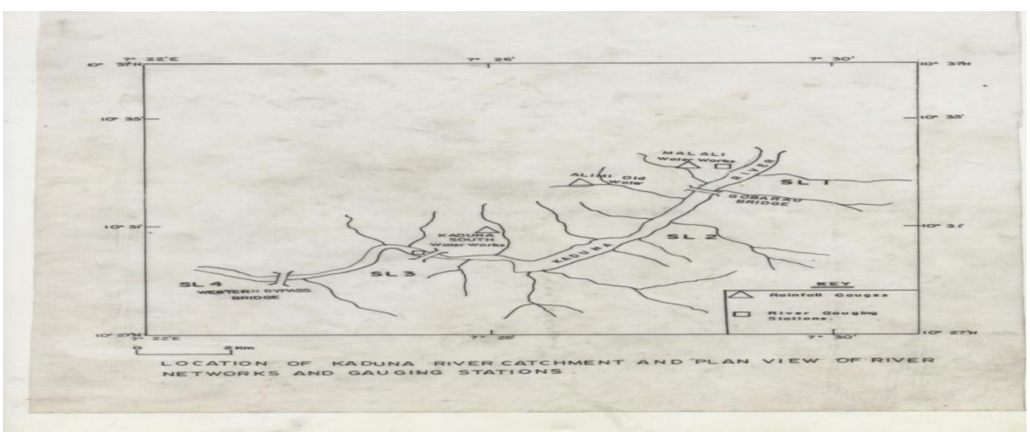

Figure 3 Kaduna South gauging station

III. GOODNESS- OF- FIT- TEST

In[9],it was recognized that many annual floods series ate too short to allow for reliable estimation of extreme events. However, [9] identified that the difficulty are related to both the identification of appropriate statistical distribution for describing the data and to the estimation of parameters of a selected distribution. [9] Therefore hypothesized that regionalization provides a means to cope with this problem. A flood frequency relationship according to [10] for a site with little or no stream flow record can be constructed by using a regionalized flood frequency model. In the method according to [9], the use of a generalized

www.ijmer.com Vol. 3, Issue. 5, Sep - Oct. 2013 pp-2848-2852 ISSN: 2249-6645

extreme value (GEV) distribution as a regional flood frequency model with an index flood approach has received considerable attention. In order to test whether the available flood data for a site are consistent with a proposed regional GEV distribution for that site, the Goodness – of- Fit Test as observed by [10] can be used to test whether the data at a particular site are consistent with a hypothesized regional distribution. [10] investigated the application of the Kolmongonov- Smirnov test, the probability plote correlation test and sample L-moment tests in testing whether a regional GEV Distribution is consistent with the available data for a site.

3.1 *The Kolmongonov-Smirnov Test*

The Kolmongonov- Smirnov goodness-of – fit – test can be used to check whether the observed flood sample at a site is consistent with a regional GEV flood distribution for the site. The advantage of the K-S test is that it gives simulation confidence interval for all the observations and therefore provides a visual goodness-of – fit- test. The K-S test procedure involves the comparison between the experimental cumulative frequency and the assumed theoretical distribution function. If the discrepancy is large compared to what is normally expected from a given sample size, the theoretical model is rejected. The test statistics for the K-S test involved determining the largest difference (Dmax) between the corresponding cumulative frequencies of the two samples. The maximum difference between the observed and theoretical predicted values (Dmax) is the measure of discrepancy between the theoretical model and observed data. Level of significance of α = 1%, α =5% and α =10% were selected and the critical value $D_{max}^{\propto}$ were computed based on the selected value of α . The K-S test determines whether for a specified level of significance α , the proposed distribution is an acceptable representation of the field data. If Dmax<$D_{max}^{\propto}$ the theoretical distribution is acceptable on the other hand, if Dmax>$D_{max}^{\propto}$ the theoretical distribution is rejected.

Results and Discussions

Table 1 Simulated mean discharge of Kaduna River

Recurrence Interval (years)	**Exceedence Probability (%)**	**95% Confidence Interval**			
		Normal Q (m^3/s)	**Log Normal Q (m^3/s)**	**Log Pearson Type 111 Q (m^3/s)**	**Gumbel Q(m^3/s)**
2	**50**	**45,000**	**40,000**	**45,000**	**40,000**
5	**20**	**75,000**	**65,000**	**70,000**	**70,000**
10	**10**	**90,000**	**85,000**	**90,000**	**90,000**
20	**5**	**100,00**	**105,000**	**115,000**	**105,000**
50	**2**	**115,000**	**135,000**	**145,000**	**130.000**
100	**1**	**120,000**	**140,000**	**150,000**	**145,000**

TABLE 1 show the annual mean discharge values in different return periods simulated with the four probability distributions functions. Evaluation of the statistical distribution of mean discharges showed that the Normal and Log Normal indicates the lowest fitting between observations and predicted values while the Log Pearson typeIII and the Gumbel showed the highest fitting.

Table 2 Kolmogonov-Smirnov (K-S) test result

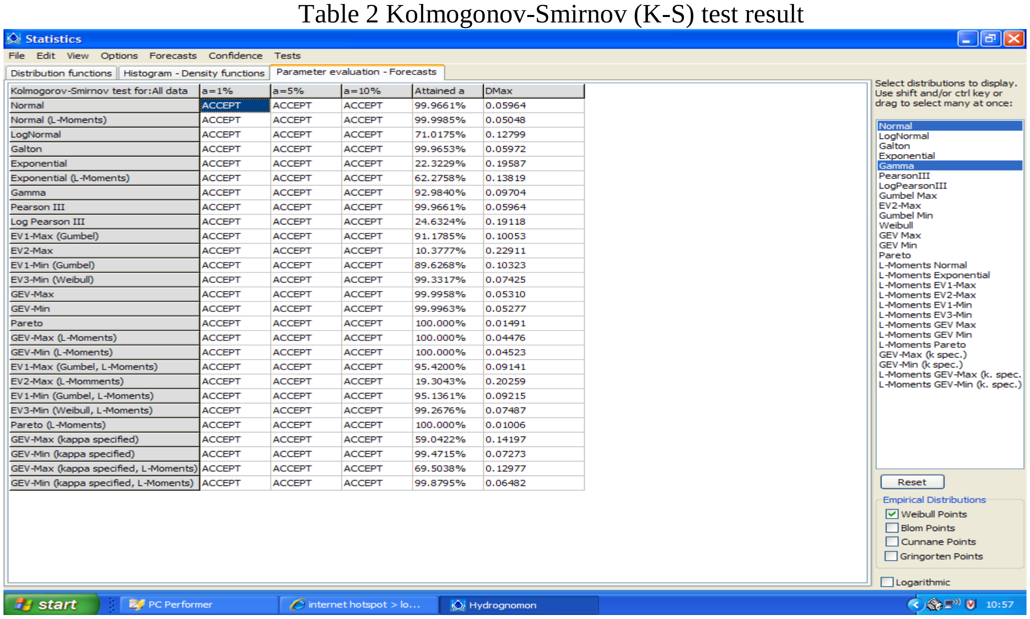

Kolmogorov-Smirnov test for:All data	a=1%	a=5%	a=10%	Attained a	DMax
Normal	ACCEPT	ACCEPT	ACCEPT	99.9661%	0.05964
Normal (L-Moments)	ACCEPT	ACCEPT	ACCEPT	99.9985%	0.05048
LogNormal	ACCEPT	ACCEPT	ACCEPT	71.0175%	0.12799
Galton	ACCEPT	ACCEPT	ACCEPT	99.9653%	0.05972
Exponential	ACCEPT	ACCEPT	ACCEPT	22.3229%	0.19587
Exponential (L-Moments)	ACCEPT	ACCEPT	ACCEPT	62.2758%	0.13819
Gamma	ACCEPT	ACCEPT	ACCEPT	92.9840%	0.09704
Pearson III	ACCEPT	ACCEPT	ACCEPT	99.9661%	0.05964
Log Pearson III	ACCEPT	ACCEPT	ACCEPT	24.6324%	0.19118
EV1-Max (Gumbel)	ACCEPT	ACCEPT	ACCEPT	91.1785%	0.10053
EV2-Max	ACCEPT	ACCEPT	ACCEPT	10.3777%	0.22911
EV1-Min (Gumbel)	ACCEPT	ACCEPT	ACCEPT	89.6268%	0.10323
EV3-Min (Weibull)	ACCEPT	ACCEPT	ACCEPT	99.3317%	0.07425
GEV-Max	ACCEPT	ACCEPT	ACCEPT	99.9958%	0.05310
GEV-Min	ACCEPT	ACCEPT	ACCEPT	99.9963%	0.05277
Pareto	ACCEPT	ACCEPT	ACCEPT	100.000%	0.01491
GEV-Max (L-Moments)	ACCEPT	ACCEPT	ACCEPT	100.000%	0.04476
GEV-Min (L-Moments)	ACCEPT	ACCEPT	ACCEPT	100.000%	0.04523
EV1-Max (Gumbel, L-Moments)	ACCEPT	ACCEPT	ACCEPT	95.4200%	0.09141
EV2-Max (L-Momments)	ACCEPT	ACCEPT	ACCEPT	19.3043%	0.20259
EV1-Min (Gumbel, L-Moments)	ACCEPT	ACCEPT	ACCEPT	95.1361%	0.09215
EV3-Min (Weibull, L-Moments)	ACCEPT	ACCEPT	ACCEPT	99.2676%	0.07487
Pareto (L-Moments)	ACCEPT	ACCEPT	ACCEPT	100.000%	0.01006
GEV-Max (kappa specified)	ACCEPT	ACCEPT	ACCEPT	59.0422%	0.14197
GEV-Min (kappa specified)	ACCEPT	ACCEPT	ACCEPT	99.4715%	0.07273
GEV-Max (kappa specified, L-Moments)	ACCEPT	ACCEPT	ACCEPT	69.5038%	0.12977
GEV-Min (kappa specified, L-Moments)	ACCEPT	ACCEPT	ACCEPT	99.8795%	0.06482

TABLE 2 showed result of Kolmongonov- Smirnov test procedure which involves the comparison between observed cumulative frequency and the four theoretical distributions functions. The K-S goodness-of-fit test was used to check whether the annual flood discharge variability at Kaduna South Water Works is consistent with the regional GEV flood distribution for the site. From the measure of discrepancy, it was observed that the difference between observed cumulative frequency values and the theoretical predicted cumulative values at level of significance of α= 1%,α =5% and α=10% with all the theoretical distribution been acceptable.

IV. CONCLUSION

A frequency analysis was performed by fitting probability distribution functions to the discharge variability of Kaduna River at Kaduna South Water Works aimed at determining the occurance frequency or return periods of extreme river floods. Estimate of the return periods of river floods are necessary in a reliability based design of flood protection structures. However, although uncertainties are important in flood analysis reliability based design.Uncertaities could be statistical due to limited amount of flood data or model uncertainty due to limited descriptive capabilities of the physical flooding process.

REFERENCES

[1] Gh Khosravi, A. Magidi and A. Nohegar. Determination of suitable probability distribution for annual and peak discharge estimations (Case Study: Minab River-Barantin Gage, Iran). *International journal of probability and statistics 2012, 1(5): 160-163.*
[2] P.H.A.J.M van Gelder, N.M Neykov, P.I Neytcher, J.K Vrijling and H Chbab. Probability distribution of annual maximum river discharges in North-Western and Central Europe, TU Deft Report 1999.
[3] D Caissie. River discharges and channel width relationship for New Brunswick Rivers. Can. Tech. Rep. Fish. Sci. 2637:26p.
[4] U Looser. River discharged standard report www.fao.org/gtos/ecv-TO/html.
[5] A.W Alayande and J.C Agunwamba. Modeling the impact of urbanization on river flooding using ST. Venant equation. *ARPN Journal of Engineering and Applied Sciences, vol 5, no 7, 2010.*
[6] W Strupczewski. Determination of probability of maximum discharges on the basin of all observed floods. Technical University of Warsaw, Warsaw Poland.
[7] O.C Izinyon and H.N Ajumuka. Probability distribution models for flood prediction in Upper Benue River Basin. *Civil and Environmental Research vol,3,No,2, 2013.*
[8] P.H.A.J.M van Gelder, J.M Noortwirk and M.T Duits. Selection of probability distribution with case study of extreme Oder River discharges. *In G.I Schueller and P Kafta; Safety and reliability proceedings of ESREL. The Tenth European Conference on Safety and Reliability, Munich Garching Germany, 1999, 1475-1480 Rotterdam Balkema.*
[9] H Garba, A Ismail and F.O.P Oriola. Calibration of hydrognomon model for simulating the hydrology of urban catchment. *Open Journal of Modern Hydrology, 3, 75-78, 2013.*
[10] J.U Chowdhung, J.R Stedinger and L.I Hsiung LU. Goodness-of- Fit Test for regional generalized extreme value flood distribution. *Water Resources Research, Vol 27, No 7, Pp 1765-1776.*

International Journal of Modern Engineering Research (IJMER)
www.ijmer.com Vol. 3, Issue. 5, Sep - Oct. 2013 pp-2853-2856 ISSN: 2249-6645

Remote Monitoring of Crop Field Using Wireless Sensor Network

V.Swathi [1], A. Krishnamurthy [2]

[1] *Asst. prof., Department of ECE, Princeton Institute of engineering and Technology for women,Ghatkesar,Ranga Reddy(dist)*

[2] *Assoc. Prof., Department of ECE, Princeton Institute of engineering and Technology for women, Ghatkesar,Ranga Reddy(dist)*

ABSTRACT: *This paper presents the design and implementation of wireless sensor network that can monitor the air temperature, Humidity, light intensity in a crop field and from remote places also. The system consists of nodes, which are equipped with small size application specific sensors and radio frequency modules. The sensor data is transmitted via radio frequency link to the centrally localized computer terminal for data logging and analysis. This data can be monitor from the remote places by uploading the data into the internet, also the sensor nodes can additionally be programmed from the computer terminal itself according to the changing needs of farmers thus preventing the need for redeployment of the wireless sensor network every time some changes are to be made. Since the energy is the main operating constraint sleep mode of the core component is utilized.*

I. INTRODUCTION

Wireless sensors will be spatially distributed with each node communicating with one another and the central unit would record the data received. The autonomous devices which use sensors to co-operatively monitor physical or environmental parameters such as temperature, light intensity, humidity, and moisture levels. Data collected from the sensors play a key role in crop field management [1]-[6] and this data can be monitor from any place by uploading this data to the remote pc's through rabbit processor. Another application of WSN in detection of forest fires and plant fires [7]-[9] forest fires can cause huge damage to the human and natural resources. Sensor nodes in WSN can determine and transmit the location of source of the fire to the fire preventing department before the fire expands to other regions. The crop growth depends upon the air temperature, humidity, light intensity and active radiation of light which plays an important role in the photosynthetic activity. Remote monitoring of crop field using WSN thus represents the class of network applications with more benefits to the end users.

II. SYSTEM ARCHITECTURE

The WSN for remote monitoring of crop field consists of set of wireless sensor nodes distributed in an area called end devices or sensor nodes. They have a stronger battery, a larger memory and more computation power, the sensor nodes collects the data from the field by using sensors and this data is send to the coordinator through routers ,the path between end devices, routers and coordinators is provided by ZIGBEE. The collected data is send to the internet and pc through Ethernet.

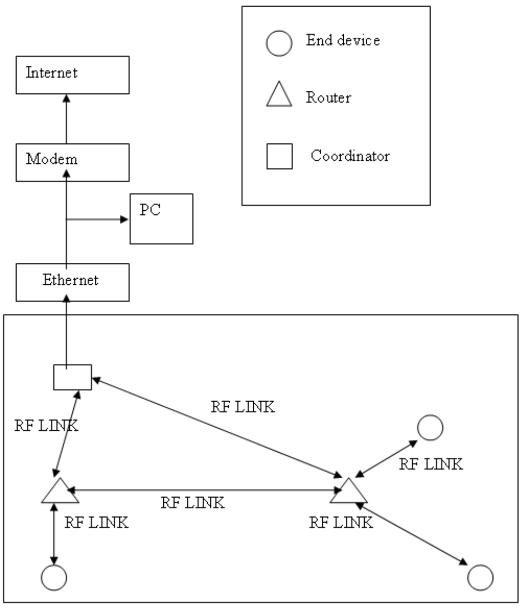

Figure 1.The structure of the WSN for remote monitoring of the crop field

III. WIRELESS SENSOR NETWORK

In the remote monitoring of parameters using WSN system consists of ZIGBEE based sensor nodes. The end devices and router are sensor part of the system, the coordinator is the controller of the system, and the topology of the WSN is shown in the figure 2.

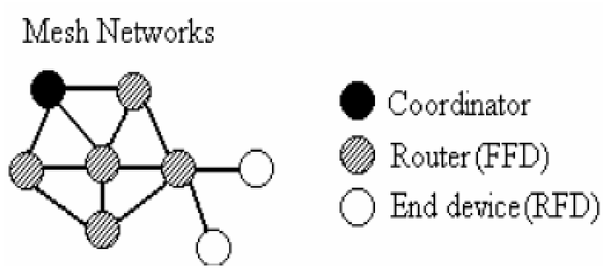

Figure 2. ZIGBEE network topology

The design of WSN system is as follows:

A. End devices

The end device is the sensor board ,this board is embedded temperature sensor, humidity sensor ,and light sensor when the ADC has transformed physiological signals into the digital signals which are sent to the 8 MHz 8 bit reduced instruction set computing cpu and then sent to 2.4 GHz IEEE 802.15.4 transceiver. The transceiver will send signals to the router. We can observer the field condition easily.

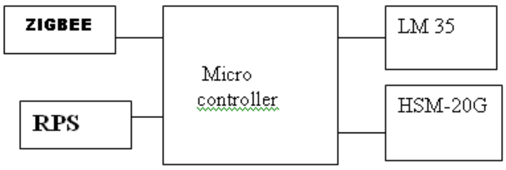

Figure 3.basic model of sensor node

(i) Sensors

Low power consumption, fast response time, tiny size, long term stability .the module HSM-20G is used as humidity sensor with measurmet accuracy /-5%RH .LM 35 is used as precision centigrade temperature sensor with directly calibrated in centigrade. Both the sensors do not require any external components for signal conditioning thereby saving valuable PCB area. Another key aspect for choosing these sensors is that the output from both the sensors is immune to noise and external disturbances due to its digital nature. The start up time in both the sensors is very low. Therefore current is not needed for a long time during initialization thereby reducing the power consumed. The power saved can be used to perform other computing tasks. Another advantage is that the sensors can be deployed quickly in the field since no calibration is needed prior to deployment.

(ii) Router

The router is used to transmit data between end device and the coordinator, when the route is received signals from the end device another router and the coordinator it will transmit signals to goals.

(iii) Coordinator

The coordinator is the controller board used to control the sensor network, the measured data of any end device appear on PC and internet via Ethernet .basic model of the coordinator is shown in Figure 4

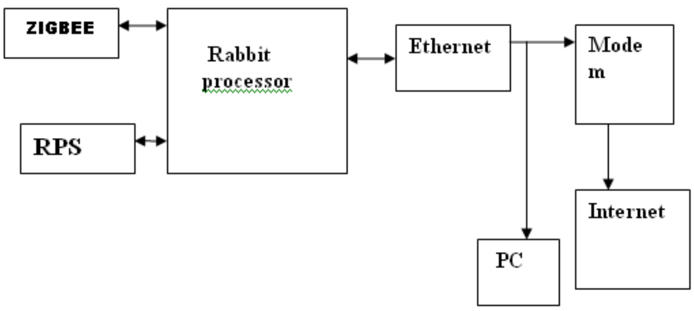

Figure 4.Basic model of coordinator

IV. RF COMUNNICATION

The ZIG BEE-PRO RF Modules [10] manufactured by Digi are used to provide the required wireless RF communication link amongst sensor nodes . The modules are engineered to meet IEEE 802.15.4 standards and provide reliable delivery of data between compatible devices. They operate within the ISM 2.4 GHz frequency band and provide a wireless communication range of 1500 m in open space. They require minimal power and support the unique needs of low-cost, low-power wireless sensor networks. The modules are programmed using dedicated programming kit to make them compatible for wireless communication.

V. RESULTS

The proposed WSN system consists of two sensor nodes which measures temperature and humidity. in order to save power and increase the life time of the nodes sleep and wake up modes are used. The collected data is displayed on web page

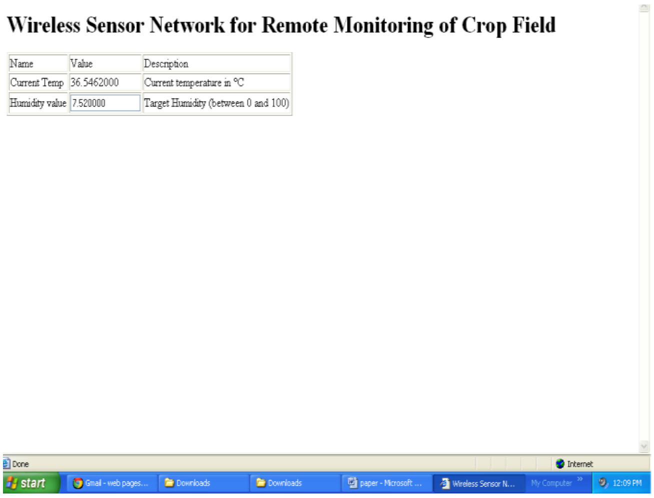

Figure 4 Web page contain results

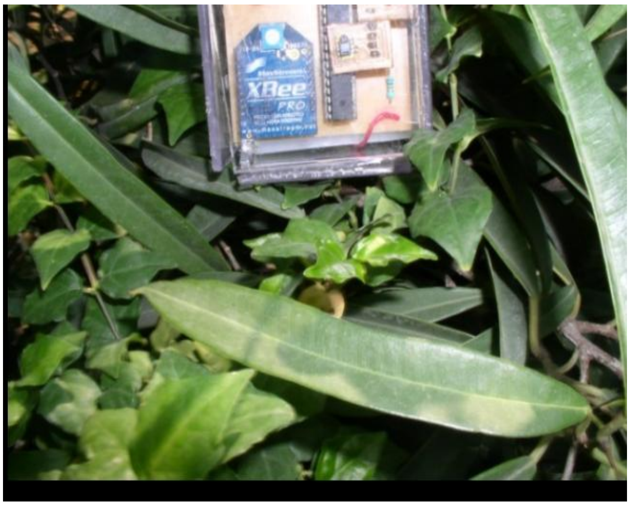

Figure 6 Basic sensor node

VI. CONCLUSIONS

Crop field monitoring is useful class of sensor network applications with enormous potential benefits for the farmers and society as a whole. This paper presents the design and the implementation of a Wireless Sensor Network that monitors the air temperature, humidity and ambient light intensity in a crop field and from remote places. The sensor data is wirelessly transmitted to a centrally located computer terminal that logs the field data within seconds. The data collected can aid the farmers in achieving maximal crop productiveness. In case the computer terminal is switched OFF, data loss is prevented by the storage of the sensor data along with the time information in non-volatile memory. We have achieved a wireless communication range of more than 1 km, which can effectively monitor a normal crop field area. To make our sensor network energy efficient, sleep mode has been used for the sensors as well as the RF modules. Long network lifetime has been achieved by including a DC boost converter in the power supply design, which provides sensor nodes a stable power supply from degrading alkaline batteries. The converter can also detect low battery level indicating the need to charge the rechargeable batteries. Other special features of the design include detection of sensor node failure

In future, we plan to expand our network by adding more sensor nodes so that the coverage of an individual node decreases.

REFERENCES

[1] W. Zhang, G. Kantor and S. Singh, "Integrated Wireless sensor/actuator networks in an agricultural applications," In Second ACM International onference on Embedded Networked Sensor Systems (SenSys), page 317, Baltimore, Maryland, USA, Nov. 2004.

[2] K. Langendoen, A. Baggio, Visser, O. Murphy, "Experiences from a pilot sensor network deployment in precision agriculture," In Proc. Of IEEE IPDPS, Rhodes Island, Greece, 2006.

[3] Richard Beckwith, Daniel Teibel and Pat Bowen, "Report from the Field: Results from an Agricultura Wireless Sensor Network," present at IEEE Workshop on Embedded Network Sensors, 2004.

[4] J. Thelen, D. Goense and K. Langendoen, "Radio wave propagation in potato fields," In First Workshop on wireless Network Measurements (co-located with WiOpt 2005), Rivadel Garda, Italy, Apr. 2005.

[5] K. Mayer, K. Taylor and K. Ellis, "Cattle health monitoring using wireless sensor networks," In Second IASTED International Conference on Communication and Computer Networks, Cambridge, Massachusetts, USA, Nov. 2004.

International Journal of Modern Engineering Research (IJMER)
www.ijmer.com Vol. 3, Issue. 5, Sep - Oct. 2013 pp-2857-2861 ISSN: 2249-6645

Mobile Operated Landrover Using Dtmf Decoder

K.V.V.S.R .Bhaskar[1], D. Sasank[2],K.Kiran Chaitanya ,G.Hari Kishore [4]
[1,2,3 &4]Department of Electronics and Communication Engineering,
R.V.R & J.C College of Engineering,Chowdavaram,Guntur

ABSTRACT: *In this project, the robot is controlled by a mobile phone that makes a call to the mobile phone attached to the robot. In the course of a call, if any button is pressed, a tone corresponding to the button pressed is heard at the other end of the call. This tone is called 'dual-tone multiple-frequency' (DTMF) tone. The robot perceives this DTMF tone with the help of the phone stacked in the robot.*

Key words: *DTMF*

I. INTRODUCTION

In this project, the robot is controlled by a mobile phone that makes a call to the mobile phone attached to the robot. In the course of a call, if any button is pressed, a tone corresponding to the button pressed is heard at the other end of the call. This tone is called 'dual-tone multiple-frequency' (DTMF) tone. The robot perceives this DTMF tone with the help of the phone stacked in the robot

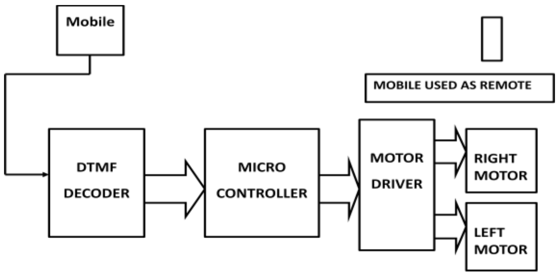

Fig 1: Block Diagram of Cell phone –Operated Land Rover

The received tone is processed by the ATmega32 microcontroller with the help of DTMF decoder MT8870 .The decoder decodes the DTMF tone into its equivalent binary digit and this binary number is sent to the microcontroller. The microcontroller is pre programmed to take a decision for any given input and outputs its decision to motor drivers in order to drive the motors for forward or backward motion or a turn.

The mobile that makes a call to the mobile phone stacked in the robot acts as a remote. So this simple robotic project does not require the construction of receiver and transmitter units.

DTMF signaling is used for telephone signaling over the line in the voice- frequency band to the call switching centre. The version of DTMF used for telephone tone dialing is known as 'Touch-Tone'. DTMF assigns a specific frequency (consisting of two separate tones) to each key so that it can easily be identified by the electronic circuit. The signal generated by the DTMF encoder is a direct algebraic summation, in real time, of the amplitudes of two sine (cosine) waves of different frequencies, i.e., pressing '5' will send a tone made by adding 1336 Hz and 770 Hz to the other end of the line. The tones and assignments in a DTMF system are shown in Table I.

Frequencies	1209 Hz	1336 Hz	1477 Hz	1633 Hz
697 Hz	1	2	3	A
770Hz	4	5	6	B
852Hz	7	8	9	C
941Hz	*	0	#	D

Table 1: Tones and Assignment in DTMF system

The important components of this mobile operated land rover are
1. DTMF Decoder
2. ATMEGA32 Microcontroller
3. Motor Driver
4. Voltage regulator
5. Regulated power supply

Let us briefly explain about the components

II. DTMF DECODER

DTMF is a generic communication term for touch tone (a Registered Trademark of AT&T). The tones produced when dialing on the keypad on the phone could be used to represent the digits, and a separate tone is used for each digit. However, there is always a chance that a random sound will be on the same frequency which will trip up the system. It was suggested that if two tones were used to represent a digit, the likelihood of a false signal occurring is ruled out.

This is the basis of using dual tone in DTMF communication. sDTMF dialing uses a keypad with 12/16 buttons. Each key pressed on the phone generates two tones of specific frequencies, so a voice or a random signal cannot imitate the tones. One tone is generated from a high frequency group of tones and the other from low frequency group. The frequencies generated on pressing different phone.

i. FEATURES:

• Complete DTMF Receiver
• Low power consumption
• Internal gain setting amplifier
• Adjustable guard time
• Central office quality

ii. APPLICATIONS:

• Receiver system for British Telecom (BT) or CEPT Spec (MT8870D-1)
• Paging systems
• Repeater systems/mobile radio
• Credit card systems
• Remote control
• Personal computers
• Telephone answering machine

iii. DESCRIPTION:

An MT8870 series DTMF decoder is used here. The MT8870D/MT8870D-1 is a complete DTMF receiver integrating both the band split filter and digital decoder functions. The filter section uses switched capacitor techniques for high and low group filters, the decoder uses digital counting techniques to detect and decode all 16 DTMF tone-pairs into a 4-bit code. All types of the MT8870 series use digital counting techniques to detect and decode all the 16 DTMF tone pairs into a 4-bit code output.

Table ii
DTMF data output

Low group(hz)	High group(hz)	digit	OE	D3	D2	D1	D0
697	1209	1	H	L	L	L	H
697	1366	2	H	L	L	H	L
697	1477	3	H	L	L	H	H
770	1209	4	H	L	H	L	L
770	1336	5	H	L	H	L	H
770	1477	6	H	L	H	H	L
852	1209	7	H	L	H	H	H
852	1336	8	H	H	L	L	L
852	1477	9	H	H	L	L	H
941	1336	0	H	H	L	H	L
941	1209	*	H	H	L	H	H
941	1477	#	H	H	H	L	L
697	1633	A	H	H	H	L	H
770	1633	B	H	H	H	H	L
852	1633	C	H	H	H	H	H
941	1633	D	H	L	L	L	L
-	-	ANY	L	Z	Z	Z	Z

III. ATMEGA32 MICROCONTROLLER

The Atmel AVR ATmega32 is a low-power CMOS 8-bit microcontroller based on the AVR enhanced RISC architecture. By executing powerful instructions in a single clock cycle, the ATmega32 achieves throughputs approaching 1 MIPS per MHz allowing the system designer to optimize power consumption versus processing speed.

i. *FEATURES:*

• High-performance, Low-power Atmel AVR 8-bit Microcontroller
• Advanced RISC Architecture
• High Endurance Non-volatile Memory segments
• JTAG (IEEE std. 1149.1 Compliant) Interface
• Peripheral Features
• Special Microcontroller Features
• I/O and Packages
• Operating Voltages
• Speed Grades
• Power Consumption at 1MHz, 3V, 25°C

The Atmel AVR core combines a rich instruction set with 32 general purpose working registers. All the 32 registers are directly connected to the Arithmetic Logic Unit (ALU), allowing two independent registers to be accessed in one single instruction executed in one clock cycle. The resulting architecture is more code efficient while achieving throughputs up to ten times faster than conventional CISC microcontrollers.

The ATmega32 provides the following features: 32Kbytes of In-System Programmable Flash Program memory with Read-While-Write capabilities, 1024bytes EEPROM, 2Kbyte SRAM, 32 general purpose I/O lines, 32 general purpose working registers, a JTAG interface for Boundary scan, On-chip Debugging support and programming, three flexible Timer/Counters with compare modes, Internal and External Interrupts, a serial programmable USART, a byte oriented Two-wire Serial Interface, an 8-channel, 10-bit ADC with optional differential input

L293 MOTOR DRIVER

The L293 is an integrated circuit motor driver that can be used for simultaneous, bi-directional control of two small motors. The L293 is limited to 600 mA, but in reality can only handle much small currents unless you have done some serious heat sinking to keep the case temperature down. Unsure about whether the L293 will work with your motor? Hook up the circuit and run your motor while keeping your finger on the chip. If it gets too hot to touch, you can't use it with your motor.

The L293 comes in a standard 16-pin, dual-in line integrated circuit package. There is an L293 and an L293D part number. Pick the "D" version because it has built in fly back diodes to minimize inductive voltage spikes. The L293D can be purchased for somewhere between $2 and $3 (quantity one) from http://www.mouser.com/ (PN 511-L293D) or http://www.digikey.com/ (PN 296-9518-5-ND). For complete information, consult the Unit rode L293 data sheet (PDF file, 626Kb).

IV. LM7805 (VOLTAGE REGULATOR)

I. FEATURE:

- 3-Terminal Regulators
- Output Current up to 1.5 A
- Internal Thermal-Overload Protection
- High Power-Dissipation Capability
- Internal Short-Circuit Current Limiting
- Output Transistor Safe-Area Compensation

V. SERIAL COMMUNICATION

Connection between the microcontroller and peripheral devices established through I/O ports is an ideal solution for shorter distances- up to several meters. But, when it is needed to enable communication between two devices on longer distances or when for any other reason it is not possible to use "parallel" connection (for example remote control of the aircraft) it is obvious that something so simple cannot be taken into account. In such and similar situations, communication through pulses, called serial communication is the most appropriate to use.

The circuit diagram of mobile operated land rover is as follows

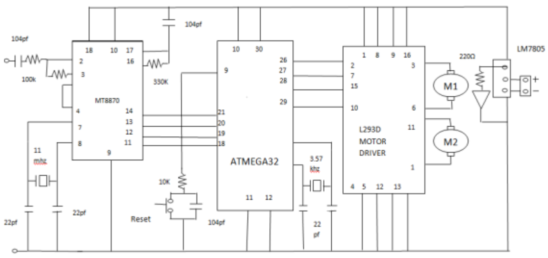

Fig2:circuit diagram of mobile operated land rover

VI. POWER SUPPLY

A variable regulated power supply, also called a variable bench power supply, is one where you can continuously adjust the output voltage to your requirements. Varying the output of the power supply is the recommended way to test a project after having double checked parts placement against circuit drawings and the parts placement guide.

VII. CONSTRUCTION

When constructing any robot, one major mechanical constraint is the number of motors being used. Either a two-wheel drive or a four-wheel drive can be used. Though four-wheel drive is more complex than two-wheel drive, it provides more torque and good control. Two-wheel drive, on the other hand, is very easy to construct. The chassis used in this model is a 10×18cm2 sheet made up of par ax. Motors are fixed to the bottom of this sheet and the circuit is affixed firmly on top of the sheet. A cell phone is also mounted on the sheet as shown in the picture. In the four-wheel drive system, the two motors on a side are controlled in parallel. So a single L293D driver IC can drive the rover. For this robot, beads affixed with glue act as support wheels.

VIII. WORKING:

In order to control the robot, make a call to the cell phone attached to the robot (through head phone) from any phone, which sends DTMF tunes on pressing the numeric buttons. The cell phone in the robot is kept in 'auto answer' mode. (If the mobile does not have the auto answering facility, receive the call by 'OK' key on the rover-connected mobile and then made it in hands-free mode.) So after a ring, the cell phone accepts the call. press any button on your mobile to perform actions as listed in Table III. The DTMF tones thus produced are received by the cell phone in the robot. These tones are fed to the circuit by the headset of the cell phone. The MT8870 decodes the received tone and sends the equivalent binary number to the microcontroller. According to the program in the microcontroller, the robot starts moving.

When you press key '2' (binary equivalent 00000010) on your mobile phone, the microcontroller outputs '10001001' binary equivalent. Port pins PD0, PD3 and PD7 are high. The high output at PD7 of the microcontroller drives the motor driver (L293D). Port pins PD0 and PD3 drive motors M1 and M2 in forward direction (as per Table III). Similarly, motors M1 and M2 move for left turn, right turn, backward motion and stop condition

TABLE III
DTMF DATA OUTPUT

Number pressed by user	Output of DTMF	Input to the micro controller	Output from micro	Actions performed
2	0X20	0X20	0XAA	Forward motion
4	0X40	0X40	0X22	Left turn
6	0X60	0X60	OX88	Right
8	0X80	0X80	OX55	Backward motion
5	0X50	0X50	0X00	stop

IX. SOFTWARE DESCRIPTION

The software is written in 'C' language and compiled using Code Vision AVR 'C' compiler. The source program is converted into hex code by the compiler. Burn this hex code into Atmega32 AVR microcontroller.

i. AVR STUDIO:

AVR Studio, with its Integrated Development Environment (IDE), is the ideal software for all AVR development. It has an editor, an assembler and a debugger and is front-end for all AVR emulators. And needs the GCC compiler i.e. WIN-AVR tool.

Two Software's are needs to install
1. AVR Studio
2. AVR GCC Compiler

ii. AVR COMPILER (WINAVR):

WinAVR is a suite of executable, open source software development tools for the Atmel AVR series of RISC microprocessors and AVR32 series of microprocessors hosted on the Windows platform. It includes the GNU GCC compiler for C and C++.

WinAVR is a collection of executable software development tools for the Atmel AVR processor hosted on Windows.
These software development tools include:

- Compilers
- Assembler
- Linker
- Librarian
- File converter
- C Library
- Programmer software
- Debugger
- In-Circuit Emulator software
- Editor / IDE

X. APPLICATIONS

- Cell phone controlled robot can be used in the borders for displaying hidden Land mines
- The robot can used for reconnaissance or surveillance
- The robot can be used anywhere there is the service provider tower of the connection provided that is mounted on robot.
- Robot is small in size so can be used for spying

XI. CONCLUSION

The primary purpose of the mobile phone operated land rover with DTMF decoder is to know the information in the places where we cannot move. The robot perceives the DTMF tone with the help of the phone stacked in the robot. It provides the advantage of robust control, working range as large as coverage area of service provider.

REFERENCES

1. "The 8051 Microcontroller and Embedded Systems" By Muhammad Ali Mazidi and Janice Gillispie Mazidi. Pearson Education.
2. *S.* Chemishkian, "Building smart services for smart home", Proceedings of IEEE 4thInternational Workshop on Networked Appliances, 2011 pp: 2 15 -224.s
3. R. Sharma, K. Kumar, and S. Viq, "DTMF Based Remote Control System," IEEE International Conference ICIT 2006, pp. 2380-2383, December 2006.
4. R.C. Luo, T.M. Chen, and C.C. Yih, "Intelligent autonomous mobile robot control through the Internet,"IEEE International Symposium ISIE 2000, vol. 1, pp. 6-11, December 2000
5. G. Arangurenss, L. Nozal, A. Blazquez, and J. Arias, "Remote control of sensors and actuators by GSM", IEEE 2002 28th Annual Conference of the Industrial Electronics Society IECON 02, vol. , 5-8 Nov. 2002,pp.2306 – 2310
6. Robotics and automation proceedings,1997 IEEE international conference on robotics & control systems .
7. Intelligent control 1989 proceedings IEEE international symposium on robotics & control systems.
8. Emerging trends in robotics and communication technologies, 2010 International conference on Robotics & control systems.

International Journal of Modern Engineering Research (IJMER)
www.ijmer.com Vol. 3, Issue. 5, Sep - Oct. 2013 pp-2862-2866 ISSN: 2249-6645

Reduction of Topology Control Using Cooperative Communications in Manets

B. Sai Manogna [1], N. Srinath Reddy[2], B. Sai Pragna[3]
#1, 3 M.TECH Scholars, VEC, Kavali
2 Associate Professor, VEC, Kavali

ABSTRACT: *A mobile ad hoc network (MANET) is a self-configuring infrastructure less network of mobile devices connected by wireless. Most of presented works on mutual communications are focused on link-level physical layer issues. The impacts of supportive communications on network-level upper layer issues, such as routing, topology control and network capacity etc. In this, we propose a Capacity-Optimized Cooperative (COCO) topology control scheme to develop the network capacity in MANETs by mutually taking into account both upper layer network capacity and physical layer mutual communications. Though the physical layer cooperative communications have more important impacts on the network capacity, and the future topology control scheme can significantly improve the network capacity in MANETs with cooperative communications and proposed optimum relay nodes selection for cooperative communication network to reduce overall power consumption of network.*

Index Terms: *Cooperative communications (CC), topology control, Optimum relay, MANET*

I. INTRODUCTION

Now a day's rapidly increasing demand for high speed wireless networks has forced the expansion of wireless ad-hoc networks. Recently, cooperative wireless communication has received tremendous interests as an untapped means for improving the performance of information transmission operating over the ever-challenging wireless medium. Cooperative communication has come forwarded as a new aspect of diversity to follow the policies designed for multiple receiver systems, since a wireless mobile device may not be capable to support multiple transmit antennas due to cost, size, or hardware limitations. By making use of the broadcast character of the wireless channel, cooperative communication permits single antenna radios to share their antennas to form a virtual antenna array, and suggests significant performance enhancements. This capable technique has been considered in the IEEE 802.16j standard, and is predictable to be integrated into Third Generation Partnership Project (3GPP) Long Term Evolution (LTE) multihop cellular networks. Network architecture and the process of abstraction go hand in hand. For most wired networks, the notion of a link has been a useful abstraction directly tied to the physical propagation medium. For wireless networks, especially the increasingly important class of MANETs, the classical notion of a link is more nebulous than in the wired case. Even so, two constraints are often imposed on network architectures to maintain it. At various levels, many current MANET protocols attempt to adapt, create, and manage a network based on a maze of point-to-point links and multihop transmission combines several intermediate links among pairs of nodes using buffer space, power, and bandwidth to route their own data as well as data from other sources. Even though an architecture based upon the classical link abstraction leads to many advantages that should not be underestimated, a number of issues occur in a wireless medium that hinder the classical link abstraction upon which these architectures are based.

Most presented works are paying attention on link-level physical layer issues, such as outage capacity and outage probability. Therefore, the impacts of CC on network level higher layer issues, such as routing, topology control and network capacity, are largely ignored. Certainly, most of present works on wireless networks attempt to adapt create and manage a network on a maze of point to point non cooperative wireless links. On the other hand recent advances in cooperative communications will present a number of advantages in flexibility over traditional techniques. Cooperation improves certain networking problems, such as routing and collision resolution and allows for simpler networks of more complex links, slightly than complicated networks of simple links.

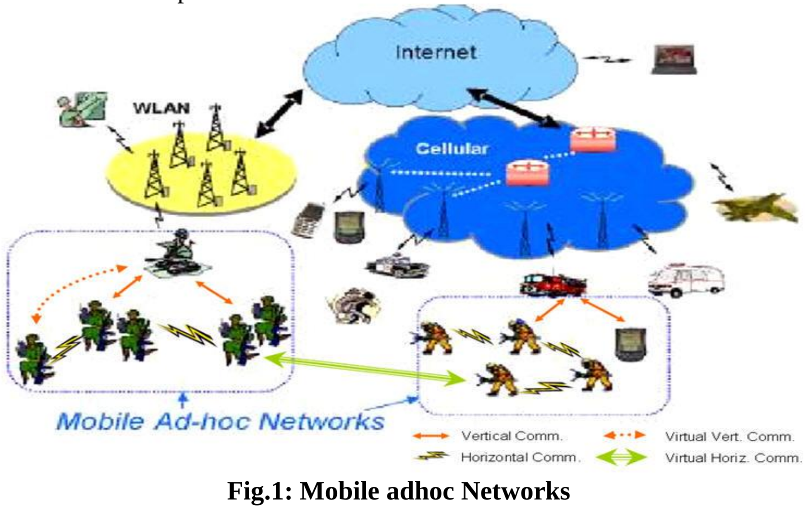

Fig.1: Mobile adhoc Networks

Due to the lack of centralized control, MANETs nodes collaborate with one another to achieve a common goal. The major activities involved in self-organization are neighbor discovery, topology reorganization and topology organization. Network topology describes the connectivity information of the entire network, including the nodes in the network and the connections between them. Topology control is very important for the overall performance of a MANET. In this presentation considering both upper layer networks capacity and physical layer cooperative communications and we study the topology control concerns in MANETs with cooperative communications. We suggest a Capacity-Optimized Cooperative (COCO) topology control scheme to develop the network capacity in MANETs by in cooperation optimizing communicate node selection, transmission mode selection and interference control in MANETs with cooperative communications. By using simulations that the physical layer cooperative communications have momentous impacts on the network capacity, and the future topology control scheme can significantly get better the network capacity in MANETs with cooperative communications.

II. MOBILE AD HOC NETWORKS WITH COOPERATIVE COMMUNICATIONS

1.1. **Cooperative Communications**

In Cooperative Communications in Existing Network Architectures, the primary network model is a MANET with an existing clustered communications, in which cooperative transmission is centrally activated and controlled by the cluster access points. All terminals communicate through a cluster access a point, which handles routing to other clusters. In the classical multihop architecture, each cluster is responsible for transmitting the message to a “gateway” node in the next cluster. In our cooperative network architecture, between clusters the access points uses multiple gateway nodes, which propagate the message providing cooperative gains compared to the single gateway solution. Better links translate into better network connectivity compared to multihop solutions. Relying on existing techniques to determine the clustering structure, our objective is to describe how the access points can select the cooperative nodes by means of matching algorithms and how this benefits the network connectivity.

Typically the cooperative communication refers to a system where users share and coordinate their resources to enhance the information transmission quality. The generalization of relay communication in which multiple sources also serve as relays for each other. At the beginning study of relaying problems appears in the information theory community to enhance communication between the source and destination. Now a day’s tremendous interests in cooperative communications are due to the increased understanding of the benefits of multiple antenna system. The Multiple Input Multiple Output (MIMO) systems have been widely acknowledged it is difficult for some wireless mobile devices to support multiple antennas due to the size and cost constraints. Recent studies show that the cooperative communications allows single antenna devices to work together to exploit the spatial diversity and reap the benefits of MIMO systems such as resistance to vanishing low transmitted power, high throughput and resilient networks. The basic idea of cooperative relaying is that some nodes which overheard the information transmitted from the source node and relay nodes the cooperative multiplicity is achieved. Communication could be implemented using two common strategies. They are Amplify and forward and Decoding and forward. In amplifying and forwarding the relay nodes simply boost the strength of the signal received from the sender and retransmit it to the receiver. In decode and forward the communicate nodes will perform physical layer decoding and then forward the decoding result to the destinations. The cooperation between multiple nodes and their antennas are employing a space time code in transmitting the relay signals. The cooperation at the physical layer can achieve full levels of diversity similar to a MIMO system and hence to reduce the interference and then increase the strength of connectivity in wireless network.

a) direct transmissions via a point-topoint conventional link;

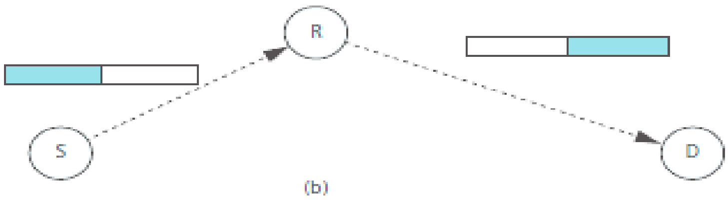

b) multi-hop transmissions via a two-hop manner occupying two time slots

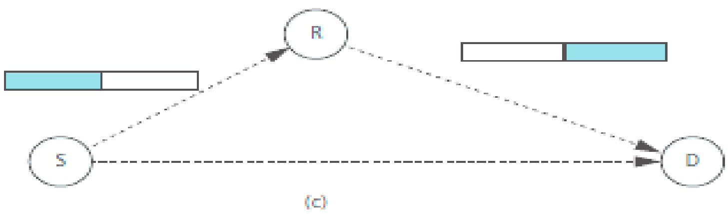

c) cooperative transmissions via a cooperative diversity occupying two consecutive slots. The destination combines the two signals from the source and the relay to decode the information.

Fig.2: Three transmission protocols

1.2. Topology Control

The network topology in a MANET is changing dynamically due to user mobility, traffic, node batteries, and so on. A MANET is controllable by adjusting some parameters such as the transmission power, channel assignment. Topology control is a method used in distributed computing to alter the understanding network in order to reduce the cost of distributed algorithms if ran over the new resulting graphs. Topology control is consumed mostly by the wireless Ad Hoc and sensor network research community. The main aspire of topology control is to save energy, reduce interference between nodes and extended lifetime of the network. Generally topology control is such a scheme to determine where to deploy the links and how the links work in wireless networks to form a good network topology which will optimize the energy consumption, the capacity of the network or end to end routing performance. A Mobile Ad hoc Network is self configuring infrastructure network of mobile devices connected by wireless. Every device in a MANET is free to shift independently in any direction and will therefore change its links to other devices regularly. Each must onward traffic not related to its own use, and as a result be a router. The primary challenge in building a MANET is equipping each device to continuously maintain the information required to properly route traffic. Such networks may work by self or may be connected to the large internet. MANETs are a kind of wireless as hoc network that usually has a routable networking environment on top of a link layer ad hoc network. The growth of laptop and 802.11/Wi-Fi wireless networking has made MANETs a popular research topic. Power control and channel control issues are coupled with topology control in MANETs while they are treated separately traditionally. Even though a mobile node can sense the available channel, it lacks of the scope to make network-wide decisions. Therefore it makes more sense to conduct power control and channel control via the topological viewpoint. Aim of topology control is then to set up interference- free connections to minimize the maximum transmission power and the number of required channels. The topology control focus on network connectivity with the link information provided by MAC and physical layers. In general a MANET can be mapped into a graph G(V,E), where V is the set of nodes in the network and E is the edge set representing the wireless links. As topology control is to determine the existence of wireless links subject to network connectivity, the general topology manage problem can be expressed as $G^*=\arg\max f(G)$, (1) According to the objective function a better topology $G^*(V, E^*)$ will be constructed as the output of the algorithm. G^* should contain all mobile nodes in G, and the link connections E^* should preserve network connectivity without partitioning the network.

III. TOPOLOGY CONTROL FOR NETWORK CAPACITY IMPROVEMENT IN MANETS WITH COOPERATIVE COMMUNICATIONS

3.1 The capacity of MANETs

There are dissimilar definitions for network capacity. There areTwo types of network capacity are introduced. The first one is transport capacity, which is parallel to the total one-hop capacity in the network. It acquires distance into deliberation and is based on the sum of bit-meter products. One bit-meter shows that one bit has been transported to a distance of one indicator toward its destination. One more type of capacity is throughput capacity, which is based on the information capacity of a channel. Clearly, it is the amount of all the data effectively transmitted during a unit time. It has been exposed that the capacity in wireless ad hoc networks is restricted. The routing not only discover paths to meet quality of service (QoS) necessities but also balances traffic load in nodes to keep away from hot spots in the network. When balancing traffic, the network may disclose more traffic flows and maximize the capacity. Since we center of attention on topology control and cooperative communications, assume an ideal load balance in the network, wherever the traffic loads in the network are uniformly distributed to the nodes in the network.

3.2. Improving Network Capacity Using Topology Control in MANETS with Cooperative Communications

We can improve MANETs network capacity with cooperative communications using topology control, we can set the network capacity as the objective function in the topology control problem in Eq.1. When cooperative network is used, a best communicate needs to be selected proactively before transmission. In this study, we agree to decode and forward relaying scheme. The source broadcasts its message to the relay and destination in the first slot. They communicate node and destination in the first slot. The relay node decodes and re-encodes the signal from the source and then forwards it to the destination in the second slot. The maximum instantaneous end to end communal information, outage probability, and outage capability can be derived. The interference model in the broadcast period of both the covered neighbors of the source and the covered neighbors of the relay and the destination have to be silent to ensure successful reception

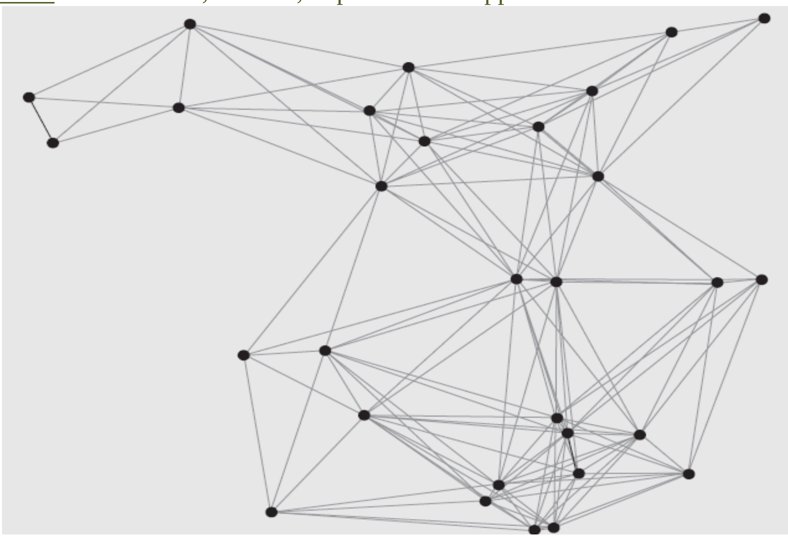

Fig.3: The original topology: A MANET with 30 nodes randomly deployed in 800 x 800 m2area

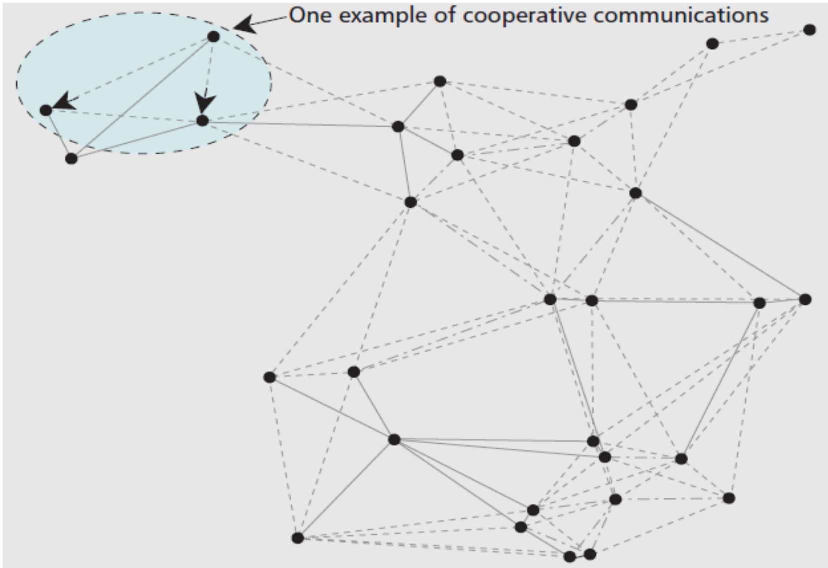

Fig.4: The final topology generated by COCO. The solid lines denote traditional direct Transmissions and multihop transmissions. The dashed lines denote the links involved in Cooperative communications

IV. PERFORMANCE ANALYSIS

In a performance analysis assume a MANET with 30 nodes randomly deployed in a 800 x 800 m2 area. The number of nodes is changed simultaneously. We evaluate the performance of the projected scheme with that of an existing well known topology control scheme called LLISE, which simply considers conventional multi-hop transmissions without cooperative communications and preserves the minimum interference path for each neighbor link locally. we furthermore show the worst network capacity between all the topology configurations for evaluation. The novel topology is shown in Fig. 3, where links exist at any time the associated two end nodes are within transmission range of each other. It is obvious that this topology lacks any physical layer cooperative communications. Fig.4. shows the resulting topology by means of the projected COCO topology control scheme. In Fig.4 the solid lines indicate links involved in cooperative communication. We can observe from Fig.4. to get the most out of the network capacity of the MANET, various links in the network are involved in cooperative communication. The example of two-phase cooperative communications is shown in the peak left corner of the outline. The Fig.4 shows the network capacity per node in different topology control schemes with different numbers of nodes in the MANET. The proposed COCO scheme has the highest network capacity regardless of the number of nodes in the network. Similar to COCO, LLISE is executed in each node distributed. Nevertheless COCO can achieve a much higher network capacity than LLISE, since LLISE only considers multi hop transmission. The gain performances of this proposed scheme comes from the joint design of relay node selection, transmission mode selection, and interference minimization in MANETs with cooperative communication.

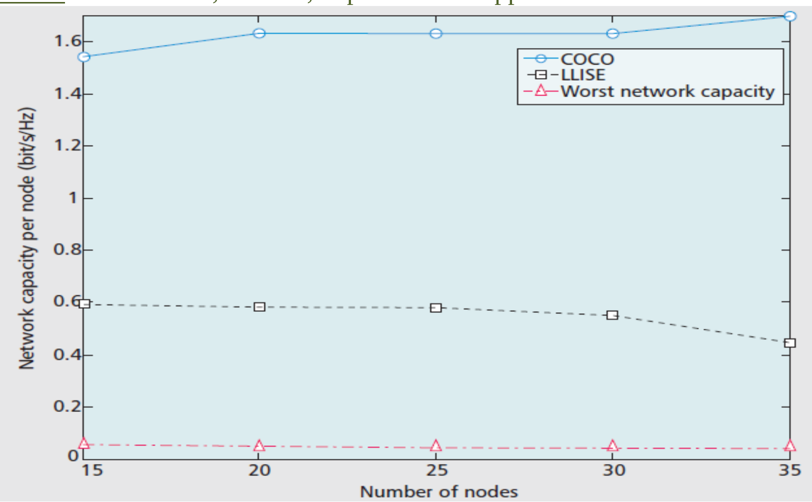

Fig.5: Network capacity versus different numbers of nodes in the MANET.

V. CONCLUSIONS AND FUTURE WORK

In this we have initiated physical layer cooperative communications, network capacity, and topology control network capacity in MANETs. To improve the network capability of MANETs with cooperative communications, we have projected a Capacity- Optimized Cooperative (COCO) topology control scheme that considers both upper layer network capacity and physical layer relay selection in cooperative communications. Simulation results have shown that physical layer cooperative communications techniques have significant impacts on the network capacity, and the projected topology control scheme can significantly get better the network capability in MANETs with cooperative communications. Prospect work is in development to consider dynamic traffic patterns in the proposed scheme to further improve the performance of MANETs with cooperative communications.

REFERENCES

[1] J. Laneman, D. Tse, and G. Wornell, "Cooperative Diversity in Wireless Networks: Efficient protocols and Outage Behavior," *IEEE Trans. Info. Theory*, vol. 50, no. 12, 2004, pp. 3062–80.
[2] P. H. J. Chong *et al.*, "Technologies in Multihop Cellular Network," *IEEE Commun. Mag.*, vol. 45, Sept. 2007, pp. 64–65.
[3] K. Woradit *et al.*, "Outage Behavior of Selective Relaying Schemes," *IEEE Trans. Wireless Commun.*, vol. 8, no. 8, 2009, pp. 3890–95.
[4] Y. Wei, F. R. Yu, and M. Song, "Distributed Optimal Relay Selection in Wireless Cooperative Networks with Finite-State Markov Channels," *IEEE Trans.Vehic.Tech.*,vol. 59, June 2010, pp. 2149
[5] Q. Guan *et al.*, "Capacity-Optimized Topology Control for MANETs with Cooperative Communications," *IEEE Trans. Wireless Commun.*, vol. 10, July 2011, pp. 2162–70.
[6] P. Santi, "Topology Control in Wireless Ad Hoc and Sensor Networks," *ACM Computing Surveys*, vol. 37, no. 2, 2005, pp. 164–94.
[7] T. Cover and A. E. Gamal, "Capacity Theorems for the Relay Channel," *IEEE Trans. Info. Theory*, vol. 25, Sept. 1979, pp. 572–84.
[8] Q. Guan *et al.*, "Impact of Topology Control on Capacityof Wireless Ad Hoc Networks," *Proc. IEEE ICCS*, Guangzhou, P. R. China, Nov. 2008.
[9] P. Gupta and P. Kumar, "The Capacity of Wireless Networks," *IEEE Trans. Info. Theory*, vol. 46, no. 2, 2000, pp. 388–404.
[10] M. Burkhart *et al.*, "Does Topology Control Reduce Interference?," *Proc. 5th ACM Int'l. Symp. Mobile Ad Hoc Networking and Computing*, Tokyo, Japan, May 2004, pp. 9–19.

Performance Analysis of Trust-Aware Routing Framework for Wireless Mesh Networks

B. Sai Pragna [1], M. Shakeel Ahmed[2], B.Sai Manogna[3]
#1,3 M.TECH Scholar, PBRVITS, Kavali
#2 Associate Professor, PBRVITS, Kavali

ABSTRACT: *Multi-hop routing in wireless sensor networks (WSNs) offer small protection against trickery throughout replaying routing information. A challenger can develop this defect to launch various harmful or even devastating attacks against the routing protocols, including wormhole attacks, sinkhole attacks and Sybil attacks. Even though important research effort has been spend on the design of trust models to detect malicious nodes based on direct and indirect confirmation, this comes at the cost of extra energy consumption. Conventional cryptographic techniques or efforts at mounting trust-aware routing protocols do not effectively address these problems. To secure the wireless sensor networks against adversaries misdirecting the multi-hop routing, we have preposed TARF, a robust trust-aware routing framework for dynamic WSNs. Without prolonged time synchronization or known geographic information, TARF offers dependable and energy-efficient route. TARF demonstrates effective adjacent to those harmful attacks developed out of identity trickery; the flexibility of TARF is verified through extensive assessment with both simulation and observed experiments on large-scale WSNs under various scenarios including mobile and RF-shielding network conditions. We have put into action a low-overhead TARF module in TinyOS; this implementation can be included into existing routing protocols with the least effort. Based on TARF, we also verified a proof-of-concept mobile target detection application that functions well next to an anti-detection mechanism.*

Index Terms: *Wireless Sensor Networks, Wireless Sensor Network, Trusted Aware Routing Framework (TARF), Congestio,. TinyOS*

I. INTRODUCTION

Wireless sensor networks (WSNs) are models for applications to report detected events of interest, such as forest fire monitoring and military surveillance. A Wireless sensor networks includes battery powered senor nodes with exceptionally limited processing abilities. With a narrow radio communication range, a sensor node wirelessly passes messages to a base station via a multi-hop path. Though, the multi-hop routing of WSNs often becomes the target of wicked attacks. An attacker may interfere nodes actually, create traffic collision with apparently valid transmission, fall or misdirect communication in routes or jam the communication channel by creating radio interference. As a risky and easy-to-implement type of attack, a malicious node basically replays all the outgoing routing packets from a applicable node to copy the latter node's uniqueness; the malicious node then uses this fake identity to contribute in the network routing, thus trouble making the network traffic. Even if malicious node cannot straightly listen in the valid node's wireless transmission, it can scheme with other malicious nodes to receive those routing packets, which is identified as a wormhole attack. A node in a Wireless sensor networks relies exclusively on the packets received to know about the sender's identity, replaying routing packets permits the wicked node to forge the individuality of this valid node. After "stealing" that valid characteristics, this malicious node is able to misdirect the network traffic. It may fall packets received, forward packets to another node not supposed toward be in the routing path, or form a transmission loop from side to side which packets are passed among a few malicious nodes infinitely.

Sinkhole attacks can be start on after thefting a applicable identity, in which a malicious node may maintain itself to be a base station through replaying all the packets from a genuine base station. Such a fake base station could attract more than half the traffic, creating a "black hole.". This technique can be engaged to conduct another strong form of attack Sybil attack: all the way through replaying the routing information of multiple legal nodes, an attacker may nearby multiple identities to the network. A valid node, if cooperated, can also launch all these attacks.

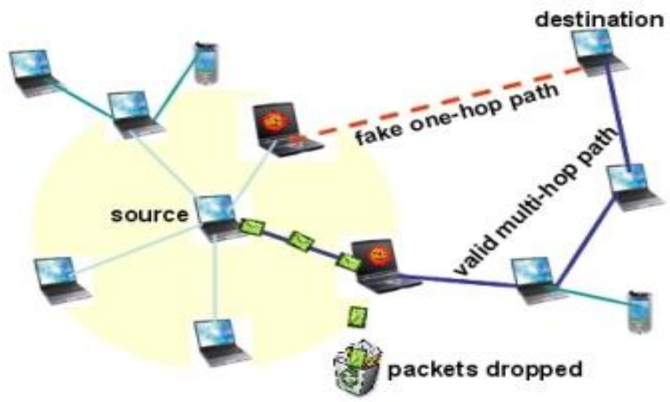

Fig.1: Attacks in multi hop routinng

Time synchronization service in wireless sensor networks has to meet challenges which are substantially different from those in infrastructure based networks. For example each sensor has a finite battery source and communication is expensive in terms of energy, an important issue of wireless sensor networks is energy efficiency. In addition, wireless sensor networks show a higher failure probability over the time than in traditional networks due to battery depletion or destruction of the sensors, and changes in the environment can severely affect radio propagation causing frequent network topology changes and network partitions. Moreover, at high densities wireless sensor networks become much more likely to suffer communication failures due to contention for their shared communication medium. These elements lead to robustness, strong energy efficiency and self configuration requirements. In the last several years, clock synchronization protocols for wireless sensor networks have been proposed based on different approaches ie., Reference Broadcast Synchronization (RBS) or hierarchical approaches, or interval based, or probabilistic approaches for energy efficiency. However, in spite of their diversity, these applications share a common viewpoint: they provide an accurate time estimate by means of periodic synchronization performed by each sensor node and based on messages exchanged with its neighbor nodes. Each clock adjustment is energy consuming since it involves transmitting messages and pay attention, besides the computational cost.

II. DESIGN CONSIDERATIONS

2.1. Assumptions

In this objective is secure routing for data collection tasks, which are one of the mainly fundamental functions of wireless sensor networks. In a data compilation task, a sensor node sends its example data to a remote base station with the help of other intermediate nodes, then there could be more than one base station, the direction-finding approach is not affected by the number of base stations that there is only one base station. An opponent may fake the identity of any legal node through replaying that node’s outgoing routing packets and spoofing the acknowledgement packets, even remotely through a wormhole. In addition, to merely simplify the introduction of TARF to assume no data aggregation is involved.

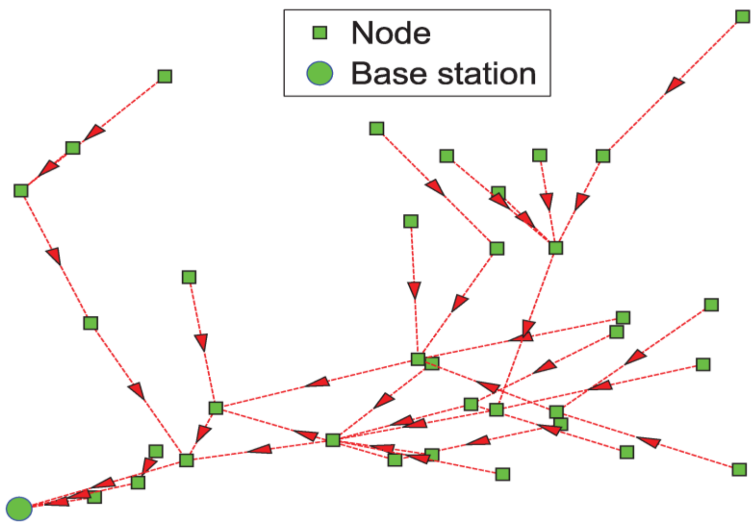

Fig. 2. Multi-hop routing for data collection of a WSN.

It is to be applied to cluster based wireless sensor networkss with static clusters, where data are cumulatively by clusters before being relayed. Cluster-based wireless sensor networkss allows for the great savings of energy and bandwidth through aggregating data from children nodes and performing routing and transmission for children nodes. In a cluster-based wireless sensor networks, the cluster headers themselves form a sub-network; after certain data arrive at a cluster header, the aggregated information will be routed to a base station only through such a sub network consisting of the cluster headers. The framework can be functional to this sub-network to achieve secure routing for cluster based wireless sensor networkss. TARF may run on cluster headers only and the cluster headers communicate with their children nodes directly since a static cluster has known relationship between a cluster header and its child nodes, even if any link-level security features may be further employed.

2.2. Authentication Requirements

Though a specific application may determine whether data encryption is needed, TARF requires that the packets are correctly authenticated, particularly the broadcast packets from the base station. The transmition from the base station is unevenly authenticated so as to guarantee that an adversary is not able to manipulate or forge a broadcast message from the base station at will. With authenticated broadcast, even with the existence of attackers, TARF may use TrustManager and the received broadcast packets about delivery information to choose trustworthy path by circumventing compromised nodes. Without being able to capturing the base station, it is generally very difficult for the opposition to manipulate the base broadcast packets from the base station is critical to any successful secure routing protocol. It can be achieved through existing irregularly authenticated broadcast schemes that may require loose time synchronization. As an example, µTESLA achieves asymmetric authenticated broadcast through a symmetric cryptographic algorithm and a loose delay schedule to disclose the keys from a key chain.

III. DESIGN OF TARF

TARF secures the multi-hop routing in wireless sensor networkss against intruders developing the repetation of routing information by evaluating the trustworthiness of neighboring nodes. It recognizes such intruders that misdirect obvious network traffic by their low trust advantage and routes data through paths circumventing those intruder to achieve reasonable throughput. TARF is also energy-efficient, highly scalable, and well flexible. Before introducing the detailed design, we initially introduce several essential notions here.

Neighbor: For a node*N*, a neighbor (neighboring node) of *N* is a node that is reachable from *N* with one-hop wireless transmission.
Trust level: For a node *N*, the trust level of a neighbor is a decimal number in [0, 1], representing *N*'s opinion of that neighbor's level of trustworthiness. Particularly, the trust level of the neighbor is *N*'s estimation of the probability that this neighbor correctly delivers data received to the base station. That trust level is indicates as *T*.
Energy cost: For a node *N*, the energy cost of a neighbor is the average energy cost to successfully deliver a unit-sized data packet with this neighbor as its next-hop node, from *N* to the base station. This energy cost is indicated as *E*.

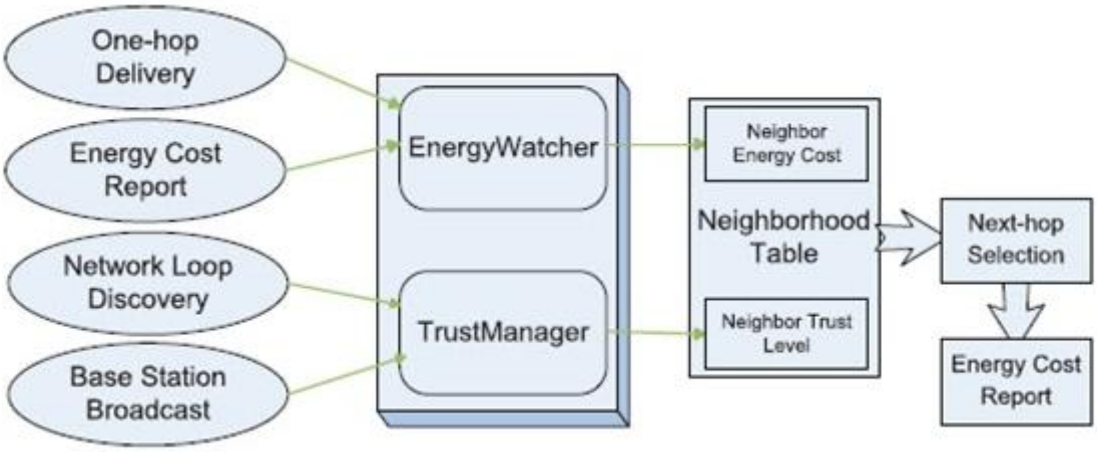

Fig. 3: Each node selects a next-hop node based on its neighborhood table, and broadcast its energy cost within its neighborhood. To maintain this neighborhood table, Energy- Watcher and TrustManager on the node keep track of related events (on the left) to record the energy cost and the trust level values of its neighbors.

3.2. Routing Procedure

TARF with as many other routing protocols, runs as a interrupted service. The length of that phase determines how regularly routing information is exchanged and reorganized. At the beginning of each period, the base station broadcasts a message regarding data release during last period to the whole network consisting of a few contiguous packets. Each such packet has a field to indicate how many packets are remaining to complete the broadcast of the current message. The achievement of the base station broadcast triggers the exchange of energy report in this new period. henever a node receives such a broadcast message from the base station, it recognizes that the most recent period has ended and a new period has just started. No fixed time synchronization is required for a node to keep track of the beginning or ending of a period. During each period, the Energy Watcher on a node monitors energy consumption of one-hop transmission to its neighbors and processes energy cost reports from those neighbors to maintain energy cost entries in its neighborhood table; its TrustManager also keeps track of network loops and processes broadcast messages from the base station about data delivery to maintain trust level entries in its locality table.

3.3. Energy Watcher & Trust Manager

In this module Cluster-based wireless sensor networks allows for the great savings of energy and bandwidth through aggregating data from children nodes and performing routing and transmission for children nodes. In a cluster-based wireless sensor network, the cluster headers themselves form a sub network, after certain information appear at a cluster header, the collective data will be routed to a base station only through such a sub network consisting of the cluster headers. Framework can then be applied to this sub-network to achieve secure routing for cluster based wireless sensor networks. A node N's Trust Manager decides the trust level of each neighbor based on the following events: broadcast from the base station about data delivery and discovery of network loops. For each neighbor b of N, TNb denotes the trust level of b in N's neighborhood table. At the opening, each neighbor is given a neutral trust level 0.5. After any of those actions takes place, the relevant neighbors' trust levels are updated. Though sophisticated loop-discovery methods exist in the presently developed protocols, they often rely on the evaluation of detailed routing cost to reject routes likely most important to loops. To minimize the attempt to put together TARF and the existing protocol and to reduce the transparency, when an existing routing protocol does not offer any anti loop mechanism, it adopts the Probabilistic Clock Reading Method to detect routing loops.

IV. IMPLEMENTATION AND EMPIRICAL EVALUATION

In order to estimate TARF in a real-world setting, we execute the TrustManager component on TinyOS 2.x, which can be included into the existing routing protocols for wireless sensor networks with the least attempt. We implemented TARF as a self-contained routing protocol on TinyOS 1.x before this second implementation.

```
//Step 1. traverse the neighborhood table for an optimal candidate for the next hop
optimal_candidate = NULL
//the cost of routing via the optimal candidate provided by the existing protocol, initially infinity
optimal_cost = MAX_COST
//the trust level of the optimal candidate, initially 0
optimal_trust = MIN_TRUST
for each candidate in the neighborhood table
    if link is congested, or may cause a loop, or does not pass quality threshold
        continue
    better = false
    if candidate.trust >= optimal_trust && candidate.cost < optimal_cost
        better = true
    //prefer trustworthy candidates
    if candidate.trust >= TRUST_THRESHOLD && optimal_trust < TRUST_THRESHOLD
        better = true
    if candidate.trust >= ESSENTIAL_DIFFERENCE_THRESHOLD + optimal_trust
        better = true
    //effective when all nodes have low trust due to network change or poor connectivity
    if candidate.trust >= 3 * optimal_trust / 2
        better = true
    //add restriction of trust level requirement
    if candidate.trust >= TRUST_THRESHOLD && candidate.trust / candidate.cost >
optimal_trust / optimal_cost
        better = true
    if better == true
        optimal_candidate = candidate
        optimal_cost = candidate.cost
        optimal_trust = candidate.trust

//Step 2. decide whether to switch from the current next-hop node to the optimal candidate found:
if optimal_trust >= currentNextHop.trust                                  \
 || currentNextHop.trust <= TRUST_THRESHOLD                               \
 || current link is congested and switching is not likely to cause loops  \
 || optimal_cost + NEXTHOP_SWITCH_THRESHOLD < currentNextHop.cost         \
    currentNextHop = optimal_candidate
```

Fig.4: Routing decision incorporating trust management.

1.1. TrustManager Implementation Details

The *TrustManager* component in TARF is enfolded into an self-determining TinyOS configuration named TrustManagerC. TrustManagerC uses a enthusiastic logic channel for communication and runs as a periodic check with a configurable period, thus not interfere with the application code. Although it is possible to implement TARF with a period always synchronized with the routing protocol's period that would cause much intrusion into the source code of the routing protocol. The current TrustManagerC utilizes a period of 30 seconds; for exact applications, by adjusting a convinced header file, the period extent may be re-configured to reflect the sensing occurrence, the energy effectiveness and trustworthiness requirement.

This new implementation integrating TARF requires moderate program storage and memory utilization. Here implemented a typical TinyOS data collection application, Multihop Oscilloscope, based on this new protocol. The Multihop Oscilloscope application, with certain modified sensing parameters for our later evaluation purpose, sometimes makes sensing samples and sends out the sensed data to a root via multiple routing hops. Originally, Multihop Oscilloscope uses CTP as its routing protocol. Now list the ROM size and RAM size necessity of both implementation of Multihop Oscilloscope on non-root Telosb motes in Table 1. The enabling of TARF in Multihop Oscilloscope increases the size of ROM by around 1.3KB and the amount of memory by around 1.2KB.

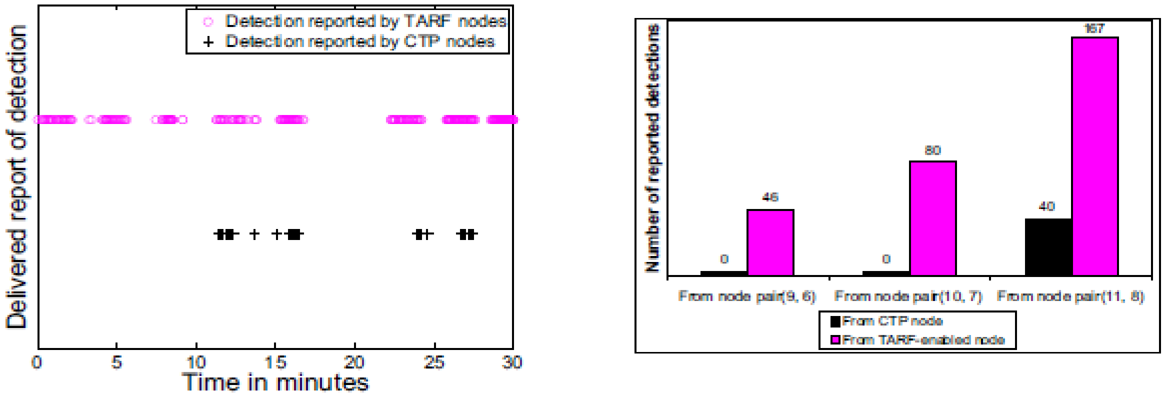

(a) Detection report. (b) Number of reported detections.

Fig. 5. Comparison of CTP and the TARF-enabled CTP in detecting the moving target.

V. CONCLUSIONS AND FUTURE WORK

We have designed and implemented a working model which is an enhanced version of TARF, a robust trust-aware routing framework for wireless sensor networks, to secure multi-hop routing in dynamic wireless sensor networks against harmful attackers exploiting the replay of routing information. TARF spotlighted on conviction worthiness and energy efficiency. With the idea of trust management, this model facilitates a node to keep track of the trustworthiness of its neighbors and thus to select a consistent route. With the idea of the energy watcher, our model calculates the total energy cost which is consumed by the packet to reach its destination. Trust manager has initiated the model of using two routing tables i.e default routing table and running routing table, with this concept its has become easy to find the attacker in the path. For provided that security in this paper we have used the new encryption technique i.e. Elliptic Curve Cryptography algorithm.

REFERENCES

[1] Guoxing Zhan, Weisong Shi, “Design and Implementation of TARF: Trust-Aware Routing Framework for WSNs” IEEE Transactions On Dependable And Secure Computing, vol. 9, no. 2, March/April 2012

[2] G. Zhan, W. Shi, and J. Deng, “Tarf: A Trust-Aware Routing Framework for Wireless Sensor Networks,” Proc. Seventh European Conf. Wireless Sensor Networks (EWSN ’10), 2010.

[3] F. Zhao and L. Guibas, Wireless Sensor Networks: An Information Processing Approach. Morgan Kaufmann, 2004.

[4] A. Wood and J. Stankovic, “Denial of Service in Sensor Networks,” Computer, vol. 35, no. 10, pp. 54-62, Oct. 2002.

[5] C. Karlof and D. Wagner, “Secure Routing in Wireless Sensor Networks: Attacks and Countermeasures,” Proc. First IEEE Int’l Workshop Sensor Network Protocols and Applications, 2003.

[6] M. Jain and H. Kandwal, “A Survey on Complex Wormhole Attack in Wireless Ad Hoc Networks,” Proc. Int’l Conf. Advances in Computing, Control, and Telecomm. Technologies (ACT ’09), pp. 555-558, 2009.

[7] I. Krontiris, T. Giannetsos, and T. Dimitriou, “Launching a Sinkhole Attack in Wireless Sensor Networks; The Intruder Side,” Proc. IEEE Int’l Conf. Wireless and Mobile Computing, Networking and Comm. (WIMOB ’08), pp. 526-531, 2008.

[8] J. Newsome, E. Shi, D. Song, and A. Perrig, “The Sybil Attack in Sensor Networks: Analysis and Defenses,” Proc. Third Int’l Conf. Information Processing in Sensor Networks (IPSN ’04), Apr. 2004.

[9] L. Zhang, Q. Wang, and X. Shu,“A Mobile-Agent-Based Middleware for Wireless Sensor Networks Data Fusion,” Proc. Instrumentation and Measurement Technology Conf. (I2MTC ’09), pp. 378-383, 2009.

[10] S. Ganeriwal, L. Balzano, and M. Srivastava, “Reputation-based framework for high integrity sensor networks,” ACM Trans. Sen.Netw., 2008.

[11] G. Zhan, W. Shi, and J. Deng, “Design, implementation and evaluation of tarf: A trust-aware routing framework for dynamic wsns,” http://mine.cs.wayne.edu/_guoxing/tarf.pdf, Wayne State University, Tech. Rep. MIST-TR-2010-003, Oct. 2010.

[12] Daniela Tulone, “A Resource–efficient Time Estimation for Wireless Sensor Networks,” Department of Computer Science University of Pisa

Developing Infrared Controlled Automated Door System

Lucky Gautam[1] Chinoy Sharma[2] Akshaj Arora[3] Pinku yadav[4]
[1,2] Department Of Electronics And Instrumentation
[3]Department Of Electronics And Communication
[4]Department Of Mechnical And Automation
[1,2,3]Amity University, Noida
[4] Vellore University, Vellore

ABSTRACT- *As a result of enhanced civilization and modernization, the human nature demands more comfort to his life. Automated doors have acquired and have become part of one's life from his office to shopping complex. Automated doors are quite common and a vast field of research now days. Many attempts are made to decrease the manufacturing cost and achieve an efficient and inexpensive output. This paper will focus upon giving a brief idea about construction of an automated door using IR sensors. A small experiment was performed which gave the desired output.*

Keywords – *IR sensor, Comparator, DC Motor, Motor driver circuit, sliding door.*

I. INTRODUCTION

Automatic door is an automated movable barrier installed in the entry of a room or building to restrict access, provide ease of opening a door or provide visual privacy. This is being achieved by various detection circuits available in the market. These detection circuits vary from basic sensors like IR sensor, force sensors to complex and expensive vision circuitry. To this end, we model and design an automatic sliding door with a room light control system to provide the mentioned needs. This was achieved by considering some factors such as economy, availability of components and research materials, efficiency, compatibility and portability and also durability in the design process. This system works on the principle of breaking an infrared beam of light, sensed by a photodiode. It consists of transmitting infrared diodes and receiving photo-diodes. The system is to detect whether someone is coming in or not. The photodiodes are connected to comparators, which give a lower output when the beam is broken and high output when transmitting normally. The general operation of the work and performance is dependent on the presence of an intruder entering through the door and how close he/she is in closer to the door. The overall work was implemented with a constructed work, tested working and perfectly functional.

II. COMPONENTS

IR SENSOR- The sensor senses whether receiver of it is receiving light from transmitter or not and feeds the result to the comparator. If any obstacle comes in between receiver or transmitter then the path of infrared between receiver and transmitter breaks off. This result of receiver receiving the light or not is sent to the comparator.

COMPARATOR- Comparator compares the analogue inputs from the sensors with a fixed reference voltage. If this voltage is higher than the reference voltage than comparator outputs a low voltage and if the voltage is lower than the reference voltage than it outputs a high voltage to the decision making element that is the microcontroller. The IC used of the comparator is LM358N.

MICROCONTROLLER- Microcontroller is pre-programmed to turn on the motors or supply required current and voltage to motors only if the condition is fulfilled. Microcontroller check when the output of comparator is low it turns the motor on as the path between receiver and transmitter is broken due to some obstacle between them. The microcontroller feeds the output to the motor driver. After providing the output to run motor it must also give some delay that can be the time for the person to pass through the gate and after the body goes away it should also run motor anticlockwise to close the door.

MOTOR DRIVER- The current supplied by the microcontroller to is not sufficient to drive the motor. Thus motor driver provides sufficient current to run motor. It can take a maximum current of 600mA per channel which is more than enough to drive two motors. The IC used for it is L293D.

Voltage Regulator: 7805IC gives the output of 5V from 9V to microcontroller and motor driver.
Thus this way you can have a black line following robot ready to perform tasks.

III. BLOCK DIAGRAM

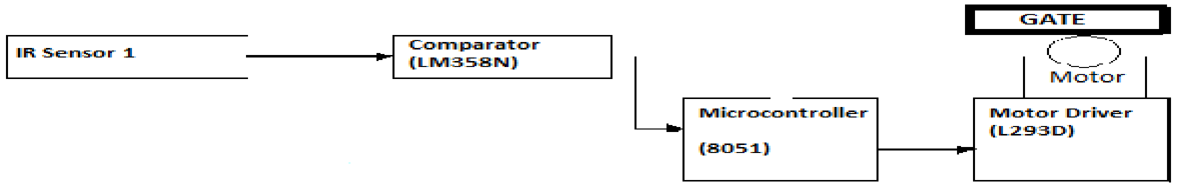

IV. SYSTEM PROGRAMMING

The program is being written in C language and the target we are trying to achieve through this program is already being defined in the above section.

```
#include <AT89X51.H>
#define L293D_A P2_0        //Positive of motor
void rotate_f(void);        //Forward run function
void rotate_b(void);        //Backward run function
void breaks(void);          //Motor stop function
void delay(void);           //Some delay

void main(){                //Our main function
   while(1){                //Infinite loop
          rotate_f();        //Run forward
          delay();           //Some delay
          breaks();          //Stop
          delay();           //Some delay
          rotate_b();        //Run Backwards
          delay();           //Some delay
          breaks();          //Stop
          delay();           //Some delay
      }                     //Do this infinitely
}

void rotate_f(){
      L293D_A = 1;          //Make positive of motor 1

}

void rotate_b(){
      L293D_A = 0;          //Make negative of motor 0
     }

void breaks(){
      L293D_A = 0;          //Make positive of motor 0

}

void delay(){               //Some delay...
   unsigned char i,j,k;
   for(i=0;i<0x20;i++)
      for(j=0;j<255;j++)
       for(k=0;k<255;k++);
}
```

V. CONCLUSION

This project gave an insight into designing of an automated door just by using IR sensors. This helped in reducing the cost spent in construction of automated doors. This project has lot of future scope like the same way we can construct a sliding door with a security system by attaching a keypad to enter password and then providing the access to the person into that secured area.

ACKNOWLEDGEMENT

This project is having lots of scope in future and it can be improved in various ways to fulfill the tasks of user. I wish to express deep sense, extreme depth of gratitude towards Rahul Kr. Verma, ECE Department, Amity University for invaluable helping hand extended to me. The work cannot be finished in such a fine manner without his help. I would also like to thank my HOD Dr. H.P Singh, EIE Dept. for the support and encouragement he provided. Lastly I would thank my whole EIE Department to give me such a wonderful platform to finish the project.

REFERENCES

[1] W.Banzhaf, P.Nordin, R.E. Keller and F.D. Francone, Genetic Progamming- An introduction; On the automatic Evolution of Computer Programs and its Applications. Morgan Kaufmann, dpunkt.verlag, 1998

[2] Jean-Francois Dupis and Marc Parizeau, Vision-Based Line-Following Robot Controller, Canada. 2006

[3] Alkar, A. Z., & Buhur, U. (2005), “An Internet Based Wireless Home Automation System for Multifunctional Devices”, *IEEE Consumer Electronics, 51*(4), pp. 1169-1174.

[4] Ciubotaru-Petrescu, B., Chiciudean, D., Cioarga, R., & Stanescu, D. (2006), “Wireless Solutions for Telemetry in Civil Equipment and Infrastructure Monitoring”, *3rd Romanian-Hungarian Joint Symposium on Applied Computational Intelligence (SACI)* May 25-26, 2006.

[5] Conte, G., & Scaradozzi, D. (2003), “Viewing ho me automation systems as multiple agents systems”, *RoboCUP2003*, Padova, Italy. Retrieved at: http://www.robosiri.it/ROBOCUP_2003/ROBOCUP-SITOSIRI/articles/pdf/Conte.pdf

[6] Kalpakjian (2008), “Automation in Manufacturing. Manufacturing processes for Engineering Materials”, 5 th Ed., Pearson Education, http://nd.edu/~manufact/MPEM%20pdf_files/Ch14.pdf

[7] Potamitis, I., Georgila, K., Fakotakis, N., & Kokkinakis, G. (2003), “An integrated system for smart-home control of appliances based on remote speech interaction”, *EUROSPEECH 2003, 8th European Conference on Speech Communication and Technology*, Geneva, Switzerland, Sept. 1-4, 2003, pp. 2197-2200.

[8] Ricardo Tesoriero, Jose A.Gallud, Maria D.Lozano, Vitor M.R. Penichet “Tracking Autonomous Entities using RFID Technology” IEEE transactions on consumer Electronics, Vol. 55, MAY2009

Design &Analysis of Pure Iron Casting with Different Moulds

Sunanda Das, Dr. Rakesh L. Himte
(MECHANICAL ENGG, RCET BHILAI/ CSVTU, INDIA)

ABSTRACT : *In the present work it has been shown that FEA software like ANSYS may play an important role in predicting cast defect before the actual casting. Transient thermal analysis and Couple-Field analysis in ANSYS can predict temperature distribution and thermal stress distribution in the casting after solidification very accurately. This fact has been proved by validating a transient thermal analysis which has been published in a reputed journal. After validating the thermal analysis, work has been extended to Couple-Field Analysis for thermal stress and shrinkage.*

After doing Couple-field analysis on sand mold, few modifications have been simulated and tested whether they are better than the configuration considered in the base paper. As first modification sand has been replaced by mullite and it has been seen that the mold shrinkage is less but the cast shrinkage is more. Thermal stress in the mullite mold is less than the sand mold. For the sand-mullite composite mold shrinkage is least as well as shrinkage for the cast is also least. But the thermal stress is more than the mullite mold.

Keywords: *Cast Solidification, Sand mold, Mullite Mold, Composite Mold, Transient thermal analysis, Couple-field analysis, ANSYS.*

I. INTRODUCTION

Technological difficulties involved in casting processes vary considerably according to the metal's melting temperature characteristics, which in turn are related to the physicochemical properties and structures of metals and alloys. These difficulties also involve a series of properties, which include differences in chemical activities between the elements that constitute the alloy, solubility of the gases, method of solidification among the chemical elements, type of molding, and coefficients of solidification shrinkage. On the other hand, the cooling process also affects the flow of cast metal, influencing the mold filling and stability, allowing the occurrence of cooling stresses and properties changes in the final product, and producing variations in the geometrical dimensions, the shape of the surface finish and the quality of the cast part.

An investigation was done by YIN-HENC CHEN and YONG-TAEK IM on the prediction of shrinkage a permanent mold casting in sand mold in the year of 1990 and their work published in Int. J. Mach. Tools Manufacture (Vol. 30, No. 2, pp. 175-189).

In the year of 1994 JYRKI MIETI'INEN and SEPPO LOUHENKILPI did a remarkable work on Calculation of Thermophysical Properties of Carbon and Low Alloyed Steels for Modeling of Solidification Processes and they published their work in METALLURGICAL AND MATERIALS TRANSACTIONS B (VOLUME 25B)

A work on Thermal stress and crack prediction was done by L.C. Würker, M. Fackeldey, P.R. Sahm and B.G. Thomas in the year of 1998.

B. J. MONAGHAN and P. N. QUESTED did a work on Thermal Diffusivity of Iron at High Temperature in Both the Liquid and Solid States in the year of 2001 and their work published in the journal named ISIJ International (Vol. 41, No. 12, pp. 1524–1528).

A very good work on Numerical Simulation of Filling Process in Die Casting was done by Y. B. Li and W. Zhou and their work got published in the journal Materials Technology in the year of 2003 (Vol. 18, No. 1, pp. 36-41).

In the year of 2005 a very excellent work was done by M. M. Pariona and A. C. Mossi on Numerical Simulation of Heat Transfer during the Solidification of Pure Iron in Sand and Mullite Molds. This work was published in a very reputed journal named "J. of the Braz. Soc. of Mech. Sci. & Eng." and this work has been referred as a base paper in the present work. The work has been extended in the present thesis over the work of this base paper on the investigation of thermal stain and shrinkage of a pure iron casting in mullite mold and a composite mold made of mullite and sand. Though many works have already been done on thermal and thermo-mechanical simulation of casting process but a thermo-mechanical simulation on a composite mold made of sand and mullite is a new one.

II. DESCRIPTION OF THE PROBLEM

In casting of an object many problems are raised during solidification. One of these problems is internal cracks of the cast object due to compressive stress generated during solidification. This compressive stress is governed by many factors of mold topology. Compressive stress generated during solidification of casting can be controlled by mold thickness, mold materials, combination of different mold materials and layer thickness, draft angle etc. So, before taking decision on above parameters it is needed to know the stress distribution of cast object after solidification. Here in this work a detailed transient (i.e. time dependent) couple-field analysis has been done on a cast object to predict thermal stress in the cast body during solidification. Moreover an investigation has been done in this work on shrinkage and thermal strain with a mold material named mullite and combination of sand and mullite.

III. MATHEMATICAL MODELING OF CAST SOLIDIFICATION

In order to formulate a mathematical model for heat transfer problem during casting, consider superheated liquid metal poured in an investment casting shell. There are two steps in which metal losses their heats,

a. First step in which metal losses its sensible heat (superheat).
b. Second step during which metal losses its heat of fusion (Hf).

Time of solidification is determined separately during each interval using different heat transfer coefficients (HTCs) and then individual times are summed up together to get total time taken for solidification.

1 Sensible Heat Transfer

When metal is poured in investment casting shell, whole of the shell is quickly heated to high temperature (temperature of molten metal), heat transfer also starts subsequently and temperature of metal starts decreasing. As a result of this, temperature of mold starts increasing. During this step total heat transfer from top and walls is

$$Q_t = Q_T \cdot t_1 \qquad (1)$$

Where Qt is the total quantity of heat lost from top and wall, QT is total rate of heat transfer by convection and radiation from top and conduction through walls and t1 is the total time taken for heat transfer (time of solidification in first step).

Heat transfer occurs by three modes namely convection, conduction and radiation; total rate of heat transfer (QT) is summation of rate of heat transfers by each mode.

$$Q_T = Q_{T1} \cdot Q_{T2} \cdot Q_{T3} \qquad (2)$$

where QT1, QT2, QT3 are the rate of heat transfers by convection and radiation from top surface, conduction through walls and convection and radiation from heated mold surface, respectively.

Rate of heat transfer by convection and radiation from top may be written as:

$$Q_{T1} = (h + h_r)_{\overline{T}} \cdot A_T \cdot (\overline{T} - T_\infty) \qquad (3)$$

where $\overline{T} = \frac{1}{2}(T_p + T_m)$, temperature at which HTCs are determined, h and hr are the heat transfer coefficients for free convection and radiation, respectively, AT is area of top surface of mold and Tα is mold temperature. Major portion of heat in this process of heat transfer is lost through top surface thus QT1 is the major rate of heat transfer during solidification. This is the reason; risers of castings are usually covered by some insulating compound or bad heat-conducting medium to keep metal liquid for a longer period of time so that proper feeding of metal could be achieved.

Rate of heat transfer by conduction may be written as:

$$Q_{T2} = \frac{(T_p - T_\infty)}{R_t} \qquad (4)$$

Where Tp and Tα are the inside and outside temperatures of mold and Rt is the thermal resistance of mold wall.

Thermal resistance of the mold here though very high, is not constant, but keeps on changing with change of temperature and contributes towards overall effect of heat transfer.

Similarly, rate of heat transfer again by convection and radiation from outer heated wall of mold may be written as:

$$Q_{T3} = (h + h_r)_{T_s} \cdot A \cdot (T_s - T_\infty) \qquad (5)$$

Where Ts is the surface temperature of the mold, Tα is the outside (surrounding) temperature of the mold [(Tα=Tr), Tr = room temperature], h and hr are heat transfer coefficients (HTCs) for free convection and radiation, respectively, and A is area of heated mold surface towards ambient. This mode of heat transfer has very little contribution towards overall rate of heat transfer during first step, as initially surface of mold is at ambient and gets heated slowly in small increments thus starts transferring heat. This mode of heat transfer also has little contribution due to high thermal resistance of mold material(s), which stops most of heat from coming out of the mold.

Putting the values in Eq. (2)

$$Q_T = (h + h_r)_{\overline{T}} \cdot A_T \cdot (\overline{T} - T_\infty) + \frac{(Tp - T_\infty)}{R_t} + (h + h_r)_{Ts} \cdot A \cdot (Ts - T_\infty) \qquad (6)$$

(3.6)

Total quantity of heat transferred (Qt) is actually the heat lost by metal as its sensible heat, which may be written as

$$Q_t = mCp\Delta T$$
$$Q_t = mCp(Tp - Tm) \qquad (7)$$

Where, Cp is specific heat of metal, Tp and Tm are pouring and melting temperatures of the metal, respectively, and m is the mass of metal being poured.

Combining Eqs. (6) and (7) and putting values in Eq. (1)

$$mCp(Tp - Tm) = (h + h_r)_{\overline{T}} \cdot A_T \cdot (\overline{T} - T_\infty) + \frac{(Tp - T_\infty)}{R_t} + (h + h_r)_{Ts} \cdot A \cdot (Ts - T_\infty) \cdot t_1$$

$$t_1 = \frac{mCp(Tp - Tm)}{(h + h_r)_{\overline{T}} \cdot A_T \cdot (\overline{T} - T_\infty) + \frac{(Tp - T_\infty)}{R_t} + (h + h_r)_{Ts} \cdot A \cdot (Ts - T_\infty)} \qquad (8)$$

This is the expression for the calculations of time for solidification of metal during pouring and subsequent freezing in investment casting molds during step in which it losses all its sensible heat.

Various factors affect this time of solidification during first step such as thermal conductivity of mold material, casting conditions, pouring temperature, specific heat of metal, etc. All these should be taken into account while designing a casting process. Soon after the release of all superheat of metal, second step of solidification begins.

2 Transfer of Heat of Fusion

When metal loses all its sensible heat (superheat) and reaches its melting temperature, a phase transformation occurs and metal starts loosing heat as heat of fusion. This heat transfer continues till whole of the metal solidifies in the mold. This is second step of heat transfer

Like first step of heat transfer, heat again transfers in three modes namely convection, conduction, and radiation. This occurs in a fashion very similar to first step of heat transfer (i.e. from top, walls and heated surface of mold). Thus, total heat transfer from top and walls may be written as:

$$Q_t = Q_T \cdot t_2 \qquad (9)$$

Where Qt is the total quantity of heat lost from top and walls, QT is total rate of heat transfer by convection and radiation from top and conduction through walls and t2 is the total time taken for heat transfer (time of solidification in second step).

Again total rate of heat transfer is the summation of rates of heat transfer by individual modes

$$Q_T = Q_{T1} \cdot Q_{T2} \cdot Q_{T3} \qquad (10)$$

where QT1, QT2, QT3 are the rate of heat transfers by convection and radiation from top surface, conduction through walls and convection and radiation from heated mold surface, respectively.

Quantities QT1, QT2 and QT3 may be determined by use of Eqs. (3) – (5) with the replacement of T with Tm in Eq. (3) as this is the temperature at which HTCs are determined during second step and Tp with Tm in Eq. (4) as this is the reference temperature from which heat is transferred during conduction in second step.

When values are inserted into Eq. (10) following is obtained,

$$Q_T = (h+h_r)_{T_m} \cdot A_T \cdot (Tm - T_\infty) + \frac{(Tm - T_\infty)}{R_t} + (h+h_r)_{Ts} \cdot A \cdot (T_s - T_\infty) \qquad (11)$$

In second step, total quantity of heat transferred (Qt) is actually the heat lost by metal as its heat of fusion, which may be written as

$$Q_t = mHf \qquad (12)$$

Where Hf is heat of fusion of metal and m is the mass of the metal.

Putting values from Eqs. (11) and (12) to Eq. (9)

$$mHf = (h+h_r)_{T_m} \cdot A_T \cdot (Tm - T_\infty) + \frac{(Tm - T_\infty)}{R_t} + (h+h_r)_{Ts} \cdot A_T \cdot (Ts - T_\infty) \cdot t_2 \qquad (12)$$

$$t_2 = \frac{mHf}{(h+h_r)_{Tm} \cdot A_T \cdot (Tm - T_\infty) + \frac{(Tm - T_\infty)}{R_t} + (h+h_r)_{Ts} \cdot A_T \cdot (Ts - T_\infty)}$$

This is the expression for the calculations of time of solidification of metal during the interval when it transforms from liquid to solid state, i.e. the time when metal losses all its heat of fusion. Factors affecting time of solidification during this step are heat of fusion of metal, thermal conductivity of mold, cooling conditions outside mold, surface area of mold exposed to ambient and extent to which mold is heated during first step.

Finally adding Eqs. (8) and (13) yields the final expression for calculating the time of solidification during whole period from liquid to solid,

$$t = t_1 + t_2 \qquad (14)$$

Prime objective in most engineering cases is to achieve a rapid rate of heat transfer as it facilitates fine grain structure in metal which imparts strength and hardness to metal/alloy. This rapid rate of heat transfer may be achieved by use of mold materials with high thermal conductivity, forced convection conditions (blowing of air on the outer surface of the mold) or rapid cooling of mold surfaces (sprinkling of water on mold surface). This rapid rate of heat transfer however, can induce brittleness in alloy along with poor impact properties. Slow rate of heat transfer on the other hand, can induce problems of segregation especially predominant in multicomponent alloys, long columnar grains and softness that are detrimental to its further applications [9]. So, in most practical conditions an optimum rate of heat transfer is desirable which should facilitate a high strength, fine-grained material with good mechanical properties. Mostly this is achieved in conjunction with post casting heat treatment.

IV. THERMAL ANALYSIS OF CAST AND SAND MOLD

In first phase of this work a transient thermal analysis has been done on an assembly of pure iron casting and sand mold. The cast object and mold design has been referred from the work of M. M. Pariona and A. C. Mossi [8]. In their work M. M. Pariona and A. C. Mossi considered a channel shaped cast object which was cast using pure iron. The drawing and solid model of the cast has been shown below.

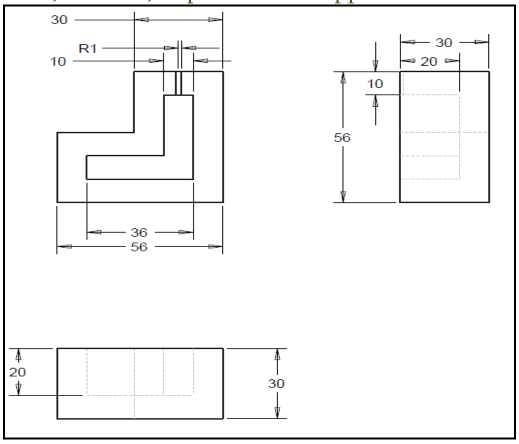

Fig 1: Drawing of cast object with mold.

As per the above drawing a solid model has been generated in Pro/Engineer software to give a clear 3-Dimensional view of the cast-mold assembly. Here only half section of the whole cast-mold assembly has been modeled to represent the assembly vividly. Blue portion is the cast object and the yellow portion is the mold object. The sprue portion though has been modeled but has not been considered in the simulation.

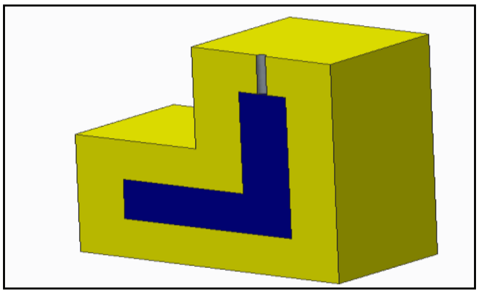
Fig 2: 3-Dimensional model of the cast-mold assembly.

Now to predict the temperature distribution of the cast-mold assembly after 1.5 hours or 5400 seconds of pouring hot and malted pure iron at 1923 K, a transient thermal simulation has been done in ANSYS software. Temperature distribution evaluated from this simulation has been verified with the result found out by M. M. Pariona and A. C. Mossi in their work (Reference [8]).

Steps followed for the transient thermal simulation in FEA software ANSYS have been explained below with relevant figures.

Simulation in any FEA software is done in three steps, namely Pre-processor, Solution and Post-Processor.

In Pre-Processor stage following jobs are done:

a. Modeling of the simulation topology.
b. Selection of Elements type.
c. Declaration of relevant material properties.
d. Discretization and Mashing of the topology.
e. Setting of boundary condition and Load data.

Modeling of the simulation topology

Due to the symmetrical shape of the cast body half portion of the whole object has been considered for the transient thermal analysis in the FEA software ANSYS. Following figure shows the topology of the object in ANSYS for simulation.

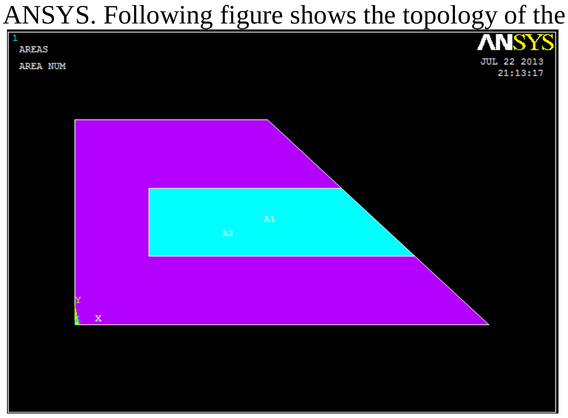

Fig 3: Topology or Geometry of the object for simulation in ANSYS.

In the above figure area with cyan color represents cast object whereas area with purple color represents sand mold portion. These two area has been assembled in ANSYS using 'Glue' command which connect both the areas for simulation but does not convert two areas in a single type because both are of different types, one of pure iron and another of silica. One thing is to be mentioned over here that in ANSYS the dimension of the symmetric geometry has been considered in 'm' whereas dimensions in the drawing in figure 3 has been mentioned in 'mm'.

After generating the topology now the topology has been discretized and meshed. Below is the meshed view of the topology.

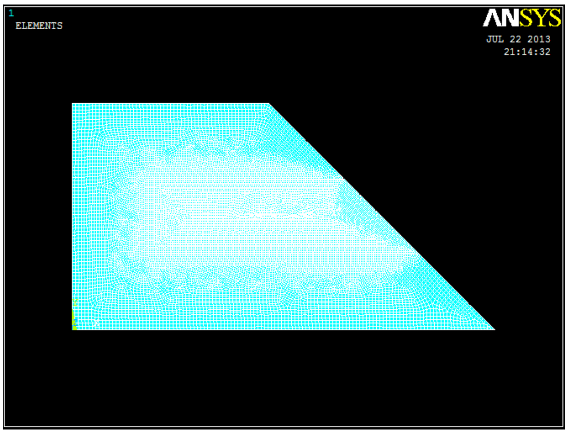

Fig 4: Meshed Topology or Geometry of the object for simulation in ANSYS.

Here meshing of the topology has been done with two different discretizing scheme. The cast object part has been meshed with 0.002 m of element length and the sand mold part has been meshed with 0.0045 m of element length. Here to mesh the topology in ANSYS 'PLANE 55' element has been used which is a thermal solid element.

After meshing the object geometry material properties have been declared. Here two types of material have been used, pure iron for the cast part and silica for sand mold. As during solidification temperature of the cast part is reduced to great extent so material properties of pure iron become function of temperature. Material properties of pure iron and silica have been mentioned below and these data has been referred from the work of M. M. Pariona and A. C. Mossi (Reference [8]), from reference [13] and from internet.

Table1: Material properties of mold materials

Properties of the pure iron			
Temperature (K)	Enthalpy (MJ/m^3)	Temperature (K)	Thermal conductivity ($W.m^{-1}.K^{-1}$)
298	0	273	59.5
373	200.75	373	57.8
473	498.87	473	53.2
573	831.83	746	49.4
673	1199.61	673	45.6
773	1602.22	773	41.0
873	2039.65	873	36.8
973	2511.91	973	33.1
1033	3200.23	1073	28.1
1073	3412.0	1273	27.6
1183	4120.86	1473	29.7
1273	4453.89		
1373	4849.96		
1473	5273.45		
1573	5724.36		
1673	6299.75		
1812	9317.24		
1812	9676.0		
Density ($kg.m^{-3}$)	7870		
Melt temperature 1812 K			
Properties of the industrial sand, AI 50/60 AFS			
Specific heat			1172.3 $J/(kg.K)$
Thermal conductivity			0.52 $W/(m.K)$
Density			1494.71 kg/m^3

After mentioning the material property data for pure iron as well as silica, temperature boundary condition has been mentioned. Here convection boundary condition has been set on the outer surface of the mold where mold is in contact with atmosphere. In this boundary condition convective heat transfer coefficient has been mentioned as 11.45 W/m2.K and bulk temperature has been considered as 300K. These data has been collected from the work of M. M. Pariona and A. C. Mossi (Reference [8]). For transient thermal simulation initial temperature has been set as 1923 K because liquid iron has been poured at 1923K temperature which is 111K super heat as melting temperature of pure iron is 1812K.

After setting the temperature boundary conditions transient simulation parameter has been set as follows.

Table2: Transient simulation setup

Total time of simulation	1.5 hours or 5400 seconds
Time step	5 seconds
Maximum Time Step	10 seconds
Minimum Time Step	1 sec

After simulation of the cast-mold assembly for 1.5 hours of solidification, temperature distribution has been evaluated for whole the region of cast-mold geometry and also separately for the cast part. Following are the figures of temperature distribution of whole the assembly and separately of the cast part.

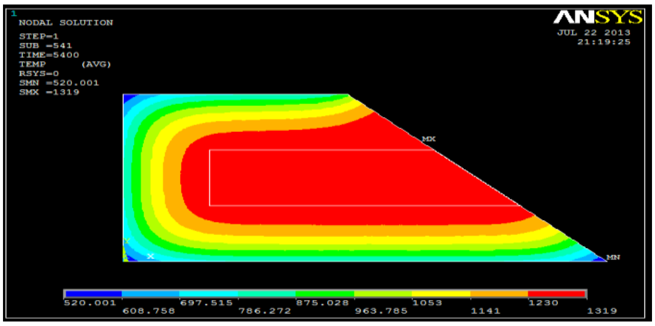

Fig 5: Temperature Distribution of the cast-mold assembly

Above figure shows the contour plotting of temperature distribution of the whole cast-mold assembly and it is clearly depicted from the figure that maximum temperature comes down to 1319 K from 1923K after 1.5 hours of solidification and mold temperature has been raised to 520 K from initial 300 K.

Now the figure below shows temperature at different point in the cast-mold assembly after 1.5 hours of solidification.

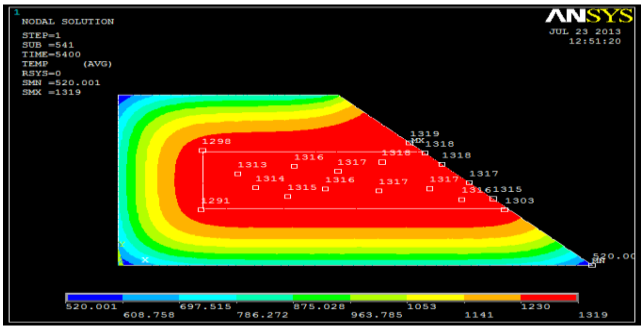

Fig 6: Temperature at different points of the cast-mold assembly.

Above result is very much in accordance with the result found out by M. M. Pariona and A. C. Mossi in their work (Reference [8]). Following figure represents the result published in reference [8].

Now with the same parameters a couple-field analysis has been done in next phase of the work to predict the thermal stress in the cast-mold assembly to take decision about mold geometry.

To know maximum temperature of the mold at different point of time in the due course of solidification a graph has been shown below which has been derived from ANSYS.

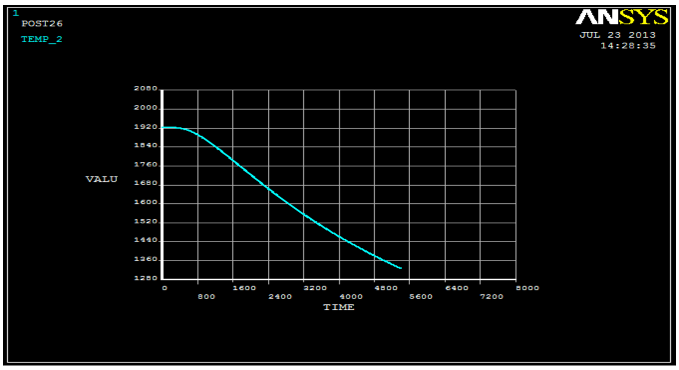

Fig 7: Graph showing max temp at different point of time in solidification process

V. COUPLE-FIELD ANALYSIS OF CAST-MOLD ASSEMBLY WITH SAND MOLD

To predict the defects in cast object and to optimize the mold thickness it is required to predict the thermal stress in the cast-mold assembly. To predict the thermal stress in the cast-mold assembly it is needed to do the couple field analysis in the whole assembly.

In this process, steps for FEA modeling and meshing in ANSYS will be same as described in previous section.

After meshing, thermal properties of both the material i.e pure iron and silica have been incorporated in ANSYS as per the method discussed in previous chapter. The thermal environment has been saved with name 'THERM' and then the environment has been switched over to structural and following structural properties of material have been mentioned in ANSYS.

Table3: Physical properties of cast iron

Young Modulus of pure iron	196×10^9 N/m^2
Poisson's Ratio of pure iron	0.29
Coefficient of linear expansion of pure iron	12×10^{-6} K^{-1}
Density of pure iron	7870 kg/m^3
Young Modulus of silica	169×10^9 N/m^2
Poisson's Ratio of silica	0.17
Coefficient of linear expansion of silica	3×10^{-6} K^{-1}
Density of silica	1494.71 kg/m^3

After incorporating all the requisite data, a simulation has been done which gives us the result for deflection and thermal stress.

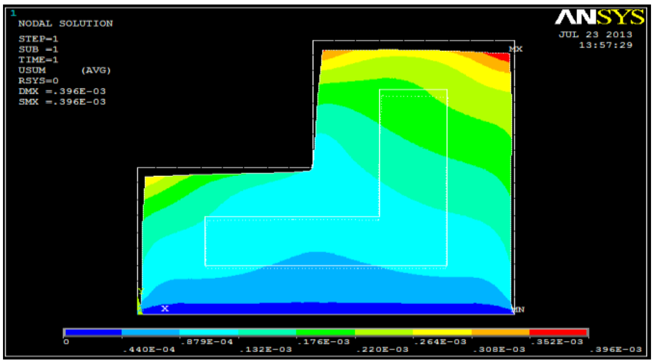

Fig 8: Deflection due to thermal load.

Figure above depicts the deflection in whole the cast object and sand mold assembly due to the thermal load created for solidification. From the above figure it is quite clear that the cast object and sand mold combination will go under a compression due to solidification.

Now due to this solidification the whole assembly will experience a compressive stress which has been presented in the figure below.

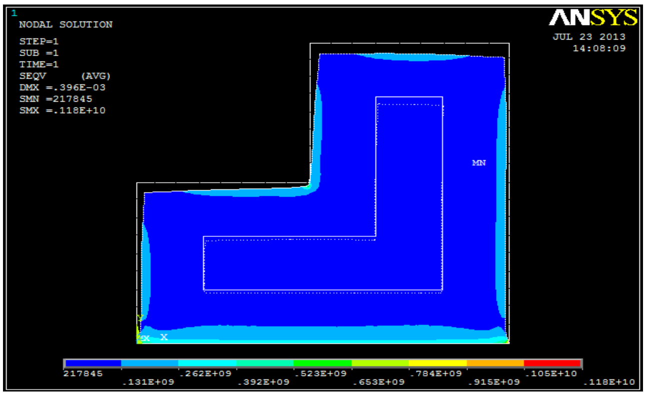

Fig 9: Thermal stress created in the cast-mold assembly.

Figure below shows the compressive stress value at different points in the cast object and sand mold assembly.

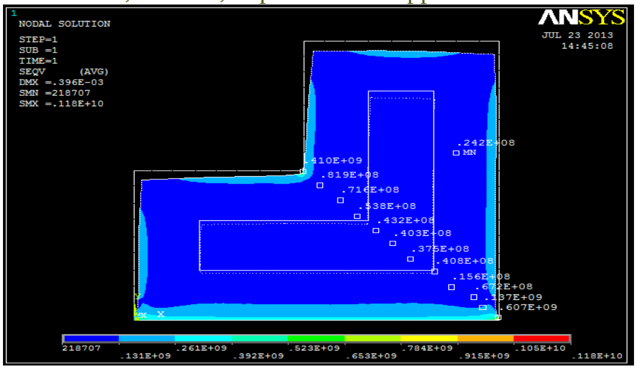

Fig 10: Value of thermal stress created at different points in the cast-mold assembly

VI. COUPLE-FIELD ANALYSIS OF CAST-MOLD ASSEMBLY WITH DIFFERENT MOLD MATERIAL

In previous section it has been shown that FEA software like ANSYS can be used successfully to predict the cast and mold deflections and stresses prior the actual casting process by a numerical simulation. This simulation results actually help a manufacturer to predict correctly about the mold defects out of a present mold design and he or she can correct it before actual manufacturing.

In this section few modifications has been tested by numerical simulation in ANSYS and those results from different modifications have been compared.

Modification-1

In this modification, dimensions of the mold have been kept similar to the dimension discussed in previous chapter but the material has been changed from sand to mullite. Following are the thermal as well as mechanical properties of mullite.

- Specific Heat : 1172.3 J/(Kg.K)
- Thermal Conductivity : 5.86 W/(m.K)
- Density : 3100 kg/m3
- Modulus of Elasticity : 151 GPa
- Poisson’s Ratio : 0.20
- Coefficient of linear expansion : 5.4×10-6 / ºC

After simulation following results have been derived and those have been presented below.

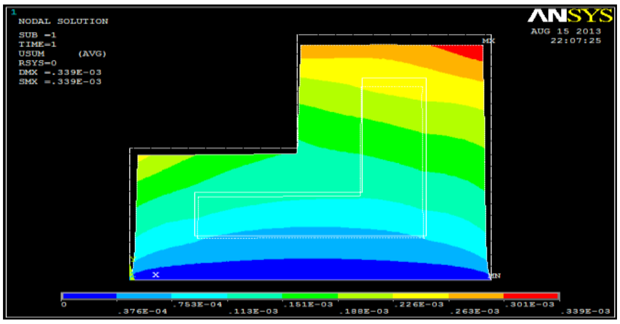

Fig 11: Deflection of the whole mullite mold.

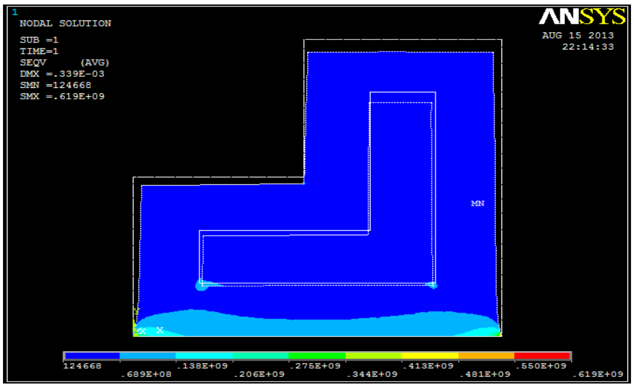

Fig 12: Von-Misses stress on whole mullite mold

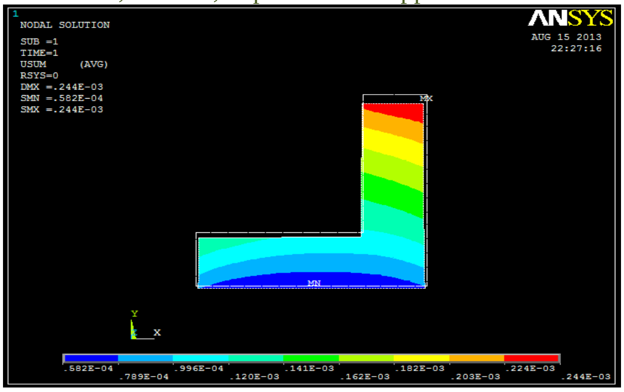

Fig 13: Deflection vector sum of cast part.

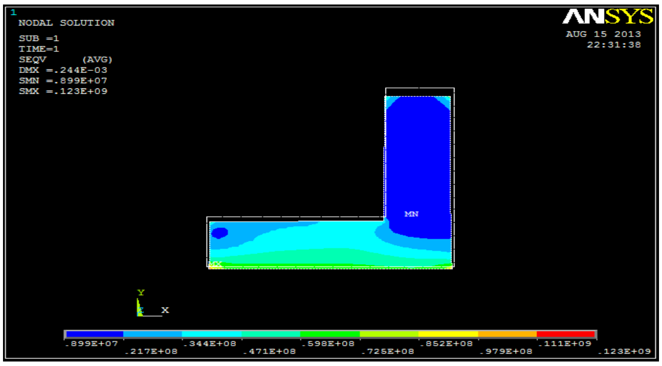

Fig 14: Von Misses stress of cast part.

Modification-2

In this modification, two layers of sand and mullite has been used to create a composite mold. Thickness of each material has been kept half of the total thickness of previously mentioned sand and mullite mold.

Now this composite mold has been modeled in ANSYS in 2D form and meshed with PLANE55 element by a process which has already been discussed in previous section.

Now after the meshing of the FEA model of the composite mold in ANSYS a couple filed analysis has been done and after simulation following results have been derived and those results have been presented below.

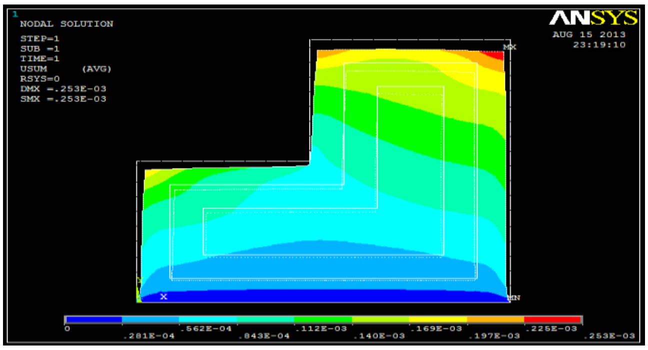

Fig 15: Deflection of whole the composite mold.

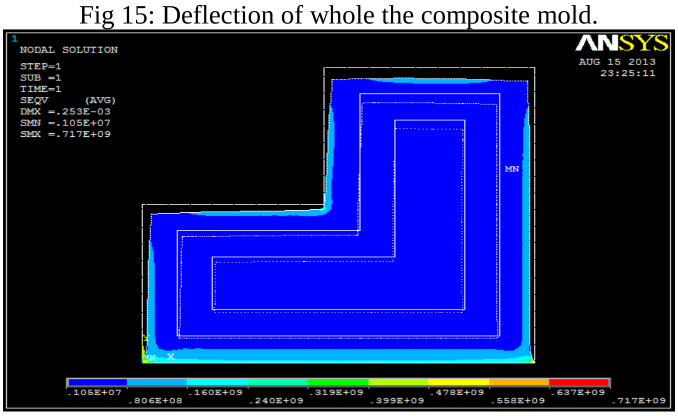

Fig 16: Equivalent stress of the composite mold.

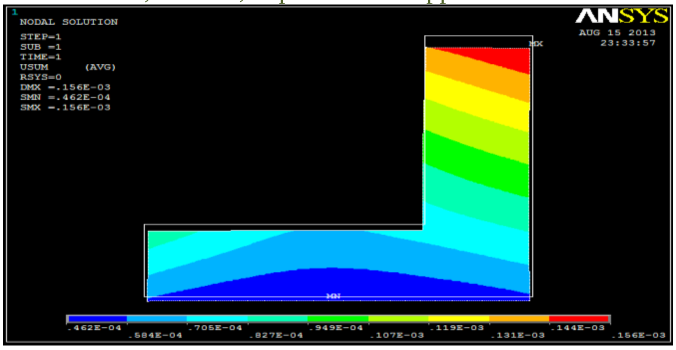

Fig 17: Deflection of the cast part of the composite mold.

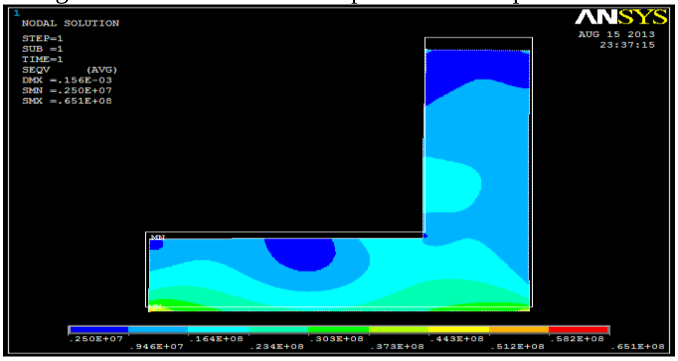

Fig 18: Equivalent stress of the cast part of the composite mold.

Now graphs have been drawn for the following parameters on the symmetry diagonal of sand mold, mullite mold and composite mold respectively.

Maximum shrinkage for whole mold body.
Maximum shrinkage for cast part.
Maximum thermal stress for whole mold body.
Maximum thermal stress for the cast part.

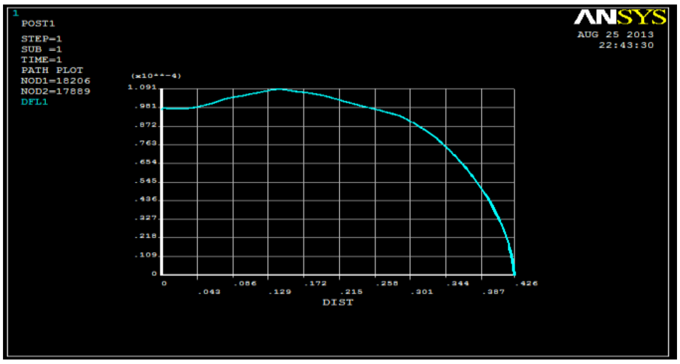

Fig 19: Shrinkage along symmetry diagonal of sand mold

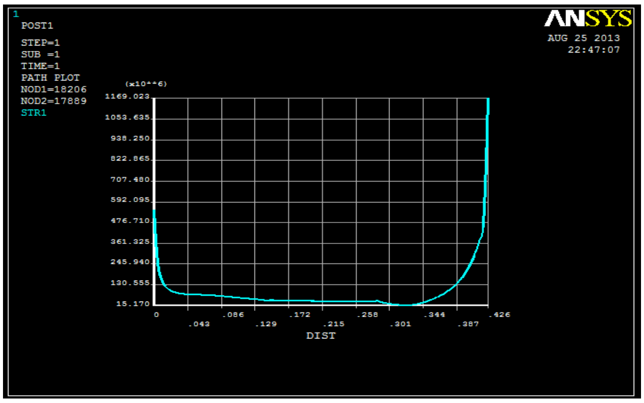

Fig 20: Thermal stress along the symmetry diagonal of the sand mold

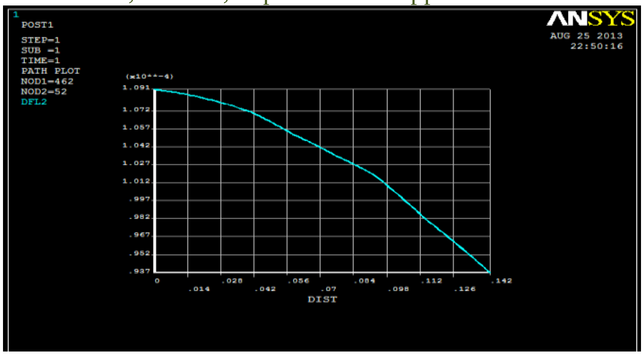

Fig 21: Shrinkage along symmetry diagonal of the cast part of a sand mold

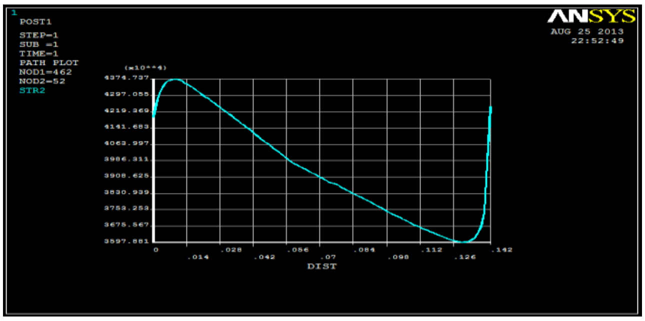

Fig 22: Thermal stress along the symmetry diagonal of cast part of the sand mold

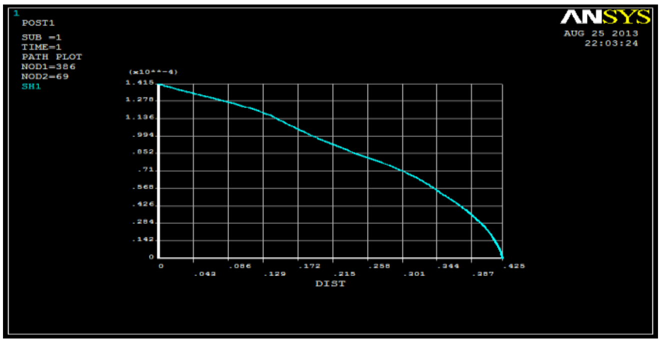

Fig 23: Shrinkage along symmetry diagonal of Mullite mold

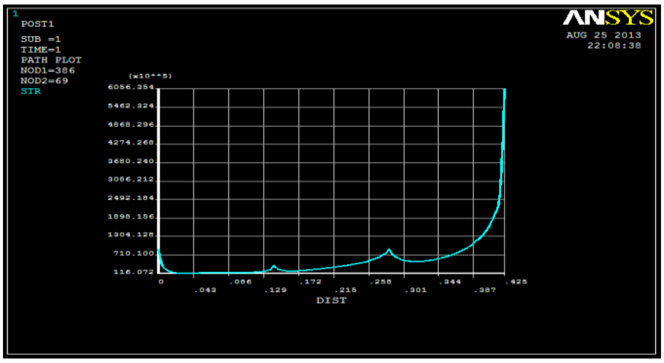

Fig 24: Thermal stress along the symmetry diagonal of Mullite mold

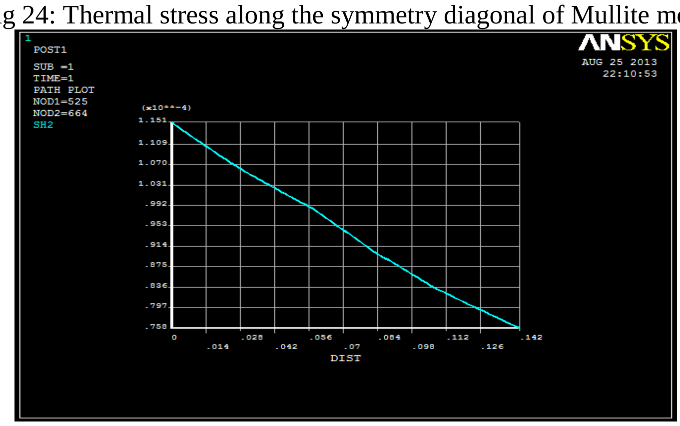

Fig 25: Shrinkage along symmetry diagonal of cast part of Mullite mold

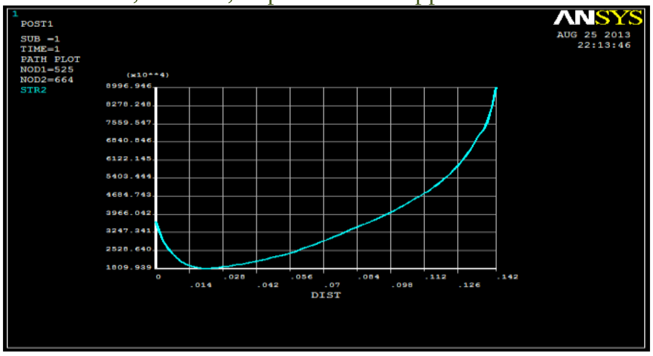

Fig 26: Thermal stress along the symmetry diagonal of cast part of the Mullite

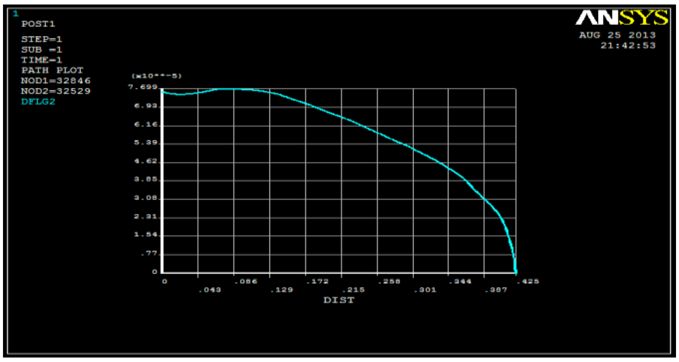

Fig 27: Shrinkage along symmetry diagonal of composite cast-mold combination

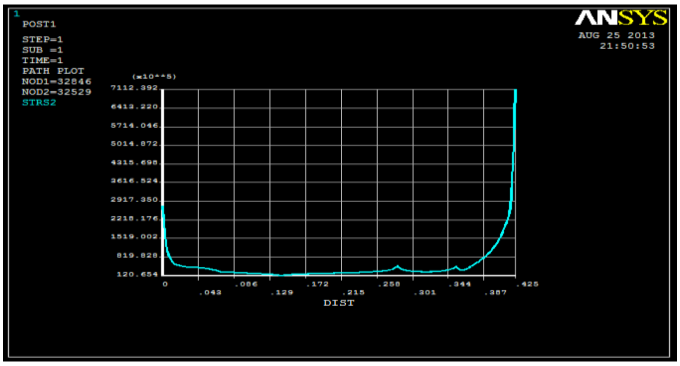

Fig 28: Thermal stress along the symmetry diagonal of the composite cast-mold combination

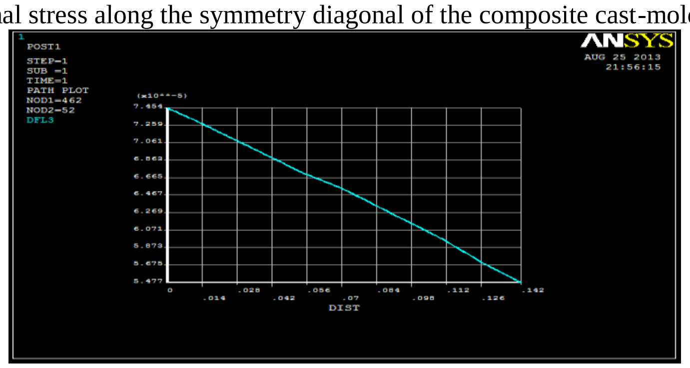

Fig 29: Shrinkage along symmetry diagonal of cast part of composite cast-mold combination

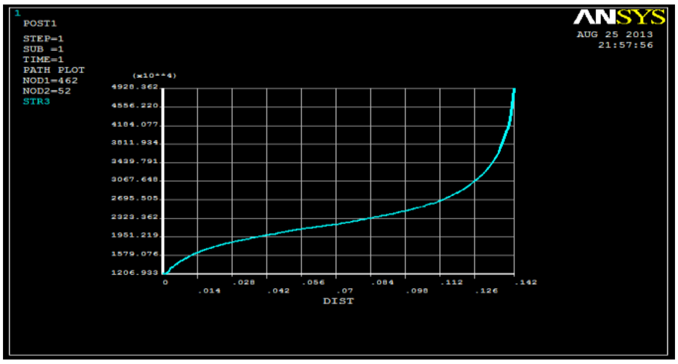

Fig 30: Thermal stress along the symmetry diagonal of cast part of the composite cast-mold

Now from the above graph we can tabulate the following result data with reference of the symmetry diagonal.

Table 6.1: Results of couple field analysis

Mold type	Whole mold cast assembly		Only Cast Part	
	Maximum Shrinkage	Maximum Thermal Stress	Maximum Shrinkage	Maximum Thermal Stress
Sand Mold	0.1091 mm	1169 MPa	0.1091 mm	43.74 MPa
Mullite Mold	0.1415 mm	605.6 MPa	0.1151 mm	89.97 MPa
Sand-Mullite Composite mold	0.07699 mm	711 MPa	0.07454 mm	49.28 MPa

From the above data it is quite evident that in sand mold cast object experience less thermal stress but than mullite and composite mold but the shrinkage on the casing is least in composite mold. So it may be concluded here the composite mold is most suitable for casting an object with pure iron.

VII. CONCLUSIONS

From the present work it can be concluded that, if it is possible to predict different output result from a casting process prior to the actual casting process then it becomes very useful to take decision on the different casting parameters for better cast product. As it has been mentioned earlier that if by any means it is possible to predict temperature distribution and thermal stress after solidification of cast object in a mold then casting defects may kept as minimum as possible.

In the present work it has been shown that FEA software like ANSYS may play an important role in this regard. Transient thermal analysis and Couple-Field analysis in ANSYS can predict temperature distribution and thermal stress distribution in the casting after solidification very accurately. This fact has been proved by validating a transient thermal analysis which has been published in a reputed journal. After validating the thermal analysis, work has been extended to Couple-Field Analysis for thermal stress.

On the basis of thermal analysis result and couple-field analysis result, work may be extended for determination of optimum mold layer thickness and best material for mold making or best combination of mold material with optimum thickness combination.

In chapter six few modifications have been simulated and tested whether they are better than the configuration considered in the base paper. As first modification sand has been replaced by mullite and it has been seen that the mold shrinkage is less but the cast shrinkage is more. Thermal stress in the mullite mold is less than the sand mold. For the sand-mullite composite mold shrinkage is least as well as shrinkage for the cast is also least. But the thermal stress is more than the mullite mold. So optimization can be done as a future work for best combination of mold materials in a composite mold with optimum thicknesses.

REFERENCES

[1] YIN-HENC CHEN and YONG-TAEK IM, "ANALYSIS OF SOLIDIFICATION IN SAND AND PERMANENT MOLD CASTINGS AND SHRINKAGE PREDICTION", Int. J. Mach. Tools Manufacture, Vol. 30, No. 2, pp. 175-189. 1990

[2] JYRKI MIETI'INEN and SEPPO LOUHENKILPI, "Calculation of Thermophysical Properties of Carbon and Low Alloyed Steels for Modeling of Solidification Processes", METALLURGICAL AND MATERIALS TRANSACTIONS B, VOLUME 25B, DECEMBER 1994—909

[3] L.C. Würker, M. Fackeldey, P.R. Sahm and B.G. Thomas, "THERMAL STRESS AND CRACK PREDICTION OF INVESTMENT CASTS ALLOYS", 1998, San Diego, CA, June 7-12, 1998, TMS, Warrendale, PA, pp. 795-802.

[4] S. I. Abu-Eishah, "Correlations for the Thermal Conductivity of Metals as a Function of Temperature", 0195-928X/01/1100-1855/0 © 2001 Plenum Publishing Corporation

[5] B. J. MONAGHAN and P. N. QUESTED, "Thermal Diffusivity of Iron at High Temperature in Both the Liquid and Solid States", ISIJ International, Vol. 41 (2001), No. 12, pp. 1524–1528.

[6] Jiarong LI, Shizhong LIU and Zhengang ZHONG, "Solidification Simulation of Single Crystal Investment Castings", Journal of Material Science and Technology, Vol. 18, No. 4, 2002

[7] Y. B. Li and W. Zhou, Numerical Simulation of Filling Process in Die Casting, Materials Technology, Vol. 18, No. 1, 2003, pp. 36-41.

[8] M. M. Pariona and A. C. Mossi, "Numerical Simulation of Heat Transfer During the Solidification of Pure Iron in Sand and Mullite Molds", J. of the Braz. Soc. of Mech. Sci. & Eng., October-December 2005, Vol. XXVII, No. 4, 399-406

[9] M.M.A. Rafique and J. Iqbal, "Modeling and simulation of heat transfer phenomena during investment casting", International Journal of Heat and Mass Transfer 52 (2009) 2132–2139

[10] Sorin-Adrian COCOLAŞ and Constantin BRATU, "EXPERIMENTAL MODEL FOR FLOWING ANALYSIS IN CASTING FERROUS ALLOY", U.P.B. Sci. Bulletin (ISSN 1454-2331), Series B, Vol. 72, Issue 2, 2010

[11] Waleed Abdul-Karem and Khalid F. Al-Raheem, "Vibration improved the fluidity of aluminum alloys in thin wall investment casting", International Journal of Engineering, Science and Technology, Vol. 3, No. 1, 2011, pp. 120-135.

[12] Taufik Roni Sahroni, Shamsuddin Sulaiman, B. T Hang Tuah Baharudin, Mohd Khairol Anuar Mohd Ariffin and Hambali Arrif, "Design and Simulation on Investment Casting Mold for Metal Matrix Composite Material", Advances in Mechanical Engineering, ISSN: 2160-0619 Volume 2, Number 4, December, 2012.

[13] "Thermodynamic Properties of Iron and Silicon" by P. D. Desai, Centre for Information and Numerical Data Analysis and Synthesis, Purdue University, West Lafayette, Indiana.

Contact Pressure Validation of Steam Turbine Casing for Static Loading Condition

Laxminarayan.k [1], Dr.M.Venkatarama Reddy [2], Dr.Kumar[3]

Department of Mechanical Engineering, Bangalore Institute of Technology, Visvesvaraya Technological University, India

ABSTRACT: *Steam Turbines are devices used to convert thermal energy of steam into mechanical energy, which may be used to produce Electrical Energy. Steam turbine generator units are being used extensively all over the world for generation of electric power and for co-generation of steam and power. Contact pressure and pretension in bolts-analysis has been made easier in recent years due to the availability of high computational capabilities and flexibility in the computational methods using finite element analysis.*

In the present work, one such analysis is carried out to evaluate the contact pressure in a high pressure steam turbine casing. The shape and design of a steam turbine casing depends on key sensitivity parameters like bolt pre-tensions, contact pressure and thickness of casing which determine the structural integrity of the casing. The preset work reviews a recent structural integrity assessment carried out on a high-pressure turbine inner casing that had suffered from temper embrittlement Conventional design of a steam turbine casing is considered. Experimental work is carried out at Maxwatt to verify the contact pressure. The assessment will be carried out to demonstrate that the casing can be safely returned to service based on custom made revised operating conditions. The experimental results will be verified through finite element Analysis results.

The project which is presented in this paper has paid special attention to employ a standard methodology to perform static analysis and experimental condition. For this purpose a new methodology called "Contact pressure" has been developed. This enables accurate and complete leak proof condition. More over due to evolution of computer software and hardware large size boundary element models can now be solved with reasonable computing time.

The goal of this paper is to estimate the contact pressure so that there should not be any leak. Pretension in bolts is considered to achieve a firm contact between the casings. The three dimensional model of steam turbine casing were created using Hypermesh Software. The cad model created was meshed using Hypermesh Software by utilizing standard quality parameters. Boundary Condition were given on the Finite element model using Hypermesh. Contact pressure analyses were performed using Radioss solver.

Contact pressure analysis of turbine casing is very important in steam turbine which needs to be addressed for structural integrity. During operating condition steam turbine casings are subjected to very high pressure and temperature which results in stress and strain distribution. If the contact pressure is not achieved as per the standards then it leads to leakage of steam which causes explosion of casing. These effects are difficult to validate experimentally, since the setup is very costly.

I. INTRODUCTION

All turbines manufactured by Maxwatt use multiple piece casings consisting of two or more pieces that are split at the horizontal centerline to facilitate inspection or removal of the turbine rotor. The casings are either cast, fabricated, or a combination of both depending on operating conditions. The casing can be of iron, carbon steel, carbon moly steel, or chrome moly steel [1].

LP casing and for redesigning it to suit the new efficient modern design of rotor. This paper presents the numerical stress analysis of the turbine casing of an aero-engine. High thermal stress gradients were found at the region of casing where fatigue cracks were detected during engine operation [2].

Has analyzing the failure of a weld repaired turbine casing after 30 years of total service including 5 years after weld repair. The casing was weld repaired by a high Cr–Ni weld metal (24Cr–32Ni–4Mn–Fe). The base metal low alloy ferritic steel (1Cr–0.5 Mo steel) with ferrite–pearlite structure did not show any abnormality to indicate significant degradation [3].

Has studied about designing of complex steam turbine low pressure casing the ever growing competition in capital intensive power sector is pressing turbine manufacturer's world over to develop new efficient steam turbine designs and to update/retrofit the old steam turbine which are in service. BHEL is also putting up major design development efforts to meet the present market challenges [4].

Holmberg and Axelson [5] presented an analysis of stresses in circular plates and rings, with applications to rigidly attached flat plates and flanges, considering the loading at bolt force point as well as gasket compression.

The ASME Code contains extensive rules for the design of pressure vessel components, including rules for non-circular pressure vessels of unreinforced and reinforced construction. These rules cover the sides, reinforcing ribs, and end plates of such vessels [6].

Russian scientists P.Shlyakhin [7], A.Kostyuk and V.Frolov [8] had proposed methods to design flanges and bolts of a steam turbine casing. The method proposed by Shlyakhin stands out since it incorporates the bolt design along with flange design.

The theory of elasticity [8] has been extensively employed in analysis and design of bolted flanged connections. Waters and Taylor [9] developed an analytical method, based on the theory of elasticity, for ring and hub flanges with straight hubs. The deflection results calculated were compared with test results to demonstrate good agreement.

Based on the theory of beam on elastic foundation, Timoshenko [10] proposed a simplified method for the analysis of bending of circular rings. The maximum circumferential stresses for ring flanges and longitudinal stresses for hub flanges can be calculated by using this method.

Development of Life Prediction System for Thermal Power Plant Based on Viscoplastic Analysis, Final report, KERPI [11].

Fig. 1 Typical configuration for steam turbine casing

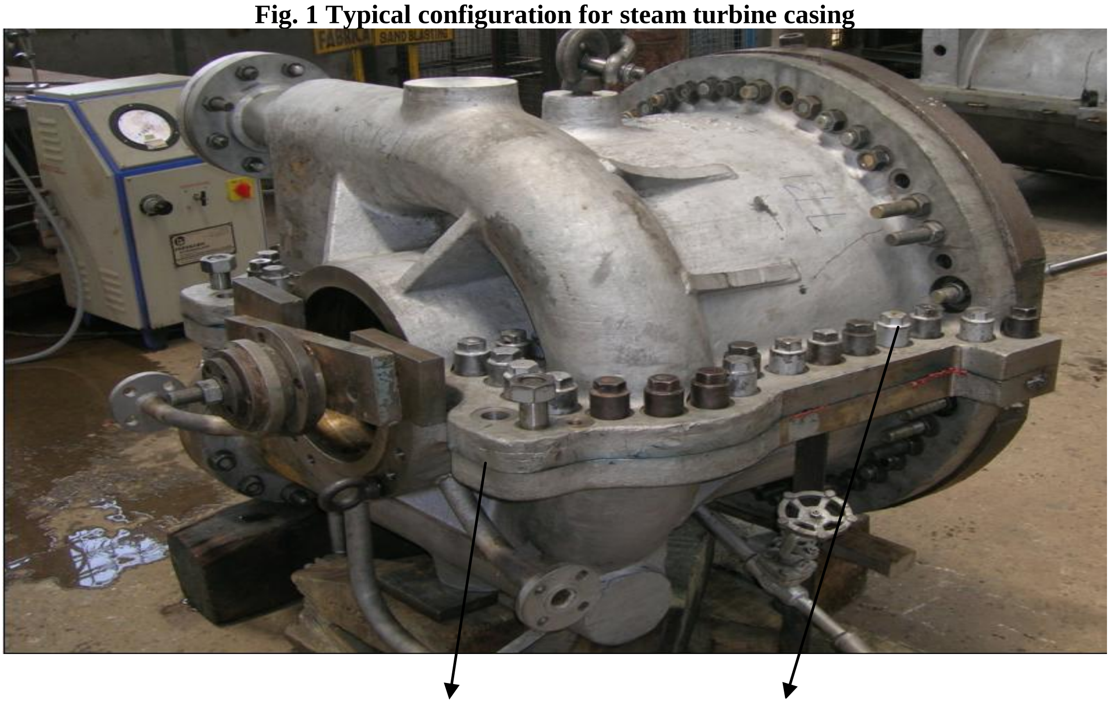

II. BOLT PRELOADING

Due to high loads, bolted connections can separate. To minimize this effect, a pretension is applied to the bolt. Pretension insures that the connection will not separate, provided the applied load remains less than the pretension. Torque tightening of bolted joint places the bolt in tension and the clamped members in compression. [6].

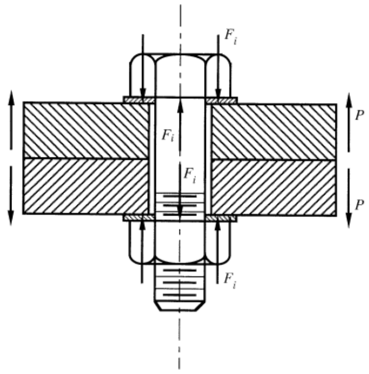

Fig.2 Forces acting upon a bolted preloaded connection

III. CALCULATIONOF PRETENSION LOAD BOLT DIAMETER.

Standard bolt diameters are considered for the calculation of pretensionload. ***Stress=PretensionLoad/Areaofbolt***
Area of bolt =πd^2/4, *stress = 232Mpa*
For 27mm diameter bolt A=572mm^2
Therefore, Pretension Load for bolt diameter 27mm = 120236.6 N. Pretension Load for bolt diameter 30mm = 163792N.
Calculated pretension value is applied
For the bolts during preprocessing.
Pretension load applied ensures that bolt is subjected to tension and the casing is subjected to compression.

IV. GEOMETRIC CAD MODELLING

Inner Diameter of Casing = 500mm
Casing Diameter thickness = 35mm
Flange thickness = 50mm

Length of Turbine = 600mm
Bolt Diameter = 27mm diameter
Bolt Length = 90mm
Capnut height = 55mm

Dimensions of the above are measured at Maxwatt to perform the FEA analysis.

It is very difficult to exactly model the steamturbine casing, in which there are still researches going on to find out the behavior of casing during operating condition at high temperature. There is always a need of some assumptions to model any complex geometry. These assumptions are made keeping in mind the difficulties involved in theoretical calculation and the importance of the parameters that are taken and those which are ignored. In modeling we always ignore the things that are of less importance and have little impact on the analysis. The assumptions are always made depending upon the details and accuracy required in the modeling. The assumptions made which are made while modeling the process are 1. Casing material is considered as homogeneous and isotropic. 2. Inertia and body force effects are negligible during the analysis.3. Structural analysis is carried out to find out the contact pressure 4. Thus stress level below yield stress is considered. 5. The analysis does not determine the life of the casing.

In an ideal scenario, CAD and FEA activities are coordinated to minimize the duplication of effort as analysis is made an integral part of the design process. The geometry built by the design team will ideally be usable FEA and all downstream applications. It is the responsibility of both the analyst and the designer, or geometry provider, to plan projects such that the optimal level of coordination between CAD and FEA is achieved. Before attempting to consider the merits of using the design model as the analysis model, the conditions listed below must be met. Design models are built in 3D solids or surfaces that fully enclosed volumes. The part can and should be meshed with tetrahedrons, or is simple enough to provide the foundation for solid mapped brick meshing or mid-plane surface extraction for building shell models.

Hydro Test Procedure as per ASTM

Component should be cleaned properly to remove machined burrs, sand, extra projections and any other foreign particles. Retapp all the tapped holes.

Close all openings by using proper flanges with gaskets/O rings.

Make provision for air release in appropriate place by fixing a valve.Hydrotest pressure will be 1.5 times the working pressure. Hold the pressure for half an hour.Take one 500gm weighing hammer and gently hammer the outer surface of the component. Ensure that there is no leakage found (by observation).offer the hydro tested component to Quality department for there approval.

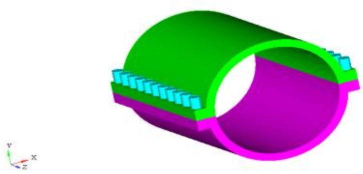

Fig.3 Cad Model of Casing and Bolts

Fig.4 Section view of actual casing and bolts during Hydro test

V. FINITE ELEMENT MODELLING AND ANALYSIS

In this part, the modeled casing is taken up for contact pressure and structural analysis. By carrying out the contact pressure analysis it will be taken care that required contact pressure is maintained at the parting plane and thus no steam leaks out of the casing [11].

By carrying out the structural analysis the stresses and deflections in the casing can be determined. Finite element analysis is a numerical technique by which the solution of a set of differential equations may be performed. The finite element method is probably the most widely used form of computer-based engineering analysis. The method can be used for analysis of a broad range of engineering problems.

Finite element methods are predominantly used to perform analysis of structural, thermal, and fluid flow situations. They are used mainly when hand calculations cannot provide accurate results. Finite element modeling involves the processes of feature suppression, model idealization and meshing of the solid model. The bottleneck of the whole process is model idealization, which is the process of generating a geometric model into an analysis model of suitable quality and reduced size so that it may be analyzed efficiently using FEA. The purpose of a finite element analysis is to re-create mathematically the behavior of an actual engineering system. In other words, the analysis must be an accurate mathematical model of a physical prototype. In the broadest sense, this model comprises all the nodes, elements, material properties, real constants, boundary conditions, and other features that are used to represent the physical system.

In FEA General Purpose programming terminology, the term model generation/finite element modeling usually takes on the narrower meaning of generating the nodes and elements that represent the spatial volume and connectivity of the actual physical prototype. ALTAIR HYPERWORKS used for the present work offers the following approaches for model generation/finite element modeling.

Default mesh control in ALTAIR HYPERMESH produces an adequate mesh for any analysis, however several mesh controls have been provided in order to achieve mesh of desired quality depending upon the requirement.

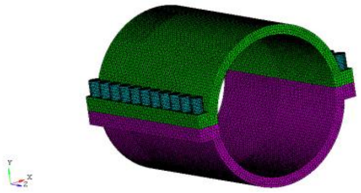

Fig.4. Meshed Model of Casing and Bolts

The meshed model of steam turbine casing is shown in Figure 4. Initially UG part file is imported to ALTAIR HYPERMESH, then meshing is carried out. In the present work we have used higher order tetra mesh for the accuracy of the results. The total mesh consists of 83999 nodes and 346571 elements. Chromium steel material is used since this material is anti corrosive and has good resistance to high temperature and pressure. Given Below are the material properties defined for the analysis.

Description	**Casing**	**Bolt**
Name	Chromium steel	Chromium steel
Density (Tonnes/mm^3)	7.8E-9	7.8E-9
Young's Modulous (MPa)	2.1E5	2.1E5
Poisson's ratio	0.3	0.3

Table 1: Material Properties

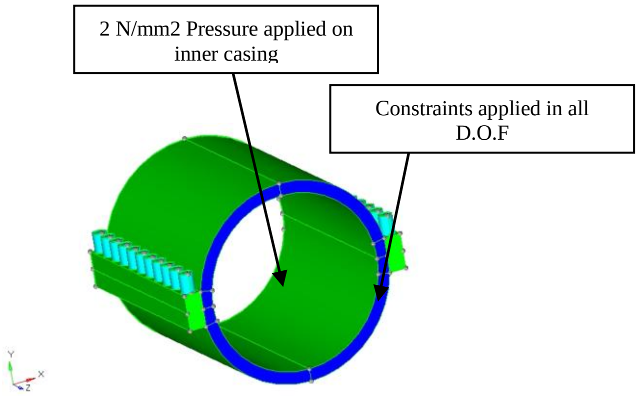

Fig.5. Boundary Conditions

VI. THEORITICAL CALCULATION

The Theoritical calculation done in this work is compared with analysis results and experimental results. i.e for the design and the casing to work on safe condition the contact pressure achieved in analysis should be greater than the calculated value. If the contact pressure achieved in the analysis is lesser than the theoretical value calculated then the design is unsafe.

For safe condition

Contact Pressure = 3 * Inner Pressure

Inner pressure applied = 2 Mpa.

Therefore Contact Pressure = 6 Mpa.

From the above calculation it is clear that contact pressure achieved in analysis should be greater than 6 Mpa or else the design is unsafe.

VII. RESULTS AND DISCUSSION

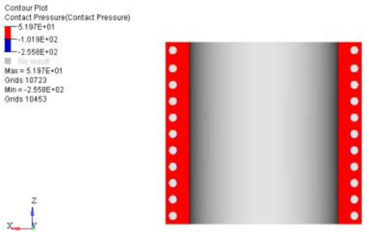

Fig.6. Contact pressure at parting plane

Figure 6 clearly shows that contact pressure achieved is 51Mpa (Red Band) which is greater than 3 times the inner pressure applied.
Since contact pressure achieved 51Mpa is greater than 6 Mpa i.e 3 times operating pressure, this ensures that there will be no leak and the casing is safe.
The same model was experimentally tested by doing Hydrotest at Maxwatt.
The test clearly showed there was no leak in the experiment and the casing is safe.

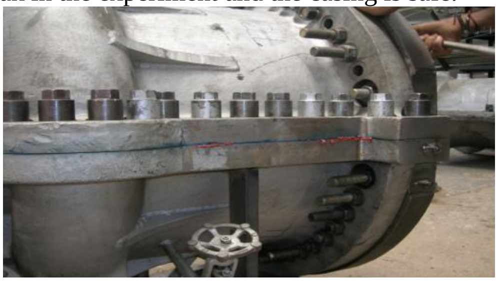

Fig.7. Contact pressure without Leak

Stress and displacement contour are also shown below.

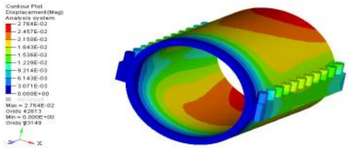

Fig.8. Displacement Contour

Displacement Contour Shown in Figure 8 shows that maximum displacement in the entire model is 0.027mm.

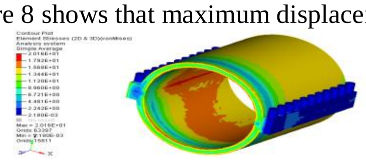

Fig.9. Von-mises Stress Contour

Von-mises Stress Contour shown in Figure9 shows that maximum Von-mises stress in the entire model is 20.16Mpa, which is less than yield stress 410 Mpa for Chromium steel. Hence the component is safe. Chromium steel is a good anti corrosive material for high temperature and pressure.

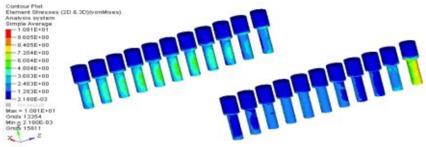

Fig.10. Von-mises Stress Contour on Bolts

Von-mises Stress Contour shown in Figure 10 shows that maximum Von-mises stress in the Bolt is 10.81Mpa, which is less than yield stress 410 Mpa for Chromium steel. Hence it shows that all the bolts are safe

VIII. COMPARISON OF RESULTS

Description	Theoritical	Analysis (Altair)
Contact Pressure	6 Mpa	51 Mpa

Table 1: Validation Table

From Table 1 result it is clear that contact pressure achieved in analysis is greater than calculated value and hence the design is safe.

IX. CONCLUSION

Validation of steam turbine casing is successfully proved theoretically, Analytically and experimental method.

- Theoretical, Analytical and experimental procedure show that this design procedure has been successful in generating an optimum design solution and thus can be easily implemented.
- The required contact pressure (wiz 3 times the pressure at respective stage) is achieved in the high pressure as well as in the intermediate pressure stages.
- It is clear from the results that the stress in the casing is well within the allowable stress of 210 MPa.
- The finite element analysis gives a complete picture of mechanical behavior of the flange structures, and design guidelines without costly experiments. The analysis results show that this design procedure has been successful in generating an optimum design solution and thus can be easily implemented.

REFERENCES

[1.] J.Ramesh,C.Vijaya Bhaskar Reddy, Dr. B. Jayachandraiah, Design and Analysis of HP steam turbine casing for Transient state condition IJCER Vol .2 issue 5.
[2.] W.S. Choi, E. Fleury, G.W.Song and J-S. Hyun, A life assessment of steam turbine rotor subjected to thermo mechanical loading using inelastic analysis,Key Eng. Mat 326-328, 601-604 (2008).Mech Engg,
[3.] “ASME Boiler and Pressure Vessel Code, Section 8, division 1,Pressure Vessels,” The American Society of Mechanical Engineering, New York, NY, 2010 Edition.
[4.] Bach, C.,”Versuche Uber die Widerstansfahigkeit ebener Platten”,Springer Variag, Berlin, Germany,1891 104 pages.
[5.] Westphal, M.,”Berchnung der Festigkeit loser und fester Flansche”,VDI-Z,Vol.41,No.36,Sept.,2008,pp.1036-1042.
[6.] Waters, E.O and J.H Taylor, “The Strength of Pipe Flanges”, Mech.Eng. Vol.49, No.5a, May2009, pp.531-542.
[7.] Timoshenko, S.,”Flat Ring and Hubbed Flanges”, Contribution to discussion of (6).Mech Engg, Vol.49, No.12, Dec,1927, pp.1343-1345 (2006).
[8.] Holmberg, E.O and K.Axelson,”Analysis of Stresses in Circular Plates and Rings”(With Application to rigidly Attached Flat Heads and Flanges),ASME Trans J.Appl.mech.Vol.54,No.2,Jan.,2009,pp.13-32.
[9.] Waters E.O., D.B.Wesstrom and F.S.G.Williams + others, ”Formulas for Stresses in Bolted Flanged Connections”,ASME Trans Vol.59,2008,pp.161-169.Discussion: Vol.60,Apr 1938, pp.267-278.
[10.] Waters E.O., D.B.Wesstrom and F.S.G.Williams+ others,” Formulas for Stresses in Bolted Flanged Connections”, Taylor Forge and Pipe Works, Chicago, 2009(printed 1949).
[11.] Mckenzie.H.W, D.J.White and C.Snell,”Design of Steam-Turbine Flanges: A Two-Dimensional Photoelastic Study”, Jour, Strain Anal., Vol.5, No.1, Jan., 2008, pp.1-13.
[12.] Blach A.E. and A.Bazergul, “Methods of Analysis of Bolted Flanged Connections- a Review”, WRC Bulletin, No.271, Oct., 2007, pp.1-15.
[13.] P.Shlyakhin, Steam Turbines: Theory and Design, Foreign Language Publishing House, Moscow (translated from Russian by A.Jaganmohan) 2010.
[14.] A.Kostyuk, V.Frolov, first published 2008, Steam and Gas Turbines.

International Journal of Modern Engineering Research (IJMER)
www.ijmer.com Vol. 3, Issue. 5, Sep - Oct. 2013 pp-2894-2900 ISSN: 2249-6645

High Speed Fault Injection Tool (FITO) Implemented With VHDL on FPGA For Testing Fault Tolerant Designs

M. Reddy Sekhar Reddy, R.Sudheer Babu (Ph.D)
M.Tech (VLSI&ES) GPREC, Kurnool.
Assistant Professor, GPREC,Kurnool.

ABSTRACT—*Fault injection is mainly used to test and evaluate the fault-tolerance based designs. In current VLSI technology fault injection has become a popular technique for experimentally verifying the fault tolerant based designs. There are fundamentally two types of fault injection methods; they are hardware-based fault injection and software-based fault injection. Both have their own limitations and advantages. The FPGA synthesizable fault injection model can give reasonable solution with high speed testing platform and also allows good controllability and observability. Even though a considerable progress has been made in research part of the fault injection algorithms, there is a little progress done in developing a tool for FPGA based fault emulation.*

In this paper an FPGA-based fault injection tool (FITO) that supports several synthesizable fault models of digital systems are implemented using VHDL. Aim is to build real time fault injection mechanism with good controllability and observability. Fault injection will be done by applying some extra gates and wires to the original design description and modifying the target VHDL model of the target system. The design will be validated with state machine based example and applying different types of faults. Analysis will be carried out studying the controllability and observability of the proposed scheme. Comparison will be carried out to estimate the speed wise improvement with respect to software simulation based fault injection method.

Modelsim Xilinx Edition (MXE) will be used for functional simulation and Xilinx ISE tools will be used for synthesis and performance analysis. Spartan-3E FPGA board will be used for on chip verification of the results with Chip scope software running on PC.

Index Terms—*VLSI, FITO, VHDL, fault modelling, Modelsim, Xilinx, GUI, Spartan 3E FPGA kit.*

I. INTRODUCTION

Fault injection is mainly used to evaluate fault tolerant mechanisms. In the last decade, fault injection has become a popular technique for experimentally determining dependability parameters of a system, such as fault latency, fault propagation and fault coverage [1].

Within the numerous fault injection approaches that have been proposed, there are two classifications of fault injection methods [2]: 1) hardware-based fault injection and 2) software-based fault injection. Software-based fault injection methods are divided into software-implemented fault injections (SWIFI) and simulation-based fault injections. In the simulation-based fault injection, faults are injected into the simulation model of the circuits using VHDL or Verilog languages. The main advantage of simulation-based fault injection as compared with other fault injection methods is the high observability and controllability [2]. However, simulation-based fault injection methods are too time-consuming. One way to provide good controllability and observability as well as high speed in the fault injection experiments is to use FPGA-based fault injection [3]. An effective FPGA-based fault injection technique should support several properties as below:

1) high controllability and observability,
2) high speed fault injection experiments with the target system running at full speed,
3) capability of injecting permanent and transient faults,
4) minimum area and time overhead into a target system. The techniques which developed for fault grading using emulators proposed in[3]. These techniques are limited to the single stuck at fault model.So they don't have the capability of injecting transient faults and don't support the e third property. In an extension to transient faults is proposed, but the approach is based on reprogramming the FPGA once for each fault. The reconfiguration, even if partial, results in a time overhead.Therefore this technique doesn't support the fourth property.[4]Perform fault injections by using the additional combinational and sequential circuits. Because of using the additional flip-flop for each fault injection location, these techniques introduce too much area overhead and don't support the fourth property. So, these techniques are not sufficient for using on the same chip with the target microprocessor after the fabrication.

The main idea of using fault injector on the same chip with the target microprocessor was proposed in [5]. Because of implementing the most part of the fault injection tool on the target microprocessor, they suffer from the main drawback of high area overhead. This paper describes the FPGA-based fault injection tool, called, FITO1 which support all of the fourth properties as mentioned above and is based on VHDL description of the systems. FITO supports several fault models into RTL- and Gate-level abstraction levels of the target system which has been described by the VHDL. For supporting high speed fault injection experiments, the fault injector part of FITO with low area overhead is implemented with synthesized microprocessor core inside the FPGA

II. DESIGN OF FITO

In this chapter the FITO design flow is explained in detail. Fault models that are implemented in our project are clearly explained

A. FITO

FITO environment consists of three parts
1) Source code modifier and fault list generator.
2) Fault injection manager
3) Results capturing with FPGA emulation

1) Source code modifier and fault list generator

Source code modifier and fault list generator are the software parts of the FITO. This is implemented with two tools.

- Eclipse editor
- C programs to insert faults on a specific port.

These are located on host (PC) computer. Separate C scripts are developed for inserting each fault. A GUI facilitates invoking the scripts by mouse right click.

2) Fault injection manager

Fault injection manger is responsible for performing the real time fault injection. The fault injection manager is implemented in VHDL. The fault injection manager

- VHDL package (dynamically updated by C programs)
- Fault scheduler
- Fault insertion components

The VHDL package is implemented to capture all the constants, type definitions, component declarations and fault injection time for each fault. The package also consists of number of total faults. This VHDL file is automatically updated by C programs every time when a fault is injected in code.The fault scheduler runs multiple counters to schedule each fault with required fault activation time and fault propagation time as per the package. The fault scheduler produces output fault number which is currently being active. This module generates the parallel fault injection signals for every fault. These signals are routed to all fault sites. Fault insertion components are gates with FIS (fault injection signal) control to inject the faults when the FIS is active high. These components instances are automatically made when ever faults are injected.

3) Results capturing with FPGA emulation

This hardware part is implemented on the FPGA board. Result analysis will be carried out with FPGA emulation results and fault list generated by C program. The analysis shall summarize the fault responses for each injected fault. The following Fig shows the fault injection process with FITO.
The golden trace data is ideal trace data (results obtained) without any faults.

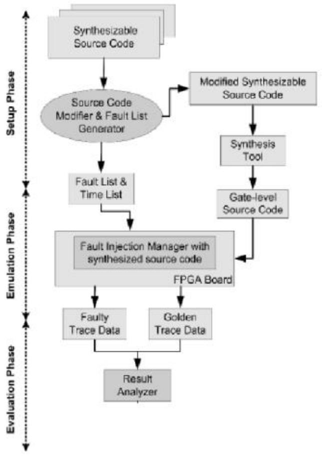

Fig. 1. FITO injection process.

B. Faults Modelled In Our Project

FITO supports the following synthesizable fault models for injecting into any HDL level designs.

- Permanent faults
- Transition faults
- Single event upset faults (or) Bit-flip

Fault injection process can be done by applying some extra gates and wires to the original design description and modifying the target VHDL model of the system. One of these extra wires is the Fault injection system (FIS) which playing the key role in the fault injection experiments. If a FIS takes the value 1, fault would be activated and if it takes the value 0, the fault would become inactive.

For example in the case of Stuck-at-0 fault when the FIS is made 1 then the signal is forced to zero, implementing the fault condition. The below section gives the detailed discussion about injecting the permanent faults.

1) Permanent faults

For supporting the permanent faults in VHDL design, FITO nominates wires for fault injection and apply the FIS signal with one extra gate,. So by selecting the FIS signal high at fault injection time, the permanent fault into the specified wire will be injected.

For example if the signal name in the original code is X then the modified signal TX will be generated as below. In all the places in the code instead of X, the TX will be replaced.

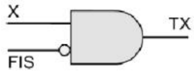

Fig. 2. Synthesizable fault model for stuck-at-0.

Similarly the following code shows the required extra gate and control signal FIS for implementing the stuck-at-1 fault.

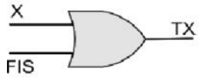

Fig. 3. Synthesizable fault model for stuck-at-1.

For each FIS there would be a path through all levels of hierarchy to its modified circuit. After modification, the final synthesizable VHDL description will be produced which is suitable to use in emulators.

2) Transient faults

The modified circuit that is suitable for transient fault injection is shown in below Fig.

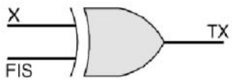

Fig. 4. Synthesizable transient fault model.

For injecting a transient fault, after reaching the fault injection time, the FIS signal will be made high and the timer, which have been loaded with the duration of the transient fault injection start to count. Therefore, the FIS will be high (at logic 1) for the specified duration of time. As similar to the permanent fault, the additional wire (TX) will be used and each wire, namely X will be replacedwithTX. The fault injection manager is responsible for managing the fault injection experiments, such as loading the timers, setting the FIS for the predetermined time, introducing additional wires and performing the fault injection.

3) Bit flip (or) single event upset (SEU)

The fault model that is used by FITO at this level is bit-flip (or single event upset). SEUs are the random events and may flip the content of the memory element at unpredictable times. FITO generate modified circuit for each memory element that is specified for fault injection. The modified circuit for supporting bit flip fault model is shown in below Fig.

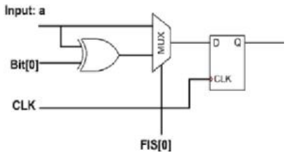

Fig. 5. Synthesizable bit-flip model.

For supporting the bit-flip model, FITO produces the additional signals such as Bit and FIS with one multiplexer. The VHDL synthesizable code for supporting this fault model is shown in above Fig. The inverted input will go to the flip-flop for the next clock when the FIS and bit are “1”.
The fault injection manager part of FITO is responsible for setting and resetting the FIS and bit signals.

C. Example Fault Tolerant Design – Redundant ALU Based Fault Tolerant Processor

In this the example fault tolerant design considered for fault injection is explained.The design uses double ALUS and to achieve fault tolerance in case of soft errors.

A soft error is also a signal or datum which is wrong, but is not assumed to imply such a mistake or breakage. After observing a soft error, there is no implication that the system is any less reliable than before. If detected, a soft error may be corrected by rewriting correct data in place of erroneous data. Highly reliable systems use error correction to correct soft errors on the fly. However, in many systems, it may be impossible to determine the correct data, or even to discover that an error is present at all. In addition, before the correction can occur, the system may have crashed, in which case the recovery procedure must include a reboot.

1) Proposed fault tolerant processor architecture:

The proposed architecture is double ALU based fault tolerant for handling soft errors. The Fig. 6. describes the detailed architecture of fault tolerant processor [6].

Definition - Fault-tolerant describes a computer system or component designed so that, in the event that a component fails, a backup component or procedure can Immediately take its place with no loss of service. Fault tolerance can be provided with software, or embedded in hardware, or provided by some combination.

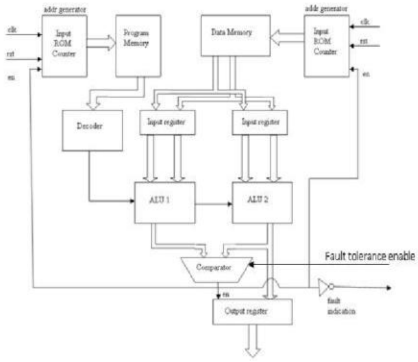

Fig. 6. Architecture of fault tolerant processor.

At a hardware level, fault tolerance is achieved by duplexing each hardware component. Disks are mirrored. Multiple processors are "lock-stepped" together and their outputs are compared for correctness. When an anomaly occurs, the faulty component is determined and taken out of service, but the machine continues to function as usual.

The same technique is used in our architecture by duplexing the ALU unit and comparing the results. An enable signal is provided by the comparator which is used to iterate the function and produce fault free results. The address generator part of the block diagram access the data and is stored in two different input registers and are processed separately by different arithmetic and logic units to achieve redundancy. The enable signal also indicates the occurrence of faulty signal. When it is assured that the fault has not occurred, the output is taken from the output register.

III. IMPLEMENTATION OF FITO MODULES

In this chapter the VHDL modules implemented for FITO are explained in detail. As explained in chapter 2 the Fault injection manger is responsible for performing the real time fault injection. The fault injection manager is implemented in VHDL. The fault injection manager

- VHDL package (dynamically updated by C programs)
- Fault scheduler
- Fault injection components

A. FITO - Package

The VHDL package is implemented to capture all the constants, type definitions, component declarations and fault injection time for each fault. The package also consists of number of total faults. This VHDL file is automatically updated by C programs every time when a fault is injected in code.

The maximum number of faults are taken to be 63 and based on that the other constants are defined. However there is no limitation of the maximum number of faults that can be inserted. Depending on the requirement one has to the constant's values in this package .Another constant is defined sto give the number of injected faults. This constant value is updated by C program every time when a new fault is inserted. FIS_vec_type defines a bus of size equal to number of faults. This bus goes through all modules such that any module can use the control lines for fault injection. It may appear that by routing 64 length wider bus to all small and big modules of design under test we are consuming high number of FPGA routing resources. But the synthesis tool can optimize the resources by only routing the lines which are used in this module. Constant by name Fault injection signal (FIS) high duration indicates the number of clock cycles for which fault will be injected in the design. FIS duration constant tells the time allotted for each fault. That is even after removing the fault we can wait for output to capture before enabling the next fault. This will be useful in cases where the fault propagation time is high. For every fault these two constants are settable in the GUI.

The constant fault_type defines the type of fault as per the below table. For each fault that is injected used will choose this option on GUI.

TABLE I: TYPES OF FAULTS.

Constant value	Fault type
0	Stuck at 0
1	Stuck at 1
2	Transient
3	Bit flip

Package also holds several component declarations. So that in all module if this package is declared then fault injection only requires to give component instantiation (no need to declare the components)

1) Fault scheduler

The fault scheduler runs multiple counters to schedule each fault with required fault activation time and fault propagation time as per the constants in FITO_package. The fault scheduler produces output fault number which is currently being active. This module generates the parallel fault injection signals for every fault. These signals are routed to all fault sites.

Fig. 7. Fault Scheduler

2) Fault injection components

Fault injection components are gates with FIS (fault injection signal) control to inject the faults when the FIS is active high. These components instances are automatically made in the selected module when ever faults are injected. Since all these components are declared in package fault injection need not add component declaration. Hence the fault insertion becomes easy to implement only the following steps.

- Generate code to declare a signal of the same size of the port on which fault need to be injected.
- Add the corresponding fault injection component instance connecting the port signal, FIS control line and output signal.
- Replace all the port signal instances with the declared new signal.

3) Random bit generator for bit flip fault

A random bit generator for bit flip fault is implemented with a Gaussian random variable generated through a Look up table. A Look up table with 127 values is taken and is used to randomly flip the bits in memory when the bit flip fault is activated.

SIMULATION RESULTS

Simulations results of Fault tolerant processor without injection of faults and with injection of faults are shown in this section.

The top level test bench module implements Fault tolerant processor with out injecting faults and after injection of faults with necessary test inputs. The following Fig shows the simulation results obtained by simulating the test bench.

A. Fault_Tolerant_Processor (Without Injecting Faults)

Fault tolerant processor with out injecting faults is implemented with VHDL and simulation results for this are shown below.

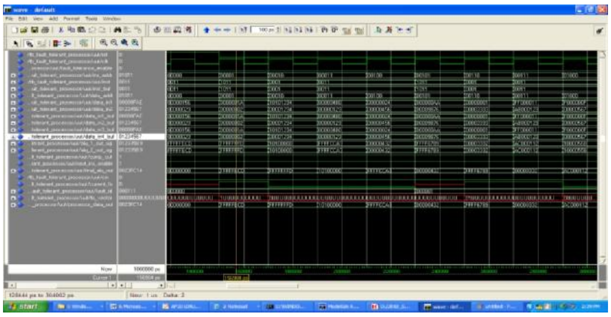

Fig. 8. The fault tolerant processor without injecting any faults.

From ins_address 00000 to 01000 the alu operations are shown in above.

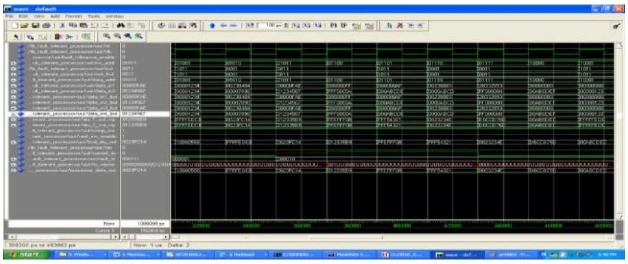

Fig. 9. The fault tolerant processor without injecting any faults (continued).

From inst_address 01001 to 10001 the alu operations which are performed are shown in above.

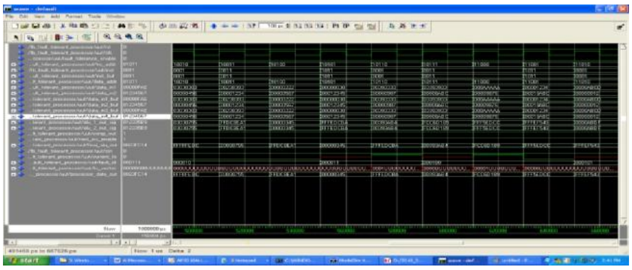

Fig. 10. The fault tolerant processor without injecting any faults (continued).

From ins_address 10010 to 11010 the alu operations which are performed are shown in above.

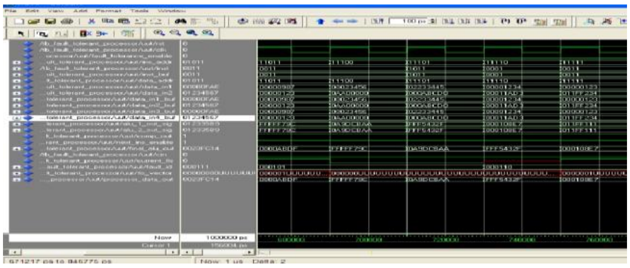

Fig. 11. The fault tolerant processor without injecting any faults (contined)

The ins_address from 01011 to 11111 the alu operations which are performed are shown in above.

B. Simulation Results of Fault tolerant Processor after Faults Have Been Injected in to the Processor are Shown Below

1) Fault tolerant processor after injection of faults

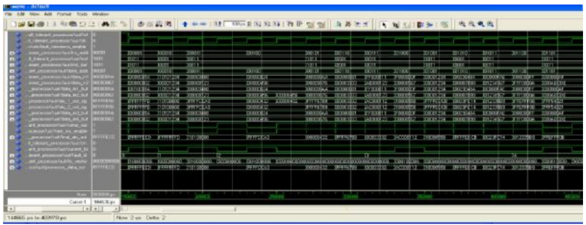

Fig. 12. Simulation results after injection of faults.

In this we injected 11faults from 0th to 10^{th} hence the fault id that is shown above is from 0 to 11.Fault id is represented presently which fault is scheduled. Current_FIS represents on each fault id how much time the current fault should be injected i.e., activated.

The 1^{st} 2^{nd} 3^{rd} 4^{th} faults are injected and results are shown in above.

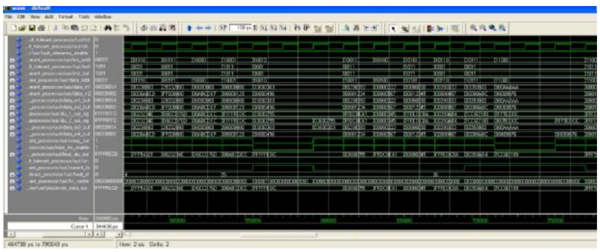

Fig. 13. Simulation results after injection the faults (contd.).

The results of 5th and 6th faults are shown in above.

The results of 7th 8th 9th and 10th fault responses and output are shown below

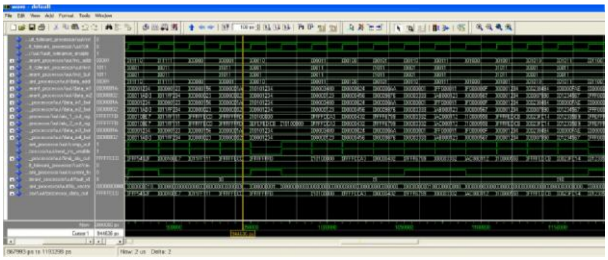

Fig. 14. Simulation Results after injection the faults(cont)

IV. CONCLUSION

The project implements the FPGA based fault called FITO for evaluating the digital systems modelled by VHDL.Fault injection with FITO is done by applying some extra gates and wires to the original design description and modifying the target VHDL model of the target system. FITO support some properties such as high speed good controllability and observability and low area overhead.We have taken a example of fault tolerant design and evaluated on FPGA and faults have been injected in to this processor and proved that really this fault tolerance feature is implemented and also proved that FITO is more faster than simulation based fault injection.

This paper is for real time application for testing the fault tolerant designs and several other fields of VLSI testing.

ACKNOWLEDGEMENT

We would like to thank the Faculty of G Pulla Reddy Engineeering College,Kurnool for their support in the Implementation of High Speed Fault Injection Tool (FITO) Implemented with VHDL on FPGA for Testing Fault Tolerant Designs

REFERENCES

[1] V. Sieh, O. Tschache, and F. Balbach, "VERIFY: evaluation of reliability using VHDL-models with embedded fault description," *Proc. of the International Symposium on Fault-Tolerant Computing*, Jun. 1997, pp. 32-36.

[2] P. Folkesson, S. Sevensson, and J. Karlsson, "A compa-rsion of simulation based and scan chain implemented fault injection," *Proc. of the Annual International Symposium on Fault-Tolerant Computing*,Jun. 1998, pp. 284-293.

[3] K.-T. Cheng, S.-Y. Huang, and W.-J. Dai, "Fault emulation:A new methodology for fault grading," *Trans. on the IEEE Computer-Aided Design of Integrated Circuits and Systems*, Oct. 1999, pp. 1487-1495.

[4] P. Civera, L. Macchiarulo, M. Rebadengo, M. S. Reorda, and M. A. Violante, "Exploiting FPGA for accelerating fault injection experiments," *Proc. of the International On-Line Testing Workshop*, 2001, pp. 9-13.

[5] B. Rahbaran, A. Steininger, and T. Handl, "Built-in fault injection hardware – The FIDYCO example," *Proc. of the IEEE International Workshop on Electronic Design, Test and applications.*

[6] "Fault tolerant Architecture Manual." [Online]. Available: http://www.opencores.org

Improving efficiency of Photovoltaic System with Neural Network Based MPPT Connected To DC Shunt Motor

J. Nagarjuna Reddy, B M Manjunatha*, Mallikarjuna Matam**
Asst Professor, EEE Dept, RGMCET, Nandyal, AP, India.
**Asst Professor, EEE Dept, RGMCET, Nandyal, AP, India.*
***Professor, EEE Dept, RYMES, Bellary, Karnataka, India.*

ABSTRACT: *A photovoltaic generator exhibits nonlinear voltage-current characteristics and its maximum power point varies with solar radiation. A boost converter is used to match the photovoltaic system to the load of dc shunt motor and to operate the pv cell array at maximum power point. This paper presents an application of a neural network for the identification of the optimal operating point of pv module maximum power tracking control. The output power from the modules depends on the environmental factors such as solar insolation, cell temperature, and so on. Therefore, accurate identification of optimal operating point and continuous control of boost converter are required to achieve the maximum output efficiency. The proposed neural network has a quite simple structure and provides a highly accurate identification of the optimal operating point and also a highly accurate estimation of the maximum power from the PV modules. This model is simulated in matlab/simulink and results are obtained.*

Keywords: *photovoltaic (PV) module, solar radiation, neural network, solar insolation maximum power point tracking (mppt) , boost converter, maximum output efficiency*

I. INTRODUCTION

Recently, as the fossil fuel exhaustion and environmental pollution are aggravated, the concern of the development of alternative energy systems, which are renewable and pollution free, has been increased continuously. Among them the photovoltaic (PV) power generation systems standout as an important solution because they produce electric power without inducing environmental pollution, by directly transforming solar irradiation into electricity. The main drawbacks of PV systems are high fabrication cost and low energy-conversion efficiency, which are partly caused by their nonlinear and temperature dependent *V–I* and *P–I* characteristics. To overcome these drawbacks, three essential approaches can be followed:

1. *Improving manufacturing processes of solar arrays*: many research efforts have been performed with respect to materials and manufacturing of PV arrays.
2. *Controlling the insolation input to PV arrays*: the input solar energy is maximized using sun-tracking solar collectors.
3. *Utilization of output electric power of solar arrays*: the main reasons for the low electrical efficiency are the nonlinear variations of output voltage and current with solar radiation levels, operating temperature, and load current. To overcome these problems, the maximum power operating point of the PV system (at a given condition) is tracked using online or offline algorithms and the system operating point is forced toward this optimal condition.

Many MPPT techniques have been proposed, analyzed, and implemented. They can be categorized as:

A) Look-up table method -- The nonlinear and time-varying nature of pv cells and their great dependency on radiation and temperature levels as well as degradation (aging, dirt) effects, make it difficult to record and store all possible system conditions.
B) Perturbation and observation (P&O) method-- Measured cell characteristics (current, power) are employed along with an online search algorithm to compute the corresponding maximum power point independent of insolation, temperature, or degradation levels.
C) Computational method -- The nonlinear *V–I* characteristics of PV panel is modeled using mathematical equations or numerical approximations. Based on the modeled *V–I* characteristics, the corresponding maximum power points are computed for different load conditions as a function of cell open-circuit voltages or cell short-circuit currents.

This paper presents an alternative method to identify the optimal operating point to achieve the maximum output efficiency of the PV modules using a neural network. The input signals are solar irradiance and the cell temperature. The Block diagram of the photovoltaic system with a neural network based maximum power point tracking is shown in Fig.1.

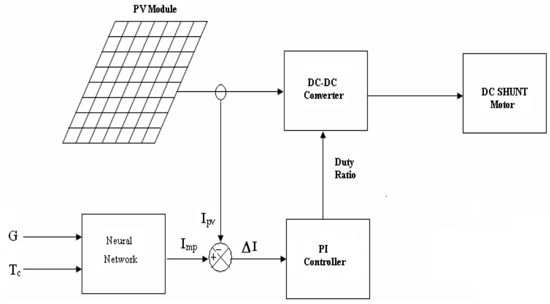

Figure 1. Block diagram of PV system

II. MODELING OF PHOTOVOLTAIC CELL

Fig.2 shows the typical equivalent circuit of PV-cell. The typical I_{pv}-V_{pv} output characteristics of PV-cell are represented as following Eq. 1.

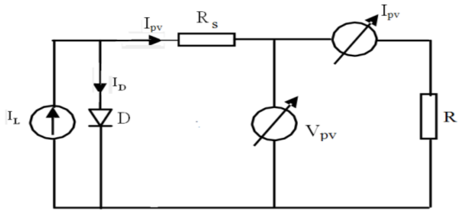

Figure.2 Equivalent model of photovoltaic cell

$$I_{PV} = I_L - I_0\left(\exp\left(\frac{V_{PV} + I_{PV}R_S}{\propto}\right) - 1\right) \ldots (1)$$

Where,

$$I_L = \frac{G}{G_{ref}}\left(I_{Lref} + \mu_{Isc}(T_C - T_{Cref})\right) \ldots (2)$$

$$I_o = I_{Oref}\left(\frac{T_{Cref} + 273}{T_C + 273}\right)^3 exp\left(\frac{e_{gap}\, q}{N_s \propto_{ref}}\left(1 - \frac{T_{Cref} + 273}{T_C + 273}\right)\right). (3)$$

I_{PV} and V_{PV} =Cell output current and voltage; I_L= Light-generated current; Io= Cell saturation current at T_r; Tc = Cell Temperature; Tref = 273K reference temperature; q = Charge of an electron; Rs = Series Resistance; e_{gap} = Band gap of the material; α = Thermal voltage timing completion factor; μ_{Isc} = Temperature coefficient of the short-circuit current.

Fig.3 shows the typical I_{pv}-V_{pv} and P-V_{pv} output characteristic curve of PV-module for a particular irradiation and cell temperature. In case the irradiation and temperature are varied, respectively from Fig. 3, we observe that the output characteristics of PV-module are nonlinear and each curve only has one MPP. Additionally, the output current of PV module is mainly affected by Solar irradiation variation, whereas the output voltage of PV-module is mainly affected by temperature variation. Therefore, to efficiently use PV module, in case the atmospheric conditions are varied, the MPP tracking of PV-module should be implemented.

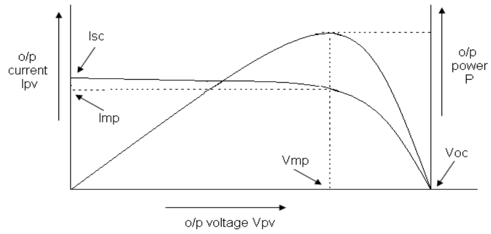

Figure 3 I_{pv}-V_{pv} & P-V_{pv} characteristics of a PV cell

III. THE NEURAL NETWORK BASED MAXIMUM POWER POINT TRACKING FOR PV-SYSTEM

The block diagram for identifying the optimal operating point is shown in Fig.4.

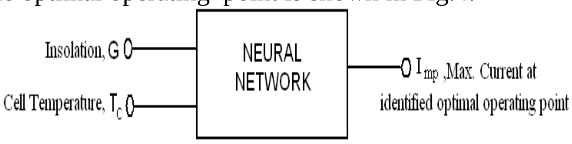

Figure.4 Block Diagram for the identification of optimal operating point

The configuration of 3-layer feed-forward neural network is shown in Fig.5. The network has 3 layers with 3 neurons in input, 4 neurons in hidden, and 1neuron in output layers [8].

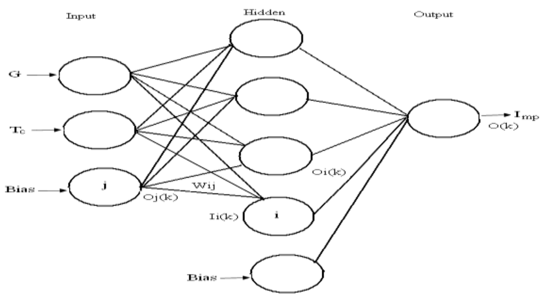

Figure.5 Configuration of a Neural Network

The node in the input layer gets the input insolation, G and Cell temperature, Tc. These signals are directly passed to the nodes in the hidden layer. The node in the output layer provides the identified maximum Imp. The nodes in the hidden layer get signals from the input layer and send their output to the node in the output layer. For each node in the hidden and the output layer, the output $O_i(k)$ is given as follows:

$$O_i(k) = \frac{1}{1 + exp\left(-I_i(k)\right)} \dots (4)$$

Where the sigmoid function is utilized for the I/P-O/P characteristics of the nodes. The term $I_i(k)$ is the input signal given to the node I at the K^{th} sampling. The input $I_i(k)$ is given by the weighted sum from the previous nodes as follows:

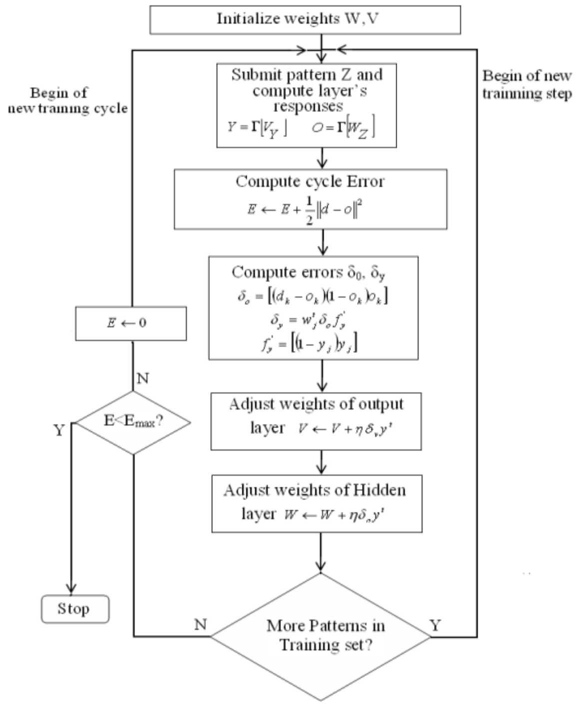

$$I_i(k) = \sum_j W_{ij}(k) O_j(k) \dots (5)$$

Figure.6: Error back propagation training algorithm flowchart

.In the training process, we need a set of I/P-O/P patterns for the neural network as shown later. All the computations are performed off-line during the training process. With the training patterns, the connection weights W_{ij} recursively until the best fit is achieved for the I/P-O/P patterns in the training data. A commonly used approach is the *generalized delta rule*, where the sum of the squared error described below is minimized during the training process.

$$E = \sum_{k=1}^{N} \left(T(k) - O(k)\right)^2 \dots (6)$$

Where N is the total number of training patterns. T(k) is the target output from the output node and O(k) is the computed one. Fig.6 illustrates the flowchart of the error back-propagation training algorithm for a basic two-layer network as shown in Fig.5.

IV. STATE SPACE MODEL OF BOOST CONVERTER

PV cells have relatively low conversion efficiency and the improvement of overall system efficiency is an important factor in the area of PV systems. This can be partly achieved by using high efficiency intermediate converters. In this paper, a boost converter coupled with PV array is presented.

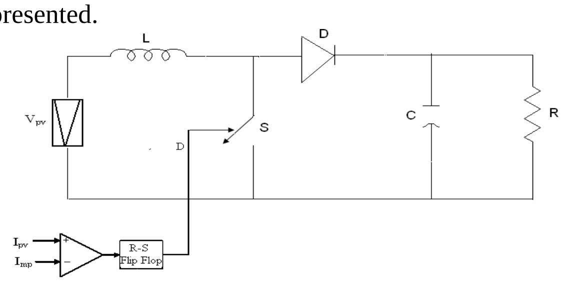

Figure.7 Circuit Diagram for Boost Converter

A state space averaging technique is used to develop linear state space models for dc-dc boost converter. The average state space model for the boost dc/dc converter can then be obtained as follows:

$$\begin{bmatrix} \frac{di_L}{dt} \\ \frac{dv_c}{dt} \end{bmatrix} = \begin{bmatrix} 0 & -\frac{(1-D)}{L} \\ \frac{1-D}{C} & -\frac{1}{RC} \end{bmatrix} \begin{bmatrix} i_L \\ V_c \end{bmatrix} + \begin{bmatrix} \frac{1}{L} \\ 0 \end{bmatrix} [v_c] \dots (7)$$

$$V_o = [0 \quad 1] \begin{bmatrix} i_L \\ V_c \end{bmatrix} \dots (8)$$

Where D = Duty ratio of the switch

V. MOTOR MODEL

The schematic diagram of a dc shunt motor is illustrated in fig.8. The fundamental equations governing the operation of the shunt dc motor are as follows:

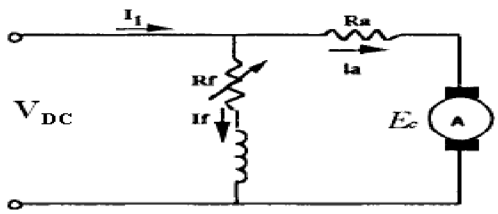

Figure.8 schematic diagram of dc shunt motor

$$V_1 = V_f = V_a = E_c + I_a R_a \dots.(9)$$

$$I_1 = I_a + I_f \dots\dots(10)$$

$$E_c = k\emptyset n \dots (11)$$

Where, V_{DC}= Terminal voltage; V_f = field voltage; V_a= armature voltage; E_c= counter emf; k=design constant; Φ= mutual air-gap flux per pole; n=rotational speed, r /min; R_a= armature resistance; $I_{1=}$ line current; I_f= field current; I_a= armature current

V. SIMULATION RESULTS

Based on the mathematical equations discussed before, a dynamic model for a PV module consisting of 153 cells in series has been developed using matlab/Simulink. The input quantities (solar irradiance G and the ambient temperature Ta) are used to determine the characteristics of a PV module.

A.PV Model Performance

The model I_{pv}-V_{pv} characteristic curves under different irradiances are given in Fig.9 at 25 °C. It is noted from the figure that the higher is the irradiance, the larger are the short-circuit current (I_{sc}) and the open-circuit voltage (V_{oc}). Obviously, the larger will be the maximum power (P), shown in Fig.10.

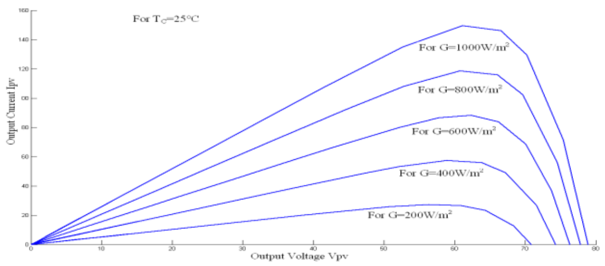

Figure.9 V_{pv}-I_{pv} characteristics for constant T_c and Varying G

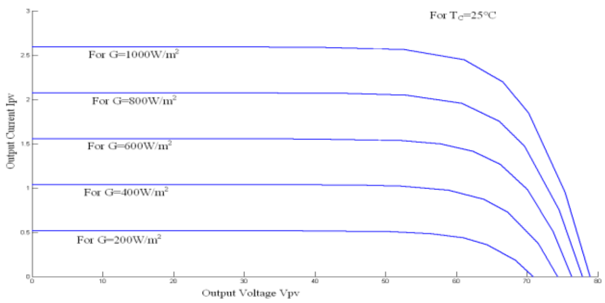

Figure 10.P-V_{pv} characteristics for constant Tc and Varying G

B. Training of a Neural Network

The training of a neural network consists of solar irradiance and cell temperature as the input patterns. The target pattern is given by measured I_{mp} for training the neural network. This calculated I_{mp} values is given as a training data to the neural network. Fig.12 shows the convergence of error during training process. During the training process, the convergence error is taken as 0.01.

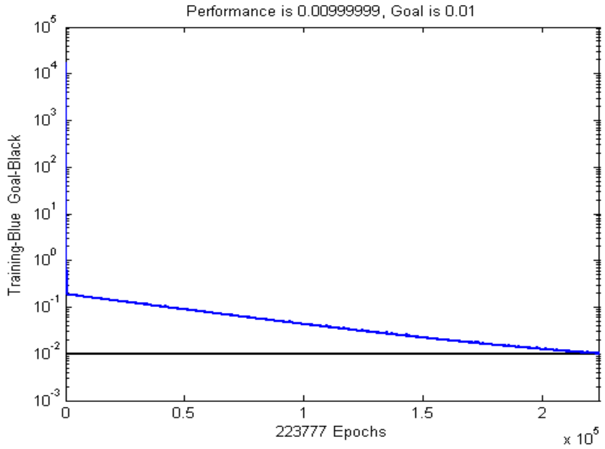

Figure.12 Training of a Neural Network

The training function used is TRAINGDX (Gradient descent w/momentum & adaptive linear backpropagation). The graphs for the I_{mp} of the neural network and the calculated values of the PV model are are combined to show the error between the two:

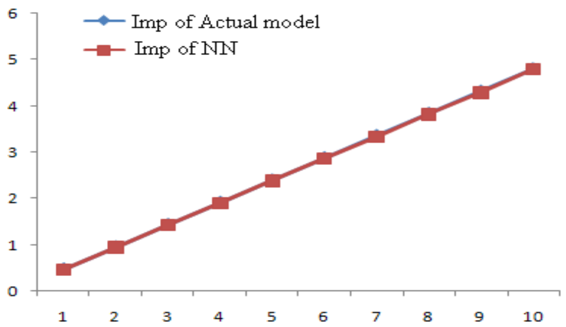

Figure 13: Combined graph of I_{mp} for both neural network and calculated

C. Optimal power point tracking for Boost converter And DC shunt motor

A Boost converter supplied by PV system has been shown in fig(1). Comprehensive simulation studies were made to investigate the influence of a boost converter as an intermediate maximum power point tracker for the PV supplied system. The PV array is simulated using a neural network as shown in figs. 4&7. **As** the studies mainly concentrate on maximum power operation of the PV module**,** a simulated modeling was developed in the matlab environment, for the PV supplied converter system employing the mathematical models developed in the preceding sections. The simulated dynamic maximum power point tracking characteristics are shown in fig.14&15 . The converter parameters considered in this paper are : L=0.06mH, C=0.4mF and R(equivalent load) =50Ω.

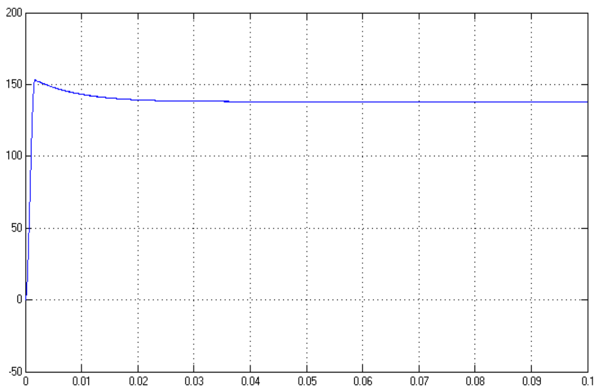

Figure.14 Simulated Dynamic characteristics of capacitor voltage to reach maximum power point

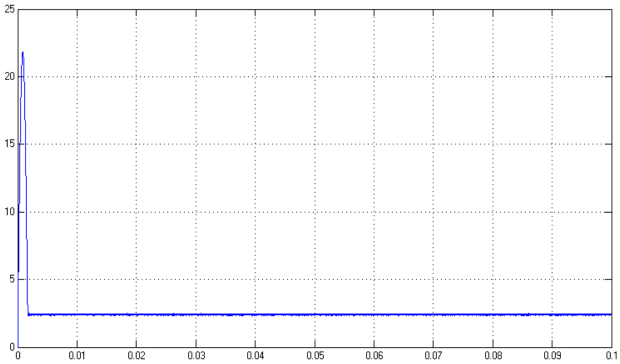

Figure.15 Simulated Dynamic characteristics of inductor current to reach maximum power point

Using the control technique discussed in previous sections the simulated waveforms of the integrated dc shunt motor for Torque and speed under no-load and load conditions are shown in fig.16 & fig.17.

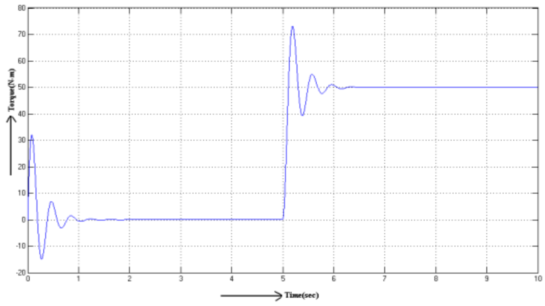

Figure 16 Torque waveform with load of 50 N-m applied at t=5 sec

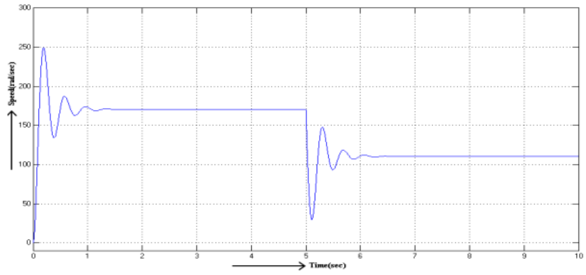

Figure 17 speed waveform with load applied at t=5 sec

VI. CONCLUSION

A Neural network based MPPT algorithm has been developed in this paper for the boost converter supplied PV system. The efficiency of the proposed neural network has been presented for identifying the optimal operating point for the maximum power tracking control of the PV modules. Despite the small set of patterns utilized for the training of the neural network, the network gives accurate predictions over a wide variety of operating modes. The accuracy is not degraded following the seasonal variations of insolation and temperature.

REFERENCES

[1] Oystein Ullberg, "Stand Alone Power Systems For the future: Optimal Design, Operation & Control of Solar-Hydrogen Systems", Ph.D. Dissertation, Norweigan University of science and technology, Trondheim, 1998.

[2] T.U.Townsend, "A Method for estimating the Long-Term Performance of Direct-coupled Photovoltaic systems', MS Thesis, University of Wisconsin, Madison, 1989.

[3] R.D Middle brook, 'Small-Signal modeling of pulse-width modulated switched-mode power converters', Proceedings of the IEEE, Vol. 76, No.4, pp.343-354, April 1988.

[4] A.Kisiovski, R.Redl, and N.Sokal, 'Dynamic analysis of switching-mode DC/DC converters, New York: Van No strand Reinhold, 1994.

[5] J.G.Kuschewski, 'Application of feed forward neural networks to dynamical system identification and control", IEEE Trans. contr.syst.Tech, vol1, no, 1, pp37-49, Mar1993.

[6] W. Shireen and M. S. Arefeen, "An utility interactive power electronics interface for alternate/renewable energy systems," *IEEE Trans. EnergyConversion*, vol. 11, no. 3, pp. 643–649, Sep. 1996.

[7] M. Tsai and W. I. Tsai, "Analysis and design of three-phase AC-to-DC converters with high power factor and near-optimum feed forward," *IEEE Trans. Ind. Electron.*, vol. 46, no. 3, pp. 535–543, Jun. 1999.

[8] *IEEE Standard for Interconnecting Distributed Resources with Electric Power Systems*, IEEE Standard 1547, 2003.

[9] H W VD Broeck, HC Skudelny, G V Stanke, 1988, "Analysis and realisation of a pulse width modulation based on voltage space vector modulation", IEEE Trans Ind, Aual ,*24*, 142-150

J.Nagarjuna Reddy was born in 1985 in India. He received the B.Tech from Dr.Paul Raj Engg. College in 2005 and Post graduated from Jawaharlal Nehru Technological University (JNTU), Hyderabad, In 2006-2008. He is currently working as a assistant professor in the department of electrical and electronics engineering in RGM college of engineering and technology, Nandyal, Andhra Pradesh, India. He has five years of teaching experience. His main areas of research include Electrical Drives & Renewable energy source.

B M Manjunath is born in 1981 in India. He is graduated from Visvwsvaraya Technological university in 2004 and Post graduated from JNTU In 2006-2008. He is currently working as a assistant professor in the department of electrical and electronics engineering in RGM college of engineering and technology, Nandyal, Andhra Pradesh, India. He has five years of teaching experience and one year of Industrial experience. His main areas of research include Renewable Energy Sources, Induction motor drives & control of special machine.

Sri Mallikarjuna Matam Basava is Working as Head of The Dept of EEE, RYM Engineering College, Bellary Since 2008 till date. He has 27 years of Experience in Teaching Electrical Engineering subjects and has presented Many papers. His areas of Academic interests are Electrical Machines, Electromagnetic Fields and Networks.

A Security Framework for Replication Attacks in Wireless Sensor Networks

T. Subramani[1], S.Ravi Varma[2], R.Kabileshwaran[3]
[1]Professor & Dean, Department of Civil Engineering, VMKV Engg College, Vinayaka Missions University, Salem, India
[2]Application Engineer, IBM Pvt. Ltd., India
[3]Application Engineer, IBM Pvt. Ltd., India

ABSTRACT: *Mobile sinks play a great role in many Wireless Sensor Network applications for efficient data accumulation, localized sensor reprogramming and for collecting data from various sensor nodes across the globe. However, in sensor networks that make use of the existing three tier security framework, elevates a new security challenge i.e an attacker can easily create a replicated node and can gain control of the data in the network. Although the three-tier security framework is more resilient to mobile sink replication attacks, it is weak against access point replication attacks. To reduce the damage caused by access node replication attack, strengthening the authentication mechanism between the sensors and access nodes is vital. For this purpose, the single polynomial pool is converted to a double polynomial pool for providing security over the existing system. Also, security is increased by separating the access points into two layers namely, access nodes-D and access nodes-I along with a more secure authentication mechanism called WHIRLPOOL that produces a 512 bit encrypted text using Miyaguchi-Preneel scheme of cipher text generation.Our proposed algorithm ensures the necessary security mechanism for Wireless Sensor Networks and also does not degrade the performance of quality of service.*

Keywords: *Security, Replication Attack, Wireless Sensor Networks, Whirlpool, Key Management*

I. INTRODUCTION

A Wireless sensor network (WSN) consists of spatially distributed autonomous sensors. These sensors are used to monitor physical or environmental conditions, such as temperature, sound, pressure, etc. To cooperatively pass their data through the network to a main location, the more modern networks are bi-directional which enables control of sensor activity. The industrial and consumer applications, such as industrial process monitoring and control, machine health monitoring, and so on. Compromising security in networks is very easy unless we supply strong authentication schemes. The idea of using single polynomial pool is certainly outdated as it opens windows to many node replication attacks. Since single polynomial authentication is compromised, we move on to create two polynomial pools namely static polynomial pool and mobile polynomial pool. Static polynomial pool will supply keys to sensor nodes and access points whereas Mobile polynomial pool will supply keys to access points and mobile sinks [7].

Using two separate key pools and having few sensor nodes that carry keys from mobile key pool will make it more difficult for the attacker to launch a mobile sink replication attack on the sensor network by capturing only few arbitrary sensor networks. Although the above security approach makes the network more resistant to mobile sink replication attack compared to single pool based key pre-distribution scheme, it is still vulnerable to stationary node replication attack. In order to resist this attack, one-way hash algorithm is paired with static polynomial pool based scheme to enhance the security.

In order to enhance the security scheme, stationary nodes (access points) are divided into two layers Access Nodes-D and Access Nodes-I consisting of nodes with direct contact and nodes with indirect contact respectively.

1.2 KEY PRE-DISTRIBUTION

The term Key Pre-distribution could be defined as loading keys into sensor nodes prior to deployment. Two nodes find a common key between them after deployment. The various challenges in key pre-distribution are memory/energy efficiency, security and scalability.

II. RELATED WORK

2.1 SECURITY IN WIRELESS SENSOR NETWORKS

Many works in past has been carried out by various researchers. Some of the important citations has been presented here. Among them, Hasan Tahir presented his work on Wireless Sensor Networks. In his work, the current applications of wireless sensor networks are in the fields of medical care, battlefield monitoring, environment monitoring, surveillance and disaster prevention. Many of these applications require that the sensor network be deployed in an area that is hostile, inaccessible and mission critical. Keeping this in mind a network administrator has to see the security risks involved and how to tackle it if a security threat arises.

Security Methods for Wireless Sensor Networks is proposed by Xiuli Ren in which wireless sensor networks can be used for a wide range of potential applications such as military target tracking, environment monitoring, patient monitoring and scientific exploration in dangerous environments. When sensor networks are deployed in a hostile terrain, security becomes extremely important, as they are prone to different types of malicious attacks. Due to the resource limitations of sensor nodes, existing network security methods, including those developed for Mobile Ad-Hoc Networks, are not well suitable for wireless sensor networks.

Routing in Wireless Sensor Networks was proposed and implemented by Rachid Ennaji. Their system in which routing takes place using protocols such as AODV and DSDV. It brings out all methods to transfer data and also the best optimum protocol for each type of data transfer.

Stephen Olariu, et al presented his work Information Assurance in Wireless Sensor Networks, that assures security. However, a Wireless Sensor Network is only as good as the information it produces. But, the most important concern is information assurance. Information sent through wireless sensor nodes may be subjected to certain risks and danger. When considering very confidential data any flaw in security can be catastrophic.

Methods for Sensors Localization in Wireless Sensor Networks was discussed by Zenon Chaczko, et al. In their work, self-organization and routing algorithms dedicated to wireless sensor networks usually assume that sensors absolute positions are unknown and all decisions are based on sensors own local information. But sooner or later we need to find the positions of the sensor nodes for various purposes such as maintenance etc., so we need effective localization algorithms to find out the relative position of the sensor nodes.

Fatemeh Nourani, et al presented his work Improved Circles Intersection Algorithm for Localization in Wireless Sensor Networks in which they determined the relative position between nodes is very difficult. In fact it is an NP problem. Each node has its own range i.e., a circular range. Their paper brings out effective algorithms to find relative positions of nodes based on intersection of ranges. This idea is used by us in differentiating the direct and indirect contact nodes in the middle layer of the architecture.

An Efficient Approach for Sensor Deployments in Wireless Sensor Network was presented Sujata Dhanorkar that describes the connectivity can be defined as the ability of the sensor nodes to reach the data sink. If there is no available route from a sensor node to the data sink then the data collected by that node cannot be processed. Most of the works discuss in this paper deal with area coverage where the objective is to maximize the coverage percentage; ratio of area covered by at least one sensor to the total area of the region of interest (ROI). In addition, the relation between the number of sensors and efficient coverage area ratio is discussed.

2.2 KEY MANAGEMENT IN WIRELESS SENSOR NETWORKS

Similarly, many works have been proposed in the past and some of them are cited here. Eric Ke Wang, et al proposed an Efficient and Secure Key Establishment Scheme for Wireless Sensor Network. The data authentication becomes very important when transferring data. Key management and generation becomes a must to do task. But public key management is not secure enough. Their paper proposes an effective way to generate keys and enhance security using diffie-helmann key exchange algorithm.

A Key Management Method ofWireless Sensor Network was proposed by Xuemei You. In his work, the actual situation of current wireless sensor network pair-wise key management research, analysis and comparison between the existing two type of pair-wise key management solution is made according to the evaluation metrics proposed in this article. This cited paper brings out the fact that proper pair wise key management can be chosen according to the environment chosen. Also, this paper also brings out the basic limitations when we are using WSN.

Kirti Sharma, et al proposed Flexible and Efficient Scheme for Static Wireless Sensor Networks. Key distribution and management is the core issue of any security approaches. Due to extremely resource-constrained SNs and lack of any infrastructure support, traditional public key based key distribution and management mechanisms are commonly considered as too expensive to be employed in WSNs. Also, they have proposed an efficient individual, pair-wise and cluster key establishment mechanisms EIPCKM for static WSNs, which enable establishing secure links between any two SNs located within their communication range. It removes the Node Addition Attack, Node Cloning Attack and also increases the security within the cluster by introducing the cluster key.

The Study on Key Distribution and Management Mechanisms in Wireless Sensor Networks presented by Liu Feng states that the polynomial pools provide a wide range of good keys. In fact polynomial based key generation is widely used in most of the authentication mechanisms in WSNs.

Walid Bechkit, et al presented an Efficient and Highly Resilient Key Management Scheme for Wireless Sensor Networks. They used the concept of probabilistic key distribution. Deterministic schemes ensure that each node is able to establish a pair-wise key with its neighbors. To guarantee determinism, protocols such as LEAP make use of a common transitory key that is preloaded into all nodes prior to deployment.

Secure and Efficient Key Management Scheme for Wireless Sensor Networks proposed by Shobhit Tiwari that provides a key management technique to ensure maximum security of the wireless sensor network and also of every individual node subject to various hostile environments and situations. This scheme ensures that compromised sensor nodes are resilient towards attack before and after mutual pairwise path establishment. It is a self-enforcing scheme and analysis shows that it is more resilient to sensor capture attacks than the previous schemes.

Walid Bechkit, et al presented a New Key Management Schemes for Resource Constrained Wireless Sensor Networks.In their paper, without effective key management and generation the authenticity of the data sent moves to a questionable state. This paper brings out a concept called Hash chaining by which key pre-distribution schemes are established.

Research on Key Pre-distribution Scheme of Wireless Sensor Networks was presented by Zhao Jinchao, et al. A novel pairwise key management scheme to enhancing the security is proposed and part of keys in the key pool are computed by using hash function and the hash value are as new keys and put back into the key pool.

Vijay Anand presented the Dynamic Key Management Method for Wireless Sensor Networks that has a static key pool which gives us a greater risk of attack. They also proposed an idea of using dynamic generation of keys to reduce an attack. But this type of generation requires more computational time and a good processor with large processor speed.

Node Replication Attacks inWireless Sensor Networks was proposed byWen Tao Zhu in which replication attack makes it possible for an adversary to prepare her own low-cost sensor nodes and induce the network to accept them as legitimate ones. The adversary only needs to physically capture one node, reveal its secret credentials, replicate the node in large quantity, and deploy these malicious nodes back into the network so as to attack the network with little effort. Their paper brings to our attention the various attacks possible with WSNs and how to develop a contingency plan if an attack takes place.

2.3 CRYPTOGRAPHIC ALGORITHMS

There are many works pertaining to cryptographic algorithms. Some of the important works have been cited in the project work. Archana Tiwari, et al presented Performance Evaluation of Cryptographic Algorithms. They presented two most widely used symmetric encryption techniques Data Encryption Standard (DES) and Advanced Encryption Standard (AES). From their paper it is very much clear that DES and AES are very much fragile because of the avalanche effect.

Modied-DES Encryption Algorithm was proposed by Walid Zibideh, et al. In their work, due to the fact that wireless channels are an open medium to intruders and their attacks, encryption is a vital process to assure security over these channels. However, using well-known encryption algorithms to encrypt data in wireless communication will result in a catastrophic error due to the avalanche effect, which is implemented in these algorithms to assure security. In their paper, we propose a modication to the Data Encryption Standard (DES) to make it secure and prone to the bit errors caused by the wireless channel. We observe that using the modied algorithm in wireless channels, improves the Bit Error Rate (BER) performance as well as security compared to DES. But we have used the simple version of DES so that it can be used to efficiently simulate an attack. Based on the above literature survey, it is found that, still there is a need for further improvements over the existing work. Hence, we propose a new security framework for replication attacks in Wireless Sensor Networks that possibly tries to prevent such attacks in this project work.

III. WIRELESS SENSOR NETWORKS

A Wireless Sensor Networks is built of ”nodes” from a few to several hundreds or even thousands, where each node is connected to one (or sometimes several) sensors. Each such sensor network node has typically several parts: a radio transceiver with an internal antenna or connection to an external antenna, a micro controller, an electronic circuit for interfacing with the sensors and an energy source, usually a battery or an embedded form of energy harvesting. A sensor node might vary in size from that of a shoe box down to the size of a grain of dust, although functioning ”motes” of genuine microscopic dimensions have yet to be created. The cost of sensor nodes is similarly variable, ranging from a few to hundreds of dollars, depending on the complexity of the individual sensor nodes. Size and cost constraints on sensor nodes result in corresponding constraints on resources such as energy, memory, computational speed and communications bandwidth.

Security is important for many sensor network applications. Wireless sensor networks (WSN) are often deployed in hostile environments, where an adversary can physically capture some of the nodes. Once a node is captured, adversary collects all the credentials like keys and identity etc. The attacker can re program it and replicate the node in order to eaves drop the transmitted messages or compromise the functionality of the network. Identity theft leads to two types attack: clone and Sybil. In particularly a harmful attack against sensor networks where one or more node(s) illegitimately claims an identity as replicas is known as the Node Replication attack. The replication attack can be exceedingly injurious to many important functions of the sensor network such as routing, resource allocation, miss-behaviour detection, etc. This paper analyses the threat posed by the replication attack, several novel techniques to detect and defend against the replication attack, and analyses their effectiveness.

Wireless sensor networks are used in many applications, in sensing the environmental conditions and transmitting it over longer distances to the base stations. When the base station is far away from the sensing field (where sensors are fixed), the data is sent by a multi-hop. As the data is passing through multiple hops, an intruder can easily cause the attack at any stage in the network.

3.1 TOOL COMMAND LANGUAGE

Tcl is a Tool Command Language in which everything is represented as a string, although the internal interpretation may be of any kind. The command set is used for assingnment in tcl. In puts statement the argument must be preceeded with the $ sign , for procedures args can be passed as both values and names. E.g. Set a 10

3.2 NETWORK ANIMATOR

Network Animator(NAM) is a tool used for network simulation traces, supports topology layout and packet level animation. Provides integrated network monitoring within the switch. Collects the network traffic statistics for real time traffic analysis, performance monitoring and trouble shooting. NS with NAM is an efficient tool for dealing the networking concepts. All the routing protocols are in NS and these protocols can be very easily visualized with the NAM. NAM Graphical editor is a latest addition to the NAM, with this there is no need to create a tcl script separately to show the animation. We can make our own network topology, simulate the traffic sources.

3.3 NETWORK SIMULATOR

Network Simulator(NS) is a simulator used for research in networks. It supports for simulating Transmission Control Protocol(TCP), routing and multicast protocols over wired and wireless networks. Software used to predict the characteristics of large scale complex network systems. Discrete event simulator uses C++ with oTcl interpreter shell (user interface) which allows the i/p model files to get executed. Almost all network elements are developed as classes. It supports a class hierarchy in C++, very similar class hierarchy in oTcl. The root of this class hierarchy is Tcl Object. User tend to create a new simulation objects through the oTcl interpreter and these objects get mirrored by corresponding objects in the class hierarchy in C++.

3.4 SPECIFICATIONS OF WIRELESS SENSOR NETWORKS

3.4.1 Access Points

These are the intermediaries in data transfer. Some of the mobile sinks acts as intermediates. They share keys from both the key pools (static and mobile key pool). Keys from the static key pool facilitates the data transfer between the sensor nodes and them, while the keys from mobile key pool provides authentication for the data transfer between them and the mobile sinks.

3.4.2 Mobile Sinks

Mobile sinks informs the sensor nodes about their location updates, frequent changes in the locations of the mobile sinks causes the sensor nodes to collide in the network. Instead of transferring the information to the entire network at each time, the sinks broadcast the update to the local LAN

.

3.4.3 Key and Key Pools

In order to maintain security, it is very important to encrypt the messages sent among the nodes, so keys must be mutually agreed by the communicating nodes. Establishing the keys for the wireless nodes is a challenging task. Key agreement schemes such as Diffie-Hellman and public key schemes are not suitable for wireless sensor networks. Key pre distribution depends upon the size of the key pool, and the maximum size of the key pool that can be used by the scheme would be s2p, where s is the size of the key pool and p is the probability that two nodes share a common key. Key pre distribution is also not possible since it consumes large amount of memory when the network size is large. So instead of assigning key prior to the data transmission, a scheme is proposed to assign keys randomly [2].

IV. ENHANCED THREE TIER SYSTEM ARCHITECTURE

Basically a sensor node in a wireless sensor networks performs some operations, gathers information and communicates with the other nodes. The main components of the sensor nodes are micro-controller, transceiver, external memory and power source. The enhanced three tier architecture scheme discussed here consists of four layers namely sensor nodes, access nodes with direct contact, and access nodes in indirect contact and mobile sinks. At the initial stage keys from the single polynomial pool has been shared between the sensor nodes and the mobile sinks for communication. Since the single polynomial has been used, the attacker can easily replicate the node, capture the key and misbehave in the network. Therefore in order to enhance the security, two polynomial pools namely static polynomial pool and mobile polynomial pool are created which is called the three tier security mechanism. Even though there is a security mechanism by sharing key from two polynomial key pool for layered communication between layers, the replication attacks still persists.

The attacks that are possible in the three tier security scheme are mobile sink replication attack and access point replication attack, out of which mobile sink replication attack is reduced to small percentage by the implementation of this scheme. In order to avoid the access point replication attack, it is divided into access points which are in direct contact with the sensor nodes mobile sinks and access points which are not in direct contact with the sensor nodes-mobile sinks. In this enhanced scheme, keys from static polynomial pool is shared by the following layers namely sensor nodes, D access nodes, I access nodes. And keys from the mobile polynomial pool are shared by the following layers namely I access nodes and mobile sinks. The access nodes which are in indirect contact share the keys from the mobile polynomial pool and some percentile of keys from the static polynomial pool. Therefore an attacker who captures an access node will get either a static key alone or both static and mobile key(hybrid key).

By capturing a node with the direct contact, which has only static key, an attacker cannot be able to send the data to intended destination because the data will be re routed. Once again an attacker capturing the access node which is indirect will get both the keys, but then also it is least possible for an attacker to reach the destination as intended. The following architecture describes the enhancement of the three tier security scheme, which is more resilient towards replication attacks [3].

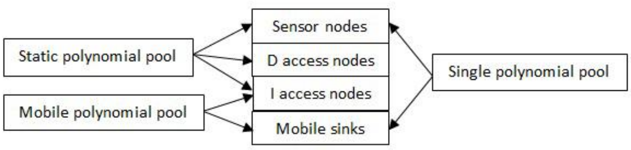

Figure 4.1 Enhanced three tier Architecture

4.1 LAYER CONSTRUCTION

In wireless sensor networks, to implement the enhanced scheme stated above three layers are to be created namely sensor nodes, access nodes and mobile sinks. Transmission control Protocol is used in communication to transfer the data between the layers. A single polynomial pool is created. Keys from this pool are used for communication between sensor nodes- access points and access points-mobile sinks. The figure 4.2 depicts the same.

4.2 KEY POOL SEGREGATION

To enhance the security scheme, two polynomial key pools are created. Keys from static polynomial pool are used for data transfer between sensor nodes and

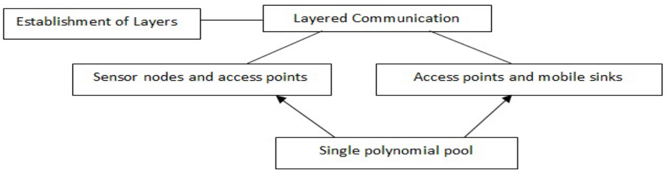

Figure 4.2 Layer Construction

access points and a key from the mobile polynomial pool is used for data transfer between access points and mobile sinks., which is described through the below block diagram in figure 4.3.

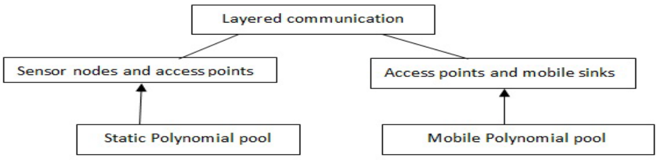

Figure 4.3 Key Pool Segregation

4.3 SECURITY ENHANCEMENT

The access point layer is separated into nodes with direct and indirect contact with respect to interference range. An enhancement of Advanced Encryption standard called the Whirlpool algorithm is used for authentication between access points and the mobile sinks. Once the layer is segregated and key distribution is done coupled with strengthening by means of Whirlpool algorithm, the probability of the attack decreases, i.e. an attacker cannot easily create a replicated node, and transfer the data. The following block diagram describes the steps to be carried out after implementing the three tier security approach.

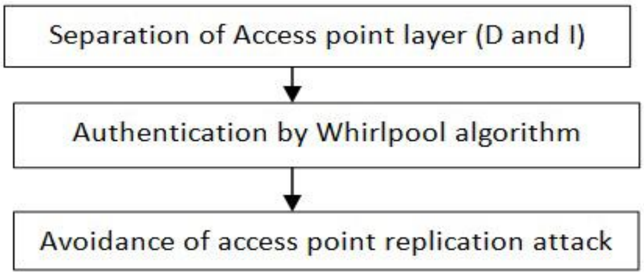

Figure 4.4 Security Enhancement

V. SECURITY MECHANISMS

5.1 DATA ENCRYPTION STANDARD

DES is a 64-bit block cipher. Both the plain text and cipher text are 64 bits wide. The key is 64-bits wide, but every eighth bit is a parity bit yielding a 54-bit key. The DES algorithm involves a step by step procedure or rounds to make up the cipher text needed. The initialization round is where the plain text is subjected to initial permutation and is split into left and right sub parts [6] [4].

Before the start of the first round the key that should be used is subjected to various processes. The 64 bit key is converted into a 48 bit key. After the key is prepared the execution of rounds start.The left and the right part of the plain text is permuted,XORED and then the output this round is given as input to the next round. The number of rounds depend on the length of the plain text. This algorithm is no longer in use because it can be easily attacked. So simulating an attack becomes easier if we use the above algorithm.

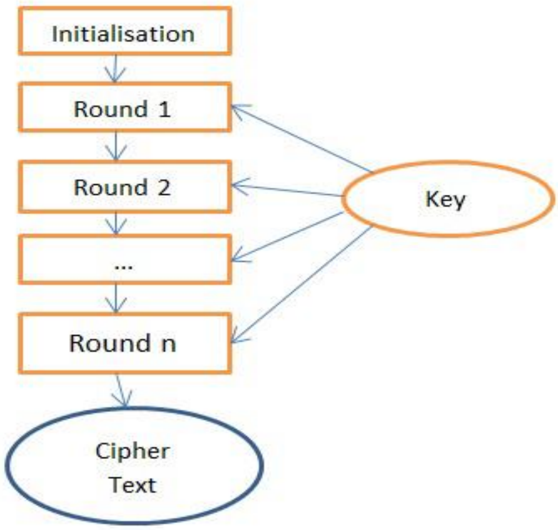

Figure 5.1 Overview of Data Encryption Standard

5.2 WHIRLPOOL

WHIRLPOOL is a hash function designed by Vincent Rijmen and Paulo S. L. M. Barreto that operates on messages less than 2256 bits in length, and produces a message digest of 512 bits. Historically, WHIRLPOOL had three versions. The first version, WHIRLPOOL-0, was submitted to the NESSIE project. Its ”tweaked” successor, WHIRLPOOL-T, was selected for the NESSIE portfolio of cryptographic primitives. A flaw in its diffusion layer reported by Shirai and Shibutani (”On the diffusion matrix employed in the Whirlpool hashing function,” NESSIE public report, 2003) was fixed afterwards, and the final version (called simply WHIRLPOOL for short) was adopted by the International Organization for Standardization (ISO) in the ISO/IEC 10118-3:2004 standard. WHIRLPOOL uses Merkle-Damgrd strengthening and the Miyaguchi-Preneel hashing scheme with a dedicated 512-bit block cipher called W. This consists of the following. The bit string to be hashed is padded with a lquo;’1’-bit, then with a sequence of ’0’-bits, and finally with the original length (in the form of a 256-bit integer value), so that the length after padding is a multiple of 512 bits. The resulting message string is divided into a sequence of 512-bit blocks m1, m2,... mt which is then used to generate a sequence of intermediate hash values H0, H1, H2, ... Ht. By definition, H0 is a string of 512 ’0’-bits. To compute Hi, W encrypts mi using Hi-1 as key, and XORs the resulting ciphertext with both Hi-1 and mi. Finally, the WHIRLPOOL message digest is Ht.

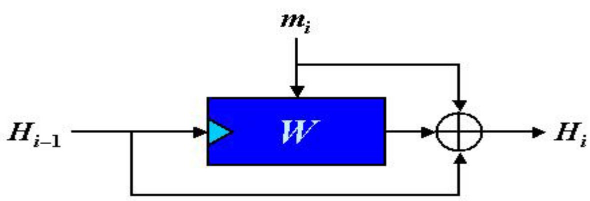

Figure 5.2 Miyaguchi-Preneel Scheme

The W block cipher used by WHIRLPOOL is very similar to the AES algorithm, RIJNDAEL, the main differences being sketched in the following table: The coding for this algorithm is very much similar to that of AES.The W S-box, which in the original submission is generated entirely at random (i.e. lacks any internal structure), by a recursive structure: the new 88 substitution box is composed of smaller 44 ”mini-boxes” (the exponential E-box, its inverse, and the pseudo-randomly generated R box). The coding for the algorithm involves the following steps.

5.2.1 Initialisation Function

The initialisation function given below creates a basic hashing state for each new input given. The hashing state defines a basic skeleton for the hashing function.

5.2.2 Addition Function

The snippet shown below declares the position of the pointers in the plain text. A buffer is also created. Also the data is processed 8 bit at a time. Before this process the data is split into blocks in such a way that each block has 512 bits. The last block is padded at the end with zeroes.

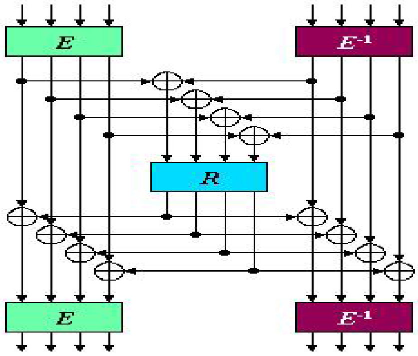

Figure 5.4 Tweaked S-Box Preparation

5.2.3 Finalising Function

The function given below generates the 512 bit cipher text by processing block by block. The above function also makes use of the miyaguchi-preneel scheme of cipher text generation.

VI. PERFORMANCE ANALYSIS

Let K1, K2 denotes the keys in the key pool.
Let Ks, Km denotes the number of keys in the static and mobile key pool.
DK1,K2 denotes the data transfer using the keys K1 and K2.
Access point involved in data transmission picks a key K1 from the Ks number of keys in the static pool and a key K2 from the Km number of keys in the mobile pool.
Selecting a key from the static key pool: Ks C1
Probability of choosing a key from the static key pool, PK1 = 1/Ks C1
Selecting a key from the mobile key pool: Km C1
Probability of choosing a key from the static key pool, PK2 = 1/Km C1
Let PCC denotes the probability of arriving at the correct combination of keys.
Let S denotes the strength of the algorithm which depends on the length of the key, length of the encrypted text and the encrypted mechanism.
Let Pbef denote the probability of access point replication attack before separation of layers.
Pbef = (1/Ks C1) + (1/Km C1) + PCC + S …(1)
Let Paft denote the probability of access point replication attack after node separation.
Direct contact nodes will share the key only from the static key pool. Let x be the small percentage of the keys gets added to the mobile key pool(Hybrid key pool)
Selecting key from the static and mobile key pool,
Y = (Km C1) * (x C1)
Paft = (1/Ks C1) + (1/Y) + PCC + S …(2)
Comparing (1) and (2), its clear that
Paft << Pbef

The factor 1/Y slightly less than 1/Km C1 which makes Paft to decrease, therefore the probability of attack after the node separation is reduced. Even though, an attacker creates the node, the chance of getting the correct combination of these is difficult i.e the attacker has to search for the correct combination of keys over large coverage of nodes. Since the keys are altered, it becomes a difficult task for the attacker to retrieve the data transferred in the network. A graph is plotted with Pbef on the Y axis and the trial number on the X axis.

From equation number 2 we then calculate Paft. A graph is also drawn with Paft on the Y axis and Trial Number on the X axis.

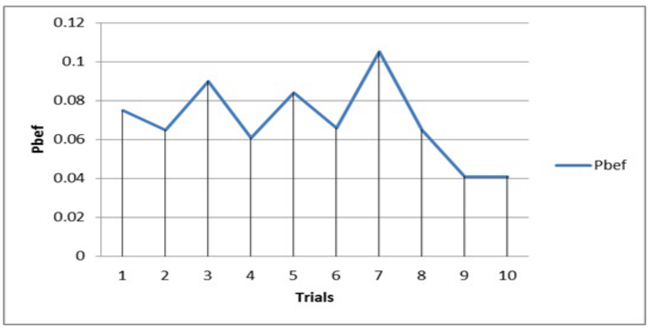

Figure 6.1 Graph of Proposed Probability Pbef

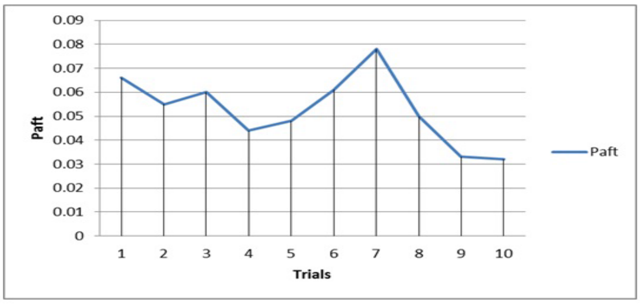

Figure 6.2 Graph of Enhanced Probability Paft

VII. CONCLUSION

The enhanced three-tier security framework has increased the security between sensor nodes and mobile sinks. By splitting the access point layer, we have achieved more resilience and protection against access point and mobile sink replication attacks. Analysis indicates that after separation of layers and key distribution, the probability of access point replication attack is reduced. The proposed scheme on polynomial pool based key pre distribution substantially improved the network resilience to mobile sink replication attacks compared to single polynomial pool based scheme. We have further improved the security performance of the proposed scheme against access point replication attack by strengthening the authentication between access nodes and mobile sinks.

7.1 FUTURE WORK

Although the enhanced three tier security scheme is more resilient towards access point replication attack, it is weak against wormhole attack. As time progresses, more type of threats will haunt WSNs. So, more complex security frameworks and stronger authentication schemes should be developed.

REFERENCES

[1] R.Mahapatra A.Rashid, "An efficient key distribution scheme for establishing pairwise key in distributed sensor networks", Proceedings of IEEE, , 2008.
[2] R.Mahapatra A.Rashid, "A key predistribution scheme for heterogenous sensor networks", IEEE Conference, 2009.
[3] R.Mahapatra A.Rashid, "The three tier security scheme in wireless sensor networks with mobile sinks", IEEE transactions, vol. 23, num. 5, pp. 958–965, 2012.
[4] L.Lamport, "Password authentication with insecure communication", Comm.ACM, vol. 24, num. 11, pp. 770–772, 1981.
[5] M.Praveen Kumar Naregalkar Akshay, "An efficient approach for sensor deployments in wireless sensor network", IEEE conference, 2011.
[6] Mustafa M. Matalgah Walid Y. Zibideh, "Modified-des encryption algorithm with improved ber performance in wireless communication", IEEE conference, 2011.
[7] E.Cayirci Y.Shankarasubramaniam, "Wireless sensor networks: A survey", Proceedings of the IEEE, vol. 38, num. 4, 2002.
[8] Wen Tao Zhu, "Node replication attacks inwireless sensor networks: Bypassing the neighbor-based detection scheme", IEEE conference, 2011.

International Journal of Modern Engineering Research (IJMER)
www.ijmer.com Vol. 3, Issue. 5, Sep - Oct. 2013 pp-2916-2919 ISSN: 2249-6645

An Effective Policy Anomaly Management Framework for Firewalls

Akula Kranthi Kumar[1], Syed Gulam Gouse[2]
[1]M.Tech, Nimra College of Engineering & Technology, Vijayawada, A.P., India.
[2]Professor, Dept.of CSE, Nimra College of Engineering & Technology, Vijayawada, A.P., India.

ABSTRACT: *Firewalls are devices or programs that control the flow of network traffic between hosts or networks that employ differing security postures. While firewalls are often discussed in the context of Internet connectivity, they may also have applicability in various other network environments. At one time, most firewalls were deployed at the network perimeters. This provided some measure of protection for internal hosts, but it could not recognize all instances and forms of attacks, and attacks sent from one internal host to another often do not pass through network firewalls. Because of these and other factors network designers now often include firewall functionality at places other than the network perimeter to provide an additional layer of network security. Due to the increasing threat of network attacks, firewalls have become important integrated elements not only in the enterprise networks but also in small-size and home networks. Firewalls have been the frontier defense for secure networks against attacks and unauthorized traffic by filtering out unnecessary network traffic coming into or going from the secured network. In this paper, we represent an effective policy anomaly management framework for firewalls, adopting a rule-based segmentation technique to identify policy anomalies and derive effective anomaly resolutions.*

Keywords: *Anomalies, FAME, Firewall, Policies.*

I. INTRODUCTION

With the global Internet connection, network security has gained significant attention in both the research and industrial communities. Due to the increasing threat of network attacks, firewalls have become important integrated elements not only in the enterprise networks but also in small-size and home networks. A firewall is a security guard placed at the point of entry between a private network and the outside Internet so that all incoming and outgoing traffic have to pass through it. A packet can be viewed as a tuple with a finite number of fields; examples of these fields are source/destination IP address, source/destination port number, and protocol type. By examining the values of these fields for each incoming and outgoing packet, a firewall accepts legal packets and discards illegitimate ones according to its configuration.

A firewall configuration defines which packets are legal and which are illegal. An error in a firewall configuration means a wrong definition of being legitimate or illegitimate for some packets, which will either allow unauthorized access from the outside Internet to the private network, or disable some legitimate communication between the private network and the outside network. How to design a correct firewall configuration is therefore a very important security issue. Firewalls have been the frontier defense for secure networks against many attacks and unauthorized traffic by filtering out unwanted network traffic coming into or going from the secured network. The filtering decision is taken according to a set of ordered filtering rules written based on the predefined security policy requirements. Although deployment of firewall technology is an important step toward securing the networks, the complexity of managing firewall policy might limit the effectiveness of firewall security. A firewall policy may include anomalies, where a network packet may match with two or more different filtering rules.

When the filtering rules are defined, serious attention has to be given to rule relations and interactions in order to determine the proper rule ordering and to guarantee correct security policy semantics. As the number of filtering rules increases, then the difficulty of writing a new rule or modifying an existing one also increases. It is very likely, in this case, to introduce the conflicting rules such as one general rule shadowing another specific rule, or correlated rules whose relative ordering determines different actions for the same packet. In addition, a typical large-scale enterprise network might involve hundreds of rules that might be written by various administrators in various times. This significantly increases the potential of the anomaly occurrence in the firewall policy, jeopardizing the security of the protected network [1]. Therefore, the effectiveness of the firewall security is dependent on providing policy management techniques and tools that enable network administrators to analyze and verify the correctness of written firewall legacy rules.

II. RELATED WORK

Effective mechanisms and tools for policy management are crucial to the success of the firewalls. Recently, policy anomaly detection has received a great deal of attention [2], [3], [4], [5]. Corresponding policy analysis tools, such as Firewall Policy Advisor [2] and FIREMAN [3], with the goal of detecting the policy anomalies have been introduced. Firewall Policy Advisor only has the capability of detecting pairwise anomalies in firewall rules. FIREMAN can detect anomalies among multiple rules by analyzing the relationships between one rule and the collections of packet spaces derived from all the preceding rules. However, FIREMAN also has several limitations in detecting anomalies [4]. For each firewall rule, FIREMAN only examines all the preceding rules but ignores all subsequent rules when performing anomaly analysis. In addition, each analysis result from FIREMAN can only show that there is a misconfiguration between oner ule and its preceding rules, but cannot accurately indicate all the rules involved in an anomaly.

A first approach to addressing our problem domain is the use of the refinement mechanisms. In this way, we can perform a top-down deployment of the rules by unfolding a global set of security policies into the configurationsof several components and guaranteeing that those deployed configurations are free of anomalies. In [6], for example, the authors present a refinement method that uses a formal model for the generation of filtering rules by transforming general rules into specific configuration rules. Indeed, the authors propose the use of roles to better define of network capabilities, and the use of an inheritance mechanism through a hierarchy of entities to automatically generate permissions and prohibitions. A second refinement approach based on the concept of roles is also presented in [7]. However, and although the authors claim that their work is based on the Role Base Access Control (RBAC) model, their specification of the network entities, roles, and permission assignments are not rigorous and does not fit any reality. Most of these limitations are solved in the approach as presented in [8], where a global set of rules based on theOrganization Based Access Control (OrBAC) model [2] are further deployed into specific firewall configuration files through a transformation process. Generally, the administrators are reluctant to set up from scratch a whole network security policy, and prefer recycling existing configurations.

III. FIREWALL POLICIES AND ANOMALIES

A firewall policy rule is defined as a set of criteria and an action to perform when a network packet matches the criteria. The criteria of a rule consist of the elements direction, protocol, source port, source IP, destination IP and destination port. Therefore a complete rule may be defined by the ordered tuple <direction, protocol, source IP, source port, destination IP, destination port, action>. Each attribute can be defined as a range of values, which can be represented and analyzed as the sets. The relation between two rules essentially mean that the relation between the set of packets they match. Thus the action field does not come into play when considering the relation between the two rules. Firewall policy anomaly is defined as the existence of two or more firewall filtering rules that may match the same packet . The existence of a rule that can never match any network packet on the network paths that cross the firewall also cause anomaly. Till date, five types of anomalies are discovered – they are: Shadowing Anomalies, Correlation Anomalies, Generalization Anomalies, Redundancy Anomalies, and Irrelevance Anomalies.

Shadowing anomaly: Two rules are said to have shadowing anomaly ,whenever the rule which comes first in the rule set matches all the packets and the second rule which is positioned after the first rule in rule set does not get chance to match any packet because the previous rule has matched all the packets.

Correlation anomaly: Two rules are said to have correlation anomaly if both of the rules matches some common packets that is the rule one matches some packets, which are also matched by the rule second.

Generalization anomaly: Two rules which are in order one of them is said to be in the generalization of another if the first rules matches all the packets which can be also matched by the second rule but the action performed is different in both the rules.

Redundancy anomaly: Two rules are said to be redundant if both of the rules matches some packets and the action performed is also the same. So there is no effect on the firewall policy if one of the redundant rules will be removed from the rule set.

Irrelevance anomaly: Any rule is said to be irrelevant if for a given time interval it does not matches any of the network packets either incoming or outgoing. Thus if any type of the packets do not match the rule then it is irrelevant i.e. there is no need to put that rule in the rule set.

IV. ANOMALY MANAGEMENT FRAMEWORK

In our proposed policy anomaly management framework is composed of two core functionalities: conflict detection and resolution, and redundancy discovery and removal, as depicted in Figure 1. Both of the functionalities are based on the rule-based segmentation technique. For conflict detection and resolution, conflicting segments are identified only in the first step. Each conflicting segment associates with the policy conflict and a set of conflicting rules. Also, the correlation relationships among the conflicting segments are identified and conflict correlation groups (CG) are derived. Policy conflicts belonging to different conflict correlation groups can be resolved separately; thus, the searching space for resolving the conflicts is reduced by the correlation process. The second step generates an action constraint for each of the conflicting segment by examining the characteristics of each conflicting segment. A strategy-based method is introduced for generating the action constraints. The third step utilizes a reordering algorithm, which is a combination of the permutation algorithm and a greedy algorithm, to discover a near-optimal conflict resolution solution for policy conflicts. Regarding redundancy discovery and removal, the segment correlation groups are first identified. Then, the process of the property assignment is performed to each rule's subspaces.

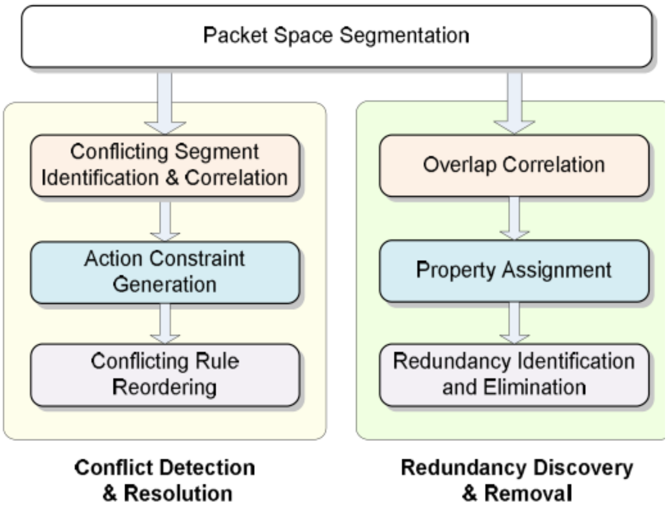

Figure 1: Policy anomaly management framework

A. Conflict Resolution

Our conflict resolution mechanism introduces that an action constraint is assigned to each of the conflicting segment. An action constraint for the conflicting segment defines a desired action (either Allow or Deny) that the firewall policy should take when any packet within the conflicting segment comes to the firewall. Then, to resolve the conflict, we only assure that the action taken for each packet within the conflicting segment can satisfy the corresponding action constraint. To generate action constraints for conflicting segments, we propose a strategy-based conflict resolution method, which generates the action constraints with the help of effective resolution strategies based on the minimal interaction with system administrators. Figure 2 shows the main processes of this method, which incorporates both automated and manual strategy selections. Once conflicts in the firewall policy are discovered and conflict correlation groups are identified, the risk assessment for conflicts is performed.

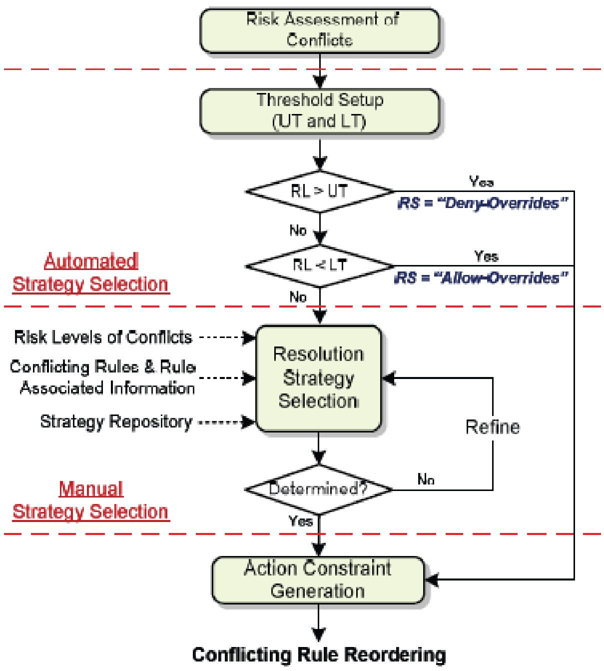

Figure 2: Strategy-based conflict resolution

B. Implementation of FAME

FAME was implemented in Java language. Based on our policy anomaly management framework, it consists of 6 components: segmentation module, correlation module, risk assessment module, action constraint generation module, rule reordering module, and property assignment module. The segmentation module takes the firewall policies as an input and identifies the packet space segments by partitioning the packet space into disjoint subspaces. Our framework is realized as a proof-of-concept prototype called as Firewall Anomaly Management Environment. Figure 3 shows a high-level architecture of FAME with two levels. The upper level is the visualization layer, which visualizes the results of the policy anomaly analysis to system administrators. Two visualization interfaces, policy conflict viewer and the policy redundancy viewer, are designed to manage policy conflicts and redundancies, respectively. The lower level of the architecture provides underlying functionalities addressed in our proposed policy anomaly management framework and relevant resources including rule information, strategy repository, network asset information, and vulnerability information.

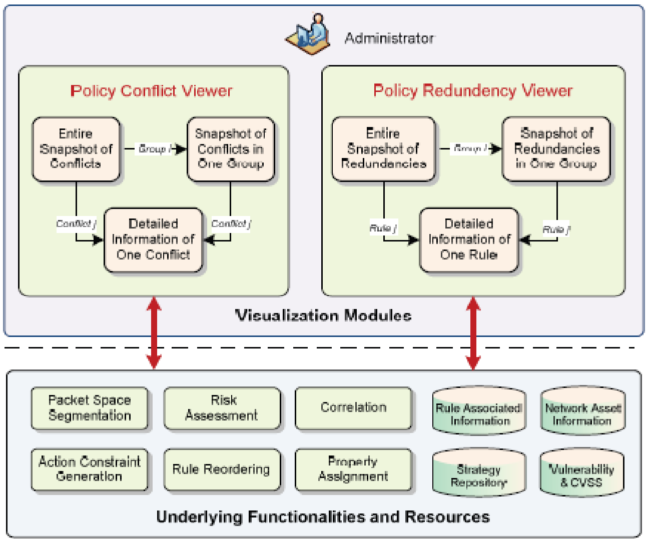

Figure 3: Architecture of FAME

V. CONCLUSION

A firewall is a system acting as an interface of a network to one or more external networks, for example, Internet. It implements the security policies of the network by deciding which packets to let through based on rules defined by the network administrator. Any error in defining the rules may compromise the system security by letting unwanted network traffic pass or blocking desired traffic. Manual definition of the rules often results in a set that contains conflicting, redundant or overshadowed rules, resulting in anomalies in the policy. Manually detecting and resolving these anomalies is a critical task but tedious and error prone task. Existing research on this problem have been focused on the analysis and detection of the anomalies in the firewall policy. A rule-based segmentation mechanism and a grid-based representation technique were introduced to achieve the goal of effective and efficient firewall anomaly analysis. In addition, it is demonstrated that our proposed work is practical and helpful for system administrators to enable an assurable network management.

REFERENCES

[1] E. Al-Shar and H. Hemed. "Firewall Policy Advisor for Anomaly Detection and Rule Editing." Proc.of IEEE/IFIP Integrated Management Conference (IM'2003), March 2003.
[2] E. Al-Shaer and H. Hamed, "Discovery of Policy Anomalies inDistributed Firewalls," IEEE INFOCOM '04, vol. 4, pp. 2605-2616,2004.
[3] L. Yuan, H. Chen, J. Mai, C. Chuah, Z. Su, P. Mohapatra, and C.Davis, "Fireman: A Toolkit for Firewall Modeling and Analysis,"Proc. IEEE Symp. Security and Privacy, p. 15, 2006.
[4] J. Alfaro, N. Boulahia-Cuppens, and F. Cuppens, "CompleteAnalysis of Configuration Rules to Guarantee Reliable NetworkSecurity Policies," Int'l J. Information Security, vol. 7, no. 2, pp. 103122,2008.
[5] F. Baboescu and G. Varghese, "Fast and Scalable ConflictDetection for Packet Classifiers," Computer Networks, vol. 42,no. 6, pp. 717- 735, 2003.
[6] Bartal, Y., Mayer, A., Nissim, K., and Wool, A. Firmato: A novel firewall management toolkit. In IEEE Symposiumon Security and Privacy, pp. 17–31, Oakland, California, May, 1999.
[7] Reed, D. IP Filter. [Online]. Available from:http://www.ja.net/CERT/Software/ipfilter/ip-filter.html
[8] Hassan, A. and Hudec, L. Role Based Network Security Model: A Forward Step towards Firewall Management.In Workshop On Security of Information Technologies, Algiers, December, 2003.

International Journal of Modern Engineering Research (IJMER)
www.ijmer.com Vol. 3, Issue. 5, Sep - Oct. 2013 pp-2920-2923 ISSN: 2249-6645

Social Tagging Of Multimedia Content A Model

Abdul Rabbani[1], P. U.V. Pavan Kumar[2], Dr. Md. Ali Hussain[3]

[1]M.Tech, Dept. of ECE, Sri Sunflower College of Engineering & Technology, A.P., India.
[2]Asst.Professor, Dept. of ECE, Sri Sunflower College of Engineering & Technology, A.P., India.
[3]Professor, Dept. of Electronics and Computer Engineering, KL University, Guntur, A.P., India.

***ABSTRACT**: Social networks are very popular now days, as it facilitates search and retrieval of multimedia features. Anyway, noisy and spam annotations often make it difficult to perform an efficient search. Users may make mistakes in tagging and irrelevant tags and content may be maliciously added for advertisement or self-promotion. This article examine recent advances in techniques for combating such noise and spam in social tagging. The trust relationship among users has a direct impact on the sharing and transmission mode of digital contents. To effectively assess direct or recommended trust between users, this paper proposed a multimedia social networks trust model based on small world theory. Online and Internet databases and early websites deployed them as a way for publishers to help users find content.*

***Keywords:** Spam, Multimedia Social Networks, Websites.*

I. INTRODUCTION

When information is exchanged on the Internet, malicious individuals are everywhere, trying to take advantage of the information exchange structure for their own benefit, while bothering and spamming others. Before social tagging became popular, spam content was observed in various domains: first in e-mail, and then in Web search networks have been also influenced by malicious peers, and thus various solutions based on trust and reputation have been proposed, which dealt with collecting information on peer behavior, scoring and ranking peers, and responding based on the scores . Today, even blogs are spammed. Ratings in online reputation systems, such as eBay, Amazon, and Epinions, are very similar to tagging systems and they may face the problem of unfair ratings by artificially inflating or deflating reputations. Several filtering techniques for excluding unfair ratings are proposed in the literature. Unfortunately, the countermeasures developed for e-mail and Web spam do not directly apply to social networks.

II. BACKGROUND

Social networks and multimedia content sharing Web sites have become increasingly popular in recent years. Their service typically focuses on building online communities of people who share interests and activities, or are interested in exploring the interests and activities of others. At the same time, they have become a popular way to share and disseminate information. For

Example, users upload their personal photos and share them through online communities, letting other people comment or rate them.

One important challenge in tagging is to identify the most appropriate tags for given content, and at the same time, to eliminate noisy or spam tags. The shared content is sometimes assigned with inappropriate tags for several reasons. First of all, users are human beings and may commit mistakes. Moreover, it is possible to provide wrong tags on purpose for advertisement, self-promotion, or to increase the rank of a particular tag in automatic search engines. Consequently, assigning free-form keywords (tags) to multimedia content has a risk that wrong or irrelevant tags eventually prevent users from the benefits of annotated content.

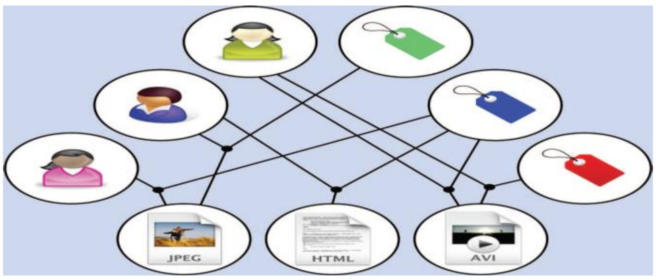

III. TRUST MODELING

The social network approach to design large-scale systems has significant benefits including scalability, low cost of ownership, robustness, and ability to provide site autonomy. However, this approach has several drawbacks as well including trust issues and lack of coordination and control among the peers. We present a trust model for a social network structured large-scale network computing system and completely define the trust model and describe the schemes used in it. Central to the model is the idea of maintaining a recommender network that can be used to obtain references about a target domain. Simulation results indicate that the trust model is capable of building and maintaining trust and also identifying the bad domains. In a social tagging system, spam or noise can be injected at three different levels: spam content, spam tag-content association, and spammer. Trust modeling can be performed at each level separately or different levels can be considered jointly to produce trust models, for example, to assess a user's reliability, one can consider not only the user profile, but also the content that the user uploaded to a social system. In this article, we categorize trust modeling approaches into two classes according to the target of trust, i.e., user and content trust modeling. Presented approaches are sorted based on their complexity from simple to advanced, separately for both content and user trust models.

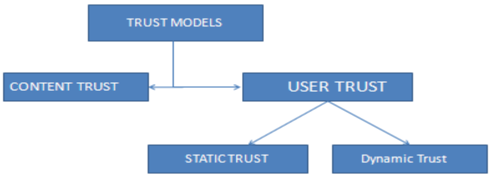

IV. CONTENT TRUST MODELING

Approaches for content trust modeling utilize features extracted from content information, users profiles and/or associated tags to detect specific spam content. Trust Rank relies on an important empirical observation called approximate isolation of the good set: good pages seldom point to bad ones. It starts from a set of seeds selected as highly qualified, credible and popular Web pages in the Web graph, and then iteratively propagates trust scores to all nodes in the graph by splitting the trust score of a node among its neighbors according to a weighting scheme. Trust Rank effectively removes most of the spam from the top-scored Web pages however it is unable to effectively separate low-scored good sites from bad ones, due to the lack of distinguishing features.

Content trust modeling is used to classify content (e.g., Web pages, images, and videos) as spam or legitimate. In this case, the target of trust is content (resource), and thus a trust score is given to each content based on its content and/or associated tags. Content trust models reduce the prominence of content likely to be spam, usually in query-based retrieval results. They try to provide better ordering of the results to reduce the exposure of the spam to users. The administrator can go a step further and remove all content contributed by the user who posted the incorrect content.

V. USER TRUST MODELING

The aforementioned studies consider users' reliability as static at a specific moment. However, a user's trust in a social tagging system is dynamic, i.e., it changes over time. The tagging history of a user is better to consider, because a consistent good behavior of a user in the past can suddenly change by a few mistakes, which consequently ruins his/her trust in tagging.

In user trust modeling, trust is given to each user based on the information extracted from a user's account, his/her interaction with other participants within the social network, and/or the relationship between the content and tags that the user contributed to the social tagging system. Given a user trust score, the user might be flagged as a legitimate user or spammer

5.1 EVALUATION

Data sets used for development and evaluation of trust modeling techniques have a wide range of diversity in terms of content, numbers of resources, tags and users, and type of spam. Some researchers dealing with bookmarks used a public data set released by BibSonomy as a part of the ECML PKDD Discovery Challenge 2008 on Spam Detection in Social Bookmarking Systems.

To model trust in other types of tagging systems, where spam is introduced through videos, tweets, or user profiles, data are usually crawled from the corresponding social network, like YouTube, Twitter, or MySpace, respectively. For example, Lee et al. [28] collected around 215,000 users and 4 million tweets from Twitter. Since this raw data are missing ground truth for evaluation, they manually labeled a small portion of users distinguishing between legitimate users,

To model trust in other types of tagging systems, where spam is introduced through videos, tweets, or user profiles, data are usually crawled from the corresponding social network, like YouTube, Twitter, or MySpace, respectively Since this raw data are missing ground truth for evaluation, they manually labeled a small portion of users distinguishing between legitimate users,

5.2 ALGORITHM

Trust modeling can be formulated as either a classification problem or a ranking problem, depending on the way of treatment. In the classification problem, the results of an algorithm can be summarized by a confusion matrix from ground-

truth data and predicted labels, which contains the number of true positives, true negatives, false positives, and false negatives. From these values, classical
measures such as a receiver operating characteristic (ROC), the area under the ROC curve (AUC), precision-recall (PR) curves, and F-measure can be derived.

VI. EXPERIMENTAL RESULTS

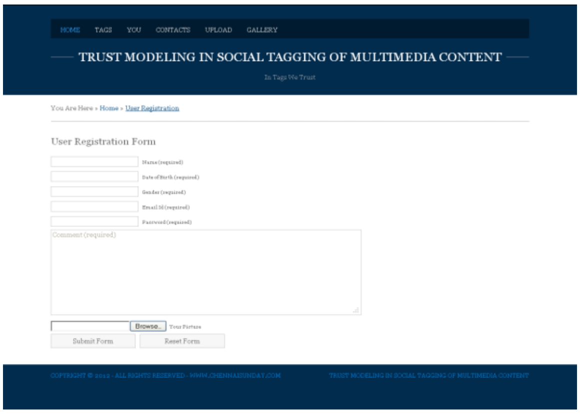

User profile

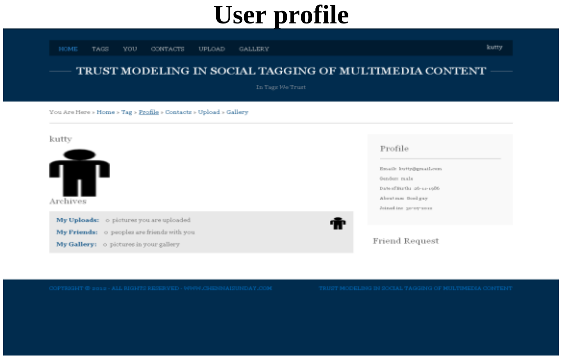

Image upload page

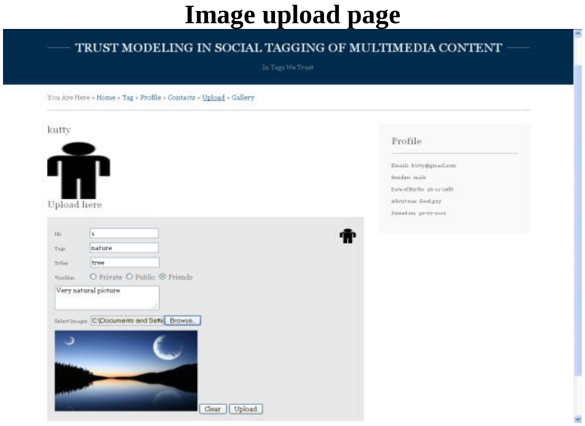

Image search page

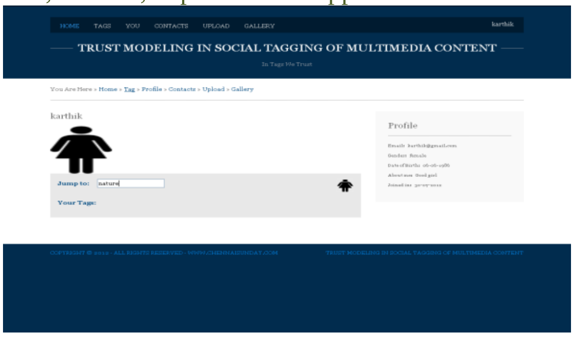

VII. CONCLUSION AND FUTURE RESEARCH

In this article, we dealt with one of the key issues in social tagging systems: combating noise and spam. We classified existing studies in the literature into two categories, i.e., content and user trust modeling. Representative techniques in each category were analyzed and compared. In addition, existing databases and evaluation protocols were re viewed. An example system was presented to demonstrate how trust modeling can be particularly employed in a popular application of image sharing and geotagging. Finally, open issues and future research trends were prospected. As online social networks and content sharing services evolve rapidly, we believe that the research on enhancing reliability and trustworthiness of such services will become increasingly important

REFERENCES

[1] Wikimedia Foundation Inc. (2011, Dec.). Flickr. [Online]. Available: http://en.wikipedia.org/wiki/Flickr.
[2] Pingdom Blog. (2011, Jan.). Internet 2010 in numbers. [Online]. Available: http://royal.pingdom.com/2011/01/12/internet-2010-in-numbers
[3] C. Marlow, M. Naaman, D. Boyd, and M. Davis, "HT06, tagging paper, taxonomy, Flickr, academic article, to read," in Proc. ACM HT, Aug. 2006, pp. 31–40.
[4] K. Liu, B. Fang, and Y. Zhang, "Detecting tag spam in social tagging systems with collaborative knowledge," in Proc. IEEE FSKD, Aug. 2009, pp. 427–431.
[5] L. S. Kennedy, S.-F. Chang, and I. V. Kozintsev, "To search or to label?: Predicting the performance of search-based automatic image classifiers," in Proc.ACM MIR, Oct. 2006, pp. 249–258.
[6] P. Heymann, G. Koutrika, and H. Garcia-Molina, "Fighting spam on social Web sites: A survey of approaches and future challenges," IEEE Internet Comput., vol. 11, no. 6, pp. 36–45, Nov. 2007.
[7] L. von Ahn, M. Blum, N. J. Hopper, and J. Langford, "CAPTCHA: Using hard AI problems for security," in Proc. Eurocrypt, May 2003, pp. 294–311.
[8] L. von Ahn, B. Maurer, C. Mcmillen, D. Abraham, and M. Blum, "reCAPTCHA: Human-based character recognition via Web security measures," Science, vol. 321,no. 5895, pp. 1465–1468, Aug. 2008.
[9] Yahoo, Inc. (2011, Dec.). Flickr—Tags. [Online]. Available: http://www.flickr.com/help/tags.
[10] G. Mori and J. Malik, "Recognizing objects in adversarial clutter: Breaking a visual CAPTCHA," in Proc. IEEE CVPR, June 2003, pp. I-134–I-141.
[11] M. Sahami, S. Dumais, D. Heckerman, and E. Horvitz, "A Bayesian approach to filtering junk e-mail," AAAI Workshop on Learning for Text Categorization,Madison: WI, Tech. Rep. WS-98-05, July 1998.
[12] D. Fetterly, M. Manasse, and M. Najork, "Spam, damn spam, and statistics:Using statistical analysis to locate spam Web pages," in Proc. ACM WebDB, June 2004, pp. 1–6.
[13] S. Marti and H. Garcia-Molina, "Taxonomy of trust: Categorizing P2P reputation systems," Comput. Netw., vol. 50, no. 4, pp. 472–484, Mar. 2006.
[14] A. Thomason, "Blog spam: A review," in Proc. CEAS, Aug. 2007.

Inverted Pendulum Control: A Brief Overview

Vijayanand Kurdekar[1], Samarth Borkar[2]
[1](Microelectronics, Goa College of Engineering, Goa University, India)
[2](Assistant professor, Goa College of Engineering, Goa University, India)

ABSTRACT: *Inverted Pendulum is a classic example of an inherently unstable system. This paper studies the Control of Inverted Pendulum. It focuses on the Mobile Inverted Pendulum. A few papers have been referred to get a brief overview of the work going on in this field. A short survey of these papers has been done for the purpose. Along with it, the basic idea of the mobile inverted pendulum and 2 control strategies have been discussed.*

Keywords: *Ball-bot, Degree of Freedom, Fuzzy control, Inverted pendulum, PID control.*

I. INTRODUCTION

Inverted pendulum is a system that is stable under specific conditions. It is inherently unstable but a few conditions can be matched to obtain stability. Much work has been done on inverted pendulum since last 50 years. In simple words, an inverted pendulum can be explained with the analogy of balancing a long stick on one finger, something that all of us have tried in childhood.

Inverted pendulum is a standard problem in Control system and is implemented in areas of precision control and robotics. The concept is applied for high precision robotic arms, launching of a rocket, control of a Vertical Take-Off and Land (VTOL) aircraft, etc. Due to the advent of humanoid robots, where this concept is applied for its balancing, recently a lot of work is being done to try and find new control methods.

Another very important place where this concept is used is the field of education. Here new students can get a very good idea of this classic problem.

The inverted pendulum has been implemented at various different levels or Degree of Freedom (DOF). The ones implementing 1st DOF are mounted on a fixed base either sliding along a straight direction (Linear Inverted Pendulum) or rotating around vertical axis (Rotary Inverted Pendulum). Other models with higher DOF (double or triple DOF) are mounted on a mobile platform or a Cart structure. Examples of which being JOE [1], Segway [2]. Segway is the commercial version of Two wheeled inverted pendulum used for personal transportation. Most papers consider a rigid pendulum, but for better precision now even the flexibility of the pendulum is being considered [3].

In recent years, people have tried to give more Degree of Freedom to this setup by making a Ball-bot [4]. Here the control and driving mechanism are placed on top of a ball, which behaves like an Omni-directional wheel for the setup. The driving mechanism consists of 3 or 4 Omni wheels that rotate the ball accordingly to keep the balance.

Most researches have mainly focused on the balance, while few have tried the driving control [5] and trajectory planning [6]. This means the controller has an additional burden of desired movement along with maintaining balance.

This paper attempts to overview the basic concepts involved in control of an inverted pendulum, along with the current work in the field. We shall focus on mobile inverted pendulum and not the fixed base ones.

II. STRUCTURE OF MOBILE INVERTED PENDULUM

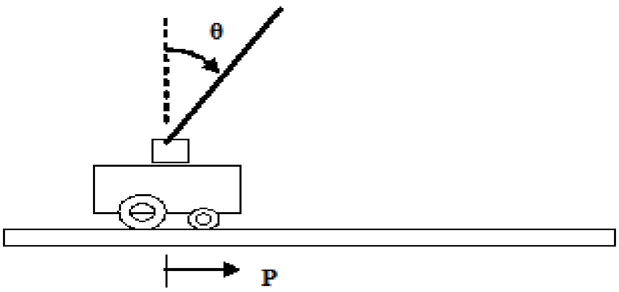

Fig. 1 Mobile Inverted Pendulum Setup

Fig. 1 shows a Four wheeled cart which has an inverted pendulum mounted on top of it. The cart is equipped with motors that provide horizontal motion. The cart position p, the tilt angle θ, the rate of tilting are measured and fed to the controller. The controller then generates and sends Pulse Width Modulated (PWM) signals to the motor drivers.

By applying the laws of dynamics on inverted pendulum system, the equations of motion obtained are [7]:

$$\ddot{p}\left(M - \frac{m_p l \cos^2(\theta)}{L}\right) = \frac{Km\,Kg}{Rr} V - \frac{Km^2\,Kg^2}{Rr^2}\dot{p} - \frac{m_p l g}{L}\cos(\theta)\sin\theta + m_p l \sin(\theta)(\dot{\theta})^2 \quad (1)$$

$$\ddot{\theta}\left(L - \frac{m_p l \cos^2(\theta)}{M}\right) - g\sin(\theta) - \frac{m_p l(\dot{\theta})^2}{L}\cos(\theta)\sin(\theta) - \frac{\cos(\theta)}{M}\left(\frac{Km\,Kg}{Rr} V - \frac{Km^2\,Kg^2}{Rr^2} p\right) \quad (2)$$

Where:-
m_c is the cart mass
m_p is the pendulum mass
I is the rotational inertia
l is the half-length of the pendulum
R is the motor armature resistance
r is the motor pinion radius
Km is the motor torque constant
Kg is the gearbox ratio

For simplicity :

$$M = m_c + m_p \qquad (3)$$

$$L = \frac{I + m_p l^2}{m_p l} \qquad (4)$$

Note that the relationship between force, F and voltage V for motor is:

$$F = \frac{Km\,Kg}{Rr} V - \frac{Km^2\,Kg^2}{Rr^2} \dot{p} \qquad (5)$$

A modification to this structure is a two wheeled inverted pendulum system, where the controller and rider (if any), form the pendulum bob. Examples of same given before: Joe [1], Segway [2].

III. CONTROL MECHANISM

Controller design is a key content of the Inverted Pendulum system. Controllers are used to stabilize the unstable system and make it robust to disturbances. Several techniques have been used for achieving the same, e.g. Sliding Mode Technique [8], Fuzzy Logic Controller [9], Partial Feedback Linearization [10], Fuzzy Servo Control Method [11], Real-Time Control [12]. We take a brief view of conventional PID type controller and rule based Fuzzy Logic controller for inverted pendulum-cart system [9]. The framework of this Inverted Pendulum-cart system Controller is presented in Fig.2.

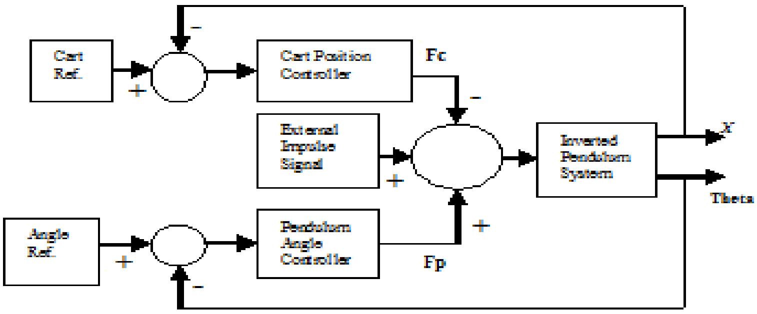

Fig. 2 Block diagram of Inverted Pendulum-cart controller system

3.1 Conventional PID Controller

An inverted pendulum-cart system, as mentioned before, is an unstable model. It can be stabilized by using the controllers. We see two PID controllers been designed, first one for Pendulum angle control and other or the Cart position control. These controllers try to correct the error between measured values and the desired values. This is done by calculating and then outputting a corrective action that can adjust the motion of the cart accordingly. For both PID controllers, the structure is taken as:

$$u = K_P\, e + K_I \int e\, dt + K_D \frac{de}{dt} \qquad (6)$$

Where:-
u is PID output control action,
e is the error i.e. difference between set point input and actual output
e = yref - yactual,
KP, KI, KD are the proportional, integral and derivative gains respectively.
We can see that the output of pendulum angle controller and the cart position controller are of opposite signs.
The selection of PID controller parameters (KP, KI, KD) is important as incorrect selection of these parameters can make controlled process input unstable. The control parameters are adjusted to optimum values for the desired response. This is called Tuning of the control loop.

3.2 Fuzzy Logic Controller (FLC)

FLC is one of the most successful applications of fuzzy set theory. It uses linguistic variables instead of numerical variables. Linguistic variables, defined as variables whose values are sentences in natural language (such as small and large) are represented by fuzzy sets. This makes the instruction set more Human.

A crisp set is one where an element can only belong to a set (full membership) or not belong to at all (no membership). A Fuzzy set is an extension of crisp set as it allows partial membership, which means that an element may partially belong to more than one set.

A fuzzy set A is characterized by a membership function µA that assigns membership to each object and it can range from 0 (no membership) to 1 (full membership), we therefore write:

$\mu A : X \rightarrow [0, 1]$

Which means that the fuzzy set A belongs to a universal set X (usually called universe of discourse) defined in a specific problem. A fuzzy set A is called a fuzzy singleton when there is only one element xo with µA(xo) = 1 , while all other elements have a membership grade which equal to zero.

This approach allows characterization of the system behaviour through simple relations (fuzzy rules) between linguistic variables. These fuzzy rules are expressed in the form of fuzzy conditional statements Ri of the type,

Ri : if x is small THEN y is large.

Where x and y are fuzzy variables, and small and large are labels of fuzzy set.

If there are i =1 to n rules, the rule set is represented by union of these rules,

R = R1 else R2 else…….Rn

A fuzzy logic controller is based on a collection of R control rules. The execution of these rules is governed by the compositional rule of inference [9].

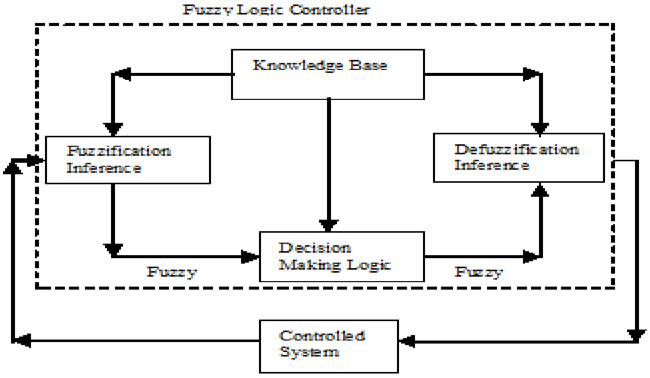

Fig. 3 Basic configuration of FLC

The general structure of an FLC is represented in Fig.3 and comprises four principle components:

1) A fuzzyfication inference converts input data into suitable linguistic values;
2) A knowledge base consists of a data base with the necessary linguistic definitions and control rule set;
3) A decision making logic infers the fuzzy control action from the knowledge of the control rules and the linguistic variable definitions;
4) A defuzzyfication inference yields a non-fuzzy control action from an inferred fuzzy controlled action.

3.3 Performance

Following figures shown are the graphical results of PID and Fuzzy Logic controller respectively. These figures have been taken from [9] for the sole purpose of comparing the two controllers. The results are from MATLAB Simulink simulations.

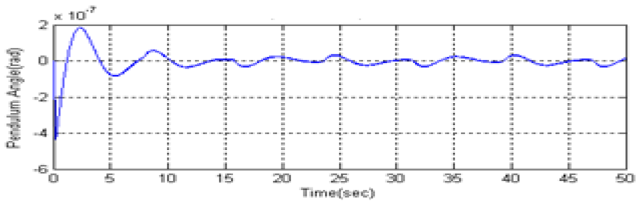

Fig. 4.a PID Response for disturbance 0.000001 unit

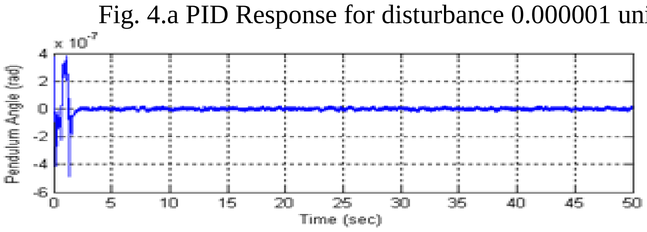

Fig. 4.b Fuzzy Response for disturbance 0.000001 unit

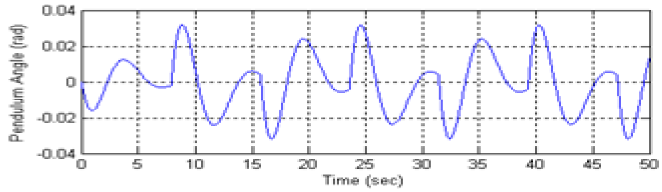

Fig. 5.a PID Response for disturbance 1 unit

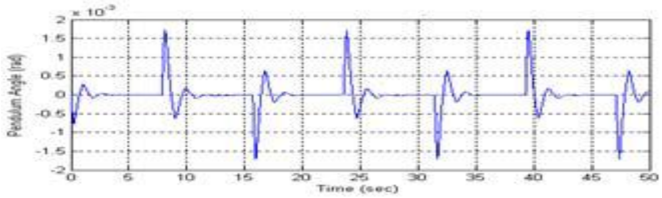

Fig. 5.b Fuzzy Response for disturbance 1 unit

The two controllers were tested for different magnitudes of disturbances for comparing their performances, two of which have been shown above. The performance comparison clearly shows that Fuzzy Controller offers a much better control as compared to the PID controller owing to its more human like approach. The PID controller does its job of maintaining the pendulum angle, but its response is sluggish as compared to the Fuzzy Controller.

IV. CONCLUSION

A brief overview of The Inverted Pendulum is taken in this paper. Two control strategies have been discussed and compared. It has been observed that the PID controller is a basic control technic with a sluggish response whereas the Fuzzy controller response is more crisp.

The paper reinstates that inverted pendulum system is a fundamental benchmark in education and research in control theory. Application of Mobile Inverted Pendulum in robotics and personal transportation has boosted the amount of work done in this field in recent times. This area of research has a lot of scope and a bright future.

REFERENCES

[1] Felix Grasser, Aldo D'Arrigo, Silvio Colombi and Alfred Rufer, "JOE: A Mobile, Inverted Pendulum", Laboratory of Industrial Electronics, Swiss Federal Institute of Technology Lausanne.
[2] Segway Human Transporter. [Online]. Available: http://www.segway.com
[3] Tang Jiali and Ren Gexue, Tsinghua Science and Technology, "Modeling and Simulation of a Flexible Inverted Pendulum System", ISSNl l 1 0 0 7 - 0 2 1 4 l1 l 0 5 / 2 1 1 lpp2 2 - 2 6, Volume 14, Number S2, December 2009.
[4] Ya-Fu Peng, Chih-Hui Chiu, Wen-Ru Tsai, and Ming-Hung Chou, "Design of an Omni-directional Spherical Robot: Using Fuzzy Control", Proceedings of the International MultiConference of Engineers and Computer Scientists 2009 Vol I, IMECS 2009, March 18 - 20, 2009, Hong Kong.
[5] Howon Lee and Jangmyung Lee, "Driving Control of Mobile Inverted Pendulum", The 9th International Conference on Ubiquitous Robots and Ambient Intelligence (URAI 2012), Nov. 26-28, 2012 in Daejeon Convention Center(DCC), Daejeon, Korea.
[6] Umashankar Nagarajan," Dynamic Constraint-based Optimal Shape Trajectory Planner for Shape-Accelerated Underactuated Balancing Systems", The Robotics Institute, Carnegie Mellon University.
[7] Johnny Lam, "Control of an Inverted Pendulum", Proceeding of University of California, Santa Barbara, June 2004.
[8] Ha Ngoc Nguyen, Tran Dinh Huy, Kang Ming Tao, Nguyen Thanh Phuong and Ho Dac Loc,," Control Of Mobile Inverted Pendulum Using Sliding Mode Technique", Ho Chi Minh City University of Technology (HUTECH), Vietnam, ISS_HUTECH – 15/04/2010.
[9] Mohan Akole, Barjeev Tyagi, "Design Of Fuzzy Logic Controller For Nonlinear Model Of Inverted Pendulum-Cart System", Electrical Engineering Department, Indian Institute of Technology (Roorkee), XXXII National Systems Conference, NSC 2008, December 17-19, 2008.
[10] Kaustubh Pathak, Jaume Franch and Sunil K. Agrawal, "Velocity and Position Control of a Wheeled Inverted Pendulum by Partial Feedback Linearization", IEEE Transactions On Robotics, VOL. 21, NO. 3, June 2005.
[11] Dazhong Wang, Shujing Wu, Liqiang Zhang and Shigenori Okubo, "Study of Inverted Pendulum Robot Using Fuzzy Servo Control Method", International Journal of Advanced Robotic Systems.
[12] S. W. Nawawi, M. N. Ahmad and J. H. S. Osman, "Real-Time Control of a Two-Wheeled Inverted Pendulum Mobile Robot", International Journal of Computer and Information Engineering 2:1 2008.

International Journal of Modern Engineering Research (IJMER)
www.ijmer.com Vol. 3, Issue. 5, Sep - Oct. 2013 pp-2928-2931 ISSN: 2249-6645

Adiabatic Logic Based Low Power Carry Select Adder for future Technologies

Mary Angel Asha Latha J(M.Tech) Prof. G.V.R.Sagar(M.Tech, P.hD)

Abstract: *Adders are of fundamental importance in a wide variety of digital systems. Many fast adders exist, but adding fast using low area and power is still challenging. This paper presents a new bit block structure that computes propagate signals called "carry strength" in a ripple fashion. Several new adders based on the new carry select Adder structure are proposed. Comparison with well-known conventional adders demonstrates that the usage of carry-strength signals allows high-speed adders to be realised at significantly lower cost and consuming lower power than previously possible. As well as in this paper we are concentrating on the heat dissipation &we are reducing the current using adiabatic logic.*

I. INTRODUCTION

The importance of a fast, low-cost binary adder in a digital system is difficult to overestimate. Not only are adders used in every arithmetic operation, they are also needed for computing the physical address in virtually every memory fetch operation in most modern CPUs. Adders are also used in many other digital systems including telecommunications systems in places where a full-fledged CPU would be superfluous. Many styles of adders exist. Ripple adders are the smallest but also the slowest. More recently, carry-skip adders [1, 2, 3] are gaining popularity due to their high speed and relatively small size. Normally, in an N-bit carry-skip adder divided into a proper number of M-bit blocks [1, 4], a long-range carry signal starts at a generic block B_i, rippling through some bits in that block, then skips some blocks, and ends in a block B_j. If the carry does not end at the LSB of B_j then rippling occurs in that block and an additional delay is needed to compute the valid sum bits. Carry-look-ahead and carry-select adders [1] are very fast but far larger and consume much more power than ripple or carry-skip adders. Two of the fastest known addition circuits are the Lynch-Swartzlander's [5] and Kantabutra's [6]. hybrid carry-look-ahead adders. They are based on the usage of a carry tree that produces carries intoappropriate bit positions without back propagation. In order to obtain the valid sum bits as soon as possible, in both Lynch-Swartzlander's and Kantabutra's adders the sum bits are computed by means of carry-select blocks, which are able to perform their operations in parallel with the carry-tree.

This paper presents two new families of adders, both based on a new bit carry Select & adiabatic structure that computes propagate signals called "carry-strength" in a ripple fashion. The first family of adders is a family of new carry-select adders that are significantly faster than traditional carry-select adders while not much larger. The second family of adders is a family of hybrid lookahead adders similar to those presented in [5, 6] but significantly smaller and still comparable in speed.

In our new type of carry-select adder, the new block structure eliminates the delay due to the rippling at the end of the life of a long-range carry signal. The main idea is, that for each bit position *k* in a block B_j we compute whether the carry-in to position *k* comes from the carry-in to block B_j, or whether this carry is internally generated in block B_j. To this purpose we will use a new type of bit block, in which we will compute propagate signals that start at the LSB of the block and end at every bit position. We find it helpful to call the complements of these "carry-strength" signals, because they indicate for each bit position whether the carry-in to that position originates within the same bit block.

In basic arithmetic computation, adder is still plays an important role though many people focus on more complex computation such as multiplier,divider,cordiccircuits. Although several algorithms and architectures are implemented in literature, there is not an general architecture for measuring performance equally. Much architectureis tested under different conditions which possibly result in variant performance even implemented with the same algorithm.

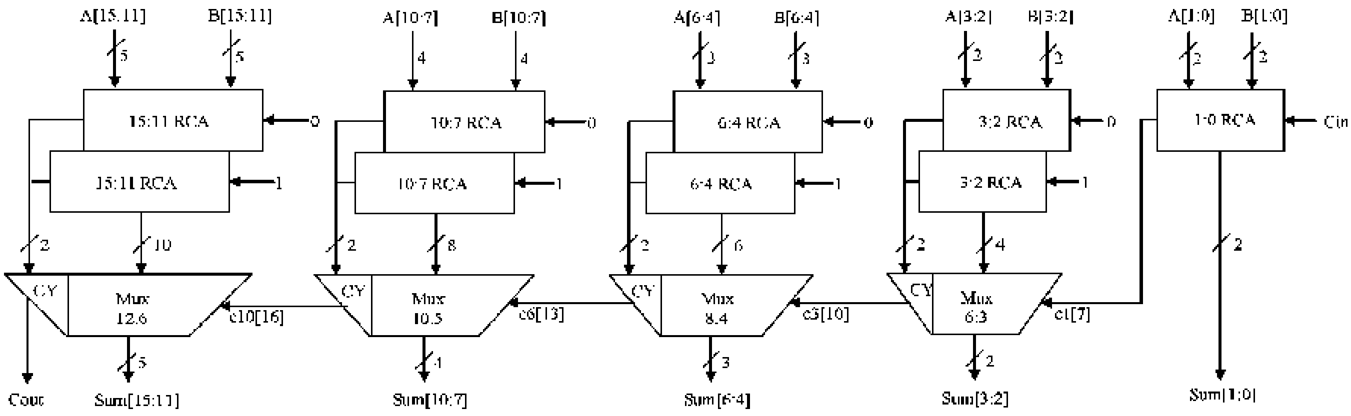

Fig1: Conventional Carry Select Adder using RCA

CLA is proved to have good performance using in high speed adder, so in many papers this architecture are used commonly. STCLA – Spanning Tree Using CLA uses a tree of 4-bit Manchester Carry-Lookaheadchains (MCC) to generate carry for different bit position. RCLCSA – Recursive CLA/CSA Adder uses the same conception as STCLA except the lengths of its carry chains are variant, not fixed. HSAC – High Speed Adder Using CLA uses Ling's adder which solves the transition of carry propagation delay.

Adder using different implementation is the most critical issue. For example, STCLA and RCLCSA use dynamic CMOS while HSAC uses static CMOS. Here, we want to implement a general architecture for measuring this three different algorithm which means we can use both dynamic CMOS and static CMOS to implement these algorithms for equal comparison. At last, I will offer my new architecture improved from the original paper.

Let me talk about the original implementation. It's based on the Adiabatic adder. But it takes advantage of the characteristics of CMOS circuit. Generally, we don't use "bar"(inverted) as we conduct every equation . But in reality, "bar" is automated added at the output of logic circuits. So, they use this special characteristic to reduce the carry propagation time

II. POSITIVE FEEDBACK ADIABATIC LOGIC

The structure of PFAL logic is shown. Two n-trees realize the logic functions. This logic family also generates both positive and negative outputs. The two major differences with respect to ECRL are that the latch is made by two pMOSFETs and two nMOSFETs, rather than by only two pMOSFETs as in ECRL, and that the functional blocks are in parallel with the transmission pMOSFETs. Thus the equivalent resistance is smaller when the capacitance needs to be charged. The ratio between the energy needed in a cycle and the dissipated one can be seen in figure 4. During the recovery phase, the loaded capacitance gives back energy to the power supply and the supplied energy decreases.

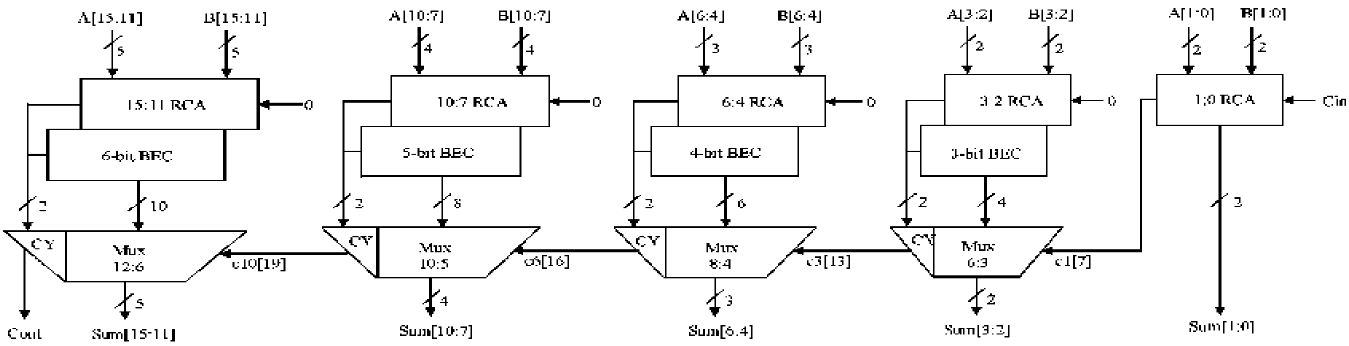

Fig1: Modified Carry select adder using BEC General schematic for PFAL family

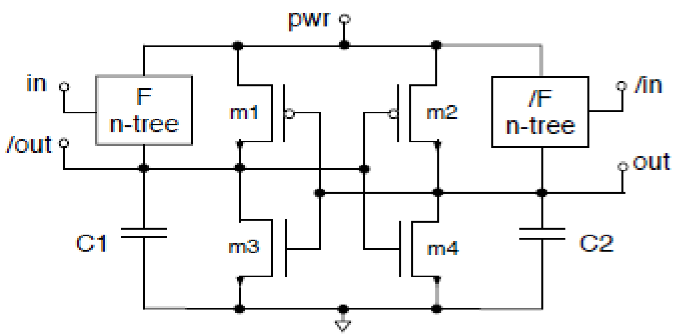

III. POWER DISSIPATION IN ADIABATIC LOGIC GATES

A limiting factor for the exponentially increasing integration of microelectronics is represented by the power dissipation. Though CMOS technology provides circuits with very low static power dissipation, during the switching operation currents are generated, due to the discharge of load capacitances, that cause a power dissipation increasing with the clock frequency. The adiabatic technique prevents such losses: the charge does not ow from the supply voltage to the load capacitance and then to ground, but it ows back to a trapezoidal or sinusoidal supply voltage and can be reused. Just losses due to the resistance of the switches needed for the logic operation still occur. In order to keep these losses small, the clock frequency has to be much lower than the technological limit.In the literature, a multitude of adiabatic logic families are proposed. Each different implementation shows some particular advantages, but there are also some basic drawbacks for these circuits.The goal of this paper is to compare di_erent adiabatic logic families and to investigate their robustness against technological parameter variations. For this purpose three adiabatic logic families are evaluated and the impact of parameter variations on the power dissipation is determined. Both intertie (and global) and intra-die (or local) parameter variations of different components in the same sub-circuit are considered. The most important factor is the threshold voltage variation, especially for sub-micrometer processes with reduced supply voltage. This was also found for low voltage CMOS circuits, cf., where the fundamental yield factor was the gate delay variation (in CMOS the power dissipation is not significantly dependent on the threshold voltage). For adiabatic circuits the timing conditions are not critical, because the clock frequency is particularly low, and therefore the outputs can always follow the clocked supply voltage. Here the yield critical requirement is the power dissipation that has a very low nominal value. Hence it exhibits large relative deviations due to parameter variations that can lead to the violation of the specifications.

The general PFAL gate consists of a two cross coupled inver-ters and two functional blocks F and /F (complement of F) dri-ven by normal and complemented inputs which realizes both normal and complemented outputs. Both the functional blocks implemented with n channel MOS transistors. The equations used to implement PFAL adder and the corres-ponding sum and carry implementations.

The logical organization of conventional and adiabatic adders is constructed by the replication of *2* and 4, 4bit blocks for %bit and 16-bit adder, respectively. Each 4bit block may be viewed as consisting of a carry unit, a sum generation unit, and a sum selection unit. (In practice, the three parts are of course not necessarily so distinctly separated.) The carries and both types of sum bits are produced using lookahead functions as much as possible. The detailed logic design of this adder can be found in [IO]. The adiabatic adder results after the substitution of the conventional CMOS adder's blocks with the corresponding adiabatic. Regarding the delay for an n-bit adiabatic carry select adder, which is constructed by mbit blocks (m<n), we obtain:

where*2t,* is the delay from the computation of the partial sum *P,* and *G*iand, *N(t+2tinv7* with *N=n/m*, the delay of carry propagation through the m-bit blocks. The design of this adder involved re-thinking of the circuit according to the principle of the adiabatic switching and no changes were held in the above equations. Also, to best of our knowledge a similar adiabatic conditional sum adder hasn't been introduced until now. Finally, following similar substitutions, for the conditional sum adder whose structure resembles that of carry select adder, we can result in another low power adiabatic adder.

The schematic and simulated waveform of the carry select adder. The energy stored at output can be retrieved by the reversing the current source direction during discharging process. Hence adiabatic switching technique offers the less energy dissipation in PMOS network and reuses the stored energy in the output load capacitance by reversing the current source direction.

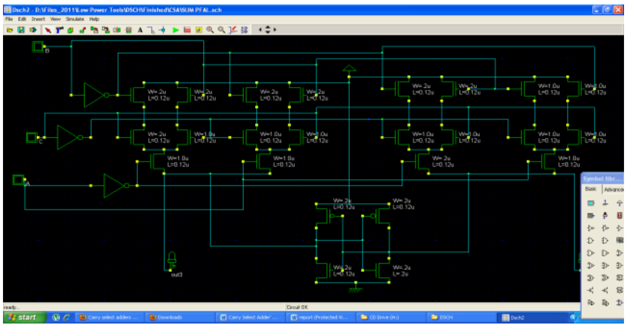

Fig 3: PFAL Sum Block

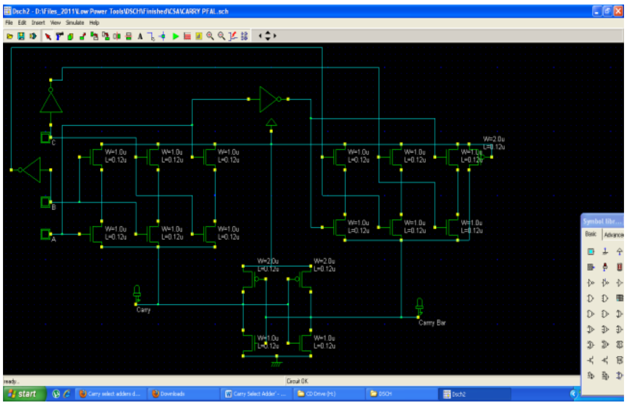

Fig4: PFAL Carry Block

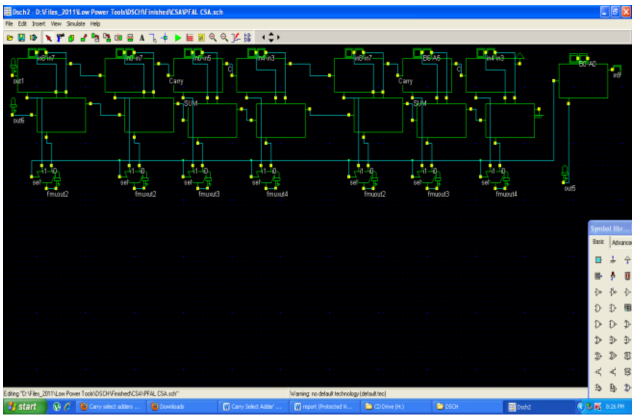

Fig5: Proposed Adiabatic CSA

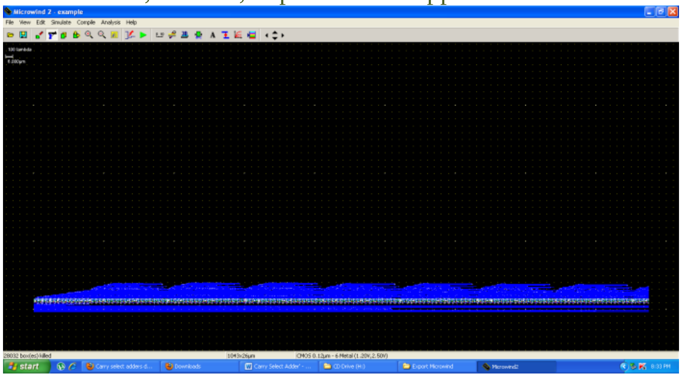

Fig6: Proposed PFAL CSA Layout with area

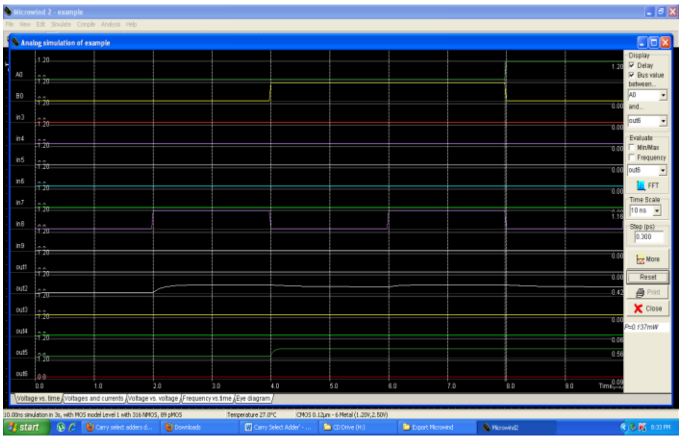

Fig7: Proposed Circuit Power Results

IV. CONCLUSION

The new implementation is based on the original architecture, so it can be used in both static CMOS and dynamic CMOS circuits. And through my architecture, I can reduce power and area consumption but sacrifice some timing (which can be neglected). By this implementation, I prove that the new architecture is really better than the traditional HSAC. After reading some papers, I realize that improving adder is very difficult now because of the transistor level. If we want to get higher performance we must reduce the complexity in transistor level.

REFERENCES

[1] KOREN, I.: “Computer arithmetic algorithms”, Prentice-Hall, 1993
[2] KANTABUTRA, V.: “Designing optimum one-level carry-skip adders”, *IEEE Trans. on Comp.*, 1993, Vol. 42, n°6, pp.759-764.
[3] CHAN, P.K., SCHLAG, M.D.F., THOMBORSON, C.D., OKLOBDZIJA, V.G.: “Delay optimization of carry-skip adders and block carry-look-ahead adders”, *Proc. of Int’l Symposium on Computer Arithmetic*, 1991, pp.154-164.
[4] NAGENDRA, C., IRWIN, M.J., OWENS, R.M.: “Area-time-power tradeoffs in parallel adders”, *IEEE Trans. CAS-II*, 43, (10), pp. 689-702.
[5] T. LYNCH, E.E. SWARTZLANDER, “A spanning-tree carry-look-ahead adder”, *IEEE Trans. on Comp.*, Vol. 41, n°8, Aug. 1992.
[6] V. KANTABUTRA, “A recursive carry-look-ahead/carry-select hybrid adder”, *IEEE Trans. on Comp.*, Vol. 42, n°12, Dec. 1993.
[7] R. Zimmermann and H. Kaeslin, “Cell-Based multilevel Carry-Increment Adders with Minimal AT- and PT-Products, unpublished manuscript. http://www.iis.ee.ethz.ch/~zimmi/
[8] Tyagi, “A reduced-area scheme for carry-select adders” *IEEE Trans. on Comp.*, Vol. 42, n°10, Oct. 1993.

International Journal of Modern Engineering Research (IJMER)
www.ijmer.com Vol. 3, Issue. 5, Sep - Oct. 2013 pp-2932-2938 ISSN: 2249-6645

Analysis and Modeling of Transformerless Photovoltaic Inverter Systems

J.Nagarjuna Reddy*, K Jyothi
*Assistant Professor, Dept. of EEE, RGMCET, Nandyal, India,
PG Student, Power Electronics/EEE, RGMCET, Nandyal, India,

ABSTRACT: *The need for a cleaner environment and the continuous increase in power demands makes decentralized renewable energy production, like solar and wind more and more interesting. Decentralized energy production using solar energy could be a solution for balancing the continuously-increasing power demands. This continuously increasing consumption overloads the distribution grids as well as the power stations. Therefore having negative impact on power availability, security and quality. The efficiency and reliability of single-phase PV inverter systems suffers from new problems related to leakage current and safety. This problem can be reduced by using transformerless inverter topologies. The work presented in this paper deals with analyzing and modeling of transformerless PV inverter systems regarding the leakage current phenomenon that can damage solar panels and pose safety problems.*

Index Terms: *DC–AC power conversion, photovoltaic(PV) systems, transformer less inverter.*

I. INTRODUCTION

Grid-connected photovoltaic (PV) systems, particularly low-power single-phase systems, are becoming more important worldwide. They are usually private systems where the owner tries to get the maximum system profitability. Issues such as reliability, high efficiency, small size and weight, and
low price are of great importance to the conversion stage of the PV system . Quite often, these grid-connected PV systems include a line transformer in the power-conversion stage, which guarantees galvanic isolation between the grid and the PV system, thus providing personal protection. Furthermore, it strongly reduces the leakage currents between the PV system and the ground, ensures that no continuous current is injected into the grid, and can be used to increase the inverter output voltage level. The line transformer makes possible the use of a full-bridge inverter with unipolar pulse width modulation (PWM). The inverter is simple. It requires only four insulated gate bipolar transistors (IGBTs) and has a good trade-off between efficiency, complexity and price. Due to its low frequency, the line transformer is large, heavy and expensive.

This paper proposes a new topology that generates no varying common-mode voltage, requires the same low-input voltage as the bipolar PWM full-bridge topology, and achieves a higher efficiency and a lower current ripple in the inductor. The topology consists of six switches and can be an advantageous power conversion stage for transformer less grid-connected PV systems.

II. COMMON-MODE CURRENTS INTRANSFORMERLESS PV SYSTEMS

When no transformer is used, a galvanic connection between the ground of the grid and the PV array exists. As a consequence a common-mode resonant circuit appears, consisting of the stray capacity between the PV modules and the ground, the dc and ac filter elements, and the grid impedance (Fig. 1). A varying common-mode voltage can excite this resonant circuit and generate a common-mode current. Due to the large surface of the PV generator, its stray capacity with respect to the ground reaches values that can be even higher than 200 nF/kWp in damp environments or on rainy days. These high values can generate ground currents with amplitudes well above the permissible levels, such as those concerning the standards. The currents can cause severe (conducted and radiated) electromagnetic interferences, distortion in the grid current and additional losses in the system. These leakage currents can be avoided, or at least limited, by including damping passive components in the resonant circuit. Obviously, additional losses will appear in the damping elements, thus decreasing the conversion stage efficiency.

The use of conversion topologies with a constant common mode voltage is another option. The instantaneous common mode voltage V_{cm} in the full-bridge inverter of Fig. 1can be calculated from the voltage of the two mid-points of both legs,

V_{AO} and V_{BO} as

$$V_{cm} = \frac{V_{AO} + V_{BO}}{2} \qquad (1)$$

To avoid leakage currents, the common-mode voltage must be kept constant during all commutation states, that is

$$V_{cm} = V_{AO} + V_{BO}$$

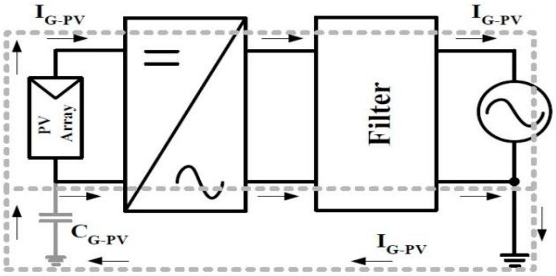

Fig.1 Common-mode currents in a transformer less conversion stage

III. MODELLING OF PV MODULE

The most commonly used model for PV-cell is one – diode equivalent circuit as shown in figure (2). Since the shunt resistance R_{sh} is large, it is normally neglected. This simplified circuit is used in this paper for modeling of a PV-cell.

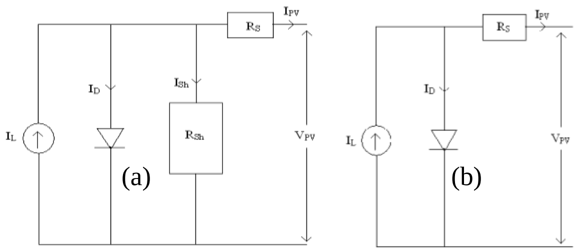

Fig.2. One-diode equivalent circuit model for a PV cell.
(a) Five parameters model;
(b) Simplified four parameters model

The non-linear of V_{pv}-I_{pv} and P-V curves are correspondingly drawn as shown below:
From figure (2.b) the relation between the output V_{pv} and the output current I_{pv} can be expressed as:

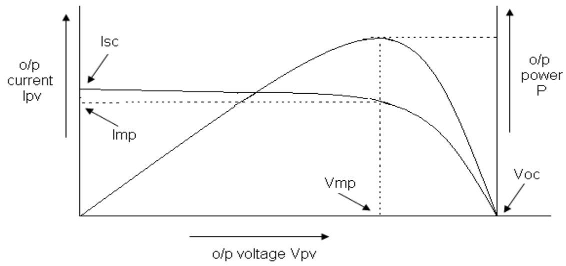

Fig.3. V_{pv}-I_{pv}& P-V_{pv} characteristics of a PV cell

From figure (2.b) the relation between the output V_{pv} and the output current I_{pv} can be expressed as:

$$I_{PV} = I_L - I_D$$

$$I_{PV} = I_L - I_0\left(\exp\left(\frac{V_{PV} + I_{PV}R_S}{\propto}\right) - 1\right) \qquad (2)$$

Where I_L= Light current; I_o= Saturation current; R_s= Series Resistance; α = Thermal voltage timing completion factor.

The above four parameters are need to be determined to obtain the I-V characteristics of PV-module. Thus, this model can be termed as Four-parameter model. The equations for determining the four parameters are given below:

A. *Light Current (I_L)*

$$I_L = \frac{G}{G_{ref}}\left(I_{Lref} + \mu_{Isc}(T_C - T_{Cref})\right) \qquad (3)$$

Where G= irradiance (W/m^2);
Gref = Reference iradiance (1000W/m^2 issued in this study);
I_{Lref} = light current at the reference condition (1000W/m^2 and 25˚C); Tc = PV cell temperature (˚C);
T_{cref} = Reference temperature (25˚C issued in this study);
μ_{Isc} = temperature coefficient of the short-circuit current (A/˚C).

From the above equation for light current it can be observed that I_L is a function of both temperature and irradiance. Both I_{Lref} and μ_{Isc} can be obtained from manufacturer data sheet.

B. Saturation Current (I_O)

$$I_0 = I_{0ref}\left(\frac{T_C+273}{T_{Cref}+273}\right)^3 \exp\left(\frac{e_{gap}\,q}{N_S \propto_{ref}}\left(1-\frac{T_{Cref}+273}{T_C+273}\right)\right) \quad (4)$$

Where I_{oref} = saturation current at the reference condition (A);
e_{gap} = band gap of the material1. 17eV for Simaterials);
N_S = number of cell sin series of a PV module;
q = charge of an electron (1.60217733×10^{-19} C);
α_{ref} = the value of α at reference condition.
I_{oref} can be calculated as:

$$I_{0ref} = I_{Lref}\exp\left(-\frac{V_{OCref}}{\propto_{ref}}\right) \quad (5)$$

Where V_{ocref} = the open circuit voltage of the PV module at reference condition (V).

C. Calculation of α

$$\propto = \frac{T_C+273}{T_{Cref}+273}\propto_{ref} \quad (6)$$

The value of α_{ref} can be calculated as:

$$\propto_{ref} \frac{2V_{mpref}-V_{ocref}}{\frac{I_{scref}}{I_{scref}-I_{mpref}}+ln\left(1-\frac{I_{mpref}}{I_{scref}}\right)} \quad (7)$$

Where
V_{mpref}= maximum power point voltage at the reference condition (V);
I_{mpref} = maximum power point current at the reference condition (A);
I_{scref} = short circuit current at the reference condition (A).

D. Series Resistance (R_S)

Some manufacturers provide the value of R_S.If not provided, the following equation can be used to estimate its value:

$$R_S = \frac{\propto_{ref}\ ln\left(1-\frac{I_{mpref}}{I_{scref}}\right)+V_{ocref}-V_{mpref}}{I_{mpref}} \quad (8)$$

R_S is taken as a constant in the model of this study.

E. *Thermal Model of PV*

From equations (1) to (7), it can be noted that the temperature plays an important role in the PV performance. Therefore, it is necessary to have a thermal model for a PV cell / module. In this study, a lumped thermal model is developed for the PV module. The temperature of the PV module varies with surrounding temperature, irradiance, and its output current and voltage, and can be written as:

$$C_{pv}\frac{dT_C}{dt} = K_{inpv}\,G - \frac{V_{pv}I_{pv}}{A} - K_{loss}(T_C - T_a) \quad (9)$$

C_{PV} = the overall heat capacity per unit area of the PV cell / module [J/ (˚C-m^2)];
K_{inpv} = Transmittance – absorption product of PV cells;
K_{loss} = overall heat loss coefficient [W/ (˚C-m^2)];
T_a = ambient temperature (˚C);
A = effective area of the PV cell / module (m^2).

IV. REVIEW OFTRANSFORMERLESS INVERTER TOPOLOGIES

Ideal transformerless inverter generates constant common mode voltage. However, if the voltage varies with time, then a leakage current is produced. For the sake of minimizing this leakage current, different topologies were studied. Among these are the full bridge with bipolar PWM, the half bridge, HERIC, H5, H6 and NPC all of which experience certain drawbacks which are discussed next.

2.1. Full Bridge Inverter

The full-bridge inverter with bipolar PWM causes high switching losses and large current ripples and does not eliminate the DC current injected into the grid that has the tendency of saturating the transformer cores. Even though, this topology is being used in some commercial transformerless inverters, it still presents quite low efficiency according to the European standards due to the losses caused by the double switching frequency.

2.2. Half Bridge Inverter

The half bridge inverter, on the other hand, requires a high input voltage and a boost converter in the DC side that would increase the inverter size and cost and reduce its efficiency down to 92% [6,8]. For this reason the half bridge is not recommended.

2.3. HERIC Inverter

Meanwhile the HERIC topology, shown in Fig. 1, combines the advantages of the unipolar and bipolar modulations. It has a three level output voltage, a high efficiency and a low leakage current. However, the HERIC topology presents low frequency harmonics and does not allow for reactive power flow. This is due to the control strategy.

2.4. H5 Inverter

This topology is based on the full bridge with an extra switch on the DC side. In this topology, the upper switches operate at grid frequency while the lower switches operate at high frequency. The extra switch operates at high frequency and guarantees the disconnection of the DC source from the grid. This topology has two main disadvantages. The first one is the high conduction losses due to the fact that three switches operate simultaneously. The second one is that the reactive power flow is not possible due to the control strategy.

2.5. NPC Inverter

The NPC inverter topology is being considered as an attractive solution in case of transformerless systems. This inverter has the advantages of no internal reactive power flow, a three level inverter output voltage and a low leakage current. However, it requires an input voltage as high as twice the input voltage required by other topologies and a boost stage which increases inverter losses and size.

V. FULL-BRIDGE INVERTER

The full-bridge inverter (Fig. 3) is a single stage dc–ac conversion topology that is used quite often in PV inverters. Different PWM techniques can be applied to this topology. Depending on the shape of the output voltage waveform, they can be classified in two groups, namely unipolar and bipolar PWM. When the full bridge is part of a conversion stage with a line transformer, unipolar PWM techniques can be applied. This is in proposed topology. Here, $S_4$is on duringthe positive half cycle, while switches S_1andS_2commutateat the switching frequency. During the negative cycle, $S_2$is on andS_3, S_4 commutate at the switching frequency. In this converter

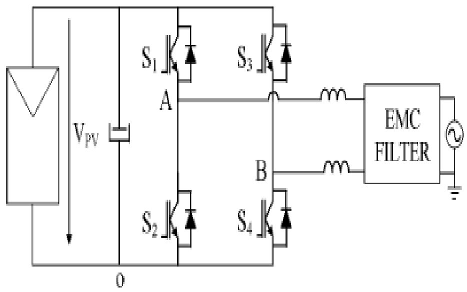

Fig 4. Full-bridge inverter

Only two switches are on at the same time, and only one IGBT and one diode commutate at the switching frequency with the whole input voltage. The main drawback, that it generates a varying common-mode voltage of amplitude $V_{pv}/2$ at the switching frequency.

In the bipolar PWM, the diagonal pairs of switches S_1- S_4 and $S_2 - S_3$are switched alternatively at the switching frequency. As a consequence

$$V_{BO} = V_{PV} - V_{Ao} \Rightarrow V_{cm} = V_{PV}/2 \quad = \text{cte}$$

If the switching actions are carried out at the same time, no changes appear in the common-mode voltage and no leakage currents are generated. However, the bipolar PWM also has draw backs. Two IGBTs and two diodes are switching at the switching frequency with the whole input voltage, therefore doubling the switching losses. Additionally, the output voltage changes between $V_{PV}$and - V_{PV}, creating a current rippletwice that obtained in the unipolar modulation.

VI. SIMULATION RESULTS

Based on the mathematical equations discussed before, a dynamic model for a PV module consisting of 153 cells in series has been developed using MATLAB/Simulink. The input quantities (solar irradiance G and the ambient temperature Ta) together with manufacturer data are used to calculate the four parameters. Then, based on equation (1), the output voltage is obtained numerically. The thermal model is used to estimate the PV cell temperature. The two output quantities

(PV output voltage V_{pv} and the PV cell temperature T_c), and the load current I_{pv}, are fed back to participate in the calculations. The model parameters used in the simulation are given in Table I

Table 1. THE PV MODEL PARAMETERS

$I_{SCref}(I_{Lref})$	2.664A
α_{ref}	5.472
R_S	1.324Ω
V_{OCref}	87.72V
V_{MPref}	70.731V
I_{MPref}	2.448A
G_{ref}	1000w/m^2
T_{cref}	25°c
C_{pv}	$5*10^4$J/(^{0}c-m^2)
A	1.5m^2
K_{inpv}	0.9
K_{loss}	30W/(^{0}c-m^2)

A. Model Performance

The model I_{pv}-V_{pv} characteristic curves under different irradiances are given in Figure (6) at 25˚C. It is noted from the figure that the higher is the irradiance, the larger are the short-circuit current (I_{SC}) and the open- circuit voltage (V_{oc}). And, obviously, the larger will be the maximum power (P), shown in Figure (7).

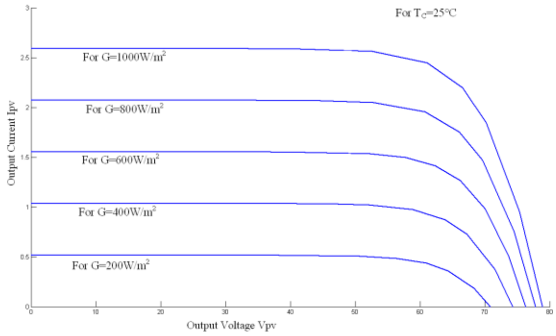

Fig6. V_{pv}-I_{pv} characteristics for constant T_c and Varying G

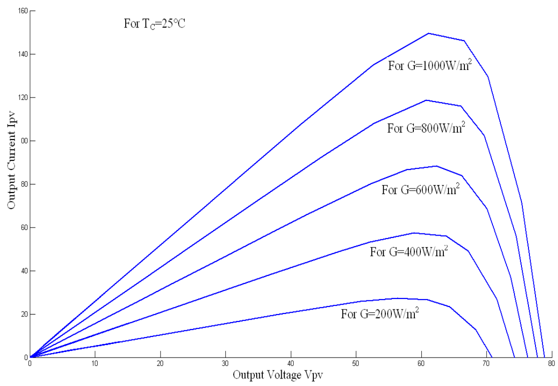

Fig.7. P-V_{pv} characteristics for constant Tc and Varying G

The simulation results of full bridge inverter with unipolar PWM and bipolar PWM te are shown in fig 8 and fig 9

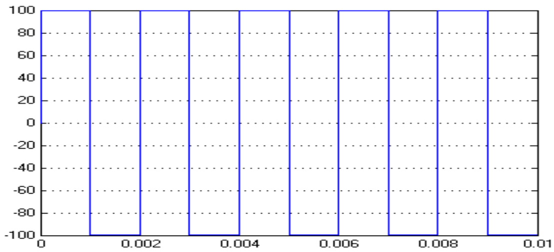

Fig 8. Output voltage in a full bridge inverter topology with bipolar PWM.

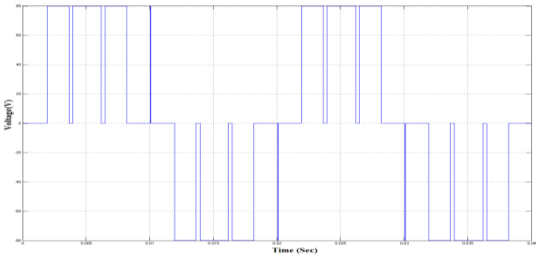

Fig 9. Output voltage in a full bridge inverter topology with unipolar PWM.

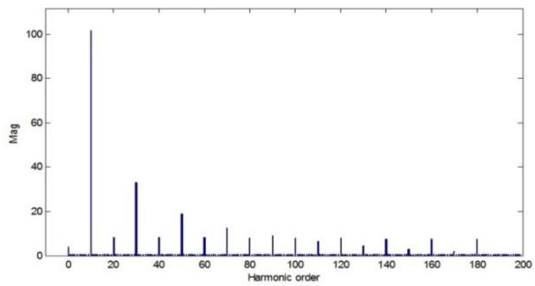

Fig 10. FFT analysis of bipolar PWM switching

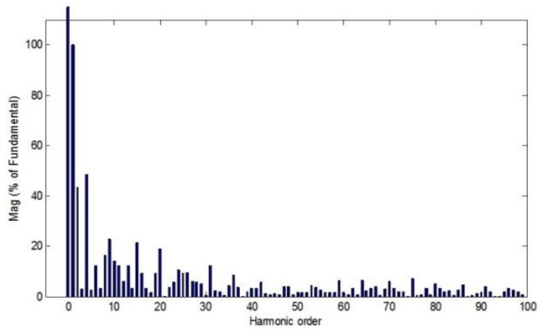

Fig 11. FFT analysis of unipolar PWM switching

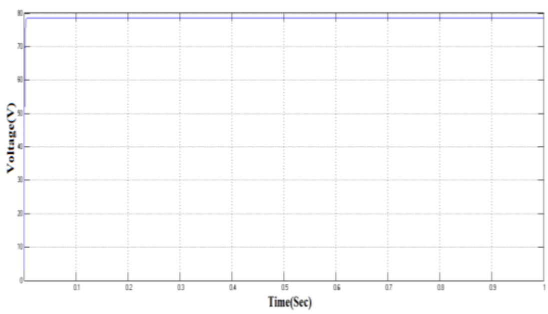

Fig 12. Output Of Pv Cell

Table 3. Lekage Currents Of Unipolar And Bipolar Switching

S.No	**Leakage Current**
PV cell With Unipolar PWM Switching	10mA
PV cell With bipolar PWM Switching	5mA

VII. CONCLUSION

This paper proposes a new transformerless, single-phase PV inverter with six switches and two diodes. The proposed topology generates no common-mode voltage, exhibits a high efficiency, and can operate with any power factor. It has been compared to other topologies and validated satisfactory results. The maximum efficiency achieved by the topology is 97.4%, As a conclusion, the proposed topology can be an advantageous power-conversion stage for transformer less, grid-connected PV systems.

REFERENCES

[1] M. Calais and V. G. Agelidis, "Multilevel converters for single-phase grid connected photovoltaic systems— An overview," in *Proc. IEEEInt.Symp. Ind. Electron.*, 1998, vol. 1, pp. 224–229.
[2] M. Calais, J. M. A. Myrzik, and V. G. Agelidis, "Inverters for single phase grid connected photovoltaic systems—Overview and prospects,"in*Proc. 17th Eur.Photovoltaic Solar Energy Conf.*, Munich, Germany, Oct. 22–26, 2001, pp. 437–440.
[3] B. Epp, "Big crowds," *Sun & Wind Energy: Photovoltaics*, pp. 69–77,Feb. 2005.
[4] J. M. A. Myrzik and M. Calais, "String and module integrated inverter for single-phase grid connected photovoltaic systems—A review," in *Proc. IEEE Power Tech. Conf.*, Bologna, Italy, Jun. 23–26, 2003, vol.2, pp. 1–8.
[5] W. N. Mohan, T. Undeland, and W. P. Robbins, *Power Electronics: Converters, Applications, and Design*. New York: Wiley, 2003.
[6] *VVerband der Elektrotechnik, Elektronik und Informations technik(VDE)*, Std. V 0126-1-1, Deutsches Institute fürNormung, Feb. 2006.
[7] *IEEE Standard for Interconnecting Distributed Resources with ElectricPower Systems*, IEEE Std. 1547, 2003.
[8] S. B. Kjaer, J. K. Pedersen, and F. Blaabjerg, "A review of single-phase grid-connected inverters for photovoltaic modules," *IEEE Trans. Ind.Appl.*, vol. 41, no. 5, pp. 1292–1306, Sep./Oct. 2005.
[9] M. F. Arman and L. Zhong, "A new, transformerless, photovoltaic array to utility grid interconnection," in *Proc. Int. Conf. Power Electron Drive Syst.*, May 26–29, 1997, vol. 1, pp. 139–143.
[10] Y. Nishida, S. Nakamura, N. Aikawa, S. Sumiyoshi, H. Yamashita, and H. Omori, "A novel type of utility-interactive inverter for photovoltaic system," in *Proc. 29th Annu. IEEE Ind. Electron. Soc. Conf.*, Nov. 2–6, 2003, vol. 3, pp. 2338–2343.
[11] Y. Chen and K. M. Smedley, "A cost-effective single-stage inverter with maximum power point tracking," *IEEE Trans. Power Electron.*,vol. 19, no. 5, pp. 1289– 1294, Sep. 2004.

J.Nagarjuna Reddy was born in 1985 in India. He received the B.Tech from Dr.Paul Raj Engg. College in 2005 and Post graduated from Jawaharlal Nehru Technological University (JNTU), Hyderabad, In 2006-2008. He is currently working as a assistant professor in the department of electrical and electronics engineering in RGM college of engineering and technology, Nandyal, Andhra Pradesh, India. He has Two years of teaching experience. His main areas of research include Electrical Drives & Renewable energy source.

K Jyothi was born in Kurnool India. He received the B.Tech (Electrical and Electronics Engineering) degree from the Jawaharla Nehru Technological University, Hyderabad in 2011 and persuing the M.Tech (Power Electronics) from Jawaharlal Nehru Technological University, Anantapur. His area of interest in the field of power electronic converters and Electric Drives. (E-mail: jyothi.kancham@gmail.com).

Influence of Skidded Distance on the Initial Velocity of Vehicle in Chain Accidents at Intersections

Robert M. Brooks[1], Mehmet Cetin[2]

[1]*Coresponding Author, Associate Professor, Department of Civil and Environmental Engineering, College of Engineering/ Temple University, USA*

[2]*Ph.D, Department of Civil and Environmental Engineering, College of Engineering / Temple University, USA*

ABSTRACT : *The objective of this study is to determine the influence of skidded distance on the initial velocity of the first vehicle in a chain accident at intersections involving three vehicles. Regression analysis on the results of these variables was conducted. Excellent correlation coefficient was found for the relationship at $\alpha = 0.05$ significance level. The influence of Skidded Distance on the Initial Velocity is shown by a quadratic equation (Initial velocity = -0.0003 Skidded distance ^{2} +0.185 Skidded Distance + 51.83) with R = 1.*

Keywords: *Accident Reconstruction, Chain Accident, Initial Velocity, Skidded Distance, Regression Analysis.*

I. INTRODUCTION

Accident reconstructing engineering is the planning, surveying, measuring, investigating, analyzing, and report making process on the intricate engineering details of how accidents occurred. The analysis and conclusions are based on the extensive application of fundamental principles of physics and engineering including Newton's Laws of Motion [1] and First Law of Thermodynamics [2]. The first law of thermodynamics when applied to accidents states that the total energy before and after the accident will be the same. The input variables include roadway, vehicle, driver and environmental conditions. Accident reconstruction engineering studies can be utilized by the industry, city and state governments for modifying the structural facilities such as roads. The modifications may include obtaining improved friction factors, increased number of lanes and lane widths and better site distances. Vehicle manufacturers use the results of the studies for developing better designs of vehicles. Some of the recent vehicles may use event data recorder containing information on the speed of the vehicle before and at the time of the accident. Some manufacturers, such as GM and Ford, allow downloading the information from these boxes after an accident [3]. The results of the accident reconstruction studies are also used for producing better navigations aids to assist the drivers.

In this study the guidelines of Accreditation Commission for Traffic Accident Reconstruction (ACTAR) [4] are used. There are many research studies on the application of accident reconstruction engineering principles. One of the most important one is that of Hurt's [5]. Hurt found that motorcyclists needed to develop their capabilities on controlling skids and proper use of helmets significantly reduced head injuries. Hurt further found that out of all the turning movements, the left turners were the most involved ones in the accidents while turning in front of the oncoming motorcycles.

II. SCOPE OF THE STUDY

The study is limited to the accidents caused by negligent drivers of cars hitting the parked cars [6,7,8]. All the accidents caused elastic deformations only [9]. There are no significant plastic deformations [10].

III. METHODOLOGY

C3 was a parked car by the side of the road. The speed limit of the road is 15 mph. C2 was parked behind C3. C1 was driven by a negligent driver. The friction coefficients of the shoulder and pavement were measured. C1 saw C2 too late and hit the brakes. C1 skidded and hit C2. C2 skidded and hit C3. C3 skidded on to the shoulder and stopped. In most of the cases C3 was damaged and its driver was injured. As the plaintiff, C3's driver sued the negligent driver of C1. In most of the cases C1 driver underestimated his or her speed at the time of the accident.

3.1. Parked vehicle Car 3

The following steps were followed.

1. Deceleration = Friction factor * acceleration due to gravity
2. Final velocity of C3 = 0
3. Initial velocity of C3 is shown in the following equation.

$$u \quad \sqrt{2 \cdot a \cdot s} \qquad (1)$$

Where, u= initial velocity of the vehicle, ft/sec
a= deceleration of the vehicle, ft/sec^2
s= skidded distance, feet

4. The total product of mass and velocity of Car2 is equal to that of Car 3 as shown in the following equation.

$$M_2 u_2 = m_3 u_3 \qquad (2)$$

Where, m_2= mass of vehicle C2 and u_2 is the velocity of C2. M_3= mass of C3 and u_3 = velocity of C3.

3.2. Car 2

Deceleration was calculated by using Equation1.
Final velocity was calculated by the following equation.

$$u \quad \sqrt{v^2 \quad 2 \cdot a \cdot s} \tag{3}$$

Where, u= initial velocity of the vehicle, ft/sec
v=final velocity, ft/sec
a= deceleration of the vehicle, ft/sec^2
s= skidded distance, feet

3.3 Car 1

Deceleration was calculated by using Equation1.
Final velocity was calculated by Equation 3.

IV. RESULTS AND DISCUSSION

The following assumptions were made in this study

1. The energy lost in sound produced by the accident is negligible.
2. The energy lost in causing the slight angular movement of the vehicle is negligible.

Professional engineering principles allow the application of the above two assumptions in the appropriate engineering calculations.

Table I shows the Engineering Calculations for Mixed Variables for Case 1 through Case 5 for Determininig the Initial Velocity while Table II gives the Engineering Calculations for Mixed Variables for Case 6 thorugh 7 for Determininig the Initial Velocity.
Engineering Calculations for Case 1 through Case 5; Case 6 through Case 10; and Case 11 through Case 15 for Determininig the influence of Skidded Distance on the Initial Velocity are given in Tables III, IV, and V respectively.
The following regression relationship was found with statistically significant correlation coefficient for predicting the performance of the engineering variables. The relationship was significant at $\alpha = 0.05$ significance level [11,12,13,14].

Fig. 1 shows the influence of Skidded Distance on the Initial Velocity. This relationship is described by a quadratic equation (Initial velocity = -0.0003 Skidded distance ^{2} +0.185 Skidded Distance + 51.83) with R = 1.

Table I. Engineering Calculations for Mixed Variables for Case 1 through Case 5 for Determininig the Initial Velocity.

	Case 1	**Case 2**	**Case 3**	**Case 4**	**Case 5**
Car3					
Final Velocity, ft/sec	**0**	**0**	**0**	**0**	**0**
Subgrade Friction	**0.38**	**0.38**	**0.38**	**0.38**	**0.38**
Skidded Distance, ft	**48**	**29**	**33**	**39**	**46**
Deceleration, ft/sec^2	**12.24**	**12.24**	**12.24**	**12.24**	**12.24**
Initial Velocity, ft/sec	**34.27**	**26.64**	**28.42**	**30.89**	**33.55**
Weight, pounds	**1800**	**2100**	**2400**	**2600**	**2500**
Car2					
Weight, Pounds	**3300**	**3100**	**3600**	**3900**	**4200**
Weight Ratio, C2/C1	**0.55**	**0.68**	**0.67**	**0.67**	**0.60**
Final Velocity, ft/sec	**18.69**	**18.05**	**18.95**	**20.60**	**19.97**
Skidded Distance, ft	**8.00**	**12.00**	**14.00**	**13.00**	**11.00**
Pavement Friction	**0.12**	**0.10**	**0.15**	**0.20**	**0.25**
Deceleration, ft/sec^2	**3.86**	**3.22**	**4.83**	**6.44**	**8.05**
Initial Velocity, ft/sec	**20.28**	**20.07**	**22.23**	**24.32**	**24.00**
Car1					
Weight, pounds	**3400**	**3700**	**4000**	**4150**	**4450**
Weight Ratio, C2/C1	**0.97**	**0.84**	**0.90**	**0.94**	**0.94**
Final Velocity, ft/sec	**19.68**	**16.82**	**20.01**	**22.86**	**22.65**
Skidded Distance, ft	**5.00**	**7.00**	**9.00**	**11.00**	**10.00**
Pavement Friction	**0.3**	**0.15**	**0.12**	**0.21**	**0.18**
Deceleration, ft/sec^2	**9.66**	**4.83**	**3.86**	**6.76**	**5.80**
Initial Velocity, ft/sec	**22.00**	**18.72**	**21.68**	**25.91**	**25.08**

Table II. Engineering Calculations for Mixed Variables for Case 6 through Case 7 for Determininig the Initial Velocity.

	Case 6	Case 7
Car3		
Final Velocity, ft/sec	**0**	**0**
Subgrade Friction	**0.38**	**0.38**
Skidded Distance, ft	**44**	**48**
Deceleration, ft/sec^2	**12.24**	**12.24**
Initial Velocity, ft/sec	**32.81**	**34.27**
Weight, pounds	**2700**	**4500**
Car2		
Weight, Pounds	**4350**	**3750**
Weight Ratio, C2/C1	**0.62**	**1.20**
Final Velocity, ft/sec	**20.37**	**41.13**
Skidded Distance, ft	**15.00**	**20.00**
Pavement Friction	**0.30**	**0.35**
Deceleration, ft/sec^2	**9.66**	**11.27**
Initial Velocity, ft/sec	**26.54**	**46.29**
Car1		
Weight, pounds	**2450**	**2750**
Weight Ratio, C2/C1	**1.78**	**1.36**
Final Velocity, ft/sec	**47.13**	**63.12**
Skidded Distance, ft	**13.00**	**19.00**
Pavement Friction	**0.1**	**0.23**
Deceleration, ft/sec^2	**3.22**	**7.41**
Initial Velocity, ft/sec	**48.01**	**65.31**

Table III. Engineering Calculations for Case 1 through Case 5 for Determininig the Relationship between Skided Distance and Initial Velocity.

	Case 1	Case 2	Case 3	Case 4	Case 5
Car3					
Final Velocity, ft/sec	**0**	**0**	**0**	**0**	**0**
Subgrade Friction	**0.38**	**0.38**	**0.38**	**0.38**	**0.38**
Skidded Distance, ft	**55**	**55**	**55**	**55**	**55**
Deceleration, ft/sec^2	**12.24**	**12.24**	**12.24**	**12.24**	**12.24**
Initial Velocity, ft/sec	**36.69**	**36.69**	**36.69**	**36.69**	**36.69**
Weight, pounds	**1800**	**1800**	**1800**	**1800**	**1800**
Car2					
Weight, Pounds	**3300**	**3300**	**3300**	**3300**	**3300**
Weight Ratio, C2/C1	**0.55**	**0.55**	**0.55**	**0.55**	**0.55**
Final Velocity, ft/sec	**20.01**	**20.01**	**20.01**	**20.01**	**20.01**
Skidded Distance, ft	**8.00**	**8.00**	**8.00**	**8.00**	**8.00**
Pavement Friction	**0.30**	**0.30**	**0.30**	**0.30**	**0.30**
Deceleration, ft/sec^2	**9.66**	**9.66**	**9.66**	**9.66**	**9.66**
Initial Velocity, ft/sec	**23.56**	**23.56**	**23.56**	**23.56**	**23.56**
Car1					
Weight, pounds	**1500**	**1500**	**1500**	**1500**	**1500**
Weight Ratio, C2/C1	**2.20**	**2.20**	**2.20**	**2.20**	**2.20**
Final Velocity, ft/sec	**51.83**	**51.83**	**51.83**	**51.83**	**51.83**
Skidded Distance, ft	**2.00**	**4.00**	**6.00**	**10.00**	**13.00**
Pavement Friction	**0.30**	**0.30**	**0.30**	**0.30**	**0.30**
Deceleration, ft/sec^2	**9.66**	**9.66**	**9.66**	**9.66**	**9.66**
Initial Velocity, ft/sec	**52.20**	**52.57**	**52.94**	**53.66**	**54.20**

Table IV. Engineering Calculations for Case 6 through Case 10 for Determininig the Relationship between Skidded Distance and Initial Velocity.

	Case 6	Case 7	Case 8	Case 9	Case 10
Car3					
Final Velocity, ft/sec	0	0	0	0	0
Subgrade Friction	0.38	0.38	0.38	0.38	0.38
Skidded Distance, ft	55	55	55	55	55
Deceleration, ft/sec^2	12.24	12.24	12.24	12.24	12.24
Initial Velocity, ft/sec	36.69	36.69	36.69	36.69	36.69
Weight, pounds	1800	1800	1800	1800	1800
Car2					
Weight, Pounds	3300	3300	3300	3300	3300
Weight Ratio, C2/C1	0.55	0.55	0.55	0.55	0.55
Final Velocity, ft/sec	20.01	20.01	20.01	20.01	20.01
Skidded Distance, ft	8.00	8.00	8.00	8.00	8.00
Pavement Friction	0.30	0.30	0.30	0.30	0.30
Deceleration, ft/sec^2	9.66	9.66	9.66	9.66	9.66
Initial Velocity, ft/sec	23.56	23.56	23.56	23.56	23.56
Car1					
Weight, pounds	1500	1500	1500	1500	1500
Weight Ratio, C2/C1	2.20	2.20	2.20	2.20	2.20
Final Velocity, ft/sec	51.83	51.83	51.83	51.83	51.83
Skidded Distance, ft	16.00	18.00	20.00	22.00	24.00
Pavement Friction	0.30	0.30	0.30	0.30	0.30
Deceleration, ft/sec^2	9.66	9.66	9.66	9.66	9.66
Initial Velocity, ft/sec	54.73	55.08	55.43	55.78	56.12

Table V. Engineering Calculations for Case 11 through Case 15 for Determininig the Relationship between Skidded Distance and Initial Velocity.

	Case 11	Case 12	Case 13	Case 14	Case 15
Car3					
Final Velocity, ft/sec	0	0	0	0	0
Subgrade Friction	0.38	0.38	0.38	0.38	0.38
Skidded Distance, ft	55	55	55	55	55
Deceleration, ft/sec^2	12.24	12.24	12.24	12.24	12.24
Initial Velocity, ft/sec	36.69	36.69	36.69	36.69	36.69
Weight, pounds	1800	1800	1800	1800	1800
Car2					
Weight, Pounds	3300	3300	3300	3300	3300
Weight Ratio, C2/C1	0.55	0.55	0.55	0.55	0.55
Final Velocity, ft/sec	20.01	20.01	20.01	20.01	20.01
Skidded Distance, ft	8.00	8.00	8.00	8.00	8.00
Pavement Friction	0.30	0.30	0.30	0.30	0.30
Deceleration, ft/sec^2	9.66	9.66	9.66	9.66	9.66
Initial Velocity, ft/sec	23.56	23.56	23.56	23.56	23.56
Car1					
Weight, pounds	1500	1500	1500	1500	1500
Weight Ratio, C2/C1	2.20	2.20	2.20	2.20	2.20
Final Velocity, ft/sec	51.83	51.83	51.83	51.83	51.83
Skidded Distance, ft	26.00	28.00	30.00	32.00	34.00
Pavement Friction	0.30	0.30	0.30	0.30	0.30
Deceleration, ft/sec^2	9.66	9.66	9.66	9.66	9.66
Initial Velocity, ft/sec	56.47	56.81	57.15	57.48	57.82

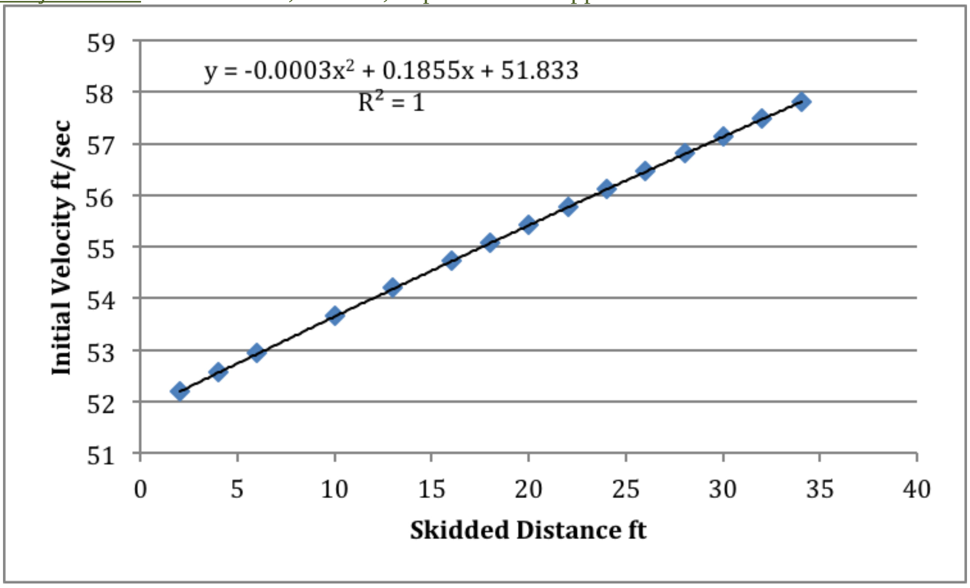

Figure 1 Influence of Skidded Distance on the Initial Velocity

V. CONCLUSIONS

The following regression relationship was found with statistically significant correlation coefficient for predicting the performance of the engineering variables.

The influence of Skidded Distance on the Initial Velocity is shown by a quadratic equation (Initial velocity = -0.0003 Skidded distance ^{2} +0.185 Skidded Distance + 51.83) with R = 1.

ACKNOWLEDGMENTS

The Republic of Turkey, Ministry of National Education Scholarships is duly acknowledged for providing scholarship.

REFERENCES

[1] Newton's Three Laws of Motion. http://csep10.phys.utk.edu/astr161/lect/history/newton3laws.html
[2] First Law of Thermodynamics. http://hyperphysics.phy-astr.gsu.edu/hbase/thermo/firlaw.html
[3] Engber, D. The Ferrari That Split in Half. 2006. http://www.slate.com/articles/news_and_politics/explainer/2006/04/the_ferrari_that_split_in_half.html
[4] Accreditation Commission for Traffic Accident Reconstruction (ACTAR). http://www.actar.org/
[5] Hurt, H. Jr. AMA Motorcycle Hall of Fame. http://www.motorcyclemuseum.org/halloffame/detail.aspx?RacerID=398
[6] Brooks R. M.; Cetin M. Determination of the Influence of Vehicles Weight Ratio on the Initial Velocity Using the Accident Reconstruction Engineering Principles. International Journal of Emerging Technology and Advanced Engineering. Volume 3, Issue 3, ISSN: 2250-2459, S. No: 159, March 2013, pp. 927-931.
[7] Brooks R. M.; Cetin M. Determination of the Influence of Pavement Friction on the Initial Velocity Using the Accident Reconstruction Engineering Principles. International Journal of Engineering Inventions. Volume 2, Issue 6, e-ISSN: 2278-7461, p-ISBN: 2319-6491, S. No: 9, April 2013, pp. 63-68.
[8] Brooks R. M.; Cetin M. Determination of the Influence of Skidded Distance on the Initial Velocity Using the Accident Reconstruction Engineering Principles. International Journal of Research and Reviews in Applied Sciences. Volume 15, Issue 3, EISSN: 2076-7366, ISSN: 2076-734X, S. No: 3, June 2013, pp 225-229.
[9] Brooks R. M.; Cetin M. Influence of Pavement Friction on the Initial Velocity of Vehicle in Chain Accidents at Intersections. International Journal of Emerging Technology and Advanced Engineering. Volume 3, Issue 7, S. No: 2, ISSN 2250-2459, July, 2013, page 10-15.
[10] Brooks R. M.; Cetin M. Pavement Friction V. Initial Velocity of Vehicle in Chain Accidents on Highways. International Journal of Engineering Inventions. Volume 3, Issue 2, e-ISSN: 2278-7461, p-ISBN: 2319-6491, S. No: 5, September 2013, pp. 27-31.
[11] Mendenhall, W., and Sincich, T., (2007) “Statistics for Engineering and the Sciences”, Prentice Hall. 5th Edition.
[12] Hogg, R. V., and Tanis, E. A., (2006) “Probability and Statistical Inference”, Prentice Hall, 7th Edition.
[13] Field, A., (2009) “Discovering Statistics Using SPSS”, Sage, 3rd Edition.
[14] Walpole, R.E., Myers, R. H., Myers, S. L., and Ye, K., (2007) “Probability and Statistics for Engineers and Scientists”, Pearson Education International. 8th Edition.

International Journal of Modern Engineering Research (IJMER)
www.ijmer.com Vol. 3, Issue. 5, Sep - Oct. 2013 pp-2944-2949 ISSN: 2249-6645

Total Harmonic Distortion Alleviation by using Shunt Active Filter

Y.Praveen Kumar Reddy, B. Kumuda, U. Shantha Kumar
Asst. Professor, Dept. of EEE, CBIT, Proddatur,Andra Pradesh, India
Asst. Professor Dept. of EEE, RYMEC, Bellary, Karnataka, India
Asst. Professor, Dept. of EEE, RYMEC, Bellary, Karnataka, India

ABSTRACT: *This paper presents a new topology for multilevel Current source converter. The new converter uses parallel connections of full-bridge cells. Also by Adding or removing the full-bridge cells, modularized circuit layout and packaging is possible, where the number of output current levels can also be easily adjusted. Using adequate levels, the multilevel current converter generates approximately sinusoidal output current with very low harmonic distortion. Based on this converter a shunt active filter has been modeled. The simulation results of the lacking shunt active filter and through shunt active filter in controlled rectifier shows that the THD alleviation by means of shunt active filter.*

Key words: *Multilevel Converter, Shunt Active Power Filter, Power Quality*.

I. INTRODUCTION

Recently multilevel power conversion technology has been a very rapidly growing area of power electronics with good potential for further developments. The most attractive applications of this technology are in the medium to high-voltage range[1] Multilevel converters work more like amplitude modulation rather than pulse modulation, and as a result:

• Each device in a multilevel converter has a much lower dv/dt The outputs of the converter have almost perfect currents with very good voltage waveforms because the undesirable harmonics can be removed easily,
• The bridges of each converter work at a very low switching frequency and low speed semiconductors can be used and
• Switching losses are very low [2].

The general function of the multilevel converter is to synthesize a desired output voltage from sev- eral levels of DC voltages as inputs. The DC volt- age sources are available from batteries, capacitors, or fuel cells. There are three types of multilevel con-verters:

• Diode-Clamped Multilevel Converter
• Flying-Capacitor Multilevel Converter
• Cascaded-Converters with Separated DC Sources

The first practical multilevel topology is the diode-clamped multilevel converter topology and first in-troduced by Nabae in 1980 [3]. The converter uses capacitors in series to divide the DC bus voltage into a set of voltage levels. To produce N levels of the phase voltage, an N −level diode-clamp converter needs N-1 capacitors on the DC bus. The flying capacitor multilevel converter proposed by Meynard and Foch in 1992 [4], [5]. The converter uses a ladder structure of the DC side capacitors where the volt-age on each capacitor differs from that of the next capacitor. To generate N −level staircase output volt-age, N − 1 capacitors in the DC bus are needed.Each phase-leg has an identical structure. The size of the voltage increment between two capacitors de-termines the size of the voltage levels in the out-put waveform The last structure introduced in the paper is a multilevel converter, which uses cascade converters with separate DC sources and first used for plasma stabilization [6], it was then extended for three-phase applications [7]. The multilevel converter using cascaded-converter with separate DC sources synthesizes a desired voltage from several independent sources of DC voltage. A primary advantage of this topology is that it provides the flexibility to increase the number of levels without introducing complexity into the power stage. Also, this topology requires the same number of primary switches as the diode-clamped topology, but does not require the clamping diode. However, this configuration uses multiple dedicated DC-busses and often a complicated and expensive line transformer, which makes this a rather expensive solution. In addition, bidirectional operation is somewhat difficult (although not impossible) to achieve [8]. Modularized circuit layout and packaging is possible because each level has the same structure, and there are no extra clamping diodes or voltage balancing capacitor. The number of output voltage levels can be adjusted by adding or removing the full-bridge cells The converters that were focused upon were volt-age source converters, with multilevel voltage wave-forms. These converters divide the total input voltage among a number switches, and allow a reduction of the voltage harmonics. As mentioned, these are the most commonly used and best-understood multilevel converters. The most multilevel converters discussed in the literature are multilevel voltage source con verters [9]. However, in many current applications, such as shunt active filters, active power line conditioners, VAR compensations etc., we need to use multilevel current converters. This paper presents a new multilevel current converter. Then the proposed multilevel current source converter is the core of a shunt active filter, which is obtained based on this converter. The proposed new multilevel current converter consists of a set of par-allel single-phase full-bridge converter units. The AC current output of each levels full-bridge converter is connected in parallel such that the synthesized current waveform is the sum of the converter outputs. In other words, for high current applications many switches can be placed in parallel, with their current summed by inductors.

II. THE PROPOSED MULTILEVEL CURRENT CONVERTER

II.1.The Proposed Topology

The full-bridge topology is used to synthesize a three-level square-wave output current waveform. The full-bridge configuration of the single-phase current source converter is shown in Fig1.

In as single-phase full-bridge configuration, four switches are needed. In full-bridge configuration, by

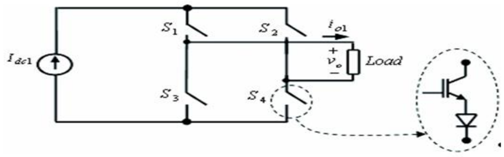

Fig.1. A multi level current converter

Turning the switches S_1 and S_4 on and S_2 and S_3 off a current of I_{dc1} is available at output i_{o1}, while reversing the ing the operation we get current of i_{dc1}. To generate zero level of a full-bridge converter, the switches $S_1$and S_3 are turned on while S_2 and S_4 are turned off or vice versa. The typical output waveform of full bridge of single-phase multilevel shown in Fig.1 is shown in Fig. 2

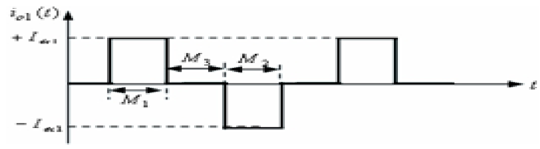

Fig.2. Typical output wave form of three level configuration

The three possible levels with respect to above discussion are shown in Table 1. Note that S_1 and S_2 should not be open at the same time, nor should S_3 and S_4. Otherwise, an open circuit would exist across the DC current source.

Table 1: output current with corresponding conditions

MODES	CONDUCTING SWITCHES	OUTPUT CURRNT
1	S1,S4	$+I_{dc1}$
2	S2,S3	$-I_{dc1}$
3	S1,S3 or S2,S4	0

Fig.3 shows equivalent circuits of the proposed topology at different modes.

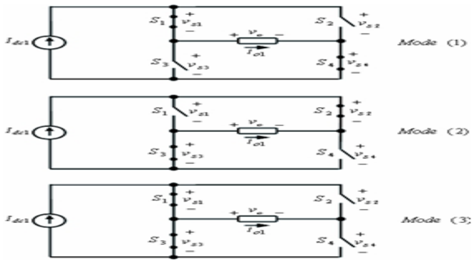

Fig.3. The Equivalent Circuits of the Proposed Topology at Different Modes

From Fig. 3, the instantaneous switches voltages of each module are given in Table2

Table 2: Instantaneous switches voltages

Mode	Vs1	Vs2	Vs3	Vs4
1	0	Vo(t)	Vo(t)	0
2	-Vo(t)	0	0	-Vo(t)
3	0	Vo(t)	0	-Vo(t)

Using parallel connections of many converters like the one shown in Fig. 1, we can synthesize multi-level current converter. The general function of this multilevel current source converter is to synthesize a desired current from several independent sources of DC currents. Fig. 3 shows a single-phase struc-ture of a parallel converter with a separate DC cur-rent source. By different combinations of the four switches, S_1−S_4, each full-bridge converter can gener-ate three different current outputs, $+I_{dc1}$, $-I_{dc1}$ and zero current. The AC outputs of each of the different level of full-bridge converters are connected in par-allel such that the synthesized current waveform is the sum of the converter outputs. An output phase current waveform is obtained by summing the output currents of the converter bridges:

$$I_{ON}(t) = i_{o1}(t) + i_{o2}(t) + \cdots + i_{on}(t) \quad (1)$$

Where N is the number of parallel bridges [10].

In the following we propose a new method for determining the levels of different DC current sources, which are used in the proposed multilevel converter.

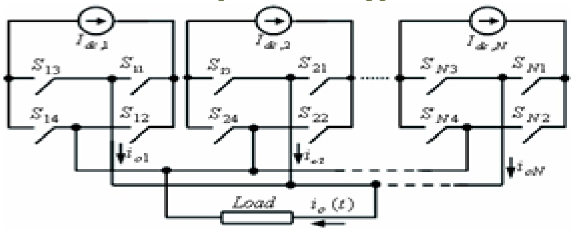

Fig.3. Single phase parllel multilevel current source converter

II.2. DETERMINING THE LEVELS

If all DC current sources in Fig. 3 are equal to I_{dc} the converter is then known as symmetric multilevel current source converter. With having a number of full-bridge converter units, this technique results in an output current of the converter that is almost sinusoidal.

The maximum output current of the N paralleled multilevel current source converter is

$$I_{MAX} = N * I_{dc} \qquad (2)$$

In this topology; the number of overall output current(S) is given by:

$$S = 1 + 2N \qquad (3)$$

For example, a 13-level multilevel current source converter using the technique can be implemented as shown in Fig. 4. In Fig. 4, i_{o1} to i_{o6} are DC current supplies, which are from either regulated inductors or separated DC sources.

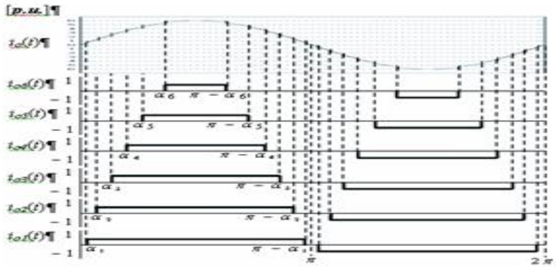

Fig.4 The 13 level converter output

III. THE SHUNT ACTIVE FILTER BASED ON MULTILEVEL CURRENT SOURCE CONVER-TER

III. 1.SHUNT ACTIVE FILTER PRINCIPLE

In recent years, the usage of modern electronic equipment has been increasing rapidly. These elect-ronic equipments impose nonlinear loads to the AC main that draw reactive and harmonic current in ad-dition to active current. In order to overcome these problems, different kinds of active power fil-ters, based on force-commutated devices, have been developed. Particularly, shunt active power filters, using different control strategies, have been widely investigated. These filters operate as current sources, connected in parallel with the nonlinear load generat-ing the current and the current harmonic components required by the load. However, shunt active filters present the disadvantages that are difficult to imple-ment in large scale where the control is also compli-cated. To reduce the drawbacks, the proposed solu-tion in this paper is to use a multilevel current source converter. A shunt active filter consists of a controllable voltage or current source. This topology is shown in fig.5 it consisting of DC link capacitor C, power electronic switch and inductor Lf.

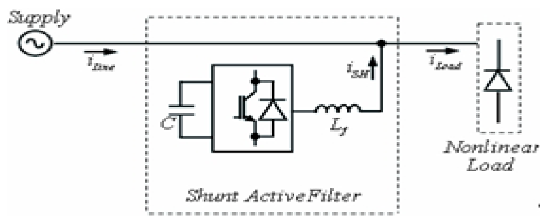

Fig.5 configuration of voltage source converter based on shunt active filter

III.2. SUGGESTED SHUNT ACTIVE FILTER

Fig.6 shows the schematic of the suggested shunt active power filter consisting of the new multilevel current source inverter with a control unit, to solve the power quality problems. The operation of the shunt current source multilevel inverters is based on the injection of current harmonic, i_{SH} , which is in phase with the load current, $i_{Load,}$ thus eliminating the harmonic current of the line(supply) current iLine. Now, suppose that the load current can be written as the sum of the fundamental and harmonic current as in equation (4)

$$i_{Load} = i_{Load\,,Fund} + i_{Load\,,Harmonics} \qquad (4)$$

Then the injected current by shunt inverter should be:

$$i_{SH} = i_{Load\,,Harmonics} \qquad (5)$$

With resulting the line current

$i_{Line} = i_{Load} - i_{SH}$ (6)

$i_{Line} = i_{Load,Found}$ (7)

As it is seen, the equation (7) only contains the fundamental component of the load current and thus free from the harmonics.

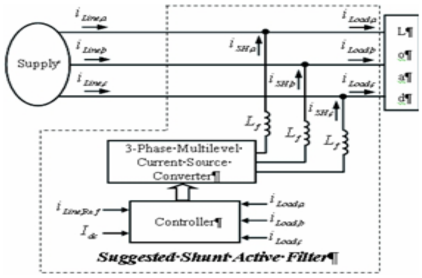

Fig.6. Suggested Shunt Active filter configuration

IV. WITHOUT SHUNT ACTIVE FILTER

The industrial loads usually have complex nonlinear dynamics. In connecting nonlinearities to a power network, they induce some undesirable distortions to the sinusoidal signal of the network. For showing this effect, a three phase controlled rectifier is used as a nonlinear load connected to grid Fig.7 shows the circuit of a three-phase controlled rectifier. The input phase voltages can be written as:

$v_a = v_m sinw_i t$ (8)

$v_b = v_m \sin(w_i t - {}^{2\pi}/_{3})$ (9)

$v_c = v_m \sin(w_i t + {}^{2\pi}/_{3})$ (10)

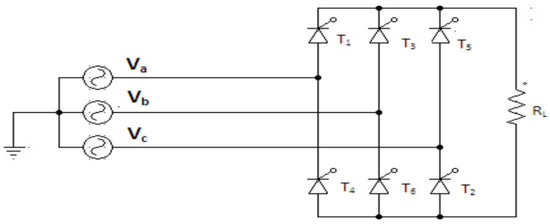

Fig.7. Three Phase Controlled Rectifier as a Nonlinear Load

If the load is assumed a pure resistance, the output current Peak is:

$$I_{MAX} = {}^{\sqrt{3}V_m}/_{R_L} \quad (11)$$

In this study, the parameters of the system are as $V_m = 110\sqrt{2}\,V, w_i = 100\pi$ and $R_L = 40$ohms Fig.8 shows waveforms of input line voltages, load current and line currents. As the Fig.8 shows, nonlinear loads may pollute power lines seriously with their high levels harmonic current and reduction in power factor. Fig.9 depicts the Fast Fourier Transform of ac utility line current Harmonics up to the 20th have been considered. The THD of the input current of the rectifier also the ac utility line current is 103.87%.

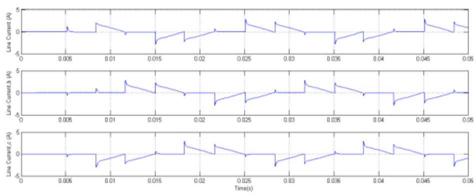

Fig.8. The Outputs of Controlled Rectifier

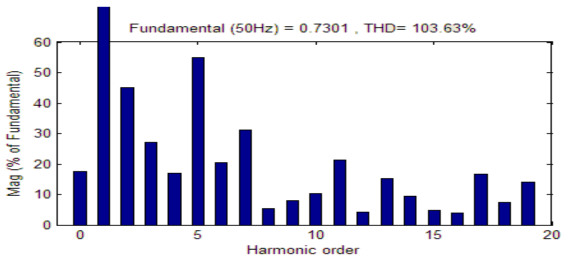

Fig.9. FFT analysis of the line current of Controlled Rectifier

V. WITH SHUNT ACTIVE FILTER

The ability of shunt active filters to suppress these problems has attracted a great deal of attention to these systems. This paper proposed a new struc-ture for shunt active filter based on multilevel cur-rent source converter. For showing the capability of the proposed shunt active filter, a 13 level multilevel current source converter as shown in Fig.10. Fig.11. Shows a single phase structure of the

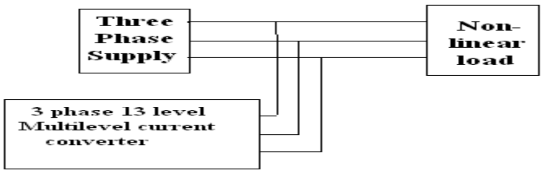

Fig.10. 13 level current converter

Multilevel converter. The converter consists of seven full-bridges with all current sources are equal to *Idc*. Fig. 12 shows the load, line and shunt active power filter output currents. The shunt active power filter with multilevel current converter is able to successfully compensates reactive power and mitigate current harmonics distortions with excellent transient performance.

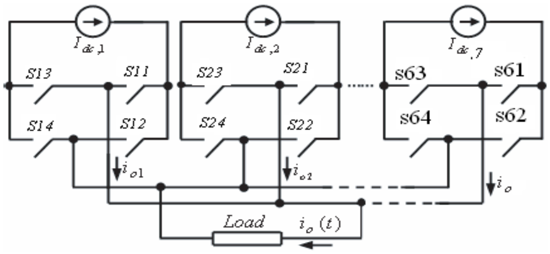

Fig.11. Single-Phase 13-Level Multilevel Current Converter Used in the Shunt Active Filter System

Fig.13. depicts the Fast Fourier Transform of ac utility line current Harmonics with shunt active filter up to the 20th have been considered. The THD of the input current of the rectifier also the ac utility line current is 12.66%.

VI. CONCLUSION

In this paper, a new topology for multilevel current source converters has been presented. The most important feature of the system is being convenient for expanding and increasing the Number of output levels. The proposed strategies generate a current with minimum error with respect to the sinusoidal reference. Therefore, it generates very low harmonic distortion.

Load currents

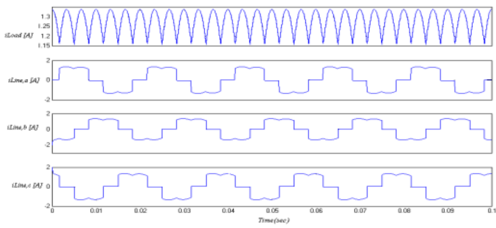

Shunt active filter currents

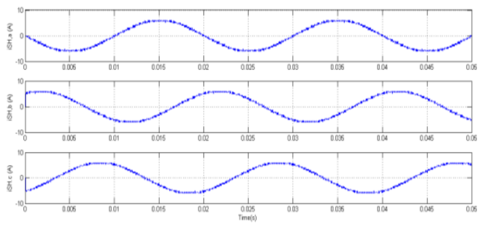

Line currents

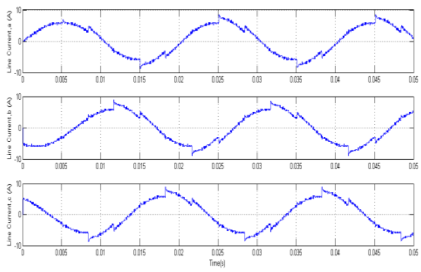

Fig.12. Load, Shunt Active Filter and Line Output Currents

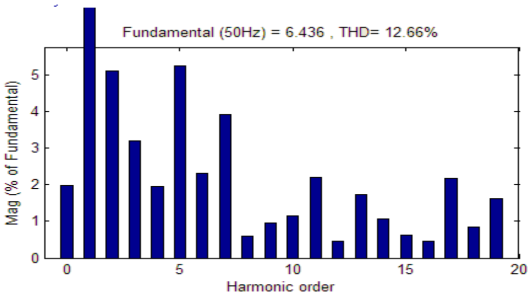

Fig.12. FFT analysis of the line current $i_{A,}$ at ac utility connected through shunt active filter

REFERENCES

[1] Nikola Celanovic, "Space Vector Modulation and Control of Multilevel Converters," Ph.D. Thesis, Blacksburg, Virginia, Sep. 2000.
[2] Giri Venkataramanan, and Ashish Bendre," Reciprocity-Transposition-Based Sinusoidal Pulse width Modulation for Diode-Clamped Multilevel Converters," IEEE Transaction on Industrial Electronics, Vol. 49, No. 5, pp. 1035-1047, Oct. 2002.
[3] Nabae, I. Takahashi and H. Akagi, "A New Neutral-Point Clamped PWM Inverter," IEEE Transactions on Industry Applications, Vol. IA-17, No.5, pp. 518-523, September=October 1981.
[4] T. Meynard and H. Foch, "Multi-Level Conversion: High Voltage Choppers and Voltage Source Inverters," IEEE PESC92, pp. 397403, 1992.
[5] T. Meynard and H. Foch"Imbricated Cells Multi-Level Voltage Source Inverters for High Voltage Applications," European Power Electronics Journal, Vol. 3, No. 2, pp. 99106, June 1993.
[6] M. Marchesoni, M. Mazzucchelli and S. Tenconi, "A Non Conventional Power Converter for Plasma Stabilization," IEEE Transactions on Power Electronics, Vol. 5, No. 2, April 1990.
[7] F. Z. Peng, J. S. Lai, J. McKeever and J. Van Coevering, "A Multilevel Voltage-Source Inverter with Separate DC Sources for Static Var Generation," IEEE-IAS Conference Record, pp. 2541-2548, 1995.
[8] J. Rodriguez, L. Moran, A, Gonzales and C.Silva,"High Voltage Converter with Regeneration Capability," IEEE-PESC Conference Proceedings, Vol. 2, pp. 1077-1082, 1999.
[9] Geoffrey R. Walker B.E. (Hons), "Modulation of Multilevel Converters," Ph.D. Thesis, Queensland, Nov. 1999.
[10] Ebrahim Babaei, Seyed Hossein Hosseini and Mahrdad Tarafdar Haque,"A Novel Approach to Multilevel Current Source Converters," Proceedings of the 2005 Electrical Engineering/Electronics, Telecommunications and Information Technology International Conference (ECTI-CON 2005), Vol. I, pp. 177-180, 12-13 May 2005, Pattaya, Choburi, Thailand.

Y Praveen Kumar Reddy received the B.E (Electrical and Electronics Engineering) degree from the Jawaharlal Nehru Technological University in 2006 and M.Tech (Power Electronics) in 2008 from the same university. Currently an Asst. Professor of the Dept. Electrical and Electronics Engineering, Chaitanya Bharathi Institute of Technology . Proddatur. Field of interest includes Renewable Energy Sources, Power Electrical & Drives,Control Systems.

B. Kumuda received the B.E (Electrical and Electronics Engineering) degree from the Visveswaraiah Technological University,Belgaum in 2008 and M.Tech (Digital Electronics) in 2011 from the same university. Currently an Asst. Professor of the Dept. Electrical and Electronics Engineering, Rao Bahadur Y Mahabaleshwarappa Engineering College ,Bellary. Field of interest includes Renewable Energy Sources, Power Electrical & Drives,Control Systems.

U. Shantha Kumar received the B.Tech (Electrical and Electronics Engineering) degree from the Jawaharlal Nehru Technological University in 2009 and M.Tech (Power Electronics) in 2012 from the same university. Currently an Asst. Professor of the Dept. Electrical and Electronics Engineering, Rao Bahadur Y Mahabaleshwarappa Engineering College,Bellary. Field of interest includes Power Systems, Power Electronics & Drives, Renewable Energy Sources.

A Novel Method for Creating and Recognizing User Behavior Profiles

Boyilla Sudheer[1], Syed Sadat Ali[2]

[1]*M.Tech, Nimra College of Engineering & Technology, Vijayawada, A.P., India.*

[2]*Assoc.Professor & Head, Dept.of CSE, Nimra College of Engineering & Technology, Vijayawada, A.P., India.*

ABSTRACT: *User profile can be defined as the description of the user interests, behaviors, characteristics, and preferences. User profiling is the practice of gathering, organizing, and interpreting the users profile information. In this paper, we propose an adaptive approach for creating user behavior profiles and recognizing computer users. We call this approach Evolving Agent behavior Classification based on Distributions of relevant events (EVABCD) and it is based on representing the observed behavior of a computer agent as an adaptive distribution of his/her relevant atomic behaviors (events). Once the model has been created, EVABCD presents an evolving method for updating and evolving the user profiles and classifying an observed user. The approach we present is generalizable to all kinds of computer user behaviors represented by a sequence of events.*

Keywords: *Classifier, EVABCD, Profiles, Trie.*

I. INTRODUCTION

A web search engine is used to search and retrieve required information from WWW and FTP servers. The needed search results that are retrieved are presented in a list of results. This information may consist of web pages, audio, video, images and other types of files [1]. Some search engines also mine the data available in various databases. Unlike web directories that maintained by human, search engines operate algorithmically or are a mixture of several algorithms and human input. Most search engines return the same results for the same query, regardless of the user's interest in that area. Since queries submitted to search engines are very short and they will not express the user's precise needs. A good user profiling strategy is a fundamental component in the search engine personalization. Search engine personalization is the act of gathering and interpreting the users profile information. Most personalization methods is based on the creation of one single profile for a user and then user have to specify his search interest in that and based on that interest ,the results will be retrieved. If his/her search interest changes, he have to update that manually.

Different queries from the user should be handled differently because a user's preferences may vary across different queries [2]. For example, a user who prefers information about a fruit on the query "apple" may not prefer the information about Apple Computer for the query "apple." Personalization strategies should be done such that it is based on user's interest, the result should be obtained. Based on the changing behavior of the user, their profiles should be updated automatically. An adaptive approach for creating behavior profiles and recognizing different computer users called Evolving Agent behavior Classification based on Distributions of relevant events (EVABCD) is used and it is based on representing the observed behavior of a computer agent as an adaptive distribution of her/his relevant atomic behaviors [3].

This paper is organized as follows: Section II provides as overview of background work. The main improvement and the development of the personalized automatic updation of the user profile are provided in Section III. Section IV describes the conclusion.

II. BACKGROUND WORK

Various approaches have been proposed as literature point of view that the user profile usually changes to recognize behavior of others in real-time. To predict, to coordinate, and to recognize human brain capacity for future actions. Different methods have been used to find out the relevant information in computer user behavior in different computer areas:

A. Discovery of navigation patterns

In [4], the authors present the Web Utilization Miner (WUM), a mining system for discovering interesting navigation patterns in website. WUM prepares the web log data for mining process and the language MINT mining the aggregated data according to the directives of the human expert [5].

B. Web recommender systems

In [6], the authors propose a system (WebMemex) that provides recommended information based on the captured history of navigation from a list of known users. WebMemex captures information such as IP addresses, user Ids and the URL accessed for future analysis.

C. Web page filtering

In [7], the authors present a technique to generate readable user profiles that accurately capture interests by observing their behavior on the Web. The proposed method is built on the Web Document Conceptual Clustering algorithm, with which profiles without an a priori knowledge of user interest categories can be acquired.

D. Computer security

In [8], the authors describe a method using queuing theory and logistic regression modeling methods for profiling computer users based on simple temporal aspects of their behavior.

International Journal of Modern Engineering Research (IJMER)
www.ijmer.com Vol. 3, Issue. 5, Sep - Oct. 2013 pp-2950-2952 ISSN: 2249-6645

III. PROPOSED WORK

In this paper, we propose a novel method for creating behavior profiles and recognizing computer users. We call this method Evolving Agent behavior Classification based on Distributions of relevant events (EVABCD) and it is based on representing the observed behavior of a computer agent as an adaptive distribution of his/her relevant atomic events. The goal of our work in the UNIX environment can be divided into two phases:

- Creating and updating user behavior profiles from the commands the users typed in a UNIX shell.
- Classifying a new sequence of UNIX commands into the predefined profiles.

The proposed work includes at each step the following two main actions:

- Creating the user behavior profiles and evolving the classifier
- User classification

Construction of the user behavior profile

In order to construct a user behavior profile in online mode from the data stream, extract an ordered sequence of acknowledged events. Commands are inherently in order, it is considered in the modelling process. According to this aspect, in order to get the most representative set of subsequence‟ s from a sequence, we propose the use of a tree data structure called trie. Building of a user profile from a single sequence of commands is done by a 3 step process:

- Segmentation of the sequence of commands.
- Storage of the subsequence’s in a tree.
- Creation of the user profile.

B. Segmentation of commands and Trie creation

First, the sequence is divided into subsequences of equal length from the first to the last element. Thus, the sequence A =A1A2 . . .An (where n is the number of unix commands of the sequence) will be segmented in the subsequences described by Ai . . .Ai+length ∀ i, i=[1,n-length+1], where length is the size of the subsequences created. The subsequences of unix commands are stored in a trie data structure. When a new model needs to be constructed, we create an empty trie, and insert each subsequence of behaviors into it, such that all possible subsequences are accessible and explicitly represented. Every trie node represents an event appearing at the end of a subsequence, and the trie nodes children represent the events that have appeared following this event. Also, each trie node keeps track of the number of times a command has been recorded into it. When a new subsequence is inserted into the trie, the existing nodes are modified and/or new nodes are created. Considering the example, the first subsequence ({ls -> date -> ls}) is added as the first branch of the empty trie (Figure 1a). Each node is labeled with the number 1 which indicates that the command has been inserted in the node once (in Figure 1, this number is enclosed in square brackets). Then, the suffixes of the subsequence ({date -> ls} and {ls}) are also inserted (Figure 1b). Finally, after inserting the three subsequences and its corresponding suffixes, the completed trie is obtained (Figure 1c).

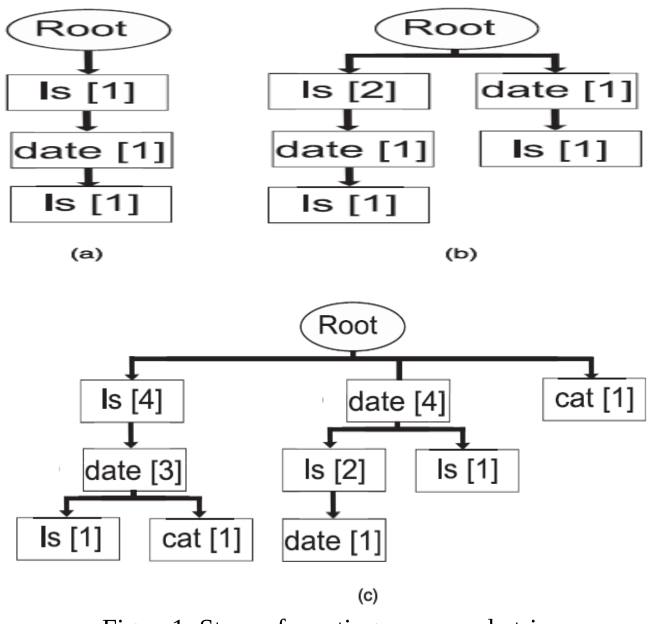

Figure1: Steps of creating an example trie

C. Creation of the User Profile

Once the trie structure is created, the subsequences that characterize the user profile and its relevance are calculated by traversing the trie. For this purpose, frequency-based methods are often used. In particular, in EVABCD, to evaluate the relevance of the subsequence, its relative frequency or support is calculated. In this step, the trie structure can be transformed into a set of subsequences labeled by its support value. In EVABCD, this set of subsequences is represented as the distribution of relevant subsequences. Thus, we assume that user behavior profiles are n-dimensional matrices, where each dimension of the matrix will represent a particular subsequence of commands. Once a user behavior profile has been created, it is then classified and used to update the Evolving-Profile-Library.

D. Evolving UNIX User classifier

A classifier is defined as a mapping from the feature space to the class label space. In the proposed classifier, the feature space is defined by the distributions of subsequences of events. Thus, a distribution in the class label space represents a specific behavior which is one of the prototypes of the EPLib. EVABCD receives observations in real time from the environment to analyze. In our case, these observations are UNIX commands and they are converted into the corresponding distribution of the subsequences online. In order to classify a UNIX user behavior, these distributions must be represented in a data space. Figure 2 explains graphically this novel idea. In this example, the distribution of the first user consists of five subsequences of commands (ls, ls-date, date, cat, and date-cat); therefore, we need a 5-dimensional data space to represent this distribution because each different subsequence is represented by one dimension. If we consider the second user, we can see that 3 of the five previous subsequences have not been typed by this user (ls-date, date, and date-cat), so these values are not available. To sum up, the dimensions of the data space represent the different subsequences typed by the computer users and they will increase according to the different new subsequences obtained.

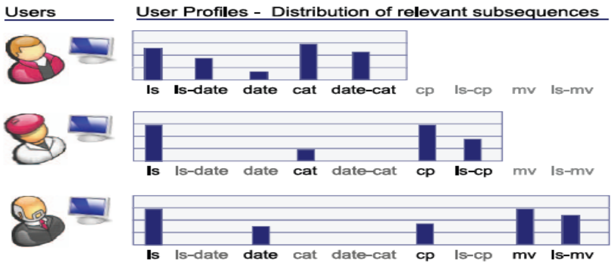

Figure 2: Distributions of subsequences of events in an evolving system approach

E. Structure of the EVABCD

Once the corresponding distribution has been created from the online stream, it is processed by the classifier. The structure of this classifier includes the following:

1. Classify the new sample in a class represented by a prototype.
2. Calculate the potential of the new data sample to be a prototype.
3. Update all the prototypes considering the new data sample. It is done because the density of the data space surrounding certain data sample changes with the insertion of each new data sample. Insert the new data sample as a new prototype if needed.
4. Remove any prototype if needed.

IV. CONCLUSION

An important result from the experiments is that user profiles with negative preferences can increase the separation between similar and dissimilar queries. And also search results retrieved based on history based search to help user to navigate the web pages easily. Our proposed method, EVABCD, to model and classify user behaviors from a sequence of events. EVABCD is recursive, and it can be used in an interactive mode; thus, it is computationally efficient and fast in updating the profile of the user. In addition, its structure is simple as well as interpretable. This personalization technique can also be used to monitor and also to detect abnormalities based on a time-varying behaviour of same users and to detect masquerades.

REFERENCES

[1] Alaniz-Macedo A., Camacho-Guerrero J.A., Graca-Pimentel M. and Truong K.N. (2003), 'Automatically Sharing Web Experiences through a Hyperdocument Recommender System', Proc. ACM Conf. Hypertext and Hypermedia (HYPERTEXT '03), pp. 48-56.
[2] Amandi A. and Godoy D. (2005), 'User Profiling in Personal Information Agents: A Survey', Knowledge Eng. Rev., vol. 20, no. 4, pp. 329-361.
[3] Gong W., Hu J., Pepyne D.L. (2009), 'User Profiling for Computer Security' Proc. Am. Control Conf., pp. 982-987.
[4] Spiliopoulou, M., Faulstich, L.C.: Wum: "A web utilization miner," In: Proceedings of EDBT Workshop WebDB 1998, pp. 109–115. Springer, Heidelberg (1998).
[5] Wexelblat, A.: "An environment for aiding information browsing tasks." In: Proc. Of AAAI Spring Symposium on Acquisition, Learning and Demonstration: Automating Tasks for Users. AAAI Press, Menlo Park (1996).
[6] Macedo, A.A., Truong, K.N., Camacho-Guerrero, J.A., da GraC¸a Pimentel, M.: "Automatically sharing web experiences through a hyperdocument recommender system," In: HYPERTEXT 2003, pp. 48–56. ACM, New York (2003).
[7] Godoy, D., Amandi, A.: "User profiling for web page filtering," IEEE Internet Computing 9(4), 56–64 (2005).
[8] Pepyne, D.L., Hu, J., Gong, W.: "User profiling for computer security," In: Proceedings of the American Control Conference, pp. 982–987 (2004).

International Journal of Modern Engineering Research (IJMER)
www.ijmer.com Vol. 3, Issue. 5, Sep - Oct. 2013 pp-2953-2955 ISSN: 2249-6645

Secure Ticket- Based Anonymity and Traceability in Wireless Mesh Networks

Ponnam Lalith Subhash[1], G.Minni[2]
[1]M.Tech, Nimra College of Engineering & Technology, Vijayawada, A.P, India.
[2]Asst.Professor, Dept.of CSE, Nimra College of Engineering & Technology, Vijayawada, A.P, India.

ABSTRACT: *Wireless Mesh Network (WMN) is a promising technology to meet the challenges of the present generation for providing flexible adaptive and reconfigurable architecture. WMN provides cost-effective business solutions. A WMN is dynamically a self-organized and self-configured system with the nodes in the network automatically establishing and maintaining mesh connectivity among themselves. However, WMN is attractive to both the service providers and users and widespread due to its low investment feature and the wireless broadband services it supports, security issues inherent in mesh network or any wireless networks need be considered before deployment and proliferation of these networks, since it is unappealing to subscribers to obtain services without a security and privacy guarantee. Anonymity can incur insider attacks since misbehaving users are no longer traceable. It provides anonymity for the honest user's and trace the users who are misbehaving using other client's identification. Moreover, the approach to ensure the network access anonymity and location privacy, our pseudonym generation does not rely on a central authority, e.g., the broker, the domain authority.*

Keywords: *Anonymity, Tickets, Traceability, WMN.*

I. INTRODUCTION

Wireless Mesh Networks (WMN) are gaining growing interest as a promising technology for ubiquitous high speed network access. The routing in wireless mesh networks is different from wired networks because of topology changes related to environmental fluctuations, limited bandwidth and battery life, partly unidirectional links, many redundant links, link quality. A WMN is dynamically a self-organized and self-configured system with the nodes in the network automatically establishing and maintaining mesh connectivity among themselves. However, WMN is attractive to both the service providers and users and widespread due to its low investment feature and the wireless broadband services it supports, security issues inherent in the mesh networks or any wireless networks need be considered before deployment and proliferation of these networks, since it is unappealing to subscribers to obtain services without a security and privacy guarantee. Wireless security has been considered as most important in many networking technologies such as the Mobile Ad-hoc Networks(MANET)[1],Vehicular AdhocNetworks(VANET)[2], wireless sensor networks. Recently, new proposals on WMN security[3] is also evolved.

Anonymity and Traceability are considered as important concept in many payment based systems. Anonymity unlinks the user identities from his/her activities and also to prevent movement tracing by hiding location information in payment based systems[4]. In unconditional anonymity, it is easier for any of the mesh network clients to misbehave and thus has not been traced. Even though there is pseudonym technique, to ensure that the network access anonymity and location privacy, it does not rely on central authority, who can derive the user's identity from his pseudonyms and illegally trace an honest user. Thus the concept of traceability is highly desirable in such systems[4]. This paper proposes a security architecture, that involves ticketing and blinding, resolve the conflicts between anonymity and traceability. Ticketing technique [5] includes Ticket Issuance and Ticket Deposit, in which the tickets are issued, based on his/her misbehavior levels of the users, using Ticket Issuance Protocol, to do any processes and using Ticket Deposit Protocol, it is deposited. The borrowed Restrictive Partially Blind Signature technique [4][6], that acts as a backbone for our architecture. In this, with the help of Restrictiveness property, the user can get the signature by blinding his personal details and thus achieves anonymity. And with the help of Partial property, Trusted Authority (TA) can view some of the user detail in case of authentication. And, the dishonest users can be easily traced with the help of the Fraud Detection protocol.

II. RELATED WORK

Sensor networks are typically characterized by limited power supplies, small memory sizes, low bandwidth and limited energy. This leads to a very demanding environment to provide security issues. Majority of security issues have not been addressed and surveyed in [7].Universal pass model [8] proposed for mesh networks, addressing countermeasures to wide range of attacks in WMNs. In [9], the TA provides free Internet access but requires the clients (CLs) to be authorized and affiliated usres generally for a long term so that Ticket –based security architecture was developed which includes: Ticket issuance, Ticket deposit. Designing a ticket-based anonymity system with traceability property; bind of the ticket and pseudonym which guarantees anonymous access control (i.e., anonymously authenticating a user at the access point and simplified revocation process ,revocation of Tickets, adoption of the hierarchical identity-based cryptography (HIBC) for inter domain authentication avoiding domain parameter certification are illustrated in [1]. Figure 1 explains the Ticket issuance and Deposit phases [9].

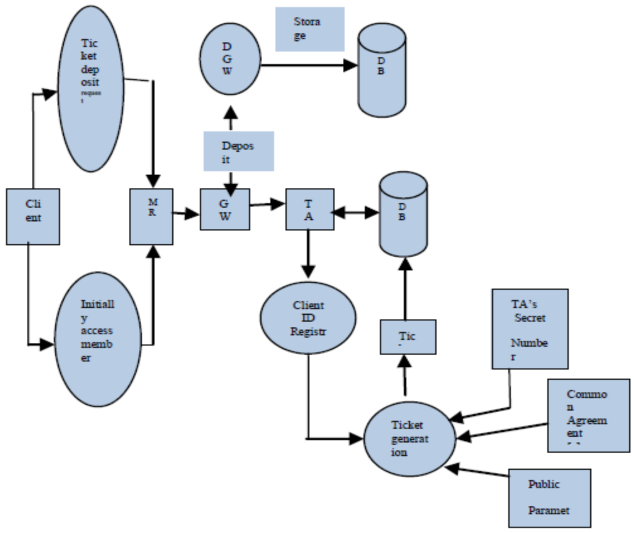

Figure 1: Ticket issuance and deposit

Here Ticket issuance occurs when the user initially attempts to access the network or when all previously issued tickets are depleted. The user or client needs to reveal his real ID to the TA(Trusted Authority) in order to obtain a ticket since the TA has to ensure the authenticity of this client. After some process TA issues the batch of Tickets to MN (mobile Node). Ticket value is the total amount of traffic that the client is allowed to generate and receive before the expiry date of the ticket Misbehavior-Ticket reuse and multiple deposits. Ticket expiry date (validity period) after obtaining a valid ticket, the user may deposit it anytime the network service is desired before the ticket expires, using the ticket deposit protocol. Misbehavior is totally different from the noncompliant behavior.

III. EXISTING SYSTEM

In wireless communication systems, it is easier for a global observer to mount traffic analysis attacks by following the packet forwarding path than in the wired networks. Thus, routing anonymity is indispensable, which conceals the secret communication relationship of two parties by building an anonymous path between them. Nevertheless, unconditional anonymity may incur insider attacks since dishonest users are no longer traceable. Therefore, traceability is highly desirable such as in e-cash systems where it is used for detection and tracing double-spenders.

Disadvantages of Existing System:

In the existing systems, there exists Conflicts between both the anonymity and traceability. The fundamental security requirements including authentication, data integrity, confidentiality and non-repudiation are not achieved in the existing systems.

IV. PROPOSED SYSTEM

In this paper, we propose a security architecture to ensure Unconditional anonymity for honest users and traceability of misbehaving users for Network authorities in wireless mesh networks (WMN). We are motivated by resolving the above security conflicts, namely anonymity and traceability concepts, in the emerging WMN communication systems. We have proposed the initial design of our security architecture, where the feasibility and the applicability of the architecture were not fully understood. As a result, we provide detailed efficiency analysis in terms of storage, communication, and computation in this paper to show that our proposed method is a practically viable solution to the application scenario of interest. We attacked Sun et al. scheme's traceability. Our analysis showed that trusted Authority (TA) cannot trace our system borrows the blind signature technique from the payment systems, and hence, can achieve the anonymity of unlinking user identities from activities, as well as the traceability of misbehaving users. Furthermore, the proposed pseudonym method renders user location information unexposed.

Our proposed work differs from previous work in that WMNs have unique hierarchical topologies and rely heavily on wireless links, which have to be considered in the anonymity design. As a result, the original anonymity method for payment systems among bank, customer, and store cannot be directly applied. In addition to the anonymity method, other security issues such as authentication, key establishment, and revocation are critical in WMNs to ensure the correct application of the anonymity scheme. Moreover, although we employ the widely used pseudonym scheme to ensure network access anonymity and location privacy, our pseudonym generation does not rely on a central authority, e.g., the broker , the domain authority , the transportation authority or the manufacturer, and the trusted authority , who can derive the user's identity from his pseudonyms and illegally trace an honest user.

A. Wireless mesh networks

The wireless mesh backbone consists of mesh routers (MRs) and gateways (GWs) interconnected by using ordinary wireless links (shown as dotted curves). Mesh routers and the gateways serve as the access points of the WMN and the last resorts to the Internet, respectively. Each network domain, or trust domain (to be used interchangeably) is managed by a domain administrator that serves as a trusted authority the central server of a campus WMN.

B. Blind Signature

In general, a blind signature technique allows a receiver to obtain a signature on a message such that both the message and the resulting signature remain unknown to the signer. The formal definition of a blind signature scheme should bear the properties of verifiability, unlinkability, and unforgeability. Blind signature scheme, where the restrictiveness property is incorporated into the blind signature scheme such that the message being signed must contain the encoded information. As the name suggests, this property restricts the client in the blind signature scheme to embed some account-related secret information into what is being signed by the bank (otherwise, the signing will be unsuccessful) such that this secret can be recovered by the bank to identify a user if and only if he double-spends. The restrictiveness property is essentially the guarantee for traceability property in the restrictive blind signature systems.

C. Ticket Issuance

In order to maintain security of the network against attacks and the fairness among users, the home server manager may control the access of each client by issuing tickets based on the misbehavior history of the user, which reflects the server manager's confidence about the client to act properly. Ticket issuance occurs when the user initially attempts to access the network or when all previously issued tickets are depleted. The client needs to reveal his/her real ID to the server manager in order to obtain a ticket since the server manager has to ensure the authenticity of this client.

D. Fraud Detection

Fraud is used interchangeably with misbehavior in this paper, which is essentially called an insider attack. Ticket reuse generally results from the client's inability to obtain the tickets from the TA when network access is desired, primarily due to the client's past misbehavior, which causes the server manager to constrain his ticket requests.

E. Fundamental security objectives

It is trivial to show that our security architecture satisfies the security requirements for data integrity, authentication and confidentiality, which follows directly from the employment of the standard cryptographic primitives, message authentication code, and encryption, in our system. We are only left with the proof of non-repudiation in this category. A fraud can be repudiated only if the client can provide a different representation, he/she knows of message from what is derived by the server manager. If the client has misbehaved, the representation he/she knows will be the same as the one derived by the server Manager which ensures non-repudiation.

V. CONCLUSION

In this paper, we propose a security architecture mainly consisting of the User ticket-based protocols, in which Ticket was generated based on user profile (anonymity requirement) which resolves the conflicting security requirements of unconditional anonymity for honest users and traceability property of misbehaving users and the single Ticket is issued to every client so that storage overhead was reduced and it enhanced with Ticket renewal process. By utilizing the tickets based on the user profile, the proposed architecture is demonstrated to achieve desired security objectives and efficiency.

REFERENCES

[1] L. Zhou and Z. J. Haas, "Securing ad hoc networks," IEEE Network Magazine, vol.13, no.6, pp. 24–30, Dec. 1999.
[2] M. Raya and J-P. Hubaux, "Securing vehicular ad hoc networks," Journal of Computer Security, Special Issue on Security of Ad Hoc and Sensor Networks, vol. 15, no.1, pp. 39–68, 2007.
[3] N. B. Salem and J-P. Hubaux, "Securing wireless mesh networks,"IEEE Wireless Communications,vol. 13, no. 2, Apr. 2006.
[4] S. Brands, "Untraceable off-line cash in wallets with observers,"in Proc. CRYPTO'93, 13th Annual Int'l Cryptology Conf. on Advances in Cryptology, pp. 302–318, Aug. 1993.
[5] J. Sun, C. Zhang, and Y. Fang, "A security architecture achieving anonymity and traceability in wireless mesh networks," IEEE Conf. on Computer Communications (INFOCOM), pp. 1687–1695,Apr. 2008.
[6] X. Chen, F. Zhang, and S. Liu, "ID-based restrictive partially blind signatures and applications," Journal of Systems and Software, vol.80, no. 2, pp. 164–171, Feb. 2007.
[7] I.F. Akyildiz, X. Wang, and W. Wang, Wireless Mesh Networks: A Survey, Computer Networks, vol. 47, no. 4, pp. 445- 487, Mar. 2005.
[8] Y. Zhang and Y. Fang, ARSA: An Attack- Resilient Security Architecture for Multihop Wireless Mesh Networks, IEEE J. Selected Areas Comm., vol. 24, no. 10, pp. 1916- 1928, Oct. 2006.
[9] Jinyuan Sun, Chi Zhang, Yanchao Zhang, and Yuguang Fang , IEEE transactions on Depentable and Secure computing vol 8, NO.2 march-april 2011 "SAT: A Security Architecture Achieving Anonymity and Traceability in Wireless Mesh Networks".

International Journal of Modern Engineering Research (IJMER)
www.ijmer.com Vol. 3, Issue. 5, Sep - Oct. 2013 pp-2956-2961 ISSN: 2249-6645

Strong Image Alignment for Meddling Recognision Purpose

Mrs. Pradnya Gajendra Kshirsagar
*(Department of computer science, Vishwabharati academy's College of Engineering , University of Pune, India)

ABSTRACT: The *Vast use of classic and modern technologies of internet causes increase the interest on systems that will protect in visual images against the wrongful manipulation that may be processed during the execution / transmission .One reason behind this problem is the verification of image received during communication. This work will be performed by strong image, and for this the image must be first registered by taking advantage of information provided by specific part of connected image. We describe strong image setting method in which there is a use of hash element (signatures) . The required signature is also attached with image before the transmission of image as well as before the image will send at destination place to get the graphical transformation of the received image. The accessor is based on the selecting the image which is having highest preference in the parameter space to recovered the graphical transformation which is used to manipulate image. The required image encodes the spaces occurred to deal with textures and contrasted strong image types.*

A block-wise strong image will be detected which occurs a graphical representation showing the visual impression of distributed of data with directed slope can be also proposed. This can be also used to build the signature for each strong image block. This new technique shows that it gives nice result as compared with state-of-art method.

Keywords: *Bag of features (BOF), forensic hash, geometric transformations, image forensics, image registration, tampering***.**

I. INTRODUCTION

The growing demand of techniques useful to protect digital visual data against malicious manipulations is induced by different episodes that make questionable the use of visual content as evidence material [1], [2]. All those, methods used for validity and authenticity of received image are required in internet communication. This strong image recognition can be make by using watermarking approach. This watermark will be inserted into the image during strong image recognition, and problems will be extracted to verify if there were any bad executions on received image. Any damage into the watermark proves that strong image is under construction

To avoid the twisting of content of image in watermarking method there is another method introduced that is signature based method. In Signature –based approach the signature must be small and strong and cannot be overlap into Image and also it must be header information of that image. Different signature-based approaches have been recently proposed in literature [3]–[10]. Most of them share the same basic scheme: 1) a hash code based on the visual content is attached to the image to be sent; 2) the hash is analyzed at destination to verify the reliability of the received image.

This method image hash is used with the help of which all the information and image content will be available in condensed way. The Hashed image must be strong against the operation allowed to it as well as its appearance also different from other image. This image hashing techniques is very useful technique for validating or checking the image authentication by using proper communication channel. Image hashing techniques are considered extremely useful to validate the authenticity of an image received through a communication channel. The binary decision task used for image authentication is not sufficient in this process. In the application, Forensic Science is fundamental to provide scientific evidence through the history of the possible manipulations ,which is applied to the original image to obtain the one, in which analysis manipulations provides required information to the end user , to decide whether the image can be trusted or not. All image manipulation information should be recovered from the short image hash signature which is one of the most challenging task. The list of manipulations provides to the end user the information needed to decide whether the image can be trusted or not. In order to perform tampering localization, the receiver should be able to filter out all the geometric transformations (e.g., rotation, scaling, translation, etc.) added to the tampered image by aligning the received image to the one at the sender[3]–[8].

The image alignment can be done randomly where only received image can be available at destination level and there is no any reference image available . At this level the geometric transformation of received image which is taken from signature must be recover which is most challenging task. At this level for better performance of image alignment and tampering localization it requires to design robust forensic hash method. Despite the fact that different robust alignment techniques have been proposed by computer vision researchers [11]–[13], these different techniques are not suitable in forensic hashing, the basic requirement is that the image signature should be as "compact" as possible to reduce the overhead of the network communications. To fit the basic condition/requirement , authors of [6] have proposed to exploit information extracted through Radon transform and scale space theory in order to estimate the parameters of the geometric transformations (i.e., rotation and scale).

To make more strong the alignment phase with respect to manipulations such as cropping and tampering, an image hash based on robust invariant features has been proposed in [7]. The latter technique extended the idea previously proposed in [8] by employing the bag of features (BOF) model to represent the features to be used as image hash. This representation of bag of features (BOF) is useful to reduce the space needed for the image signature, by maintaining the performances of the alignment component. In [4] a more robust approach based on a cascade of estimators has been introduced; it is able to better handle the replicated matchings in order to make a more robust estimation of the orientation parameter. The use of the cascade of estimators, which allows a higher precision in estimating the scale factor, this is the more effective way to deal with the problem of wrong matchings has been proposed in [3], where a filtering strategy based on the scale-invariant feature transform (SIFT) dominant directions combined in cascade with a robust estimator based on a voting strategy on the parameter space is presented. Taking into account the technique in [3], we propose to extend the underlying approach by encoding the spatial distribution of the image features to deal with highly textured and contrasted tampering patterns.

The proposed estimator is based on a voting procedure in the parameter space of the model which is used to recover the geometric transformation occurred into the manipulated image. The proposed method of tampering detection obtains satisfactory results with a significant margin in terms of estimation accuracy with respect to [4] and [7]. Further, by encoding spatial distribution the proposed method performs the original method proposed in [3] when strongly contrasted and/or texture regions are contained into the image. I also propose a block-wise tampering detection based on histograms of oriented gradients representation ,which makes the use of a non-uniform quantization to build the signature of each image block for tampering purposes. Experimental results confirm the effectiveness of the non-uniform quantization in terms of both compactness of the final hash signature and tampering detection accuracy. The main contributions of the paper can be summarized as follows.

1) Lu et al. [7] simply consider only the single matching in the first estimation and refine the results later considering the remaining ones. Although the refinement can be useful, the correctness of the final estimation heavily depends on the first estimation (only a refinement is performed later). Our approach does not discard replicated matchings retaining their useful information. The ambiguity of the matching is solved considering all the possible pairs with the same. As discussed also in [4], this solution introduces additional noise (i.e., incorrect pairs) that has to be properly taken into account employing the voting procedure.

2) The strong image estimator is based on a signature voting strategy. This voting strategy under parameter space allows to map the matchings from the image coordinate space to the parameters space novel. Specifically, the equations related to the similarity model have been combined and reduced with respect to the simple application of the voting procedure in the four-dimensional parameters space.

3) Feature selection based on their spatial distribution. In previous works (Lu et al. [7], Roy et al. [8], Battiato et al.[4]) the features were selected considering only their contrast properties. The proposed approach introduces a novel selection strategy that considers both contrast properties and spatial distribution of the features.

4) Complex dataset of tampered images.

II. REGISTRATION

The Alignment of received image is one of the conmen steps of image tampering detection. Registration of image is little but difficult job since all the other tasks (e.g., tampering localization) usually assume that the received image is aligned with the original one, and hence could fail if the registration is not properly done. Because of limited information can be used like no any original image is available at destination and image hash should be as short as possible ,Classical registration approaches [11]–[13]cannot be directly employed in the considered context.

The schema of the proposed registration component is shown in Fig. 1. As in [3], [4], and [7], we adopt a BOF-based representation [15] to reduce the dimensionality of the descriptors we employ a transformation model and a voting strategy to retrieve the geometric manipulation [16].

In the proposed system, a codebook is generated by clustering the set of SIFT [17] extracted on training images. The clustering procedure points out a centroid for each cluster. The set of centroids represents the codebook to be used during the image hash generation. The computed codebook is shared between sender and receiver (Fig. 1).

This codebook is built only once, and then used for all the communications between sender and receiver (i.e., no extra overhead for each communication).The sender can extracts all SIFT features and sorts them in descending order with respect to their contrast values. After extracting of all features , the top SIFT are selected and associated to the label corresponding to the closest centroid belonging to the shared codebook. At last, the final signature for the alignment component is created by considering the label, the dominant direction, and the key point coordinates for each selected SIFT (Fig. 1).

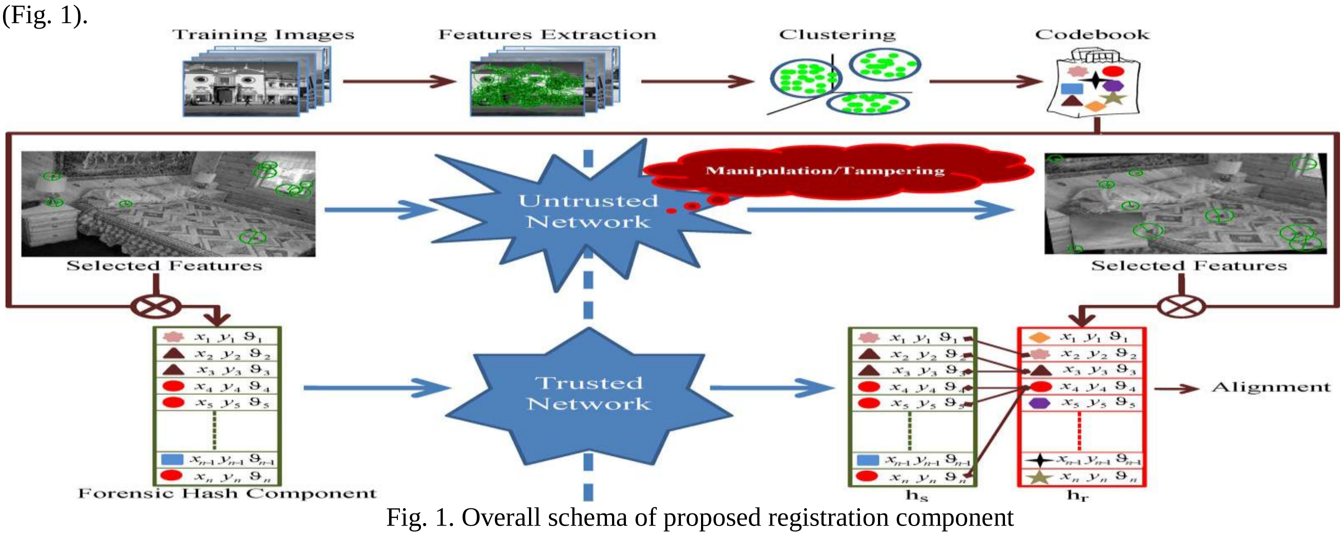

Fig. 1. Overall schema of proposed registration component

The source image and the corresponding hash component for the alignment are sent to the destination. As in [5] the system assumes that the image is sent over a network consisting of possibly untrusted nodes, whereas the signature is sent upon request through a trusted authentication server which encrypts the hash in order to guarantee its integrity.

After reaching the image at its destination, the receiver generates the related hash signature for registration by using the same procedure employed by the sender. Then, the entries of the hashes and are matched by considering the values (see Fig. 1,The alignment is performed by employing a similarity transformation of key point pairs corresponding to matched hashes entries (1) &(2). The earlier transformation is used to model the geometrical manipulations which have been done on the source image during the untrusted communication. Source image points are transforms with destination image point by combining rotate on, scaling and translation process.

III. INDENTATIONS AND EQUATIONS

The image signature to be used for alignment component must be strong enough against malicious manipulations. As well as, the image hash should be that much strong to handle different visual content to be encoded like (textures, contrast variations, etc.).

For the communication purpose a small subset of the strong image features is retained to compose the image hash for the alignment component. Fig. 4 shows an example of malicious tampering which deludes the typical SIFT-based systems presented in [3], [4], [7], and [8]. In Fig. 4(a) the image at the source is shown, whereas the malicious pattern added during the transmission is reported in Fig. 4(b). Sixty SIFT selected by the approach discussed in Section II, at both source and destination, are shown in Fig. 4(c) and Fig. 4(d).

As demonstrated by the figures, all the SIFT extracted by the sender which are used to build the alignment signature are concealed at destination, since all the 60 SIFT . The alignment procedure is hence invalidated, and all further processing to verify the authenticity of the image, to localize the tampered regions, and in general to tell the history of the manipulations of the image, will be unreliable. In order to improve the strongness of the registration phase we suggest modifying the initial step.

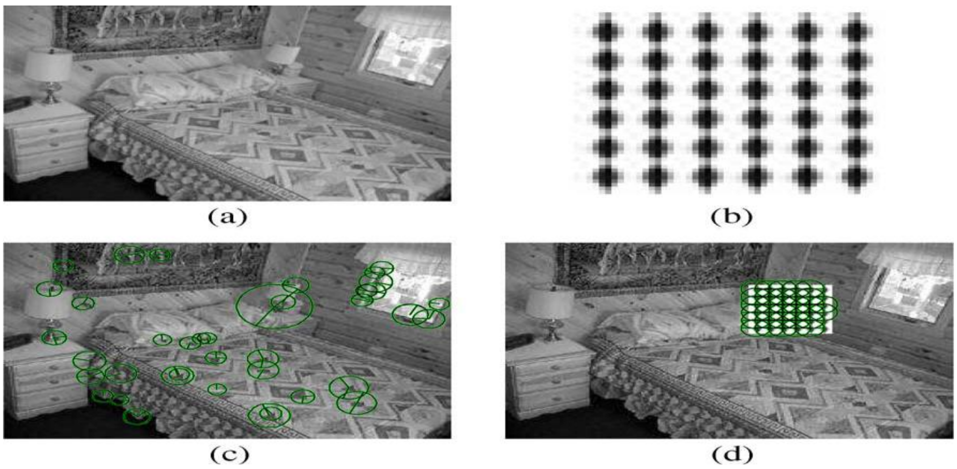

Fig. 4. Concealing true local features: (a) Original image, (b) tampering pattern,
(c) 60 SIFT selected by ordering contrast values on the original image.(d)
The 60 SIFT selected by ordering contrast values on tampered image.

As reported in [19]–[21] the spatial distribution of the features on the entire image is a property that registration algorithms have to take into account. The proposed spatial-based selection process works as follows: first the SIFT are extracted and then grouped taking into account the spatial coordinates of the obtained feature key points. The grouping can be done employing a classic clustering algorithm (k-means, hierarchical clustering, etc.). For each cluster, the best SIFT in terms of contrast value is selected. In this way, the proposed feature selection procedure allows us to extract high contrasted features (corresponding to the clusters) well distributed in the image in terms of spatial position.

IV. FIGURES AND TABLES

The composition of the considered dataset allows for coping with the high scene variability needed to properly test methods in the context of application of this paper. The training set used in the experiments is built through a random selection of 150 images from the aforementioned dataset. Specifically, ten images have been randomly sampled from each scene category. Training and test sets are available for experimental purposes.1 The following image transformations have been considered (Table I): cropping, rotation, scaling, translation, seam carving, tampering, linear photometric transformation and JPEG compression. The considered transformations are typically available on image manipulation software. Tampering on the [22] subset has been performed through the swapping of blocks (50 50) between two images randomly selected from the training

The registration results can be obtained by employing the proposed alignment approach (with and without spatial clustering) with hash component of different size (i.e., different number of SIFT) are reported in Table II

TABLE I
IMAGE TRANSFORMATIONS

Operations	Parameters
Rotation (α)	3, 5, 10, 30, 45 degrees
Scaling (σ)	factor = 0.5, 0.7, 0.9, 1.2, 1.5
Orizontal Traslation (T_x)	5, 10, 20 pixels
Vertical Traslation (T_y)	5, 10, 20 pixels
Cropping	19%, 28%, 36%, of entire image
Tampering	block size 50x50
Malicious Tampering	block size 50x50
Linear Photometric Transformation (a*I+b)	a = 0.90, 0.95, 1, 1.05, 1.10 b = -10, -5, 0, 5, 10
Compression	JPEG Q=10
Seam Carving	10%, 20%, 30%
Realistic Tampering [16]	
Various combinations of above operations	

TABLE II
REGISTRATION RESULTS OF PROPOSED APPROACH

	Mean Error α			
Number of SIFT	15	30	45	60
Unmatched Images	10.99%	3.85%	2.02%	1.56%
Lu et al. [7]	7.3311	7.9970	7.8600	7.4125
Battiato et al. [4]	3.4372	2.4810	2.4718	1.9581
Proposed approach without spatial clustering	1.1591	0.8206	0.5485	0.4634
Proposed approach with spatial clustering	1.7933	0.8288	0.5735	0.4318

TABLE III
COMPARISON WITH RESPECT TO UNMATCHED IMAGES

	Proposed approach							
Number of SIFT	15		30		45		60	
Unmatched Images	5.00%		1.90%		1.04%		0.83%	
Spatial Clustering	without	with	without	with	without	with	without	with
Mean Error α	1.3826	1.9911	0.8986	0.8627	0.6661	0.6052	0.5658	0.4518
Mean Error σ	0.0462	0.0593	0.0306	0.0302	0.0241	0.0200	0.0208	0.0164
Mean Error T_x	2.7672	3.3191	1.8621	1.9504	1.5664	1.5626	1.4562	1.4227
Mean Error T_y	2.6650	3.2428	1.9409	2.0750	1.7009	1.7278	1.6008	1.5944

TABLE IV
AVERAGE ROTATIONAL ERROR

	Unmatched Images			
Number of SIFT	15	30	45	60
Lu et al. [7]	7.87%	2.77%	1.52%	1.16%
Battiato et al. [4]	0.86%	0.48%	0.25%	0.08%
Proposed approach without spatial clustering	3.00%	1.35%	0.87%	0.73%
Proposed approach with spatial clustering	2.53%	0.64%	0.18%	0.10%

TABLE V
AVERAGE SCALING ERROR

	Mean Error σ			
Number of SIFT	15	30	45	60
Unmatched Images	10.99%	3.85%	2.02%	1.56%
Lu et al. [7]	0.0619	0.0680	0.0625	0.0592
Battiato et al. [4]	0.0281	0.0229	0.0197	0.0179
Proposed approach without spatial clustering	0.0388	0.0281	0.0214	0.0183
Proposed approach with spatial clustering	0.0541	0.0287	0.0195	0.0161

As reported in Table III, by increasing the number of SIFT points the number of unmatched images decreases (i.e., image pairs that the algorithm is not able to process because there are no matchings between and) for all the approaches. In all cases the percentage of images on which our algorithm (with and without spatial clustering) is able to work is higher than the one obtained by the approach proposed in [7].

Tables IV and V show the results obtained in terms of rotational and scale estimation through mean absolute error. In order to properly compare the methods, the results have been computed taking into account the images on which all approaches were able to work (the number of unmatched images is reported into the tables). The proposed approach (with and without spatial clustering) out performs [4] and [7] obtaining a considerable
gain both in terms of rotational and scaling accuracy. Moreover, the performance of our approach significantly improves with the increasing of the extracted feature points (SIFT).

A good gain in terms of performance is also obtained with respect to the scale factor (Table V).

TABLE VI
PERCENTAGE OF UNMATCHED IMAGES OBTAINED THROUGH MALICIOUS MANIPULATION

	Unmatched Images			
Number of SIFT	15	30	45	60
Lu et al. [7]	90.50%	87.71%	81.01%	73.74%
Battiato et al. [4]	68.72%	54.19%	29.61%	9.50%
Proposed approach without spatial clustering	87.15%	86.03%	74.86%	64.25%
Proposed approach with spatial clustering	0%	0%	0%	0%

TableVI shows the percentage of malicious manipulated images that cannot be considered by the different approaches (i.e., there are no matchings between and), whereas Tables VII and VIII report the results obtained y the different approaches on the malicious manipulated images have been found.

TABLE VII
AVERAGE ROTATIONAL ERROR ON IMAGES OBTAINED THROUGH MALICIOUS MANIPULATION

	Mean Error α			
Number of SIFT	**15**	**30**	**45**	**60**
Lu et al. [7]	85.6844	79.9884	88.4555	97.4700
Battiato et al. [4]	86.9447	92.0451	92.5144	91.8478
Proposed approach without spatial clustering	35.6087	33.6800	42.5111	38.5156
Proposed approach with spatial clustering	1.2458	0.0000	0.0000	0.0000

In Table IX the different approaches are compared taking into account only the images on which all the approaches are able to find matchings The results demonstrate that robustness can be obtained embedding spatial information during the selection of the features to be used as a signature for the alignment component. The embedded spatial information helps to deal with tampered images obtained by adding patches containing a highly texturized and contrasted pattern.

A novel test dataset has been hence built by using (16) and (17) for shear and (18) and (19) for the anisotropic scale (see Table XI). As reported in Tables XII and XIII the accuracy of the proposed affine solution, although dependent on the degree of the affine warping, can be considered satisfactory. Finally, the results obtained with the affine model by considering the dataset containing all the transformation in Tables I and XI are reported in Table XIV. The obtained results confirm the effectiveness of the proposed approach.

TABLE XI
IMAGE TRANSFORMATIONS

Operations	**Parameters**
Anisotropic Scaling (σ_x or σ_y)	0.7, 0.9, 1.2
Shear (k)	0.05, 0.1, 0.15

TABLE XIV
AVERAGE ERRORS OBTAINED BY PROPOSED SOLUTION BASED ON AFFINE MODEL. SIXTY SIFT HAVE BEEN CONSIDERED IN IMA HASH GENERATION PROCESS

Proposed approach with spatial clustering and affine estimation	
Unmatched	0.0824
Mean Error α	0.2093
Mean Error σ_x	0.0109
Mean Error σ_y	0.0069
Mean Error k	0.0274
Mean Error T_x	1.2210
Mean Error T_y	1.2742

V. CONCLUSION

The main contribution of this paper is related to the alignment of images in the context of distributed forensic systems. A strong image registration component which exploits an image signature based on the BOF paradigm has been introduced. The proposed hash encodes the spatial distribution of features to better deal with highly texturized and contrasted tampering patches. Moreover, a non-uniform quantization of histograms of oriented gradients is exploited to perform tampering localization. The proposed framework has been experimentally tested on a representative dataset of scenes. Comparative tests show that the proposed approach out performs recently appeared techniques by obtaining a significant margin in terms of registration accuracy, discriminative performances and tampering detection. Future works should concern a more in-depth analysis to establish the minimal number of SIFT needed to guarantee an accurate estimation of the geometric transformations and a study in terms of bits needed to represent the overall image signature.

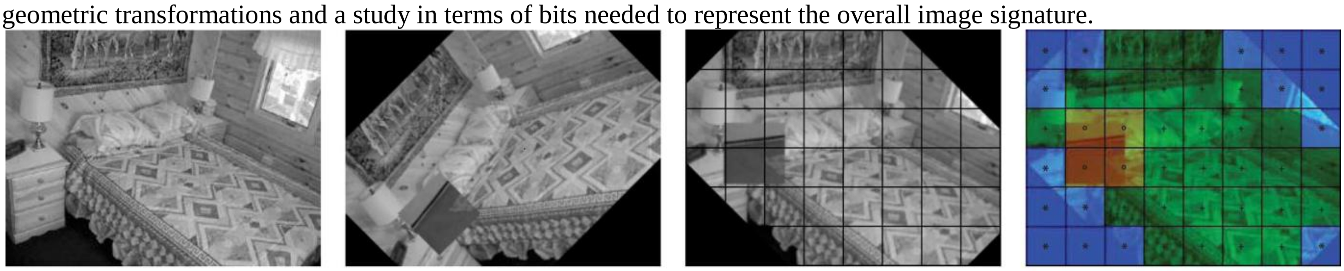

(a) Original image. (b) Tampered image. (c) Image registration. (d) Tampering localization

Fig. 9. Example of proposed tampering detection workflow. In (d) orange indicates recognized tampered blocks, whereas green indicates blocks detected as not tampered. Blue indicates image blocks falling on border of images after registration. The 32 grid in (c) and (d) has been over imposed just for visual assessment. This result has been obtained employing alignment with spatial clustering and non-uniform quantization for tampering detection. (a) Original image. (b) Tampered image. (c) Image registration. (d) Tampering localization.

ACKNOWLEDGEMENTS

I would like to thank all the authors.

REFERENCES

Journal Papers:

[1] Photo tampering throughout history [Online]. Available: www.cs.dartmouth.edu/farid/research/digitaltampering/

[2] H. Farid, "Digital doctoring: How to tell the real from the fake," Significance,vol. 3, no. 4, pp. 162–166, 2006.

[3] S. Battiato, G.M. Farinella, E.Messina, and G. Puglisi, "Robust image registration and tampering localization exploiting bag of features based forensic signature," in Proc. ACM Multimedia (MM'11), 2011.

[4] S. Battiato, G. M. Farinella, E. Messina, and G. Puglisi, "Understanding geometric manipulations of images through BOVW-based hashing," in Proc. Int. Workshop Content Protection Forensics (CPAF 2011), 2011.

[5] Y.-C. Lin, D. Varodayan, and B. Girod, "Image authentication based on distributed source coding," in Proc. IEEE Computer Soc. Int. Conf. Image Processing, 2007, pp. 3–8.

[6] W. Lu, A. L. Varna, and M. Wu, "Forensic hash for multimedia information," in Proc. SPIE Electronic Imaging Symp.—Media Forensics Security, 2010.

[7] W. Lu and M.Wu, "Multimedia forensic hash based on visual words," in Proc. IEEE Computer Soc. Int. Conf. Image Processing, 2010, pp. 989–992.

[8] S. Roy and Q. Sun, "Robust hash for detecting and localizing image tampering," in Proc. IEEE Computer Soc. Int. Conf. Image Processing, 2007, pp. 117–120.

[9] N. Khanna, A. Roca, G. T.-C. Chiu, J. P. Allebach, and E. J. Delp, "Improvements on image authentication and recovery using distributed source coding," in Proc. SPIE Conf. Media Forensics Security, 2009, vol. 7254, p. 725415.

[10] Y.-C. Lin, D. P. Varodayan, and B. Girod, "Didstributed source coding authentication of images with affine warping," in Proc. IEEE Int. Conf. Acoustics, Speech, and Signal Processing (ICASSP 2009), 2009, pp. 1481–1484.

[11] M. Irani and P. Anandan, "About direct methods," in Proc. Int. Workshop Vision Algorithms, held during ICCV, Corfu, Greece, 1999, pp. 267–277.

[12] P. H. S. Torr and A. Zisserman, "Feature based methods for structure and motion estimation," in Proc. Int.Workshop Vision Algorithms, held during ICCV, Corfu, Greece, 1999, pp. 278–294.

[13] R. Szeliski, "Image alignment and stitching: A tutorial," Foundations Trends in Computer Graphics Computer Vision, vol. 2, no. 1, pp. 1–104, 2006.

[14] S. Battiato and G. Messina, "Digital forgery estimation into DCT domain— Acritical analysis," in Proc. ACMConf.Multimedia 2009, Multimedia in Forensics (MiFor'09), 2009.

[15] G. Csurka, C. R. Dance, L. Fan, J. Willamowski, and C. Bray, "Visual categorization with bags of keypoints," in Proc. ECCV Int. Workshop Statistical Learning Computer Vision, 2004.

[16] G. Puglisi and S. Battiato, "A robust image alignment algorithm for video stabilization purposes," IEEE Trans. Circuits Syst. Video Technol., vol. 21, no. 10, pp. 1390–1400, 2011.

[17] D. G. Lowe, "Distinctive image features from scale-invariant keypoints," Int. J. Computer Vision, vol. 60, no. 2, pp. 91–110, 2004. L. Shapiro and G. Stockman, Computer Vision. Upper Saddle River, NJ: Prentice-Hall, 2001.

[18] M. Brown, R. Szeliski, and S. Winder, "Multi-image matching using multi-scale oriented patches," in Proc. IEEE Conf. Computer Vision Pattern Recognition, 2005, vol. 1, pp. 510–517.

[19] L. Gruber, S. Zollmann, D.Wagner, D. Schmalstieg, and T. Hollerer, "Optimization of target objects for natural feature tracking," in Proc. 20th Int. Conf. Pattern Recognition (ICPR 2010), Washington, DC,2010, pp. 3607–3610.

[21] S. Gauglitz, L. Foschini, M. Turk, and T. Hllerer, "Efficiently selecting spatially distributed keypoints for visual tracking," in Proc. IEEE Int.Conf. Image Processing (ICIP 2011), 2011.

[22] S. Lazebnik, C. Schmid, and J. Ponce, "Beyond bags of features: Spatial pyramid matching for recognizing natural scene categories," in Proc. IEEE Computer Soc. Conf. Computer Vision Pattern Recognition, 2006, pp. 2169–2178.

[23] J. Bi and K. P. Bennett, "Regression error characteristic curves," in Proc. Int. Conf. Machine Learning, 2003, pp. 43–50.

[24] S.Maji, A. Berg, and J.Malik, "Classification using intersection kernel support vector machines is efficient," in Proc. IEEE Int. Conf. Computer Vision Pattern Recognition, 2008, pp. 1–8.

International Journal of Modern Engineering Research (IJMER)
www.ijmer.com Vol. 3, Issue. 5, Sep - Oct. 2013 pp-2962-2970 ISSN: 2249-6645

High Speed Infra Red Furnace

1, Mr.Amalorpava Dass. J, 2, Mr.Mohanraj.N 3, Mr. Senthil Vel.C, Mr.Gugan raja.PL)

1.Asst.Professor Aalim Muhammed Salegh College of Engineering,IAF, Avadi, Chennai-600055,
2..Asst.Professor Sri Krishna College of Technology, Covaipudur, Coimbatore-641042.
3. Asst.Professor Aalim Muhammed Salegh College of Engineering,IAF, Avadi, Chennai-600055,
4. Lecturer, VKS College of engineering and technology, desiyamangalam, kulithalai,karur-639120.

ABSTRACT *This project is designed to improve Electrical versus Thermal efficiency. Nowadays electrical heating system converts 65% of the electrical power into thermal power. We have introduced infrared penetration heating system to improve efficiency up to 95% thermal efficiency and 100% electrical efficiency.*

We are going to construct a furnace model to improve our system. A real fabrication model is to analyze IR heating system. The capacity of infrared lamps used inside the furnace will be about 500watts. IR lamps will be used to provide heat.

From the furnace, the temperature is sensed by the thermocouple, which is based on the principle of Seeback effect. The function of a thermocouple is to convert heat energy to mill voltage and it is fed to a signal conditioner to improve the sensitivity and also to improve the non-linear Property of thermocouple. Temperature acquired from the thermocouple is indicated on the screen of the computer. The computer will also compare the temperature acquired with the set temperature and control action if any will be done by the solid-state relay that avoids instantaneous heating. The infrared (IR) heating has the potential to be used for solutionizing of metal forgings with benefits of reduced energy consumption, increased productivity, and improved microstructure and mechanical properties.

In our project, we have integrated heat treatment, annealing, oven and furnace operations are done in a single device. So that the cost of equipment for each process and time taken are reduced.

Key words: *Infrared lamp; Radiation; Furnace; Heat transfer.*

I. INTRODUCTION

1.1. GENERAL

A furnace is a device used for heating. The term furnace is used exclusively to mean industrial furnaces which are used for many things, such as the extraction of metal from ore (smelting) or in oil refineries and other chemical plants, for example as the heat source for fractional distillation columns.

The term furnace can also refer to a direct fired heater, used in boiler applications in chemical industries or for providing heat to chemical reactions for processes like cracking. The benefits of infrared (IR) heating, including short heat-up times, good temperature control, and energy efficiency. Significantly higher heating rates and better temperature control is possible than in conventional convection furnaces. Since heating is on a demand basis, reduced energy consumption is a major advantage, in addition to the shorter production times. For solution treating of forged alloy parts, the improved control at higher heating rates provides the flexibility to solutionize at temperatures closer to the solidus, and for shorter soak times.

The projected savings from IR heating for this application due to reductions in energy consumptions and lead times are about 50%. In addition, it has been shown that enhanced mechanical properties can be obtained by using infrared heating for processing of forgings.

The absence of standard solutionizing procedures using IR furnaces prevents industry from implementing and taking full advantage of this process.

Short soak solution treatment, and fluidized bed solution treatment of aluminum alloy castings are some of the current related work exploring improvements in thermal processing. Improvements in microstructure and mechanical properties using rapid heating have also been explored for other alloy system.

II. FURNACE

2.1 HISTORY

A furnace is a device used for heating. The term furnace is used exclusively to mean industrial furnaces which are used for many things, such as the extraction of metal from ore (smelting) or in oil refineries and other chemical plants, for example as the heat source for fractional distillation columns. The term furnace can also refer to a direct fired heater, used in boiler applications in chemical industries or for providing heat to chemical reactions for processes like cracking and are part of the Standard English names for many metallurgical furnaces worldwide, upto 1709, furnaces could only use charcoal to produce iron. However, wood (which is what charcoal is made from) was becoming more expensive, as forests were being cleared for farmland and timber.

Coal was a possible alternative to wood, but although it was cheap and plentiful, it wasn't a feasible fuel for making iron, because it contained sulphur, and this made the iron too brittle to be of any use.

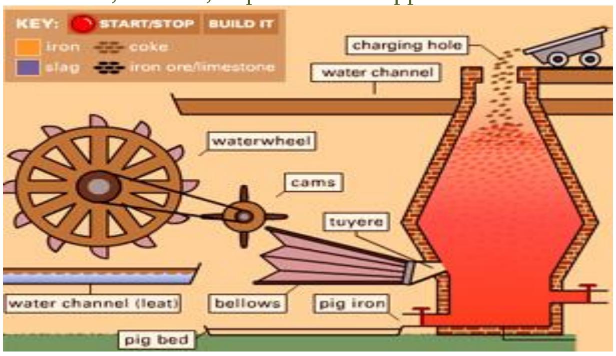

Fig.1

However, in 1709, a man called Abraham Darby finally succeeded in smelting iron using coke (see list of terms below) as fuel, and he bought all his workers beer, in celebration of his discovery. This technological achievement allowed a major expansion of the iron trade, and ultimately it helped lead to the Industrial Revolution. After 1709, Coalbrookdale saw other achievements, such as the first cast-iron bridge - built over the River Severn - and the first cast-iron framed building - built in Shrewsbury.

2.2 TYPES

2.2.1BELLEFONTE FURNACE

Bellefonte Furnace was a hot blast iron furnace located in Bellefonte, Pennsylvania. Founded in 1888, it was the first hot blast, coke-fuelled iron furnace to be built in Centre County, Pennsylvania. While its founders hoped to transform Centre County's iron industry with modern technology, the furnace struggled to operate at a profit and was out of operation from 1893 until 1899. Thereafter, it operated more or less continuously until 1910, and was demolished four years later. It should not be confused with the charcoal-fuelled Bellefonte Furnace and Forge on Logan Branch, which was replaced by Valentine Furnace.

2.2.2INDUCTION FURNACE

An induction furnace is an electrical furnace in which the heat is applied by induction heating of metal. The advantage of the induction furnace is a clean, energy-efficient and well-controllable melting process compared to most other means of metal melting. Most modern foundries use this type of furnace and now also more iron foundries are replacing cupolas with induction furnaces to melt cast iron, as the former emit lots of dust and other pollutants. Induction furnace capacities range from less than one kilogram to one hundred tonnes capacity and are used to melt iron and steel, copper, aluminium and precious metals.

Since no arc or combustion is used, the temperature of the material is no higher than required to melt it; this can prevent loss of valuable alloying elements.

The one major drawback to induction furnace usage in a foundry is the lack of refining capacity; charge materials must be clean of oxidation products and of a known composition and some alloying elements may be lost due to oxidation (and must be re-added to the melt).

Operating frequencies range from utility frequency (50 or 60 Hz) to 400 kHz or higher, usually depending on the material being melted, the capacity (volume) of the furnace and the melting speed required. Generally, the smaller the volume of the melts, the higher the frequency of the furnace used; this is due to the skin depth which is a measure of the distance an alternating current can penetrate beneath the surface of a conductor. For the same conductivity, the higher frequencies have a shallow skin depth - that is less penetration into the melt. Lower frequencies can generate stirring or turbulence in the metal.

2.2.3ELECTRIC ARC FURNACE (EAF)

An electric arc furnace (EAF) is a furnace that heats charged material by means of an electric arc. Arc furnaces range in size from small units of approximately one ton capacity up to about 400 ton units used for secondary steelmaking. Arc furnaces used in research laboratories and by dentists may have a capacity of only a few dozen grams. Industrial electric arc furnace temperatures can be up to 1,800 ° C, (3272 °F) while laboratory units can exceed 3,000 °C. (5432 °F) Arc furnaces differ from induction furnaces in that the charge material is directly exposed to an electric arc, and the current in the furnace terminals passes through the charged material.

2.2.4BLAST FURNACE

A blast furnace is a type of metallurgical furnace used for smelting to produce industrial metals, generally iron. In a blast furnace, fuel, ore, and flux (limestone) are continuously supplied through the top of the furnace, while air (sometimes with oxygen enrichment) is blown into the bottom of the chamber, so that the chemical reactions take place throughout the furnace as the material moves downward.

The end products are usually molten metal and slag phases tapped from the bottom, and flue gases exiting from the top of the furnace. The downward flow of the ore and flux in contact with an up flow of hot, carbon monoxide rich combustion gases is a counter current exchange process. However, the term has usually been limited to those used for smelting iron ore to produce pig iron, an intermediate material used in the production of commercial iron and steel.

2.3 IR FURNACE HISTORY

In 1800 William Herschel, a German astronomer and composer, while testing filters to observe sun spots passed sunlight through a prism, observed a heating effect in the visible red portion of the spectrum. Testing further, he detected the presence of the greatest amount of heat in the area just beyond the red end of the visible spectrum now called Near-Infrared (NIR). He wrote two papers detailing his findings and later that year, presented his discovery of invisible "Calorific rays" to the Royal Society of London. Thirty-five years later Andre-Marie Ampere employed the newly invented thermocouple to demonstrate that near-IR (NIR) radiation was in fact invisible light. It wasn't until 1900 that the term infrared was applied to the part of invisible spectrum contiguous to the red end of the visible spectrum that comprises wavelengths from 0.74 microns to 300 microns.

- Near IR

IR was first used in an industrial process in the 1930's in automotive paint curing applications. It was discovered that NIR (Near Infrared) wavelengths, which are the shortest form of infrared radiation generate the greatest amount of heat. NIR can penetrate most

- Near IR Furnaces

Over 30 years ago, Radiant Technology Corporation pioneered the development of short wavelength infrared continuous belt ovens and furnaces. In the '70's RTC introduced the first high-temperature infrared furnace capable of operating at 1000°C with extremely tight temperature control from 1972 to 2006 RTC became the undisputed leader in infrared heating technology and developed precise, efficient, and reliable thermal processing equipment for the photovoltaic, semiconductor processing.

2.4 OVEN

An oven is a thermally insulated chamber used for the heating, baking or drying of a substance. It is most commonly used for cooking. Kilns and furnaces are special-purpose ovens. The first being used mainly for the fabrication of pottery and the second being used for forging.

A furnace can be used either to provide heat to a building or used to melt substances such as glass or metal for further processing. A blast furnace is a particular type of furnace generally associated with metal smelting (particularly steel manufacture) using refined coke or similar hot-burning substance as a fuel, with air pumped in under pressure to increase the temperature of the fire.

A kiln is a high-temperature oven used in wood drying, ceramics and cement manufacturing to convert mineral feedstock (in the form of clay or calcium or aluminum rocks) into a glassier, more solid form. In the case of ceramic kilns, a shaped clay object is the final result, while cement kilns produce a substance called clinker that is crushed to make the final cement product. (Certain types of drying ovens used in food manufacture, especially those used in malting, are also referred to as kilns.)

An autoclave is an oven-like device with features similar to a pressure cooker that allows the heating of aqueous solutions to higher temperatures than water's boiling point in order to sterilize the contents of the autoclave.

Industrial ovens are similar to their culinary equivalents and are used for a number of different applications that do not require the high temperatures of a kiln or furnace. A wood-fired pizza oven, a type of masonry oven.

III. DESIGN OF WORKING MODEL

3.1 OBJECTIVE

In our project we intend using Infra Red Heating. Heating process is attained through infra red lamps. At a wavelength of 680nm of the infra red lamp, the heating effect starts. We are applying a wavelength of 980 nm. This method offers following advantages over the conventional heating:

- 90% of energy is transmitted as infrared
- Lamp lifetime 5000 hours
- Instant, accurately controllable radiant heat
- Easy installation
- Simple, safe and clean heat source
- High-efficiency, low energy costs

Apart from the heating accuracy and speed provided by the Infra Red lamps the solid state relay also has major advantages in controlling the temperature. Temperature in the furnace is usually controlled by a conventional relay. But a conventional relay is said to work for only one million operations and hence the lifetime is very less. In order to avoid this difficulty and control the temperature for N number of operations and N number of years, we are using a solid-state relay, which is a combination of OPTO TRIAC and SCR connected back to back.

The furnace consists of the infra red lamp which is the heat source. The temperature of the component which is heated is measured using a thermocouple. The output of the thermocouple is conditioned and amplified using signal conditioning equipment. The amplified output is sent to the controller.

The controller receives the signal and displays the temperature for the user to see. It also compares the temperature to the required set point temperature and controls the solid state relay accordingly.

The solid state relay controls the input to the lamp in the furnace according to the command of the controller. If the actual temperature is lesser than the set temperature, the lam is switched ON. If the actual temperature exceeds the required temperature then power to the infra red lamp is cut OFF.

3.2 SPECIFICATIONS

3.2.1 FURNACE SPECIFICATION

- Max. Temperature : 325°C.
- Furnace cube material :Mildsteel sheet(18gauges)
- Insulation material : Mineral wool.
- Inner coating : Berger Alloy coating.
- Area occupied : 1 ½ Feet square.
- Utilization area : 1 feet square

3.2.2 INFRA RED LAMP SPECIFICATION

- Number of lamps : 2.
- Heating type : Radiation heating.
- Input power : 500 watts.
- Wavelength : 980 nm.
- Max. Temperature : Up to 1000°C.

3.2.3 THERMOCOUPLE SPECIFICATION

- Type : K type thermocouple.
- Composition : Ni Chromel- Ni Alumel.
- Range : 0 - 1350°C.
- Speed : 1 microsecond

3.2.4 CIRCUIT SPECIFICATION

- Control action : ± 1°C.
- Interface : LCD/PC display.
- Switching : Solid state relay.
- A to D converter : 12- BIT Channel.
- Interface : embedded controller with serial port.

3.3 COMPONENTS USED

- Furnace cubes
- Insulator material
- Furnace door
- Infra red lamps
- Lamp holders
- Berger alloy coating
- External paint
- Thermocouple

3.3.1 FURNACE CUBES

The furnace cubes are made from mild steel sheets of thickness 18 gauge. The oven is of double walled construction, the gap between the two walls being 50 mm. The sheets are folded and welded to form two identical cubes. One of the cubes is made larger than the other. The inner cube is made closed on all sides except the front. It is made to the dimensions of 1 feet cube. That is 1 feet on all sides. The outer cube is made 1 ½ feet on all sides. The edges are welded and the closing side of the outer cube is bolted closed. Mild steel sheets can handle high temperatures and also form a hard structure to the furnace.

3.3.2 INSULATOR MATERIAL

The insulator used in the furnace is mineral wool. This is a very effective insulator. It is similar to glass wool but more effective. Insulator material is packed in between the outer and inner mild steel cabins. The insulator is loosely packed. It has very low thermal conductivity of k = 0.06 W/mk. Since the mineral wool is loosely packed, the air packets will further increase the thermal resistance, thereby reducing the conduction losses. It may be pointed that air is an excellent insulator having k = 0.02 W/mk. Mineral wool is also called marganite wool. This insulator is so effective that when the inner cabin is at a temperature of around 325°C, the outer surface of the cabin remains only slightly higher than the room temperature. This makes this type of furnace safer and environment friendly.

3.3.3 FURNACE DOOR

The furnace door is made similar to the furnace cube itself. The door is made like a hollow mild steel block by welding the mild steel plates in that form. A gap of half an inch is maintained between the steel plates on both sides. One side of the door is left open initially to insert the insulator material. After the insulator is filled the side is closed using bolts. The door is screwed to the furnace on one side using normal hinges and a small handle is also provided. The door remains closed with the help of a ball-socket type of joint. This allows the door to opened and closed easily

3.3.4 POWER RATING:

The oven has a rating of 500W and can be operated on 230V, single phase, AC supply. The maximum temperature inside the oven is restricted to 325 degree Celsius.

3.3.5 INFRA RED LAMP:

Industrial manufacturing processes are becoming more and more rationalized. Automation increases and production rates rise. To gain the competitive edge, industry today demands innovative, effective heating solutions that will optimize cost of ownership. Infrared heat is transferred from the heat source to the object to be heated without any intermediary.

In our project we have used two Infra Red Lamps each having a capacity of 250 Watts. They transfer heat on to component by means of radiation heat transfer as described in the operation section of our project.

Features:

- 90% of energy is transmitted as infrared
- Lamp lifetime 5000 hours
- Instant, accurately controllable radiant heat
- Easy installation

3.3.6 THERMOCOUPLE

- Two strips of dissimilar metals joined to form junction called thermocouple. If the junction is heated and a milli-voltmeter is connected across the free ends away from the junction, there will be found a voltage present. This voltage is caused by the different work -function of the metals forming the junction and is dependent upon both the temperature and the types of metals used.
- Since the voltage across the thermocouple junction is proportional to temperature we may use it in thermometry. The standard metals and pairs have been adopted for thermocouple construction.

These are:

- Chrome - Alumel
- Iron - Constantan
- Copper - Constantan
- Platinum - Platinum-Rhodium

Additional properties:

It is extremely important that polarity be observed when making connections. There is only one method of determining polarity and that is by knowing which wire is which the wires can be identified by testing them with a permanent magnet. Alumel is slightly magnetic; iron is strongly magnetic, constantan not at all. Copper can be identified by its color.

K TYPE THERMOCOUPLE:

Type K (chromel–alumel) is the most commonly used general purpose thermocouple. It is inexpensive and owing to its popularity They are available in the −200 °C to +1200 °C range. The type K was specified at a time when metallurgy was less advanced than it is today. Another potential problem arises in some situations since one of the constituent metals is magnetic. The characteristic of the thermocouple undergoes a step change when a magnetic material reaches its Curie point. This occurs for this thermocouple at 354°C.

IV. FABRICATION OF WORKING MODEL

4.1 MANUFACTURING PROCESSES

- Furnace fabrication involves bulk deformation processes like sheet metal bending, deep drawing, etc. to obtain the outer casing of the furnace. The first process is the bending of sheet using highly precise anvil. The material used is 18 SWG Mild Steel sheet. This material is strong to enough to withstand very high temperatures and also well suited for the manufacture furnace casing. Since the material is to be deformed to bring it to the required shape, plastic deformation and yield criteria need to be developed upon.
- Plastic deformation of a material depends upon two principal laws of solid mechanics namely, Von – Misces Theory and Guest – Tresca Theory. Both these theories give us the yielding criteria for a specimen based on maximum shear stress and maximum normal stress respectively.
- The process involves bending and deforming the sheet to the required specifications and dimensions as given by the customer. Sheets of sizes 400mm and 300mm are made from huge cold rolled sheet to make the furnace casing. The reason behind using cold rolled sheets is that material undergoes heat treatment processes in cold rolling process and hence is devoid of any porosity. The sheets are bent to the required dimensions. Once the shaped is obtained the inner and outer casing are welded together using clamps within the gap between the walls. The joining process used here welding is highly precis.

4.2 OPERATION

Mass production of painted components can be achieved either by dip coating on a conveyor or spray painting using spray painting booths. After spray painting the component has to be baked at a required temperature as recommended by the paint manufacturer.

This being a project, the operation is intended to be carried out on small components using a prototype oven. The initial warm-up time may be about 30 minutes to 45 minutes. After this the component is placed inside the oven. There will be a temperature drop and it may take about 10 minutes for the oven to attain the set temperature. The subsequent holding time in conventional heating is about 20 minutes to make sure that the baking has been uniform. In Infra Red heating, because of the advantages outlined in section it is seen that the time for baking is only 7 minutes.

4.3 MECHANISM OF HEAT TRANSFER

RADIATION:

The method of heat transfer is primarily through radiation which is governed by Stefan- Boltzmann law, Wien's law and Planck distribution law. Radiation heat transfer is caused as a result of vibrational and rotational movements of molecules, atoms and electrons. The energy is transported by electromagnetic waves (photons). Radiation requires no medium for propagation, therefore can take place also in vacuum. All matters emit radiation as long they have a finite temperature.

The rate at which radiation energy is emitted is usually quantified by Stefan – Boltzmann law

$q = \varepsilon\sigma AT4$

Where the emissivity ε, is a property of the surface characterizing how effectively the surface radiates compared to a black body.

- ❖ σ – Stefan - Boltzmann constant (W/m2 K4).
- ❖ T - absolute temperature of the surface in Kelvin.

A portion of the electromagnetic radiation spectrum is shown below. Thermal radiation lies in the range of 0.1 to 100 micro metres. It includes ultra – violet radiation, visible light and Infra Red radiation. As said above the propagation of thermal radiation takes place in the form of discrete quanta, each having energy of

$E = h\nu$

Where h is the Planck's constant given by h = 6.625*10^-34 joule second.

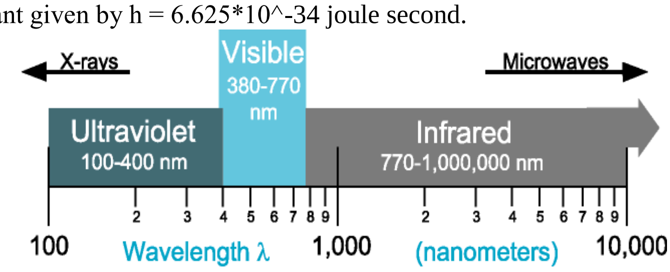

Fig. 1.1 The optical portion of the electromagnetic spectrum

4.4 CIRCUIT OPERATION

- ❖ The temperature of the component is measured by a thermocouple which works on the principle of seebeck effect.
- ❖ According to seebeck " When two dissimilar metals in a circuit are maintained at different temperatures an emf is produced in the circuit"
- ❖ The emf obtained can be calibrated to give the temperature of the component.
- ❖ The e.m.f induced is of small amplitude and there is no linearity. This problem is solved by using a signal conditioner.
- ❖ The signal conditioning equipment may be required to perform linear processes such as amplification, attenuation, integration, differentiation, addition or subtraction. They are also required to do non linear processes such as modulation, demodulation, sampling, filtering, clipping, clamping and etc.
- ❖ After suitable conditioning, the signal is sent to the microcontroller. The micro controller in a small size controller which is embedded into the system to control the input to the furnace.
- ❖ The micro controller is linked to a LCD display through an analog to digital converter to provide interface for easier operation.
- ❖ The TRIAC is a kind of transistor and SCR stands for Silicon Controlled Rectifiers. The solid state relay is used control the power supply to the furnace. They receive input from the micro controller.
- ❖ Conventional heaters work indirectly by warming the air in a room which in turn warms the people and the objects in it. This type of convection heat not only wastes energy by having to warm the air first before the heat is felt, but you also don't feel the benefits of the heater as soon as it is turned on. It might take quite a few minutes for a room to heat up before you feel warmth.
- ❖ Infrared heat on the other hand is a radiant heat which heats you and the objects in the room directly at the speed of light and is not dependent on heating the air first in order for you to feel warmth. You feel the warmth almost instantly once the heater is turned on. This principle makes infrared heaters far more efficient than conventional heaters.
- ❖ Another unique property of infrared heat that makes it so efficient and effective is that the heat is distributed evenly throughout the space and from floor to ceiling. The infrared waves heat the water molecules in the air directly and quickly and because water molecules are denser than air, the heat stays more evenly distributed throughout the room.

Also, water and objects retain heat longer than air, so the heat is not lost as quickly through poor insulation, windows, doors and cracks. The heated air is quickly dissipated through windows, doors, cracks and gaps, so a conventional heater has to work much harder to keep the room at a constant temperature than an infrared heater, making conventional heating methods less efficient and less effective.

V. PROCESS

5.1 HEAT TREATMENT

Heat treating is a group of industrial and metalworking processes used to alter the physical, and sometimes chemical, properties of a material. The most common application is metallurgical. Heat treatments are also used in the manufacture of many other materials, such as glass. Heat treatment involves the use of heating or chilling, normally to extreme temperatures, to achieve a desired result such as hardening or softening of a material. Heat treatment techniques include annealing, case hardening, precipitation strengthening, tempering and quenching. It is noteworthy that while the term heat treatment applies only to processes where the heating and cooling are done for the specific purpose of altering properties intentionally, heating and cooling often occur incidentally during other manufacturing processes such as hot forming or welding.

5.2 Annealing

Annealing is a rather generalized term. Annealing consists of heating a metal to a specific temperature and then cooling at a rate that will produce a refined microstructure. Annealing is most often used to soften a metal for cold working, to improve machinability, or to enhance properties like electrical conductivity.

In ferrous alloys annealing is usually accomplished by heating the metal beyond the upper critical temperature and then cooling very slowly, resulting in the formation of pearlite. In both pure metals and many alloys that can not be heat treated, annealing is used to remove the hardness caused by cold working. The metal is heated to a temperature where recrystallization can occur, thereby repairing the defects caused by plastic deformation. In these metals, the rate of cooling will usually have little effect. Most non-ferrous alloys that are heat-treatable are also annealed to relieve the hardness of cold working. These may be slowly cooled to allow full precipitation of the constituents and produce a refined microstructure.

Ferrous alloys are usually either "full annealed" or "process annealed." Full annealing requires very slow cooling rates, in order to form coarse pearlite. In process annealing, the cooling rate may be faster; up to, and including normalizing. The main goal of process annealing is to produce a uniform microstructure. Non-ferrous alloys are often subjected to a variety of annealing techniques, including "recrystallization annealing," "partial annealing," "full annealing," and "final annealing." Not all annealing techniques involve recrystallization, such as stress relieving.[17]

5.3 Normalizing

Normalizing is a technique used to provide uniformity in grain size and composition throughout an alloy. The term is often used for ferrous alloys that have been heated above the upper critical temperature and then cooled in open air.[17] Normalizing gives harder and stronger steel, but with less ductility for same composition, than full annealing.

5.4 Quenching

Quenching is a process of cooling a metal very quickly. This is most often done to produce a martensite transformation. In ferrous alloys, this will often produce a harder metal, while non-ferrous alloys will usually become softer than normal.

To harden by quenching, a metal (usually steel or cast iron) must be heated above the upper critical temperature and then quickly cooled. Depending on the alloy and other considerations (such as concern for maximum hardness vs. cracking and distortion), cooling may be done with forced air or other gases, (such as nitrogen). Liquids may be used, due to their better thermal conductivity, such as water, oil, a polymer dissolved in water, or a brine. Upon being rapidly cooled, a portion of austenite (dependent on alloy composition) will transform to martensite, a hard, brittle crystalline structure. The quenched hardness of a metal depends on its chemical composition and quenching method. Cooling speeds, from fastest to slowest, go from polymer (i.e.silicon), brine, fresh water, oil, and forced air.

VI. PURPOSE OF THE PERFORMANCE TEST

• To find out the efficiency of the furnace
• To find out the Specific energy consumption

The purpose of the performance test is to determine efficiency of the furnace and specific energy consumption for comparing with design values or best practice norms. There are many factors affecting furnace performance such as capacity utilization of furnaces, excess air ratio, final heating temperature etc. It is the key for assessing current level of performances and finding the scope for improvements and productivity.

Heat Balance of a Furnace

Heat balance helps us to numerically understand the present heat loss and efficiency and improve the furnace operation using these data. Thus, preparation of heat balance is a pre-requirement for assessing energy conservation potential.

Performance Terms and Definitions

1. Furnace Efficiency, η $= \frac{\text{Heat output}}{\text{Heat input}} x100$

$= \frac{\text{Heat in stock (material) (kCals)}}{\text{Heat in fuel / electricity (kCals)}} x100$

2. Specific Energy Consumption $= \frac{\text{Quantity of fuel or energy consumed}}{\text{Quantity of material processed}}$

Reference Standards

In addition to conventional methods, Japanese Industrial Standard (JIS) GO702 "Method of heat balance for continuous furnaces for steel" is used for the purpose of establishing the heat losses and efficiency of reheating furnaces.

Furnace Efficiency Testing Method

The energy required to increase the temperature of a material is the product of the mass, the change in temperature and the specific heat. i.e. Energy = Mass x Specific Heat x rise in temperature. The specific heat of the material can be obtained from a reference manual and describes the amount of energy required by different materials to raise a unit of weight through one degree of temperature.

If the process requires a change in state from solid to liquid, or liquid to gas, then an additional quantity of energy is required called the latent heat of fusion or latent heat of evaporation and this quantity of energy needs to be added to the total energy requirement. However in this section melting furnaces are not considered.

The total heat input is provided in the form of fuel or power. The desired output is the heat supplied for heating the material or process. Other heat outputs in the furnaces are undesirable heat losses.

The various losses that occur in the furnace are listed below.

1. Heat lost through exhaust gases either as sensible heat or as incomplete combustion
2. Heat loss through furnace walls and hearth
3. Heat loss to the surroundings by radiation and convection from the outer surface of the walls
4. Heat loss through gases leaking through cracks, openings and doors.

The efficiency of a furnace is the ratio of useful output to heat input. The furnace efficiency can be determined by both direct and indirect method.

Direct Method Testing

The efficiency of the furnace can be computed by measuring the amount of fuel consumed per unit weight of material produced from the furnace.

$$\text{Thermal efficiency of the furnace} = \frac{\text{Heat in the stock}}{\textit{Heat in the fuel consumed}}$$

The quantity of heat to be imparted (Q) to the stock can be found from the formula

$$Q = m \, x \, C_p \, x (t_2 - t_1)$$

Where

Q = Quantity of heat in kCal

m = Weight of the material in kg

C_p = Mean specific heat, kCal/kg^{o}C

t_2 = Final temperature desired, ^{o}C

t_1 = Initial temperature of the charge before it enters the furnace ^{o}C

Indirect Method Testing

Similar to the method of evaluating boiler efficiency by indirect method, furnace efficiency can also be calculated by indirect method. Furnace efficiency is calculated after subtracting sensible heat loss in flue gas, loss due to moisture in flue gas, heat loss due to openings in furnace, heat loss through furnace skin and other unaccounted losses from the input to the furnace.

In order to find out furnace efficiency using indirect method, various parameters that are required are hourly furnace oil consumption, material output, excess air quantity, temperature of flue gas, temperature of furnace at various zones, skin temperature and hot combustion air temperature. Efficiency is determined by subtracting all the heat losses from 100.

Measurement Parameters

The following measurements are to be made for doing the energy balance in oil fired reheating furnaces (e.g. Heating Furnace)

- Weight of stock / Number of billets heated
- Temperature of furnace walls, roof etc
- Flue gas temperature
- Flue gas analysis
- Electricity consumption Instruments like infrared thermometer, fuel consumption monitor, surface thermocouple and other measuring devices are required to measure the above parameters.

Reference manual should be referred for data like specific heat, humidity etc.

VII. ADVANTAGES

- Rigidness
- No chance of short circuit failure
- Globally compatible transducer
-

VIII. DISADVANTAGES

- Nonlinear
- Requires cold junction compensation
- Poor sensitivity

IX. CONCLUSION

We have designed and fabricated a prototype of an infra red furnace in which heat radiated from infra red lamp is used to achieve quicker and effective heating. Thus we have developed a method to improve the heat treatment process and at the same time decrease the cost of production. Moreover the life of the furnace and components is also increased. The electrical circuit is also accurate and durable hence reducing the cost of maintenance and repair which is a problem with the existing furnaces.

REFERENCES

[1] Phillip F. Ostwald, Jairo Muñoz, Manufacturing Processes and Systems (9th Edition), John Wiley & Sons, 1997 ISBN
[2] 1st Electric Arc *Furnace*; ^ www.worldsteel.org; ^ Preston, R., American Steel. Avon Books, New York, 1991;
[3] Pennsylvania Iron *Furnace* Sourcebook, bibliographical *reference* sources to the Iron *Furnaces* and Iron Works of Pennsylvania.
[4] http://www.freek*heaters*.com/products/infrared_heaters/infrared_heaters.php; ^ Hirsch, Edwin Walter (1922)
[5] History of *Infrared Heating* **...** In good old ancient tradition in postwar Germany, 'stone *heaters*'
[6] Raymond Kane, Heinz Sell Revolution in *lamps*: a chronicleof50**...**http://www.prothermind.com/*InfraredQuartzTubeHeaters*
.
[7] Welty, James R.; Wicks, Charles E.; Wilson, Robert Elliott (1976). Fundamentals of momentum, *heat*, and mass *transfer* (2 ed.).
[8] H. C.: *Radiant Heat* Transmission, in William H. McAdams (ed.) **...** of Some Common Spacecraft Thermal-Control Coatings," NASA *Reference* Publication 1121.

International Journal of Modern Engineering Research (IJMER)
www.ijmer.com Vol. 3, Issue. 5, Sep - Oct. 2013 pp-2971-2977 ISSN: 2249-6645

Automation of Ration Shop Using Plc

Dhanoj Mohan[1], Rathikarani[2], Gopakumar[3]
[1] *Asst Professor, Vimal Jyothi Engineering College, Kannur*
[2] *Asst Professor, Annamali University, Chidambaram*
[3] *Professor, TKM Engineering College, Kollam*

ABSTRACT: *Automatic Ration Dispensing System presented here is an advanced system useful for the automatic & more efficient way of ration distribution. This project is designed to minimize the manual intervention in the process of ration distribution, so that more transparency & efficiency can be maintained*

Our project focuses on design and implementation of Automation of Ration Shop. In recent scenario, all the public and private sectors go for automation in their process. Civil Supplies Corporation is the major public sector which manages and distributes the essential commodities to all the citizens. In that system various products like Rice, sugar and kerosene are distributed using conventional ration shop system. Some of the limitations of conventional ration shop system are Due to the manual measurements in the conventional system, the user can not able to get the accurate quantity of material.

And also there is a chance for the illegal usage of our products in the conventional system. i.e. the materials are robbed by making wrong entries in the register without the knowledge of the ration card holder. Due to that large amount of money given by government gets wasted. The Ration shops cannot able to meet the requirements of the user due to the over population of our country. So the processing speed is low As a result, there is always crowd of people in the ration shop.

I. INTRODUCTION

Automatic Ration Dispensing System presented here is an advanced system useful for the automatic & more efficient way of ration distribution. This project is designed to minimize the manual intervention in the process of ration distribution, so that more transparency & efficiency can be maintained.

Our project focuses on design and implementation of Automation of Ration Shop. In recent scenario, all the public and private sectors go for automation in their process. Civil Supplies Corporation is the major public sector which manages and distributes the essential commodities to all the citizens. In that system various products like Rice, sugar and kerosene are distributed using conventional ration shop system. Some of the limitations of conventional ration shop system are Due to the manual measurements in the conventional system, the user can not able to get the accurate quantity of material.
And also there is a chance for the illegal usage of our products in the conventional system. i.e. the materials are robbed by making wrong entries in the register without the knowledge of the ration card holder. Due to that large amount of money given by government gets wasted. The Ration shops cannot able to meet the requirements of the user due to the over population of our country. So the processing speed is low As a result, there is always crowd of people in the ration shop. Due to the human operations the working hours of the ration shops are restricted, so that the user cannot able to get the material at any time i.e. 24 * 7 basis. To overcome these problems we go for the automation of the ration shops using embedded PLC. In our project, we have desired to control the parameters Level and Load by GEFANUC PLC. Some of the commodities distributed under Public Distribution system are Rice, Kerosene and Sugar

To overcome those problems, we are going for the Automation of ration shop. In our project we designed the hardware for two commodities namely Sugar and Kerosene. These two commodities are stored in reservoir tanks and they are measured and supplied to the user as and when required. The user has to enter the required product and quantity using a keypad andLCD display. For the measuring purposes, we use load cell for sugar and Resistance type Ball float Level Sensor for Kerosene. And these parameters are controlled by the Embedded PLC GEFANUC. Motorized gate valves are used for the measurement and delivery operations. Four tanks are designed, two of them are reservoir tanks and another two of them are delivery tanks.

II. BLOCK DIAGRAM

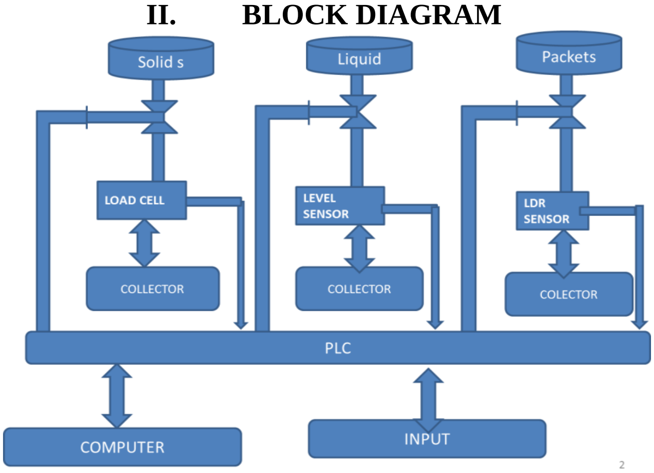

Fig.1: Block Diagram of automatic ration shop system

In automatic ration shop we use PLC for controlling purpose. Three different commodities like sugar/rice, oils and packets/soaps can be counted using three measuring set ups. For programing purpose we use personal computer. Inputs are given directly from mechanical switches and sensors. The controller outputs are used to drive motors and solenoid valves. Different sensor assemblies used are,

III. LEVEL SENSOR

The level station consist of three containers ;

- Reservoir/storage tank
- Measuring chamber
- Collecting flask

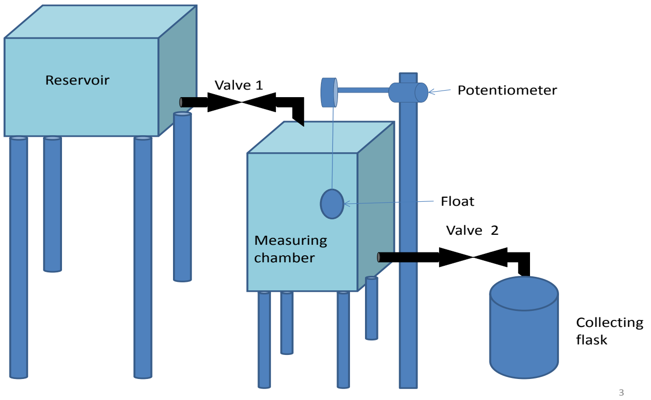

Fig 2: level station

Before the starting of measuring process, the measuring tank level should be a the specified reference level it can be achieved by the operation of on/off valve connected between the reservoir and collecting chamber .Before the starting measuring process the PLC check whether the measuring chamber level is at the reference level. If thru, then measuring process starts by opening the valve V2 it remains open until the specified amount of liquid is discharged from the measuring chamber or collected at the collecting flask.. If the condition is false, then the measuring chamber level is adjusted to the reference level by opening valve V1.

IV. COUNTING STATION

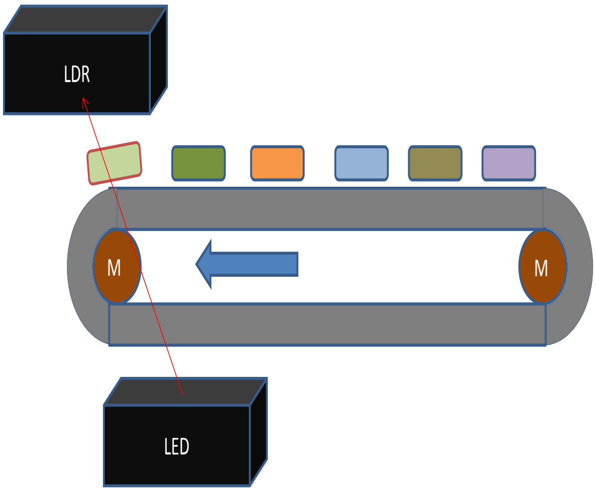

Fig 3: counting station

In counting station we use a LDR sensor circuitry and a conveyer system, the chain conveyer is driven by a high torque 24v dc motor. The rotation of the motor is controlled by PLC output. In LDR sensor setup a LED and LDR are placed in opposite position. When packed items moves through the conveyer, the intensity of light falling on the LDR changes, this change is sensed by the sensor circuitry and counted by PLC. The counting speed of the setup is depends on the sensitivity of LDR so the motor speed should be adjusted with the sensitivity of LDR.

V. LDR SENSING CIRCUIT

This circuit uses a popular timer I.C 555. I.C 555 is connected as comparator with pin-6 connected with positive rail, the output goes high(1) when the trigger pin 2 is at lower then 1/3rd level of the supply voltage. Conversely the output goes low (0) when it is above 1/3rd level. So small change in the voltage of pin-2 is enough to change the level of output (pin-3) from 1 to 0 and 0 to 1. The output has only two states high and low and cannot remain in any intermediate stage. Pin

4, 6 and 8 is connected to the positive supply and pin 1 is grounded. To detect the present of an object we have used LDR and a source of light. LDR is a special type of resistance whose value depends on the brightness of the light which is falling on it. It has resistance of about 5k ohm when in total darkness, but a resistance of only about 1k ohms when brightness illuminated. It responds to a large part of light spectrum. We have made a potential divider circuit with LDR and 4.7K variable resistance connected in series. We know that voltage is directly proportional to conductance so more voltage we will get from this divider when LDR is getting light and low voltage in darkness. This divided voltage is given to pin 2 of IC 555. Variable resistance is so adjusted that it crosses potential of 1/3rd in brightness and fall below 1/3rd in darkness.
Sensitiveness can be adjusted by this variable resistance. As soon as LDR gets dark the voltage of pin 2 drops1/3rd of the supply voltage and pin 3 gets high and LED or buzzer which is connected to the output gets activated.

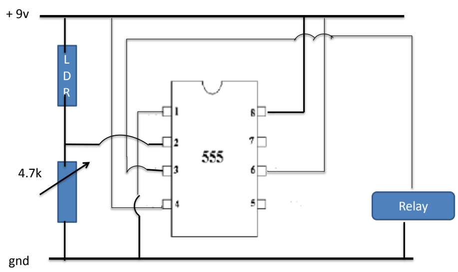

Fig 4: LDR sensing circuit.

When light falls on the LDR then its resistance decreases which results in increase of the voltage at pin 2 of the IC 555. IC 555 has got comparator inbuilt, which compares between the input voltage from pin2 and 1/3rd of the power supply voltage. When input falls below 1/3rd then output is set high otherwise it is set low. Since in brightness, input voltage rises so we obtain no positive voltage at output of pin 3 to drive relay or LED, besides in poor light condition we get output to energize

VI. AMPLIFYING CIRCUIT

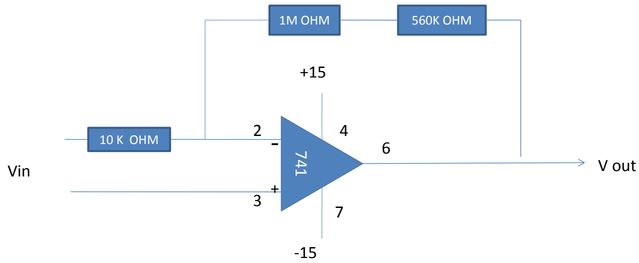

VII. COMPONENT SPECIFICATION

VII.1. LOAD CELL

The Wheatstone bridge configured above is a simple diagram of a load cell. The resistors marked T1 and T2 represents train gauges that are placed in tension when load is applied to the cell. The resistors marked C1 and C2 represent strain gauges which are placed in compression when load is applied. The +In and -In leads are referred to as the +Excitation (+Exc) and -Excitation (-Exc) leads. The power is applied to the load cell from the weight indicator through these leads. The most common excitation voltages are 10 VDC, and15 VDC depending on the indicator and load cells used. The +Out and -Out leads are referred to as the +Signal (+Sig) and -Signal (-Sig) leads. The signal obtained from the load cell is sent to the signal inputs of the weight indicator tobe processed and represented as a weight value on the indicator's digital display.

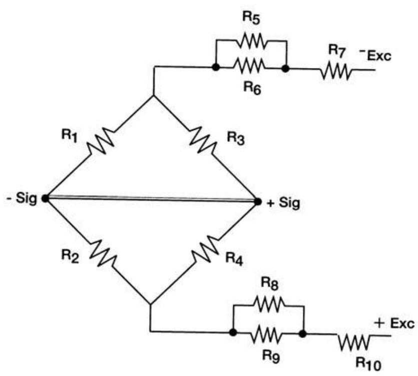

Fig 6: Load cell circuit

As weight applied to the load cell, the gauges C1 and C2 compress. The gauge wire becomes shorter and its diameter increases. This decreases the resistances of C1 and C2. Simultaneously, gauges T1 and T2 are stretched. This lengthens and decreased the diameter of T1 and T2, increasing their resistances.

Fig.7: Strain gauge load cell

COLOUR	TERMINAL
RED	+ INPUT
GREEN	+ OUTPUT
WHITE	- OUTPUT
BLACK	- INPUT

Table 1: load cell output

These changes in resistances cause more current to flow through C1 and C2 and less current to flow through T1 and T2. Now a potential difference is felt between the outputs or signal leads of the load cell. Let’s trace the current flow through the load cell. Current is supplied by the indicate through the -In lead. Current flows from -In through C1 and through -Out to the indicator. From the indicator current flows through the +Out lead, through C2 and back to the indicator at +In.

VII.2. LIGHT DEPENDING RESISTOR

LDR (Light dependent resistor) Engineering is a technique of making several electronics circuits following the logic of a simple light and dark sensor using transistors, 555 IC and 741 IC. Out of several optical sensors, light dependent resistor can be used for making light/dark sensors. A dark sensor switches on transistor or LED whenever the incident light intensity is decreased, whereas a light sensor works in opposite way.

In LDR Engineering, we first understand the working principle of any circuit using LDR, and then we replace the LDR with a fixed resistor or some other electronic component that makes the simple automatic light/dark sensor work as a completely different device.

Making automatic light/dark sensor circuits using different methods can make you observe several electronics components. On the other hand, modifying those automatic light/dark sensor circuits to some functionally different circuits like touch switch,water level indicator, clap switch, etc. can make you understand about those circuits. In this article, we will see how we can use the concept of a dark sensor to make a touch and a clap switch

VII.3. RELAY

A relay is an electrically operated switch. Many relays use an electromagnet to operate a switching Mechanism mechanically, but other operating principles are also used. Relay are used where it is necessary to control a circuit by a low-power signal or where several circuit must be controlled by one signal. The first relays were used in long distance telegraph circuits, repeating the signals coming in from one circuit and retransmitting into another. Relays were used extensively in telephone exchanges and early computers to perform local operations.

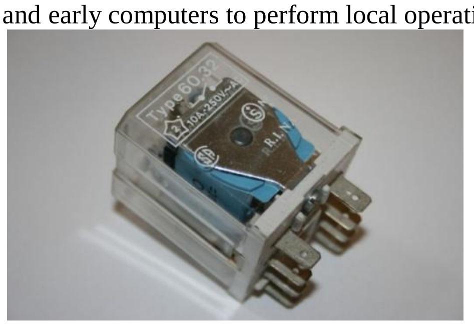

Fig.8: relay

A type of relay that can handle the high power required to directly control an electric motor is called a conductor. Sol id state relays control power circuit with no moving parts instead using a semiconductor device to perform switching. Relays withcalibrated operating characteristics and sometimes multiply operating coils are used to protect electrical circuits from over load or faults; in modern electric power systems this functions are performed by digital instruments still called “protective relays”.

VII.3.1 BASIC DESIGN AND OPERATION

A simple electromagnetic relay consist of a coil of wire surrounding a soft iron core, an iron yoke which provides a low reluctance path for magnetic flux, a movable iron armature, and one or more sets of contacts. The armature is hinged to the yoke and mechanically linked to one or more sets of moving contacts. It is held in place by spring so that when the relay is de-energized there is an air gap in the magnetic circuit. In this condition, one of the two sets of contacts in the relay pictured are closed, and the other is open.

Other relays may have more or fewer sets of contacts depending on their functions. The relay in the picture also has a wire connecting the armature to the yoke. This ensures continuity of the circuit between the moving contacts on the armature, and the circuit track on the printed circuit via the yoke, which is soldered to the PCB.

When an electric current is passed through coil it generates a magnetic field that attracts the armature and the consequent movement of the movable contact either makes or breaks a then movement opens the contacts and breaks the conWhen the current to the coil is switched off, the armature is returned by the force approximately half as strong as the magnetic force, to its position relaxed position. Usually this force is provided by a spring, but gravity is also used commonly in industrial motor starters. Most relays are manufactured to operate quickly. In a low voltage application this reduces noise; ina high voltage or current application it reduces arcing.

When the coil is energized with direct current a diode often placed across the coil to dissipate the energy from the collapsing magnetic field at deactivation, which would otherwise generate a voltage spike dangerous to semiconductor circuit components. Some automotive relays include a diode inside the relay case. Alternatively, a contact protection network consisting of a capacitor and resistor in series may absorb the surge. If the coil is designed to be energized with alternating current, a small copper “shading ring” can be climbedto the end of the solenoid
section, andvice versa if the contacts were open ., creating a small out- of-phase current which increases the minimum pull on the armature during the AC cycle. A solid state relay uses a thyristor or other solid state switching device, activated by the control signal, to switch the control load instead of a solenoid

VII.4. POTENTIOMETERS

The humble potentiometer (or pot, as it is more commonly known) is a simple electro-mechanical transducer. It converts rotary or linear motion from the operator into a change of resistance, and this change is (or can be) used to control anything from the volume of a hi-fi system to the direction of a huge container ship.

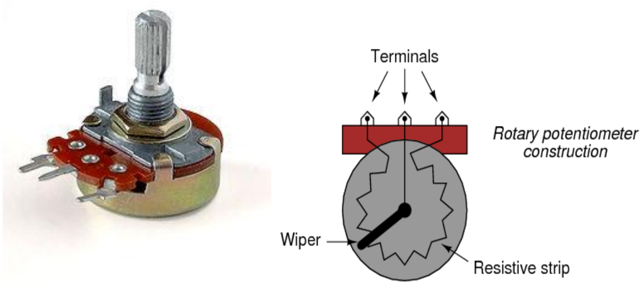

Fig.9: potentiometer

The pot as we know it was originally known as a rheostat (or rheostat in some texts) - essentially a variable wire wound resistor. The array of different types is now quite astonishing, and it can be very difficult for the beginner (in particular) to work out which type is suitable for a given task. The fact that quite a few different pot types can all be used for the same task makes the job that much harder - freedom of choice is at best confusing when you don't know what the choices actually are, or why you should make them. This article is not about to cover every aspect of pots, but is an introduction to the subject. For anyone wanting to know more, visit manufacturers' web sites, and have a look at the specifications and available types.

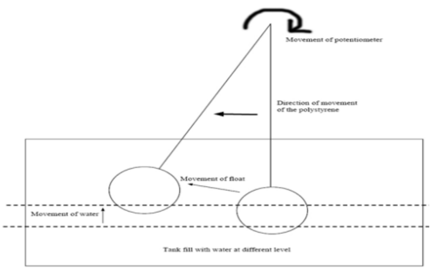

Fig.10: potentiometer movement with level

The very first variable resistors were either a block of carbon (or some other resistive material) with a sliding contact, or a box full of carbon granules, with a threaded screw to compress the granules. More compression leads to lower resistance, and vice versa. These are rare in modern equipment, so we shall limit ourselves to the more common types

VII.5 SOLENOID VALVES

The type of solenoid valve refers to whether that valve is a 2-way, 3-way or 4-way. A 2-way valve (Figure 1) has two port connections-a pressure or input port (port 1) and an outlet port (port 2). These valves are used to stop the flow of a fluid or start the flow of a fluid in a piping configuration. Usually, a 2-way valve is referred to as a 2/2 valve, which means the valve has two ports and two positions. The positions are: 1) on or energized and 2) off or de-energized.

Fig.11: solenoid valve

Three-way valves (Figure 2) are those that have three ports-a pressure or inlet port (port 1), a cylinder port (port 2) and an exhaust port (port 3). A 3-way valve's most common application is for process valve automation. The solenoid valve sends air to a spring return actuator or cylinder, which creates rotational or linear movement to open or close a process valve.In this case, the media is usually compressed air or gas that is creating work, which is where the term "fluid power" is derived. The power of a compressed gas or pressurized liquid is controlled to create mechanical work. Three-way valves are usually referred to as 3/2 valves-they have three ports and two positions.
Operation is a word used to describe if a valve is normally open (NO), normally closed (NC) or universal (U). NO and NC refers to the state of a 2-way solenoid valve when de-energized or off. NO, NC or U is used to describe the state of a 3-way valve when it is de-energized or off. Below is a table that describes operation modes of 2-way and 3-way valves.

VII.6. HIGH TORQUE DC GEARED MOTOR 100RPM

- High torque DC motor with Metal Gear box and off centered shaft.
- 100 12V DC geared motors for robotic application.
- It gives a massive torque of 35 Kgcm.
- The motor comes with metal gear box and off centered shaft.
- 6mm diameter shaft with M3 thread hole.
- Gear box diameter 37mm.
- Motor diameter 28.5mm.
- Length 63mm without shaft.
- Shaft length 15mm.
- 150gm Wight.
- No load current 800mA, load current up to7.5A.

VIII. FLOW CHART

VIII.1 LEVEL STATION

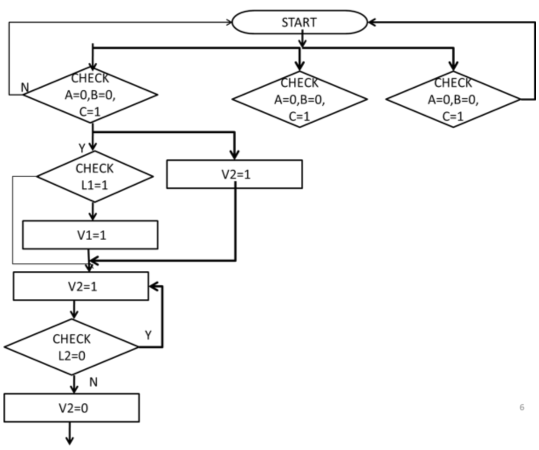

VIII.2. WEIGHING SECTION

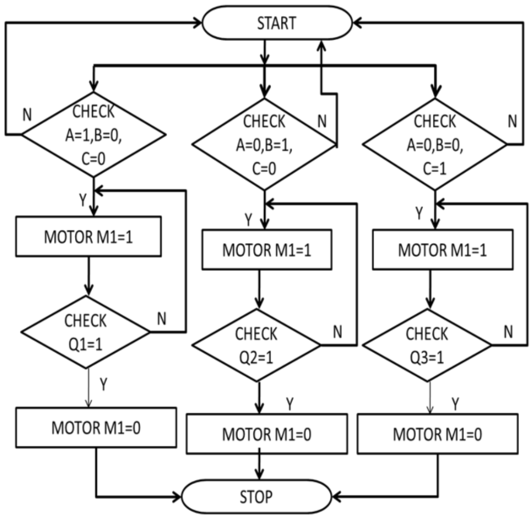

VIII.3. COUNTING STATION

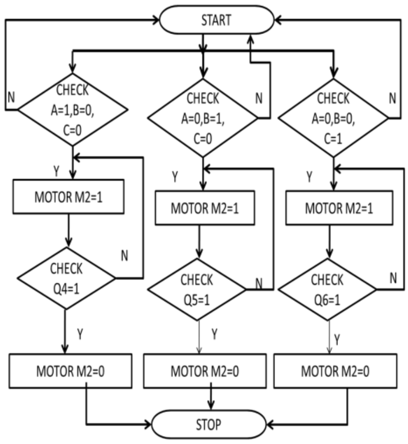

IX. ADVANTAGES

- Reliability
- PLC/DCS along with upper computer raises the system reliability.
- The upper computer is not with the real time control process of PLC/DCS, except gives the order of initial process parameters and control; therefore, the upper computer is off-line, PLC/DCS can successfully go through the production.
- Mixed programming with high-level and assembly languages.
- Not only ensure the system reliability, but also benefit for software upgrade;
- Make operation easy and intuitive;
- Visualization
- Flexibility
- Bring transparent.

X. CONCLUSIONS

Our project focuses design and implementation of Automation of Ration Shop. In recent scenario, all the public and private sectors go for automation in their process.. In that system various products like Rice, sugar and kerosene are distributed using conventional ration shop system. Some of the limitations of conventional ration shop system are Due to the manual measurements in the conventional system, the user can not able to get the accurate quantity of material.Through our project we are overcome these problems.

REFERENCES

[1.] Process measurement and analysis by liptak, Mcgraw Hill
[2.] Mechatronics by W Bolton,pearson education ltd
[3.] Programmable logic controller principles and applications by john W.Webb prentice hall of india
[4.] http:/www.youtube.com/watch?v=mus7uqfqk
[5.] http:/www.youtube.com/watch?v=YBwvkaswynm
[6.] en.wikipedia.org/wiki/relay
[7.] ikalogic.com/ldr_sensor.php

Experimental Comparison Study for Savonius Wind Turbine of Two & Three Blades At Low Wind Speed

Mohammed Hadi Ali
Lecturer University of Mustansiriya

ABSTRACT: *In this project, experimental comparison and investigations were carried out to study the performance and to make a comparison between two and three blades Savonius wind turbine.*
For this purpose, two models of two and three blades were designed and fabricated from Aluminum sheet, each of them has an aspect ratio of (A_s = H/D =1), the dimension is (H = 200 mm height and diameter D = 200 mm) and the blades were made of semi – cylindrical half of diameter (d = 100 mm). The two models were assembled to have (overlap e = 0 and a separation gap $e' = 0$).

These two models were tested and investigated by using a subsonic wind tunnel that was fabricated for this purpose under a low wind speed due to many reason mostly that the savonius wind turbine has its maximum performance at (λ = TSR = 1) and a high starting torque at low wind speed.

It was observed from the measured and calculated results that the two blades savonius wind turbine is more efficient, it has higher power coefficient under the same test condition than that of three blades savonius wind turbine.
The reason is that increasing the number of blades will increase the drag surfaces against the wind air flow and causes to increase the reverse torque and leads to decrease the net torque working on the blades of savonius wind turbine.

I. INTRODUCTION:

The renewable energy is considered as a new technology and an alternating energy source to be used instead of fossil fuel, its continuous rising cost of it and due to growing concern to reduce the effects of climate change, such as global warming, generated by extensive and deliberate use of fossil fuels, mainly in the electric power generating plants and transport.

Global warming will continue unless dependence on fossil is reduced, thus the Wind power has a key role in reducing greenhouse gas emissions [ref. 1].

Today, the most commonly used wind turbine is the Horizontal Axis Wind Turbine (HAWT), where the axis of rotation is parallel to the ground. However, there exist other types of wind turbines, one of which will be the primary focus of this paper, the Vertical Axis Wind Turbine (VAWT). These devices can operate in flows coming from any direction, and take up much less space than a traditional HAWT [ref. 2], and VAWT are definitely a credible source of energy for the future [ref. 1].

VAWTs have a number of advantages over HAWTs, such as [ref. 3]:
1) Simple construction, they can be made from oil barrels cut in two halves.
2) Extremely (low cost), simplicity reduces cost of construction, and aids installation.
3) They can accept wind from any direction, thus eliminating the need for re-orienting towards the wind.

VAWTs work well in places with relatively low wind strength, and constant winds, VAWTs include both a drag-type configuration, such as the Savonius rotor, and a lift-type configuration, such as the Darrieus rotor [ref. 4].

II. PRINCIPLES OF SAVONIUS ROTOR WIND TURBINE:

Savonius turbines are one of the simplest turbines. Aerodynamically, they are drag-type devices, consisting of two or three blades (vertical – half cylinders). A two blades savonius wind turbine would look like an "S" letter shape in cross section (figure 1).

The savonius wind turbine works due to the difference in forces exert on each blade. The lower blade (the concave half to the wind direction) caught the air wind and forces the blade to rotate around its central vertical shaft. Whereas, the upper blade (the convex half to wind direction) hits the blade and causes the air wind to be deflected sideway around it.

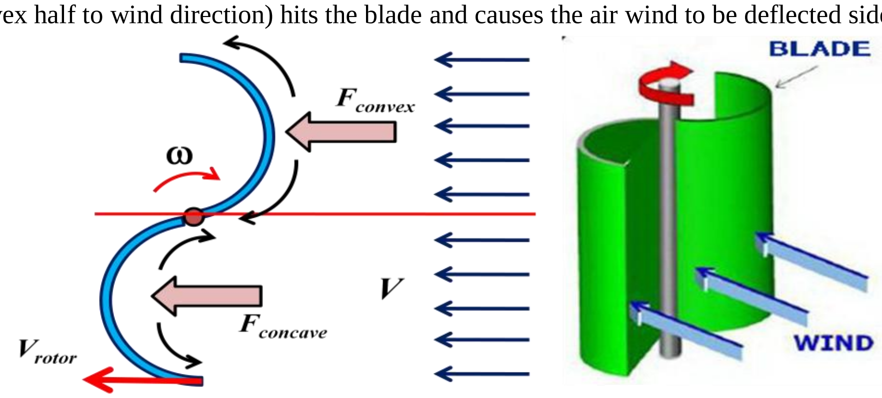

Figure (1): Schematic drawing showing the drag forces exert on two blade Savonius.

Because of the blades curvature, the blades experience less drag force (F_{convex}) when moving against the wind than the blades when moving with the wind ($F_{concave}$). Hence, the half cylinder with concave side facing the wind will experience more drag force than the other cylinder, thus forcing the rotor to rotate. The differential drag causes the Savonius turbine to spin. For this reason, Savonius turbines extract much less of the wind's power than other similarly sized lift type turbines because much of the power that might be captured has used up pushing the convex half, so savonius wind turbine has a lower efficiency.
Similarly, the three blade savonius wind turbine is constructed from three half cylinders, they are arranged at (120^o) relative to each other as shown in figure (2).

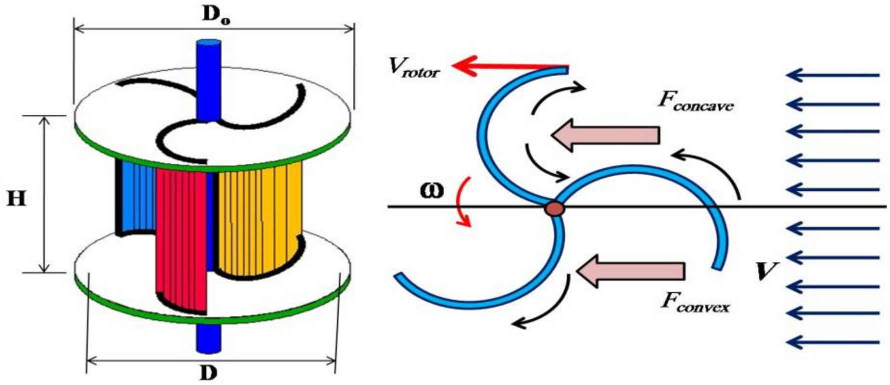

Figure (2): Schematic drawing showing the drag forces exert on three blade Savonius.

III. THE RESEARCH GOAL:

The goal of this research is to carry out a study and make a comparison in performance between two and three blades savonius wind turbine at low wind speed, the reasons to study them at low speed are:

1. In many areas in the world apart from coastal region, the average wind speed is relatively low and varies appreciably with seasons. It is around 20 km/h.
2. A Savonius rotor requires (30 times) more surface for the same power as a conventional rotor blade wind turbine. Therefore it is only useful and economical for small power requirements [ref. 5].
3. It has a high starting torque; a Savonius rotor can theoretically produce energy at low wind velocities [ref. 6].
4. It is difficult to protect them from extreme winds [ref. 7].
5. The peak power coefficient for any Savonius rotor occurs at a tip speed ratio (less than 1) [ref. 7].
6. Lower wind speeds found at lower heights, thus VAWT like savonius can be installed close to the ground without an extended post with the generator and the driven train mounting at the base near the ground level which makes these components easier to service and repair.

IV. EXPERIMENTAL RIG DESIGN:

The Wind Tunnel:

A subsonic wind tunnel was designed and fabricated for the experimental part of this research as shown in the schematic drawing and the experimental rig construction [figure 3]. The wind tunnel was designed using plywood modeling and fabricated at laboratory workshop. The wind tunnel is (250 cm) long which consists of fan section (with circular mouth entry), rectangle section, converging section and square exit section with straightener section.

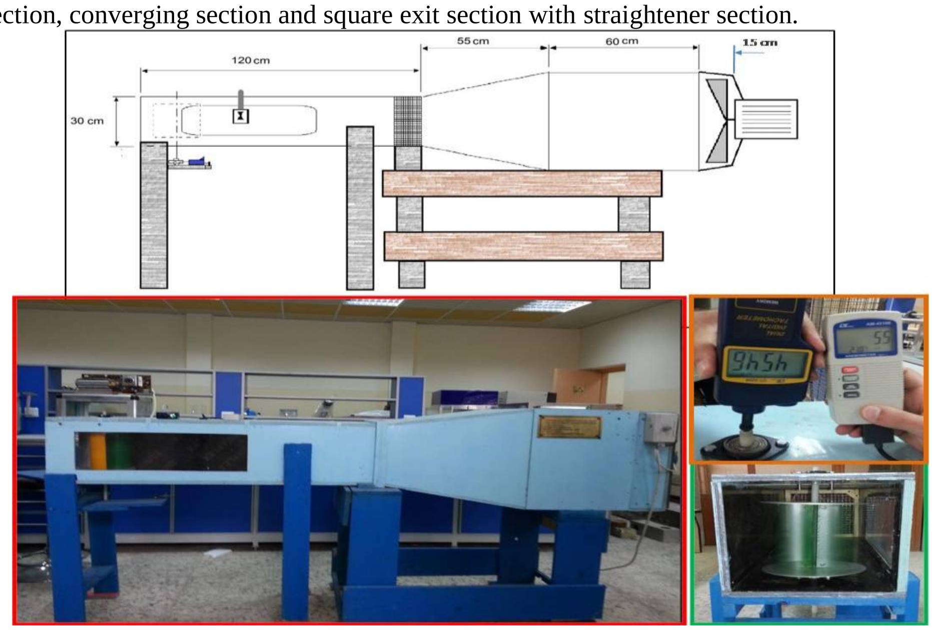

Figure (3): Schematic drawing & the Experimental rig with Savonius blade model.

www.ijmer.com Vol. 3, Issue. 5, Sep - Oct. 2013 pp-2978-2986 ISSN: 2249-6645

a) The Fan section – The axial flow fan is mounted and encased in a circular mouth casing. The capacity of the fan is 4500 m^3/hour at 1500 rpm. The fan is driven by a single phase 0.5 kW motor.
b) The Rectangular section – it is made of plywood to make the entry of the air blowing from the fan into the diverging section and to decay turbulence.
c) The Diverging section – it is a contraction zone made of plywood to produce a uniform velocity distribution with weak turbulence in Straightener section.
d) The Straightener section – it is at the entrance of the test section to break the large scale disturbances and eddies. The Straightener comprises a number of plastic sheet meshed together to form a square cells shape to straighten the air flow and their axis parallel with the direction axis of the tunnel.
e) Test Section - it has four sides made of plywood. One of the vertical sides has a window with glass plate for seeing the testing models. Part of the upper side can be opened to change the testing models. There is a hole in the upper plate for inserting a wind speed instrument. The four sides make square section of dimension (30 cm X 30 cm) with a length of (120 cm).
f) The Air Speed Regulator – it used to control the air speed flowing through the wind tunnel to represent a change in wind speed.

The Savonius rotor blades:

The savonius rotor blades (the model) was designed and fabricated. The model was tested in the wind tunnel for various air flow speed conditions.
The material choice to fabricate such models for two and three savonius wind turbine depends mainly on many criterions. Aluminum is the best choice due to its light weight, corrosion resistance, rigidity, recyclable materials, easy to construct and low cost [ref. 8].
The dimensions of these rotors were selected to have an aspect ratio (A_a = H / D = 1), thus the blades (scoops) were made of semi-cylindrical scoops of diameter (d = 100 mm), height of (H = 200 mm) and thickness of (0.079 mm).
These blades were assembled and mounted on two Aluminium disc sheets (End plates) of diameter (D_o = 210 mm) and thickness of (1.59 mm) to obtain a better performance (figure 4). Both the semi- cylindrical blades and the two end plates were assembled to a central shaft.

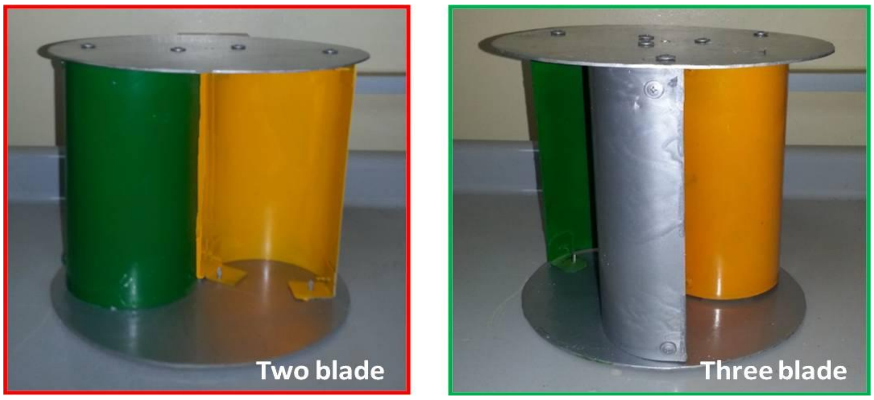

Figure (4): The fabricated models of two & three blades Savonius wind turbine.

The measuring instruments:

The experiment was carried out at different wind speeds [V = 2 m/s, to V = 6 m/s] and data was recorded at room temperature.
Different digital instruments were used to measure and record the required data. The rotational speed (N) of the rotor blade speed was measured using a photo - contact tachometer (model: DT-2268). The rotational speed was measure by using a digital tachmeter to calculate the angular velocity (□) and then the rotor tip velocity (V_{rotor}). The wind speed (V) was determined using the digital Thermo – Anemometer (model: AM-4210E). The anemometer vane was mounted and fixed in the wind tunnel - test section between the straightener and the testing savonius wind turbine.
The static torque was measured by measuring the tangential force exerted on the savonius rotor shaft by digital electronic force meter (*WeiHeng* model).

V. THE BASIC CONCEPTS:

The performance of savonius wind turbine can be explained according to the following three basic rules that are still applicable [ref. 7]:

1. The speed of the blade tips is ideally proportional to the speed of wind.
2. The maximum torque is proportional to the speed of wind squared.
3. The maximum power is proportional to the speed of wind cubed.

The performance of any kind of wind turbine can be expressed in the form of torque coefficient (C_t) and the coefficient of power (C_p) versus the tip speed ratio ( ).

The swept area (A_s):

As the rotor turns, its blades generate an imaginary surface whose projection on a vertical plane to wind direction is called the *swept area* [ref. 9].

The amount of energy produced by a wind turbine primarily depends on the rotor area, also referred to as cross-sectional area, swept area, or intercept area.

The swept area for Savonius wind turbine can be calculated from the dimensions of the rotor (Figure 5).

Savonius area = The swept area = $A_s = H * D$

Where: H = the rotor height (m).

D = the rotor diameter (m).

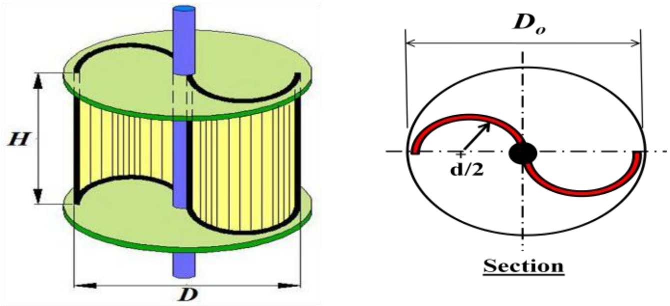

Figure (5): Schematic diagram of Savonius rotor wind turbine.

The Tip speed ratio ( ):

The tip speed ratio is the ratio of the product of blade radius and angular speed of the rotor to the wind velocity [ref. 10]. The tip peripheral velocity of the rotor (V_{rotor}) is defined as (Figure 6):

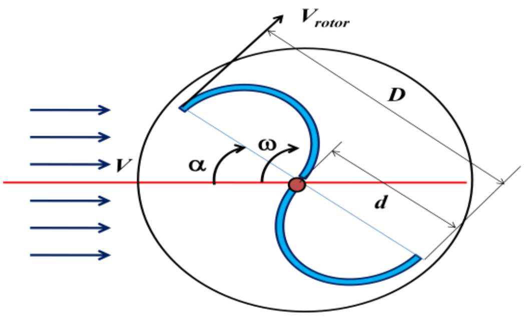

Figure (6): Scheme of a Savonius rotor showing the tip velocity of the rotor.

$$V_{rotor} = \omega * d$$

Where: V_{rotor} = the tip speed (the peripheral velocity of Savonius rotor) (m/sec)

ω = the angular velocity of Savonius rotor (rad/sec).

d = the diameter of the semi-cylindrical Savonius rotor (m).

Now the Tip Speed Ratio (TSR) of a turbine is expressed as:

$$\textit{The tip speed ratio } (TSR) = \lambda = \frac{V_{rotor}}{V} = \frac{\omega * d}{V}$$

Where: V = the wind speed (m/sec)

The Torque Coefficient (C_t):

It is defined as the ratio between the actual torque developed by the rotor (T) and the theoretical torque available in the wind (T_w) [ref. 11], thus the torque coefficient (C_t) is given by:

$$C_t = \frac{\textit{the rotor Torque}}{\textit{the wind Torque}} = \frac{T}{T_w} = \frac{T}{\frac{1}{4}\rho * A_s * d * V^2}$$

Where: C_t = the torque coefficient

T = the rotor torque (N . m)

T_w = the wind available torque (N . m)

ρ = the air density (kg/m^3)

Another concept that can used to measure the wind turbine performance is the static torque (T_s), which measures the self-starting capability of the turbine. Static torque is defined as a maximum value of the torque when rotor is blocked i.e. without ability to rotate [ref. 12]. So, the static torque coefficient is given by:

$$C_{ts} = = \frac{T_s}{T_w} = \frac{T_s}{\frac{1}{4}\rho * A_s * d * V^2}$$

Where: C_{ts} = the static torque coefficient

T_s = the rotor static torque (N . m)

The static torque of different angle of attack (α) relative to the wind direction was measured at every (30^o) to (360^o). Figure (7) shows the angle of attack (α) for both two and three blades savonius wind turbine.

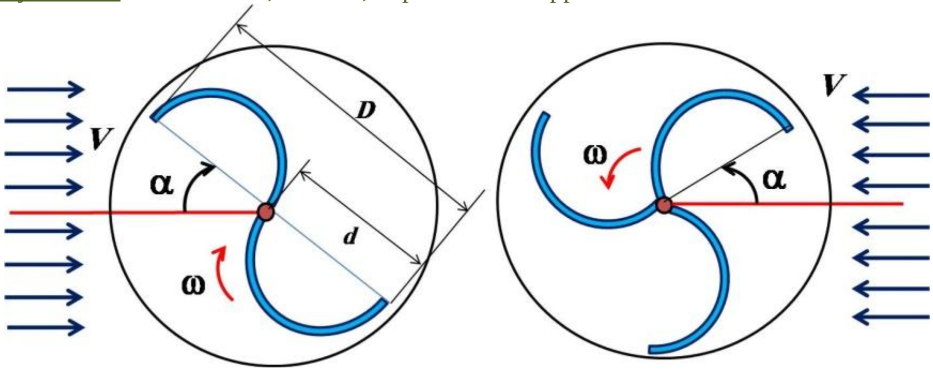

Figure (7): Scheme of a Savonius rotor showing the angle of attack ( ).

The torque is defined as the force acting tangentially over the rotor blade, operating at a distance of rotor radius (*d*) from the centre, it is given as:

$$T = I \, . \, \alpha$$

Where: I = the rotor moment of inertia [(kg . m^2) or (N . m . s^2)]

 = the rotor angular acceleration (1 / s^2)

The moment of inertia tells us "how much energy is stored in a rotating shaft or about how much energy it will take to accelerate the shaft to a particular velocity. This is called the second moment or moment of inertia" and it is equal to [ref. 13]:

$$dI = r^2 * dm$$

Referring to (figure 8), the moment of inertia for a semi-circular blade shape can be calculated according to the following equation:

$$I_b = \int r^2 \, . \, dm$$

Where: r = the radius (the distance of the infinitesimal element of mass from the origin) (m)

$= d * cos\emptyset$

dm = the infinitesimal element of mass (kg)

$= \rho \, . H \, . t \, . d \, . cos\emptyset \; d\emptyset$

t = the blade thickness (m)

Therefore, the moment of inertia for one blade (I_{1b}) becomes equal to:

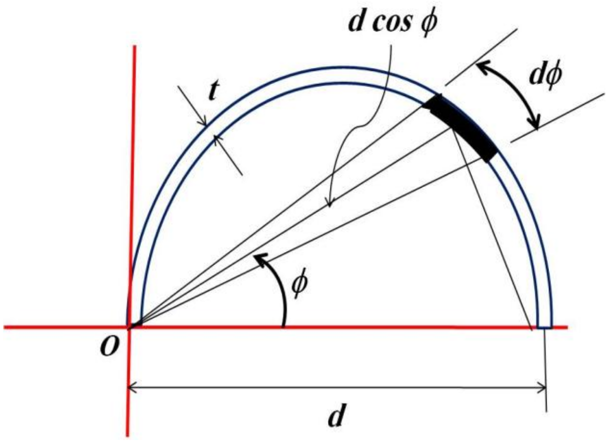

Figure (8): Schematic drawing for a semi-circular shape for moment of inertia calculation.

$$I_{1b} = \int_0^{\pi/2} \rho \, . H \, . t \, . d^3 . cos^3\emptyset \, . d\emptyset = \rho \, . H \, . t \, . d^3 \int_0^{\pi/2} cos^3\emptyset \, . d\emptyset$$

$$I_{1b} = \frac{2}{\pi} \, m \, . d^2 \int_0^{\frac{\pi}{2}} cos^3\emptyset \, . d\emptyset = \frac{4}{3\pi} \, m \, . d^2$$

Where: $m = \frac{\pi}{2} \, \rho . H . t . d$ (kg)

Thus, the moment of inertia for two and three blades of savonius becomes:

$$I_{2b} = \frac{8}{3\pi} \, m \, . d^2 \qquad and \qquad I_{3b} = \frac{4}{\pi} \, m \, . d^2$$

Referring to figure (9), the total moment of inertia for the savonius wind turbine is equal to:

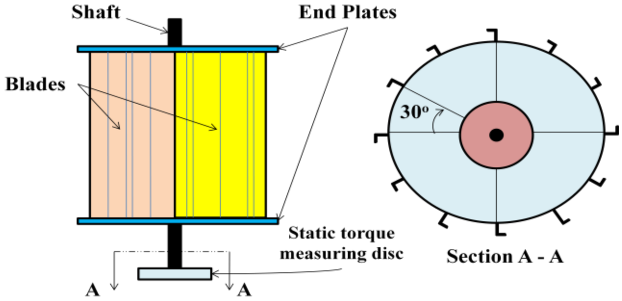

Figure (9): Schematic drawing for a semi-circular shape for moment of inertia calculation.

$$I = I_b + 2\,I_p + I_s + I_d$$

Where: I_b = the two or three blades moment of inertia (kg. m^2)

I_p = the end plates moment of inertia (kg. m^2)

I_s = the shaft moment of inertia (kg. m^2)

I_d = the torque measuring disc moment of inertia (kg. m^2)

The angular acceleration (□), is given as:

$$\omega_2 = \omega_1 + \alpha\,.\,\tau$$

$$\alpha = \frac{\omega_2 - \omega_1}{\tau} \quad \rightarrow \quad \alpha = \frac{\omega_2}{\tau} \quad when\ \omega_1 = 0$$

Where: τ = the time (sec.)

ω_1 = the initial angular velocity (1/ s)

ω_2 = the final angular velocity (1/ s)

Power Coefficient (C_p) Analysis:

Power coefficient, (C_p) of a wind turbine is the ratio of maximum power obtained from the wind to the total power available in the wind [ref. 14].

This hypothesis shows the relationship between the power coefficient (C_p) and the wind speed (V), which expresses the basic theory of the Savonius wind turbine. Principally the power that the savonius rotor can extract from the wind (P_w) is less than the actual available from the wind power (P_a).

The available power (P_a), which is also the kinetic energy (KE) of the wind, can be defined as:

$$K_E = P_a = \frac{1}{2}\ m_a\,.\,V^2 \qquad \text{(Watt)}$$

$$P_a = \frac{1}{2}\ \rho\,.\ A_s\,.\,V^3$$

Where: m_a = wind mass flow rate striking the swept area of the wind turbine (kg/sec).

$= \rho\ .\ A_s\ .\ V$

But, the swept area ($A_s = H * D$), therefore the actual power becomes:

$$P_a = \frac{1}{2}\ \rho\,.\ H\,.\,D\,.\,V^3$$

The power that the rotor extracts from the wind is:

$$P_w = T * \omega \qquad \text{(Watt)}$$

Where: P_w = the power that the rotor extracts from the wind (Watt).

The power coefficient (C_p) is given by:

$$C_p = \frac{\text{the extracted power from the wind}}{\text{the available power of the wind}} = \frac{P_w}{P_a}$$

VI. RESULTS & DISCUSSION:

The experiment's procedure was carried out and tested in the wind tunnel and the required measurement were obtained to study the performance of the two blades and three blades savonius wind turbine and makes the comparison between them to see which one is better in performance than the other.

The performance [the dimensionless parameters torque coefficient (C_t) and power coefficient (C_p)] was evaluated as function of the dimensionless parameter the tip speed ratio (λ) at low wind speeds in terms of starting acceleration and maximum no-load speed.

Figure (10) shows the plot between the wind (air) speed and the rotor revolution (rpm) for both two and three blades savonius wind turbine, it appears that as the wind speed increases from [(0 m/s) upto (3 m/s)] where the savonius wind turbine is initiated and starts to move. At this wind velocity where the wind turbine starts to move, the wind velocity is called the cut in speed, the low cut-in speed for this type of wind turbine which is about (2.5 m/s) and two blades savonius is a little bit lesser than three blades.

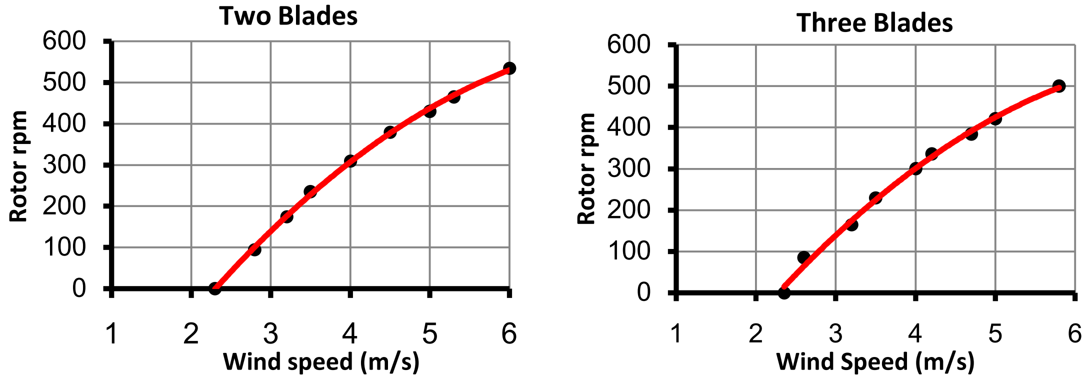

Figure (10): The graph showing the rotor rpm versus wind speed for two & three blade.

Figure (10) shows high rotational speed, the cause is that slim rotor with small diameter can get higher rotational speed but lower torque, and vice versa rotor with bigger rotational diameter produces a bigger torque but a lower rotational speed.

It is observed from figure (11) that static torque for two blade savonius wind turbine varies with the angle of attack [angle of rotation (α)] for a wind speed of (V = 5.3 m/s) , the static torque was measured at every (30^o to 360^o), it appears the torque that can be produced during each revolution is an oscillatory torque.

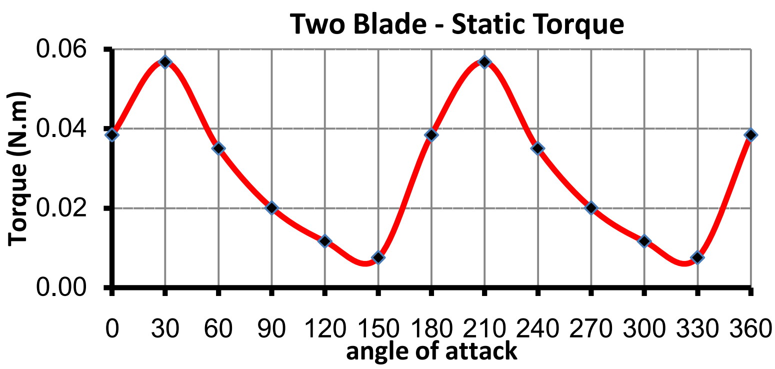

Figure (11): The static torque variation with angle of rotation for two blade savonius wind turbine.

Figure (12) shows the static torque coefficient for two blade savonius wind turbine for different wind speed (5.3 & 4.6 m/s), the static torque coefficient varies with increasing the angle of rotation, it starts to increase from (0^o to 30^0) to reach its maximum value of (0.83 & 0.65) respectively and then goes down to decrease from (30^o to 150^o) to reach it lowest value of (0.11 & 0). It is noticeable that torque values are yielding the symmetry for flow angles higher than (180° to 360^o). At angle of (150^o and 330^o), the static torque coefficient has it lowest value and for lower wind speed it may has a negative torque.

Figure (12): The static torque coefficient variation with angle of rotation for two blade savonius wind turbine at different wind speed.

Figure (13) shows the static torque coefficient for three blade savonius wind turbine for (5 m/s) wind speed, the static torque coefficient varies with increasing the angle of rotation, it starts to increase from (0^o to 60^0) and then goes down to decrease from (60^o to 120^o), It is noticeable that torque values are yielding the symmetry for flow angles higher than (120°) from (120^o to 210^o) and (240^o to 330^o).

The static torque for both two and three blade is found to be positive at any angle, high enough to obtain self-starting conditions.

Figure (14) shows the torque coefficient for two and three blades savonius wind turbine, it appears that the torque coefficient for two blades has a noticeable increasing values than the three blades.

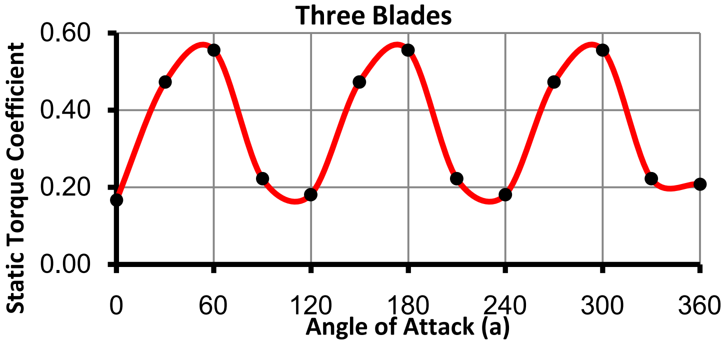

Figure (13): The static torque coefficient variation with angle of rotation for three blade savonius wind turbine.

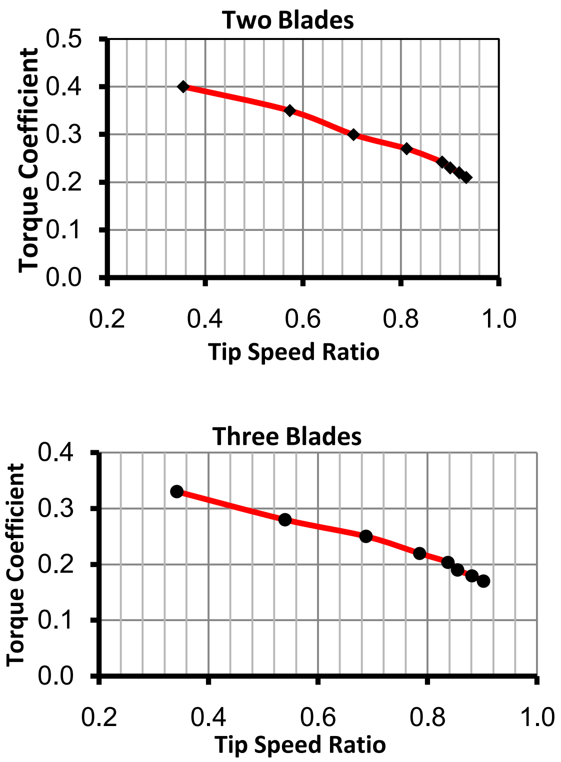

Figure (14): The torque coefficient variation with the tip speed ratio for two & three blades savonius wind turbine.

The reason is that increasing the number of blades will increase the drag surfaces against the wind air flow and causes to increase the reverse torque that leads to decrease the net torque working on the blades of savonius wind turbine.

Figure (15) shows the power coefficient for both two and three blades savonius wind turbine, it appears that the power coefficient for two blades has a noticeable increasing values than the three blades. It appears that the two blades savonius wind turbine has it highest value of (0.21) at the tip speed ratio of (0.8), the three blades has a value of (0.17) at the tip speed ratio of (0.8).

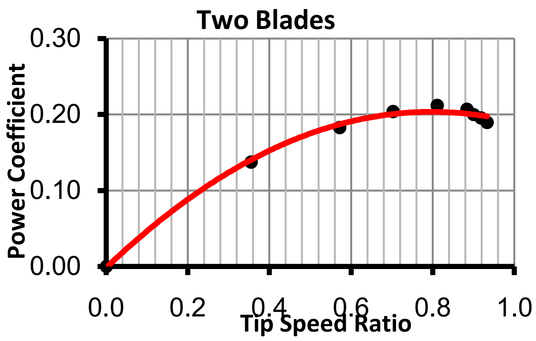

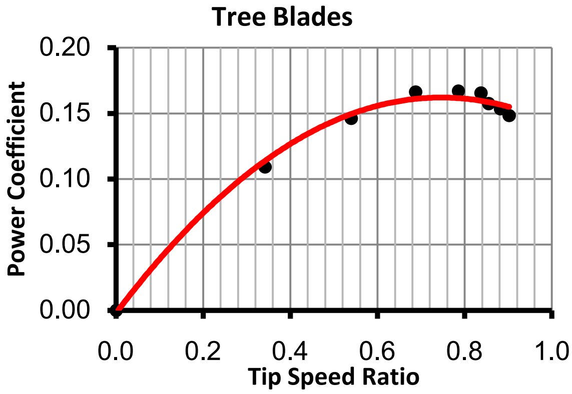

Figure (15): The power coefficient variation with the tip speed ratio for two & three blades savonius wind turbine.

REFERENCES:

[1.] John O. Ajedegba, 2008 "Effects of Blade Configuration on Flow Distribution and Power Output of a Zephyr Vertical Axis Wind Turbine", thesis submitted for a degree of M. Sc. to University of Ontario Institute of Technology.
[2.] http://wenku.baidu.com/view/5862f727bcd126fff7050bf7.html
[3.] Wei Kiat Chen & Genki Kondo, 2010 "Aerodynamics of a Drag Type Vertical Axis Wind Turbine", http://www.downloadpdffree.com/viewpdf/AERODYNAMICS-OF-A-DRAG-TYPE-VERTICAL-AXIS-WIND-TURBINE
[4.] R. Gupta, R. Das & K.K. Sharma, " Experimental Study of a Savonius- Darrieus Wind Machine", Proceedings of the International Conference on Renewable Energy for Developing Countries-2006.
[5.] http://www.wrapwind.com/download/vawt/Gupta.pdf
Khandakar Niaz Morshed, 2010" Experimental and Numerical Investigations on Aerodynamic Characteristics of Savonius Wind Turbine With Various Overlap Ratios", A Thesis Submitted for a degree of M. Sc. to Georgia Southern University.
[6.] http://dspaceprod.georgiasouthern.edu:8080/jspui/bitstream/10518/3541/1/morshed_khandakar_n_201001_ms.pdf
[7.] Robert E. Wilson, Peter B. S. Lissaman, "Applied Aerodynamics of Wind Power Machine", National Science Foundation, 1974.
[8.] http://wind.nrel.gov/designcodes/papers/WilsonLissaman_AppAeroOfWindPwrMach_1974.pdf
[9.] Joachim Peinke, Peter Schaumann and Stephan Barth, "Wind Energy", Proceedings of the Euromech Colloquium, Springer-Verlag Berlin Heidelberg 2007.
[10.] J.F. Manwell, J,G. McGowan and A,L. Rogers, "Wind Energy Explained, Theory, Design and Application" , 2nd edition, John Wiley & Sons Ltd, UK 2009.
[11.] Md. Jahangir Alam and M. T. Iqbal, 2010 "A Low Cut – In Speed Marine Current Turbine", The Journal of Ocean Technology, 5 (4). pp. 49-61. ISSN 1718-3200.
[12.] David A. Spera, "Wind Turbine Technology, Fundamental Concepts of Wind Turbine Engineering", 2nd edition, ASME press, 2009, NY.
[13.] A.R. Jha, Ph.D., "Wind Turbine Technology", CRC press Taylor & Francis Group, 2011, New York.
[14.] Sathyajith Mathew, "Wind Energy, Fundamentals, Resource Analysis and Economics", Springer-Verlag Berlin Heidelberg 2006, Netherlands.
[15.] Nemanja Komatinovic, "Investigation of the Savonius-type Magnus Wind Turbine", thesis submitted for a degree of M. Sc. to Technical University of Denmark, October 2006
[16.] http://www.mek.dtu.dk/sektioner/fvm/upload/institutter/mek/fvm/fm/eksamensprojekter/nemanjakomatinovic2006.pdf
[17.] George B. Thomas, Maurice D. Weir, Joel Hass, Frank R. Giordano, "Thomas' Calculus", 11th edition, Addison Wesley, 2004.
[18.] Ibrahim Al-Bahadly, "Wind Turbines", InTech Open Access Publisher, 2010, Croatia.

International Journal of Modern Engineering Research (IJMER)
www.ijmer.com Vol. 3, Issue. 5, Sep - Oct. 2013 pp-2987-2991 ISSN: 2249-6645

Investigations of Surface Dissolution on Fatigue Crack Nucleation in Ni-22Cr-2Fe Alloy

Aezeden Mohamed
Faculty of Engineering and Applied Science, Memorial University, St. John's, NL, A1B 3X5, Canada

ABSTRACT : *Ni-Cr-Fe alloy specimens were fatigued in a hydrochloric acid solution cell at pH 5.6 ±0.1. Results show that the number of surface slip bands forming, extending, and widening increased with the number of cycles. Results also indicated that, initially, cracks initiated as transgranular features but took on intergranular forms as the number of cycles increased.*

Keywords: *Corrosion, cycle to failure, fatigue, intergranular crack initiation, slip band broadening*

I. INTRODUCTION

Fatigue crack initiation in aqueous solutions has been shown to be affected by a number of mechanisms. However, surface pitting [1, 2] is the primary method of attack on many metallic materials that have poor resistance to pitting corrosion of surface oxides, i.e. passive film breakdown [3,4].

The corrosion resistance of the alloy that is the topic of this paper, Ni-22Cr-2Fe, can be significantly affected by cold working, alloy composition, inclusions, heat treatment, precipitates, and, most importantly, the severity and concentration of the test solution and test conditions [5]. Many researchers who have studied corrosion and corrosion fatigue have reported that solution and concentration acidity enhance the pitting corrosion of alloys contains chromium such as stainless steel alloys and nickel based chromium alloy. There are studies reporting the detrimental influence of solutions concentration on the pitting corrosion resistance of alloys contain chromium content such as stainless steels and nickel based chromium alloys [6,7]. Each of these mechanisms and their interaction with fundamental fatigue processes has been recently reviewed with the conclusion that little is actually known about the fundamentals of corrosion and corrosion fatigue in strong solutions [8].

The current study examines the characteristics of corrosion fatigue in an aggressive solution of hydrochloric acid and the evidence of accelerating formation of surface slip bands, pitting, crack initiation, and crack propagation in Ni-22Cr-2Fe alloy specimens.

II. EXPERIMENTAL PROCEDURES

Corrosion test of Ni-22Cr-2Fe alloy in hydrochloric acid solution HCl with pH value 5.6 ±0.1 was performed prior to fatigue test study as indicated in Figure 1. Axial tension-tension fatigue test were conducted on as received quenched specimens in hydrochloric acid solution as shown in Figure 2. Specimens were carefully polished prior to testing.

III. RESULTS AND DISCUSSIONS

Figure 1 shows polarization test result for Ni-22Cr-2Fe alloy in hydrochloric acid solution HCl at pH 5.6. Test results indicated that corrosion potential (E_{corr}) is -0.4 (V) and corrosion current (I_{corr}) is $5x10^3$ (NA/Cm^2).

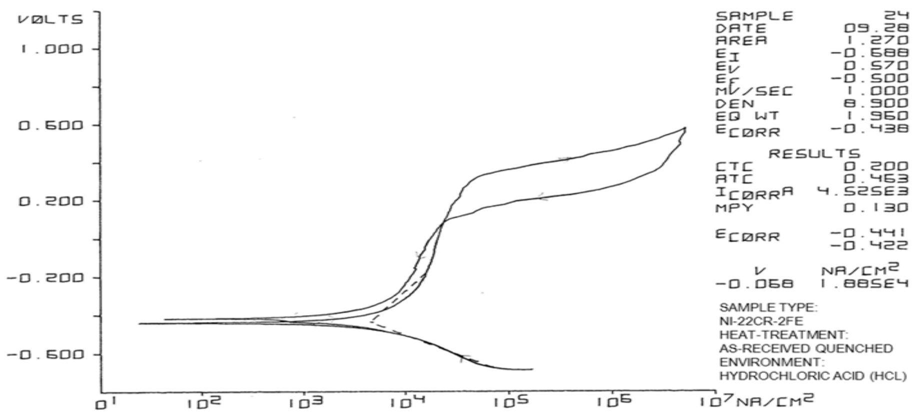

Figure 1 Polarization curve of Ni-22Cr-2Fe alloy in diluted HCl solution at pH 5.6.

Corrosion fatigue design is based on use of S-N curves, which were obtained from corrosion fatigue tests in laboratories. The design S-N curve is developed from data points, each point representing a specimen tested up to fracture. It should be pointed out that a few points were deleted because they were anomalous, being well off the trend of other the majority of points. Corrosion fatigue results were summarized in a S-N curve of stress versus number of cycles as shown in Figure 2.

For simple fatigue test specimens the testing is performed until the specimens fracture. This means that most of the fatigue life is associated with growth of a small surface crack that grows faster due to hydrochloric acid solution in contact with the specimen surface as the crack size increases until fracture.

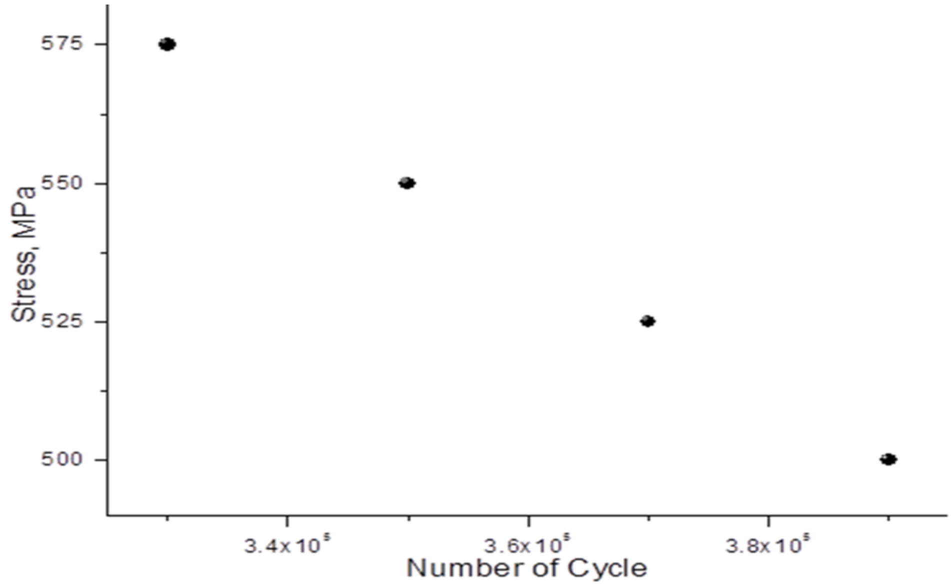

Figure 2 Stress versus number of cycles of Ni-22Cr-2Fe alloy fatigued in HCl solution.

An examination of fatigue specimens after testing in the hydrochloric acid solution revealed the generation of a large number of surfaces slip bands with very intense markings in the initial stages of cyclic deformation (Figure 3). This early damage resulted in the formation of slip band cracks oriented nearly normal to the direction of applied stress. Further cycling led to the amplification of many of the surface slip bands. Thus, some surface slip bands remained active in hydrochloric acid solution and these eventually culminated in crack nucleation as shown in Figure 3 and Figure 4.

Intergranular cracking in Ni-Cr-Fe alloys has usually been associated with the application of large number of cycles and consequent increasing corrosion of grain boundaries. These corroded grain boundaries are sites for initiation of intergranular cracking which ultimately leads to fracture. On the other hand, researchers have shown that preferential sites for transgranular initiation, even in long lived fatigue tests [9-11], occur and are attributed to the dislocation substructure associated with the grain boundaries. The intergranular cracking may be associated with alloy ductility and to the large number of cycles. In addition, the intergranular cracking tends to be most dominant in corrosion cracking and corrosion fatigue cracking. The preferential removal of metal atoms associated with dislocations can be expected, as in the case of transgranular attack, in the unlocking of otherwise static dislocation arrays and the subsequent multiplication of dislocation sources. Thus, the state of strain in a small volume of material adjacent to the boundary may be greater than that in the interior [12]. These features are observed to be primarily intergranular along the broadening slip bands as shown, notably in Figure 8.

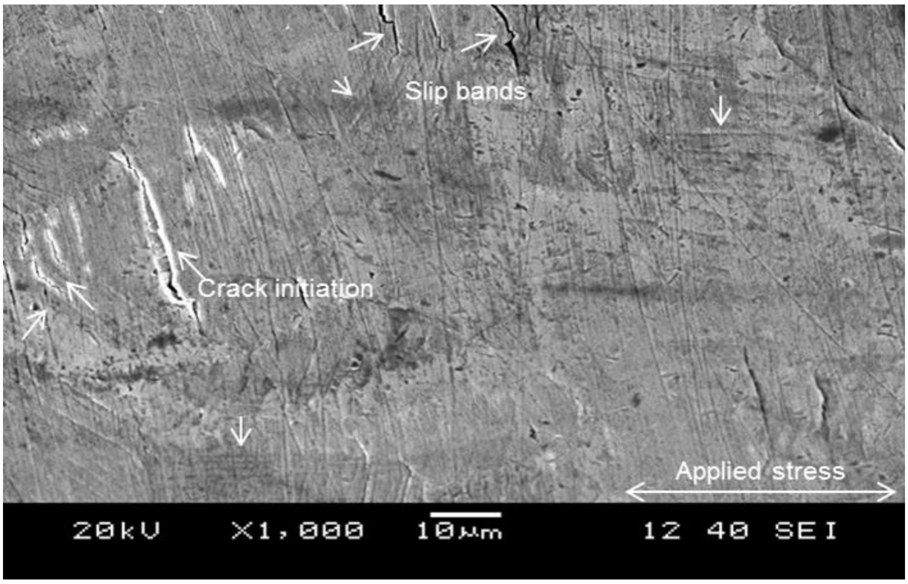

Figure 3 SEM micrograph showing slip band formation and premature crack nucleation in slips generated from corrosion fatigue of Ni-22Cr-2Fe alloy in HCl solution at $3.29x10^5$cycles.

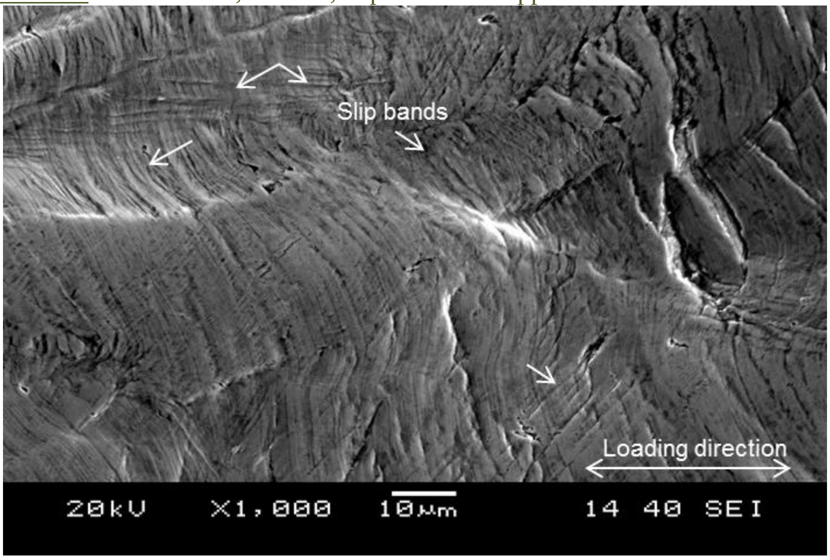

Figure 4 SEM micrograph showing surface slip band broadening on specimen of Ni-22Cr-2Fe alloy in HCl solution at $3.55x10^5$cycles.

As the test progresses, slip bands broaden and further attack is observed (Figure 5) with broadening or development of surface slip bands. Increases in the number of cycles, for example, in Figure 5 and Figure 6, are associated with slip band amplification or an increasing density and broadening of slip bands. At some point, crack initiation and propagation occur.

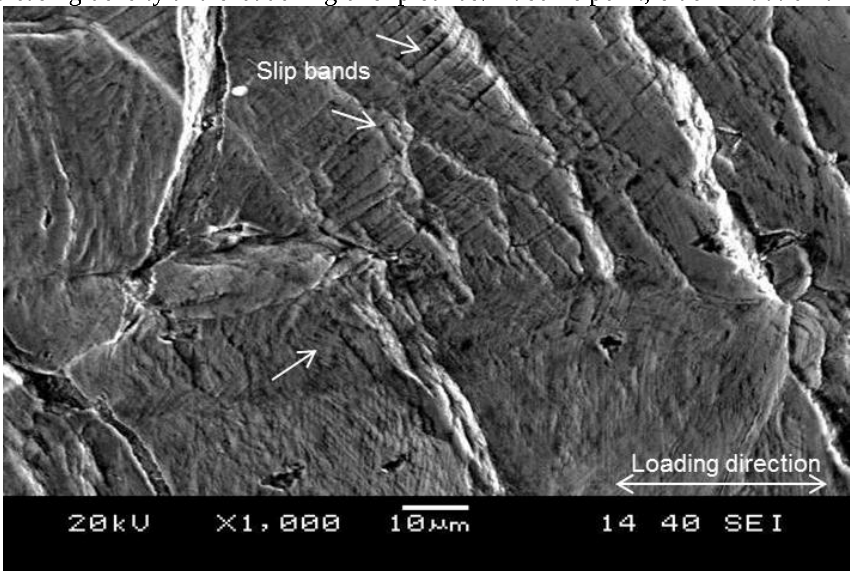

Figure 5 SEM micrograph showing slip bands and crack nucleation Ni-22Cr-2Fe in HCl solution showing slip intensification at $3.55x10^5$cycles.

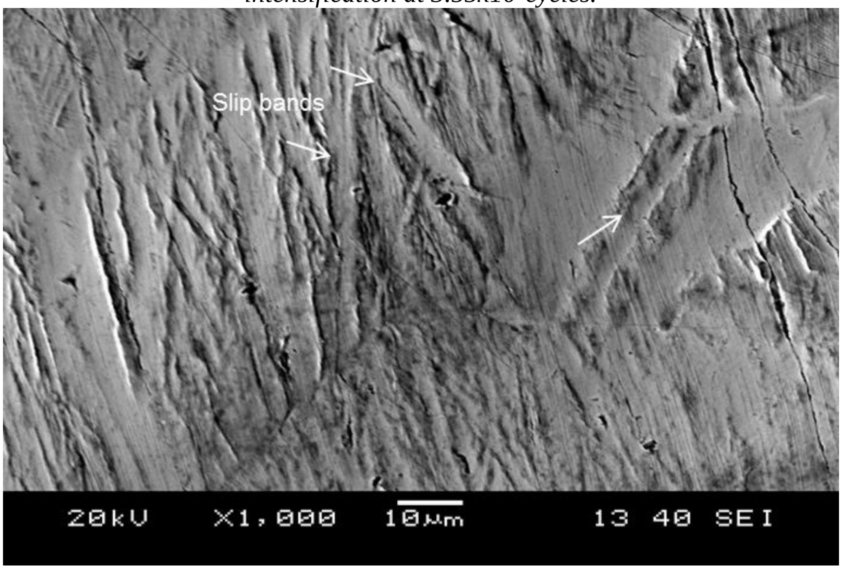

Figure 6 SEM micrograph showing surface slip band in specimen of Ni-22Cr-2Fe in HCl solution, at $3.62x10^5$ cycles.

Slip band development results in transgranular fatigue crack initiation and growth with a resulting reduction in fatigue life. Slip bands are attacked by the hydrochloric acid solution and primarily intergranular crack initiation and propagation occurs (Figure 7).

It can be seen that broadening or development surface slip bands increases with the number of cycles to failure. For example, Figure 4 and Figure 5 shows slip band amplification or an increasing density and broadening of slip bands with number of cycles to failure respectively.

At some point, crack initiation and propagation show transgranular and intergranular tracks. Slip band development results in intergranular fatigue crack initiation and growth with a resulting reduction in fatigue life. Slip bands are attacked by a diluted hydrochloric acid solution and primarily intergranular crack initiation and propagation occurs mainly along the surface slip bands (Figure 7).

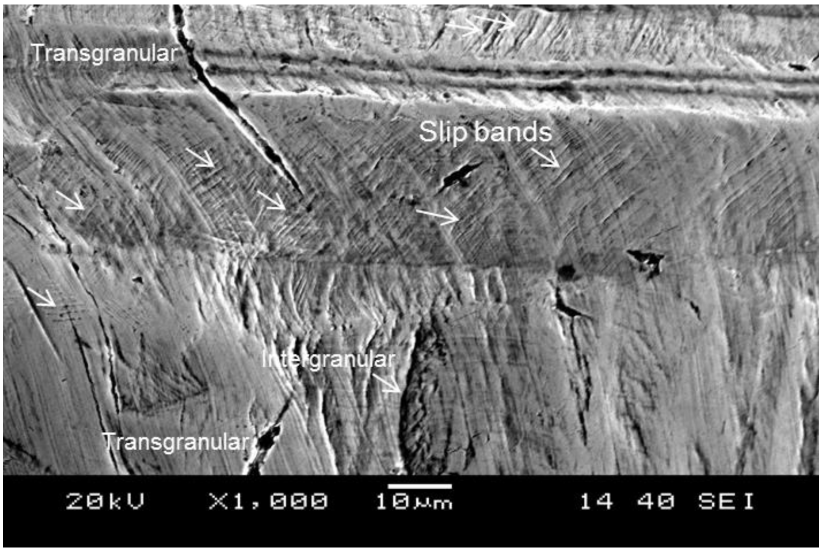

Figure 7 SEM micrograph showing surface slip band in specimen of Ni-22Cr-2Fe in HCl solution, at $3.69x10^5$ cycles.

With increasing fatigue cycles the intergranular cracks and the crack population along slip bands increases. In HCl solution, surface slip bands develop on the specimen surface and are preferentially attacked. This mechanism is responsible for the slip band broadening observed in this study. It is likely that the preferential corrosion fatigue is associated with slip bands. It is also possible that the slip bands are associated with fatigue striations which can be seen especially in Figure 8.

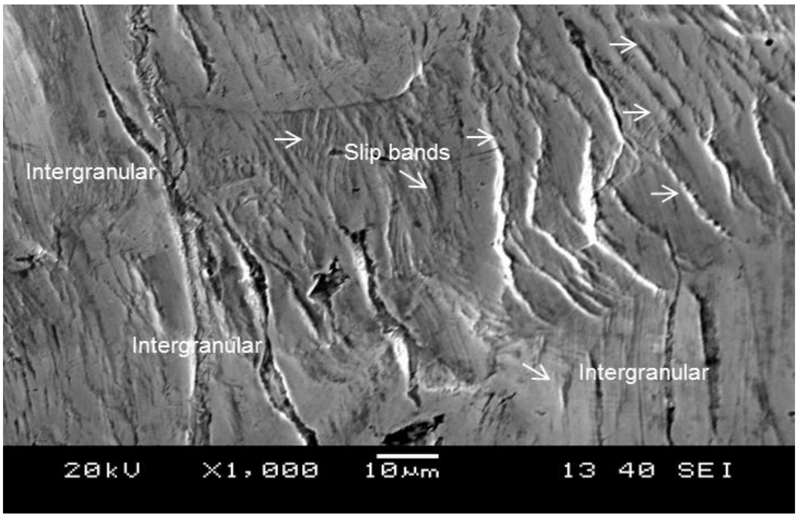

Figure 8 SEM micrograph showing surface slip band in specimen of Ni-22Cr-2Fe in HCl solution, at $3.83x10^5$ cycles.

After fatigue specimen fracture, the fracture specimens were loaded to scanning electron microscopy for surface observations. The area of interest of the current study were mainly two sides of the specimen one represent surface slip bands observation and another side represent fracture surface observation as shown in Figure 9 (a) and (b) respectively.

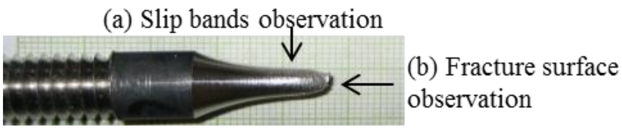

Figure 9 Fatigue fracture indicates, (a) slip bands and (b) fracture surface side.

Fracture surface of Ni-22Cr-2Fe alloy appeared as ductile fracture like formed by depressions, called dimples, in the microstructure. Intergranular dimple rupture occurs along grain boundaries due to nucleation and coalescence of voids at grain boundaries or at other interfaces such as in slip bands. Final fracture occurs in association with broad slip bands near crack initiation and crack propagation total dimples sites as shown in Figure 10 (a) and (b) respectively.

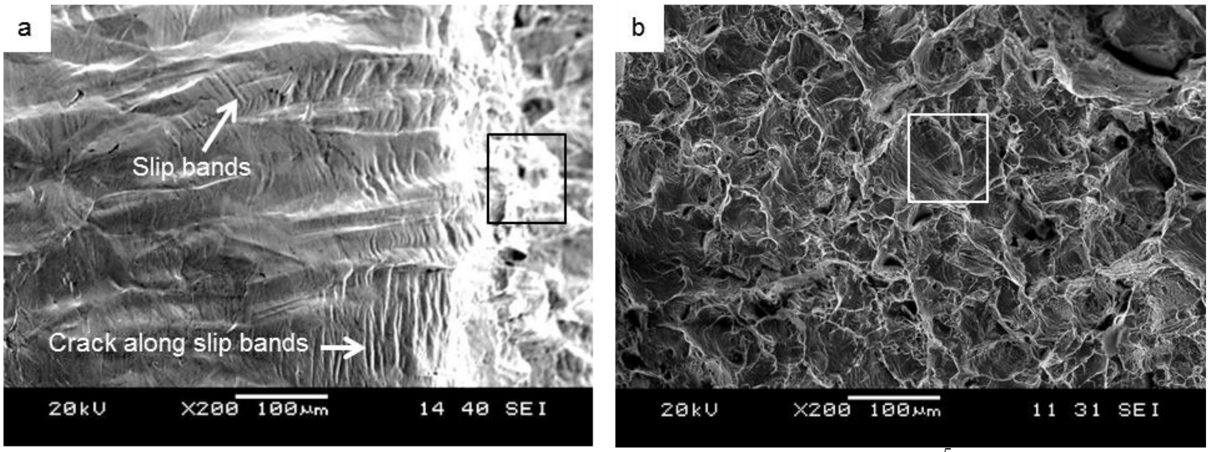

Figure 10 Fatigue fracture surface of specimen of Ni-22Cr-2Fe in HCl solution, at 3.62x10^5 cycles. (a) Indicates slip bands and partially fracture surface, (b) ductile fracture surface.

IV. Conclusion

Ni-22Cr-2Fe alloy specimens fatigued in diluted hydrochloric acid HCl solution at a pH value of 5.6 developed surface slip bands which broadened and widened with increasing number of cycles. In addition, crack initiation was observed to occur along the slip bands with increasing number of cycles.

References

[1] D. J. McAdam, and G. W. Geil, “Pitting and the Effect on the Fatigue Limit of Steel Corroding under Various Conditions”, *Proceedings American Society Testing Materials ASTM STP 41, ASTM*, Philadelphia, PA, Vol. 41, 1970, pp. 696-731.
[2] D. J. McAdam, Jr., G.W. Geil, and D. H. Woodard," Influence of Strain Rate and Temperature on the Mechanical Properties of Monel Metal and Copper”, *Proceedings American Society Testing Materials*, 46, 1946, pp. 90-92
[3] U.R. Evans and M. T. Simnad, "The Mechanisms of Corrosion Fatigue of Mild Steel,” *Proceedings of the Royal Society*, London, A188, 1947, pp. 372-392.
[4] V. Likhtman, E. Shehukin, and P. Rebinder, “Physiocochemical Mechanics of Metals”, *Academy of Sciences USSR*, Israel Program for Scientific Translations, Jerusalem, 1964.
[5] T. Pyle, V. Rollins, and D. Howard, Proceedings International Conference on Corrosion Fatigue, Storrs, Conn., 1971. pp. 312-313.
[6] C. Laird and G. C. Smith, “Initial Stages of Damage in High Stress Fatigue in Some Pure Metals”, *Philosophical Magazine*, Vol. 8, 1963, pp. 1945-1950.
[7] P. Lukas, M. Klesnil, and J. Krejci, “Dislocation Structure Associated with Fracture Surface of Fatigued Copper Single Crystal”, *Philosophical Magazine*, Vol. 27, 1968, pp. 545-546.
[8] C. Laird and D. J. Duquette, “Corrosion Fatigue”, *Proceedings International Conference on Corrosion Fatigue”*, 1972, pp. 88-100.
[9] A. Mohamed, “Fatigue and Corrosion Fatigue Behavior of Nickel Alloys in Saline Solutions”, *International Journal of Modern Engineering Research*, Vol. 3, 2013, pp-1529-1533.
[10] D. H. Avery and W. A. Backofen, “Fracture of Solids”, *Gordon and Breach*, 1963, pp.339-340.
[11] C. E. Felmer and P. Beardmore, “Achievement of High Fatigue Resistance in Metals and Alloys”, *ASTM STP*, no. 467, 1970, pp. 77-80.
[12] H. Masuda, and D. J. Duquette, “The Effect of Surface Dissolution on Fatigue Crack Nucleation in Polycrystalline Copper”, *Metallurgical Transactions A*, Vol. 6A, 1975, pp. 87-94.

International Journal of Modern Engineering Research (IJMER)
www.ijmer.com Vol. 3, Issue. 5, Sep - Oct. 2013 pp-2992-2995 ISSN: 2249-6645

Cloud in the sky of Business Intelligence

Anamitra Das
IT Specialist, IBM India Pvt Ltd, India

ABSTRACT : *The Modern day business is highly information driven. At one side the volume of data is growing by leaps and bounds and at the other side it is becoming more and more unstructured. Information is not limited to tabular format now. It is in the form of images, MP3 files, videos and social media snippets. To tame this giant we must adopt a more scalable, cheap, and robust way of processing where cloud computing is the answer. Again, the business intelligence is a process which processes raw data to produce information that help in forecasting and decision making. Organizations are striving to become intelligent and achieve competition advantages through the use of Business Intelligence (BI) solutions. The present paper identifies the key factors responsible for evolution of Business Intelligence on the Cloud, the various models available to port BI solution on Cloud, the primary drivers for Cloud BI, the impact of implementing Cloud BI.*

Keywords: *Business Intelligence, Cloud Computing, Cloud Infrastructure, Data warehouse, Return of Investment*

I. INTRODUCTION

Business environment has totally changed today. In this changing world business houses are drifting towards more scalable, robust, flexible information technology architecture. Each organization is thriving to become an intelligent organization and at gaining competition advantage on the market by the use of new and innovative Business Intelligence (BI) solutions. Today, business intelligence (BI) has been under mounting pressure to evolve as an all pervasive information and analytics agent. On the other hand, in the wake of the present economic crisis organizations are reducing IT budget which is practically compelling to have concretized its strategic relationship with business with the reintroduction of grid technology in the form of cloud computing. Popular solutions based on Cloud Computing, called Cloud BI or BI services on demand are increasingly popular.

II. WHAT IS CLOUD COMPUTING

The time you started using Picasa you started using it. The moment you created your account in Facebook and entered the world of social networking you started using it. It, starting with a big 'I' is no other than "Cloud Computing".

Cloud computing refers to the delivery of computing resources over the Internet. The term 'cloud' is analogical to internet. Instead of keeping data on your own hard drive or updating applications for your needs, you use a service over the Internet, at another location, to store your information or use its applications.

It can reduce the cost (isn't it the sufficient reason where every big business house is slashing IT Infrastructure budget?) and complexity of owning and operating computers and networks. Since cloud users do not have to invest in information technology infrastructure, purchase hardware, or buy software licenses, the benefits are low up-front costs, rapid return on investment, rapid deployment, customization, flexible use, and solutions that can make use of new innovations. In addition, cloud providers that have specialized in a particular area (such as e-mail) can bring advanced services that a single company might not be able to afford or develop. Some other benefits to users include scalability and efficiency. Scalability means that cloud computing offers unlimited processing and storage capacity. Cloud computing is often considered efficient because it allows organizations to free up resources to focus on innovation and product development.

2.1 Service Models : What we see is what we get

The bottom-line of the technology is to share resources. Use the unused, release after using so that others can use, and do this seamlessly without heavy management intervention are the basics of cloud computing. Now what are the services available to reuse, which model one can adapt so that it fits the bill? May be I need a book for a lazy evening and my friend has a hamburger to offer? Here we chose from the three service models that are available.

Software as a Service (SaaS) - We can use applications running on a cloud infrastructure from either a thin client interface, such as a web browser, or a program interface without managing or controlling the underlying infrastructure including network, servers, operating systems or storage.

Platform as a Service (PaaS) - We can deploy applications (self created or acquired) onto the cloud infrastructure using programming languages, libraries, services, and tools supported by the provider, without managing network, servers, operating systems, or storage, but have control over the deployed applications and hosting environment.

Infrastructure as a Service (IaaS) - We can use processing, storage, networks, and other fundamental computing resources and deploy or run arbitrary software, which can include operating systems and applications. Consumer has control over operating systems, storage, and deployed applications but does not manage the underlying infrastructure.

2.2 What the infrastructure should guarantee

So we see the backbone is 'Cloud Infrastructure' which has to be managed by the providers and above there are different layers of services that we can use as consumer. It should have the following characteristics.

- Computing capabilities, like network storage, server time should be available automatically when needed without any manual or human interaction with provider. This is what we say **"on-demand self-service"**
- Infrastructure should be built on **"broad network access"**, meaning capabilities are over the network and can be accessed through standard mechanisms like laptops, mobile phones etc.
- **"Resource pooling"** is an essence of cloud computing. Resources are pooled to serve multiple consumers using a multi-tenant model, with different physical and virtual resources dynamically assigned and reassigned according to consumer demand.
- The capabilities available must appear to be unlimited and can be appropriated in any quantity at any time. So the capability must support **"Rapid elasticity"** - it must be elastically provisioned and released between consumers.
- Should support **"Measured service" for** automatically controlling and optimizing resource usage by leveraging a metering facility. This is also required to enable consumer to use and pay for the infrastructure.

III. CLOUD BI – AN OPPORTUNITY UNLEASHED

3.1 Challenges of modern day BI

BI is an umbrella term that includes the applications, infrastructure and tools, and best practices that enable access to and analysis of information to improve and optimize decisions and performance. Roots of business intelligence are found in relational databases, data warehouses and data marts that help organizing historical information in the hands of business analysts to generate reporting that informs executives and senior departmental managers of strategic and tactical trends and opportunities [1].

When we talk about information analysis, it's important to think about where the data actually resides. While the scope of traditional BI is limited to structured data that can be stuffed into columns and rows on a data warehouse, the fact is that over 90% of today's data is unstructured in the form of images, MP3 files, videos and social media snippets. Also, much of the data that organizations need to look at is not necessarily "owned" by them - it exists within various social computing services like Twitter and Facebook, it's hidden within Web logs, sensor output, and call detail records. Finding exactly what you need within such an enormous stream can be like finding a needle in a haystack.

In recent times, business intelligence (BI) has been under enormous pressure to evolve as an all pervasive information and analytics agent. From mass quantities of transactional data, Web data, and growing volumes of "machine-generated" information, such as sensor and log data, volumes are expanding into the petabyte range. As the data center strains under the need for more storage and faster performance (all while keeping costs in check,) cloud computing, open source technologies and other emerging approaches are presenting compelling new ways to manage data and consume IT services [2].

3.2 Cloud BI – An architectural Overview

Cloud BI is the new way to do Business Intelligence: instead of implementing expensive and complex software on-site, the BI software runs in the Cloud. It is accessible via any web browser in a SaaS model. There is no need to install software, or to buy any hardware. And when you're computing needs grow, the system will automatically assign more resources. This elastic scale is what makes Cloud BI so powerful – user pay for what he use as opposed to always paying to provision for peak load. With business intelligence software running in the cloud, it is still possible to make comprehensive integration with back-end systems – both within User Company and in the cloud [3].

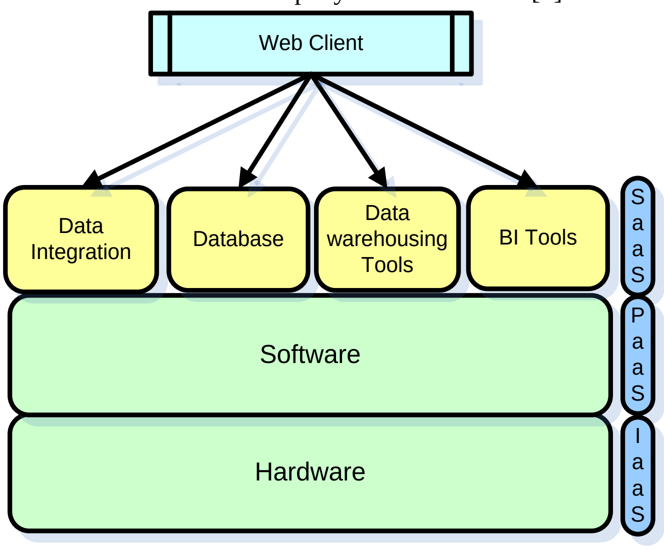

Fig 1 : BI on the Cloud - The Basic Architecture

Hardware : refers to processing, storage, and networks
Software : refers to the operating systems and drivers required to handle the hardware
Data integration : refers to the tools needed to perform the ETL and data cleansing processes
Database : refers to the relational or multidimensional database systems that administer the information
Data warehousing : set of applications that allow the creation and maintenance of the data warehouse
BI tools : are the set of front-end applications that enable the final users to access and analyze the data
Web Client : finally, since all the architecture is going to be accessed through the Internet, there is no need for thick clients or preinstalled applications, because all the content and configuration can be reached through traditional internet browsers

3.3 Why adopt Cloud BI

The small and medium level companies or big houses can leverage the below benefits of cloud BI for reducing implementation and operating IT cost.

Accelerating BI technology adoption: the cloud becoming the default platform for evaluating new software.
Easier evaluation: the cloud enables software companies to make new technology available to evaluators on a self-services basis, avoiding the need to download and set up free software downloads [4].
Increased short-term ad-hoc analysis: avoiding data marts spawned as a result of new business conditions or events. Where short term needs [weeks or months] for BI is required, cloud services are ideal. A data mart can be created in a few hours or days, used for the necessary period, and then the cloud cluster cancelled, leaving behind no redundant hardware or software licenses. The cloud makes short term projects very economical [5].
Increased flexibility: due to the avoidance of long term financial commitments, individual business units will have the flexibility to fund more data mart projects. This is ideal for proof of concept, and ad-hoc analytic data projects on-demand. This agility enables isolated business units to respond to BI needs faster than their competitors and increase the quality of their strategy setting and execution.

The strengths of the cloud model have led many BI vendors to introduce cloud services as a clear and distinctive extension to the on-premise and on-demand BI applications [6]. Companies like Amazon and Google offer unlimited processing power and storage thus allowing any business to cater to its increasing information stack while keeping the IT related costs under control. In addition, a number of innovative SaaS and "cloud-friendly" BI and analytic solutions are cropping up, which means that organizations can take advantage of the cloud to not only store their data, but also crunch it. Depending on the organization's specific requirements, there's more than one flavor of cloud like

Private Cloud - The cloud infrastructure is operated solely for a specific organization, and is managed by the organization or a third party. It offers greater security and control.
Public Cloud - Offered over the Internet and are owned and operated by a cloud provider. It is affordable and highly scalable.
Community Cloud - The service is shared by several organizations and made available only to those groups.
Hybrid Cloud - It is a combination of different methods.
The best approach will ultimately depend on what's most important to the target organization.

IV. ANALYSIS OF THE OPPORTUNITY OF USING A CLOUD BI SOLUTION

By analyzing risks and associated costs and benefits a Cloud BI solution can be evaluated. There are different types of cost-benefit analyses where models are limited mainly to the measurement of costs and savings. The approach proposed in this article provides a perspective on the calculation of ROI (Return of Investment) indicator associated to a BI solution in the Cloud environment, stressing the difference between the traditional practice and Cloud.

$$ROIBI = (TB - TC)/ ITC \qquad (1)$$

where *TB* represents the total benefits following implementation of the BI solution, *TC* represents the total costs , and *ITC* – initial total costs of the solution.

$$ROICloudBI = (IPB + DCB - CloudTC)/ CloudTC \qquad (2)$$

where *IPB* represents the benefit obtained as a result of increased profit, *DCB* represents the benefit obtained as a result of decreasing costs by the use of a Cloud solution, *CloudTC* represents the total costs generated by the Cloud environment (after [7]).

The benefit reached by decreasing costs through the use of a Cloud BI solution may be calculated according to the formula:

$$DCB = \triangle IHC + \triangle ISC + \triangle IIC \qquad (3)$$

where *IHC* represents the initial hardware costs, *ISC* represents initial software costs, and *IIC* initial implementation costs for a traditional BI solution, detailed in [8]. Within these costs an important role is that of decreasing number of hardware equipments, of costs generated by the spaces used and of the license costs.

The benefit obtained as a result of increasing profit following the use of intangible advantages of a Cloud BI solution may be calculated according to the formula:

$$IPB = IAB + ISB + MB + CB + RB + GITB + UTB, \quad (4)$$

where *IAB* represents the benefit obtained by increased agility, *ISB* – same as a result of increased scalability, *MB* – same from reducing the time of response to the market demands , *ISB* – same as a result of increased clients' satisfaction, *CB* – same as a result of focusing business on the main competences, *RB* – same as a result of disaster recovery, *GITB* – same as a result of using Green IT, *UTB* – same as a result of better use of time, detailed in [7].

V. CONCLUSION

Cloud computing is an essential platform for the future Business Intelligence and offers several advantages in terms of cost, flexibility, availability and speed of implementation. It also can be an answer to the challenges of the cost cutting and economic crisis. Organizations – small, medium or large – may consider this consolidation at two levels: onto shared hardware infrastructure and onto shared and standardized platforms, the choice can be driven their by strategies. At the infrastructure level, organizations can consolidate by sharing hardware through virtualization, reaping benefits such as lower hardware, power, cooling and data-center costs. However, to reduce the cost and complexity of the heterogeneous application and data siloes running on top of virtualized servers will require standardization and consolidation at a platform level, creating a single database architecture capable of handling both data warehousing and OLTP workloads across the enterprise. This further boosts IT productivity, agility and responsiveness to business needs and shifting market conditions. Finally, consolidating workloads in the cloud delivers dramatic cost savings by minimizing the human costs of IT systems management. Like consolidating many databases into one reduces IT costs as the organization's need for database administrators, vendor support, and time allocated to upgrades and patches is greatly reduced if not eliminated all together.

REFERENCES

[1] J. Dibbern, T. Goles, R. Hirschheim, and B. Jayatilaka, "Information Systems Outsourcing. A Survey and Analysis of the Literature," 2004.

[2] Don Deloach, *It's a Brave New World for Business Intelligence.* Available: http://cloudcomputing.sys-con.com/node/1927082

[3] M Peter and G Timothy, *The Nist Definition of Cloud Computing (draft) (2011).* National Institute of Standards and Technology Special Publication, 800 -145

[4] R. Buyya, C. S. Yeo, and S. Venugopal, "Market-Oriented Cloud Computing: Vision, Hype and Reality for Delivering IT Services as Computing Utilities." *Future Generation Computer Systems*, vol. 25, pp. 599-616, 2009.

[5] P. Relan and Sibbingz, "Business intelligence for the cloud software stack helps gaming sites quickly adapt to evolving customer needs,"2009.

[6] Bharat Chandra and Meena Iyer, *BI in the Cloud – Defining the Architecture for Quick Wins.* Available: http://www.infosys.com/infosys-labs/publications/Documents/BI-in-a-cloud.pdf

[7] Misra, S.C., Mondal, A. (2010), Identification of a company's suitability for the adoption of cloud computing and modelling its corresponding return on investment, Mathematical and Computer Modelling, doi:10.1016/j.mcm.2010.03.037

[8] Ghilic-Micu, B., Stoica, M., Mircea, M. (2008), A framework for measuring the impact of BI solution, The 9th WSEAS Int. Conf. on Mathematics And Computers In Business And Economics, Bucharest, Romania, ISBN 978-960- 6766-76-3, ISSN 1790-5109, 68-73

.

An Efficient Mechanism of Handling MANET Routing Attacks using Risk Aware Mitigation with Distributed Node Control

Sk.Rahima Sulthana[1], D.Srujan Chandra Reddy[2],T.Bharath Manohar[3]

[1]*M.Tech 2ndyr,Dept of CSE,PBRVITS(Affiliated to JNTU Anantapur), Kavali,Nellore.Andhra Pradesh.India.*
[2] *Assoc. Prof.,Dept of CSE, PBRVITS(Affiliated to JNTU Anantapur), Kavali,Nellore.Andhra Pradesh.India.*
[3] *Asst.Professor,Dept of CSE, CMR College of Engineering &Technology,*
(Affiliated to JNTU Hyderabad)Hyderabad.Andhra Pradesh.India.

ABSTRACT*— Mobile Ad hoc Networks (MANET) have been highly vulnerable to attacks due to the dynamic nature of its network infrastructure. Among these attacks, routing attacks have received considerable attention since it could cause the most devastating damage to MANET. Even though there exist several intrusion response techniques to mitigate such critical attacks, existing solutions typically attempt to isolate malicious nodes based on binary or naıve fuzzy response decisions. However, binary responses may result in the unexpected network partition, causing additional damages to the network infrastructure, and naıve fuzzy responses could lead to uncertainty in countering routing attacks in MANET. In this paper, we propose a risk-aware response mechanism to systematically cope with the identified routing attacks. Our riskaware approach is based on an extended Dempster-Shafer mathematical theory of evidence introducing a notion of importance factors. In addition, our experiments demonstrate the effectiveness of our approach with the consideration of several performance metrics.*

Keywords— *Mobile Ad Hoc Networks, Intrusion Response, Risk Aware, D-S Theory*

I. INTRODUCTION

MOBILE Adhoc Networks (MANET) is utilized to set up wireless communication in improvised environments without a predefined infrastructure or centralized administration. Therefore, MANET has been normally deployed in adverse and hostile environments where central authority point is not necessary. Another unique characteristic of MANET is the dynamic nature of its network topology which would be frequently changed due to the unpredictable mobility of nodes. Furthermore, each mobile node in MANET plays a router role while transmitting data over the network. Hence, any compromised nodes under an adversary's control could cause significant damage to the functionality and security of its network since the impact would propagate in performing routing tasks. Several work [1], [2] addressed the intrusion response actions in MANET by isolating uncooperative nodes based on the node reputation derived from their behaviors. Such a simple response against malicious nodes often neglects possible negative side effects involved with the response actions. In MANET scenario, improper countermeasures may cause the unexpected network partition, bringing additional damages to the network infrastructure. To address the abovementioned critical issues, more flexible and adaptive response should be investigated. The notion of risk can be adopted to support more adaptive responses to routing attacks in MANET [3]. However, risk assessment is still a nontrivial, challenging problem due to its involvements of subjective knowledge, objective evidence, and logical reasoning. Subjective knowledge could be retrieved from previous experience and objective evidence could be obtained from observation while logical reasoning requires a formal foundation. Wang et al. [4] proposed a naive fuzzy cost-sensitive intrusion response solution for MANET. Their cost model took subjective knowledge and objective evidence into account but omitted a seamless combination of two properties with logical reasoning. In this paper, we seek a way to bridge this gap by using Dempster-Shafer mathematical theory of evidence (D-S theory), which offers an alternative to traditional probability theory for representing uncertainty [5]. D-S theory has been adopted as a valuable tool for evaluating reliability and security in information systems and by other engineering fields [6], [7], where precise measurement is impossible to obtain or expert elicitation is required. D-S theory has several characteristics. First, it enables us to represent both subjective and objective evidences with basic probability assignment and belief function. Second, it supports Dempster's rule of combination (DRC) to combine several evidences together with probable reasoning. However, as identified in [8], [9], [10], [11], Dempster's rule of combination has several limitations, such as treating evidences equally without differentiating each evidence and considering priorities among them. To address these limitations in MANET intrusion response scenario, we introduce a new Dempster's rule of combination with a notion of importance factors (IF) in D-S evidence model. In this paper, we propose a risk-aware response mechanism to systematically cope with routing attacks in MANET, proposing an adaptive time-wise isolation method. Our risk-aware approach is based on the extended D-S evidence model. In order to evaluate our mechanism, we perform a series of simulated experiments with a proactive MANET routing protocol, Optimized Link State Routing Protocol (OLSR) [12]. In addition, we attempt to demonstrate the effectiveness of our solution.

II. MOTIVATION

Existing System

Several work addressed the intrusion response actions in MANET by isolating uncooperative nodes based on the node reputation derived from their behaviors. Such a simple response against malicious nodes often neglects possible negative side effects involved with the response actions. In MANET scenario, improper countermeasures may cause the unexpected network partition, bringing additional damages to the network infrastructure. To address the above-mentioned critical issues, more flexible and adaptive response should be investigated. The notion of risk can be adopted to support more adaptive responses to routing attacks in MANET. Subjective knowledge could be retrieved from previous experience and objective evidence could be obtained from observation while logical reasoning requires a formal foundation. Wang et al. proposed a naïve fuzzy cost-sensitive intrusion response solution for MANET. Their cost model took subjective knowledge and objective evidence into account but omitted a seamless combination of two properties with logical reasoning.

Disadvantage of Existing System

However, risk assessment is still a nontrivial, challenging problem due to its involvements of subjective knowledge, objective evidence, and logical reasoning.

Proposed System

We formally propose an extended D-S evidence model with importance factors and articulate expected properties for Dempster's rule of combination with importance factors (DRCIF). Our Dempster's rule of combination with importance factors is nonassociative and weighted, which has not been addressed in the literature. We propose an adaptive risk-aware response mechanism with the extended D-S evidence model, considering damages caused by both attacks and countermeasures. The adaptiveness of our mechanism allows us to systematically cope with MANET routing attacks. We evaluate our response mechanism against representative attack scenarios and experiments. Our results clearly demonstrate the effectiveness and scalability of our risk-aware approach.

III. LITERATURE SURVEY

In this section, we overview the OLSR and routing attacks on OLSR.

OLSR Protocol

The major task of the routing protocol is to discover the topology to ensure that each node can acquire a recent map of the network to construct routes to its destinations. Several efficient routing protocols have been proposed for MANET. These protocols generally fall into one of two major categories: reactive routing protocols and proactive routing protocols. In reactive routing protocols, such as Adhoc On Demand Distance Vector (AODV) protocol, nodes find routes only when they must send data to the destination node whose route is unknown. In contrast, in proactive routing protocols, such as OLSR, nodes obtain routes by periodic exchange of topology information with other nodes and maintain route information all the time. OLSR protocol is a variation of the pure Link-state Routing (LSR) protocol and is designed specifically for MANET. OLSR protocol achieves optimization over LSR through the use of multipoint relay (MPR) to provide an efficient flooding mechanism by reducing the number of transmissions required. Unlike LSR, where every node declares its links and forward messages for their neighbors, only nodes selected as MPR nodes are responsible for advertising, as well as forwarding an MPR selector list advertised by other MPRs.

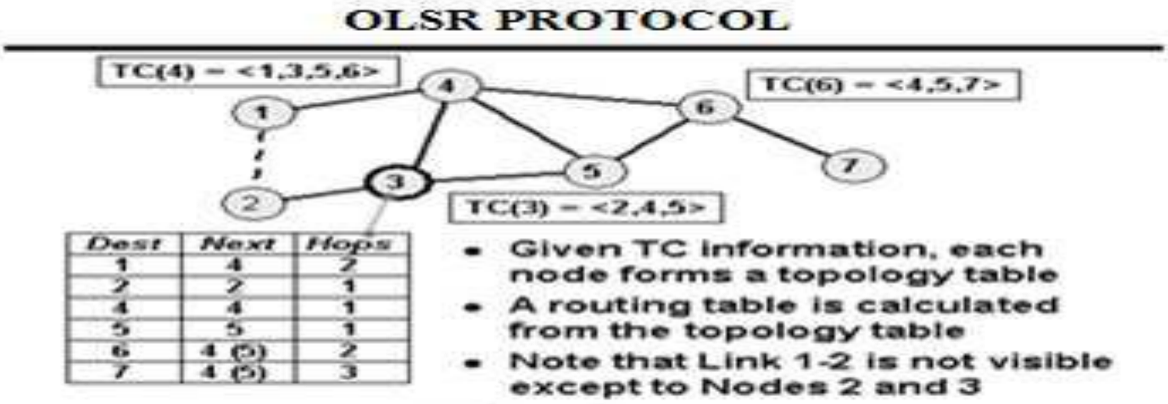

Fig: OLSR Protocol

Routing Attack on OLSR

Based on the behavior of attackers, attacks against MANET can be classified into passive or active attacks. Attacks can be further categorized as either outsider or insider attacks. With respect to the target, attacks could be also divided into data packet or routing packet attacks. In routing packet attacks, attackers could not only prevent existing paths from being used, but also spoof non existing paths to lure data packets.

IV. SYSTEM ANALYSIS

Extended Dempster-Shafer Theory of Evidence

The Dempster-Shafer mathematical theory of evidence is both a theory of evidence and a theory of probable reasoning. The degree of belief models the evidence, while Dempster's rule of combination is the procedure to aggregate and summarize a corpus of evidences.

Dempster's Rule

1. Associative. For DRC, the order of the information in the aggregated evidences does not impact the result. As shown in [10], a nonassociative combination rule is necessary for many cases.
2. Nonweighted. DRC implies that we trust all evidences equally [11]. However, in reality, our trust on different evidences may differ. In other words, it means we should consider various factors for each evidence.

Importance Factors and Belief Function

In D-S theory, propositions are represented as subsets of a given set. When a proposition corresponds to a subset of a frame of discernment, it implies that a particular frame discerns the proposition. First, we introduce a notion of importance factors.

Definition 1

Importance factor (IF) is a positive real number associated with the importance of evidence. Ifs are derived from historical observations or expert experiences.

Definition 2

An evidence E is a 2-tuple hm; IFi, where m describes the basic probability assignment [5].Basic probability assignment function m is defined as follows: m(Φ)=0 and Σm(A)=1 (1) and Σm(A)=1 (2) According to [5], a function Bel:2θ ->[0,1] ,a belief function over θ if it is given by (3) for some basic probability assignment m:2θ->[0,1] Bel(A)=Σm(B) for all A ϵ 2 θ , Bel(A),describes a measure of the total beliefs committed to the evidence A. Given several belief functions over the same frame of discernment and based on distinct bodies of evidence, Dempster's rule of combination, which is given by (4), enables us to compute the orthogonal sum, which describes the combined evidence. Suppose Bel1 and Bel2 are belief functions over the same frame θ, with basic probability assignments m1 and m2.Then, the function m : 2 θ->[0,1]; defined by m(θ)=0 and m(C)=(ΣAi ∩ Bj =Cmi (Ai) m2 (Bj))/(1- ΣAi∩Bj=Φm1(Ai)m2(Bj)) (4) for all nonempty C ⊆θ,, m(C) is a basic probability assignment which describes the combined evidence. Suppose IF1 and IF2 are importance factors of two independent evidences named E1 and E2, respectively. The combination of these two evidences implies that our total belief to these two evidences is 1, but in the same time, our belief to either of these evidences is less than 1. This is straightforward since if our belief to one evidence is 1, it would mean our belief to the other is 0, which models a meaningless evidence. And we define the importance factors of the combination result equals to (IF1+ IF2)=2.

Definition 3

Extended D-S evidence model with importance factors: Suppose E1=<m1, IF1> and E2 =< m2, IF2> are two independent evidences. Then, the combination of E1 and E2 is E = <m1 Θ m2,(IF2+IF2)/2>, where Θ is Dempster's rule of combination with importance factors.

Expected Properties for Our Dempster's Rule of Combination with Importance Factors

The proposed rule of combination with importance factors should be a superset of Dempster's rule of combination. In this section, we describe four properties that a candidate Dempster's rule of combination with importance factors should follow. Properties 1 and 2 ensure that the combined result is a valid evidence. Property 3 guarantees that the original Dempster's Rule of Combination is a special case of Dempster's Rule of Combination with importance factors,where the combined evidences have the same priority. Property 4 ensures that importance factors of the evidences are also independent from each other. Property 1. No belief ought to be committed to in the result of our combination rule m'(Φ)=0 (5) Property 2. The total belief ought to be equal to 1 in the result of our combination rule Σm'(A)=1 (6) Property 3. If the importance factors of each evidence are equal, our Dempster's rule of combination should be equal to Dempster's rule of combination without importance factors m'(A,IF1,IF)= m(A); if IF1= IF2 (7) for all Aϵ θ, where m(A) is the original Dempster's Combination Rule. Property 4. Importance factors of each evidence must not beexchangeable m'(A1, IF1, IF2) ≠ m'(A,IF2,IF1) if (IF1 ≠ IF2) (8)

Dempster's Rule of Combination with Importance Factors

In this section, we propose a Dempster's rule of combination with importance factors. We prove our combination rule follows the properties defined in the previous section.

Theorem 1. Dempster's Rule of Combination with Importance Factors:

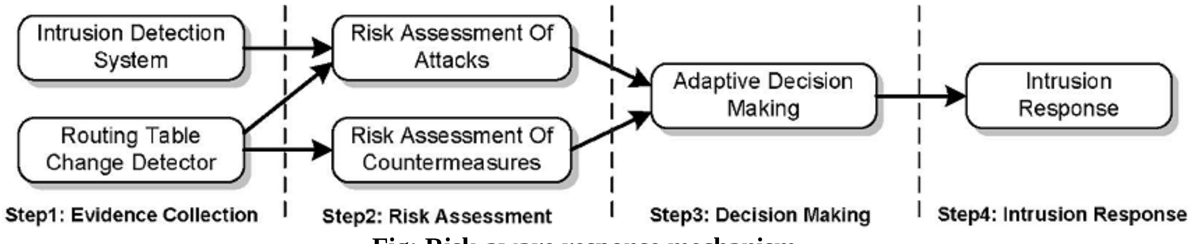

Fig: Risk-aware response mechanism.

Suppose Bel1 and Bel2 are belief functions over the same frame of discernment, with basic probability assignments m1 and m2. The importance factors of these evidences are IF1 and IF2. Then, the function m defined by our proposed DRCIF is non associative for multiple evidences. Therefore, for the case in which sequential information is not available for some instances, it is necessary to make the result of combination consistent with multiple evidences. Our combination

www.ijmer.com Vol. 3, Issue. 5, Sep - Oct. 2013 pp-2996-3004 ISSN: 2249-6645

algorithm supports this requirement and the complexity of our algorithm is O (n), where n is the number of evidences. It indicates that our extended Dempster-Shafer theory demands no extra computational cost compared to a naive fuzzy-based method. The algorithm for combination of multiple evidences is constructed as follows:

Algorithm 1. MUL-EDS-CMB

INPUT: Evidence pool Ep

OUTPUT: One evidence

$|Ep| =$ sizeof(Ep);
While $|Ep| > 1$ do
  Pick two evidences with the least IF in Ep, named E_1 and E_2;
  Combine these two evidences, $E = \langle m_1 \oplus m_2, (IF_1 + IF_2)/2 \rangle$;
  Remove E_1 and E_2 from Ep;
  Add E to Ep;
end
return the evidence in Ep

Risk-Aware Response Mechanism

In this section, we articulate an adaptive risk-aware response mechanism based on quantitative risk estimation and risk tolerance. Instead of applying simple binary isolation of malicious nodes, our approach adopts an isolation mechanism in a temporal manner based on the risk value. We perform risk assessment with the extended D-S evidence theory.

Overview

Because of the infrastructure-less architecture of MANET, our risk-aware response system is distributed, which means each node in this system makes its own response decisions based on the evidences and its own individual benefits. Therefore, some nodes in MANET may isolate the malicious node, but others may still keep in cooperation with due to high dependency relationships. Our risk aware response mechanism is divided into the following four steps shown in Fig. 3. Evidence collection. In this step, Intrusion Detection System (IDS) gives an attack alert with a confidence value, and then Routing Table Change Detector (RTCD) runs to figure out how many changes on routing table are caused by the attack. Risk assessment. Alert confidence from IDS and the routing table changing information would be further considered as independent evidences for risk calculation and combined with the extended D-S theory. Risk of countermeasures is calculated as well during a risk assessment phase. Based on the risk of attacks and the risk of countermeasures, the entire risk of an attack could be figured out. Decision making. The adaptive decision module provides a flexible response decision-making mechanism, which takes risk estimation and risk tolerance into account. To adjust temporary isolation level, a user can set different thresholds to fulfill her goal.

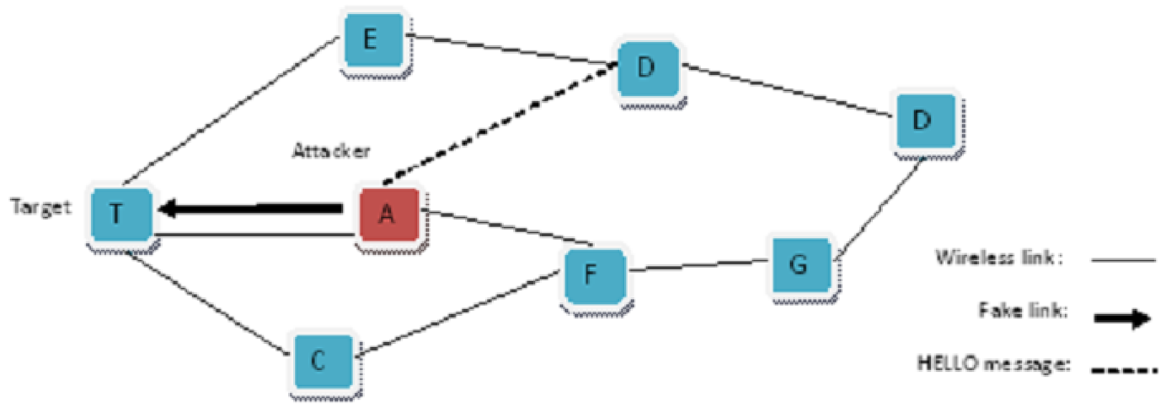

Figure 2: Link spoofing attack

Intrusion response.With the output from risk assessment and decision-making module, the corresponding response actions, including routing table recovery and node isolation, are carried out to mitigate attack damages in a distributed manner.

Response to Routing Attacks

In our approach, we use two different responses to deal with different attack methods: routing table recovery and node isolation. Routing table recovery includes local routing table recovery and global routing recovery. Local routing recovery is performed by victim nodes that detect the attack and automatically recover its own routing table. Global routing recovery involves with sending recovered routing messages by victim nodes and updating their routing table based on corrected routing information in real time by other nodes in MANET. Routing table recovery is an indispensable response and should serve as the first response method after successful detection of attacks. In proactive routing protocols like OLSR, routing table recovery does not bring any additional overhead since it periodically goes with routing control messages. Also, as long as the detection of attack is positive, this response causes no negative impacts on existing routing operations. Node isolation may be the most intuitive way to prevent further attacks from being launched by malicious nodes in MANET. To perform a node isolation response, the neighbours of the malicious node ignore the malicious node by neither forwarding packets through it nor accepting any packets from it. On the other hand, a binary node isolation response may result in negative impacts to the routing operations, even bringing more routing damages than the attack itself. For example, in Fig, Node 1 behaves like a malicious node. However, if every other node simply isolates Node 1, Node 6 will be disconnected from the network. Therefore, more flexible and fine-grained node isolation mechanism is required. In our risk-aware response mechanism, we adopt two types of time-wise isolation responses: temporary isolation and permanent isolation.

Risk Assessment

Since the attack response actions may cause more damages than attacks, the risks of both attack and response should be estimated. We classify the security states of MANET into two categories: {Secure, Insecure}. In other words, the frame of discernment would be {_, {Secure}, {Insecure}, {Secure, Insecure}}. Note that {Secure, Insecure} means the security state of MANET could be either secure or insecure, which describes the uncertainty of the security state.

Selection of Evidence

Evidence choice approach considers subjective proof from experts' information and objective proof from routing table modification. we have a tendency to propose a unified analysis approach for evaluating the risks of each attack (RiskA) and step (RiskC). Take the arrogance level of alerts from IDS because the subjective information conspicuous one. In terms of objective proof, analyze whole completely different routing table modification cases. There area unit staple items in OLSR routing table (destination, next hop, distance). Thus, routing attack can cause existing routing table entries to be unintelligible, or any item of a routing table entry to be changed. We illustrate the possible cases of routing table change and analyze the degrees of damage in Evidences 2 through 5.

Evidence 1: Alert confidence. the boldness of attack detection by the IDS is provided to deal with the likelihood of the attack incidence.

Evidence 2: Missing entry. This proof indicates the proportion of missing entries in routing table. Link withholding attack or node isolation step will cause potential deletion of entries from routing table of the node.

Evidence 3: ever-changing entry I. This proof represents the proportion of fixing entries within the case of next hop being the malicious node.

Evidence 4: ever-changing entry II. This proof shows the proportion of modified entries within the case of various next hops (not the malicious node) and therefore the same distance.

Evidence 5: ever-changing entry III. This proof points out the proportion of fixing entries within the case completely different of various} next hop (not the malicious node) and therefore the different distance. Like proof four, each attacks and countermeasures might end in this proof.

Combination of Evidence

Call the combined evidence for an attack, EA and the combined evidence for a countermeasure, EC. Thus, BelA(Insecure) and BelC(Insecure) represent risks of attack (RiskA) and countermeasure (RiskC), respectively. The combined evidences, EA and EC are defined and the entire risk value derived from RiskA and RiskC

$EA = E1 \oplus E2 \oplus E3 \oplus E4 \oplus E5,$

$EC = E2 \oplus E4 \oplus E5,$

where $\oplus$ is Dempster's rule of combination with important factors defined in Theorem 1

Risk = RiskA - RiskC = BelA(Insecure) –BelC(Insecure).

Adaptive Decision Making

The response level is as well divided into multiple bands. each band is said to academic degree isolation degree, that presents a special amount of your time of the isolation action. The response action and band boundaries unit all determined in accordance with risk tolerance and may be changed once risk tolerance threshold changes. the upper risk tolerance threshold (UT) would be associated with permanent isolation response. The lower risk tolerance threshold (LT) would keep each node intact. The band between the upper tolerance threshold and lower tolerance threshold is said to the temporary isolation response, inside that the isolation time (T) changes dynamically supported the assorted response level given by following equation where n is that the vary of bands which i is that the corresponding isolation band.

V. SYSTEM DESIGN & ARCHITECTURE DIAGRAMS

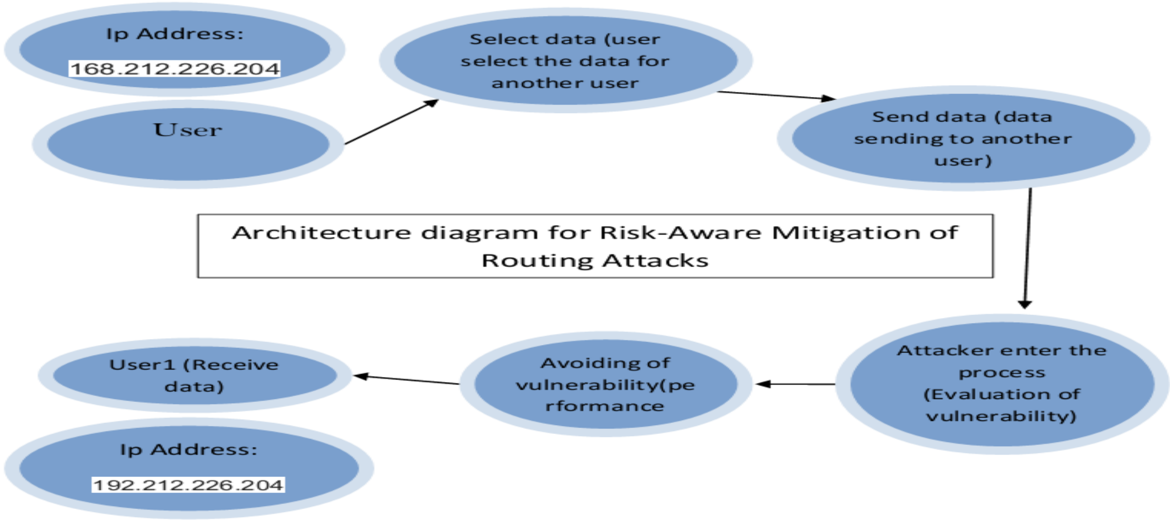

Fig: Architecture diagram for mitigation of Routing attacks

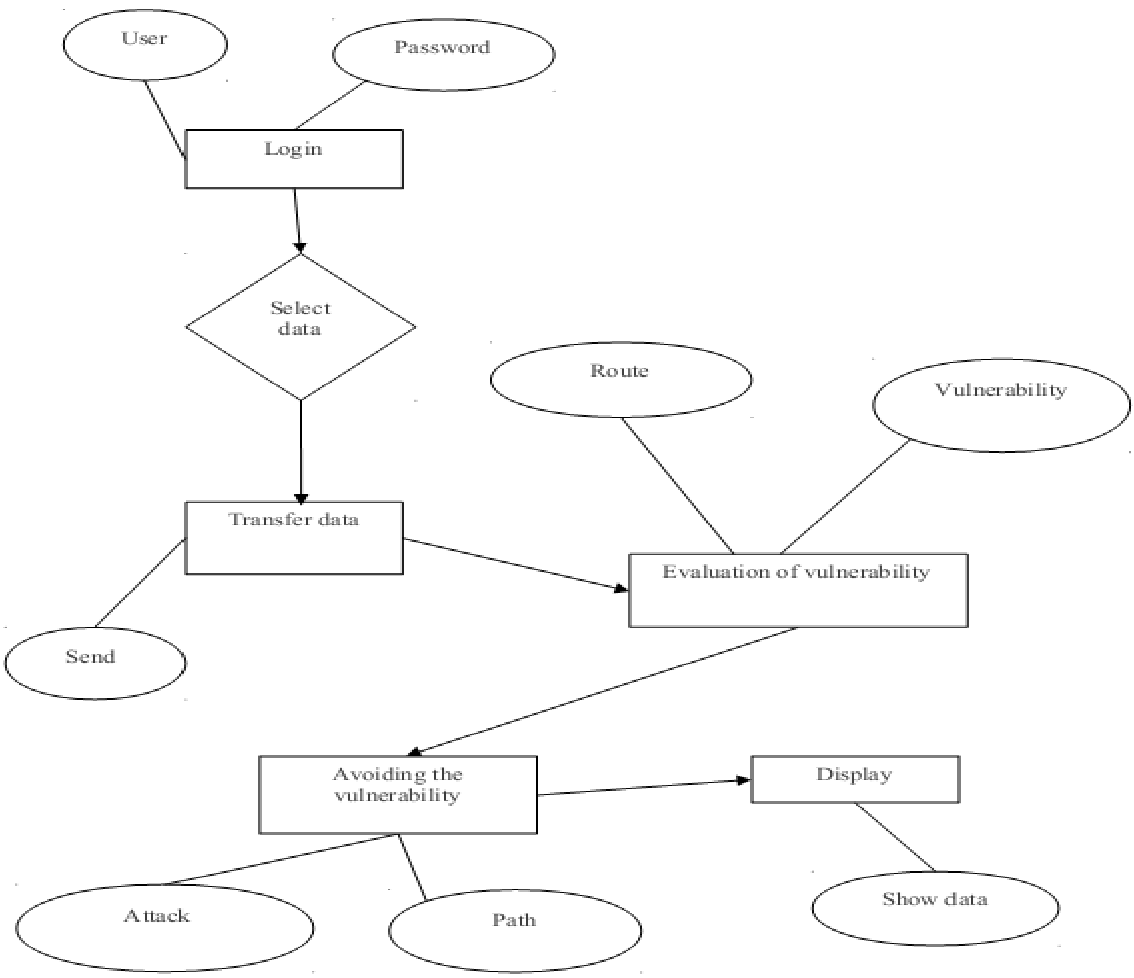

Fig: Overall Architecture

VI. EXPERIMENT & RESULT

The performance ends up in these random network topologies of our risk-aware approach with DRCIF, riskaware approach with DRC and binary isolation approach. In Fig. 5, because the range of nodes will increase, the packet delivery magnitude relation conjointly will increase as a result of their square measure a lot of route decisions for the packet transmission. Among these 3 response mechanisms, we have a tendency to conjointly notice the packets delivery magnitude relation of our DRCIF riskaware response is on top of those of the opposite 2 approaches.

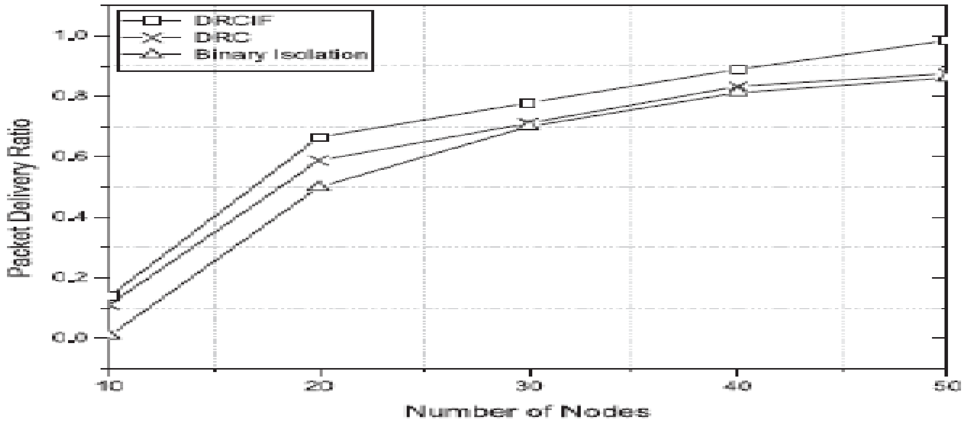

Fig: Packet delivery ratio

In Fig we are able to observe that the routing price of our DRCIF risk-aware response is under those of the opposite 2 approaches. Note that the fluctuations of routing price shown in Fig. three are caused by the random traffic generation and random placement of nodes in our realistic simulation. In our DRCIF risk-aware response, the amount of nodes that isolate the malicious node is a smaller amount than the opposite 2 response mechanisms.

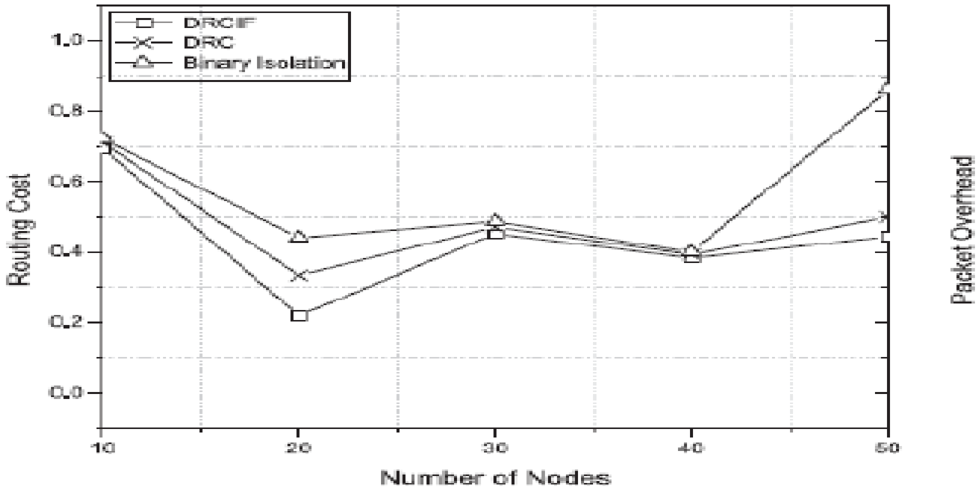

Fig: Routing cost

In Fig that's the reason why we can also notice that as the number of nodes increases, the packet overhead and the using our DRCIF risk-aware response are slightly higher than those of the other two response mechanisms.

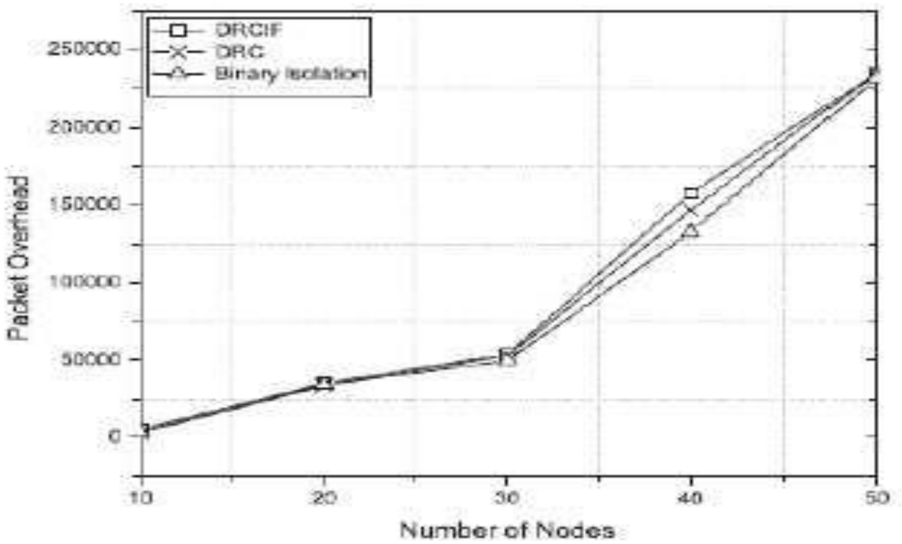

Fig: Packet Overhead

In Fig The mean latency victimization our DRCIF risk-aware response is over those of the opposite 2 response mechanisms, once the amount of nodes is smaller than twenty. However, once the amount of nodes is bigger than twenty, the mean latency victimization our approach is a smaller amount than those of the opposite 2 response mechanisms.

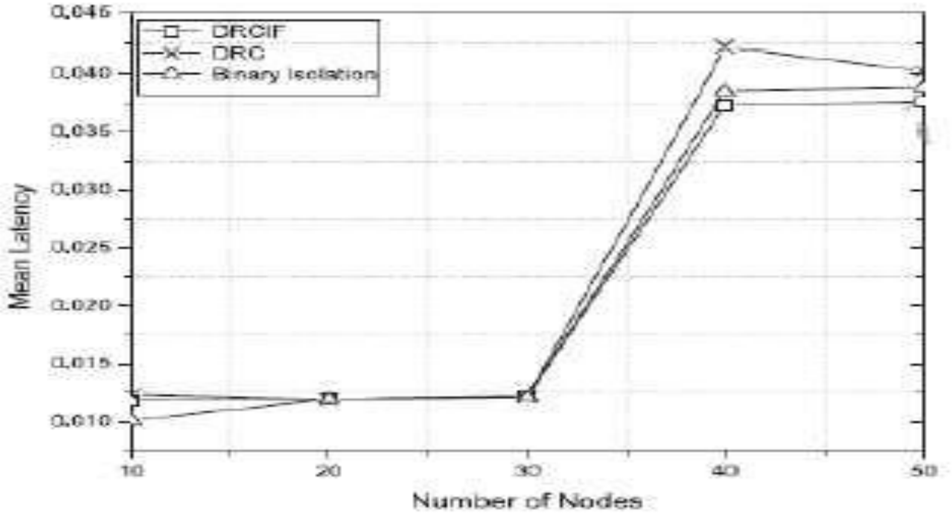

Fig: Mean Latency

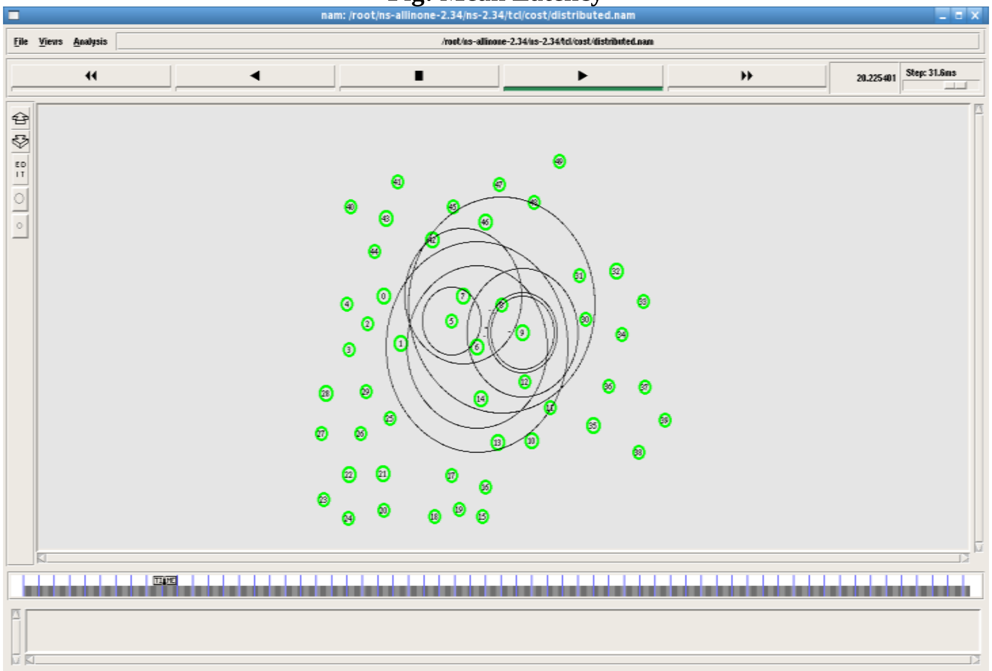

Screen shot 1: Node communication

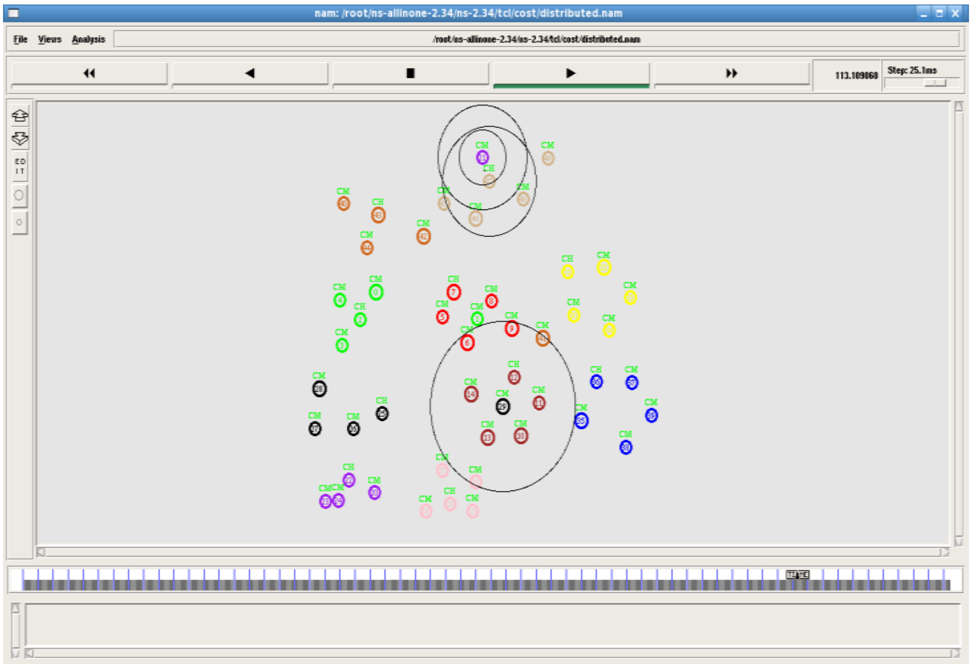

Screen shot 2: Attack detection

VII. CONCLUSION

Handling MANET Routing Attacks Using Risk Aware Mitigation Mechanism with Distributed Node Control. Especially, our approach considered the potential damages of attacks and countermeasures. so as to live the danger of each attacks and countermeasures, we tend to extended D-S theory of proof with a notion of importance factors. Supported many metrics, we tend to additionally investigated the performance and utility of our approach and also the experiment results clearly incontestable the effectiveness and quantifiable of our risk aware approach. Supported the promising obtained through these experiments.

ACKNOWLEDGMENT

I would like to express my sincere thanks to my Guide and my Co-Authors for their consistence support and valuable suggestions.

REFERENCES

[1] Y. Sun, W. Yu, Z. Han, and K. Liu, "Information Theoretic Framework of Trust Modeling and Evaluation for Ad Hoc Networks," IEEE J. Selected Areas in Comm., vol. 24, no. 2,pp. 305-317, Feb.2006.
[2] M. Refaei, L. DaSilva, M. Eltoweissy, and T. Nadeem, "Adaptation of Reputation Management Systems to Dynamic Network Conditions in Ad Hoc Networks," IEEE Trans. Computers, vol. 59, no. 5,pp. 707-719, May 2010.
[3] P. Cheng, P. Rohatgi, C. Keser, P. Karger, G. Wagner, and A.Reninger, "Fuzzy Multi-Level Security: An Experiment on Quantified Risk-Adaptive Access Control," Proc. 28th IEEE Symp.Security and Privacy, 2007.
[4] S. Wang, C. Tseng, K. Levitt, and M. Bishop, "Cost- Sensitive Intrusion Responses for Mobile Ad Hoc Networks," Proc. 10th Int'l Symp. Recent Advances in Intrusion Detection (RAID '07), pp. 127-145, 2007.
[5] G. Shafer, A Mathematical Theory of Evidence. Princeton Univ., 1976.
[6] L. Sun, R. Srivastava, and T. Mock, "An Information Systems Security Risk Assessment Model under the Dempster-Shafer Theory of Belief Functions," J. Management Information Systems,vol. 22, no. 4, pp. 109- 142, 2006.
[7] C. Mu, X. Li, H. Huang, and S. Tian, "Online Risk Assessment of Intrusion Scenarios Using D-S Evidence Theory," Proc. 13th European Symp. Research in Computer Security (ESORICS '08),pp. 35-48, 2008.
[8] K. Sentz and S. Ferson, "Combination of Evidence in Dempster-Shafer Theory,"technical report, Sandia Nat'l Laboratories, 2002.
[9] L. Zadeh, "Review of a Mathematical Theory of Evidence," AIMagazine, vol. 5, no. 3, p. 81, 1984.
[10] R. Yager, "On the Dempster-Shafer Framework and New Combination Rules_1," Information Sciences, vol. 41, no. 2, pp. 93- 137, 1987.
[11] H. Wu, M. Siegel, R. Stiefelhagen, and J. Yang, "Sensor Fusion Using Dempster-Shafer Theory," Proc. IEEE Instrumentation and Measurement Technology Conf., vol. 1, pp. 7-12, 2002.
[12] T. Clausen and P. Jacquet, "Optimized Link State Routing Protocol," Network Working Group, 2003.
[13] C. Perkins, E. Belding-Royer, and S. Das, "Ad Hoc On- Demand Distance Vector Routing," Mobile Ad-Hoc Network Working Group,vol. 3561, 2003.

A Graphical Password Scheme using Persuasive Cued Click Points

Moulisai Rachagundla[1], Syed Gulam Gouse[2]
[1]M.Tech, Nimra College of Engineering & Technology, Vijayawada, A.P., India.
[2]Professor, Dept.of CSE, Nimra College of Engineering & Technology, Vijayawada, A.P., India.

ABSTRACT: *Despite the ubiquity of password systems, knowledge-based authentication mechanism remains an important and active research area. Many current systems have low level security, and even then users often devise insecure coping strategies in order to compensate for memorability and usability problems. Alternatives such as tokens or biometrics raise other issues such as privacy and loss. Various graphical password mechanisms have received considerable attention in response. A systematic review of the literature on graphical passwords shows no consistency in the usability and security evaluation of various schemes. The situation is similar for text passwords, making fair comparison between methods nearly impossible. This paper presents a graphical password scheme using persuasive cued click points. This method is based on knowledge based authentication.*

Keywords: *Authentication, Cued click points, Graphical password, Persuasive technology.*

I. INTRODUCTION

To validate the end user for authentication, we usually prefer to adopt the knowledge-based authentication mechanism, which involves text based passwords. The text based passwords [1] are vulnerable to be hacked. The hackers can easily guess the text passwords with other details of the system. If we want to avoid this, the system can assign a strong password, which the hacker cannot guess. But the system assigned passwords are very difficult to memorize and also remembered by the user. The study on the graphical password mechanisms states that the click point passwords are hard to guess by the attacker and easy to remember for the users. So the password authentication system should encourage the strong password selection scheme while maintaining the memorability of the user. This paper proposes the idea of persuasive technology [2] cued click point authentication with dynamic user blocks.

This mechanism influence the user to set a random password which cannot be guessed and also being graphical, the user can easily remember. In practical situations the same user will require different level of security for different types of applications over the internet. But the existing system provides a concrete security level, which is same for all users and the applications. It sets the threshold value as a fixed one whose size cannot be changed. In the proposed system the size of the threshold value is set by the user, depending upon his/her current requirement, with the help of dynamic user blocks. To increase the memorability of the user, audio support can also be provided, i.e. each click point is randomly associated with an audio sound clip. So that legitimate user can be alarmed for wrong clicks.

II. LITERATURE SURVEY

A. Token based Methods

The traditional user name /password or personal identification number (PIN) based authentication scheme is an example of the Token Based. It is based on “something You possess”. For example, Smart Cards, a driver's license, credit card, a university ID card etc. It allows users to enter their user name/ password in order to obtain a token which allows them to fetch a specific resource- without using their user name and password. Once their token has been obtained, then the user can offer the token-which offers access to a specific resource for a time period- to the remote site[3].

B. Biometrics

Biometrics is the study of automated methods for uniquely recognizing human beings based upon one or more intrinsic physical or behavioral traits. It is based on “something you are”. It uses physiological or behavioral characteristics like facial or fingerprint scans and iris or voice recognition to identify users[4].

C. Knowledge based Authentication

Knowledge based authentication are the most extensively used authentication techniques and include both text based and picture based passwords KBA is based on “something You Know to identify you”. The major drawback of token-based and biometric- based authentication methods are expensive and requires special devices. Graphical- based password methods have been proposed as a potential alternative to text-based techniques, supported partially by the fact that humans can remember images better than text Psychologists have confirmed that in both recognition and recall scenarios, the images are more memorable than text. Therefore, graphical- based authentication mechanisms have higher usability than other authentication techniques In general, the graphical password methods can be classified into two categories: Recognition-based[5] and Recall- based graphical techniques [6].

D. Click based Graphical Password

Graphical password mechanisms are a type of knowledge-based authentication that attempts to leverage the human memory for visual information. A precursor to Persuasive cued click points(PCCP) was designed to reduce patterns and to reduce the usefulness of hotspots for attackers. Rather than five click- points on one image, CCP uses one click-point on five different images shown in the sequence[7].The next image displayed is based on the location of the previously entered cued click-point (Figure. 1), creating a path through an image set. Users select their images only to the extent that their cued click-point determines the next image. Creating a new password with different cued click-points results in a different image sequence[8].

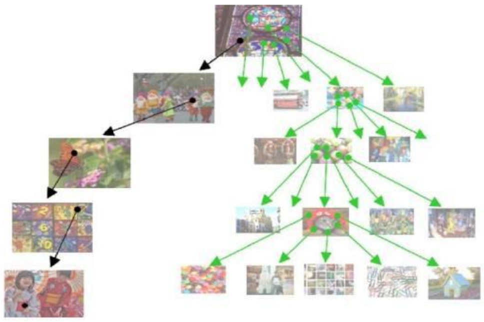

Figure 1: A user navigates through images to form a CCP password

E. Persuasive Technology

Persuasive Technology is a technology to motivate and influence people to behave in a desired manner. An authentication method which applies Persuasive Technology should guide and encourage users to select stronger passwords, but not impose system-generated passwords. To be effective, the users must not ignore the persuasive technology elements and the resulting passwords must be memorable. As detailed below, PCCP accomplishes this by making the task of selecting a low level(weak) password more tedious and time consuming [7]. The path of least resistance for users is to select a strong password (not comprised entirely of known hotspots or following a predictable pattern).The formation of hotspots across various users is minimized since click-points are more randomly distributed.

III. PERSUASIVE CUED CLICK POINT MECHANISM

Using a skewed password distribution the hackers can guess the password in the previous graphical password schemes. Without the system guidance most of the users clicks on the hotspot in each selected image. In this method the system influence the user to select more random clicks, and also maintains the memorability of the user. In this method when the image is displayed the randomly selected block called the view port only clearly seen out. All the other parts of the image are shaded, so that the user can click only inside the view port of the image. This is how the PCCP influence the user to select the position of the cued click point. The view ports of the image are selected by the system randomly for each image to create a graphical password. It will be very hard for the hackers to guess the click point in all the images.

The users are allowed to click anywhere in the view port of the image. There is an option for changing the viewport (Figure 2) position also. This option is called as "Shuffle". There is a limit on the number of times the shuffle option to be used by the user. While users may shuffle as often as desired, this significantly slows down the password creation. The viewport and shuffle button appear only during password creation process. During later password entry, the images are displayed normally, without shading or the view port, and the users may click anywhere on the images. Like Pass Points and CCP, login click-points must be within the defined tolerance squares of the original points in the image. The theoretical password space for a password system is the total number of unique passwords that could be generated according to the given system specifications.

Ideally, a larger theoretical password space would lowers the likelihood that any particular guess is correct for a given password. Whereas text passwords have very skewed distributions resulting in an effective password space much smaller than the theoretical space, therefore PCCP is specifically designed to significantly reduce such skews. The recall studies of the PCCP approach proved that remembrance of the graphical password methods is much better than the text-based passwords.

Figure 2: PCCP Create Password interface. The viewport highlights part of the image

IV. USABILITY EVALUATION AND SECURITY ANALYSIS

A. Usability of PCCP

PCCP has similar success rates to the other authentication mechanisms evaluated (CCP, PassPoints, and text). PCCP password entry takes a similar time to the other mechanisms in the initial lab sessions, but the results indicate longer recall times for PCCP when recalling passwords beyond the initial session. Users who shuffled more had significantly higher success rates in the PCCP Lab study, but the difference in success rates between high and low shufflers was not statistically significant for the two week or the web studies. Furthermore, users reported favorable opinions of PCCP in the post-task questionnaires; a general trend indicates that larger images or more click- points negatively impacts the password entry time. No clear pattern emerges between the 6 conditions for success rates, providing no evidence that either manipulation affects success rates in a consistent manner.

B. Security of PCCP

Given that click-point clustering and hotspots are significantly less prominent for PCCP than for CCP and Pass-Points, guessing attacks based on these characteristics are less likely to succeed. Taking into account PCCP's sequence of images rather than a single image offers further reduction in the efficiency of the guessing attacks. For capture attacks, PCCP is susceptible to shoulder surfing and malware capturing user input during the password entry. However, we expect social engineering and phishing to be more difficult than for other cued recall graphical password methods due to PCCP's multiple images.

V. CONCLUSION

Graphical password schemes essentially use images or representation of images as passwords. Human brain is good in remembering images (pictures) than textual character. There are various graphical password methods or graphical password software's are available in the market. Therefore, this paper work merges persuasive cued click points and the password guessing resistant protocol. The major goal of this work is to reduce the guessing attacks as well as encouraging users to select more random, and difficult passwords to guess by attackers. Well known security threats like brute force attacks and the dictionary attacks can be successfully abolished using this method.

REFERENCES

[1] S. Chiasson, A. Forget, E. Stobert, P. van Oorschot, and R. Biddle, "Multiple Password Interference in Text and Click-Based Graphical Passwords," Proc. ACM Conf. Computer and Comm. Security (CCS), Nov. 2009.

[2] A. Forget, S. Chiasson, P. van Oorschot, and R. Biddle, "Improving Text Passwords through Persuasion," Proc. Fourth Symp. Usable Privacy and Security (SOUPS), July 2008.

[3] Wazir Zada Khan, Mohammed Y. Aalsalem and Yang Xiang ―A Graphical Password Based Systems for Small Mobile Devices, IJCS Issues, vol 8,Issue 5, No. 2, September 2011.

[4] Neil Yager and Ted Dunstone ―The Biometric Menagerie‖ IEEE Transactions on Pattern Analysis and Machine Intelligence, Vol 32, No. 2 February 2010.

[5] Sadiq Almuairrfi, Prakash Veeraraghavan and Naveen Chilamkurti ―Implicit Password Authentication System ― 2011 Workshops of International Conference on Advanced Information Networking and Applications.

[6] Xiaoyuan Suo Ying Zhu and G. Scott. Owen ―Graphical Passwords : A Survey.

[7] S. Chiasson, A. Forget, R. Biddle, and P. van Oorschot, "Influencing Users towards Better Passwords: Persuasive Cued Click-Points," Proc. British HCI Group Ann. Conf. People and Computers: Culture, Creativity, Interaction, Sept. 2008.

[8] X.S. Zhou and T.S. Huang, ― Relevance feedback For Image Retrieval: A Comprehensive Review,Multimedia systems, vol.8, no. 6 Apr. 2003.

International Journal of Modern Engineering Research (IJMER)
www.ijmer.com Vol. 3, Issue. 5, Sep - Oct. 2013 pp-3008-3011 ISSN: 2249-6645

3D Median Filter Design for Iris Recognition

K. Ganesh Kumar[1], Dr. K. Kiran Kumar[2]
[1]M. Tech (ES), Dept. of ECM, KL University, Guntur Dist., A.P., India.
[2]Professor, Dept. of ECM, KL University, Guntur Dist., A.P., India.

ABSTRACT - *In many applications user authentication has to be carried out by portable devices. These kinds of devices must deal with constraints like computational performance, power consumption while also maintaining high performance rates in the authentication process. This paper provides solutions to designing such personal tokens where biometric authentication is required. In this paper, a 3D median filter design for iris biometrics has been chosen to be implemented due to the low error rates.*
Keywords *– Biometric authentication, 3D median filter.*

I. INTRODUCTION

Biometrics is the science of automated recognition of persons based on one or more physiological or behavioral characteristics. Possible biometrics methods include face, fingerprint, iris, hand shape, gait, signature, etc. Biometrics is widely used in many applications, such as access control to secure facilities, verification of financial transactions, welfare fraud protection, law enforcement, and immigration status checking when entering a country. Biometrics is the only method capable of recognizing human beings using the real features of the user instead of his or her knowledge (e.g., passwords) or belongings (e.g., a magnetic stripe card) [1]. Among currently existing biometric modalities, iris recognition is considered to be one of the most secure and reliable technologies [2], [4], [6], [5]; however, while matching algorithms in iris recognition are straightforward, the signal processing prior to matching requires a significant amount of processing power.

IRIS ACQUISITION

Iris recognition is an automated method of biometric identification that uses mathematical pattern-recognition techniques on video images of Irises of an individual's eyes, whose complex random patterns are unique and can be seen from some distance.

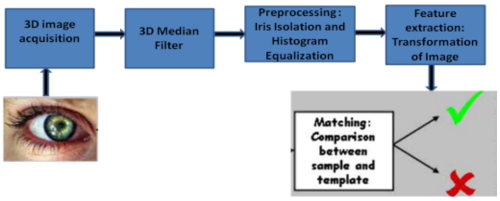

Fig.1. Block diagram of a biometric system

Iris biometrics systems do not use laser-scans to capture the image of the human eye. Instead, an infrared photo or video camera is used at a set distance to capture a high quality image of the iris. Working in the infrared range provides many advantages when compared to the visible range: iris ridges, nerves, and crypts are more evident, the border between the iris and the pupil is more pronounced; and users are not exposed to annoying flashes.

A 3D median filter takes input as 2D or 3D image this can be done using a Stereo camera.
A stereo camera is that which captures the iris image in 3D.

IRIS SEGMENTATION

The main purpose of this process is to locate the iris on the image and isolate it from the rest of the eye image for further processing. Some other important tasks that are also performed in this iris segmentation block include image quality enhancement noise reduction, and emphasis of the ridges of the iris.

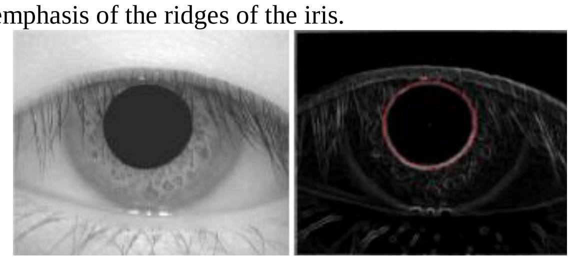

(a) (b)

Fig.2 Input image (a), detected pupil edge

FEATURE EXTRACTION

Feature extraction involves simplifying the amount of resources required to describe a large set of data accurately. When performing analysis of complex data one of the major problems stems from the number of variables involved.

Analysis with a large number of variables generally requires a large amount of memory and computation power or a classification algorithm which overfits the training sample and generalizes poorly to new samples. Feature extraction is a general term for methods of constructing combinations of the variables to get around these problems while still describing the data with sufficient accuracy.

II. MEDIAN FILTER

Median filter is windowed filter of nonlinear class that is used for image quality improvement. Median filter[8] is used “salt and pepper” noise reduction and in some cases to suppress speckle noise. The median filter is a nonlinear digital filtering technique, often used to remove noise. Such noise reduction is a typical pre-processing step to improve the results of later processing (for example, edge on an image).

Median filtering is very widely used in digital image processing because, under certain conditions, it preserves edges while removing noise like salt and pepper noise

WORKING:

Like the mean filter, the median filter considers each pixel in the image in turn and looks at its nearby neighbors to decide whether or not it is representative of its surroundings. Instead of simply replacing the pixel value with the mean of neighboring pixel values, it replaces it with the *median* of those values. The median is calculated by first sorting all the pixel values from the surrounding neighborhood into numerical order and then replacing the pixel being considered with the middle pixel value. (If the neighborhood under consideration contains an even number of pixels, the average of the two middle pixel values is used.)

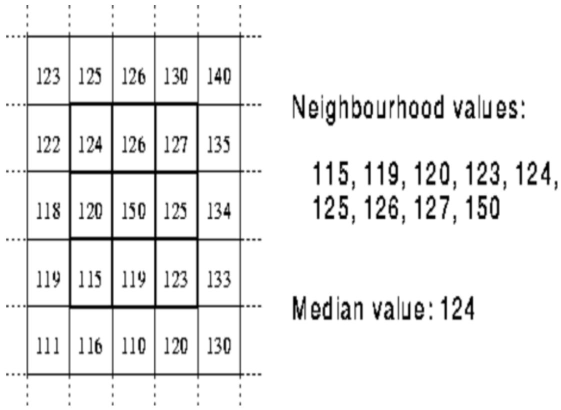

Fig.4 calculating the median value of a pixel neighborhood.

As can be seen, the central pixel value of 150 is rather unrepresentative of the surrounding pixels and is replaced with the median value: 124. A 3×3 square neighborhood is used here; larger neighborhoods will produce more severe smoothing.
By calculating the median value of a neighborhood rather than the mean filter, the median filter has two main advantages over the mean filter:

1) The median is a more robust average than the mean and so a single very un-representative pixel in a neighborhood will not affect the median value significantly.
2) Since the median value must actually be the value of one of the pixels in the neighborhood, the median filter does not create new unrealistic pixel values when the filter straddles an edge. For this reason the median filter is much better at preserving sharp edges than the mean filter.

SALT AND PEPPER NOISE

Salt and pepper noise[3] is a form of noise typically seen on images. It represents itself as randomly occurring white and black pixels. An effective noise reduction method for this type of noise involves the usage of a median filter, morphological filter or a contra harmonic mean filter. Salt and pepper noise creeps into images in situations where quick transients, such as faulty switching, take place.
As a stereo camera is used in getting iris image it gives a 3D image of iris which contains salt and pepper noise

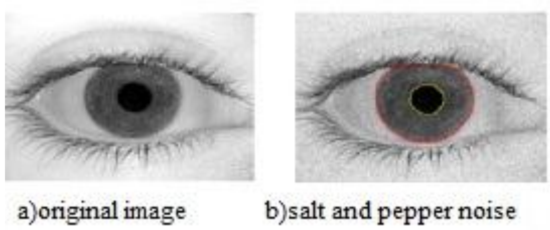

Fig.3 Iris image with salt and pepper noise

3D MEDIAN FILTER

3D median filter[9] uses 3D parallelepiped window to process volume image elements.

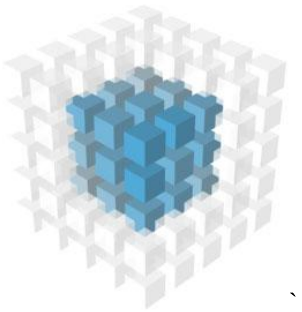

Fig. 4 Window or mask of size 3×3×3 in 3D

In special cases we can analyze and process sequences of image frames corrupted with different levels of noise. These frames of images can be stored in the selected three-dimensional matrix X3(1: M; 1: N; 1: K). The operation of a moving three-dimensional array mask is illustrated in algorithm presented.

```
for i=1:M-2
    for j=1:N-2
      for k=1:K-2
           B (1:3, 1:3, 1:3) =...
              X3(i-1:i+1,j-1:j+1,k-1:k+1);
           Y ( i, j, k)= med(B(:));
          end
       end
 end
```

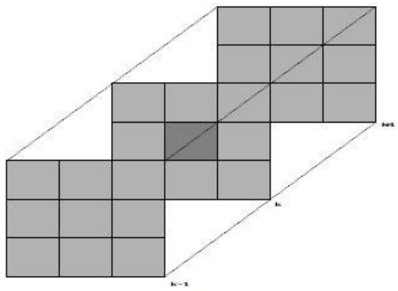

Fig.5 The three-dimensional median filter masken

Estimation of Statistical Parameters

The parameters which are used in estimation of performance are Signal to Noise Ratio (SNR), Root Mean Square Error (RMSE), and Peak Signal to Noise Ratio (PSNR) [7].

A. Estimation of SNR

SNR compares the level of desired signal to the level of background noise. The higher the SNR, the lesser the noise in the image and vice versa [7].

$$SNR = 10 \log (\sigma_g^2/\sigma_e^2)$$

Where, σ_g^2 is the variance of the original image and

σ_e^2 is the variance of error between the original and image denoised with some filter.

B. Estimation of RMSE

Mean square error (MSE) is given by

$$MSE = \sum_{i=j=1}^{N} [f(i,j) - F(i,j)]^2 / N^2$$

Where, f is the original image F is the image denoised with some filter and N is the size of image [7].

RMSE = √MSE

C. Estimation of PSNR

PSNR gives the ratio between possible power of a signal and the power of corrupting noise present in the image [7]. Higher the PSNR gives lower the noise in the image i.e. higher image quality.

PSNR = 20 log10 (255/RMSE)

APPLICATIONS:

Median filter is having following applications in image processing applications.
1. Median filtering extensively used for Salt & Pepper noise filtering purpose.
2. Its edge preserving quality makes it to useful in cases where edge blurring is unacceptable.
3. This filter also used to remove speckle noise from images

ADVANTAGES
1. Simple to understand.
2. Preserves brightness difference resulting in minimal blurring of regional boundaries.
3. Median computer algorithm can be customized.

DISADVANTAGES
1. Less effective in removing Gaussian or random intensity noise.
2. High computational cost.
3. Removes noise only if the noisy pixel occupies less than one half of neighbor- hood area.

III. CONCLUSION

As previously used 2D median filter doesn't gives a much efficient filtering of noise in images it can be replaced by an 3D median filter for better noise removal.

As the theoretical studies give that a 3D median filter is most efficient in removing salt and pepper noise in 3D ultrasound images. It can be applied to an iris biometric system for more efficient de-noising if images.

REFERENCES

[1] A. Jain, R. Bolle, and S. Pankanti, , S. P. A. Jain and R. Bolle, Eds., *Biometrics: Personal Identification in a Networked Society*. Norwell, MA: Kluwer, 1999.

[2] M. Faundez-Zanuy, "Biometric security technology," *IEEE A&E Syst. Mag.*, vol. 21, no. 6, pp. 15–26, Jun. 2006.

[3] Salt-and-Pepper Noise Removal by Median-Type Noise Detectors and Detail-Preserving Regularization Raymond H. Chan, Chung-Wa Ho, and Mila Nikolova; IEEE TRANSACTIONS ON IMAGE PROCESSING, VOL. 14, NO. 10, OCTOBER 2005 1479.

[4] P. Phillips, W. T. Scruggs, A. J. O'Toole, P. J. Flynn, K. W. Bowyer, C. L. Schott, and M. Sharpe, "FRVT 2006 and ICE 2006 large-scale results," Nat. Inst. Standards Technol.,2007. [Online].

[5] Independent Biometric Group, "Comparative biometric testing round 6 public report," 2006 [Online]. Available: http://www.biometricgroup.com/reports/public/comparative_biometric_testing.html..

[6] K. Bowyer, K. Hollingsworth, and P. Flynn, "Image understanding for iris biometrics: A survey," *Comput. Vision Image Understand.*, vol.110, no. 2, pp. 281–307, 2008.

[7] Z. Wang, A. Bovik, H. Sheikh, and E. Simoncelli, "Image quality assessment: From error measurement to structural similarity," *IEEE Trans. Image Process.*, vol. 13, no. 4, pp. 600–612, Apr. 2004.

[8] NON-LINEAR MEDIAN FILTERING OF BIOMEDICAL IMAGES V. Musoko and A. Prochiazka; IJCSI International Journal of Computer Science Issues, Vol. 8, Issue 5, No 3, September 2011.

[9] High-performance 3D median filter architecture for medical image despeckling November 23 2006 Jiang, M. Sch. of Electron., Queen"s Univ. Belfast Crookes, D. Volume: 42 .

[10] Iris Biometrics for Embedded Systems Judith Liu-Jimenez, *Student Member, IEEE*, Raul Sanchez-Reillo, *Member, IEEE*, and Belen Fernandez-Saavedra, *Student Member*, IEEE TRANSACTIONS ON VERY LARGE SCALE INTEGRATION (VLSI) SYSTEMS, VOL. 19, NO. 2, FEBRUARY 2011.

[11] Karakas DG, Trahnias, Trahanis PE, "Generalized Multichannel Image-Filtering Structures," *IEEE Trans. On Image Process.*, vol 6, no. 7, pp1038-45,1997.

[12] V.Ponomaryyov, A.Rosales-Silva and V. Golikov, "Adaptive and Vector Directional Processing Applied to Video Colour Images," *Electronic Letters*,vol. 42, no. 11 pp 131-32,May 2006.

[13] Dang D. and Luo W., "Color Image Noise Removal Algorithm Utilizing Hybrid Vector Filtering," *Int. Journal of Electronics and Comm.*, vol. 62, no. 1, pp 63-71.

[14] Jin L. and Li D., "A Switching Vector Median Filter Based on CIELAB color Space for Color Image Restoration," *Signal Process. Letters*, vol. 87, no. 6, pp 1345-54.

[15] Rajoo Pandey, Awdesh Kumar Singh and Umesh Ghanekar, "Local Pixel Statistics Based Impulse Detection and Hybrid Color Filtering for Restoration of Digital Color Images," *Intl. Journal of Electronics and Comm., in Press Corrected Proof*, Available online on 29 April 2011.

International Journal of Modern Engineering Research (IJMER)
www.ijmer.com Vol. 3, Issue. 5, Sep - Oct. 2013 pp-3012-3019 ISSN: 2249-6645

A Survey of User Authentication Schemes for Mobile Device

Hezal Lopes[1], Madhumita Chatterjee [2]
**(Computer, Universal College/Mumbai University, India)*
*** (Department of Computer Engineering, Mumbai University, India)*

***ABSTRACT**: Personal mobile devices (PMDs) have become ubiquitous technology. There, steadily increasing computational and storage capabilities have enabled them to over an increasingly large set of services. Mobile devices offer their users lots of possibilities and a feeling of freedom. However, this freedom comes along with new security threats. Sensitive data might be stolen and abused, if an unauthorized person gets unrestricted access to such devices. Considering their significance, it's necessary to ensure that they aren't misused. Therefore, user authentication mechanisms are required. Unfortunately, a less effective and inconvenient PIN based authentication system is used to protect them against their misuse. So far authentication mechanisms like PINs and passwords do not take into account the limited capabilities of user interfaces of mobile devices. So, it is necessary to create and develop specially adapted mechanisms, which are designed to be usable under these restrictions. In this paper, we have tried to identify what are possible approaches for authenticating users on mobile device and highlight their pros and cons in terms of security and usability.*

***Keywords:** User authentication, Graphical method, Image based method, Audio based method.*

I. INTRODUCTION

Mobile devices support us in our everyday life. The main advantage of these devices is that we can take them with us and use them almost everywhere and at any time. We can check our e-mails, read online news, communicate via social networks and do many other things on the go. To support their owners mobile devices create and store a lot of sensitive personal data.

Today, mobile devices are ubiquitous, but are potentially accessible to unauthorized persons. To avoid misusage it is important to implement and use reliable authentication mechanisms. Widely used knowledge-based mechanisms like PINs and passwords are not well suited for mobile devices as the capabilities of user interfaces are very limited.

It is necessary to understand the capabilities and limitations of mobile devices beforehand. It is important to develop new authentication mechanisms specially adapted to the limitations and options of mobile devices.

In this paper we have discussed possible user authentication mechanisms for mobile devices their deficiencies.

II. A USER AUTHENTICATION SCHEMES

User authentication is the primary line of defence for a handheld device [1] that comes into the hands of an unauthorized individual. Password or Personal Identification Number (PIN) based authentication is the leading mechanism for verifying the identity of actual device users but this method has been shown to have considerable drawbacks. For example, users tend to pick PIN or passwords that can be easily guessed. On the other hand, if a password is hard to guess, then it is often hard to remember. To address this problem in handheld devices, some researchers have developed comparatively more secure, affordable and memorable authentication schemes based on graphical assistance, images and audio.

Security of user authentication associated issues comes into view over the use of mobile and handheld devices, handheld devices progressively build up sensitive information and over time gain access to wireless services and organizational intranets. Because of their small size, handheld devices may be misplaced, lost, or stolen, and thus out in the open to an unauthorized individual. If user authentication is not enabled, a general default, the devices contents and network services fall under the control of whoever holds it. Even if user authentication is enabled, the authentication mechanism may be weak (e.g., a four number PIN) or easily guessed. Typing passwords are difficult especially those that are long and complex and the users are limited to one handed typing. Shoulder surfing attack is also a bigger problem with these devices because someone can gain access with ease. User Authentication schemes for mobile and handheld devices can be divided into three broad classes. They are as follows:

- Graphical-based Authentication
- Image based Authentication
- Audio-based Authentication.

II.I Graphical-based Authentication

Many of the deficiencies of password authentication systems arise from the limitations of human memory. If humans were not required to remember the password, a maximally secure password would be one with maximum entropy: it would consist of a string as long as the system allows, consisting of characters selected from all those allowed by the system. Some passwords are very easy to remember, but also very easy to guess with dictionary searches. In contrast, some passwords are very secure against guessing but difficult to remember. This scheme is divided into three categories. [1].

- Password with Graphical Assistance
- Draw-A-Secret
- 3D Graphical Password.

II.I.I Password with Graphical Assistance

Password with Graphical Assistance scheme is stronger than textual passwords [1]. Figure 1(a) shows, step 0 is the initial row of blanks, and steps 1-6 indicate the temporal order in which the user fills in the blanks. The password can be placed in the normal, left-to-right positions as shown in Figure 1(a). Due to the graphical nature of the input interface, however, the user could enter the password in other positions, as well. For example, Figure 1(b) shows a modification in which the user enters the password in a left-to-right manner, but starting from a different initial position than the leftmost. Figure 1(c) shows entering the password in an outside-in strategy. And, of course, these variations can be combined in the obvious way, as shown in Figure 1(d).

0. 1. t 2. t o 3. t o m 4. t o m a 5. t o m a t 6. t o m a t o (a) Left-to-right	0. 1. t 2. o t 3. o m t 4. o m a t 5. o m a t t 6. o m a t o t (b) Rotated left
0. 1. t 2. t o 3. t m o 4. t m a o 5. t m t a o 6. t m t o a o (c) Outside-in	0. 1. t 2. o t 3. m o t 4. m a o t 5. m t a o t 6. m t o a o t (d) A complex example

Figure 1: Password with Graphical Assistance [1]

Advantage

The power of graphical input abilities while yielding a scheme that is convincingly stronger than textual passwords.

Disadvantage

Long and random passwords are hard to remember also it has complex function.

III.I.II Draw-A-Secret

A technique, called "Draw - a - secret (DAS)", which allows the user to draw their unique password [2]. A user is asked to draw a simple picture on a 2D grid. The coordinates of the grids occupied by the picture are stored in the order of the drawing. During authentication, the user is asked to re-draw the picture. If the drawing touches the same grids in the same sequence, then the user is authenticated. Jermyn, et al. suggested that given reasonable-length passwords in a 5 X 5 grid, the full password space of DAS is larger than that of the full text password space.

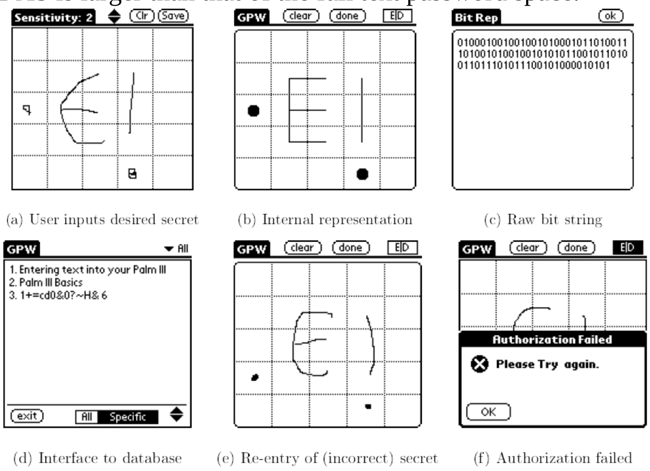

Figure 2: Draw a secret [2]

Advantage

DAS password scheme is hard to crack in practice than the conventional textual scheme.DAS passwords of length 8 or larger on a 5 x 5 grid may be less susceptible to dictionary attack than textual passwords. This approach is alphabet independent. Users are freed from having to remember any kind of alphanumeric string.

Disadvantage

DAS passwords (for some reasonable number of primitives) constitute a larger space than that of textual-based password.

II.I.III 3D-Graphical Passwords

A special feature in this scheme the user is permitted to rotate the drawing canvas (grid) [3]. The rotation is performed on the z-axis, which gives a noticeable clockwise or counter-clockwise motion using either mouse or stylus. The grid is displayed in the window and the user may draw directly on it. The slider may be dragged up or down to adjust the existing rotation angle of the grid. The user rotates the canvas at an angle of, say in the clockwise direction and then for an angle of 90 in the same direction. This is equivalent to (has the same encoding as) a single rotation of 135 in the clockwise direction. However, if the user switches direction, the consecutive rotations are modelled as two distinct events. Hence, rotating the canvas, say in the clockwise direction for 45 and then rotating equivalent to not rotating at all. Such equip-angular bi-directional rotations in-between strokes are encoded differently and generate a different password from drawing the same picture with no rotations at all.

(c) Rotation of -90° and another stroke drawn: (-90)(5,1)(5,2)(5,3)(5,4)(5,5)(6)

(d) Rotation of +90°, rotation of -45°, then another stroke drawn: (+90)(-45)(1,1)(1,2)(1,3)(1,4)(1,5)(6)

Figure 3: 3D Graphical Password [3]

Advantage

This scheme increases the password space to very large extent and hence promises to provide extended security. This scheme provides a higher level of security without compromising user convenience. The same mirror-symmetric drawings with different intermediate rotations are encoded as different passwords, making it difficult for the attacker to form the dictionary simply based on mirror symmetry. Also, rotation of the drawing grid introduces resistance to shoulder-surfing attacks. Consider where an attacker manages to get a glimpse of the final drawing on the canvas when the user is trying to log in. The attacker would try to guess the sequence in which the strokes were made (including the direction of the strokes) by the user while drawing the picture. (Knowing whether the user is right-handed or left-handed might help the attacker guess the direction of the strokes.) If the attacker guesses the sequence and direction of the strokes correctly, he would succeed in getting the user's password. However, the added dimension of rotation makes it significantly difficult for the attacker to guess the password by just looking at the final drawing on the canvas.

Disadvantage

Password space increases around 20 times than draw a secret.

II.II Image based Authentication

Images are more readily recalled than words [1] alphanumeric passwords are harder to remember, especially if they are changed every few months. Instead of letters and numbers for passwords, images can be selected as password in Image-based authentication schemes, these schemes suits to handheld devices those have special security needs.

II.II.I Passface

To log in, users select their Passfaces from a grid of faces displayed on the screen [4]. This study uses the standard implementation of the Passfaces demonstration toolkit, requiring participants to memorise 4 faces, and correctly select all 4: one in each of 4 grids of nine faces (see Figure 4 for an example grid). The grids are presented one at a time on the screen, and the order of presentation remains constant, as do the faces contained in each grid. However, no grid contains faces found in the other grids, and the order of faces within each grid is randomised. These features help secure a user's Passface combination against detection through shoulder-surfing and packet-sniffing.

Figure 4: Passfaces [4]

Advantages

Passfaces have been shown to be very memorable than traditional passwords. Passfaces offer better performance than passwords for users who log in infrequently (less than once every two weeks). These features help secure a user's Passface combination against detection through shoulder-surfing and packet-sniffing.

Disadvantages

The increasing power of computing infrastructure is inevitable. As the increase occurs, the resources that Passfaces require will become ubiquitous. Passfaces should therefore be tested with up to date hardware and software facilities. If these facilities are not available, speed of the authentication mechanisms' responses to user input should be measured and included in analyses, and response times made similar by retarding the password mechanism. Pass face-based log– in process took longer than text passwords and therefore was used less frequently by users. However the effectiveness of this method is still the graphical passwords created using the Passface technique and found obvious patterns among these passwords. For example, most users tend to choose faces of people from the same race. This makes the Passface password somewhat predictable.

1) II.II.II Passclick

A graphical password scheme in which a password is created by having the user click on several locations on an image [5]. During authentication, the user must click on the approximate areas of those locations. The image can assist users to recall their passwords and therefore this method is considered more convenient than unassisted recall a user can click on any place on an image (as opposed to some pre-defined areas) to create a password. A tolerance around each chosen pixel is calculated. In order to be authenticating, the user must click within the tolerance of their chosen pixels and also in the correct sequence.

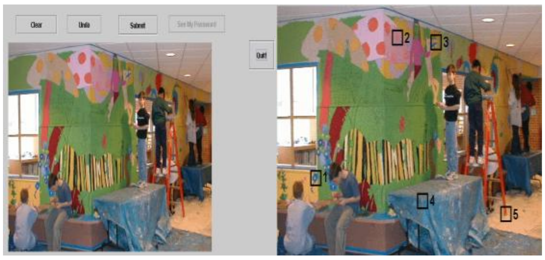

Advantage

There are no multiple rounds of images, just a single image. In an implementation of this scheme the image had predefined click objects or regions that were outlined by thick boundaries. The users chose the password from these objects and logged in using them (although thick boundaries were not visible when logging in). A click anywhere within the boundary was considered correct.

Disadvantage

A problem with this scheme was that the number of predefined click regions was relatively small so the password had to be quite long to be secure (e.g., 12 clicks). Also, the use of pre-defined click objects or regions required simple, artificial images, for example cartoon-like images, instead of complex, real-world scenes. If we have some complicated or crowded image then it takes more time to scan the image to identify their password points. They probably also had to observe the area of their password points very carefully to identify the exact place to click. Consider figure 6 which is very complicated image. So here difficult to identify exact place user has click.

II.III Audio-based Authentication

Audio signal are one of the most useful and effective features for user authentication in mobile environments [1]. Human ability to recall and recognize the audio signal is much higher than remembering words, hence different user authentication schemes are being developed using audio and voice signal. The voice signal conveys many levels of information to the listener. At the primary level, speech conveys a message via words, but at other levels speech conveys information about the language being spoken and the emotion, gender, and, generally, the identity of the speaker. While speech recognition aims at recognizing the words spoken in speech, the goal of automatic speaker recognition systems is to extract, characterize, and recognize the information in the speech signal conveying speaker identity.

II.III.I Voice Verification

Voice Verification [1] presents a user with a series of randomized phrases to repeat so the system can verify not only the voice matches but also the required phrases match. Voice verification, also known as speaker recognition, determines the identity of the speaker. Enrolment requires an individual to say a set of specific words, typically a numeric value, in succession and usually repeated several times. A template is extracted from this input using an acoustic model, which defines the characteristic of the voice. Once enrolled, authenticating to the system is done by prompting the individual to speak into a microphone and vocalize a randomly drawn set of digits, as they appear in the display.

Advantage

Audio signal are one of the most useful and effective features for user authentication in mobile environments. Human ability to recall and recognize the audio signal is much higher than remembering words. The voice signal conveys many levels of information to the listener. At the primary level, speech conveys a message via words, but at other levels speech conveys information about the language being spoken and the emotion, gender, and, generally, the identity of the speaker. While speech recognition aims at recognizing the words spoken in speech, the goal of automatic speaker recognition systems is to extract, characterize, and recognize the information in the speech signal conveying speaker identity.

Disadvantage

While many handheld devices incorporate a built-in sound card and microphone, they typically lack the processing power (i.e., floating point hardware) to perform the needed calculations quickly enough. Other drawbacks to this type of solution include environmental sounds, individual speaker variability in pronunciation (e.g., for the number 12, saying one-two versus twelve), the significant amount of time needed for enrollment compared to other isometric mechanisms, and the larger size templates that are needed. On the other hand, speech is a behavioral signal that may not be consistently reproduced by a speaker and can be affected by a speaker's health (cold or laryngitis). The varied microphones and channels that people use can cause difficulties since most speaker verification systems rely on low-level spectrum features susceptible to transducer/channel effects. The mobility of system likes uncontrolled and harsh acoustic environments (cars, crowded airports), which can stress the accuracy.

II.III.II Audio and Image Authentication

In considering how both audio and visual information can be used to authenticate a user, it was assumed that an individual would make a visual association when a particular piece of music is heard [6]. AVAP protocol is used for this type of authentication. AVAP is based on the following hypothesis: mnemonic associations between audio and visual information can be exploited to authenticate a user. A prototype was developed to authenticate users entering a particular website. The prototype records a number of associations during enrolment, and requests those associations to authenticate users for subsequent website accesses. Five image-sound associations were required. Users were given a randomly-selected sound and required to relate it to one of a corresponding set of 10 images. These associations have to all be recalled at subsequent site entries.. Audio controls were displayed to facilitate repeated audio activation. Audio clips were chosen deliberately to provoke an association within a particular image set, and tended to mirror the general mood of a category (e.g.,. epic orchestral music corresponding to dramatic imagery of the cosmos). Nine audio clips were associated with groups of 10 images, six of which were semantically similar (i.e., same subject matter) and three random. We expected that grouping semantic images together would increase security by reducing the predictability of an association. For instance, it may be trivial to guess that an individual may choose an image of plant life for a given piece of music, but it may not be so easy to select what type of plant life an individual would select from a set of ten semantically-similar images. The three random categories were included to measure the relative performance of associations made using a random image set to those made using a semantically-similar set.

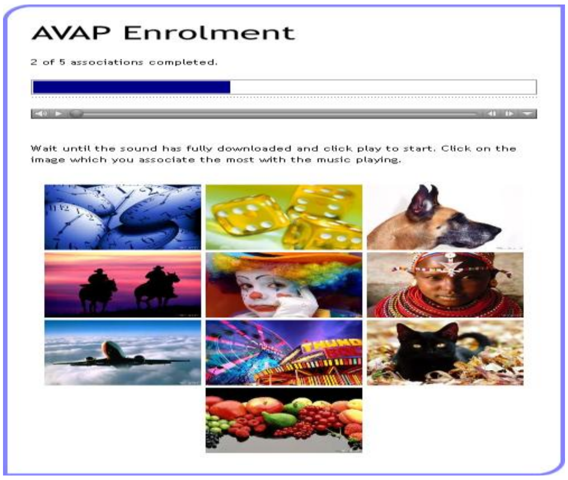

Figure 7: AVAP [6]

Advantage

Exciting and relaxing to use to be more enjoyable and relaxing. The beauty of this scheme is that it is harder for the user to record their password, thus it increases the security of the scheme.

Disadvantage

Users did not always listen to the audio, but only chose pictures they liked. Users became irritated with the time taken for the images to download at each site access. Users struggled to distinguish between semantically similar images and thus made frequent errors. Images were deemed to be too abstract.

II.III.III Audio Visual Person Authentication Using Speech and Ear Images

Figure 8 shows multimodal person authentication system using speech and ear images [7]. Audio and visual data are respectively converted into feature vectors. Each set of features is matched with both a claimed person model and a speaker independent (SI) model. Then, audio and visual scores are integrated with appropriate weighting and a decision is made whether he/she is a true speaker or an impostor. If the score is larger than a threshold value, the speaker is accepted as a claimed speaker.

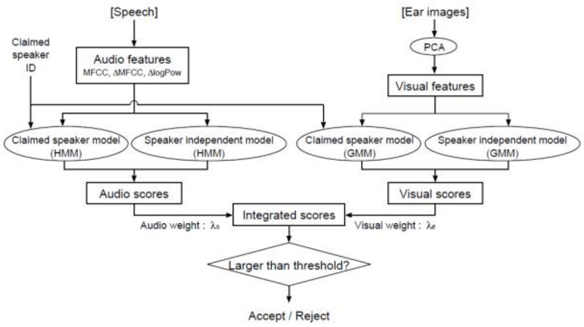

Figure 8: Multimodal Authentication Scheme[7**]**

Advantage

Although most of them use "face" information in combination with speech, the face features also change due to make-up, beard, hair styles and so on, and derives degradation of the performance. Therefore, it is worth investigating other biometric features with high permanence. ear shape hardly changes over time. Ear shape of person does not change over time that increases robustness of person authentication.

Disadvantage

Ear images are more changeable than face images by a tilt of the camera, since the ear surface is more irregular than face surface.

III. COMPARATIVE ANALYSIS OF USER AUTHENTICATION SCHEMES FOR MOBILE AND HANDHELD DEVICES

This table is used to give analysis of all user authentication schemes that we saw above.

	User Authentication Schemes	**Authentication process and usability**	**Memorability /Usability**	**Possible Attacks/ Security Issues**	**Analysis**
Graphical Based Authentication	Alphanumeric Password	Type the password	Complex function, Long and random passwords are hard to remember.	Brute force search, Spy ware, shoulder surfing, etc	Vulnerable to dictionary attacks(simple password)
	Draw a Secret	Users draw something on a 2D grid.	Drawing sequence is hard to remember	Guess, Shoulder Surfing, different password attack methods are not successful	Approach is alphabet independent, Users are freed from having to remember any kind of alphanumeric string
	3D graphical Password	Users draw something on a 3D grid and allowed to rotate the drawing canvas on z axis in clockwise or Counter clockwise motion.	The drawing sequence is hard to Remember. Password space Increase around 20 times than draw a secret scheme.	Guess, Shoulder Surfing, because this scheme include graphical input different password attack methods Are not successful.	Increase the password space to very large extent and hence promise to provides extended security
Image	Pass faces	Recognize and pick the preregistered	Faces are easier to remember, but the choices are	Dictionary (Face) attack, Face brute force	Images are more easily recalled than

Based Authentication		pictures; takes longer than text based password	still predictable. Memorability mainly depends on the total number of rounds in the process and the face selection	search, Guess, shoulder Surfing	words.
	Pass clicks like Blonder scheme Passlogix, Passpoint, visual Key.	Click on several pre registered locations of a picture in the right sequence	If the selected image has limited memorable points in it, pass clicks can be hard to remember. Memorability depends on the image selection	Guess, brute force search, Shoulder surfing. Because this scheme include graphical input different password attack Methods are not successful.	Instead of arbitrary images, user can click on any place on an image.
Audio Based Authentication	Audio Authentication (Voice system and Voice Verification)	Voice signal work as password, voice may be speech or any audio. Process can be fast or slow depend on user.	Depends on the Voice password. Long and random passwords are hard to remember, but Long song, poems are easy to member.	Dictionary attack, Brute force search, Guess, spy ware, Shoulder surfing, etc.	Human ability to recall and recognize the audio signal is much higher than remembering words
	Audio and Image Authentication	Images can be associated with a particular piece of music as a password	The Images and music association. Number of associations chosen by user improve Security but reduces memorability.	Brute force search, Guess, spy ware, Shoulder surfing, etc.	Environmental noise, pronunciation style, speech depends on speaker health, speaker system
	Audio-Visual Person Authentication using Speech and Ear Images	The image of ear shape of a user is integrated with user speech information, high Increases the robustness of user authentication.	Not Applicable Comes under the biometrics user authentication.	Speech is deteriorated by acoustic Noises and time. Ear shape feature changes with time.	Speech can go down by acoustic noise and feature changes over time. Ear shape of person does not change over time that increases robustness of person authentication.

IV. CONCLUSION

Authenticating users on mobile devices can be challenging and many solutions currently being used by mobile applications either compromise security or usability. When mobile devices connect to business networks, user and endpoint authentication play critical roles in preventing misuse, abuse and attack. With effective use of authentication methods, organizations and individuals can cost-effectively guard against current and emerging threats, while retaining optimal productivity and flexibility in their use of mobile devices.

The authors do not support for any particular solution here because the best solution depends on users application's requirements. For example, the security requirements for an online banking application that performs funds transfers are different from the security requirements for student just using mobile for playing games. Additionally, the ultimate security of user application is depending on many implementation details.

REFERENCES

Journal Papers:

[1] M. N. Doja, Naveen Kumar,"User authentication schemes for mobile and handheld Devices", Jamia Millia Islamia - New Delhi,2007.

[2] Jermyn, I., Mayer, A., Monrose, F., Reiter, M.K., Rubin, A.D. "The design and analysis of graphical passwords", In: Proceedings of the Eighth USENIX Security Symposium, pp. 114,1999.

[3] Saikat Chakrabarti, George V. Landon, and Mukesh Singhal. "Graphical Passwords: Drawing a Secret with Rotation as a New Degree of Freedom", To appear in The Fourth IASTED Asian Conference on Communication Systems and Networks (AsiaCSN 2007).

[4] Brostoff, S. and Sasse, M. A. "Are Passfaces more usable than passwords: a field trial investigation", in People and Computers XIV – Usability or Else: Proceedings of HCI. Sunderland, UK: Springer-Verlag, 2000.

[5] Wiedenbeck, S., Waters, J., Birget, J.C., Brodskiy, A. and Memon, N. "Authentication using graphical passwords: Effects of tolerance and image choice", in Symposium on Usable Privacy and Security (SOUPS), at Carnegie-Mellon Univ., Pittsburgh, 6-8 July2005.

[6] Liddell, J., Renaud, K. and De Angeli, A. "Using a combination of sound and images to authenticate web users." Short Paper HCI 2003. 17th Annual Human Computer Interaction Conference. Designing for Society. Bath, England. 8-12 Sept 2003.

[7] Koji Iwano, Tomoharu Hirose,Eigo Kamibayashi, and Sadaoki Furui. "Audio Visual Person Authentication Using Speech and Ear Images", Tokyo Institute of Technology, Department of Computer Science, 2-12-1 Ookayama, Meguro-ku, Tokyo, 152-8552 Japan.

International Journal of Modern Engineering Research (IJMER)
www.ijmer.com Vol. 3, Issue. 5, Sep - Oct. 2013 pp-3020-3025 ISSN: 2249-6645

Implementation of Low Power and High Speed encryption Using Crypto-Hardware

G.VijayaBharathi, *K.VasuBabu, M.tech,*
Asst.Prof, VVIT, Nambur, Guntur.

ABSTRACT: *Cryptographic algorithms such as International Data Encryption Algorithm (IDEA) have found various applications in secure transmission of the data in networked instrumentation and distributed measurement systems. Modulo 2n +1 multiplier and squarer play a pivotal role in the implementation of such crypto-algorithms. In this work, an efficient hardware design of the IDEA (International Data Encryption Algorithm) using novel modulo 2n + 1 multiplier and squarer as the basic modules is proposed for faster, smaller and low-power IDEA hardware circuits. Novel hardware implementation of the modulo 2n + 1 multiplier is shown by using the efficient compressors and sparse tree based inverted end around carry adders is given. The novel modules are applied on IDEA algorithm and the resulting implementation is compared both qualitatively and quantitatively with the IDEA implementation using the existing multiplier/squarer implementations. Experimental measurement results show that the proposed design is faster and smaller and also consume less power than similar hardware implementations making it a viable option for efficient hardware designs.Yet,despiteitssophistication,manyfutureattemptsat crackingDESshowedsignificant signsofsuccess.Forexample, thedistributive computing approachofspreadingcracking computationpoweroverthe Internet earnedRockeVerserandMichael Sandersthe prize ofthe1997DESChallenge.DESChallenge II wasalso crackedthefollowingyear.WiththeinventionoftheElectronic FrontierFoundationDESCracker, itwasshownthat a 56-bit keyprotectionisinsufficient againstexhaustivesearchemployedwithtoday'stechnology.Therefore,there wasanurgentcallforastrongersecret-keyencryptionalgorithm.IDEAwasone ofthe algorithmstoanswerthatcall.*

Key words **—**modulo 2*n* + 1 multiplier; International Data Encryption Algorithm (IDEA); Sparse-tree adder; Power/area/speed measurement;

I. INTRODUCTION

Thedemand for highsecurityincommunicationschannels,networkedInstrumentationanddistributedmeasurement systemsisevergrowing rapidly.Theconfidentiality andsecurityrequirementsarebecomingmoreandmoreimportant to protectthedata transmittedandreceived. Thisleadsto the need for efficient design of cryptographic algorithms whichofferdataintegrity, authentication, non-repudiationand confidentialityof the encrypteddataacrossthe communication channels.Variouscryptographic algorithmshavebeenstudied andimplemented toensuresecurityofthesesystems.Inthis paper,modulo2n+1multiplier hasbeenmuchfocusasithas found itsimportant roleinIDEAalgorithm. Forexample,the threemajoroperationsthatdecidetheoverallperformanceand delayoftheIDEA [1,4,15]aremodulo2^{16} addition,bitwise XOR and modulo2^{16}+1multiplicationand the GF(2^n) Montgomerymultiplicationandmodularexponentiationcan beimplementedusingrepeatedmultiplication andsquaringof thevectors.Amongtheseoperations, improvingthedelayandpowerefficiencyofthemodulo2^n +1multiplicationoperation leadstosignificant increaseintheperformanceoftheentirecryptographiccipher.

Numeroushardware implementationsofthe IDEAalgorithmareproposedintheliteratureusingdifferentmodulo 2^{16}+1multiplierarchitectures.TheIDEAalgorithmhasbeen implementedinsoftware[3]onIntelPentiumII445MHzwith encryptionrateof23.53Mb/Sec.Later,IDEAwasrealized on hardwarechipbyCurigeret al [1]withencryptionratesup to 177Mb/sec.Byusingabit-serialimplementation [4],which enablestheIDEAtobefully,pipelinedtheencryption rates reached500Mb/sec with125MHzclockrate.Theefficiency oftheIDEAciphercanstillbeimprovedifefficient basic modules suchasmodulomultipliers and addersareused. Theefficient implementationofthemodulo2^n+1multiplier basedonnovelcompressorsandsparsetreebasedinverted end around carry adders is presentedin [7]. Even though thearchitecture ofthemodulomultiplierisveryefficiently proposedin[6],thehardwareimplementationandoptimization areconsiderablyimprovedin[7].Thisisresulted byreplacing thefulladder arrayswiththenovelcompressors andthefinal stageadderwiththesparsetreebasedinvertedendaround carryadder.

Thepaperisorganizedasfollows;Section II-A introducesmultiplexer-basedcompressors. InSectionII-B,thehardware implementationofmodulo2^n+1multiplierisgiven.Section IIIdiscussestheproposedimplementationoftheIDEAcipher whichusesmodulo2^{16} +1multiplier.Acomparisonofourimplementationtoa recentlyproposedimplementationismade inSectionIV.OurconclusionsaredrawninsectionV.

II. PRELIMINARIES AND REVIEW

Novelmultiplexor(MUX)basedcompressorsand2^n +1 multiplierdesignhavebeenreported in[7]andarebriefly reviewedinthissectionasfollows:

A. Compressors

1) MUXvs.XOR:

ExistingCMOSdesignsof2-1MUX and2-inputXORareshowninFig.1.According to[8], the CMOSimplementation ofMUXperformsbetterintermsofpoweranddelaycomparedtoXOR.Suppose,XandY are inputstotheXORgate,theoutputisXY+XY.Thesame XORcanbeimplementedusingMUXwithinputsX,Xand selectbitY.Theefficientimplementationofcompressors[9] isachievedbyusingbothoutputanditscomplement ofthese gates.Thisalsoreducesthetotalnumberofgarbageoutputs.

2) DescriptionofCompressors:
A(p,2)compressorwith pinputsX1,X2 ...Xp andtwooutputbitsSumandCarry alongwithcarryinputbitsandcarryoutputbitsis governedbytheequation:

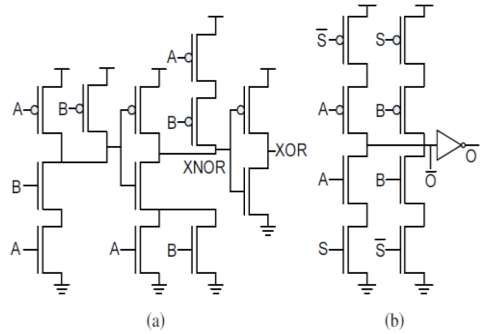

Fig. 1: CMOS implementation of 2-input (a) XOR (b) MUX

$$\sum_{i=1}^{p} X_i + \sum_{i=1}^{t} (C_{in})_i = Sum + 2(Carry + \sum_{i=1}^{p} (C_{out})_i)$$

Blockdiagramofa5:2compressorisshowninFig.2.Efficient designoftheexistingXOR-based 5:2compressor [10,11], whichtakes5inputs and2carryinputs, isshowninFig.3(a). Thecriticalpathdelayofthisexistingcompressoris4Δ-XOR (delaydenotedbyΔ).

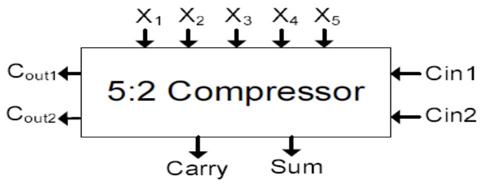

Fig. 2: Block Diagram of a 5:2 compressor

Thenewlydesignedcompressorsusemultiplexersinplace ofXORgates,resultinginhighspeedarithmetic. Also,as showninFig.3(a)inalltheexistingCMOSimplementations oftheXORandMUX gatesboththeoutput anditscomplementareavailablebutthedesignsofcompressors availablein literaturedonotusetheseoutputsefficiently. IntheCMOS implementation of the MUX if both the selectbit and its complementaregeneratedinthepreviousstage thenitsoutput isgeneratedwithmuchless delaybecausetheswitchingofthe transistorisalreadycompleted. Andalsoifboththeselectbit anditscomplementaregeneratedinthepreviousstagethentheadditionalstage oftheinverteriseliminatedwhichreducesthe overalldelayinthecriticalpath. ThenewMUX-based design of5:2compressors[9] isshownin Fig.3(b),the delayof which isΔ-XOR+3Δ-MUX CGEN blockusedinFig.3(b) canbe obtainedfromtheequationCout1=$(x_1+x_2)\cdot x_3+x_1\cdot x_2$andtheCMOSimplementationisgiveninFig.4.

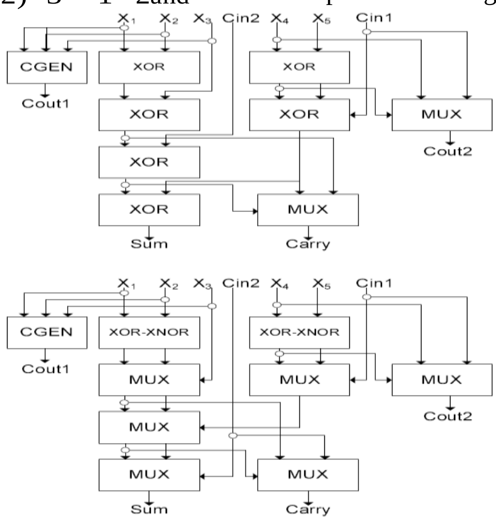

Fig. 3: 5:2 compressors: (a) existing XOR-based design; (b) new MUX-based design

B.Hardware Implementation of the mod 2^n+1 Multi plier/Squarer

The hardwareimplementationofthe modulomultiplier consistsofthreemodules.Firstmoduleistogeneratepartial products,second module is to reduce the partial products to two final operands and the last module is to add the Sum and Carry operands from partial products reduction to get the final result.

1) Partial products generation: The n × n partial products matrix is obtained from the n + 1-bitinput vectors. This partialproduct matrix is generated after repositioning the bits of the initial partial product matrix based on several observations presented in [6]. The final partial products matrix after applying all the observations is shown in Fig. 5. The partialproductbits can becomputedfrom AND,OR andNOT gates. The most complexfunctionof partialproduct generationmoduleis$p_{n-1,n-1} V_{q_{n-2}}$,where$p_{i,j}=a_i b_j$and$q_i=p_{n,i} V p_{i,n}$

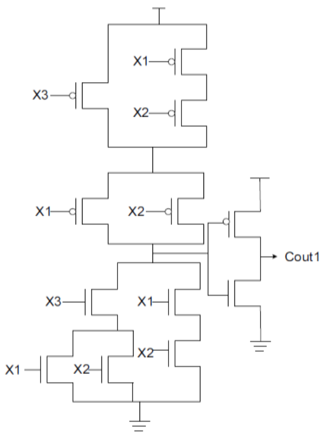

Fig. 4: CMOS implementation of carry generator block (CGEN) for the proposed design.

2^{n-1}	2^{n-2}	2^{n-3}
$PP_0 = p_{n-1,0} \vee q_{n-1}$	$p_{n-2,0}$	$p_{n-3,0}$
$PP_1 = p_{n-2,1}$	$p_{n-3,1}$	$p_{n-4,1}$
$PP_2 = p_{n-3,1}$	$p_{n-4,2}$	$p_{n-5,2}$
....	....	....
$PP_{n-2} = p_{1,n-2}$	$p_{0,n-2}$	$\overline{p_{n-1,n-2} \vee q_{n-3}}$
$PP_{n-1} = p_{0,n-1}$	$\overline{p_{n-1,n-1} \vee q_{n-2}}$	$p_{n-2,n-1}$

2^2	2^1	2^0
$p_{2,0}$	$p_{1,0}$	$p_{0,0} \vee q_{n-1} \vee p_{n,n}$
$p_{1,1}$	$p_{0,1}$	$\overline{p_{n-1,1} \vee q_0}$
$p_{0,2}$	$\overline{p_{n-1,2} \vee q_1}$	$\overline{p_{n-2,2}}$
....	....	....
$\overline{p_{4,n-2}}$	$\overline{p_{3,n-2}}$	$\overline{p_{2,n-2}}$
$\overline{p_{3,n-1}}$	$\overline{p_{2,n-1}}$	$\overline{p_{1,n-1}}$

Fig. 5: Final n×n partial product matrix showing 2^{n-1}, 2^{n-2}, $2^{n-3} \ldots 2^2$, 2^1 and 2^0 columns.

2) Partialproductsreduction: Thisisthemostimportant modulewhichlargelydeterminesthecriticalpathdelayand theoverallperformance ofthemultiplier.Hencethismodule needsto be designedso as to get minimumdelayandconsume lesspower. Theimplementations fromtheliterature[5,6,13]usefull adders(FA)andhalfadders(HA)toconstructthismodule. Theseriesoffulladdersinanycolumncanbereplacedby thenovelcompressorsthattakethesamenumberofinputs.In theproposedimplementationuseofsuggestedcompressorsis done which not only reduces the delay and power consumptionbut also the area of the circuit. For a modulo 2^{16} + 1multiplier in IDEA cipher the Carry Save Adder (CSA) arrayimplementation using Full Adders requires fifteen full addersin series in any column, these fifteen full adders can bereplaced by two 7:2 compressors, one 5:2 compressor and two3:2 compressors.

Correction factor computation is an important step while generating the partial products matrix. The full adder implementation [6] and the compressor based implementations [7]result in the same value. Because of the space constraints, computation of the correction factor COR for full adder implementation [6] is not given in this paper. COR computation for compressor implementation involves computingonly COR2, because COR1 is obtained based on repositioning of the partial productterm, which issame for both implementations. The correctionfactor COR2 computation for FA implementation which has n-1 stages of additions is shown in [6]. And the COR2 computation for the proposed multiplier implementation using the compressors also yields the same result. Since, any (p, 2) compressor can be primarily designed using *p*- 2 FAs which give *p* - 2 carry outs with 2^nweight. Hence, the overall correction factor COR computation for CSA array FA implementation and compressor implementation yield the same result i.e., 3 as shown in [5].

3) Final Stage addition*:*The partial product reduction module gives one n-bit carry vector and one n-bit sum vector which need to be added in the final stage addition module. Very efficient parallel prefix adders are designed to do this operation [2].

Suppose S and C are sum and carry vectors produced after the partial product reduction section. As it is shown in the work of Zimmerman [2] that

$$|S + C + 1|_{2^n+1} = |S + C + \overline{Cout}|_{2^n} \quad (1)$$

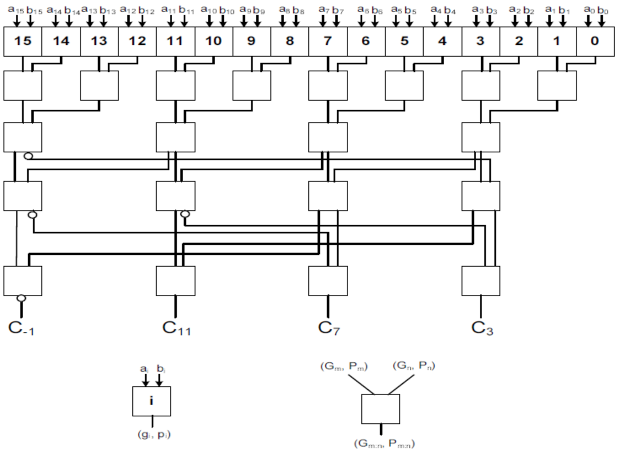

Fig. 6: Inverted EAC adder implemented using sparse tree structure

Equation (1) can be implemented using an invertedEnd-Around-Carry adder [2, 5, 6]. Even though the propagation delay of this adder is in the order of *log*2*n*, it has a drawback of high interconnect complexity and high fan-out. This can be overcome by sparse tree adder [12, 16] based on the prefix network logic. The sparse tree adder generates the carry for every four bits instead of generating it at every stage and using a carry select block for selecting the final carry after the prefix network. This sparse tree adder was proven to be much more efficient in terms of both delay and power when compared with the existing prefix tree based adders [14]. Hence this sparse tree can be used to design Inverted-End-Around-Carry adder. The newly designed Inverted-End-Around-Carry adder using sparse tree adder structure is shown in Fig. 6. This Inverted-EAC adder is used in the final stage addition of the modulo 2*n*+1 multiplier. Theproposed implementation of the modulo 216 + 1 multiplier for IDEA cipher is shown in Fig. 7 and $R_{16}R_{15} : : :R_2R_1R_0$ represents the final product of the modulo 216 + 1 multiplier.

III. NOVEL IMPLEMENTATION OF IDEA CIRCUIT USINGTHE PROPOSED MODULO 2^N+ 1 MULTIPLIER/SQUARER

The modulo 2*n* + 1 computation is an integral part of the International Data Encryption Algorithm (IDEA) where *n* =16 [1, 4, 15]. Three major operations that decide the overall delay and performance of IDEA cipher are:
1) Modulo 216 addition;
2) Bitwise-XOR;
3)Modulo 216 + 1 multiplication/squaring.

As the first two operations take less time and are easy to implement, the delay and power efficiency of the entire IDEA cipher depends significantly on the modulo 216 + 1 multiplication/squaring operation. Hence, the IDEA cipher is implemented using the proposed modulo multiplier and compared with the existing implementations.

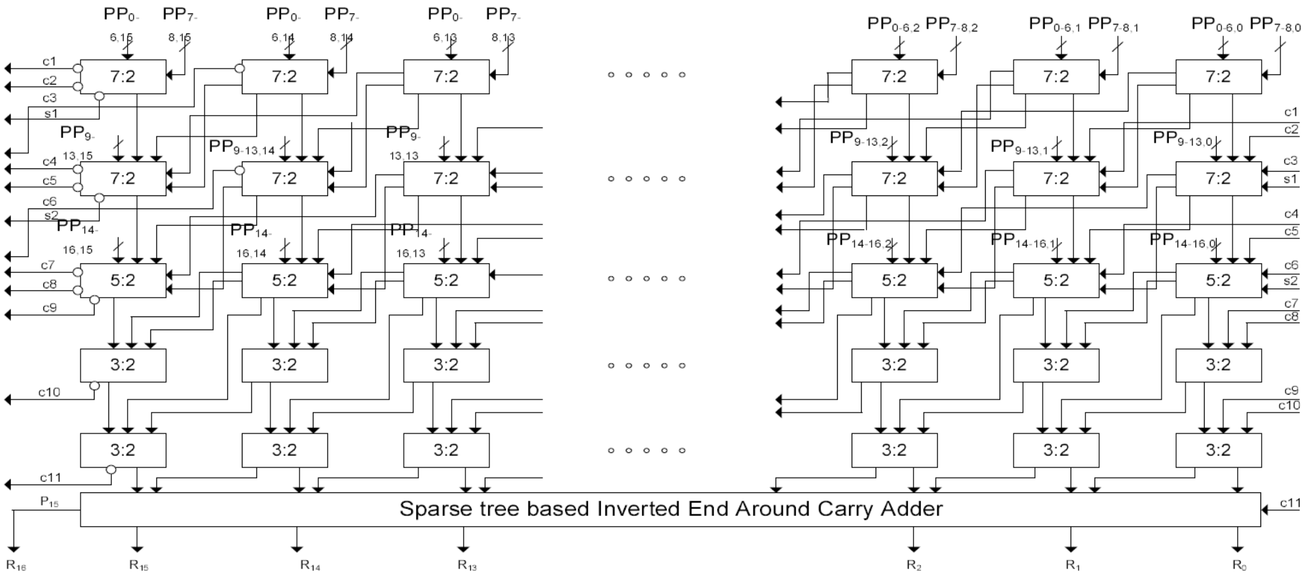

Fig. 7: Novel implementation of the modulo 2^{16}+1 multiplier using efficient compressors

Toencrypt adatablockusingIDEAcipher,thedatashould be processed through three modulo multiplication operationsin a single round and the manipulated data again shouldPass through seven such rounds iteratively and a final outputtransformation to produce the final encrypted output. TheIDEA cipher takes 64-bit input data and produces a 64-bitcipher text with a 128-bit key. The encryption and decryptionalgorithms in IDEA are almost identical except they utilizetwo different sets of sub key generated by the same key with different processes. The IDEA encryption and decryptionprocesses consist of eight rounds of data manipulation usingsubkeys and a final output transformation stage. In this cipher,all the operations are carried out on 16-bit sub-blocks. In theencryption process, the input data block of 64-bits is dividedinto 4 sub blocks of 16-bits each ($X1;X2;X3;X4$). 52 sub-keys for the encryption process are generated from the original128-bit key by shifting a part of it. Out of the 52 subkeys, sixdifferent subkeys (i.e., $Z_1^{(r)};Z_2^{(r)};Z_3^{(r)};Z_4^{(r)};Z_5^{(r)}$ and $Z_6^{(r)}$,where r is the roundnumber) are used for each round and theremaining 4 subkeys are used in the final output transformationstage. The 16-bit outputs at each round are represented as$Y_1^{(r)}$; $Y_2^{(r)}$; $Y_3^{(r)}$; $Y_4^{(r)}$and W_1; $W2$; $W3$; $W4$ are the outputs of the final output stage transformation. The 52 subkeys used for the decryption process are obtained using a different algorithm[17]. As shown in Fig. 8, the critical path consists ofthreemodulo 216 + 1 multiplication operations, two modulo 216addition operations and two 16-bit XOR operations in eachround. In the final output transformation stage, critical path consists of a single modulo 216 + 1 multiplication operation.The throughput of the IDEA cipher can be improved, if thedelay of the modulo 216+1 multiplication operation is reduced in the pipelined implementation of the IDEA cipher. Fig. 8shows the data path of encryption process of the IDEA cipherand datapath of a single round with 4 pipeline stages with the proposed modulo multiplier.

IV. EXPERIMENTAL SIMULATIONAND RESULTS

The proposed design of the IDEA cipher with four pipelinestages using novel modulo $2n+1$ multipliers is used to analyse and compare with the well-known IDEA cipher implementations. The use of the novel modulo multiplier improves thethroughput and performance of the IDEA cipher significantly.

A. Simulation environment

All the simulations have been carried out using MentorGraphics ASIC (Application-Specific IC) design suite. Theproposed IDEA cipher design is specified using Verilog HDLand the multiplier descriptions are mapped on a 0.18 _mCMOS standard cell library usingLeonardo Spectrum synthesis tool from Mentor Graphics.

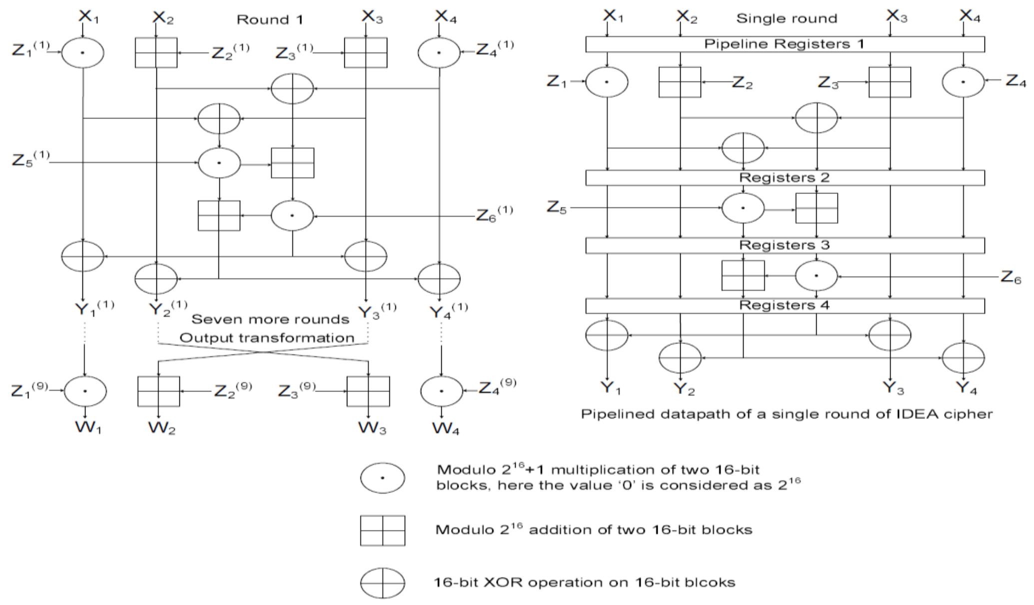

Fig. 8: Datapath of IDEA cipher with 4 pipeline stages

The design is optimized forhigh speed performance. Netlists generated from synthesis toolare passed on to standard route and place tool; the layouts areiteratively generated to get the circuits with minimum area.The calculation of power and delay are carried out using theEldosimulation tool. The proposed experimental simulationhas been performed at 1.8V with all inputs fed at a frequency of 25MHz.

B. Simulation results

The IDEA cipher is implemented using both the proposedmultiplier and the multipliers presented in [6]. Various performancemeasurements includingencryptionrate,delayand areafortheIDEAcipherusingboththeproposedmultiplier and theexisting multiplierareparametricallyobtainedand listed inTableI. As expected, theproposedIDEA circuit implementationachievessignificantimprovementsintermsof throughput(i.e.,encryption rate),latency(i.e.,criticalpath delay)andarea(i.e.,circuitarea).

TABLE I: Comparison of the performance measurements for IDEA cipher

Performance Measurement	Using proposed multipliers	Using the multipliers in [6]	% Improvement
Encryption Rate (Mb/sec)	460.25	412.15	11.25
Critical path delay (nS)	4.372	5.168	15.4
Area of the cipher (mm^2)	3.68	4.22	12.79

V. CONCLUSION

A hardware implementation of the IDEA cipher using novelmodulo 2^n+1multipliers ispresented in this paper. It isshown that the proposed modulo 2n+1 multiplier improvestheperformance of the variouscryptographic algorithms used insecure communication systems of networked instrumentationand distributed measurement systems. Efficient compressorsandsparsetreebasedinvertedendaroundcarryaddersare usedtoreducethedelayandcomplexity ofthemultiplier. Simulations areperformedontheknownimplementation and theproposedimplementation.Thepresentedimplementation isproven toperform betterthantheexistingoneinvarious aspects,(i.e., throughputandcriticalpathdelay).

REFERENCES

[1] R. Zimmermann, A. Curiger, H. Bonnenberg, H. Kaeslin, N. Felber andW. Fichtner, A 177 Mb/s VLSI implementation of the international dataencryption algorithm, IEEE J. Solid-State Circuits, 1994, 29, (3), pp.303-307

[2] R. Zimmerman, Efficient VLSI implementation of modulo (2^n _ 1)addition and multiplication, IEEE trans. Comput., 2002, 51, pp. 1389-1399.

[3] O. Cheung, K. Tsoi, P. Leong and M. Leong, Tradeoffs in parallel andserial implementations of the international data encryption algorithmIDEA, Lecture Notes in Computer Science, vol. 2162, pp. 333-340,2001.

[4] M. Leong, O. Cheung, K. Tsoi, and P. Leong, A bit-serial implementation of the international data encryption algorithm IDEA, 2000 IEEESymposium on Field-Programmable Custom Computing Machines, pp.122-131, 2000.

[5] C. Efstathiou, H. Vergos, S. Dimitrakopoulos and D. Nikolos, Efficientdiminished-1 modulo 2^n+ 1 multipliers, IEEE Trans. Comput., 2005,54, pp. 491-496.

[6] H. Vergos and C. Efstathiou, Design of efficient modulo 2^n+ 1multipliers, IETComput. Digit. Tech., 2007, 1, (1), pp. 49-57.

[7] R. Modugu, N. Park and M. Choi, A Fast Low-Power Modulo2^n+ 1 Multiplier Design, 2009 IEEE International Instrumentationand Measurement Technology Conference, pp.951-956, May 2009.

[8] R. Zimmermann and W. Fichtner., Low-power logic styles: CMOSversus pass-transistor logic, IEEE J. Solid- State Circuits, vol. 32, pp.1079-1090, July 1997.

[9] S. Veeramachaneni, L. Avinash, M. Rajashekhar and M. Srinivas,Efficient Modulo (2k _1) Binary to Residue Converters System-on-Chip for Real-Time Applications, The 6th International Workshop onDec. 2006 pp.195 - 200.

[10] C. Chang, J. Gu and M. Zhang, Ultra low-voltage lowpower CMOS4-2 and 5-2 compressors for fast arithmetic circuits, IEEE J. Circuitsand Systems I, Vol. 51, No. 10, pp. 1985- 1997, 2004

[11] M. Rouholamini, O. Kavehie, A. Mirbaha, S. Jasbi and K. Navi, ANew Design for 7:2 Compressors, Computer Systems and Applications,2007. AICCSA '07. IEEE/ACS International Conference on 13-16 May2007 Page(s):474 - 478.

[12] S. Mathew, M. Anders, R. Krishnamurthy and S. Borkar, A 4-GHz130-nm address generation unit with 32-bit sparse-tree adder core,IEEE Journal of Solid-State Circuits, Volume 38, Issue 5, May 2003Page(s):689 - 695.

[13] Zhongde Wang, Graham A. Jullien, William C. Miller., An efficient treearchitecture for modulo 2n +1 multiplication, VLSI Signal Processing14(3): 241-248 (1996).

[14] P. Kogge and H. S. Stone., A parallel algorithm for the efficient solutionof a general class of recurrence equations, IEEE Trans. Comput., vol.C-22, pp. 786-793, Aug 1973.

[15] A. Curigeret. al., VINCI: VLSI Implementation of the New Secret-keyBlock Cipher IDEA, Proc. of the Custom Integrated CircuitsConference, San Diego, USA, May 1993

[16] Yan Sun, DongyuZheng, Minxuan Zhang, and Shaoqing Li HighPerformance Low-Power Sparse-Tree Binary Adders, 8*th* InternationalConference on Solid state and Integrated Circuit Technology, ICSICT2006.

[17] Yi-Jung Chen, Dyi-Rong Duh, Yunghsian Sam Han: Improved Modulo(2^n+1) Multiplier for IDEA, J. Inf. Sci. Eng. 23(3):911-923(2007)

Role of IT in Lean Manufacturing: A brief Scenario

*G T Padmane, **M T Sohel, ***P D Patil

*Lecturer in Mech. Dept. Government Polytechnic, Murtizapur, Akola, India
**Lecturer in Mech. Dept Government Polytechnic Murtizapur, Akola, India,
***Lecturer in Mech. Dept Government Polytechnic Murtizapur, Akola, India

ABSTRACT: *A concept of Lean can be seen as a loosely connected set of potentially competing principles whose goal is cost reduction by the elimination of waste, and organise the possible effort to utilise waste of all kinds in a productive way. The avoidance and then lateral removal of waste has a long history, and as such this history forms much of the basis of the philosophy now known as "Lean". Many organisations are implementing 'lean manufacturing' (LM) with the objective of achieving a superior competitive advantage over other organisations. Few companies have attained their objective, while many of them did not. One of the reasons for failure is that the managers of these organisations have not understood clearly: how the performance measures of an organisation are affected, when it gets transformed through LM.*

Lean can be elevated through optimized utilization of Information Technology. Lean IT is the extension of lean manufacturing and lean services principles to the development and management of information technology (IT) products and services along with other manufacturing sectors . Its central concern, applied in the context of IT, is the elimination of waste, where waste is work that adds no value to a product or service. Although lean principles are generally well established and have broad applicability, their extension from manufacturing to IT is only just emerging. Indeed, Lean IT poses significant challenges for practitioners while raising the promise of no less significant benefits. And whereas Lean IT initiatives can be limited in scope and deliver results quickly, implementing Lean IT is a continuing and long-term process that may take years before lean principles become intrinsic to an organization's culture. This paper is an attempt to summarise the various components of lean manufacturing, role of IT in lean manufacturing and a brief overview of lean and I T.

Keywords: *lean services, smart automation, wasteful, unevenness, overburden, business building, etymologically, world class manufacturing.*

I. Introduction

Is is observed that the things in many ways goes waste which directly affects the cost and quality of the product . So it becomes essential on the part of manufacturers to reduce the waste from all possible angles and accordingly they have stepped up the waste elimination movement in possible manner. But the results were not creating any sensation in entire role of waste elimination. By that time Lean principles came from the Japanese manufacturing industry. The term was first coined by John Krafcik in a Fall 1988 article, "Triumph of the Lean Production System," published in the Sloan Management Review and based on his master's thesis at the MIT Sloan School of Management.

Lean manufacturing, lean enterprise, or lean production, often simply, "Lean," is a production practice that considers the expenditure of resources for any goal other than the creation of value for the end customer to be wasteful, and thus a target for elimination. Working from the perspective of the customer who consumes a product or service, "value" is defined as any action or process that a customer would be willing to pay for. Lean manufacturing concepts were developed over the last five to six decades, primarily in Japan, particularly for the Toyota production system. These concepts met various tests for many years and passed the test of time very easily.

Lean manufacturing revolutionaries the manufacturing process. It was not a fine tuning of the existing manufacturing processes. These manufacturing techniques are conceptually different from the traditional process.

Lean manufacturing is a variation on the theme of efficiency based optimizing flow; it is a present-day instance of the recurring theme in human history toward increasing efficiency, decreasing waste, and using empirical methods to decide what matters, rather than uncritically accepting pre-existing ideas.

The difference between these two approaches is not the goal itself, but rather the prime approach to achieving it. The implementation of smooth flow exposes quality problems that already existed, and thus waste reduction naturally happens as a consequence. The advantage claimed for this approach is that it naturally takes a system-wide perspective, whereas a waste focus sometimes wrongly assumes this perspective.

II. A 'LEAN' CULTURE

2.1. Brief Overview

Also known as the flexible mass production, mainly it has two pillar concepts, Just-in-time (JIT) or "flow", and "autonomation" (smart automation). The smooth flowing delivery of value achieves all the other improvements as side-effects. If production flows perfectly then there is no inventory; if customer valued features are the only ones produced, then product design is simplified and effort is only expended on features the customer values. The other of the two pillars is the very human aspect of autonomation, whereby automation is achieved with a human touch. The "human touch" here meaning to automate so that the machines/systems are designed to aid humans in focusing on what the humans do best. It is now possible to give the machines enough intelligence to recognize when they are working abnormally and flag this for human attention. Thus, in this case, humans would not have to monitor normal production and only have to focus on abnormal, or fault, conditions.

Lean implementation is therefore focused on getting the right things to the right place at the right time in the right quantity to achieve perfect work flow, while minimizing waste and being flexible and able to change. These concepts of flexibility and change are principally required to allow production levelling, using tools like SMED, but have their analogues in other processes such as research and development (R&D). The flexibility and ability to change are within bounds and not open-ended and therefore often not expensive capability requirements. More importantly, all of these concepts have to be understood, appreciated, and embraced by the actual employees who build the products and therefore own the processes that deliver the value. The cultural and managerial aspects of Lean are possibly more important than the actual tools or methodologies of production itself. There are many examples of Lean tool implementation without sustained benefit, and these are often blamed on weak understanding of Lean throughout the whole organization.

Lean aims to make the work simple enough to understand, do and manage. To achieve these three goals at once there is a belief held by some that Toyota's mentoring process,(loosely called Senpai and Kohai, which is Japanese for senior and junior), is one of the best ways to foster Lean Thinking up and down the organizational structure. This is the process undertaken by Toyota as it helps its suppliers improve their own production. The closest equivalent to Toyota's mentoring process is the concept of "Lean Sensei," which encourages companies, organizations, and teams to seek outside, third-party experts, who can provide unbiased advice and coaching.

2.2. Lean goals and strategy
Some commonly mentioned goals are:-
Improve quality: To stay competitive in today's marketplace, a company must understand its customers' wants and needs and design processes to meet their expectations and requirements.
Eliminate waste: Waste is any activity that consumes time, resources, or space but does not add any value to the product or service. See Types of waste, above.
Reduce time: Reducing the time it takes to finish an activity from start to finish is one of the most effective ways to eliminate waste and lower costs.
Reduce total costs: To minimize cost, a company must produce only to customer demand. Overproduction increases a company’s inventory costs because of storage needs.

2.3 Lean Manufacturing Metrics
The goal of Lean Manufacturing is the creation of "World Class" level of manufacturing operations metrics. The following chart shows typical world class manufacturing metrics:

Measure	Performance	Measure	Performance
Manufacturing Lead Time	<1 day	Delivered Quality	3 PPM
Delivery Performance	99+ %	Inventory Turns	>50
Conversion Costs	25-40% less than mass	Manufacturing Space	35-50% less than mass producers
New Product Development	<6 months	Skill Trades Response	<2 minutes
Production Skilled Trades Ratio	>20:1	Changeover Time	<TAKT Time

Table No. 1 world class manufacturing metrics

2.4 Principles of lean
The five-step thought process for guiding the implementation of lean techniques is easy to remember, but not always easy to achieve:

- Specify value from the standpoint of the end customer by product family.
- Identify all the steps in the value stream for each product family, eliminating whenever possible those steps that do not create value.
- Make the value-creating steps occur in tight sequence so the product will flow smoothly toward the customer.
- As flow is introduced, let customers pull value from the next upstream activity.

Fig. No.1 Principles of lean

- As value is specified, value streams are identified, wasted steps are removed, and flow and pull are introduced, begin the process again and continue it until a state of perfection is reached in which perfect value is created with no waste.

III. LEANMANAGEMENT AND WASTE

While the elimination of waste may seem like a simple and clear subject it is noticeable that waste is often very conservatively identified. This then hugely reduces the potential of such an aim. The elimination of waste is the goal of Lean .Diagram given below refers to forms of waste and components of lean production system.

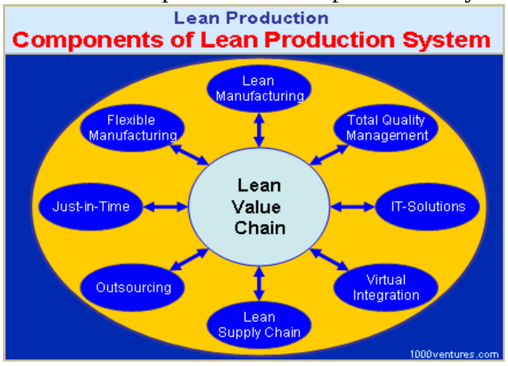

Fig. No.2 Lean Value Chain

3.1 Muda (wasteful)

Is a traditional Japanese term for an activity that is wasteful and doesn't add value or is unproductive, etymologically none or un-useful in practice or others. Muda has been given much greater attention as waste than the other two which means that whilst many Lean practitioners have learned to see muda they fail to see in the same prominence the wastes of mura(unevenness) and muri (overburden).

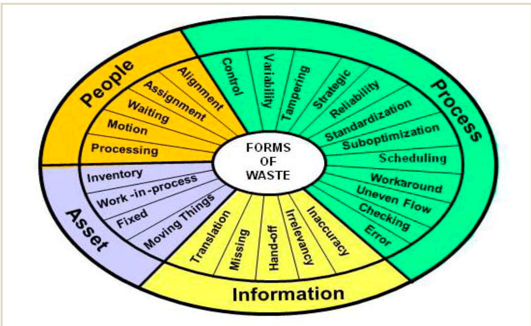

Fig. No.3 Forms Of Waste

3.2 Mura (unevenness)

Is traditional general Japanese term for unevenness, irregularity or inconsistency in physical matter or human spiritual condition. It is also a key concept in performance improvement systems such as the Toyota Production System. Mura is one of the three types of waste. Waste reduction is an effective way to increase profitability. Mura, in terms of business/process improvement, is avoided through Just In Time systems which are based on keeping little or no inventory, rather supplying the production process with the right part, at the right time, in the right amount, and first-in, first out component flow. Just in Time systems create a "pull system" in which each sub-process withdraws its needs from the preceding sub-processes, and ultimately from an outside supplier. When a preceding process does not receive a request or withdrawal it does not make more parts. This type of system is designed to maximize productivity by minimizing storage overhead.

3.3 Muri(overburden)

Muri is all the unreasonable work that management imposes on workers and machines because of poor organization, such as carrying heavy weights, moving things around, dangerous tasks, even working significantly faster than usual. It is pushing a person or a machine beyond its natural limits. This may simply be asking a greater level of performance from a process than it can handle without taking shortcuts and informally modifying decision criteria. Unreasonable work is almost always a cause of multiple variations.

Firstly, muri focuses on the preparation and planning of the process, or what work can be avoided proactively by design. Next, mura then focuses on how the work design is implemented and the elimination of fluctuation at the scheduling or operations level, such as quality and volume. Muda is then discovered after the process is in place and is dealt with reactively. It is seen through variation in output. It is the role of management to examine the muda, in the processes and eliminate the deeper causes by considering the connections to the muri and mura of the system. The muda and mura inconsistencies must be fed back to the muri, or planning, stage for the next project.

IV. LEAN AND IT

4.1 Need and Scope

As lean manufacturing has become more widely implemented, the extension of lean principles is beginning to spread to IT (and other service industries). Industry analysts have identified many similarities or analogues between IT and manufacturing. whereas the manufacturing function manufactures goods of value to customers, the IT function "manufactures" business services of value to the parent organization and its customers. Similar to manufacturing, the development of business services entails resource management, demand management, quality control, security issues, and so on. Moreover, the migration by businesses across virtually every industry sector towards greater use of online or e-business services suggests a likely intensified interest in Lean IT as the IT function becomes intrinsic to businesses' primary activities of delivering value to their customers. Already, even today, IT's role in business is substantial, often providing services that enable customers to discover, order, pay, and receive support. IT also provides enhanced employee productivity through software and communications technologies and allows suppliers to collaborate, deliver, and receive payment.

The relationships between lean manufacturing and information technology is now building a new concept of business building. Software industry and IT can get great lessons from lean. On the other hand lean manufacturers can use IT to help their efforts in the journey. First of all it is important to understand that software alone will not make you lean or even efficient. In most of the cases IT plays an important support role. Good processes can be made more effective and efficient with software and application of IT not the other way around. It is important to know where IT can explore lean concept to a greater extent. Some major areas in this regard are given below.

- Information Technology can be used in communicating data fast and accurately. Sharing the same piece of truth is very important to run a lean system effectively.
- Collection and processing of data is another very important area where IT can help the lean manufacturer. Collecting data and analysis will help you in better decision making.
- Some of the work can be automated using the IT technology. For an example rather than creating a purchase order every time, the system can be configured in such a way that it can pass the requirement to the suppliers in a predefined interval based on the TAKT time.
- When implementing complicated IT systems it is important to make sure the systems also are following the concepts of lean. For an example;
- Collecting and accumulating data which are not used for decision making will increase the workload for people and machinery and also will serve no purpose; hence it creates the wastes of over processing and inventory.

Systems must be made to update just in time and possibilities of erroneous data into the systems must be eliminated making the system error proofed.

In simple terms implementing an IT system will not solve your problem or will not make you a lean manufacturer. You have to put the processes in place first to be facilitated by IT in true lean manner. Like in lean manufacturing, it is important to apply the concepts of lean in designing the suitable IT systems for you. Good IT systems and good lean processes will make you a better lean manufacturer.

4.2 Types of Waste in Lean IT

Lean IT promises to identify and eradicate waste that otherwise contributes to poor customer service, lost business, higher than necessary business costs, and lost employee productivity. To these ends, Lean IT targets eight elements within IT operations that add no value to the finished product or service or to the parent organization

Each element in the table can be a significant source of waste in itself, linkages between elements sometimes create a cascade of waste (the so-called domino effect). For example, a faulty load balancer (waste element: Defects) that increases web server response time may cause a lengthy wait for users of a web application (waste element: Waiting), resulting in excessive demand on the customer support call center (waste element: Excess Motion) and, potentially, subsequent visits by account representatives to key customers' sites to quell concerns about the service availability (waste element: Transportation). In the meantime, the company's most likely responses to this problem — for example, introducing additional server capacity and/or redundant load balancing software), and hiring extra customer support agents — may contribute yet more waste elements (Overprovisioning and Excess Inventory).

Waste Element	**Examples**	**Business Outcome**
Defects	Unauthorized system and application changes. Substandard project execution.	Poor customer service, increased costs.
Overproduction	Unnecessary delivery of low-value applications and services.	Business and IT misalignment, Increased costs and overheads: energy, data center space, maintenance.
Waiting	Slow application response times. Manual service escalation procedures.	Lost revenue, poor customer service, reduced productivity.
Non-Value Added Processing	Reporting technology metrics to business managers.	Miscommunication.
Transportation	On-site visits to resolve hardware and software issues. Physical software, security and compliance audits.	Higher capital and operational expenses.
Inventory (Excess)	Server sprawl, underutilized hardware. Multiple repositories to handle risks and control. Benched application development teams.	Increased costs: data center, energy; lost productivity.
Motion (Excess)	Fire-fighting repeat problems within the IT infrastructure and applications.	Lost productivity.
Employee Knowledge (Unused)	Failing to capture ideas/innovation. Knowledge and experience retention issues. Employees spend time on repetitive or mundane tasks.	Talent leakage, low job satisfaction, increased support and maintenance costs.

Table No. 1 Targets of Waste in Lean IT

4.3 .Implementation of lean IT

Implementation begins with identification and description of one or more IT value streams. It is essential to generate a date base which must includes the detailed information of time and motion supplies, customer demand, process flow and product families. The database should have a facility to update and edit the data contents as per requirement of the lean . The generated data is to be analyzed for capacity plan, value stream map current status , vale stream map future status , work balance and layout proposal. The final stage is of project implementation wherein the above discussed steps are to be followed to create foolproof A schematic layout given below can refer to basic theme of Lean It implementation.

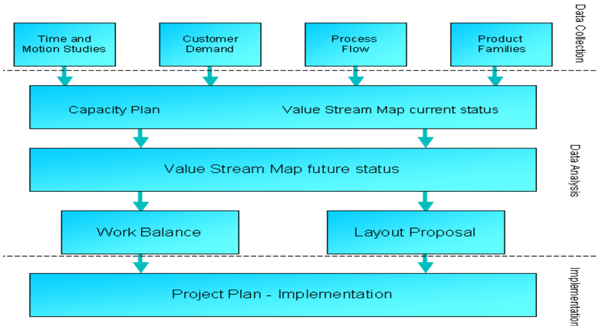

Fig. No.4 Implementation of lean IT

V. CONCLUSION

It now essential to tie up lean manufacturing with information technology so as to expedite lean management movement. The industries and service sectors in totality should move forward to take up this task and must execute possible efforts to update the various events through lean principles . It is now high time to move up for stability as far as global scenario is concerned. It is not that much difficult or complicated to opt for lean management drive. This will not only help the industries and service sectors to downsize the waste to a greater extent but also will enhance the quality of work culture . It has been proved by number of companies that lean manufacturing is a need of today and future of tomorrow.

REFERENCES

[1] A B Womack, James P., Daniel T. Jones, and Daniel Roos (1990). "The Machine That Changed the World".
[2] A B Holweg, Matthias (2007). "The genealogy of lean production". Journal of Operations Management 25 (2): 420–437. doi:10.1016/j.jom.2006.04.001.
[3] Bailey, David. "Automotive News calls Toyota world No 1 car maker". Reuters.com. Reuters. http://www.reuters.com/article/businessNews/idUSN2424076820080124. Retrieved 19 April 2008.
[4] Krafcik, John F. (1988). "Triumph of the lean production system". Sloan Management Review 30 (1): 41–52.
[5] Ohno, Taiichi (1988). Toyota Production System. Productivity Press. p. 8. ISBN 0-915299-14-3.
[6] Suprateek Roy (1988), p 4
[7] Suprateek Roy (1988), p 6
[8] "Problems continue at Heathrow's Terminal 5", New York Times, March 31, 2008 article [1]
[9] Andrew Dillon, translator, 1987. The Sayings of Shigeo Shingo: Key Strategies for Plant Improvement).
[10] (Charles Buxton Going, preface to Arnold and Faurote, Ford Methods and the Ford Shops (1915))
[11] Ford, Henry; with Crowther, Samuel (1922). My Life and Work. Garden City, New York, USA: Garden City Publishing Company, Inc. http://www.gutenberg.net/etext/7213. Various republications, including ISBN 9781406500189. Original is public domain in U.S.
[12] Bennett, Harry; with Marcus, Paul (1951). We Never Called Him Henry. New York: Fawcett Publications. LCCN 51-036122.
[13] Womack, James P.; Daniel T. Jones (2003). Lean Thinking. Free Press.
[14] A B Ruffa, Stephen A. (2008). Going Lean: How the Best Companies Apply Lean Manufacturing Principles to Shatter Uncertainty, Drive Innovation, and Maximize Profits. AMACOM. ISBN 0-8144-1057-X. http://books.google.com/?id=_Q7OGDd61hkC.
[15] Hounshell, David A. (1984), From the American System to Mass Production, 1800-1932: The Development of Manufacturing Technology in the United States, Baltimore, Maryland, USA: Johns Hopkins University Press, ISBN 978-0-8018-2975-8, LCCN 83-016269 . pp 248 ff.
[16] Toyota Production System, Taichi Ohno, Productivity Press, 1988,, p. 58
[17] Womack, James P.; Daniel T. Jones (2003). Lean Thinking. Free Press. p. 352.
[18] Bicheno, John; Matthias Holweg (2009). The Lean Toolbox. PICSIE Books. ISBN 978-0954124458.
[19] Toyota Vision and Philosophy[dead link]
[20] Pat Lancaster of Lean Thinking's Lanchester Technologies reference implementation
[21] Maskell & Baggaley (December 19, 2003). "Practical Lean Accounting". Productivity Press, New York, NY.
[22] The Gold Mine, F & M Ballé, The Lean Enterprise Institute, 2005, p196
[23] Michael Ballé & Freddy Ballé (2009) The Lean Manager, Lean Enterprise Institute
[24] Adsit, Dennis. "Cutting Edge Methods Target Real Call Center Waste". isixsigma.com. Archived from the original on 2008-04-14. http://web.archive.org/web/20080414194658/http://www.isixsigma.com/library/content/c070611a.asp. Retrieved 19 April 2008.
[25] Hanna, Julia. "Bringing 'Lean' Principles to Service Industries". HBS Working Knowledge. October 22, 2007. (Summary article based on published research of Professor David Upton of Harvard Business School and doctoral student Bradley Staats: Staats, Bradley R., and David M. Upton. "Lean Principles, Learning, and Software Production: Evidence from Indian Software Services.". Harvard Business School Working Paper. No. 08-001. July 2007. (Revised July 2008, March 2009.)
[26] Radnor, Dr Zoe; Paul Walley, Andrew Stephens, Giovanni Bucci. "Evaluation Of The Lean Approach To Business Management And Its Use In The Public Sector". scotland.gov.uk. http://www.scotland.gov.uk/Publications/2006/06/13162106/0. Retrieved 19 April 2008.
[27] Radnor & Bucci (2010) " Analysis of Lean Implementation in UK Business Schools and Universities", Association of Business Schools, http://www.wbs.ac.uk/downloads/news/2011/03/abs-lean-report-exec-summary-march-2011-13008.pdf
[28] E G Liker, J.K., 2004. The Toyota Way: 14 Management Principles from the World's Greatest Manufacturer, New York: McGraw-Hill., Feld, W.M., 2001. Lean Manufacturing: Tools, Techniques, and How to Use Them, Boca Raton: St. Lucie Press., Ohno, T., 1988. Toyota Production System: Beyond Large-Scale Production, Portland: Productivity Press., Monden, Y., 1998. Toyota production system: an integrated approach to just-in-time, London: Chapman & Hall., Schonberger, R.J., 1982. Japanese Manufacturing Techniques: Nine Hidden Lessons in Simplicity, New York: Free Press., Shingo, S., 1984. A Study of the Toyota Production System from an Industrial Engineering Viewpoint, Tokyo: Japan Management Association.
[29] E.G . Womack, J.P., Jones, D.T. & Roos, D., 1990. The Machine That Changed the World: The Story of Lean Production, New York: Rawson Associates., Womack, J.P. & Jones, D.T., 2003. Lean Thinking: Banish Waste and Create Wealth in Your Corporation, New York: Free Press., Bicheno, J., 2004. The new lean toolbox: towards fast, flexible flow, Buckingham: PICSIE Books., Dennis, P., 2002. Lean Production Simplified: A Plain Language Guide to the World's Most Powerful Production System, New York: Productivity Press., Schonberger, R.J., 1982. Japanese Manufacturing Techniques: Nine Hidden Lessons in Simplicity, New York: Free Press.
[30] Pettersen, J., 2009. Defining lean production: some conceptual and practical issues. The TQM Journal, 21(2), 127 - 142.
[31] a b c Thinking of Lean Manufacturing Systems MacInnes, Richard L. (2002) The Lean Enterprise Memory Jogger Page, Julian (2003) Implementing Lean Manufacturing Techniques

International Journal of Modern Engineering Research (IJMER)
www.ijmer.com Vol. 3, Issue. 5, Sep - Oct. 2013 pp-3032-3040 ISSN: 2249-6645

Analysis of the Effects of Infectious Disease in a Closed Population

R.A. Kareem, T.S. Nurudeen, S.O. Salawu and A.A. Abdurasid
Department of Mathematics, Lagos State Polytechnic, Ikorodu, Nigeria

ABSTRACT: *This work focuses on the analysis of the effects of infectious disease in a closed population. We considered a Drilling rig company in Nigeria positioned several hundred meters from the coast. Because of their remoteness we are worried about the effect of an epidemic among the staff. We formulated a problem base on a typical rig practice in Nigeria. We look at the effect of the epidemic among the staff and the provision the company should make to mitigate the effects of an outbreak of some infectious diseases. Here individual do not come in contact with people from outside the community under consideration.*

I. INTRODUCTION

The diseases and any study about them can be very helpful and important for human beings. Specially, mathematical modeling can be a good and suitable instrument for having a better life. The basic SIR model has a long history. At first Kermak and Mckendrich introduced SIR model in 1927 [8]. Now, SIR model is developing more and more that you can even find it discussed in some introductory calculus text books [5]. SIR model can be very useful and helpful in characterizing some diseases. More numbers of these mathematical models can be seen in [2, 3, 13, 14, and 15].

Epidemics have ever been a great concern to human kind and we are still moved by the dramatic descriptions that arrive to us from the past. A single epidemic outbreak (as opposed to disease endemic) occurs in a time span short enough not to have the demographic changes perturbing the dynamics of the contacts between individuals [7, 9, 10]. The mathematical techniques used to understand, forecast, and control the spread of infectious diseases like influenza are diverse and growing rapidly. Some techniques have been newly developed, whereas others build upon existing methods from diverse fields including dynamical systems, stochastic processes, statistical physics, graph theory, statistics, operations research, and high-performance computing [12]. Here, we considered an epidemic in a fraction of the population in a community especially in a drilling rig company in Nigeria where individual did not come in contact with people from the community.

II. MATHEMATICAL MODEL

At any given time, the population may be divided into three groups: the Susceptible, S, (i.e. those who have not yet been infected by the disease), the Infectives, I, (i.e. those who are currently suffering from the disease, who may pass it on to others), and the Removal, R, (i.e. those who have had the disease and either died, become immune or been isolated from the rest of the population). The rates at which these transfer take place can be assumed to obey the following equations [5, 11]

$$\frac{dS}{dt} = -rSI \qquad (1)$$

$$\frac{dI}{dt} = rSI - aI \qquad (2)$$

$$\frac{dR}{dt} = aI \qquad (3)$$

Let systems (1) - (3) be **Model A**,

Where $r > 0$ is the infection rate and $a > 0$ is the removal rate of infectives.

The population size is constant and is given as

$$\frac{dS}{dt} + \frac{dI}{dt} + \frac{dR}{dt} = 0$$

$$S(t) + I(t) + R(t) = N$$

Where N is the total size of the population

The initial conditions attached to the mathematical formulation of the epidemic problem in (1) - (3) are

$$S(0) = S_0 > 0, I(0) = I_0 > 0, R(0) = R_0 = 0 \qquad (4)$$

III. PROBLEM FORMULATION

In this work, we considered a drilling rig company in Nigeria with staff strength of 100 employees each of whom spend 5 months at a time on the rig. Each month 20 employees leave the rig and are replaced by 20 others. It is these newcomers which could bring infection to the staff of the rig. It is estimated that an infection rate, r, of 0.1 would be typical for most viral diseases under the current conditions of the rig and that current practice on the rigs would lead to a removal rate, a, of 0.5. Both of these rates are based on a time-scale measured in days. Using the initial conditions $S(0)=90, R(0)=0, I(0)=10$, we investigate the effect of more or fewer of the 20 new arrivals being infected, the effect of the removal rate on the spread of the epidemic, effect of adopting safer behavior patterns on the spread of the epidemic and to ensure that there are never fewer than 60% of the staff available for work at any one time.

IV. INVESTIGATIONS

At each month, 20 employees leave the rig and are replaced by 20 others. Then the following cases can be investigated.

(a) 0.1 infection rate within the new 20 arrivals i.e.

$$\frac{10}{100}\times 20 = 2 \text{ People are infected}$$

(b) 0.2 infection rate within the new 20 arrivals i.e.

$$\frac{10}{100}\times 20 = 18 \text{ People are susceptible}$$

(c) 0.3 infection rate within the new 20 arrivals i.e.

$$\frac{10}{100}\times 20 = 2 \text{ People are infected}$$

We investigate three cases of the infection

Case 1: Susceptible = 18, Infected = 2

0 month [0 1]

$$S(0)=90, R(0)=0, I(0)=10$$

[S I R] = [90 10 0]

1st month [1 2]

$$S(1)=0, R(0)=31, I(1)=69$$

S: $0.2\times 0 = 0 \Rightarrow$ home
$0.8\times 0 = 0 \Rightarrow$ remain
I: $0.2\times 69 = 14 \Rightarrow$ home
$0.8\times 69 = 55 \Rightarrow$ remain
R: $0.2\times 31 = 6 \Rightarrow$ home
$0.8\times 31 = 25 \Rightarrow$ remain

[S I R] = [18 57 25]

2nd month [2 3]

$$S(2)=0, R(2)=54, I(2)=46$$

S: $0.2\times 0 = 0 \Rightarrow$ home
$0.8\times 0 = 0 \Rightarrow$ remain
I: $0.2\times 46 = 9 \Rightarrow$ home
$0.8\times 46 = 37 \Rightarrow$ remain
R: $0.2\times 54 = 11 \Rightarrow$ home
$0.8\times 54 = 43 \Rightarrow$ remain

[S I R] = [18 39 43]

3rd month [3 4]

$$S(3)=0, R(3)=64, I(3)=36$$

S: $0.2\times 0 = 0 \Rightarrow$ home
$0.8\times 0 = 0 \Rightarrow$ remain
I: $0.2\times 36 = 7 \Rightarrow$ home
$0.8\times 36 = 29 \Rightarrow$ remain
R: $0.2\times 64 = 13 \Rightarrow$ home
$0.8\times 64 = 51 \Rightarrow$ remain

[S I R] = [18 31 51]

4th month [4 5]

$$S(4)=0, R(4)=69, I(4)=31$$

S: $0.2\times 0 = 0 \Rightarrow$ home

$0.8\times 0 = 0 \Rightarrow$ remain
I: $0.2\times 31 = 6 \Rightarrow$ home
$0.8\times 31 = 25 \Rightarrow$ remain
R: $0.2\times 69 = 14 \Rightarrow$ home
$0.8\times 69 = 55 \Rightarrow$ remain
[S I R] = [18 27 55]

Case 2: Susceptible = 16, Infected = 4

0 month [0 1]
$$S(0) = 90, R(0) = 0, I(0) = 10$$
[S I R] = [90 10 0]
1st month [1 2]
$$S(1) = 0, R(1) = 31, I(1) = 69$$
[S I R] = [16 59 25]

2nd month [2 3]
$$S(2) = 0, R(2) = 54, I(2) = 46$$
[S I R] = [16 41 43]
3rd month [3 4]
$$S(3) = 0, R(3) = 64, I(3) = 36$$
[S I R] = [16 33 51]
4th month [0 1]
$$S(4) = 0, R(4) = 69, I(4) = 31$$
[S I R] = [16 29 55]

Case 3: Susceptible = 14, Infected = 6

0 month [0 1]
$$S(0) = 90, R(0) = 0, I(0) = 10$$
[S I R] = [90 10 0]
1st month [1 2]
$$S(1) = 0, R(1) = 31, I(0) = 69$$
[S I R] = [14 61 25]
2nd month [2 3]
$$S(2) = 0, R(2) = 54, I(2) = 46$$
[S I R] = [14 43 43]
3rd month [3 4]
$$S(3) = 0, R(3) = 64, I(3) = 36$$
[S I R] = [14 35 51]
4th month [4 5]
$$S(4) = 0, R(4) = 69, I(0) = 31$$
[S I R] = [14 31 55]

V. OBSERVATION FOR MODEL A

1. A close look at the plots in figures 1 – 4 show that at the beginning the infection rate increase and later fall towards the end with no number of susceptible and the removal rate is increased and reduced over a period of time. So between 0 and 20 people are susceptible and this implies that no number of susceptible people can go home or remain at the rig.

For the infected, 14 people will go home and 55 will remain and this implies that between 0 and 20 people of the new arrivals are infected. That is between 55 and 75 people are infected after the arrival of the new employees at the rig. So if between 1 and 14 people are infected it means we have the same number of people or less infected at the rig. Also more people will be infected at the rig if more than 14 are infected. Assuming no removal will arrive, then six people will go home and 25 remain.

For all the graphs plotted in the epidemic model the following colours represent the lines:
Blue: Susceptible
Green: Infected
Red: Removed
Light blue: Recovery

Yellow: Those available to work

S(0) = 90; I(0) = 10; R(0) = 0

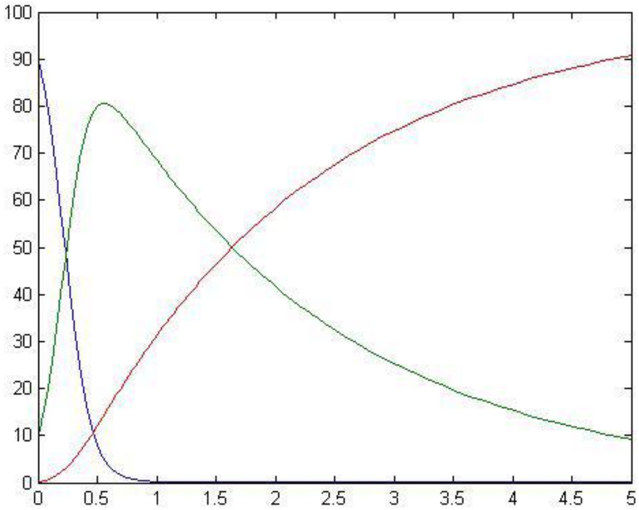

Figure 1: r = 0.1; a = 0.5

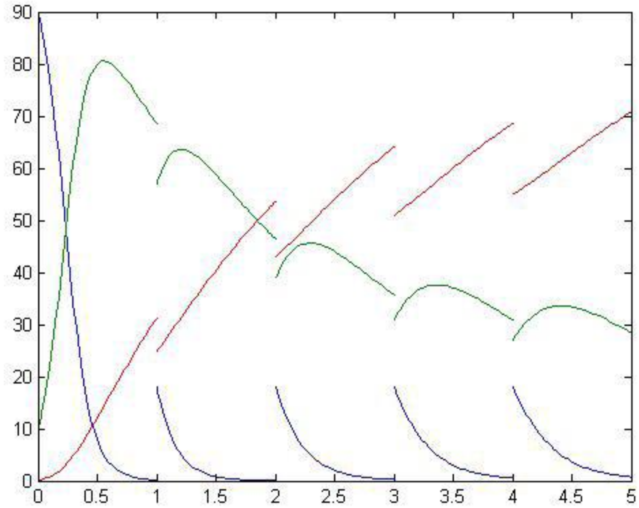

Figure 2: r = 0.1; a = 0.5

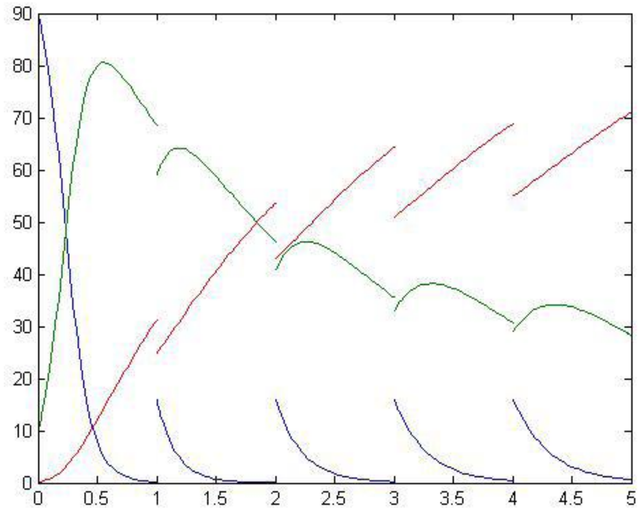

Figure 3: r = 0.1; a = 0.5

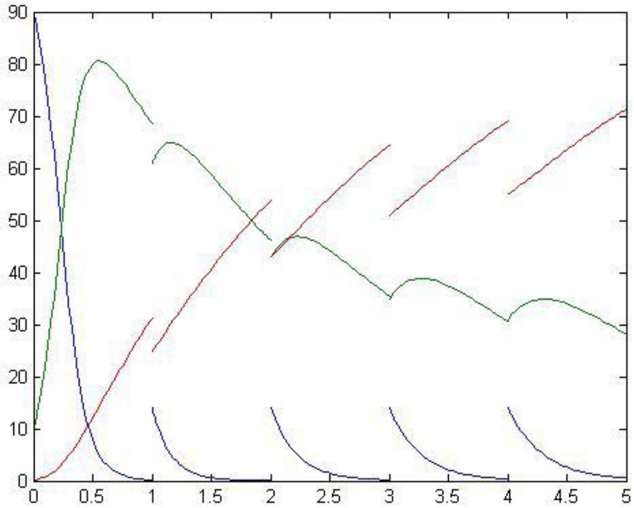

Figure 4: r = 0.1; a = 0.5

2. As there is increase in removal rate it is observed in figures 5 - 8 that the numbers of susceptible is the same for the period of time. For the infected, the rate is the same with reduction in the number of staff infected.

$$S(0)=90, R(0)=0, I(0)=10$$

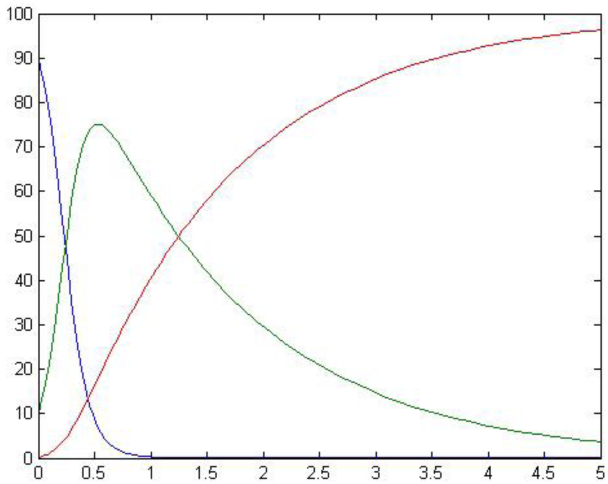

Figure 5: r = 0.1; a = 0.7

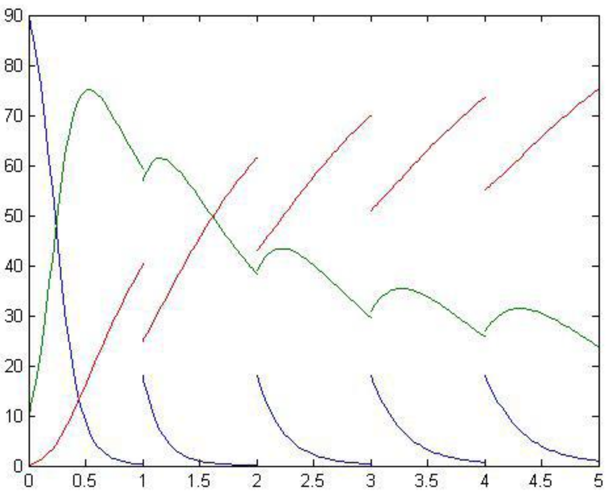

Figure 6: r = 0.1; a = 0.7

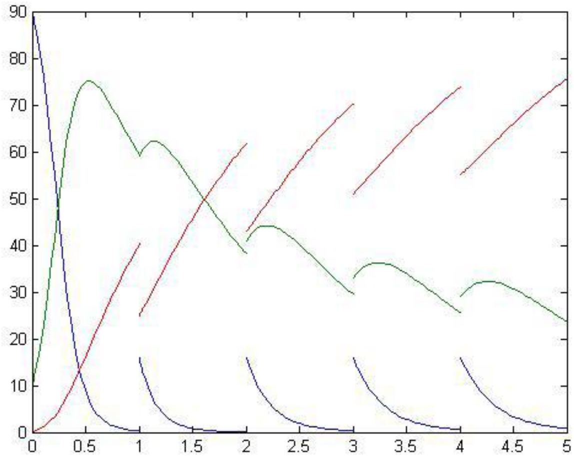

Figure 7: r = 0.1; a = 0.7

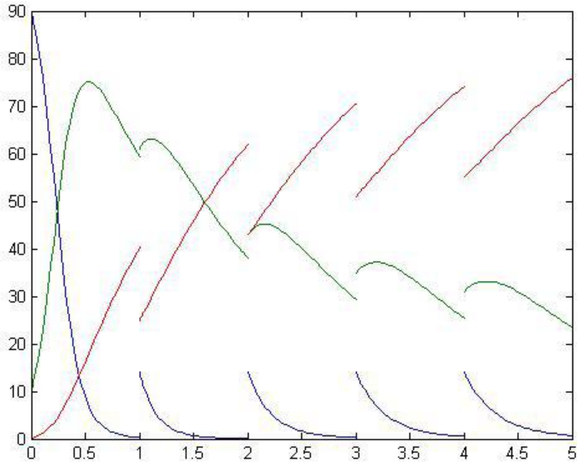

Figure 8: r = 0.1; a = 0.7

3. Figures 9 – 12 show that over a period of time, the infection rate is reduced. This means that there are less people being infected at the beginning. Also the maximum numbers of infected people are smaller to that of figures 1 – 4. Immediately after the maximum point the line is not so steep and number of infected people is a bit higher at the same time. So as there are less people infected at the same time in the beginning, less people will be removed. And towards the end, as more people are infected, more are removed. Hence the lines move closer.

$$S(0) = 90, R(0) = 0, I(0) = 10$$

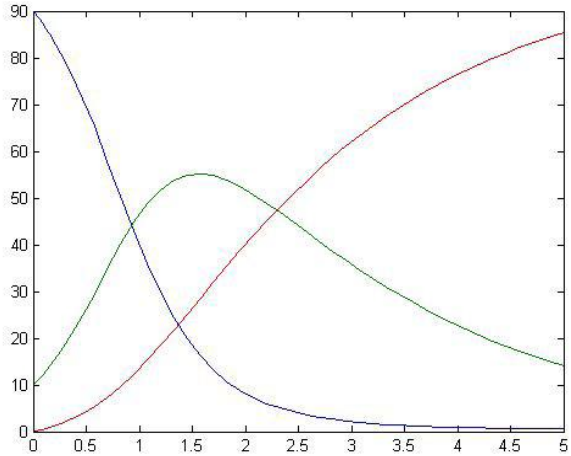

Figure 9: r = 0.03; a = 0.5

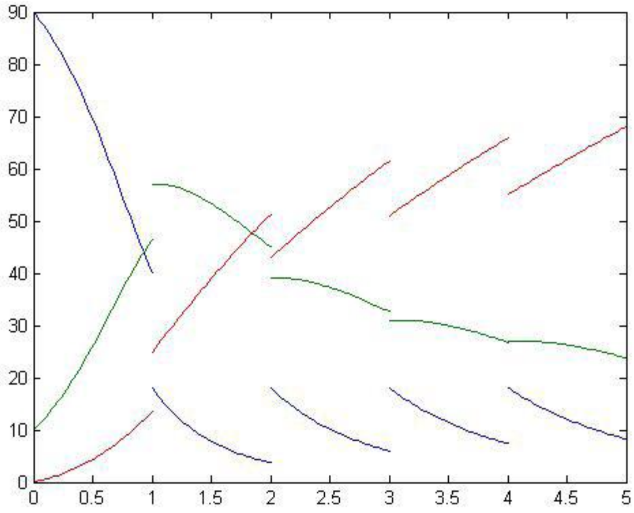

Figure 10: r = 0.03; a = 0.5

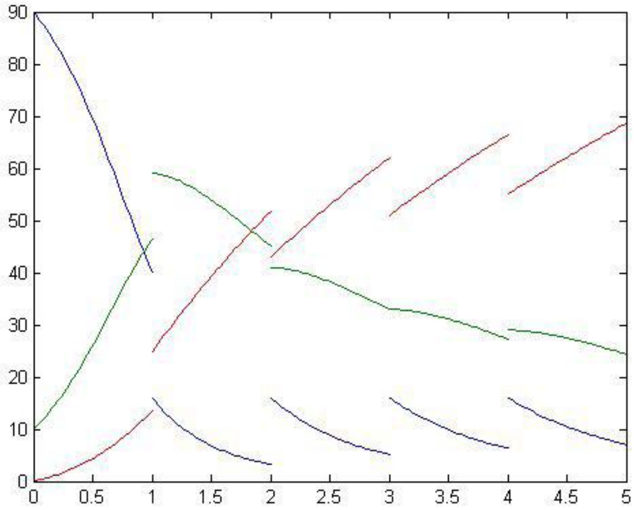

Figure 11: r = 0.03; a = 0.5

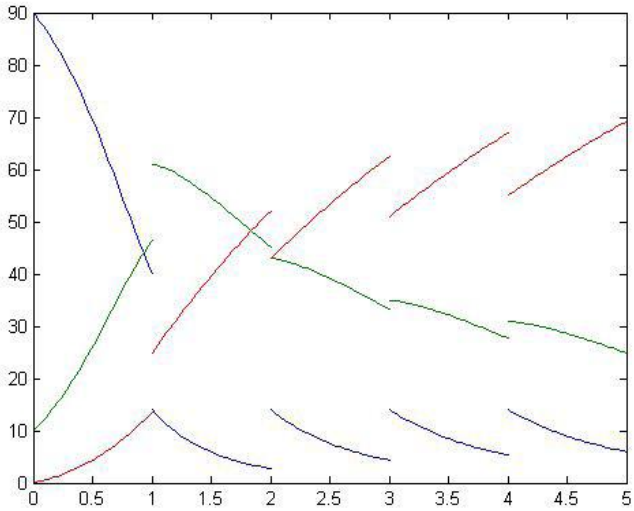

Figure 12: r = 0.03; a = 0.5

To ensure that there are fewer than 60% of the staff available for work at any one time, system 1 – 3 is modified and called **Model B**, i.e.

Model B

$$\frac{dS}{dt} = -rSI$$

$$\frac{dI}{dt} = rSI - aI \qquad \frac{dR}{dt} = aI - vR$$

$$\frac{dC}{dt} = vR$$

Where v is the recovery rate and C is the recovery group.

$r = 0.03, a = 0.7, v = 0.03$

VI. OBSERVATION FOR MODEL B

It is observed in figures 13 – 15 that fewer than 60% of staff will always be available for work assuming a constant recovery rate within the removed group as shown in Model B, and this is not in the best interest of Drilling company as their interest is to ensure that there are never fewer than 60% of the staff available for work at any time.

In figure 13, the recovery group (light blue line) is very low which implies that many of the infected are not recovered within the removed group. In figure 14 the recovery group falls a little bit without much significance on the infected being recovered. The number of susceptible increases a little bit at a constant recovery rate and figure 15 shows that the Drilling company will always have less than 60% of its staff available for work (yellow line) at any time.

S(0) = 90, I(0) = 10, R(0) = 0, C(0) = 0

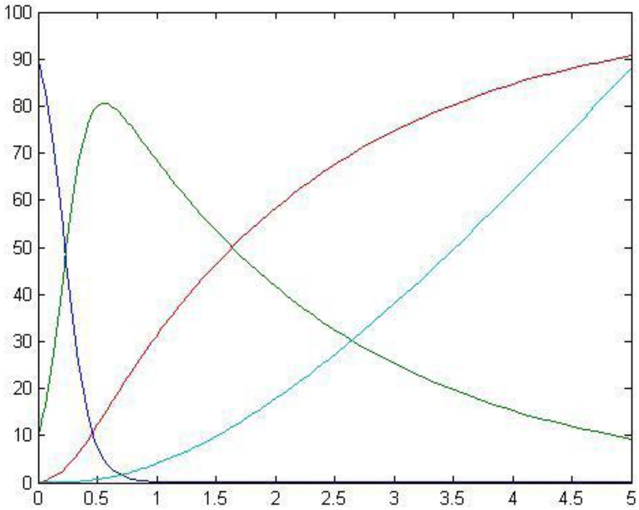

Figure 13: r = 0.1; a = 0.5; v = 0.3

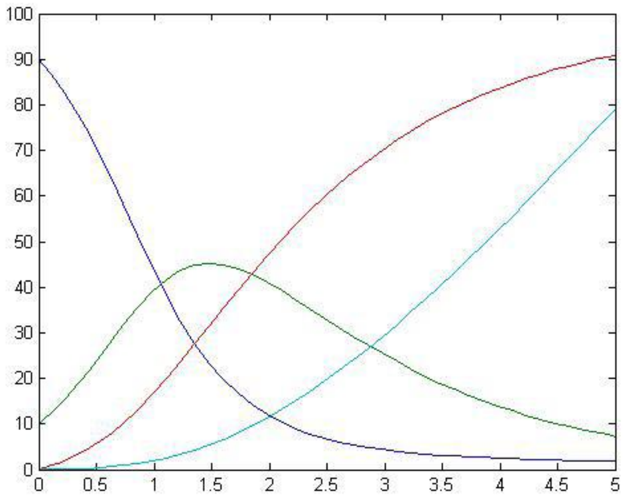

Figure 14: r = 0.03; a = 0.7; v = 0.3

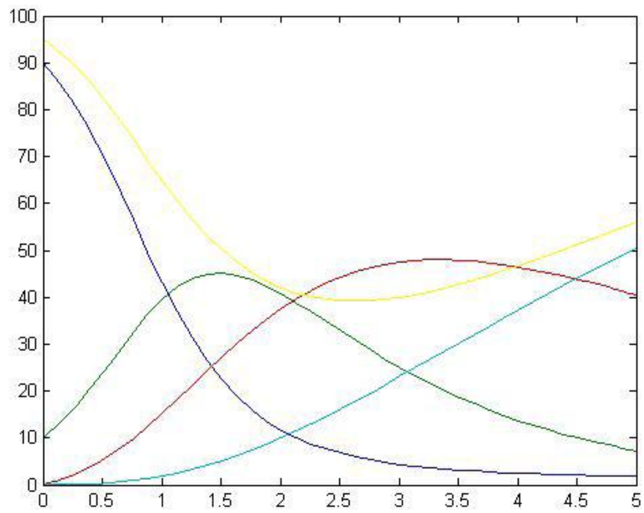

Figure 15: r = 0.03; a = 0.7; v = 0.3

VII. CONCLUSION

As a remedy to Drilling company situation, a thorough medical test should be carried out on the new comers of employees that are to replace the outgoing ones, to screen out those that may possibly have any trace of the disease before being introduced to the other staff working at the rig.

To ensure that more people are available for work, it is recommended that the company should make a research that all the 20 people leaving the rig are in the removed group. That is those who have had the disease and either died or the infected, that is those who are suffering from the disease.

REFERENCES

[1] Brauer.F and Van Den Driessche. P and Wu. J, Mathematical Epidemiology, Springer, 2008.
[2] Capasso. V, Mathematical Structures of Epidemics Systems, Lecture Notes in Biomaths 97, Berlin: Springer-Verlag, 1993.
[3] Delisi. Ch, Mathematical Modeling In Immunology, Ann. Rev. Biophys. Bioeng. 12: 117-138, 1983. *A Mathematical Model* for *an Epidemic* without Immunity 61
[4] Farkas. M, Dynamical Models in Biology, Academic Press, 2001.
[5] Guillermo Abramson, Mathematical Modeling of the Spread of Infectious Diseases. PANDA, UNM, Nov. 2011
[6] Hethcote, H.W, Three Basic Epidemiological Models. In: Levin, S.A., Hallam, T., Gross L.J. (Eds.) Applied Mathematical Ecology. Springer Verlag (1989).
[7] Hethcote, H.W.: The Mathematics of Infectious Diseases. SIAM Review 42, 599{653 (2000).
[8] Hughes-Hallett. D, Gleason. A. M, Lock. P. F, Flath. D. E, Gordon. S. P, Lomen. D. O, Lovelock. D, Mccallum. W. G, Osgood, B. G, Quinney.D, Pasquale. A, Rhea. K, Tecosky- Feldman. J, Thrash. J. B, Tucker. T. W Applied Calculus, Wiley, Toronto, Second Edition 2002.
[9] Kermack. W. O and Mckendrick. A. G, Contributions to the Mathematical Theory of Epidemics, Proc. Royal Soc. A, 115: 700-721, 1927.
[10] Mimmo Iannelli, Mathematical Models in Life Science: Theory and Simulation. (Bolzano-Italy), July, 2005.
[11] Murray J.D. Mathematical Biology Base on an Epidemic Model, Lecture Note.
[12] Nedialko B. Dimitroa and Lauren Ancel Meyers, (Mathematical Approches to Infectious Diseases, Prediction and Control). Operation Research INFORMS 2010.
[13] Okubo. A, Diffusion and Ecological Problems: Mathematical Models, Berlin: Springer-Verlag, 1980.
[14] Rowe. G, Theoretical Models In Biology, Oxford: Clarendon Press, 1994.
[15] Shahshahani. S, A New Mathematical Framework for the Study for the Study Of Linkagr And Selection. Memoirs Amer. Math. Soc. 211,1979.
[16] Willems. J.L, Stability Theory of Dynamical Systems, New York: Wiley, 1970.

International Journal of Modern Engineering Research (IJMER)
www.ijmer.com Vol. 3, Issue. 5, Sep - Oct. 2013 pp-3041-3041 ISSN: 2249-6645

An Introductory Comment on Wave Relativity

Umasankar Dolai
Assistant Teacher, Dwarigeria Pry. School, Garhbeta South C.L.R.C., Satbankura-721253, West Bengal, India

ABSTRACT: *Wave criterion of special and general relativity can be introduced in this paper. A report can be drawn; about wave mechanical relativistic idea in it.*

Keywords: *Four-Dimensional wave Equation, Invariant Quantity, Special and General Relativity, Riemannian and Euclidean metrics, Summary.*

I. INTRODUCTION

When a wave can travel in a four-dimensional time space continuum, then its wave equation is $\Diamond^2\psi=0$; where $\Diamond^2$ is a mechanical operator and ψ is wave function. Here operator $\Diamond^2 = \partial^2/\partial x^2_1 + \partial^2/\partial x^2_2 + \partial^2/\partial x^2_3 + \partial^2/\partial x^2_4 = \partial^2/\partial x^2 + \partial^2/\partial y^2 + \partial^2/\partial z^2 - 1/c^2 \cdot \partial^2/\partial t^2$; where c is the velocity of light.

II. INVARIANT OPERATOR

The special theory of relativity shows that operator $\Diamond^2$ is invariant under Lorentz transformation i.e. $\Diamond^2 = \partial^2/\partial x^2 + \partial^2/\partial y^2 + \partial^2/\partial z^2 - 1/c^2 \cdot \partial^2/\partial t^2 = \partial^2/\partial x'^2 + \partial^2/\partial y'^2 + \partial^2/\partial z'^2 - 1/c^2 \cdot \partial^2/\partial t'^2$; where the equations of Lorentz transformation are : $x'=\gamma(x-vt)$, $y'=y$, $z'=z$ and $t'=\gamma\,(t-vx/c^2)$; here $\gamma=(1-v^2/c^2)^{-1/2}$. Thus operator $\Diamond^2$ be called invariant operator. Obviously the operator $\Diamond^2$ can develop a new mode of relativity; then $\Diamond^2$ may be defined as relativistic operator of this new way of relativity. So now relativity can be expressed by operator $\Diamond^2$ in a new mode of algebraic operation.

III. WAVE INVARIANT QUANTITY

If the both sides of relation $\Diamond^2 = \partial^2/\partial x^2_1 + \partial^2/\partial x^2_2 + \partial^2/\partial x^2_3 + \partial^2/\partial x^2_4$ can be multiplied by wave function ψ, then the formulation $\Diamond^2\psi = \partial^2\psi/\partial x^2_1 + \partial^2\psi/\partial x^2_2 + \partial^2\psi/\partial x^2_3 + \partial^2\psi/\partial x^2_4$ is obtained. Now the quantity $\Diamond^2\psi$ may be called wave invariant quantity. This relation can reveal wave interpretation of Special relativity.

IV. INTRODUCTORY WAVE RELATIVITY

However it is known that $\Diamond^2\psi = \partial^2\psi/\partial x^2_1 + \partial^2\psi/\partial x^2_2 + \partial^2\psi/\partial x^2_3 + \partial^2\psi/\partial x^2_4 = 0$. Moreover this equation can reveal an idea about special wave relativity. Actually the above formulation can give a real meaning or a real situation of four-dimensional continuum even if $\Diamond^2\psi$ does not vanish. Moreover this situation can make $\Diamond^2\psi$ as a physically meaningful quantity. It can be done by concept of particular procedure of operator algebra such a way that $\Diamond^2\psi$ is not equal to zero. This is the actual reality of wave relativity especially general wave relativity.

V. GENERAL FORM OF WAVE RELATIVITY

If the unit of time can be considered such a way that c=1 and the time $t = x_4$, then the formulation $\Diamond^2\psi = \partial^2\psi/\partial x^2 + \partial^2\psi/\partial y^2 + \partial^2\psi/\partial z^2 - 1/c^2 \cdot \partial^2\psi/\partial t^2$ gives the form $\Diamond^2\psi = \partial^2\psi/\partial x^2_1 + \partial^2\psi/\partial x^2_2 + \partial^2\psi/\partial x^2_3 - \partial^2\psi/\partial x^2_4$. It is written in this way that $\Diamond^2\psi = \partial/\partial x_1.\partial\psi/\partial x_1 + \partial/\partial x_2.\partial\psi/\partial x_2 + \partial/\partial x_3.\partial\psi/\partial x_3 - \partial/\partial x_4.\partial\psi/\partial x_4$. Now the above metric may be assumed as a general Riemannian metric of the form $\Diamond^2\psi = \sum^{n=4}_{i,j=1} g_{ij}\ \partial\psi/\partial x_i \partial\psi/\partial x_j$; where g be a symmetric tensor. Here $g_{ij} = \langle\partial/\partial x_i, \partial/\partial x_j\rangle$ being the coefficients of the above metric form.

VI. CONCLUSION

Thus the wave invariant $\Diamond^2\psi$ can suggest perfect wave criterion of gravity as well as general wave relativity. The situation may be expressed by invention of a new proposed operator algebraic system in four-dimensional continuum to reveal a real and general meaning of $\Diamond^2\psi$ and to define wave relativity. Here special wave relativity is nothing but a specific situation of general wave relativity where $\Diamond^2\psi = 0$. i.e. $\Diamond^2\psi = \sum^{n=4}_{i,j=1} g_{ij}\ \partial\psi/\partial x_i \partial\psi/\partial x_j$ for general wave relativity and $\Diamond^2\psi = \sum^{n=4}_{i,j=1} g_{ij}\ \partial\psi/\partial x_i \partial\psi/\partial x_j = 0$ for special wave relativity. However the latter metric form may be considered as a form of Euclidian metric.

ACKNOWLEDGEMENT

I indebt to thank Mr. Sujoy Pandit, Computer Operator, Sweet Heart, Daspur for his helps to type this paper and to search information from internet for me.

REFERENCES

[1] U.Dolai, *Proposal of New Operator in Four-Dimensional Wave Equation*, IOSR journal of Applied Physics (IOSR-JAP), vol.4, Issue 2, PP 31-32 (Jul.-Aug. 2013).
[2] S. Banerji and A. Banerjee, *The Special Theory of Relativity*, chapter-2, PP 73,74,75, Published by Asoke K. Ghosh, Prentice – Hall of India Private Limited, M-97, Connaught Circus, New Delhi-110001 (Third Printing – June, 2006).
[3] A. Einstein, *ideas and opinions*, PP 283, 284, 308, 309, 350, Rupa Paperback (1979), Twenty – Second Impression (2006).

International Journal of Modern Engineering Research (IJMER)
www.ijmer.com Vol. 3, Issue. 5, Sep - Oct. 2013 pp-3042-3048 ISSN: 2249-6645

Scan-Based Delay Measurement Technique Using Signature Registers

Telukutla Sahithi[1], Mr. V. T. Venkateswarlu[2] M. Tech., [Ph.D.],
[1]*PG Student,*[2]*Associate professor, Department of ECE, Vasireddy Venkatadri Institute of Technology, Nambur, Guntur (Dt.), Andhra Pradesh, India*

ABSTRACT: *With the scaling of semiconductor process technology, performance of modern VLSI chips will improve significantly. However, as the scaling increases, small-delay defects which are caused by resistive-short, resistive-open, or resistive-via become serious problems. The proposed method uses a signature analysis and a scan design to detect small delay defects. The proposed measurement technique measures the delay of the explicitly sensitized paths with the resolution of the on-chip variable clock generator. The proposed scan design realizes complete on-chip delay measurement in short measurement time using the proposed delay measurement technique and extra latches for storing the test vectors.*

Index terms: Very large scale integration (VLSI), signature register, design for testability (DFT).

I. INTRODUCTION

Semiconductor process technology has developed rapidly to improve the performance of modern VLSI chips. As a continuous process scaling produces large-scale chips. With the rapid development of semiconductor technology, delay testing has become a critical problem. The major types of delays are occurred because of resistive-shorts, resistive-open and resistive-vias. These small delays can cause a fail of a system if they are activated for a longer time. Furthermore their life time become very short. Therefore to overcome these drawbacks some embedded delay measurement techniques have been proposed. Scan-based delay measurement technique with variable clock generator is one of these on-chip delay measurement techniques. The delay of path is measured by continuous sensitization of path under measurement with test clock width reduced gradually. The advantage of this technique is its high accuracy. This technique has some drawbacks. Therefore we present a scan-based delay measurement technique which uses signature registers.

A.EXISTING SYSTEM

These days, various methods for small-delay defect detection have been proposed. Scan-based delay measurement technique with variable clock generator is most widely used. In this technique the delay of path is measured by continuous sensitization of path under measurement with test clock width reduced gradually by resolution. In this technique the accuracy is high. The reason of the high accuracy is that the technique measures just the period between the time when a transition is launched to the measured path and the time when the transition is captured by the flip flop connected to the path, directly. The variation of the measured value just depends on the variation of the clock frequency of the clock generator. Therefore, if the clock generator is compensated the influence of the process variation, the measured value does not depend on the process variation.

B. DRAWBACKS OF EXISTING SYSTEM

Disadvantages of existing system are as follows.

- The gap between the functional clock and scan clock frequency increases. Therefore the measurement time becomes too long to make it practical.
  Area reduction technique of the self testing scan-FFs is also proposed. The flip flop reduces the required number of scan operations, which makes the measurement time practical.
- However, the area overhead of these methods is still expensive compared with the conventional scan designs.

C. PROPOSED SYSTEM

We present a scan-based delay measurement technique using signature registers for small-delay defect detection. The proposed method does not require the expected test vector because the test responses are analyzed by the signature registers. The overall area cost is of the order of conventional scan designs for design for test (DFT). The measurement time of the proposed technique is smaller than conventional scan-based delay measurement. The extra signature registers can be reused for testing, diagnosis, and silicon debugging.

D. ADVANTAGES OF PROPOSED SYSTEM

- Proposed method does not require expected test vectors.
- The measurement time is smaller.

- The overall area cost is of the order of conventional scan designs for design for test (DFT).

E. VARIABLE CLOCK GENERATOR

In the proposed method, the clock width should be reduced continuously by a constant interval. It is difficult for an external tester to control this clock operation. Therefore an on-chip variable clock generator is used for the proposed method. In this paper, we use the on-chip variable clock generator. Figure1 illustrates the circuit. The circuit consists of the arbitrary clock frequency generator and the 2-pulse generator. The arbitrary clock frequency generator generates an arbitrary clock width. The 2-pulse generator generates 2-pulse test clocks with arbitrary timing in response to a trigger signal.

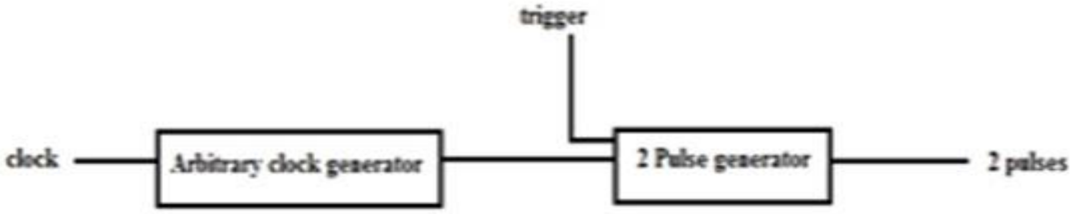

Figure 1: variable clock frequency generator

II.DELAY MEASUREMENT TECHNIQUE USING SIGNATURE REGISTER

The proposed measurement is scan-based delay measurement. The difference from the existing one is use of signature registers and additional latches. In this measurement latches are used to store test vector after scan-in operation.

A.SCAN FLIP FLOPS

An important flip-flop function for ASIC testing is so-called scan capability. The idea is be able to drive the flip-flop's D input with an alternate source of data during device testing. When all of the flip-flops are put into testing mode, a test pattern can be "scanned in" to the ASIC using the flip-flops' alternate data inputs. After the test pattern is loaded, the flip-flops are put back into "normal" mode, and all of the flip-flops are clocked normally. After one or more clock ticks, the flip-flops are put back into test mode, and the test results are "scanned out. Figure2 shows the gate level description of scan flip flop. The lines D, Q, and clk are the input, output, and clock lines, respectively. When se0=0, the flip flop is in normal operation mode. When se0=1 and se1=1, the flip flop is in scan operation mode. When se0=1, se1=0, the flip flop loads the value stored in the latch connected to the latch line. The lines si and s0 are the input and output for constructing the scan path.

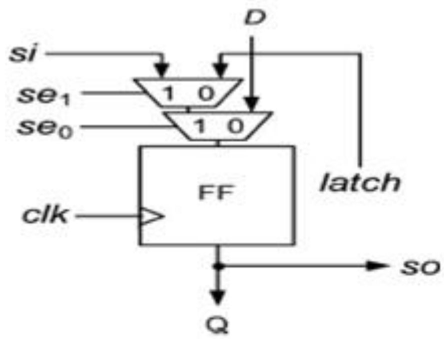

Figure 2: scan flip flop

B.RECONFIGURABLE SIGNATURE REGISTER

Signature analysis registers are often used in combination with standard LFSRs for on-chip self test of VLSI circuits. The signature register for the proposed measurement requires the following functions to meet the demand of the proposed measurement.

• Capturing the test response in arbitrary timing.
• Shifting out the signature data in arbitrary timing.

Figure3 shows the architecture of the signature register for the proposed measurement. It has four flip flops FF0, FF1, FF2, and FF3. . When sge = 1 , it works as a signature register. When sge=0, it works as a shift register. The line in is the input of the signature register. The clock line is controlled by sck . When sck = 0 , the signature register does not capture the input value. When sck = 1 , the signature register captures the input value synchronizing with the positive edge of clk . By controlling sck, the signature registers capture only the target test response. The output is sg0. The measurement system requires multiple signature registers generally.

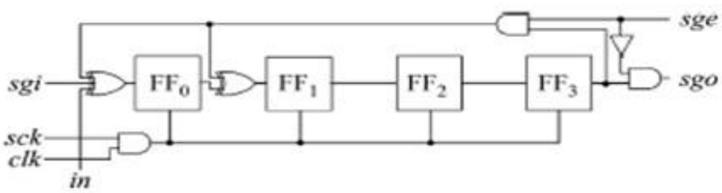

Figure3: 4- bit reconfigurable signature register

III.DELAY MEASUREMENT SYSTEM

Delay measurement system is shown figure 4. The proposed system consists of the low cost tester and the chip with the variable clock generator (VCG) explained in and a BCD decoder. The chip is assumed to have single functional clock in the proposed method, and the chip has two reset lines for initializing the flip flops and the signature registers independently. The reset operations are controlled by the tester. The low cost tester controls the whole measurement sequence. The clock frequency tck is slower than the functional clock. The line sg0 retrieves the signature data from the signature registers to estimate the measured delay. The line sci sends the test vectors to the scan input of the chip. The line sc0 gets the data of the flip flops from the scan output of the chip. In the proposed measurement sequence, sc0 is not used. However, it is used to check the flip flops or the additional latches before the measurement. The line cs is the clock control line. The proposed measurement uses both the slow tester clock tck and the fast double pulse generated by on-chip VCG. The line selects the slow and fast clock. If cs is 1, the fast clock is sent to the clock line clk of the components. Otherwise the slow tester clock tck is sent. The lines trg and cnt are the input lines for VCG. The fast double pulse is launched synchronizing with the positive edge of trg . The line cnt controls the width of the double pulse. The line se controls the scan flip flops. The line lck controls the latches for storing test vectors. The lines scj_0, scj1…..scj_{l-1} are the inputs for the encoded data to control the capture operation of the signature registers. The BCD decoder decodes the encoded input data to the control data of the signature registers sck0…sck_{m-1}. As explained later, the decoder is used to reduce the input lines for the control data of the signature registers. The sge is the enable signal for the signature registers. The control lines of the signature registers are connected to the BCD decoder.

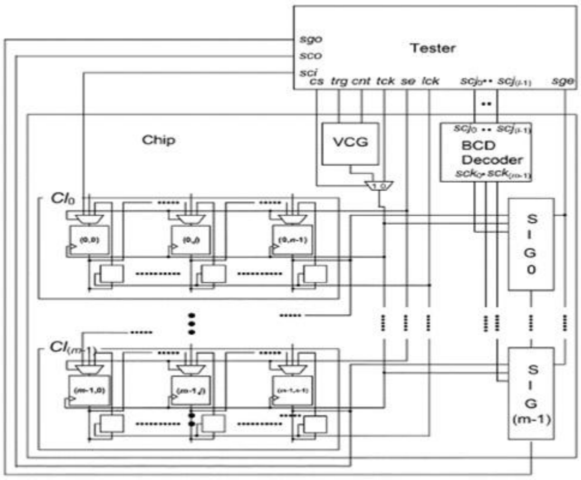

Figure 4: measurement system

A. MEASUREMENT SEQUENCE PER TEST VECTOR

When the measurement system has m signature registers, m paths can be measured in parallel maximally. The measurement strategy using the example is depicted in figure5. In this example, the proposed method consists of six flip flops FF_0-FF_5.the flip flops are classified to the two clusters cl_0 andcl_1. Each cluster has its own signature register $SIG_0$and SIG_1 respectively. The pathsp_1, p_2, p_3 , p_5 are sensitized by the test vector ($FF_0, FF_1, FF_2, FF_3, FF_4, FF_5$) = (0, 0, 1, 0, 1, 1).The test response ofp_i, is captured byFF_i. The expected test response is $(FF_0, FF_1, FF_2, FF_3, FF_4, FF_5) = (1,1,0,1,0,0)$. The paths p_1 and p_2 are measured by SIG_0. The paths $p_3$and p_5 are measured by SIG_1. The combination of two paths, one of which is selected from p_1 andp_2, the other which is selected from p_3 and p_5, can be measured simultaneously. First, the test vector is set to the flip flops with scan-in operation. After that, the values of flip flops are set to extra latches. Second, the first stage is performed. Third the second stage is performed. In each stage, the paths under measurement are tested multiple times with reducing test clock width. Steps (b) and (c) show the state after test execution. The flip flops hold the test response. The latches hold the test vector. After testing, the responses are shifted to signature registers with clock operation ofclk. The number of required shift clocks varies in each stage.

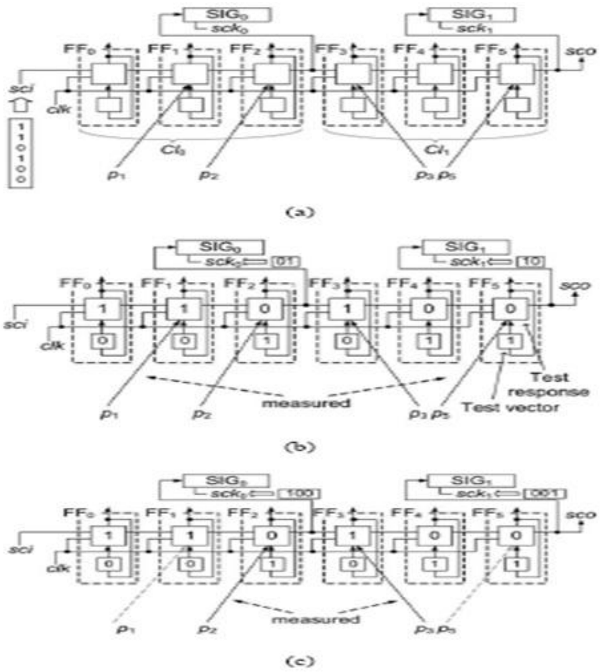

Figure 5: measurement of paths sensitized in attest vector in parallel. (a) scan-in test vector and store it in latches. (b) Sending test responses of p_1 and p_5 to SIG_0 andSIG_1. (c) Send test responses of p_2 and p_3 SIG_0 and SIG_1.

Figure6 shows the timing chart of operation. The low cost tester controls the whole measurement sequence. For measurement both VCG clock and tester clock are used. The clock controlled by cs. The triggered signal trg and control signal cnt are provided to VCG. The control data cnt is updated after each testing operation. In STG_0, SIG_0 captures the test response in second shift-out clock. Therefore sck_0 turns to 1 synchronizing with the negative edge of first clock of the shift-out operation. The latch clock lck captures the value of the flip flops just after scan-in operation is finished.

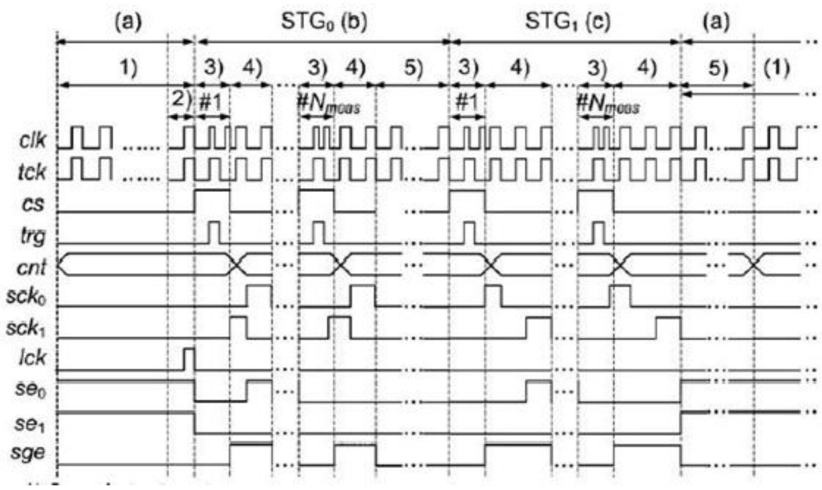

1) Scan-in test vector.
2) Set initial vector to L_j.
3) Apply test clock.
4) Transfer test responses to signature registers.
5) Retrieve signature data.

Figure 6: timing chart of the sequence of figure5.

B.WHOLE MEASUREMENT SEQUENCE

Let us assume that the test set for measurement TS has N_{TV} test vectors$tv_0, \ldots\ldots tv_{NTV-1}$. The number of stages of tv_i is$N_{st(i)}$. Before measurement, we have to check if the flip flops, the latches, and the clock generator work correctly by applying test vectors. After that the following measurement sequence is executed.

Step 1: Initialize the variable$i = 0$.

Step 2: if i is equal toN_{TV}, finish, otherwise initialize the variable j to0, and set tv_i to the flip flops with scan-in operation.

Step 3: send the values of flip flops to the latches.
Step 4: the paths included in STG_j are measured simultaneously. After that, $j$is updated to $(j+1)$.
Step 5: if j equal to $N_{st(i)}$, go to step 6, otherwise load the test vector from the latches to flip flops, and go to step 4.
Step 6: i is updated to $i+1$, and go to step 2.

C.TESTER CHANNEL REDUCTION

If sck of each signature register is directly fed to the inputs of the chip, it requires the same number of extra inputs as the number of the signature registers. It increases tester channel width. To keep the tester channel width short, we use BCD decoder. The decoder circuit transforms n bit binary code in to the corresponding 2^n width decimal code. The example to encode sck bit sequences to the corresponding binary code is shown in figure7. It consists of three clusters $cl_0, cl_1,$ and cl_2. Each cluster has three flip flops. Consider the case that test response of sensitized paths are captured in $FF_{01}, FF_{12}, FF_{20}$.in the shift out operation after a testing, the test response of FF_{01} is captured by SIG_0 two clocks later. Therefore the bit sequence “010” should be sent to sck_0 .the test response of FF_{12} is captured by SIG_1 one clock later. Therefore the bit sequence “100” should be sent to sck_1 . The test response of $FF_{02}$is captured by SIG_2 three clocks later. Therefore bit sequence “001” should be sent to sck_2. Each bit value of this bit sequence is grouped. The group of 0th bit value is $sck_0 sck_1 sck_2 = 010$. Those of first bit values and second bit values are $sck_0 sck_1 sck_2 = 100$, $sck_0 sck_1 sck_2 = 001$, respectively. We call each group slice. Here, sl_i represents the slice of i^{th} bit. Finally the decimal codes are transformed to binary code. The 0th slice sl_0 “010” is transformed to “10”. The 1st slice sl_1 “100” is transformed to “10”. The second slice sl_2 “001” is transformed to “11”. As a result the bit width of data is reduced from 3 bit to 2 bit by transformation. Generally, the width of the slice of sck is n, the width of encoded slice of scj is $[log_2 n]$. However, for the encoding, each slice is permitted only 1 bit with the value 1. More than two bits with the value are not permitted.

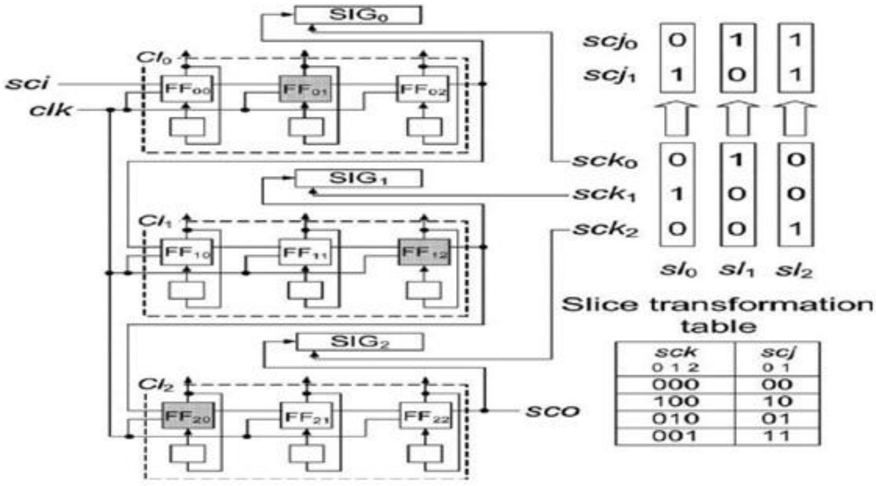

Figure 7: encoding the output data of BCD decoder

D.TEST RESPONSE TRACING

The target paths of proposed measurement are single-path sensitizable. In single path sensitizable measurement, it is guaranteed that once the test fails the test with higher frequency than the failing frequency is fail. Let L_{SIG} be the length of the signature register, the measurement sequence of a path with test response tracing mode is described as follows.
Step1: SIG is initialized.
Step2: Test vector is loaded from the latches.
Step3: Test clock width T is set to normal clock width.
Step4: Test clock is applied.
Step5: The test response is sent to SIG with scan-out operation.
Step6: If testing is equal to N_{meas} or multiple number of L_{SIG} , the values of flip flops of SIG is retrieved. After that, if testing time is equal to N_{meas} , go to step 7, otherwise go back to step 2after the test clock width T is updated to $T - \Delta T$.
Step 7: The delay value is estimated by comparing the retrieved signature value and the signature table.

IV.SIMULATION RESULTS

In this section, on-chip path delay under different process variations will be simulated and measured. During the simulation we measure the delay of each path under test. Random faults were injected in circuits to generate erroneous data. Random input patterns were applied to the ISCAS-89 benchmark circuits and compared with proposed method. The length of the signature register is 8 bit. The test set consists of test vectors which detects all single-path sensitizable transition faults. The paths sensitized by these test vectors are measured. The measurement times using the proposed scan design and is calculated by Tsig =time required for {whole scan-in + double pulse + SIG data}

Simulation results of delay measurement using signature register are shown in figure8 and figure9

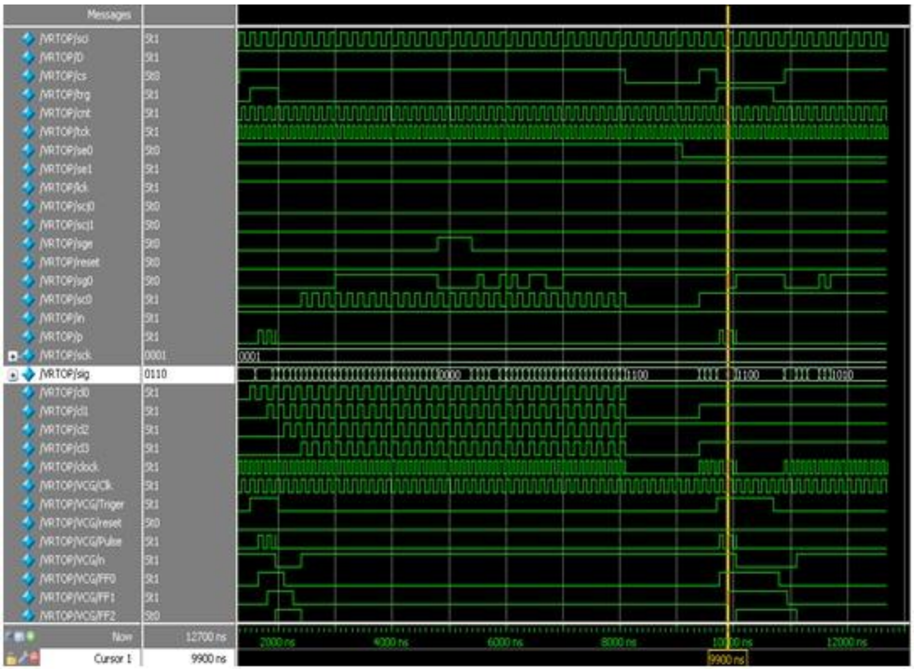

Figure 8: Simulation results

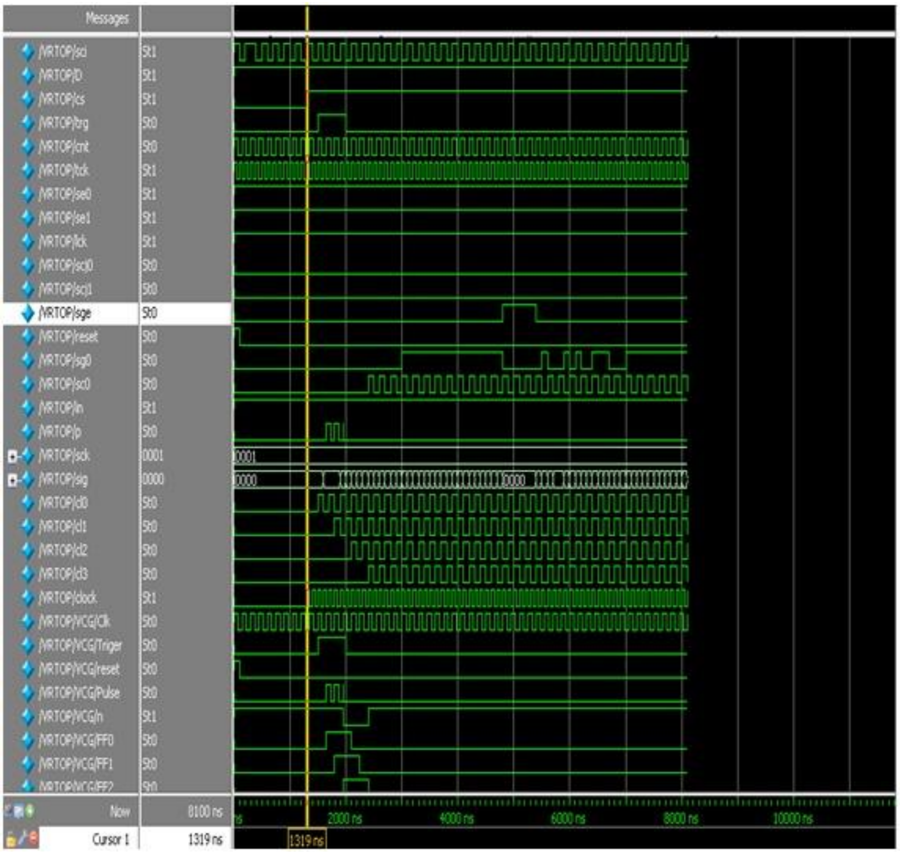

Figure9: simulation results

The device utilization summary for the delay measurement technique is shown in Table I

Logic utilization	*used*	*available*	*Utilization*
Total number of slice register	43	7,168	1%
Number used as flip flop	31		
Number used as latches	12		
Number of 4 input LUTs	47	7,168	1%
Number of occupied cells	47	3,584	1%
Number of slices containing only related logic	47	47	100%
Number of slices containing unrelated logic	0	47	0%
Number of 4 input LUTs	47	7,168	1%
Number of bonded IOBs	13	141	9%
Number of BUFGMUXs	3	8	37%
Average fan out non clock nets	2.76		

Table I: device utilization summary

CONCLUSION

- The proposal of the delay measurement method using signature analysis and variable clock generator.
- The proposal of a scan design for the delay measurement of internal paths of SOC.

The first proposal can be applied not only SOC but also field programmable gate array (FPGA). A future work is the low cost application of the proposed measurement to FPGA. When we measure short paths the measurement error can increase for the IR drop induced by higher test clock frequency. It can reduce the test quality. Another future work is the reduction and the avoidance of the measurement error caused by the IR drop.

REFERENCES

[1] N. Ahmed and M. Tehranipoor, Nanometer Technology Designs: High-Quality Delay Tests. New York: Springer, 2007.
[2] K. Noguchi, K. Nose, T. Ono, and M. Mizuno, “A small-delay defect detection technique for dependable LSIs,” in Proc. IEEE Symp. VLSI Circuits, 2008, pp. 64–65.
[3] B. I. Dervisoglu and G. E. Stong, “Design for testability: Using scanpath techniques for path-delay test and measurement,” in Proc. IEEE Int. Test Conf. (ITC), 1991, pp. 365–374.
[4] K. Noguchi, K. Nose, T. Ono, and M. Mizuno, “An area reduction technique of self-testing FFs for small-delay defects detection,” The Inst. Electron., Inf. Commun. Eng. (IEICE), Tech. Rep. DC2009-16, 2009.
[5] A. Krstic and K.-T. Chen, Delay Fault Testing for VLSI Circuits. Norwell, MA: Kluwer, 1998.
[6] J.-J. Liou, L.-C. Wang, and K.-T. Cheng, “Enhancing test efficiency for delay fault testing using multiple-clocked schemes,” in Proc. Des. Autom. Conf. (DAC), 2002, pp. 371–374.
[7] H. Yan and A. D. Singh, “Evaluating the effectiveness of detecting delay defects in the slack interval: A simulation study,” in Proc. IEEE Int. Test Conf. (ITC), 2004, pp. 242–251.
[8] J. Lee and E. J. McCluskey, “Failing frequency signature analysis,” in Proc. Int. Test Conf. (ITC), 2008, pp. 1–8.
[9] R. Tayade and J. A. Abraham, “On-chip programmable capture for accurate path delay test and characterization,” in Proc. IEEE Int. Test Conf. (ITC), 2008, pp. 148–159.
[10] M. Beck, O. Barondeau, X. Lin, and R. Press, “Logic design for on-chip test clock generation-implementation details and impact on delay test quality,” in Proc. IEEE Des., Autom. Test Eur. Conf. Exhib. (DATE), 2005, pp. 56–61.

A Comparative Study of Low Cost Solar Based Lighting System and Fuel Based Lighting System for Remote off Grid Location in India

Biswajit Biswas[1], Sujoy Mukherjee[2]

[12]*Department of AEIE, Murshidabad College of Engineering & Technology, India,*

ABSTRACT: *A number of villages in India is yet to be electrified due to its location. At the same time it is also important to mention that grid connection to those areas is very expensive and time consuming. The source of lighting in those areas are conventional fuel based lighting system i.e. mainly kerosene based lantern. It has immense health hazard and environmental impact. To meet the energy demand of the off grid locations in India, solar energy can play vital role. The aim of the present study is to design an efficient and low cost solar based lighting system for the off grid location in India. The solar based lighting system was compared to the kerosene based lantern and found much efficient as far as lighting flux is concerned. The cost of the solar based system and payback period is also studied. The payback period definitely indicates the opportunity to utilize solar based lighting system for off grid locations in India.*

Keywords: *Energy Efficiency, LED Lighting, Payback Period, Single Diode Model, Solar Cell*

I. Introduction

Energy is the integral part of life. Energy demand increases day by day but it is a big challenge to distribute energy in usable form in all part of the country. It is found that, around 25,000 villages are located in remote and inaccessible areas and hence could not be electrified through conventional grid extension in India. But, it is essential to provide energy to those people who are living in off grid area. At the same time it is very much expensive to connect those areas though grid connection because of their inaccessible geographical location. The concept of mini grids is advantageous in some remote areas to provide sustainable, reliable electricity and cost effective electricity [1]. But this concept is also a long term process to meet the energy demand of the remote locations. To overcome this problem, it is beneficial to generate off grid power to meet the minimum energy requirement using available alternative sources of energy. The Ministry of New and Renewable Energy (MNRE) in India is implementing the 'Remote Village Electrification Program' (RVEP) to electrify such remote villages by installing solar photovoltaic (PV) home lighting systems in all the states. It is found that solar home lighting system in the remote village can influence the standard of living of people very significantly in the remote areas. It also reduces the expenditure on kerosene of the households of all income groups due to solar home lighting system [4]. A study in the household sector of Kanyakumari District of Tamil Nadu reveals that the consumption pattern of energy sources wholly depends upon the availability of the energy sources, and the level of income of the people [2]. It is found that decentralized energy planning (DEP) is one of the options for meeting the rural and small scale energy needs in a reliable, affordable and environmentally sustainable way. The main aspect of the energy planning at a decentralized level is to prepare an area based DEP to meet energy needs and development of alternate energy sources at least cost to the economy and environment [3]. In the rural area, domestic household sector accounts for nearly 75 percent of the energy use in rural areas [5]. In a study it is found that the employment of a solar lighting system of 3 W lamp and battery backup can successfully be used for small scale lighting applications in remote areas that are far away from the power grid. [6]. A study to quantify the energy saving potential possible with changing in illumination schemes, it found that the adoption of LED lighting scheme has huge energy saving potential, and reasonable payback period [8].

Hence conjugation of LED as a means of illumination with solar photovoltaic system will give a highly efficient system as alternative lighting for remote inaccessible areas in India. The scheme will definitely improve the lighting energy utilization pattern in the remote off grid location and hence the standard of living of the people.

II. Sources of lighting energy in off grid area in India

A huge no of remote villages are not connected yet with grid connection to meet the energy demand of that locations. This is mainly due to inaccessibility of the areas due to geographically backward location. The main means of lighting in those areas is burning fossil fuels. A very few number of people uses solar energy for lighting. In the present study it is found that solar energy is one of the important resources to meet the lighting energy demand of households with low initial investment and payback period. Our study is based on the solar energy utilization as highly efficient lighting system in a cost effective manner.

III. Sun as source of energy

Sun is the source of all energy in this universe. The energy received from the sun is in the form of radiation. The intensity of solar radiation available on the earth surface varies significantly with seasonal change. The intensity of solar radiation is measured in watt per square metre. The available energy from sun can be converted into usable energy by solar thermal application or by solar photovoltaic application. In the present study, concentration is given towards use of solar photovoltaic cell to directly convert the solar energy into usable electrical energy and hence to meet the lighting demand of remote off grid areas.

IV. Design of low cost domestic lighting system for off grid area

The schematic design for the domestic lighting system is shown in the figure. The main objective of the design is to provide lighting energy with very low cost as a large section of the people in remote areas belongs to economically backward section. It comprises of a solar cell array, solar charger, a battery backup system, LED as scheme of illumination.

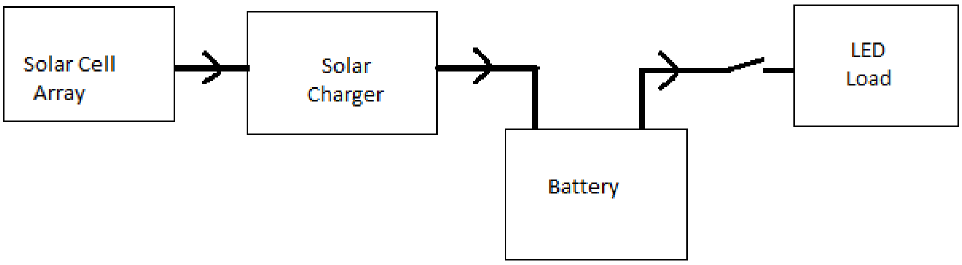

Figure 1: Schematic diagram of the system designed

4.1 Solar cell array

PV cells are grouped in larger units called PV panels which are further interconnected in a parallel-series configuration to form PV arrays. Each of these cells is basically a p-n junction capable of converting solar energy into electrical energy. The conventional technique to model solar cell is to establish mathematical expressions based on the equivalent circuits of the cell. Circuit of a single diode model of solar cell is shown in Fig 2 [9]. In single diode model, there is a current source parallel to a diode. The current source represents light generated current, which varies linearly with solar irradiation. This is the simplest and most widely used model as it offers a good compromise between simplicity and accuracy.

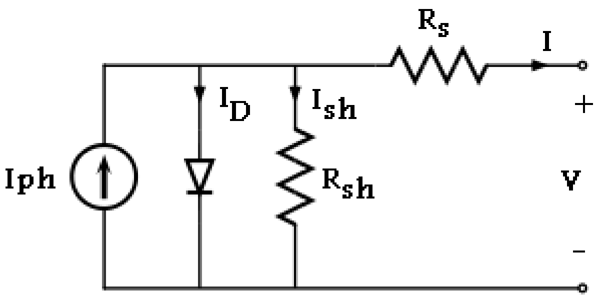

Figure 2: single diode model of solar cell

From the Fig.2 the following equations can be written to mathematically describe the model of the solar cell:

$$I = I_{ph} - I_D - I_{sh} \quad (1)$$

$$I_D = I_s \left(exp \frac{q(V_D + R_s I)}{NKT} - 1 \right) \quad (2)$$

$$I_{sh} = \frac{(V + R_s I)}{R_{sh}} \quad (3)$$

$$I = I_{ph} - I_s \left(exp \frac{q(V_D + R_s I)}{NKT} - 1 \right) - \frac{(V + R_s I)}{R_{sh}} \quad (4)$$

In these equations, I_{ph} is the photo current, I_s is the reverse saturation current of the diode, q is the electron charge, V_D is the voltage across the diode, K is the Boltzmann's constant, T is the junction temperature, N is the ideality factor of the diode, and R_s and R_{sh} are the series and shunt resistors of the cell, respectively. In the present work a solar cell specifications are mentioned in Table 1.

Table 1: Solar cell parameters

Parameters	Values
Maximum Power (P_{max})	5W
Voltage at max. Power (V_{max})	8.8 V
Current at max. Power (I_{max})	0.57 A
Short circuit current (I_{sc})	0.61 A
Open circuit voltage (V_{oc})	10 V

4.2 Solar charger

A solar charger is designed to charge a sealed and maintenance fee (SMF) battery during the presence of day light. It will also limit the current and protect the battery to discharge through the solar cell in absence of day light.

4.3 Battery

The battery is used here to store energy generated in the solar cell and use the same in absence of sunlight i.e. mainly during the night time. The battery used is a sealed and maintenance free battery of 4 Ah capacities.

4.4 LED as lighting source

LED is a semiconductor device which emits light when connected to power source. Basically it is a PN junction diode. In forward biased condition it emits energy in the form of light. The collour of the emitted light depends on the material used to develop the LED. The efficacy of light source is measured in lumens/watt. The efficacy of LED is compatible with the present light source but the efficiency of LED lighting is very high. As there is no heat developed in LEDs hence power towards heat will be reduced. The losses taking place will be in driver circuits which account for 10-15% losses, thus a higher efficiency in the range of 85-90 % can be obtained. It makes LED as an energy efficient source of lighting of coming days [8]. Power consumption of the designed light system is 3w.

V. Results

From the study it is found that the developed system can deliver power for four hours per day when the battery is charged during the day time on a sunny day. The available solar radiation profile for a particular sunny day during 5:00 a.m. to 5:00 p.m. is shown in Fig.3. From the Fig.3 it is seen that the duration of effective day light is around seven hours to charge the battery.

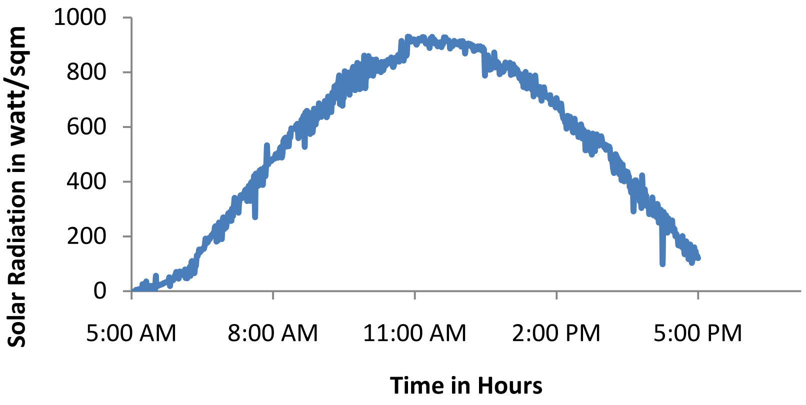

Figure 3: Variation of solar radiation on a sunny day

The scheme of measurement of output LUX of the lighting source has been shown in Figure 4. Lighting source is placed on different vertical height and measurement of light flux has been taken in two positions namely A and B in the Figure 4. Position A indicates the lighting flux on the working plane just under the lighting source. It is obvious that this position will be the maximum LUX point on the working plane. Position B is the point on working plane at some defined horizontal distances from the maximum LUX point. The vertical distance from source to working plane and horizontal distance between position A and B on the working plane are 1, 2 and 3 feet respectively.

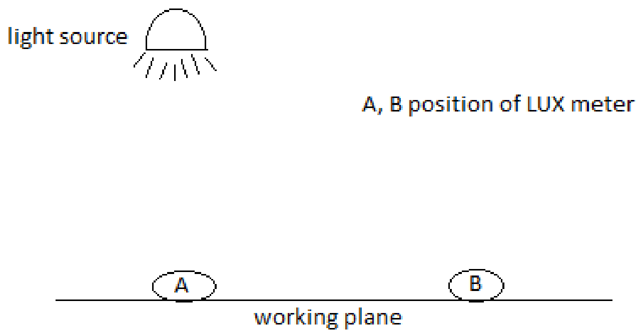

Figure 4: Illumination measurement in working plane

The output light flux for the designed system at different distances is shown in Table 2. The conventional lighting system i.e. kerosene based lamp for the remote off grid area is also studied and shown in Table 3. Kerosene lantern is placed on the working plane to quantify the available lighting flux. The measurement has been taken at 1, 2 and 3 feet distance with LUX meter facing towards source and LUX meter placed on the working plane. From the comparative study it is clear that the designed system is much better as far as lighting flux is concern. It is also important to mention that it can avoid the health hazard on the occupants caused due to burning of fossil fuel.

Table 2: Illumination level on the working plane with the designed system

Sl. No.	Distance (in feet)	Illumination level when LUX meter at position A (in LUX)	Illumination level when LUX meter at position B (in LUX)
1	1	125	30
2	2	33	7
3	3	13	3

Table 3: Illumination level on the working plane with the conventional kerosene lantern

Sl. No.	Distance (in feet)	Illumination level when LUX meter at position faced towards the source (in LUX)	Illumination level when LUX meter is placed in working plane (in LUX)
1	1	10	5
2	2	5	2
3	3	2	1

VI. Calculation

Cost of the system designed is around Rs. 700. Now the cost of kerosene based hurricane lantern used in the rural area for lighting is around Rs. 100. On an average the fuel consumption per household to run a lantern round the year is around 40 litres. Now the yearly cost of fuel i.e. kerosene in this case is Rs.15X40 = Rs.600 assuming the cost of kerosene per litre with Government subsidy as Rs. 15. Hence the replacement of kerosene based lantern with solar photovoltaic based lighting system will demand a reasonable initial investment with payback period of 700/600 = 1.16 year i.e. one year two months.

VII. Conclusion

From the present study it can be concluded that the developed lighting system will eliminate the health hazard of using low intensity kerosene based lighting system in the remote villages in India. At the same time, the study shows the amount of savings kerosene and the initial investment of the system which reflects a reasonable payback period.

References

[1] R.K. Viral, T. Bahar, M. Bansal, Mini grid development for rural electrification in remote India, *International Journal of Emerging Technology and Advanced Engineering*, Volume 3, Special Issue 3, Feb 2013, 356-361.
[2] Dr. M. Murugan, An analysis of rural household energy consumption in Kanyakumari district – Tamilnad, *International Journal of Multidisciplinary Research*, Vol.1, Issue 7, November 2011, 130-139.
[3] R.B. Hiremath, B. Kumar, P. Balachandra, N.H. Ravindranath, Implications of Decentralized Energy Planning for Rural India, *Journal of Sustainable Energy & Environment*, Vol. 2, 2011, 31-40.
[4] Tarujyoti Buragohain, Impact of Solar Energy in Rural Development in India, *International Journal of Environmental Science and Development,* Vol. 3, No. 4, August 2012, 334-338.
[5] Ajay Kumar Vinodia, Dr. Najamuddin, Promotion of renewable energy in rural India, *ITPI JOURNAL*, 3: 2, 2006, 21-28.
[6] L. Suresh, G. R. S. Naga Kumar, Dinesh. V. R. Gopal Krishna, Design, Development & Simulation of Solar Lighting System, *International Journal of Engineering Research and Applications*, Vol. 1, Issue 3, 991-996.
[7] U. E. Asuquo, E. P. Obot, Construction and Operation of a Solar Lighting System, *Global Journal of Pure and Applied Sciences*, Vol. 15, No. 3, 2009, 417-420.
[8] Narendra B Soni, P. Devendra, The transition to LED illumination: A case study on energy conservation, *Journal of Theoretical and Applied Information Technology*, 2005 - 2008 ,1083-1087
[9] Sree Manju, B Ramaprabha, R Mathur B.L, Design and Modeling of Standalone Solar Photovoltaic Charging System, *International Journal of Computer Applications*, Volume 18– No.2, March 2011,0975 – 8887.

International Journal of Modern Engineering Research (IJMER)
www.ijmer.com Vol. 3, Issue. 5, Sep - Oct. 2013 pp-3053-3059 ISSN: 2249-6645

Regression analysis of shot peening process for performance characteristics of AISI 304 austenitic stainless steel

Dr. Lakhwinder Singh[1], Dr. RA Khan[2] Dr. ML Aggarwal[3]

Associate Professor, Department of Mechanical Engineering, YMCA University of Science & Technology, Faridabad -121006, Haryana , India

[2]Retd. Professor, Department of Mechanical Engineering, Jamia Millia Islamia, New Delhi-110025

[3] Professor, Department of Mechanical Engineering, YMCA University of Science & Technology, Faridabad -121006, Haryana , India.

ABSTRACT: *The surface fibers of the material are yielded in tension by the impact of shots in shot peening process. Below the surface fiber an even thin skin surface layer of material is deformed and this layer is highly stressed in compression. It results in the improvement of surface and mechanical properties of the material. Regression analysis is the statistical modeling technique, and it is suitable for the majority of predicting problems. It is valuable for quantifying the impact of various simultaneous influences upon a single dependent variable. In the present study quantification of performance characteristics were carried out, by developing the mathematical models of logarithmic nature using regression analysis. MINITAB 14 is a statistical tool which is used for the complete analysis. The analysis includes pressure, shot size, exposure time, nozzle distance and nozzle angle as process parameters. The complete analysis will be helpful to the manufacturer in deciding the shot peening parameters for desired performance characteristics. It helps the manufacturer to reduce the cost and improve its productivity.*

Keywords: *AISI 304 austenitic stainless steel, ANOVA, Regression analysis and Shot peening*.

I. Introduction

Stainless steel is iron-base alloys containing chromium and nickel. Chromium makes the surface passive by forming a surface oxide film [1, 2], which protects the underlying metal from corrosion. This is because when the metal is scratched; the oxide layer re-forms quickly, hence protecting it from corrosion. However, chromium is a ferrite stabilizer. To counteract this, nickel is added as an austenite stabilizer, so that the microstructure at ambient temperature remains as austenitic [3].The stainless steel attains its stainless characteristics due to the formation of an invisible and adherent chromium-rich oxide surface film. The austenitic stainless steel is used in verity of applications due to its corrosion resistance, ductility, good weldability and resistance to high and low operating temperatures [4]. The heat treatment processes make austenitic stainless steel soften. Further the addition of carbon results in sensitization. Austenitic stainless steel is usually cold worked to enhance the mechanical properties [5, 6, 7]. Kirk and Payne [5] concluded in their work that martensite formation was easily induced by plastic deformation in austenitic stainless steel.

Shot peening is a cold working process in which the surface of a part is bombarded with small spherical media with high speed called shot. Each shot striking the material acts as a tiny peening hammer, imparting to the surface a small indentation or dimple. The surface fibers of the material are yielded in tension by the impact of shots. Below the surface fiber an even thin skin surface layer of material is deformed and this layer is highly stressed in compression. It develops a residual compressive stress in this thin skin surface layer [8, 9]. Shot peening is one of the most versatile tool to strengthen the metal parts against tensile strength, impact strength, surface hardness, compressive residual stress, damping, surface roughness, fatigue failure and corrosion. Shot peening is a well-known cold working process that affecting thin skin surface layer of the materials [10, 11, 12]. The layer is called the depth of deformed layer. The shot peening variables like shot material, shot quality, shot intensity, shot coverage etc. effect on mechanical properties [10, 13]. Kapoor and Tiwari [14] discussed some basic aspects of shot peening. They overviewed the shot peening process and mentioned its critical impacts. It is used now days in hundreds of different components of automobiles, aircraft and marine industries like railway and automobile leaf spring, helical spring, gears, axle bearing, crankshafts, milling cutters, connecting rod, cylinder block, valve springs, washers etc. [4].

The controlled shot peening parameters helps in enhancing the surface and mechanical properties of the material. T. Dorr et al. and M. Obata et al. discussed the increase in surface hardness and surface roughness with increase in shot size and the peening intensity [15, 16]. K.B. Prakash et al. have made study on shot peening for precision-machined steels with high strength to weight ratio [11]. As per the guidelines given by Champaine [13], the exposure time is an important factor to achieve desired peening coverage for the material.

The development of complex non-linear predictive model using regression analysis is well established approach to predict the performance characteristics. The researchers [17, 18] developed a mathematical model and the adequacy of the model was verified using ANOVA. Meguid et al. [19] developed a mathematical model for shot peening related to single and double impact events. Seceleanu et al. [20] pointed out the influence of some metallurgical factors on the phase transformation and properties of cast iron. They determined the mechanical properties of a S.G. cast iron and developed mathematical modeling using the regression analysis. Schiffner and Helling [21] constructed a simplified model to simulate the evolution of residual stress caused by shot peening. Delijaicov et al. [9] developed a mathematical model to describe the relationship between the shot peening process variables (shot diameter, impact velocity, static preload and coverage) and the curvature of the specimens made of aluminium 7050 and 7475 alloys.

The main objective of the present work is to investigate the effects of shot peening for improving the mechanical and surface properties of AISI 304 austenitic stainless steel. It is required to develop the mathematical models for multi performance characteristics of AISI 304 austenitic stainless steel. Therefore, an attempt was made in this study to find out the synergetic effect of different process parameters on performance characteristics. The investigation is helpful to the manufacturers for reduction of cost, performance variation and scrap to increase productivity.

II. Experimental set up

The material AISI 304 austenitic stainless steel is used for various tests. The composition of the material is shown in Table 1. The mechanical properties of the material are: tensile strength 617MPa, fatigue strength 228MPa and surface hardness 271VHN.

Table 1: Chemical composition (wt %) of AISI 304 austenitic stainless steel

Austenitic stainless steel	**C**	**Si**	**Mn**	**P**	**S**	**Ni**	**Cr**	**Mo**	**V**
AISI 304	0.08	0.57	1.6	0.021	0.02	9.83	18.78	0.25	0.07

A 10mm thick flat plate was used for making various specimens for determining the tensile strength. The dimension of specimen for tensile strength test is shown in Fig. 2. These specimens were required to perform the tensile test at different process parameter levels.

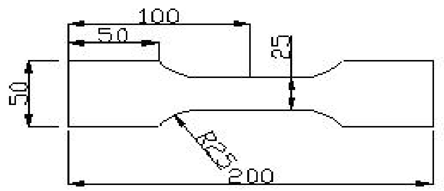

Fig. 2: Specimen for tensile test (all dimensions in mm).

Vickers hardness test was carried on the surface of specimens. The hardness measurements were performed on specimens of 20mm by 60mm by 10mm thickness using WOLPERT universal hardness testing machine dia tester – 2, model 2RC. The average values of three readings of surface hardness were taken for different peening parameters. The fatigue life of the USP and SP was tested by an axial fatigue-testing machine. Stress ratio (R) equal to 0.1 was used during fatigue testing.

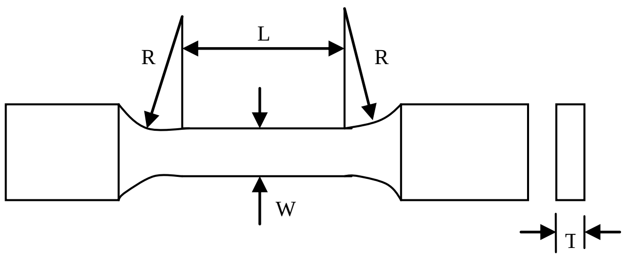

T = 5mm W = 2.6T L = 3.23W R= 117 mm

Fig. 3: ASTM flat specimen for fatigue strength.

The dimension of specimen for plotting S-N curve is shown in Fig. 3. The dimensions of the specimens were according to the ASTM standards. Fifteen specimens were tested in order to plot an S/N curve. Only the average points were presented for each level. The specimens were testing in axial fatigue testing machine MTS model 810, at a frequency 30Hz, at room temperature. The other specifications of the machine are:

Type : Servo hydraulic system
Force Capacity : $\pm$ 285kN
Column space : 460 mm
Test space : 978mm

III. Selection of shot peening parameters

The selection of process parameters is most important step in Design of Experiments (DoE). Shot peening process constitutes a multiple impacts of small sized spherical balls onto a surface to achieve better surface and mechanical properties. In shot peening process the parameters are divided into two categories one is controlled before the start of the process i.e. shot size and nozzle angle and the remaining are evaluated after shot peening process i.e. intensity, saturation, coverage etc. The desired magnitude of intensity, saturation, velocity and coverage are controlled by the air pressure, shot mass flow rate, nozzle type, feed rate of the nozzle along the work piece, nozzle distance from the work piece, and the work piece table speed. Therefore in the present investigation pressure, shot size, exposure time, nozzle distance and nozzle angle (θ) (considered in the analysis as sin θ i.e. impact of normal component of force) are the controllable influential process parameters under consideration. These shot peening parameters along with their levels are shown in Table 2.

Table 2: Process parameter and their levels

Process Parameter	**Parameter Designation**	**Levels**		
		L1	L2	L3
Pressure (MPa)	P	0.196	0.392	0.588
Shot Size (mm)	S	0.85	1.00	1.85
Exposure Time (Sec)	T	80	120	160
Nozzle Distance (mm)	D	80	100	120
Nozzle Angle θ (Sin θ)	E	60^0 (0.866)	75^0 (0.966)	90^0 (1.000)

An air-blast shot peening machine was used for shot peening of the specimens. The hardness of shots was 56HRC to 60HRC.

IV. Design of experiments (DoE)

The DoE was based on full factorial design considering five factors each at three levels. An orthogonal array is a fractional factorial matrix that ensures a balanced comparison of levels of any parameter. In the present analysis a L27 orthogonal array is used. For three levels of each five factors there are 27 runs. The experimental results for tensile strength (TS), surface hardness (VHN) and fatigue strength (FS) are depicted in Table 3 for different 27 runs.

Table 3: Experimental results for different shot peening parameters.

Exp. No.	**P**	**S**	**T**	**D**	**E**	**TS**	**VHN**	**FS**
1	1	1	1	1	1	760.8	361.2	270.5
2	1	1	1	1	2	778.4	381.4	281.3
3	1	1	1	1	3	793.5	390.6	295.6
4	1	2	2	2	1	790.4	370.1	292.4
5	1	2	2	2	2	802.5	382.7	301.8
6	1	2	2	2	3	815.6	395.4	315.2
7	1	3	3	3	1	799.1	360.4	282.6
8	1	3	3	3	2	825.1	381.1	291.3
9	1	3	3	3	3	840.7	395.7	305.1
10	2	1	2	3	1	722.5	370.5	267.3
11	2	1	2	3	2	738.3	386.4	278.2
12	2	1	2	3	3	750.4	397.6	289.6
13	2	2	3	1	1	805.7	391.2	295.6
14	2	2	3	1	2	815.8	403.1	318.2
15	2	2	3	1	3	826.9	415.2	310.3
16	2	3	1	2	1	685.8	355.9	245.7
17	2	3	1	2	2	698.3	375.8	258.4
18	2	3	1	2	3	720.6	381.3	264.6
19	3	1	3	2	1	788.6	390.8	280.8
20	3	1	3	2	2	800.1	412.3	320.5
21	3	1	3	2	3	835.7	419.8	308.2
22	3	2	1	3	1	670.5	362.4	239.1
23	3	2	1	3	2	681.4	377.2	252.4
24	3	2	1	3	3	695.3	389.7	261.3
25	3	3	2	1	1	740.8	399.1	258.1
26	3	3	2	1	2	750.3	416.2	272.6
27	3	3	2	1	3	758.8	426.8	283.8

V. Regression analysis of performance characteristics

Regression analysis is a statistical tool to establish a mathematical relationship between the variables. The technique is helpful for the quantification of the performance characteristics. The present investigation involves the regression analysis of tensile strength, surface hardness and fatigue strength for AISI 304 austenitic stainless steel by using statistical software MINITAB 14. These models can be used for the selection of a set of shot peening parameter for desired performance characteristics.

The log transformed response variables are assumed for formulating the correlation. The following model is assumed for performance characteristics:

$$\ln(Y) = \beta_0 + \beta_1 \ln(P) + \beta_2 \ln(S) + \beta_3 \ln(T) + \beta_4 \ln(D) + \beta_5 \ln(E) \quad (1)$$

where Y is the performance characteristic and β_0, β_1, β_2, β_3, β_4, β_5 are the regression coefficients.

The log transformed response variables to formulate the correlation for AISI 304 austenitic stainless steel are shown in Table 4-5. Table 4 represents the log transformed response for process parameters and Table 5 represents log transformed response for performance characteristics.

5.1 Quantification of tensile strength

The quantification of each performance characteristic is established by regression analysis using statistical software MINITAB 14. The regression analysis outputs are tabulated in Table 6-8 for each performance characteristic. The regression results for tensile strength are shown in Table 6. It shows the following correlation between the tensile strength and the process parameters:

$$\ln(TS) = 6.27 - 0.0684 \ln(P) - 0.0265 \ln(S) + 0.178 \ln(T) - 0.114 \ln(D) + 0.249 \ln(E) \quad (2)$$

The exponential form of the equation is as follows:

$$(TS) = 528.47\ (P)^{-0.0684}\ (S)^{-0.0265}\ (T)^{0.178}\ (D)^{-0.114}\ (E)^{0.249} \quad (3)$$

Table 4: Log transformed response table for process parameters.

P	ln(P)	S	ln(S)	T	ln(T)	D	ln(D)	E	ln(E)
0.196	-1.6296	0.85	-0.1625	80	4.3820	80	4.3820	0.866	-0.1441
0.196	-1.6296	0.85	-0.1625	80	4.3820	80	4.3820	0.966	-0.0348
0.196	-1.6296	0.85	-0.1625	80	4.3820	80	4.3820	1.000	0.0000
0.196	-1.6296	1	0.0000	120	4.7875	100	4.6052	0.866	-0.1441
0.196	-1.6296	1	0.0000	120	4.7875	100	4.6052	0.966	-0.0348
0.196	-1.6296	1	0.0000	120	4.7875	100	4.6052	1.000	0.0000
0.196	-1.6296	1.85	0.6152	160	5.0752	120	4.7875	0.866	-0.1441
0.196	-1.6296	1.85	0.6152	160	5.0752	120	4.7875	0.966	-0.0348
0.196	-1.6296	1.85	0.6152	160	5.0752	120	4.7875	1.000	0.0000
0.392	-0.9365	0.85	-0.1625	120	4.7875	120	4.7875	0.866	-0.1441
0.392	-0.9365	0.85	-0.1625	120	4.7875	120	4.7875	0.966	-0.0348
0.392	-0.9365	0.85	-0.1625	120	4.7875	120	4.7875	1.000	0.0000
0.392	-0.9365	1	0.0000	160	5.0752	80	4.3820	0.866	-0.1441
0.392	-0.9365	1	0.0000	160	5.0752	80	4.3820	0.966	-0.0348
0.392	-0.9365	1	0.0000	160	5.0752	80	4.3820	1.000	0.0000
0.392	-0.9365	1.85	0.6152	80	4.3820	100	4.6052	0.866	-0.1441
0.392	-0.9365	1.85	0.6152	80	4.3820	100	4.6052	0.966	-0.0348
0.392	-0.9365	1.85	0.6152	80	4.3820	100	4.6052	1.000	0.0000
0.588	-0.5310	0.85	-0.1625	160	5.0752	100	4.6052	0.866	-0.1441
0.588	-0.5310	0.85	-0.1625	160	5.0752	100	4.6052	0.966	-0.0348
0.588	-0.5310	0.85	-0.1625	160	5.0752	100	4.6052	1.000	0.0000
0.588	-0.5310	1	0.0000	80	4.3820	120	4.7875	0.866	-0.1441
0.588	-0.5310	1	0.0000	80	4.3820	120	4.7875	0.966	-0.0348
0.588	-0.5310	1	0.0000	80	4.3820	120	4.7875	1.000	0.0000
0.588	-0.5310	1.85	0.6152	120	4.7875	80	4.3820	0.866	-0.1441
0.588	-0.5310	1.85	0.6152	120	4.7875	80	4.3820	0.966	-0.0348
0.588	-0.5310	1.85	0.6152	120	4.7875	80	4.3820	1.000	0.0000

5.2 Quantification of surface hardness

The regression analysis results for surface hardness are tabulated in Table 7. It shows the following correlation between the surface hardness and the process parameters:

$\ln(VHN) = 6.17 + 0.0427 \ln(P) - 0.00518 \ln(S) + 0.0826 \ln(T) - 0.114 \ln(D) + 0.479 \ln(E)$ (4)

The exponential form of the equation is as follows:

$(VHN) = 478.19\ (P)^{0.0427}\ (S)^{-0.00518}\ (T)^{0.0826}\ \ln(D)^{-0.114}\ (E)^{0.479}$ (5)

5.3 Quantification of fatigue strength

Similarly, the regression analysis results for fatigue strength are tabulated in Table 8. It shows the following correlation between the fatigue strength and the process parameters:

$\ln(FS) = 5.21 - 0.0599 \ln(P) - 0.0692 \ln(S) + 0.196 \ln(T) - 0.114 \ln(D) + 0.545 \ln(E)$ (6)

The exponential form of the equation is as follows:

$(FS) = 183.09\ (P)^{-0.0599}\ (S)^{-0.0692}\ (T)^{0.196}\ (D)^{-0.114}\ (E)^{0.545}$ (7)

The resulting regression analysis equations 3, 5 and 7 determine the values of tensile strength, surface hardness and fatigue strength of parent AISI 304 austenitic stainless steel. These mathematical models help in selecting the process parameters for the desired performance characteristics.

Table 5: Log transformed response table for performance characteristics.

TS	ln(TS)	VHN	ln(VHN)	FS	ln(FS)
760.8	6.6344	361.2	5.8894	270.5	5.6003
778.4	6.6572	381.4	5.9438	281.3	5.6394
793.5	6.6765	390.6	5.9677	295.6	5.6890
790.4	6.6725	370.1	5.9138	292.4	5.6783
802.5	6.6877	382.7	5.9473	301.8	5.7098
815.6	6.7039	395.4	5.9799	315.2	5.7532
799.1	6.6835	360.4	5.8872	282.6	5.6440
825.1	6.7155	381.1	5.9431	291.3	5.6744
840.7	6.7342	395.7	5.9807	305.1	5.7206
722.5	6.5827	370.5	5.9149	267.3	5.5885
738.3	6.6044	386.4	5.9569	278.2	5.6283
750.4	6.6206	397.6	5.9854	289.6	5.6685
805.7	6.6917	391.2	5.9692	295.6	5.6890
815.8	6.7042	403.1	5.9992	318.2	5.7627
826.9	6.7177	415.2	6.0288	310.3	5.7375
685.8	6.5306	355.9	5.8746	245.7	5.5041
698.3	6.5486	375.8	5.9291	258.4	5.5544
720.6	6.5801	381.3	5.9436	264.6	5.5782
788.6	6.6703	390.8	5.9682	280.8	5.6376
800.1	6.6847	412.3	6.0218	320.5	5.7699
835.7	6.7283	419.8	6.0398	308.2	5.7307
670.5	6.5080	362.4	5.8927	239.1	5.4769
681.4	6.5241	377.2	5.9328	252.4	5.5310
695.3	6.5443	389.7	5.9654	261.3	5.5657
740.8	6.6077	399.1	5.9892	258.1	5.5533
750.3	6.6205	416.2	6.0312	272.6	5.6080
758.8	6.6317	426.8	6.0563	283.8	5.6483

Table 6: Coefficients and intercepts for tensile strength

Predictor	Coef	SE Coef	T	P
Constant	6.2672	0.1055	59.43	0.000
ln(P)	-0.068376	0.007166	-9.54	0.000
ln(S)	-0.026452	0.009704	-2.73	0.013
ln(T)	0.17818	0.01143	15.59	0.000
ln(D)	-0.11445	0.01960	-5.84	0.000

ln(E)	0.24894	0.05294	4.70	0.000
S = 0.0168889 R-Sq = 95.0% R-Sq(adj) = 93.8%				

Table 7: Coefficients and intercepts for surface hardness.

Predictor	**Coef**	**SE Coef**	**T**	**P**
Constant	6.16796	0.08756	70.44	0.000
ln(P)	0.042685	0.005949	7.17	0.000
ln(S)	-0.005179	0.008057	-0.64	0.527
ln(T)	0.082557	0.009490	8.70	0.000
ln(D)	-0.11442	0.01627	-7.03	0.000
ln(E)	0.47902	0.04396	10.90	0.000
S = 0.0140223 R-Sq = 93.4% R-Sq(adj) = 91.8%				

Table 8: Coefficients and intercepts for fatigue strength

Predictor	**Coef**	**SE Coef**	**T**	**P**
Constant	5.2125	0.1373	37.96	0.000
ln(P)	-0.059897	0.009331	-6.42	0.000
ln(S)	-0.06917	0.01264	-5.47	0.000
ln(T)	0.19636	0.01488	13.19	0.000
ln(D)	-0.11358	0.02552	-4.45	0.000
ln(E)	0.54518	0.06894	7.91	0.000
S = 0.0219920 R-Sq = 94.0% R-Sq(adj) = 92.5%				

VI. Discussion and validation

ANOVA, R-sq value and R-sq (adj) value are used for the validation of the models obtained by regression analysis. The ANOVA is the statistical treatment applied to determine the significance of the regression model. The R-sq is used in the context of statistical models whose main purpose is the prediction of future outcomes on the basis of other related information. It is the proportion of variability in a data set that is accounted for by the statistical model. It gives the information about goodness of fit for a model. In regression, the R-sq is a statistical measure of how well the regression line approximates the real data points. An R-sq of 1.0 indicates that the regression line perfectly fits in the data. Unlike R-sq, an R-sq (adj) allows for the degrees of freedom associated with the sums of the squares. Therefore, even though the residual sum of squares decreases or remains the same as new independent variables are added, the residual variance does not. For this reason, R-sq (adj) is generally considered to be a more accurate goodness-of-fit measure than R-sq. R-sq (adj), is a modification of R-sq that adjusts for the number of explanatory terms in the model.

The results of ANOVA, R-sq and R-sq (adj) are obtained by regression analysis using MINITAB 14 and are shown in the following sections. The results show the significance of the analysis. It is observed from Tables 9-11 that p-values for the response tensile strength, surface hardness and fatigue strength is less than 0.05, which shows that it is at 95% confidence level. R-sq is the statistical measure of the exactness at which the total variation of dependent variables is explained by regression analysis. The obtained values of R-sq and R-sq (adj) (Table 6-8) are more than 0.90 and quite near to 1.0 for the performance characteristics, it indicate a good fit. This confirms that the model adequately describes the observed data.

Table 9: ANOVA for tensile strength

Source	**DF**	**SS**	**MS**	**F**	**P**
Regression	5	0.113433	0.022687	79.54	0.000
Residual Error	21	0.005990	0.000285		
Total	26	0.119423			

Table 10: ANOVA for surface hardness

Source	**DF**	**SS**	**MS**	**F**	**P**
Regression	5	0.058154	0.011631	59.15	0.000
Residual Error	21	0.004129	0.000197		
Total	26	0.062283			

Table 11: ANOVA for fatigue strength

Source	**DF**	**SS**	**MS**	**F**	**P**
Regression	5	0.158428	0.031686	65.51	0.000
Residual Error	21	0.010157	0.000484		
Total	26	0.168584			

VII. Conclusion

Logarithmic regression models for shot peened AISI 304 austenitic stainless steel properties with a wide scope have been developed and can help the engineers with relative success in future. These models are tested with various experiments to investigate how the different inputs influenced the mechanical behaviour. Analysis shows good agreement with the literature. Hence the models are considered to be a good reflection of properties of shot peened AISI 304 austenitic stainless steel. MINITAB 14, the response optimizer is used for maximizing the response based on the selected regression model. All analysis results, including, best parameter level combinations, 95% confidence intervals, R-sq and R-sq (adj) of the regression models are estimated. The best chosen regression models for AISI 304 austenitic stainless steel are shown in equations 3, 5 and 7 for tensile strength, surface hardness and fatigue strength respectively. Regression models correlating tensile strength, surface hardness and fatigue strength with process parameters have obtained with R-sq and R-sq (adj) value more than 0.90. The results obtained for optimum process parameters by these equations are near to the experimental values. Hence equations provide a useful guide for setting proper values of process parameters so as to obtain desired tensile strength, surface hardness and fatigue strength.

References

[1] R.W.K. Honeycombe, and H.K.D.H. Bhadeshia, *Steels - Microstructure and Properties*, (Second Edition, Edward Arnold, 1995).

[2] P.J. Cunat, "A New Structural Material for Passenger Cars: Stainless Steel", *Auto Technology*, 2002, 40-42.

[3] T. Oshima, Y. Habarai, and K. Kuroda, "Efforts to save nickel in austenitic stainless steels", *ISIJ International, Vol. 47, No. 3*, 2007, 359-364.

[4] A. Kyröläinen, M. Vilpas, and H. Hänninen, "Use of stainless steels in bus coach structures", *Journal of Materials Engineering and Performance, Vol. 9(6)*, 2000, 669-677.

[5] D. Kirk, and N.J. Payne, "Transformation induced in austenitic stainless steels by shot peening", *ICSP-7. Warsaw, Poland*, 1999, 15-22.

[6] M. Milad, N. Zreiba, F. Elhalouani, and C. Baradai, "The effect of cold work on structure and properties of AISI 304 stainless steel", *Journal of Materials Processing Technology, 203*, 2008, 80-85.

[7] A. Hedayati, A. Najafizadeh, A. Kermanpur, and F. Forouzan, "The effect of cold rolling regime on microstructure and mechanical properties of AISI 304L stainless steel", *Journal of Materials Processing Technology*, *210*, 2010, 1017-1022.

[8] Y. Maheshwari, "Basics of shot peening and important design features of a centrifugal peening machine", *International conference on shot peening and blast cleaning, Bhopal, India*, 2001, 210-221.

[9] S. Delijaicov, A.T. Fleury, and Martins, "Application of multiple regression and neural networks to synthesize a model for peen forming process planning", *Journals of Achievements in Materials and Manufacturing Engineering, Vol. 43, Issue 2*, 2010, 651-656.

[10] H. Olivier, "Correlation of shot peening parameters to surface characteristic", *ICSP-9, France*, 2005, 28-35.

[11] K.B. Prakash, B.M. Sunil, B.M., and Y.S. Chandrakant, "Shot peening: state-of-the-art", *ICAMMP conference, IIT Kharagpur*, 2006, 296-303.

[12] M. Milad, N. Zreiba, F. Elhalouani, and C. Baradai, 2008, "The effect of cold work on structure and properties of AISI 304 stainless steel", *Journal of Materials Processing Technology, 203*,2008, 80-85.

[13] J. Champaigne, *Controlled shot peening*, (2nd edn., The shot peener, Mishawaka, USA, 1989).

[14] V. Kapoor, and A. Tiwari, "Basic aspects of shot peening", *International conference on shot peening and blast cleaning. Bhopal, India*, 2001, 99-106.

[15] T. Dorr, M. Hilpert, P. Beckmerhagan, A. Kiefer, and L. Wagner, "Influence of shot peening on fatigue performance of high-strength aluminum-and magnesium alloys", *Proceedings of the ICSP-7 conference*, Warsaw, Poland, 1999.

[16] M. Obata, and A. Sudo, "Effect of shot peening on residual stress and stress corrosion cracking for cold worked austenitic stainless steel", *Proceedings of the ICSP-5 conference*, Oxford, UK, 1993.

[17] T. L. Ginta, A.K.M. Amin, and Mohd. H.C.D. Radzi, 2009, "Tool life prediction by response surface methodology in end milling titanium alloy Ti-6Al-4V using uncoated WC-Co inserts", *European Journal of Scientific Research, Vol. 28 No. 4*, 2009, 533-541.

[18] P. S. Sivasakthivel, V.V. Murugan, and R. Sudhakaran, "Prediction of tool wear from machining parameters by response surface methodology in end milling", *International Journal of Engineering Science and Technology, 2(6)*, 2010,1780-1789.

[19] S. A. Meguid, G. Shagal, and J.C. Stranart, "Finite element modeling of shot-peening residual stresses", *Journal of Materials and Processing Technology, 92/93*, 1999, 401-404.

[20] D. Seceleanu, I. Milosan, and R. Dobrota, "Some aspects about the mathematical modeling results of an S.G. cast iron with special properties", *Journal of Materials Processing Technology, 143-144*, 2003, 175-178.

[21] K. Schiffner, and C.D. Helling, "Simulation of residual stress by shot peening", *Computers and Structures, 72*, 1999, 329-340.

International Journal of Modern Engineering Research (IJMER)
www.ijmer.com Vol. 3, Issue. 5, Sep - Oct. 2013 pp-3060-3062 ISSN: 2249-6645

Stability of the Equilibrium Position of the Centre of Mass of an Inextensible Cable - Connected Satellites System in Circular Orbit

Vijay Kumar[1], Nikky Kumari[2]
*(Assistant Professor, Department of Mathematics, Shobhit University, Gangoh, Saharanpur,India)
** (Research Scholar, Department of Mathematics, Dayalbagh Educational Institute, Agra, India)

ABSTRACT: *In this paper we have studied the motion and stability of the centre of mass of a system of two satellites connected by inextensible cable under the influence of air resistance and magnetic force in the central gravitational field of oblate earth in circular orbit. We have obtained an equilibrium point which has been shown to be stable in the sense of Liapunov.*

Keywords: *Perturbative forces, stability, interconnected satellites, Equilibrium point, and Circular orbit.*

I. INTRODUCTION

This paper is devoted to study the equilibrium position under the influence of air resistance and magnetic force of oblate earth in case of circular orbit of the centre of mass of the system.

For this, firstly we have derived equations of motion in case of circular orbit of the centre of mass of the system under perturbative forces mentioned above and then Jacobian integral for the problem is obtained. Equilibrium Position has been obtained shown to be stable in the sense of Liapunov. This work is direct generalization of works done by V.V. Beletsky; R. B. Singh; B. Sharma; S. K. Das; P. K. Bhattacharyya and C.P.Singh.

II. EQUATIONS OF MOTION OF ONE OF THE TWO SATELLITES IN ELLIPTIC ORBIT

The equations of motion of one of the two satellites when the centre of mass moves along a keplerian elliptical orbit in Nechvill's co-ordinate system have been derived in the form.

$$x''-2y'-3\rho x=\bar{\lambda}_\propto\rho^4x-\frac{4Ax}{\rho}-\frac{B\cos i}{\rho}-f\rho\rho'$$

$$y''+2x'=\bar{\lambda}_\propto\rho^4y-\frac{A}{\rho}y-\frac{B\rho'\cos i}{\rho^2}-f\rho^2$$

$$z''+z=\bar{\lambda}_\propto\rho^4z-\frac{A}{\rho}z-\frac{B}{\rho}\left[\frac{\rho'}{P}\cos(v+w)+\frac{1}{\mu_E}\left(3p^3\rho^2-\mu E\right)\sin(v+w)\right]\sin i \qquad \text{……....... (2.1)}$$

Where,

$\bar{\lambda}_\propto=\frac{p^3}{\mu}\lambda_\propto=\frac{p^3}{\mu}\frac{\lambda(m_1+m_2)}{l_0m_1m_2}$: λ being Lagrange's multiplier's and m_1, m_2 being masses of two satellites.

l_0 being the length of cable connected by two satellites

$\rho=\frac{R}{p}=\frac{1}{1+e\cos v}$; p being focal parameter and e eccentricity of the orbit of centre of mass

R = Radius vector of the centre of mass from the attracting centre

v = True anomaly of the centre of mass

i = Inclination of the orbit of centre of mass with the equatorial plane of the earth

$A=\frac{-k_2}{p^2}$ = oblateness force parameter

B = $\frac{m_1}{m_1+m_2}\left[\frac{Q_1}{m_1}\frac{-Q_1}{m_2}\right]\frac{\mu_E}{\sqrt{\mu p}}$ = magnetic force parameter

$f=\frac{a_1p^3}{\sqrt{\mu p}}$ = Air resistance force parameter

Here, dashes denote differentiations w.r. to true anomaly v.

The condition of constraint is given by

$$x^2+y^2+z^2\le\frac{1}{\rho^2} \qquad \text{.................. (2.2)}$$

Since the general solution of the system of differential equations given by (2.1) is beyond our reach so we restrict ourselves to the case of circular orbit of the centre of mass of the system in equatorial plane (i = 0) and hence we get from (2.1) on putting.

$\rho = \frac{1}{1+e\cos v} = 1$, $\rho' = 0$ and $i = 0$ (for equatorial plane)

$$x'' - 2y' - 3x = \bar{\lambda}_\alpha x - 4Ax - B$$

$$y'' + 2x' = \bar{\lambda}_\alpha y + Ay - f$$

$$z'' + z = \bar{\lambda}_\alpha z + Az \qquad \text{……………… (2.3)}$$

The condition of constraint given by (2.2) takes the form

$$x^2 + y^2 + z^2 \le 1 \qquad \text{.................. (2.4)}$$

Thus if inequality sign holds in (2.4) then the motion takes place with loose string and the motion is called free motion. If the equality sign holds in (2.4), then the motion takes place with tight string and the motion is called constrained motion.

We are actually interested in stability due to constrained motion. Thus, motion takes place on unit sphere given by -

$$x^2 + y^2 + z^2 = 1 \qquad \text{.................. .(2.5)}$$

Differentiating (2.5), we get

$$xx^1 + yy^1 + zz^1 = 0 \qquad \text{.................. (2.6)}$$

To obtain Jacobian integral of the problem, we multiply the first, second and third equation of (2.3) by x', y' and z' respectively and add them together, we get after integrating on using (2.5) and (2.6)

$$x'^2 + y'^2 + z'^2 - \left(3x^2 - z^2\right) = 5Ax^2 - 2Bx - 2fy + h \qquad \text{.................. (2.7)}$$

Which is known as Jacobian integral and can be interpreted as energy equation with modified potential given by

$$V = -\frac{1}{2}\left(3x^2 - z^2\right) - \frac{5A}{2}x^2 + Bx + fy \qquad \text{.................. (2.8)}$$

Differentiating (6) with respect to v, we get

$$x'^2 + y'^2 + z'^2 = -\left(xx'' + yy'' + zz''\right) \qquad \text{.................. (2.9)}$$

Multiplying the first, second and the third equations of (2.3) by x, y and z respectively and adding we get on using (2.5)

$$xx'' + yy'' + zz'' = 2\left(xy' - x'y\right) + \left(3x^2 - z^2\right) - \left(5x^2 - 1\right)A + \bar{\lambda}_\propto - Bx - fy \qquad \text{................ (2.10)}$$

Using (2.9) in (2.10), we get

$$-\bar{\lambda}_\propto = \left(x'^2 + y'^2 + z'^2\right) + 2\left(xy' - x'y\right) + \left(5x^2 - 1\right) + \left(3x^2 - z^2\right) - Bx - fy\,. \qquad \text{................. (2.11)}$$

To simplify (2.7) and (2.8), we use spherical polar coordinate on unit sphere:

$$x = \cos\phi\cos\psi : y = \cos\phi\sin\psi \text{ and } z = \sin\phi \qquad \text{.................. (2.12)}$$

Using (2.12), (2.7) and (2.8) become respectively

$$\phi'^2 + \psi'^2\cos^2\phi = \left(3\cos^2\psi + 1\right)\cos^2\phi - 5A\cos^2\phi\cos^2\psi - 2B\cos\phi\cos\psi - 2f\cos\phi\sin\psi + h_1$$

.... (2.13)

Where,

$h_1 = h - 1$, and

$$V\left(\phi,\psi\right) = -\left(3\cos^2\psi + 1\right)\cos^2\phi + 5A\cos^2\phi\cos^2\psi + 2B\cos\phi\cos\psi + 2f\cos\phi\sin\psi \qquad \text{............... (2.14)}$$

III. PARTICULAR SOLUTION AND STABILITY

For equilibrium positions, (2.14) can be taken as modified potential energy.

The equilibrium positions are given by the stationary values of $v\left(\phi,\psi\right)$ and hence, we have

$$\frac{\partial V}{\partial \phi} = 0 \qquad \text{.................. (3.1)}$$

$$\frac{\partial V}{\partial \psi} = 0 \qquad \text{.................. (3.2)}$$

Differentiating (2.14) partially with respect to ϕ and using (3.1), we get

Sin ϕ = 0 i.e. ϕ = 0 ....(3.3)

Also, we have

$$\left[\frac{\partial V}{\partial \psi}\right]_{\psi=\psi_0}^{\phi=0} = 3\cos\psi_0 \sin\psi_0 - 5A\cos\psi_0 \sin\psi_0 - B\sin\psi + f\cos\psi = 0 \qquad \text{...................} \quad (3.4)$$

For smallest value of ψ_0, we have from (3.4) on putting $\cos\psi_0$ =1 and sin $\psi_0 = \psi_0$

$$\psi_0 = \frac{-f}{3-5A-B} \qquad \text{...................} \quad (3.5)$$

Thus, the equilibrium point is given by

$$\phi = \phi_0 = 0 \qquad \text{and} \qquad \psi = \psi_0 = \frac{-f}{3-5A-B} \qquad \text{...................} \quad (3.6)$$

To test the stability to the equilibrium position given by (2.6), we have

$$\left[\frac{\partial^2 V}{\partial \phi^2}\right]_{\psi=\psi_0}^{\phi=0} = 2\left(3\cos^2\psi_0 + 1\right) - 10A\cos^2\psi - 2B\cos\psi_0 - 2f\sin\psi_0 \qquad \text{...................} \quad (3.7)$$

$$\left[\frac{\partial^2 V}{\partial \psi^2}\right]_{\psi=\psi_0}^{\phi=0} = 6\cos 2\psi_0 - 10A\cos 2\psi_0 - 2B\cos\psi_0 - 2f\sin\psi_0 . \qquad \text{..................} \quad (3.8)$$

and

$$\left[\frac{\partial^2 V}{\partial \psi \partial \phi}\right]_{\psi=\psi_0}^{\phi=0} = 0 = \left[\frac{\partial^2 V}{\partial \phi \partial \psi}\right]_{\psi=\psi_0}^{\phi=0} \qquad \text{...................} \quad (3.9)$$

For equilibrium point given by (3.6) to be stable in the sense of Liapunov, we have to show that

$$\begin{vmatrix} \left[\frac{\partial^2 V}{\partial \psi^2}\right]_{\psi=\psi_0}^{\phi=0} & \left[\frac{\partial^2 V}{\partial \phi \partial \psi}\right]_{\psi=\psi_0}^{\phi=0} \\ \left[\frac{\partial^2 V}{\partial \phi \partial \psi}\right]_{\psi=\psi_0}^{\phi=0} & \left[\frac{\partial^2 V}{\partial \phi^2}\right]_{\psi=\psi_0}^{\phi=0} \end{vmatrix} > 0 \qquad \text{...................} \quad (3.10)$$

Using (3.7), (3.8) and (3.9) in (3.10) it can be easily seen that (3.10) is positive if 5A + B < 3. .

Conclusion: we conclude that the equilibrium point

$$\phi = \phi_0 = 0 ; \qquad \psi = \psi_0 = \frac{-f}{3-5A-B}$$

is stable in the sense of Liapunov if 5A + B < 3.

REFERENCE

[1] V. V. Beletsky, About the relative motion of two connected bodies in orbit, Kosmicheskiye Isseldovania,vol.7, No. 6 (1969),827-840(Russian)

[2] R. B. Singh, The three dimensional motion of two connected bodies in an elliptical orbit, Bulletin of Moscow state university, Mathematic-Mechanics. No.4, 59-64, 1973(Russian)

[3] B. Sharma, The motion of a system of two cable - connected satellites in the atmosphere, Ph.D. Thesis submitted to B.U. Muzaffarpur. (1974).

[4] S. K. Das, and P. K .Bhattacharya, Effect of magnetic force on the motion of a system of two cable connected satellites in orbit, Proc. Nat. Acad. Sci. India. (1976), 287-299

[5] C. P Singh, Motion and stability of inter-connected satellites system in the gravitational field of oblate earth. Ph.D. Thesis submitted to B.U. Muzaffarpur (1983)

[6] V. Kumar and N. Kumari, Stability of Equilibrium point of the centre of mass of an extensible cable connected satellites system in case of circular orbit in three dimensional, IJSER,Vol-4,Issue 9, (2013),1802-1808

Characterization, Classification and Standardization of Fly Ash of Kosovo Lignite-Fired Power Stations as Industrial Construction Product

Mevlan Qafleshi[1], Lulezime Aliko[2]

[1] *Faculty of Mathematical Engineering and Physical Engineering, Polytechnic University of Tirana, Tirana, Albania*
[2] *Faculty of Mathematical Engineering and Physical Engineering, Polytechnic University of Tirana, Tirana, Albania*

ABSTRACT**:** *Kosovo generates around 6000 GWh of electrical energy annually. Over 97% of this is produced by lignite-fired power-plants and less than 3% by hydro-plants. The lignite combustion, around 8 Mt/a, besides the emission of gases, produces a residue ash, fly ash and bottom ash. Since the first operation of power-plants in 1962 up to now, this ash was removed and stockpiled as a waste without utilization, which presents a great threat as pollutant for people and environment. It is a fact that many countries utilize their fly ash as cement substitute in concrete production and/or as additive in concrete for achieving specific properties in construction sector; as fill material in road construction; industry as filler etc. But in Kosovo, the Fly ash is literally only a waste. In the world, the cement is the second most consumed substance after water, and its production emits around 5% of CO_2 globally; from 900 kgCO_2/t- 935 kgCO_2/t of cement. The results show that for 1kg of cement substituted by 1kg fly ash, we will have 1kg less CO_2 in atmosphere, i.e. less green house gases, less global warming. The core part of this paper is to classify the Kosovo fly ash based on its chemical and mineralogical analyzes, and standardize this waste to an industrial product conform international standards, specifically European and American standards. If we standardize this waste to a construction product, then the utilization of Fly ash from Kosovo TPP would be of a great importance environmentally and economically.*

Keywords: *Kosovo, fly ash, characterization, classification, standardization*

I. INTRODUCTION

In Kosovo the first lignite-fired power plant unit Kosova A1 started operating in 1962 and all over the years other units A2, A3, A4, A5, and B1 and B2. These units combusting lignite as fuel generate up to 97% of electrical energy in Kosovo. This is a significant indicator that Kosovo is profoundly dependent from the energy produced by thermal power plants (TPP) since the contribution of electricity produced by hydro-power plants (HPP) is very of low with a participation of less than 3%. The orientation of Kosovo for a sustainable energy production by TPP is based on the fact that Kosovo possesses huge lignite reserves around 14 bt [1], the third place in Europe after Germany and Poland. This abundance of Kosovo with lignite as fuel has made the Kosovo Government to plan the construction of one other TPP unit “The New Kosovo”, with anticipated installed capacity 1000 MW in the first phase, and with another 1000 MW in the second phase [2].This unit of New Kosovo is anticipated to be operational in 2016. Since the first operation of TPP units in 1962 till 2012, the energy production of all units sums 158,829,841 MWh [3]. This energy production annually consumes around 7-8 Mt lignite [4]. In other terms, for the production of 1 MWh of electrical energy approximately 1.4 t of lignite is consumed as fuel, i.e. 1.4t/MWh for Kosovo B units and 1.8t/MWh for Kosova A units.[3][5].

The burning process of lignite besides the emission of gases generates an amount of ash as combustion byproduct. Around 80% of this ash flies with flue gases and before exiting the stack gets captured by Electrostatic Precipitators-ESP (or electro-filters) in the form of Fly Ash. 20% of ash falls down as bottom ash. Both ashes are waste and for decades have been transported and dumped to the stockpiles; they have not been utilized at all. From the analyses of Kosovo lignite, the content of ash in lignite is around 14-17% by mass [6]. This indicates that from burning of 1ton lignite the residue ash is around 160 kg. A calculation shows that up to 2012, in Kosovo there are around 27 Mt of unutilized fly ash. Only in 2012 the lignite combustion in TPP produced around 1 Mt of fly ash. The aim of this paper is to characterize, based on its chemical and mineralogical composition, and standardize this unutilized fly ash to an industrial beneficial product and produce with it environmentally friendly concrete-green concrete.

II. ELECTRICITY GENERATION IN KOSOVO

Basically Kosovo’s power demand is supplied by thermal power plants (TPP) combusting lignite as fuel and a small amount is a contribution from hydro-power plants (HPP). In terms of percentage 97% of electricity is provided by Kosovo Energy Corporation KEK (in Albanian: Korportata Energjetike e Kosovës), which is a public owned enterprise situated in the central part of Kosovo, and the 3% is supplied by low capacity HPP in different regions. [4].
Table I. Energy production by Kosovo TPP and HPP in a period from 2002-2012 [5][3]

	Energy produced by TPP		Energy produced by HPP		TPP+HPP GWh
	GWh	%	GWh	%	
2002	3151.7	97.52	80	2.48	3231.7
2003	3221.1	98.44	51	1.56	3272.1
2004	3481.1	96.88	112	3.12	3593.1
2005	3999.5	97.32	110	2.68	4109.5
2006	3970.5	97.54	100	2.46	4070.5
2007	4309.5	97.88	93.2	2.12	4402.7
2008	4505.8	98.35	75.7	1.65	4581.5
2009	5260.0	98.34	88.7	1.66	5348.7
2010	5481.0	97.94	115.5	2.06	5596.5
2011	5696.4	98.69	75.4	1.31	5771.8
2012	5847.2	98.90	65.0	1.10	5912.2

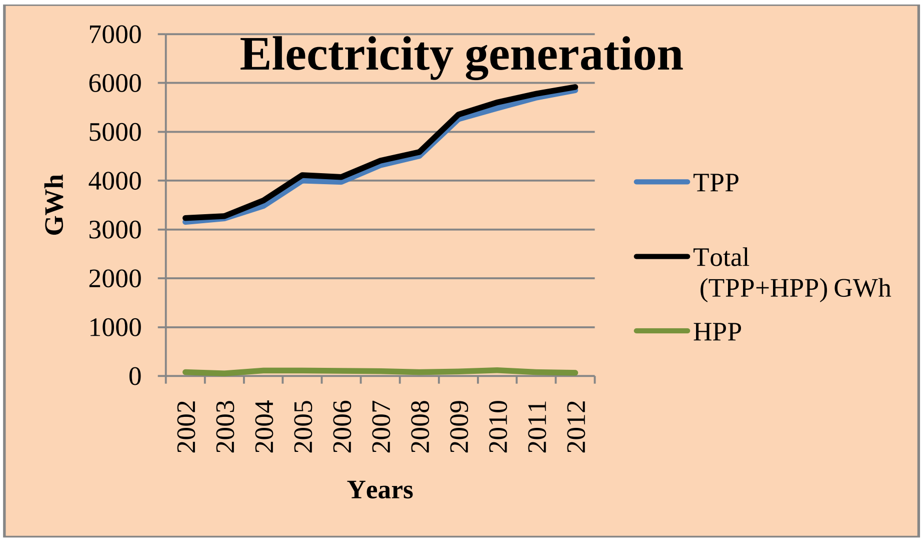

Figure1: Electricity generation from TPP and HPP in Kosovo

From the Table I and the Fig. 1 it can be seen that, for a decade, 97.98 % of electrical energy is produced by TPP and only 2.02 % is the contribution of HPP. This low electrical generation from HPP dictates the prospect of Kosovo energy to be basically oriented towards a sustainable generation from TPP.

As it is shown in Table I, the greater quantity of electrical energy in Kosovo is produced by Thermo Power Plants-lignite-fired power plants. The construction of KEK units was done over the period since 1962 till 1984. The Kosovo Energy Corporation-KEK consists of two thermal power plants Kosova A with five Units: A1, A2, A3, A4, A5 and Kosova B with two generating units: B1 and B2.

The overall installed power capacity of TPP Kosova A and B is 1478 MW and for each generating unit is given in the table below

Table II. Overview of installed capacity of Kosova (A+B) TPP [7]

TPP	**Unit**	**Commission year**	**Installed capacity MW**	**Available capacity**		**Technical minimum load MW**	
				Generator	Entry	Generator	Entry
Kosova A	A1	1962	65	0	0	0	0
	A2	1965	125	0	0	0	0
	A3	1970	200	135	110	110	100
	A4	1971	200	135	110	110	100
	A5	1975	210	135	110	100	97
Total Kosova A			800	405	330	320	297
Kosova B	B1	1983	339	290	265	200	182
	B2	1984	339	280	265	200	182
Total Kosova B			678	570	530	400	364

Since the capacity of HPP is very low, only 52.15 MW**,** in regard to the requirements in Kosovo, the electricity production generally is covered by KEK TPPs. The energy which is converted in thermo power plants to electrical energy is the energy of lignite with which Kosovo is abundant, thus lignite represents an outstanding source for energy generation in Kosovo and will remain as principal fuel for electricity generation in the long term future.

III. LIGNITE OF KOSOVO

With 14,700 Mt, Kosovo possesses the world's fifth-largest proven reserves of lignite. Lignite deposits of Kosovo are distributed across Kosova (here Kosova as a region within the Republic of Kosovo), Dukagjini and Drenica Basins. The Kosovo lignite open-cast mines are operated as one as most favorable lignite deposits in Europe due to its geological condition. The average stripping ratio for 1 ton of coal is 1.7 m^3 of top soil overburden, and the average deposits thickness of 40 m. With an average of net calorific value (NCV) of 7.8 MJ/kg, lignite of Kosovo is considered of high quality for exploitation and utilization for electricity generation. These parameters of lignite make the generation of electricity to be of a low cost comparing to the countries in region [1].

A study "Energy Strategy and Policy of Kosovo", by EU Pillar, PISG Energy Office, ranks Kosovo as third in Europe with 10000 Mt economically exploitable resource of lignite. Thus Kosovo represents one of the richest sources of lignite in Europe. In the Table IV below it is shown the ranking of some European countries based on lignite exploitable resources.

Table IV: Exploitable lignite reserves in European countries in Bt [6]

Country	**Germany**	**Poland**	**Kosovo**	**Hungary**	**Turkey**	**Greece**	**Czech R.**	**Romania**	**Bulgaria**	**Macedonia**	**Slovakia**	**BiH**	**Slovenia**	**Spain**
Bt	42.8	14.0	10.0	7.8	5.9	4.2	3.5	3.0	2.5	1.7	0.38	0.31	0.15	0.04

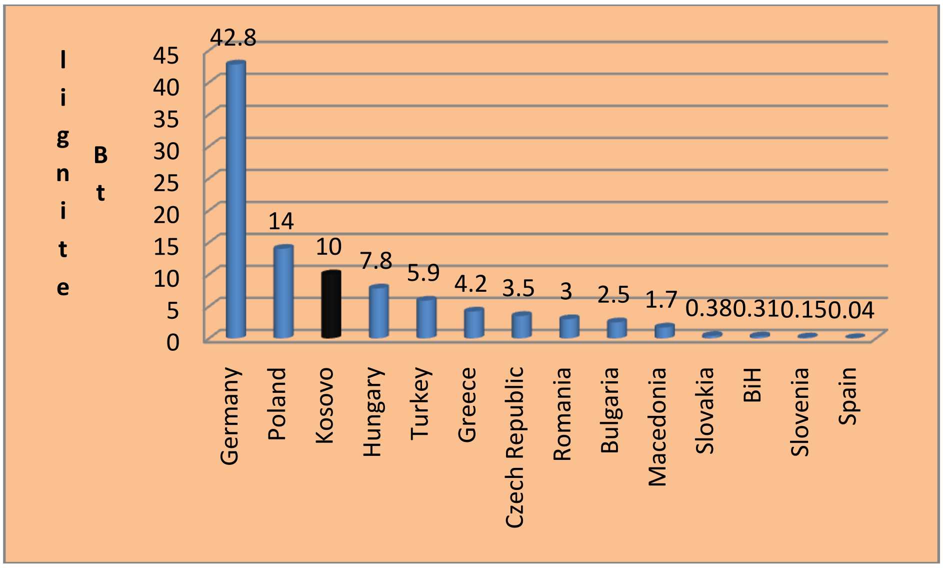

Figure 2: Lignite reserves of Kosovo comparing to European countries

Annually the lignite consumption from TPP Kosova A and TPP Kosova B is 7-8 Mt/a. The Table V below shows the annual lignite consumption for a period from 2002 to 2012.

Table V: The overall lignite consumption in TPP Kosova A and Kosova B [3][5].

	Year	2002	2003	2004	2005	2006	2007	2008	2009	2010	2011	2012
Lignite consumption	**Mt**	5.23	5.64	5.59	6.27	6.35	7.11	7.46	8.41	9.34	9.11	9.35

Note: The calculations for 2009, 2010, 2011 and 2012 are done from specific average of coal consumption for Kosova A 1.83 t/MWh, and Kosova B 1.4t/MWh , taking the specific average for both Kosova A and Kosovo B as 1.6 t/MWh.

In the Table VI there are presented some parameters and characteristic to feature the lignite as the main fuel used in the process of generation of electricity in Kosovo TPP

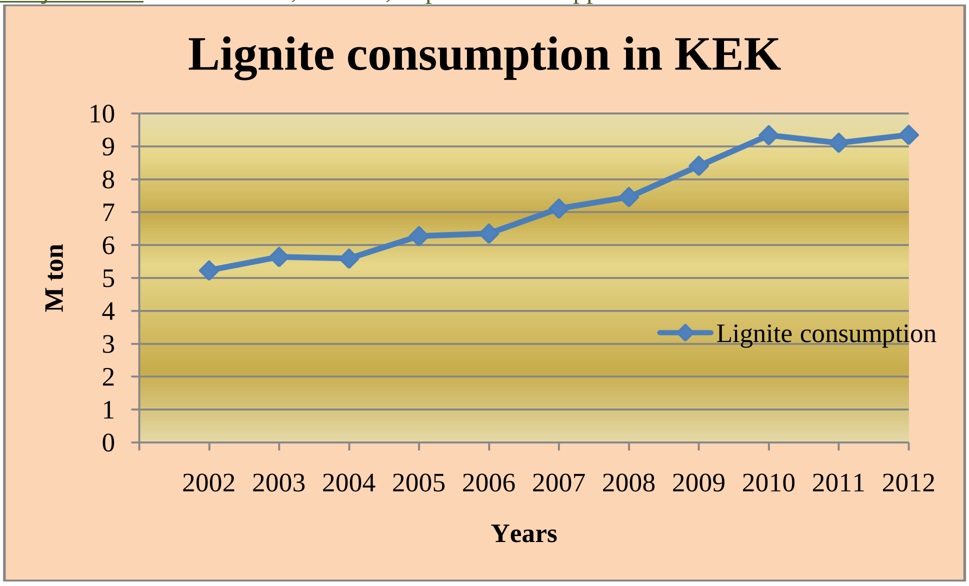

Figure 3: Total Lignite consumption in TPP Kosova A and Kosova B

Table VI: Kosovo lignite quality and parameters [6]

Ash content	12-21%. The average values 14-17%		
Moisture content	35-50%		
Heating values	Bardh -Mirash	7800 KJ/kg	
	Sibovc	8100 KJ/kg	
	Total reserves	29%	> 8.4 MJ/kg
		43%	7.7-8.4 MJ/kg
		25%	5.8-7.7 MJ/kg
Sulfur content	1 %. In all deposits/mines. The average content of combustible sulfur is 0.35%		
Lime	The concentration of lime is sufficient to absorb the SO_x gas emitted during combustion- no need for desulfurization of flue gases		

IV. FLY ASH AS LIGNITE COMBUSTION BYPRODUCT AT TPP KOSOVA A AND KOSOVA B

Lignite, after extraction from the deposits, is transported through a system of conveyers to the TPP. There it undergoes a drying process; grinding-pulverization up to baking flour sized particles and sprayed to the combustion chamber of the TPP. The pulverized lignite combustion process heats up the water steam that is beneficial for pressure steam turbine rotation and finally the generation of electrical energy in generators, which are connected to the transmission system. This is advantage and benefit of usage of lignite.

The combustion process is associated, apart from energy release, with the emission of some other combustion byproducts:

- gaseous products: carbon dioxide (CO_2), sulfur oxides (SO_X), nitrogen oxides (NO_X),
- lignite ash (particulate matter-PM): fly ash, bottom ash

The aim of this study is lignite ash that is a mineral residue from the combustion process of lignite in Kosova TPPs. The coal ash from lignite fired power plants depends from the ash content of lignite and boiler operation. The emission of PM for the coal with high ash content depends more on the coal ash than combustion efficiency [8], whilst the coal, lignite in this case, with low ash content depends more on the combustion efficiency.

Bottom ash, which represents 10-15% [9] of the overall coal ash, is a coarse granular ash almost sand like material. It is the noncombustible residue of lignite combustion. It is called bottom ash because during the high temperature combustion, some of the ash melts and accumulates on the boilers walls and steam tubes and then it is collected from the bottom of the boiler where the combustion takes place.

Fly ash is also a noncombustible residue from the combustion of lignite in the TPP. It is the finest of coal ash particles which constitutes 85-90% of the overall ash. [9]

The control of dust (PM) in most lignite fired TPP is done through Electrostatic precipitators (ESP). The designed efficiency of ESP in TPP B is 99.14 %, for TPP 98% [10]. The fly ash is carried together with other flue gases (this why it is called "**fly**") and before exiting the stack it is collected by ESP.

Fly ash features cementitious (property of a material to harden when mixed with water) and pozzolanic (the property of material that in the presence water reacts with calcium hydroxide at ordinary temperatures to form compounds possessing cementitious properties. The definition of fly ash in EN 450-1[11], which is the European standard for Fly ash in Concrete, is:

"Fine powder of manly spherical, glassy particles derived from burning of pulverized coal, with or without co-combustion materials, which has pozzolanic properties and consists essentially of SiO_2 and Al_2O_3" [11].
The properties of fly ash resulting from its chemical composition and reaction make it of a great use either in concrete production as cement substitute or aggregate.
As it is known that in the world, the cement is the second most consumed substance after water [12][13], and during the cement production a great quantity of CO_2 is emitted, approximately from 900 kgCO2/t- 935 kgCO2/t of cement. This means that for 1kg of cement replaced by 1kg Fly ash, we have 1kg less CO2 released in our air we breath, i.e. less green house gas, less global warming [14].
Many countries in the world utilize Fly ash (and bottom ash as aggregate substitute) as cement replacement in concrete production and as additive in concrete to archive specific properties in construction sector; as fill material in road construction; industry as filler in plastic, paint sealing material etc. But in Kosovo, the Fly ash is literally only a waste with health and environmental consequences.
The core part of this paper is to classify and standardize this waste to a product conform other international recognized standards, specifically European and American standards. If we standardize this waste to a construction product, then the utilization of Fly ash from KEK TPP would be of a great importance, economically and environmentally, for Kosovo industry and environment. Up to now, there is no evidence of its utilization in Kosovo, i.e. our Fly ash is only a threatening waste that waits for exploitation.

V. FLY ASH OF KOSOVA B TPP

Fly ash as a residue of combustion of lignite for generating electrical energy comprises of fine particles that rise with flue gases, but these particle (Particulate matter) before exiting the stack get captured by ESP or electro-filters, and then can be carried to storage or silos. In Kosovo none of these, the fly ash is stockpiled ore better said dumped.

The sample for analyses are taken from Kosovo B TPP and the chemical, physical and mineralogical analyses were conducted at laboratory **ZAG, Department of materials, Laboratory for cement, mortar and ceramics, Lubljana, Slovenia**. The analyses were conducted in conformity with European Standards SIST EN 450-1:2005 5.2 and 5.3 [11].

Conform EN 450-1 the fly ash is defined as Fine powder of mainly spherical, glassy particles derived from burning of pulverized coal, with or without co-combustion material, which has pozzolanic properties and consists essentially of SIO_2 and Al_2O_3.

According to ASTM C618 12a [15], Standard chemical requirements there are two classes of fly ash determined by the content by mass of lime:

- Class F: lime (CaO) content less than 20% by mass
- Class C: lime (CaO) content more than 20% by mass

5.1. Chemical composition of Kosovo Fly Ash

Table VII: Chemical composition of TPP Kosova B Fly Ash.

Constituent	% by mass	Requirements of SIST EN 450-1 cl.5.2	Test method
Loss on ignition	**2.09**	≤5.0%, A category	SIST EN 196-2 cl. 7
SiO_2 total	**29.7**	≥75%*	SIST EN 196-2 cl.13.6
SiO_2soluble	**0.27**		SIST EN 196-2 cl. 13.8
Al_2O_3	**10.65**		SIST EN 196-2 cl.13.11
Fe_2O_3	**6.18**		SIST EN 196-2 cl. 13.10
CaO	**32.92**	-	SIST EN 197-1 cl.3.1
MgO	**5.93**	≤4.0%	SIST EN 196-2 cl. 13.13
SO_3	**9.98**	≤3.0%	SIST EN 196-2 cl. 8
Na_2O	**0.74**	-	SIST EN 196-2 cl. 17
K_2O	**0.61**	-	SIST EN 196-2 cl. 17
Na_2O equivalent	**1.14**	≤5.0%	Calculated
Insoluble residue	**5.65**	-	SIST EN 196-2 cl. 10
CaO free	**6.49**	≤1.5%**	SIST EN 451-1
CaO reactive	**24.62**	≤10.0 %	
SiO_2 reactive	**26.30**		SIST EN 197-1 cl. 3.2
Cl^-	**0.019**	≤0.10 %	SIST EN 196-2 cl. 14
P_2O_5 soluble, mg/kg	**0.00**	≤0.100 mg/kg	
Added ml NaOH (1 mol/l)	**0.00**	-	SIST EN 450-1, Annex C

*for Siliceous fly ash (Class F), 50% for Calcareous fly ash class C
**≤1.5% with the SIST EN 450-1 New this is changed from ≤1.0% to 1.5% [24].

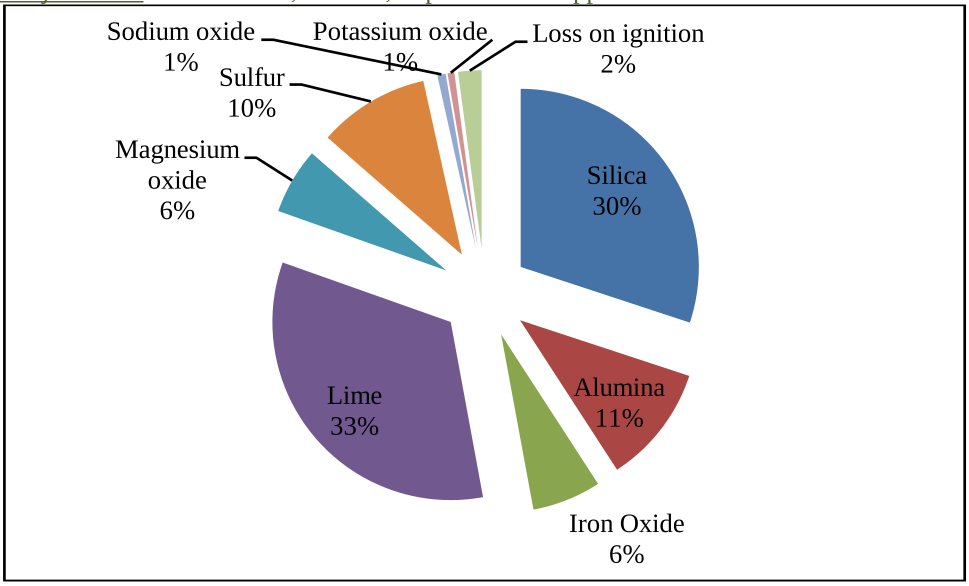

Figure 4: Chemical composition in %/weight of Kosovo Fly Ash

VI. CLASSIFICATION OF KOSOVO B TPP FLY ASH

Fly ash produced from the combustion of lignite generally is composed of silica, alumina, small quantities of oxides of magnesium, iron, calcium and some other elements. The percentage of its constituents depends. The general classification of Fly ash is done by the percentage content of CaO, which depends on the type of the fuel. This fly ash that is produced from burning lignite showed to have 32.92 % CaO (testing method SIST EN 197-1, clause 3.1) and conform this percentage value, the Kosovo B TPP Fly ash belongs to Class C**.** Class C Fly ash in addition of pozzolanic properties has also cementitious properties.

Cementitious property is the property of a material (in this case fly ash) that in the presence of water to harden, whilst the pozzolanic property is the property that in the presence of water and other activating agent (cement, quicklime, or hydrated lime) to react chemically and have cementitious properties.

These properties make Kosovo Fly ash very useful for utilization as substitute of cement in concrete production industry.

Note: the other Class F of Fly ash has less then 10% CaO and has only pozzolanic properties. This is produced when other types of fuel are burned.

VII. CHARACTERIZATION AND STANDARDIZATION OF FLY ASH OF TPP KOSOVA B

7.1. Loss on Ignition 2.09%

Loss on ignition indicates the content of unburned carbon in fly ash. This property of fly ash is very important because the carbon content has a significant influence on the effect of air-entraining admixtures that are used for the improvement of concrete to the freezing and thawing. Generally portland cement concrete has less than 3% entrapped air. The presence of fly ash in concrete lowers the content of air by 05.-1 % [16].

Carbon absorbs the air-entraining admixture, resulting with lower entrapped air in concrete, which directly affects the resistance to free-thaw cycles.

The SIST EN 450-1 cl.5.2 requirement is ≤5.0%, and the Loss on ignition determined conform SIST EN 196-2 cl. 7 of Kosovo fly ash is 2.09 that is absolutely compatible with European standard and American standard ASTM C618.

7.2. Calcium Oxide (CaO)

7.2.1. Total calcium oxide 33 %

From the analyses shown in the table and graph, the Kosovo Fly ash has high lime content (33%), which under the specification of American Standard ASTM **C618** this is greater than 20% by mass and is classified as calcareous fly ash-Class C. This lime content makes the Kosovo fly both pozzolanic and cementitious, and presents hydraulic properties [17].

7.2.2. Free calcium oxide 6.49 %

This is determined in conformity by the method prescribed by European Standard **SIST EN 451-1[**11], as stipulated in **EN 197-1:2000, cl. 3.1[**18]. The test result for Kosovo Fly ash is 6.49 % by mass. Here the test result shows a fluctuation of the result from the standard **SIST EN 450-1 cl.5.2.**requirement value of ≤1.0%. This implies that fly ash shall be tested for conformity to the requirements for soundness in 5.3.3 of the standard [11].

7.2.3. Reactive calcium oxide 24.62 %

This is determined conform **EN 197-1:200, Cl. 3.1,** which limits this not to exceed 10% by mass. This is greater than the standard requirement. This also implies that the fly ash should be tested for conformity, to the requirements for soundness in 5.3.3.

In our case the fly ash is Class C, i.e. calcareous fly ash, and the sum of silica, alumina and ferric oxide is almost 50%, the content of reactive calcium oxide should no be expected to be less than 10% [19].

7.3. Total content of Silica (SiO2), Alumina (Al2O3) and Iron oxide (Fe2O3) 46.53%

The sum of these oxides expressed as percentage by mass of fly ash has been determined conform SIST EN 196-2 cl.13.6, SIST EN 196-2 cl.13.11 and SIST EN 196-2 cl. 13.10 respectively. The requirement of SIST EN 450-1 cl.5.2 for the sum of all above three constituents of Fly ash is to be greater than 75%. But, in accordance with ASTM C618, for Class C fly ash, this sum shall be equal or greater than 50% by mass. This indicates that ASTM C618 for the content of three oxides requires the value of 70% for Class F of Fly ash. According to ASTM C618, Kosovo Fly ash is almost compatible with the standard's requirements. The Indian Standard, Bureau of Indian Standard (BIS), IS: 3812 part-1 2003 requires this value to be 50% too.

7.4. Reactive silicon dioxide 26.30%

Reactive silica is the key parameter for determining the pozzolanic ability of fly ash. This is the property that flies ash tends to react with available calcium hydroxide to form hydration products with binding properties [20].

According to EN 450-1+A1:2007, and the new revised EN 450-1: New, the content of reactive silica as described in SIST EN 197-1 cl. 3.2 must no be lees than 25 % by mass. The content of reactive silica of Kosovo Fly ash (26.30 %) is in compliance with this standard.

7.5. Alkalis content Na_2O-0.74%, K_2O-0.61%, Na_2O equivalent -1.14%

The present alkalis in fly ash (concrete) react with free silica of the aggregate and the result is the formation of alkali silica gel with properties of capturing the water and causing local expansion of concrete. This expansion causes the deterioration-cracking of concrete.

The alkalis content has been determined conform SIST EN 196-2 cl. 17 and calculated as Na_2O (equivalent). The requirement of SIST EN 450-1 cl.5.2 is less than 5%, and Kosovo fly ash is absolutely compatible with EN 450-1:2005+A1:2007.

7.6. Magnesium oxide 5.93%

The content of MgO has been determined in accordance with SIST EN 196-2 cl. 13.13 and the requirement of SIST EN 450-1 cl.5.2 is ≤4.0%. The Kosovo fly ash has a slight higher content of MgO, i.e. a little fluctuation from the European standard requirement. This excessive content of magnesium oxide may have some deleterious effect; can cause expansion of concrete. But for Class C fly ash this value is almost within the limits. In some countries this limit is up to 5% [21]. The testing method of ASTM C151-74 for detecting unsoundness caused by CaO and MgO, shows that the expansion of concrete affected by the presence of these two oxides is smaller than the actual expansion that can occur under field conditions [22].

7.7. Sulfur Trioxide (SO3) 9.98%

The requirement SIST EN 450-1 cl.5.2 for SO_3 in fly ash is less than 3%, which represents a high fluctuation. But, ASTM C 618 for both Class C and F limits this to 5% maximum. It is known that fly ash inhibits the ASR, and the content of SO_3 is known to be one of the factors of this inhibition. So, care must be taken for this value when fly ash with this content of SO_3 is used in concrete production as hydraulic material or blended cement [23].

7.8. Soluble phosphate (P2O5) 0.00%

The requirement of **SIST EN** 450-1 cl.5.2 for soluble phosphorous pentoxide in fly ash is 100 mg/kg, and Kosovo fly ash is fully compatible with European Standard.

The text of EN 450-1: New reads:

"The content of total phosphate (P_2O_5) shall be determined in accordance with EN 196-2 and shall not be grater than 5.0% by mass. Fly ash obtained from combustion of pulverized coal only shall be deemed to satisfy this requirement". Although there is no known effect of phosphate in concrete performance, it is stated that fly ash may contain up to 5% by mass of P_2O_5 [24].

7.9. Chloride (expressed as Cl^-) 0.019%

The content of chloride has been determined in accordance with SIST EN 196-2 cl. 14 and the obtained value of 0.019 % is lower than 0.10 % by mass, which in fact is the requirement of SIST EN 450-1 cl.5.2. Thus Kosovo fly ash with this content of chlorides is suitable for use in cement-concrete industry.

VII. CONCLUSIONS

Kosovo electrical energy is basically generated by TPP. This process produces a huge quantity of unprocessed waste-fly ash which has a very deleterious impact in environment especially in the central Kosovo where the TPPs are situated. The fly ash, since the beginning of TPP operation has been not utilized at all. Thus, due to its huge quantity produced every year it represents not only a waste that should be stockpiled it also represents an industrial pollutant of environment that must be considered seriously.

By this study, through the chemical analyzes this waste-fly ash can be turned to be a construction-industrial product either as direct substituent of cement in concrete industry or as admixture in concrete. The basics of Kosovo Fly ash, its chemical and mineralogical composition generally prove to be suitable for utilization in concrete industry. The composition of Kosovo Fly ash in many aspects is compatible with two basic standards referred in this paper: European Standard EN 450-1 and American Standard ASTM C 618 for use of fly ash in concrete.

The percentage by mass of three oxides SiO_2, Al_2O_3 and Fe_2O_3 according to standards classify Kosovo fly ash in the category of high lime content, which in terms of classification belongs to Class C fly ash. This class C fly ash is calcareous fly ash. The carbon content expressed as LOI, is one of the most important factor for the utilization of fly ash in concrete industry since the carbon content of fly ash affects many properties of concrete, and Kosovo fly ash meets the chemical requirements of standards regarding the LOI, i.e. carbon content.

The content of CaO, MgO and SO_3 represent some fluctuations from standards requirements. This excessive content of these three components may have some undesired effects in concrete-unsoundness. By considering this and testing the concrete for soundness, concrete produced with a specific percentage of fly ash as cement substituent, can make fly ash utilizable as construction material. The alkalis content of Kosovo fly ash is in complete accordance with the standards requirements showing that Kosovo fly ash represents no threat to possible alkali silica reaction that could cause cracking of concrete, i.e. unsoundness of concrete. Also, the chloride content that can affect the PH of concrete is in full accordance with requirements of standards that depict requirements of utilization of fly ash in cement-concrete industry.

This in-depth chemical analyze, compared to the requirements of standards, prove that Kosovo Fly ash could not be a threatening waste to Kosovo environment, but it can be very useful for utilization as cement substituent in certain percentage for producing concrete, or as concrete admixture. Finally, the Kosovo fly ash with these chemical properties can be used as cement substituent in concrete production industry.

ACKNOWLEDGEMENTS

The authors would like to thank the managers of laboratory IPE ProIng, Prishtina, Kosovo for their support.

REFERENCES

[1] Independent Commission for Mines and Minerals, R. of Kosovo, http://www.kosovo-mining.org/ kosovoweb/ en/mining.html.
[2] V. Sofiu, A. Pervizaj, B.Selimi, E. Erxhepi, The Strategy of energy as a good opportunity for protection of the environment in the republic of Kosovo, *International Journal of Modern Engineering Research*, *3(5*), 2013, 2591-2599.
[3] Kosovo Energy Corporation, KEK statistical data, Strategic development office.
[4] The Government of Kosovo, Ministry of Energy and Mines of Kosovo.
[5] Kosovo Agency of Statistics, Energy Balance in Kosovo Q4 2012, Kosovo, 2013.
[6] Energy Strategy and Policy of Kosovo, EU Pillar, PISG Energy Office.
[7] Republic of Kosovo, Ministry of Economic Development, Annual Energy balance of R of Kosovo for the year 2013, 2013.
[8] S. Isufi, *Emission Controls at Kosovo's Thermal Power Plants, Current and Future Capabilities*, AUK, Pristina, 2010.
[9] P. Sahu, *Characterization of coal combustion byproducts (CCBs) for their effective management and utilization, department of mining engineering*, National Institute of technology, Orissa, 2010.
[10] B. Gjurgjeala, *Efficiency of TPP* (Prishtina, 2007).
[11] European standard for fly ash in concrete 450-1, 2007.
[12] World Business Council for Sustainable development (WBCSD), Cement technology roadmap, 2009
[13] UNEP, Greening cement production. United Nations Environment Programme, Carbon emissions reductions up to 2050, 2009 P.2.
[14] IPCC, CO_2 Emission Trends in the Cement Industry: An International Comparison, 2002, Kim and Worell, Mitigation and adaptation strategies for global change, &: 115-133.p.120. 2007.
[15] ASTM, American Society for Testing and Materials, Standard Specification for Coal Fly Ash and Raw or Calcined Natural Pozzolan for Use in Concrete.
[16] R.O. Lane, J.F. Best, Properties and use of fly ash in portland cement concrete, *Concrete International 4(7*), 1981, 81-92.
[17] N. K. Koukouzas, C. Vassilatos, I. Glarakis, *Mixture of Lignite Fly ash in Concrete: Physical and Mineralogical characterization*, Case Study from Ptolemais, Northern Greece , *American Coal Association*, 2005.
[18] European standard for Cement EN 197-1:2000**.**
[19] NTPC Limited, *Fly ash for cement Concrete, Resource for high strength and durability of structures at lower cost*, Ash utilization division, India, 2010.
[20] S.K. Antiohos, T. Tsimas, *Reactive silica of fly ash as an indicator for the mechanical performance of blended cements*, Athens, Greece.
[21] V.M Malhotra, A.A. Ramezanianpour, *Fly Ash in Concrete*, MSL 94-45(IR), CANMET, Canada Center for Mineral and Energy Technology, Natural Resources Canada, Ottawa, Ontario, Canada, (1994), 307 pp.
[22] J.L. Alonso, K. Wesche, *Characterization of fly ash- Fly ash in concrete, properties and performance* (Champan & Hall, London, 2005).
[23] P. Klieger, S. Gebler, *Fly Ash and Concrete Durability, Concrete Durability*: Katharine and Bryant Mather International Conference, SP100-56, J.M. Scanlon, ed., American Concrete Institute, Detroit, MI, (1987), pp. 1043-1069.
[24] Fly ash for concrete the new EN 450, background to the revision of EN 450-1 and EN 450-2, EUROCOALASH, Copenhagen, 2010.

International Journal of Modern Engineering Research (IJMER)
www.ijmer.com Vol. 3, Issue. 5, Sep - Oct. 2013 pp-3071-3078 ISSN: 2249-6645

Anartificial Neural Network for Prediction of Seismic Behavior in RC Buildings with and Without Infill Walls

Mohammad ParsaeiMaram, [1]Dr. K Rama Mohan Rao[2], Ali Poursalehi[3]
[1]Master of Technology in Structural EngineeringDepartment of Civil Engineering, Jawaharlal NehruTechnological University, Hyderabad– 500085, India
[2]Professor & Director. BICSDepartment of Civil Engineering, Jawaharlal NehruTechnological University, Hyderabad–500085, India
[3]Master of Computer ScienceDepartment of Mathematics, Osmania University, Hyderabad, India

ABSTRAC:*In this study the influence of masonry infill walls on the seismicbehavior of RC frames with help of ETABS software were studied.Pushover analysis on buildings with five, seven, nine and eleven storey with symmetrical in the plan was carried out.And trial model with thirteenstorey was created for testing in ArtificialNeural Network (ANN).Each structure was modeled in two different types, such as RC bare frame and RC frame with masonry infill walls.In the present paper infill walls are modeled as equivalent diagonal strut. In this type of molding infill wall behaves like compression strut, as suggested in FEMA 365, 2000.*

Nonlinear analysis in according with IS1893, 2002 code is realized to sketch pushover curves and results at Immediate Occupancy, Life Safety and Collapse Prevention onperformances level were determined.

Thisstudy reports seismic behavior of RC building due to increase height of the buildings.For this purpose, one of the significantly techniques, Artificial Neural Network(ANN), was used.Result of this study using ANNis used for prediction of seismicbehavior of structures.The trial model with thirteen storey was modeled by ETABS to compare with result of ANN.

KEY WORRDS:*Nonlinear analysis, Masonry infill, Equivalent diagonal strut, ArtificialNeural Networks.*

I. INTRODUCTION

Motivation of this study is assessment of vulnerability of the building with and without unreinforcedmasonry infill walls. And behavior of a thirteen storey building is predicted by Artificial Neural Network (ANN) technique.

ANN is a branch of artificial intelligence which attempt to mimic the behavior of the human brain and nerves system. A neural network can be considered as a black box that is able to predict an output pattern when it recognizes a given input pattern. Neural networks are able to detect similarities in input, even though a particular input may never have been seen previously. This property allows for excellent interpolation capabilities, especially when the input data is noisy[1].

It is estimate that, effect of infill walls is important on the building performance, but structural engineers, during the design process, ignore the effect of infill wall in the structural analysis. According to the FEMA guideline the masonry unreinforced infill walls have a significant effect on the stiffness of building [2].In this study advantages and disadvantages of infill walls will be investigated.

Masonry infill walls are frequently used as interior partitions and architectural elements.In the design and assessment of the building infill walls are usuallytreated as non-structural elements and the presence of infill walls are usually neglected in conventional design because they are assumed to be beneficial to the structural responses. Therefore, their influences on the structural response are generally ignored. However, their stiffness and strength are not negligible, and they will interact with the boundary frame when the structure is subjected to ground motion. This interaction may or may not be beneficial to the performance of the structure and it has been a topic of much debate in the last few decades. [3].

II. DESCRIPTION OF STRUCTURAL MODEL

2-1 Building Models

In this studysymmetrical floor plans layout of 3D reinforced concrete residential building with moment resisting RC frames was selected as shown in fig 1. Thebuildings consist of five, seven, nine and eleven, but the plan was unaltered to avoid any irregularity effects. Buildingsare located inseismic zone IV, and soil profile type was assumed to be medium.

Response reduction factor for the special moment resisting frame has taken as 5.All the four models are designed and analyzed as per IS456, 2000. Further inputs include unit weight of the concrete is 25 KN/m^3, elastic modulus of concrete is $25*10^6$ KN/m^2, compressive strength of concrete is 25 N/mm^2 (M25), yield strength of steel is 415 N/mm^2 (Fe 415),elastic modulus of steel is $2*10^8 KN/mm^2$. The loading of building was assumed to be dead load 5.5 KN/m^2, live load 2.0 KN/m^2, and weight of floor finishes is 1 KN/m^2. Percentage of imposed load to be considered in seismic weight calculation 25.The support condition of columns was assumed to be fixed at ground level. All columns and beams had different dimensions in height, dimension of columns vary between 0.40*0.40 m and 0.50*0.50 m , dimension of beam vary between 0.40*0.30 m and 0.30*0.30 m and thickness of slab is 0.15m. finally the example structure used in this study are following as shown in fig1 to 9.

1. Fivestorey with two models: - Model 1-0: Bare frame.
- Model 1-1: RC frame with brick masonry infill.
2. Sevenstorey with two models: - Model 2-0: Bare frame.
- Model 2-1: RC frame with brick masonry infill.

3. Ninestorey with two models:- Model 3-0: Bare frame.
- Model 3-1: RC frame with brick masonry infill.

4. elevenstorey with two models: - Model 4-0: Bare frame.
- Model 4-1: RC frame with brick masonry infill.

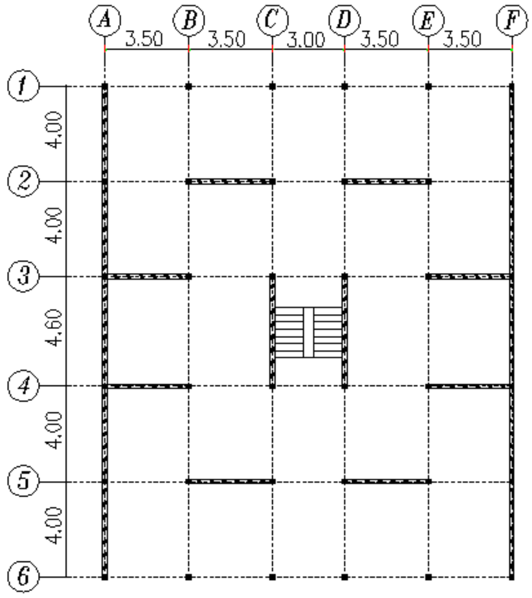

Fig 1: Typical plan of Buildings

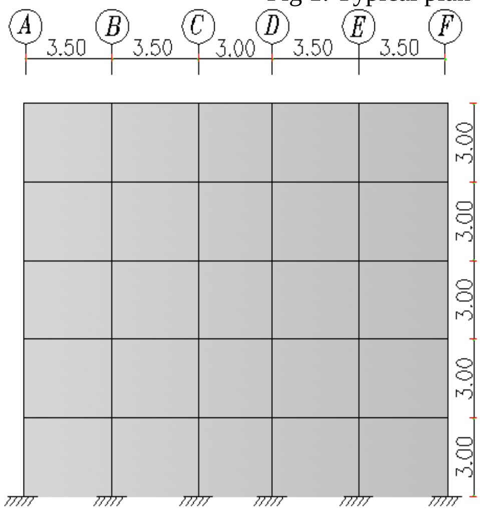

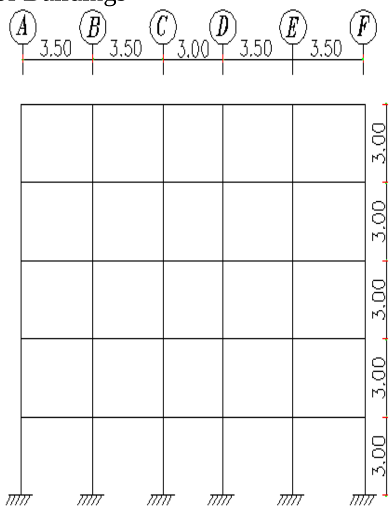

Fig2: Model 1-1Fig 3: Model 1-0

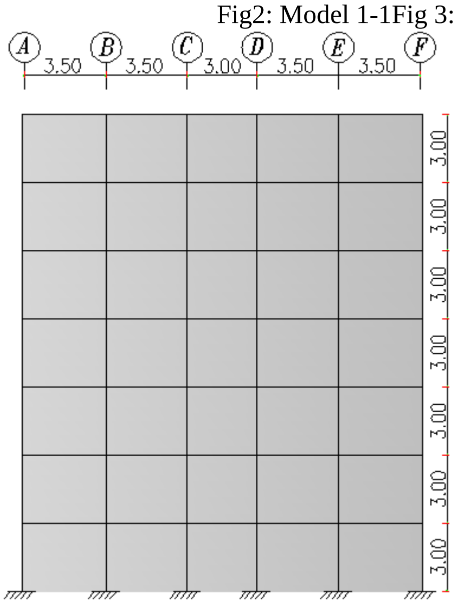

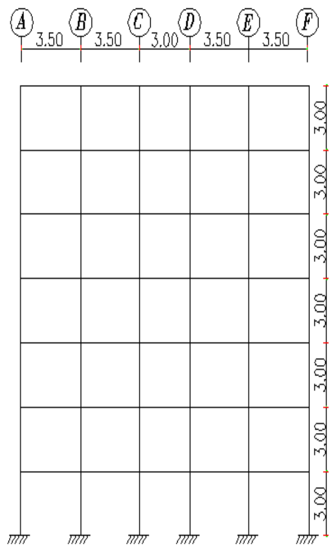

Fig 4: Model 2-1Fig5: Model 2-0

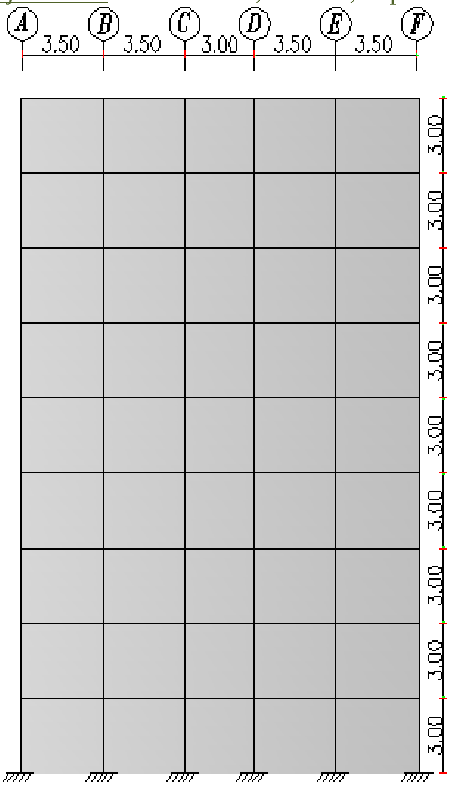

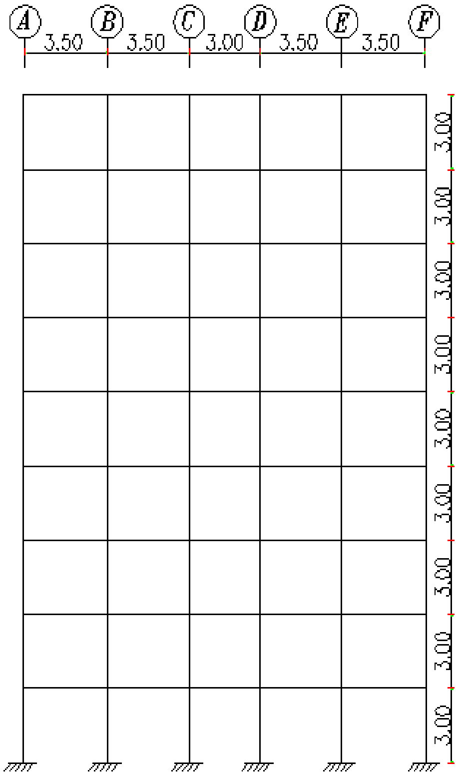

Fig 6: Model 3-1Fig 7: Model 3-0

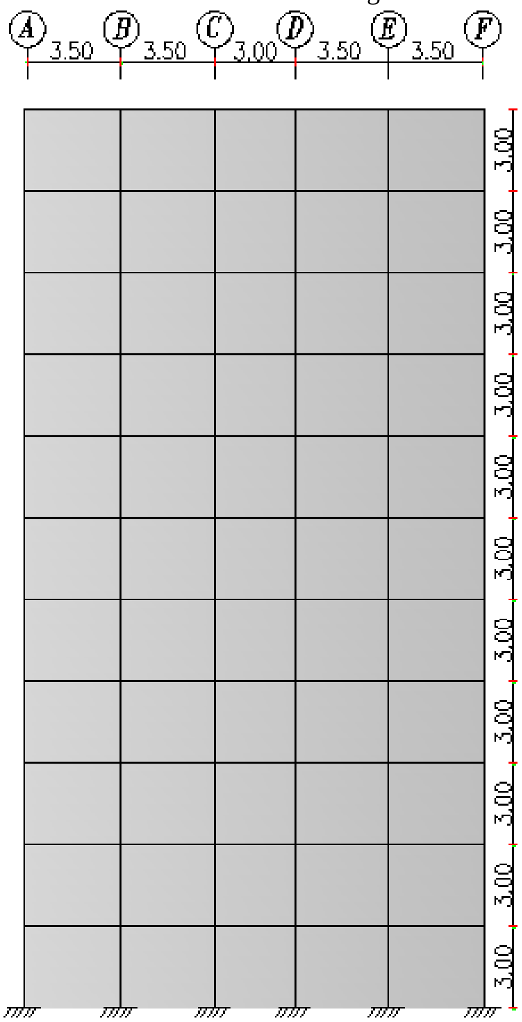

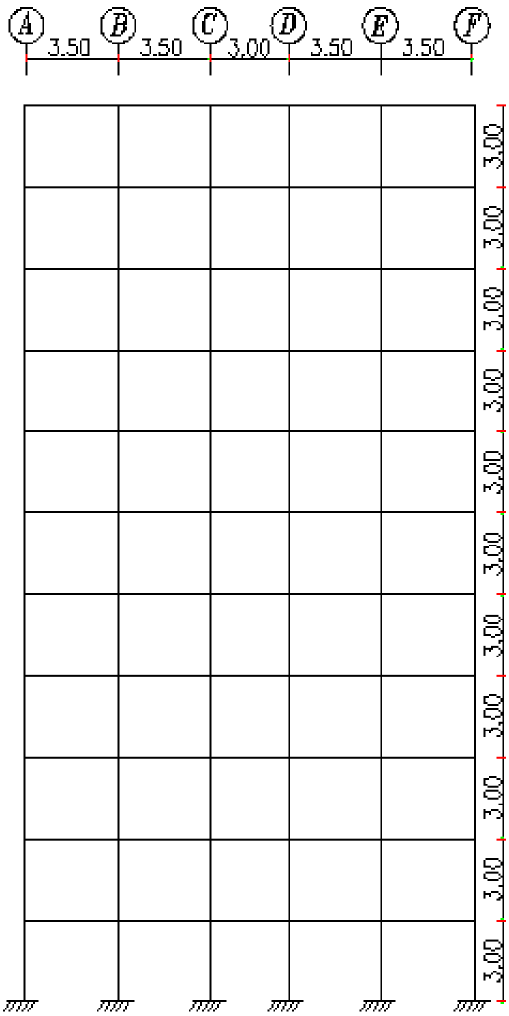

Fig8: Model 4-1Fig9: Model 4-0

2-2 modeling of infill masonry infill walls

Infill walls in this study can be generally categorized in to two types, masonry infill walls with and without opening. Only masonry infill walls without opening were considered as lateral load resistant element with shaded areas as shown in fig1. Infill walls with opening that prevent diagonal strut [2] formation are considered as dead loads only [4]. Window opening are assumed tiny relative to the overall wall area, thus not included in the as they have no appreciable bearing on the general behavior of the structure[5]. Usually in a building of the structure 40% to 60% presence of masonry infillsare effective as the remaining portion of the masonry infills are meant for functional purpose such as doors and window openings [6].In this study, buildings were modeled using 40% masonry infill.

The model for masonry infill walls can be classified as finite element method (micro) and static equivalent strut (macro).in this study equivalent compression strut used instead of masonry infill walls, this strut is a compression diagonal. The single strut model is the most widely used as it is simple and evidently most suitable for large structure [7]. Thus RC frames with unreinforced masonry walls can be modeled as equivalent braced frames with infill walls replaced by equivalent diagonal strut which can be used in rigorousnonlinearpushover analysis using the theory of beams on elastic foundations [8]suggested a non-dimensional parameter to determine the width and relative stiffness of diagonal strut according to FEMA306, 1997 the strut area A_e is given by following expression as shown in fig10.

$A_e = W_e\ t$

$W_e = 0.175(\lambda h)^{-0.4} w$

$$\lambda = \sqrt[4]{\frac{E_m t \sin(2\theta)}{4 E_f I_c h'}}$$

E_m =The modulus of elasticity of the infill material
E_f =The modulus of elasticity of the frame material
I_c =The moment of inertia of column
t =The thickness of infill
h =The center line height of frame
h' =The height of infill
w =The diagonal length of infill panel
θ =The slope of infill diagonal to the horizontal.

In this study, the following material properties were used for solid brick masonry infill walls. Unit weight of masonry is 20 KN/m3, elastic modulus of masonry infill is E_m =550f_m =2275 KN/mm2.

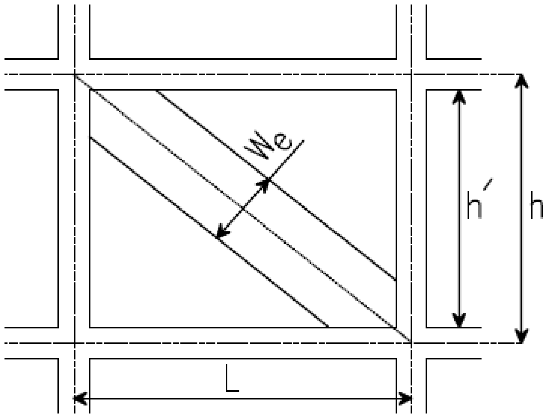

Fig10: Equivalent diagonal strut model [9].

III. ARTIFICIAL NEURAL NETWORKS

One efficient way of solving complex problems is following the lemma “divides and conquers”. A complex system may be decomposed into simpler elements, in order to be able to understand it. Alsosimple elements may be gathered to produce a complex system [10]. Artificial Neural Networks (ANNs) are one approach for achieving this. The scope of this study is to create a brief induction to ANNs for training buildings which there are no analysis of them. Displacement and performance points were prediction using ANN.

IV. NONLINEAR STRUCTURAL ANALYSIS

Nonlinear analysis is performed for eight models of the building in this study. Nonlinear static pushover analysis has been performed to determine the structural earthquake behavior using ETABS nonlinear version 9.7 program[11]. However the earthquake response is determined by one of the structural analysis method as nonlinear analysis. This method is included two ways as nonlinear static pushover analysis and nonlinear dynamic time history analysis.

Nonlinear static pushover analysis has been suggested in FEMA365 and ATC40.

The guidelines ATC and FEMA mentioned in this paper include modeling procedures, acceptance criteria and analysis procedures for pushover analysis. These documents define force – deformation criteria for potential locations of lumped inelastic behavior, designated as plastic hinges used in pushover analysis.

ETABS implements the plastic hinge properties described in FEMA365 and ATC40 as shown in fig 11.five points labeled A, B, C, D and E define force–deformation behavior of the plastic hinge and performance level are Immediate Occupancy (IO), Life Safety (LS), Collapse Prevention (CP), A, B are performance points before immediate occupancy (elastic range), B, Care related to yieldand ultimate curvatures (plastic range) and D, E performance point beyond collapse are used to define the acceptance criteria for the hinge.[2,12].

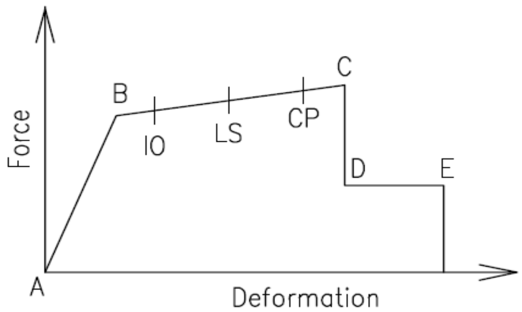

Fig11. Force – Deformation Relation for plastic Hinge in Pushover Analysis

V. ANALYSIS AND RESULTS

The nonlinear static pushover analysis was performed for all models; models were designed and checked as per IS456,[13]. The comparative results of story displacement,fundamental natural time period as per IS1893,[14]capacity curves along with performance levels as IO, LS and CP and neural networks for prediction of seismic behavior for all models are shown,tabulated in table 1 to 4.

5-1Storeydisplacement

The lateral displacement at top storey of various models is tabulated in table1.Displacement depends on the stiffness of each model, table 1 shows that where stiffness of infill walls are considered have significantly lower displacement as compared to bare frame. From table 1 it is observed that infill wall decreases displacement due to its stiffness, stiffness of infill walls decreases displacement from 25.87%, 24.62%, 17.1%, to16.01% for five, seven, nine, eleven stores (respectively), with respect to bare frame.

Table 1: Displacement at top storey level of various structural systems

Type of Structures	Model 1-0	Model 1-1	Model 2-0	Model 2-1	Model 3-0	Model 3-1	Model 4-0	Model 4-1
DispAt top story(cm)	1.38	1.023	1.99	1.50	2.28	1.89	2.81	2.36

5-2 fundamental natural period:

The approximate fundamental natural period of vibration from the empirical expression of the IS1893,[14] is compared with the analytical time period. As shown in table 2 analytical time period do not tally with empirical time period (caudal). The analytical natural period depends on the mass and stiffness, but empirical time period depends on the height of the building.

For models with stiffness of infill walls observed that analytical natural period have lower time period as compared to bare frame, and for models with higher level, empirical period have higher time period. Table 2 shows that analytical fundamental natural time period for models with infill walls are 1.94 to 1.88 times higher than empiricaltime period.

Table 2: Empirical and Analytical time period in all models

Type of Structures	Model 1-0	Model 1-1	Model 2-0	Model 2-1	Model 3-0	Model 3-1	Model 4-0	Model 4-1
Analytical	0.913	0.64	1.23	0.88	1.535	1.12	1.85	1.36
Caudal	0.572	0.33	0.736	0.45	0.888	0.59	1.033	0.72

5-3 Capacity curves along with performance level:

The capacity curves, displacement capacity and performance point values of each model obtained from pushover analysis.Pushover curves are given in fig 12 and also tabulated in table 3. From the data presented in table 3, the models with infill walls have the highest capacity as compared with bare frame. Pushover curves in fig 12 show that buildings with lower height have parabolic curves with clear life safety points. And they show that due to enhance height of the buildings parabolic curves transform in to the straight line with unclear point at life safety.

Performance point was determined from pushover analysis. The status of plastic hinges formed in the structure according to force – deformation curve define performance of the structure at performance point,when the structure reaches its performance point.

Table 4 shows status of hinges at performance point. From the data presented in table 4 for models with infill wall the number of plastic hinges in LS-CP stage are very less in number as compared with models without infill wall.

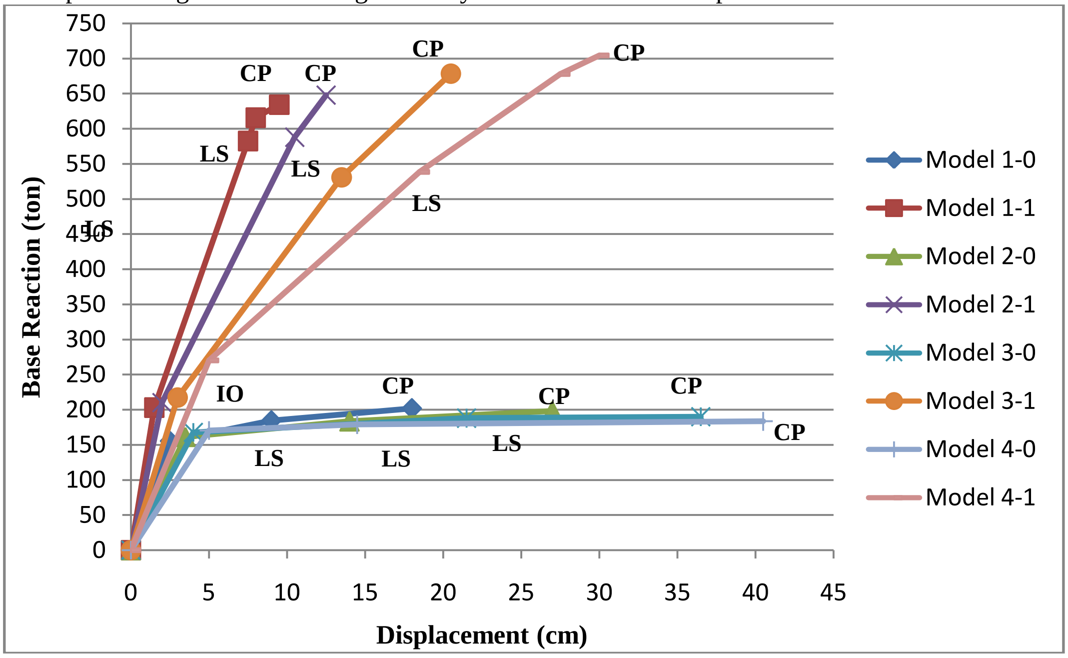

Fig12: Pushover curves for all models.

Table 3: Base shear (ton) and Displacement (cm) at Performance level for all models.

Typeof Structures			Model 1-0	Model 1-1	Model 2-0	Model 2-1	Model 3-0	Model 3-1	Model 4-0	Model 4-1
Performance Level	IO	Base Shear	155.5	203	161.3	210	167.7	217.5	170.5	270
		Disp	2.5	1.50	3.6	2.0	4.0	3.0	5.0	5.0
	LS	Base Shear	184.3	615.7	183.4	588	188	530.9	178	678
		Disp	9.0	8.0	14.0	10.5	21.5	13.5	14.5	27.5
	CP	Base Shear	201.6	634.1	198.2	648	190	678.3	183.4	704.2
		Disp	18.0	9.5	27	13	36.5	20.5	40.5	30.0

Table 4: Hinge status at performance point in x-direction for all models

Type of models	Disp (cm)	Base Shear (ton)	A-B	B-IO	IO-LS	LS-CP	CP-C	C-D	D-E	>E	Total
Model 1-0	13.3	192.2	803	32	113	192	0	0	0	0	1140
Model 1-1	8.11	601.3	727	206	205	2	0	0	0	0	1140
Model 2-0	17.9	187.6	1149	62	85	299	0	1	0	0	1596
Model 2-1	11.4	594	1062	262	263	9	0	0	0	0	1596
Model 3-0	23.4	187.5	1512	0	120	420	0	0	0	0	2052
Model 3-1	14.6	551.3	1300	321	347	84	0	0	0	0	2052
Model 4-0	27.8	183.4	1855	148	145	360	0	0	0	0	2508
Model 4-1	17.6	520	1542	397	328	241	0	0	0	0	2508

5-4 Neural networks for prediction of seismic behavior:

MATLAB software is used to createneural network. For creation the network, totally 32 data set are used which are listed in table 5. These data sets were generated analytically using structures with infill walls. The network was trained and then tested by 4 and 4 data sets for displacement and base shear (respectively), at performance pointwhich are tabulated in table 6. And for trial model with thirteen storey input data are listed in table 7.Displacement and base shear at performance point predicted for building with thirteen storey using ANN is compared with actual values of ETABS output as shown in table 8. The result clearlyshows that predicted values using neural networkat displacement and base shear on the performance point are 3.0(cm) and 500(ton),(respectively) are close to actual value 2.86(cm) and 490(ton). It can be observed that overall prediction is very good.

Table 5: Data set used input for model with infill wall.

Input	Model 1-1	Model 2-1	Model 3-1	Model4-1
Number of storey	5	7	9	11
Height(m)	15	21	27	33
Seismic coefficient	0.051	0.0382	0.0292	0.024
Total weight(ton)	2103	3010	3882	4776
Total cross section of column(m^2)	22.67	34.85	55.8	72.42
Total cross section of beam(m^2)	31.5	44.1	56.7	69.3
Total area of reinforcement steel(m^2)	0.3617	0.7034	1.0852	1.7245
Total trust area(m^2)	12.67	17.738	22.806	27.874

Table 6: Data set used target for model with infill wall.

Target	Model 1-1	Model 2-1	Model 3-1	Model4-1
Displacement(cm)	1.023	1.50	1.89	2.36
Performance point(v)(ton)	601.3	594	551.27	520

Table 7: Data set used input for trial model.

Input	Trial model 5-1
Number of storey	13
Height(m)	39
Seismic coefficient	0.02
Total weight(ton)	5667
Total cross section of column(m^2)	88.255
Total cross section of beam(m^2)	89.1
Total area of reinforcement steel(m^2)	2.11
Total trust area(m^2)	32.942

Table 8: Displacement and Base shear at performance point in x-direction for trial model

Trial Model(thirteen storey)	Displacement atTop(cm)	Base shear at Performance Point(ton)
Model 5-1(ETABS Value)	2.86	490
Model 5-1(ANN Value)	3.0	500

VI. CONCLUSIONS

1. Due to presence of the infill wall displacement at top storey decreasesfrom 25.87%, 24.62%, 17.1%, to 16.01% for five, seven, nine, eleven stores (respectively) with respect to bare frame.From the above observationit can be seen that due to enhance height of the building influence of stiffness of the infill wall will be less, thus it should be used more lateral load resistant system to increase the stiffness of the multi storey building. And results show that stiffness of the infill walls is efficient for building with low and medium height.
2. It is observed that performance of all structures in elastic range have definite values for model with and without infill walls at immediateoccupancy,and performance of the structures with low-rise building in plastic range have clear point at life safety in comparison with multi storey buildings that have unclear point at life safety.
3. It can be seen that the performance of all the models lies in between life safety and collapsepervasion.Overall the performances of these models are satisfactory and some of the elements in some models require retrofitting.

4. The predicted values in displacement and base shear at performance point for trial building using artificial neural network vary only marginally maximum of 4.89% and 2.04% (respectively), from the actual values. The values show that prediction by artificial neural network is satisfactory.

REFERENCES

[1] T N SINGH ET AL. Prediction of p- wave velocity and anisotropic property of rock using artificial neural network technique. journal of scientific & industerial reserch, v. vol,63, p. pp, 32-38, 2004.

[2] FEMA365. prestandard and Commentary for theSseismic Rehabilitation of Buildings, Federai Emergency Management Agancy, 2000.

[3] Mehrabi A. B. and shing P. B.(2002). Behaviour and masonry-infilled frames. Prog. struct. Engng Mater 4,320-331., 2002.

[4] MEHMET INEL AND HAYRI BO ZMEN. Effect ofIinfill Wall on Soft Story Behaviour in Mid-Rise RC Buildings, 2008.

[5] S.K., Murty C. V. R, Arlekar, J.N, Sinha, R, Goyal, A., and jain, C.K., (1997),"Some Observations on Engineering Aspects of the Jabalpur Earthquake of 22 May a997", EERI Special Earthquake Report, EERI Newsletter, Vol.31, No.8, August 1997, pp 1-8., 1997.

[6] Pauley, T. and Priestley, M.J.N (1992) "seismic design of reinforced and masonry buildings" WileyInterscienceInc, USA, 1992, 1992.

[7] Das, D., Murty, C. V. R. (2004) "Brick masonry infil in seismic design of Rc framed buildings :part 1-Cost implications" The indian concrete journal july 2004, vol78 No7 : 39-43l, 2004.

[8] Smith, S. B. & carter, 1969. A method of analysis for infilled frames. proc. of Institution of Civil Engineering part 2, 44, 1969:31:48, 1969.

[9] FEMA306. Evaluation of Earthquake damaged cocrete and masonry wall building - Basic procedures manual. Washington, D.C. : Federal Emergency Management Agency., 1997.

[10] BARYAM. Dynamicc of Complex Systems. Addison-Wesley, 1997.

[11] ETABS9.7.0. Nonlinear Version 9.7.0. 2000. Extended 3-D analysis of the Bbuilding Systems computers and structures Inc. 2000 Berkeley, california, 2000.

[12] ATC40. seismic evaluation and Retrofit of Cocrete Buildings, Applied Technology Council, redwood City, CA., 1996.

[13] IS456. Bureau of Indian Standards code, IS456-2000,"Plain and reinforced concrete-code of Practic",Bureau of Indian Standards, New Delhi, India., 2000.

[14] IS1893. Bureau of indian Standards code, IS1893-2002, "Criteria for earthquake resistant design of structures", part I: General Provisionsand Buildings, Fifth revisio, Bureau of Indian Standards, New delhi, India., 2002.

International Journal of Modern Engineering Research (IJMER)
www.ijmer.com Vol. 3, Issue. 5, Sep - Oct. 2013 pp-3079-3085 ISSN: 2249-6645

Spectrophotometric Determination of Cardiovascular Drugs

K. Sayanna[1], G. Venkateshwarlu[2]
[1]Department of Chemistry, Nizam college/Osmania University, Hyderabad –500001,India
[2]Department of Chemistry, Nizam college/Osmania University, Hyderabad –500001,India

ABSTRACT: *Simple, sensitive, accurate and precise spectrophotometric methods for quantitative determination of cardiovascular drugs viz., Dobutamine Hydrochloride (DOB), Ramipril (RAM), Telmisartan (TEL), Verapamil Hydrochloride (VER) were developed. The method of each drug depends upon oxidation of drugs by Ce (IV) (Excess) and estimating the amount of un reacted Ce (IV) by amaranth dye at 523nm. The calibration curves obeyed Beer's law over the concentration range of 1.6-12µg ml^{-1} (DOB), 8-56 µg ml^{-1} (RAM), 2-14 µg ml^{-1} (TEL) & 2-12 µg ml^{-1} (VER). The method has been validated in terms of guidelines of ICH and has been applied to analysis of pharmaceuticals.*

Keywords: *Cerium (IV), Amaranth dye couple, drugs, Determination, UV-VIS Spectrohotometry*

I. INTRODUCTION

1.1. Dobutamine hydrochloride

Dobutamine hydrochloride, [Fig.1 (a)], is chemically as 4-(2-((1-methyl-3-(4-hydroxybenzene) propyl) amido) ethyl)-1,2-di-hydroxybenzene hydrochloric salt, is an adrenalin receptor concussion medicine indicated obvious curative effect for coronary heart disease, acute miocardial infarction and expansionary cardiomyopathy [1].

The literature survey reveals that several analytical methods such as enzymatic catalytic spectrofluorimetry [2], Spectrophotometry [3,4,5], high performance liquid chromatography [6,7] and flow-injection chemiluminescence method [8] have been developed for determination of Dobutamine hydrochloride

1.2. Ramipril

Ramipril chemically is (2*S*,3*aS*,6*aS*)-1-[(2*S*)-2-{[(2*S*)-1-ethoxy-1-oxo-4-phenylbutan-2-yl]amino}propanoyl]-octahydrocyclopenta[*b*]pyrrole-2-carboxylic acid, is a highly lipophilic, long acting angiotensin converting enzyme (ACE) inhibitor, [Fig.1(b)]. It effectively reduces both supine alterations in the pulse rate. It is indicated for Hypertension and cardiac failure [9].

Some methods for the analysis of ramipril are Spectrophotometry [10,11,12], High-performance liquid chromatographic and chemometric based spectrophotometry [13] and simple colorimetry [14] have been employed.

1.3. Telmisartan

Telmisartan or (2-(4-{[4-methyl-6-(1-methyl-1*H*-1,3-benzodiazol-2-yl)-2-propyl-1*H*-1,3-benzodiazol-1-yl]methyl}phenyl)benzoic acid or [Fig.1(c)] is a cardiovascular drug, indicated for hypertension [15].

Because of its physiological importance many physical and instrumental techniques have been developed for the quantification of TEL like HPLC [16-22], Spectrophotometry [23-26], LC-MS/MS [27] and HPTLC [28,29].

1.4. Verapamil Hydrochloride

Verapamil Hydrochloride [Fig.1(d)] is chemically known as 5-[N-(3, 4-dimethoxy-phenethyl)-N-methyl-amino]-2-(3,4-dimethoxyphenyl)-2-isopropylvaleronitrile hydrochloride. It is a calcium-channel blocker, has been indicated for anti-arhythmic drug to manage supra ventricular tachyarrhythmias[30] and it is a anti-anginal drug.

Some analytical methods for quantitative determination of VER are described *viz.*, capillary electrophoresis [31], tandem mass spectrometry detection (LC-MS/MS) [32, 33], HPLC [34] and Inverse volt-ampere method [35].

Through survey of literature revealed that oxidative method of quantification of these drugs by Ce (IV) have been not reported yet, although the methods simple sensitive, precise and accurate [36,37].

II. ABOUT THE METHOD

Cerium (IV) is a good oxidizing agent like $KMnO_4$, $K_2Cr_2O_7$ *etc.*, it has been used for quantitative determination of drugs based on the oxidation of drugs. The spectrophotometric methods involved addition of excess Ce(IV) and un reacted cerium is estimated by suitable dyes, which should be oxidized by cerium *viz.*, Indigo Carmine, Methyl Orange, Safranin-O and Xylene cyanol.

Amaranth dye is suitable for estimation of unreacted Ce (IV) absorbance at 523 nm.

III. EXPERIMENTAL

3.1. Apparatus

Spectral and absorbance measurements were made on a thermo electron corporation single beam U.V.-Vis spectrophotometer by using 1 cm quartz cells.

3.2. Materials and methods

All reagents used were of analytical-reagent grade and distilled water was used throughout the investigation.

3.2.1. Cerium (IV) solution

Cerium (IV) sulphate ($CeSO_4.2H_2O$, 99.9 % pure) was prepared by dissolving 750 mg of chemical (merck, mumbai, india) in 2 N $H_2SO_4$with the aid of heat and filtered using glass wool, and diluted to 250 ml with the same acid and standardized and cerium is standardized by ferrous ammonium sulphate and ferroin indicator. The solution was then diluted appropriately with 2 *N* H_2SO_4 to get working concentrations of 4.0x 10^{-3} M (0.25%).

3.2.2. Amaranth dye

Aqueous solutions of 0.8x10^{-3} *M* of Amaranth dye was prepared by dissolving an appropriate weight of 0.0483 grams in 100 ml bi distilled water.

3.2.3. Sulphuric acid

Prepared by diluting the concentrated acid (Merck, Mumbai, India, Sp. gr. 1.84, 98.0 %) with water appropriately to get 2 *N* acid.

3.2.4. Preparation of drug solution

Standard drug solution (200 µgml^{-1}) was prepared by dissolving 20 mg of drug with distilled water to the mark in 100 ml standard flask. The stock solution was diluted appropriately to get the working concentration.

IV. PROCEDURE

Aliquots containing 1.6 — 56.00 µg ml^{-1} of drug were transferred into a series of 10 ml standard flasks using a micro burette. To this, 1 ml of CAS was followed by 1 ml of 2N H_2SO_4 and contents were shaken well. After 30 minutes, 1 ml of 0.02% of amaranth added to the content. Then contents were shaken well and diluted up to the mark. The absorbance of each solution was measured at 523 nm against the corresponding reagent blank.

V. ASSAY OF DRUG PURE SAMPLE

To the test the accuracy and precision of the methods developed pure sample solutions containing drug in the Beer's Law limit were chosen. For this study 1.6-12 µgml^{-1} of DOB, 8-56 µgml^{-1} of RAM, 2-14 µgml^{-1} of TEL, 2-12µgml^{-1} of VER have been taken. To each of the solution 1 ml of 250 µg ml^{-1} of cerium, 1 ml of 2 N of H_2SO_4 were added and the un reacted cerium is analyzed as described above using amaranth dye.

VI. PROCEDURE FOR ANALYSIS OF PHARMACEUTICALS

6.1. Dobutamin Hydrochloride

Two Cardiject injection (50mg/4ml/injection)s of DOB were placed in a boiling tube and worked out to get working standard solutions of 1.6 µgmL^{-1}. Quantification was performed using 1.5, 3.0, 4.5 & 6.0 µg ml^{-1} of Dobutamine hydrochloride.

6.2. Ramipril

To determine the content of Ramipril in pharmaceutical preparations, 20 tablets of Cosrpil (lable claim : 5 mg/tablet) were weighed and finely powdered. A portion of the powder equivalent to 50mg. ramipril was stirred with 50 ml doubly distilled water and let stand for 10 minutes. The residue was filtered on Whatmann No.42 filter paper and wash with doubly distilled water. This solution was further diluted as necessary to complete the analysis concentration solutions for assay.

6.3. Telmisartan

Four tablets (Teli: 20mg/tablet) were weighed and powdered. Accurately weighed quantity of tablet powder equivalent to about 25 mg of telmisartan was transferred into 50 ml volumetric flask, added 25 ml of acetonitrile and shaken for ten minutes, the volume was then adjusted to mark with acetonitrile and mixed, the solution was filtered through Whatmann filter paper No.42 and the filtrate was then appropriately diluted with acetonitrile to get a final concentration of 2 µg ml^{-1} of telmisartan.

6.4. Verapamil Hcl

Two tablets of Veramil (themis chemicals:40mg/tablet) were accurately weighed and finely powdered. The powder equivalent to 20 mg of VER was transferred into 100ml volumetric flask and dissolved in 0.2 M H_2SO_4 . then the solution was filtered using whatmann No.41 filter paper and further diluted with distilled water to obtain working standard solutions.

VII. METHOD OF VALIDATION

The each method developed quantification of drugs has been validated in terms of precision, accuracy, limit of detection, limit of quantification, linearity, selectivity and ruggedness. Absorbance time curves were drawn, initial rate and fixed time methods were used to assess the recovery of the drug. To assess the precision each experiment was repeated at least 5 times and accuracy is estimated in terms of percent recovery and percent RSD. Excellent percent recovery and RSD being less than 2 for each drug demonstrates accuracy and precision of the methods. Further t-test and F-test values have also been calculated using a standard reference method. The closeness of t-test and F-test values is less than that they permissible range indicating high accuracy of the methods [Table 2].

As mentioned earlier limit of detection is the minimum limit that can be detected but not necessarily quantified is determined for each drug.

LOD is determined from the standard deviation of y-intercepts of regression lines of replicate determinations.

LOD = 3.3 s/S

Where s = standard deviation of intercept (n=6)

S = slope of linearity plot

LOQ the minimum concentration of analyst using calibration curve is also determined.

LOQ = 10s/S.

Limits of linearity of calibration curves are mentioned in the [Fig. 2] under the title Beer's law limit. To test the selectivity known excipients of each drug are added to the pure drug sample and recovery experiments were performed. Ruggedness is resistance of method for a small change in variables like instrument, and analyst or both to test the Ruggedness of the method absorbance data was collected using 3 different instrument and 2 analysts no significant changes were observed either by change of instrument or analyst hence the method may be taken as robust.

VIII. FACTORS EFFECTING ABSORBANCE

8. 1. Effect of acid concentration

To study the effect of acid concentration, different types of acids were examined (H_2SO_4, $H_3PO_4$and CH_3COOH) to achieve maximum yield of Redox reaction. The results indicated that the sulphuric acid was the preferable acid with Ce (IV) as oxidant. The reaction was performed in a series of 10 ml volumetric flask containing 8.0 μgml^{-1} 0f the cited drugs, different volumes (0.5–2.5 ml) of 2.0 N H_2SO_4 and 1 ml of Ce(IV) (4.0x 10^{-3}*M*) were added. After 5.0 min of heating time at 60 ± 2°C in a water bath, the solution was cooled for about 3.0 min, 1.0 ml of amaranth dye were added, then complete to 10 ml total volume with water. It was found that the maximum absorbance was obtained at 1 ml of 2 N H_2SO_4. Above this volume, the absorbance decreased therefore, a volume of 1 ml of 2 N H_2SO_4 was used for all measurements.

8.2. Effect of heating time

In order to obtain the highest and most stable absorbance, the effect of heating time on the oxidation re-action of drugs were catalyzed by heating in a water bath at 60 ± 2°C for the periods ranging for 2.5-20 min. the time required to complete the reaction and maximum absorbance was obtained after 5.0 min of heating. After oxidation process, the solution must be cooled at least for 3.0 min before addition of dye.

8.3. Effect of oxidant concentration

When a study on the effect of Ce (IV) on color development was performed, it was observed that in both cases the absorbance increased with increase in the volume of Ce (IV). It reached maximum when 1 ml of 200 µg ml^{-1} Ce (IV) solution was added to a total volume of 10 ml for drugs solutions. The color intensity decreased above the upper limits. Therefore, 1 ml of 200 µg ml^{-1} Ce (IV) was used for all measurements.

8.4. Effect of dye concentration

In order to ascertain the linear relationship between the volume of added Ce (IV) and the decrease in absorbance of Amaranth dye, experiments were performed using 1 ml of 2 *N* H_2SO_4 with varying volumes of Ce (IV). The decrease in absorbance was found to be linear up to the 1 ml of 200 µg ml^{-1} Ce (IV) with optimum volume 1.0 ml of Amaranth dye for fixed concentration drug solution. The color was found to be stable up to 24 hours.

IX. ANALYSIS OF PHARMACEUTICALS

To the test the applicability of the method developed solution of pharmaceutical tablets solutions containing drug in the Beer's Law limit were chosen. To assess the precision each tablet analysis was repeated at least 6 times and accuracy is estimated in terms of percent recovery and percent RSD. Excellent percent recovery and RSD being less than 2 for each drug demonstrates applicability of the methods for pharmaceutical analysis [Table 3]. Further t-test and F-test values have also been calculated using a standard reference method. The closeness of t-test and F-test values is less than that they permissible range indicating excellent applicability of the methods for pharmaceutical analysis [Table 4]. The excellent recovery studies indicate that methods developed can be applied to pharmaceutical analysis without hesitation.

X. RESULTS AND DISCUSSION

The ability of cerium (IV) sulphate to oxidize drugs, and bleach the color of amaranth dye is the basis of the indirect spectrophotometric method developed here. In this method the drugs were reacted with a measured excess of cerium(IV) sulphate in acidic medium and the unreacted oxidant was determined by reacting with amaranth followed by absorbance measurement at 523 nm (scheme 1). The absorbance increased linearly with increasing concentration of drug, when increasing amounts of each drug were added to a fixed amount of 0.25% of CAS, consumed the latter and there occurred a concomitant fall in its concentration. When fixed amount of the dye was added to decreasing amount of oxidant, an concomitant increase in the concentration of dye resulted. This was observed as a proportional increase in absorbance at the respective λ_{max} with increasing concentration of each drug. One ml of 2N acid was used in the reaction, as this concentration was found ideal.

D + Ce $(IV)_{excess}$ → D oxidation product + Ce (III) + Ce $(IV)_{unreacted}$: (1)

Ce $(IV)_{unreacted}$ + amaranth → oxidation product of amaranth + uncreated amaranth : (2)

Measured spectrophotometrically at λ_{max} =523 nm

Scheme 1: Reaction Scheme of the indirect determination of drug by oxidation with Ce (IV) sulphate

XI. ANALYTICAL DATA

A linear correlation was found between absorbance at λ_{max} and concentration ranges, and sensitivity parameters such as molar absorptivity, Sandal's sensitivity, detection limit and quantification limit are presented in Table 1. Regression analysis of Beer's law data using the method of least squares was made to evaluate the slope (b), intercept (a), correlation coefficient (r) and is also given in [Table 1].

XII. ACCURACY AND PRECISION

The accuracy and precision of the methods were established by analyzing the pure drug solution at 6 different levels (with working limits). The relative error (%) which is a measure of accuracy & RSD (%) a measure of precision are summarized in Table 2 and reveal the high accuracy and precision of the methods.

XIII. CONCLUSION

The present study described the successful development of new, simple, sensitive, selective, accurate and rapid spectrohotometric method for the accurate determination of drugs each one in its pharmaceutical forms Cerium (IV) sulphate as the oxidizing reagent. There is no interference from additives and excipients. The method thus can be used in the determination of these drugs in pure and pharmaceutical formulations. So, it is the good alternative to the reported methods for the determination of these drugs.

ACKNOWLEDGEMENT

We are grateful to Head, Department of Chemistry and Principal, Nizam College, Osmania University for providing facilities.

REFERENCES

[1] Liu, Haiyan; Zhang, Ling; Zhou, Jingming; Hao, Yuhong; He, Pingang; Fang, Yuzhi, Flow injection chemiluminescence determination of dobutamine hydrochloride injection using luminolferricyanide/ferrocyanide system, *Analytica Chimica Acta , 541(1-2),*2005, 125-129.

[2] Tian Feng-Shou; Chen Ya-Hong; Liang Hai-Yan, Determination of dobutamine hydrochloride by enzymatic catalytic spectrofluorimetry, Luminescence : *the journal of biological and chemical luminescence (2013)*.

[3] Rao, K. V. Kanna; Reddy, M. N., Spectrophotometric determination of dobutamine hydrochloride in pharmaceutical formulations, *Asian Journal of Chemistry (2001), 13(4),* 1535-1538.

[4] El-Kommos, Michael E., Spectrophotometric method for the determination of dobutamine hydrochloride, *Analyst (Cambridge, United Kingdom) (1983), 108(1284)*, 380-5.

[5] Rao, K. V. Kanna; Murthy, T. K.; Rao, S. S.; Reddy, M. N., Spectrophotometric determination of dobutamine hydrochloride in pharmaceutical formulations, *Acta Ciencia Indica, Chemistry (2001), 27(4),* 187-189.

[6] Zhang, Yingxue; Chen, Funan; Zhang, Zhujun, Chemiluminescence determination of dobutamine hydrochloride in human serum by high performance liquid chromatographic separation connected with ultrafiltration technology, *Fenxi Huaxue (2004), 32(6),* 769-771.

[7] Li, Guodong; Zhang, Jianming; Xu, Fu; You, Yingwei; Gao, Shen, Determination of dobutamine hydrochloride glucose injection by HPLC, *Zhongguo Yiyao Gongye Zazhi (2002), 33(10),* 497-498.

[8] Tang, Guo-feng; Huang, Yu-ming; Shi, Wen-bing; Liu, Wei-bing, Determination of dobutamine hydrochloride by flow-injection chemiluminescence method, *Xinan Shifan Daxue Xuebao, Ziran Kexueban (2004), 29(4),* 638-641.

[9] Nafisur Rahman,1 Yasmin Ahmad,1 and Syed Najmul Hejaz Azmi1, Kinetic Spectrophotometric Method for the Determination of Ramipril in Pharmaceutical Formulations, *AAPS PharmSciTech 2005; 6 (3)* Article 68

[10] Pratapareddy, A. J.; Muralikrishna, Ch.; Chakravarthi, I. E., New spectrophotometric determination of ramipril in bulk and pharmaceutical dosage form, *Asian Journal of Chemical and Environmental Research (2012), 5(1-2),* 5-9.

[11] Afieroho, O. E.; Okorie, O.; Okonkwo, T. J. N., A spectrophotometric method for the determination of ramipril in solid dosage forms, *Tropical Journal of Pharmaceutical Research (2012), 11(2),* 275-279.

[12] Kalyana Ramu, B.; Raghubabu, K., Extractive visible spectrophotometric determination of ramipril in pharmaceutical preparations, *Asian Journal of Pharmaceutical and Clinical Research (2011), 4(3),* 82-85.

[13] Gowda, Nagaraj; Tekal, Raju; Thangavelu, Radhasri; Vipul, Kalamkar; Rajashree, Mashru, Validated high-performance liquid chromatographic and chemometric based spectrophotometric determination of ramipril and atorvastatin in pharmaceutical dosage forms, *Journal of Food and Drug Analysis (2012), 20(3),* 577-587.

[14] Kalyanaramu, B.; Raghubabu, K.; Vamsikumar, Y., Development of a simple colorimetric determination of ramipril from pharmaceutical formulations, *Journal of Chemical and Pharmaceutical Research (2011), 3(2),* 863-869.

[15)] Kumbhar, S. T.; Chougule, G. K.; Gajeli, G. B.; Tegeli, V. S.; Thorat, Y. S.; Shivsharan, U. S., Visible spectrophotometric determination of telmisartan from urine, *International Journal of Pharmaceutical Sciences and Research (2011), 2(5),* 1254-1258.

[16] Gupta, A.; Charde, R. M.; Charde, M. S., Determination of Telmisartan and forced degradation behavior by RP-HPLC in tablet dosage form, *International Journal of Pharmaceutical Chemistry (2012), 2(3),* 93-99.

[17] He, Haixia; Zhou, Yuanda; Li, Juan, Determination of telmisartan concentration in human plasma by HPLC, *Zhongguo Yaofang (2012), 23(2),* 129-131.

[18] Charde, M. S.; Gupta, A.; Chakole, R. D., Determination of Telmisartan in pharmaceutical formulations by reverse phase-high performance liquid chromatography, *International Journal of Phytopharmacy (2012), 2(2),* 61-67.

[19] Virkar, Prasad S.; Pingale, Satish G.; Mangaonkar, Kiran V., Development and validation of a High Performance Liquid Chromatography method for determination of telmisartan in rabbit plasma and its application to a pharmacokinetic study, *Journal*

of Analytical & Bioanalytical Techniques (2012), 3(3), 133.

[20] Varma D., P. S. R. C. H. N. P.; Lakshmana Rao, A.; Dinda, S. C., Stability indicating RP-HPLC method for simultaneous determination of telmisartan and hydrochlorothiazide in pharmaceutical dosage form, *International Journal of Pharmaceutical, Chemical and Biological Sciences (2012), 2(3),* 382-391

[21] Lin, Hangjuan, Determination of telmisartan in compound telmisartan capsules by HPLC, Zhongguo Yaoye (2011), 20(11), 25-26.

[22] Wang, Yongchun; Fei, Pingxia; Xi, Yunfei; Tian, Yuning, Determination of telmisartan in human plasma by RP-HPLC, *Xibei Yaoxue Zazhi (2011), 26(1),* 1-3.

[23] Huang, Yan-li, Spectrophotometric determination of telmisartan,*Lihua Jianyan, Huaxue Fence (2012), 48(7),* 818-819, 822.

[24] Qin, Zong-hui; Xia, Hong-mei; Xie, Bing; Qin, Xiu-rong; Gan, Xiang-qing; Pang, Xiang-dong; Wan, Bang-jiang, Spectrophotometric determination of telmisartan by its reaction with cresol red, *Lihua Jianyan, Huaxue Fence (2012), 48(1),* 90-92, 101.

[25] Xie, Bing; He, Yi-heng; Tan, Rong; Gan, Xiang-qing; Pang, Xiang-dong; Qin, Zong-hui, Determination of telmisartan by spectrophotometry with solid green FCF, *Fenxi Shiyanshi (2011), 30(2),* 74-77.

[26] Wan, Bang-jiang; Gan, Xiang-qing; Xie, Bing; Pang, Xiang-dong; Wang, Yang-mei; Qin, Zong-hui, Spectrophotometric method for the determination of telmisartan with chlorophosphonazo I, *Fenxi Kexue Xuebao (2010), 26(6),* 693-696.

[27] Wang, Guocai; Zhang, Dan; Yang, Man; Zheng, Tianlei; Wang, Tao; Wang, Zhenlong; Han, Jing; Liu, Huichen, Determination of telmisartan in human plasma by LC-MS/MS and bioequivalence study of it, *Zhongguo Yaofang (2011), 22(46),* 4365-4368.

[28] Maria Irene Yoshida 1, Elionai Cassiana Lima Gomes 1, Cristina Duarte Vianna Soares 2, Alexandre Frinhani Cunha 3 and Marcelo Antonio Oliveira 3*, Thermal Analysis Applied to Verapamil Hydrochloride Characterization in Pharmaceutical Formulations, *Molecules 2010, 15,* 2439-2452.

[29] Parmar, Kreny E.; Mehta, R. S.; Patel, Nikita D.; Parmar, Kreny E., Development and validation of HPTLC method for simultaneous determination of Telmisartan and Chlorthalidone in bulk and pharmaceutical dosage form, *International Journal of Pharmacy and Pharmaceutical Sciences (2013), 5(2),* 420-425

[30] Vekariya, N. R.; Patel, G. F.; Dholakiya, R. B., Stability-indicating HPTLC determination of telmisartan in bulk and tablets, *Research Journal of Pharmacy and Technology (2010), 3(3),* 900-904

[31] Liang, Ru-Ping; Zhu, Xiao-Yan; Tao, Yi-Wen; Wang, Jing-Wu, Separation and determination of verapamil hydrochloride by capillary electrophoresis with end-column electrochemiluminescence detection, *Fenxi Huaxue (2010), 38(9),* 1305-1310.

[32] Chen, Yao; Tan, Zhirong; Wang, Yicheng; Deng, Xiaolan; Zhang, Wei; Zhou, Honghao, LC-MS/MS determination of verapamil in human plasma and its application in bioequivalence evaluation, *Zhongguo Yaoxue Zazhi (Beijing, China) (2012), 47(7),* 546-550.

[33] Baviskar, Dheeraj; Sharma, Rajesh; Jain, Dinesh, Determination of verapamil in human plasma by tandem mass spectrometry, *Asian Journal of Chemistry (2009), 21(9),* 6785-6791.

[34] Milenovic, Dragan M.; Milosevic, Snezana P.; Duric, Svetlana Lj.; Naskovic, Daniela C.; Mitic, Snezana S., Development and validation of an HPLC method for the determination of verapamil residues in supports of cleaningProcedure, *Journal of Analytical Chemistry (2013), 68(6),* 545-551.

[35] Gusakova, A. M.; Ivanovskaya, E. A.; Krasnova, N. M.; Idrisova, E. M.; Karpov, R. S., *Inverse volt-ampere method for determination of verapamil hydrochloride concentration in blood,* Russ. (2009), RU 2354962 C1 20090510,

[36] Sara Abdulgader Mohammed Ebraheem , Abdalla Ahmed Elbashir, spectrophotometric method for the determination of ofloxacin and levofloxacin in pharmaceutical formulations, *American Academic & Scholarly Research Journal Vol. 4, No. 2,* March 2012

[37] B Narayana & K Ashwini, Spectrohotometric determination of frusemide by its oxidation with ceric ammonium sulphate, *Indian journel of chemical technology vol.17,* march-2010,pp 150-153

a) DOBUTAMINE HCl	b) RAMIPRIL
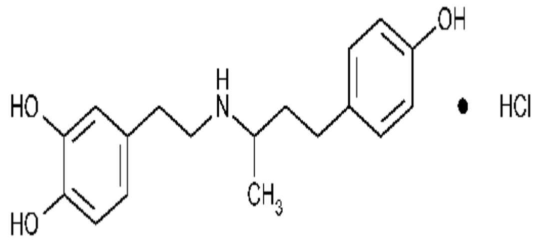	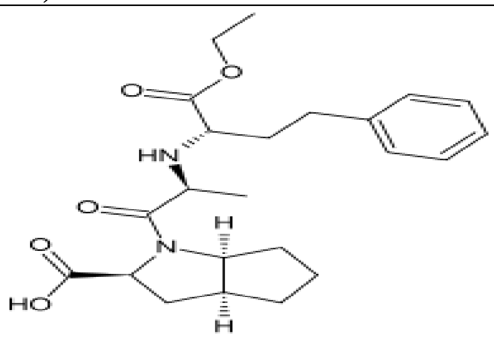
c) TELMISARTAN	d) VERAPAMIL HCl
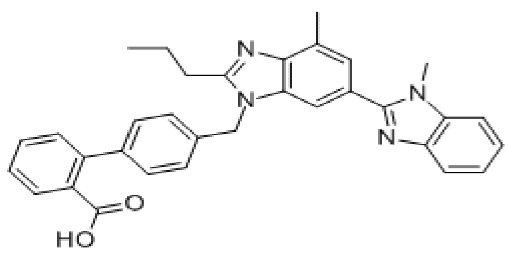	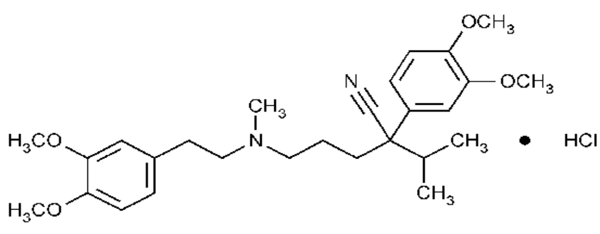

Figure 1 : Structures of Drugs

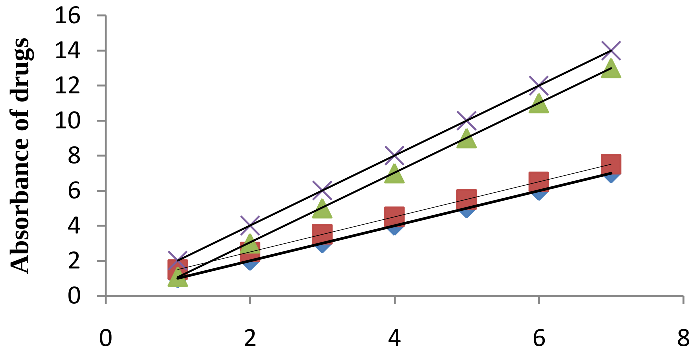

Fig.2 Calibration curves

Table 1: Analytical and Regression parameters of Spectrophotometric method

Name of drug Property	DOB	RAM	TEL	VER
λ_{max}	523	523	523	523
Beer's law limits (μg ml^{-1})	1.6-12	8-56	2-14	2-12
Sandell's sensitivity (μg cm^{-2})	0.0127	0.0833	0.0204	0.0172
Std.Dev. Of intercepts	0.0306	0.0273	0.0204	0.0788
LOD (μg ml^{-1})	1.2763	7.5158	1.3704	4.4823
LOQ (μg ml^{-1})	3.8678	22.775	4.1527	13.5828
Slope (b)	0.079	0.012	0.049	0.058
Intercept (a)	0.089	0.025	0.171	0.061
Correlation coefficient	0.988	0.98	0.99	0.969
Regression equation Y = a + bx	0.215	0.121	0.269	0.177

*Limit of determination as the weight in µg per mL of solution, which corresponds to an absorbance of A = 0.001 measured in a cuvette of cross-sectional area 1 cm 2 and path length of 1 cm. Y** = a+bX, where Y is the absorbance and X=concentration of drug (µg ml^{-1})

Table 2: Determination of Accuracy and Precision of the methods on pure Drug Samples

Name of the Drug	Amount Taken (µg ml^{-1})	***Amount Found*** (µg ml^{-1})	% er	% Recovery	RSD %	Proposed method mean ± SD
DOB	1.5 3.0 4.5 6.0	4.51 2.99 4.46 6.01	0.67 0.33 0.88 0.16	100.67 99.67 99.11 100.17	0.6696	100.01 ± 0.671
RAM	1.0 2.0 4.0 6.0	0.99 2.01 3.98 5.97	1.00 0.50 0.50 0.50	99.00 100.50 99.50 99.50	0.6316	99.59 ± 0.622
TEL	3.0 5.0 7.0 9.0	2.99 4.97 6.98 8.99	0.33 0.60 0.28 0.11	99.67 99.40 99.71 99.89	0.2031	99.70 ± 0.199
VER	3.0 5.0 7.0 9.0	3.02 5.01 6.99 8.96	0.67 0.20 0.14 0.44	100.67 100.20 99.86 99.56	0.4762	100.18 ± 0.469

Table 3: Results of assay of tablets by the proposed methods and statistical evaluation and recovery experiments by standard addition method

Pharmaceuticals/ tablets/ injection	Drug in tablet (µg ml^{-1})	Drug added (µg ml^{-1})	Total found (µg ml^{-1})	er %	Recovery %	RSD%	Reference method mean ±SD	Proposed method ±SD
DOB	2.0 4.0 6.0 8.0	1.0 1.0 0.0 0.0	2.98 4.99 5.98 7.99	0.67 0.20 0.33 0.13	99.33 99.88 99.67 99.88	0.261	101 ± 1.0	99.7 ± 0.257
RAM	08.0 10.0 12.0 14.0	1.0 1.0 0.0 0.0	8.98 11.01 11.99 14.00	0.22 0.10 0.08 0.00	99.98 100.09 99.92 100.00	0.070	100.96 ± 0.672	100.10 ± 0.07
TEL	3.0 5.0 7.0 9.0	1.0 1.0 0.0 0.0	3.98 6.02 6.99 8.98	0.50 0.33 0.43 0.22	99.50 100.33 99.57 99.78	0.377	100.5 ± 0.393	99.80 ± 0.361
VER	2.0 4.0 6.0 8.0	1.0 1.0 0.0 0.0	3.02 5.0 5.98 7.99	0.50 0.0 0.33 0.16	100.67 100.0 99.67 99.88	0.432	98.93 ± 0.37	100 ± 0.396

Table 4: Student's t-test and f-test values for Pharmaceutical analysis

Pharmaceuticals/ tablets/ injection	DOB	RAM	TEL	VER
Student's t-test	1.327 (1.42)	1.396 (1.393)	0.074 (1.45)	0.059 (1.19)
f-test	0.066 (3.15)	0.011 (4.02)	0.841 (3.85)	1.145 (3.24)

Nose Tip Detection Using Shape index and Energy Effective for 3d Face Recognition

Sawsen Abdulhadi Mahmood[1],Rana Fareed Ghani[2], Abdulamir Abdullah Kerim[3]
Computer Science Department, University of Technology, Baghdad,Iraq

Abstract:*Nose tip detection is an essential point in 3d face alignment, pose estimation and the discrimination process. A method to determine nose tip location based on exploiting local descriptors(shape index) from each point cloud on the 3d surface mesh is presented in this paper. Furthermore, theeffective energy constraint was appliedover each 3d mesh data point. Then NN-Nearest Neighbour classification methodwas applied in order to locate the nose tip and nose region based 3d feature extraction techniques.The detection method is also characterized by the refining of candidate points for nose tip regions and is robust against pose and expression variations.All computations were based on the pure 3D mesh data points of a face without texture information. The proposed method was tested using a 3d face image sample database FRAV3d, and GAVADB database. The experimental results show 96% and 76% correct nose tip detection for FRAV3d and GAVADB databases respectively.*

I. INTRODUCTION

The detection of three dimensional facial landmarks is an important stage in biometric applications, computer vision and computer graphics. In order to perform face registration, recognition, facial expression recognition, facial shape analysis and segmentation in 3d face recognition systems,the facial landmarks must be located. Compared to other facial landmarks the nose tipis one of the most important and critical landmarks because of its distinct shape and symmetrical property. Technically in a 3D face environment, the nose tip is the point with the maximum depth value.In reality, the nose tip point (region) has a maximum depth value which is true only in the frontal image[1].

A lot of researches have been done to locate the nose tip of 3d faces. Breitenstein et al. [12] proposed an approach to detect an invariant pose for the nose tip. For each point in the acquisitioned image, the shape signature was calculated and the corresponding pose hypotheses were generated in parallel. Then, the nose tip was selected using error function which compares the input range image to the pre-computed pose images of an average face model.

Zhu et al.[10] assumed the protuberant points as nose tip candidates. Since only frontal faces were considered, symmetry calculation was performed in order to obtain the nose tip location, which was implemented using the direction comparison of normal vectors.

Werghi et al.[9] investigated a method of nose tip detection and frontal face extraction by estimating mesh quality. They measured and assessed mesh surface quality by extracting groups of triangular facets. The nose tip was detected by identifying the single triangular facet using a cascaded filtering framework mostly based on simple topological rules.

Bagchi et al. [8] used HK classification to detect the nose tip and eye corner which is based on curvature analysis of the entire facial surface.

In this paper,a nose tip detection approach is presented for 3d facial data points.This approach is based on a simultaneous filtering technique. The extraction of local geometry information from the 3d data point is carried out, at the same time that the effective energy constraint is computed for nose tip candidates.Therefore, the two region points which are deduced from the two approaches feed into NN-Nearest Neighbour classifier to obtain the nose tip location on the 3d facial image.

II. 3D SHAPE DESCRIPTORS

Surface curvature is a property of the local surface, which has the advantage of being invariant against rigid transformation (translations and rotations)[15].Therefore the shape descriptors derived from curvature have been adopted in this work.Curvature based measures, which are related to second-order derivatives of theraw depth measurements, were used to extract features from 3D facial images. To understand principal curvatures, imagine the normal on a surface and an infinite set of planes (a *pencil of planes*) each of which contains this normal. Each of these planes intersects the surface in a plane curve and the principal curvatures are defined as the maximum curvature K_1, and minimum curvature $K_2$of this infinite set of plane curves. The directions that correspond to maximum and minimum curvatures are always perpendicular and are called the principal directions of the surface. Principal curvatures are in fact the eigenvalues of the *Weingarten matrix*, which is a 2 × 2 matrix containing the parameters of aquadratic local surface patch fitted in a local plane that is aligned to the surface tangentplane[4].

III. THE PROPOSED NOSE TIP DETECTION METHOD

The proposednose tip detection method is based on the extraction of local descriptors and statistical characteristics from 3d data points. Figure (1) shows the outlines of the proposed method.The process starts with the acquisition of the 3d face data by a face scanner. In the next stage the3d data is filtered and smoothed by median noise removal. Preprocessed 3d data is fed into the next stage in order to perform the calculation of the local shape index and effective energy. At the final stage, the nose tip location and nose regionare extracted by applying the NN-Nearest Neighbour classification method on the two candidate regions. The details of these stages are given in the following sections.

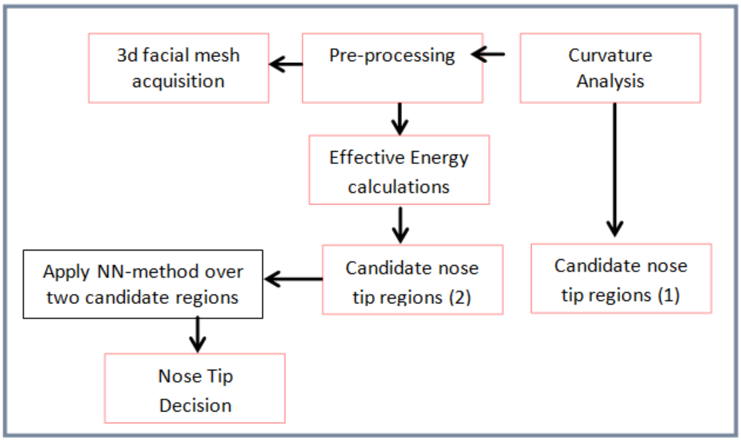

Fig 1. Block Diagram of The Proposed nose tip detection method

1. Pre-processing

Preprocessing is an important stage of the recognitionsystems, since all the features will be extracted from theoutput of this step [3].The 3d face images are obtained by 3d scanner.Each captured image (mesh) is composed of 3d coordinate points, set of faces (polygons), normal of vertex, and may also contain texture information. Therefor the first step is to remove spikes formacquisition datausing filtering techniques. A 2d median filter is used to smooth 3d data which is applied to Z-values.This technique will remove spikes from the 3d facial image.

2. Curvature Analysis

The local curvature information about a point is independent of the coordinate system. The feature points and geometry information of the 3d surface is captured by calculatingthe shape index of each 3d point. Shape index is extensively used for 3D landmark detection [14].And is a scale independent component derived from principle curvatures.In other words the shape index values represent continuous mapping of principal curvature values(K_{max} , K_{min})of a 3D face pointPinto the interval [0,1],and can be computed as follows:

$$SI = \frac{1}{2} - \frac{1}{\pi}\frac{(K_{max} + K_{min})}{(K_{max} - K_{min})} \dots\dots\dots (1)$$

The principle curvatures (K_{max} , K_{min})are in fact the eigenvalues of the *Weingarten matrix*, which is a 2×2 matrix containing the parameters of a quadratic local surface patch [4]. The surface patch equation is:

$$f(x,y) = z = ax^2 + by^2 + cxy + dx + ey + f \quad \dots\dots.(2)$$

Since (x_i, y_i, z_i) are neighbouring points and a,b,c,d,e,f are thesurface parameters to be found by the least square fitting technique. The Weingarten matrixformula is:

$$W = \begin{bmatrix} a & b \\ b & c \end{bmatrix} \quad \dots\dots\dots (3)$$

The shape index captures the curvature value for each point on the surface. Every distinct surface shape corresponds to aunique value of shape index, except the planar shape. Points on a planar surfacehave an indeterminate shape index, since$K_{max} = K_{min} = 0$. In fact there are five well-known shape types and their locations on the shape index scale are shown in figure(2):

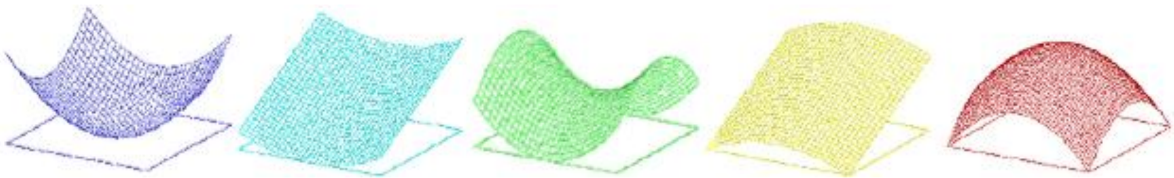

Spherical cup=0.0 Rut = 0.25 Saddle = 0.5Ridge = 0.75 Spherical cap = 1.0

Fig 2.Sample representative shapes on the shape index scale[13]

After calculating shape index values for all 3d facial data points, the surface points that have a shape index within a threshold range are extracted, which indicates the convex regions of thesurface of the face.The low values of the shape index represent a spherical cup while a high values representsa spherical cap.
This step will reduce the search space for nose tip candidate regions and produce at the same time what is called candidate nose tip regions(1).

3. Effective Energy Calculations

The usual method to find the nose tip candidate region on 3d face images is to select N points with highestZ-value from the entire 3d mesh data points [7]. This process will reduce the possible candidate nose tipregions significantly.However with pose variation this processwilllead to incorrect regionlocations.As a resultthe *effective energy*constraint which wasadopted in[2]was applied over 3d mesh data points in order to collect the points which satisfy the locally protuberant conditions and to locate convex regions in the facial image. First of all the neighbours for each vertex$P$ in the polygons mesh should be found.This is done by finding the faces that share this vertex.The *effective energy*d_i for each neighbour pointsP_i is calculated using the following formula:

$$d_i = (P_i - P) \cdot N_p = \|P_i - P\| \cdot \cos\theta \; \dots \dots \dots (4)$$

Where θ is the angle between $(P_i - P)$ vector and the normal vectorN_p isthe normal vector of the vertex P, which is calculated according to the common method based on a weighted average of theadjacent faces normal n_f for a face composed of vertices **v**1, **v**2 and **v**3.The face normal is given by the formula (5) which is given in [4]:

$$n_f = \frac{(v1 - v2) \times (v1 - v3)}{\|(v1 - v2) \times (v1 - v3)\|} \dots \dots \dots (5)$$

Next the points that have a negative value of d_i (peaked region)are selected,which leadsto a reduction in the searching space for the nose tip candidate points.The Effective Energy constraint removes most of the points which are unlikely to be the nose tip.

3.1 Local characteristic

There are severalpossible nose tip regionsdue to the fact that the other regions like (chine, cheeks, forehead, ...) have a negative effective energy also. Since the effective energy measure is based on distance and angle,a nose tip candidate vertex should have a small variance value (the amount of dispersion in relation to neighbouring vertices). The next step is to select the vertex with smaller variance value from nose tip candidate regions as shown in figure (3). The mean and variance for each candidate region is calculated as follows:

$$\mu = \frac{1}{n}\sum_{i=1}^{n} d_i \qquad \dots \dots \dots \dots (6)$$

$$\sigma^2 = \frac{1}{n}\sum_{i=1}^{n} (d_i - \mu)^2 \dots \dots \dots \dots (7)$$

Whereμ is the mean,σ^2 is the variance, n is the number of neighbouring vertex and $d_i$is *the effective energy*for a neighbours.

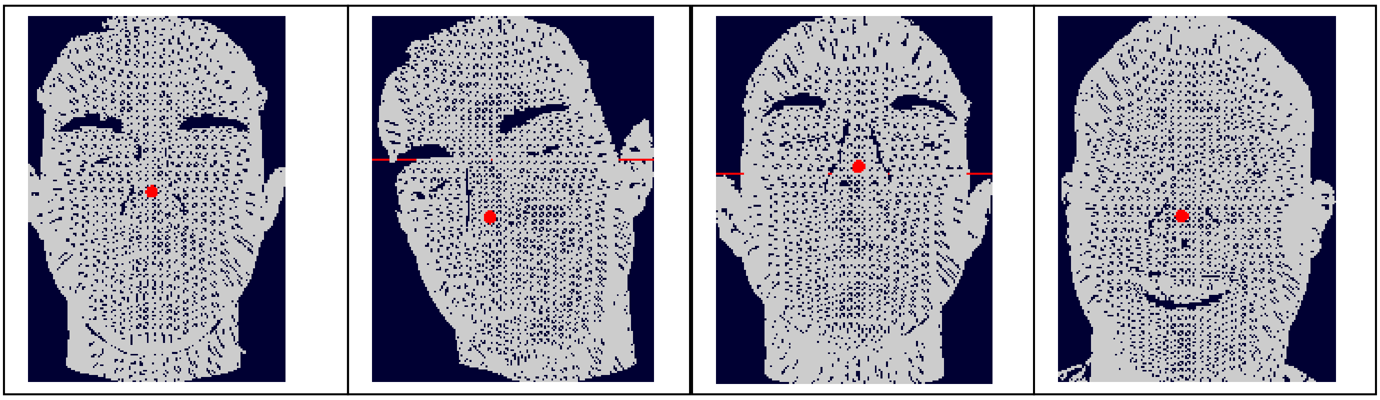

(a)

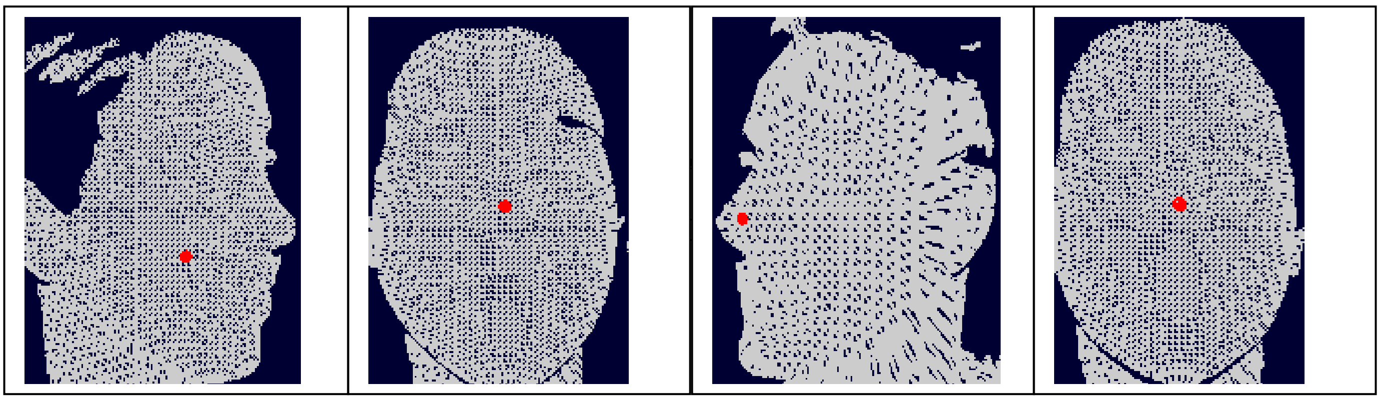

(b)

Fig 3. Nose tip detection based on effective energy calculation a) for FRAV3D database, b)for GAVADB database

4. Nose Tip Detection

The last step in the proposed method for locating nose tip is to apply the Nearest Neighbour algorithm on two candidate regions.The results shown inFigure (4).Figure (4-a) represent the result values that come from two techniquespresented, the green points represent the nose tip candidate which are extracted using the EE method,while the red points represent the nose tip candidate points which are extracted using the shape index descriptor. Figure (4-b)represents the result values after applying the NN-classifier.

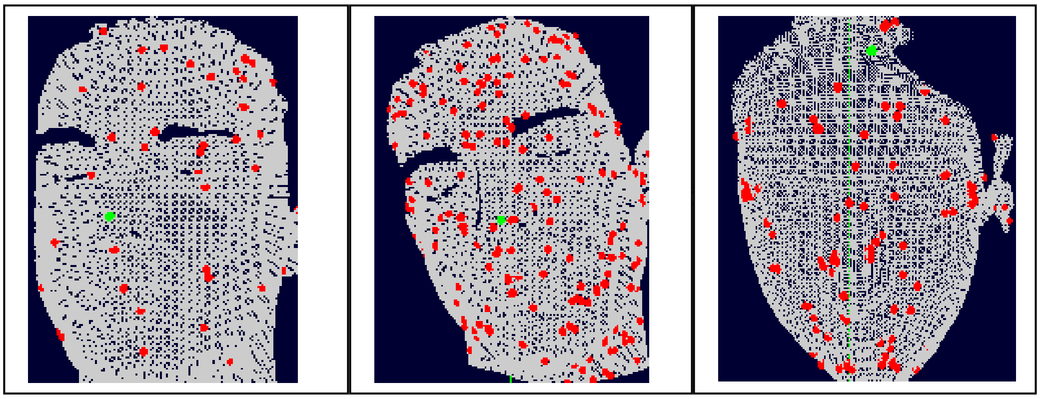

(a) Before applying NN-classifier

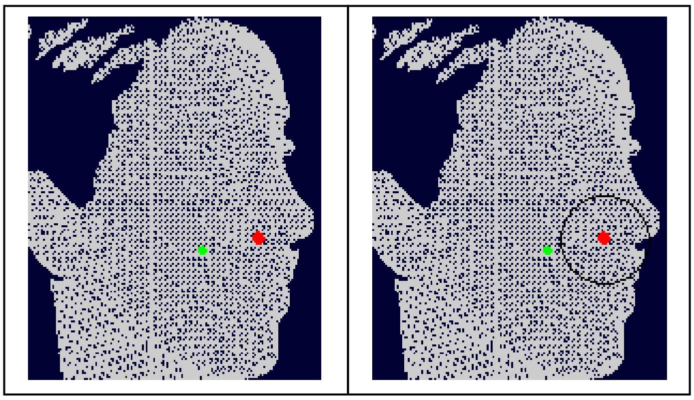

(b) After applying NN-classifier.

Fig 4. Presentation for values of two candidate regions (a) Before applying NN-classifier,(b) After applying NN-classifier.

IV. DATABASE

The proposed nose detection methodwasappliedto two different 3d facial databases: the FRAV3D and GAVADB database[5][6]. The FRAV3D database containeda 3D point cloud of106subjects,with 16 captures per person. In addition, each subject had a different pose (rotation about x-axis,y-axis,z-axis),
which includes facialscans with frontal(1,2,3,4), 25° right turn in Y direction (5,6),5° left turn in Y direction(7,8), severe right turn in Zdirection(9), small right turn in Z direction(10), smilinggesture(11), open mouth gesture(12), looking up turn in Xdirection(13), looking down turn in X direction(14), frontal
images with uncontrolled illumination(15,16) as shown in [5] [11].
Furthermore the experimentshave been conducted over 40 random subjectsof the GAVADB database. Thiscontained 61 individual(45 male and 16 female)including (9)a 3d faceimage for each individual, whereby each image consisted ofa 3dmesh representing thefacial surface. This database did not contain normal of vertices, the normal for each face in a 3d face mesh was found in order to obtain the normal of verticesas described in section 2.3.

The required programmes werewritten in Visual C++ platformwith assistedOpengl graphic library.

V. EXPERIMENTAL RESULTS

Experiment 1: The first test was performed with the FRAV3D and GAVADB databases, which included locating the nose tip of the input 3d facial images using energy effective constraint for N- highest Z-values.The results shown in table (1) representthe detection rate for the nose tip in both databases.

Experiment 2: The second test was performed with theGAVADB database,which included the following:

- Locating nose tipfor the frontal 3d face image and profile sides withnon-acute rotation angles$-35^{\circ} to +35^{\circ}$around (x-axis, y-axis, z-axis)
- Detecting the nose region for non-frontal 3d face images with acute rotation angles$-90^{\circ} to +90^{\circ}$around y-axis.

The testwas performed based on EE constraint and a local shape descriptor for 3d data points. The results shown in table (2) (3) represent the detection rate for the nose tip and nose region respectively.

DB Name	Nose tip detection rate
FRAV3d	96%
GAVADB	66.6

Table 1. Nose tip Detection rate based on EE constraint calculation

DB. Name	Frontal and non frontal posses $(-35^{\circ} to + 35^{\circ})$	
	EE constraint	EE & shape index
GAVADB	66.6%	96%

Table 2.Nose tip Detection rate using EE constraint and Shape index for

DB. Name	Profile Posses $(-90^{\circ} \& + 90^{\circ})$	
	EE constraint	EE & shape index
GAVADB	66.6%	76.8%

Table 3.Nose Region Detection

VI. CONCLUSIONS

In this paper, acombinedschemefor determining nose tip and nose region in a three dimensional facial image has been presented with the presence of expression and pose variations. The local shape information was exploited from each data point using ashape index descriptor.The vertices which have a shape index value within a threshold range were selected.This step produced the first candidate region of the nose tip. Furthermore the energy effective for each neighbouring vertex was calculated.Next, the candidate points that had negative EE and the smallest variance value were selected to collect the second candidate regions of the nose tip.

The final step in the proposed method wasthe application of the Nearest Neighbour classification method on the two candidate regions.In this stepa detection process for nose tip location and nose region was performedwith high rate detection for frontal and semi frontal posses.

REFERENCES

[1] Panagiotis P., Georgios P., Theoharis T. and Ioannis “A 3D Facial Landmark Detection & Face Registration, A 3D Facial Landmark Model & 3D Local Shape Descriptors Approach”, CGL Technical Report, No. TP-2010-01, January 2010.

[2] ChenghuaXu., Yunhong W., Tieniu T. and Long Q., ” Robust Nose Detection In 3D Facial Data Using Local Characteristic”, Image Processing, ICIP '04. International Conference, pp.(1995 – 1998), Vol. 3, 2004.

[3] Parvin A., Ahmad A., Siamak A. and ReihanehA.i, ” The Novel Approach for 3D Face Recognition Using Simple Preprocessingmethod”,InternationalMulticonference of Engineers and Computer Scientist , March (16-18),Hong Kong, 2011.

[4] Ajmal M. and Nick P., “3d Imaging and analysis”, Book, Springer-Verlag London 2012.

[5] http://www.frav.es/databases/FRAV3D/

[6] http://gavab.escet.urjc.es

[7] Yeunghak L. andTaihong Y., “3D Face Recognition Using Multiple Features For

[8] Parama B., Debotosh B., Mita N. and Dipak K.,”A novel approach to nose-tip and eye corners detection using H-K Curvature analysis”, Third International Conference on Emerging Applications of Information Technology (EAIT),IEEE ,2012.

[9] Naoufel W., Haykel B., Youssef M. and Harish B., “ Nose Detection and Face Extraction from 3D Raw Facial Surface Based on Mesh Quality Assessment”,2010.

[10] Wenhao Z., Yanyun W., and BaogangW.,“Nose Detection based Feature Extraction on both Normal and Abnormal 3D Faces”,Computer and Information Technology, IEEE. 2008.

[11] B. H.Shekar , N.Harivinod , M.SharmilaK.andK.Raghurama H.,”3D Face Recognition using Significant Point based SULD Descriptor”,Recent Trends in

[12] Michael D. B., Daniel K., Thibaut W. and Luc V. G., “Real-Time Face Pose Estimation from Single Range Images”,Computer Vision and Pattern Recognition, IEEE Conference ,2008.

[13] C. Dorai and A.K. Jain, “COSMOS—A Representation Scheme for 3D Free-Form Objects” ,IEEE Trans. Pattern Analysis and Machine Intelligence, vol. 19, no. 10, pp.

[14] J. Koenderink and A. van D., “Surface Shape and Curvature Scales,” Image and Vision Computing, vol. 10, pp. 557-565, Oct. 1992.

[15] Augusto S., Alexander C., and Flavio P., “3D Curvature-Based Shape Descriptors for Face Segmentation”,An Anatomical-Based Analysis”, ISVC, pp. 349–358, 2010.

International Journal of Modern Engineering Research (IJMER)
www.ijmer.com Vol. 3, Issue. 4, Jul – Aug. 2013 pp-3091-3095 ISSN: 2249-6645

Vision Based Deep Web data Extraction on Nested Query Result Records

L. Veera Kiran[1], Dr. S. Muralikrishna[2]

[1] *M. Tech (II CSE), MITS, Madanapalle – 517325, A.P, INDIA*

[2]*head & professor, Department of Computer Science & Engineering, MITS, Madanapalle – 517325, A.P, INDIA*

ABSTRACT: *Web data extraction software is required by the web analysis services such as Google, Amazon etc. The web analysis services should crawl the web sites of the internet, to analyze the web data. While extracting the web data, the analysis service should visit each and every web page of each web site. But the web pages will have more number of code part and very less quantity of the data part. In this paper we propose a novel vision based deep web data extraction on nested Query Result Records. This technique extract the data from web pages using different font styles, different font sizes and cascading style sheets after extracting the data the entire data will be aligned into a table using alignment algorithms. The algorithms are pair-wise alignment algorithm, holistically alignment algorithm and nested-structure alignment algorithm.*

Key words: *extracting data, data record alignment, Query Result Records, cascading style sheets.*

I. INTRODUCTION

Data extraction is where data is analyzed and crawled through to retrieve relevant information from data sources (like a database) in a specific pattern. Further data dispensation is done, which involves adding metadata and other data integration; another process in the data workflow. The majority of data extraction comes from unstructured data sources and different data formats. This shapeless data in any form, such as tables, indexes, and analytics. Data extraction development can be challenging. Every organization has important data hidden in corners of the company, sometimes spread across over the world. Once the raw data is grouped, the real work begins. If the association wants to use this information to produce reports, make product decisions, or make intelligent business decisions, must extract the relevant data from source documents, web sites, business news, and many of other sources.

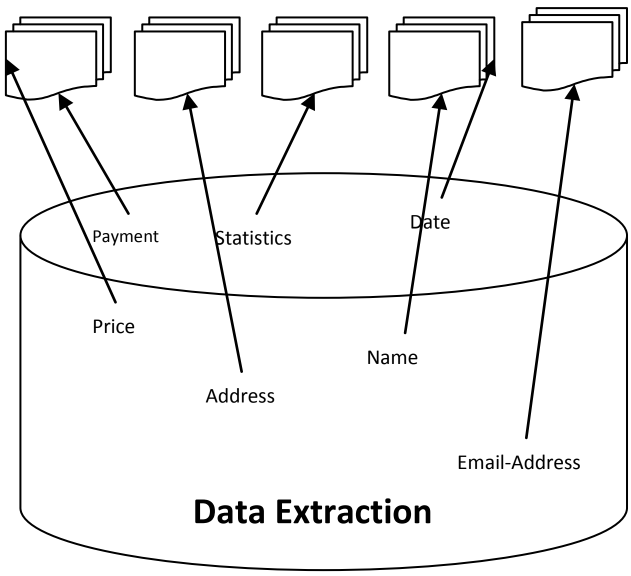

Fig:1. Data Extraction

The above figure explains how the data can be extracted from the data sources and it shows where the data can be retrieved from different online databases. The approach automatically extracts the query result records (QRRs) from HTML pages (to a user query) dynamically generated by a deep web site. The goal is to remove the immaterial information from a query result page. Component 1: Ontology construction for a given domain (fully automatic). Component 2: Data Extraction[1,2,3] using the ontology (fully automatic). Only when the data are extracted and stored in a database can they are easily compared and aggregated using traditional database querying techniques. Accordingly, an accurate data extraction method is vital for these applications to operate correctly. The goal is therefore to acquire sufficient domain knowledge from the query interfaces and query result pages in a domain and to use the acquired knowledge to extract the data instances from the query result pages of the domain. In capable of processing zero or few query results. Almost all existing data extraction methods[1] rely on tag or visual regularity features to do the data extraction. As a result, they require at least two records in a query result page Vulnerable to optional and disjunctive attributes. Optional and disjunctive attributes affect the tag and visual reliability, which may cause data values to be aligned incorrectly. In capable of processing nesting data structures. Many methods can only process a flat data structure and fail for a nested data structure. No label assignment. Though, label assignment is important for many applications that need to know the meaning (i.e., the semantics) of the data. Uses both the query interfaces and the query result pages of web sites from the same domain to automatically construct domain ontology. Identifies query result section in a query result page using the ontology. Segments the query result section into query result records (QRRs), and Aligns and labels the data values in the query result records into a table so that the data values for the same attribute in each record are put into the same column in the table.

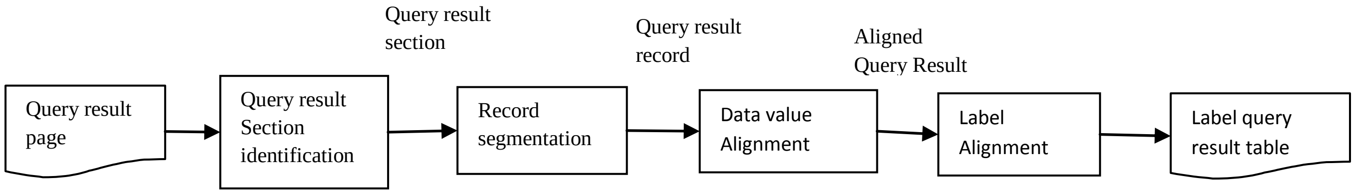

FIG: 2 QRR EXTRACTION FRAMEWORK

The above figure explains about the QRR extraction framework contains a query result page, tag tree construction module constructs a tag tree. Query result section identification identifies all possible data regions, which contain dynamically generated data. Record segmentation module segments the identified data regions into data records. Query result section module selects one of the merged data regions as the one of the merged data regions as the QRRs.

II. BACKGROUND AND RELATED WORK

We propose a systematic approach to build an interactive system for semi-automatic construction of wrappers for Web information sources, called XWRAP. The goal of our work can be informally stated as the transformation of difficult" HTML input[4,5] into program-friendly" XML output, which can be parsed and understood by sophisticated query services, mediator-based information systems, and agent-based systems. A main technical challenge is to discover boundaries of meaningful objects (such as regions and semantic tokens) in a Web doucment, to distinguish the information content from their metadata description, and to recognize and encode the metadata explicitly in the XML output. Our main contribution here is to provide a set of interactive mechanisms and heuristics for generating information extraction rules with a few clicks, and a way to combine those information extraction rules into a method for generating an executable wrapper program

State-of-the-art ontology matching has been designed to cope with nicely structured and well defined ontologies in order to produce high-quality mappings for one pair of sources from one specific domain at a time. Instead, in the case of data that stems from the web, we need approaches that can (simultaneously) deal with heterogeneous and incomplete vocabulary definitions from many different sources dealing with various topics. Further, the vocabularies from the LOD cloud as a whole allow a holistic view on the web of vocabulary terms and thus to create alignments depending on other alignments and dependencies. Resulting alignment information across many sources can be used for web query answering or the discovery of sources with respect to specific topics. However, it is a major scalability challenge to deal with very many vocabulary terms gathered from the linked data web. Therefore, we tackle one the major challenges in ontology matching, namely the matching at a very large scale. We further add the requirement to be applicable to real world web data from various origins instead of two specific sources.

Web pages are intended to be human readable, there are some common conventions for structuring HTML documents. For instance, the information on a page often exhibits some hierarchical structure; furthermore, semi structured information is often presented in the form of lists of tuples, with unambiguous separators used to distinguish the different elements. With these observations in mind, we developed the embedded catalog (EC) formalism, which can describe the structure of a wide-range of semi structured documents.

Web information gathering robots/crawlers, meta-search engines etc; To facilitate the development of these information addition systems, we need good tools for information grouping and extraction. Consider a data has been collected from different Web sites, a conservative approach for extracting data from various Web pages would have to write programs, called “wrappers” or “extractors”, to extract the contents of the Web pages based on a priori knowledge of their format. we have to observe the extraction rules in person and write programs for each Web site.

III. PROBLEM STATEMENT

It cannot process when an advertisement code exists in the middle of Query Result Record (QRR) [1]. The problem is to identify the data part and should extract the web data from the web sites.QRR alignment is performed by a novel three-step data alignment method that combines tag and value similarity.

1. Pairwise QRR alignment aligns the data values in a pair of QRRs to provide the evidence for how the data values should be aligned among all QRRs.
2. Holistic alignment aligns the data values in all the QRRs.
3. Nested structure processing identifies the nested structures that exist in the QRRs.

Semi-structured data can be described as data which is neither raw nor very strictly typed as in traditional data-base systems. In case of HTML, predefined markup tags could be used to control the appearance of untyped text. Therefore we could formalize HTML documents as a class of labeled unordered trees. A labeled unordered tree is a di-rected acyclic graph $T = (V, E, r, \delta)$ where V denotes a set of nodes with a distinguished node r called the root, $E \subseteq V \times V$ a set of edges between two different nodes and a label function $\delta : V \times L$ where L is a string.

3.1. Pre-Processing:

To enhance the pattern extraction accuracy in HTML documents pre-processing has to be performed. For instance, numerous Web pages are not even well-formed with respect to their HTML syntax. We used the Open Source Mozilla Browser and its underlying rendering engine Gecko to convert HTML documents into valid XHTML. The reason is that most HTML authors verify their pages with standard browsers before publishing their sites. To analyze T^* we work on an abstract representation where each HTML tag is restricted to its tag name ignoring attributes. Moreover, trimmed text between two tag elements is represented by a new abstract element denoted as <TEXT> element tag.

3.2. Pattern Search Strategy:

One common technique to measure the similarity between two plain sequences Si, Sj with length n,m, respectively, is the edit-distance, which computes the minimal cost to transform one sequence into the other, utilizing uniform cost operations insert, delete and rename. Using Dynamic Programming techniques we can compute an n×m edit distance matrix D in O(nm) time. A typical characteristic of data records is that single data record instances vary in optional or repetitive subparts. For instance, optional or multiple authors in the description of a book data record.

3.3. Primitive Tandem Repeats:

Consequently tandem repeats build an array of consecutive repeats. If we additionally claim that the repeats have to be primitive then α may not contain shorter repeats. In the context of HTML tags we only consider primitive tandem repeats with $|\alpha| \geq 3$. For the running example we disregard this condition owing to space constraints. We implemented the algorithm described in based on suffix trees to identify all z primitive tandem repeats in a sequence of length n in O(n + z) time be-fore computing the edit-distance. This assures that additional repetitive subparts contained in both sequences do not unduly increase the edit-distance.

IV. EXTRACTION RULE GENERATOR:

The system includes three components, an extraction rule generator which accepts an input Web page, a graphical user interface, called pattern viewer, which shows repetitive patterns discovered, and an extractor module which extracts desired information from similar Web pages according to the extraction rule chosen by the user.

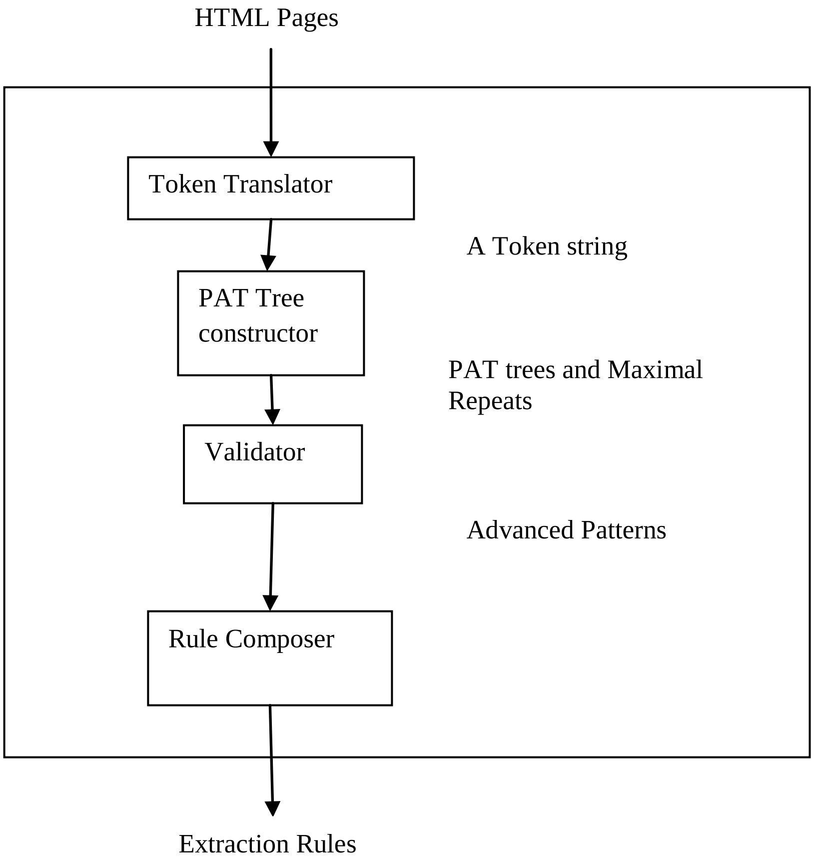

Fig:3 EXTRACTION RULE GENERATOR:

The core techniques of pattern mining are implemented in the rule generator. It includes a translator, a PAT tree constructor, a blueprint discover, a prototype validator, and an extraction rule composer. The results of regulation extractor are extraction rules discovered in a Web page. The GUI can allow users to view the information extracted by each extraction rule. Once the user selects a objective extraction rule conforming to his information desire, the extractor module can use it to take out information from other pages having similar structure with the input page.

4.1. Translator:

HTML tags are the basic components for document presentation and the tags themselves carry a certain arrangement information, it is spontaneous to examine the tag token string formed by HTML tags and regard other non-tag text content between two tags as one single token called TEXT. Tokens often observe in an HTML page include tag tokens and text tokens, denoted as Hyper Text Markup Language(<tag_name>) and Text(_), respectively.

4.2. PAT Tree Construction:

PAT tree to discover repeated patterns in the encoded token string. A PAT tree is a Practial tree (Practical Algorithm to Retrieve Information Coded in Alphanumeric) constructed over all the possible suffix strings. A Practical tree is a particular implementation of a compressed binary (0,1) digital tree such that each internal node in the tree has two branches: zero goes to left and one goes to right. Like a suffix tree, the Patricia tree stores all its data at the external nodes and keeps one integer in each internal node as an indication of which bit is to be used for branching.

4.3. Pattern Discoverer:

All the leaves in a subtree share a regular prefix, for the path that leads from root to the root of the subtree. Each path label of an interior node represents a repeated sequence in the input. Therefore, to discover recurring model, to discover only needs to examine path labels to determine whether or not they are maximal repeats. Since every inner node in a PAT tree indicates a branch, it implies a different bits are common prefix between two suffixes.

V. RESULTS:

Web database generates a webpage which can stores the users data, automatically it extracts when the data needs for users.

FIG: 4 Front Page for Amazon Books World

The above figure explains that whatever the data needs from the webpage the information will extracts from the database, multiple databases are internally linked with each other to get much more information from the users webpage. From the URL maintains the link which is helpful for opening the webpage to extract the required information. If any information is needed the url link can be modified in the Amazon browser. The whole data can be stored in the mysql server only. This is the backup for storing the required data.

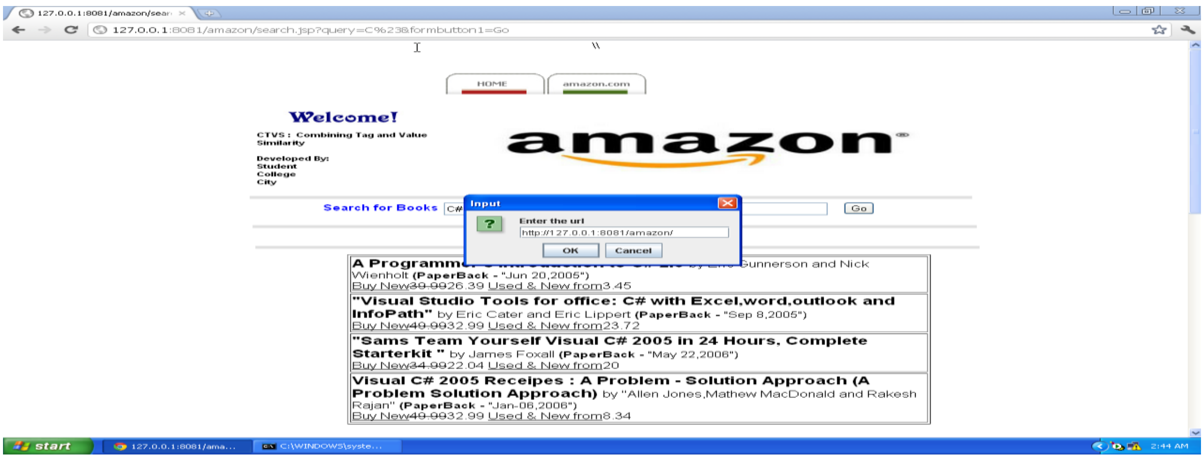

FIG: 5 Amazon Books World Webpage Extraction of Records from Website

VI. CONCLUSION

The ontology for a domain is constructed by matching the query interfaces and the query result pages among different web sites. The ontology is used to do the data extraction. For query result section identification, Ontology assisted data extraction finds a subtree, which has the maximum correlation with the ontology, in the HTML tag tree. For data value alignment and label task, it uses a maximum entropy model, environment, tag structure and visual information are used as features for the maximum entropy model. Experimental results show that ODE is very effective and can satisfactorily. we propose a novel vision based deep web data extraction on nested Query Result Records. This technique extract the data from web pages using different font styles, different font sizes and cascading style sheets after extracting the data the entire data will be aligned into a table using alignment algorithms.

REFERENCES

[1] "Combining Tag and Value Similarity for Data Extraction and Alignment" Weifeng Su, Jiying Wang, Frederick H. Lochovsky, Member, IEEE Computer Society, and Yi Liu IEEE TRANSACTIONS ON KNOWLEDGE AND DATA ENGINEERING, VOL. 24, NO. 7, JULY 2012.

[2] A. Arasu and H. Garcia-Molina, "Extracting Structured Data from Web Pages," Proc. ACM SIGMOD Int'l Conf. Management of Data, pp. 337-348, 2003.

[3] R. Baeza-Yates, "Algorithms for String Matching: A Survey," ACM SIGIR Forum, vol. 23, nos. 3/4, pp. 34-58, 1989.

[4] R. Baumgartner, S.Flesca, and G. Gottlob, "Visual Web Information Extraction with Lixto," Proc. 27th Int'l Conf. Very Large Data Bases, pp. 119-128, 2001.

[5] M.K. Bergman, "The Deep Web: Surfacing Hidden Value," White Paper, BrightPlanet Corporation, http://www.brightplanet. com/resources/details/deepweb.html, 2001.

[6] P. Bonizzoni and G.D. Vedova, "The Complexity of Multiple Sequence Alignment with SP-Score that Is a Metric," Theoretical Computer Science, vol. 259, nos. 1/2, pp. 63-79, 2001.

[7] D. Buttler, L. Liu, and C. Pu, "A Fully Automated Object Extraction System for the World Wide Web," Proc. 21st Int'l Conf. Distributed Computing Systems, pp. 361-370, 2001.

[8] K.C.-C. Chang, B. He, C. Li, M. Patel, and Z. Zhang, "Structured Databases on the Web: Observations and Implications," SIGMOD Record, vol. 33, no. 3, pp. 61-70, 2004.

[9] C.H. Chang and S.C. Lui, "IEPAD: Information Extraction Based on Pattern Discovery," Proc. 10th World Wide Web Conf., pp. 681-688, 2001.

[10] L. Chen, H.M. Jamil, and N. Wang, "Automatic Composite Wrapper Generation for Semi-Structured Biological Data Based on Table Structure Identification," SIGMOD Record, vol. 33, no. 2, pp. 58-64, 2004.

[11] W. Cohen, M. Hurst, and L. Jensen, "A Flexible Learning System for Wrapping Tables and Lists in HTML Documents," Proc. 11th World Wide Web Conf., pp. 232-241, 2002.

[12] W. Cohen and L. Jensen, "A Structured Wrapper Induction System for Extracting Information from Semi-Structured Documents," Proc. IJCAI Workshop Adaptive Text Extraction and Mining, 2001.

[13] V. Crescenzi, G. Mecca, and P. Merialdo, "Roadrunner: Towards Automatic Data Extraction from Large Web Sites," Proc. 27th Int'l Conf. Very Large Data Bases, pp. 109-118, 2001.

[14] D.W. Embley, D.M. Campbell, Y.S. Jiang, S.W. Liddle, D.W.Lonsdale, Y.-K. Ng, and R.D. Smith, "Conceptual-Model-Based Data Extraction from Multiple-Record Web Pages," Data and Knowledge Eng., vol. 31, no. 3, pp. 227-251, 1999.

[15] A.V. Goldberg and R.E. Tarjan, "A New Approach to The Maximum Flow Problem," Proc. 18th Ann. ACM Symp. Theory of Computing, pp. 136-146, 1986.

[16] D. Gusfield, Algorithms on Strings, Trees, and Sequences: Computer Science and Computational Biology. Cambridge Univ. Press, 1997.

Network Forensic Investigation of HTTPS Protocol

Manesh T[1], Brijith B[1], Bhraguram T M[1], R Rajaram[1], Bhadran V K[2]
[1]*Shankara Centre for Research in Information Science*
Adi Shankara Institute of Engineering & Technology,Kalady, Ernakulum, Kerala-683574,
[2]*Resource Center for Cyber Forensics CDAC Trivandrum, Kerala-695033*

ABSTRACT : *Nowadays a large amount of personal and business transactions are done electronically through secured internet communication with HTTPS Protocol. The internet offers computer users access to a wealth of information and reaches in to the heart of many organizations. In this context, there are many possibilities for having different malicious activities or attacks that may occur through the HTTPS protocol. Usually it is very difficult to see or recreate HTTPS network sessions to verify its content as part of the forensic analysis. Network analysts must be able to see and test the packet data when a malicious network usage is identified and produce actual session by recreating the original data between users as part of forensic analysis. So we need an efficient forensic system to perform this kind of content analysis. The proposed novel technique can be used for content level observation of HTTPS protocol and regenerate original malicious HTTPS session between users for network forensic investigations.*

Keywords: *Network Forensics, Packet Reordering, HTTPS Traffic Analysis, TLS Parser, Pcap File.*

I. INTRODUCTION

Network forensics is the study of analyzing network activity in order to discover the source of security policy violations or information assurance breaches [3]. Analysis of the individual traffic flows and their content is essential to a complete understanding of network usage. Many tools let you view traffic in real time, but real-time monitoring at any level requires significant human and hardware resources, and doesn't scale to networks larger than a single workgroup. It is generally more practical to archive all traffic and analyze subsets as necessary. The data stored in the networks can give us a lot of information about the interests, patterns of behavior and even whereabouts of the attacker .This process is known as reconstructive traffic analysis, or network forensics [3]. In practice, it is often limited to data collection and packet level inspection; however, a network forensics analysis tool (NFAT) can provide a richer view of the data collected, allowing you to inspect the traffic from further up the protocol stack. Capturing network activity for forensic analysis is simple in theory, but relatively trivial in practice. Not all the information captured or recorded will be useful for analysis. Identifying key features that reveal information deemed worthy for further intelligent analysis is a problem of great interest to the researchers in the field. Tools like Wire Shark, Packetizer will give enough information for the forensic investigator. But the amount of time that he needs to spend

On these tools is very high for processing large volume of data. So it is often impractical to perform a complete forensic analysis on the entire data due to time constraints and limited human resources. However, good analysis method, visual interfaces and visualizations can vastly improve the time it takes to complete a task, reduce errors, increase concentration and allow a better knowledge of the data. Now day's majority of the network traffic in the internet started using encrypted channels like SSL for communication. Majority of the tools which are performing the analysis of this traffic is doing that in real time, which requires significant human and hardware resources [6] .So a tool is required for performing this analysis in offline mode. A network that has been prepared for forensic analysis is easy to monitor, to trace its security vulnerabilities and configuration problems. In this proposed work, a tool for network forensic investigation of HTTPS protocol is developed which has been successful in recreating the original HTTPS network sessions for tracing any malicious activities. It also allows the best possible analysis of security violations. Most importantly, analyzing a complete record of your network traffic with the appropriate reconstructive tools provides context for other breach-related events. Rest of the paper is organized as follows; section 2 deals with related work, section 3 describes HTTPS traffic analysis process, Section 4 gives detailed working of HTTPS Analyzer, Section 5 provides performance evaluation of proposed tool with existing packet analysis tools, Section 6 gives conclusion followed by references.

II. RELATED WORK

2.1 Network Forensic Analysis

Network Forensic Analysis Tools permits administrators and investigators to monitor networks, gather all information about anomalous traffic, assist in network crime investigation and help in generating a suitable incident response. Forensic tools also provide support in analyzing the inside illegal network event and misuse of resources, predict network pattern in near future, executes risk assessment processes, judging the network performance, and thus help in protecting the intellectual propriety. An ideal network forensic investigation tools is expected to trace out what exactly happened during a recently past network sessions [5]. This may include replaying of network session, identifying different protocols, sessionizing and auditing the network, locating source of any illegal network activities and monitoring network characteristics etc. Network forensics is being researched for a decade but it still seems to be very young science and many issues like IP spoofing, Mac spoofing etc, are not very clear, ambiguous and found to be still an open problem.

2.2Existing Network Forensic Analysis Environments

There exist many network forensic investigation tools which are suitable to investigate different type of protocol and networks. These tools may contain important modules like network monitoring, packet capturing, packet sessionizing, packet reordering, packet reconstruction specific to internet protocols, traffic auditing and evidence manipulation etc. An extensive study on various approaches is made about the development of network forensic investigation tools and corresponding packet reordering methods which are given at the end of this section. Most of these methods are found to be shareware with limited functions, and uses comparatively complex methods for reordering the packets and managing the retransmitted or duplicate packets.

Vicka Corey and Charles Peterman (2004) initially proposed a network forensic analysis tool which addresses how to integrate network security tools and forensic tools to work towards generating valuable evidences in an efficient manner. They presented some security, legal issues and how to manage with forensic tools. They make use of output from security tools, scanners and intrusion detection system as input to forensic section for analysis. They also presented how to sessionize the network capture and parsing of protocols in an efficient manner [3].

Jacob Pennock (2005) proposed an approach for developing remote forensic system to monitor and perform forensic investigation remotely in the network. This proposal mainly concentrates on how data can be collected and preserved for further forensic analysis remotely. This method also addresses execution of forensic analysis in three modes like on demand, periodically and automatic in response to an incident.

Endicott-Popovsky (2007) presents a conceptual framework for embedding digital forensics [11] in the enterprise, where policies, procedures, practices, mechanisms, and awareness training are driven by a system goal expressed as' preserving the ability to prosecute malicious cyber intrusion successfully, while reducing current effort expended on digital forensic investigations that have become too resource intensive. This results in a forensically ready network or network forensic readiness.

J. Scott Haugdahl (2007) proposed an approach towards network forensics which provides detailed case study in identifying many faces of forensics, different possible areas of an organization or network from which probable evidences can be found easily. The proposal includes the psychological, technical, organizational, and contextual factors in developing the forensic tools.

Carol Taylor and Deborah A Fricke (2007) proposed an approach towards digital forensics specification based on forensic policy definition. Their methodology borrows from computer security policy specification, which has accumulated a significant body of research. They first define the process of specifying forensics properties through a forensics policy and then present an example application of the process. This approach lends itself to formal policy specification and verification, which would allow for more clarity and less ambiguity in the specification process.

III. HTTPS TRAFFIC ANALYSIS PROCESS

HTTP traffic analysis is increasingly hampered by the ubiquitous use of encrypted channels by legitimate and illegitimate network traffic. Both types of traffic are frequently tunneled over application-layer encryption mechanisms, generally using the ubiquitous TLS (SSL) protocol. While it is highly desirable to secure http traffic in this way, it is not an unmitigated benefit as this generally implies that monitoring will be considerably less effective unless special precaution is taken. As a result the traditional network forensics tools are largely limited to recording external characteristics (source and origin addresses and ports, time and traffic patterns), but with little insight into content and purpose of the traffic [8].This section of the tool is dealing with the analysis of the HTTPS traffic in the LAN and to obtain the information from the encrypted traffic that is passing through the network. This section contains two activities for performing this analysis. One is a HTTPS certificate handler (MITM) and the other is HTTPS analyzer. The design of the section is shown in the figure (1).

3.1 System Design for HTTPS Analysis

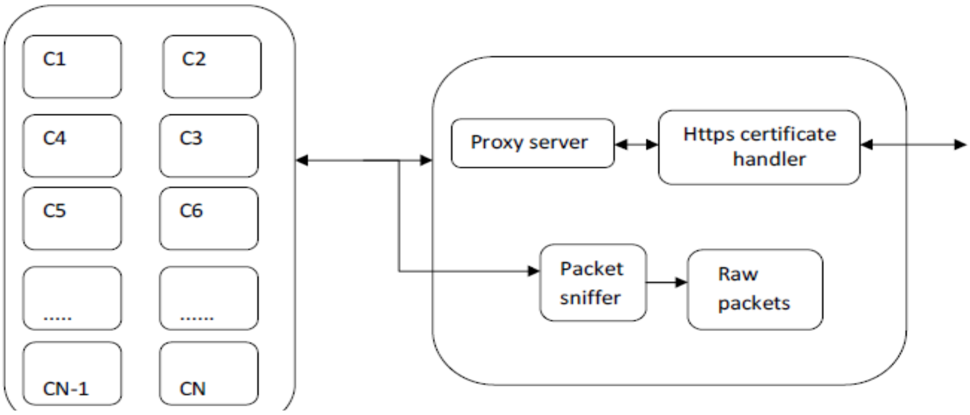

Fig 1. System Design for HTTPS analysis

3.2 Working of SSL

SSL is an Enterprise Standard adopted by millions of websites to safeguard their online transaction. It ensures the privacy and integrity of transmitted data during the transaction process. Each web server requires one SSL certificate to protect its safety of linkage. SSLscheme uses public and private keys to create an encrypted channel and can be setup at the time of the transaction. Figure (2) shows corresponding SSL Handshake process.

3.3 SSL Handshake Process

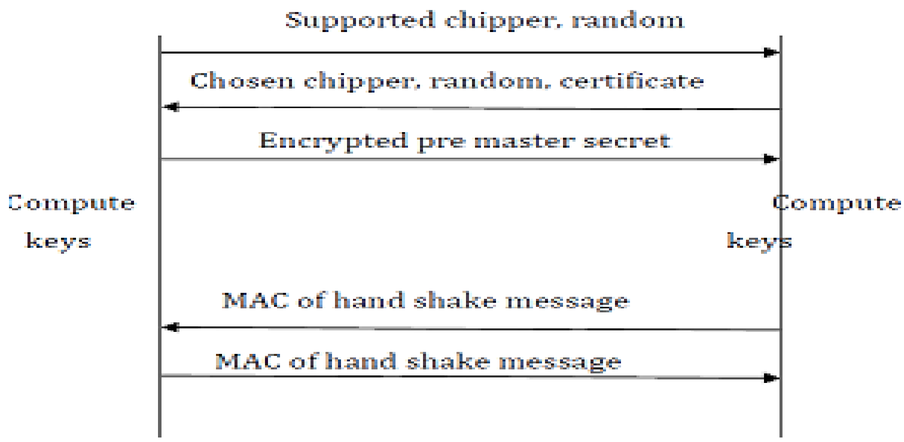

Fig 2. SSL Initial handshake process

The connection establishment is as follows

1. The client sends the server a list of the algorithms its willing to support, along with a random number used as the input to the key generation process
2. The server chooses a chipper out of the list and sends it back along with a certificate containing server's public key.

The certificate also provides servers identity for authentication purpose and the server supplies a random number which
is used as part of the key generation process

3The clients verify the server's certificate and extract the server's public key. The client then generates a random secret
string called pre master secret and encrypts it using the server's public key. It sends the encrypted per master secret
to the server

4 The client and server independently compute the encryption and Mac keys from the pre master secret and the client and server random values

5. The client send a mac of all the hand shake message to the server

6. The server sends a mac of all hand shake messages to the client

The main goals of these steps are to agree on a set of algorithm and to establish a set of cryptographic keys. Step 1 and 2 accomplishes the first goal. Second goal is accomplished by step 2 and 3.in step two the server provide the client with its certificate, which allows the client to transmit a secret to the server. After step 3 the client and the server both will share the premaster secret. Step 3 is the key step in the whole handshake. All the data that is going to be protected depends on the security of the pre master secret. The proposed tool willtry to exploit this section so as to decrypt the traffic and perform the web forensic analysis

3.4 Certificate Handler

This section is used for handling the SSL certificate and thereby providing facility for HTTPS analyzer to analyze the encrypted SSL traffic. From the above steps of SSL hand shake, it is identified that the MAC key is used for the encryption of the SSL channel. Fromthe step four, it is observed that the Mac keys are calculated using the pre master secret, servers and client's random number from which two random numbers are directly derived. But there master secret in encrypted using the server's public key. So in order to get the premaster secret it needs to have server's private key [1]. In order to decrypt the encrypted premaster secret key value, the methods exploiting the step three of the hand shaking. Here, tool uses a man in the middle type of attack as shown in figure (3) in which the *certificate handler* will be acting MITM attacker. Certificate handler acts as a proxy to the targeted PC/suspect. All traffic from the targeted PCor suspect will be redirected to the certificate handler. Therefore, it can collect the genuine certificate from SSL Server if the targeted PC access to the SSL Server. At the meantime, the certificate handler returns with its own generated certificate, i.e. the certificate handler will intercept the hand shaking process and it will establish two separate SSL connections

- One from the client to the certificate agent
- Another from the certificate agent to the server

In the first connection the certificate agent will use its own fake SSL certificate and the second connection will be using the original certificate from the server

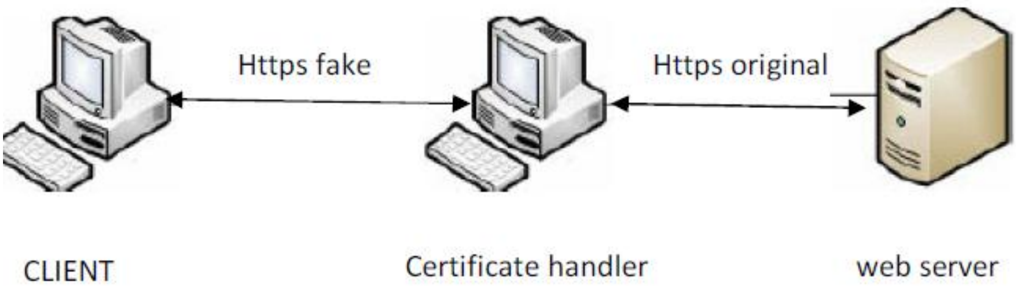

Fig 3. MITM attack using certificate handler

The certificate handler will have a root certificate (CA certificate) that is made as trusted in the target host system. For each site the client trying to access through the SSL connection the certificate handler will dynamically create a self-signed certificate with the certificate handlers CA extensions using OpenSSL library using the same private key. As the tool have already made the CA certificate as trusted in the target host the browser will not give any exception. So the user will not get any https error message. The steps for making the root certificate as trusted in the target host are given in the next section.3.5 Adding the Root Certificate to the Trust Store in the Target HostSetup a Local Certificate Management Console:

- Start, Run: mmc
- From the Microsoft Management Console:
- File, Add/Remove Snap-in…
- Click Add…
- Select Certificates and click Add
- Make sure My User Account is selected and click Finish
- Again, make sure Certificates is selected and click Add
- This time select Computer Account and click Next
- Make sure Local Computer is selected and click Finish
- Click Close

- Click OK

Now we have a Management Console that looks like as figure (4).

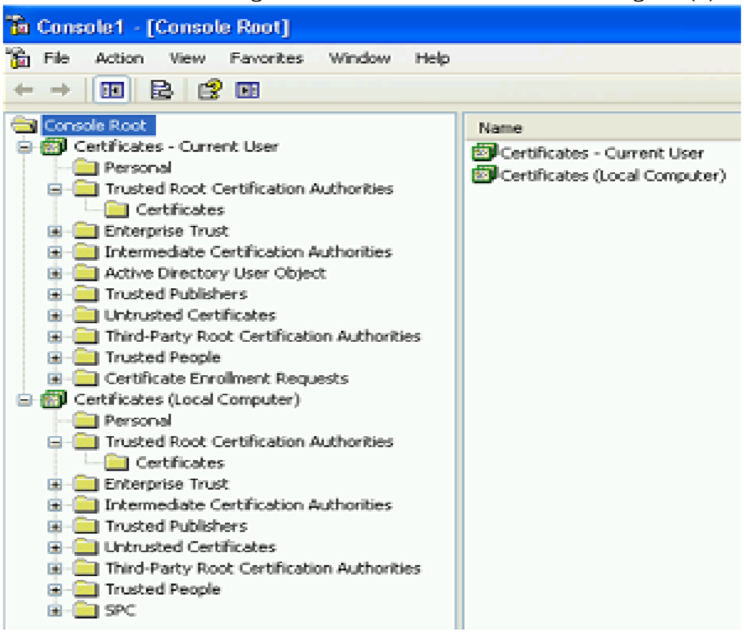

Fig 4. Certificate management console

You can now save this:

- File, Save
- Enter a name: Local Certificate Management
- Click Save
- Copy the root certificate (CA certificate)to the target system
- Open the Local Certificate Management Console that we setup earlier.
- Open Certificates – Current User, Trusted Root Certification Authorities, Certificates
- Right click in the Certificate Area on the right and choose All Tasks, Import…
- Browse to the root certificate file
- For Certificate Store, make sure place all certificates in the following store is selected
- with Trusted Root Certification Authorities
- Click Yes to the security warning
- We can now see this certificate in our Personal Trusted Root Certification Authority
- Store.

Now this certificate is added to the trust store in the target computer. So it will not give anyhttps error while the certificate handler is performing the MITM attack.

IV. Working of Https Analyzer

This is the main section of HTTPS analysis process. HTTPS analyzer works on the raw packets that are collected from the proxy system and perform https analysis on those packets. The main goals of this section are to calculate the session key used for the traffic encryption, decrypt the encrypted HTTPS traffic and produce the forensic result of the traffic. The session keys are calculated on the basis of the initial handshake messages that are used for establishing the SSL session between the client and the server [1]. In order to calculate the session key, section needs to have the private key of the certificate used for the SSL connection .So only the legitimate users who are having access to private key can perform this task. The following flow diagram will give an idea about the steps followed by the HTTPS analyzer for performing the HTTPS forensic analysis.

4.1. Work Flow Diagram for Https Analyzer

4.1.1 Pcap File

This file consists of all the Ethernet packets that we have captured from the Ethernet card. This can be done by using the capture section in our software or using some other software's like Wire shark that support Pcap format. The analysis process is performed on this file. This can be done either using our software in the system in which the analysis is to be performed or by capturing the packets using some other software and export that file to a system that contains our software. If the tool needs to get all the packets that are passing through the Ethernet card then the tool must perform the capture in promiscuous mode.

4.1.2. Filter HTTPS Packets
This is done on the basis of the port that is set on the proxy for the HTTPS traffic. The tool will filter those TCP packets that having either the source port or the destination port as the HTTPS port

4.1.3. Separation of each Section
In order to perform the analysis process, the tool separates each connection that is created for the http traffic. This can be done using the combination of the source port and the destination port

4.1.4 Reordering the packets
Due to the multipath routing or parallelism at the routers, the packets that we have collected in the Pcap file may be out of order. So in order to perform the analysis, this section reorders those packets. The algorithm is given below briefly as Work flow diagram of HTTPS analyzer. It consists of two phases. First four steps constitutes first phase and second phase starts at fifth step onwards.

4.1.5 Work Flow diagram of HTTPS Analyzer

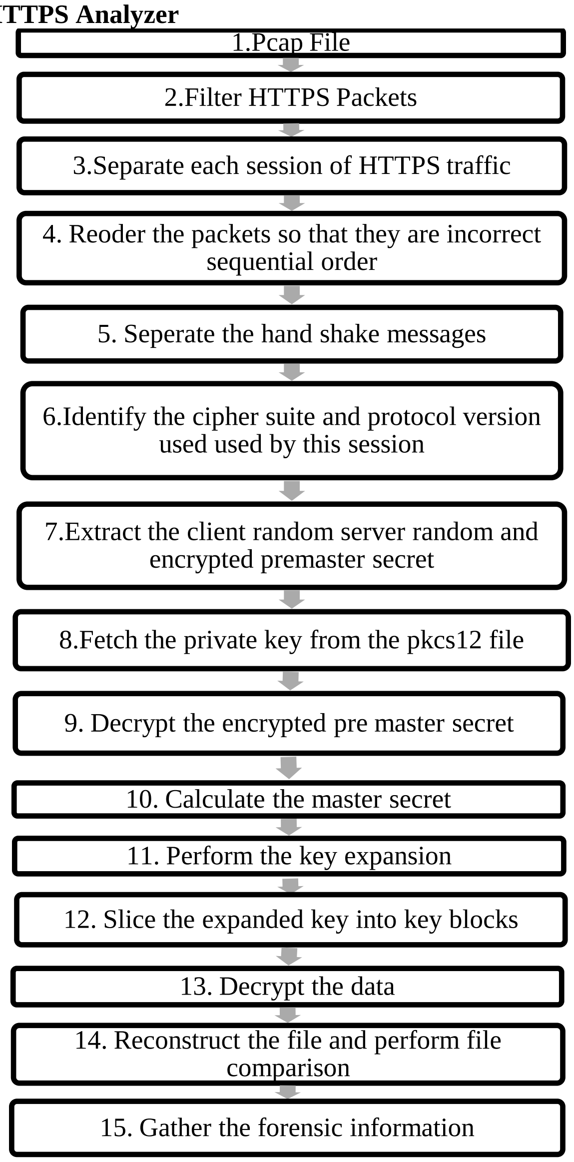

Fig.5 Flow diagram of HTTPS Analyzer

4.1.6 Separating the hand shake messages and extracting required fields

This section needs to collect the handshake message from client to server and from server to client. This is done using a TLS parser. The design of TLS parser will be explained later. Using this TLS parser, the tool extracts the protocol version, cipher suite, client random, server random and the encrypted premaster secret. These five fields are required for the key generation process and the decryption of the traffic [4]. In order to extract these fields, the tool needs to parse three types of handshake message Client hello, Server Hello, Client key Exchange .Details of these messages are given below

4.1.7 Client Hello Message

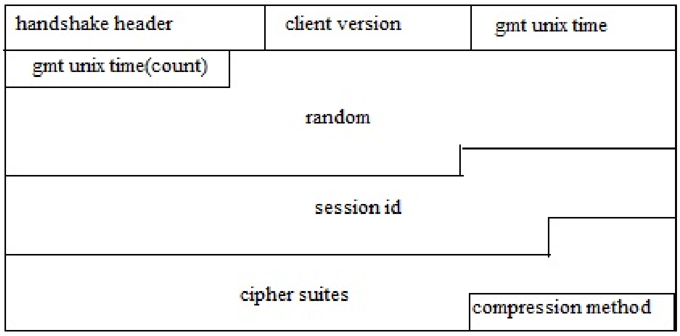

Fig 6. Format of Client Hello Message

The client hello message as shown in figure (6) is sent when a client connects to a server to initiate the handshake. After the common handshake header is the client version, which specifies the highest version of the protocol that the client supports. SSL and TLS Implementations need to support all previous versions of the protocol as well. Then comes a random number which consists of the current GMT time-stamp and 28 bytes generated by a cryptographically secure pseudo number generator. After the random number comes the session id. If supplied, this can be used to perform an abbreviated handshake sequence by reusing key material that was previously negotiated between the client and the server. Next comes the list of cipher suites that the client is prepared to use. Cipher suites define the encryption and hashing functions that will be used by the connection once the handshake concludes as well as the key exchange method used during the handshake. They are represented by two 8bit numbers which is documented in the SSL or TLS specification or by some additional specification. For example TLS RSA WITH RC4 128 SHA is a cipher suite that uses RSA for key exchange, RC4 as the bulk encryption algorithm, SHA1 as the hashing function for the MAC. From this client hello, the tool extracts the client random number.

4.1.8 Server Hello Message

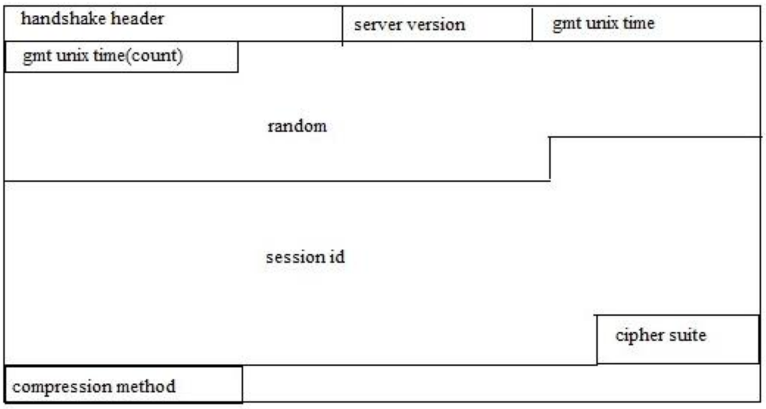

Fig 7. Format of Server Hello Message

The server hello shown in figure (7) is sent by the server in response to a client hello. The server version is the client version if it is supported by the server, else the highest version supported by the server. Then there is a random number consisting of the GMT time-stamp and 28 bytes generated by a cryptographic random number generator. Next is the optional session ID. If this is the same as the session ID sent by the client in the client hello then an abbreviated handshake will be performed using key material cached by both the client and the server. If empty, it indicates that the server is not willing to perform an abbreviated key handshake. If the session ID not empty then tool cannot decrypt the traffic because the traffic is using the cached key material. Finally the message includes the cipher suite and compression method selected by the server from the lists provided in the client hello. From this message, tool extracts the protocol version, cipher suite and the server random number.

4.1.9 Client key exchange

Th3 client key exchange message format is shown in figure (8) is sent immediately after the client certificate is sent. It has two variants, one for when RSA is used as the key-exchange algorithm, and one for when Diffie-Hellman is used. Here the tool uses RSA. When RSA is used, the client key exchange message consists of the header handshake followed by PKCS #12 encoded pre-master secret that is encrypted using the server's key, as sent in the server certificate message. The handshake header is not encrypted. The pre-master secret consists of the maximum version supported by the client followed by 48 random bytes generated by a cryptographic random number generator. Here the tool extracts encrypted premaster secret.

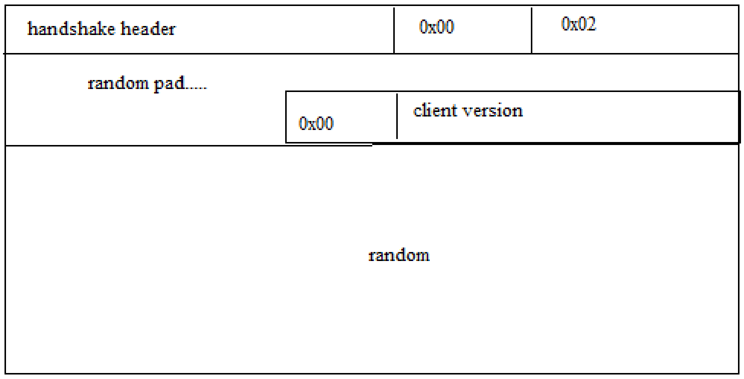

Fig8 Client key exchange packet format

4.1.10. TLS Parser Overview

A TLS parser is developed for separating the fields in the HTTPS connection so that the tool can retrieve the basic information about the connection and the data required for the decryption on the HTTPS traffic. The basic functionality of the TLS parser is to retrieve features from the data like server random number, client random number, cipher suit, protocol version, encrypted application data, encrypted premaster secret [4]. The TLS parser will first convert the data in to corresponding hex value .This hex value is parsed in order to get the details. The structure of the parser is shown in the figure (9) below.

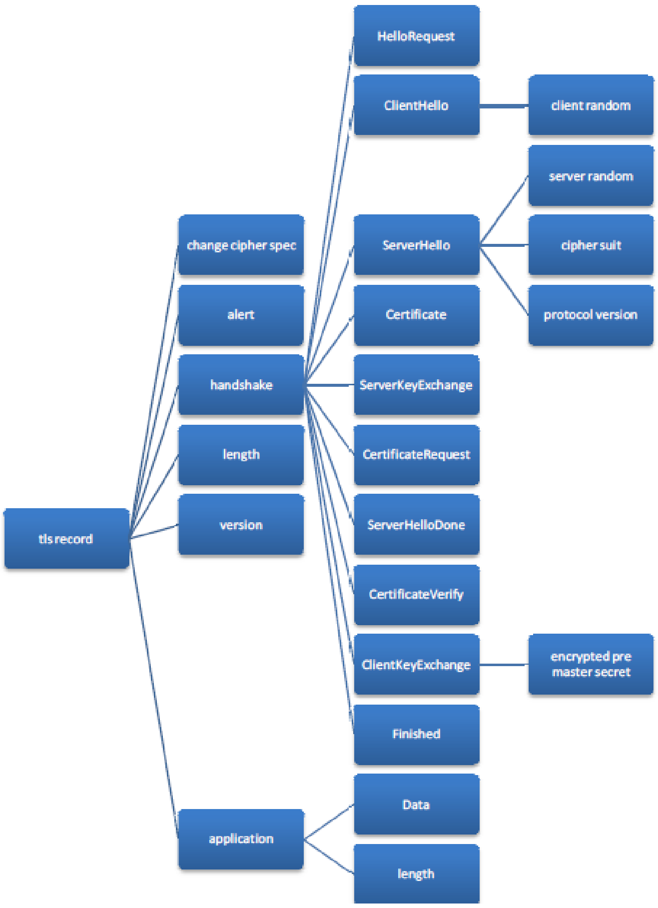

Fig 9. TLS Parser Design

4.1.11 Decryption of the premaster secret

As already specified in the third step of the SSL handshake the pre master secret is encrypted using the server's public key. As the key with us in the pkcs12 file, the tool fetches the private key from the file. At this point, tool will identify the algorithm used for encryption of the premaster secret from the cipher suite and perform the decryption operation of the encrypted premaster secret using the specified algorithm and obtain the original premaster secret.

4.1.12 Key Material Generation

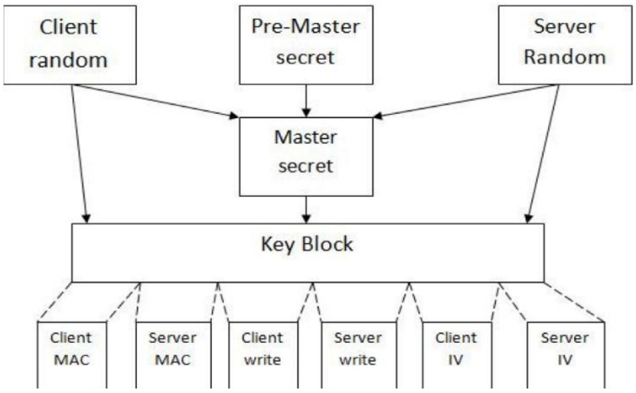

Fig10. Key Derivation

Key material generation as shown in figure (10) is used to generate the secret material that will be used as keys and input vectors to encrypt and verify records. The inputs to key generation are the client and server random, and the pre-master secret, sent in the client and server hello, and client key exchange messages respectively. The first step in the key material generation is to transform the pre master secret in to the master secret. This is done by applying the pseudo random function PRF to the pre master secret, client random and server random: Master_Secret=PRF (pre_master_secret, “master secret” ,client_random + server_ random)[0..47]. Now the tool uses the PRF with the master secret to obtain the key block. Key_block=PRF (Master_Secret, “key expansion”, server_ random +client_random). The key block is as many bytes long as is needed and is divided up into MAC secrets, symmetric encryption keys, and input vectors for blocking used with symmetric encryption [11]. These are, in order, the client write MAC secret, server write MAC secret, client write key, server write key, client write IV and server write IV. Unneeded values are omitted.

4.1.13 Pseudo Random Function (PRF)

Pseudo Random Function (PRF) is at the heart of key material generation. It takes three arguments, a secret a fixed ASCII string and a seed as in PRF (secret, label, seed). First the secret part is split in to two halves S1 and S2.Each half is used as a secret component in an expansion function P_Hash which is based on HMAC. P_hash generates an arbitrary length byte string by the process shown below.
P_hash(secret,seed)=HMAC_hash(secret,A(1),A(0))+
HMAC_hash(secret,A(2),A(0))+
HMAC_hash(secret,A(3),A(0))+….
A(): A(0)= seed
A(i)=HMAC_hash(secret,A(i-1))
HMAC_hash means HAMC using a given hash algorithm,e.g..,
HMAC_MD5 means HMAC using MD5. This is run as many times as desired. So to produce 48 bytes of output, it would be run 3 times for MD5, and for SHA-1 it would also be run 3 times and the last 12 bytes of output would be discarded. Now PRF is constructed by XORing a P_MD5 and a P_SHA-1:
PRF (secret, label, seed) =P_MD5 (S1, label + seed)$\oplus$ P_SHA-1(S2, label + seed); [11].
14) SSL v3 key derivation
SSL v3 Key derivation is similar to TLS key derivation, except that the PRF is replaced with a series of expansion functions based on a combination of MD5 and SHA-1[11]. The use of constants “A”, “BB”, etc. ensures that the output of each digest is different, even though the secret data is the same. The process is shown below Master Secret = MD5 (pre master secret + SHA1 (“A”+ pre master secret +client random +server random)) + MD5 (pre master secret + SHA1 (“BB”+ pre master secret +client random +server random)) + MD5 (pre master secret + SHA1 (“CCC”+ pre master secret +client random +server random)).
Key_Block= MD5 (Master Secret + SHA1 (“A”+ Master Secret + server random +client random)) + MD5 (Master Secret + SHA1 (“BB”+ Master Secret + server random +client random)) + MD5 (Master Secret + SHA1 (“CCC”+ Master Secret + server random +client random)) +….

4.1.14Decryption of the application data

Final step of the HTTPS analysis is the decryption of the application data using the key blocks that is being generated in the previous step (Key material derivation) [11]. At first tool separates the traffic in to two parts one coming from the Server (certificate handler) and the other goingto the Server (certificate handler).Now these two section are send to the TLS parser separately. The TLS parser will parse the application data messages and fetches the data part from it and write it to a file. Now we will be having two files one containing encrypted data from server to client and the other containing encrypted data from client to server. Now this section performs the decryption on these two data files with the appropriate keys. If the file contains the data from server to client then, the tool uses the server write key and the server IV for decryption otherwise we will use client write key and the client IV for decryption purpose [7].

4.1.15 Reconstruction of data and Comparing the File

In this step, the tool is reconstructing the data by separating the header and data field form the decrypted data that have been passed through the network and identify the file type of that data and save them in the specified folder in the hard disk. Now this reconstructed file is compare with the given file. If a match is found then it will be reported in the forensic details section.

4.4.16 Gathering and displaying the forensic details

Once the original session is reconstructed, the tool will trace the forensic details of the HTTPS data that has been reconstructed in the packet and display those details in the GUI so that the user can understand what has happened to that system during a particular network session. Forensic details are displayed in four separate windows for the easiness of analysis. One window contains the header details which will give the idea about the HTTP headers that has been transferred in those connections. The second window will give the details of each packet with its time of arrival or departure source and destination IP, Mac ID, and ports. The third window will display the hex code of the data that has been reconstructed. The hex code represents the pattern of the data which can be used by other pattern matching software's for further analysis purpose. The fourth window gives an over view of the total no of files created its location its file path file type and length. The fifth window will display the in-depth forensic details of each file. It contains the file name, file type, the length of the file, the time at which the file is downloaded or uploaded, the source mac address, source IP, source port, the destination mac address destination IP, destination port etc. Thus the aim of proposed work is to identify the system and then to handover the case to police with exact malicious network stream reconstructed (proof) for further investigations.

V. PERFORMANCE EVALUATION OF PROPOSED TOOL WITH EXISTING PACKET ANALYSIS TOOLS

A brief comparison on the performance of packet stream reassembly of proposed tool with other freely available packet analysis tools is done in this section. The proposed tool is named as Network Forensic Analysis Tool Kit (NFATK). The other tools which are considered are not purely used for forensic analysis, but used for packet analysis or session analysis. Some tools give session reconstruction facility. Figure (11) provides time taken to reconstruct HTTPS streams with average number of packets in seconds and proves that the proposed method is much efficient in regenerating corresponding HTTPS stream.

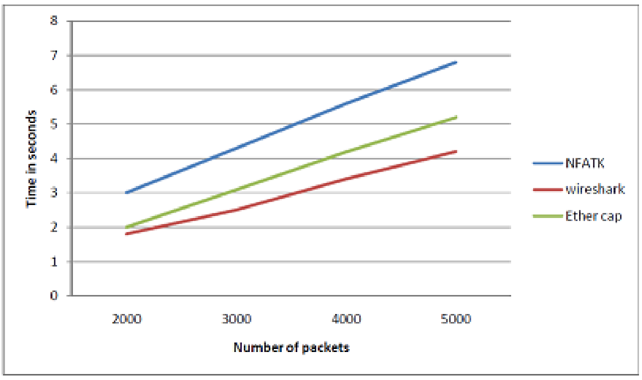

Fig11. Time Analysis for HTTPS Reconstruction.

VI. CONCLUSIONS

The proposed methodology is a strategic approach for the session recreation of HTTPS analysis as part of network forensic process and further related investigation. Thus this forensic analysis would recreate all transactions through HTTPS protocol to check whether it is malicious or not. This tool can be effectively used by network administrators, forensic investigators to identify any kind of network traffic breaches or sessions based on above mentioned protocol and to perform internet or network traffic content analysis.

REFERENCES

[1] Alberto Ornaghi, Marco Valleri (2003). “Man in the middle attack demos.” black hat conference USA.
[2] E. Anderson, M. Arlitt (2006). “Full Packet Capture and Offline Analysis on 1 and 10 Gb/s Networks” HP Laboratories Palo Alto HPL-2006-156
[3] Vicka Corey, Charles Peterman (2002). “Network Forensics Analysis” IEEE INTERNET COMPUTING
[4] Eric Rescorla (2006). “SSL and TLS Design and Building Secure Systems.” Addison Wesley.
[5] Ka-CheongLeung, Li, V.O.K.Daiqin (2007). “An Overview of Packet Reordering in Transmission Control Protocol (TCP): Problems, Solutions and Challenges.” IEEE Transactions On Parallel And Distributed Systems.
[6] Kefei Cheng, MengGao, RuijieGuo (2010). “Analysis and Research on HTTPS Hijacking Attacks.” Second International Conference on Networks Security, Wireless Communications and Trusted Computing.
[7] Moxie Marlinspike (2009). “New Tricks For Defeating SSL In Practice.” Black hat conference DC
[8] Natarajan Meghanathan, Sumanth Reddy Allam (2009). “Tools And Techniques For Network Forensics.” International Journal of Network Security & Its Applications (IJNSA), Vol .1
[9] Seung-hoon Kang, Juho Kim (2008). “Network Forensic Analysis Using Visualization Effect.” IEEE International Conference on Convergence and Hybrid Information Technology
[10] Barbara E. Endicott-Popovsky ,Deborah A. Frincke (2007) “Embedding Forensic Capabilities into Networks: Addressing Inefficiencies in Digital Forensics Investigations.” IEEE Workshop on Information Assurance United States Military Academy, West Point, NY
[11] ThawatchaiChomsiri (2007). **“**HTTPS Hacking Protection.” IEEE Advanced Information Networking and Applications Workshops (AINAW)

International Journal of Modern Engineering Research (IJMER)
www.ijmer.com Vol. 3, Issue. 5, Sep - Oct. 2013 pp-3107-3115 ISSN: 2249-6645

An Improved Optimization Techniques for Parallel Prefix Adder using FPGA

O.Anjaneyulu[1], L.Swapna[2], C.V.Krishna Reddy[3],
Member, IEEE KITS,Warangal[12], NNRESGI-Hyd[3] Andhra Pradesh, India

ABSTRACT*—In this paper, Carry Tree Adders are Proposed. Parallel prefix adders have the best performance in VLSI Design. Parallel prefix adders gives the best performance compared to the Ripple Carry Adder (RCA) and Carry Skip Adder (CSA). Here Delay measurements are done for Kogge-Stone Adder, Sparse Kogge-Stone Adder and Spanning Tree Adder. Speed of Kogge-Stone adder and Sparse Kogge-Stone adder have improved compared to the Ripple Carry Adder (RCA) and Carry Skip Adder (CSA). Model Simulator-Altera 6.6d and Xilinx 10.1 tools were used for simulation and synthesis of the design.*

Index Terms *–Carry Skip Adder (CSA), Kogge-Stone adder, Ripple carry adder (RCA), sparse Kogge-Stone adder and Spanning tree adder.*

I. INTRODUCTION

In VLSI implementations, parallel-prefix adders are known to have the best performance. Reconfigurable logic such as -Field Programmable Gate Arrays (FPGAs) has been gaining in popularity in recent years because it offers improved -performance in terms of speed and power over DSP-based and microprocessor-based solutions for many practical designs involving mobile DSP and telecommunications applications. Parallel-prefix adders will have a different performance than VLSI implementations. In particular, most modern FPGAs employ a fast-carry chain which optimizes the carry path for the simple Ripple Carry Adder (RCA).

An efficient testing strategy for evaluating the -performance of these adders is discussed. Several tree-based adder structures are implemented and characterized on a FPGA and compared with the Ripple Carry Adder (RCA) and the Carry Skip Adder (CSA). Finally, some conclusions and suggestions for improving FPGA designs to enable better tree-based adder performance are given.

II. CARRY-TREE ADDER DESIGNS

Parallel-prefix adders, also known as carry-tree adders, pre-compute the propagate and generate signals [1]. These signals are variously combined using the *fundamental carry operator* (fco) [2].

$$(G_L, P_L) \square (G_R, P_R) = (G_L + P_L \bullet G_R, P_L \bullet P_R) \quad (1)$$

Due to associative property of the fco, these operators can be combined in different ways to form various adder structures. For, example the four-bit carry-look ahead-generator is given by:

$$c_4 = (g_4, p_4) \square [(g_3, p_3) \square [(g_2, p_2) \square (g_1, p_1)]] \quad (2)$$

A simple rearrangement of the order of operations allows parallel operation, resulting in a more efficient tree structure for this four bit example:

$$c_4 = [(g_4, p_4) \square (g_3, p_3)] \square [(g_2, p_2) \square (g_1, p_1)] \quad (3)$$

It is readily apparent that a key advantage of the tree structured adder is that the critical path due to the carry delay is on the order of log2N for an N-bit wide adder. The arrangement of the prefix network gives rise to various families of adders. For a discussion of the various carry-tree structures, see [1,3].

For this study, the focus is on the Kogge-Stone adder [4]
Here we designate BC as the black cell which generates the ordered pair in equation (1); the grey cell (GC) generates the left signal only, following [1]. The interconnect area is known to be high, but for an FPGA with large routing overhead to begin with, this is not as important as in a VLSI -implementation. The regularity of the Kogge-Stone prefix network has built in redundancy which has implications for fault-tolerant designs [5]. The sparse Kogge-Stone adder, shown in Fig 2, is also studied. This hybrid design completes the summation process with a 4 bit RCA allowing the carry prefix network to be simplified.

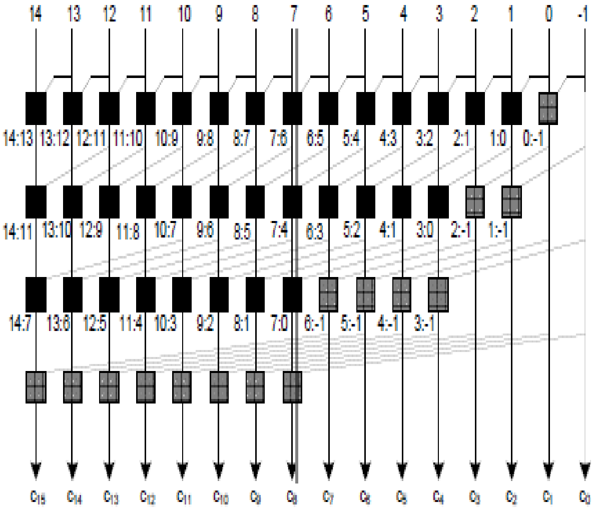

Fig1.16 bit Kogge-Stone adder

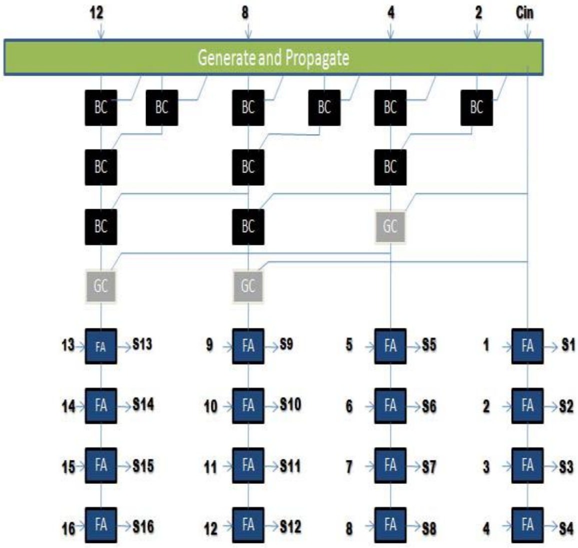

Fig2. sparse 16 bit Kogge-Stone adder

Another carry-tree adder known as the spanning tree carry-look ahead (CLA) adder is also examined [6]. Like the sparse Kogge-Stone adder, this design terminates with a 4- bit RCA. As the FPGA uses a fast carry-chain for the RCA, it is interesting to compare the performance of this adder with the sparse Kogge-Stone and regular Kogge-Stone adders. Also of interest for the spanning-tree CLA is its testability feature [7].

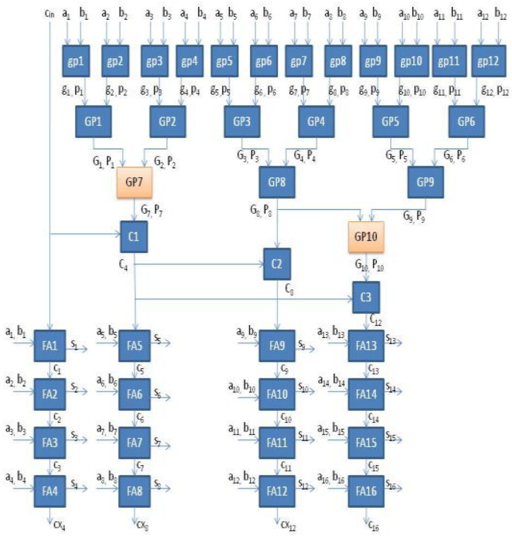

Fig3. Spanning Tree Carry Look ahead Adder (16 bit)

III. METHOD OF STUDY

The adders to be studied were designed with varied bit widths up to 128 bits and coded in VHDL. The functionality of the designs were verified via simulation with Model Simulator. The Xilinx ISE 10.1 software was used to synthesize the designs onto the Spartan 3E FPGA. In order to effectively test for the critical delay, two steps were taken. First, a memory block (labelled as ROM in the figure below) was instantiated on the FPGA using the Core Generator to allow arbitrary patterns of inputs to be applied to the adder design. A multiplexer at each adder output selects whether or not to include the adder in the measured results, as shown in Fig A switch on the FPGA board was wired to the select pin of the multiplexers. This allows measurements to be made to subtract out the delay due to the memory, the multiplexer. And interconnect (both external cabling and internal routing).

Second, the parallel prefix network was analysed to determine if a specific pattern could be used to extract the worst case delay. Considering the structure of the Generate-Propagate (GP) blocks (i.e., the BC and GC cells), we were able to develop the following scheme, by considering the following subset of input values to the GP blocks.

Table1: Subset of (g, p) Relations Used for Testing

(gL,pL) (gR,pR)	**(gL + pL gR, pL pR)**
(0,1) (0,1)	**(0,1)**
(0,1) (1,0)	**(1,0)**
(1,0) (0,1)	**(1,0)**
(1,0) (1,0)	**(1,0)**

If we arbitrarily assign the (g, p) ordered pairs the values (1,0) = True and (0, 1) = False, then the table is self-contained and forms an OR truth table. Furthermore, if both inputs to the GP block are False, then the output is False; conversely, if both inputs are True, then the output is True. Hence, an input pattern that alternates between generating the (g, p) pairs of (1, 0) and (0, 1) will force its GP pair block to alternate states. Likewise, it is easily seen that the GP blocks being fed by its predecessors will also alternate states. Therefore, this scheme will ensure that a worse case delay will be generated in the parallel prefix network since every block will be active. In order to ensure this scheme works, the parallel prefix adders were synthesized with the "Keep Hierarchy" design setting turned on (otherwise, the FPGA compiler attempts to reorganize the logic assigned to each LUT). With this option turned on, it ensures that each GP block is mapped to one LUT, preserving the basic parallel prefix structure, and ensuring that this test strategy is effective for determining the critical delay. The designs were also synthesized for speed rather than area optimization.

IV. DISCUSSION OF RESULTS

The simulated adder delays obtained from the Xilinx ISE synthesis reports are shown in Fig. An RCA as large as 160 bits wide was synthesizable on the FPGA, while a Kogge-Stone adder up to 128 bits wide was implemented. The carry-skip adders are compared with the Kogge-Stone adders. The actual measured data appears to be a bit smaller than what is predicted by the Xilinx ISE synthesis reports. An analysis of these reports, which give a breakdown of delay due to logic and routing, would seem to indicate that at adder widths approaching 256 bits and beyond, the Kogge-Stone adder will have superior performance compared to the RCA. Based on the synthesis reports, the delay of the Kogge-Stone adder can be predicted by the following equation:

$t_{KS} = (n+2)\Delta_{LUT} + \rho_{KS}(n)$ **(4)** where $N = 2n$, the adder bit width, ΔLUT is the delay through a lookup table (LUT), and $\rho_{KS}(n)$ is the routing delay of the kogge-Stone adder as a function of n. The delay of the RCA can be predicted as:

$t_{RCA} = (N-2)\Delta_{MUX} + \tau_{RCA}$ **(5)**

where ΔMUX is the mux delay associated with the fast-carry chain and τ_{RCA} is a fixed logic delay. There is no routing delay assumed for the RCA due to the use of the fast-carry chain. For the Spartan 3E FPGA, the synthesis reports give the following values: ΔLUT = 0.612 ns, ΔMUX = 0.051 ns, and τ_{RCA} = 1.715 ns. Even though ΔMUX << ΔLUT, it is expected that the Kogge-Stone adder will eventually be faster than the RCA because $N = 2n$, provided that $\rho_{KS}(n)$ grows relatively slower than $(N-2)\Delta$MUX. Indeed, Table II predicts that the Kogge-Stone adder will have superior performance at N =256.

Table2 : Delay Results for the Kogge-Stone Adders

N	**Synth. Predict**	**Route Delay**	**Route Fitted**	**Delay *tKS***	**Delay *tRCA***
4	**4.343**	**1.895**	**1.852**	**4.300**	**1.817**
16	**6.113**	**2.441**	**2.614**	**6.286**	**2.429**
32	**7.607**	**3.323**	**3.154**	**7.438**	**3.245**
64	**8.771**	**3.875**	**3.800**	**8.696**	**4.877**
128	**10.038**	**4.530**	**4.552**	**10.060**	**8.141**
256	**–**	**–**	**5.410**	**11.530**	**14.669**

(all delays given in ns)

The second and third columns represent the total predicted delay and the delay due to routing only for the Kogge-Stone adder from the synthesis reports of the Xilinx ISE software. The fitted routing delay in column four represents the predicted routing delay using a quadratic polynomial in n based on the $N = 4$ to 128 data. This allows the $N = 256$ routing delay to be predicted with some degree of confidence as an actual Kogge-Stone adder at this bit width was not synthesized. The final two columns give the predicted adder delays for the Kogge-Stone and RCA using equations (4) and (5), respectively. The good match between the measured and simulated data for the implemented Kogge-Stone adders and RCAs gives confidence that the predicted superiority of the Kogge-Stone adder at the 256 bit width is accurate. This differs from the results in [10], where the parallel prefix adders, including the Kogge-Stone adder, always exhibited inferior performance compared with the RCA(simulation results out to 256 bits were reported). The work in [10] did use a different FPGA (Xilinx Vertex 5), which may account for some of the differences. The poor performance of some of the other implemented adders also deserves some comment. The spanning tree adder is comparable in performance to the Kogge-Stone adder at 16 bits. However, the spanning tree adder is significantly slower at higher bit widths, according to the simulation results, and slightly slower, according to the measured data. The structure of the spanning tree adder results in an extra stage of logic for some adder outputs compared to the Kogge-Stone. This fact coupled with the way the FPGA place and route software arranges the adder is likely the reason for this significant increase in delay for higher order bit widths. Similarly, the inferior performance of the carry-skip adders is due to the LUT delay and routing overhead associated with each carry-skip logic structure. Even if the carry-skip logic could be implemented with the fast-carry chain, this would just make it equivalent in speed to the RCA. Hence, the RCA delay represents the theoretical lower limit for a carry-skip architecture on an FPGA.

V. SIMULATION RESULTS

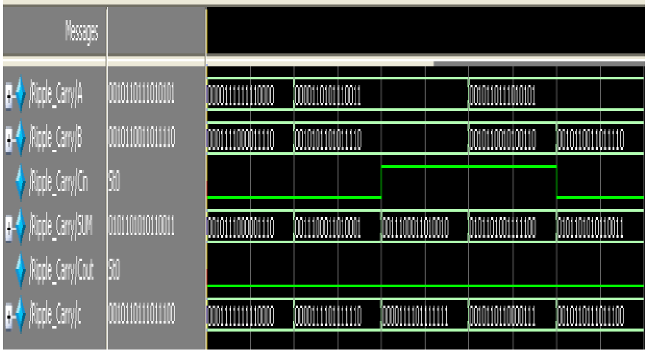

(a)Ripple-Carry Adder

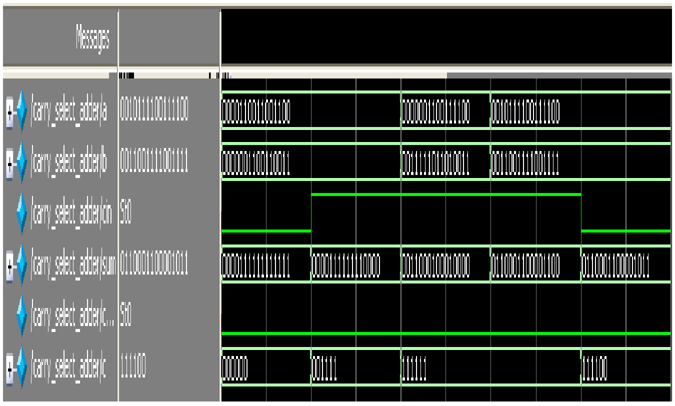

(b) Carry-Select Adder

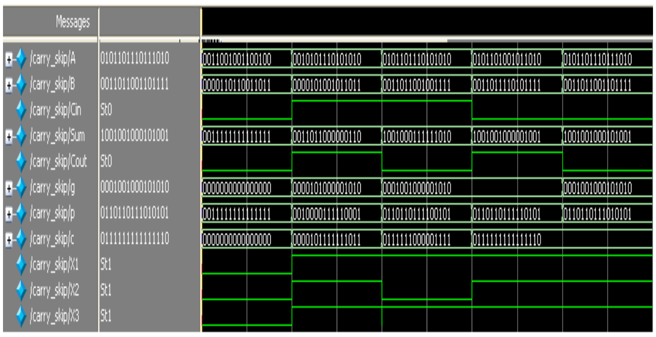

(c) Carry-Skip Adder

International Journal of Modern Engineering Research (IJMER)
www.ijmer.com Vol. 3, Issue. 5, Sep - Oct. 2013 pp-3107-3115 ISSN: 2249-6645

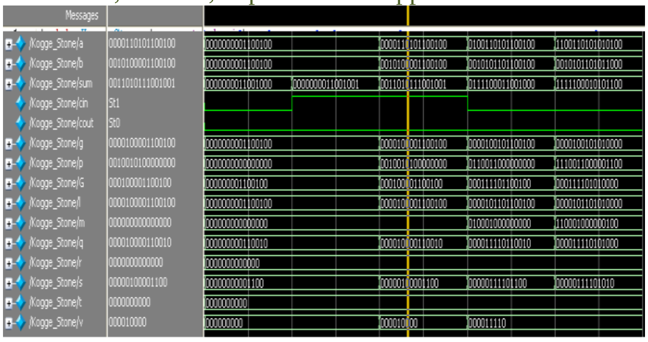

(d) Kogge-Stone Adder

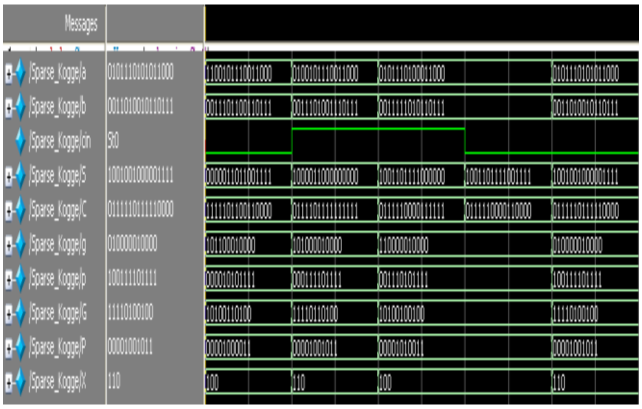

(e) Sparse Kogge-Stone Adder

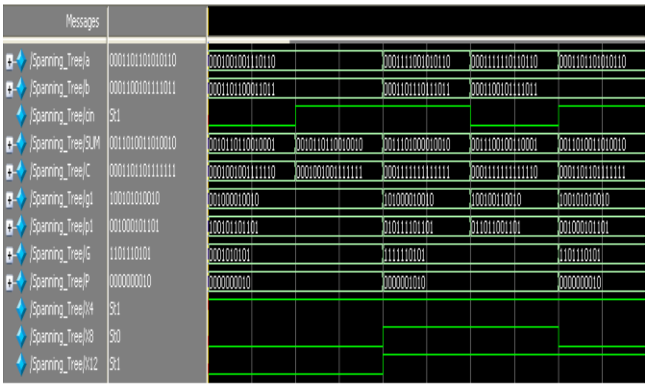

(f) Spanning Tree adder

Figure: (a)-(f): A 16-bit parallel prefix adder simulation result for all combinations outputs.

For the HDL structural design, the test vectors for excitation has been provided, and the response is as shown in Figure. Here the input reference vector is a=0010110111010101,b=0010110011011110,for Ripple carry adder, a=0010111100111100, b=0011001111001111, for Carry select adder, a=0101101110111010,b=0011011001101111 for Carry skip adder.
a=0000110101100100,b=0010100001100100 for Kogge stone adder,
a=0101110101011000,b=0011010010110111 for sparse kogge stone adder,
a=0001101101010110,b=0001100101111011 for panning tree adder.

VI. SYNTHESIS REPORT

Final *Results*

RTL Top Level Output File Name : ripple carry adder.ngr
Top Level Output File Name : ripple carry adder
Output Format : NGC
Optimization Goal : Speed
Keep Hierarchy : No

Design Statistics

IOs : 50

Cell Usage :

#	BELS	: 32
#	LUT3	: 32
#	IO Buffers	: 50
#	IBUF	: 33
#	OBUF	: 17

Timing constraints

Delay: 21.69ns (Levels of Logic = 18)
Source: B<0> (PAD)
Destination: C out (PAD)
Data Path: B<0> to C out

Cell: In_>Out	Fan out	Gate delay	Net delay	Logic Name(Net Name)
IBUF:I->O	2	1.106	0.532	B_0_IBUF (B_0_IBUF)
LUT3:I0->O	2	0.612	0.449	FA0/cout1 (c<0>)
LUT3:I1->O	2	0.612	0.449	FA1/cout1 (c<1>)
LUT3:I1->O	2	0.612	0.449	FA2/cout1 (c<2>)
LUT3:I1->O	2	0.612	0.449	FA3/cout1 (c<3>)
LUT3:I1->O	2	0.612	0.449	FA4/cout1 (c<4>)
LUT3:I1->O	2	0.612	0.449	FA5/cout1 (c<5>)
LUT3:I1->O	2	0.612	0.449	FA6/cout1 (c<6>)
LUT3:I1->O	2	0.612	0.449	FA7/cout1 (c<7>)
LUT3:I1->O	2	0.612	0.449	FA8/cout1 (c<8>)
LUT3:I1->O	2	0.612	0.449	FA9/cout1 (c<9>)
LUT3:I1->O	2	0.612	0.449	FA10/cout1 (c<10>)
LUT3:I1->O	2	0.612	0.449	FA11/cout1 (c<11>)
LUT3:I1->O	2	0.612	0.449	FA12/cout1 (c<12>)
LUT3:I1->O	2	0.612	0.449	FA13/cout1 (c<13>)
LUT3:I1->O	2	0.612	0.449	FA14/cout1 (c<14>)
LUT3:I1->O	1	0.612	0.357	FA15/cout1 (c<15>)
OBUF:I->O		3.169		Cout_ OBUF (Cout)

Final *Results*

RTL Top Level Output File Name : kogge-stone adder.ngr
Top Level Output File Name : kogge-tone adder
Output Format : NGC
Optimization Goal : Speed
Keep Hierarchy : No

Design Statistics

IOs : 50

Cell *Usage*:

#	BELS	: 41
#	GND	: 01
#	LUT3	: 27
#	LUT4	: 9
#	IO Buffers	: 50
#	IBUF	: 33
#	OBUF	: 17

Timing constraints

Delay: 20.262ns (Levels of Logic = 17)
Source: b<1> (PAD)
Destination: Sum<14> (PAD)
Data Path: b<1> to Sum<14>

Cell: in->out	Fan out	Gate delay	Net delay	Logic name(Net Name)
IBUF:I->O	**4**	**1.106**	**0.651**	**b_1_IBUF (b_1_IBUF)**
LUT4:I0->O	**1**	**0.612**	**0.000**	**GC2/G1_SW01 (GC2/G1_SW0)**
MUXF5:I1->O	**2**	**0.278**	**0.410**	**GC2/G1_SW0_f5 (q<1>)**
LUT3:I2->O	**2**	**0.612**	**0.532**	**GC2/G1 (q<2>)**
LUT3:I0->O	**2**	**0.612**	**0.532**	**GC6/G_SW0_SW0 (s<3>)**
LUT3:I0->O	**2**	**0.612**	**0.532**	**GC7/G_SW0_SW0 (s<4>)**
LUT3:I0->O	**2**	**0.612**	**0.532**	**GC8/G_SW0_SW0 (s<5>)**
LUT3:I0->O	**2**	**0.612**	**0.410**	**GC9/G_SW0_SW0 (s<6>)**
LUT3:I2->O	**3**	**0.612**	**0.603**	**GC9/G_SW0 (v<7>)**
LUT3:I0->O	**2**	**0.612**	**0.410**	**GC9/G_SW1 (v<8>)**
LUT3:I2->O	**2**	**0.612**	**0.410**	**GC9/G (v<9>)**
LUT3:I2->O	**2**	**0.612**	**0.532**	**GC12/G_SW0 (v<10>)**
LUT3:I0->O	**2**	**0.612**	**0.410**	**GC12/G_SW1 (GC13/G5)**
LUT3:I2->O	**2**	**0.612**	**0.410**	**GC12/G (GC14/G9)**
LUT3:I2->O	**2**	**0.612**	**0.410**	**GC14/G18 (GC13/G34)**
LUT3:I2->O	**1**	**0.612**	**0.357**	**Mxor_sum<14>_Result1 (sum_14_OBUF)**
OBUF:I->O		**3.169**		**sum_14_OBUF (sum<14>)**

Final *Results*

RTL Top Level Output File Name: sparse kogge-stone Adder.ngr

Top Level Output File Name : sparse kogge

Output Format : NGC

Optimization Goal : Speed

Keep Hierarchy : No

Design *Statistics*

IOs : 65

Cell *Usage*:

- # BELS : 54
- # LUT2 : 02
- # LUT3 : 30
- # LUT4 :19
- # MUXF5 :03
- # IO Buffers : 65
- # IBUF : 33
- # OBUF : 32

Timing constraints

Delay: 15.916ns (Levels of Logic = 13)

Source: a<6> (PAD)

Destination: C<6>t (PAD)

Data Path: a<6> to C<16>

Cell: in_>out	**Fan out**	**Gate delay**	**Net delay**	**Logic Name(Net Name)**
IBUF:I->O	**4**	**1.106**	**0.651**	**a_6_IBUF (a_6_IBUF)**
LUT4:I0->O	**2**	**0.612**	**0.449**	**BC8/G18 (BC8/G18)**
LUT4:I1->O	**1**	**0.612**	**0.000**	**BC8/G461 (BC8/G461)**
MUXF5:I1->O	**3**	**0.278**	**0.603**	**BC8/G46_f5 (BC8/G46)**
LUT4:I0->O	**1**	**0.612**	**0.387**	**GC3/C13 (GC3/C13)**
LUT3:I2->O	**1**	**0.612**	**0.360**	**GC3/C21 (GC3/C21)**
LUT4:I3->O	**1**	**0.612**	**0.426**	**GC3/C46 (GC3/C46)**
LUT4:I1->O	**2**	**0.612**	**0.449**	**GC3/C77 (GC3/C77)**
LUT3:I1->O	**3**	**0.612**	**0.520**	**FA13/cout1 (C_13_OBUF)**
LUT3:I1->O	**3**	**0.612**	**0.520**	**FA14/cout1 (C_14_OBUF)**
LUT3:I1->O	**3**	**0.612**	**0.520**	**FA15/cout1 (C_15_OBUF)**
LUT3:I1->O	**1**	**0.612**	**0.357**	**FA16/cout1 (C_16_OBUF)**
OBUF:I->O		**3.169**		**C_16_OBUF (C<16>)**

VII. IMPLEMENTATION AND RESULTS

The proposed design is functionally verified and the results are verified. The timing report was obtained. The Simulation Verified in Modelsim and Synthesis was verified in Xilinx.

N	Delay t_{RCA}	Delay t_{KS}	Delay t_{SKS}
16	**21.690ns**	**20.262ns**	**15.916ns**

VIII. CONCLUSION

In this paper An improved optimization techniques for parallel prefix adder has been proposed and implemented. The design of the proposed prefix adders is done using Ripple carry adder and Kogge-stone adder, Sparse kogge tone adder and panning tree adder. speed of parallel prefix adder is increased compared to the Ripple carry adder. The functional verification of the proposed design of the An improved optimization techniques for parallel prefix adder is performed through simulations using the Verilog HDL flow in ModelSim for prefix adders and Synthesis done using Xilixn.The design of An improved optimization technique for parallel prefix adder has been performed. The proposed design of An improved optimization techniques for parallel prefix adder can perform ripple carry adder,kogge stone adder,spare kogge adder,spanning tree adder ,parallel adder give the better result compared to the ripple carry adder.

REFERENCES

[1] N. H. E. Weste and D. Harris, CMOS VLSI Design, 4th edition, Pearson –Addison-Wesley, 2011.
[2] R. P. Brent and H. T. Kung, “A regular layout for parallel adders,” IEEE Trans. Comput., vol. C-31, pp.260-264, 1982.
[3] D. Harris, “A Taxonomy of Parallel Prefix Networks,” in Proc. 37th Asiloma r Conf. Signals Systems and Computers, pp. 2213–7, 2003.
[4] P. M. Kogge and H. S. Stone, “A Parallel Algorithm for the Efficient Solution of a General Class of Recurrence Equations,” IEEE Trans. on Computers, Vol. C-22, No 8, August 1973.
[5] P. Ndai, S. Lu, D. Somesekhar, and K. Roy, “Fine Grained Redundancy in Adders,” Int. Symp. on Quality Electronic Design, pp. 317-321, March 2007.
[6] T. Lynch and E. E. Swartzlander, “A Spanning Tree Carry Lookahead Adder,” IEEE Trans. on Computers,vol. 41, no. 8, pp. 931-939, Aug. 1992.
[7] D. Gizopoulos, M. Psarakis, A. Paschalis, and Y. Zorian, “Easily Testable Cellular Carry Lookahead Adders,” Journal of Electronic Testing: Theory and Applications 19, 285-298, 2003.
[8] S. Xing and W. W. H. Yu, “FPGA Adders:Performance Evaluation and Optimal Design,” IEEE Design & Test of Computers, vol. 15, no. 1, pp. 24-29,Jan. 1998.
[9] M. Bečvář and P. Štukjunger, “Fixed-Point Arithmetic in FPGA,” Acta Polytechnica, vol. 45, no. 2, pp. 67-72, 2005.
[10] K. Vitoroulis and A. J. Al-Khalili, “Performance of Parallel Prefix Adders Implemented with FPGA technology,” IEEE Northeast Workshop on Circuits and Systems, pp. 498-501, Aug. 2007.

International Journal of Modern Engineering Research (IJMER)
www.ijmer.com Vol. 3, Issue. 5, Sep - Oct. 2013 pp-3116-3117 ISSN: 2249-6645

An Effective Strategy of Firewall Based Matching Algorithm

Rathod.Sangeetha[1], J.Rajeshwar[2]Azmeera Rajesh[3]

[1]*M.Tech Student, Dept of CSE,Vijay Rural Engineering College, Rochis Valley, Manikbhandar, Nizamabad, A.P, India*
[2]*Professor, Dept of CSE,Vijay Rural Engineering College, Rochis Valley, Manikbhandar, Nizamabad, A.P, India*

ABSTRACT: *Here the perimeter oriented to the network based strategy where the crossing of the traffic plays a major role in its implementation based aspect in a well oriented fashion respectively. Therefore there is a necessity of the implementation of the system with respect to the implementation and the proper filtering based aspect where this particular thing has to be well effective controlled n a well oriented fashion respectively. Here the main strategy of the system is to improve the performance oriented strategy of the system followed by the risk aware strategy of the bottleneck in a well respective fashion takesplace in the system respectively. Here the matching related to the packet based on the firewall strategy through which where the problem is analyzed with a well respective locative point respectively where the rule based on the matching oriented strategy in a well effective manner in which there is an implementation of the strategy related to the aspect of the a proper cross verification takesplace in the system in a well efficient manner and also the against firewall based strategy in a well effective manner respectively. There is an application of the algorithms related to the aspect oriented with respect to the strategy of the implementation based aspect by which there is an analysis oriented with the prefect fashion takes place in the system. In order to overcome the above problem based strategy in a well efficient manner by which algorithm based on the classical strategy through which domain based on the firewall based phenomena is not implemented here in a well respective analysis take splace in the system based aspect respectively.Experiments have been conducted on the present method and a lot of analysis is made on the present method by the help of the large number of the data sets in a well oriented fashion with respect to the improvement in the performance based strategy followed by the outcome of the entire system in a well respective fashion through the entire system based aspect respectively.*

Key Words: *Communication of the network strategy, Security and the protection in the network level aspect respectively.*

I. INTRODUCTION

Here the technologies related to the centralized based phenomena and is applied n the well oriented fashion through the help of the control based access related to the high level of the strategy based implementation oriented analysis followed by the networks related o the organizational based strategy respectively [1][2]. Here the matching related to the aspect of the packet based phenomena in a well oriented aspect by which there is an analysis with respect to the system based strategy of the well known orientation of the scenario which includes involvement of the matching oriented firewall in a well oriented fashion by which it is applied n the many fields based aspect in a well oriented fashion respectively.Here there is an accurate involvement of the protocol basedon the standards of the TCP based aspect followed by the header of the packet oriented information packet in a well respective fashion takesplace in the system respectively[3][4].

II. BLOCK DIAGRAM

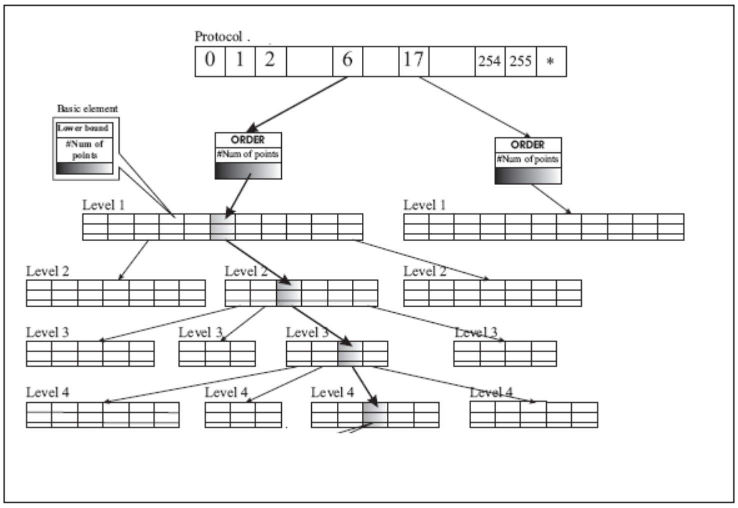

Fig 1:Shows the block diagram of the present method respectively

III. METHODOLOGY

In this paper a method is designed with a well efficient framework oriented strategy in which there is an improvement in the performance based strategy followed by the entire system based outcome in a well oriented fashion respectively [5][6]. Here the implementation of the present method is shown in the below figure in the form of the block diagram and explains in the elaborative fashion respectively. There is a huge challenge for the present method in which the present method is implement in well respective fashion followed by the improvement in the outcome of the entire system in a well oriented fashion respectively. Here the present method is effective and efficient in terms of the design oriented strategy of the reduced power oriented scenario followed by the improvement in the speed plays a major orle in the system based aspect respectively [9].

IV. EXPECTED RESULT

A lot of analysis is made between the present method to that of the several previous methods and a huge computations have been applied on the well oriented fashion for the effective improvement in the performance based strategy followed by the outcome of the entire system based aspect in a well oriented fashion respectively. Comparative analysis is made between he present method to that of the several previous methods as shown in the below figure in the form of the graphical representation and is explained in the elaborative fashion respectively. Here we finally conclude that the present method completely overcome the drawbacks of the several previous methods in a well oriented fashion and improvement in the analysis respectively [7][8].

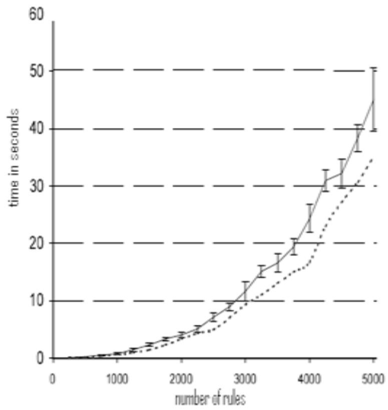

Fig 2:Shows the graphical representation of the present method respectively

V. CONCLUSION

Here a new technique is proposed based on the strategy of the implementation of the system based aspect which is a powerful method mainly implemented for the purpose of the accurate analysis of the outcome based strategy followed by the performance is a major concern respectively. Here a new technique is presented based on the strategy of the based on the algorithm oriented with the GEM based phenomena in a well oriented fashion by which it is efficient in terms of the implementation based phenomena in a well effective manner followed by the implementation of the algorithm related to the practical strategy in a well efficient manner where there is a matching of the packet based firewall oriented phenomena respectively. Here this particular technique based aspect is implemented by the help of the kernel oriented with the linux based strategy in a well efficient manner with respect to the test bed oriented strategy in a well effective manner through the implementation aspectrapidly increasing the matching strategy oriented with the packet based phenomena in a well effective manner where the matching rule is based on the GEM large scale phenomena in awell efficient manner respectively.Here the present method completely overcome the drawbacks of the several previous methods in a well oriented fashion respectively.

REFERENCES

[1] M. Smid, "Dynamic rectangular point location with an application to the closest pair problem," Information and Computation, vol. 116, no. 1, pp. 1–9, Jan. 1995.
[2] V. Srinivasan, "A packet classification and filter management system," in Proc. IEEE INFOCOM, 2001, pp. 1464–1473.
[3] V. Srinivasan, S. Suri, and G. Varghese, "Packet classification using tuple space search," in Proc. ACM SIGCOMM, 1999, pp. 135–146.
[4] V. Srinivasan and G. Varghese, "Faster IP lookups using controlled prefix expansion," in ACM Conference on Measurement and Modeling of Computer Systems, 1998, pp. 1–10.

AUTHORS

R.Sangeetha: I am pursuing mtech in vrecnizamabad.i have more then three year experience in teaching field.i scored in btech first class with distinction.i attend many national conference and work shop.
Prof J Rajeshwar:I am pursuing my phd at jntu.i am head&professer of csit at vrecnzb.i published so many papers national amdinternationali have more then 15 year experience in teaching field.

A Rajesh:I am working as asst professor in vcew,nzb.i am complited my mtech in power systems.i attend four international and national conference.i published two paper in international journal also.my interesting area is facts

International Journal of Modern Engineering Research (IJMER)
www.ijmer.com Vol. 3, Issue. 5, Sep - Oct. 2013 pp-3118-3128 ISSN: 2249-6645

Effect Of Water On Slope Stability And Investigation Of □ □w Drainage Techniques Applied To Sections Of Egnatia Odos.

Tzarouchi Sophia[1], Basile Christaras[2], Georgios Dimopoulos[3],

[1]*Geologist, MSc, Greece,*
[2]*Professor AUTH, Supervisor,*
[3]*Professor AUTH, Member of the Tripartite Advisory Committee.*

ABSTRACT: *This study is to explore the drainage possibility of physical and technical landslide slopes, with the help of draining projects implementation, which operate without energy consumption and contribute significantly to their stabilization. We investigated the function, the general assumptions of application and the construction methodology of these new drainage techniques, i.e. the Drainage Gravel Piles. In addition, we investigated their applicability in a landslide area of Egnatia Odos: Section 3.1 (Peristeri - Anthochori), Area B (1+100-1+600), with the unsaturated background of a buried riverbed, and calculated the most suitable distance between them, in order to drain it. After observing their function and evaluating the results of our study, we reached some important conclusions such as: 1. The positive effect of drainage gravel piles on the drainage of a landslide area, in the presence of high water-bearing capacity aquifers within these materials and the existence of unsaturated permeable background, through the attainment of draining these landslide materials in this permeable background. 2. The groundwater drawdown and the reduction of pore pressure that they cause, in the landslide area, are inversely proportional to the distance between them and directly proportional to the depth which the landslide materials reach. 3. The drainage of a landslide area, highlighting failures in various positions without their hydraulic communication, is achieved by applying groups of drainage gravel piles in these sub-positions. 4. In the areas where landslide incidents are recurrently manifested and take up large areas, these drainage projects contribute to a greater extent than other measures to the stabilization of the situation and to further balance restoration.*

Keywords: *Drainage gravel piles, Landslide materials, unsaturated permeable background, Pumping tests, Drawdown, Landslide Stabilization.*

I. INTRODUCTION

Through the detailed description of the ground conditions and the effect of surface water and groundwater on mechanisms activating failures, the way in which the application of new drainage measures can alter local conditions, by reducing the pore pressure and inhibiting ground motions resulting in halting landslide phenomena, is investigated and additionally the operating principles of these new projects are analyzed. That is, we tried to attain without additional cost the same result as the one attained by pumping tests. That is to say achieve the draining of the landslide mass with the simultaneous channeling of the leachate in underlying unsaturated aquifers and not in the ground surface by pumping. The investigation of the function of these new ground drainage techniques that were called Drainage Gravel Piles was performed under certain conditions which concerned:

- Having loose landslide ground materials.
- Having an unconfined aquifer formation in landslide materials and thus presence of impermeable underlying formation.
- Having an unsaturated aquifer underlying the impervious layer.

II. DRAINAGE GRAVEL PILES

2.1 Operating Principle

- The operating principle of the drainage gravel piles is based on the principle of the flow into water drilling works, in which the empirical methods of Dupuit and Thiem on pumping tests are applied for the calculation of their hydraulic parameters according to the type of the aquifer and the flow status.
- Darcy's law must apply and is expressed by the relationship: $\mathbf{Q = kiF}$ where:

Q = the water supply that flows through the cross-sectional area F in m^3/sec,
$i = h_1 - h_2 / I$ = the hydraulic gradient along the water flow, where I the length of run,
k = the permeability coefficient of porous media in m/sec
F = the cross-sectional area vertically to water flow in m^2

- Drainage gravel piles are vertical drainage wells, filled with a graded gravel material (of a diameter of 5 to 20mm), washed and free of fine ingredients. The method is consisted in displacing a column of ground material on the spot and replacing it with gravel material, i.e. a gravel pile is created. Due to the high permeability of the gravel material in relation to the environment, the gravel piles function as vertical strainers facilitating the defusing of pore overpressures. Each well displays a drawdown aquifer cone (cone of depression) in its perimeter, for a specific impact radius, which concerns the drainage area. Therefore, the draining of a delimitated landslide area achieved through a specific grid or provision of drainage wells. The method is mostly applied to relatively cohesive, soft and compressible silt and clay soils.
- The monitoring of the drawdown is carried out by installed satellite piezometers of the drainage gravel piles, while the certification of ground motions is monitored by the pre-existing inclinometer measurements in each area. By the

application of the drainage wells both the drawdown, as well as the reduction of ground motions, is achieved. [1, 6, 7 & 14]

2.2 General assumptions of application

In order for the above to be applied we accept some general assumptions concerning [1, 7 & 13]:

- Having an unconfined aquifer of infinite extent
- Having a state of equilibrium
- Accepting homogeneity and isotropy throughout the length of the ground profile, as such in conjunction with the consideration state e.g. the landslide ground materials are considered heterogeneous at cm^3 level, at m^3 level, however, they are considered homogeneous and isotropic.
- Accepting the presence of a steady hydraulic load surrounding the project. Since this is theoretically impossible to be achieved, the situation becomes acceptable, with the assumption that the drawdown variation becomes negligible over time, after an extended pumping.
- The Thiem-Dupuit equation is therefore valid: $$Q=\frac{\pi k\,(h_2^2 - h_1^2)}{\ln(r_2/r_1)} \qquad (1)$$
- There is a continuation of the cone of depression to the water surface in the well. Even if this suggestion deviates from reality, but as we move away from the wellhead, these deviations are diminished, not affecting our calculations, since we are not interested in the precise form of the unconfined surface in close proximity to the drainage gravel piles.
- The vadose zone above the water table, the effect of the capillary zone, as well as the effect of the vertical component of velocity.
- Finally, we accept that the permeable background is practically horizontal, unsaturated and not under pressure.

2.3 Construction methodology

The general procedure is as follows (Fig. B1):

- we begin perforation with diameter 100cm, minimizing him progressively up to the end of drilling in Φ15´´ and placing them corresponding fence tube,
- following that, is the installation of galvanized filter tube, with grommet, Φ6″ and 4mm thick, with conical edge of 0.5m length and Φ6″ and blind the first 3 metres of the tube, while in the upper rim, of the lowest three-meters long filter tube, a piezometric galvanized tube is placed, heavy duty with grommet, Φ1½´´diameter,
- around the filter tube, the removal of the fence tube is performed and the filling of the vacuum with the graded gravel filter (5-20mm), with a simultaneous water circulation to prevent block formation,
- then, the protruding parts of the tubes are cut and in the heads of the gravel piles galvanized casings Φ10″ and concrete foundations with dimensions of 2X2X0.24m are placed,
- restoration of the surrounding area and coating using gravel,
- finally, a moat is constructed perimetrically for the collection of surface water.

- Daily measurements are carried out in the piezometers, at various stages of their construction, in order to label potential problems and to monitor their effectiveness.
- While, with the completion of the perforation works, test measurements concerning the level changes are performed by channeling water (2.5 m^3) through them, a procedure which operates as an evaluation criterion for their proper construction and function.

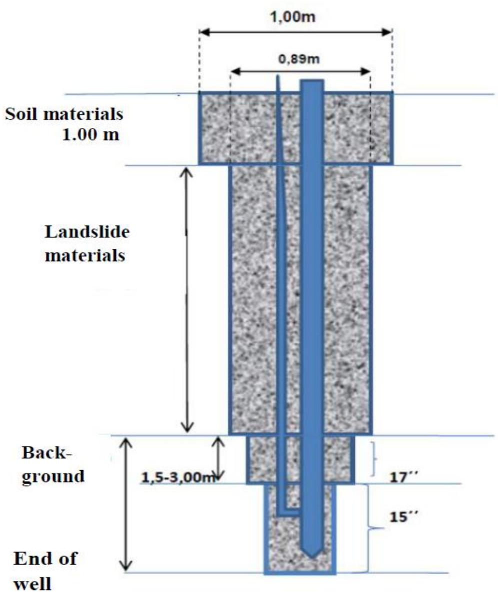

Figure B1: Schematic representation of the Drainage Gravel Piles.

III. AREA OF DRAINAGE GRAVEL PILES APPLICATION (SECTION 3.1 OF EGNATIA HIGHWAY, AREA B' –C.H. 1+100-1+900)

3.1 General data

In the category of major infrastructure projects all the highways across Europe are included and part of this trans-European transportation network is also Egnatia Highway. It happens to be one of the most difficult engineering projects. The Igoumenitsa port is its starting point and has a total length of about 680 km to Alexandroupoli and about 780 km to Ormenio. The special geotechnical problems (landslide areas) that were found at the opening up of the Highway, are rather remarkable and combined with the intense mountainous terrain, make the situation even more difficult. The Peristeri landslide is also one of them (Area B', from C.H. 1+100 to 1+900), which is found in Section 3.1 of Egnatia Highway. This project necessitated immediate treatment and stabilization in order for the road to be constructed (Map A1). It concerns a riverside landslide area, with Metsovitikos River its most important morphogenetic event. [2]

Map A1. Section 3.1 of Egnatia Highway:Peristeri – Anthochori, Area B' C.h. 10+100-10+660, (Area of application Drainage Gravel Piles)

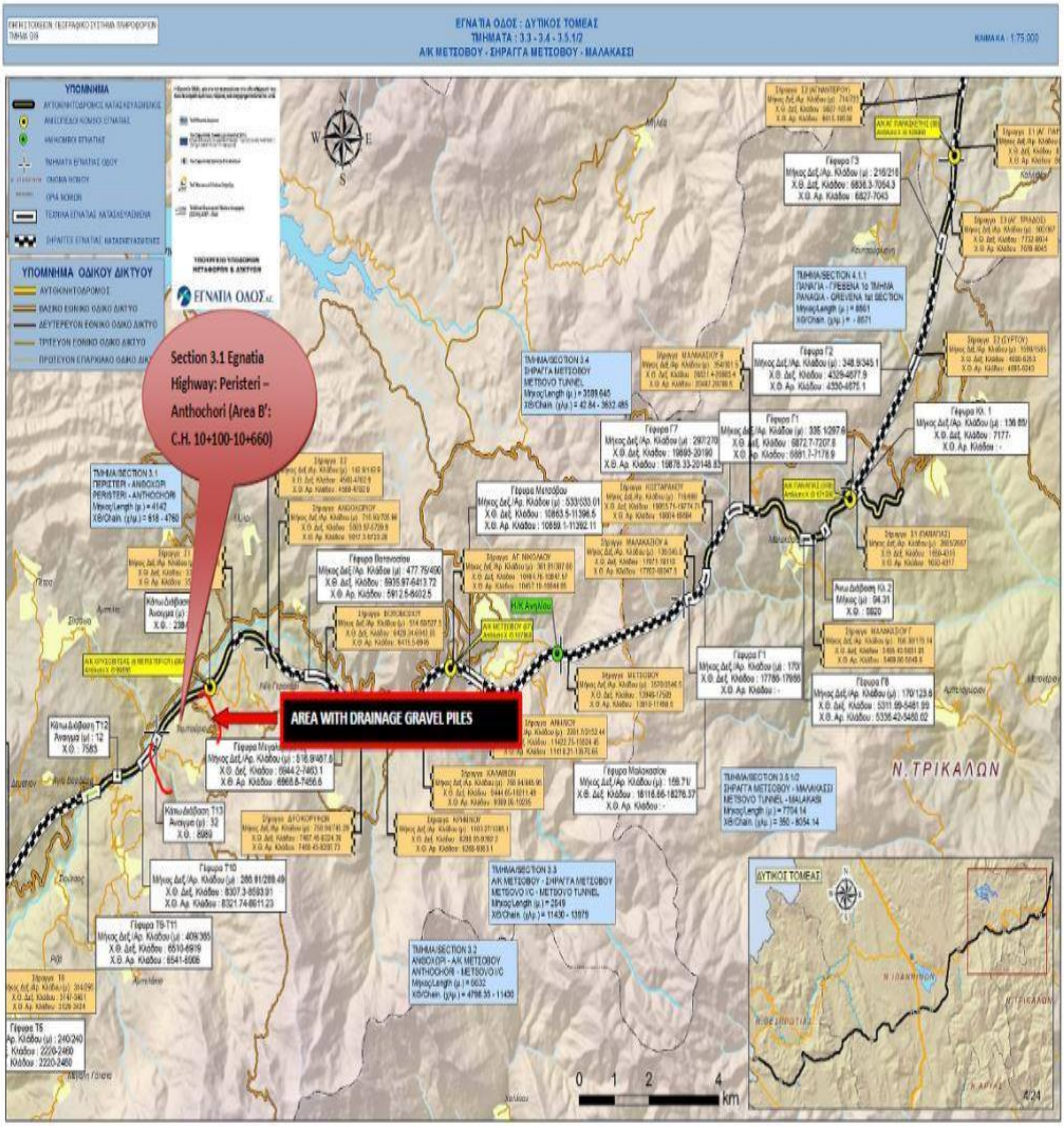

3.2 Peristeri Landslide (Area B', 1+100 CH - 1+900 CH)

3.2.1 Geological structure and Geotectonic framework of the landslide area

More than one factors usually interact in order for landslides to occur. Soils consisting of alternations of several heterogeneous layers are more likely to display landslide phenomena, to others consisting of a single layer. Regions with alternations of permeable and impermeable formations, as well as zones of intense neotectonic activity, also display a similar behavior. Our study area is a combination of these, as it is structured with a large variety of formations concerning: **materials of anthropogenic origin** and **quaternary deposits** (current and past deposits of Metsovitikos River). In the highest (southernmost) part of the area the **formations of the geotectonic zone of Pindos** appear (limestone and hornstone formations and magmatic andesitic and cave rocks) obduct onto the **flysch formations of the Ionian zone** (average - to thin layer siltstones, sectioned and highly plicate in the highest section of the abutment and relatively of small thickness intercalations sandstone and conglomerate) (F. C1).

Photo C1: Landslide Area B pigeons (soil material instabilities).

This overthrust constitutes the main tectonic fact of the area. The area is divided into two sub-regions of different tectonic origin: the lower region, which extends from the bed of Metsovitikos River up to an altitude of about 800m and it is structured by flysch formations of the Ionian zone on which the landslides appear and the higher region (over 800m altitude) which is structured by obducted formations of Pindos. The main cause of the landslide development is the erosive process of Metsovitikos River. It is estimated that in past years it formed a deep engulfment towards the interior of the abutment, resulting in its undermining, in the development of landslide phenomena (in the degraded flysch formations) and in the displacement of the abutment to the north. The estimate inclination of the surface slope ranges between 20-22^{o}, in the highest landslide section, and between 10-15^{o} to its lower section (F. C2).

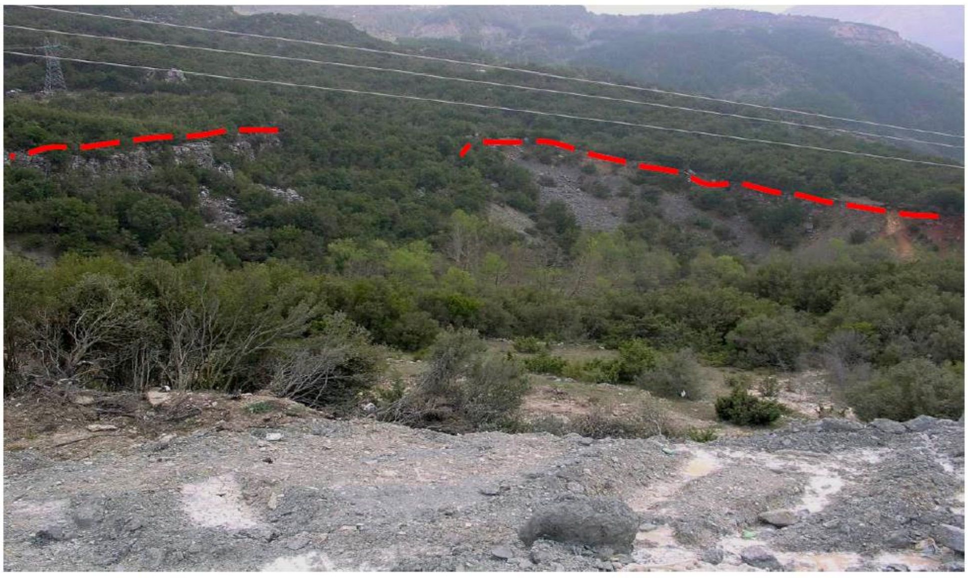

Photo C2: Landslide Peristeriou (the red dashed line shows the landslide).

A typical geological intersection is illustrated in Map A2. [4, 8, 11 & 12]

3.2.2 Hydraulic groundwater conditions and surface water indications

The formations that structure the area, from a hydrogeological point of view, are classified as of **very small to zero permeability** formations (landslide materials and flysch background which are found in the lower section of the abutment, from the Metsovitikos riverbed to an altitude of +800) and as of **average permeability** formations (small brecciaed limestone with green stones, intercalations of pelagic limestone, cherts and andesites). Finally, they are also classified as of **high permeability formations** (limestone formations and their side screes of Pindos zone and materials from the current and prior bed of Metsovitikos River, in the highest section of the abutment). Many water discharge points and springs of high supply have been spotted, especially in the highest section of the abutment, which overflow during the winter months, as well as evidence of stagnant waters (gathering of clayey silt materials in flats), especially in posts where phenomena of instability occur. [3, 4, 9 & 12]

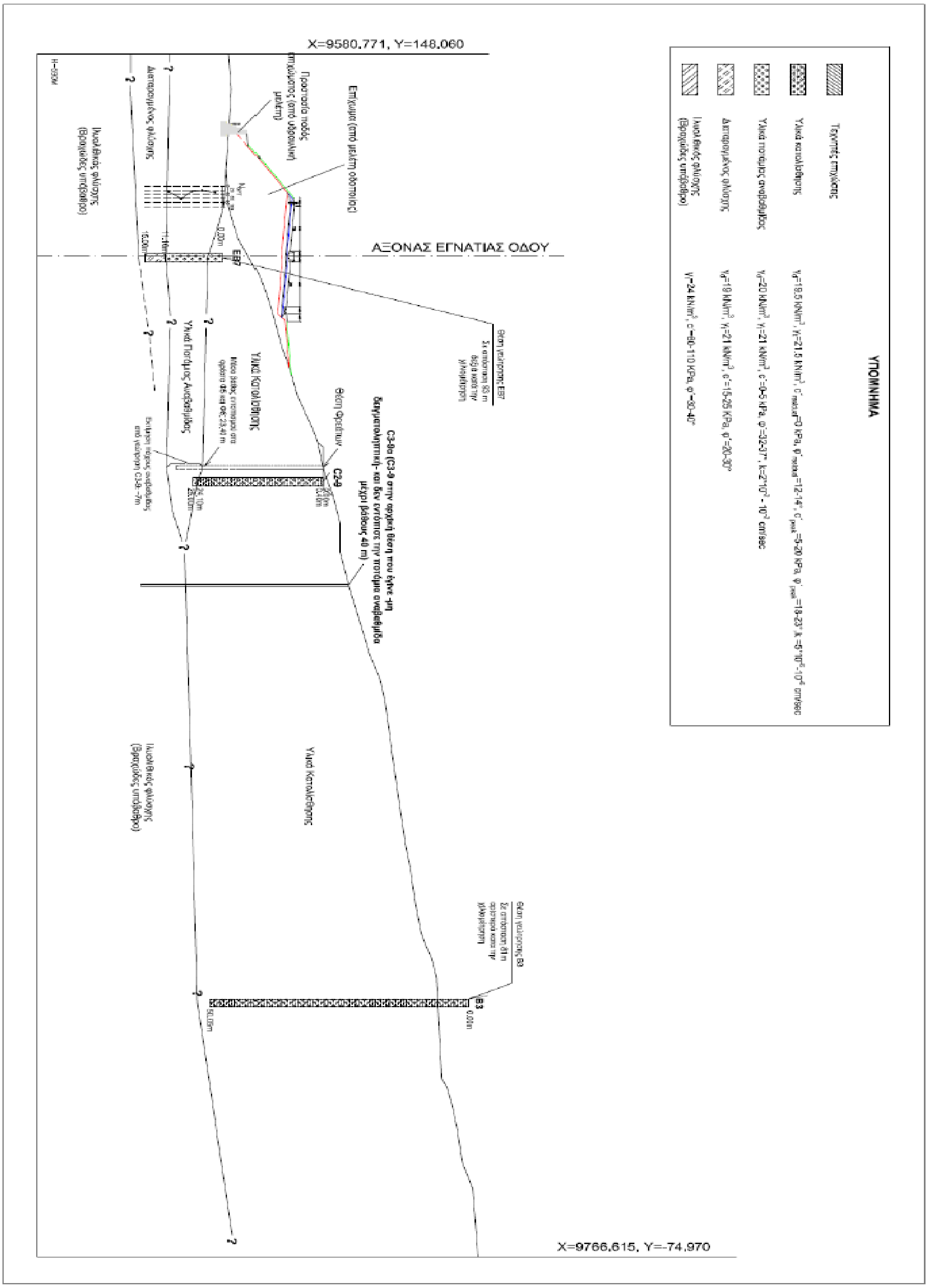

Map A2: Geological intersection of the landslide's area (Area B': C.H. 1+100 – 1+900) of section 3.1 of the Egnatia Highway (Edafos Engineering Consultans S.A., 2003).

www.ijmer.com Vol. 3, Issue. 5, Sep - Oct. 2013 pp-3118-3128 ISSN: 2249-6645

3.3 Investigation of the Drainage Gravel Piles application

According to the above we ascertain that, in this specific landslide, apart from many heterogeneous layers, the main manifestation mechanism of ground motions is related directly to the change of the additional, mostly, hydrostatic pressures and the hydrological conditions, as well as the gradient changes of landscaped slopes that cause flashing of water and lead to local or generalized failures. This was the pretext to investigate new types of drainage measures, the so-called **Drainage Gravel Piles**. These operate as the amount of water inserted in them, by the pierced landslide materials, is channeled into the river terrace which characterized by high permeability and this provide a satisfactory level of security against landslide.

The hydrogeological overview of the region is characterized by the supernatant drainage materials, of high water-bearing capacity but low permeability ($k \sim 2{,}0 x 10^{-5}$cm/sec) and the shallow well horizon, because of the underlying flysch formations, the clay composition of which are responsible for the very slow (practically zero) rate of groundwater drainage in the buried river terrace. So, between the supernatant drainage materials and the impermeable flysch background, a distinctive slide surface is created. (Fig. B2).

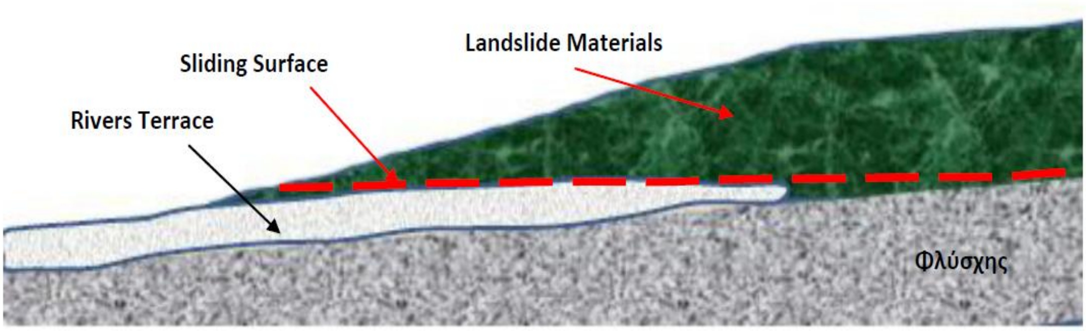

Figure B2: Hypothetical range of materials overlying landslide buried river terrace.

Based on the above assumption, the problem of dimensioning the drainage wells is basically reduced to the study of the change in flow of groundwater in an aquifer well, which is caused by the well function that reach the impervious background. The assessment of groundwater drawdown due to ongoing pumping tests is investigated, both in the wells, as well as in their surrounding area. For this reason, we represented schematically the level change caused by the pumping of the surface, in an unconfined underground aquifer (Fig. B3) and the level change caused by water channeling, in the underlying (buried) river terrace, in the case of Gravel Piles application in an area (Fig. B4).

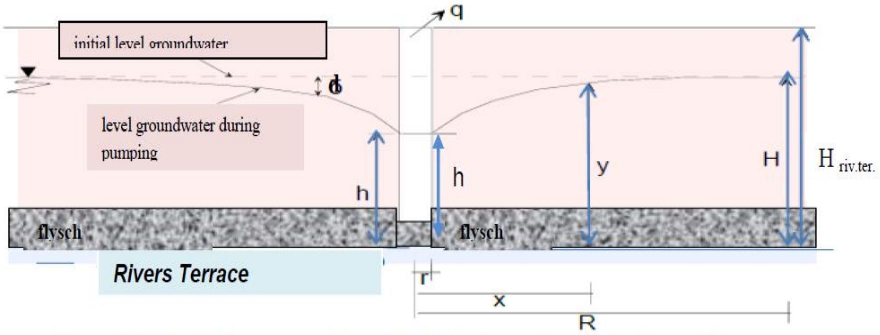

Figure B3: Typical case pumping well - level change in aquifer free surface

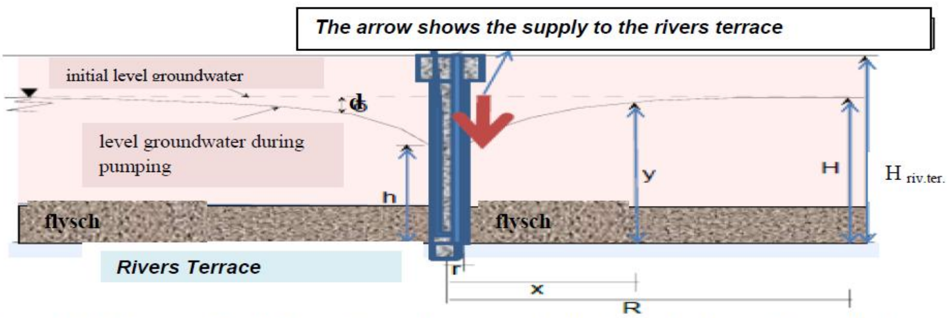

Figure B4: Schematic level change by applying gravel piles instead of pumping well - in aquifer free surface

Of these figures indicate the correlation of level change in both cases which are takes the shape of an inverted cone. In the second case, concerning the real under study problem, the pumping is regarded as groundwater channeling in the river terrace. Therefore, the pump supply is estimated based on gravel piles test runs, by channeling within them an amount of water of about 2,5m^3 and measuring its reduction rate.

The results of these tests can be used when the “quality” of the river terrace, on which the desired rate is mainly depended, is the same throughout the research area. Let us use for example 15´ as an indicative average time required for the water drawdown in the gravel piles. The pump supply is consequently given the value $\mathbf{q = 2.5m^3 /15 \ X \ 60sec = 0.0028 \ m^3/sec}$.

Due to the correlation of the two above cases the Thiem equations, of pumping tests, apply, so according to the symbolizations in Fig. B3 & B4, we get:

$$q = \frac{\square k (\square^2 - y^2)}{\ln (R/x)} \qquad (2)$$

$$k = \frac{q}{\square (H^2 - h^2)} \ln \frac{R}{r} \qquad (3)$$

The level of the aquifer which is obtained during design is the level which corresponds to the most “wet” period of the year, so the rainwater supply is intentionally disregarded [5 & 10]. We therefore apply the known relations and laws of underground hydraulics, for the application of which the assumptions of paragraph 2.2 are endorsed and they should be satisfied by the actual hydrogeological conditions of the area. The recommended arrangement among the Gravel piles is the ***linear*** one, ***because***:

- ❖ The area is riverine, so the further we move away towards the interior of the slope the biggest the likelihood of non-detecting the terrace gets and penetration adequacy of the gravel piles is not provided in the underlying river terrace.
- ❖ Throughout the mass of the landslide materials there is a distinctive equable distribution of pore pressure, resulting in *the identification of the free surface of the permeable layer and the level of the river*.

Note that the drainage in a landslide area with failures in various posts, without their hydraulic communication, is achieved by applying groups of Drainage Gravel Piles in these sub-positions.

3.4 Calculation of the suitable distance between the Gravel Piles

For the investigation of the requisite arrangement of the drainage gravel piles, a good knowledge of geotechnical conditions, as well as hydraulic parameters of the landslide area is required. These data are obtained from executing sample drillings and by installing piezometers and inclinometers within them. The former is used for level measurements and their changes and the second for the certification of ground motions, as well as for the verification of their reduction, after the application of the drainage program, and therefore for the achievement of the goal of our study.

As mentioned above, the precise mathematical model of free surface flows is described by the Thiem equation (equation 1), with a series of assumptions. The solution of this equation, for a typical pumping case of a well in an aquifer, gives the following equations for the calculation of the supply and the change of free surface (in different forms and based on the symbolizations in Fig. B4):

$$q = \frac{\square k (\square^2 - y^2)}{\ln (R/x)} \qquad (4)$$

$$q = \frac{\square k (\square^2 - h^2)}{\ln (R/r)} \qquad (5)$$

$$q = \frac{\square k (y^2 - h^2)}{\ln (x/r)} \qquad (6)$$

From the equality of the two equations (5) and (6) => $\frac{\pi k (H^2 - h^2)}{\ln (R/r)} = \frac{\pi k (y^2 - h^2)}{\ln (R/r)}$ =>

$$y^2 = h^2 + \frac{H^2 - h^2}{\ln (R/r)} \ln(x/r) \qquad (7)$$

where:
H = the initial level of the aquifer, before pumping,
h = the water level in the well, during pumping,
r = the distance from the centre of the well, in which the depth of the aquifer is equal to h and which coincides with the radius of the drainage well,
R = the impact radius of the well, i.e. the distance beyond which no drawdown due to pumping is observed,
x = the distance from the centre of the well, in which the depth of the aquifer is equal to y.

From equation (7) by solving for x we get the equation:

$$x = \exp\left(\ln \frac{R}{r} \times \frac{y^2 - h^2}{H^2 - h^2} + \ln r\right) \qquad (8)$$

The solution of equations 4-7 requires the estimation of sizes H, R and h. In point of the initial level H of the aquifer, before the pumping, it depends on the occurrence depth of the river terrace (= $\mathbf{H_{riv.ter.}}$). During designing, the initial level of the aquifer is measured, $\mathbf{H_{in.lev.}}$, so we get:

$H = H_{riv.ter.} - H_{in.lev.}$
*Porchet after a lot of trials of pumping proposed, suggested the approximate, empirical relation **ln (R/r) = 4.651*** (which also we use). It has also been estimated that there is a specific value for the water level h, h_{cruc}, beyond which it can no longer be reduced and it equals: ***$h_{cruc} \approx ⅓H \div ⅔ H = ½ H$.*** Thus solving equation (6) the q_{cruc}= … *m^3/s* is estimated. Also, for flow rates higher than q_{cruc}, and therefore for the actual pump supply as well, the value of h does not drop below h_{cruc}, hence the design value ***$h = h_{κριτ} = 0,5 X H$.*** [5] is accepted. The relegation by β m of the initial level of the aquifer is examined, so that under the drainage conditions created by the simultaneous operation of the gravel piles arrangements, proposed, to find itself below the level of the slide surface. A linear arrangement is selected, with α the axial distance of the gravel piles (Fig. B5). The distance x from the centers of the specific gravel piles equals x = a/2 => a **= 2x**.

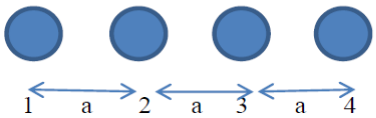

Figure B5: Order gravel piles fixed axial distance a

For the proper function of the gravel piles arrangement we set as a target that the final level value, at a random point inside the study zone, should come of the calculation of the overall drawdown at this point, due to their simultaneous function, that serves the objective of the slope stability. So, the goal of our study is reduced to the calculation of distance x and subsequently by equation (8), distance a [6 & 12]:

$$a=2x=2 \exp\left(\frac{\ln R}{r} \times \frac{y^2-h^2}{H^2-h^2}+\ln r\right) \qquad (9)$$

From results, of a georesearch program has preceded, we estimated the average occurrence of the river terrace: **$H_{riv.ter.}$ =25m** and the underground water level in the landslide materials: **$H_{in.lev.}$ =17m.** We also want the function of a single gravel pile to induce a drawdown equal to half the required value, that is d=b/2m and b= required level- $H_{in.lev.}$ and because of Fig. B4: y=H–d => y=H-d/2. The required level is related to the **occurrence depth of the slide surface** which occurs on the interfacial boundary of landslide materials-flysch background (i.e. **about 20 to 22m deep)**. Thereby, the minimum required level for the area stability should be in 22m deep, so:
$q=2,5m^3$ /sec (we put the inserted water amount during tests as the pump supply).
$H_{riv.ter.}$= 25m
$H_{in.lev.}$ = 17m => H = $H_{riv.ter.}$ – $H_{in.lev.}$= 25-17m = 8m
b=required level - $H_{in.lev.}$= 22m – 17m = 5m => d = b/2 = 2,5m, The following also apply:
ln R/r = 4.651 h = 0.5 x H = 0.5x 8m=4m και y = H- b/2 = 8 – 2,5m = 5,5m
r=d/2=1m/2=0.5m (we use the drill diameter, on ground surface)
By applying then relationship (2), we get:

$$\mathbf{a = 2x=2 \exp\left(\frac{\ln R}{r} \times \frac{y^2-h^2}{H^2-h^2}+\ln r\right) = 2 \exp\left(4.651 \times \frac{5,52-42}{82-42}+\ln 0,5\right) = 2 \exp 0,71=4,3m}$$

The required distance between the gravel piles is therefore ~4.5m.

3.5 Application of Drainage Gravel Piles

The general picture given by the measurements of the already installed instruments in the area confirmed that this is a slope of limit equilibrium. Amongst other measures proposed for the stabilization of the slope were also the deep drainage works, which concerned the drainage wells of the 1st and 2nd group (Drainage Gravel Piles). These permeate the landslide materials and reach down about 3 to 5m within the river terrace gravels. By monitoring and the estimating the optimal operating distance of the gravel piles, it was resulted and proposed that of 5.0 m. They are arranged into two rows, the downstream and the upstream row (Map A3). The upstream well row included wells Φ99 to Φ134, at axial distances, with very few exceptions, of about 5m. They are 33 in total (102&104 are missing) and they were drilled in 10th/2007. The upstream row included wells Φ135 to Φ217 and after a modification they were drilled one well at a time, so, in total 42 wells were drilled in 9th/2007. [4]

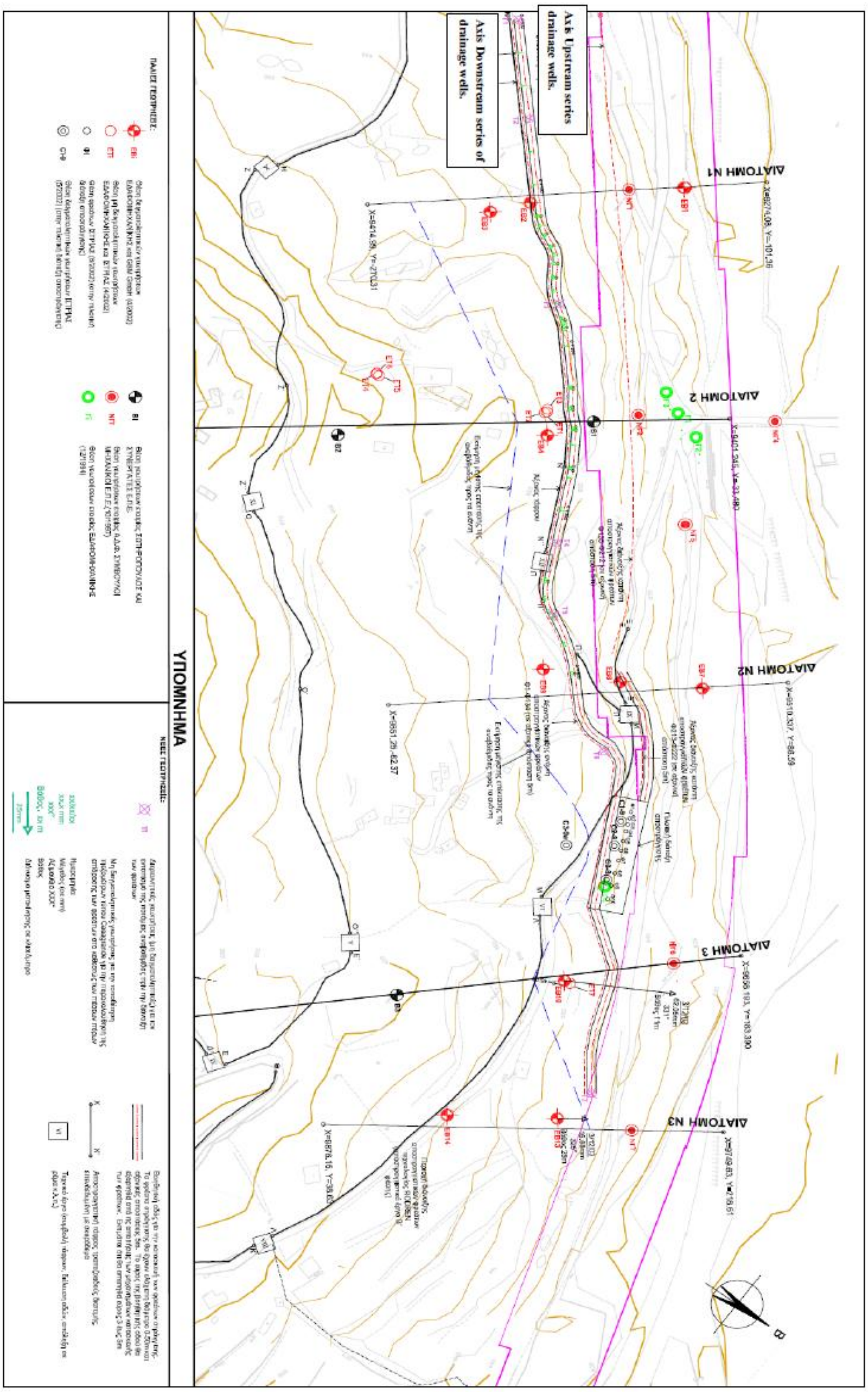

Map A3: Horizontiography of the landslide area (1+100 – 1+900) of the section 3.1 of the Egnatia Highway (Distinguished the drainage pilot program and axes opening of downstream and upstream wells series). (Egnatia Highway S.A. Measurement Department of the Geotechnical Instruments).

3.6 Effects of the Drainage Gravel Piles application on the landslide area

As part of our study, we monitored the progress of the landslide phenomenon through constant observation and evaluation of the measurements of the piezometers and inclinometers for many years (up to five years 3rd/2012, since the deep drainage works construction). In this way, we investigated the success of the drainage project by monitoring the groundwater level, while, at the same time, we observed the reduction of ground motions and consequently the stabilization of the greater landslide area. More specifically, from the evaluation of these measurements- some tables are given indicatively in annex D- we ascertain that ***after the completion of the project a drawdown is observed and this drawdown trend goes on throughout the whole observation period*.** Thus therefore, observing the measurements of the installed piezometers (ET4, ET5, ET6, ET7), in the greater landslide area B, from 2002 up to their last measurement 3rd/2012, we observe humiliation of level. This drawdown ranges from a minimum decrease of 1m (ET4) up to the maximum decrease of 8.43m (ET5) or an up to 96% decrease, after the Drainage Gravel Piles construction (9th/2007). There are of course intermediate values of drawdown e.g. a 2.9m decrease (ET6), or a 1.82m decrease (ET7), (**Table D1**).

Table D1: Measurements level of ET-piezometers in the area of the landslide.

	Days	Depth instrument (m)	Water level from ground	Level reduction after the wells	Remarks
ET4 (Days installation 18/4/02)	22/10/02	6	5,20	**0,80**	Dry
	13/3/12		Dry		
ET5 (Days installation 18/4/02)	10/9/02	13	4,57	**8,43**	
	13/3/12		Dry		Dry
ET6 (Days installation 24/4/02)	9/6/05	21	16,52	**2,91**	* Blocked in 21m
	13/3/12		19,43		
ET7 (Days installation 24/4/02)	10/9/02	13	2,20	**1,82**	
	15/2/11		4,02		

After the construction of the Gravel Piles, previously installed piezometers in the area also exhibit a drawdown (EB2, EB3, EB5, EB6, EB9, EB12 & EB13), with minimal reduction of 0.14m (EB2) and maximum reduction of 3.11m (EB2). Intermediate reductions of approximate 2.59m (EB3) and 0.87m (EB5) are also observed. We stress out that the greatest drawdowns concern the piezometers closest to wells area, while it is worth noting that though the level may not be reduced enough, it never reaches, however, its initial price, not even in winter or the rainy spring months (March-April), e.g. piezometer EB3. Also the levels of the two row wells of deep drainage works remain stable at low prices even in winter months, on all these years. From the measurements of pore pressures we obtained from the Casagrande piezometers, we notice, in the downstream wells NΠ15 and NΠ17 and upstream wells NΠ6-2 NΠ6-3, ***reductions in pore pressures in depths greater than 10m*** (depth of interest), from ***a minimum of 6% (NΠ17) up to a maximum of 21% (NΠ15),*** (**Table D2**).

Table D2: Measurements of NΠ-Casagrande piezometers in the area of the landslide.

NΠ6-2 Days installation 5/10/06 - Depth instrument 19,50m.		**NΠ15 Days installation 11/10/06 - Depth instrument 23m.**	
Days	**kPa**	**Days**	**kPa**
1/3/2007	117,692	**13/7/2007**	100,607
24/9/2007	112,230	**24/9/2007**	91,148
14/12/2007	109,929	**24/4/2009**	86,370
13/3/2012	109,796	**16/2/2011**	Destroyed
NΠ6-3 Days installation 5/10/06 – Depth instrument 29,50m.		**NΠ17 Days installation 04/10/06 - Depth instrument 22m.**	
Days	**kPa**	**Days**	**kPa**
1/3/2007	80,870	**13/7/2007**	133,240
24/9/2007	66,726	**24/9/2007**	128,791
14/12/2007	69,053	**13/3/2012**	128,083
13/3/2012	69,713		

Finally, **in Table D3**, we see characteristically some of the installed inclinometers of the deep drainage project area. We observe a reduction in ground motions after the deep drainage project construction. The inclinometers that did not display any motion or distortion prior to the construction of the wells, such as ***EB8 & EB9, continued to show the same behavior after their construction***. On the contrary, in the inclinometers of the drills (***EB3, EB10, EB11 and EB13***) that ***had recorded motions before the drainage gravel piles construction, a significant decrease, tending to zero, was noted after their construction***. More specifically: the motion rate ***completely stopped in inclinometer EB11***, in inclinometer ***EB3 the motion decreased from 7mm per year to 0.80mm per year*** and in inclinometer ***EB13 from 20-25mm per year to 7.3mm per year***. The ***EB10*** inclinometer ***was destroyed*** (on 06.08.2004) due to heavy distortions and was replaced by ***EB10N, and the motion decreased from ~ 21mm per year to 7.5mm per year***. Regarding the newest inclinometers which are mounted in the drills in the upstream wells area NK1, NK2, NK4 & NK6 ***we observed motion only in the NK***, with an observed ***move decrease from 1.71mm per year to 0.46mm per year***.

Table D3: Speed movement and maximum movements derived from measurements of inclinometer in the area of the landslide.

inclinometer	Depth motion (m)	Moving speed (mm/month) Days installation-10/07	Moving speed (mm/month) 10/07-03/12	Maximum movement (mm)	Remarks
EB 3	3,0-5,00	0,00-0,94 **(M.O. 7mm/year)**	0,01-0,41 **(M.O. 0,8mm/year)**	**7,75**	
EB 10	11,00	0,06-13,75	**Maximum movement 89,76 mm (**destroyed 6/04 and replaced by EB10N).		
EB 10N	11,00	0,05-1,57 **(M.O. 21mm/year)**	0,18-0,92 **(M.O. 7,57mm/year)**	**41,05**	
EB 11	30,00	0,00-1,60	**Maximum movement 8,35mm** (until 14/5/07, Since there is no development of the phenomenon).		
EB 13	25,00	0,34- (-4,75) **(M.O. 20-25mm/year)**	0,13-3,39 **(M.O. 7,30 mm/year)**	**Maximum movement 71,24mm** (until 15/4/09, Since there is no development of the phenomenon).	
NK6	22,00	0,00-0,80 **(M.O. 1,71 mm/year)**	0,00-0,12 **(M.O. 0,46mm/year)**	9,42	
EB 8	2,00-4,00	0,04	After 8/12/06 destroyed due asphalt paving.		
EB 9	25,00-35,00	**Strong deformations until 20/11/2004,** thereafter showed no particular development.			

From the monitoring and the evaluation of the measurements of the geotechnical instruments, for many years, confirm the success of this project. Namely, the construction of two rows of drainage wells (Drainage Gravel Piles) manage to drain the landslide materials within the river terrace materials, resulting in drawdown or immersion of the aquifer and the rate decrease of ground motions, thus the beginning of the stabilization of the landslide area.

IV. CONCLUSIONS

Finally, we conclusively report that:

- ***The drainage gravel piles, whether of minor range or of an extensive landslide***, in the presence of high water-bearing capacity within its structuring materials in cases of underlying unsaturated permeable body (e.g. buried river terrace), ***achieve the drainage of landslide materials in this permeable background, through the groundwater drawdown, the reduction of pore pressure and the consequential reduction of ground motions, therefore the beginning of landslide stabilization***.
- The drainage gravel piles achieve a ***greater groundwater drawdown or reduction of pore pressure, within the mass of the landslide materials, as the distance between the wells decreases and as the depth increases in the mass of the landslide materials***.
- ***The drainage of landslide areas***, in which failures are pointed out in various posts without their hydraulic communication, ***is achieved by applying groups of drainage gravel piles***.
- ***Finally, the study and application of the Drainage Gravel Piles*** in the abovementioned area of Egnatia Odos ***certify that these projects may not be sufficient on their own to entirely stop in time the motion of the landslide*** which occupies a large area and manifests recurrent landslide incidents, ***they contribute however to a greater extent than others to the stabilization of the situation and to further restoration of the equilibrium***.

REFERENCES

[1] Voudouris K. (2011), “Exploitation And Management Of Groundwater – Pumping Tests”, (Pp. 3-17), Thessaloniki.
[2] Egnatia Odos S.A. (2002), “Egnatia Odos – Information Note”, (P. 3), Thessaloniki.
[3] Edafos Engineering Consultants S.A. (1999), “Final Geotechnical Study Of Area B, From 1+100 Ch To 1+900 Ch”, Athens.
[4] Associated Engineering Consultants : Edafos Engineering Consultants S.A. - Geologiki Epostirixi S.A. - Galeridis K.,-Bourbos E. & Associates E.E. – Anodos Ete Karavokiris G. & Associates Engineering Consultants S.A. (2004), “Landslide Investigation At 1+100 Ch ÷ 1+900 And Final Editing Of Road Construction Study, Hydraulic And Geotechnical Works, 0+617 Ch ÷ 2+460 At Peristeri Ic, In The Peristeri-Anthochori Section Of Egnatia Odos”, Athens.
[5] Exarchou - Nikolopoulos - Bensasson Engineering Consultants S.A. (2002), “Evaluation Report On Drainage Pilot Project In Landslide Area In Section 1.1.3 (Likopodi-Makrichora) Of The E.O. From 10+100 Ch-10+660”, Athens.
[6] Exarchou - Nikolopoulos - Bensasson Engineering Consultants S.A. (2000), “Geotechnical Surveys, Studies Of Supporting Techniques And Stabilization Work Study In Landslide Area In Section 1.1.3 (Likopodi-Makrichora) Of The Nr From 10+100 Ch-10+660”, Athens.
[7] Dimopoulos G. (2008), “Engineering Geology”, (Pp. 21-52), Publisher: Kyriakidis Brothers Sa, Auth.
[8] Kallergis G., Koukis G. (1985), “Engineering Geology”, Publisher: O.E.D.B.., Athens.
[9] Katsikatsos G.C. (1992), “Geology Of Greece”, University Of Patras.
[10] Latinopoulos Π. Δ., “Groundwater Hydraulics”, (Pp.61-151), Thessaloniki.
[11] Mountrakis D. (1982), “Geology Of Greece Courses”, University Of Thessaloniki.
[12] Papanikolaou D. (1986), “Geology Of Greece”, University Of Athens.
[13] Porchet, “The Inversed Auger-Hole Method” Is A Technique For Determining Hydraulic Conductivity Above The Groundwater Table (Wells 1989).
[14] Stournaras G. (2007), “Water: Environmental Dimension & Trail’’, (Pp.257-278), Athens.

International Journal of Modern Engineering Research (IJMER)
www.ijmer.com Vol. 3, Issue. 5, Sep - Oct. 2013 pp-3129-3133 ISSN: 2249-6645

Real Time Vision Hand Gesture Recognition Based Media Control via LAN & Wireless Hardware Control

Tarachand Saini,Savita Sivani
Dept. of Software Engineering, Suresh Gyan Vihar University Jagatpura mahal, jagatpura, Jaipur(raj.), India

ABSTRACT: *Gesture (Ges-ture) means a movement of part of body. Gesture Recognition is the technology that recognize the movement of body. It recognize hand, arms, head or any part of the body. So the goal of Gesture Recognition is to provide interface of human body with computer via mathematical algorithm.*

This paper gives a real time vision based method for recognizing human body motion using MATLAB. It also gives the working details of recognizing process using Edge detection and Skin detection algorithms. In this paper Gesture Recognition used to control the media application over LAN connectivity and wireless hardware interface technology employed allow us to control home appliances formed in a wireless network via Hand gesture movement only, this opens a new pleothera of avenues in real time vision based home automation system.

I. INTRODUCTION

Gesture Recognition recognize meaningful expression of motion by a human body, involving the hands, arms, face, head or body. Gesture Recognition is important in designing efficient human computer interface. Its provides a bitter bridge between machine and human than primitives tent user interface or event GUI(graphical user interface).

One of the attractive methods for providing natural human-computer interaction is the use of the hand as an input device rather than the cumbersome devices such as keyboards and mice, which need the user to be located in a specific location to use these devices. Since human hand is an articulated object, it is an open issue to discuss. The most important thing in hand gesture recognition system is the input features, and the selection of good features representation. This paper presents a review study on the hand postures and gesture recognition methods, which is considered to be a challenging problem in human computer interaction context and promising as well. Many applications and techniques were discussed here with the explanation of system recognition framework and its main phases. This section defines the literature review of real time media control application LAN control and hand gesture recognition with wireless network to control hardware. Appearance based technology is used for recognize a gesture. Appear based technology read appearance of image of hand and compare this image parameters with the extracted image feature from input video. Gesture recognition does not require the user to wear any special equipment or attach any devices to the body. The gestures of the body are read by a camera instead of sensors attached to a device.

We control media application or utility application through LAN. In recent years LAN connectivity of computer system is commonly used in all fields like Education, Business, Medical and Banking etc. Application sharing and open same application on many systems is common task. Gesture Recognition makes it easy to control media application (audio, video etc.) or utility application (notepad, word sheet or business purpose application) to share or open on different computers connected through LAN. A hand gesture is used on one system and its controls all LAN connected system. This paper gives and implements a idea of media application controlled over LAN network by a simple hand gesture recognition.

This paper also gives the idea of wireless hardware control. It controls hardware over wireless network. In any building or big companies to control the hardware like (fan, light, gates etc.) take more time and man work. We control hardware by gesture recognition manually or automatically through wireless connectivity. It is also used in home appliance to control like TV, Radio, Light, Fan, and Door through a gesture without use of switch. To understand gesture recognition two things are important.

I. **Human Gesture Introduction** - Human band gestures provide the most important means for non-verbal interaction among people. They range from simple manipulative gestures that are used to point at and move objects around to more complex communicative ones that express our feelings and allow us to communicate with others. Hand gesture recognition based man-machine interface is being developed vigorously in recent years. Due to the effect of lighting and complex background, most visual hand gesture recognition systems work only under restricted environment. Many methods for hand gesture recognition using visual analysis have been proposed for hand gesture recognition. Sebastiean Marcel, Oliver Bernier, Jean Emmanuel Viallet and Danieal Collobert have proposed the same using Input-output Hidden Markov Models. Xia Liu and Kikuo Fujimura have proposed the hand gesture recognition using depth data. For hand detection, many approached uses color or motion information. Attila Licsar and Tamas Sziranyi have developed a hand gesture recognition system based on the shape analysis of the static gesture. Another method is proposed by E. Stergiopoulou and N. Papamarkos which says that detection of the hand region can be achieved through color segmentation. Byung-Woo Min, Ho-Sub Yoon, Jung Soh, Yun-Mo Yangc and Toskiaki Ejima have suggested the method of Hand Gesture Recognition using Hidden Markov models. Another very important method is suggested by Meide Zhao, Francis K.H. Quek and Xindong Wu. There is another efficient technique which uses Fast Multi-Scale Analysis for the recognition of hand gestures as suggested by Yikai Fang, Jian Cheng, Kongqiao Wang and Hanqing Lu, but this method is computationally expensive. Chris Joslin et. al. have suggested the method for enabling dynamic gesture recognition for hand gestures. Rotation Invariant method is widely used for texture classification and recognition. Timi Ojala et. al. have suggested the method for texture classification using Local Binary Patterns.

II. GESTURE RECOGNITION

Gestures are expressive, meaningful body motions – i.e., physical movements of the fingers, hands, arms, head, face, or body with the intent to convey information or interact with the environment. There are several aspects of a gesture that may be relevant and therefore may need to be represented explicitly. Hummels and Stappers (1998) describe four aspects of a gesture which may be important to its meaning.

• Spatial information – where it occurs, locations agesture refers to.
• Pathic information – the path that a gesture takes.
• Symbolic information – the sign that a gesture makes
• Affective information – the emotional quality of a gesture.

In order to infer these aspects of gesture, human position, configuration, and movement must be sensed. Gesture recognition is the process by which gestures made by the user are made known to the system. Gesture recognition is also important for developing alternative human-computer interaction modalities. It enables human to interface with machine in a more natural way. Gesture recognition is a technique which used to take computers 'see' and interpret intelligently is becoming increasingly popular. Dynamic gesture recognition isn't something entirely new.

III. SYSTEM MODEL

Input: The input of the gesture recognition is hand gesture image that taken by a webcam or camera. This is a motion of hand or body part that is captured and processed by edge detection algorithm. Before preprocessing first we initialize variable and parameters.

Preprocessing: Preprocessing is applied to images before we can extract features from hand images. It is a step by step process to recognize and matching appearance of the image that is previously stored.

STEP 1: Captured image is a gray scale image converted into equal binary form or frames. Ostu algorithm is used to convert gray scale into binary form. In computer vision and image processing, Otsu's method is used to automatically perform histogram shape-based image thresholding or the reduction of a gray level image to a binary image. The algorithm assumes that the image to be threshold contains two classes of pixels or bi-modal histogram (e.g. foreground and background) then calculates the optimum threshold separating those two classes so that their combined spread (intra-class variance) is minimal.
The result of this step is in the figure show below.
STEP 2: After applying the Otsu algorithm on the original gray scale image, we find that some noise occurs in binary image or frames. These errors create problems in detection of hand gesture. So we need remove these errors. Morphological filtering approach is done to remove these errors. In the morphological filtering, we apply a rule on the binary image. The value of any given pixel in the output image is obtained by allying set of rules on the neighbors in the input image.
STEP 3: After finding the real binary image features extraction is perform. Features extraction is a process of find the edge of detected image. Canny edge detection algorithm is used for find the edge of detected image.
STEP4: The detected edge of image is used to match the appearance of hand gesture and give the result to the output hardware or media application.

IV. FLOW CHART

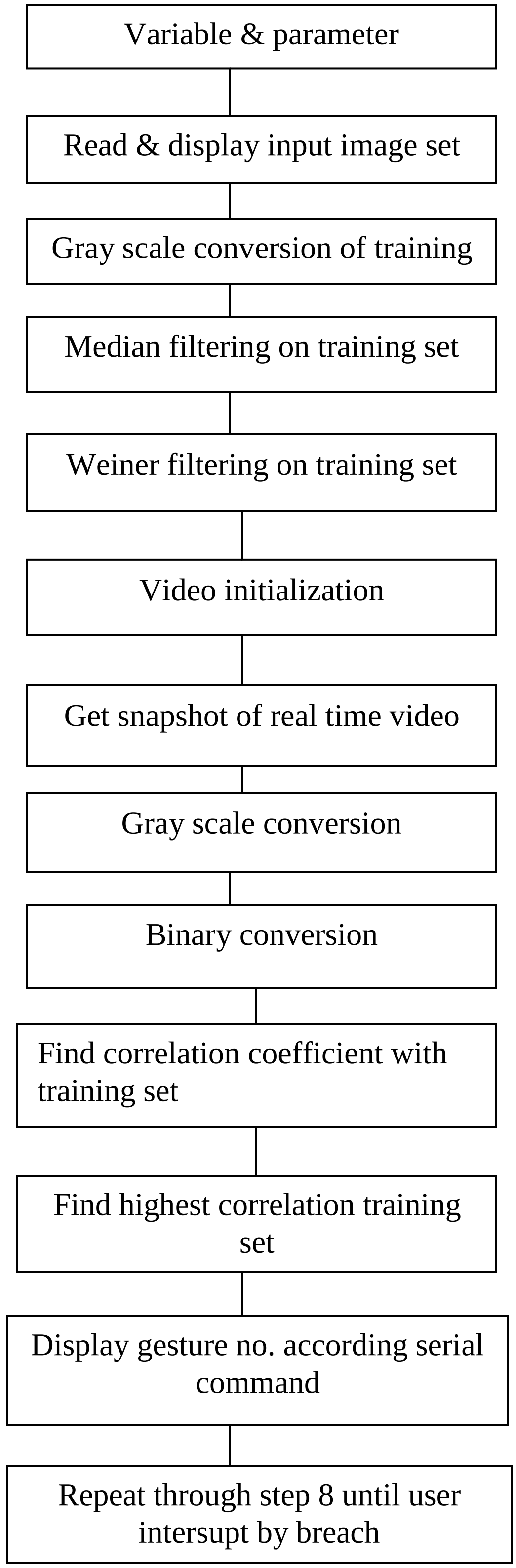

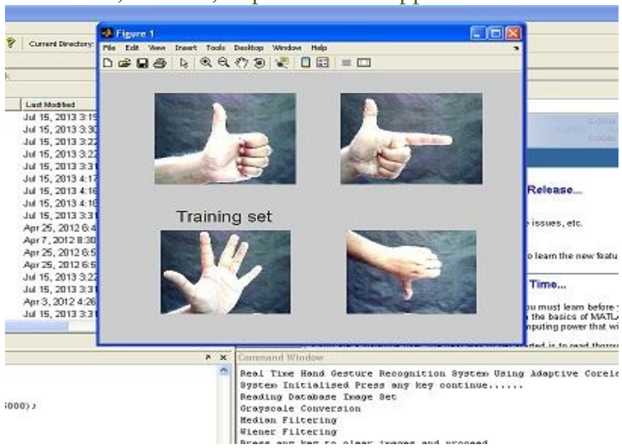

TRAINING SET

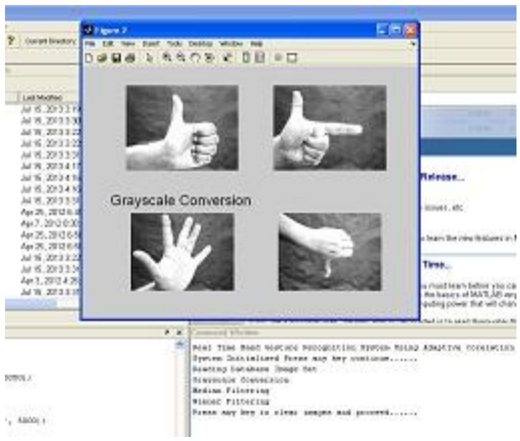

GRAY SCALE CONVERSION

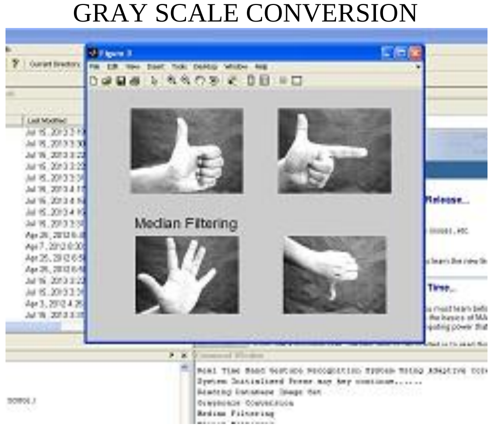

MEDIAN FILTERING

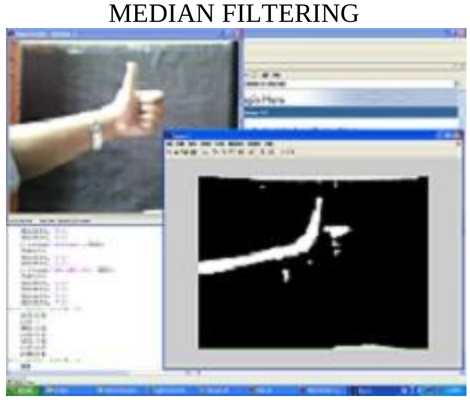

BINARY IMAGE

V. FURTHER RESRARCH

Further detail research is focused on providing security machenism through gesture. We use body motion for authentication purpose or provide security to access the information or data with CCTV camera. It will be a multipurpose system. Recognize a pattern of body motion with CCTV camera and used to provide security to system not extra webcam is used.

REFERENCE

[1] P. Jenifer Martina1, P. Nagarajan2, P. Karthikeyan3, "Hand Gesture Recognition Based Real-time Command System" 1P.G Scholar/Applied Electronics, Dept of ECE, PSNA College of Engineering and Technology Dindigul, Tamilnadu, India,April 2013.

[2] Sushmita Mitra, Senior Member, IEEE, and Tinku Acharya, "Gesture Recognition: A Survey" Senior Member, IEEE, May 2007.

[3] Carl A. Pickering*, Keith J. Burnham†, Michael J. Richardson*,"A Research Study of Hand Gesture Recognition Technologies and Applications for Human Vehicle Interaction", Coventry University, UK, Control Theory and Applications Centre, Priory Street, Coventry.

[4] Qing Chen, Nicolas D. Georganas, Emil M. Petriu, "Real-time Vision-based Hand Gesture Recognition Using Haar-like Features", School of Information Technology and Engineering University of Ottawa, March 2007.

[5] X. Zabulisy, H. Baltzakisy, A. Argyroszy, "Vision-based Hand Gesture Recognition for Human-Computer Interaction", Institute of Computer Science Foundation for Research and Technology - Hellas (FORTH) Heraklion, Crete, Greece.

[6] J. Canny,"A computational approach to edge detection," IEEE Trans. Pattern Anal. Machine. Intell., vol. 8, no. 6, pp. 679–698, Nov. 1986.

[7] Bill Green "Canny Edge Detection Tutorial.", http://www. pages. drexel.edu/~weg22/can tut.html ,2002.

Mislaid character analysis using 2-dimensional discrete wavelet transform for edge refinement

Kushal Kumar[1], Anamika Yadav[2], Himanshi Rani[3], Yashasvi Nijhawan[4]

[1](Electronics and Communication Engineering, Jaypee University of Engineering and Technology, India, 2013)
[2](Electronics and Communication Engineering, Bhagwan Parshuram Institute of Technology, GGSIPU, Delhi, India, 2012)
[3](Electronics and Communication Engineering, Vellore Institute of Technology, Chennai, India, 2015)
[4](Electronics and Communication, Jaypee University of Information Technology, Waknaghat, India, 2013)

ABSTRACT: *Character recognition is an important tool used for many purposes limited only by imagination, some of them being automatic number plate recognition and digital conversion of texts. In the present methods, edge detection techniques perform well but they are time consuming and have errors if the data provided is not up to the mark. In this paper, a novel method is proposed to minimize those errors and perform the edge detection of characters using 2-dimensional wavelet transform pre-processing.*

Keywords: *2-dimensional wavelets, Character recognition, Machine vision, Image processing, ANPR.*

I. INTRODUCTION

Today, many character recognition systems are used worldwide. The system works fine too in most of the cases, but sometimes the characters on given image aredifficult to identify because of many reasons like bad lightning, or mislaid/broken characters. In this paper, a vehicle number plate with difficult to detect characters is taken and, a novel image processing method for detection of characters using wavelet pre-processing is proposed to segment the characters from that image. The criterion used to compare different methods is touse the number of pixels of the characters the method could detect with the conventional edge detection techniques to emphasize the benefit of 2D-DWT over those methods.

A series of steps in wavelet pre-processed edge detection are performed in a systematic way which detects the characters. Edge detection is almost a prerequisite in various recognition tasks, like automatic number plate recognition, which we have done in this paper. Edge is a boundary between two homogeneous surfaces. Fig.1 shows the text which was used for edge detection in the proposed method and the conventional edge-detection methods (Sobel, Prewitt and Canny). Various conventional techniques for edge detection of IC's are available in literature[1]. Huang et al. (2011) proposes an improved algorithm for canny edge detection. It uses an improved switch median filter algorithm instead of Gaussian filter algorithms for filtering. [2]Somyot et al.(2012) used wavelet transforms to compress the image before edge detection.

II. EDGE DETECTION

An edge is an abrupt change in the intensity level, which characterizes high frequency component in an image. Noise is an unwanted signal which can cause inefficiency in edge detection.

In practice due to imperfection in image acquisition or sampling, the edges get blurred and tend to become thick. However the derivatives play an important role in detecting the edges and locating the edge pixels in an image. The first derivative is positive at the point of intensity variation and zero in the areas of constant intensity. The magnitude of first derivative can be used to detect the presence of an edge. The second derivative is positive if the transition occurs on the dark side of an edge and it is negative if transition is on the light side of an image. Hence, a second derivative can be used to locate the edge pixels. For edge detection second derivative can also be used but its sensitivity towards noise limits its application in edge detection. In the subsequent sections we will be discussing about the approximated first derivative operators that are used for edge detection in the present investigation.

III. CONVENTIONAL EDGE DETECTION METHODS

The edge detection methods used in this paper are Sobel, Prewitt and Canny, which are compared to each other and then the best one of them is compared to the proposed algorithm. The algorithms are compared based on how much amount of the character data can they extract from the given image. So, first we should know briefly what these methods are and how do they work. Next, we extract the pin information from the original image as well as segmented edge-detected image in the form of number of pin-pixels and compare which method extracts the maximum pin-information for analysis. In the original image, the no. of pixels contained by the characters are 1882.

3.1 SOBEL

The Sobel edge detector is an approximated, first derivative two dimensional edge detector. It calculates gradient in X and Y direction. It uses a convolutional mask to calculate the gradients as in equation (1) and gradient directions as in equation (2). The masks are slid over the image and gradient values are calculated. In Sobel the centre coefficient of the mask uses a weight of two, it is used so as to achieve a smoothing by giving more weightage to the central term of the mask. The segmented image obtained by using a Sobel operator is shown in Fig.2. The number of pin-pixels detected by this algorithm was 203.

$|G|=|G_X|+|G_Y|$ (1)

$\Theta=\tan^{-1}[\frac{G_Y}{G_X}]$ (2)

3.2 PREWITT

Prewitt edge detector is also an approximated first derivative two dimensional edge detector. It uses aconvolutional mask to calculate the gradient in X and Y directions respectively. The segmented image obtained by using Prewitt operator is shown in Fig.3. The number of pin-pixels detected by this algorithm was 201.

3.3 CANNY

Canny edge detection is another method of edge detection. It follows a series of steps. In the first step it eliminates the noise from the Image by filtering the Image using Gaussian filter. In the second step it calculates the gradient and the edge direction of the Image using Sobel edge detection. In the third step it performs non-maximum suppression. The pixels along the edge direction which do not satisfy (3) are set to 0 or considered as non-edge pixel. Further suppression is done using hysteresis. Hysteresis uses two thresholds. T1 and T2. If the magnitude is below the first threshold then it is set to 0 (non-edge pixel). If the magnitude is above threshold T2 then it is considered as an edge pixel. If the magnitude lies between T1 and T2 then depending upon the path between the current pixel and the pixel with magnitude greater than T2 the pixel is considered as an edge pixel or non-edge pixel. The segmented image obtained by using a canny edge detector is shown in Fig.4. The number of pin-pixels detected by this algorithm was 978.

IV. WAVELETS

Wavelets are a small portion of the wave. Wavelet transform uses wavelets to capture different frequency components of the signal whose resolution matches up with its scale. This technique is known as multi-resolution Analysis. It comprises of a scaling function and a wavelet function. Scaling function gives the series of approximation of the signal, where each approximated signal differs by a factor of two. Wavelet functions are used to add the detailed information in the difference of the two neighbouring approximations. Hence in wavelet analysis we get the approximated part and the detailed part of the signal.

In case of Images the wavelet analysis is carried out in two dimensions. In X and Y direction respectively, the two dimensional wavelet decomposition is shown in the form of an image in Fig. 5. It is known as filter bank analysis. It consists of high pass and low pass filters. First the analysis is done along the columns and then along the rows. The output of the low pass filter gives the approximated coefficients and the output of the high pass filter gives detailed coefficients. The approximated coefficients at scale j+1 are used to construct the detailed and approximated coefficients at scale j. In case of two dimensions we get three sets of detailed coefficients (rest three squares) and one set of approximated coefficient (upper left square).

V. PROPOSED METHOD

In the proposed method, we have first subjected the image to a 2-Dimensional discrete wavelet transform (2-D DWT). Doing this, we get a set of 4 images, one is the set of approximated coefficients and the other three are set of detailed coefficients. We ignore the approximated coefficient and reconstruct the image using the set of detailed coefficients, i.e. we take inverse 2-D DWT. The image is now ready to be edge-detected using any conventional algorithm like Canny in this case. So, we choose the best one of the conventional methods, which comes out to be Canny and then compare it with our proposed method in Fig. 6. The number of pin-pixels detected by this algorithm was 5636, i.e. 84.25% of the pin-information is accurately extracted.

VI. FIGURES

Fig.1 Original IC image**.**

Fig.2Character segmentation on Sobel edge-detected image.

Fig.3 Pin segmentation on Prewitt edge-detected image

Fig.4 Character segmentation on Canny edge-detected image.

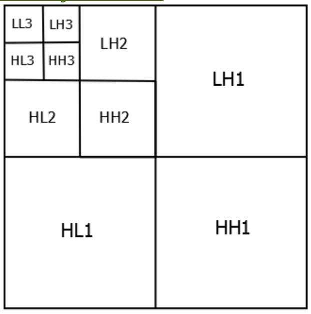

Fig.5 2-D DWT illustration.

Fig.6 Pin segmentation on Wavelet pre-processed Canny edge-detected image.

VII. CONCLUSION

Based on the results the following inferences can be made. When wavelet pre-processing was not performed, canny edge detection, Fig.4 was found to be the most efficient method followed by Sobel, Fig.2 and Prewitt, Fig.3, which are pretty close to each other. When wavelet pre-processing was used, the results obtained are as shown in Fig. 6 which arefar more accurate than the results obtained without using wavelet pre-processing as in Fig. 2, 3 and 4. The proposed method detects over 50% of the pixels while the conventional methods could detect only about 10%. On using wavelet pre-processing the low frequency component of the image was removed and high frequency components were retained during reconstruction. The edges which comprises of high frequencies were efficiently detected. Thus the choice of using wavelet pre-processing made edge detection more efficient. Better and efficient extraction of IC pin information was achieved.

Many sectors could benefit from this approach, like the traffic regulation sector or the handwriting analysis sector. The number of man-hours will be greatly reduced and the results would be more accurate than any of the current methods. This method could be implemented over existing hardware.

ACKNOWLEDGMENTS

I, Kushal Kumar, would like to thank Dr. Sudha Radhika who was an inspiration for me to take up this project.

REFERENCES

[1] Ying Huang, Qi Pan,Qi Liu,XinPeng He,Yun Feng Liu,Yong Quan Yu, “Application of Improved Canny Algorithm on the IC Chip pin Inspection”,Advanced Materials Research Vols. 317-319 (2011) pp 854-858.

[2] K. Somyot, S. Anakapon and K. Anantawat, “Pattern recognition technique for IC pins inspection using wavelet transform with chain code discrete Fourier Transform and signal correlation”, International Journal of Physical Sciences, Vol.7 (9), pp. 1326-1332, 23 February 2012.

[3] Tim Edwards, “Discrete Wavelet Transform: Implementation and theory”, Stanford University, September 1991.

[4] Rafael C. Gonzalez, Richard E. Woods Digital Image Processing (ISBN-13: 978-0131687288,3rd Edition, 2007)

[5] Barroso, J. ; Seccao de Engenharias, Dagless, E.L. ; Rafael, A. ; Bulas-Cruz, J., “Number plate reading using computer vision”, ISIE '97., Proceedings of the IEEE International Symposium on Industrial Electronics, 1997.

Effective Searching Policies for Web Crawler

Suyash Gupta, KrishanDev Mishra, Prerna Singh
(Department of Information Technology, Mahamaya Technical University, India)
(Department of Information Technology, Mahamaya Technical University, India)
(Department of Information Technology, Mahamaya Technical University, India)

ABSTRACT: *As we know search engines cannot index every Web page, due to limited storage, bandwidth, computational resources and the dynamic nature of the web. It cannot monitored continuously all parts of the web for changes. Therefore it is important to develop effective searching policies. In this technique there is the combination of different searching technique to form a effective searching policies. These combined techniques are best first search, focused crawling, info spiders, recrawling pages for updation, crawling the hidden web page.This combined technique also includes Selection policy such as page rank, path ascending, focused crawling Revisit policy such as freshness , age Politeness , Parallelization so that it allow distributed web crawling.*

Keywords: *Best first search, recrawling pages for updation, crawling the hidden web page, focused crawling, Revisit policy, Politeness, Parallelization.*

I. INTRODUCTION

A Web crawler is a software program that helps in locating information stored on a computer system, typically based on WWW. Web crawlers are mainly used to create a copy of all the visited pages for later processing by a search engine that will index the downloaded pages to provide fast searches. Crawlers can also be used for automating maintenance tasks on a Web site, such as checking links or validating HTML code. Also, crawlers can be used to gather specific types of information from Web pages, such as harvesting e-mail addresses.

Given an initial set of seed URLs[5], it recursively downloads every page that is linked from pages in the set. A focused web crawler[10] downloads only those pages whose content satisfies some criterion also known as a web spider, bot, harvester.Web crawlersare commonly known as a Web Spider or a Web Bot. The crawler is an automated program that is designed to scan the World Wide Web. These crawlers are used by search engines like Google, Yahoo or MSN.

It provided these engines with update knowledge of the sites that are on the web. The crawlers begin with a list of sites to scan, these are called seeds. When the crawler comes to the sites it first identifies the hyperlinks on the page and then puts them on another list of the Url's called the crawl frontier. There are a couple of factors that may affect the way a crawler crawls a site. If there is a large volume of information it may take the crawler a bit of time to send the downloads. So the crawler will have to see what information it wants to send down first.

Another thing a crawler will notice is if the site has undergone a change since the last time it has crawled that site. There may have been pages added or removed during this time, which is a good thing because a search engine want to see a fresh site as long as you remove old pages. It is single piece software with two different functions building indexes of web pages and navigate the web automatically on demand.

Our goal is to have the crawler for our site in order to get a good rank. It can take a crawler weeks or a few months to change a rank but in that time there could be changes that have been made to the site. The crawler will already have taken this into consideration. You may have added or removed some content. Try to keep the site the same until your index changes. You can add pages because search engines love new content.They help us in getting track or getting updated information which we want to access.

II. HISTORY OF WEB CRAWLER

WebCrawler was the first web search engine. It was used to provide full text search. It was bought by America Online on June 1, 1995 and sold to Excite on April 1, 1997. Excite was born in February 1993 as a university project called Architext seeking to use statistical analysis of word relation to improve relevancy of searches on the internet. Then, web crawler was acquired by InfoSpace in 2001 after Excite, went bankrupt. InfoSpace also made to operates the metasearch engines DogPile and MetaCrawler. More recently it has been repositioned as a metasearch engine, providing a composite of separately identified sponsored and non-sponsored search results from most of the popular search engines.WebCrawler also changed its image in early 2008, scrapping its classic spider mascot.In July 2010, WebCrawler was ranked the 753rd most popular website in the U.S., and 2994th most popular in the world by Alexa. Quantcast estimated 1.7 million unique U.S. visitors a month, while Compete estimated 7,015,395 -- a difference so large that at least one of the companies has faulty methods, according to Alexa.[2][3][4]

III. WORKING OF WEB CRAWLER

Web crawler collects all the documents from the web to build a searchable index for the search engine. After collection and build a searchable index the web crawler identifies all the hyperlinks in the pages and adds them to the list of URLs to visit. The web crawler continuously populates the index server. The process of the search engines queries are firstly, the web server sends the query to the index servers that tell which pages contain the words that match the query.

Secondly, the query travels to the doc server, which actually retrieve the stored documents, snippets are generated to describe each search result. Thirdly, the search results are returned to the user. It recursively downloads every page that is linked from pages in the set. Our main goal is that the crawler comes to our site in order to get a good rank (i.e. highly ranked) for you. It can be done by having something on our site that a crawler will not see kind of defeats the purpose of having a site. It can take a crawler weeks or a few months to change a rank but in that time there could be changes that have been made to the site. In this there are combination of different technique for parameter tuning so that it shows the results of the searches as per the highly rank. It will also help to remove unwanted pages on the web[6].

IV. CATEGORIES OF SEARCH ENGINE : in terms of how they work

Crawler based search engine: These search engines create their listings automatically. Examples are Google, Yahoo. The Google web crawler will enter your domain and scan every page of your website, extracting page titles, descriptions, keywords, and links – then report back to Google IQ and add the information to their huge database. They crawl or spider the Web to create directory of information. People can search through the directory created in the above process. When changes are made to page, such search engines will find these changes eventually because they are automatically go from one web server to other looking for information, based on whatever information it can find their it will try to build up a directory. Later on whenever user submit a query the directory will be consulted to return the result. And if some pages are updated then the next time when the crawler again visit the web the new updated version will be consulted on the directory. It can serve automatically[8].

Human powered search engine: These depend on humans for the creation of directory. Example: OpenDirectory. One submits a short description (contain keyword and other information) for the web site to be listed to the directory. When searching is response to some user queries, only the description submitted are searched for. This process has been carried out by the person who had created the web page.Alternatively, editors can write reviews for some web sites. The editors will be taken a responsibility of submitting a information to the directory service, so that the web page is to be indexed. When changes are made to the page, it has no effect on the listing[8].

Hybrid search Engine: It can accept both types of result based on web crawlers andbased on human-powered listings. Hybrid search engine can look through dictionaries which are created by web crawlers and also using human power listing so both these are allowed there. But however most of such hybrid engines can assign prioritiesout of the web crawler and human powered listing which one should given higher priority. For example MSN search (product of Microsoft) gives priority to human powered listings and the technology of the tool that is LookSmart.MSN search also presents crawler based search results for complex queries. So it first look for the human powered listings and then for other one. The tools that it uses for crawler based search are Inktomi, SubmitExpress[8].

V. COMPONENTS OF CRAWLER BASED SEARCH ENGINES

Broadly they have three major elements first one is**crawler or spider**[1] that implies crawler will crawl from one web site to other. Usually this crawling is based on the hyperlinks that are present on one web page. It visits a web page, retrieves it, and follows the hyperlinks to other pages within the site. It visit the site regularly(once in every month) and look for changes that had taken place on the pages since the last time it was visited. Second one is **Index or catalog**[7]. It is like a huge book containing a copy of every web page that the crawler finds. It means the crawler whatever pages it retrieves it get stored in the index or catalog. Once stored it will remain there and it will be updated when a page changes. Indexing is an important step until a page is indexedit is not available for search. The Third one is **search engines software**is the actual softwarethrough which the user submit the queries. This program searches through the million of entries in the index because the index will typically contain huge number of entries to find the matches to a search. It can also rank the matches based on relevance (they should be mechanism for us to tell or to find out whether the particular page is relevant for search or not or given alternate pages). All crawler-based engines have above basic components, but differ in the ways these are implemented are tuned.

VI. EVALUATION OF CRAWLER

In a general,a crawler may be evaluated on its ability to retrieve good pages. However, a major hurdle is the problem of recognizing these good pages. The real users may judge the relevance of the pages as these are allowing the users to determine if the crawled was successful or not in an operational environment.

As we know the evaluation of crawler is quiet difficult because the main purpose of the crawler is to retrieve good pages, in the sense that are beneficial to the user for which they looked for. It is very important to judge the relevance of the pages that are crawled by crawler. Search engines cannot index every WEB page due to limited bandwidth, storage and computational resources and to the dynamic nature of the WEB, therefore it is important to develop effective crawling methods to assign priorities of the pages to be indexed. Since here we are not involving any real users, here we use topics instead of queries, each represented by a collection of seed URLs (uniform resource locator). Now it is clear that we clear the issues by moving from queries to topics. Let us consider we may lose any clues to user context and goals that queries may provide. However, this approach of beginning with the seed URLs is increasingly common in crawler research. We assume that if a page is on topic then it is a good page. There are also some limitations with assumption. All the assumption may not be sufficient condition according to user relevance. For example, a user who has already viewed a topical page may not consider it relevant since it lacks novelty. While we don't under rate these criteria, given the reasons stated above we choose to focus only on topic as an indicator of relevance for the extent of this research.[9][10]

VII. CONCLUSIONS

In past there is not very well documented in the written that every web crawler is scalable and also everything in the world has some limitation. These limitations are like parameter tuning, remove unwanted pages, paid crawl ordering, deep web. So in order to remove this limitation we have to make the effective searching policies for web crawler get accurate result. In this method we combine different technique which results into one can easily get the appropriateresult, it will also help to remove the unwanted web pages because of finite storage capacity.

REFERENCES

[1] He, H., Meng, W., Yu, C., and Wu, Z. WISE-Integrator*: A System for Extracting and Integrating Complex Web Search Interfaces on the Deep Web*. In Proceedings of the 31th VLDB Conference. 2005.
[2] Webcrawler.com Site Info Alexa, 2010
[3] Webcrawler.com-- Quantcast Audience Profile", Quantcast, 2010
[4] Site Profile for webcrawler.com, Compete, 2010
[5] A. Broder, M. Najork, and J. Wiener, "*Efficient URL caching for World Wide Web crawling,*" in Proceedings of the 12th International World Wide Web Conference, 2003.
[6] Grossan, B. "*Search Engines: What they are, how they work, and practical suggestions for getting the most out of them*," February1997. http://www.webreference.com.
[7] C. Duda, G. Frey, D. Kossmann, and C. Zhou, "*AJAXSearch: Crawling, indexing and searching web 2.0 applications*," in Proceedings of the 34th International Conference on Very Large Data Bases, 2008.
[8] I.Sengupta, "*Search Engine And Web Crawler*", Dept of computer science and engineering, Indian Institute of Technology Kharagpur.
[9] FilippoMenczer, Gautam Pant, PadminiSrinivasan, Miguel E. Ruiz," *Evaluating TopicDriven Web Crawlers*", Department of Management Sciences, School of Library and Information Science, The University of Iowa, Iowa City, 2001
[10] Y. Yang. "*An evaluation of statistical approaches to text categorization*", Information Retrieval, 1(1):69-90,1999.

Impact of the Hydrographic Changing in the Open Drains Cross Sections on the Hydraulic Efficiency of Open Drains

Esam El-Deen .Y. El-Azab[1], Hosam Ibrahim[2], Mohamed.M.F.Sobeih[3], Mahmoud Zayed[4]
[1,3](Department of Irrigation and Hydraulic, Civil Engineering/ Minoufia University, Egypt)
[2,4] (Channel Maintenance Research Institute, National Water Research Center, Egypt)

ABSTRACT : *Drained water is collected through 16000 km of open drains spread all over Egypt. Therefore, drains hydraulic problems lead to reduce their efficiency and ability to the free drainage of cultivated land. The work of the present investigation is based mainly on field data measurements along a group of selected drains. The derived relations were developed taking into consideration the degree of the drains. The main objective of this study is to carry out a research program include a group of Egyptian open drains. The developed new relations help in giving a set of rules that control the cross – section and gradient of regime alluvial drains in Egypt to improve its efficiency, achieve the highest operating efficiency of open drains, increase the ability of open drains cross sections for conveyance and identify scientifically study about the maintenance program of open drains.*

Keywords: *Hydraulic Efficiency, Open Drains, Hydraulic Parameters, Hydrographic Changing, Field Measurements.*

I. INTRODUCTION

Drainage of agricultural land is one of the pillars of the sustainability of agricultural production and protection of land degradation as a result of the high ground water level and the accumulation of salts. Therefore, the hydraulic problems of open drains affect the efficiency of drains, which leads to the existence of economic, environmental and social consequences. Molesworth and Yenidunia (1922) recommended an empirical formula for Egyptian trapezoidal drains. Preliminary investigations revealed that the previous empirical equations may not be valid for the present condition, where the suspended material of the river Nile decreased to value of less than 100 part per million after construction of High Dam. Therefore, improving the hydraulic efficiency of the drainage network in Nile Delta region is the most important concern for Ministry of Water Resources and Irrigation to raise efficient use and conservation of water loss.

II. INDENTATIONS AND EQUATIONS

Dimensional analysis is used in the derivation of general equation to compute the hydrographic changing in the open drains cross sections on the hydraulic efficiency of open drains were studied, This equation may be written in the following form:

$$\frac{K_d}{K_a} = f\left(\frac{y_d}{y_a}, \frac{T_d}{T_a}, \frac{R_d}{R_a}, \frac{A_d}{A_a}, \frac{P_d}{P_a}, \frac{d_{50}}{y_a}\right) \ldots\ldots(1)$$

$$\frac{R_d}{R_a} = f\left(\frac{y_d}{y_a}, \frac{T_d}{T_a}, \frac{A_d}{A_a}, \frac{K_d}{K_a}, \frac{P_d}{P_a}, \frac{d_{50}}{y_a}\right) \ldots\ldots(2)$$

Where: (y_d) is the design water depth of the channel, (y_a) is the actual water depth of the channel,(T_d) is the design top width of the channel,(T_a) is the actual top width of the channel,($K_d= (A_dR_d)^{2/3}$) is the design factor of hydraulic efficiency, ($K_a= (A_aR_a)^{2/3}$) is the actual factor of hydraulic efficiency, (R_d) is the design hydraulic radius of the channel, (R_a) is the actual hydraulic radius of the channel, (A_d) is the design channel area, (A_a) is the actual channel area,(P_d) is the design wetted perimeter of the channel ,(P_a) is the actual wetted perimeter of the channel and (d_{50}) is the median size of bed material.
A definition sketch for these hydraulic parameters is shown in Fig (1, 2).

III. FIELD MEASUREMENT AND DATA COLLECTION

To achieve the main goal of this study seven drains have been chosen to represent the operating conditions at west Delta in Egypt. They are chosen to cover the main drains and branches drains. These drains are El-Umum main drain and its branches Hares, Deshody, Troga, Ganabia El Umum El Bahrea, Shereshra and Abo Homes branch drains as shown in Fig (3) and Table (I) illustrate the characteristic design parameters of the selected drains at out let . The work program that implemented was divided into two parts, field and laboratory measurements.

For field measurements, the velocity measurements were accomplished by means of a calibrated electro-megnatic current meter at 0.2 and 0.8 of at least 15 vertical local water depth. Afterward, the discharge value was calculated using the simultaneous velocity and the water depth measurements. The boat equipped with echo-sounding apparatus to trace the shape of the drain cross-section at the selecting stations simultaneously with the velocity measurements. GPS was used to conduct the hydrographic measurements and it connected with the satellite and give high survey efficiency. From these data, the geometrical elements of the drain section such as water depth, cross sectional area, side slope, top width of water, hydraulic mean depth, and hydraulic radius are measured and calculated. The surface Water slope was calculated along a sufficient length of straight reach. Also full survey was carried out for the selected reaches of drains to identify degree of infestation and types of aquatic weed. Results and information obtained showed that, about 35 % of reaches are infested by emergent weeds In general, it can be concluded that state of weeds was acceptable and of negligible effect of flow.

For soil samples analysis, a series of laboratory tests were carried out for samples collected from bed and sides of the open drains to determine the grain size distribution particles. Sieve analysis tests were done for soil fraction retained by sieve 200 while for soil passed sieve No. 200, the hydrometer analysis was used. The total solid suspension in water samples was also determined. Table (II) illustrate the soil analysis for the selected drains.

IV. ANALYAIS OF THE RESULTS

For achieving the main objective of the present study, the field measurements and laboratory tests were analyzed to correlate the variable such as cross section area, water depth, top width, hydraulic radius, wetted parameter and Median size of bed material). The relationships represented for the studied main drain and branch drains between the hydraulic efficiency that represented by the section factor (K_a/K_d)= ($(A_aR_a)^{2/3}$/ $(A_dR_d)^{2/3}$), and the expression of the hydraulic efficiency represented by the hydraulic radius (R) versus the different hydraulic parameters.

4.1 Relationship between the Hydraulic Efficiency of Sections and Cross Section Area

By plotting the values of the hydraulic efficiency of sections versus the cross section area ratio (A_a/A_d) as shown in Fig (4) and (5), where these curves were obtained, with the following equations:

Hydraulic Efficiency % = 100.51(A_a / A_d) -15.057…………………..…..(3)

For open main drain with correlation coefficient R^2 = 0.98

(R_a / R_d) = 0.9586 (A_a / A_d) + 0.0753 ……………………………………..…(4)

For open main drain with correlation coefficient R^2 = 0.89

Hydraulic Efficiency % = 93.749(A_a / A_d) -9.5612……………………..…..(5)

For open branch drains with correlation coefficient R^2 = 0.93

(R_a / R_d) = 0.6556 (A_a / A_d) + 0.1369 ………..………...…………..……..(6)

For open branch drains with correlation coefficient R^2 = 0.80

4.2 Relationship between the Hydraulic Efficiency of Sections and Water Depth

By plotting the values of the hydraulic efficiency of sections versus the water depth ratio (y_a/y_d) as shown in Fig (6) and (7), where these curves were obtained with the following equations:

Hydraulic Efficiency % = 121.72(y_a / y_d) -24.268……..……..………….(7)

For open main drain with correlation coefficient R^2 = 0.929

(Ra / Rd) = 0.7816 (y_a / y_d) + 0.0547 ………....…………………………(8)

For open main drain with correlation coefficient R^2 = 0.977

Hydraulic Efficiency % = 146.87(y_a / y_d) -10.536……………......……..(9)

For open branch drains with correlation coefficient R^2 = 0.68

(Ra / Rd) = 1.246 (y_a / y_d) - 0.0187 …………………...…………………(10)

For open branch drains with correlation coefficient R^2 = 0.914

4.3 Relationship between the Hydraulic Efficiency of Sections and Hydraulic Radius

The relation between the hydraulic efficiency of sections versus the hydraulic radius ratio (R_a/R_d) was plotted in Fig (8) and (9), where these curves were obtained with the following equations:

Hydraulic Efficiency % = 96.692(R_a / R_d) -18.473……………..……….(11)

For open main drain with correlation coefficient R^2 = 0.938

Hydraulic Efficiency % = 126.94(R_a / R_d) -15.421……………………….(12)

For open branch drains with correlation coefficient R^2 = 0.777

4.4 Relationship between the Hydraulic Efficiency of Sections and the Wetted Perimeter

By plotting the values of the hydraulic efficiency of sections versus the wetted perimeter ratio (P_a/P_d) as shown in Fig (10) and (11), where these curves were obtained with the following equations:

Hydraulic Efficiency % = 138.53(P_a / P_d) -85.092……………………...(13)

For open main drain with correlation coefficient R^2 = 0.63

(R_a / R_d) = 1.5898 (P_a / P_d) - 0.849 …………………………....………(14)

For open main drain with correlation coefficient R^2 = 0.63

Hydraulic Efficiency % = 94.194(P_a / P_d) -39.951…...……....……...(15)

For open branch drains with correlation coefficient R^2 = 0.624

(R_a / R_d) = 0.5743 (P_a / P_d) + 0.0153……………..……................…(16)

For open branch drains with correlation coefficient R^2 = 0.618

4.5 Relationship between the Hydraulic Efficiency of Sections and Top Width

By plotting the values of the hydraulic efficiency of sections versus the top width ratio (T_a/T_d) as shown in Fig (12) and (13), where these curves were obtained with the following equations:

Hydraulic Efficiency % = 127.08(T_a / T_d) -77.52…………..…...….(17)

For open main drain with correlation coefficient R^2 = 0.63

$(R_a / R_d) = 1.0415 (T_a / T_d) - 0.396$ ……………………........………(18)
For open main drain with correlation coefficient $R^2 = 0.55$
Hydraulic Efficiency % = $236.3(T_a / T_d) -182.88$..…..…………….….(19)
For open branch drains with correlation coefficient $R^2 = 0.63$
$(R_a / R_d) = 0.4897 (T_a / T_d) + 0.0638$……………..……….......…(20)
For open branch drains with correlation coefficient $R^2 = 0.51$

4.6 Relationship between the Hydraulic Efficiency of Sections and the Median Size of Material to Water Depth

The relation between the hydraulic efficiency of sections versus the median size of bed material (d_{50}/y_a) was plotted in Fig (14) and (15), where these curves were obtained with the following equations:
Hydraulic Efficiency % = $- 100333(d_{50}/y_a) +52.311$……..……......(21)
For open main drain with correlation coefficient $R^2 = 0.70$
$(R_a / R_d) = - 919.73 (d_{50}/y_a) + 0.71$……… …….…………….......…(22)
For open main drain with correlation coefficient $R^2 = 0.66$
Hydraulic Efficiency % = $- 56678 (d_{50}/y_a) + 71.747$….……………..(23)
For open branch drains with correlation coefficient $R^2 = 0.70$
$(R_a / R_d) = - 608.82 (d_{50}/y_a) +0.8195$…….…………………..….......…(24)
For open branch drains with correlation coefficient $R^2 = 0.73$

V. FIGURES AND TABLES

Table I: The Characteristic Design Parameters of the Selected Drains at Out Let

Section No.	Drains Name	Area Served (Fed)	Discharge (m3\s)	Area (m2)	Water Depth (m)	Bed Width (m)	Water slope (cm/km)	Side Slope
1	El-Umum	400000	78.75	169.65	4.25	40	3	2:1
2	Hares	69000	19.44	42.24	2.01	18	10	3:2
3	Deshody	17500	5.64	15.46	1.79	6	9	2:1
4	Troga	15500	2.62	10.82	1.5	5	6	3:2
5	Ganabia El-Umum	31500	8.32	18.89	2.1	8	8	3:2
6	Shereshra	136000	34.89	74.34	3.3	18	6	2:1
7	Abo Homos	13000	4.05	12.35	1.05	5	9	3:2

Table II: Soil Analysis

Section No.	Drains Name	Type of Soil	
		Bed	Bank
1	El- Umum	Sand to Sandy Loam	Cohesive
2	Hares	Sand to Sandy Loam	Cohesive
3	Deshody	Sand to Sandy Loam	Cohesive
4	Troga	Sand to Sandy Loam	Cohesive
5	Ganabia El-Umum	Sand to Sandy Loam	Cohesive
6	Shereshra	Sand to Sandy Loam	Cohesive
7	Abo Homos	Sand to Sandy Loam	Cohesive

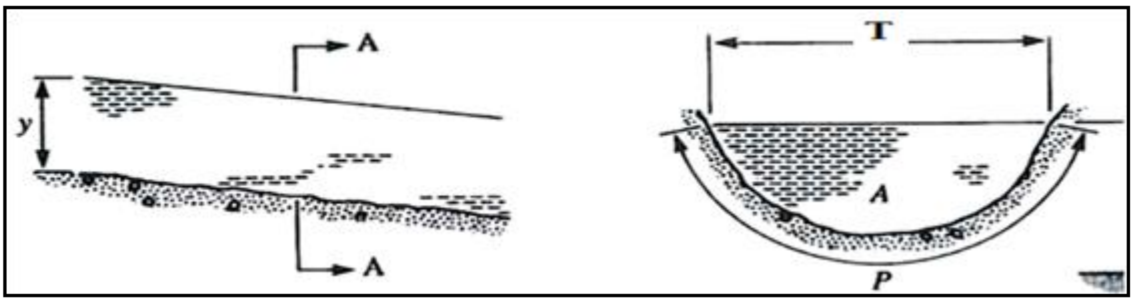

Figure 1: Definition sketch of actual geometric channel properties

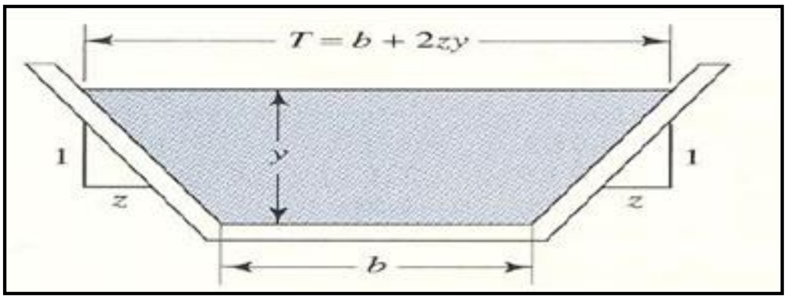

Figure 2: Definition sketch of design geometric channel properties

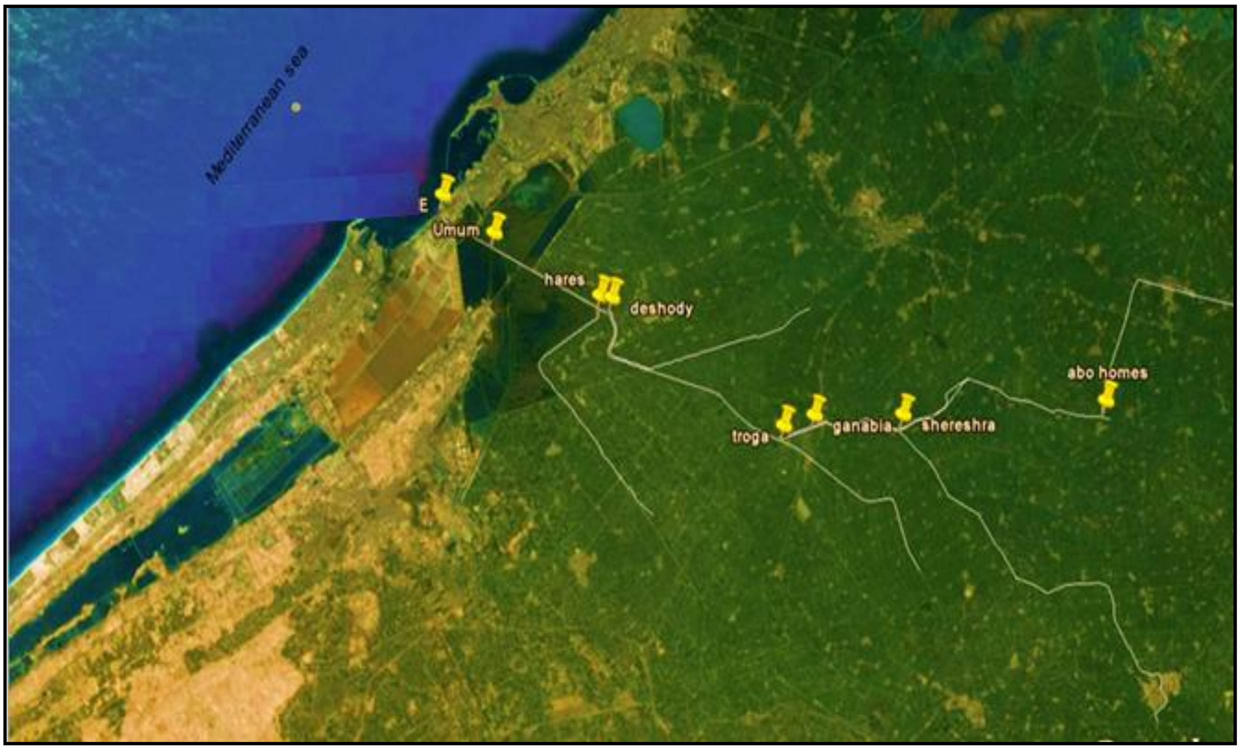

Figure 3: Google earth map of the selected drains under investigation

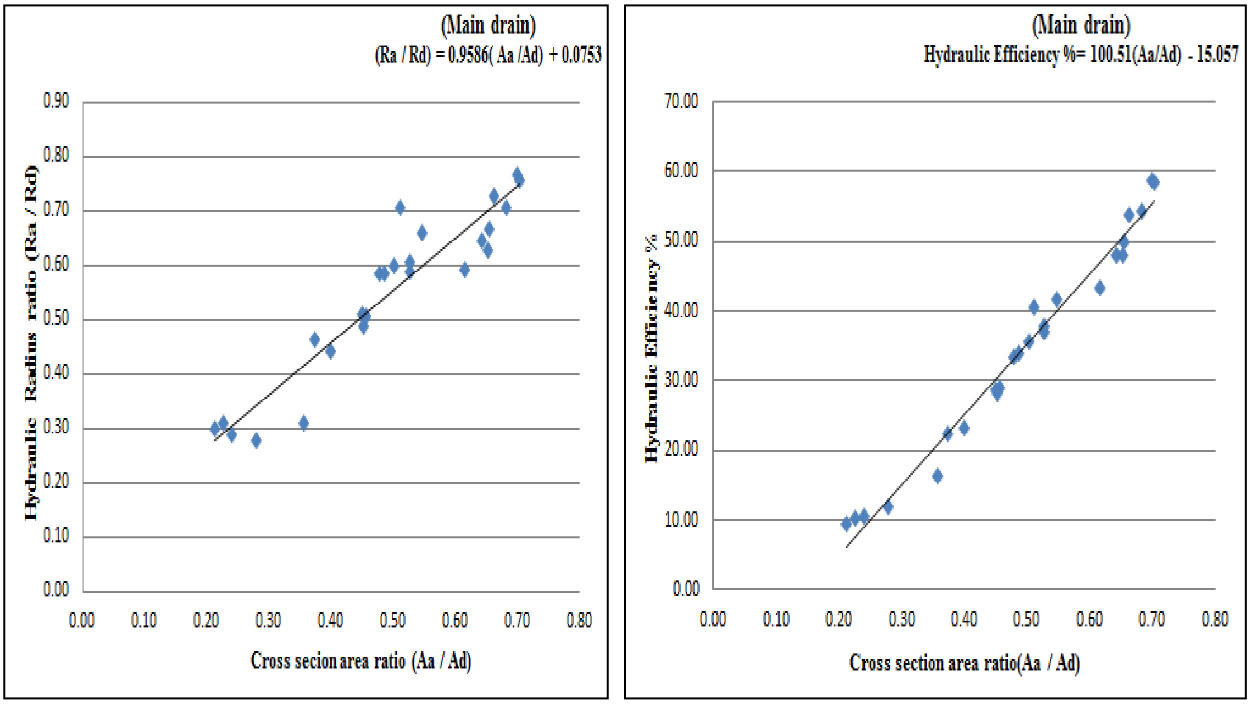

Figure 4: Relationship between hydraulic efficiency and hydraulic radius versus cross section area of main drain

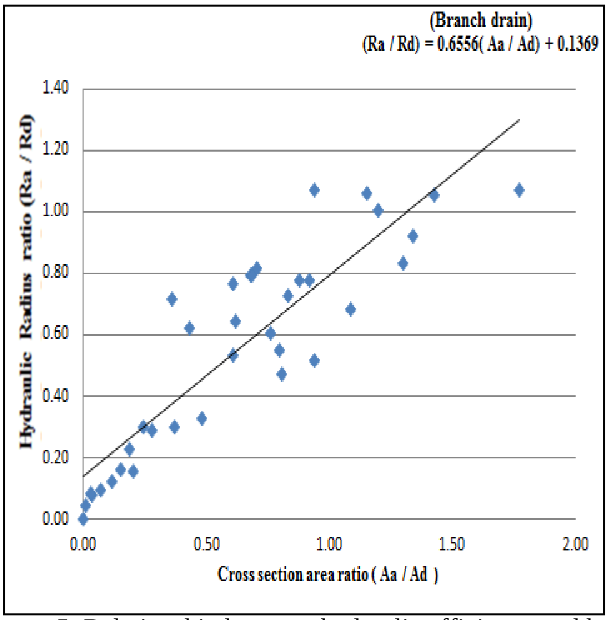

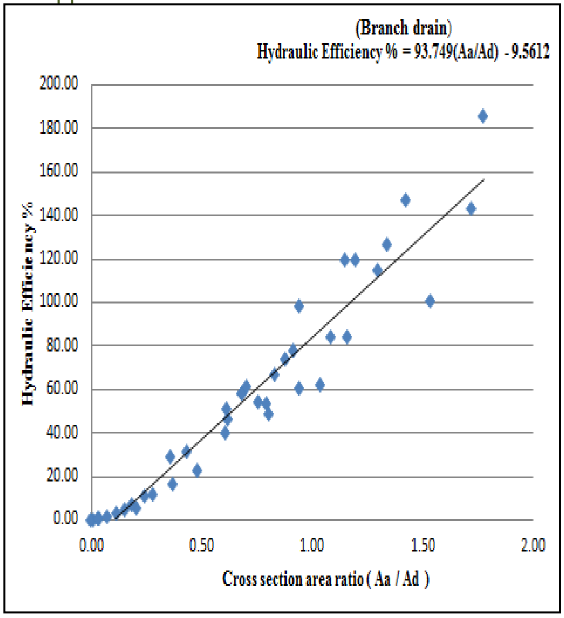

Figure 5: Relationship between hydraulic efficiency and hydraulic radius versus cross section area of branch drains

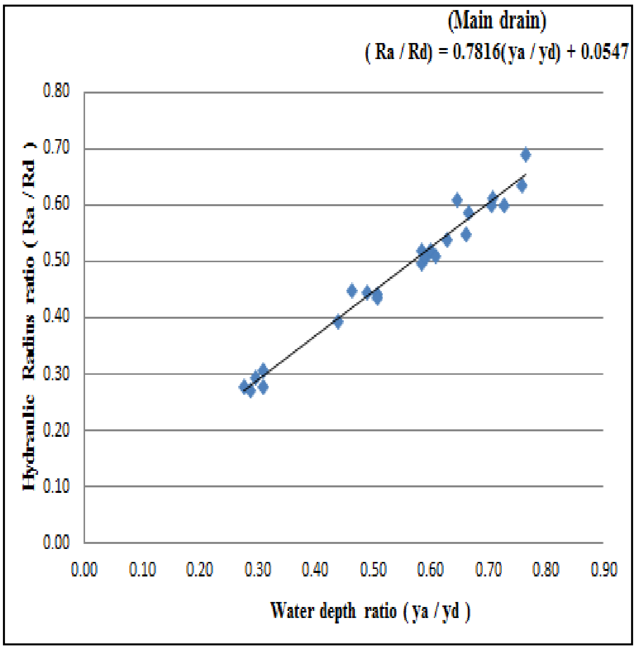

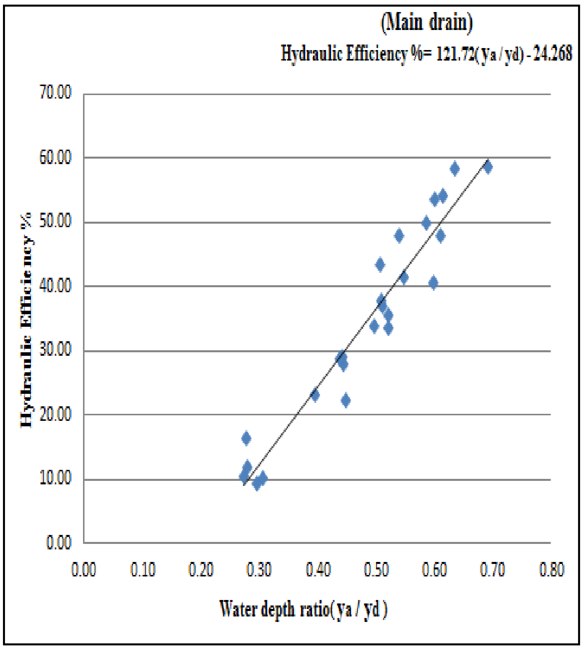

Figure 6: Relationship between hydraulic efficiency and hydraulic radius versus water depth of main drain

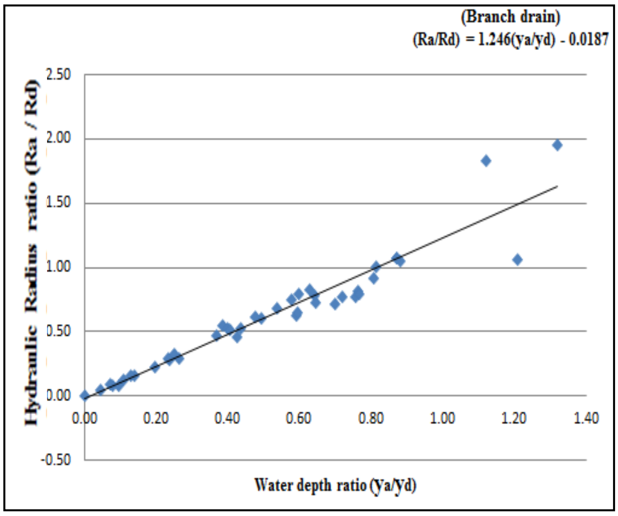

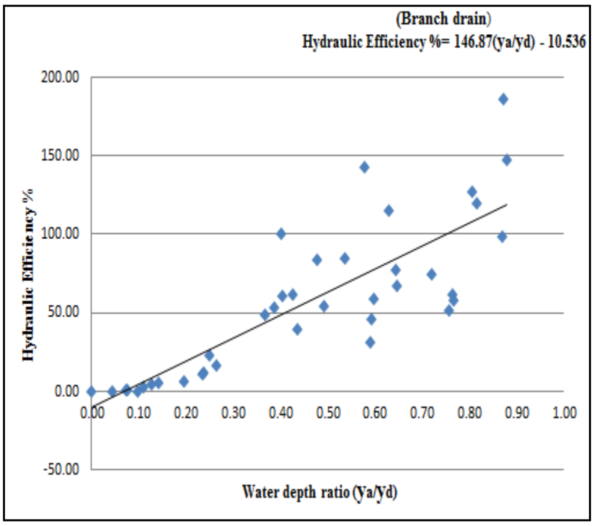

Figure 7: Relationship between hydraulic efficiency and hydraulic radius versus water depth of branch drains

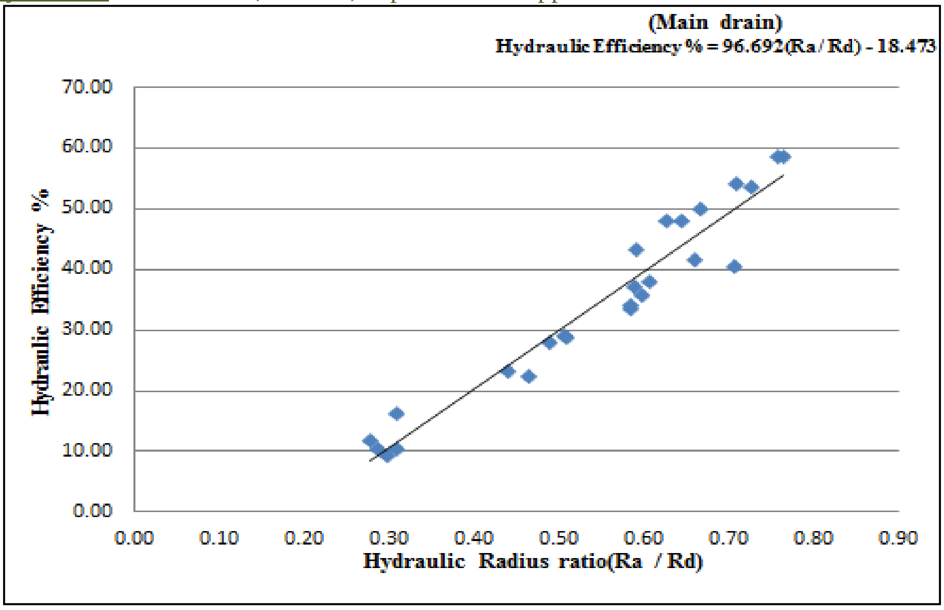

Figure 8: Relationship between hydraulic efficiency versus hydraulic radius of main drain

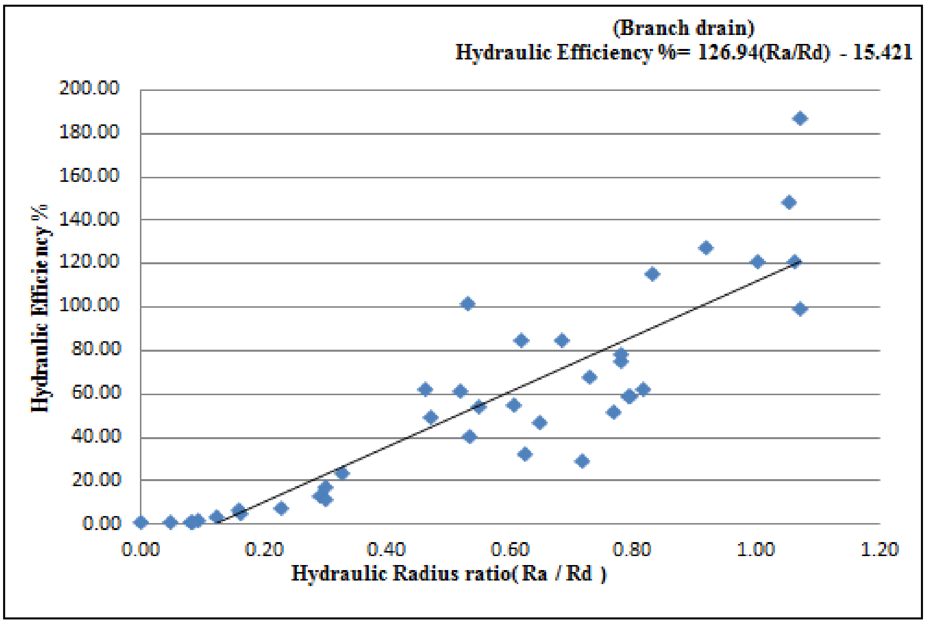

Figure 9: Relationship between hydraulic efficiency versus hydraulic radius of branch drains

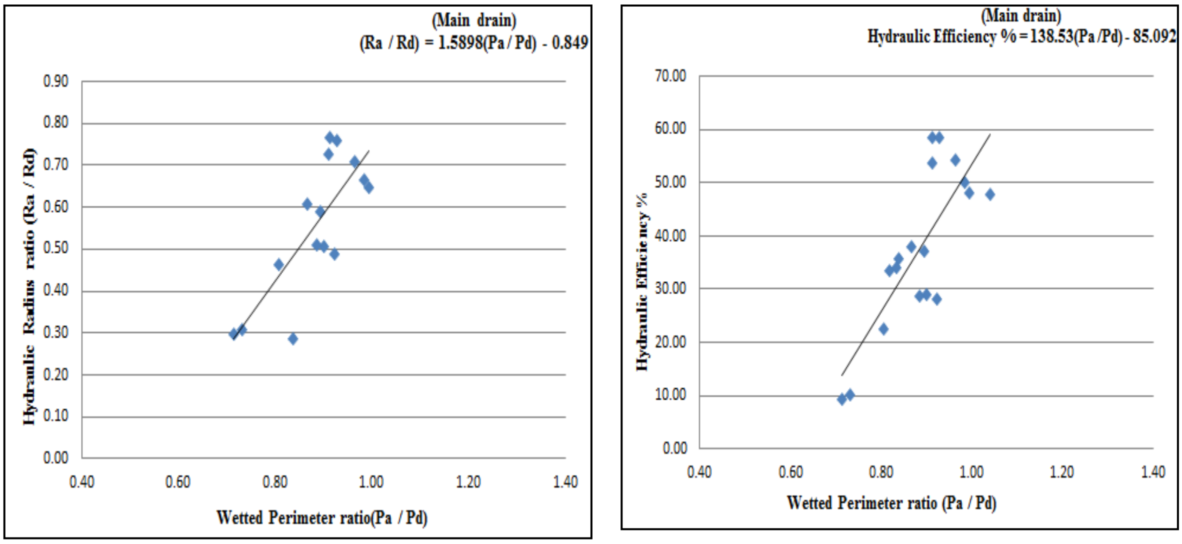

Figure 10: Relationship between hydraulic efficiency and hydraulic radius versus wetted perimeter of main drain

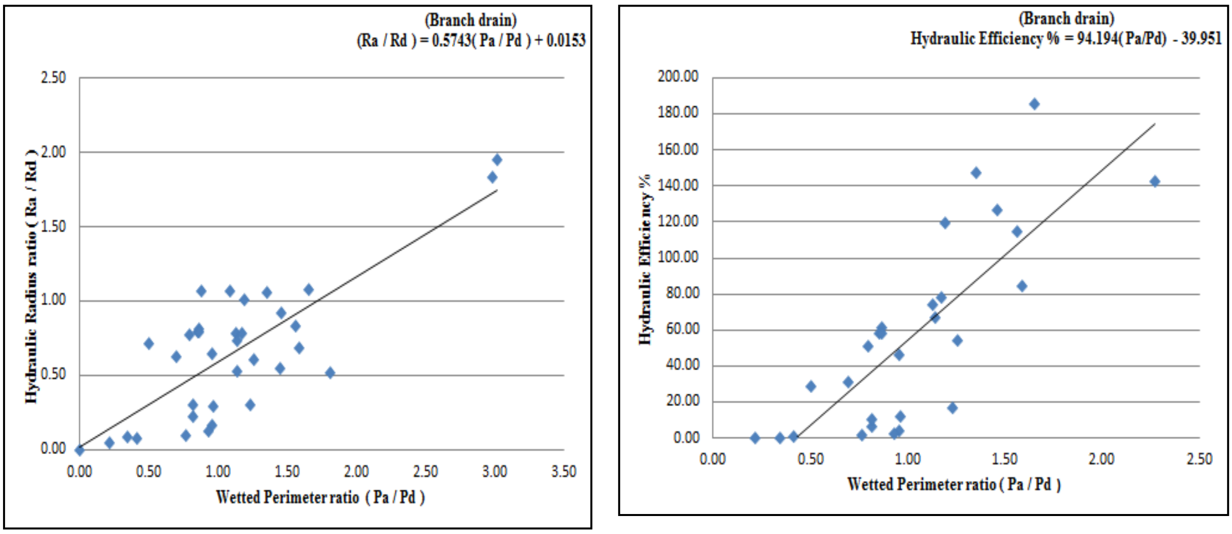

Figure 11: Relationship between hydraulic efficiency and hydraulic radius versus wetted perimeter of branch drains

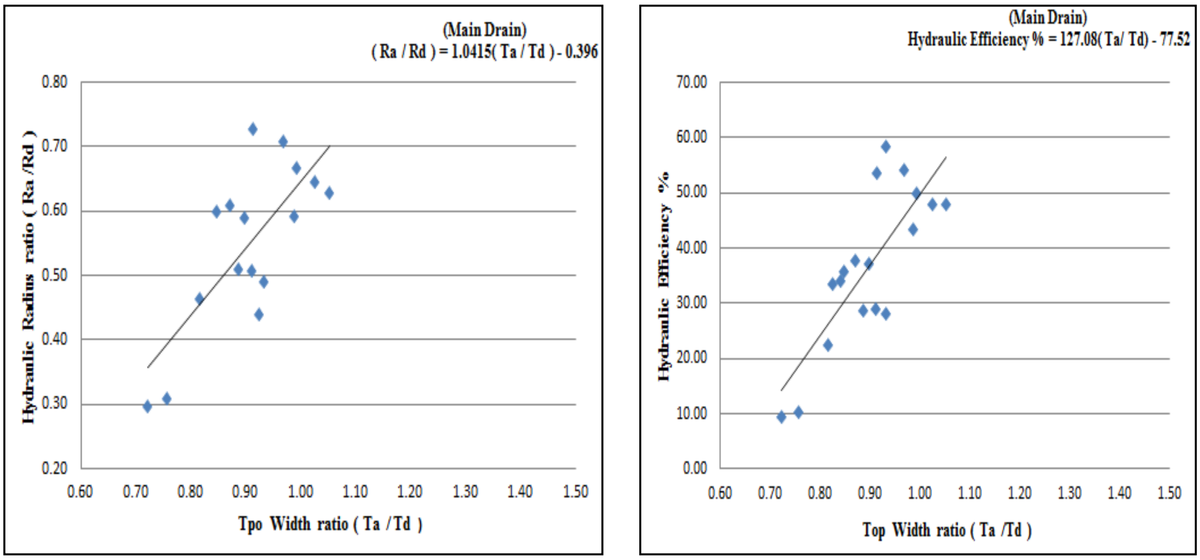

Figure 12: Relationship between hydraulic efficiency and hydraulic radius versus Top width of main drain

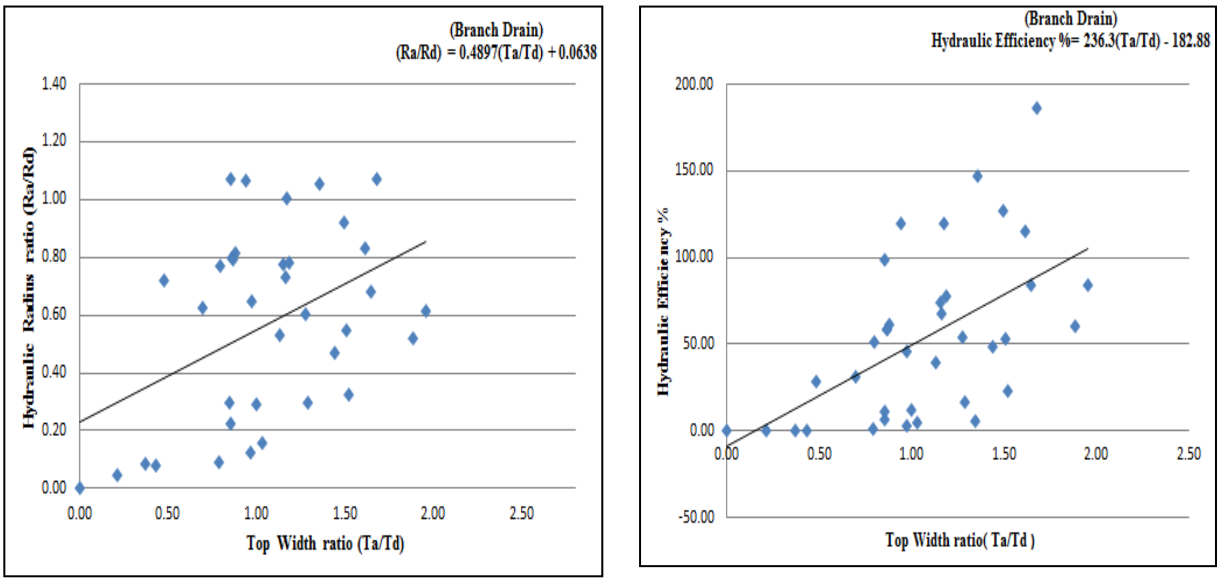

Figure 13: Relationship between hydraulic efficiency and hydraulic radius versus top width of branch drains

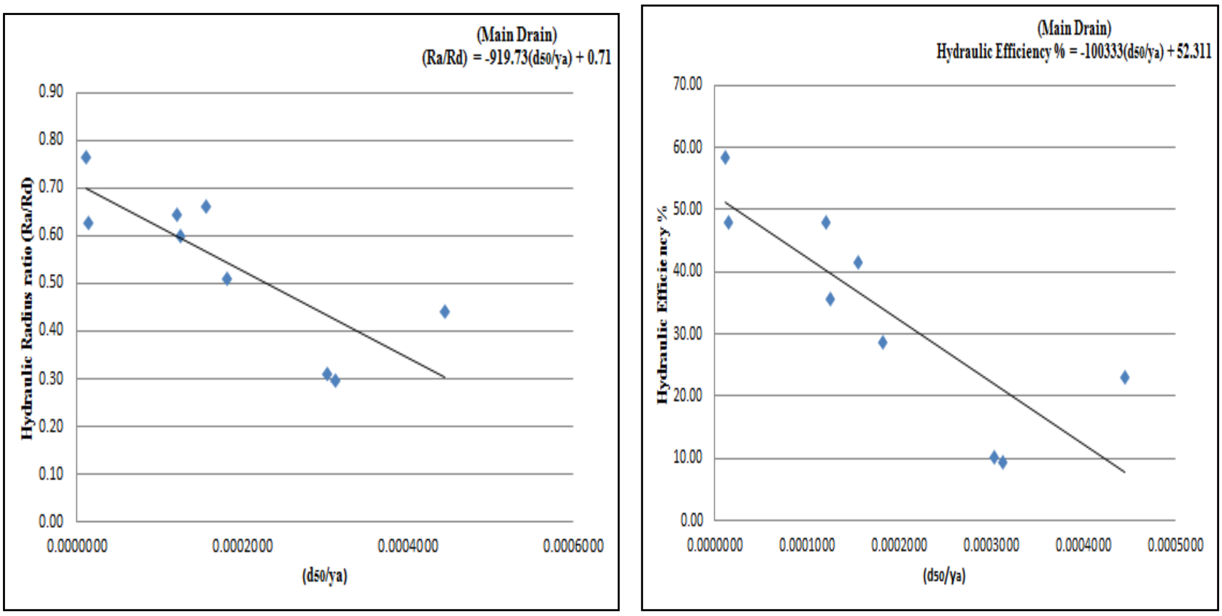

Figure 14: Relationship between hydraulic efficiency and hydraulic radius versus median size of material to water depth of main drain

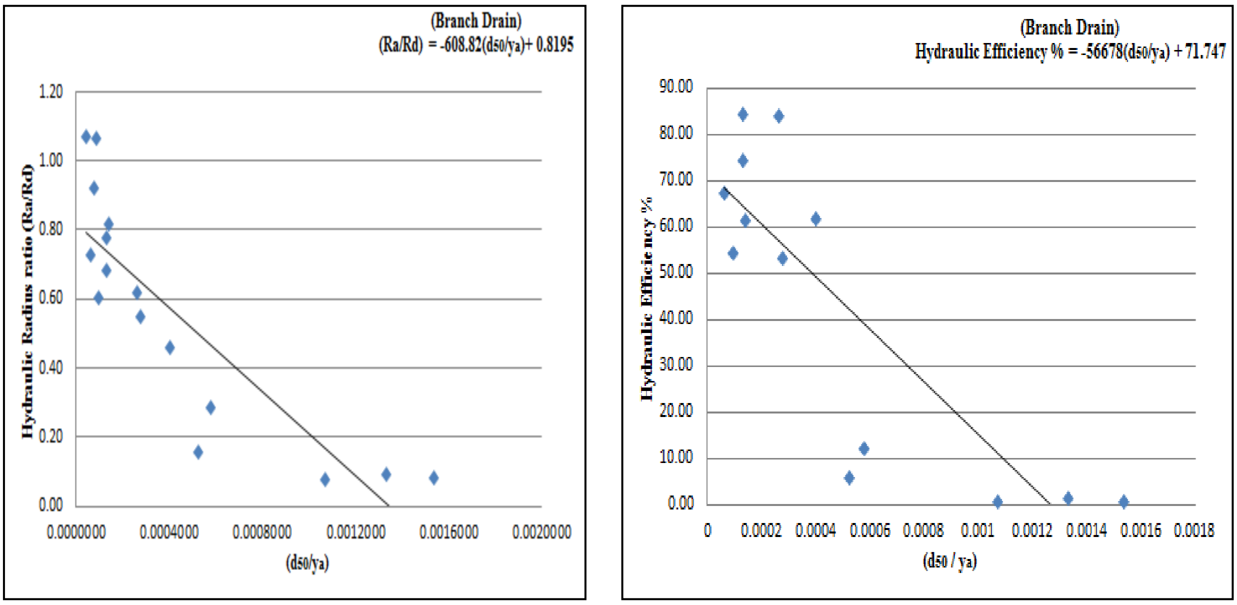

Figure 15: Relationship between hydraulic efficiency and hydraulic radius versus median size of material to water depth of branch drains

VI. CONCLUSION

Field work study was conducted to investigate the possibility of minimizing the drains hydraulic problems that lead to reduce their efficiency and ability to the free drainage of cultivated land, by identifying the most effective parameters that affect the hydraulic efficiency in order to achieve the highest operating efficiency of open drains, increase the ability of open drains cross sections for conveyance and give scientifically study about maintenance program of open drains. The developed equations are only valid for the limited range of conditions upon which they are based as follows:

- The designs of flow discharge along these selected drains are ranging among 2.62 m^3/s – 78.75 m^3/s and the side slope of the selected drains are 2/1 and 3/2.
- The boundary condition between the design and actual cross sections are the design water level. For applying the deduced relations all actual and design parameters are calculated till the design water level, to reserve the levels of earth banks and collectors out fall without any flooding for banks and submerging of collectors out fall.
- The main drains in Egypt having sandy loam beds and silty clay bank represents about 10% of the total length for Egyptian open drains. While the Branch open drains having cohesive beds and banks. Represent about 30% of Egyptian open drains. The boundary is considered as a sandy type when the medium diameter d_{50} range from 0.06 to 0.40 mm with 0.5 – 1% clay and 5-6% silt. A sandy loam type is considered when the percentage of the silt and clay

in the hydrometer analysis are ranging from 20% to 30%. Also a cohesive bed and bank types are considered when the percentage of the silt and clay in the hydrometer analysis are ranging from 50% to 65%.

ACKNOWLEDGEMENTS

This research and included work would never have been completed without the financial and technical support of the staff of Channel Maintenance Research Institute, National Water Research Center, Cairo, Egypt.

REFERENCES

Journal Papers:

[1] Bakry, M.F , The hydraulic roughness of stable alluvial canals in Egypt, *Water Science, National Water Research Center, 11th ISSUS*, April 1992, *pp. 41-46*.

Books:

[2] Chow, V.T, *Open channel hydraulics*(McGraw-hill, new York, N.Y,1959).

Theses:

[3] El-Syaed . A.H, *Design of Open Drains In Egypt*, M.Sc. Thesis, Ain Shams Univ., Cairo, Egypt,1998.

Proceedings Papers:

[4] Hosny, M.M, Regime design concept of Egyptian earthen channels: *Militray technical college, Third International Conference on Civil and Architecture Engineering*, Egypt, March 1999.

Proceedings Papers:

[5] Khattab,A.F, M.M.Abu sieda, Z. El- Gharably ,M.M.Bakry, New design for the egyptian canals system the construction of High Aswan Dam: *5^{th} Afro-Asian Regional Conference*, Townsville, (Australia),1985.

Books:

[6] MPWWR, *Drainage policy in Egypt*(Ministry of Irrigation, Cairo, Egypt, 1981 in Arabic).

International Journal of Modern Engineering Research (IJMER)
www.ijmer.com Vol. 3, Issue. 5, Sep - Oct. 2013 pp-3149-3155 ISSN: 2249-6645

Evaluating phase level for critical success factors of BPM-system implementation: a case study in a Saudi government organization

Abdullah Al-Dahmash, Saleh Al-Saleem
Department of Information Systems, College of Computers and Information Sciences
King Saud University, Riyadh, KSA

ABSTRACT*: Nowadays, many organizations rely on a business process management system (BPMS) since it provides a systematic approach to aligning organization's processes with the customers' needs. There has been much research to study the critical success factors (CSFs) of implementing a BPMS in an organization. To our knowledge, this is the first published study that attempts to study the CSFs for BPMS implementation for each project phase independently. This research will present and study a case of BPMS implementation, located in a Saudi government organization. There was a survey conducted to analyze the CSFs of BPMS for each implementation project phase. Also, this research aims to present the importance of studying CSFs for BPMS implementation not in the whole project but rather for each project phase and to suggest success factors for each phase.*

Keywords: *BPM implementation, BPMS, case study, success factors*

I. INTRODUCTION

In the last decade, many organizations around the world have attempted to implement a system that can tackle business process management (BPM) concerns. Gartner's study in 2009 identified BPM as the number one priority of (chief information officer) s(CIOs) globally [1]. From this study and other studies, BPM is considered one of the biggest information technology (IT) trends today. BPM has been known as a systematic approach to managing the basic activities in an organization. A business process is a set of activities that must be accomplished in order to achieve a collection of predefined objectives, such as the production of a product or delivery of a service. The activities within BPM may be performedmanually by people or automatically by anIT system [2].

There have been many researches to identify the CSFs for BPMS. As far as we know, this is the first published research to study the CSFs of a BPMS implementation project at the phase level. One of our aims of this study is to present the CSFs for each project phase independently ordered by importance and impact. We aim also to provide the relationship between the project progress and status with the success factor. We will be using the Markus model [3] to identify the BPMS implementation project phases. The Markus model spouses that each enterprise system (ES) (e.g., ERP, CRM, and BPMS) implementation project consists of four phases: project chartering phase, project (configuration and rollout) phase, shakedown phase, and the onward and upward phase. The Markus model and its phases will be discussed further in literature review section.

In this research, we will study the CSFs of implementing BPMS by studying and analyzing a BPMS implementation case. Our case study was a BPM system implementation project which was located in a Saudi government organization. There has been a survey conducted of different stakeholders in the studied project. The survey's result will be used to study the CSFs of the BPMS project for each project phase.

Do the CSFs for implementing BPMS have the same importance to the BPMS implementation project during all the project's phases? Are the CSFs playing the same role regardless of project progress or status? Did the project phases all have the same success factors in order to end the phase with success? What are the critical success factors that the BPM systems implementers and researchers need to focus on more during each project's phase? We will answer these questions by doing a phase level evaluation for critical success factors of BPM-system implementation.

This research will consistof four sections. The first section is a literature review on the history of BPM and process modeling and the development of BPM systems. The second section will provide the case study description and analysis. The third section will discuss the conducted survey results and the experimental results. The last section in this research will be the conclusion of the work and the future works.

II. LITERATUREREVIEW

Michael Hammer defined process management as a systematic approach to performance improvement that focuses on organization's business processes. All the business processes should be organized and work together in order to satisfy the customer needs [4]. Each business process must have structure, input, output, and owner. Business processes are built from an organization's functions and operation flow (internally or externally) [5].

What is business process management (BPM)? There is no one agreed definition of BPM. Zairi answered this question: BPM is a systematic approach to managing and improving basic activities of an organization, such as manufacturing, marketing, etc. He also suggests that BPM should governed by list of rules. For example, BPM should focus on customer needs, it should be a continued approach, and it's about changing culture not only building a good structure [6]. According to Werth et al., [7] BPM is a requirement engineering approach which used IT services to take care of business needs. Therefore, according to Werth et al., IT plays the most important role in BPM by facilitating process automation.

Currently off-the-shelf software, such as ERPsystems and CRM systems, already provides automated processes following the best practices in the industry.

Business process management system is considered as a new era in enterprise applications (EA) and has attracted a lot of academic researches. Most of the researchers consider the BPM systems to be the next step after ERP and workflow systems. As per Fanbo et al., [8]BPMS can be defined as an information system supporting business processes by using techniques and tools to control and improve the process. A BPMS can be defined also as enterprise software that provides the ability to model, improve, and manage sets of processes based on a complete and an automated mechanism. An enterprise's defined processes can be modified and improved using BPMS at any time. BPMS can be seen as the evolution of the ERP systems and the WFM systems. Processes in an organization managed by BPMS can be divided into three main categories: core processes, support processes, and management processes [9].

Business processes are the main core of today's and tomorrow's enterprises. Enterprises must be ready to focus on their business processes in order to improve the quality of their services. Due to the importance of modeling the processes, many business process modeling techniques and tools have been introduced in the research society and the market. Figure [1] presents the benefits of using BPM system for an enterprise.

Figure [1] Benefits of using Business Process Management System

Identifying the critical success factors (CSFs) is a well-studied subject in information systems research. After each IS's system or solution matures in research and practice, there is a need to identify CSFs to implement that system or solution. In BPM studies there are many researchers who tried to identify the CSFs of implementing a BPMS in an organization. It is important to discuss what success in BPMS implementation means before we could discuss the CSFs to implement a BPM system. Based on Bandara et al.[10], a BPMS implementation project is considered a success project if it is effective and efficient. The implementation project can be considered effective if it accomplishes its objectives. The implementation project can be considered efficient if it is completed within an assigned time and budget.

The literature always offers similar CSFs for BPM. The critical success factors for BPM are similar to the critical success factors for any other enterprise system such as ERP and CRM. According to Yanhong [11], the IBM China Research Institute of Commercial value conducted a survey of around 200 companies to analyze the key factors of implementing an enterprise system business in China. The survey showed that the key success factors are top-management support, organizational strategy, organizational culture regarding the new system, technology (the new system), and project management. However, top management support was considered to be the most important CSF for BPM [12]. There are many CSFs for BPM listed in the literature. Table1 contains the CSFs for BPM that we will consider in our study.

Critical Success Factor	Literature Citation
Top Management Support	[13];[14];[12];[15];[16];[17]
Project Management Skills/ Methodology	[16];[13];[18];[19];[17]
Communication	[17];[13];[18];[19];[12]
User Participation/Involvement	[13];[17];[19];[12]
Organizational Culture	[12];[15];[11]
Training	[17];[16];[15]
Effective Change Management	[13];[17];[12]

Table[1]: CSFs for BPMS Implementation

Most of the researches on CSFs for BPMS or any Enterprise System studied the factors in the whole project life cycles. To our knowledge, this is the first published study that attempts to study the CSFs for BPMS implementation in each project's phase. Markus in [3] has introduced a project life cycle model for an enterprise system implementation. We will use this project model to study our case study and the CSFs in each phase.

The Markus model is a very well-known model with many citations in the relevant literature. The proposed model was built to provide a framework for an enterprise system implementation project. Based on the Markusmodel, any enterprise system implementation project consists of the following phases: project chartering phase, project (configuration and rollout) phase, the shakedown phase, and the onward and upward phase.

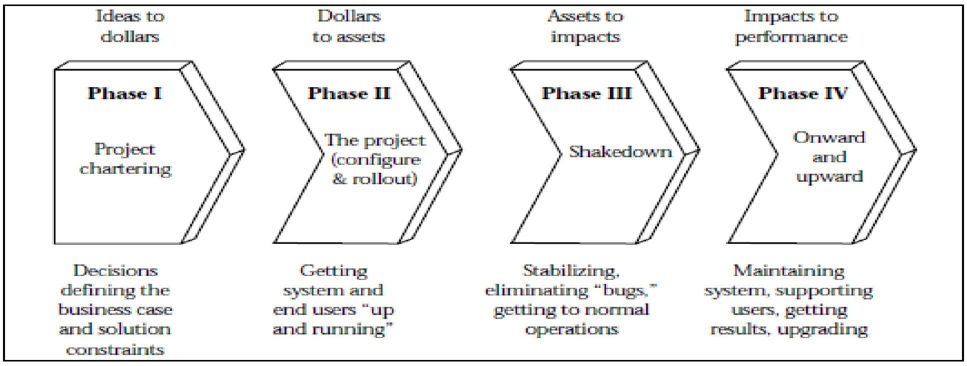

Figure [2] Markus model: Enterprise System Life Cycle [3]

III. CASE STUDY

Research Methodology

The research methodology is based on implementing the Marcus model for a BPMS implementation project. Semi-structured interviews and surveyshave been used for data collection. Several individual interviews and meetings have been conducted with end users and top management to understand and present the case. There has been a survey built in order to study the CSFs for each project phase. The results from the survey will be used to find the relationships among those CSFs and to present the importance of identifying the CSFs for each project phase, using the Marcus and Tanis model.

Case Description

Our case study, which we will discuss in this research, was located in a Saudi government agency. This agency or authority was established by a royal order in 2004 to be fully operational officially in 2010. The agency plays an important role in the Saudi healthcare industry with more than 2,000 staff members. The business process management implementation project, which we will study in our research, was started in 2010. The agency decided to implement BPMS using an external implementer (vendor). Also, they have decided to use ORACLE SOA as a BPMS tool. However, they have different possibilities for BPMS tools. We will discuss the process of selecting the BPMS tool and the vendor in detail. Project duration was 16 months, and the project ended within the time and budget as per the input from the executives with whom I met. Project team members included approximately 11 people.

There were many causes and business needs that led the organization to implement a BPMS. One of the goals was to unify the process across the organization. For example, they found that the same process might be completed within a different time frame and a varied workload. Also, there was a pressure from top management to define realistic measurements for the organization's processes. There was a need to improve the productivity and reduce the time for each process, and implementing a new business process management system was intended to help in that. Also, the organization aims to be able to make better predictions of time, budget, and teams in case a new process will be implemented in the organization's future.

There was a strategic decision to implement BPMS using a commercial off-the-shelf (COTS) software package and using offshore implementer support. This decision was made for many reasons: lack of resources and the cost of in-house development,as well as the core business of the organization is not IT and in-house implementation of a BPM system would require a huge IT budget and team.

The phase of selection of the BPMS tool and vendor is an important phase for any BPMS implementation project. However, in our case, the organization didn't spend enough time and effort on this phase. For the BPMS tool, they decided to use Oracle Solution for BPM because they had a long contract with Oracle. Also, their IT platforms (databases, ERP system, and CRM system) were with Oracle. One of the IT executives I met said, "We didn't have many possibilities, so we decided to go with Oracle due to the successful history in implementing our ERP and CRM systems." It is clear to me that they didn't take the selection of the BPMS tool seriously. Also, the name-recognition of the brand may have distracted them from considering what they really needed from implementing a BPM system.

Study Marcus Model Phases on the Case:

- **Project chartering phase:**

In our case, this phase starts with the agreement on the business case document. A business case document is a document where all the business needs and requirements are written at a very high level. In this project, the business case document clearly mentioned that the agency needs to have a system that will help to improve and automate the current business processes. After that, the project team starts to prepare for brainstorming workshops, and it will invite all of the project's stakeholders to participate. These workshops aim to involve all the stakeholders in the process of preparing the Request-For-Proposal (RFP) document and the agreement on the new system's specification (hardware and software specifications). As per the project manager, the participation in the workshops was perfect and above what they expected as a project team.

After that, there were several meeting between the executives and the project team. By the end of those meetings, the project budget and the project timeline were adopted. Since the agency does not have any previous, similar projects on BPMS, they were forced to compare the project with other BPMS projects' budgets and time plans. The selection of the BPMS tool was a top management decision, where the project team participated as well. By end of this, they agreed to go with Oracle's solution for the BPMS. Oracle's tool was selected due to many reasons: the successful history of support the agency received in previous IT projects with Oracle, the familiarity (platforms and staff knowledge) with Oracle that the agency has, and the budget and time comparisons with other BPMS tools. After the agreement on budget and time, RFPs were sent to five interested vendors.

By the end of chartering phase, the project team defines the performance indicators and the success measurements of the project. The performance indicators were to increase the productivity of the processes after using the system, and to increase the agency's ability to predict the time and cost, as well as the resources required for each new process. In addition, one of the performance indicators was to reduce the human inputs and resource the costs by fully automating the process. One more indicator was reducing the steps and time required to finish the process by using the benefits of automation.

The success measurements of the project were, first, the ability to finish the project within the reserved budget and time. The second success measurement was to achieve the suggested to-be improvements to the business processes after using the implemented BPM system. Third, success required increased availability and the friendly-of-use to the agency's processes, for its customers and staff. Fourth, increase the agency staff's ability to automate any business process within the agency, after the end of this project and the vendor's consultants are gone. Finally, improve the agency's culture and attitude to be more process-oriented than function-oriented.

- **Project configuration and rollout phase:**

By the end of the project configuration and rollout phase, the implemented system should be up and running. In our case, there were many activities during this phase. Since the decision has been made to go with a commercial off-the-shelf (COTS) BPM tool, there have been no development activities other than some system configuration tasks. The system configuration consists of several activities: system installation on the server Oracle BPM tool is working on either UNIX servers or WINDOWS servers; fortunately, both are available without requiring a new platform. Database platform creation required Oracle as a database and, fortunately, the agency's database platform was Oracle, which reduces the amount of work in this activity. The tool customization to fit the agency's business processes and rules, and other technical details required for any software configuration were important system configuration activities as well. At this phase, business process modeling and business process reengineering activities (where required) have been started. The project team started modeling the matured and the agreed processes. Some of the business processes required reengineering, which is done with the help of the vendor's consultants.

- **Shakedown phase:**

The shakedown phase starts when the system goes live and runs until the system has achieved normal operations. In our case, it started from the pilot go-live on the selected department's processes until the new system covered all organization's processes. Upon reaching this time, the vendor leaves the agency as per the implementation contract. At this stage, the project team has agreed on an action plan to cover all the remaining processes in the new implemented BPMS. There was agreement from the top executives to not pressure the agency departments to use the new BPM system. By that time, they figured out how the new system helped the pilot department. Thus, after that each department start looking forward to automate and model its business processes using the new system. The agreed-on action plan mentions that they have to send a request to the IT department to start using the new BPMS.

By the time our BPMS take the confidence from all the agency's different departments that the system will help them. For example, for one of the processes, which was in the project pilot phase, after the use of the new BPMS the number of weekly procedures jumped from 120 procedures to 700 procedures. After the heavy use of the system, there were some performance and delay complaints from users. After looking into those complaints, the root causes for the delay were identified by the project team. As per the project manager's input, the performance issues were coming from the integration tasks, which were implemented during the project phase. The project team reviewed the integration and those issues were resolved. One of the business users I had met mentioned that the performance of the system clearly improved after this enhancement.

With the increased system usage across the agency's business processes, more licenses from the tool vendor were required to overcome the usage expansion. This cost for more licenses was within the project budget, since the increased system usage was considered during the project chartering phase. By the end of the shakedown phase, the system had reached normal operations and the number of raised issues and requests was reduced.

- **Onward and upward phase:**

The onward and upward phase is the time when the organization decides that its investment has successfully met its goals or business needs. This is also the time to evaluate the system under normal operations, which was reached at the shakedown phase. In our case, a high-level committee has been established to review the project. This committee produced many recommendations. We will list the three main recommendations, which are the following: the project of implementing the BPM system at the agency successfully ended within budget and schedule, achievements were reached in process automation that satisfied the agency's needs, and the agency's business needs from the project were successfully addressed.

This system went smoothly and the majority of the agency's business processes are implemented using the new BPM system. Until the time of writing this research, there was no decision to upgrade the system or implement any new support system, since the current BPMS successfully meets the agency's requirements. However, there was an agreement to improve business processes continuously using the improved capabilities in the newly implemented BPMS. Moreover, there was a decision to provide additional user skills building, if required. The required skills include process improvement, process modeling, and process reengineering. Based on the Marcus model, the onward and upward phase might be a continuous phase, even if the project has ended.

IV. DISCUSSION AND EXPLORATION RESULTS

A questionnaire survey has been conducted to evaluate the critical success factors of implementing BPMS. The survey was built to do a phase-level evaluation for the CSFs in implementing the BPM system. The success factors for BPMS will be evaluated for each of the following project phases: the project chartering phase, project (configuration and rollout) phase, shakedown phase, and onward and upward Phase. The survey was administered to all of the project's stakeholders, accounting for their different perspectives and backgrounds. Thus, the survey studies the CSF for each phase and the survey results will determine the relations between the project phases, the success factors, and the importance of studying the CSF at a phase level.

The survey results show differences in the importance of success factors across the various phases. Based on the survey results, we will present the importance (range from 0 to 1) for each of the critical success factors in each project phase. In the following, we will propose the importance of each success factor in each project phase. This will help to prioritize the success factors for each phase, based on the importance and the impact of each success factor in that phase:

Project Chartering Phase:

Survey results have shown that the critical success factors during the chartering phase are ordered by the importance of the following:

Chartering Phase	Important Factor
1. User Involvement	0.938
2. Top Management support	0.933
3. Project Management	0.905
4. Communication	0.888
5. Culture	0.766
6. Change Management	0.622
7. Training	0.538

Table [2] CSFs for project chartering phase

The survey results show how that user involvement and top management support are the most important critical success factors among the different CSFs during the chartering phase. Project management factor and communication factor come in third and fourth, with importance factors of 0.90 and 0.88, respectively. After that, factors like culture, change management, and training exhibit lower importance factors. From this result, we conclude that user involvement is essential to achieving success during the chartering phase. It is also clear from these results that having top management support and project management skills are required to ensure this phase's success, after the end users are involved. Results also showed that the communication factor plays almost the same role during all the BPMS project phases.

Project Configuration and Rollout Phase:

Survey result has shown that the critical success factors during project configuration and rollout phase are ordered by the importance as the following:

Project Configuration phase	Important Factor
1. Project Management	0.9
2. Communication	0.872
3. Culture	0.872
4. User Involvement	0.861
5. Top Management Support	0.727
6. Change Management	0.705
7. Training	0.583

Table [3] CSFs for project configuration and rollout phase

The project configuration phase is the phase where the technical issues are tackled. Activities, such as the system setup, integration with other systems, and package customization, are the main activities during this phase. As shown from the survey, those activities do not required high levels of top management support or training. However, it is clear from this result that the most important success factors for configuration phase are, in order, project management, communication, and culture. The results show that user involvement still affects this phase, but much less than the effects user involvement had on the chartering phase. In addition, the importance of top management support clearly decreased from the chartering phase to the configuration phase. Change management and training factors are less important than other CSFs during the configuration phase.

Shakedown Phase:

The survey results show that the critical success factors during the shakedown phase are ordered by the importanceof the following:

Shakedown Phase	Important Factor
1. Change Management	0.938
2. Culture	0.905
3. Training	0.888
4. Communication	0.838
5. Project Management	0.788
6. User Involvement	0.716
7. Top Management support	0.666

Table [4] CSFs for shakedown phase

The shakedown phase begins after the BPM system goes live. Thus, the survey results highlight the greater importance of soft factors, such as change management, culture, and training, in comparison to the other factors, such as project management and top management support. These results show that change management, culture, and training are the most important success factors during the shakedown phase. After the start of the new BPMS, which is during the shakedown phase, the project team should be ready for many change management tasks and organizational culture changes, as well as redefined activities. There is a decrease in the importance of success factors like user involvement and top management support. This is reasonable because the implemented system in the shakedown phase is in use, thus there will be no big demand to have the user involved or to have top management support. It is clear from this result that the project management success factor during the shakedown phase has less impact than it does during the chartering or configuration phases.

Onward and Upward Phase:

The critical success factors during the onward and upward phase are ordered by the importance and impact of the following:

Onward & upward Phase	Important Factor
Change Management	0.95
Training	0.938
Culture	0.916
Communication	0.894
Top Management support	0.8
Project Management	0.688
User Involvement	0.666

Table [5] CSFs for onward and upward phase

The results show that, during the onward and upward phase, the most important critical success factor is change management. In addition to change management, training has greater importance and impact during the onward and upward phase. This result could help academics and practitioners to focus more on change management, training, and culture during this phase. With regard to the communication factor, it continues to have almost the same impact during all phases of the BPMS implementation project.

The result shows that there is a clear increase in the importance of top management support in this phase, with value of 0.8. The importance of top management support during the onward and upward phase comes from the need to improve the system or to update the current system package, requires top management support and commitment. Factors like project management and user involvement continue to have almost the same impact during the shakedown phase. Since the onward and upward phase is almost like a monitoring and improving phase, it is reasonable to expect less importance and impact on factors like project management and user involvement.

V. CONCLUSION AND FUTURE WORKS:

During the last decade, business process management (BPM) was considered a global IT trend. BPMS is defined as an information system supporting business processes in an organization, through methodologies, techniques, and tools, which are used to model, automate, control, and improve the business processes. While there has been much research on process management techniques and tools, there has been little research on the critical success factors (CSFs) of implementing business process management systems. To our knowledge, this is the first published study that attempts to evaluate the phase level of CSFs for a BPMS implementation project, with each project phase considered independently. The project phases are followed the Marcus Model, which assumes that each BPMS implementation project consists of four phases: the project chartering phase, project configuration phase, shakedown phase, and onward and upward phase.

This research presented and studied a case study, which is the BPMS implementation project located in a Saudi governmental organization. The selected project studied in this research using the Marcus model. A survey was conducted to study CSFs for BPMS implementation project for each project phase. The survey's participants included the project stakeholders, IT specialists, BPM specialists, executives, consultants, and vendors. The survey results are used to analyze and study each critical success factor in the four project phases. In addition, the survey results are used to presents the critical success factors, ordered by the importance and the impact for each project phase.

Survey results showed that the different levels of importance and impact for each success factor depend on the BPMS implementation project status and progress. The top management support factor played a more important role during the chartering phase and the onward and upward phase than in other phases. Project management skills and methodology factors, and the user involvement factor, have the greatest importance and impact during the early stages of the BPMS project. The communication factor has almost the same impact and importance during the entire BPMS implementation project life cycle. The more the BPMS project progresses, the greater the importance and impact will be for the following factors: change management, training, and organizational culture.

This research suggests and presents the critical success factors for each project phase ordered by their importance. For the project chartering phase, the critical success factors are ordered as follows: user involvement / participation, top management support, project management, communication, culture, change management and, lastly, training. The critical success factors during the project configuration phase are ordered as follows: Project Management, Communication, Culture, User Involvement, Top Management support, Change Management and lastly Training. For the shakedown phase, the critical success factors are ordered as follows: Change Management, Culture, Training, Communication, Project Management, User Involvement and lastly Top Management support. Finally, the critical success factors during the onward and upward phase are ordered: Change Management, Training, Culture, Communication, Top Management support, Project Management and lastly User Involvement.

Further studies may focus on building a framework for using the Marcus model to present the BPMS implementation project's life cycle. The reasons for differences in critical success factors' importance between projects phases might be studied in future research as well. Future research may study the relations between the success factors for a BPMS implementation project.

REFERENCES

[1] Gartner Report. (2009). Meeting the challenge: *The 2009 CIO Agenda*.
[2] Gerth, C. (2013). Introduction in Business Process Models. Change Management (pp. 1–12). Berlin, Heidelberg: Springer.
[3] Markus, M. L., & Tanis, C. (2000). The enterprise system experience — From adoption to success. Framing the Domains of IT Management: Projecting the Future...Through the Past (pp. 173–207). Pinnaflex Educational Resources Inc.
[4] Hammer, M. (2002). Process management and the future of Six Sigma.*MIT Sloan Management Review*, 43, 26–32.
[5] Al-Mashari, M., & Zairi, M. (2000). Revisiting BPR: holistic review of practice and development.*Business Process Management Journal*, 6(1) 10–42.
[6] Zairi, M. (1997). Business process management: A boundaryless approach to modern competitiveness. *Business Process Management Journal*, 3(1), 64–80.
[7] Werth, D., Leyking, K., Dreifus, F., Ziemann, J., &Martin, A. (2007). Managing SOA through business services–A business-oriented approach to Service-Oriented Architectures.*Proceedings of Service-Oriented Computing ICSOC 2006, 4th International Conference*, Chicago, USA, Springer Berlin Heidelberg, 3-13.
[8] Fanbo, M., Minli, J., &Wuliang, P. (2010). A business process management system based on workflow technologies.*Intelligent Networks and Intelligent Systems International Conference (ICINIS)*, 68–172.
[9] Akhavan, M. (2012). ,IT's role in business process management (BPM). *International Journal of Business and Management Tomorrow*, 2(8).
[10] Bandara, W., Gable, G. G., & Rosemann, M. (2005). Factors and measures of business process modelling: Model building through a multiple case study. *European Journal of Information Systems*, 14(4), 347–360.
[11] Yanhong, Z. (2009). ERP implementation process analysis based on the key success factors. *Proceedings of International Forum on Information Technology and Applications IFITA'09*, 3, Chengdu, China, 25–27.
[12] Trkman, P. (2010). The critical success factors of business process management. *International Journal of Information Management*, 30(2), 125-134.
[13] Kappelman, L. A., McKeeman, R., & Zhang, L. (2006). Early warning signs of IT project failure: The dominant dozen. *Information Systems Management*, 23(4), 31–36.
[14] Glaser, J. (2004). Management's role in IT project failures. Healthcare Financial Management: *Journal of the Healthcare Financial Management Association*, 58(10).
[15] Al-Mashari, M., Al-Mudimigh, A., & Zairi, M. (2003).Enterprise resource planning: A taxonomy of critical factors. *European Journal of Operational Research*, 146(8), 352–364.
[16] Zhang, L., Lee, M., & Banerjee, P. (2002). Critical success factors of enterprise resource planning systems implementation success in China. *Proceedings of 36th Hawaii International Conference on System Sciences*, Hawaii, USA, 236–244.
[17] Nah, F., Lau, J., &Kuang, J. (2001).Critical factors for successful implementation of enterprise systems. *Business Process Management Journal*, 7(3), 285–296.
[18] Humphrey, W. S. (2005). Why big software projects fail: The 12 key questions.
[19] Charette, R. N. (2005). Why software fails [software failure]. *Spectrum, IEEE*, 42(9), 42–49.

Performance Analysis of Three Phase Cascaded H-Bridge Multi Level Inverter for Voltage Sag and Voltage Swell Conditions

[1]Ganesh Pashikanti, [2]Sudha Dasari
[1]P.G Scholar, [2]Assistant Professor, [1,2]Vathsalya Institute of Science and Technology

ABSTRACT: *A Multilevel Inverter is a power electronic device built to synthesize a desired AC voltage from several levels of DC voltages. Nowadays, modern industrial devices are mostly based on electronic devices such as programmable logic controllers and electronic drives. The electronic devices are very sensitive to disturbances and become less tolerant to power quality problems such as under voltage and over voltage conditions. In general under voltage and over voltage conditions will occur more at source side. In this paper a closed loop Control system is designed using PI controller in order to maintain load voltage constant for under voltage and Over voltage conditions. The triggering pulses to Cascaded H-Bridge (CHB) MLI is given using multi carrier phase shifted technique and MATLAB simulations have been carried out.*

Keywords: *Multilevel Inverter (MLI), Carrier based Pulse Width Modulation (PWM), Phase Shifted (PS), Under Voltage, Over Voltage.*

I. INTRODUCTION

Multilevel inverters have gained more attention in high power applications because it has got many advantages [1-4]. It can realize high voltage and high power output by using semiconductor switches without the use of transformer and dynamic voltage balance circuits. When the number of output levels increase, harmonic content in the output voltage and current as well as electromagnetic interference decrease. The basic concept of a Multilevel inverter is to achieve high power by using a series of power semiconductor switches with several lower dc voltage sources to perform the power conversion by synthesizing a staircase voltage waveform [1,5]. To obtain a low distortion output voltage nearly sinusoidal, a triggering signal should be generated to control the switching frequency of each power semiconductor switch. A three phase Cascaded H-bridge Multi (five) Level Inverter has been taken. Fig.1 shows a three-phase five-level Cascaded H-Bridge MLI. It requires a total of six dc voltage sources.

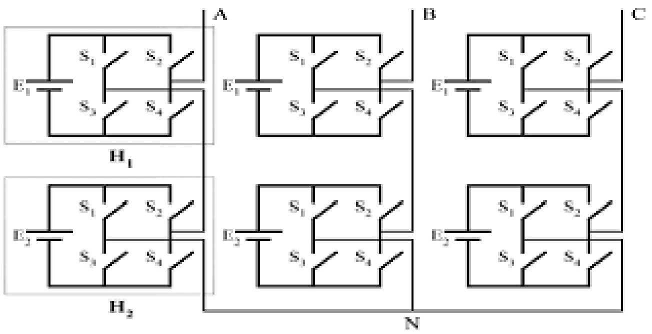

Fig.1 Conventional Three Phase 5-Level Cascaded H-Bridge Multilevel Inverter.

As Multilevel inverter is made up of semiconductor switches which are very sensitive to disturbances and become less tolerant to power quality problems such as under voltage and over voltage conditions this paper investigates an approach of designing a closed control system using PI controller to maintain load voltage constant for under voltage and Over voltage conditions.

II. CONTROL TECHNIQUES OF MLI

There are different control techniques available for a CHB MLI [13, 15] as shown in Fig.2 Among all those techniques, PWM control technique which produces less total harmonic distortion (THD) values is most preferable. In PWM technique also, sinusoidal PWM is used for generating triggering pulses to MLI. In sinusoidal PWM pure sinusoidal wave as modulating signal and multi carrier signal which is of triangular in shape have been considered [10, 14, 15]. For an m-level MLI, (m-1) carrier signals are required.

2.1 Multi carrier Sinusoidal PWM: For generation of triggering pulses to the MLI, carrier signals can be constructed using various control techniques like APOD, POD, PD, PS, Hybrid and can be modulated using sine wave [6-7]. As phase shifted technique is best suitable for CHMLI, is used in this paper for generation of triggering pulses to CHMLI [7-9]. Multilevel sinusoidal PWM can be classified as shown in Fig.3 [14-19].

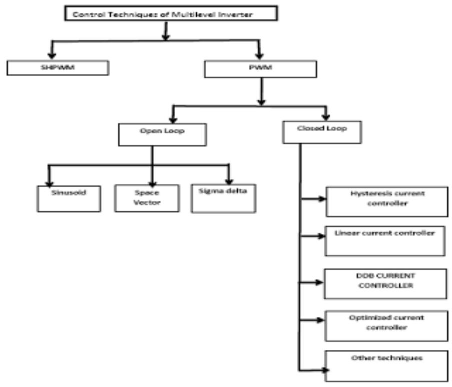

Fig.2 Control Techniques for a Cascaded H-Bridge MLI

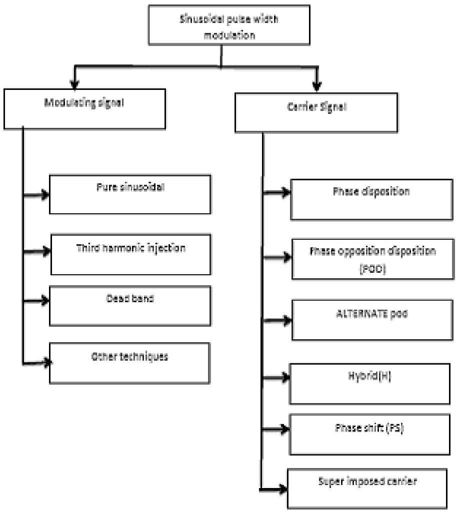

Fig.3 Classification of Sinusoidal PWM

Amplitude Modulation

$$M_a = \frac{A_m}{A_c(m-1)}$$

Frequency Modulation

$$M_f = \frac{F_c}{F_r}$$

Here A_m = Amplitude of Modulating Wave (Sine)
A_c = Amplitude of Carrier Wave (Triangular)
F_c = Carrier Frequency
F_r = Reference Frequency

2.2 Modes of Operation: For generating triggering pulses, sine wave (reference) can be modulated with phase shifted carrier technique in bipolar and uni polar mode. As in
this paper bi polar mode of operation is used, carrier signals arrangement using PS control technique in bipolar mode of operation is shown in Fig.4 In bi polar mode, four carrier signals of triangular in nature and one sine wave are used [6,15].

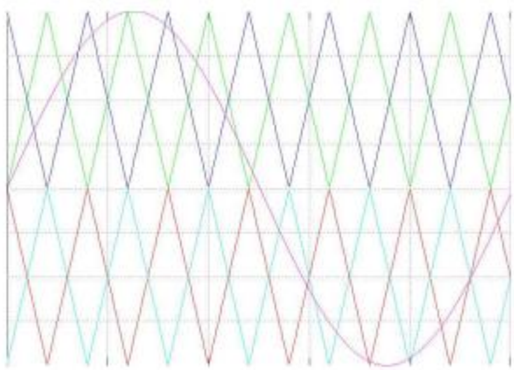

Fig.4 Carrier Arrangement for Bi-Polar Mode in PS Technique

For a five level MLI, in PS Technique the carrier signals are Phase Shifted by 90 Degrees $\frac{360}{(m-1)}$

III. POWER QUALITIES

Power Quality is the concept of powering and grounding sensitive equipment in a matter that is suitable to the operation of that equipment according to IEEE Std 1100. Power quality is mainly concerned with deviations of the voltage from its ideal waveform (voltage quality) and deviations of the current from its ideal waveform (current quality). Power quality phenomena can be divided into two types; they are 1) Variations 2) Events.

Voltage and Current variations are relatively small deviations of voltage or current characteristics around their nominal or ideal values. The two basic examples are voltage magnitude and frequency. Events are phenomena which only happen every once in a while. An interruption of the supply voltage [IEEE Std.1159] is the best-known example.

3.1 Under Voltage: Under voltages of various duration are known under different names. Short duration under voltages are called “voltage sags” or “voltage dips”. Long duration under voltage is normally simply referred to as “under voltage”. Voltage sag is a reduction in the supply voltage magnitude followed by a voltage recovery after a Short period of time. Reduction of voltage magnitude of short duration can be called as voltage sag. For the IEEE voltage drop is only a sag if the during sag voltage is between 10% and 90% of the nominal voltage. Voltage sags are mostly caused by short circuit faults in the system and by starting of large motors. Voltage sag is generally characterized by depth and duration. The depth of the sag depends on the system impedance, fault.

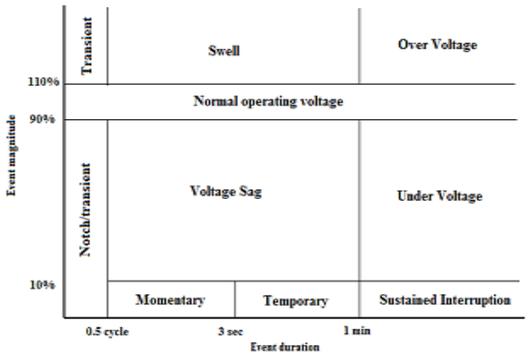

Fig.5 Voltage Magnitude Events as Used in IEEE Std. 1159-1995

Distance, system characteristics (grounded or ungrounded) and fault resistance. The duration of the sag depends on the time taken by the circuit protection to clear the fault.

3.2 Over Voltage: Just like with under voltage, overvoltage events are given different names based on their duration. Over voltages of very short duration, and high magnitude, are called “Transient Over Voltages”, “Voltage Spikes,” or sometimes “Voltage Surges.” When the output voltage exceeds 110% of the rated voltage & with duration More than 1 minute is called Over Voltage. Long and Short over voltages originate from, lightning strokes, switching operations, sudden load reduction, single phase short circuits, and nonlinearities. A resonance between the nonlinear magnetizing reactance of a transformer and a capacitance (either in the form of a capacitor bank or the capacitance of an underground cable) can lead to a large overvoltage of long duration. This phenomenon is called Ferro resonance, and it can lead to serious damage to power system.

In this paper the three phase ac voltage supply is taken directly and is given to three dc voltage is given as a input to Cascaded H-bridge 5 level Multilevel Inverter and the output of MLI is given to load.

In closed loop control the supply voltages and load voltages are both compared and error value is given to PI Controller. Output of PI controller is imposed on the phase shifted carrier phase controlled rectifier which converts ac supply to controlled pulsated dc voltage and this is given to low pass filter. Low pass filter is a device which converts pulsated dc voltage to pure dc voltage and this pure

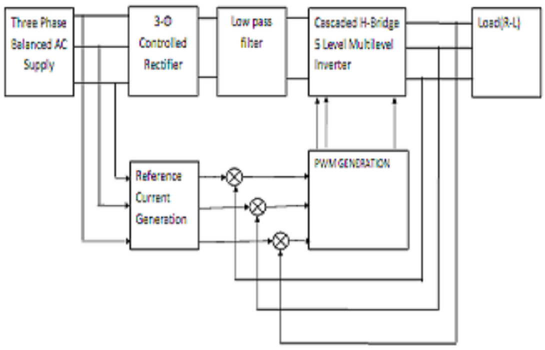

Fig.6 Closed Loop Block Diagram

So as to get pulses. These pulses are given to MLI for each phase. Here we are using three PI controllers for three phases MLI. The desired voltage at the load bus is maintained at 1pu.

3.3 PI Controller: To regulate the load-bus voltage, a PI controller is employed that contains a feedback signal derived from the voltage at the load bus V.

$$Z_c = K_p e + K_i \int edt$$

Where,
K_p = Proportional Constant
K_i = Integral Constant
E = Error Value

3.4 Design of Filter: LC Filter is the combination of two filters & provides a lower ripple than which is possible with either L or C alone. As it is known, in an inductor filter, ripple increases with RL but decreases in a capacitor filter. So the combination of both L and C filter lowers the ripple content. Here,

$$C = \frac{10}{2 * w(R_L^2 + (2W_L L_L)^2}$$

$$VRF = \frac{\sqrt{2}}{3} \frac{1}{(2 * W)^2 LC - 1}$$

Where VRF is Voltage Ripple Factor

IV. SIMULATION RESULTS

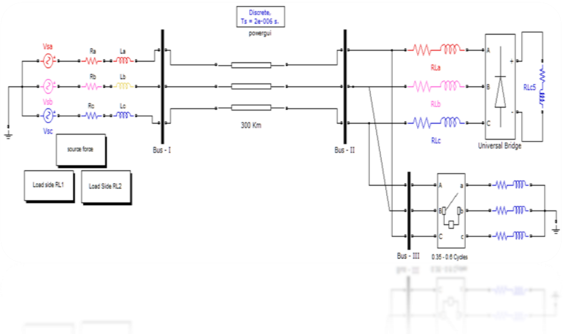

Fig.7 Simulink Diagram of Open Loop System for Voltage Sag

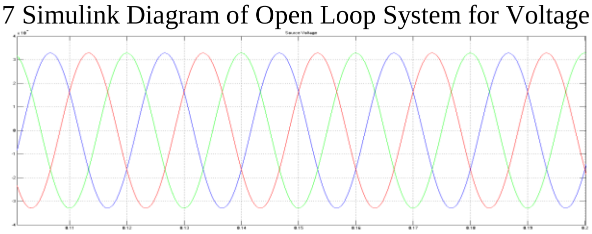

Fig.8 Supply Voltages

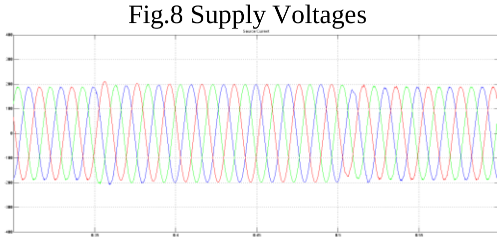

Fig.9 Supply Current

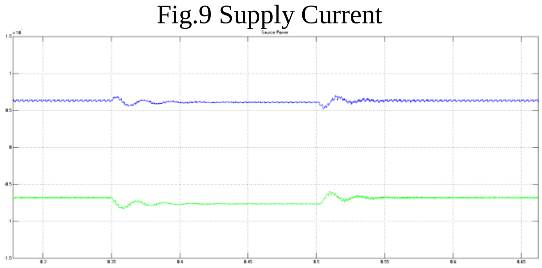

Fig.10 Source Active Power & Reactive Power

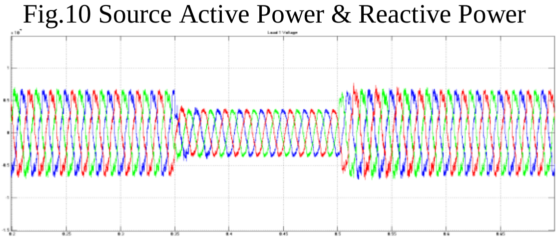

Fig.11 Load Voltage

International Journal of Modern Engineering Research (IJMER)
www.ijmer.com Vol. 3, Issue. 5, Sep - Oct. 2013 pp-3156-3163 ISSN: 2249-6645

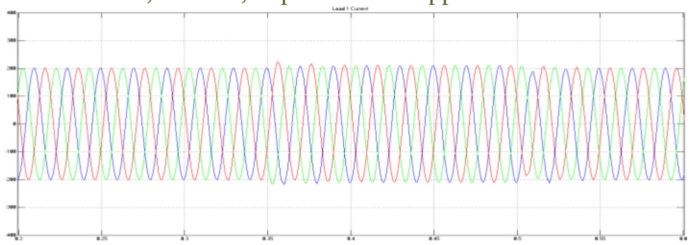

Fig.12 Load Current

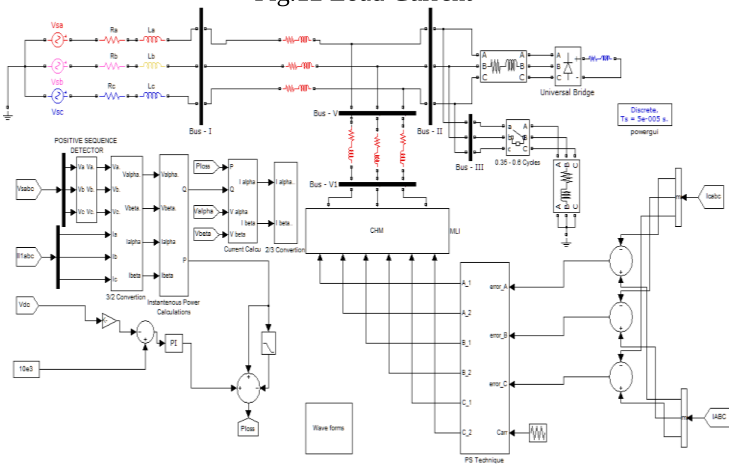

Fig.13 Voltage Sag Closed Loop

Fig.14 Closed loop Current

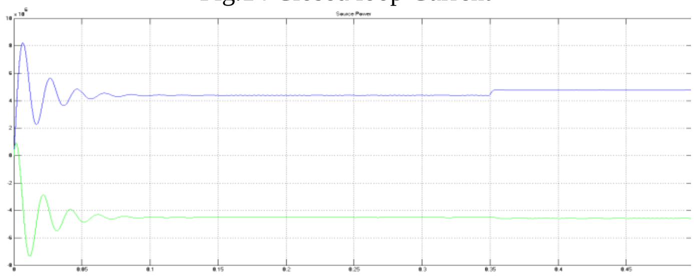

Fig.15 Active & Reactive Powers

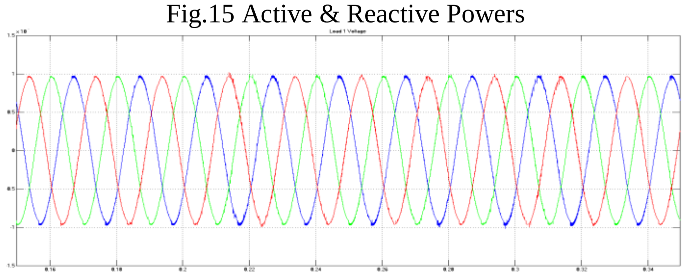

Fig.16 Load Voltage

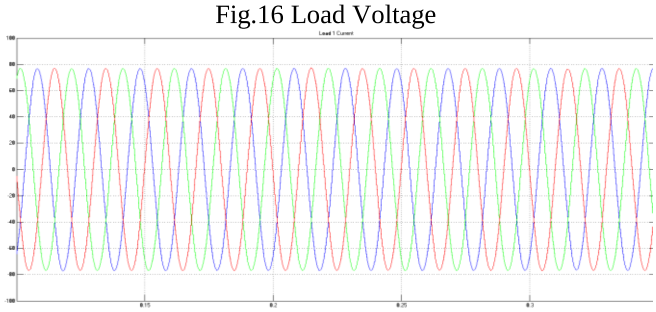

Fig.17 Load Current

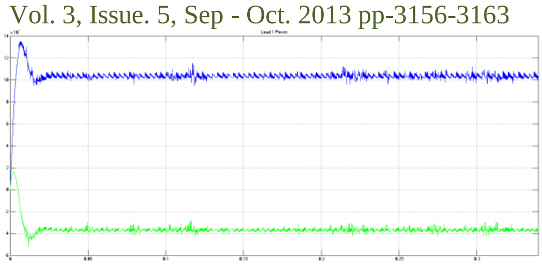

Fig.18 Active & Reactive Powers at Load Side

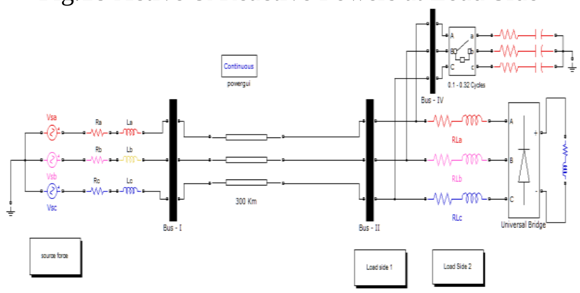

Fig.19 Voltage Swell Open Loop

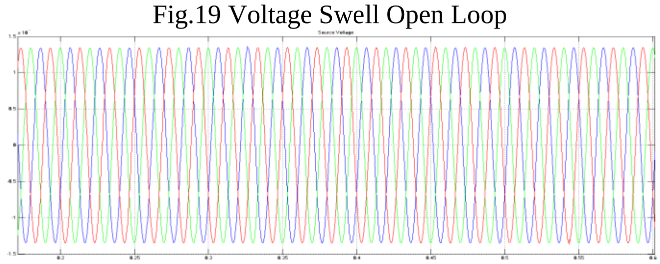

Fig.20 Source Voltage

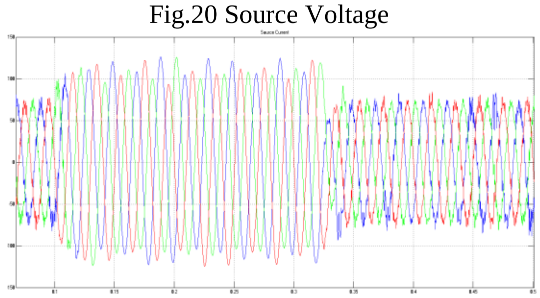

Fig.21 Source Current

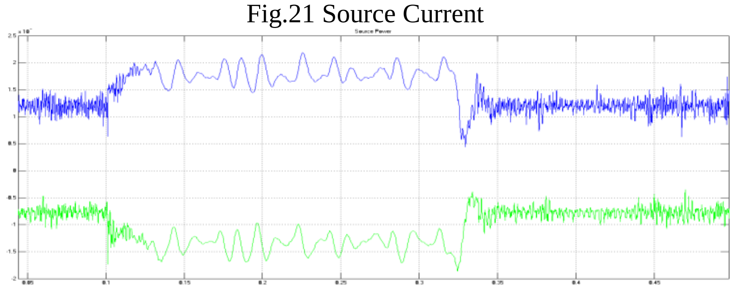

Fig.22 Source Active & Reactive Power

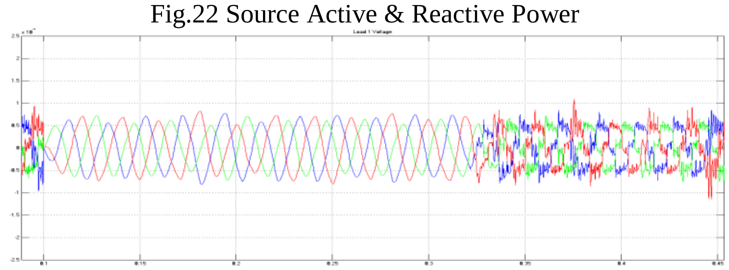

Fig.23 Load Voltage

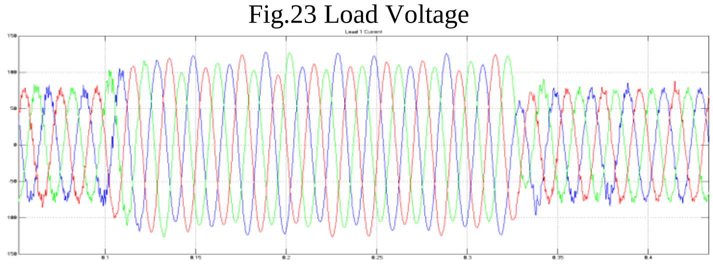

Fig.24 Load Current

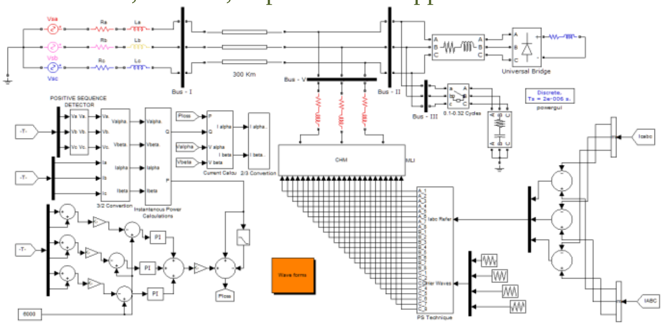

Fig.25 Voltage Swell Closed Loop

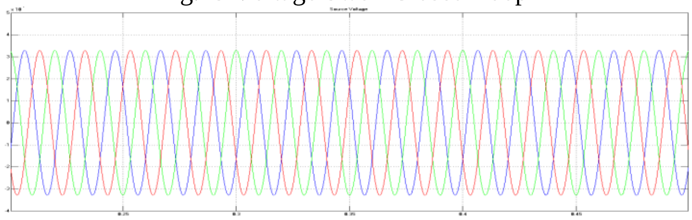

Fig.26 Source Voltage

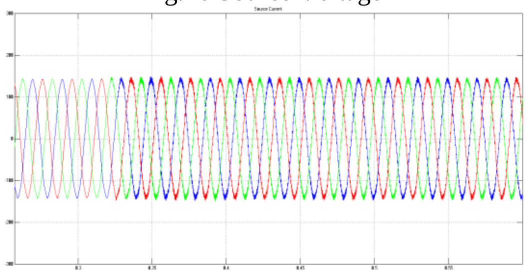

Fig.27 Source Current

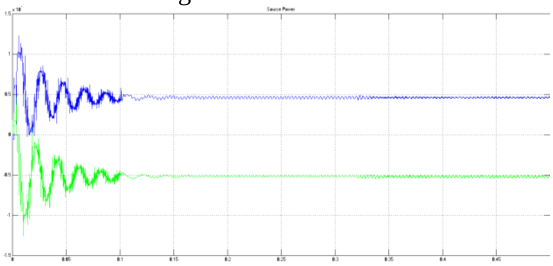

Fig.28 Source Active & Reactive Power

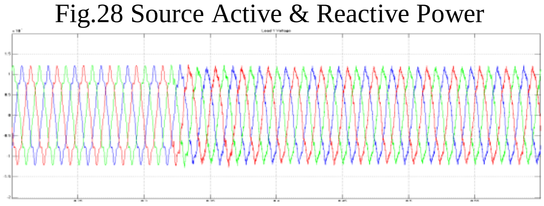

Fig.29 Load Voltage

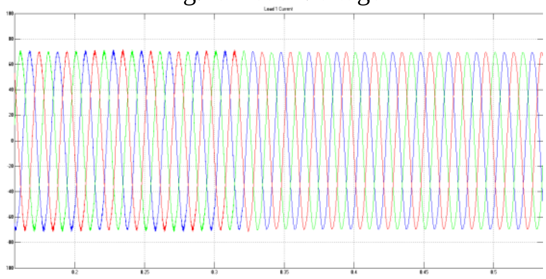

Fig.30 Load Current

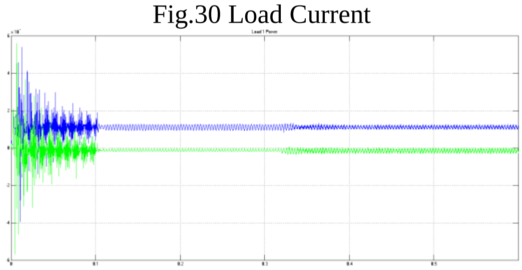

Fig.31 Load Active & Reactive Power

V. CONCLUSION

In this paper three phase Cascaded H-Bridge Multilevel inverter is simulated using multi carrier Phase Shifted technique and analyzed for Under Voltage and Over Voltage conditions. In the open loop system under voltage and over voltages were introduced at the supply side and the changes in the load voltages are analyzed from the observed waveform. In the closed loop system, with the help of PI Controller the load voltage is maintained constant during under voltage and over voltage conditions which can be observed from the above simulated figures.

REFERENCES

[1] D. A. Rendusara, E. Cengelci, P. N. Enjeti, V. R. Stefanovic, and J.W. Gray. "*Analysis of common mode voltage—neutral shift in medium voltage PWM adjustable Speed drive (MV-ASD) systems*," IEEE Trans. Power Electronics, vol.15, no.6, pp.1124-1133, Nov. 2000.

[2] Fang Zheng Peng, Jih-Sheng Lai, and Rodriguez J. "*Multilevel inverters: A survey Of topologies, controls, and applications*", Industrial Electronics, IEEE Transactions, Vol. 49, issue: 4, pp. 724-738, Aug 2002.

[3] Holmes, D.G, McGrath, B.P. "*Multi carrier PWM strategies for multilevel inverters*" Industrial Electronics, IEEE Transactions, Vol. 49, issue: 4, pp.858-867, Aug 2002.

[4] Leon M. Tolbert, Fang Zheng Peng, Tim Cunnyngham, and John N.Chiasson. "*Charge balance control schemes for cascade multilevel converter in hybrid electric vehicles*" IEEE Trans. Industrial Electronics, vol.49, no.5, pp.1058- 1064, Oct. 2002.

[5] Yan Deng, Hongyan Wang, Chao Zhang, Lei Hu and Xiangning He, "*Multilevel PWM Methods Based On Control Degrees of Freedom Combination And Its Theoretical Analysis*", IEEE IAS 2005 Conference record no.:0-7803-9208-6/05, pp.1692 – 1699, 2005.

[6] Alan Joseph, et al. "*A 24-pulse rectifier cascaded multilevel inverter with minimum number of transformer windings*," IEEE Fourtieth IAS Annual Meeting ,vol.1, Oct. 2005, pp.115-120.

[7] J. Rodriguez, B. Wu, S. Bernet, J. Pontt, and S. Kouro, "*Multilevel voltage source-converter topologies for industrial medium-voltage drives*," IEEE Trans. Ind.Electron., vol. 54, no. 6, pp. 2930–2945, Dec. 2007.

[8] S. Khomfoi, L. M. Tolbert, "*Multilevel Power Converters*," Power Electronics Handbook, 2nd Edition Elsevier, 2007, ISBN 978-0-12- 088479-7, Chapter 17, pp.451-482.

[9] Samir Kouro, Student Member, IEEE, Pablo Lezana, Member, IEEE,Mauricio Angulo, and Jose Rodriguez, Senior Member, IEEE Transactions on Power Electronics, Vol. 23, No. 1, January 2008 "*Multicarrier PWM With DC-Link Ripple Feed forward Compensa. for Multilevel Inverters*".

[10] Panagiotis Panagis, Fotis Stergiopoulos, Pantelis Marabeas and Stefanos Manias "*Comparison of State of the Art Multilevel Inverters*". 978-1-4244-1668-4/08/2008 IEEE

[11] Ge Baoming,and Fang Zheng Peng,"*An Effective Control Technique for Medium-Voltage High Power Induction Motor Drives*", 978-1-4244-1766-7/08-2008 IEEE.

[12] "*A 5-Level Cascaded Hybrid Multilevel Inverter for Interfacing with Renewable Energy Resources*" Surin Khomfoi1, Chatrchai Aimsaard 978-1-4244-3388- 9/09/2009 IEEE

[13] "*Optimized Hybrid Phase Disposition PWM Control Method for Multilevel Inverter*" C. Govindaraju and Dr. K. Baskaran Internatio. Journal of Recent Trends in Engineering, Vol 1, No. 3, May 2009 49

[14] "*A modular power electronic transformer based on a cascaded H-bridge multilevel converter*" H. Iman-Einia,b, Sh. Farhangia, J.-L. Schanenb, M. Khakbazan-Fardc H. Iman- Eini et al. / Electric Power Systems Research 79 (2009) 1625–1637.

International Journal of Modern Engineering Research (IJMER)
www.ijmer.com Vol. 3, Issue. 5, Sep - Oct. 2013 pp-3164-3169 ISSN: 2249-6645

Efficient Implementation of Low Power 2-D DCT Architecture

[1]Kalyan Chakravarthy. K , [2]G.V.K.S.Prasad
[1] *M.Tech student, ECE, AKRG College of Engineering and Technology, Nallajerla, INDIA*
[2]*Assistant professor, ECE, AKRG College of Engineering and Technology, Nallajerla, INDIA*

ABSTRACT*: This Research paper includes designing a area efficient and low error Discrete Cosine Transform. This area efficient and low error DCT is obtained by using shifters and adders in place of multipliers. The main technique used here is CSD (Canonical Sign Digit) technique.CSD technique efficiently reduces redundant bits. Pipelining technique is also introduced here which reduces the processing time.*

I. INTRODUCTION

Multimedia data processing, which encompasses almost every aspects of our daily life such as communication broad casting, data search, advertisement, video games, etc has become an integral part of our life style. The most significant part of multimedia systems is application involving image or video, which require computationally intensive data processing. Moreover, as the use of mobile device increases exponentially, there is a growing demand for multimedia application to run on these portable devices. A typical image/video transmission system is shown in the Figure 1.

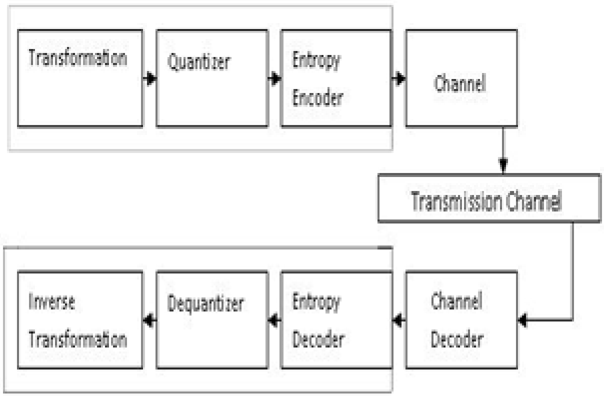

Figure1. Image/Video Transmission System

In order to reduce the volume of multimedia data over wireless channel compression techniques are widely used. Efficiency of a transformation scheme can be directly gauged by its ability to pack input data into as few coefficients as possible. This allows the quantizer to discard coefficients with relatively small amplitudes without introducing visual distortion in the reconstructed image.

In image compression, the image data is divided up into 8x8 blocks of pixels. (From this point on, each color component is processed independently, so a "pixel" means a single value, even in a color image.) A DCT is applied to each 8x8 block. DCT converts the spatial image representation into a frequency map: the low-order or "DC" term represents the average value in the block, while successive higher-order ("AC") terms represent the strength of more and more rapid changes across the width or height of the block. The highest AC term represents the strength of a cosine wave alternating from maximum to minimum at adjacent pixels.

II. JPEG ENCODER

The JPEG encoder is a major component in JPEG standard which is used in image compression. It involves a complex sub-block Discrete Cosine Transform (DCT), along with other quantization, zigzag and Entropy coding blocks. In this architecture, 2-D DCT is computed by combining two 1-D DCT that connected by a transpose buffer. The architecture uses 4059 slices, 6885 LUT, 58 I/Os of Xilinx Spartan-3 XC3S1500 FPGA and works at an operating frequency of 65.55 MHz.

Vector processing using parallel multipliers is a method used for implementation of DCT. The advantages in the vector processing method are regular structure, simple control and interconnect, and good balance between performance and complexity of implementation. For the case of 8 x 8 block region, a one-
dimensional 8- point DCT followed by an internal transpose memory, followed by another one dimensional 8-point DCT provides the 2D DCT architecture. Here the real time DCT coefficients are used for matrix multiplication. Using vector processing, the output Y of an 8 x 8 DCT for input X is given by $Y = C*X* C^T$, where C is the cosine coefficients and C^T are the transpose coefficients. This equation can also be written as $Y=C * Z$, where $Z = X*C^T$.
The calculation is implemented by using eight multipliers and storing the co-efficients in ROMs. At the first clock, the eight inputs xOO to x07 are multiplied by the eight values in column one, resulting in eight products (POO _0 to POO 7). At the eighth clock, the eight inputs are multiplied by the eight values in column eight resulting in eight 586 products (P07 0 to P07 7). From the equations for Z, the intermediate values for the first row of Z are computed. The values for ZO (0 -7) can be

calculated in eight clock cycles. All 64 values of Z are calculated in 64 clock cycles and then the process is repeated. The values of Z correspond to the 1-DDCT of the input X. Once the Z values are calculated, the 2D-DCT function Y can be calculated from Y = C*Z.

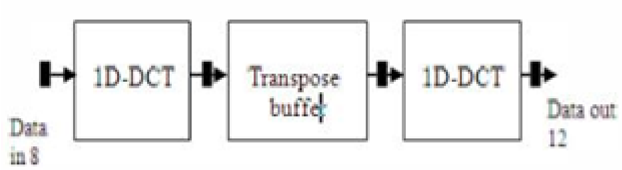

Figure 2. 2-D DCT Architecture

The maximum clock frequency is 65. 55 MHz when implemented with a Spartan FPGA XCS1500 device.

III. MULTIPLIER-LESS 2-D DCT/IDCT ARCHITECTURE FOR JPEG

The Discrete Cosine transform is widely used as the core of digital image compression. Discrete Cosine Transform attempts to de-correlate the image data. After de-correlation, each transform co-efficient can be encoded independently without losing compression efficiency. In this paper we present VLSI Implementation of fully pipelined multiplier less architecture of 8x8 2D DCT/IDCT. This architecture is used as the core of JPEG compression hardware. The 2-D DCT calculation is made using the 2-D DCT separability property, such that the whole architecture is divided into two 1-D DCT calculations by using a transpose buffer. The architecture described to implement 1-D DCT is based on Binary-Lifted DCT. The 2-D DCT architecture achieves an operating frequency of 166 MHz. One input block of 8x8 samples each of 8 bits each is processed in 0.198µs. The pipeline latency of proposed architecture is 45 Clock cycles.

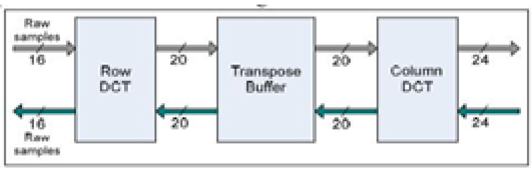

Figure 3 Architecture of 2-D DCT

Figure 2. shows the architecture of 2-D DCT. 2D-DCT/IDCT design is divided into three major blocks namely Row-DCT, Transpose Buffer, and Column-DCT. Row-DCT and Column-DCT contains both 1DDCT (Figure 4) by Row . Access of Transpose buffer DCT and Column DCT is efficiently managed to achieve the performance and minimal usage of resources in terms of area.

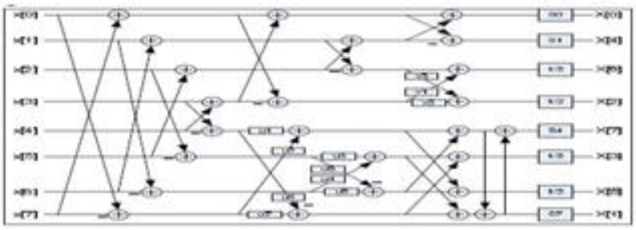

Figure 4. Architecture of 1-D DCT

During Forward transform, 1D-DCT structure (Figure 4) is functionally active. Row-DCT block receives two 8-bit samples as an input in every cycle. Each sample is a signed 8- bit value and hence its value ranges from -128 to 127. The bit width of the transformed sample is maintained as 10-bit to accommodate 2-bit increment.

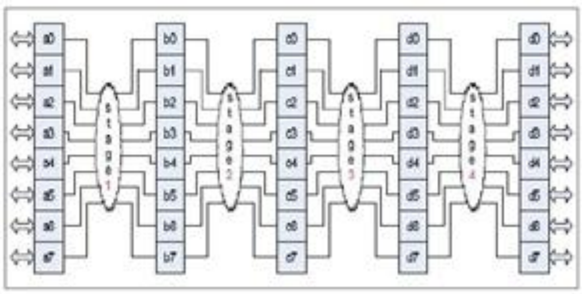

Figure 5. Four stage pipeline 1D-DCT.

1D-DCT computation architecture (Figure 4) has a four stage internal pipeline shown in

Figure 5.Transpose Buffer receives two 10-bit samples as an input every cycle. Each sample is a signed 10-bit value and hence its value ranges from -512 to 511. Since there is no data Manipulation in the module the output sample width remains as input sample width i.e. 10-bit. Transpose buffer has sixty-four 10-bit registers to store one 8X8 block 1D-DCT

samples. Transpose operation on 8X8 block data is performed by writing the transformed samples in row-wise and reading them in column-wise and vice versa. Transpose Buffer block guarantees that the nth 8X8 block data will be written into the registers after (n-1) th 8X8 block data has been completely read out for further processing. The latency of the block is 31 cycles since the data can be read only after full 8X8 block is written in the registers. Column DCT block receives two 10-bit samples as an input in every cycle. Input samples are internally buffered.
The 2D-DCT/IDCT architecture efficiently operates up to 166MHz. Pipeline latency for the initial 8x8 block with each element of 8 bits is 45 clock cycles which is due to 7 cycles at Row-DCT, 31 cycles for Row-DCT operation to complete, 7 cycles at Column-DCT. Effectively to perform complete 2D DCT on one 8x8 will take 33 Clock cycles on availability of continuous input data to process. For operating frequency of 166 MHz, the processing time of 8x8 blocks is 0.198μs.

IV. QUANTIZATION ARCHITECTURE

Two dimensional DCT takes important role in JPEG image compression. Architecture and VHDL design of 2-D DCT, combined with quantization and zig-zag arrangement, is described. The architecture is used in JPEG image compression. The output of DCT module needs to be multiplied with post-scaler value to get the real DCT coefficients. Post-scaling process is done together with quantization process. 2-D DCT is computed by combining two 1-D DCT that connected by a transpose buffer. This design aimed to be implemented in cheap Spartan 3E XC3S500 FPGA. The 2-D DCT architecture uses 3174 gates, 1145 Slices and 11 multipliers of one Xilinx Spartan-3E XC3S500E FPGA and reaches an operating frequency of 84.81 MHz. One input block with
8 x 8 elements of 8 bits each is processed in 2470 ns and pipeline latency is 123 clock cycles.

This architecture adopts the scaled 1-D DCT algorithm. It means the DCT coefficients produced by the algorithm are not the real coefficients. To get the real coefficients, the scaled ones must be multiplied with post-scaler value. Equation (1) is showing scaled 1-D DCT process.

$$\mathbf{y'} = \mathbf{C}\,\mathbf{x} \qquad (1)$$

Variable **x** is 8 point vector. **C** is Arai's DCT matrix and **y'** is vector of scaled DCT coefficients. To get the real DCT coefficients, y' must be element by element multiplicated with post-scaling factor. It is shown in (2).

$$\mathbf{y} = \mathbf{s}\ .\!*\ \mathbf{y'} \qquad (2)$$

Constant **s** is vector of post-scaling factor. Figure 6 shows the block diagram representation of the entire system.

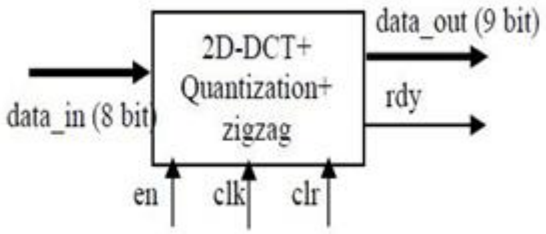

Figure 6. Block Diagram of entire system

The DCT input/output has 8 points and data has to be entered and released in sequential manner, it takes 8 clock cycles for each input and output process. Totally, 8 points 1D-DCT computation needs 22 clock cycles. 1D-DCT computation is done in pipeline process. Figure 7 shows 1-D DCT architecture with pipelining.

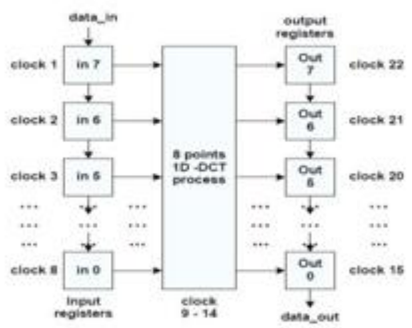

Figure 7. 1-D DCT with pipelining

The 2-D DCT architecture was described in VHDL. This VHDL was synthesized into an Xilinx Spartan 3E family FPGA. According to synthesis result, maximum time delay produced is 5.895 ns. That constraint yields minimum clock period 11.790 ns. Maximum clock frequency can be used is 84.818 MHz. The 2-D DCT architecture uses 3174 gates, 1145 Slices and 11 multipliers.
The stronger operator, multiplication is transformed to simple shift and adds operations by applying
Horner's rule. This reduces the power consumption. For example, consider the cosine coefficients c and g, **c *X**

= $2^5 + 2^4 + 2^2 + 1$ (X) = (2^4 (**3**) + **5**) (X) and **g*X** = $2^3 + 2^2$ (X)= 2^2(**3**) (X) and the common terms they share is 3X. The common terms among the cosine basis are the partial outputs. These blocks are termed as *precomputing* units and an unit is shown in the Figure 3. The intermediate results from the precomputing blocks are added in the final stage yielding the DCT coefficients. The 3A is constructed by expressing it as 3A = 1A+2A = {1A + (1A<<1)}. Similarly the 5A can be expressed as {1A + (1A<<2)}.

A. Low Power Odd And Even Architecture

The stages involved in the determination of 1-D DCT coefficients are precomputing, odd DCT and even DCT. The proposed architecture is a multiplier less architecture. The representation of cosine basis in CSD format reduces power consumption as it has less number of ones. Each multiplication of the cosine coefficients with the sequence are expressed using Horner's rule [6].

The sub structure sharing is carefully done so that it contains the actual sequence i.e. 1A prevalently. This keeps the result of the shift and adds nearly matching the direct multiplication of the cosine basis with the sequence. The Odd DCT precomputing units have 1A, -1A, 3A, and 5A structures to be shared. 3A can be expressed as ($1A+2^1A$) and 2^1A is obtained by left shifting A by 1 place to the left. Similarly 5A=1A+(A<<2).

The even DCT contains the DC part of the transformed image i.e. in frequency domain. Hence care should be taken in calculating the Z0 value. The corresponding cosine basis is d and is represented as d = $2^5 + 2^3 + 2^2 + 1$. The precomputing unit of the even DCT consists of 1A, -1A and 3A only.

The odd and even modules use four precomputing instances each. The outputs from the precomputing units are fed to the final adder stage. The final adder outputs are the desired DCT coefficients. The image pixel value is represented in 8-bits and hence the output of the adder and subtractor has 9-bits.The input to the row DCT has 9-bits and its output is chosen to have 12 bits. Thus the column DCT is fed by 12-bit inputs. The DCT coefficients are quantized to have 12-bits.

B. Synthesis Results

The 2-D DCT architecture is implemented with Verilog HDL and simulated using MODELSIM for functional verification. Finally it is synthesized using QUARTUS II tool and mapped on to a Cyclone III device (65 nm). The simulated results are shown below. The DCT coefficients obtained through this architecture is verified against MATLAB results.

evice Utilization Summary

Flow Status	Successful - Tue Jun 19 12:56:31 2012
Quartus II Version	9.0 Build 132 02/25/2009 SJ Web Edition
Revision Name	twodf
Top-level Entity Name	dct2d
Family	Cyclone III
Device	EP3C5F256C7
Timing Models	Final
Met timing requirements	N/A
Total logic elements	4,758 / 5,136 (93 %)
Total combinational functions	4,605 / 5,136 (90 %)
Dedicated logic registers	2,106 / 5,136 (41 %)
Total registers	2106
Total pins	172 / 183 (94 %)
Total virtual pins	0
Total memory bits	0 / 423,936 (0 %)
Embedded Multiplier 9-bit elements	0 / 46 (0 %)
Total PLLs	0 / 2 (0 %)

Power Analysis Report

PowerPlay Power Analyzer Summary	
PowerPlay Power Analyzer Status	Successful - Thu Aug 23 11:48:37 2012
Quartus II Version	11.0 Build 208 07/03/2011 SP 1 SJ Web Edition
Revision Name	qa
Top-level Entity Name	dct_algorithm
Family	Cyclone III
Device	EP3C16F484C6
Power Models	Final
Total Thermal Power Dissipation	80.09 mW
Core Dynamic Thermal Power Dissipation	0.00 mW
Core Static Thermal Power Dissipation	51.82 mW
I/O Thermal Power Dissipation	28.26 mW
Power Estimation Confidence	Low: user provided insufficient toggle rate data

A low complexity 2-D DCT architecture has been designed. The sub structure sharing removes the redundancy in the DCT calculation. The architecture can be pipelined to meet high performance needs such as applications in HD televisions, satellite imaging systems.

V. IMPLEMENTATION OF THE PROPOSED APPROACH

Raw image data used in applications such as high definition television, video conferencing, computer communication, etc. require large storage and high speed channels for handling huge volumes of image data. In order to reduce the storage and communication channel bandwidth requirements to manageable levels, data compression techniques are inevitable. To meet the timing requirements for high speed applications the compression has to be achieved at high speeds.

A. Pipelining

The speed of the system depends on the time taken by the longest data path which is known as the critical path. To increase the speed of the architecture, pipelining technique can be used. Pipelining is the technique of introducing latches along the data path so as to reduce the critical path. Reduction in the critical path increases the speed of operation. Pipelining latches can only be placed across any feed-forward cutest of the architecture graph. The clock period is then limited and the critical path may be between i.An input and a latch, ii.A latch and an output, iii. Two Latches an input and an output.

In this architecture, the pipelining is of fine grain type as the pipeline latches are introduced inside the 1-D module. The critical path of the 1-D module is from the input to the output. This includes the computational time of precomputing modules and the final adders as well. The critical path time is from the onset of the input xi±xj and the arrival of zk (i=0,1,,2,3;j=4,5,,6,7 and k=0 to 7). The speed can be improved if latches are introduced between the shifter and adder module of precomputing modules. After pipelining the critical path is from the input(X) to 3X generator.

The architecture is synthesized into Stratix family EP1S10 device (for high performance needs). The results are shown in the Table1

Design Unit	FMAX Summary
2-D DCT Without Pipelining	126.25MHz
2-D DCT With Pipelining	295.95MHz

Table 1. Frequency summary

B. Device Utilization Summary (Non Pipelined 2-D DCT)

Flow Summary	
Flow Status	Successful - Thu Aug 23 11:46:39 2012
Quartus II Version	11.0 Build 208 07/03/2011 SP 1 SJ Web Edition
Revision Name	qa
Top-level Entity Name	dct_algorithm
Family	Cyclone III
Total logic elements	1,660 / 15,408 (11 %)
Total combinational functions	1,628 / 15,408 (11 %)
Dedicated logic registers	454 / 15,408 (3 %)
Total registers	454
Total pins	171 / 347 (49 %)
Total virtual pins	0
Total memory bits	0 / 516,096 (0 %)
Embedded Multiplier 9-bit elements	0 / 112 (0 %)
Total PLLs	0 / 4 (0 %)
Device	EP3C16F484C6
Timing Models	Final

Design Unit	Frequency Report
2-D IDCT	115.85MHz

C. Image Analysis Results

Figure 8. Original Image

Figure 9. Reconstructed From DCT Coefficients

VI. CONCLUSION

The 2-D DCT and 1D-DCT architectures which adopts algorithmic strength reduction technique to reduce the device utilization pulling the power consumption low have thus been designed. The DCT computation is performed with sufficiently high precision yielding an acceptable quality. The pipelined 2-D DCT architecture achieves a maximum operating frequency of 185.95 MHz. The first eight 2-D coefficients arrived at the nineteenth clock cycle and for the full 64 coefficients, it took about 26 clock cycles to compute. The future work can be oriented towards developing an encoder by architecting a quantizer, based on the strength reduction technique and an entropy encoder.

REFERENCES

[1]. Enas Dhuhri Kusuma, Thomas Sri Widodo "FPGA Implementation of Pipelined 2D- DCT and Quantization Architecture for JPEG Image Compression" Proceedings of 978-1-4244-6716-7/10/$26.00 ©2010 IEEE
[2]. Vijay Kumar Sharma, K. K. Mahapatra and Umesh C. Pati "An Efficient Distributed Arithmetic based VLSI Architecture for DCT"
[3]. Chidanandan, Bayoumi, M, "Area-Efficient NEDA Architecture for The 1-D DCT/IDCT" ICASSP 2006 Proceedings. 2006 IEEE International Conference.
[4]. Zhenyu Liu Tughrul Arslan Ahmet T. Erdogan "A Novel Reconfigurable Low Power Distributed Arithmetic Architecture for Multimedia Applications" Proceedings of 1-4244-0630-7/07/$20.00 C 2007 IEEE.
[5]. S.Saravanan, Dr.Vidyacharan Bhaskar, P.T.Lee ,"A High Performance Parallel Distributed Arithmetic DCT Architecture for H.264 Video Compression" European Journal of Scientific Research ISSN 1450- 216X Vol.42 No.4 (2010), pp.558-564 EuroJournals Publishing, Inc. 2010
[6]. VLSI Digital Signal Processing Systems: Design And Implementation (Hardcover) By Keshab K Parhi
[7]. Vijaya Prakash.A.M, K.S.Gurumurthy "A Novel VLSI Architecture for Digital Image Compression Using Discrete Cosine Transform and Quantization", IJCSNS International Journal of Computer Science and Network Security, VOL.10 No.9, September 2010

Santosh Sanjeevannanavar, Nagamani A.N , "Efficient Design and FPGA Implementation of JPEG Encoder using Verilog HDL" 978-1-4673-0074- 2/11/$26.00 @2011 IEEE 584

International Journal of Modern Engineering Research (IJMER)
www.ijmer.com Vol. 3, Issue. 5, Sep - Oct. 2013 pp-3170-3176 ISSN: 2249-6645

Design Of Hybrid Series Active Filters for Harmonic Reduction in Single Phase Systems

P. Kishore Kumar[1], M.Sharanya[2]
*(M.Tech student in Vignana Bharathi institute of Technology, India)
** (Associate professor in EEE dept in Vignana Bharathi institute of technology, India)

***ABSTRACT**: In this paper, Design of Hybrid series active filter (HSAF) for Harmonic reduction and reactive power compensation in single phase systems is represented. The HSAF consists of the series combination of two single tuned LC filters which are tuned to 3rd and 5th harmonics and an active filter. Discrete Fourier transformation is used as the control technique. Simulation results using MATLAB shows the effectiveness of control technique. On getting the simulation results the value of THD is very low (2.75%), which is very negligible. So the power quality is said to be improved.*

***Keywords:** Hybrid series active filter, active filter, harmonic reduction, reactive power compensation, Discrete Fourier transformation, power quality.*

I. INTRODUCTION

With the wide use of power electronic equipments and nonlinear loads, the power quality has been lost in distribution system. Current harmonics cause serious harmonic problems in distribution feeders for sensitive consumers. Some technology solutions have been reported in order to solve power quality problems. Initially, lossless passive filters have been used to mitigate harmonics and for compensation of reactive power at nonlinear loads. However, passive filters have the drawbacks of fixed compensation, large size and resonance with the supply system.

Active filers have been explored in shunt and series configurations to compensate different types of nonlinear loads; nevertheless, they have some demerits. As a case in point, their power rating is sometimes close to load, and thus it becomes a costly option for power quality improvement. Many analysts have classified various types of nonlinear loads and have suggested different filter options for their compensation. In response to these factors, a series of hybrid filters has been evolved and widely used in practice as a cost effective solution for the compensation of nonlinear loads. Mainly shunt active filters consisting of voltage-fed pulse width modulated (PWM) inverters using IGBT or GTO thyristors are operating successfully in all over the world. These filters provided the required harmonic filtering, reactive power compensation, and etc [1-2].

The most important technology for the power quality improvement is the detecting method of harmonics to decrease the capacity of the various energy storage components. Different control methods are presented in recent publications for this type of active filters [3-16].The control method presented in this thesis is depends upon the calculation of the real part of the fundamental load current while this is helpful in some configurations such as hybrid series active filter, since it cannot compensate reactive power completely and needs many complicate calculations. The active power filter proposed in this thesis uses a dc capacitor voltage closed- loop control and used a modified phase-locked loop for extraction of the reference current. In the cited references, the computation involves various control parameters or needs complex calculations. Also, the dynamic performance of the compensator is not desire in the case of fast-changing loads. The least compensation current control method presented in [9] is based on detection of the harmonics and reactive current of the active power filter. In [10], genetic algorithm and extended analysis optimization techniques were applied for switched capacitor active filters. The combined genetic algorithm/conventional analysis control methods [11] have been considered as a recent control approach. These control methods have a common demerit of concerning the global stability of the closed-loop system. In [12], the control technique is based on the calculation of average power; this wants to know some information regarding system and requires some intense calculation. The sliding-mode control technique proposed in [13] solves the stability problem; however, the calculation technique for compensation of current reference is complex and switching rate is variable. In [14], a digital repetitive control approach is presented to obtain high gain for the current loop; nevertheless, the control strategy in this method is based on a linearized replica of the active filter and does not direct to global stability. A deadbeat control strategy is presented in [15] for the current loop of single-phase active filters. Even though this process has a rapid current control due to the deadbeat nature, it dependence on parameters is a basic drawback. Furthermore, the call for prediction of the current reference requires adaptive signal processing techniques, complicating the execution of this technique. Passivity based controllers [16] based on phasor models of system dynamics have also been projected in an attempt to improve the stability properties of active filters.

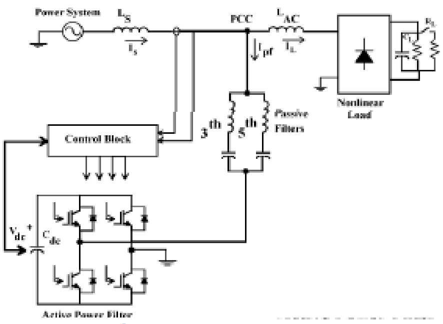

Fig. 1. System configuration.

This paper uses a Discrete Fourier transform for single phase active power filters (APF) that is organized as follows: section II show the hybrid series active filter (HSAF) pattern for harmonic reduction and reactive power compensation; Section III presents the control method; section IV shows stability study of the proposed pattern; section V shows frequency response of the projected pattern; section VI presents the simulation outcome of this technique for a hybrid series active filter, and section VII presents the experimental outcome of this method for a HSAF.

TABLE I. System parameters used in simulations

Parameter	Values
Power source voltage : V_s(V)	220
System equivalent inductance: L_s(mH)	0.48
Load input inductor: L_{AC}(mH)	3
Filter capacitor of 3^{rd}: C_{3f}(μf)	25
Filter inductance of 3^{rd}: L_{3f}(mH)	45
Filter capacitor of 5^{rd}: C_{3f}(μf)	25
Filter inductance of 5^{rd}: L_{5f}(mH)	16
dc capacitor: C_{dc}(μf)	1500
Load capacitor: C_L(μf)	2100
Load resistance: R_L(Ω)	40
Power system fundamental frequency : (Hz)	50

Fig. 1 shows the pattern of the HSAF and nonlinear load planned in this paper and, its parameters are given in Table I. The HSAF consists of a series combination of an active filter and two parallel single tuned passive filters. Two passive filters are tuned in dominants harmonic frequencies of 3rd and 5th. The effectiveness of the proposed method in harmonic elimination and reactive power compensation is shown using HSAF for a non linear load. In the following sections control method and design process and simulation results are given.

II. HYBRID SERIES ACTIVE FILTER (HSAF) FOR HARMONIC REDUCTION

The active filters are divided into pure active filters and hybrid active filters in terms of their circuit pattern. Most pure active filters in their power circuit use either a voltage-source pulse width-modulated (PWM) converter set with a dc capacitor or a current-source PWM converter set with a dc inductor. At present, the voltage-source converters are more positive than the current-source converters in terms of cost, physical size, and efficiency. A hybrid active filter consists of single or multiple voltage-source PWM converters and passive elements such as capacitors, inductors, and/or resistors. The hybrid filters are more favorable than the pure filters in harmonic reduction from both feasibility and economical points of view, particularly for high-power applications. However, single-phase active filters attract much less attention than three-phase active filters because single phase versions are restricted to low-power applications except for electric traction or rolling stock [17].execution of an APF is to use a consistent method for current/voltage reference generation. Presently, there is a great variety of practical achievement supported by various theories.

III. COMPENSATION STRATEGY

The control technique has to extract the harmonic components with minimum phase shift and attenuate the fundamental component. In this paper discrete Fourier transformation (DFT) is used to extract the source current harmonics with assuming N samples in a cycle, as

$$X_1 = \sum_{k=0}^{N-1} x_k e^{\frac{j2\pi k}{n}}$$

$$x_{k1} = \frac{1}{N} X_1 e^{\frac{-j2\pi k}{N}}$$

Where upper equation is DFT and lower equation is inverse DFT. After extracting the fundamental component, it is subtracted from source current to get harmonic components as:

$$i_{Sh} = i_S - i_{S1}$$

Fig. 2 represents the control circuit. If active filter is placed along the passive filter, an extra voltage reference is added to q component. As seen from this figure, a component with 90 degree lead the load terminal voltage is summed to reference voltage to control the dc link voltage capacitor.

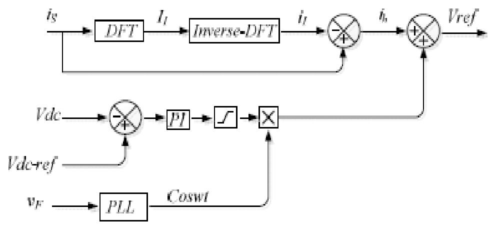

Fig. 2. Control circuit of hybrid series active filter.

IV. POWER SYSTEM STABILITY ANALYSIS

Fig. 3 shows entire power system block diagram. Active filter shows zero impedance against fundamental component of the source current while it shows very high impedance against harmonics. In Fig. 3, analog to digital converters which are placed in the control circuit give some delays in system. Also, it takes a little bit of time to take out harmonic components by the microcontroller. Assuming that all the delays in the system as τ, Fig. 4 shows the system control diagram. So, the open-loop transfer function will be as:

$$G(s)=\frac{K}{sL+Z_F}e^{-s\tau}$$

Above equation represents that if τ is zero, the system is always stable. However, the noise is not eliminated. Fig. 5 represents the relationship between system critical time (τ) and system impedance for various values of K. As seen in from this figure, as K increases, the system critical time is decreased to avoid instability; however, the source current THD gets reduced. Fig. 6 represents the system frequency response. From this figure, it is concluded that the system is stable and its phase margin is about 90 degree.

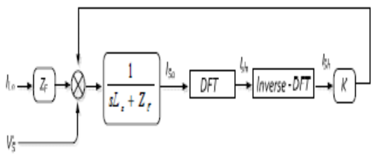

Fig. 3. Block diagram of the whole system.

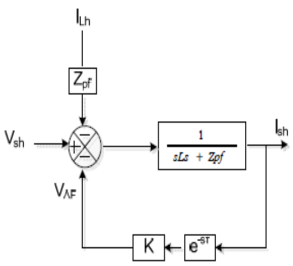

Fig. 4. Control diagram of the system with constant delay τ.

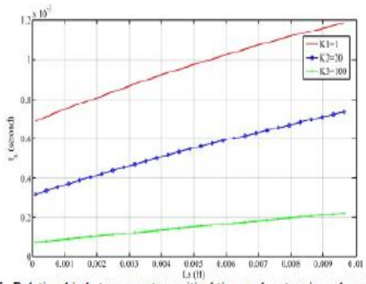

Fig. 5. Relationship between system critical time and system impedance.

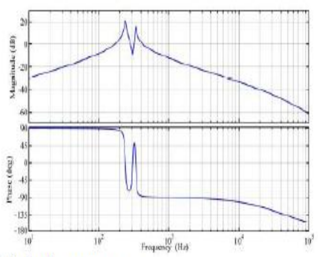
Fig. 6. System frequency response.

V. FREQUENCY RESPONSE OF THE POWER SYSTEM

Single phase harmonic equivalent circuit of the power system, given in Fig. 1, is explained in Fig. 7. In the figure, the voltage source harmonics are represented as Vsh, and it is in series with the Thevenin impedance (Zs) of the power system.

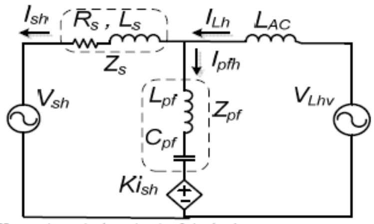

Fig. 7. Harmonic equivalent circuit of single phase system.

Here nonlinear load is a diode rectifier with a resistive capacitive load on its output. This load has typically a voltage source characteristic because an inductor is on rectifier input, and this makes it as a current source type load characteristic. The load is modeled by harmonic voltage VLhv in series with inductor LAC. The series active filter behaves as a damping resistor which is responsible for elimination of resonance between the parallel passive filter and the source impedance. It also prevents allowing of harmonic currents to the power source by experiencing zero impedance at the fundamental frequency and a high resistance K at the power source or load harmonics. So, the series active filter is modeled by a resistor, K, and its output reference voltage as:

$$V_{af} = Ki_{sh}$$

where Ish is the harmonic current flowing from the power source, produced by both the load harmonic current (ILh) and the power source harmonic voltage (VSh). Consequently, from the model shown in Fig. 7, the harmonic current of the power source is calculated as:

$$I_{sh} = \frac{Z_{pf}}{Z_s + Z_{pf} + K} I_{Lh} + \frac{V_{sh}}{Z_s + Z_{pf} + K}$$

where Zs and Zpf are power source and passive filter equivalent impedance, respectively. Based on above equation, when K is large enough greater than Zs and Zpf, the power source harmonic currents will be equal to zero (ISh=0). In information, in this case the source impedance (Zs) has no effect on the parallel passive filter characteristic, and the power source current harmonics will be reduced . If the power source voltage harmonics (VSh) are not considered, the load current will be separated between the passive filter and the power source; in this case, the ratio between the power source harmonic current and the load harmonic current is:

$$\frac{I_{sh}}{I_{Lh}} = \frac{Z_{pf}}{Z_S + Z_{pf} + K}$$

Fig. 8 represents the frequency response for various values of K. As seen in this figure, when the passive filter is used alone (K=0), then two resonances occur between the parallel passive filter and the power source impedance at around 130 Hz and 240 Hz. Also, when the series active filter is placed along with the passive filter, since the series active filter behaves as damping resistor, so there is no resonance in the system.

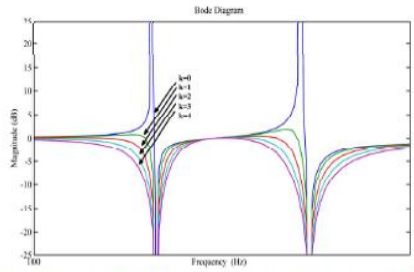

Fig. 8. Frequency response of the hybrid series active filter for different values of K.

VI. SIMULATION RESULTS AND OBSERVATION

Harmonic reduction and reactive power compensation by HSAF is publicized in this section through simulation. A HSAF with the procedure offered above is simulated in MATLAB. In this simulation two single tuned passive filters which are tuned to 3^{rd} and 5^{th} harmonics were used with the parameters specified in Table I.

Fig. 9 shows the simulation outcome when the active filter is in off-line mode. The power source current THD (iL) without compensation is calculated about 70 %. Also, in passive filter compensation manner, the THD of the power source current (is) reduced from 70% to about 41 %. Still, this THD value has not been less than the recommended value in standards such as IEEE 519-1992 [21] and IEC61000 [22].

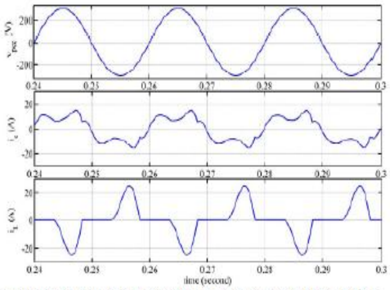

Fig. 9. Simulated waveforms of compensated system with passive filter.

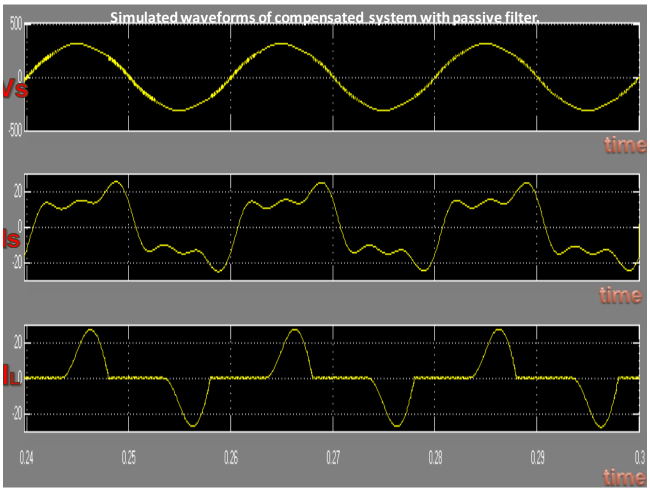

To further reduce the value of the THD, the active filter is placed in the circuit with the dc capacitor voltage of 85 V. Fig. 10 shows the simulation results for this case. The THD of the power source current (is) reduced from 41% in off-line active filter mode to about 2.75 % in on-line active filter mode.

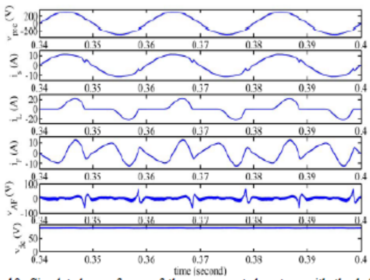

Fig. 10. Simulated waveforms of the compensated system with the hybrid series active filter.

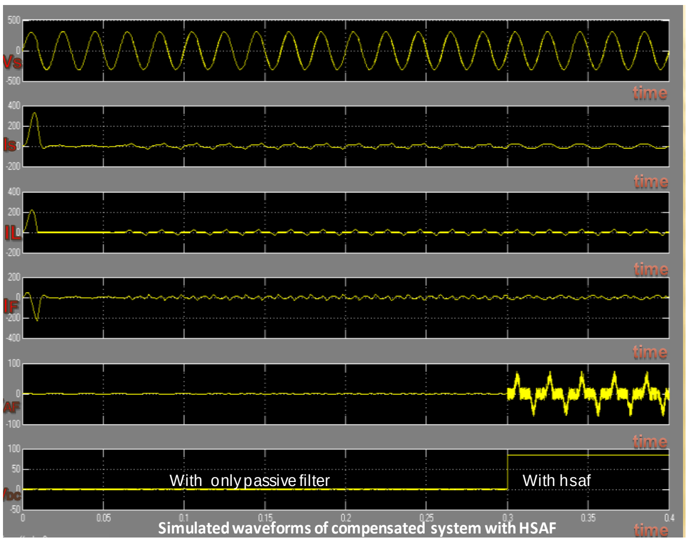

VII. EXPERIMENTAL OUTCOME.

A. System Configuration

It is renowned that the passive filter utilized in this execution is tuned to get rid of 3rd and 5th harmonics. The dc bus voltage is 65 V, and the IGBT switch is employed in the active filter. The projected control technique was implemented with a digital signal processor (TMS320F2812 DSP). Initially, the DSP calculates the reference voltage for the active filter; next, the calculated reference voltage is helpful to produce PWM gate signals for the IGBT switches as the modulation index is 0.5.

B. Experimental Results

Fig. 12 shows the investigational waveform of the power source current without any compensation. In this regards, the THD of the power source current is calculated as 78%. In Fig. 13 the similar current with passive filter is verified with the THD of about 21 %. Fig. 14 shows the power source current with together the active filter as well as the passive filter. In this regards, the THD decreased to about 6.3 %.

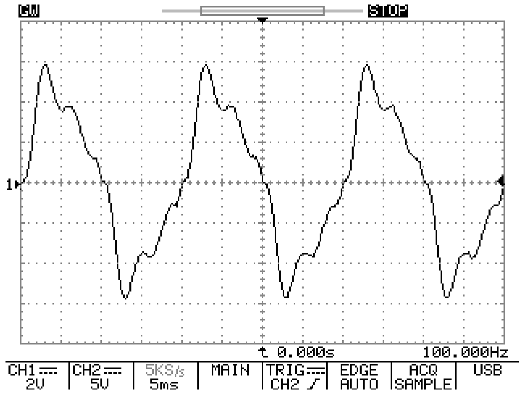

Fig. 13. Experimental waveform of the power source current with the passive filter only.

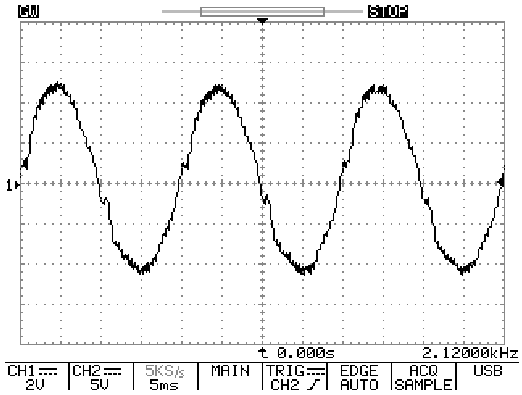

Fig.14. Experimental waveform of the power source current with both the active and the passive filter.

VIII. CONCLUSION

This thesis presents HSAF for harmonic reduction and reactive power compensation in a single phase system with a control method as Discrete Fourier Transformation.. This method is applicable in both single and three phase systems. The main advantage of the presented Hybrid series active filter is that its filter's power rating is 10% of the load making it a cost-effective solution for high power applications. The value of the Total harmonic Distortion is around 2.75%. The effectiveness of the present method is simulated by using MATLAB /Simulink.

REFERENCES

[1] B. Singh, A. Chandra and K. Al.haddad, "Hybrid Filters for Power Quality Improvement," IEE Proc. Gener. Transm. Distrib., vol. 152, pp. 365 - 378, no. 3, May 2005.

[2] Fang Z. Peng, "harmonic sources and filtering approaches," IEEE Industry Applications Magazine, vol. 7, pp. 18 – 25, Jul. /Aug. 2001.

[3] J. C. Wu and H. J. Jou, "Simplified control method for single-phase active power filter," Proc. Inst. Elect. Eng., vol. 143, pp. 219 - 224, no. 3, May 1996.

[4] H. L. Jou, J. C.Wu, and H. Y. Chu, "New single-phase active power filter," Proc. Inst. Elect. Eng.—Electr. Power Appl., vol. 141, pp. 129–134, no. 3, May 1994.

[5] C. Y. Hsu and H. Y. Wu, "A new single-phase active power filter with reduced energy-storage capacity," Proc. Inst. Elect. Eng.—Electr. Power Appl., vol. 143, pp. 25–30, no. 1, Jan. 1996.

[6] J. Barros, E. Perez ," An Adaptive Method for Determining the Reference Compensating Current in Single-Phase Shunt Active Power Filters," IEEE Trans. Power Del., vol. 18, pp. 1578 – 1580, no. 4, Oct. 2003.

[7] M. Karimi-Ghartemani, H. Mokhtari, and M. R. Iravani, "A signal processing system for extraction of harmonics and reactive current of single phase systems," IEEE Trans. Power Del., vol. 19, pp. 979–986, no. 3, Jul. 2004.

[8] M. K. Ghartemani and M. R. Iravani, "A nonlinear adaptive filter for online signal analysis in power system: application," IEEE Trans. Power Del., vol. 17, pp. 617–622, no. 2, Apr. 2002.

[9] L. Zhou and Z. Li, "A novel active power filter based on the least compensation current control method," IEEE Trans. Power Elec., vol. 15, pp. 655–659, No. 4, Jul. 2000.

[10] M. Welsh, P. Mehta, and M. K. Darwish, "Genetic algorithm and extended analysis optimization techniques for switched capacitor active filters - Comparative study," Proc. Inst. Elect. Eng.—Electr. Power Appl., vol. 147, pp. 21–26, no. 1, Jan. 2000. [11] M. El-Habrouk and M. K. Darwish, "A new control technique for active power filters using a combined genetic algorithm/conventional analysis," IEEE Trans. Ind. Elec., vol. 49, pp. 58–66, no. 1, Feb. 2002.

[12] L. P. Kunjumuhammed, M. K. Mishra, "A Control Algorithm for Single-Phase Active Power Filter under Non-Stiff Voltage Source," IEEE Trans. Power Elec., vol. 21, pp. 822 -825 No. 3, May 2006.

[13] D. A. Torrey and A. M. A. M. Al-Zamel, "Single-phase active power filters for multiple nonlinear loads," IEEE Trans. Power Elec., vol. 10, pp. 263–272, no. 3, May 1995.

[14] R. C. Castello, R. Grino, and E. Fossas, "Odd-harmonic digital repetitive control of a single-phase current active filter," IEEE Trans. Power Elec., vol. 19, pp. 1060–1068, no. 4, Jul. 2004.

[15] K. Nishida, M. Rukonuzzman, and M. Nakaoka, "Advanced current control implementation with robust deadbeat algorithm for shunt single-phase voltage-source type active power filter," IEE Proc. Elect. Eng. - Electr. Power Appl., vol. 151, pp. 283–288, no. 3, May. 2004.

[16] A. M. Stankovic, G. Escobar, and P. Mattavelli, "Passivity-based controller for harmonic compensation in distribution lines with nonlinear loads," in Proc. IEEE Power Elec. Specialists Conf. (PESC), vol. 3, pp. 1143–1148, Jun. 2000,

[17] H. Akagi, "Active Harmonic Filters," in Proc. IEEE, vol. 93, pp. 2128 – 214, no. 12, Dec. 2005.

[18] S. Bhattacharya and D. M. Divan, "Synchronous frame based controller implementation for a hybrid series active filter system," Ind. App. Conf., Thirtieth IAS Annual Meeting, IAS '95., vol. 3, pp. 2531 - 2540, Oct.1995.

[19] Wu Longhui, Zhuo Fang, Wang Zhaoan, "Soft Phase Locked Loop for Active Power Filter Applied in Small Rating Stand-alone Power System," Power Elec. Specialists Conf. (PESC 2007). , pp. 2600 - 2606,Jun. 2007.

[20] F. D. Freijedo, J. Doval-Gandoy, O. Lopez and J. Cabaleiro, "Robust Phase Locked Loops Optimized for DSP Implementation in Power Quality Applications," Ind. Elec. 34th Annual Conf. of IEEE (IECON 2008), pp. 3052-3057, Nov. 2008.

[21] IEEE Std. 519-1992, "IEEE Recommended Practice and Requirements for Harmonic Control in Electric Power Systems," Published by IEEE, 1992.

[22] Electromagnetic Compatibility (EMC)—Part 3–4 Limits—Limitation of Emission of Harmonic Current in Low-Voltage Power Supply Systems.

International Journal of Modern Engineering Research (IJMER)
www.ijmer.com Vol. 3, Issue. 5, Sep - Oct. 2013 pp-3177-3180 ISSN: 2249-6645

Evaluation of Tensile and Flexural Properties of Polymer Matrix Composites

S. Channabasavaraju[1], Dr. H. K. Shivanand[2], Santhosh Kumar .S[3]

[1]*Research Scholar, UVCE, Bangalore University, Bangalore—01, India*
[2]*Associate Professor, UVCE, Bangalore-01, India*
[3]*Assistant Professor, RNSIT, Bangalore-98, India*

ABSTRACT: *The work presented in this project is to evaluate tensile and flexural properties of Glass, Graphite and Kevlar fiber reinforced polymer matrix composites. Behaviour of different fibre-reinforced composite materials are studied with respect to different thickness. The test specimens are fabricated by simple hand lay-up technique followed by vacuum bag moulding and prepared according to ASTM standards.*

Keywords: *Graphite fiber, Epoxy resin, Glass fiber, Kevlar fiber*

I. INTRODUCTION

The Technology advancements are necessitating exploring materials of unusual combination of properties (mechanical, electrical, corrosion, optical, magnetic, semi conducting dielectric etc). taking cue from natural composite such as wood (which is a composite of cellulose fibers in lignin matrix) and bone (a composite of soft protein called collagen in which hard appetite particles are naturally embedded by bio mineralization process), man has synthesized composite materials to meet the ever increasing property spectrum. This property spectrum is otherwise not obtainable by using metal, ceramics and polymeric materials alone.

The most remarkable features of wood and bones are that the low density, strong and stiff fibers are embedded in a low density matrix resulting in a strong, stiff and light weight composite. Wood and bones in many respects may be considered as predecessors to modern man made composites. The main characteristics of wood and bones are that they are fiber-reinforced composites having low weight and directional properties. Early man used rocks, wood and bones effectively in their struggle for existence against natural and various kinds of other forces. The primitive people utilized these materials to make weapons, tools and many utility articles and also built shelters. Later on they utilized several other materials such as vegetable fibers, shells, clays as well as horns, teeth, skins and sinews of animals. Natural fibers like straws from grass plants and fibrous leaves were used as roofing material. The limitations experienced in using these materials and search for better materials taught them to combine two or more materials to obtain a more efficient material with better properties. This is turn laid the foundation for development of man made modern composite materials. Composite materials have been used from earliest know civilization.

Composite materials were recognized for their strength and lightweight when used in the construction of the first all composite, radar proof airplane. Honeycomb exemplifies natural sandwiched composites which was guided man to build airframe structure. Composite materials in the form of sandwich construction showed that primary aircraft structures could be fabricated from these materials. World War II gave birth to glass-fiber polyester composites for secondary aircraft structures, such as doors and fairings, which were designed and produced. Glass fiber composites were recognized as valid materials for fabrication and production of Polaris submarine missile casings. In the 1950s, fiber technology identified the need for fibers that could compete in strength and stiffness when the state –of- the –art development led to high performance glass fibers, in the late 1950s, research efforts focused on lightweight elements in the search for fibers of even greater strength that could compete successfully in the market place with aluminum and titanium. Boron fibers were the result of this effort (1963), followed by carbon, beryllium oxide, and graphite. A material such as aluminum that served as a matrix surrounded these filaments. These developments, by the collective efforts of government, NASA, industry and universities, gave rise to advanced composites. With continuing quest for new generation of materials, which have improved properties over conventionally available materials, vigorous research activities were pursued in this over conventionally available materials, vigorous research activities [3] were pursued in this desired direction to develop a new class of materials, having light weight, higher strength and a lower costs, the result of extensive research in this specialized field led to the development of composites.

By the broadest definition, a composite material in one in which two or more materials that are different are combined to form a single structure with an identifiable interface, the properties of that new structure are dependant upon the properties of the constitutes material as well as the properties of the interface. In the most familiar world of metals, the mixing of different materials typically forms bonds at the atomic level (alloys); composites typically form molecular bonds in which the original materials retain their identity and mechanical properties.

II. HEADINGS

The Polymer matrix composites are predominantly used for the aerospace industry, but the decreasing price of carbon Fibres is widening the applications of these composites to include the automobile, marine, sports, biomedical, construction, and other industries [4]. Carbon Fibre polymer-matrix composites have started to be used in automobiles mainly for saving weight for fuel economy. The so-called graphite car employs carbon Fibre epoxy-matrix composites for body panels, structural members, bumpers, wheels, drive shaft, engine components, and suspension systems. This car is 570 kg lighter than an equivalent vehicle made of steel. It weighs only 1250 kg instead of the conventional 1800 kg for the average American car. Thermoplastic composites with PEEK and polycarbonate (PC) matrices are finding use as spring elements for car suspension systems [5]. An investigation was conducted by Issac M Daniel et.al [6] on failure modes and criteria for their occurrence in composite columns and beams. They found that the initiation of the various failure modes depends on the material properties, geometric dimensions and type of loading. They reported that the loading type or condition determines the state of stress throughout the composite structure, which controls the location and mode of failure. The appropriate failure criteria at any point of the structure account for the biaxiality or triaxiality of the state of stress. Jeam Marc et.al [7] investigates the modeling of the flexural behavior of all-thermoplastic composite structures with improved aesthetic properties, manufactured by isothermal compression moulding. A four noded plate element based on a refined higher order shear deformation theory is developed by Topdar et.al [8] for the analysis of composite plates. This plate theory satisfies the conditions of inter-laminar shear stress continuity and stress free top and bottom surfaces of the plate. Moreover, the number of independent unknowns is the same as that in the first order shear deformation theory. Banerji and Nirmal [9] reported an increase in flexural strength of unidirectional carbon Fibre/ Poly(methyl methacrylate), composite laminates having polyethylene Fibres plies at the lower face.

III. INDENTATIONS AND EQUATIONS

The reinforcing material such as plain weave bi-woven glass fibres, plain weave bi-woven graphite fibres and plain weave bi-woven kevlar fibres are cut into required size and are laid on the flat surface of the mould. The fibres of the required size are laid along the required direction as per the design requirements. The resin that is LY556 and hardener HY 951 are mixed in the proportions as recommended by the manufacturer in the required proportions that is in the proportions of 10:1 as suggested by the manufacturer is mixed thoroughly and is applied on the laminated surface to be laminated. The resin is spread evenly on the reinforcing fibres, the resin is squeezed evenly on the surface using a roller and compressed thoroughly with the roller it self. The reinforcing fibres are stacked one above the other and the above mentioned procedure is repeated repeatedly. The laminated composite material is enclosed in a bagging and a recommended vacuum pressure is applied on the laminate to remove the entrapped air bubbles in the layers of the laminated composites. The laminated composites are allowed to cure for 24 hours. These laminated composites are post cured at a temperature of 120^0c for 2 hours to ensure the even distribution of the resin and to ensure the proper percolation of the matrix into the reinforcing material. The laminate is ready and this laminate is cut into required size as per ASTM standard and subjected to various tests.

Fig. 1: Vacuum Bag Moulding

Fig. 2: Tensile test specimens before and after test

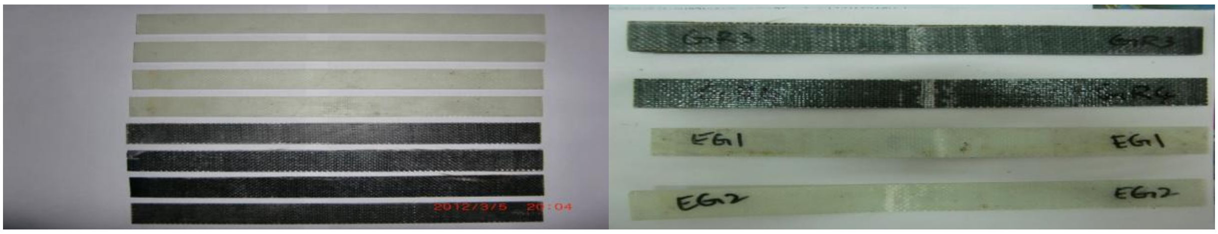

Fig. 3: Flexural test specimens before and after test

IV. FIGURES AND TABLES

Table : 1: Tensile Test Results

Specimen No.	Width (b) mm	Thickness (d) mm	Span length (L) mm	Maximum load (F) (kN)	Deflection at Max. load (mm)	Tensile strength (σ) N/mm^2
EG1	25.2	2.25	50	21.40	13.5	377.43
EG2	24.05	2.25	50	20.08	9.8	371.08
EG3	24.92	3.47	50	32.96	11.2	381.16
EG4	24.62	3.39	50	30.36	12.6	363.76
GR5	25.2	1.83	50	19.80	7.5	429.35
GR6	25.08	1.83	50	18.40	7.6	400.90
GR7	24.96	4.8	50	42.76	13.9	356.90
GR8	24.84	4.8	50	44.72	13.3	375.07
K1	12.73	1.99	50	8.36	9.2	330.01
K2	12.71	2	50	10.64	12.2	418.57
K3	12.99	2.98	50	15.92	12.7	411.26
K4	13.09	2.88	50	14.00	12.8	371.36

EG: E-Glass Laminates, GR: Graphite Laminates, K: Kevlar Laminates

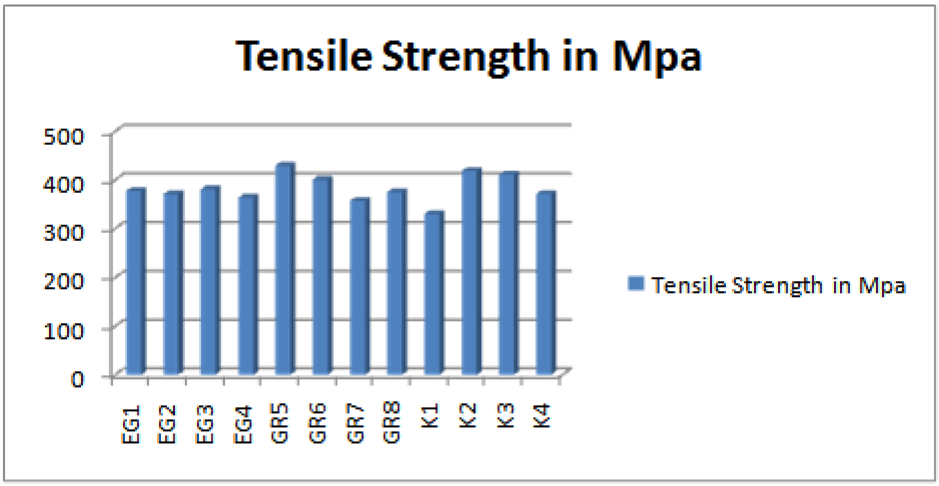

Graph: 1: Tensile strength vs specimen

As a preliminary method of investigation, the tension test is conducted on the three types of the specimens that is, glass, graphite and kevlar reinforced laminates. The basic desired mechanical property like the tensile strength and % elongation of the specimen is evaluated by performing the tension test on the three different types of the laminates for 2mm and 4mm thick specimens. Table shows the ultimate tensile strength and % elongation for glass fibre reinforced laminates, graphite fibre reinforced laminate and kevlar fibre reinforced laminate. The graphite fibre reinforced laminates show greater strength when compared with glass fibre reinforced laminates. The graphite fibre reinforced laminates exhibit less strength than kevlar fibre reinforced laminates. Glass fibre reinforced laminates shows a moderate strength under tension strength but satisfies the required value of strength requirement for the mechanical applications that can be used for the sheet moulded components. The different strength values are attributed to their basic properties of the reinforcement materials. Glass fibre reinforced specimen exhibits more elongation than the graphite and kevlar reinforced laminates.

Table : 2: Flexural Test Results

Specimen No.	Width (b) mm	Thickness (d) mm	Span length (L) mm	Maximum load (F) (kN)	Deflection at Max. load (mm)	Stiffness (P/Δ) N/mm	Flexural strength (σ) MPa
EG1	24.9	2.2	100	0.27	18.5	20	336
EG2	24.8	2.2	100	0.27	16.5	22	337
EG3	24.3	3.5	100	0.72	10.2	70	363
EG4	25.5	3.5	100	0.78	11.0	76	375
GR1	25.3	2.2	100	0.23	13.5	17	282
GR2	25.2	2.2	100	0.22	13.8	15	270
GR3	25.4	3.5	100	0.65	8.8	75	313
GR4	25.3	3.5	100	0.66	9.4	75	319
K4	11.0	2.1	100	0.071	16.0	8.6	220
K5	12.1	2.1	100	0.070	15.8	8.4	197
K7	12.5	3.0	100	0.142	9.5	29	190
K8	12.5	3.0	100	0.132	8.5	28	176

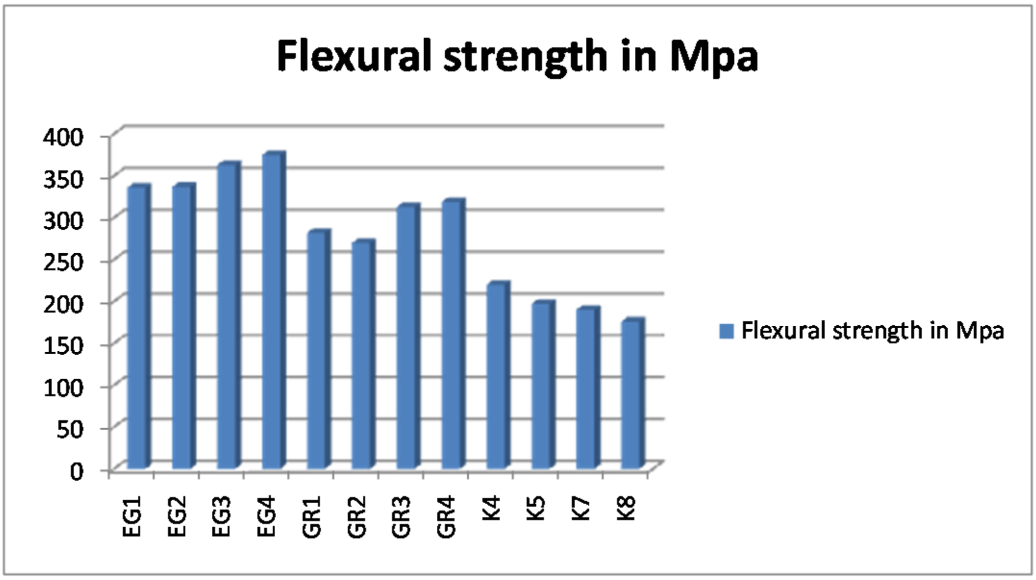

Graph: 1: Flexural strength vs specimen

Table 2 shows the influence of the reinforcing fibre type and thickness used that is the influence of the glass, graphite and kevlar Fibres on the flexural properties of the specimen. It was observed that glass Fibre reinforced laminates dominates in its flexural properties with other fibres having the lower value in the series. But when these laminates compared with some of the auto parts (presently used in automotive vehicles), the laminated composites made of bi- woven fabrics of glass, graphite and kevlar laminates exhibited excellent properties. Even the glass Fibre laminates with 4mm thickness which recorded the highest flexural strength is observed to be having better flexural properties.

V. CONCLUSION

- A simple tensile and flexural test was conducted to estimate the tensile and flexural strength in variety of Composites with varying thicknesses.
- The graphite fibre reinforced laminates show greater strength when compared with glass fibre reinforced laminates. The graphite fibre reinforced laminates exhibit less strength than kevlar fibre reinforced laminates. Glass fibre reinforced specimen exhibits more elongation than the graphite and kevlar reinforced laminates.
- Possible Failure modes of the composite specimens with different fibres have been analyzed and maximum load corresponding to the Failure mode that can occur have been computed and compared with the non-linear point of the load versus deflection plot and excellent agreement has been found.
- The tensile and flexural test conducted illustrated that with increase in thickness of the specimen of the same type there is an increase in the tensile and flexural properties of the specimens.
- The studies further showed that with the variation in the fibre type used has a significant effect on the tensile and flexural properties of the specimens, the three varieties of fibres used are plain bi-woven glass fibre reinforced laminate, plain bi-woven graphite fibre reinforced laminate and plain bi-woven kevlar Fibre reinforced laminate.

REFERENCES

[1]. *Composite materials Hand book* by Schwarz /670/N841, pp1.2
[2]. Schwarz, M.M.1997 Composite *materials processing, Fabrication and application* USA;Prentice Hall
[3]. Kelly .A.C Zweben and T.W.Dyne 2000 *Comprehensive Composite Materials volume Metal matrix composites* UK: Pergamon.
[4]. Mallick P.K., *Composite Engineering Handbook*, 1997, Marcel Dekker Inc., NY, USA.
[5]. Gill, R.M., 1973, *Carbon Fibers in Composite Materials*, Page Bros (Norwich) Ltd, England.
[6]. Isaac M. Daniel, Emmanuel E. Gdoutos, *Deformation and Failure of Composite Structures,* Journal of Thermoplastic Composite Materials 2003; 16; 345.
[7]. Jean-Marc Scanzi and Bruno Hilaire "*All-Thermoplastic Composite Sandwich Panels – Part II:* Modeling of Bending Behavior" Journal of Sandwich Structures and Materials 2004; 6; 423.
[8]. Topdar, A. H. Sheikh and N. Dhang *Finite Element Analysis of Composite and Sandwich Plates* Using a Continuous Inter-laminar Shear Stress Model P. Journal of Sandwich Structures and Materials 2003; 5; 207.
[9]. Nirmal Saha, Amar Nath Banerjee*, "Flexural behavior of unidirectional polyethylene-carbon fibers-PMMA hybrid composite laminates,"* J. App. Poly. Sci. vol.60, 1996, pp. 139-142.

International Journal of Modern Engineering Research (IJMER)
www.ijmer.com Vol. 3, Issue. 5, Sep - Oct. 2013 pp-3181-3187 ISSN: 2249-6645

Effect Estimation Method of Parallel Computing Based on Dynamic Generation of Equivalent Transformation Rules

Hiroshi Mabuchi[1]
[1](Software and Information Science, Iwate Prefectural University, Japan)

ABSTRACT: *Recent studies in parallel computing have mainly focused on physically producing multiple computing sites for computational speed-up and not considered theories and methodologies, which are the essence of parallel computing, and correctness as well. It means that the studies have mostly considered cost-effectiveness, that is, how many computing sites are produced determines how much computing speed improves. This study proposes an algorithm to estimate the effectiveness of parallel computing based on the model with established theories and methodologies, which are the essence of parallel computing, and with assured correctness, instead of exploring such cost-effectiveness. Moreover, we will demonstrate the effectiveness of the proposed method by applying it to one of constraint satisfaction problems, Pic-a-Pix Puzzle, and comparing sequential computing time with estimated parallel computing time based on the dynamic generation of equivalent transformation (ET) rules.*

Keywords: *parallel Computing, Effect Estimation Algorithm, Equivalent Transformation Rule, Rule Dynamic Generation.*

I. INTRODUCTION

Recently, there has been an increase in study of parallel computing and in its importance [1,5,6,8]. Parallelization can be mainly divided in two categories: in local area (LAN) and in CPU [12,14]. The former speeds up the computation by using a supercomputer to make the master processor and multiple slave processors share the computing. The latter executes multithreaded applications on the multi-core processor.

Recent studies in parallel computing have mainly focused on physically producing multiple computing sites for computational speed-up and not considered theories and methodologies, which are the essence of parallel computing, and correctness as well [5,7,8]. It means that the studies have mostly considered cost-effectiveness, that is, how many computing sites are produced determines how much computing speed improves. The purpose of this study is to propose an algorithm to estimate the effectiveness of parallel computing based on the model with established theories and methodologies, which are the essence of parallel computing, and with assured correctness, instead of exploring such cost-effectiveness. Specifically, we adopt the parallel computing model (with multiple processors and CPUs) based on the dynamic generation of equivalent transformation (ET) rules, which is on the basis of the sequential computation model (with one processor) [2,3,9] based on the dynamic generation of ET rules [4]. This model executes costly generation of ET rules in dynamic and parallel way in multiple computing sites. ET is to preserve the meaning of the problem and to transform it to another simplified problem. An ET rule is a meaning-preserving transformation rule. It operates by, first, rewriting a definite clause by replacement of its body and, then, making clause specialization. Based on this model, it is possible that we conduct actual measurement of the effectiveness of parallel computing using with multiple slave processors and CPUs. However, this study provides the model with multiple abstract computing sites and independently operating virtual CPUs and proposes an algorithm to estimate the effectiveness of parallel computing without actual measurement.

Moreover, we will demonstrate the effectiveness of the proposed method by applying it to one of constraint satisfaction problems [10,11,13,15], Pic-a-Pix Puzzle [16], and comparing sequential computing time with estimated parallel computing time based on the dynamic generation of ET rules.

II. SEQUENTIAL COMPUTING MODEL BASED ON THE DYNAMIC GENERATION OF ET RULES

This study is based on a sequential computing model on the basis of the dynamic generation of ET rules, and the sequential computing model is used for a comparison in the experiment. We will define, therefore, the sequential computing model first in this section, then outline “Pic-a-Pix Puzzle [16]”, which is used in the experiment of this study, and describe the generation of ET rules with the specific example.

2.1 Definition of The Sequential Computing Model

A sequential computing model is a model which successively simplifies problems in order to obtain solutions in the end by repeating the following process: if there is an applicable rule in a pre-constructed ET rule set (program), the rule will be applied to the problem; if not, a new rule will be generated dynamically and the rule will be applied to the problem. Fig. 1 shows the outline of this model [2,3].

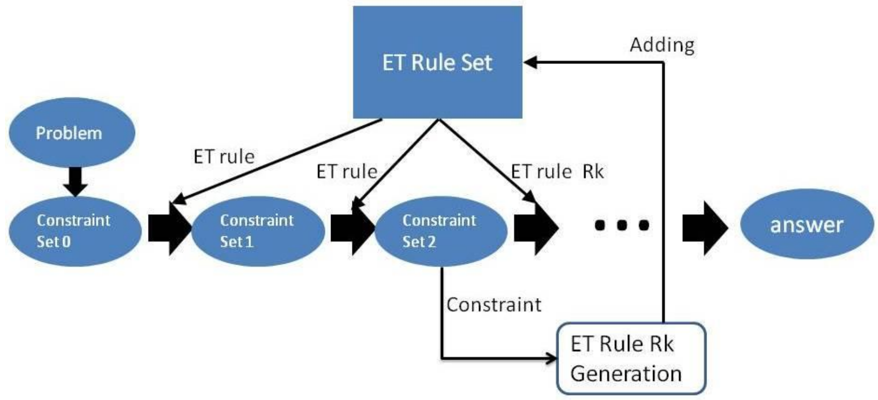

Fig. 1 Sequential Computing Model

ET is to preserve the meaning of the problem and to transform it to another simplified problem. The first step of sequential computing corresponds to the application of ET rules.

In Fig. 1, there is no applicable rule to the constraint set 2. A new ET rule, then, will be generated, added to the ET rule set and applied to the constraint set 2 so that equivalent transformation will proceed.

2.2 Pic-a-Pix Puzzle

Consider a Pic-a-Pix puzzle in Fig.2. It consists of a blank grid and clues, i.e., block patterns, on the left of every row and on the top of every column, with the goal of painting blocks in each row and column so that their length and order correspond to the patterns and there is at least one empty square between adjacent blocks.

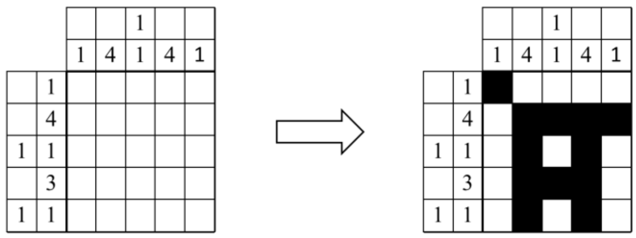

Fig. 2 A Pic-a-Pix Puzzle

For example, the constraints in Fig. 1 in Section 2.1 correspond to each row or column of the puzzle, and all the constraints are computed with the same algorithm. This will allow each constraint of the problem to be shared and computed in a number of computing sites.

2.3 ET Rule

An ET rule is a meaning-preserving transformation rule.

The following is a format of ET rules.

H , {Cs} → {Es} , Bs.

Here, H is an atom, and each of Cs, Es, and Bs is an atom string. An atom means an indivisible minimum sentence and is represented as a sequence of a predicate and zero or more of arguments. H , Cs, and Es is called head, condition part and execution part, respectively, and an atom which is an element of Bs is called replaced atom. Connecting atoms (string) with an arrow means replacing an atom (string) with another atom (string).

2.4 ET Rule Generation

This section describes a method of generating ET rules with an example of Pic-a-Pix Puzzle.

Dynamic generation of ET rules is that if there is no applicable rule during the process of ET by applying ET rules in the problem, a new rule will be dynamically generated. Adding the new rule to the program will allow the ET to be continued. It is shown in the part of Fig. 1, that is, generating ET rule Rk from "Constraint Set 2" and adding it to ET rule set.

In the case of Pic-a-Pix Puzzle, as shown in Fig. 2, rules are generated with the following algorithm depending on each sequence of numbers of the puzzle.

(1) From the list (row or column) consisting of the first argument, which is the number of blocks to be painted, and the second argument, which is n elements (block), the common part of the list is obtained, and if it is determined, a rule is generated.

(2) From the beginning of the list, sort out undetermined elements with each case, apply 1 or 0 to every case, specialize the common part depending on the number of blocks to be painted and determine either 1 or 0.

For the fourth row of the puzzle shown in Fig. 2, Fig. 3 shows a method of generating ET rules.

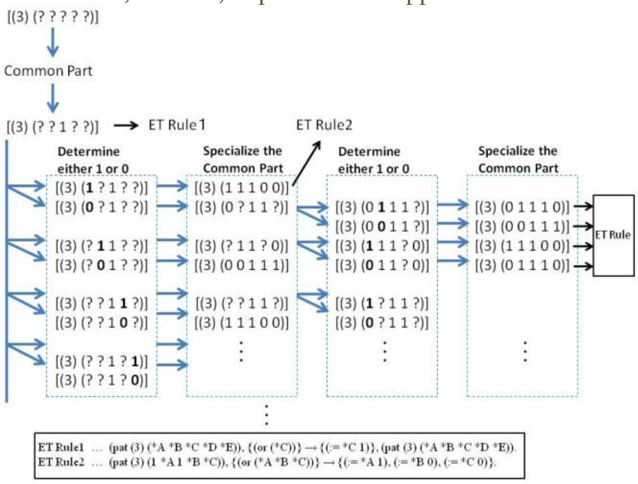

Fig. 3 An Example of Rule Generation

ET Rule1 and ET Rule2 shown in Fig. 3 are explained.

ET Rule1 is a rule which transforms the list consisting of "the number of painted block is three" and "five blank blocks" into a predicate which suggests painting the common part, the third (*C) block. ET Rule2 is a transformation rule in which the list consisting of "the number of painted block is three" and "the first and third blocks are painted" transforms into "the second block is painted {(:= *A 1)}" and "the fourth and fifth blocks become blank {(:= *B 0) , (:= *C 0)} in order to satisfy the condition to paint three consecutive blocks.

III. PARALLEL COMPUTING MODEL BASED ON THE DYNAMIC GENERATION OF ET RULES

A parallel computing model based on the dynamic generation of ET rules [4] consists of the Master computer and multiple computing sites (Slaves). Costly rule generation is done in each computing site, and the fastest generated ET rule is applied to the constraint sets to obtain a new more simplified constraint set. A solution will be obtained by repeating this operation. Fig. 4 shows the outline of this model.

The computation of this model follows from 1 through 4 below.

1. Generate a set of constraints (Constraint Set 0) to solve a constraint satisfaction problem.
2. Each atom of the constraint set is sent to multiple computing sites (Slaves) and costly ET rule generation is done in each Slave.
3. Apply the first generated ET rule of the ET rules generated in 2 to the constraint sets successively and obtain a new simplified constraint set.
4. If the solution of the problem is obtained, the computing is finished. If not, it goes back to 2.

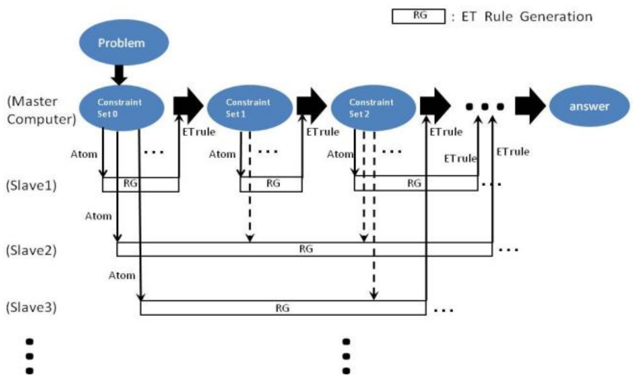

Fig.4 Parallel Computing Model

IV. EFFECT ESTIMATION OF PARALLEL COMPUTING BASED ON THE DYNAMIC GENERATION OF ET RULES

This section proposes a method to estimate to what extent the computing become more efficient in the case of parallelization.

4.1 Effect Estimation Method of Parallel Computing

An effect estimation method of parallel computing is a method in which operations will be continued repeatedly until no constraint of the problem (atom) exists, and when no atom exists, an estimated parallel computing time is output.

First, an ET rule is generated for each atom in constraint sets, then the fastest generated ET rule is applied to the constraint set, and a new constraint set is obtained. The applied ET rule is deleted.

An algorithm to estimate the effect of parallel computing is shown below.

Given a set C of atoms. Here, T is an estimated parallel computing time. S is a set of pairs of a generated rule and a time. rt is a time for rule r to be generated. t is the time taken until a new constraint set is obtained after the rule is applied to the constraints sets.

(1) T= 0, S = {}.
(2) while C =/= {} do
(2-1) For any atom a in C
gen(a) = (rt, r). // rule r is generated.
S = S ∪ {(T + rt +τ+ t, r)} // τ is a delay for sending and receiving.
(2-2) S' = sort(1, S). // sort by the first argument.
(2-3) Let (rt, r) be the first pair in S'.
(2-4) If T < rt, then T = rt.
(2-5) Apply the rule r to an atom in C to have new C. (The time at this point is t.)
(2-6) S = S - {(rt, r)}.
(3) return T

This algorithm is explained.
(1) Initialize an estimated parallel computing time and a set of pairs of a generated rule and a time.
(2) Repeat the operation from (2-1) to (2-6) until no atom in the problem exists.
(2-1) For each atom, create a pair of an ET rule and its generating time. Then, create a set of pairs of T, rt, τ, t and an ET rule.
(2-2) Sort the set created in (2-1) by ascending order of total time of T, rt, τ and t.
(2-3) Take out the first sorted pair of S'.
(2-4) If rt is more than T, let rt be T.
(2-5) Apply the rule taken out in (2-3) to the atom and obtain a new atom.
(2-6) Delete the applied pair of the ET rule and generating time.
(3) When there is no atom in the problem, return the estimated parallel computing time as a solution.

4.2 Estimation of Parallel Computing Time in Pic-a-Pix Puzzle

Fig. 5 shows the estimated parallel computing time based on dynamic generation of ET rules which was obtained using a 7 x 7 Pic-a-Pix Puzzle (let τ, which is defined in Section 4.1, be 0msec).

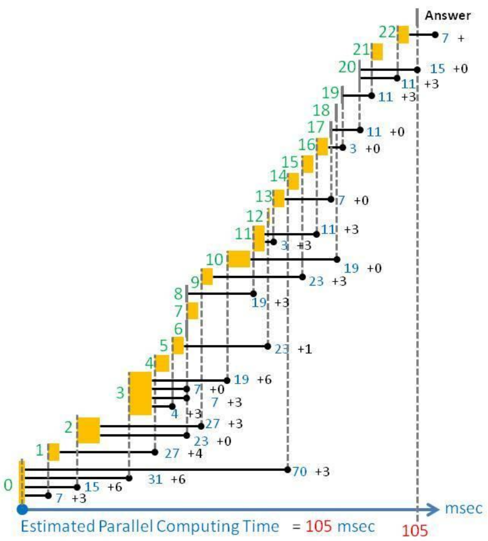

Fig.5 Calculation of Estimated Parallel Computing Time
Fig. 5 is explained based on Section 4.1.

The numbers from 0 to 22 represent the constraint set number. For example, four ET rules are generated in the constraint set 0. The fastest generated rule (in this case, it is the bottom of four rules in Fig. 5, which is generated in 7msec) is applied an atom (constraint), and a new atom is generated. The time to generate this new atom is 3msec. That is, it takes 10msec (= 7+3) to the obtainment of a new atom from the generation of the bottom rule and the application of it to an atom.

Next, the fastest generated rule in the sum of the rules of the unused rule set generated in the constraint set 0 and the rule set generated in the constraint set 1 (in this example, the second rule from the bottom generated in the constraint set 0) is applied to an atom, and a new atom is obtained. In this case, it takes 15msec to generate the rule, and 6msec from the application of the rule to an atom to the obtainment of a new atom.

Next, the fastest generated rule in the sum of the rules of the unused rule set generated in the constraint set 0, that in the constraint set 1 and the rule set generated in the constraint set 2 (in this example, the third rule from the bottom generated in the constraint set 0) is applied to an atom, and a new atom is obtained. In this case, it takes 31msec to generate the rule, and 6msec from the application of the rule to an atom to the obtainment of a new atom. Repeat the same process and obtain the Answer by applying the generated rule in constraint set 20(the rule above the two rules generated in the constraints set 20).

The followings show "Constraint set before the rule is applied → The rule which is applied → Constraint set after the rule is applied ･･･ Estimated time" from the constraint set 0 to the Answer.
Constraint Set 0 → Apply the second rule from the top generated in the Constraint Set 0
→ Constraint Set 3 ･･･ 37msec (= 31 + 6)
Constraint Set 3 → Apply the second rule from the top generated in the Constraint Set 3
→ Constraint Set 8 ･･･ 7msec (= 7 + 0)
Constraint Set 8 → Apply the rule generated in the Constraint Set 8
→ Constraint Set 11 ･･･ 22msec (= 19 + 3)
Constraint Set 11 → Apply the rule under the rules generated in the Constraint Set 11
→ Constraint Set 13 ･･･ 6msec (= 3 + 3)
Constraint Set 13 → Apply the rule generated in the Constraint Set 13
→ Constraint Set 17 ･･･ 7msec (= 7 + 0)
Constraint Set 17 → Apply the rule generated in the Constraint Set 17
→ Constraint Set 20 ･･･ 11msec (= 11 + 0)
Constraint Set 20 → Apply the above the rules generated in the Constraint Set 20
→ Answer ･･･ 15msec (= 15 + 0)

The total of these estimated parallel computing times is 105msec(= 37 + 7 + 22 + 6 + 7 + 11 + 15). The sequential computing time for this example is 1920msec. Then, if the sequential computing time is set to 1, the estimated parallel computing time becomes 0.05. The computing time, thus, is found to be greatly reduced.

V. CALCULATION OF THE PARALLEL ESTIMATED COMPUTING TIME TAKING INTO ACCOUNT THE COMMUNICATION TIME

In this section, it is studied how the estimated parallel computing time changes if the communication time is taken into account. That is, τ defined in section 4.1 is considered.

5.1 Calculation of The Estimated Time Taking into The Fixed Communication Time

In this section, set the communication time to 10msec in the example in section 4.2 and calculate the estimated parallel computing time. The result is shown in Fig. 6. The process flow of the parallel computing time and the estimated time change by adding the communication time of 10msec for the calculation made in Fig. 5. For instance, in Fig. 6, four rules are generated in the constraint set 0. The bottom rule, which is generated in the fastest time, 7msec, is applied to an atom, and a new atom is obtained. The time for this is 3msec and the communication time is 10msec. The process flow to obtain the estimated parallel computing time until the solution is obtained is the same as that in Fig. 5.

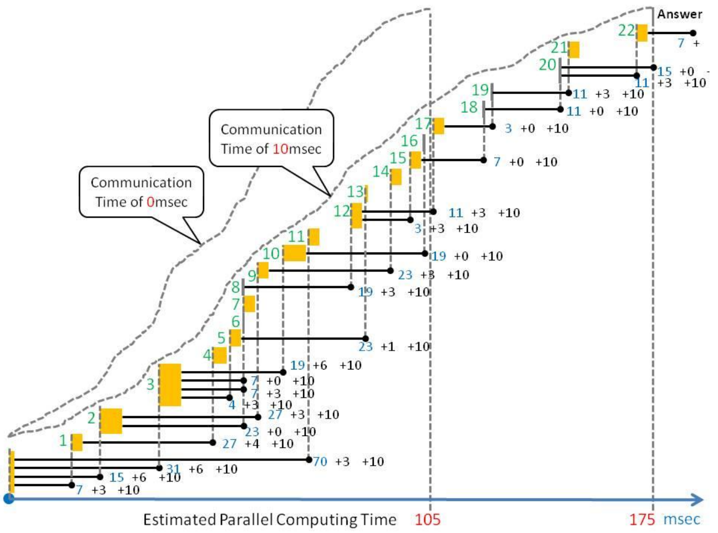

Fig.6 Calculation of Estimated Parallel Computing Time (Taking into Account Communication Time of 10msec)

Fig. 6 shows that in the case of taking into account the communication time of 10msec, the estimated parallel computing time is 175msec. When the sequential computing time is set to 1, the estimated parallel computing time becomes 0.09, and the computing time is greatly reduced.

5.2 The Change of The Estimated Time Due to The Change of The Communication Time

In this section, it is studied how the estimated time changes when the communication time is changed from 0msec to 200msec. The result is shown in Fig. 7. This graph shows that the communication time of which the range is from 0msec to 30msec greatly affects the computing time, however, the communication time over 30msec does not much affect it.

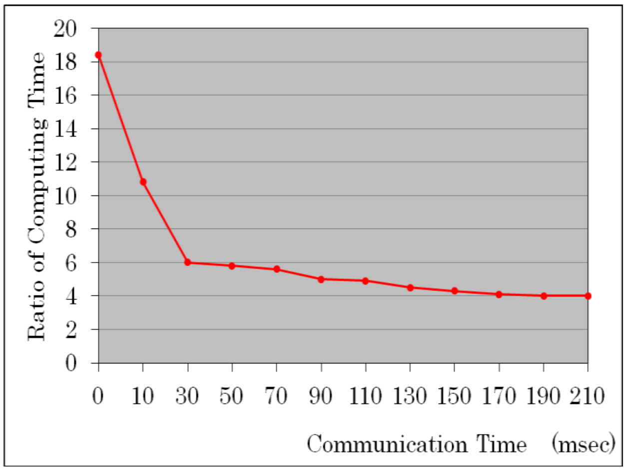

Fig.7 Changes in Computing Time with Communication Time

VI. CALCULATION OF THE ESTIMATED PARALLEL COMPUTING TIME BY THE PROGRAM

This section compares the estimated computing time with the sequential computing time when a Pic-a-Pix Puzzle is solved with the program, which is created using an ET programming language [17] to obtain the estimated parallel computing time.

As experimental data, we chose five 15 x 15-size Pic-a-Pix Puzzles from http://starscafe.net/riddle/logic/ [16] and compared the average sequential computing time of ten times with the average estimated parallel computing time of ten times. The result is shown in Table 1. Here, Table 1 shows the ratio of the estimated parallel computing time when the sequential computing time is set to 1.

Problem	Sequential Computing Time	Estimated Parallel Computing Time
Problem 1	1	0.72
Problem 2	1	0.2
Problem 3	1	0.05
Problem 4	1	0.04
Problem 5	1	0.01

Table 1 Comparison of Computing Time

It can be found from Table 1 that the parallel computing time is greatly reduced compared with the sequential computing time. It is assumed that this is because ineffective rules which make computational efficiency lower were not applied to the problem when the problem was solved with the parallel computation. Available rules are applied regardless of anything else in sequential computing, whereas such ineffective rules can be eliminated in parallel computing.

VII. CONCLUSIONS

We proposed an algorithm to estimate the effect of parallel computing using a parallel computing model based on the dynamic generation of ET rules. This study provided a model with multiple abstract computing sites and independently operating virtual CPUs and estimated the effect of parallel computing on the model. Furthermore, we have demonstrated the effectiveness of the proposed method by creating a program which estimates the effect of parallel computing, solving several Pic-a-Pix Puzzles with the program and comparing the sequential computing time with the parallel computing time. This study used Pic-a-Pix Puzzles as examples of constraint satisfaction problems. We would like to demonstrate the effectiveness of the proposed method by applying it to various examples in the future.

REFERENCES

[1] T. Abe, T. Hiraishi, Y. Miyake, T. Iwashita. Job-level Parallel Executions for Satisfying Distributed Constraints. *Information Processing Society of Japan, Vol.59*, 2011, 1- 8.

[2] K. Akama and E. Nantajeewarawat. Formalization of the equivalent transformation computation model. *Journal of Advanced Computational Intelligence and Intelligent Informatics, 10*, 2006, 245-259.

[3] K. Akama, E. Nantajeewarawat, and H. Ogasawara. A Processing Model Based on Equivalent Transformation and a sufficient Condition for Program Correctness. *International Journal of Foundations of Computer Science 3*, 2010.

[4] K. Akama, E. Nantajeewarawat, H. Koike. Constructing Parallel Programs Based on Rule Generators. *The First International Conference on Advanced Communications and Computation*, 2011, 173-178.

[5] Guy E. Blelloch. Programming parallel algorithms. *Magazine Communications of the ACM CACM Homepage archive, Vol. 39, Issue 3*, 1996.

[6] D.C.Gras and M.Hermenegildo. Non-strict independence-based program parallelization using sharing and freeness information. *Theoretical Computer Science, 410*, 2009, 4704-4723.

[7] G.Gupta, E.Pontelli, K.Ali, M.Carlsson, and M.Hermenegildo. Parallel execution of Prolog programs: a survey. *ACM Transactions on Programming Languages and Systems, 23*, 2001, 472-602.

[8] W. Daniel Hillis, Guy L. Steele, Jr. Data parallel algorithms. *Magazine Communications of the ACM - Special issue on parallelism CACM Homepage archive, Vol. 29, Issue 12*, 1986.

[9] H. Mabuchi, K. Akama, and T. Wakatsuki. Equivalent transformation rules as components of programs. *International Journal of Innovative Computing, Information and Control, 3*, 2007, 685-696.

[10] Y. Makoto, K. Hirayama. Distributed Breakout: Iterative Improvement Algorithm for Solving Distributed Constraint Satisfaction Problem (Special Issue on Parallel Processing). *Information Processing Society of Japan, Vol.39, No.6*, 1998.

[11] . Makoto, E.H.Durfee, T.Ishida, K.Kuwabara. The distributed constraint satisfaction problem: formalization and algorithms. *IEEE Transactions on Knowledge and Data Engineering, Vol. 10*, 1998, 673-685.

[12] K. Minami. Performance Improvement of Application on the "K computer". *IEICE Transactions, 95(2)*, 2012, 125-130.

[13] S. Nishihara. Fundamentals and Perspectives of Constraint Satisfaction Problems. *Japanese Society for Artificial Intelligence, Vol.12, No.3*, 1997, 351-358.

[14] N. Nishimura. Grid Computing and Parallel Computing. *Journal of The Japan Society for Computational Engineering and Science, 10(3)*, 2005, 1198-1202.

[15] K. Uchino, S. Kubota, H. Konoh, S. Nishihara. Classifying CSPs On the Basis of Parallelism. *Information Processing Society of Japan, Vol.35*, 1994, 2676-2684.

[16] http://starscafe.net/riddle/logic/

[17] http://assam.cims.hokudai.ac.jp/eti/index.html

Noise Tolerant and Faster On Chip Communication Using Binoc Model

Arun Arjunan.[1], Karthika Manilal.[2]

[1]*PG Scholar, Dept.of Electronics and Communication Engg, TKM Institute of Technology, Kollam, Kerala, India.*
[2]*Asst.Professor, Dept. of Electronics and Communication Engg, TKM Institute of Technology, Kollam, Kerala, India.*

ABSTRACT: *Network on chip (NoC) has become the most promising and reasonable solution for connecting many cores in system on chips (SoC). In conventional NoC architectures neighbouring routers are connected via hard wired unidirectional communication channels. Due to unpredictable and uneven traffic patterns in NoC one of the channels may be overflowed due to heavy traffic in one direction while the other unidirectional channel is idling and thus causing inefficient resource utilization, data loss and degradation in performance. So as a remedy for this situation a bidirectional NoC (BiNoC) can be used, which uses bidirectional channels to connect adjacent routers and it also supports runtime reconfiguration of channel direction according to traffic demand by using channel direction control (CDC) protocol. Since data communication through Network on Chip is susceptible to noise due to the presence of various noise sources, the incorporation of a hybrid error control scheme in which combined approach of error correction and retransmission is used which increases the reliability of the system. This architecture will allow the NoC structure to handle massive data transmission by effectively increasing the communication bandwidth, resource utilization capability and speed of NoC communication together with the increased reliability. The architecture is modelled using VHDL.*

I. INTRODUCTION

With vigorous advancement in semiconductor processing technologies, the chip integration has reached a stage where a complete system can be placed in a single chip. A system on chip (SoC) is an integrated circuit (IC) that integrates all components of an electronic system into a single chip. Applications of these systems are in the area of telecommunications, multimedia, and consumer electronics where it has to satisfy real time requirements. As technology scales toward deep sub-micron, mare and more number of computational units will be integrated onto the same silicon die, causing tight communication requirements on the communication architecture. Due to this fact the traditional solution for inter core communication in SoCs such as shared bus systems and point to point links were not able to keep up with the scalability and performance requirements. As a result "Network on Chip" (NoCs) emerged which has some reasonable and promising features for application to giga-scale system on chips such as modularity, scalability, high band width availability, despite the increased design complexity. NoC consists of components such as IP Cores, Network Interface (NI), and Routers or switch which routes the packets of data through the Network according to a routing algorithm and interconnecting channels or wires. Packets of data to be communicated through the NoC are transmitted through the NoC via routers and channels to reach the destination IP core from the source IP core of the SoC.

The city block style, tiled NoC architecture is the most popular type of NoC and is considered in most of designs due to its flexibility, simplicity, scalability and performance advantages. In this type of architecture, the wires and routers are arranged like street grids of a city, while the resources (logic processor cores) are placed on city blocks separated by wires. Here neighbouring routers are connected together using a pair of unidirectional communication channels where each channel is hard-wired to handle either outgoing or incoming traffic only. At run time quite often one channel may be overflowed with heavy traffic in one direction, while the channel in the opposite direction remains idling. This leads to performance loss, inefficient resource utilization, reduced throughput of the system and wastage of bandwidth in City Block style Network on Chip architectures. As a solution for these problems the concept of reversible lanes in city traffic can be implemented in Network on chip (NoC). A counter flow lane is one in which the driving directions are changed using some electronics signs in-order to provide high capacity to the direction with heavier traffic volume. Such a Network on chip (NoC) which implements the idea of reversible lanes in city traffic to configure the direction of channel according to the traffic inside the system is termed as Bidirectional Network on Chip (BiNoC) [1]. The channels are made dynamically self reconfigurable at real time by using a protocol called as Channel direction control protocol (CDC). This project targeted the Bidirectional NoC having dynamically self reconfigurable channels to reduce the limitations of conventional NoC architecture such as inefficient resource utilization, reduced channel bandwidth availability for massive unidirectional communication and it also increases the effective throughput of the network on chip without using additional channels for interconnection.

II. RELATED WORKS

By borrowing the ideas from real world computer networks in the chip level communication issue the concept of Network on chip evolved. Network-on-Chip (NoC) provides scalable bandwidth requirement where number of simultaneous bus requesters is large and their required bandwidth for interconnection is more than the bus based design [7][8]. When we are moving to the era of nano scale technology one of critical issues is a wiring delay. While the speed of basic elements such as gate delay becomes much faster, the wiring delay is growing exponentially because of the increased capacitance caused by narrow channel width and increased crosstalk [10]. In designing NoC systems, there are several issues to be concerned with, such as topologies, switching techniques, routing algorithms, performance, latency, complexity and so on. Mesh Topology is a Feasible topology and is easily expandable by adding new nodes [1][6][9][3]. A routing algorithm determines the direction of Packet Transmission in NoCs [2][4]. The algorithm determines to what direction packets are routed during every stage of the routing. XY routing is a dimension order routing which routes packets first in x- or horizontal direction to the correct column and then in y- or vertical direction to the receiver [4][6].The performance of NoC communication architecture is dictated by its flow-control mechanism. Wormhole flow control has advantages such as less memory requirement and less latency. In wormhole routing packets are divided to small and equal sized flits (flow control digit or flow control unit). . After first flit the route is reserved to route the remaining flits of the packet. This route is called wormhole.

In conventional tiled NoC structures neighboring routers are connected using hardwired unidirectional communication channels which can handle data only in a single direction i.e. either output data or input data [1]. While considering the case of basic NoC structure one channel may be overflowed with heavy unidirectional traffic, while the channel in the opposite direction remains idling since the channels or links that connect the neighboring routers together are hardwired in such a way to handle traffic in only one particular direction [2]. This causes performance degradation and inefficient resource utilization in traditional city block style NoC architectures. Thus Traditional tiled NoC structures are not up to the mark in handling a heavy flow of traffic in single direction although it is equipped by resources to handle the situation.

As we move to consider Deep Submicron NoCs (DSM NoCs), communication becomes unreliable because of the increased sensitivity of interconnects to on-chip noise sources, such as crosstalk and power-supply noise [5].In DSM SoCs; low swing signaling reduces signal-to-noise ratio thus making interconnects more sensitive to on-chip noise sources such as cross-talk, power supply noise, electromagnetic interferences, soft errors, etc [5]. A common practice to increase the reliability of NoC is to incorporate error detection and correction schemes into the design. . Hamming codes [5] are the first class of linear codes devised for error correction and have been widely employed for error control in digital communication and data storage systems. When the transmitted codeword is received, an error detecting stage checks the parity bits. If a correction stage is applied, the exact location of the error can be identified so that the corrupted bit can be restored. A distance- 3 Hamming code can be easily modified to increase its minimum distance to 4, adding one more check bit, chosen so that the parity of all of the bits, including the new one, is even to form Single Error Correction and Double Error Detecting hamming Code (SECDED)[5]. This version of the Hamming code is traditionally used for single error correction and double error detection.

In this Paper a noise tolerant and faster on chip communication is proposed using bidirectional Network on Chip (BiNoC) having dynamically self reconfigurable channels. The noise toleration capability of the system is to be increased by using a hybrid scheme of error detection/correction and retransmission schemes. The packet switched Bidirectional NoC prototype design considers the design constraints such as two dimensional mesh topology, XY routing algorithm, and wormhole flow control mechanisms.

III SYSTEM ARCHITECTURE

Network on Chip provides the infrastructure for the communication in multicore single chip systems. A NoC consists of resources and switches that are connected using channels so that they are able to communicate with each other by sending messages. Here the topology used is mesh, which is a simplest layout; also routing in a two-dimensional mesh is easy. [2]. Figure: 1 shows the basic structure of a tiled, city block style network on chip. The inter router communication in conventional NoC design is accomplished by using two unidirectional communication channels that are hardwired for handling traffic only in a single direction. This causes problems such as performance degradation and ineffective resource utilization in conventional tiled NoC architectures. In a BiNoC, each communication channel allows itself to be dynamically reconfigured to transmit flits in either direction [2]. This promises better bandwidth utilization, lower packet delivery latency, and higher packet consumption rate for the network. The flow direction at each channel is controlled by a channel-direction-control protocol (CDC protocol).Figure: 2 shows the basic block diagram of a 3*3 grid array structure of Bidirectional NoC in which routers are interconnected together using bidirectional channels.

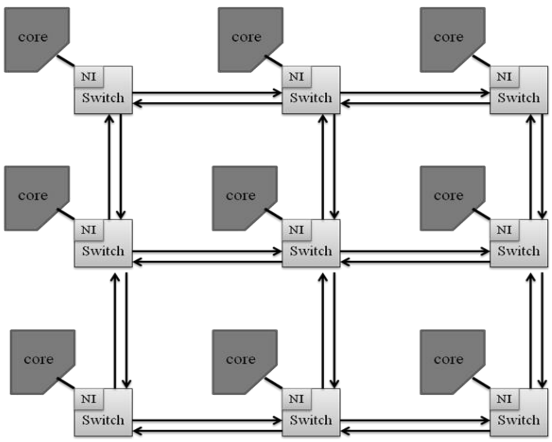

Figure:1 Basic structure of 4*4 array of NoC.

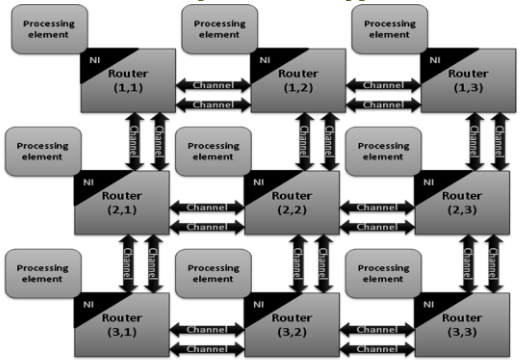

Figure: 2 Block diagram of 3*3 2D-Mesh BiNoC

A. Existing Conventional NoC router Architecture

The network on chip routers which are connected together using communication links are the most vital part in a NoC design. These routers are responsible for the correct switching of data to the destination resource by using a routing protocol. The architecture of a basic tiled network on chip is shown in Figure: 3. The Router used in basic city block style NoC will have five ports corresponding to the directions North, East, South, west and a local PE(Processing Element). Each port is having its input and output channel, and each input and output channel is having its control and decoding logic, which supports five parallel connections at the same time simultaneously. The input channel consists of three parts i.e. FIFO, FSM, and XY logic. The FIFO is used as input buffer to store the data temporarily. XY Logic is used for comparing the coordinates stored in header flit with the locally stored coordinates and thus finds out the direction to which the packet has to be switched. There is a switch present inside the router which switches the data from the input port of a particular direction of router to the output port of the desired location calculated by the XY routing algorithm. An Arbiter is used in output channel to overcome the problem of multiple input requests coming at single output port. Arbiter is based on rotating priority scheme in which each port get reduced its priority once it has been served.

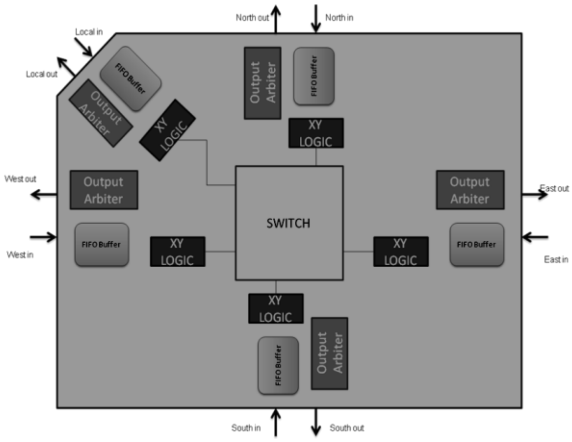

Figure: 3 Five Port Router in Basic Tiled NoC

B. BiNoC Router Architecture

Modifications to the five port router structure when used in Bidirectional network on chip are:

1. All the ports of router will be bidirectional ports.
2. Buffers should be placed in every port to store data temporarily.
3. FIFO buffer capacity should be made higher to accommodate heavy traffic.
4. A high priority finite state machine (HP FSM) and a low priority finite state machine (LP FSM) will be connected at each port to dynamically configure the channel direction according to the traffic needs.

Architecture of five port router used in BiNoC is shown in Figure: 4.Which has the capability of dynamically self reconfiguring the directions of its bidirectional port according to the traffic needs. The direction of data transmission of a bidirectional channel needs to be self-configured, at run time based on local traffic demands. To achieve this goal a distributed CDC (Channel direction Control) protocol is used. Configuration of a bidirectional channel direction is controlled by a pair of FSMs in the channel control blocks of the routers at both ends. Opposite priorities are assigned to FSMs on the other channel of same pair of adjacent routers. The operations of adjacent FSMs synchronized against a common clock.

The two FSMs exchange control signals through a pair hand-shaking signals: input−req (input request) and output−req (output request). When the sending end router has data packet to transmit the output−req is made '1'. The output−req signal from one router becomes the input−req signal to the FSM of the other router. Each FSM also receives a channel−req (channel request) signal from the internal routing computation module as there is a grant given to a particular port to output data. channel−req = 1 when a data packet in the local router is requesting the current channel.

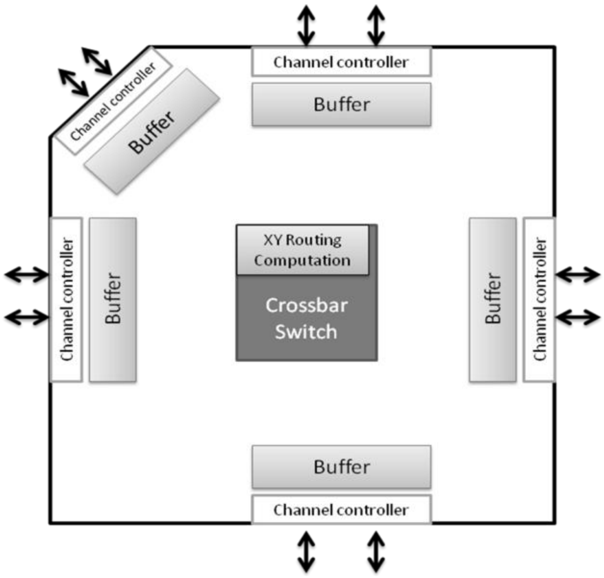

Figure: 4 Architecture of BiNoC Router

The state transition diagram of high priority FSM and low priority FSM are shown in Figure: 5. Each FSM consists of three states: Free, Wait, and Idle, defined as:

1. Free State: the channel is available for data output to the adjacent router.
2. Idle State: the channel is ready to input data from the adjacent router.
3. Wait State: an intermediate state preparing the transition from the idle state with an input channel direction to the Free State with an output channel direction.

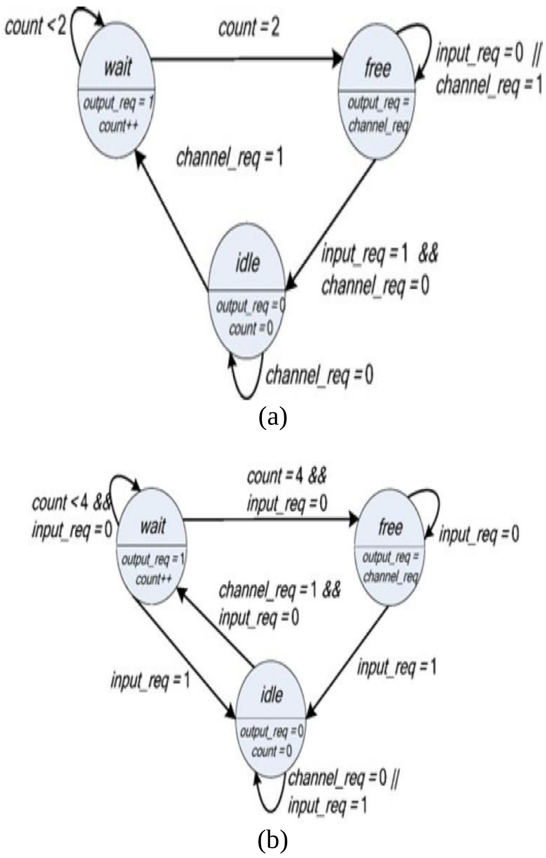

Figure: 5 state transition diagram of HP and LP FSMs

The inter router channel direction control scheme is shown in figure: 6.

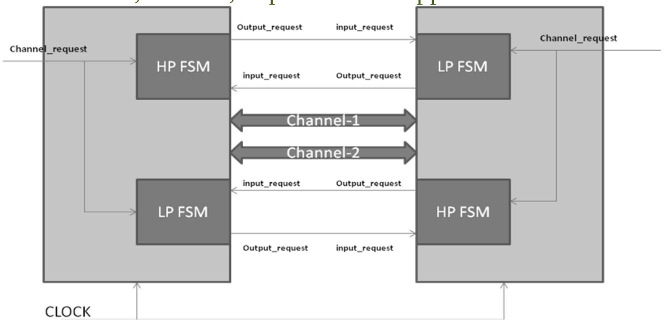

Figure: 6 channel Direction control scheme(CDC)

C. Flit Structure

As this project uses worm hole flow control mechanism, the data packet will be divided into equal sized flits (flow control units). A packet of data will contain a header flit having the information of source, destination PEs and if needed it may contain length of packets [9] followed by the data flits which carry the actual data to be communicated and finally there will be a tail flit which indicates the completion of packet. In this proposed system the flit structure is considered in the way that the first bit shows the flit to be the header-trailer or the data. When the first bit equals one, this flit is a header or trailer. In this case, the 2nd bit determines which one is the header and which one is the trailer. The data flit will have first bit as zero. The sizes of flits considered in this project are of 16 bits each.

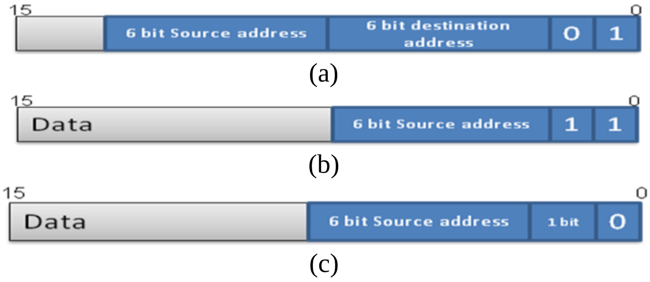

Figure 7 (a) Header, (b) Tail and (c) Data Flit structures

D. Error Control

Hamming codes are the widely used error detection and correction code in network on chip due to its simplicity, short timing delay and less area overhead. SEC-DED Hamming code is used here for error detection and correction of errors. A retransmission scheme in which the receiver acknowledges the sender to transmit the data again is also implemented in NoC designs to increase the reliability. For Retransmission scheme the Network Interface (NI) of sender will be having additional Retransmission Buffers which will store the packets that have been transmitted.

When considering the switch to switch and end to end error control policy [7], end to end error control policy has less latency and area overhead. So in this project an end to end and hybrid scheme of error detection, correction and retransmission are considered for increasing the reliability of the NoC communication. Since wormhole flow control mechanism is been used in this project error detection and correction will be occurring in flit by flit basis so it assures more reliability than packet by packet error control mechanism.

Flit size considered is 16 bit so for a SEC-DED hamming code will have 5 check bits and one overall parity bit. he codeword generated by the SEC-DED Hamming encoder (22, 16) will be of 22 bits containing 16 data bits 5 check bits and one overall parity bit.Here p1,p2,p4,p8,p16 are the check bits occupying the 2^n positions of codeword while p is the overall parity bit of the data to be transmitted. Structure of codeword generated by SEC-DED hamming encoder is shown in Figure 8.

P	d15	d14	d13	d12	d11	P16	d10	d9	d8	d7	d6	d5	d4	P8	d3	d2	d1	P4	d0	P2	P1

Figure: 8 structure of (22, 16) SEC-DED hamming codeword

Hamming decoder is more complex than encoder. The Hamming Decoder block recovers a binary message vector from a binary Hamming codeword vector. (22, 16) SEC_DED Hamming decoder takes 22 bit codeword and it calculates the syndrome and overall parity and decides whether an error has occurred or not in a transmitted code word. Since the error control scheme used in this work is a hybrid scheme of error correction and retransmission in which if certain number of uncorrectable errors are found to be occurred in the received data packet then the hybrid SEC-DED decoder has to generate the retransmission request.

IV. SIMULATION RESULTS

The modules are modeled using VHDL in Xilinx ISE Design Suite 12.1 and the simulation of the design is performed using Modelsim SE 6.2c to verify the functionality of the design. Analysis of the results obtained is discussed in this section.

In Figure 9, five port router used in conventional NoC designs is shown. The five port router designed here is the one used in basic tiled NoC architecture. The router consists of five input and five output ports. The structure of router is shown in Figure: 3.6. The routing decision is taken by the router according to the XY routing logic present in the router module. The 8 bits from 3rd bit of the header flit is analyzed to find out the address of destination router and it is compared to find the direction of switching inside the router. Switching is made into effect by a crossbar switch inside the NoC router. There may be multiple requests for one particular output port at a time, but when using an arbiter only one request is served once. Since Wormhole flow control is used in this router once a request is granted then the data from that port is switched till a tail flit is encountered.

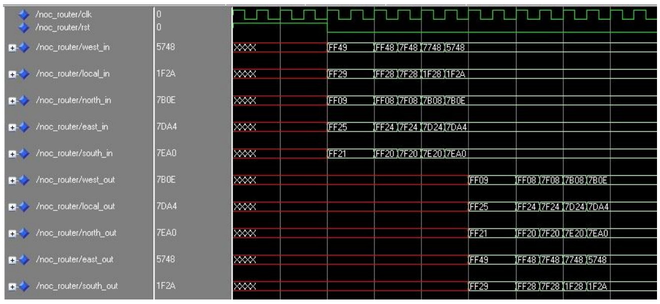

Figure:9 Five port Router Simulation

In Figure:10 the simulation results of high priority and Low priority FSM are shown which dynamically configures the direction of bidirectional channels that interconnects the adjacsent routers in BiNoC structure.

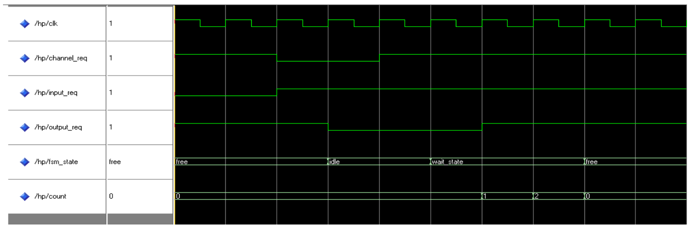

Figure:10a Simulation result of HP FSM

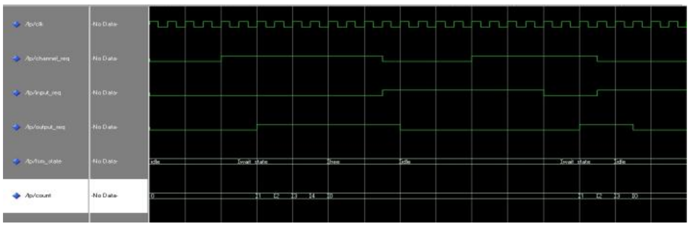
Figure:10b Simulation result of LP FSM

Simulation result of BiNoC router is shown in figure: 9 which show the switching of data flits through bidirectional ports of the router. The direction of bidirectional ports are configured according to the distributed CDC protocol consisting of high priority and low priority FSMs at run time.

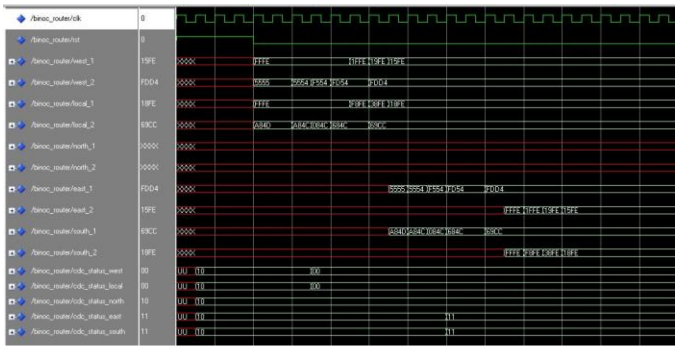
Figure: 11 Simulation result of BiNoC Router

Figure:12 shows the simulation result of Single Error Correction-Double Error Detecting (SEC-DED)Hamming encoder. The hamming encoder designed here is a (22, 16) SEC-DED hamming encoder. Encoder inputs are 16 bit flits and its output is 22 bit codeword consisting of check bits, data bits and an overall parity bit.

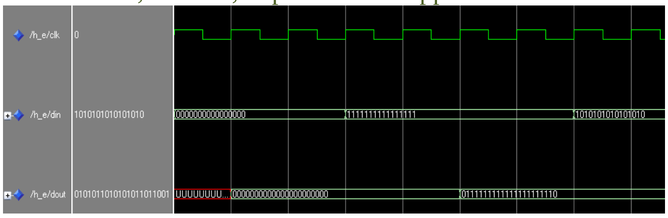

Figure: 12 Simulation result of Hamming Encoder

Decoder designed here is a SEC-DED hamming decoder with forward error correction and retransmission. Decoder module takes 22 bit codeword and calculates the syndrome as well as overall parity and makes decisions.

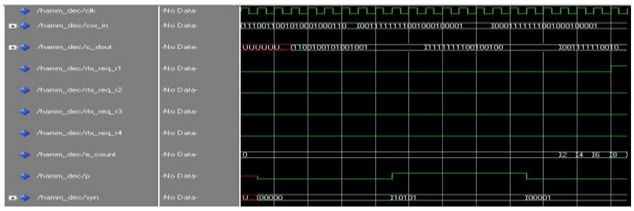

Figure: 12 Simulation result of Hamming Encoder

Figure 13 shows the simulation result of 2*2 BiNoC with hybrid error control scheme. Here communication is established between router having address (1, 1) and router having address (2, 2) via router having address (1, 2). Here the channels and buffers will be having more width to accommodate the hamming encoded flits than normal BiNoC. The Header and data flits are injected in the router R1 (1, 1) and the flits are switched through the network by using both the channels in the path. At the receiver end i.e. R4 (2, 2) the encoded flits are decoded by the hybrid decoder and if single bit errors are detected then it is corrected and if two bit errors are occurring then errors are counted and a Retransmission Request signal is made HIGH which reaches NI of the sender router.

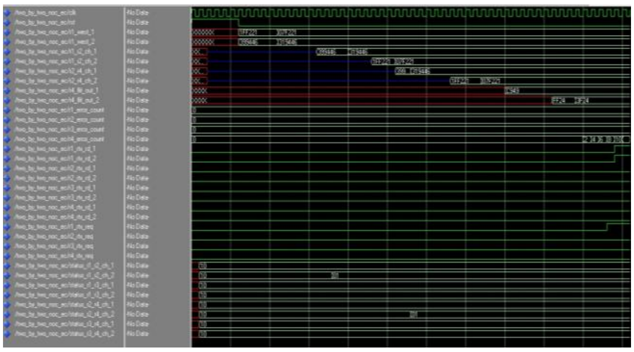

Figure: 5.13 Simulation result of 2*2 BiNoC with Hybrid Error Control Scheme

Table: 1 shows the comparison of flit switching speed and resource utilization of Basic NoC router and BiNoC router. Flits where injected into the west port of routers and switching was done to the ports in east direction for both the routers.

Type of Router	No of Clocks	No of flits switched	No o f channels configured
Basic NoC Router	50	44	1
BiNoC Router	50	84	2

Table: 1 Flit Switching Speed Comparison of Basic NoC Router Vs BiNoC Router.

Table: 2 shows the details of clock cycles, channels used and number of flits switched by the 2*2 Bidirectional NoC when a communication was established form Router R1 (1, 1) to R4 (2, 2).

2*2 BiNoC	No of clocks	No of flits reaching destination	No of channels used
Communication from R1 to R4	100	146	4

Table: 2 BiNoC (2*2) flit switching from R1 (1, 1) to R4 (2, 2).

V. CONCLUSION

This paper focuses on the development of Bidirectional Network on Chip prototype for faster on chip communication than conventional city block style NoC. The system also incorporates a noise toleration scheme by using SEC-DED hamming code and for increasing the reliability, a hybrid scheme of error detection/correction and retransmission of packets is employed in the system. Wormhole routing mode based basic 5 port NoC router and 5 port BiNoC router having bidirectional ports which are dynamically configurable to either direction by using CDC protocol are designed and simulated. Routing algorithm considered is XY routing algorithm. Comparative analysis of Basic NoC router with BiNoC reveals that the flit switching speed and resource utilization capability of BiNoC router is almost double for massive unidirectional communications. 2*2 BiNoC was developed by interconnecting the routers together in mesh topology and communication through network based on XY routing algorithm and wormhole flow control was established. The error control policy considered in this work is End to End Error Control Policy since its area overhead and delay overhead for packet transfer are less. For error correction and detection SEC-DED hamming code is used which can correct single bit errors and detect two bit errors. By using BiNoC having hybrid scheme of error control a faster and reliable on chip communication is achieved. The whole architecture is designed using VHDL, synthesized using Xilinx ISE 12.1 and simulated using ModelSim 6.2c simulator.

REFERENCES

[1] Y. C. Lan, S. H. Lo, Y. C. Lin, Y. H. Hu, and S. J. Chen, “BiNoC: A bidirectional NoC architecture with dynamic self-reconfigurable channel,” *IEEE Trans. Comput.-Aided Des,*vol. 30, No. 3, Pp. 421–434, March 2011.

[2] Wen-Chung Tsai, Ying-Cherng Lan, Yu-Hen Hu, and Sao-Jie Chen “Networks on Chips:Structure and Design Methodologies” Hindawi Publishing Corporation Journal of Electrical and Computer Engineering, Volume 2012, Article ID 509465

[3] Ankur Agarwal, Cyril Iskander, Ravi Shankar, “Survey of Network on Chip (NoC) Architectures & Contributions” journal in engineering, computing and architecture, volume 3, issue 1, 2009

[4] Ville Rantala, Teijo Lehtonen, Juha Plosila, “Network on Chip Routing Algorithms “TUCS Technical Report No 779, August 2006

[5] Davide Bertozzi, Luca Benini, Giovanni De Micheli, “Error Control Schemes for On-Chip Communication Links: The Energy–Reliability Tradeoff”, IEEE Transactions on Computer-Aided Design Of Integrated Circuits and Systems, Vol. 24, No. 6, June 2005.

[6] M.Mirza Aghatabar, S.Koohi, S. Hessabi, M.Pedram, “An Empirical Investigation of Mesh and Torus NoC Topologies Under Different Routing Algorithms and Traffic Models” Sharif University of Technology, Tehran, Iran, University of Southern California, CA, USA

[7] Erno Salminen, Ari Kulmala, and Timo D. H¨am¨al¨ainen “On network-on-chip comparison” Erno Salminen, Ari Kulmala, and Timo D. H¨am¨al¨ainen Tampere University of Technology, Finland.

[8] Dan Marconett “A Survey of Architectural Design and Implementation Tradeoffs in Network on Chip Systems”, University of California, Davis, CA 95616, USA

[9] Tobias Bjerregaard and Shankar Mahadevan “A Survey of Research and Practices of Network-On-Chip” Technical University of Denmark

[10] Jun Ho Bahn “Overview of Network-on-Chip”

International Journal of Modern Engineering Research (IJMER)
www.ijmer.com Vol. 3, Issue. 5, Sep - Oct. 2013 pp-3196-3199 ISSN: 2249-6645

A Novel Approach To Answer Continuous Aggregation Queries Using Data Aggregations

K. Suresh[1], Sk. Karimulla [2], B. Rasagna[3]
1, M.TECH Scholar, QCET, Nellore
2, Assistant Professor, QCET, Nellore
3, Assistant Professor, MLRITM, Hyderabad

ABSTRACT: *Decision making can be regarded as the reflective development consequential in the selection of a course of action among several alternative scenarios. Continuous and uninterrupted aggregation queries are used to monitor the changes in data with time varying for online decision making. Usually a user requirements to obtain the value of some aggregation function larger than distributed data items, for example, to be familiar with value of portfolio for a client; or the average of temperatures sensed by a set of sensors. In these queries a client identifies a coherency requirement as measurement of the query. In this we suggested a low-cost, scalable technique to answer continuous aggregation queries using a network of aggregators of dynamic data items. Such a network of data aggregators, each and every data aggregator gives out a set of data items at specific coherencies. Just as a variety of fragments of a dynamic web pages are served by one or more nodes of a content allocation network, our proposed method involves decomposing a client query into sub-queries and carry out sub-queries on sensibly chosen data aggregators with their individual sub query incoherency boundaries. We present that a technique for getting the optimal set of sub queries with their incoherency boundaries which gratifies client query's coherency obligation with least number of refresh messages driven from aggregators to the client. For approximation the number of refresh messages, we put together a query cost model which can be used to calculate approximately the number of messages required to gratify the client specified incoherency bound.*

Index Terms— *Algorithms, Continuous Queries, Data Dissemination, Coherency, Performance, Distributed Query Processing*

I. INTRODUCTION

Applications such as sensors-based monitoring, auctions, personal portfolio valuations for financial decisions, route planning depends on traffic information, etc., make wide use of dynamic data. For such type of applications, data from one or more independent data sources may be aggregated to determine if some action is warranted. Given the growing number of such type of applications that make use of highly dynamic data, there is imperative interest in systems that can efficiently deliver the relevant updates repeatedly. In these continuous query applications, users are probably to bear some incorrectness in the results. That is, the exact data values at the equivalent data sources need not be reported as long as the query results gratify user specified accuracy requirements.

Data incoherency: Data accuracy can be specified in terms of incoherency of a data item, defined as the complete dissimilarity in value of the data item at the data source and the value known to a client of the data. Let $v_i(t)$ indicate the value of the i^{th} data item at the data source at time t; and let the value the data item known to the client be $u_i(t)$. Then, the data incoherency at the client is given by $|v_i(t)- u_i(t)|$. For a data item which needs to be refreshed at an incoherency bound C a data refresh message is sent to the client as soon as data incoherency exceeds C, i.e., $|v_i(t)- u_i(t)| > C$.

Network of data aggregators (DA): Data refresh from data sources to consumers can be done using push or pull based mechanisms. In a push based system data sources send bring up to date messages to clients on their own while in a pull based system data sources send messages to the customer only when the client makes a request. In this assume the push based system for data transfer between data sources and clients. For scalable management of push based data distribution, network of data aggregators are proposed.

In this assume that each data aggregator maintains its configured incoherency bounds for different data items. From a data distribution capability point of vision, each and every data aggregator is characterized by a set of (d_i, c_i) pairs, where d_i is a data item which the DA can disseminate at an incoherency bound c_i. The configured incoherency bound of a data item at a data aggregator can be maintained using any of following methods:
1) The data source refreshes the data value of the DA whenever DA's incoherency bound is about to get violated. This method has scalability problems. 2) Data aggregator with tighter incoherency bound help the DA to maintain its incoherency bound in a scalable manner

1.1. Aggregate Queries and Their Execution

While executing continuous multi data aggregation queries, using a network of data aggregators, with the objective of minimizing the number of restores from data aggregators to the client. First, we give two motivating scenarios where there are various options for executing a multi data aggregation query and one must select a particular option to minimize the number of messages.

1.2. Problem statement & contributions

Our simulation studies show that for continuous aggregation queries:

- Our method of dividing query into sub queries and executing them at individual DAs requires less than one third of the number of refreshes required in the existing schemes.
- For reducing the number of refreshes more dynamic data items should be part of a sub query involving larger number of data items.

Our method of executing queries over a network of data aggregators is practical since it can be implemented using a mechanism similar to URL-rewriting in content distribution networks (CDNs). Just like in a content distribution networks, the client sends its query to the central site. For getting appropriate aggregators (edge nodes) to answer the client query (webpage), the central site has to first determine which data aggregators have the data items required for the client query. If the client query cannot be respond by a single data aggregator, the query is divided into sub queries (fragments) and each sub query is assigned to a single data aggregator. In case of a content distribution networks webpage's division into fragments is a page design issue, whereas, for permanent aggregation queries, the issue has to be handled on per query basis by considering data dissemination capabilities of data aggregators.

This strategy ignores the fact that the client is interested only in the aggregated value of the data items and various aggregators can disseminate more than one data item. Second, if a single Data Aggregator (DA) can disseminate all three data items required to answer the client query, the Data Aggregator can construct a compound data item corresponding to the client query and disseminate the result to the client so that the query incoherency bound is not violated. It is obvious that if we obtain the query result from a single Data Aggregator, the number of refreshes will be (as data item updates may cancel not in each other, thereby maintaining the query results within the incoherency bound). Further, even if an aggregator can refresh all the data items, it may not be capable to satisfy the query coherency requirements. In such cases the query has to be implemented with data from multiple aggregators.

II. DATA DISSEMINATION COST MODEL

To estimate the number of refreshes required to disseminate a data item while maintaining a certain incoherency bound. There are two most important factors affecting the number of messages that are needed to maintain the coherency requirement:

1) The coherency requirement itself

2) Dynamics of the data.

1.3. Incoherency Bound Model

Consider a data item which needs to be distributed at an incoherency bound C that is new value of the data item will be pushed if the value deviates by more than C from the last pushed value Thus, the number of dissemination messages will be proportional to the probability of | v(t)- u(t) | greater than C for data value v(t) at the source/aggregator and u(t) at the client, at time t. A data item can be replicated as a discrete time random process where each step is correlated with its previous step. In a push-based distribution, a data source can follow one of the following schemes:

1. Data source pushes the data value whenever it differs from the last pushed charge by an amount more than C.
2. Client estimates data value based on server specified parameters. The source drives the new data value whenever it differs from the (client) estimated value by an amount more than C.

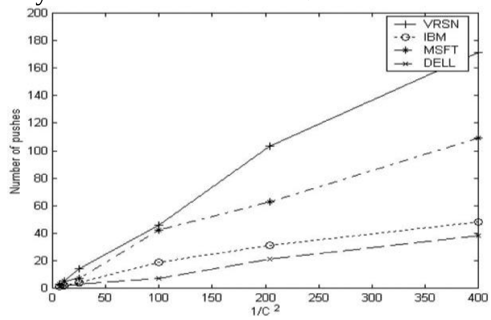

Fig.1: Number of pushes versus incoherency bounds

In both these cases, value at the source can be modeled as a random process with average as the value known at the client. In case 2, the server and the client estimate the data value as the mean of the modeled random process, whereas in case 1 difference from the last pushed value can be modeled as zero mean process.

2.2. Data dynamics Model

Two possible options to model data dynamics, as a first option, the data dynamics can be quantified based on standard deviation of the data item values. Suppose both data items are disseminated with an incoherency bound of 3. It can be seen that the number of messages required for maintaining the incoherency bound will be 7 and 1 for data items d1 and d2, respectively, whereas both data items have the same standard deviation. Thus, we need a measure which captures data changes along with its temporal properties. This motivates us to examine the second measure. As a second option we considered Fast Fourier Trans- form (FFT) which is used in the digital signal processing domain to characterize a digital signal. FFT captures number of changes in data value, amount of changes, and their timings. Thus, FFT can be used to model data dynamics but it has a problem. To estimate the number of refreshes required to disseminate a data item we need a function over FFT coefficients which can return a scalar value. The number of FFT coefficients can be as high as the number of changes in the data value. Among FFT coefficients, 0th order coefficient identifies average value of the data item, whereas higher order coefficients represent transient changes in the value of data item.

Validating the hypothesis: We did simulations with different stocks being disseminated with incoherency bound values of $0:001, 0.01, and 0.1. This variety is 0.1 to 10 times the regular standard deviation of the share price values. Number of invigorate messages is plotted with data sum diff (in $) the linear relationship appears to exist for all incoherency bound values. To enumerate the measure of linearity we used Pearson product moment correlation coefficient (PPMCC), a widely used measure of association, measuring the quantity of linearity between two variables.

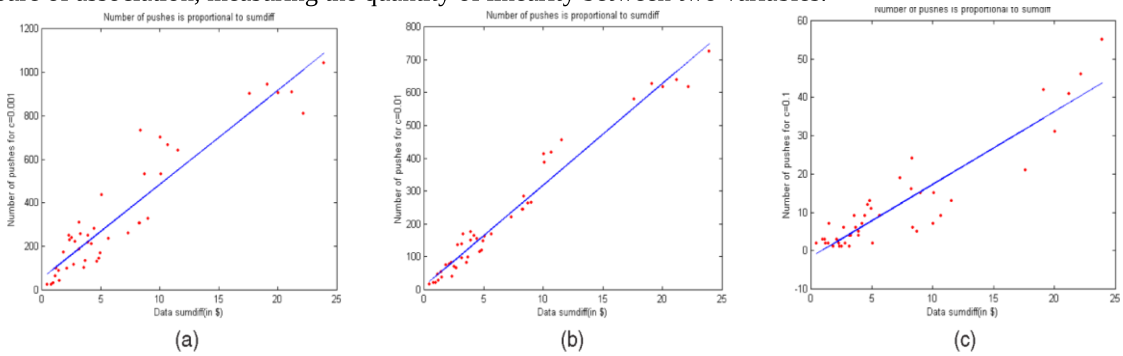

Fig.2: Number of pushes versus data sumdiff (a) C ¼ 0:001, (b) C ¼ 0:01, and (c) C ¼ 0:1.

It is calculated by summing up the products of the deviations of the data item values from their mean. PPMCC varies between 1 and 1 with higher (absolute) values signifying that data points can be considered linear with more confidence. For three principles of incoherency bounds 0.001, 0.01, and 0.1; PPMCC values be 0.94, 0.96, and 0.90, respectively and average deviation from linearity was in the range of 5 percent for low values of C and 10 percent for high values of C. Thus, we can conclude that, for lower values of the incoherency bounds, linear relation- ship between data sum diff and the number of refresh messages can be assumed with more confidence.

2.3 Combining Data Dissemination Models

Number of refresh messages is proportional to data sumdiff R_s and inversely proportional to square of the incoherency bound (C^2). Further, we can see that we need not disseminate any message when either data value is not changing ($R_s = 0$) or incoherency bound is unlimited ($1/C^2 = 0$). Thus, for a given data item S, disseminated with an incoherency bound C, the data distribution cost is proportional to R_s/C^2. In the next section, we use this data dissemination cost model for developing cost model for additive aggregation queries.

III. QUERY PLANNING

A query plan is an ordered set of steps used to access or modify information in a SQL relational database management system. This is a detailed case of the relational model concept of access plans. Since Oracle is declarative, there are typically a large number of alternative ways to execute a specified query, with extensively varying performance. When a query is suggested to the database, the query optimizer appraises some of the unlike, accurate possible plans for executing the query and returns what it considers the best alternative. Thus to get a query plan we need to perform following tasks.
1. Determining sub queries: For the client query get sub queries for each data aggregator.
2. Dividing incoherency bound: Divide the query incoherency bound among sub queries to get the value of sub query.

Optimization objective:

Number of refresh messages is minimized. For a sub query the estimated number of refresh messages is given by the ratio of sum diff of the sub query and the incoherency bound assigned to it and the proportionality factor k. Thus the total no of refresh messages is estimated as the summation of the ratio of the sub query of a given query and in coherency bound associated to it.

Constraint1: q_k is executable at ak: Each DA has the data items required to execute the sub query allocated to it, i.e., for each data item d_q k_i required for the sub query

Constraint2: Query incoherency bound is satisfied: Query incoherency should be less than or equal to the query incoherency bound. Meant for preservative aggregation queries, value of the consumer query is the sum of sub query values. As different sub queries are distributed by different data aggregators, we need to ensure that sum of sub query incoherencies is less than or equal to the query incoherency bound.

Constraint3: Sub query incoherency bound is satisfied: Data incoherency bounds at ak should be such that the sub query incoherency bound can be satisfied at that data aggregator. The tightest incoherency bound, which the data aggregator ak can satisfy for the given sub query q_k. For satisfying this constraint we ensure the following is the outline of our approach for solving this constraint Optimization problem we prove that determining sub queries at the same time as minimizing Zq, as specified by is NPhard.

IV. PERFORMANCE EVOLUTION

4.1 Comparison of Algorithms

We consider various other query plan options. Each query can be executed by distributing individual data items or by getting sub query values from network of data aggregators. Set of sub queries can be selected using sumdiff-based approaches or any other random selection. Sub query (or data) incoherency bound can either be pre decided or optimally allocated. Various arrangements of these proportions are covered in the following algorithms:

1. No sub query, equal incoherency bound (naive): In this the client query is performed with each data item being disseminated to the client independent of other data items in the query. Incoherency bound is separated evenly among the data items. This algorithm proceeded as a baseline algorithm.
2. No sub query, optimal incoherency bound (optc): In this algorithm as well data items are distributed independently but incoherency bound is separated among data items so that total number of invigorate can be minimized.
3. Random sub query selection (random): In this case, sub queries are obtained by randomly selecting a network of data aggregators in the each iteration of the greedy algorithm. This algorithm is designed to see how the random selection works in comparison to the sumdiff-based algorithms.
4. Subquery selection while minimizing sumdiff (mincost)
5. Subquery selection while maximizing gain (maxgain)

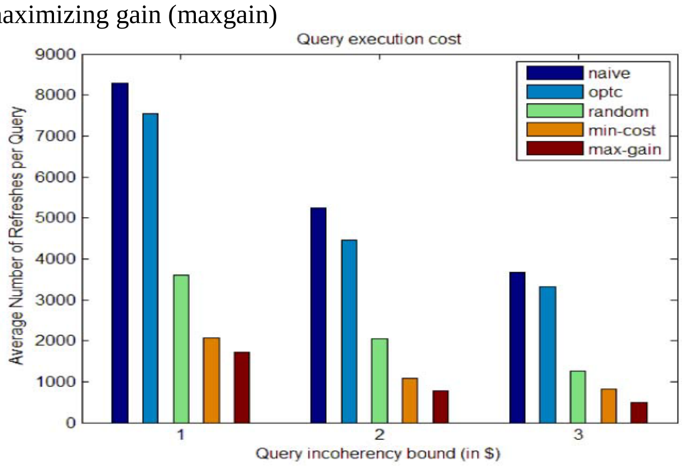

Fig. 5: Performance evaluation of algorithms.

IV. CONCLUSION

Here current a cost-based approach to minimize the number of refreshes required to execute an incoherency bounded uninterrupted query. We assume the continuation of a network of data aggregators, where each Data Aggregator is accomplished of distributing a set of data items at their pre specified incoherency bounds. We developed an important measure for data dynamics in the form of sum diff which is a more appropriate measure compared to the widely used standard deviation based measures. For optimal query implementation we divide the query into sub queries and evaluate each sub query at a thoughtfully chosen data aggregator.

REFERENCES

[1] A. Davis, J. Parikh, and W. Weihl, "Edge Computing: Extending Enterprise Applications to the Edge of the Internet," Proc. 13th Int'l World Wide Web Conf. Alternate Track Papers & Posters (WWW), 2004.
[2] D. VanderMeer, A. Datta, K. Dutta, H. Thomas, and K. Ramamritham, "Proxy-Based Acceleration of Dynamically Generated Content on the World Wide Web," ACM Trans. Database Systems, vol. 29, pp. 403-443, June 2004.
[3] J. Dilley, B. Maggs, J. Parikh, H. Prokop, R. Sitaraman, and B. Weihl, "Globally Distributed Content Delivery," IEEE Internet Computing, vol. 6, no. 5, pp. 50-58, Sept. 2002.
[4] S. Rangarajan, S. Mukerjee, and P. Rodriguez, "User Specific Request Redirection in a Content Delivery Network," Proc. Eighth Int'l Workshop Web Content Caching and Distribution (IWCW), 2003.
[5] S. Shah, K. Ramamritham, and P. Shenoy, "Maintaining Coherency of Dynamic Data in Cooperating Repositories," Proc. 28th Int'l Conf. Very Large Data Bases (VLDB), 2002.
[6] T.H. Cormen, C.E. Leiserson, R.L. Rivest, and C. Stein, Introduction to Algorithms. MIT Press and McGraw-Hill 2001.
[7] Y. Zhou, B. Chin Ooi, and K.-L. Tan, "Disseminating Streaming Data in a Dynamic Environment: An Adaptive and Cost Based Approach," The Int'l J. Very Large Data Bases, vol. 17, pp. 1465-1483, 2008.
[8] "Query Cost Model Validation for Sensor Data,"www.cse.iitb.ac. in/~grajeev/sumdiff/ RaviVijay_BTP06.pdf, 2011.
[9] R. Gupta, A. Puri, and K. Ramamritham, "Executing Incoherency Bounded Continuous Queries at Web Data Aggregators," Proc. 14th Int'l Conf. World Wide Web (WWW), 2005.
[10] A. Populis, Probability, Random Variable and Stochastic Process. Mc. Graw-Hill, 1991.
[11] C. Olston, J. Jiang, and J. Widom, "Adaptive Filter for Continuous Queries over Distributed Data Streams," Proc. ACM SIGMOD Int'l Conf. Management of Data, 2003.
[12] S. Shah, K. Ramamritham, and C. Ravishankar, "Client Assignment in Content Dissemination Networks for Dynamic Data," Proc. 31st Int'l Conf. Very Large Data Bases (VLDB), 2005.
[13] NEFSC Scientific Computer System, http://sole.wh.whoi.edu/ ~jmanning//cruise/serve1.cgi, 2011.

International Journal of Modern Engineering Research (IJMER)
www.ijmer.com Vol. 3, Issue. 5, Sep - Oct. 2013 pp-3200-3206 ISSN: 2249-6645

An Approach for Project Scheduling Using PERT/CPM and Petri Nets (PNs) Tools

Amer A. M. Boushaala
(Department of Industrial and Manufacturing Systems Engineering / University of Benghazi, Libya)

ABSTRACT: *The Petri Nets are more powerful models as compared to the PERT/CPM charts. The Petri Nets show the same type of scheduling constraints as the PERT/CPM charts does. We can easily convert a PERT/CPM networks to a Petri Net model.This work shows how to use Petri net's for modeling and verifying project management networks. Software for a functional analysis of a Petri Net model is developed. The developed software enables analyzing of a system for its various properties irrespective of time. The software analysis is based on some approaches used to determine the various properties of PN model: livens, safeness, reach-ability and conservativeness. This paper proposes a PN based modeling approach to provide a formal way to verify that all the activities are well connected in the project network. This PN model can then be analyzed through (PN based) scheduling techniques, used to find the critical path, used as a basis to develop algorithms for resource-constrained project management, and used for other decisions related to project management. The proposed PN based approach enables the project manager to consider not only resources but also all different types of variables/constraints related to a project, e.g. costs of activities.*

Keywords: *CPM, PERT, Petri Net's, Verifications*

I. INTRODUCTION

CPM/PERT are major tools for project management. They are networks that show precedence relations of activities of a project with the activity times. They are used to find project completion time, which is the longest path in the network. They are also used to find other related information about the activities, e.g., slack time, earliest start and end time. All these analyses are made based on the infinite resource assumption. Then, resource allocation of the project is carried out. That is, finite resources are allocated to the project activities whose time requirements were calculated based on the infinite resource assumption. However, instead of this two-step approach to the resource-constrained project management, a one-step approach, through Petri nets (PNs), is possible. Furthermore, CPM/PERT; do not provide a formal way to verify that all the activities are well connected in the project network.

Liang, Chen and Wang [1] introduced a project model, called SPREM, which extends CPM/PERT's notation to four types of vertices to express the non-deterministic and iterative behaviors of software engineering projects. They compared it with PNs, and discussed its analysis and behavioral properties. These properties are verified through several algorithms they proposed. However, as discussed in section 5, the well known place (transition) invariants help verify some of these properties without any additional algorithms.

Desrochers and Al-Jaar [2] give some advantages of PNs: PNs capture the precedence relations; conflicts and buffer sizes can be modeled easily; PN models represent a hierarchical modeling tool with a well-developed mathematical and practical foundation. These advantages help model and verify (resource-constrained) project networks.

Several PN based approaches to project management were proposed in the literature. Jeetendra et al. [3] evaluate conventional project management tools, state their inadequacies and list advantages of using PNs for project management. Chang and Christensen [4] propose PM-Net for software development, which adopts the basic concepts of PNs with extensions to represent both decisions and artifacts. Ashok Kumar and Ganesh [5] also describe project management models with their inadequacies, and propose a new model based on PNs and demonstrate its usefulness for real-time activity scheduling in a resource-constrained project environment. However, these approaches need to modify and extend basic PN semantics and add new tools to analyze the project network. For example, Jeetendra et al. [3] change PN semantics through a precedence matrix they developed. Conflicting transitions in traditional PNs behave concurrently in their definition. This matrix is then used to help determine floats and the critical path and to find deadlocks. Ashok Kumar and Ganesh [5] also add several features to basic PN semantics for project management.

The proposed PN based approach facilitates modeling (resource-constrained) projects, and verifying some properties of the projects networks, exploiting the well known place (transition) invariants, through the basic PN definitions. That is, contrary to some approaches in the literature, there is no need to modify the basic PN semantics to model activities and decisions related to a project. This increases the capability of the basic PNs, without any extension in the theory, to model projects. Transitions are used to model all the preconditions, for an activity to start, which is modeled via a place. The place invariants are then used to verify some properties of the projects, as discussed in section 5. This model can then be analyzed through (PN based) scheduling techniques [6, 7], and used to find the critical path [8], and used as a basis to develop algorithms for resource-constrained project management [9, 10]. These considerations are beyond the scope of this paper. The aim of this paper is to show how to model project networks with PNs without any modification or extension in the basic PN semantics, and how to compute the critical path and verify some project properties through the well known place invariants.

II. PERT/CPM ACTIVITY NETWORKS

The foundation of the approach came from the Special Projects Office of the US Navy in 1958. It developed a technique for evaluating the performance of large development projects, which became known as PERT - Project Evaluation and Review Technique. Other variations of the same approach are known as the Critical Path Method (CPM) or Critical Path Analysis (CPA) [11, 12].

The heart of any PERT chart is a network of tasks needed to complete a project, showing the order in which the tasks need to be completed and the dependencies between them. This is represented graphically as shown in Fig. 1. The diagram consists of a number of circles, representing events within the development lifecycle, such as the start or completion of a task, and lines, which represent the tasks themselves. Each task is additionally labeled by its time duration. Thus the task between events 4 and 5 is planned to take 3 time units. The primary benefit is the identification of the critical path. The critical path = total time for activities on this path is greater than any other path through the network (delay in any task on the critical path leads to a delay in the project). Diagram Symbols illustrated in Fig. 2.

Project network complexity is often recognized way, but not completely understood by everyone. Boushaala [13] proposed a new measure of project complexity. The developed measure showed more sensitivity to the changes in the network data and give accurate quantified results in evaluating the project complexity where the critical activities, the critical paths, number of critical activities to the total number of project activities, the length of critical path, the resource types and their availability are considered.

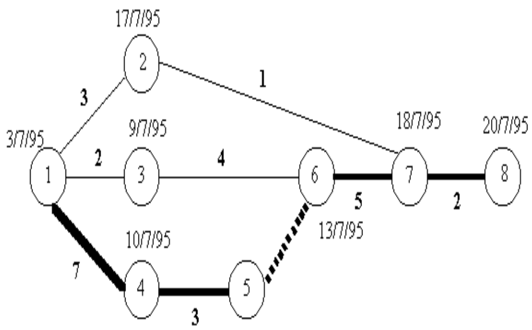

Fig. 1 Example of an activity network

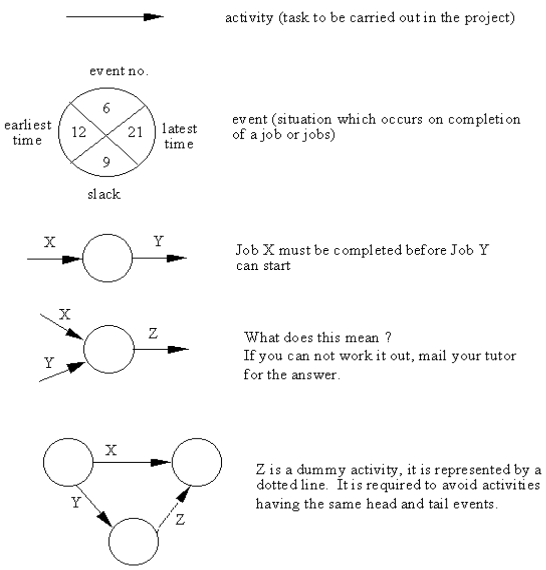

Fig. 2 Symbols used in activity networks

III. MODELING WITH PETRI NET'S

A Petri net (PN) is formally defined as a four-tuple C= (P,T, I,O) where P is a finite set of places p, T is a finite set of transitions t, I is a mapping from transitions to a subset of places (bag of input places) such that I(t) represents input places for transition t, and O is a mapping from transitions to a subset of places (a bag of output places) such that O(t) represents output places for transition t. Multiple occurrences of each in the input and output bags are allowed [14, 15].

A PN can also be described by a bipartite directed graph with two types of nodes: circles for places and bars for transitions. Directed arcs connected places and transitions. Let B (p, t) and F (p, t) be, respectively, the number of occurrences of places P in the input and output bags of transition t. Then B, F and D = F - B, respectively, define the backward, forward and incidence matrices of the PN. These matrices define the topology of the PN. The dynamics of the PN are defined by marking μ of the PN; μ is a state vector with $\mu(p)$ is the number of tokens in place p. The dynamics of the PN are controlled by the execution of that PN. A PN executes by firing its transitions. A transition fires by removing tokens from its input places and depositing tokens at its output places. A transition may fire if it is enabled. A transition t is enabled in marking μ if $\mu \geq B.f_t$ where $f_t = (0, 0, ... ,1 , 0, ..., 0)$ with 1 corresponding to transition t. If μ' is a new marking after firing transition t, then $\mu' = \mu + D.f_t$ defines the dynamics of the PN. For a sequence σ of n transitions, the dynamics equation becomes $\mu_n = \mu_0 + D.f_t$ where $f = \sum_{t\in\tau} f_t$, τ is a set of n transitions and μ_0 is the initial marking; f is called the firing vector of the sequence. Each marking defines a state. Firing a transition may result in a new state. All the possible states define the state space of the PN. From an analytical perspective, it is quite important to determine all the reachable states. It is also important to determine whether or not the PN is live or dead-lock free, bounded (number of tokens in any place is finite in any marking), conservative (the weighted number of tokens in any marking is fixed and finite) and consistent (there is a firing vector with all positive elements). A live and consistent PN is cyclic, which is typical property of manufacturing systems. One may also be interested in other features of a PN as a controller, such as recoverability and fairness. Some of these properties can be mathematically analysed through the P-and T-invariants of the PN [15, 16].

3.1 Marked Graph

A marked graph is a PN in which each place is an input for exactly one transition and an output for exactly one transition. Alternatively, we can say that each place exactly one input and one output [16, 17].

Definition: A marked graph is a PN C = (P,T,I,O) such that for each $p_i \in P$, $|I(pi)| = |\{t_j/p_i\ O(t_j)\}| =1$ and $|O(pi)| = |\{t_j/p_i\ I(tj)\}| =1$.

Marked graphs can model concurrence and synchronization but cannot model conflict or data-dependent decisions. The properties which have been investigated for marked graphs have been Livens, safeness, and reach-ability. Marked graphs can model concurrence and synchronization but cannot model conflict or data-dependent decisions. The properties which have been investigated for marked graphs have been Livens, safeness, and reach-ability. In the investigation of these properties, the major structural parts of a marked graph of interest are its cycles. A cycle in a marked graph is a sequence of transitions $t_{j1}t_{j2}...t_{jk}$ such that for each t_{jr} and t_{jr+1} in the sequence there is a place p_{ir} the $p_{ir} \in O(t_{jr})$ and $p_{ir} \in I(t_{jr+1})$ and $t_{j1} = t_{jk}$. A cycle is such a closed path from a transition back to that same transition.

If $P` \subset P$ is a subset of places that compose a cycle, then the characteristic vector U= ( $u_i | i = \{ 1, 2, ..., n\}$ such that $crd_i\ U = 1$ for $p_i \in P`$, is a p- invariant of PN. If U' and U'' are P- invariants of PN, then U = U' + U'' + ... is also a P-invariant of PN, where $crd_i\ U = u_i$ for $U=(u_1,u_2,...,u_i,...,u_r)$ [16].

3.2 P – Invariant

U is said to be a P-invariant of a PN if and only if $U=(u_1,u_2,...,u_n)$ is a vector such that D*U=0 and $u_i \geq 0$ for I =1,2,...,n and D is the incidence matrix. The following theorem provides the condition allowing solving the reachability problem states. Given a Petri net C =(P,T,I,O,μo) with marking μ (R (C,μo)) and marking μ` ( R ( C,μo ) ). The problem is if μ` is reachable from μ , i.e. μ`(R (C,μ)) [10,18].

Theorem (1): Let μ_0 be an initial marking and let μ (R (C,μ_0)). If U is an P-invariant, then $\mu_0 U^T = \mu U^T$

The above theorem provides the condition allowing solving the so called reachability problem. The problem can be stated as following. Given a PN C = (P,T,I,O,μo) with marking μ (R (C,μ_0)) and marking μ`( R ( C,$\mu_0$ ) ). Is μ` reachable from μ, i.e. μ`(R (C,μ))?.As shown in Fig. 3[19].

3.3 Software for a Functional Analysis of a Petri Net Model

The developed software enables analyzing of a system for its various properties irrespective of time. Functional analysis has been used in the Petri net to refer to this type of analysis. The software analysis is based on some approaches used to determine the various properties of PN model: livens, safeness, reach-ability and conservativeness. Fig. 3 shows the flow chart of computing P-invariants.

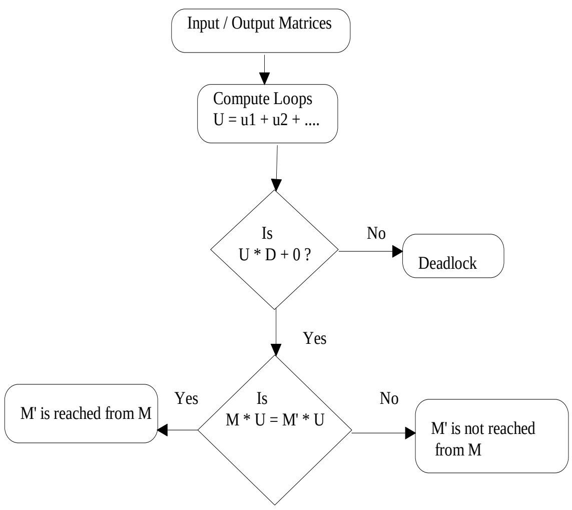

Fig. 3: Flow chart of computing P-invariants

IV. HEADINGS CONVERSION OF PERT/CPM CHARTS INTO EQUIVALENT PETRI NET MODEL

The Petri Nets show the same type of scheduling constraints as the PERT/CPM charts does. We can easily convert a PERT/CPM networks to a Petri Net model. Each activity in the PERT chart is represented by a place, while the precedence constraints are represented by the transitions. In CPM chart each event is represented by place (transition), while the activity is represented by transition (place). The Petri Net is excellent vehicle to represent the concurrency and precedence constraints of the PERT chart. In modelling the PERT chart with the Petri Net, activities that are represented by places and transitions are reserved to model multiple resources of limited amounts. Fig. 4 demonstrates the conversion process of PERT/CPM charts into Petri net chart.

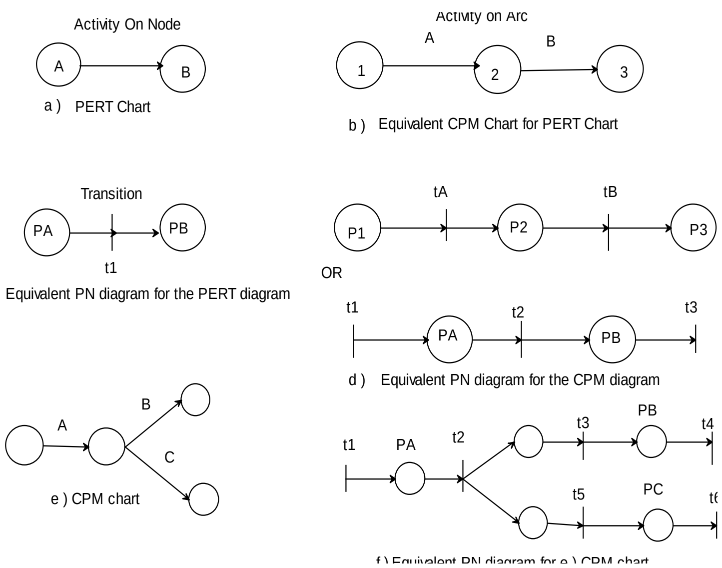

Fig. 4: Conversion of PERT/CPM charts into Petri net chart

The Petri Nets are more powerful models as compared to the PERT/CPM charts. The following reasons may be given for it:

- The repeated performance of activities, if necessary, can be modelled by the PN.
- Required resources per activity appear explicitly as tokens in representation.
- Non-deterministic aspects can be dealt with. For example: the order in which a particular resource performs some tasks may not be totally specified.

V. MODELING PROJECT NETWORKS THROUGH PETRI NETS

By definition of a project, the project is completed when all the activities are processed exactly once. In PN terminology, this means that all the transitions must fire exactly once, i.e. U.D = 0 for U = 1, where 1 is a column vector with all entries being one. This transition invariant verifies that the precedence relations among the activities are well established (the nodes are strongly connected), i.e. the project can be completed. Note that because the PN model of a project is a marked graph, the transition invariant is also a sufficient condition. D.1 = 0 means that the sum of each and every row of D should be zero. Hence, to verify that the project can be completed, it is sufficient to show that the incidence matrix of the PN model of the project has this property and that the PN is a marked graph. The following demonstrates this through an illustrative example. Consider a project consists of 8 activities A, B, C, D, E, F, G, and H with their times of completion as shown in Table 1 [18].

The project will be finished after 21 weeks, which is the CPM network contains two of critical paths. The first critical bath consists of 4 activities A, B, E, and H, and the second critical bath consists of 5 activities A, B, D1, F, and H. The activities D1 and D2 were dummies with zero duration. Fig. 5 shows A CPM project network for Table 1 with completion time for the project.

Table 1: The sequence of the project activities

Activity	Precedecessor(s)	Duration (Weeks)
A	------	3
B	A	6
C	A	4
D	A	3
E	B	4
F	B, C, D	4
G	B	1
H	E, F	8

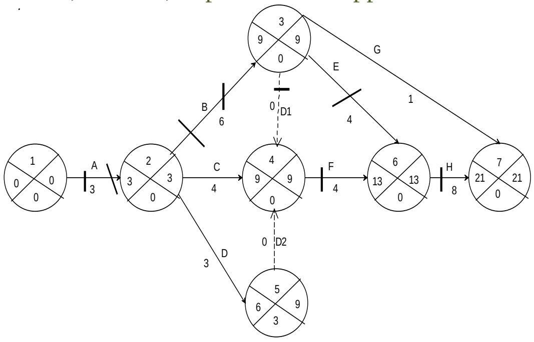

Fig. 5: A CPM project net work for table 1 with completion time for the project [13]

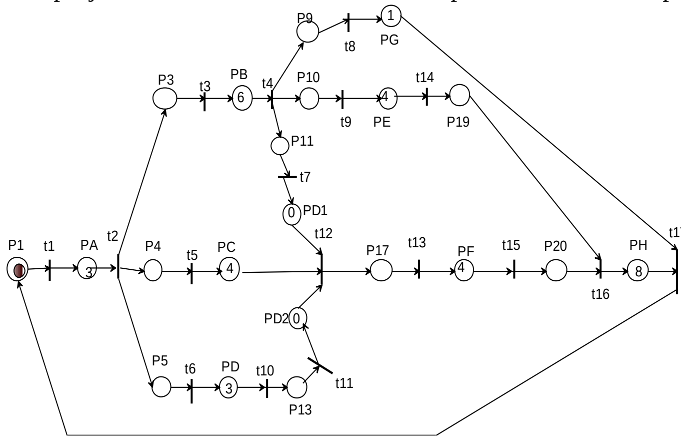

Fig. 6: Petri net (PN) model of figure 5

Fig. 6 shows the PN model of the project network in Fig. 5. For example activity A (PA) needs 3days to be completed. Activity times are denoted within the circles (places), which model the timed places. The bars denote immediate transitions, which model logical conditions (transitions t1 and t2 were pre and post conditions of PA) and take zero time to fire. The same as for the other activities from B through H including dummy activities D1 and D2 have pre and post conditions represented in transitions. All other places P1, P3, P4, … , and P20 were connection places between all the project activities, for example P3 is the connection between the two activities PA and PB through t2 which is post condition of PA and t3 which is precondition of PB, as well as for the other remaining places (e.g. P4, P5, … , P20) and needs zero time to be completed.

The incidence matrix of Fig. 6 is shown below. The sum of each and every row of the incidence matrix should be zero and each and every column should have at least one -1 and +1 entry to verify that the corresponding PN models the project correctly, i.e. all the activities, hence the project, can be completed

	t1	t2	t3	t4	t5	t6	t7	t8	t9	t10	t11	t12	t13	t14	t15	t16	t17
p1	−1	0	0	0	0	0	0	0	0	0	0	0	0	0	0	0	1
pA	1	−1	0	0	0	0	0	0	0	0	0	0	0	0	0	0	0
p3	0	1	−1	0	0	0	0	0	0	0	0	0	0	0	0	0	0
p4	0	1	0	0	−1	0	0	0	0	0	0	0	0	0	0	0	0
p5	0	1	0	0	0	−1	0	0	0	0	0	0	0	0	0	0	0
pB	0	0	1	−1	0	0	0	0	0	0	0	0	0	0	0	0	0
pC	0	0	0	0	1	0	0	0	0	0	0	−1	0	0	0	0	0
pD	0	0	0	0	0	1	0	0	0	−1	0	0	0	0	0	0	0
p9	0	0	0	1	0	0	0	−1	0	0	0	0	0	0	0	0	0
p10	0	0	0	1	0	0	0	0	−1	0	0	0	0	0	0	0	0
p11	0	0	0	1	0	0	−1	0	0	0	0	0	0	0	0	0	0
pD1	0	0	0	0	0	0	1	0	0	0	0	−1	0	0	0	0	0
p13	0	0	0	0	0	0	0	0	0	1	−1	0	0	0	0	0	0
pD2	0	0	0	0	0	0	0	0	0	0	1	−1	0	0	0	0	0
pE	0	0	0	0	0	0	0	0	1	0	0	0	0	−1	0	0	0
pG	0	0	0	0	0	0	0	1	0	0	0	0	0	0	0	0	−1
p17	0	0	0	0	0	0	0	0	0	0	0	1	−1	0	0	0	0
pF	0	0	0	0	0	0	0	0	0	0	0	0	1	0	−1	0	0
p19	0	0	0	0	0	0	0	0	0	0	0	0	0	1	0	−1	0
p20	0	0	0	0	0	0	0	0	0	0	0	0	0	0	1	−1	0
pH	0	0	0	0	0	0	0	0	0	0	0	0	0	0	0	1	−1

$$-u_1 + u_{17} = 0$$
$$u_1 - u_2 = 0$$
$$u_{16} - u_{17} = 0$$

In order to illustrate the application of the approach proposed, let consider the example provided in the previous example of Fig. 6. An event graph (like PN in general) said to be strongly connected if there is a directed path joining any node A to any node B of the graph. The event graph presented in Fig. 6 strongly connected. We also define an elementary circuit in a strongly connected event as a directed path goes from one node, i.e. a place or transition, back to the same node, which any other node is not repeated. For instance, Fig. 6 exposes five elementary circuits, namely:

γ_1 = (p1, t1;pA ,t2; p3 ,t3; pB ,t4;p9 ,t8;pG ,t17;)

γ_2 = (p1,t1;pA ,t2;p3 ,t3;pB ,t4;p10 ,t9;pE ,t14;p19 ,t16;pH ,t17;)

γ_3 = (p1,t1;pA ,t2;p3 ,t3;pB ,t4;p11 ,t7;pD1 ,t12;p17 ,t13;pF ,t15;p20 ,t16;pH ,t17;)

γ_4 = (p1,t1;pA ,t2;p4 ,t5;pC ,t12;p17 ,t13;pF ,t15;p20 ,t16;pH ,t17;)

γ_5 = (p1,t1;pA ,t2;p5 ,t06;pD ,t10;p13 ,t11;pD2 ,t12;p17 ,t13;pF ,t15;p20 ,t16;pH ,t17;)

If the number of tokens in a marking remains fixed for all markings in the reachability set, the Petri net is then said to be strictly conservative. An immediate consequence of conservativeness is boundedness of the Petri net. The boundedness property implies that the number of tokens in any place does not increase beyond a limit. This in turn guarantees a finite reachability set for the Petri net. If there exist an U with all positive elements the Petri net is then said to be conservative.

If U = (1,...,1) then the Petri net is strictly conservative. The total number of tokens in γ_i (i=1,2,…,5) is then:

$n_1(\gamma_1) = \mu(p_1) + \mu(pA) + \mu(p_3) + \mu(pB) + \mu(p_9) + \mu(pE) + = 1 + 0 + 0 + 0 + 0 + 0 = 1$

$n_2(\gamma_2) = \mu(p_1) + \mu(pA) + \mu(p_3) + \mu(pB) + \mu(p_{10}) + \mu(pG) + \mu(p_{19}) + \mu(pH) = 1 + 0 + 0 + 0 + 0 + 0 + 0 + 0 = 1$

$n_3(\gamma_3) = \mu(p_1) + \mu(pA) + \mu(p_3) + \mu(pB) + \mu(p_{11}) + \mu(pD1) + \mu(p_{17}) + \mu(pF) + \mu(p_{20}) + \mu(pH) = 1 + 0 + 0 + 0 + 0 + 0 + 0 + 0 + 0 + 0 = 1$

$n_4(\gamma_4) = \mu(p_1) + \mu(pA) + \mu(p_4) + \mu(pC) + \mu(p_{17}) + \mu(pF) + \mu(p_{20}) + \mu(pH) = 1 + 0 + 0 + 0 + 0 + 0 + 0 + 0 = 1$

$N_5(\gamma_5) = \mu(p_1) + \mu(pA) + \mu(p_5) + \mu(pD) + \mu(p_{13}) + \mu(pD2) + \mu(p_{17}) + \mu(pF) + \mu(p_{20}) + \mu(pH) = 1 + 0 + 0 + 0 + 0 + 0 + 0 + 0 + 0 + 0 = 1$

Therefore, the total P – invariants of all loops U = (5, 5, 3, 1, 1, 3, 1, 1, 1, 1, 1, 1, 1, 3, 3, 1, 3, 4).

By applying the equations : U * D = (0,0,0,0,0,0,0,0,0,0,0,0,0,0,0,0,0,0), this means that the system is deadlock free. To compute the total time for each loop to find the critical path(s) as follows:

γ_1 = (p1, pA , p3 , pB ,p9 ,pG) = 0 + 3 + 0 + 6 + 0 + 1 = 10 weeks

γ_2 = (p1, pA ,p3 ,pB ,p10 ,pE ,p19 ,pH) = 0 + 3 + 6 + 0 + 4 + 0 + 8 = 21 weeks

γ_3 = (p1, pA ,p3 ,pB ,p11 ,pD1 ,p17 ,pF ,p20 ,pH ,) = 0 + 3 + 0 + 6 + 0 + 0 + 0 + 4 + 8 = 21 weeks

γ_4 = (p1,pA ,p4 ,pC ,p17 ,pF ,p20 ,pH) = 0 + 3 + 0 + 4 + 0 + 4 + 0 + 8 = 19 weeks

γ_5 = (p1,pA ,p5 ,pD ,p13 ,pD2 ,p17 ,pF ,p20 ,pH) = 0 + 3 + 0 + 3 + 0 + 0 + 0 + 4 + 0 + 8 = 18 weeks

Then there is two critical paths $\underline{\gamma_2}$ and $\underline{\gamma_3}$, as the same as of the CPM network Figure 5.

VI. CONCLUSIONS AND REMARKS

The proposed PN based approach to project management facilitated modeling (resource-constrained) projects, and verifying some properties of the projects networks, exploiting the well known place (transition) invariants, through the basic PN semantics. That is, contrary to some approaches in the literature, there is no need to modify the basic PN semantics to model activities and decisions related to a project. This increases the capability of the basic PNs, without any extension in the theory, to model projects. Places were used to model all the preconditions, including resources, for an activity to start, which was modeled via a place (transition). The place (transition) invariants were then used to verify some properties of the projects. This PN model can then be analyzed through (PN based) scheduling techniques, used to find the critical path, used as a basis to develop algorithms for resource-constrained project management, and used for other decisions related to project management.

The transition invariant means that the sum of each and every row of the incidence matrix should be zero. Hence, to verify that the project can be completed, it is sufficient to show that the sum of each and every row of the incidence matrix is zero, and that each and every column has at least one -1 and +1 entry.

The proposed PN based approach enables the project manager to consider not only resources but also all different types of variables/constraints related to a project, e.g. costs of activities. Any of these variables can be considered fuzzy as well. In this case, fuzzy arc weights cause the firing rule to be modified. These are possible future research directions.

REFERENCES

[1] B.S., Liang, J.N., Chen, and F.J., Wang, A project model for software development, *Journal of Information Science and Engineering, 16,* 2000, 423 – 446.

[2] A.A., Desrochers, and R.Y, Al-Jaar, *Application of Petri nets in manufacturing systems: modeling, control, and performance analysis* (New York: IEEE Press, 1995).

[3] V.A., Jeetendra, O.V., Chetty, and J., Reddy, Petri nets for project management and resource leveling, *International Journal of Advanced Manufacturing Technology, 16,* 2000, 516-520.

[4] C.K.,Chang and M., Christensen, A net practice for software project management, *IEEE Software, November/ December,* 1999, 80-88.

[5] V.K., Kumar, and L.S., Ganesh, Use of Petri nets for resource allocation in projects, *IEEE Transactions on Engineering Management, 45(1),* 1998, 49 – 56.

[6] W.M.P., Van der Aalst, Petri net based scheduling, *OR Spectrum, 18,* 1996, 219-229.

[7] W., Herroelen, and R., Leus, Project scheduling under uncertainty: Survey and research potentials, *European Journal of Operational Research, 165*, 2005, 289-306.
[8] S.M., Chen, and T.H., Chang, Finding multiple possible critical paths using fuzzy PERT, *IEEE Transactions on System Management, and Cybernetics Part B: Cybernetics, 31 (6)*, 2001, 930 – 937.
[9] K.W., Kim, Y.S., Yun, J.M., Yoon, M., Gen, and G., Yamazaki, Hybrid genetic algorithm with adaptive abilities for resource-constrained multiple project scheduling, *Computers in Industry, 56,* 2005, 143- 160.
[10] V., Valls, F., Ballestín, and S., Quintanilla, Justification and RCPSP: A technique that pays, *European Journal of Operational Research, 165*, 2005, 375-386.
[11] Erik and Will, *Project scheduling a research handbook*, (Kulwer Academic Publishers : New York, Boston, London, Moscow, and Dordrecht, 2002).
[12] J.P., Lewis, *Project planning, scheduling and control*, (Mc Graw – Hill Companies, Inc., 2001).
[13] A. M., Boushaala, Project complexity indices based on topology features, *Al-satil Journal, 4 (8)*, 2010, 137-150.
[14] T., Peterson, *Petri Net Theory and the Modeling of Systems* (Prentice Hall, 1981).
[15] Z., Banaszak and K., Jedrzejek, Rule – based knowledge verification using Petri nets, 3rd *Turkish Symposium on AI and Networks*, June 1994.
[16] P.M., del Foyo and J. R., Silva, Using timed Petri nets for modeling and verification of timed constrained workflow systems, *ABCM Symposium Series in Mechatronics*, *3*, 2008, 471-478.
[17] Y., Chen, P., Fsu, and Y., Chang, A Petri net approach to support resource assignment in project management, *IEEE Transactions on Engineering Management, 38(3),* 2008, 564 – 574.
[18] I. Amiruddin, K. Abdul Rashid, and J. Wisam, Literature review in resource – constrain critical path method technique, *European Journal of Scientific research*, *29(2),* 2009, 222-236.
[19] I. M., Buseif, *An approach to FMS design using SADT and PN tools*, doctoral diss., Faculty of Production Engineering, Warsaw University of Technology, Warsaw – Poland, 1997.

International Journal of Modern Engineering Research (IJMER)
www.ijmer.com Vol. 3, Issue. 5, Sep - Oct. 2013 pp-3207-3215 ISSN: 2249-6645

Theoretical and graphical analysis of abrasivewater jetturning

G.Ramu[1]B.Bapiraju[2]M.Leela Kumari[3]

[1]*vitam engineering college,Mechanical Engineering, JNTUK,AP.*
[2]*swamyVivekananda engineering college, Faculty of Mechanical Engineering,JNTUK, AP.*
[3]*vitam engineeringcollege, Faculty of Mechanical Engineering, JNTUK, AP.*

ABSTRACT: *Recent developments in the materials technology, as well as the requirements for more complex and economic machining processes, demand new approaches to the machining of materials. The machining of lightweight materials, specialty metals, ceramics, and advanced metal matrix composites requires careful machining strategy to maximize performance, minimize tool wear and avoid material distortion or destruction due to thermally induced oxidation, shear stresses, thermal stresses, vibration. It will be of great importance to develop a machine tool that is less sensitive to material properties, has virtually no thermal effects, imposes minimal stresses, is free of vibrations and provides acceptable surface finish. Abrasive water jet (AWJ) technology offers the potential for the development of such a tool.An explicit finite element analysis (FEA) of a single abrasive particle impact on stainless steel in abrasive water jet (AWJ) machining. In the experimental verification, the shapes of craters on the workpiece material were observed and compared with FEA simulation results by means of crater sphericity. The influences of the impact angle and particle velocity were observed.Especially the impact angle emerged as a very suitable process parameter for experimental verification of FEA simulation, where crater sphericity was observed. Results of the FEA simulation are in good agreement with those obtained from the experimental verification. The presented workgives the basis for further FEA investigation of AWJ machining, where influences such as particles rotation and other process parameters will be observed.The objective of the present work is to develop a mathematical model, considering the variation in jet impact angle and the kerf profile, for predicting the final diameter achieved in AWJ turning process for ductile and brittle materials. Various distributions that can represent the kerf shape and the best distribution among them is identified by comparing the predicted kerf shape with the observed kerf shape. It was observed that a sine function could represent the observed kerf geometry better than exponential and cosine functions. The proposed model is validated by comparing the predicted final diameters with experimental results obtained literature.*

Keywords*:AWJ turning, Kerf, Modeling.Explicit finite elements analysis*

I. INTRODUCTION

Manufacturing industry is being ever more time conscious with regard to the global economy. The need for rapid prototyping and small production batches is increasing in modern industries. These trends have placed a premium in the use of new and advanced technologies for quickly turning raw materials in to usable goods; with no time being required for tooling. Abrasive water jet (AWJ) machining technology has been found to be one of the most recent developed advanced non-traditional methods used in industry for material processing with the distinct advantages of no thermal distortion; high machining versatility, high flexibility and small cutting forces. There are several distinguished advantages of AWJ technique. It is less sensitive to material properties and hence does not cause chatter, has no thermal effects, imposes minimal stresses on the work piece, and has high machining versatility and flexibility.Further, several requirements such as tight tolerances on the machined parts and effective utilization of these advanced materials motivated one to look for certain alternatives to these advanced machining processes. In conventional methods of machining, a solid tool, made of higher hardness than work piece, makes a direct contact with the work piece material. In contrast to this, unconventional methods of machining make use of different forms of energy to process the materials and do not make any direct contact with the work material. Among the several unconventional machining processes, electro-chemical machining, electro-discharge machining, ultrasonic machining, abrasive jet machining, abrasive water jet machining, chemical machining and laser beam machining are the most popular ones. Among them, abrasive water jet machining process is gaining lot of popularity due to its ability to process a range of materials in different ways. An abrasive water jet is a jet of water, which contains abrasive material. Usually the water exits a nozzle at a high speed and the abrasive material is injected into the jet stream. This process is sometimes known as entrainment in that the abrasive particles become part of the moving water much as passengers become part of a moving train. Hence as with a train the water jet becomes the moving mechanism for the particles. However high speed jet of a pre-mixture of the abrasive and the water would also be defined as an abrasive water jet The purpose of the abrasive water jet is to perform some machining or finishing operation such as cutting, boring, turning, etc.

II. HEADINGS

1.1 Introduction Manufacturing industry is being ever more time conscious with regard to the global economy. The need for rapid prototyping and small production batches is increasing in modern industries. These trends have placed a premium in the use of new and advanced technologies for quickly turning raw materials in to usable goods; with no time being required for tooling. Abrasive water jet (AWJ) machining technology has been found to be one of the most recent developed advanced non-traditional methods used in industry for material processing with the distinct advantages of no thermal distortion; high machining versatility, high flexibility and small cutting forces. There are several distinguished advantages of AWJ technique. It is less sensitive to material properties and hence does not cause chatter, has no thermal effects, imposes minimal stresses on the work piece, and has high machining versatility and flexibility.

1.2 Abrasive Water Jet Turnin Abrasive water jets are extensively employed for cutting of different materials such as soft and ductile materials to hard and brittle materials. It has become the state of the art in many industries such as automobile, aerospace and many consumable product making industries .Attempts made on AWJ turning include the turning of long and small diameter parts and the production of threads on difficult-to-machine materials like ceramics, composites, glass, etc.

1.3 present works The present work is to develop a mathematical model, considering the variation in jet impact angle and kerf geometry, for predicting the final diameter in AWJ TURNING process for ductile and brittle materials.

2.1 Introduction Many researchers developed a stable abrasive water jet turning process in the field of manufacturing in order to generate high quality products. However extensive works have been reported by varying different process parameters in Abrasive Water Jet Turning.This chapter highlights the literature available on abrasive water jet machining, especially focusing on abrasive water jet turning. It also gives the classification of different types of water jets and discusses the relevance of these jets for abrasive water jet turning. It also includes the description of various components of abrasive water jet machining system, the various theories proposed for explaining the mechanism of material removal in abrasive water jet machining.The water jet cutting, also called hydrodynamic machining, technology was developed in 1968 by Dr. Norman Franze, followed by the first commercial system in 1971. A breakthrough was made by adding abrasive particles to the high pressure stream of water in the early 1980s, immediately followed by the introduction of the first commercial abrasive water jet (AWJ) system in 1983.

2.2 The AWJM Process

An abrasive water jet is a jet of water that contains some abrasive material. Abrasives are particles of special materials like aluminum oxide, silicon carbide, sodium bicarbonate, dolomite and/or glass beads with varying grain sizes. Usually the water exits a nozzle at a high speed and the abrasive material is injected into the jet stream. This process is sometimes known as entrainment in that the abrasive particles become part of the moving water much as passengers become part of a moving train. The added abrasives drastically increase the range of materials that can be cut with a water jet. Materials like super alloys, ceramics, glass, and refractory material are typically machined by this process. This process aids in achieving higher traverse speeds, machining of thicker materials, and better edge quality.The abrasive water jet-cutting process is characterized by a large number of process parameters that determine the efficiency, economy and quality of the entire process. In general, the parameters in the abrasive water-jet cutting process can be divided into four categories 1. Hydraulic parameters,– Pump pressure (p)– Water-orifice diameter (do)– Water flow rate (mw)2. Mixing and acceleration parameters– Focus diameter (df)– Focus length (lf)3. Cutting parameters– Traverse rate (v)– Number of passes (np)– Standoff distance (x)– Impact angle (φ)4. Abrasive parameters– Abrasive mass flow-rate (ma)–Abrasive particle diameter (dp)– Abrasive particle size distribution (f (dp))– Abrasive particle shape– Abrasive particle hardness (Hp)

III. PROCESS PARAMETER ESTIMATION

Determining the optimal process parameters by testing/ experimentation is a time consuming and cost ineffective procedure. The knowledge of a mathematical function that relates the cutting parameters to the cutting results is necessary for a computer controlled cutting process. An important aspect is to estimate some of the most crucial output process parameters using the input parameters. One of the critical input parameters is the depth of cut (dc), which reflects the thickness of the work-piece material to be removed. Many complex mechanisms of material removal and a huge quantity of particles involved in the process produce a strongly nonlinear and stochastic behavior of the system. The generated surface depends on several machining parameters and work piece properties. Because the AWJ process is a dynamic system, the interactions of the system inputs (machining parameters and work piece properties) play an important role on process evolution.From the technological point of view, the most interesting machining parameters are the cutting head traverse rate, the water pressure, the abrasive mass flow rate and the stand-off distance between the mixing tube and the work piece. All these parameters can be controlled during AWJ machining. Other parameters, like cutting head components' geometry, abrasive properties and work piece material properties are unchanged during the process.As explained earlier by many researchers in the field of abrasive water jet turnining, much work is to be carried out to find the critical diame

3.1 Introduction: Abrasive water jet turning (AWJT) is a new process that holds promise for efficient machining of difficult to machine materials. The process uses abrasive water jet as a cutting tool that deflects from its trajectory upon interaction with the work piece. Therefore, the final work piece diameter, in addition to depth of cut, is a function of abrasive water jet, work piece and turning parameters. Here an initial attempt is made to model the AWJ turning process that is based on existing models of erosion. A new approach is to predict the process parameters in Abrasive Water Jet (AWJ) turning. The methodology involves the application of Finnie's theory of erosion for estimation of volume of material removed assuming the impact of jet on the work piece surface at an angle to account for the curvature of work piece.

3.2 Characteristics of AWJ machining: AWJ machining technology has been increasingly used since it has various distinguished advantages over other cutting processes

- ✓ No thermal damage or distortion. The heat generated is instantaneously carried away by the water. As a result, no temperature rise occurs in the work piece. This is especially useful for cutting thermal sensitive materials and other metals where excessive heat may change the properties of the material.

- ✓ Ability to produce contours. Abrasive water jets are exceptionally good at two-dimensional machining. It is possible to cut very complicated shapes or bevels of any angle in addition to three-dimensional profiling because the process is unidirectional.
- ✓ High machining versatility. An abrasive water jet can cut virtually any materials, particularly for machining many difficult-to-machine materials such as pre-hardened steels, titanium alloys, copper, brass and aluminum, brittle materials like glasses, ceramics and quartz..
- ✓ High initial capital and operating costs. For most industrial applications, the investment and operating costs are very high.
- ✓ **Low nozzle life:** The AWJ nozzle suffers from wearing by particles, which tends to produce unacceptable cut quality.
- ✓ **Low energy efficiency:** In the AWJ machining process, material removal is caused primarily by abrasives. The kinetic energy of abrasives is less than 10% of the total energy of the water stream in an AWJ system. The water stream retains a significant amount of energy until it is collected in an energy-dissipating container.
- ✓ **Low energy efficiency:** In the AWJ machining process, material removal is caused primarily by abrasives. The kinetic energy of abrasives is less than 10% of the total energy of the water stream in an AWJ system. The water stream retains a significant amount of energy until it is collected in an energy-dissipating container.

3.3 Mechanism of Material Removal in AWJ Machining. Material removal in the case of AWJs is due to the erosion caused by the impact of high velocity abrasive particles on the material. Abrasives strike the work piece at approximately one million collisions per second thus transferring a large amount of kinetic energy to the work material. The damage caused to the material by the high speed impact of particles entrained in a fluid system is called erosion.

3.4 Micro cutting mechanisms.

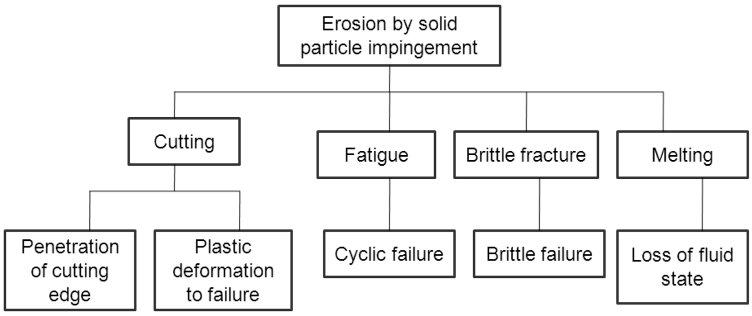

3.5.Abrasive Water Jet Turning .A novel turning technique that employs abrasive water jet as cutting tool was proposed [6]. Abrasive water jet turning (AWJT) is a new process that holds promise for efficient machining of difficult to machine materials. The configuration of AWJ turning is similar to that of a conventional lathe, except that an AWJ is used as a cutting tool. An AWJ is formed by mixing solid abrasive particles with high velocity water jet in a specially designed nozzle assembly. The high velocity water jet is obtained by passing water at pressure upto 380 MPa through a small sapphire orifice less than 1 mm in diameter. The abrasive particles are entrained in water downstream of the orifice with the help of a vacuum pressure that exits around the water jet. The impact of high velocity abrasive particles with the work piece causes material removal, which can generally be classified as erosive wear.

3.6 PARAMETERS INVOLVED IN AWJ CUTTING
3.6.1 Input parameters:

- Hydraulic parameters:Water jet pressure , Water jet diameter
- Target material: Fracture strength, Hardness , Ductility
- Mixing parameters: Mixing tube diameter , Mixing tube length
- Cutting parameters: Traverse speed , Standoff distance ,Angle of attack
- Abrasive parameter :Abrasive particle size ,Abrasive material ,Abrasive flow rate ,Abrasive condition (dry or slurry)

3.6.2. Output parameters:

- Kerf characteristicsSurface waviness ,Kerf width and taper ,Burr formation ,Surface finish, Depthofcut
- Geometrical and dimensional accuracy ,Material removal rate

3.7 MOTIVATION:

- ✓ AWJ TURNING is the promising method to machine hard, brittle and difficult to machine material
- ✓ Scope for optimizing the parameters to improve the process efficiency [4].
- ✓ Very few attempts to model the AWJ TURNING.
- ✓ The existing AWJ turning models [2] does not considering varying impact angle.

3.8. OBJECTIVE and SCOPE OF THE WORK: The objective of the present work is to develop a mathematical model, considering the variation in jet impact angle and kerf geometry, for predicting the final diameter in AWJ TURNING process for ductile and brittle materials. The scope of the present work is limited to the development of an approach for predicting the overall geometry of kerf and final diameter achieved while turning ductile materials using AWJ.

IV. INDENTATIONS AND EQUATIONS

4.2..IMPORTANCE OF MATHEMATICAL MODELING The important controlling process parameters in AWJ cutting include water pressure (P), jet traverse rate (V), abrasiveflowrate(M_f)anddiameteroffocusingnozzle(d_f). Inthisstudy,depthof cuthasbeenchosenasthemainprocess response characteristicstoinvestigatetheinfluenceof theaboveparameters.We firstdevelopa mathematicalmodelto relatetheprocesscontrolparametersto theprocessresponse characteristics. The empiricalmodel for the prediction of depth ofcutinterms ofthecontrolling parameters willbe establishedbymeansofpiecewiselinearregressionanalysis.

4.2.1 Solving Ansari and Hashish [2] model using numerical methods It was attempted in the present work to solve the existing model to obtain the final results using numerical methods through a MATLAB program. While solving that equation by using numerical methods, results of the solved equation are imaginary and do not have reasonable values. Hence, a modified approach was developed based purely on the geometry of the part to predict the final diameter of part turned using AWJ.

4.2.2 Modified approach: From the geometry

$$\cos\alpha = \left(\frac{r_i-\delta}{r}\right)$$

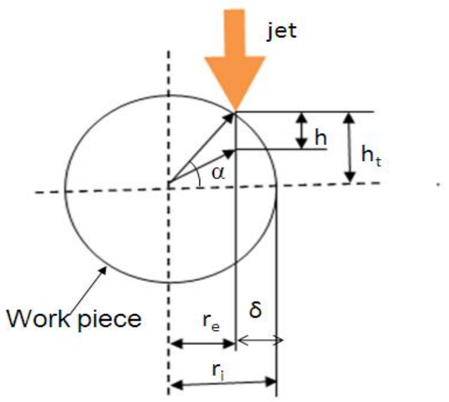

$$\sin\alpha = \left(\frac{h_t-h}{r}\right)$$

$$r^2 = (r_i-\delta)^2 + (h_t-h)^2$$

$$r^2 = (r_i-\delta)^2 + \left\{\left[r_i^2-(r_i-\delta)^2\right]^{1/2} - h\right\}^2$$

$$h_t = \left(r_i^2-(r_i-\delta)^2\right)^{1/2}$$

Fig.4.1 Work piece geometry

$$r^2 = (r_i-\delta)^2 + (h_t-h)^2$$

so,

$$r^2 = (r_i-\delta)^2 + \left\{\left[r_i^2-(r_i-\delta)^2\right]^{1/2} - h\right\}^2$$

,By solving

$$r = \left(r_i^2 - 2hh_t + h^2\right)^{1/2}$$

Differentiating above eqn. so

$$dr = \frac{(h-h_t)}{\left(r_i^2-2hh_t+h^2\right)^{1/2}}dh$$

Elemental volume removal rate (from the geometry):

$$d\dot{v} = -2\pi r(dr)u$$

$$d\dot{v} = 2\pi(h_t-h)udh$$

When solving above eqn., the result is quartic

$$Ah^4 + Bh^3 + Ch^2 + Dh + E = 0 \qquad \text{(I)}$$

Where

$$A = 1 \qquad B = -\left(4h_t\right)$$

$$C = \left(4h_t^2 + r_i^2\right) \qquad D = -\left(2h_t r_i^2 + 2Kr_e\right) \qquad r_e = r_i - \delta$$

$$E = \left(3Kr_e^2 + 2Kr_e h_t\right) \qquad K = \frac{m_a v_a^2}{8\sigma\pi u}$$

4.3 MODELING OF KERF GEOMETRY. In the previous chapter, it was seen that modified approach was discarded. In order to estimate the volume of material removed, previous works (Manu & Ramesh Babu) [4] assumed kerf profile to be rectangular. Analysis of kerf profile using optical profile projector showed that this is not true. The purpose of this work is to develop an approach for predicting the overall geometry of kerf turned with AWJs. Since the geometry of kerf depends on several process parameters such as water pressure, abrasive mass flow rate and jet traverse rate, it is essential to consider all these parameters for developing suitable relations for predicting the kerf geometry.

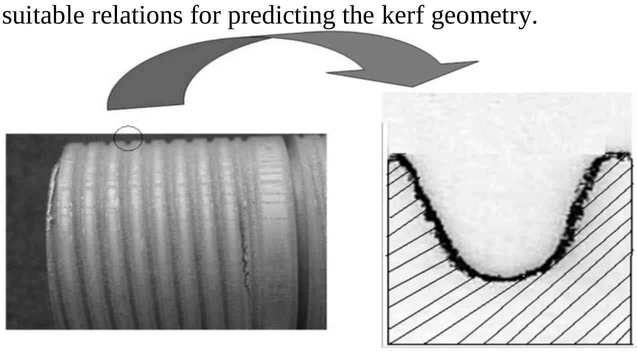

Fig. 4.3 Kerf profile got from optical profile projector

4.5 PREDICTION OF KERF PROFILE . To predict the shape of kerf produced by AWJ traversed over the work material, the proposed analysis first considers a uniform distribution of energy in the jet to predict the kerf shape and then introduces a function to obtain the kerf shape with non-uniform distribution of energy in the jet.

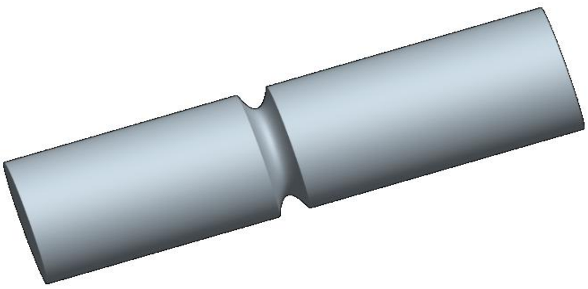

Fig. 4.4 Sschematic diagram showing the kerf formation in abrasive water jet turning

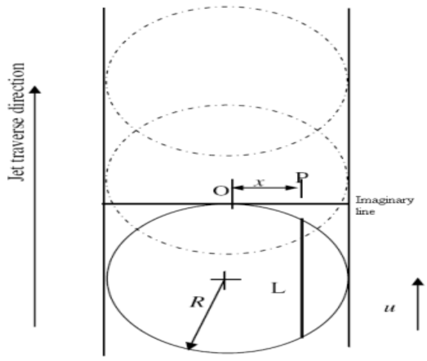

Fig. 4.5 Jet moving on imaginary line L\

4.5.1 Uniform distribution of energy: Kerf profile produced on the material with AWJ having uniform distribution of energy can be determined with the above relation. By substituting x= 0 and x = R, one can determine the maximum and minimum depth of kerf at the center and at the edges and are given by

$$h_i(0) = \frac{2k_i}{s} R \qquad (4.3)$$

$$h_i(R) = 0$$

For uniform distribution of energy across the jet, Kerf shape showing depth *hi*(*x*) at a distance x

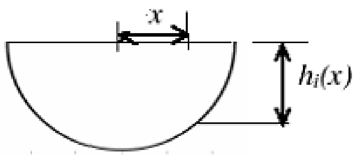

Fig. 4.6 kerf shape for uniform distribution of energy across the jet

4.5.2 Non-Uniform distribution of energy: Let the EI is the rate of energy per unit area per unit time at any radius r in the cross section of the jet. E_{max} is the maximum rate of energy per unit area per unit time in the cross section of jet. Let the variation in the energy of the jet over its cross section be represented by a function fI

$$f(r) = \frac{\dot{E}(r)}{\dot{E}_{max}} \qquad (4.4)$$

The value of fI varies from 0 to 1 from the periphery to center of the jet

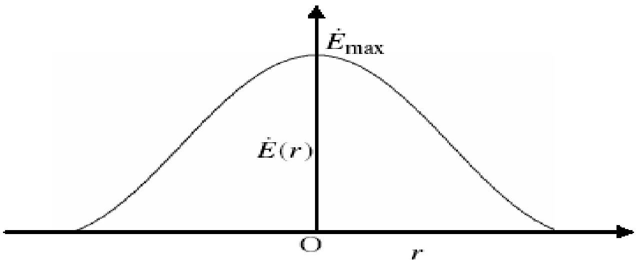

Fig. 4.7 Distribution of energy in abrasive water jet having non-uniform energy distribution

V. FIGURES AND TABLES

To develop these relations, AWJ having non-uniform energy distribution was considered. In fact, the energy distribution in the jet is non-uniform and is the resultant of the bell shaped distribution of velocity in the jet. The present work considers different non-uniform distributions while developing the relation for predicting the kerf shape produced by AWJs. By comparing the predicted shape of kerf with the shape of kerf observed from the experiments, the function that represents the distribution of energy in the jet was chosen. After identifying the distribution of energy in the jet, this particular jet produces a kerf on a particular material. The width of kerf is considered as the effective diameter of jet that interacts with material in generating kerf. This chapter covers the predicted results, discussion validation.

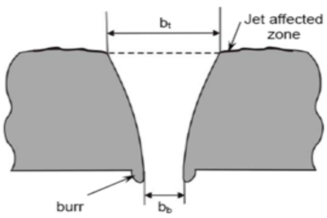

Schematic of AWJM kerf

5.2 SELECTION OF ENERGY DISTRIBUTION FUNCTION IN THE JET

Here function meansthe variation in the energy of the jet over its cross section be represented by a function f(r). To determine the function f(r), various distributions such as Gaussian, exponential, sine and cosine functions were considered to predict the kerf shape. As it is important to know the distribution of energy in the jet for developing the relations for predicting the geometry of kerf, the distribution of energy in the jet was identified by comparing the kerf observed on the material with the kerf predicted with different distributions. As explained earlier, a set of experiments were conducted to produce kerf on work material at various surface speeds, for the purpose of comparing these kerf profiles with the kerf predicted using the various functions (*f*(*r*)) like sine, cosine and exponential functions for representing the non-uniform variation of energy in the jet.The function *f*(*r*) is chosen in such a way that the predicted kerf profile is closest to observed kerf profile. The simulation experiments were conducted by varying the surface speeds 1000mm/s, 2000 mm/s, 3000 mm/s, 4000 mm/s. The different functions that were chosen to represent the energy distribution are given in table below.Profiles with the kerf predicted using the various functions (*f*(*r*)) like sine, cosine and exponential functions for representing the non-uniform variation of energy in the jet.The function *f*(*r*) is chosen in such a way that the predicted kerf profile is closest to observed kerf profile. The simulation experiments were conducted by varying the surface speeds 1000mm/s, 2000 mm/s, 3000 mm/s, 4000 mm/s. The different functions that were chosen to represent the energy distribution are given in table below

Distribution	**Function f(r)**
Sine	(1-sin(πr/2R))
Exponential	(1-exp((r/R)-1))
Cosine	0.5* (1+cos (πr/R)

.By substituting the above functions in equation (3.16) and then integrating that equation, the height of kerf at any point on the kerf can be determined. A MATLAB program was written for predicting the kerf profile and finding the area under the kerf for each function.

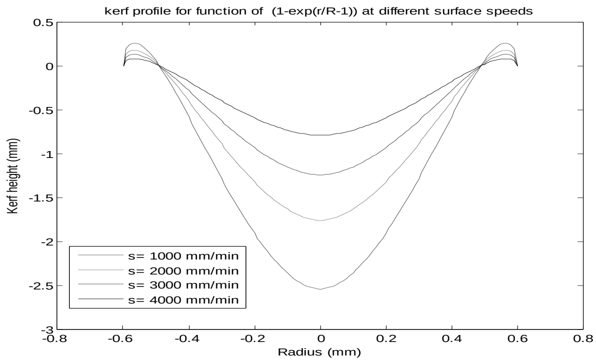

$$\left(1-e^{((r/R)-1)}\right)$$

the kerf profile generated using exponential function $\left(1-e^{((r/R)-1)}\right)$ It can be seen that in some region the profile depth is taking a positive depth, whereas the kerf profile depth must be negative

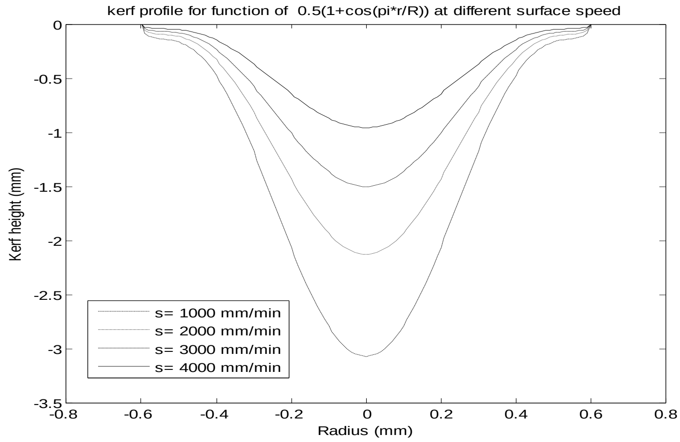

$$0.5\times\left(1+\cos\left(\pi r/R\right)\right)$$

Profile comparison for function at different traverse rate presented the profiles obtained using cosine and sine functions respectively. It can be seen that profiles are similar to observed kef profiles. Here also max. depth of kerf decrease with increase in surface speed. Profile shown in Figs 5.2, 5.3 and 5.4 satisfy the boundary condition i.e at the centre of the jet (radius =0) kerf height is maximum and at the extreme ends of the jet (radius =R and radius = -R) kerf height is zero.

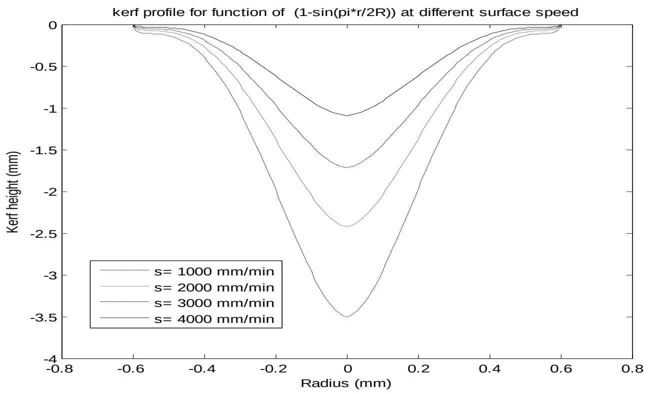

$$\left(1-\sin\left(\pi r/2R\right)\right)$$

Fig. 5.4 Profile comparison for function $\left(1-\sin\left(\pi r/2R\right)\right)$ at different traverse rate

Fig.5.5 Profile comparison for 3 functions

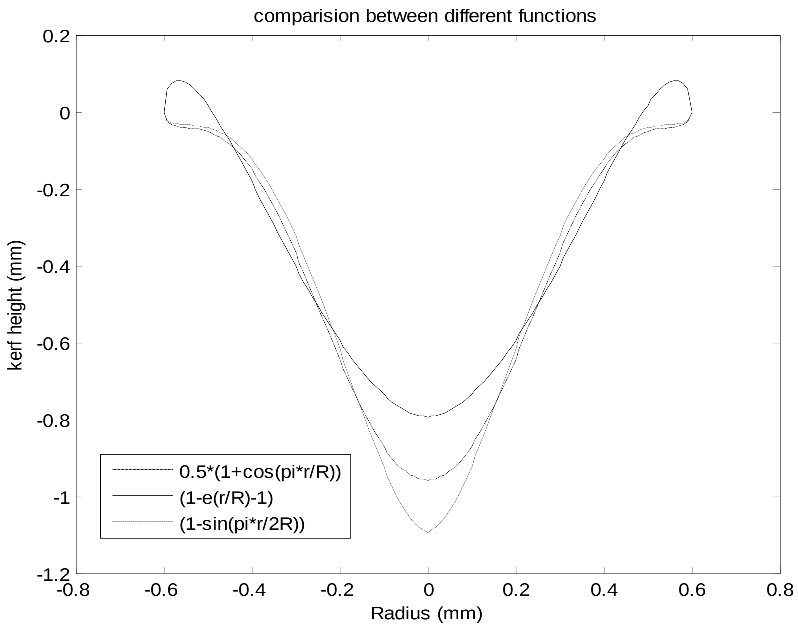

Fig. 5.5 presented the comparison of the 3 profiles obtained using 3 different distribution functions. In order to selected the most suitable one to represent the actual kerf profile , the area under each profile is compared with the actual area of the kerf. Here the atual area of the kerf is taken from the 'kerf shape drawn with optical profile projector'. That profile is redrawn on graph paper and the area obtained by counting the no. of units inside the kerf. Where as area for the particular function is obtained directly from the MATLAB program.

	Functions			
Surface speed (mm/min)	**0.5*(1+ cos(□r/R))**	**1-sin(□r/2*R))**	**1-e$^{((r/R)-1)}$**	**Actual**
s = 4000	0.5152	0.5166	0.4512	0.5600
s = 3000	0.8082	0.8104	0.7078	0.9220
s = 2000	1.1444	1.1482	1.0102	1.1684
s = 1000	1.6532	1.6576	1.4478	1.6320

Table 5.2 Comparison of kerf area in mm^2

From the table 4.2 it can be seen that sine function is closest to actual area of the kerf. So the sine function is considered as energy distribution function in the jet. By substituting the sine function in eqn. (3.16). Final equation for the Kerf profile depth at any distance x from the center of kerf is obtained as

$$h(x)=$$

$$\frac{\pi}{R^2(\pi^2-8)}0.5\times M v_a^2 \frac{1}{\varepsilon s} * f(\theta) \int_{-\sqrt{R^2-x^2}}^{\sqrt{R^2-x^2}} \left(1-\sin\left(\pi\sqrt{(x^2+y^2)}\Big/_{2R}\right)\right) dy \qquad (5.1)$$

Table 5.3 Error unpredicted kerf area for selected function

	Functions		
Surface speed (mm/min)	**1-sin(□r/2*R))**	**Actual**	**Error (%)**
s = 4000	0.5166	0.5600	-7.75
s = 3000	0.8104	0.9220	-12.104
s = 2000	1.1482	1.1684	-1.73
s = 1000	1.6576	1.6320	1.57

VI. CONCLUSION

- In the present work, a new approach to predict the kerf geometry in Abrasive Water Jet Turning has been developed.
- The nature of interaction of jet with material and the material removal from part surface could be represented using Finnie's theory of erosion.
- The energy distribution in the jet has been used as the basis for predicting the kerf geometry.
- Among the various distributions considered, the sine function was found to represent the variation of energy in the abrasive water jet very well, predicting the kerf shape close to the observed shape.
- The predicted maximum depth of kerf was in turn used to estimate the final diameter of turned part under various process parameter combinations.
- The final diameters predicted using this approach were in agreement ($R^2 = 0.94$) with experimental results from literature.

FUTURE WORK

- Modification of the developed model employing other theories of erosion
- Employing other functions for representing kerf profile
- Modeling of AWJT of brittle materials.
- Modeling of AWJT using FEM.

REFERENCES

[1.] Hualui, *A Study of the cutting performance in Abrasive Water jet Contouring of Alumina Ceramics and Associated Jet Dynamic Characteristics*, Ph. D thesis, (Queensland University of Technology) .

[2.] Ajmal I Ansari , Mohamed Hashish, *On the modeling of abrasive water jet turning*, Jet Cutting Technology, edited by A. Lichtarowicz, Proceedings of the Published by Kluwer Academic Publishers, Dordrecht, Nethelands, 1992, pp.555-576.

[3.] N. Prasankumar ,*Modeling and analysis of pockets milled with abrasive water jet*, M.S Thesis, (IIT Madras) .

[4.] R. Manu and N. Ramesh Babu, *Estimation of Process Parameters in Abrasive Water Jet Turning of Parts*, Tehran International Congress on Manufacturing Engineering (TICME2005) December 12-15, 2005, Tehran, Iran.

[5.] Hashish M (1998) Water jet advances in field and factory. Proceedings of 5th Pacific Rim International Conference on Water jet Technology, New Delhi, India 231-246

[6.] Hashish M (1984) A modeling study of metal cutting with abrasive water jets. Transactions of ASME Journal of Engineering for Industry 106:88-100

[7.] Louis H (1998) Abrasive water jets: A Review. Proceedings of 5th Pacific Rim International Conference on water jet technology, New Delhi, India 321-329

[8.] Momber A, Kovacevic R (1988) Principles of abrasive water jet machining. Springer-Verlag, London

[9.] Hashish M (1991) Optimization factors in abrasive water jet machining. Transactions of ASME Journal of Engineering for Industry 113:29-37

[10.] Momber A. Pfeiffer, Kovacevic R, Schunemann (1996) The Influence of abrasive grain size distribution parameters on the abrasive water jet machining process. Proceedings of the 1996 24th NAMR1 conference, Society of Manufacturing Engineers MR96 (115): 1-6

[11.] Member A, Kovacevic R (2000) Particle size distribution influence in high speed erosion of aluminum. Particle Science and Technology 18:199-212

[12.] Labus T, Neusen K, Alberts D, Gores T (1991) Factors influencing the particle size distribution in an abrasive water jet. Transactions of the ASME, Journal of Engineering for Industry 113:402-411

[13.] KrishnaiahChetty OV, Ramesh Babu N (1999) some investigations on abrasives in abrasives water jet machining. Proceeding of 10th American waterjet conference, Waterjet Technology Association, USA: 419-430

[14.] KanthaBabu M, KrishnalahChetty OV (2001) Studies on the use of local abrasives in abrasive waterjet machining. Proceedings of 17th International conference on CAD/CAM, Robotics and Factories of Future, Durban, South Africa: 150—156

[15.] KanthaBabu M, KrishnaiahChetty OV (2001) Abrasive water jet machining of aluminium with local abrasives. Proceedings of 1 lth American Water Jet Conference, Water Jet Technology Association, Minneapolis, USA: 325-341

[16.] Guo N, Louis H, Meier G, Ohlsen J (1992) Recycling capacity of abrasives in Abrasive Water Jet cutting. Proceedings of 1 lth International conference on Jet Cutting Technology, Scotland 503-523

[17.] Hashish M (1989) A model for abrasive water jet machining. Transactions of the ASME, Journal of Engineering Materials and Technology 111:154—162

[18.] Matsumoto K, Arasawa H, Yamaguchi S (1998) A study of the effect of abrasive material on cutting with abrasive water jet. Proceedings of 9th International symposium of jet cutting technology, Sendal, Japan 255-269

[19.] KanthaBabu M, KrishnaiahChetty OV (2002) Studies on recharging of abrasives in abrasive waterjet machining. International Journal of Advanced Manufacturing Technology, Springer-Verlag, London 19:697-703

[20.] KanthaBabu M, KrishnaiahChetty OV (2003) A study on recycling of abrasives in abrasive waterjet machining. International Journal of Wear, Elsevier Science, Ireland 254:763-773

[21.] KanthaBabu M, KrishnaiahChetty OV (2003) Studies on abrasive water jet machining of black granite through design of experiment. International Journal of Experimental Techniques, September: 49-54

International Journal of Modern Engineering Research (IJMER)
www.ijmer.com Vol. 3, Issue. 5, Sep - Oct. 2013 pp-3216-3224 ISSN: 2249-6645

Design, Simulation and Implementation of Flyback based, True Single Stage, Isolated, Power Factor Corrected AC-DC Converter for Solar Array Simulators

Gowrishankara C.K.[1], Gaurav Yadav[2], Chandan S.[3]
[1,2]*Spacecraft Checkout Group*
ISRO Satellite Centre, Bangalore-560 017
[3]*St. Joseph Engineering College- Mangalore*

ABSTRACT*: Presently most of the Power Factor correction circuits are based on boost topology. They consist of two stages, one being the power factor correction (pre-regulator) and later DC-DC conversion stage. This paper presents the design of a true single stage, isolated, power factor corrected, 110V-3.5A AC-DC converter as front end of Solar Array Simulators [7]. Flyback topology is used to achieve power factor correction as well as DC regulation in single step, and thus it simplifies two stage structure down to single stage. Single stage power factor corrected AC-DC converter has many advantages in term of cost and power density.*

Keywords: *Power factor, AC-DC Converter, Solar Array Simulator, Harmonics*

I. INTRODUCTION

Power can be divided mainly into 3 forms:-
1. **True Power** which is measured in Watts and it is a function of dissipative elements (R).
2. **Reactive Power** which is measured in VAR and it is a function of reactive elements (X).
3. **Apparent Power** which is measured in VA and it is a function of total impedance (Z).

Power factor is a dimensionless quantity which can be defined as the ratio of the real power flowing to the load to the apparent power input to the circuit. More physically, power factor measures how efficiently the current is being converted into real power. For eg. A circuit with power factor of 0.7, the apparent power required by the circuit will be 1.4 times the real power used by the load.

Power simulators required in any satellite checkout are Battery simulators, Battery chargers and Solar Array Simulators. All these power simulators use front end AC-DC converters. If conventional AC-DC converters are used, their power factor will be poor and associated problems like current spikes which lead to imminent EMI/EMC problems.

From the instrumentation point of view, the term power factor basically consists of two components namely [2]
1. Displacement Power Factor (DPF).
2. Harmonic Power factor(HPF)

The True Power Factor (TPF) of any system is product of both of them.

TPF = DPF * HPF

Presently, boost converter based Power Factor Corrected (PFC) AC-DC converters are popular, whose block diagram [2] is shown in figure-1

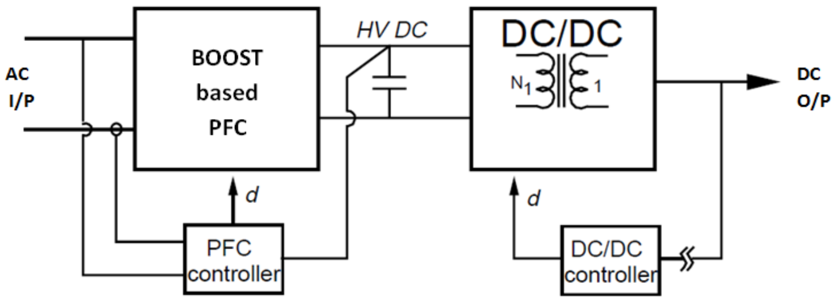

Fig. 1 Conventional two-stage AC-DC Converter

The paper presents the design, simulation and hardware implementation of true single stage, isolated PFC AC-DC converter. Flyback converter is used to simplify the two stage front end design to a single isolated PFC conversion stage, by integrating the PFC stage with the DC-DC conversion stage. Additionally the isolation is inherent to fly back converter. The single stage fly-back PFC design offers the following advantages:-
1. Reduction in component count and size.
2. Inherent isolation in the design.

Basic conceptual block diagram of the single stage is shown in figure-2

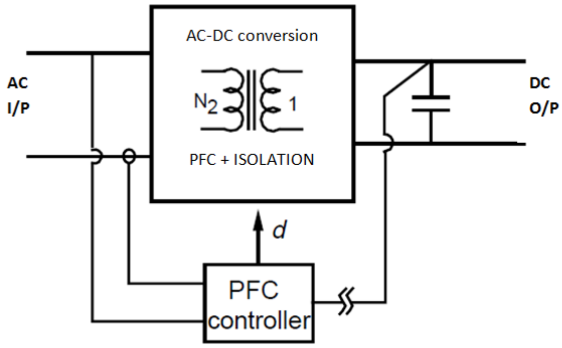

Fig. 2 Conceptual block diagram of single stage AC-DC converter

II. SINGLE STAGE ARCHITECTURE

The single stage architecture is divided into two parts:-

1. O/P Voltage regulation Loop :-

This loop is an outer loop which maintains DC output voltage. It sets the reference for the inner current loop by multiplying the output of the first loop with incoming scaled down sinusoidal signal. A linear isolator is used to isolate the feedback (Output voltage) from the secondary ground. A isolated feedback voltage and reference is fed to the error amplifier, which generates error signal. The variation in the outer loop changes the magnitude of the current drawn from the mains.

2. Power factor correction and current loop :-

The inner control loop is the one, which implements Power factor correction and output voltage control, by modulating the ON and OFF times of the semiconductor switch. The reference for this loop is from the multiplier. The current feedback is derived from a current sense resistor which is in series with line of AC supply. The magnitude of the multiplier output will decide magnitude of the line current and the shape of the multiplier output will dictate the phase and shaping of the line current.

Functional block diagram of single stage AC-DC converter architecture is shown in figure 3

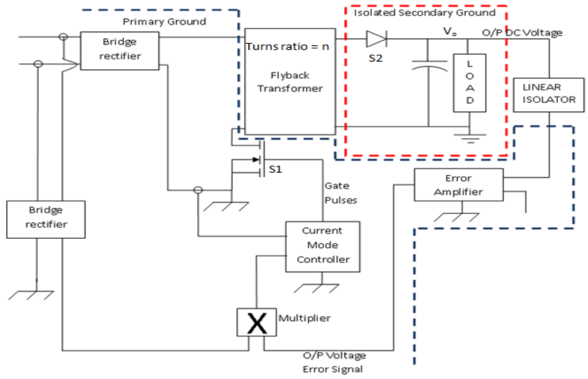

Fig. 3 Functional block diagram of single stage, flyback converter based AC-DC converter

III. DESIGN REQUIREMENTS

Design inputs:

1. Input AC voltage : 230V ± 10%.
2. Input AC Frequency : 50 ± 2 HZ.
3. Output ripple Voltage : 1V.
4. Output Voltage (Vo) : 110V DC.
1. Output Current : 0.5 – 3.5A DC.
2. Switching Frequency : 20KHz
3. No. of Stages : Single Stage

Determination of Fly-back transformer turns ratio:

The optimum turns ratio of fly-back transformer is selected considering the voltage stress on switches S1 and S2 (refer figure 3).

Let Vs1 be the voltage stress on switch S1 (MOSFET) placed on the primary side. It consists of two terms,

1. Vin max
2. Reflection of output voltage on the primary side which can be given by (Vo/n)

Thus voltage stress on switch S1 can be given as

$$Vs1 = Vin\ max + \left(\frac{Vo}{n}\right), \text{----------------------} (1)$$

Where,

V_{S1} is the voltage across the MOSFET,
$V_{in\ max}$ is the maximum input voltage to the chopper,
Vo is the output DC voltage,
n = (N_2/N_1)Turns ratio of fly-back transformer/coupled inductor
Similarly, let Vs2 be the voltage stress on the switch S2 (diode) placed on the secondary side, and it is given as

$$Vs2 = Vo + (Vin\ max * n) \text{, ----------------------------- (2)}$$

Where,
$V_{s2} \rightarrow$ Reverse voltage stress (PIV) across the secondary rectifier diode
Using the above equations the computed values of voltage stress is given in the table below.

Stress on switch S1 Vs1(V)	**Stress on switch S1 Vs2(V)**	**Total stress (Vs1 + Vs2) (V)**	**N2/ N1**
907.8	181.6	1089.4	0.2
724.4	217.3	941.7	0.3
632.7	253.2	885.9	0.4
577.7	288.9	866.6	0.5
541.1	324.7	865.8	0.6
514.9	360.5	875.4	0.7
495.3	396.2	891.5	0.8
480	432.0	912	0.9
467.7	467.8	935.5	1

Table 1 Voltage Stress on S1 (MOSFET) and S2 (Diode)

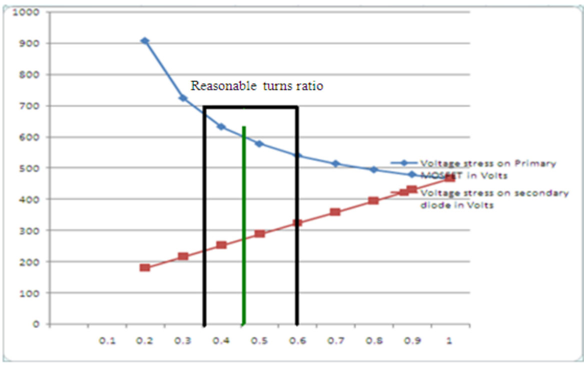

Fig. 4 Stress Vs Turns Ratio

Figure 4 shows the stress on individual semiconductor switches. It can be noted that the stress on S1 (primary MOSFET) reduces exponentially turns ratio. Whereas the stress on S2 (output diode) increases linearly with turns ratio. Table 4 shows the total stress (Vs1 + Vs2) is minimum for turns ratio of 0.4 to 0.6. Thus based on simplicity of design, n = 0.5 is chosen.

Calculation of Minimum Duty cycle (Dmin):
We have

$$Vo = n * Vin\ max * \left(\frac{D}{1-D}\right) \text{--------------------- (3)}$$

At maximum input AC voltage duty cycle will be minimum, therefore from eq. (3) we can have

$$Vo = \left[n * Vin\ max * \left(\frac{Dmin}{1 - Dmin}\right)\right]$$

$$110 = \left[0.5 * 253 * \left(\frac{Dmin}{1 - Dmin}\right)\right]$$

We get D*min* = 0.464 or 46.4%
Therefore minimum duty cycle is 46% i.e. $[(50 * 10^{-6}) * 0.464] = 0.23\mu s.$

Determining the value of the primary inductance (Lp) and secondary Inductance of fly-back transformer (Ls)
We have,

$$L_p = \frac{V_o * D}{\Delta I_L * f_s} \text{ --- (4)}$$

Where,
$L_p \rightarrow$ Primary inductance

$V_0 \rightarrow$ Output DC voltage
$\Delta I_l \rightarrow$ Output ripple DC current
$f_s \rightarrow$ Switching Frequency
Therefore the value of the primary inductance will be

$$L_p = \frac{110 * 0.464}{0.5 * 20 * 10^3}$$

$L_p = 5.104$ mH.

For secondary inductance
We have the relation,

$$\frac{N_1}{N_2} = \sqrt{\frac{L_P}{L_S}}$$

$$L_S = L_P * \left(\frac{N_1}{N_2}\right)^2$$

$$L_S = 2.552 \text{ mH.}$$

Calculation of the primary peak current and secondary peak current:
Secondary current:

We have the relation,

$$I_0 = \left(\frac{I_{S-} + I_{S+}}{2}\right) * (1 - D) \text{------------------------------ (5)}$$

Substituting the values of the corresponding terms we get,

$$3.5 = \left(\frac{I_{S-} + I_{S+}}{2}\right) * (1 - 0.46)$$

Thus,

$$(I_{S-} + I_{S+}) = 12.96 \text{ A.} \text{---------------------------------- (6)}$$

Equating the energy stored in the inductor we get,

$$P_O * T_S = \left(\frac{1}{2}\right) * L_S({I_{S+}}^2 - {I_{S-}}^2)$$

Substituting the values we get,

$$770 * 50 * 10^{-6} = 2.552 * 10^{-3} * 12.96 * (I_{S+} - I_{S-})$$

On solving the above equation we get,

$$(I_{S+} - I_{S-}) = 1.164 \text{ A.} \text{---------------------------------- (7)}$$

We also have the relation,

$$I_{S+} = \left(\frac{I_O}{1 - D}\right) + \left(\frac{V_O * (1 - D)}{2 * L_S * f_S}\right)$$

And

$$I_{S-} = \left(\frac{I_O}{1 - D}\right) - \left(\frac{V_O * (1 - D)}{2 * L_S * f_S}\right)$$

Solving eq. (5), (6), (7) , we get,

$$I_{S+} = 7.069 \text{ A.} \text{-- (8)}$$

$$I_{S-} = 5.891 \text{ A.} \text{-- (9)}$$

Similarly for primary current we have,

$$I_{P+} - I_{P-} = \left(\frac{V_I * D}{L_P * f_S}\right) \text{------------------------------------ (10)}$$

Substituting the values we will get,

$$I_{P+} - I_{P-} = 1.14 \text{ A} \text{------------------------------------ (11)}$$

Again equating the energy stored in the inductor we get,

$$P_O * T_S = \left(\frac{1}{2}\right) * L_P * (I_{P+} - I_{P-}) * (I_{P+} + I_{P-})$$

Thus we get

$$(I_{P+} + I_{P-}) = 6.616\ A \quad (12)$$

For input current we have,

$$I_{in} = \left(\frac{I_{P+} + I_{P-}}{2}\right) * D$$

Thus, solving eq. (8), (9), (10)

$$I_{in} = 1.521\ A.$$

$$I_{P+} = \left(\frac{I_{in}}{D}\right) + \left(\frac{V_i * D}{2L_p * f_s}\right)$$

$$I_{P+} = \left(\frac{1.521}{0.46}\right) + \left(\frac{253 * 0.46}{2 * 5.104 * 10^{-3} * 20 * 10^{3}}\right)$$

$$I_{P+} = 3.876\ A. \quad (13)$$

$$I_{P-} = \left(\frac{I_{in}}{D}\right) - \left(\frac{V_i * D}{2L_p * f_s}\right)$$

$$I_{P-} = \left(\frac{1.521}{0.46}\right) - \left(\frac{253 * 0.46}{2 * 5.104 * 10^{-3} * 20 * 10^{3}}\right)$$

$$I_{P-} = 2.736\ A. \quad (14)$$

Calculation of output filter capacitance (Co):

Using the specification of the output voltage ripple we can calculate output capacitance(Co),

$$C_o = \frac{I_o * (1 - D)}{\Delta V_o * f_s}$$

Substituting the values we get,

$$C_o = \frac{3.5 * (1 - .46)}{0.3 * 20 * 10^{3}}$$

$$C_o = 31.5\ mF$$

IV. SIMULATION

The proposed circuit topology is simulated in SIMULINK/MATLAB. The figure 5 below shows the simulink model of single stage fly back PFC circuit with simple ON-OFF control. The results are shown in the subsequent figures. The Total Harmonic Distortion of the input current is also analyzed.

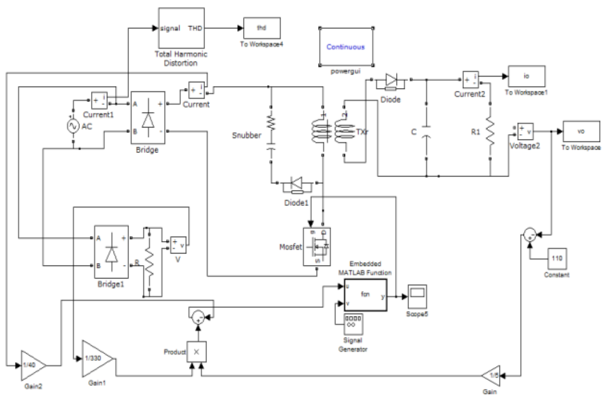

Fig. 5 SIMULINK Block diagram

V. SIMULATION RESULTS

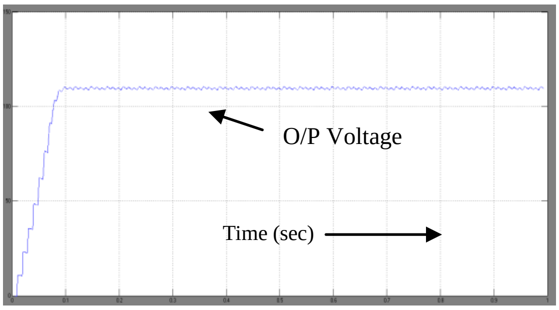

Fig. 6 O/P Voltage

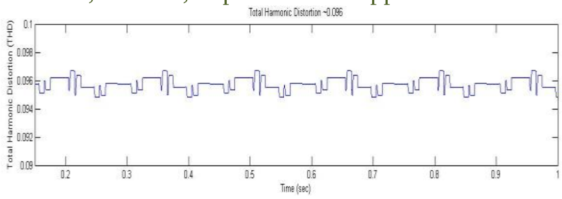

Fig. 7 Total Harmonic Distorion (THD)

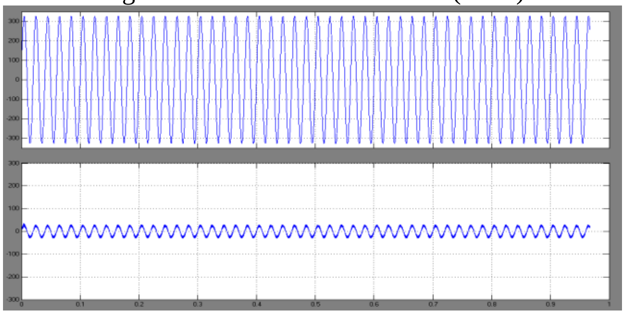

Fig. 8 I/P voltage and I/P current

VI. HARDWARE RESULTS

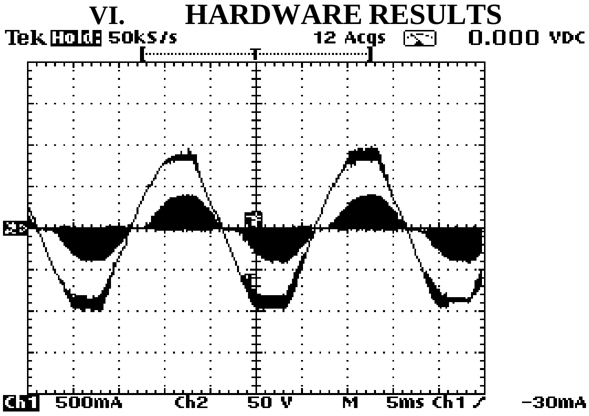

Fig. 9 (a) Open Loop Output of the flyback converter

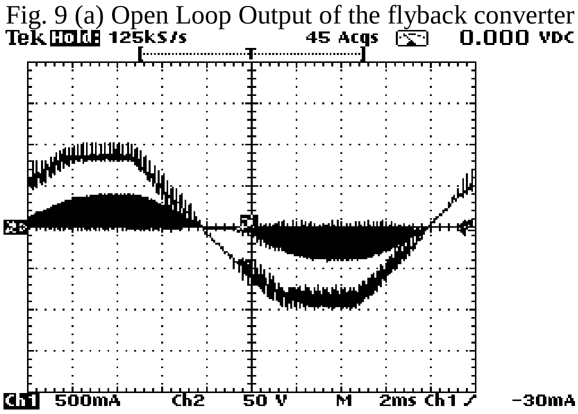

Fig. 9(b) Open Loop Output zoomed

Figure 9 (a)&(b) show the open loop output of the flyback converter. It is observed that the current is delayed w.r.t voltage by around 1.8milisecond which corresponds to a Displacement Power Factor of 0.87.

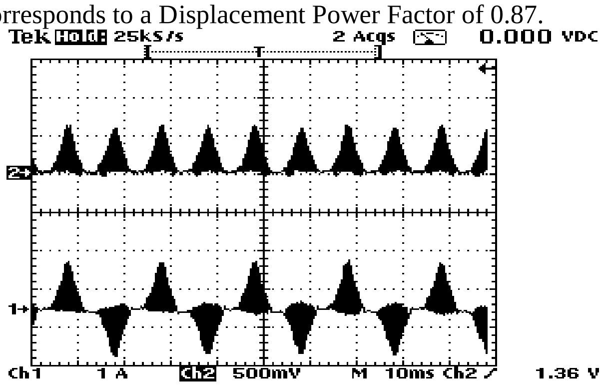

Fig. 10 Input current reference

In the above figure 10, channel 1 shows the actual input current and channel 2 shows the input current reference to the current mode controller IC.

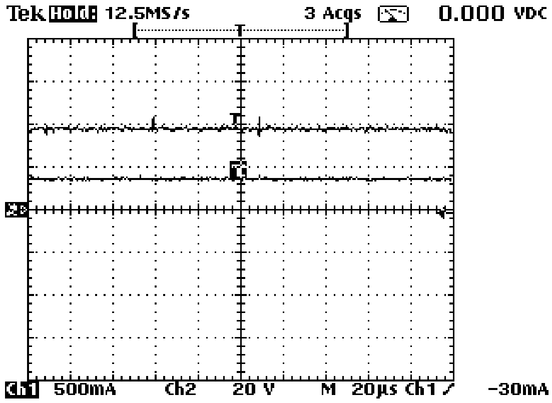

Fig. 11 Output voltage and current

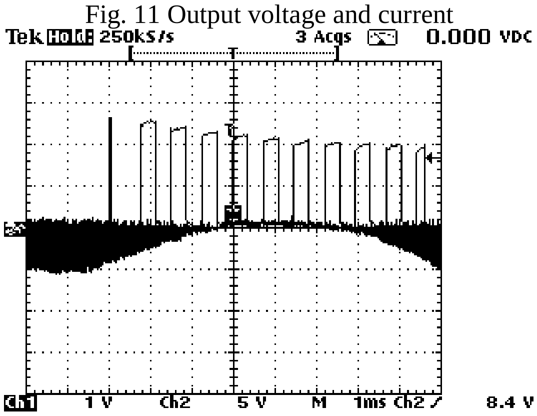

Fig. 12 Duty cycle variation with current feedback

Figure 12 shows the variation of the PWM duty cycle variation with respect to the input current variation. It is observer that at lower current the duty cycle is maximum and it reduces as the current reference becomes higher.

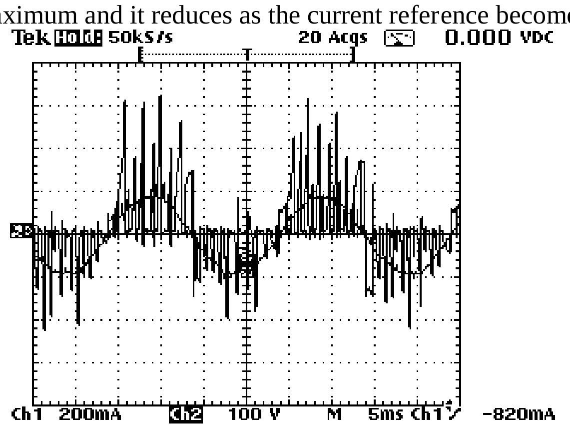

Fig. 13 Input current vs Input voltage

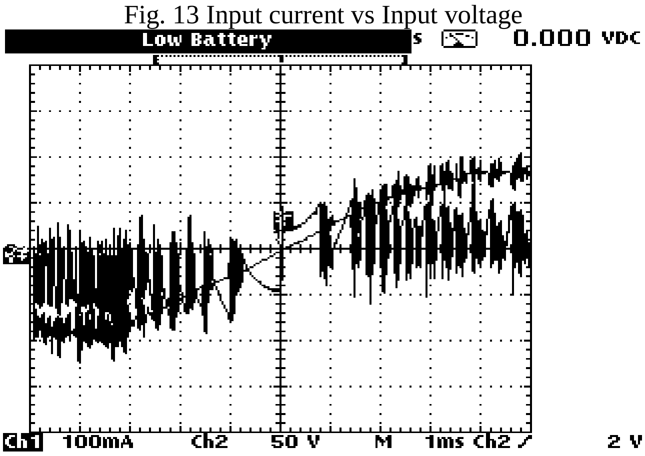

Fig. 14 Displacement between I/P current and I/P voltage

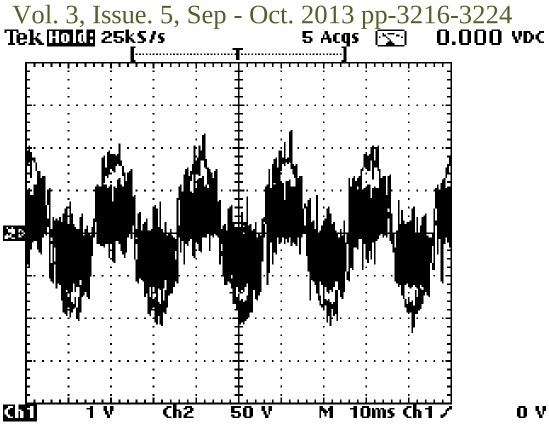

Fig. 15 I/P voltage vs I/P current

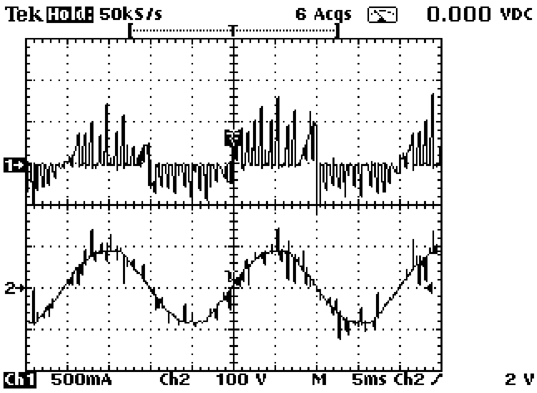

Fig. 16 I/P voltage vs I/P current

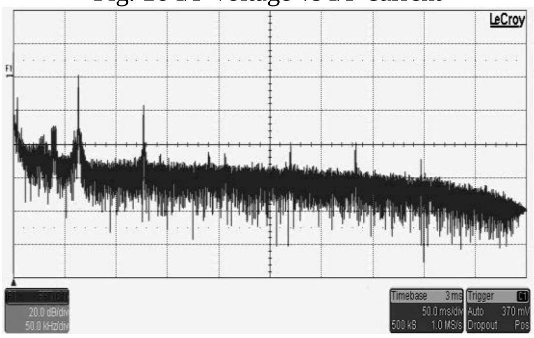

Fig. 17 FFT of the I/P current (switching component)

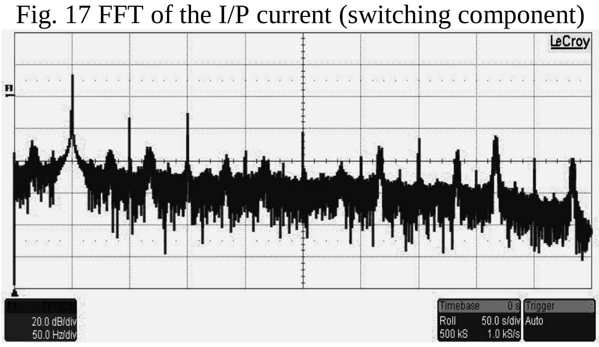

Fig. 18 FFT of the I/P current (Fundamental and its components)

VII. DISCUSSION

Simulation results shows that the Displacement power factor of the circuit is equal to 0.99 and the Total harmonic distortion is near 0.09. Thus the Harmonic power factor (HPF) can be calculated as,

HPF = 1/[sqrt (1+ (THD^2))]

HPF = 0.995

Displacement Power Factor = 0.99

True Power Factor = 0.99*0.995 = 0.98

Practically, the displacement power factor is improved to 0.99. The figures 17 and 18 shows the FFT of the I/P current. From the FFT, the Total Harmonic distortion was found to be 1%.

Thus the Harmonic power factor was also improved to 0.99, which results in true power factor of 0.98.

VIII. CONCLUSION

The design of a true single stage, isolated, power factor corrected,110V-3.5A AC-DC is successfully completed and simulated using SIMULINK-MATLAB®. A power factor of 0.98 is achieved in simulation model.
Practically a single stage Power Factor Corrected 40V-2A AC-DC converter is designed and developed using suitable components and the displacement power factor was improved from 0.87 to 0.99. The harmonic power factor is also considerably improved. The final achieved power factor is 0.98 which is very close to unity.

ACKNOWLEDGMENT

The authors are thankful to K.B.A.R.Sarma, Group Director SCG, Usha Bhandiwad, Division Head, CSAD-SCG, N.Reviraj Section Head, GCS-3-GCD-SCG, ISAC Bangalore for their valuable support and encouragement for this work. Authors also wish to thank their section heads for their support during the work.

REFERENCES

[1] Ned Mohan, Tore M. Underland, William P. Robbins,"Power ElectronicsConverters, Applications and Design", Third Edition.
[2] M. H. Rashid, Power Electronics Handbook: Circuits, Devices and Applications, 2nd Edition, (Prentice Hall, 1993).
[3] L.Umanand, Power Electronics: essentials & Applications.
[4] R. Ridley, "Average small-signal analysis of the boost power factor correction circuit," Virginia Power Electronics Center Seminar, pp. 108-120, 1989.
[5] W. Tang, Y. Jiang, G.C.Hua and F.C.Lee, "Power Factor Correction With Flyback Converter Employing Charge Control", APEC Conf. Proc., 1993, pp. 293-298.
[6] W. Tang, F. C. Lee, R. Ridley and I. Cohen, "Charge control: modelling, analysis and design," IEEE Power Electronics Specialists Conference Record, pp. 503-511, 1992.
[7] Gowrishankara C.K. et al., "Advanced Solar Array Simulator," Journal of Spacecraft Technology

AUTHORS

[1]Gowrishankara.C.K. Project Manager SCOS-Hylas, Mainframe checkouts of GSAT-6, GSAT-14 & GSAT-11 Received M.E In Power Electronics from Bangalore University. He Joined SDSC-SHAR Centre and worked in the field of process instrumentation and Industrial electronics. Presently he is with ISRO Satellite Centre and working in the area of spacecraft checkout. His work areas include development of power and signal simulators for spacecraft testing, SMPS and Process-Instrumentation.

[2]Gaurav Yadav, Received B.Tech In Avionics from IIST, Trivandrum. He joined ISAC and working in the field of power electronics and spacecraft test instruments. His work areas include development of power simulators for spacecraft testing and Analog circuit design.

[3]Chandan S, is student of MTech (Power Electronics) from St. Joseph Engineering College- Mangalore. His interest areas include development of Switched Mode Power Supplies, PCB designing and analog circuit design.

A novel approach for performance parameter estimation of face recognition based on clustering, shape and corner detection

1.Smt.Minj Salen Kujur , 2.Prof. Prashant Jain,
Department of Electronics & Communication Engineering college Jabalpur

ABSTRACT: *The aim of this research is to solve face recognition problem in area of biometric by using CSC hybrid method. In our work first we make the cluster of face key points and parallely apply shape and corner method for detection boundary of face and the corner of face objects. Our work is performing both face identification and recognition on large face database. It is better than other previous work because our FAR, FRR and EER less than. Also we calculate the recognition time in our work.*

Keywords: *Face Recognition, Clustering, Shape Descriptor, Corner Detection, RGB Image, Image Processing, Color Model, Binary Image, 4-Connected Component.*

I. INTRODUCTION

Image of outdoor scenes are Now a day's face recognition is play very crucial role in recent technology like mostly companies are adopting the biometric identification for login but when images are degraded than the performance of our system is reduced. This study gives some idea about steps by steps face recognition algorithm how face is recognized but when quality of an image is degrade due to some noise or any external reason than matching process will not give accurate result for this reason we adopt some restoration and enhancement techniques like retinex theory for degrade image to improve quality for better performance in next part of my work.

Pattern recognition is the scientific discipline whose goal is the classification of *objects* into a number of categories or classes [1]. Depending on the application, these objects can be images or signal waveforms or any type of measurements that need to be classified. We will refer to these objects using the generic term *patterns*. Pattern recognition has a long history, but before the 1960s it was mostly the output of theoretical research in the area of statistics [6].

We have studied a face recognition system using the Principal Component Analysis (PCA) algorithm with Euclidean distance as a classifier and secondly Linear Discriminant Analysis (LDA) with Euclidean distance as a classifier. Face recognition systems try to find the identity of a given face image according to their memory. The memory of a face recognizer is generally simulated by a training set. Independent Component Analysis (ICA) is similar to PCA except that the distribution of the components is designed to be non-Gaussian. Maximizing non-Gaussianity promotes statistical independence.

The problem of face recognition can be stated as follows: Given still images or video of a scene, identifying one or more persons in the scene by using a stored database of faces [3]. The problem is mainly a classification problem. Training the face recognition system with images from the known individuals and classifying the newly coming test images into one of the classes is the main aspect of the face recognition systems.

II. FACE RECOGNITION

The face plays a major role in our social intercourse in conveying identity and emotion. Face Recognition (FR) [1,3] is a challenging task and has been one of the most successful applications of image analysis and understanding in many fields such as computer vision, pattern recognition. Image-based face recognition techniques can be divided into two groups according to the face representation which they use, which being the appearance-based approach and the feature-based approach, among which the appearance-based is more popular, that use holistic texture features [2,7]. With automatic face recognition there are many applications in human computer interaction, biometrics and security, etc. Over the decades, many computer systems that can recognize faces have been developed, some of which have been in commercial use. Generally, appearance-based face recognition techniques are finished with image matching in the space of compressed image. If image matching done in the original space, it will result in the curse of dimensionality in addition to the problems of large computational complexity and memory Face recognition has received considerable interest as a widely accepted biometric, because of the ease of collecting samples of a person, with or without subject's intension . Face recognition [10,11] refers to an automated or semi automated process of matching facial images. This type of technology constitutes a wide group of technologies which all work with face but use different Scanning techniques. Most common by far is 2D face recognition which is easier and less expensive compared to the other approaches.

There are four steps in face recognition process as shown in flow chart:

1. Acquiring a sample: In a complete, full implemented biometric system, a sensor takes an observation. The sensor might be a camera and the observation is a snapshot picture. In our system, a sensor will be ignored, and a 2D face picture [8, 11] "observation" will supplied manually.

2. Extracting Features: For this step, the relevant data is extracted from the predefined captured sample. This is can be done by the use of software where many algorithms are available. The outcome of this step is a biometric template which is a reduced set of data that represents the unique features of the enrolled user's face.

3. Comparison Templates: This depends on the application at hand. For identification purposes, this step will be a comparison between a given picture for the subject and all the biometric templates stored on a database. For verification, the biometric template of the claimed identity will be retrieved (either from a database or a storage medium presented by the subject) and this will be compared to a given picture.

4. Declaring a Match: The face recognition system will return a candidate match list of potential matches. In this case, the intervention of a human operator will be required in order to select the best fit from the candidate list. An illustrative analogy is that of a walk-through metal detector, where if a person causes the detector to beep, a human operator steps in and checks the person manually or with a hand-held detector.

III. PREVIOUS WORK

A. Facial-Image Acquisition

In our research, original images were obtained using a charge coupled devices (CCD) camera with image dimensions of 384×243 pixels encoded using 256 gray-scale levels.

In image acquisition, the subject sits 2.5 m away from a CCD camera. On each site of the camera, two 200-W lamps are placed at $30_{\circ}$ angles to the camera horizontally. The original images are shown in Fig. 1.

B. Lighting Compensation

We adjusted the locations of the lamps to change the lighting conditions. The total energy of an image is the sum of the squares of the intensity values. The average energy of all the face images in the database is calculated. Then, each face image is normalized to have energy equal to the average energy

$$\text{Energy} = \sum (\text{Intensity})_2. \qquad (1)$$

C. Facial-Region Extraction

We adopt the face-detection method presented in the method of detecting and extracting the facial features in a gray-scale image is divided into two stages. First, the possible human eye regions are detected by testing all the valley regions in an image. A pair of eye candidates is selected by means of the genetic algorithm to form a possible face candidate. In our method, a square block is used to represent the detected face region. Fig. 2 shows an example of a selected face region based on the location of an eye pair. The relationships between the eye pair and the face size are defined as follows:

$$h_{\text{face}} = 1.8 d_{\text{eye}}$$
$$h_{\text{eye}} = \frac{1}{5} h_{\text{face}}$$
$$w_{\text{eye}} = 0.225 h_{\text{face}}.$$

Then, the symmetrical measure of the face is calculated. The nose centerline (the perpendicular bisector of the line linking the two eyes) in each facial image is calculated. The difference between the left half and right half from the nose centerline of a face region should be small due to its symmetry. the symmetrical measure is less than a threshold value, the face candidate will be selected for further verification.

After measuring the symmetry of a face candidate, the existences of the different facial features are also verified. The positions of the facial features are verified by analyzing the projection of the face candidate region. The facial feature regions will exhibit a low value on the projection. A face region is divided into three parts, each of which contains the respective facial features. The y-projection is the average of gray-level intensities along each row of pixels in a window. In order to reduce the effect of the background in a face region, only the white windows, as shown in Fig. 3, are considered in computing the projections. The top window should contain the eyebrows and the eyes, the middle window should contain the nose, and the bottom window should contain the mouth. When a face candidate satisfies the aforementioned constraints, it will be extracted as a face region. The extracted face image is shown in Fig. 4.

D. Principal Component Analysis (PCA)

Let a pattern Z_i be a two-dimensional (2-D) $m \times m$ array of intensity values. A pattern may also be considered as a vector of dimension m^2. Denote the database of n patterns by $Z = (Z_1 Z_2 \ldots Z_n) \in \Re^{m^2 \times n}$. Define the covariance matrix as follows [4].

$$\Gamma = \frac{1}{n}\sum_{i=1}^{n}(Z_i - \bar{Z})(Z_i - \bar{Z})^T = \phi\phi^T$$

Proposed Work

We present the model of the our work is given below

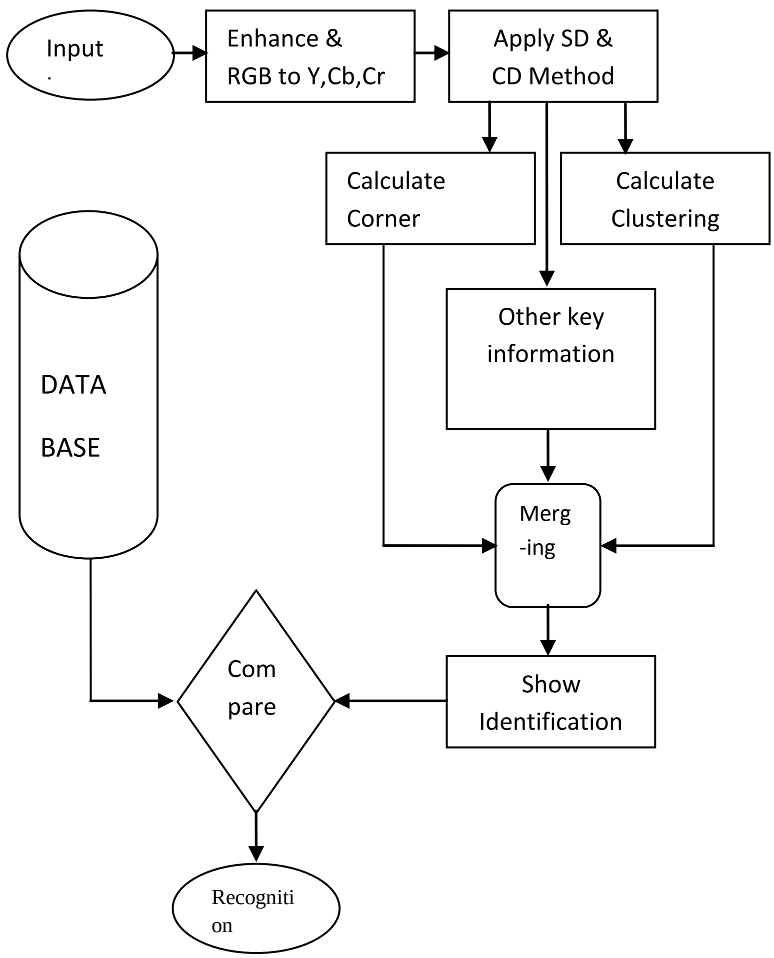

Algorithm

Step1. we take query image.

Step2. Image enhancement (Filtering)

Step3. Convert into Y, Cb, Cr model.

Step4. By this process (step 3), we get three picture of this query image (luminance, chrome blue & chrome red)

Step5. Then we apply shape discripter on luminance image.

Step6. Now we apply colour discripter on Cb(chrome blue) &Cr.

Step7. Merging of result no.5&6 steps.

Step7. By step 7 we detect the face.

Step8. Now we save the detected shape in variables (For subsequent analysis) c o m p l e t e

Step9. Prepare predefind database of 40 image.

Step10. Now we apply step 2-9 on prepare database image.

Step11. Now we apply C-Means clustering on step 9& step 10 (parallely)

Step12. If no. of clusters, clusters position, cluster size are same then show recognition done and also show recognize person name.

Step13. Determine no. of detected & no. of non face.Image will be count & then calculate FAR,FRR & EER.

IV. EXPERIMENTAL RESULT

Below figure show the GUI of our work, that getting the face image for analysis. Next figure calculate the only face of the face image. After that we apply our methodology on this query image and finally archive the matching face image, name of image person, clustering on face image and diagram of FAR,FRR.

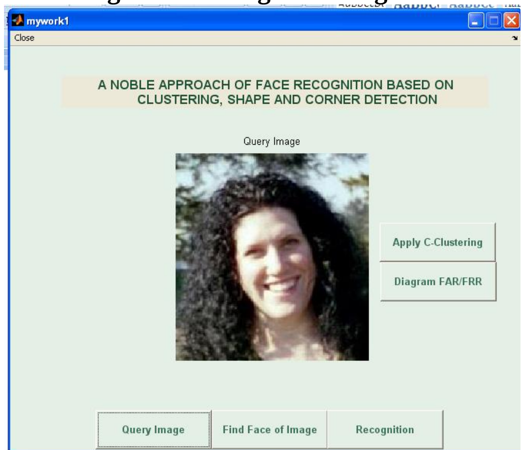

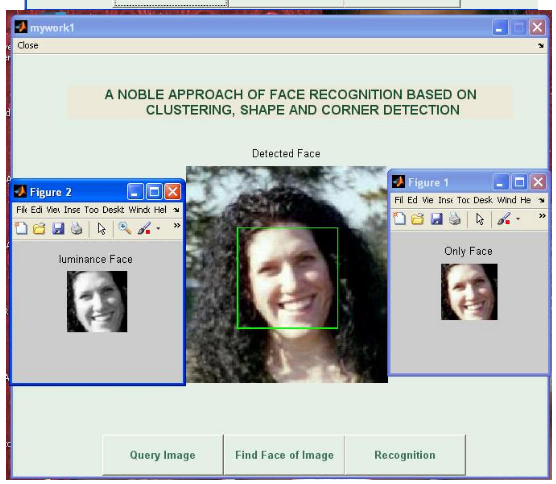

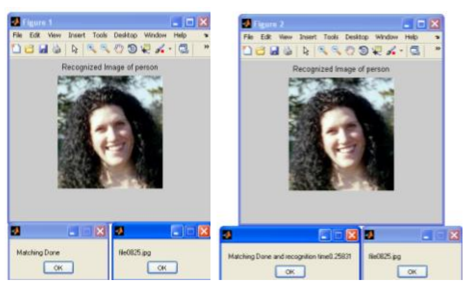

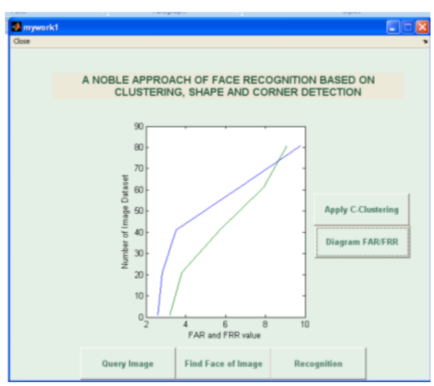

V. CONCLUSION

In this paper, we have developed a hybrid method that is very effectively work on face image. It selects a face image then find the only face image and matching with respect to database. It reduces the deficiency of existing methods like PCA, correlation based etc. This hybrid method gives better result than all the other individual method. In this work we calculate FAR and FRR. In future we add some other concept like 2D cross correlation and moment invariants of face, with this approach and get a very good result for fingerprint matching.

REFFERENCE

[1] R. Brunelli, T. Poggio, Face recognition: features versus templates,IEEE Transactions on Pattern Analysis and Machine Intelligence 15(10) (1993) 1042–1052.
[2] M. Turk, A. Pentland, Eigenfaces for recognition, Journal of Cognitive Science 1991; 71–86.
[3] P.N. Belhumeur, J.P. Hespanha, D.J. Kriegman, Eigenfaces vs. fisherfaces: recognition using class specific linear projection, IEEE Transactions on Pattern Analysis and Machine Intelligence 19 (7) (1997) 711–720.
[4] M.S. Bartlett, H.M. Lades, T.J. Sejnowski, Independent component representations for face recognition, Proceedings of the SPIE Conference on Human Vision and Electronic Imaging III, San Jose, CA, 1998 pp. 528–539.
[5] Y. Moses, Y. Adini, S. Ullman, Face recognition: the problem of compensating for changes in illumination direction, IEEE Transactions on Pattern Analysis and Machine Intelligence 19 (7) (1997) 721–732.
[6] G.C. Feng, P.C. Yuen, D.Q. Dai, Human face recognition using PCA on wavelet subband, SPIE Journal of Electronic Imaging 9 (2) (2000) 226–233.
[7] J. Tang, R. Nakatsu, S. Kawato, J. Ohya, A wavelet-transform based asker identification system for smart multi-point tele-conferences, Journal of the Visualization Society of Japan 20 (1) (2000) 303–306.
[8] C. Garcia, G. Zikos, G. Tziritas, Wavelet packet analysis for face recognition, Image and Vision Computing 18 (4) (2000) 289–297.
[9] B. Li, Y. Liu, When eigenfaces are combined with wavelets, International Journal of Knowledge-Based Systems 15 (5/6) (2002) 343–347.
[10] J.T. Chien, C.C. Wu, Discriminant waveletfaces and nearest feature classifiers for face recognition, IEEE Transactions on Pattern Analysis and Machine Intelligence 24 (12) (2002) 1644–1649.
[11] P.J. Phillips, Matching pursuit filters applied to face identification, IEEE Transactions on Image Processing 7 (8) (1998) 1150–1164.
[12] A. Hyva¨rinen, E. Oja, Independent component analysis: algorithms and applications, Neural Networks 13 (2000) 411–430.
[13] J. Kittler, M. Hatef, R.P. Duin, J.G. Matas, On combining classifiers, IEEE Transactions on Pattern Analysis and Machine Intelligence 20 (3) (1998) 226–239.
[14] I. Daubechies, Ten lectures on wavelets, CBMS-NSF Regional Conference Series in Applied Mathematics, vol. 61, SIAM Press, Philadelphia, 1992.
[15] T. Sim, S. Baker, M. Bsat, TheCMUpose, illumination, and expression (PIE) database, Proceedings of the IEEE International Conference on Automatic Face and Gesture Recognition, May 2002.
[16] P.J. Phillips, H. Moon, S.A. Rizvi, P.J. Rauss, The FERET evaluation methodology for face-recognition algorithms, IEEE Transactions on Pattern Analysis and Machine Intelligence 22 (10) (2000) 1090–1104.

Design and Implementation of Multiplier Using Kcm and Vedic Mathematics by Using Reversible Adder

V S Kumar Chunduri[1], G.Sree Lakshmi[2], Dr.M.J.C.Prasad[3]

*(PG Student, Dept. of DSCE(ECE), Malla Reddy Engineering College/Autonoumous,India)

** (Assoc.Professor, Dept. of ECE, Malla Reddy Engineering College/Autonoumous,India)

***(professor & Head of the Department, Dept. of ECE, Malla Reddy Engineering College/ Autonoumous,India)

ABSTRACT : *This work is devoted for the design and FPGA implementation of a 16bit Arithmetic module, which uses Vedic Mathematics algorithms. For arithmetic multiplication various Vedic multiplication techniques like Urdhva Tiryakbhyam Nikhilam and Anurupye has been thoroughly analyzed. Also Karatsuba algorithm for multiplication has been discussed. It has been found that Urdhva Tiryakbhyam Sutra is most efficient Sutra (Algorithm), giving minimum delay for multiplication of all types of numbers. Using Urdhva Tiryakbhyam, a 16x16 bit Multiplier has been designed and using this Multiplier, a Multiply Accumulate (MAC) unit has been designed. Then, an Arithmetic module has been designed which employs these Vedic multiplier and MAC units for its operation. Logic verification of these modules has been done by using Model sim 6.5.Further, the whole design of Arithmetic module has been realized on Xilinx Spartan 3E FPGA kit and the output has been displayed on LCD of the kit. The synthesis results show that the computation time for calculating the product of 16x16 bits is 10.148 ns, while for the MAC operation is 11.151 ns. The maximum combinational delay for the Arithmetic module is 15.749 ns. The further extension of this 8 x 8 Array multiplication and Urdhava multiplication can be implemented by using reversible DKG adder replacing with adders(H.A or F.A), and by using 16 x 16 – bit, 32 X 32 – bit are more than that. It can be dumped in to Xilinx tools, and also finding the comparison between the adders like power consumption, speed etc..,*

Keywords: KCM; Urdhava; Vedic Maths; Array Multiplier; DKG Adder; FPGA.

I. INTRODUCTION

Multiplication is one of the more silicon-intensive functions, especially when implemented in Programmable Logic. Multipliers are key components of many high performance systems such asFIR filters, Microprocessors, Digital Signal Processors, etc. A system's performance is generally determined by the performance of the multiplier,because the multiplier is generally the slowest element in the system. Furthermore, it is generally the most area consuming. Hence, optimizing the speed and area of the multiplier is a major design issue.Vedic mathematics [I] is the ancient Indian system of mathematics which mainly deals with Vedic mathematicalformulae and their application to various branches of mathematics. The word 'Vedic' is derived from the word 'Veda' which means the store-house of all knowledge. Vedic mathematics was reconstructed from the ancient Indian scriptures (Vedas) by Sri Bharati Krshna Tirthaji (1884-1960), after his eight years of research on Vedas [1]. According to his research, Vedic mathematics is mainly based on sixteen principles or word-formulae which are termed as Sutras. This is a very interesting field and 978-1-4577-0697-4/12/$26.00 ©2012 IEEE presents some effective algorithms which can be applied tovarious branches of Engineering such as Computing and Digital Signal Processing.

II. VLSI DESIGN

The complexity of VLSI is being designed and used today makes the manual approach to design impractical. Design automation is the order of the day. With the rapid technological developments in the last two decades, the status of VLSI technology is characterized by the following

A steady increase in the size and hence the functionality of the ICs:

• A steady reduction in feature size and hence increase in the speed of operation as well as gate or transistor density.
• A steady improvement in the predictability of circuit behavior.
• A steady increase in the variety and size of software tools for VLSI design.

The above developments have resulted in a proliferation of approaches to VLSI design.

Final step in the development process, starting in the 1980s and continuing through the present, was in the early 1980s, and continues beyond several billion transistors as of 2009. In 1986 the first one megabit RAM chips were introduced, which contained more than one million transistors. Microprocessor chips passed the million transistor mark in 1989 and the billion transistor mark in 2005.The trend continues largely unabated, with chips introduced in 2007 containing tens of billions of memory transistors. The complexity of VLSIs being designed and used today makes the manual approach to design impractical. Design automation is the order of the day. With the rapid technological developments in the last two decades, the status of VLSItechnology is characterized by the following [Wai-kai, Gopalan]:

•A steady increase in the size and hence the functionality of the ICs.
•A steady reduction in feature size and hence increase in the speed of operation as well as gate or transistor density.
•A steady improvement in the predictability of circuit behavior.
•A steady increase in the variety and size of software tools for VLSI design. The above developments have resulted in a proliferation of approaches to VLSIdesign. We briefly describe the procedure of automated design flow [Rabaey, Smith MJ]. The aim is more to bring out the role of a Hardware Description Language (HDL) in the design process. An abstraction

based model is the basis of the automated design. The model divides the whole design cycle into various domains. With such an abstraction through a division process the design is carried out indifferent layers. The designer at one layer can function without bothering about the layers above or below. The thick horizontal lines separating the layers in the figure signify the compartmentalization. As an example, let us consider design at the gate level. The circuit to be designed would be described in terms of truth tables and state tables. With these as available inputs, he has to express them as Boolean logic equations and realize them in terms of gates and flip-flops. In turn, these form the inputs to the layer immediately below.

III. ARRAY MULTIPLIER

In Array multiplier , AND gates are used for generation of the bit-products and adders for accumulation of generated bit products. All bit-products are generated in parallel and collected through an array of full adders or any other type of adders. Since the array multiplier is having a regular structure, wiring and the layout are done in a much simplified manner. Therefore, among other multiplier structures, array multiplier takes up the least amount of area. But it is also the slowest with the latency proportional to O(Wct), where Wd is the word length of the operand.

Example 1:

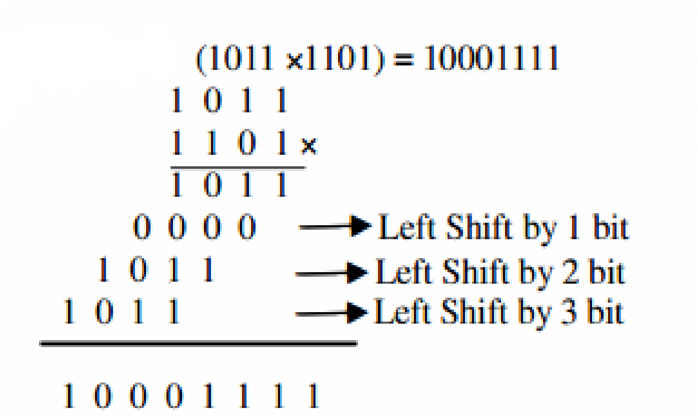

Example1 for Array multiplier 4*4

Example 2:

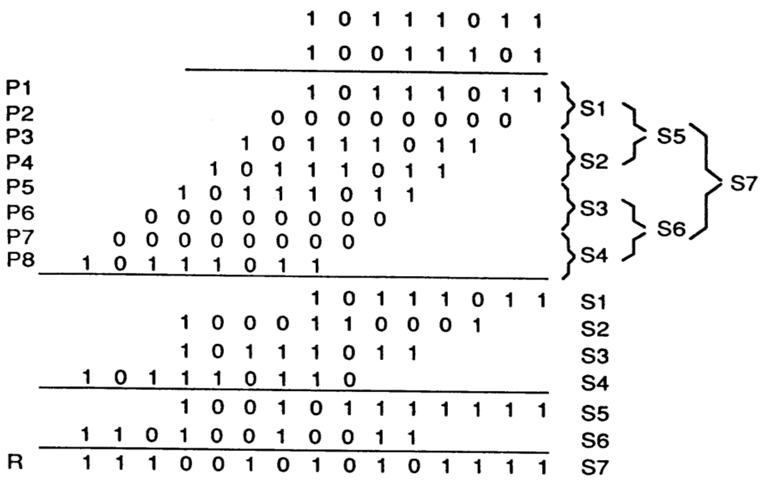

Example2 for Array multiplier 8*8

Instead of Ripple Carry Adder (RCA), here Carry Save Adder (CSA) is used for adding each group of partial product terms, because RCA is the slowest adder among all other types of adders available. In case of multiplier with CSA , partial product addition is carried out in Carry save form and RCA is used only in final addition. Here from the above example it is inferred that partial products are generated sequentially, which reduces the speed of the multiplier. However the structure of the multiplier is regular.

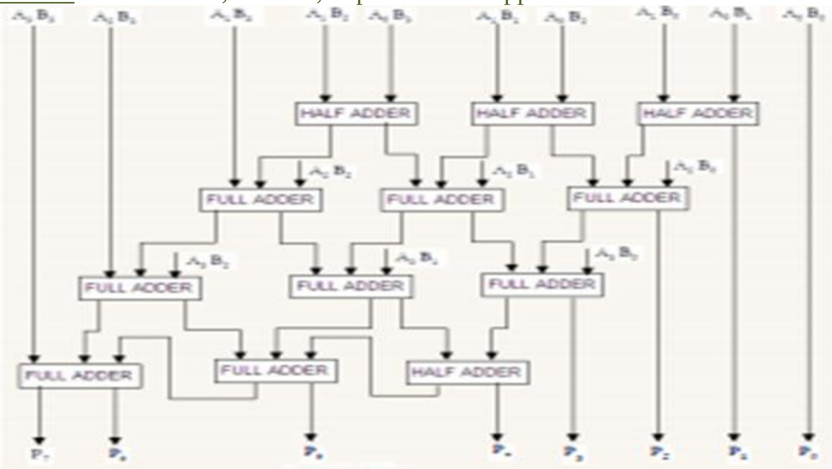

Fig : 1 Array Multiplier 4 * 4 using CSA Hardware Architecture.

In this method, for the first 3 numbers a row of full adder are used. Then a row of full adder is added for each additional number. The final results, in the form of two numbers sum and carry, are then summed up with a carry propagate adder or any other adder. An example 4 numbers addition is shown in Fig 1.There are many cases where it is desired to add more than two numbers together. The straight forward way of adding together m numbers (all n bits wide) is to add the first two, then add that sum to the next, and so on. This requires a total of m − 1 additions, for a total gate delay of (assuming look ahead carry adders). Instead, a tree of adders can be formed, taking only gate delays. Using carry save addition, the delay can be reduced further still. The idea is to take 3 numbers that we want to add together, x + y + z, and convert it into 2 numbers c + s such that x + y + z = c + s, and do this in time. The reason why addition cannot be performed in time is because the carry information must be propagated. In carry save addition, we refrain from directly passing on the carry information until the very last step. We will first illustrate the general concept with a base 10 example. To add three numbers by hand, we typically align the three operands, and then proceed column by column in the same fashion that we perform addition with two numbers. The three digits in a row are added, and any overflow goes into the next column. Observe that when there is some non-zero carry, we are really adding four digits (the digits of x ,y and z, plus the carry).In many cases we need to add several operands together, carry save adder are ideal for this type of addition. A carry save adder consists of stand-alone full adders, and carries out a number of partial additions. The principal idea is that the carry has a higher power of 2 and thus is routed to the next column. Doing addition with carry save adder saves time and logic.In this method, for the first 7 numbers a row of full adder are used. Then a row of full adder is added for each additional number. The final results, in the form of two numbers sum and carry, are then summed up with a carry propagate adder or any other adder.

IV. URDHAVA MULTIPLIER

In Urdhava Tiryakbhyam is a Sanskrit word which means vertically and crosswire in English. The method is a general multiplication formula applicable to all cases of multiplication. It is based on a novel concept through which all partial products are generated concurrently. Fig. Demonstrates a 4 x 4 binary multiplication using this method. The method can be generalized for any N x N bit multiplication. This type of multiplier is independent of the clock frequency of the processor because the partial products and their sums are calculated in parallel.The net advantage is that it reduces the need of microprocessors to operate at increasingly higher clock frequencies. As the operating frequency of a processor increases the number of switching instances also increases. This results more power consumption and also dissipation in the form of heat which results in higher device operating temperatures. Another advantage of Urdhava Tiryakbhyam multiplier is its scalability T.

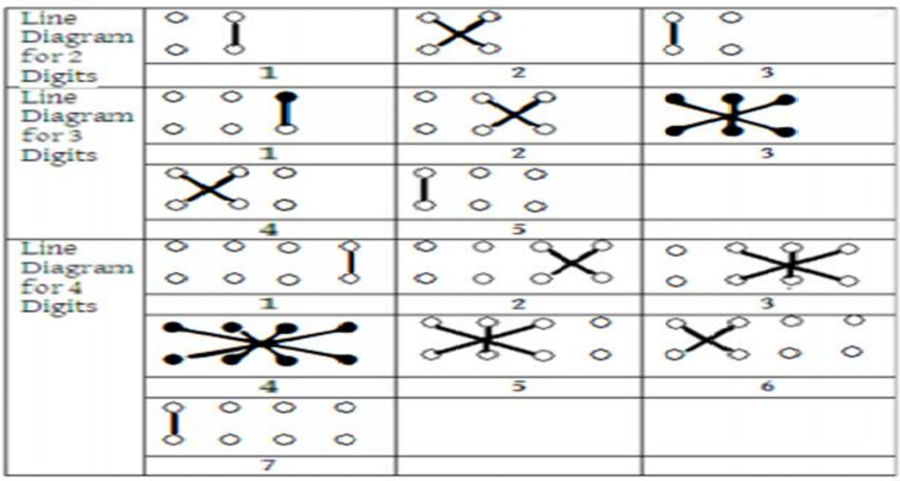

Fig: 2 Line Diagram for Urdhava Multiplication.

The processing power can easily be increased by increasing the input and output data bus widths since it has a regular structure. Due to its regular structure, it can be easily layout in a silicon chip and also consumes optimum area. As the number of input bits increase, gate delay and area increase very slowly as compared to other multipliers. Therefore Urdhava Tiryakbhyam multiplier is time, space and power efficient.

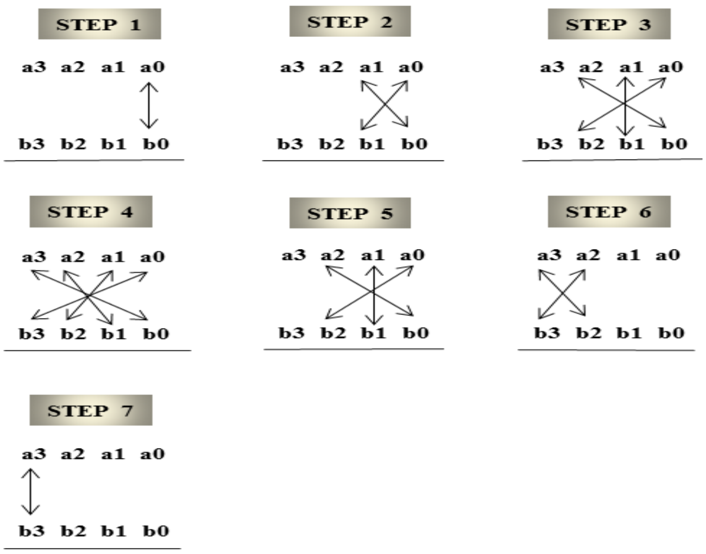

Fig : 3 Multiplication of two 4 bit numbers using Urdhava Tiryakbhyam method

Example 3:

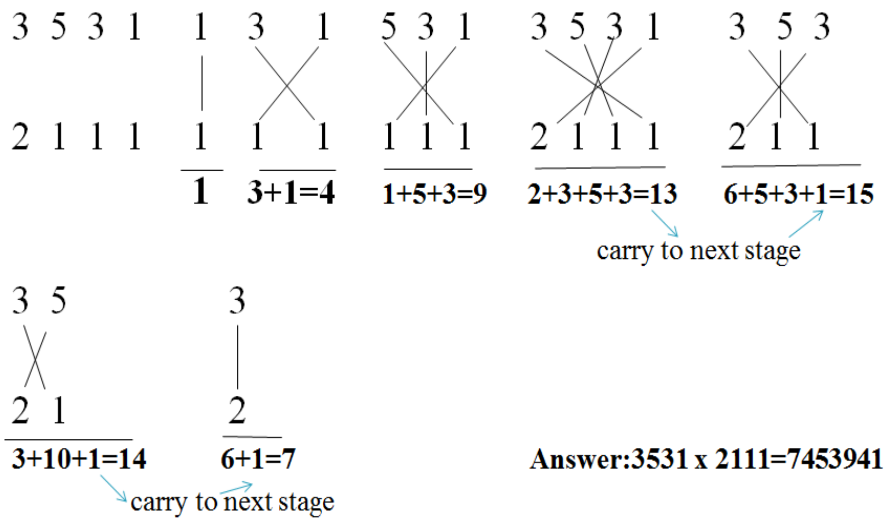

Example3 for the Multiplication of two 4 bit numbers using Urdhava Tiryakbhyam method

The line diagram in fig. 3 illustrates the algorithm for multiplying two 4-bit binary numbers a3, a2, a1, a0 and b3, b2, b1, b0. The procedure is divided into 7 steps and each step generates partial products. Initially as shown in step 1 of fig. 2, the least significant bit (LSB) of the multiplier is multiplied with least significant bit of the multiplicand (vertical multiplication). This result forms the LSB of the product. In step 2 next higher bit of the multiplier is multiplied with the LSB of the multiplicand and the LSB of the multiplier is multiplied with the next higher bit of the multiplicand (crosswire multiplication). These two partial products are added and the LSB of the sum is the next higher bit of the final product and the remaining bits are carried to the next step. For example, if in some intermediate step, we get the result as 1101, then 1 will act as the result bit(referred as rn) and 110 as the carry (referred as cn). Therefore cn may be a multi-bit number. Similarly other steps are carried out as indicated by the line diagram. The important feature is that all the partial products and their sums for every step can be calculated in parallel. Thus every step in fig. 3.1 has a corresponding expression as follows:

$$r0=a0b0. \quad (1)$$
$$c1r1=a1b0+a0b1. \quad (2)$$
$$c2r2=c1+a2b0+a1b1 + a0b2. \quad (3)$$
$$c3r3=c2+a3b0+a2b1 + a1b2 + a0b3. \quad (4)$$
$$c4r4=c3+a3b1+a2b2 + a1b3. \quad (5)$$
$$c5r5=c4+a3b2+a2b3. \quad (6)$$
$$c6r6=c5+a3b3 \quad (7)$$

With c6r6r5r4r3r2r1r0 being the final product. Hence this is the general mathematical formula applicable to all cases of multiplication and its hardware architecture is shown in fig. 3. In order to multiply two 8-bit numbers using 4-bit multiplier we proceed as follows.

Consider two 8 bit numbers denoted as AHAL and BHBL where AH and BH corresponds to the most significant 4 bits, AL and BL are the least significant 4 bits of an 8-bit number. When the numbers are multiplied multiplied according to Urdhava Tiryakbhyam (vertically and crosswire) method, we get,

AH AL
BH BL

(AH x BH) + (AH x BL + BH x AL) + (AL x BL).

The digits on the two ends of the line are multiplied and the result is added with the previous carry. When there are more lines in one step, all the results are added to the previous carry.

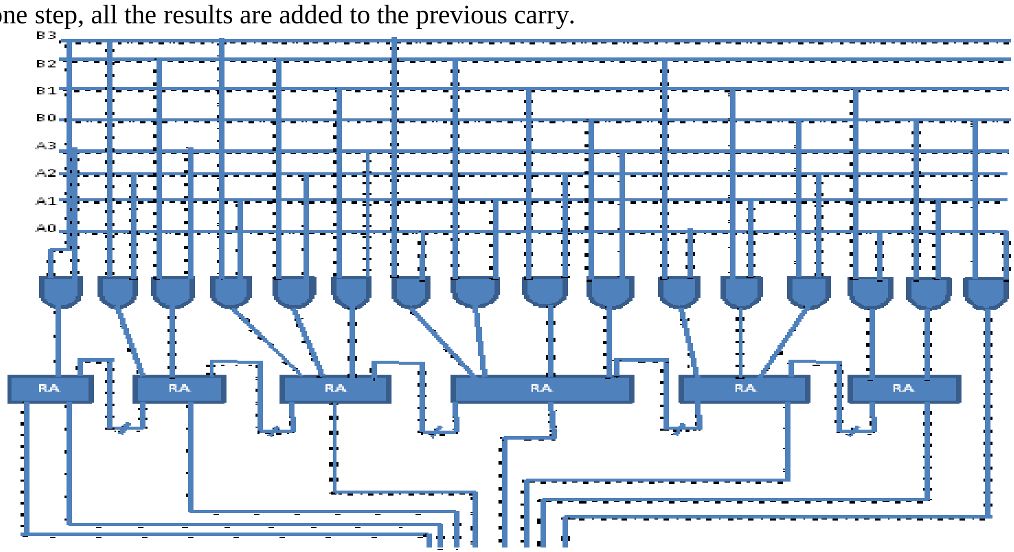

Fig: 4 Hardware architecture of 4 X 4 Urdhava Tiryakbhyam multiplier using reversible DKG added.

Thus we need four 4-bit multipliers and two adders to add the partial products and 4-bit intermediate carry generated. Since product of a 4 x 4 multiplier is 8 bits long, in every step the least significant 4 bits correspond to the product and the remaining 4 bits are carried to the next step. This process continues for 3 steps in this case. Similarly, 16 bit multiplier has four 8 x 8 multiplier and two 16 bit adders with 8 bit carry. Therefore we see that the multiplier is highly modular in nature. Hence it leads to regularity and scalability of the multiplier layout. The multiplier architecture is based on this Urdhava tiryakbhyam sutra. The advantage of this algorithm is that partial products and their sums are calculated in parallel. This parallelism makes the multiplier clock independent. The other main advantage of this multiplier as compared to other multipliers is its regularity. Due to this modular nature the lay out design will be easy. The architecture can be explained with two eight bit numbers i.e. the multiplier and multiplicand are eight bit numbers. The multiplicand and the multiplier are split into four bit blocks. The four bit blocks are again divided into two bit multiplier blocks. According to the algorithm the 8 x 8 (AH x BH) bit multiplication will be as follows.

AH = AHH - AHL, BH = BHH - BHL
AH=AH7AH6AH5AH4AH3AH2AH1AH0,
BH = BH7BH6BH5BH4BH3BH2BH1BH0,
AHH = AH7AH6AH5AH4,
AHL = AH3AH2AH1AH0
BHH = BH7BH6BH5BH4, BHL = BH3BH2BH1BH0

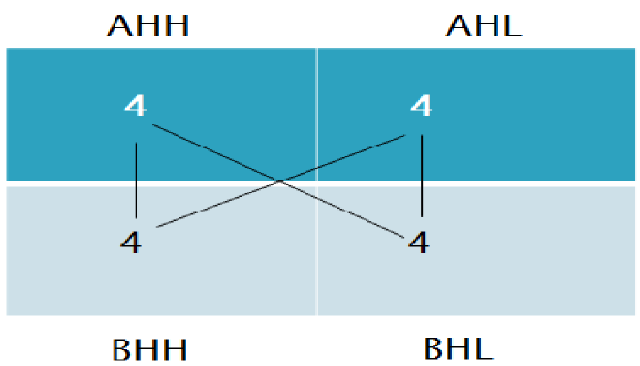

Fig : 5 Multiplication of two 8 bit numbers using Urdhava Tiryakbhyam method

By the algorithm, the product can be obtained as follows.
Product of AH x BH = AHL x BHL + (AHH x BHL + AHL x BHH) + AHH x BHH
Thus 8 x 8 multiplications can be decomposed into 2 x 2 multiplication units. By using this algorithm any complex N x N multiplication can be implemented using the basic 2 x 2 multiplier units.

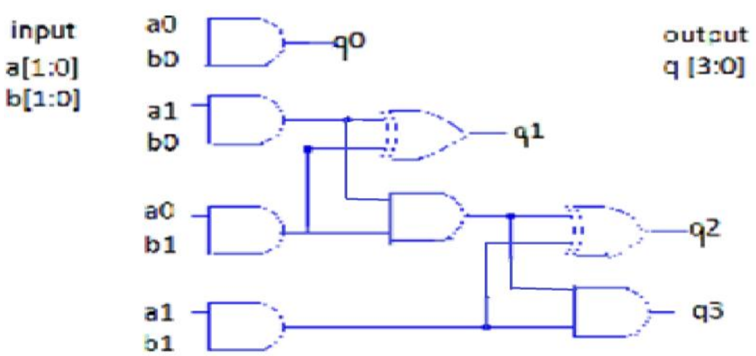

Fig: 6 Hardware Realization of 2x2 block

Hear a0=AL, a1=AH;
b0=BL, b1=BH;

For Multiplier, first the basic blocks, that are the 2x2 bit multipliers have been made and then, using these blocks, 4x4 block has been made and then using this 4x4 block, 8x8 bit block, 16x16 bit block. Urdhava Tiryakbhyam Sutra is a general multiplication formula applicable to all cases of multiplication. It means "Vertically and Crosswise". The digits on the two ends of the line are multiplied and the result is added with the previous carry. When there are more lines in one step, all the results are added to the previous carry. The least significant digit of the number thus obtained acts as one of the result digits and the rest act as the carry for the next step. Initially the carry is taken to be as zero. The line diagram for multiplication of two 4-bit numbers is as shown in Fig.

8 X 8 Bit Multiplication Using Urdhava Triyakbhyam (Vertically and crosswise) for two Binary numbers

Consider two binary numbers A and B of 8 bits as respectively

A = $\mathbf{A_7A_6A_5A_4}$ $\mathbf{A_3A_2A_1A_0}$
(X_1) (X_0)
B = $\mathbf{B_7B_6B_5B_4}$ $\mathbf{B_3B_2B_1B_0}$
(Y_1) (Y_0)

Which can be viewed as two four bit numbers each, i.e. A can be viewed as X_1 X_0 and B can be viewed as Y_1 Y_0 respectively, as shown above, thus the multiplication can be written as

X_1 X_0
* Y_1 Y_0

EDC

Where, CP= C = X_0Y_0
CP= A = X_1Y_0
CP = B = X_0Y_1
CP= D = A+B
CP= E = X_1Y_1 here CP= Cross Product

Thus, A*B= EDC, is achieved using Urdhava Triyakbhyam (Vertically and crosswise) sutra.

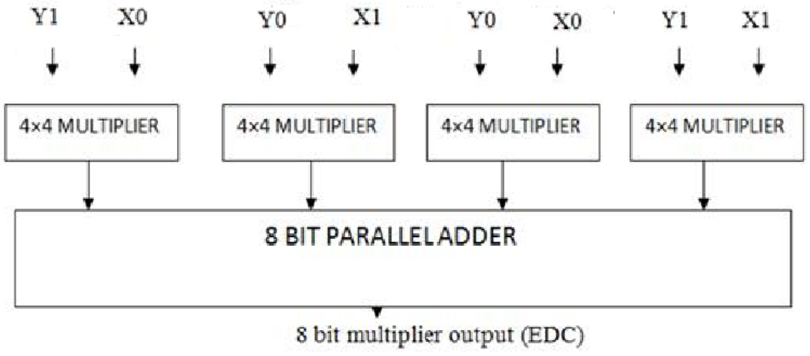

Fig :7 Hardware architecture of 8 X 8 Urdhava Tiryakbhyam multiplier.

Now we will extend this Sutra to binary number system. For the multiplication algorithm, let us consider the multiplication of two 8 bit binary numbers A7A6A5A4A3A2A1A0 and B7B6B5B4B3B2B1B0. As the result of this multiplication would be more than 8 bits, we express it as ...R7R6R5R4R3R2R1R0. As in the last case, the digits on the both sides of the line are multiplied and added with the carry from the previous step. This generates one of the bits of the result and a carry. This carry is added in the next step and hence the process goes on. If more than one lines are there in one step, all the results are added to the previous carry. In each step, least significant bit acts as the result bit and all the other bits act as carry. For example, if in some intermediate step we will get 011, then I will act as result bit and 01 as the carry.

V. REVERSIBLE LOGIC GATES

There exist many reversible gates in the literature. Among them 2*2 Feynman gate , 3*3 Fredkin gate, 3*3 Toffoli and 3*3 Peres is the most referred. The detailed cost of a reversible gate depends on any particular realization of quantum logic. Generally, the cost is calculated as a total sum of 2*2 quantum primitives used. The cost of Toffoli gate is exactly the same as the cost of Fredkin gate and is 5. The only cheapest quantum realization of a complete (universal) 3*3 reversible gate is Peres gate and its cost is 4.

Controlled NOT (CNOT) gate is an example for a 2*2 gate. The Reversible 2*2 gate with Quantum Cost of one having mapping input (A, B) to output (P = A, Q = A B)

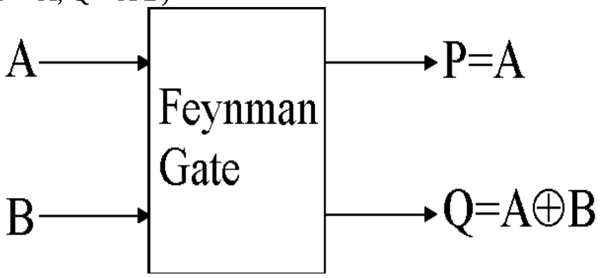

Figure 8: 2*2 Feynman gate

Reversible 3*3 gate maps inputs (A, B, C) to outputs (P=A, Q=A'B+AC, R=AB+A'C) having Quantum cost of 5 and it requires two dotted rectangles, is equivalent to a 2*2 Feynman gate with Quantum cost of each dotted rectangle is 1, 1 V and 2 CNOT gates.

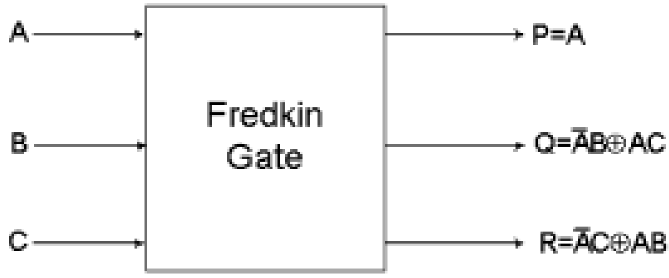

Figure 9: 3*3 Fredkin gate

The 3*3 Reversible gate with three inputs and three outputs. The inputs (A, B, C) mapped to the outputs (P=A, Q=B, R=A.BC)

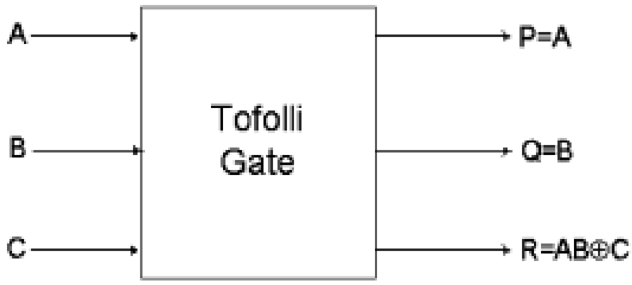

Figure 10: 3*3 Toffoli gate

The three inputs and three outputs i.e., 3*3 reversible gate having inputs (A, B, C) mapping to outputs (P = A, Q = A B, R = (A.B) C). Since it requires 2 V+, 1 V and 1 CNOT gate, it has the Quantum cost of 4.

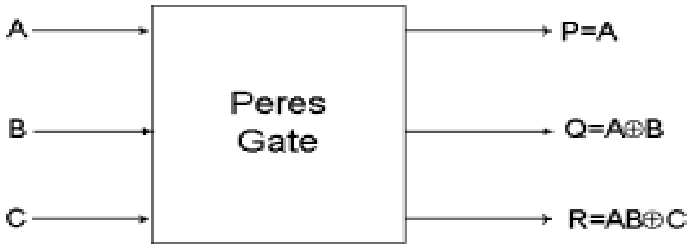

Figure 11: 3*3 Peres gate

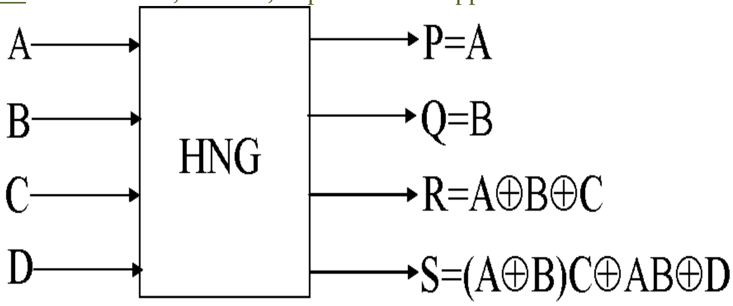

Figure 12: 4*4 HNG gate

Reversible DKG Gate:

Reversible DKG gate has 4 inputs and 4 outputs, so it is called Reversible 4*4 DKG gate, A 4* 4 reversible DKG gate that can work singly as a reversible Full adder and a reversible Full subtractor is shown in Fig . It can be verified that input pattern corresponding to a particular output pattern can be uniquely determined. If input A=0, the proposed gate works as a reversible Full adder, and if input A=1, then it works as a reversible Full subtractor. It has been proved that a reversible full-adder circuit requires at least two garbage outputs to make the output combinations unique figures.

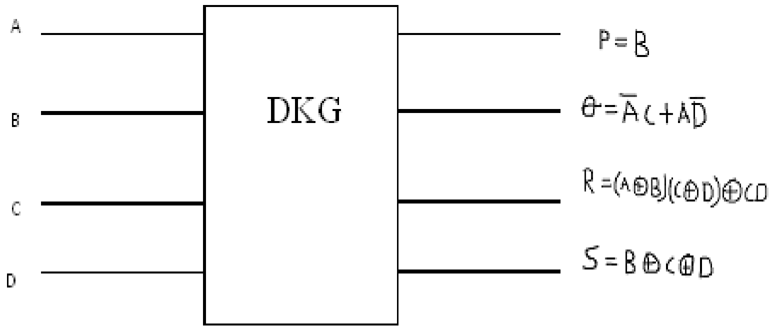

Figure 13: Reversible DKG gate

DKG gate with inputs A, B, C, D and outputs are P, Q, R, S. This gate is known as DKG gate. Figure 8 shows the DKG gate with 4*4 inputs and outputs. The binary Full adder/subtractor is capable of handling one bit of each input along with a carry in/borrow in generated as a carry out/ borrow from addition of previous lower order bit position. If two binary numbers each consisting of n bits are to be added or subtracted, then n binary full adders/subtractors are to be cascaded.

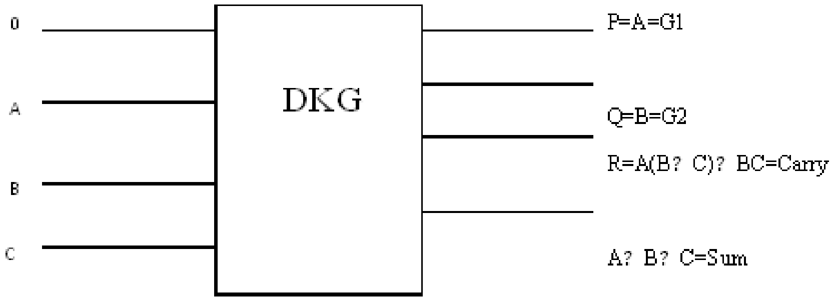

Figure 14: DKG gate implemented as Full adder

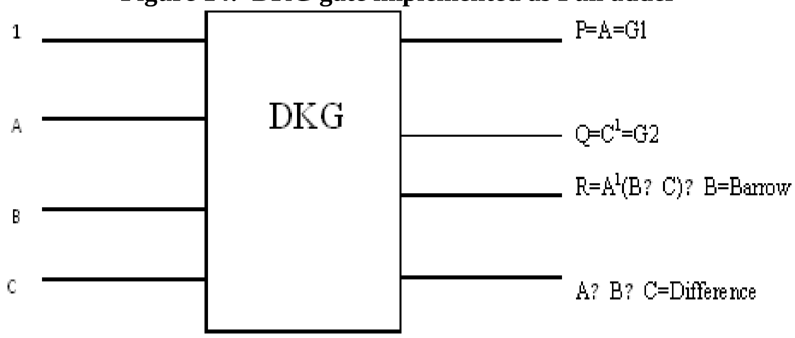

Figure 15: DKG gate implemented as Full subtractor

The binary Full adder/subtractor is capable of handling one bit of each input along with a carry in/borrow in generated as a carry out/ borrow from addition of previous lower order bit position. If two binary numbers each consisting of n bits are to be added or subtracted, then n binary full adders/subtractors are to be cascaded. A Parallel adder/subtractor is an interconnection of full adders/subtractors and inputs are simultaneously applied. The carry/borrow generated at a stage is propagated to the next stage. Thus, delay is more in such type of adders/subtractors. A 4 bit reversible parallel adder/subtractor is implemented using the reversible DKG gate and shown in Fig 10a. When the control input A=0, the circuit acts as a parallel adder, produces a 4 bit sum and a carry out, as shown in Fig 10b. If the control input A=1, the circuit acts as a parallel subtractor, produces a 4 bit difference and borrow out, as shown in Fig. The same design can be extended to n bits.

VI. PROPOSED MULTIPLIER

The proposed method is based on ROM approach however both the inputs for the multiplier can be variables. In this proposed method a ROM is used for storing the squares of numbers as compared to KCM where the multiples are stored.

operation:

To find (a x b), first we have to find whether the difference between 'a' and 'b' is odd or even. Based on the difference, the product is calculated.

In case of Even Difference

Result of Multiplication= [Average]^2- [Deviation]^ 2

In case of Odd Difference

Result of Multiplication = [Average x (Average + 1)] -[Deviation x (Deviation+ I)]

Where

Average = [(a+b)/2]

Deviation = [Average -smallest(a, b)]

Example 4 (Even difference) and Example 5 (Odd difference) depict the multiplication process. Thus the two variable multiplication is performed by averaging, squaring and subtraction. To find the average[(a+b)/2], which involves division by 2 is performed by right shifting the sum by one bit.

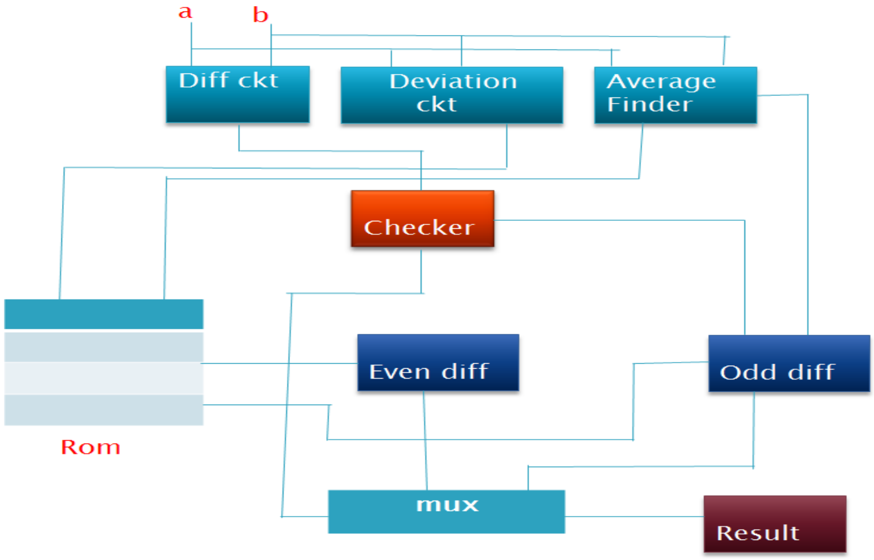

Fig : 16 Block diagram for proposed multiplier.

If the squares of the numbers are stored in a ROM, the result can be instantaneously calculated. However, in case of Odd difference, the process is different as the average is a floating point number. In order to handle floating point arithmetic, Ekadikena Purvena - the Vedic Sutra which is used to find the square of numbers end with 5 is applied. Example 4 illustrates this. In this case, instead of squaring the average and deviation, [Average x (Average + 1)] - [Deviation x (Deviation+ I)] is used. However, instead of performing the multiplications, the same ROM is used and using equation the result of multiplication is obtained.

n(n+l) = (n2+n) ... (10)

Here n2 is obtained from the ROM and is added with the address which is equal to n(n+l)

Example 4:

16 x 12 = 192

1) Find the difference between (16-12) = 4 ----Even Number

2) For Even Difference, Product = [Average]^2- [Deviation]^2

i. Average = [(a+b)/2] = [(16+12)12] = [28/2] = 14

ii. Smallest(a,b) = smallest(l6,12) =12

iii. Deviation = Average - Smallest (a,b) = 14 -12 =2

3) Product = 14^2- 2^2= 196 - 4 = 192.

Example 5:
15 x 12 = 180
I) Find the difference between (15-12)=3 -7 Odd Number
2) For Odd Number Difference find the Average and Deviation.
i.Average = [(a+b)/2] = [(12+15)/2] = 13.5
ii.Deviation = [Average - smallest(a, b)] = [12.5 - smallest(l3,12)] = [13.5 - 12] = 1.5
3)Product = (l3xI4) - (lx2) = 182 - 2 =180.

VII. SIMULATION RESULTS AND TABLES

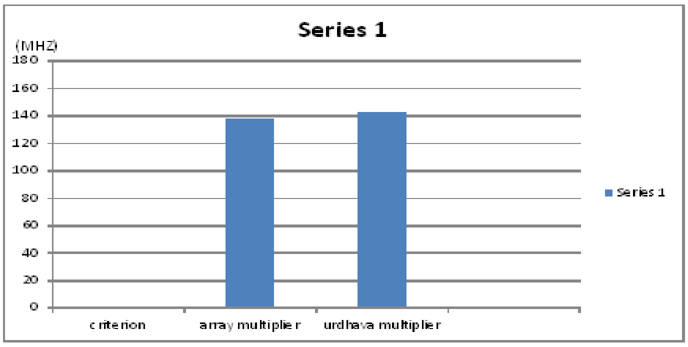

Fig : 17 Speed Comparison for (8x8)

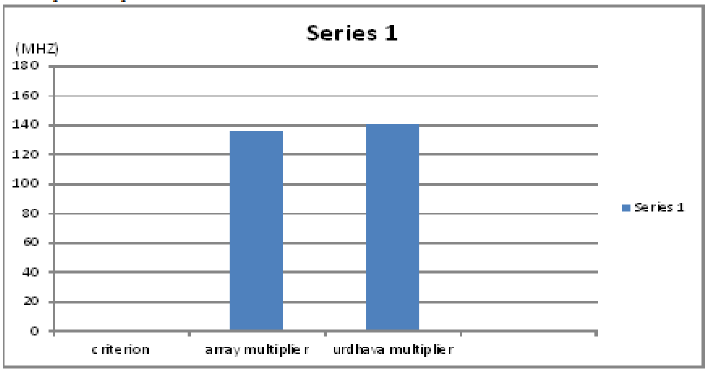

Fig : 18 speed comparison for DKG (8*8)

Simulation result

The comparison is carried out in between the reversible and conventional logic gates by using XILINX 9.1and program is written in VERILOG language. . In reversible logic we use DKG and TSG gates for both adder/subtractor as it has low power consumption and less garbage output as already discussed in the section3. The comparison is carried out for the four operand four bit adder/subtractor in reversible and conventional gates.

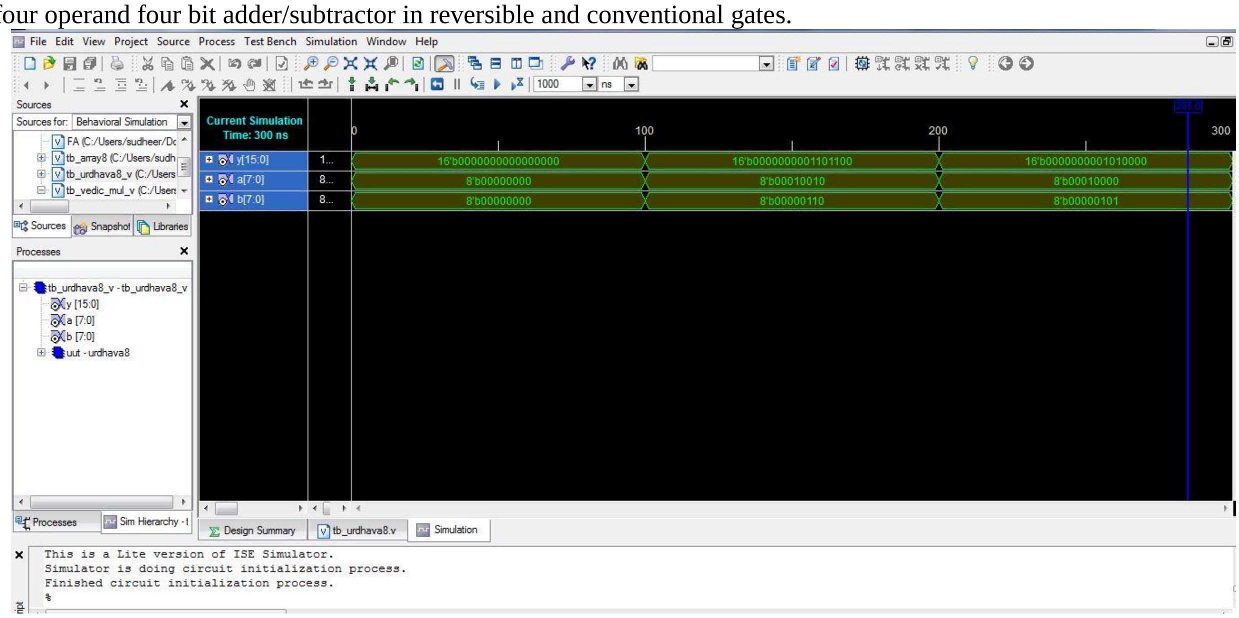

Fig 19 : 8 bit Array multiplier using DKG

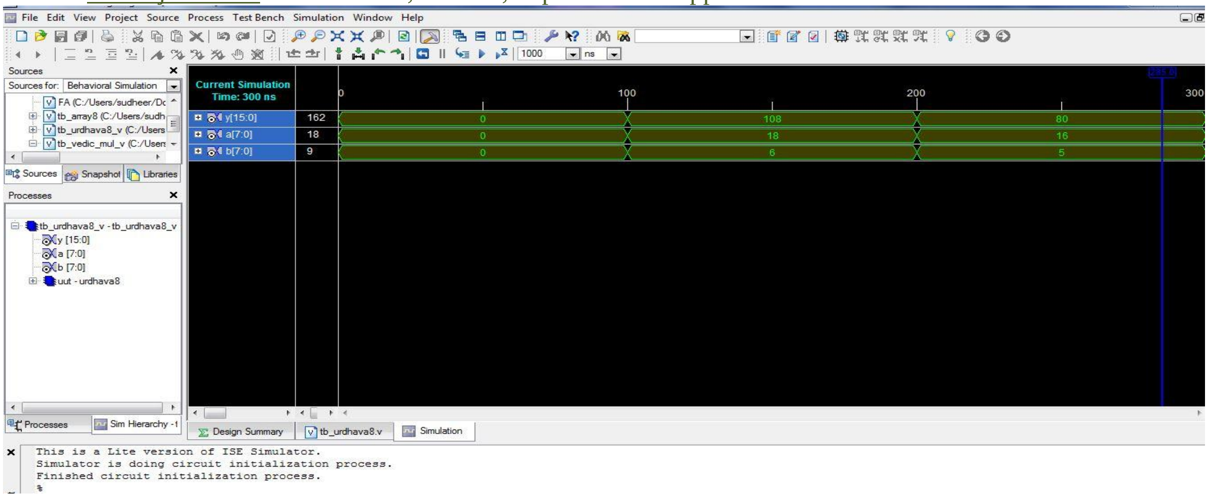

Fig 20: 8 bit Urdhava multiplier using DKG

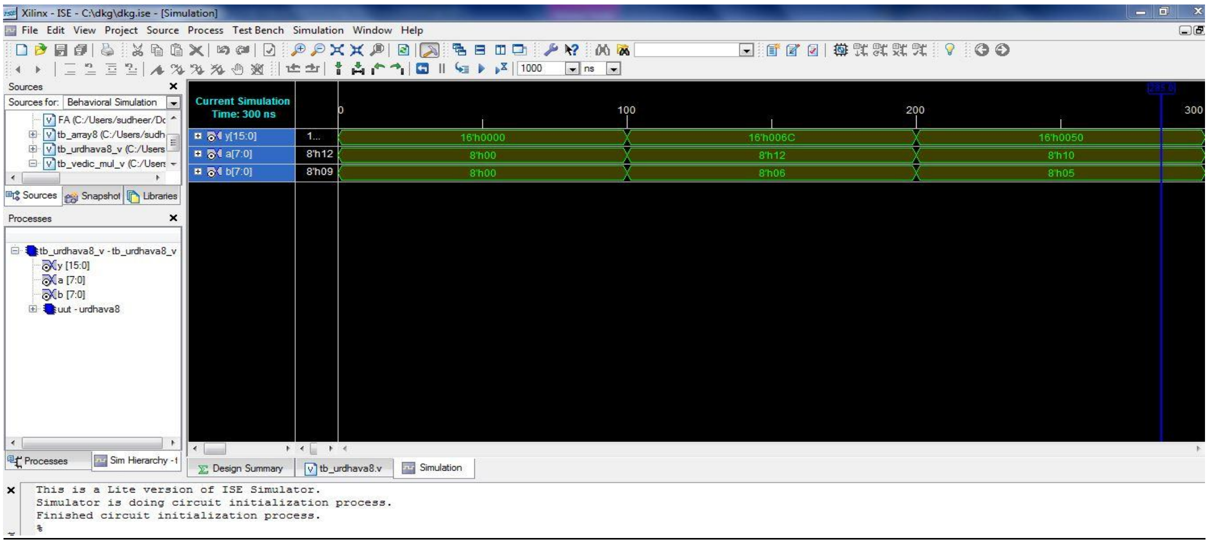

Fig 21: 8 bit proposed multiplier

Criterion	Array Multiplier	Urdhava Multiplier
Area	126	180
Total Combinational Functions	163	149
Dedicated Logic Registers	48	48
Total Memory Bits(Kb)	0	0
Transitions	1557	1501
Speed(After Pipelining)(MHz)	137.46	142.67
Power	100	90
temperature	27c	27c

Table1: results for 8x8 multiplier

Criterion	Array Multiplier	Urdhava Multiplier
Area	126	180
Total Combinational Functions	158	146
Dedicated Logic Registers	46	46
Total Memory Bits(Kb)	0	0
Transitions	1551	1547
Speed(After Pipelining)(MHz)	139.35	145.03
Total Power	90	82
temperature	27c	27c

Table 2: Results For Dkg 8*8 multiplier

VIII. CONCLUSION

Thus the proposed multiplier provides higher performance for higher order bit multiplication. In the proposed multiplier for higher order bit multiplication i.e. for 16x16 and more, the multiplier is realized by instantiating the lower order bit multipliers like 8x8. This is mainly due to memory constraints. Effective memory implementation and deployment of memory compression algorithms can yield even better results.

ACKNOWLEDGMENTS

I am very grateful to my project guide **Mrs. G.SREE LAKSHMI, Associate prof** of Electronic & Communication Engineering, Malla Reddy Engineering College, for her extensive patience and guidance throughout my project work. Also having provided the freedom to use all the facilities available in the department, especially the laboratories and the library.

I am happy to express my since thanks to Mrs. P.S. INDRANI, Associate prof, PG coordinator of Electronic & Communication Engineering department.

I would like to thank Dr. M. Jagdissh Chandra Prasad, Professor & HOD, Department of Electronics and communication engineering, Malla Reddy Engineering College, for their timely suggestions, healthy criticism and motivation during the course of this work.

I am happy to express my deep sense of gratitude to the principal of the college **Dr. S. Sudhakara Reddy,** professor for having provided us with facilities to pursue our project.

I sincerely thank to all teaching and non- teaching staff of the department of Electronics & Communication Engineering for their timely suggestions, healthy criticism and motivation during the course of this work.

Finally, I express my immense gratitude with pleasure to other individual who having directly or indirectly contributed to my need at right time for the development and success if this project work.

REFERENCE

[1.] Bharati Krshna Tirthaji, Vedic Mathematics. Delhi: Motilal Banarsidass Publishers, 1965.

[2.] Harpreet Singh Dhillon and Abhijit Mitra "A Digital MultiplierArchitecture using Urdhava Tiryakbhyam Sutra oj Vedic Mathematics" IEEE Conference Proceedings,2008.

[3.] Asmita Haveliya "A Novel Design ./i)r High Speed Multiplier .fi)r Digital Signal Processing Applications (Ancient Indian Vedic mathematics approach)" International Journal of Technology AndEngineering System(IJTES):Jan - March 2011- Vo12 .Nol

[4.] P. D. Chidgupkar and M. T. Karad, "The Implementation oj Vedic Algorithms in Digital Signal Processing", Global J. oj /c'ngg. /c'du., vol. 8, no.2, pp. 153-158, 2004.

[5.] J.Bhasker, "Verilog HDL Primer" BS P Publishers, 2003.

[6.] M. Ramalatha, K. Deena Dayalan,P. Dharani, S. Deborah Priya,"High Speed Jc'nergy ElJzcient AL U Design using Vedic Multiplication Techniques", ACTEA 2009, Zouk Mosbeh, Lebanon.

[7.] Landauer, R., 1961. Irreversibility and heat generation in the computing process, IBM J. Research and Development, 5 (3): 183-191.

[8.] Thaplyal, H. and M.B. Srinivas, 2006. Novel Reversible Multiplier Architecture Using Reversible TSG gate. IEEE international Conference on Computer Systems and Applications, pp: 100-103.

[9.] Shams, M., M. Haghparast and K. Navi, 2008. Novel Reversible Multiplier Circuit in Nanotechnology. World Appl. Sci. J., 3 (5): 806- 810.

[10.] D. MASLOV, G. W. DUECK, AND D. M. MILLER, Synthesis of Fredkin-Toffoli Reversible Networks, *IEEE Trans. VLSI Systems*, **13**(**6**), pp. 765-769, 2005.

[11.] C.H. Bennett , "Logical Reversibility of Computation", IBM J.Research and Development, pp. 525-532, November 1973.

[12.] Himanshu Thapliyal, M.B Srinivas and Hamid R. Arabnia, " A Reversible Version of 4 x 4 Bit Array Multiplier With Minimum Gates and Garbage Outputs ", The 2005 International Conference on Embedded System and Applications(ESA'05), Las Vegas, U.S.A, June 2005,pp-106-114.

[13.] Saiful Islam and Rafiqul Islam., 2005. Minimization of Reversible Adder Circuits. Asian Journal of Information Technology 4 (12): 1146-1151.

[14.] Fredkin, E. and Toffoli, T. (1982). Conservative logic. Int. Journal of Theoretical Physics, 21, 219–253.

[15.] Md. Saiful Islam, Md. Rafiqul Islam, Muhammad Rezaul Karim, Abdullah Al Mahmud and Hafiz Md. Hasan Babu, "Minimization of Adder Circuits and Variable Block Carry Skip Logic using Reversible Gates", In Proc. of 7th International Conference on Computer and Information Technology, ICCIT 2004, Brac University, Dhaka, Bangladesh, 26-28 December, 2004, pp. 378- 383.

Analytic Model of Wind Disturbance Torque on Servo Tracking Antenna

Tushar Golani[1], Suresh Sabhapathy[2]
[1]*Spacecraft Checkout Group, ISRO Satellite Centre, Bangalore 560 017*
[2]*Giant Metrewave Radio Telescope, Tata Institute of Fundamental Research, Pune 410 504*

ABSTRACT: *The paper develops an analytic wind disturbance torque model that can be used to simulate antenna servo errors. The forces due to wind acting on antenna induce torque that creates servo errors which become significant in slow tracking antennas. The model developed is based on the vector sum of torque acting on the antenna and is analytically computed by disintegrating the forces due to wind in mutually orthogonal directions. The demarcation between the existing field models of wind disturbances and the model presented in this article is brought out by the generalization of torque induced with the only variable antenna specific parameter being the porosity.*

Keywords: *Antenna servo errors, antenna torque, field model, mutually orthogonal, wind disturbance*

I. INTRODUCTION

Large antennas are required to capture feeble signals, especially those received from space. Radio telescopes that track astronomical phenomenon and inter planetary satellite tracking antennas fall under these categories. These tracking antennas require very high pointing accuracies and thereby a robust servo control system. The large structures associated with these antennas in ideal conditions require a second-order time invariant feedback controller[1]. However, these large structures are affected by torques generated by wind disturbances. The torque results in large servo errors, which reduce the pointing accuracies of antennas. The requirement of high pointing accuracy antennas call for wind torque disturbance models that can accommodate the induced servo errors. The existing models[2] are field models specific to antennas and thus, require extensive fieldwork before they can be used for designing the servo control loop. The model presented here is generalized for large antenna structures and depends only on one antenna specific parameter. The parameter is the resistance offered by the antenna to wind and is characterized by the porosity of the antenna[2].

The article presented develops an analytic method which employs vector mechanics to calculate the torques generated about a point. The model was conceptualized at Tata Institute of Fundamental Research during servo control design for 45 meter Giant Meterwave Radio Telescope at Pune.

II. THE ANALYTIC MODEL FOR WIND DISTURBANCE TORQUE

The wind disturbance generates torque that is the main cause of servo errors for tracking antenna. The wind torque generated can be analytically expressed as vector sum of torques generated in two mutually perpendicular axes. The determination of wind force from wind velocity is the preliminary modeling step. The force due to wind is calculated using the pressure exerted by wind by virtue of its velocity.

2.1 Obtaining Wind Force from Wind Velocity

An antenna exposed to uniformly blowing wind is acted upon by pressure given by $1/2\ \rho v_w^2$ where
$\rho$is the density of air;
$v_w$is the uniform velocity with which wind is blowing.
The force acting on an area A due to pressure P in quantized as the product of the P and A. Generalized force on antenna of cross sectional area A due to wind is given by Eqn (1).

$$F = \eta_1 \eta_2 PA \tag{1}$$

Where
η_1 is a measure of porosity of the antenna
η_2 is a factor less than 1 that takes into account the relative orientation of the wind, w.r.t. the antenna.
Fig 1 illustrates the interaction of wind with the cross sectional area of an antenna.

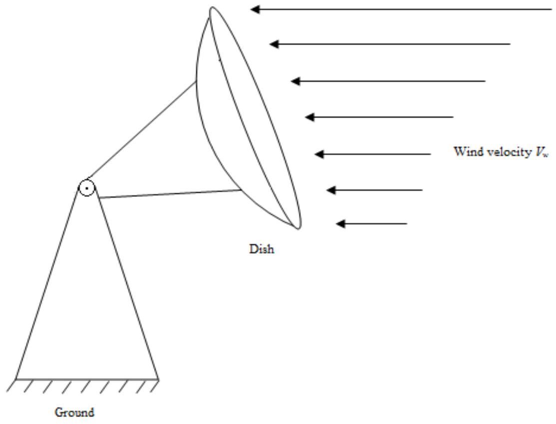

Fig 1: The force generated is a function of wind velocity, area offered by the antenna against wind, porosity of the antenna and the relative orientation of the antenna w.r.t wind.

The wind velocity so far is assumed to be constant. However, it is a function of the height above ground level. The forces experienced by the antenna therefore, vary along the height. The unbalanced forces at the top of the antenna and bottom of the antenna generate torque. The unbalanced force vectors are illustrated in Fig 2.

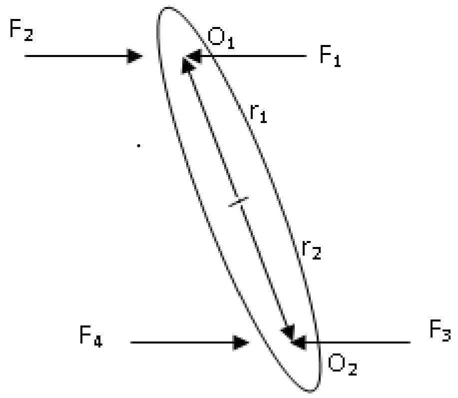

Fig 2: Unbalanced forces due to varying wind velocity generate torque.

The force due to wind is distributed over the entire area of the antenna. However, single vector sum of forces acting on O_1 and O_2 can be calculated which shall produce the same torque as distributed forces would have produced. The vectors are given by Eqns (2-3).

$$\overrightarrow{F_1} - \overrightarrow{F_2} = \overrightarrow{F_{up}} \quad (2)$$

$$\overrightarrow{F_3} - \overrightarrow{F_4} = \overrightarrow{F_{down}} \quad (3)$$

O_1 and O_2 are points on the upper and lower half of discs, where a resultant single vector force shall produce the same effects as distributed force.

2.2 Variation of Wind Velocity: Hellman's Equation

Hellman's equation relates the velocity of wind w.r.t altitude above the earth's surface. (The equation is assumed valid as long as density of air remains constant, within the altitude range or in other words, thinning of air as one goes up is not taken into consideration).

$$v_w(h) = v_o\left(\frac{h}{h_o}\right)^{\alpha} \quad (4)$$

Where
α is the Hellman coefficient
v_o is velocity of wind at reference altitude
$v_w(h)$ is velocity of wind at height h
α can be measured on a day when winds are steady. To measure α , velocity at two points of antenna can be measured and the equation can be solved for α. The measurement can be repeated for precision. To further nullify the effect of wind-gusts, velocity of wind can be taken over finite time duration and wind-gusts being random the velocity of wind will deviate about the steady state wind velocity. Since wind gusts follow Davenport spectrum, the measured α deviates as dictated by Davenport spectrum.

2.3 The Case of Face on Wind: Perpendicular Attack

The perpendicular attack case is the worst case as the whole cross-section of the antenna is exposed to the wind. Fig 3 illustrates the case of perpendicular attack. To calculate force we need an elemental area over which the force is constant. The area is basically a horizontal strip that is at a distance x from the center and is of width dx. The strip subtends an angle θ at the center of parabolic disc. The strip's center subtends an angleϕ at O as illustrated in Fig 4. The strip is the differential element for torque calculation.

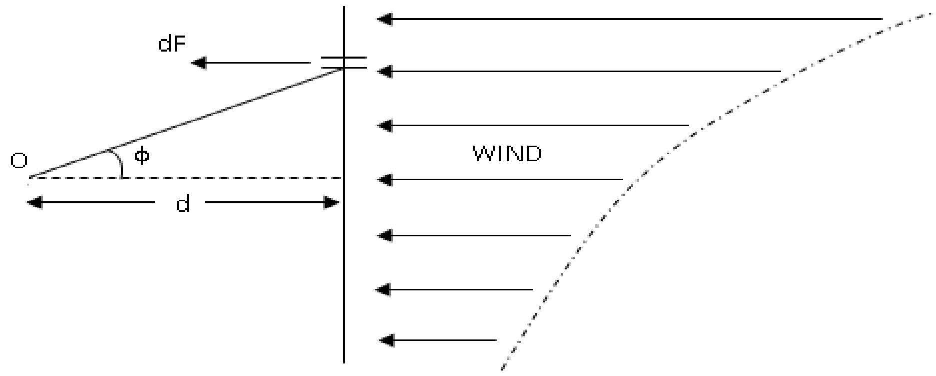

Fig 3: The varying wind velocities are illustrated with different vector lengths. The shaded strip is the part of antenna that encounters equal velocity wind. The differential element for torque calculation is the strip that faces perpendicular force of wind.

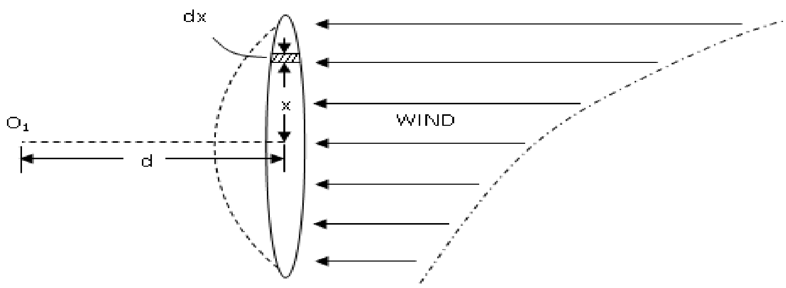

Fig 4: The differential element subtends an angle of ϕat O, which is the point about which the moment is calculated. O being *d* distance away from the center of disc.

Torque calculation requires calculating the force acting on the elemental strip as a function of wind velocity and distance from the center of the parabolic disc A. Fig 5 serves as reference for further analysis.

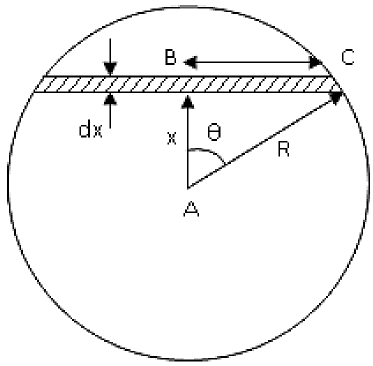

Fig 5: The elemental strip faces constant velocity wind. The center of the circular cross-section is A. The strip subtends θ at A, is *x* distance away from A and is of width *dx.*

The area of the elemental strip in polar coordinates is given by Eqn (5).

$$dA = -2R^2 sin^2\theta d\theta \quad (5)$$

The inclination of antenna is 90° w.r.t wind. Therefore, $\eta_2$is 1. Referring to Eqn (1) the force on the elemental strip can be given as in Eqn (6).

$$dF = 1/2\, \eta_1 \rho v_w^2 \times dA \quad (6)$$

The velocity of wind as a function of height above ground level can be substituted as per Eqn (4), while the elemental area of the strip is substituted from Eqn (5). Eqn (6) modifies to Eqn (7).

$$dF = 1/2\,\eta_1\rho\left(v_o\left(\frac{h}{h_o}\right)^{\alpha}\right)^2 \times (-2R^2 sin^2\theta d\theta) \quad (7)$$

If center of the circle shown in Fig 5 is taken as the reference, the height parameter in Eqn (7) equals *x*. Substituting *x* in polar coordinates in Eqn (7) in place of *h* yields Eqn (8).

$$dF = 1/2\,\eta_1\rho\left(v_o\left(\frac{Rcos\theta}{h_o}\right)^{\alpha}\right)^2 \times (-2R^2 sin^2\theta d\theta) \quad (8)$$

The force on the differential element produces a turning moment about the hinge of antenna. The magnitude of the generated torque is analytically found by multiplying the rotational arm length for the element or the distance of the differential element from O with the component of *dF* perpendicular to the rotational arm. Fig 6 illustrates the force vectors and the rotational arm lengths about O.

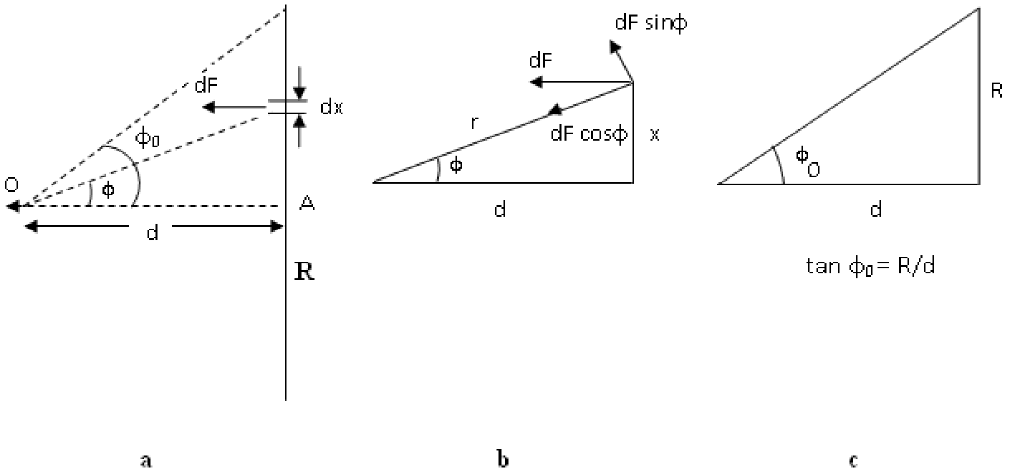

Fig 6: (a) Figure illustrating the angular span of the parabolic disc about O. The radius of the dish being R. (b) Figure showing the resolution of forces perpendicular to the rotational arm *r*. (c) Figure illustrating the relation between radius R of the antenna dish, angular span ϕ_o and distance *d*.

The elemental torque ($d\tau_{up}$) on the elemental strip in the upper half of the parabolic strip is given by Eqn (9).

$$d\tau_{up} = dFsin\phi \times r \quad (9)$$

The force on the elemental strip is calculated in Eqn (8) and substituting *r* as $^{d}/_{cos\emptyset}$ from Fig 6, we have the torque on the elemental strip as

$$d\tau_{up} = -1/2\,\eta_1\rho\left(v_o\left(\frac{Rcos\theta}{h_o}\right)^{\alpha}\right)^2 \times 2R^2 sin^2\theta d\theta \times d \times tan\emptyset \times d\emptyset \quad (10)$$

Integrating Eqn (10) with limits for θ and $\emptyset$ the torque on the upper half disc can be calculated as shown in Eqn (11).

$$\int_0^{\tau} d\tau_{up} = \int_{\theta=0}^{\pi/2}\int_{\phi=0}^{\phi_o}\eta_1\rho\left(v_o\left(\frac{Rcos\theta}{h_o}\right)^{\alpha}\right)^2 \times R^2 sin^2\theta d\theta \times d \times tan\emptyset \times d\emptyset\, d\theta \quad (11)$$

The limits for θ are reversed to absorb the negative sign in *dF* expression. The torque for the lower half of the dish can be found by placing proper limits and appropriate expression for the velocity of wind. The antenna here faces the wind perpendicularly; however, tracking antenna may be inclined at some angle to the wind velocity. The next section takes into account the parameter η_2.

2.4 Antenna Inclined w.r.t the Wind: Angular Attack

The most generalized torque generating case is that of an inclined antenna against arbitrary direction of wind. The assumption here is that the wind follows Hellman's velocity relation, only the direction is arbitrary. Consider the antenna to be inclined at angle ξ as illustrated in Fig 7. Wind force is resolved into three mutually perpendicular components and torque due to each component is measured and generalized for parameter ξ.

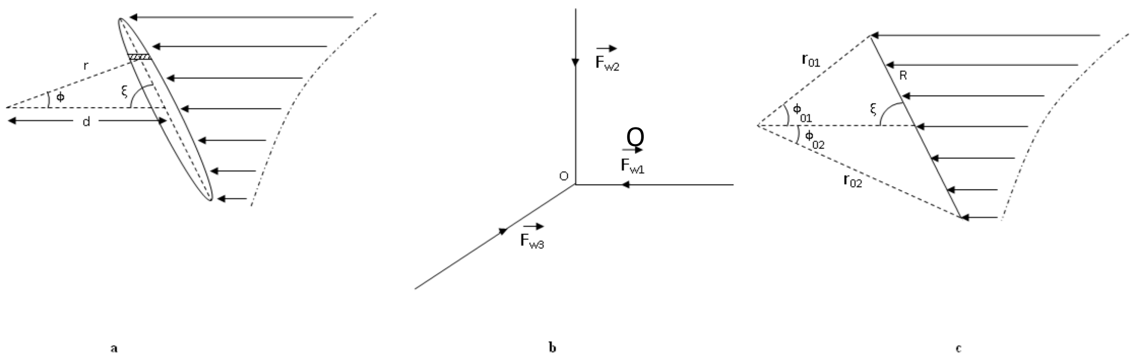

Fig 7: (a) Figure illustrating the inclination of the antenna w.r.t wind. (b) The resolved components of force vector. (c) Figure illustrating the angular span of the antenna about reference O.

The three mutually perpendicular force vectors are depicted in Fig 7 (b). F_{w1} is the direction considered earlier for perpendicular attack. F_{w3} sees the parabolic lateral face analyzed in the next section and F_{w2} is in the vertical direction. The case of wind blowing vertically is seldom encountered and especially when the region experiences tornados and hurricanes.

The differential force on the element is illustrated in Fig 8. The corresponding parameters are depicted in the triangle. The component of the force perpendicular to the moment arm is $dF_{w1} sin\phi$. The element is at a distance r from O. As compared to the case of perpendicular case the element is at an inclination of ξ w.r.t the wind. InΔABO, the relation between sides and angles can be determined by applying Sine Law as in Eqn (12).

$$\frac{r}{sin\xi} = \frac{d}{\sin\left(\pi-(\phi+\xi)\right)} \qquad (12)$$

Applying Sine Law for the triangles in Fig 7 (c) we arrive at Eqns (13-14)

$$\frac{R}{sin\,\phi_{01}} = \frac{d}{\sin\left((\phi_{01}+\xi)\right)} \qquad (13)$$

$$\frac{R}{sin\,\phi_{02}} = \frac{d}{\sin\left((\xi-\phi_{02})\right)} \qquad (14)$$

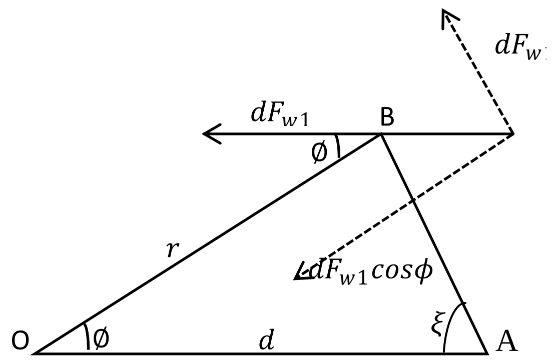

Fig 8: Figure illustrating the force vectors for the differential element. *r* is the distance of the element from O, *d* is the distance of center A from O. and being the angle subtended by the elemental strip at O and A respectively.

The differential torque is given by Eqn (9). Substituting *r* from Eqn (12) and *dF* from Eqn (8) in Eqn (9), the differential torque on the element can be expressed by Eqn (12).

$$d\tau_{up} = -\eta_1 \rho \left(v_o \left(\frac{Rcos\theta}{h_o}\right)^{\alpha}\right)^2 \times R^2 sin^2\theta d\theta \times \frac{dsin\xi}{\sin(\xi+\phi)} \times sinØ \times dØ \qquad (15)$$

The torque on the upper half of the antenna can be obtained by integrating Eqn (15) with limits for θ and ϕ. The limits for ϕ is from *0* toϕ_{01}, where $\phi_{01}$is obtained from Eqn (13).

$$\int_0^{\tau} d\tau_{up} = \int_{\theta=0}^{\pi/2}\int_{\phi=0}^{\phi_{01}} \eta_1 \rho \left(v_o \left(\frac{Rcos\theta}{h_o}\right)^{\alpha}\right)^2 \times R^2 sin^2\theta d\theta \times \frac{dsin\xi}{\sin(\xi+\phi)} \times sinØ \times dØ\, d\theta \qquad (16)$$

2.5. Torque on the Lateral Surface

The antenna employed for tracking is mostly a parabolic antenna. The lateral cross- section thus is a parabola. Fig 9 shows the parameters for a parabolic cross-section. The parabola can be mathematically represented by Eqn (17).

$$y = \frac{K}{R^2} m^2 \qquad (17)$$

The elemental area in this case is the product of length of the strip with its width and can be expressed by Eqn (18)

$$dA = l \times dx \qquad (18)$$

The length of the strip is mathematically the difference between the depth of the parabola *K* and *z*.

$$l = K - z = K\left(1 - \left(\frac{x^2}{R^2 cos^2\xi}\right)\right) \qquad (19)$$

The differential area thus obtained can be substituted in the expression for torque dictated by Eqn (10). The porosity of the antenna may differ as the lateral side now offers resistance to wind. The moment arm in this case is *x* as the torque is generated about *mm'*

$$d\tau_{up} = 1/2\, \eta_{1'} \rho \left(v_o \left(\frac{Rcos\theta}{h_o}\right)^{\alpha}\right)^2 \times K\left(1 - \left(\frac{x^2}{R^2 cos^2\xi}\right)\right) \times dx \times x \qquad (20)$$

Eqn (20) can be integrated over the upper half antenna to obtain the total torque experienced by the upper half part of the dish. Since, this expression does not use polar coordinates the torque expression is a single integral as shown in Eqn (21).

$$\int_0^{\tau_{up}} d\tau_{up} = \int_{x=0}^{Rsin\xi} 1/2\, \eta_{1'} \rho \left(v_o \left(\frac{Rcos\theta}{h_o}\right)^{\alpha}\right)^2 \times K\left(1 - \left(\frac{x^2}{R^2 cos^2\xi}\right)\right) \times dx \times x \qquad (21)$$

The torque for the lower half of the antenna can be expressed with the same equation but with different limits.

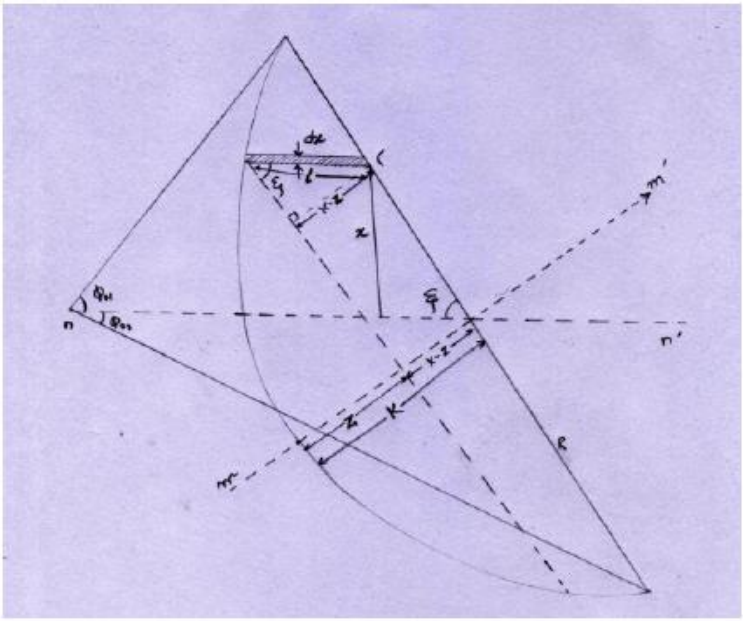

Fig 9: Figure illustrating the lateral cross-section of the parabola with its parameters

III. CONCLUSION AND FUTURE SCOPE

The paper develops a mathematical model for wind disturbance torque on tracking antenna. The vector approach to torque calculation in case of antenna requires only porosity of the antenna as the variable parameter to be as compared to the numerous antenna specific coefficients that need to be calculated while opting for field models of wind disturbance torques. The model here has considered antenna as a single entity, however, a finite element analysis of antenna structure still needs to be explored.

REFERENCES

[1.] W. Gawronski, "Wind Gust Models Derived From Field Data," The Telecommunications and Data Acquisition Progress Report 42-123, July–September 1995, Jet Propulsion Laboratory, Pasadena, California, pp. 30–36, November 15, 1995.
[2.] W. Gawronski and J. A. Mellstrom, "Control and Dynamics of the Deep Space Network Antennas," in Control and Dynamics Systems, C. T. Leondes, ed.,vol. 63, San Diego, California: Academic Press.
[3.] W. Gawronski, B. Bienkiewicz, and R. E. Hill, "Pointing-Error Simulations of the DSS-13 Antenna Due to Wind Disturbances," The Telecommunications and Data Acquisition Progress Report 42-108, October–December 1991, Jet Propulsion Laboratory, Pasadena, California, pp. 109–134, February 15, 1992.
[4.] Norman S. Nise, Control System Engineering, 4th edition, Wiley Education Press.
[5.] BC Joshi,"Simulation Study of Servo Control System of 45 meter Giant Metrewave Radio Telescope".
[6.] www.ncra.tifr.res.in

ABOUT THE AUTHOR

Tushar Golani received his B.Tech from Indian Institute of Space Science and Technology, Thiruvananthapuram. He joined ISRO Satellite Centre in 2011 and is currently working in Spacecraft Checkout Group. His areas of interest include control systems, analog and digital circuit design and embedded systems. He is elected as a life member of the Astronautical Society of India (ASI) and Associate Member of the Aeronautical Society of India (AeSI).

Suresh Sabhapathy is appointed as Engineer-'F' at the Giant Metrewave Radio Telescope facility of TIFR. He is the group coordinator of the servo control systems group and is actively working in the field of linear and non-linear control of large structures. He has guided several students in the field of servo control systems.

Optimized, Low-Power Dissipative and Precise Pulsating Constant Current Source Based Temperature Measurement System

Gowrishankara.C.K[1], Tushar Golani [2]
Spacecraft Checkout Group, ISRO Satellite Centre Bangalore-560 017, INDIA

ABSTRACT: *A constant voltage source based temperature measurement system; using PRT-1000 is one of the currently used methods to measure the temperature of subsystems in Indian Satellites. One such subsystem which uses PRT-1000 is solar panels. This paper describes a constant current source based temperature measurement system and the advantages it offers in terms of linearity, sensitivity and power dissipation. Simulations using MATLAB and Simulink® are carried out to illustrate the differences between the two methods. To overcome self-heating effects in the resistor a pulsating constant current source based temperature measurement system is described.*

Keywords: *Linearity, pulsating constant current source, PRT-Platinum Resistance Thermometry, SADA- Solar Array Drive Assembly, self-heating, sensitivity.*

I. INTRODUCTION

Remote Sensing as well as Geostationary satellites use deployable solar panels [1], [2], [3] to convert solar energy to electrical energy. The solar panels at a time either face the sun or the dark space. The orientation thus, leads to a large temperature variation of about 400 ºC (-200 ºC to +200 ºC). This temperature variation is sensed using PRT-1000 and associated circuitry. The paper presents two methods that can be used with PRT-1000 namely constant voltage source method and constant current source method.

II. CONSTANT VOLTAGE SOURCE METHOD

The constant voltage source method employs the PRT-1000 as one of the resistor of a voltage divider circuit and maps the associated voltage change to the corresponding temperature changes. The following circuit setup is currently used. R_{SADA} is the resistance offered by the slip rings of the rotary power transferring assembly called SADA.

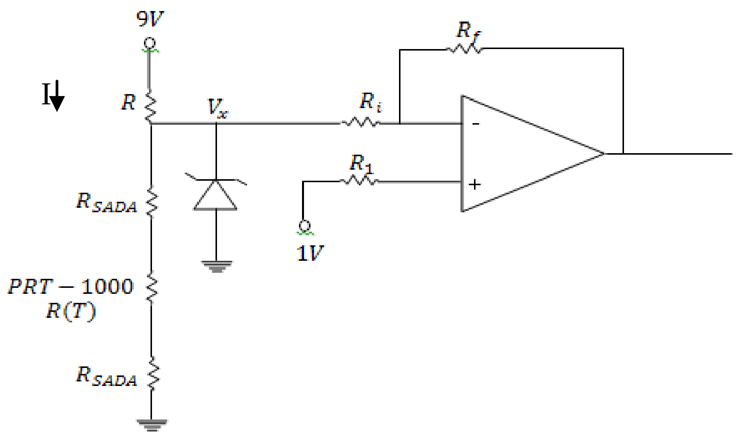

Fig 1: Temperature measurement system using constant voltage source and PRT-1000

2.1 Mathematical analysis

Let a current I flow as shown. If R= 10K, then by Ohm's Law and assuming infinite input impedance for the op-amp:-

$$I = \frac{9V}{10K + R(T)} \tag{1}$$

where R(T) is the resistance of the PRT-1000 that varies with temperature.
We have

$$V_x = V + V_{NOISE} \tag{2}$$

where
V_x is the voltage at one end of R_{in}
V is the voltage induced by the voltage divider circuit
V_{NOISE} is the voltage noise added due to SADA. It is approximately 10mV/Amp.
We have, the voltage at the Zener due to voltage divider circuit as:-

$$V = \left(\frac{R(T)}{10K + R(T)}\right) \times 9V \tag{3}$$

Writing Kirchoff's loop equation for the op-amp, we obtain

$$\frac{V_x - 1}{R_{in}} = \frac{1 - V_{out}}{R_f} \tag{4}$$

Simplifying the above equation and rearranging the terms, we obtain

$$V_x - 1 = \beta(1 - V_{out}) \tag{5}$$

Where

$$\beta = \frac{R_{in}}{R_f} \tag{6}$$

Solar Array Drive Assembly (SADA) of the satellite introduces voltage noise that is proportional to the current flowing through it and given as:-

$$V_{NOISE} = 10\frac{mV}{A} \times I$$

Taking into account the negative path SADA, we have

$$V_{NOISE} = 2 \times 10mv \times \left(\frac{9v}{10k + R\,(T)}\right)$$

$$V_x = \left(\frac{R(T)}{10K + R(T)}\right) \times 9V + 2 \times 10mV \times \left(\frac{9V}{10K + R(T)}\right) \tag{7}$$

The linearity of the system can be measured by analyzing the differential of the system w.r.t the variable parameter. If the differential is constant, the system linearly depends on the variable parameter. Differentiating (5) w.r.t temperature (T), we obtain

$$\frac{dV_x}{dT} = -\beta \frac{dV_{out}}{dT} \tag{8}$$

Substituting, V_x from equation (7), equation (8) modifies to

$$\frac{dV_x}{dT} = \frac{d}{dT}\left\{\left(\frac{R(T)}{10K + R(T)}\right) \times 9V\right\} + \frac{d}{dT}\left\{\left(\frac{0.02}{10K + R(T)}\right) \times 9\right\} \tag{9}$$

Simplifying equation (9)

$$\frac{dV_x}{dT} = \frac{d}{dT}\left\{\left(\frac{(9R(T) + 0.18)}{10K + R(T)}\right)\right\} \tag{10}$$

$$\frac{dV_x}{dT} = \frac{(90K - 0.18)}{\left(10K + R(T)\right)^2} \times \frac{dR(T)}{dT} \tag{11}$$

The differential term $\frac{dR(T)}{dT}$ represents the differential variation of resistance of PRT w.r.t temperature. The relation between the resistances of PRT w.r.t temperature is a complex n-th order equation in temperature. However, the higher order equations are negligible and can be ignored; thus reducing the dependence of R (T) to first order equation as shown below

$$R(T) = R_o(1 + \alpha dT) \tag{12}$$

Differentiating equation (12) we obtain $\frac{dR(T)}{dT}$ as

$$\frac{dR(T)}{dT} = R_o\alpha \tag{13}$$

Substituting values of R_o and α, in equation (13), and thereafter substituting the result in (11), we have

$$\frac{dV_x}{dT} = \frac{(90K - 0.18)}{\left(10K + R(T)\right)^2} \times 3.85 \tag{14}$$

$$\frac{dV_x}{dT} = \frac{(90K - 0.18)}{\left(10K + 1000(1 + 3.85\Delta T)\right)^2} \times 3.85 \tag{15}$$

Equation (15) illustrates that the change in voltage w.r.t is not constant and varies with change in temperature. However, for a linear system the differential should be constant to yield a linearly varying integral (or the system). The output depends on the input as given by equation (16)

$$V_{out} = \frac{\beta + 1 - V_x}{\beta} \tag{16}$$

The linear relationship between V_{out} and V_x makes V_{out} nonlinear w.r.t temperature. Thus, it can be concluded that a constant voltage source based temperature measurement system is non-linear method of measurement.

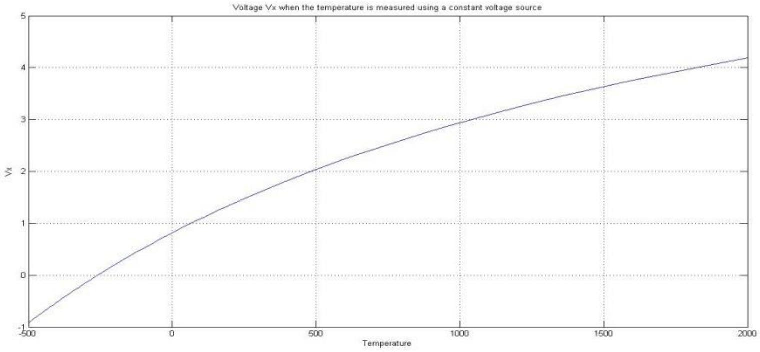

Fig 2: MATLAB simulation depicting nonlinear curve between Vx and Temperature (T) when constant voltage source based temperature measurement system is employed

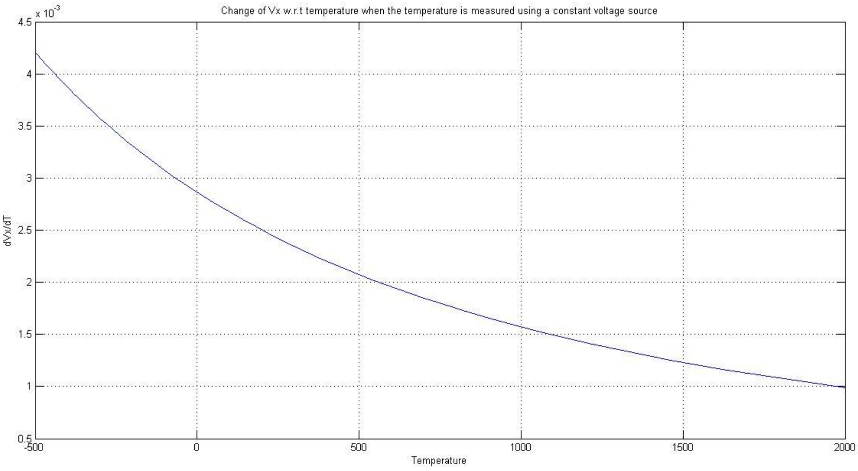

Fig 3: MATLAB simulation showing the nonlinear behavior of the differential of Vx w.r.t Temperature (T) when constant voltage based temperature measurement system is employed

2.2 Sensitivity Analysis

Sensitivity discussed in this section refers to the variation of the output voltage with changes in temperature. By equation (8) it is evident that the change in output voltage is proportional to the change in V1 w.r.t temperature. Sensitivity in the output voltage is a factor multiplied to the sensitivity of $V_{X..}$ The analysis here shown that the voltage source based temperature measurement system lacks an optimized discrete value of R for which the system is most sensitive. Keeping the fixed resistor of the voltage divider as the optimizing parameter, we differentiate V_X w.r.t temperature.

Applying Ohm's Law and assuming infinite input impedance for the op-amp, we have:

$$V = \frac{R(T)}{R + R(T)} \times 9V \tag{17}$$

Taking into account the noise introduced by SADA:

$$V_x = V + V_{NOISE} \tag{18}$$

Differentiating equation (18), w.r.t temperature

$$\frac{dV_x}{dT} = \frac{d}{dT}\left\{\left(\frac{R(T)}{R + R(T)}\right) \times 9V\right\} + \frac{d}{dT}\left\{\left(\frac{0.02}{R + R(T)}\right) \times 9\right\} \tag{19}$$

Clubbing the derivatives of summation terms from equation (19), we arrive at equation (20) as:

$$\frac{dV_x}{dT} = \frac{d}{dT}\left\{\left(\frac{(9R(T) - 0.18)}{R + R(T)}\right)\right\} \tag{20}$$

Simplifying equation (20), gives the derivatives in terms of $\frac{dR(T)}{dT}$, R and $R(T)$ as written in equation (21)

$$\frac{dV_x}{dT} = \frac{(9R(T) - 0.18)}{\left(R + R(T)\right)^2} \times \frac{dR(T)}{dT} \tag{21}$$

Substituting $\frac{dR(T)}{dT}$ as 3.85 $\Omega/^0$C

$$\frac{dV_x}{dT} = \frac{(9R(T) - 0.18)}{\left(R + R(T)\right)^2} \times 3.85 \tag{22}$$

The change in Vx is maximum when the differential of Vx w.r.t T is zero, i.e. to say the second derivative of Vx w.r.t T should be zero. Therefore, differentiating equation (22)

$$\frac{d^2V_x}{dT^2} = \frac{d}{dT}\left(\frac{(9R(T) - 0.18)}{\left(R + R(T)\right)^2} \times 3.85\right) = 0 \tag{23}$$

Simplifying

$$\frac{d^2V_x}{dT^2} = \frac{-(9R - 0.18) \times \left(R + R(T)\right) \times 3.85 \times 2}{(R + R(T))^4} = 0 \tag{24}$$

Solving equation (24) yields R in terms of R(T) which itself varies with temperature. Thus, there is no optimized value of R for which the circuit is most sensitive, i.e. to say R should also change over temperature so that the output voltage experiences maximum change with corresponding change in temperature.

III. CONSTANT CURRENT SOURCE METHOD

A constant current source based temperature measurement system proposes the following advantages over constant voltage source based temperature measurement system:

(a) Linear Relationship between V_{out} and temperature.
(b) Greater sensitivity independent of R.
(c) Reduced power dissipation.

The following setup shows a constant current source based temperature measurement system.

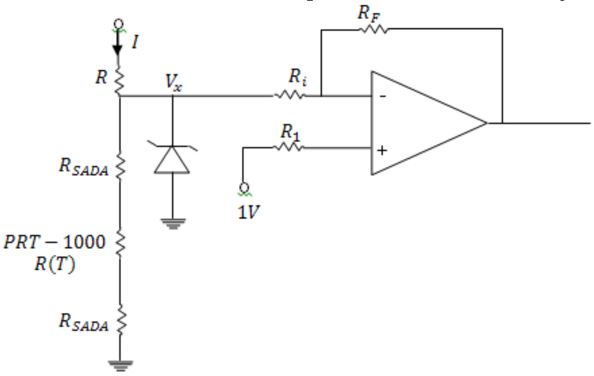

Fig 4: Temperature measurement system using constant current source and PRT-1000

3.1 Mathematical analysis

The mathematical analysis is aimed to prove the linearity of a constant current source based temperature measurement system. The approach is similar to the one followed for constant voltage source based temperature measurement system. Here too, the aim is to prove the linearity of the system, by showing that the derivative of Vx is constant w.r.t temperature.

Let a constant current I flow as shown. The voltage induced due to PRT, because of a constant current flowing is

$$V = IR(T) \tag{25}$$

The voltage observed at the zener is the sum of V and the noise introduced by the SADA resistances. This is given as:

$$V_x = V + V_{NOISE} \tag{26}$$

$$V_x = V + \frac{10I}{1000}V \tag{27}$$

Substituting V from equation (25) into (27)

$$V_x = IR(T) + \frac{I}{100} \tag{28}$$

Writing KVL for the inverting input of the op-amp

$$\frac{V_x - 1}{R_i} = \frac{1 - V_{out}}{R_f} \tag{29}$$

$$V_x - 1 = \beta(1 - V_{out}) \tag{30}$$

$$V_{out} = \frac{\beta + 1 - V_x}{\beta} \tag{31}$$

Where

$$\beta = \frac{R_{in}}{R_f}$$

The linearity of the system can be found by differentiating equation (31) w.r.t temperature (T). We have

$$\frac{dV_{out}}{dT} = \frac{d}{dT}\left(\frac{\beta + 1}{\beta}\right) - \frac{d}{dT}\left(\frac{V_x}{\beta}\right) \tag{32}$$

Substituting Vx from equation (28)

$$\frac{dV_{out}}{dT} = \frac{-1}{\beta}\frac{d}{dT}\left(IR(T) + \frac{I}{100}\right) \tag{33}$$

Since, I is constant its differential is zero w.r.t 'T'

$$\frac{dV_{out}}{dT} = -\frac{I}{\beta}\left(\frac{dR(T)}{dT}\right) \tag{34}$$

$\frac{dR(T)}{dT}$ is the change of PRT resistance with temperature, and first order relation between R(T) and T, we have

$$\frac{dV_{out}}{dT} = -\frac{R_o \alpha I}{\beta} \tag{35}$$

Equation (35) clearly illustrates that the change of Vout w.r.t is constant, i.e. Vout varies linearly with temperature. The following equations derive the linear relation between the output voltage and temperature.

$$V_{out} = \frac{\beta + 1 - V_x}{\beta} \tag{36}$$

$$V_{out} = \frac{\beta + 1 - IR(T) + {}^{I}/_{100}}{\beta} \tag{37}$$

$$V_{out} = c - \frac{I}{\beta}R(T) \tag{38}$$

$$c = \frac{\beta + 1 + {}^{I}/_{100}}{\beta} \tag{39}$$

Equation is an equation of line. Proper op-amp biasing will make the circuit perfectly linear.

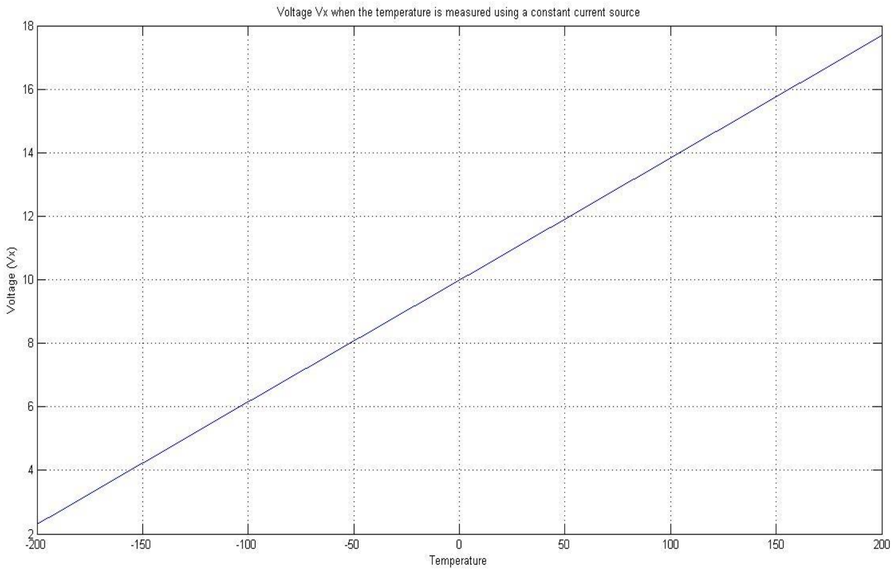

Fig 5: MATLAB simulation depicting nonlinear curve between Vx and Temperature (T) when constant voltage source based temperature measurement system is employed

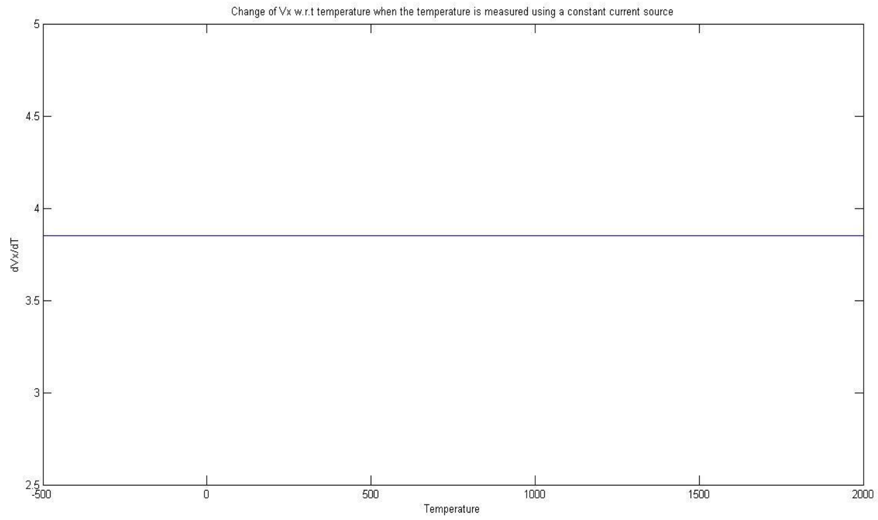

Fig 6: MATLAB simulation showing the nonlinear behavior of the differential of Vx w.r.t Temperature (T) when constant voltage based temperature measurement system is employed

3.2 Sensitivity Analysis
The constant current source based temperature measurement system can be simplified to the following.
We have

$$V = IR(T) \tag{40}$$

We observe that V is independent of R and thus sensitivity depends only on R(T). R can be chosen so as to address power dissipation issues.

IV. OP-AMP BASED CONSTANT CURRENT SOURCE

A constant current source can be realized using a power op-amp and a current sense resistor. The following circuit setup shows a constant current source realization.

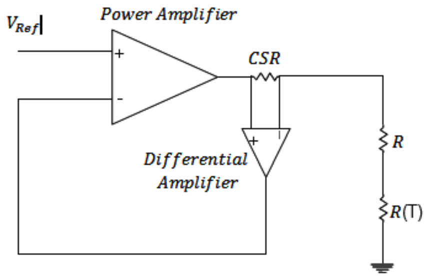

Fig 7: A constant current source using power op-amps

The voltage drop across the CSR is monitored using a differential amplifier. Any change in current I, causes a change in the voltage across the CSR. This change is sensed using a differential amplifier and is fed back to the power op-amp. The op-amp adjusts its output voltage so as to maintain constant current through the CSR. The CSR is typically of very small value, so as to minimize power dissipation.

V. CONSTANT CURRENT PULSES BASED TEMPERATURE MEASUREMENT METHOD

A constant current source based temperature measurement system proposes several advantages over constant voltage source based temperature measurement system. However, it suffers from the self-heating effects of PRT, which causes erroneous temperature measurement. This can be overcome by a pulsating constant current source based temperature measurement system.

Microcontroller based pulsating constant current source

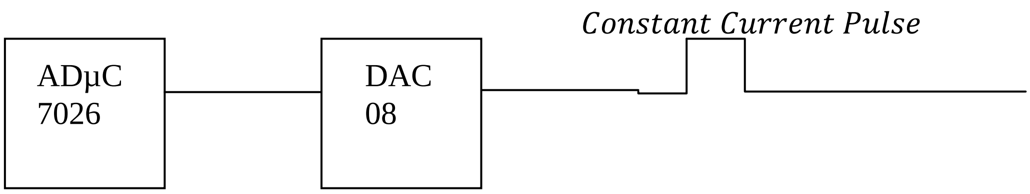

Fig 8: A pulsating constant current source using power op-amps

Pulsating constant current source is realized using a microcontroller (ADµC 7026) and DAC 08. DAC 08 is a voltage to current conversion chip. It produces small current proportionally to the voltage fed to it. Constant signal pulses are programmed and sent through the microcontroller periodically (Appendix B) and these pulses are converted to current pulses. These current pulses when passed through the PRT generate corresponding voltages and can be used to measure the resistance and in turn to temperature.

VI. CONCLUSION

The paper draws a comparative picture between a constant voltage source based temperature measurement system and a constant current source based temperature measurement system. The constant current source has been proved to be linear analytically as well as through simulations. A constant current source based temperature measurement system induces power dissipation in PRT and leads to self-heating . A constant pulsating current source based temperature measurement system is proposed over constant current source based temperature measurement system. The later method highlights the following:

- An optimized temperature measurement system that eliminates the effect of constant series resistance from the sensitivity of the circuit.
- A constant current pulse of short duration leads to low power dissipation and reduces the self-heating effect of PRT, thereby making the system more precise.

ACKNOWLEDGEMENTS

The authors are thankful to Group Director Spacecraft Checkout Group, ISAC Bangalore, for his valuable support, technical discussions and encouragement for this work.

REFERENCES

[1] Jones P A, Spence B R. Spacecraft solar array technology trends. Aerospace Conference Proceedings, 1998 IEEE. 1998; 141-152.
[2] Kwak M K, Heo S, Kim H B. Dynamics of satellite with deployable rigid solar arrays. Multibody System Dynamics 2008; 20(3): 271-286.
[3] Jorgensen J R, Louis E L, Hinkle J D, et al. Dynamics of an elastically deployable solar array: ground test model validation. AIAA-2005-1942, 2005.
[4] Patel, Mukund R., Wind and Solar Power Systems, CRC Press, 1999

ABOUT THE AUTHOR

Gowrishankara.C.K. Project Manager SCOS-Hylas, Mainframe checkouts of GSAT-6, GSAT-14 & GSAT-11. He received his M.E in Power Electronics from Bangalore University. He Joined SDSC-SHAR Centre and worked in the field of process instrumentation and industrial electronics. He is presently with ISRO Satellite Centre and is working in the area of spacecraft checkout. His work areas include development of power and signal simulators for spacecraft testing, SMPS and Process-Instrumentation.

Tushar Golani received his B.Tech from Indian Institute of Space Science and Technology, Thiruvananthapuram. He joined ISRO Satellite Centre in 2011 and is currently working in Spacecraft Checkout Group. His areas of interest include control systems, analog and digital circuit design and embedded systems. He is elected as a life member of the Astronautical Society of India (ASI) and Associate Member of the Aeronautical Society of India (AeSI).

International Journal of Modern Engineering Research (IJMER)
www.ijmer.com Vol. 3, Issue. 5, Sep - Oct. 2013 pp-3255-3266 ISSN: 2249-6645

Tannin gel derived from Leaves of Ricinus Communis as an adsorbent for the Removal of Cu (II) and Ni (II) ions from aqueous solution

M. Makeswari[1], T. Santhi[2]
Department of chemistry, Karpagam University, Coimbatore 641021, Tamil Nadu, India.

ABSTRACT: *The biosorption of Cu (II) and Ni (II) ions from aqueous solutions by Tannin gel derived from Leaves of Ricinus Communis was investigated as a function of $pH_{ZPC,}$ Initial pH, adsorbent dose, contact time and metal ion concentration. The aim of this study was to prepare the adsorbent and to find a suitable equilibrium isotherm and kinetic model for the removal of Cu (II) and Ni (II) ions in a batch reactor. The maximum percentage of adsorption for the removal of Cu (II) ion was found to be 76.92% at 7.04 pH and for the removal of Ni (II) ion was 71.74% at 7.12 pH. The adsorption of Cu (II) and Ni (II) ions followed the Pseudo-second-order and Intra particle diffusion rate equations and fits the Langmuir, Freundlich and Frenkel-Halsey-Hill isotherm equations well. The effects of the presence of one metal ion on the adsorption of the other metal ion were investigated in binary and ternary mixture and then the results were compared with single system. We investigate the recovery of the used adsorbent for its reusing is of great importance for environmental and economical reasons. i.e., TGLRC will be recovered by desorption method by using proper desorption agent like H_2O by batch mode study. Activated carbon developed from Ricinus Communis leaves can be an attractive option for heavy metal removal from water and waste water since test reactions made on stimulated waste water sowed better removal percentage of Cu (II) and Ni (II) ions.*

Keywords: *Adsorption; Tannin gel; Ricinus communis leaves; Binary and Tertiary; Desorption.*

I. INTRODUCTION

The pollution of water resources due to the indiscriminate disposal of heavy metals has been causing worldwide concern for the last few decades. It is well known that some metals can have toxic or harmful effects on many forms of life. Among the most toxic metals are chromium (Cr), copper (Cu), lead (Pb), zinc (Zn) and mercury (Hg), which is one of the 11 hazardous priority substances in the list of pollutants contained in the Water Framework Directive (Directive 2000/60/EC) [1]. Many industries discharge heavy metals such as lead, cadmium, copper, nickel and zinc in their wastewaters [2]. Metals such as copper and nickel are known to be essential to plants, humans and animals, but they can also have adverse effects if their availability in water exceeds certain threshold values.

Therefore, it is urgent to remove heavy metals such as copper and nickel from wastewater. Although heavy metal removal from aqueous solutions can be achieved by conventional methods, including chemical precipitation, oxidation/reduction, electrochemical treatment, evaporative recovery, filtration, ion exchange and membrane technologies, they may be ineffective or cost-expensive, especially when the metal ion concentrations in solution are in the range of 1–100 mg/L [3, 4]. Recently, adsorption technology has become one of the alternative treatments in either laboratory or industrial scale [5, 6]. There are many adsorbents in use. Activated carbons (AC) are known as very effective adsorbents due to their highly developed porosity, large surface area, variable characteristics of surface chemistry, and high degree of surface reactivity [7]. However, due to their high production costs, these materials tend to be more expensive than other adsorbents. This has led a growing research interest in the production of activated carbons from renewable and cheaper precursors. The choice of precursor largely depends on its availability, cost, and purity, but the manufacturing process and intended applications of the product are also important considerations [8]. Several suitable agricultural by-products (lignocellulosics) including fruit stones, olive waste cake, pine bark, rice husks, pistachio-nut shells and wheat bran have been investigated in the last years as activated carbon precursors and are still receiving renewed attention.

In recent years, considerable attention has been focused on the removal of heavy metals from aqueous solution using natural raw materials are an interesting potential source of low-cost adsorbents [9-11]. Tannins, natural biomass containing multiple adjacent hydroxyl groups and exhibiting specific affinity to metal ions, can probably be used as alternative, effective and efficient adsorbents for the recovery of metal ions. During the last years, the interest on biomaterials and specifically in tannins was growing.

The term tannins cover many families of chemical compounds. Traditionally they have been used for tanning animal skins, hence their name, but one also finds several of them used as water treatment agents. Their natural origin is as secondary metabolites of plants [12], occurring in the bark, fruit, leaves, etc. While Acacia and Schinopsis bark constitute the principal source of tannins for the leather industry, the bark of other non-tropical trees such as Quercus ilex, suber, and robur, Castanea, and Pinus can also be tannin-rich.

Tannin gelification is a chemical procedure that inmobilizes tannins in an insoluble matrix [13, 14] so their properties involving, e.g. metal chelation, are available then in an efficient adsorbing agent. In addition, the resulting material from gelification (sometimes called tannin rigid gel) presents interesting properties from the point of view of resistance, nonflammability or mechanical undeformability [15, 16]. Gelifications of tannins have been widely reported either in scientific literature or in patents. Experimental conditions of gelification may imply the use of formaldehyde or other aldehyde in a basic or acidic environment. Examples of basic gelification are shown in scientific literature previously [17-19] and in patents such as US patent 5,158,711 [20]. Acid gelification is also presented by other researchers [21, 22].

The chemical basis of the tannin gelification is widely reported [23]. Formaldehyde and other aldehydes react with tannins to induce polymerization through methylene bridge linkages at reactive positions on the tannin flavonoid molecules.

Agricultural by-products are high volume, low value and underutilized lignocellulosic biomaterials, and contain high levels of cellulose, hemicellulose and lignin. *Ricinus communis* is a species of flowering plant in the spurge family, Euphorbiaceae. It belongs to a monotypic genus, Ricinus, and subtribe, Ricininae.

Ricinus communis grows throughout the drier parts and near drainages of India. Annual production of *Ricinus communis* is estimated to be more than 1.0 tons globally, of which India accounts for 60% of the production. The adsorption ability of *Ricinus communis leaves was* previously investigated for the adsorption of Cu^{2+} ion and Ni^{2+} ion from aqueous solution [24, 25].

In this study, Tannin gel has been prepared from the cheap and abundantly available agricultural waste product leaves of *Ricinus communis* (TGLRC) and applied them to remove heavy metals such as Cu (II) and Ni (II) ions from waste water.

The objective of this study is to systematically examine adsorption mechanisms, adsorption isotherms, adsorption kinetics and properties of a tannin gel adsorbent synthesized from leaves of *Ricinus communis* (TGLRC) for removal of Cu (II) and Ni (II) ions from aqueous solutions.

II. MATERIALS AND METHODS

Preparation of Adsorbent

Tannin extracts

The *Ricinus communis leaves* were obtained from the agricultural form in Tirupur district (Tamil Nadu). It was air-dried and powdered in a grinder. Dried *Ricinus communis* with the mass of 100 g were mixed with 600 mL of water. Then 5 g of NaOH were added and the mixture was stirred in magnetic stirrer at 90°C for 1 h. Solids was separated by filtration and liquid fraction was dried in oven (65°C) overnight. The resultant was considered the tannin extract.

Tannin gel preparation (TGLRC)

Tannin gels were prepared according to the basis of Nakano et al. [17]. Five grams of tannin extract were dissolved in 32mL of NaOH (PANREAC) 0.125 mol L−1 and 30mL of distilled water at 80 ◦C. When mixture was homogeneous, certain amount of aldehyde (Formaldehyde) was added and reaction was kept at the same temperature for 8 h until polymerization was considered completed. Then, the apparent gummy product was lead to complete evaporation of water remain and dried in oven (65º C) overnight. After drying, tannin rigid gels were crushed to small particles. They were washed successively with distilled water and 0.01 molar HNO_3 was used to remove unreacted sodium hydroxide. Finally, the adsorbent was dried again in oven. Differences are found between this preparation way and the description made by Yurtsever and Sengil [26], mainly concerning the amount of formaldehyde.

Preparation of stock solution

Samples of potassium chromate (K_2CrO_4), copper sulphate penta hydrate ($CuSO_4.5H_2O$) and Nickel sulphate hexa hydrate ($NiSO.6H_2O$) was obtained from Aluva, Edayar (specrum reagents and chemicals pvt. Ltd). All other chemicals used in this study were analytical grade and Purchased from Aluva, Edayar (specrum reagents and chemicals pvt. Ltd)

A Stock solution of 1000 mg/L was prepared by dissolving accurately weighed amounts of potassium chromate (K_2CrO_4) in doses of 1000 mL double-distilled water. Working copper and Nickel solutions were prepared just before used by appropriate dilutions of stock solution.

Characterization of the adsorbent

The point of zero surface charge characteristic of TGLRC was (pH_{ZPC}) determined by using the solid addition method. A Fourier transform infrared spectroscopy (SHIMADZU, IR Affinity-1) with KBr pellet was used to study the functional groups available on the surface of TGLRC, with a scanning range of 4000-400cm^{-1}. The crystalline structure of TGLRC was evaluated by X-ray diffractometer, by using Cu K_α radiation (1.54060 Å) at 45 kV and 30 mA with a scan analysis. The concentration of Cu (II) and Ni (II) ions was determined using UV-vis spectrophotometer (SHIMADZU UV-2450).

Batch adsorption studies

The adsorption experiments were carried out in a batch process to evaluate the effect of pH, contact time, adsorbent dose, adsorption kinetics, adsorption isotherm, influence of other metal ions in single and binary system and regeneration of Cu (II) and Ni (II) ions onto TGLRC.

Batch equilibrium studies

To study the effect of parameters such as adsorbent dose, metal ion concentration and solution pH for the removal of adsorbate on TGLRC, batch experiments were performed. Stock solutions of $CuSO_4.5H_2O$ and $NiSO_4.6H_2O$ was prepared and further diluted to the 25 – 200 mg/ L concentrations for the experiments. pH adjustment was fulfilled by adding 0.1 M HCl or 0.1 M NaOH into the solutions with known initial metal concentrations. Batch adsorption experiments were conducted in asset of 250 mL stoppered flasks containing 200 mg adsorbent and 50 mL of metal solutions with different concentrations (25-200 mg / L) at the optimum solution pH. The flasks were agitated using a mechanical orbital shaker, and maintained at room temperature for 2 h at a fixed shaking speed of 120 rpm until the equilibrium was reached. The suspensions were filtered and metal concentrations in the supernatant solutions were measured using a Digital photo colorimeter (model number-313). From the initial and final concentrations, percentage removal can be calculated by use of the formula:

$$\% \text{ of Removal } = \frac{(C_0 - C_f)}{C_0} \times 100 \qquad (1)$$

where C_o is the initial concentration of Cu (II) and Ni (II) ions in mg/L and C_f is the final concentration of Cu (II) and Ni (II) ions in mg/L. The results obtained in batch mode were used to calculate the equilibrium metal uptake capacity. The amounts of uptake of Cu (II) and Ni (II) ions by TGLRC in the equilibrium (q_e) were calculated by the following mass-balance relationship:

$$q_e = \frac{(C_0 - C_e)}{W} \times V \qquad (2)$$

where q_e is the equilibrium uptake capacity in mg/g, V is the sample volume in liters, C_o is the initial metal ion concentration in mg/L, C_e the equilibrium metal ion concentration in mg/L, and W is the dry weight of adsorbent in grams.

III. RESULTS AND DISCUSSION

Characterization of TGLRC adsorbent

Zero point charges (pH_{ZPC})

The zero surface charge characteristics of TGLRC were determined by using the solid addition method [27]. The experiment was conducted in a series of 250 mL glass stoppered flasks. Each flask was filled with 50 mL of different initial pH $NaN0_2$ solutions and 200 mg of TGLRC. The pH values of the $NaN0_2$ solutions were adjusted between 2 to 10 by adding either 0.1 M HNO_3 or 0.1 M NaOH. The suspensions were then sealed and shaken for 2 h at 120 rpm. The final pH values of the supernatant liquid were noted. The difference between the initial pH (pH_i) and final pH (pH_f) values ($pH = pH_i - pH_f$) was plotted against the values of pH_i. The point of intersection of the resulting curve with abscissa, at which pH of 0, gave the pH_{zpc}.

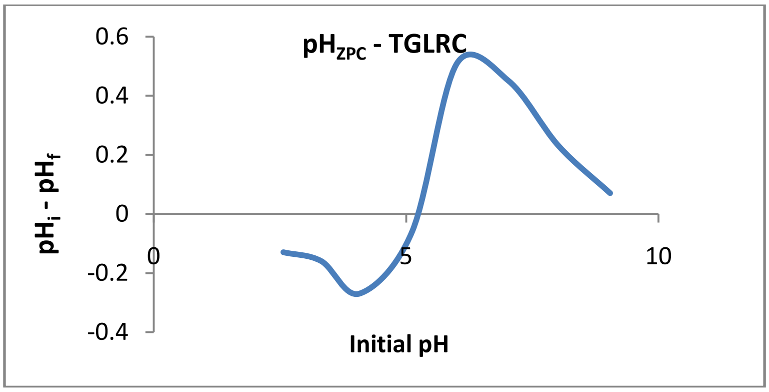

Figure. 1. Zero point charge of TGLRC.

The pH_{ZPC} of an adsorbent is a very important characteristic that determines the pH at which the adsorbent surface has net electrical neutrality. *Fig.1.* shows that the plot between ΔpH, i.e. ($pH_i - pH_f$) and pH_i for pH_{ZPC} measurement. The point of zero charge for TGLRC is found to be 5.12. This result indicated that the pH_{ZPC} of TGLRC was depended on the raw material and the activated agency. The zero point charge ($pH_{ZPC} = 5.12$ for TGLRC) is below the solution pH (pH = 7.04 for Cu (II) and 7.12 for Ni (II) ion adsorption) and hence the negative charge density on the surface of TGLRC increased which favours the adsorption of Cu (II) and Ni (II) ions [28].

FTIR analysis of TGLRC

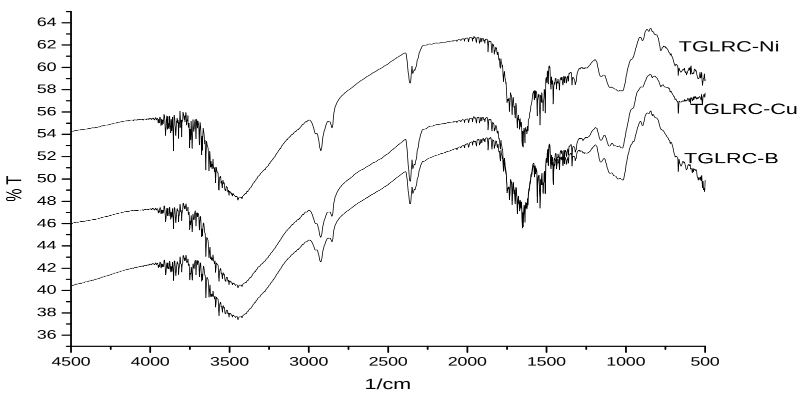

Figure. 2. FTIR spectra for TGLRC before and after adsorption of Cu (II) and Ni (II) ions.

Surface functional groups were detected by Fourier-transform infrared spectroscopy. The *Fig. 2* shows the FTIR spectra of TGLRC before and after adsorption of Cu (II) and Ni (II) ions from aqueous solution. The functional groups of the adsorbents and the corresponding infrared absorption frequency are shown in *Table 1.* These spectra contain peaks at 3421-3462 cm^{-1}. This indicates the presence of hydrogen-bonded OH groups. The peak 3421 cm^{-1} which is originated from TGLRC before adsorption of Cu (II) and Ni (II) ions is shifted to 3462 cm^{-1} in TGLRC-Cu (after adsorption of Copper) and shifted to 3446 cm^{-1} in TGLRC-Ni (after adsorption of Nickel). The intense bent at about region 2852-2854 cm^{-1} for the precursor was attributed to the asymmetric and symmetric vibration modes of methyl and methylene group (C-H group)[29]. The peak around 1647-1653 cm^{-1} can be assigned to aromatic ring vibrations. The peak at 1018-1047 cm^{-1} is related to lignin. Therefore it is possible that cellulose, hemicelluloses as well as lignin, having many OH groups in their structure, make up most of the absorbing layer.

Table 1. The FTIR spectral characteristics of TGLRC before and after adsorption of Cu (II) and Ni (II) ions.

IR Peak	Frequencies (cm^{-1})	Assignment
1	3447	Bonded –OH groups
2	2852	Aliphatic C-H groups
3	1647	Aromatic ring vibrations
4	1022	-C-C group

X-ray diffraction analysis

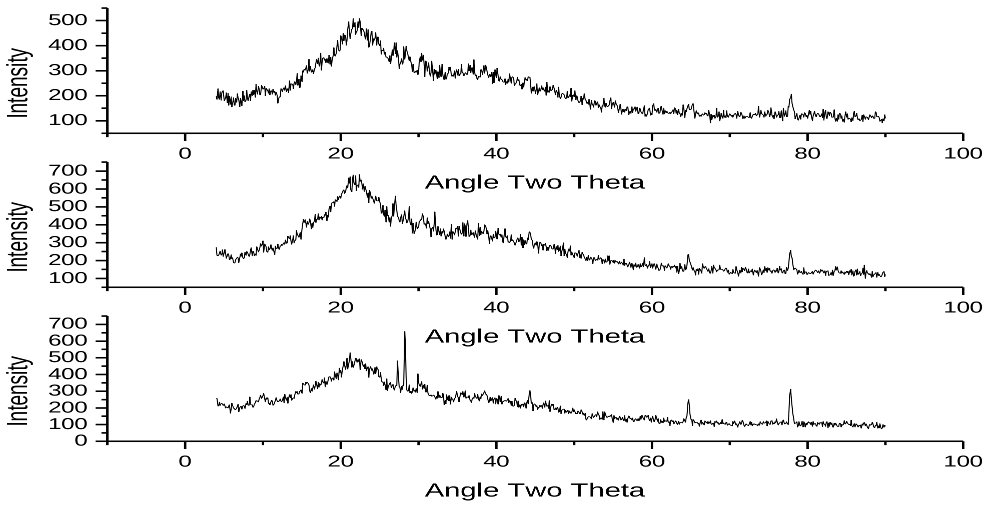

Figure. 3. XRD pattern of TGLRC before and after adsorption of Cu (II) and Ni (II) ions.

Adsorption reaction may lead to changes in molecular and crystalline structure of the adsorbent and hence an understanding of the molecular and crystalline structures of the adsorbent and the resulting changes thereof would provide valuable information regarding adsorption reaction. Hence, XRD patterns of the adsorbent before and after adsorption of Cu (II) and Ni (II) ions have been studied.

As a representative case the XRD patterns of TGLRC before and after treatment with Cu (II) and Ni (II) ions are shown in *Fig. 3.* The results indicated that the diffraction profiles of TGLRC before and after adsorption of Cu (II) and Ni (II) ions exhibited broad peaks and the absence of a sharp peak revealed a predominantly amorphous structure, the broad peak seems to be appear at around 2θ = 21, 22, 26 and 28° which was similar to the peak of crystalline carbonaceous structure such as graphite. It is evident from the figure that the XRD pattern of TGLRC loaded with Cu (II) and Ni (II) ions exhibits no variation in the crystal structure and this suggests that the Cu (II) and Ni (II) ions might diffuse into micropores and sorbs mostly by physisorption without altering the structure of the adsorbent. From the XRD analysis for the adsorbent (TGLRC), we concluded that the tannin gel preparation was completed. The above observation corroborated well with batch sorption experiments.

Batch adsorption studies

Effect of solution pH

The zeta-potentials of the TGLRC particles in water were measured at different pH. It was found that TGLRC particles are positively charged at low pH and negatively charged at high pH, having a point of zero charge (pH_{zpc}) at pH 5.12 for TGLRC. Therefore, it can be expected that positively charged metal ions are likely to be adsorbed by the negatively charged TGLRC particles at a pH > ZPC.

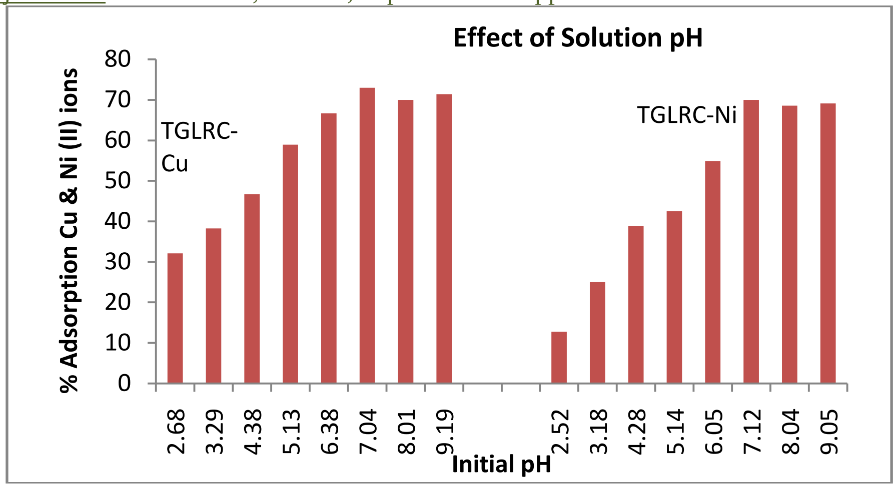

Figure. 4. Effect of solution pH on the adsorption of Cu (II) and Ni (II) ions on TGLRC.

The pH of the aqueous solution has been identified as the most important variable governing metal adsorption onto adsorbents. This is partly due to the fact that hydrogen ions themselves are a strongly competing adsorbate and because the solution pH influences the ionization of surface functional groups. In order to establish the effect of pH on the adsorption of Cu (II) and Ni (II), the batch equilibrium studies at different pH values were carried out in the range of 2–9 (*Fig. 4*). We note that as the pH of the solution increased from 2.0 to 9.0, the adsorption capacity of TGLRC increased up to pH 7.0 for the adsorption of Cu (II) and Ni (II) ions by TGLRC and then decreased at pH > 6.0. The amount adsorbed increased as pH increased from 2.0 to 7.0 may be due to the presence of negative charge on the surface of the adsorbent that may be responsible for metal binding. However, as the pH is lowered, the hydrogen ions compete with the metal ions for the sorption sites in the sorbent; the overall surface charge on the adsorbent becomes positive and hinds the binding of positively charged metal ions [30]. At pH higher than 7.0, the precipitation of insoluble metal hydroxides takes place restricting the true adsorption studies [31].

However, when the pH of the solution was increased, the uptake of metal ions was increased. It appears that a change in pH of the solution results in the formation of different ionic species, and different carbon surface charge. At pH values lower than 5, the metal ions can enter into the pore structure may be due to its small size. So, an optimized pH of 7.04 for the removal of Cu (II) ions and 7.12 for the removal of Ni (II) ions by TGLRC adsorbent is taken for all the adsorption experiments.

Effect of contact Time

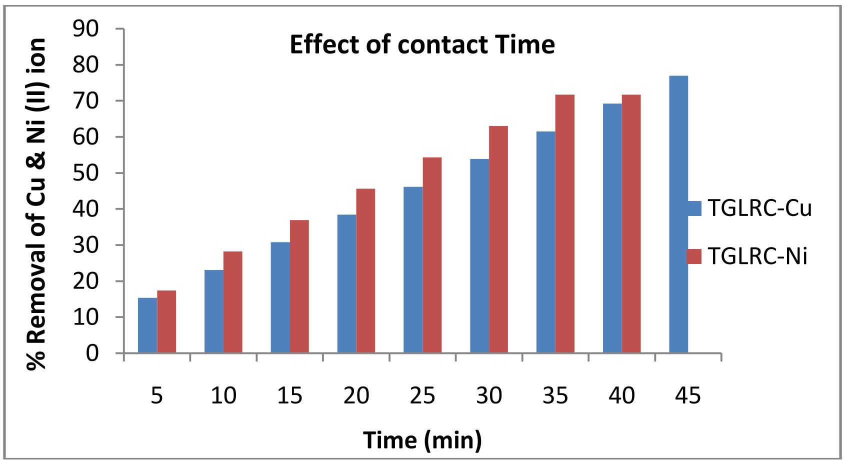

Figure. 5. Effect of Contact time on the adsorption of Cu (II) and Ni (II) ions onto TGLRC.

The uptake of Cu (II) and Ni (II) ions onto TGLRC as a function of contact time is shown in *Fig. 5*. The effect of contact time between the adsorbents and Cu (II) and Ni (II) ions showed that the Cu (II) was removed within 45 min by TGLRC and Ni (II) ions was removed within 40 min by TGLRC and remains almost constant even up to an hour.

This may be due to the attainment of equilibrium condition at 45 min of contact time for Cu (II) removal with TGLRC and 40 min for the removal of Ni (II) with TGLRC, which are fixed as the optimum contact time. At the initial stage, the rate of removal of Cu (II) and Ni (II) ions was higher, due to the availability of more than required number of active sites on the surface of carbons and became slower at the later stages of contact time, due to the decreased or lesser number of active sites.

Effect of adsorbent dose

The effect of adsorbent dose on the percentage removal of Cu (II) and Ni (II) ion was studied at initial Cu (II) and Ni (II) ion concentration of 100 mg/L by allowing a contact time of 60 min and at the solution pH of 7.04 for Cu (II) and 7.12 for Ni (II) ions. The results are presented in *Fig. 6.* It is showed that the percentage removal of Cu (II) and Ni (II) ion increased with increase in adsorbent dose from 200 mg/50mL to1000 mg/50mL. This increase in Cu (II) and Ni (II) ion removal is due to the availability of higher number of Cu (II) and Ni (II) ions per unit mass of adsorbent (TGLRC), i.e., higher metal ions/ adsorbent ratio. Thus, further experiments were carried out using 200 mg of adsorbent per 50 ml of Cu (II) and Ni (II) ion solution, as it exhibits appreciable removal capacity, for the optimization of adsorption parameters.

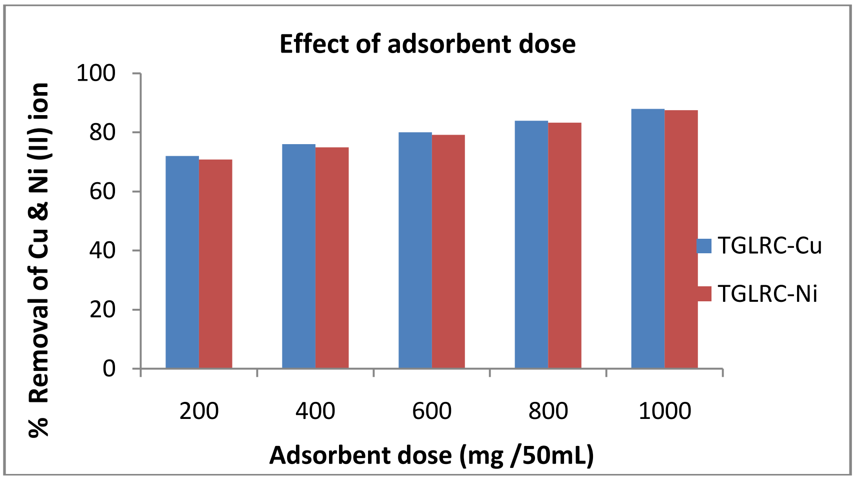

Figure. 6. Effect of adsorbent dose on the adsorption of Cu and Ni (II) ions by TGLRC.

Effect of metal ion concentration

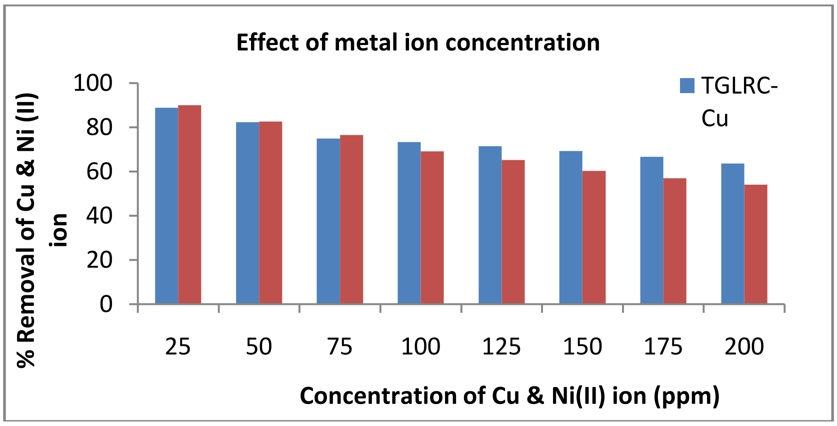

Figure. 7. Effect of metal ion concentration on the adsorption of Cu (II) and Ni (II) ions by TGLRC.

The effect of initial metal ion concentration on adsorption capacity of TGLRC was carried out at a carbon dosage of 200 mg/ 50 mL, pH 7.04 for Cu (II) ion removal and 7. 12 for Ni (II) ion removal by TGLRC, contact time 1 h, temperature 303K for different initial metal ion concentration from 25 to 200 mg/50mL and is shown in *Fig. 7.* As shown, the amount of metal uptake per unit weight of the adsorbent increases with increasing initial metal ion concentration showing the maximum adsorption capacity of 5.48 mg /50mL to 31.32 for Cu (II) ion removal and the maximum adsorption capacity of 5.53 mg/50mL to 26.57 mg/50mL for Ni (II) ion removal by TGLRC. This is because at higher initial concentrations, the ratio of initial number of moles of metal ions to the available adsorption surface area is high. This may be attributed to an increase in the driving force of the concentration gradient with increase in the initial metal ion concentration [32] .

Adsorption isotherms

Adsorption isotherm is the most important information which indicates how the adsorbate molecules distribute between the liquid phase and the solid phase when adsorption process reaches on Equilibrium state. When the system is at Equilibrium is of importance in determining the maximum sorption capacity of TGLRC towards metal solution. Equilibrium data are a basic requirement for the design of adsorption systems and adsorption models, which are used for the mathematical description of the adsorption equilibrium of the metal ion by the adsorbent. The results obtained for adsorption of Cu (II) and Ni (II) ions were analyzed by use of well-known models given by the Langmuir, Freundlich, Temkin, Dubinin–Radushkevich, Harkin-Jura and Frenkel-Halsey-Hill adsorption isotherm models [34 - 38]. For the sorption isotherms, initial metal ion concentration was varied whereas solution pH and amount of adsorbent were held constant. The sorption isotherms for Cu (II) and Ni (II) ions were obtained for TGLRC at solution pH 7.04 and pH 7.12, respectively.

$$\frac{C_e}{q_e} = \frac{1}{q_{max}b} + \frac{C_e}{q_{max}} \quad \textit{Langmuir model} \quad (4)$$

$$log\, q_e = \frac{1}{n} log(C_e) + log\, K \quad \textit{Freundlichmodel} \quad (5)$$

$$q_e = \beta \ln \alpha + \beta \ln C_e \quad \textit{Temkin model} \quad (6)$$

$$\ln q_e = \ln Q_m - K\varepsilon^2 \quad \textit{Dubinin} - \textit{Radushkevich model} \quad (7)$$

The mean adsorption energy, *E* (kJ/mol) is calculated with the help of following equation:

$$\mathrm{E} = \frac{1}{\sqrt{-2\bar{\mathrm{Y}}}} \quad (8)$$

$$\frac{1}{q_e^2} = \left(\frac{B_2}{A}\right) - \left(\frac{1}{A}\right) \log C_e \quad \textit{Harkin} - \textit{Jura model} \quad (9)$$

$$\ln q_e = \frac{1}{n} \ln K - \frac{1}{n} \ln C_e \quad \textit{Frenkel} - \textit{Halsey} - \textit{Hill model} \quad (10)$$

where C_e is the Cu (II) and Ni (II) ion concentration in the solution (mg/L), q_e is the Cu (II) and Ni (II) concentrations in the solid adsorbent (mg/g), q_m is the maximum adsorption capacity (mg/g), K_f is a constant related to the adsorption capacity ($mg^{1-1/n}$ $L^{1/n}$/g), b is a constant related to the energy of adsorption (L/g), n is a constant related to the energy of adsorption, α (L/g) is Temkin constant representing adsorbent–adsorbate interactions and β (mgL-1) is another constant related with adsorption heat, ε is the Polanyi potential (kJ^2 mol^2) and *E* (kJ/mol) is the mean adsorption energy. B_2 is the isotherm constant, represented by Harkin-Jura isotherm model. The adsorption isotherm parameters for all the six isotherm models are calculated and the values are summarized in *Table 2.*

Table 2. Adsorption isotherm parameters for the adsorption of Cu (II) and Ni (II) ions.

Isotherm model	Parameters	Cu (II) ion	Ni (II) ion
Langmuir	Q_m (mgg^{-1})	43.47	30.303
	b (Lmg-1)	0.0160	0.0201
	R^2	0.9390	0.9790
Freundlich	n	1.8382	2.3364
	K_f (mgg^{-1})	3.0690	3.8994
	R^2	0.9950	0.9960
Temkin	α (Lg-1)	0.1093	0.3424
	β (mgL-1)	8.0810	5.8130
	b	311.73	433.36
	R^2	0.9230	0.9690
Dubinin-Radushkevich	Q_m (mgg^{-1})	21.019	19.005
	K (x10-5mol2kJ-2)	0.2	0.2
	E(kJmol-1)	0.625	0.625
	R^2	0.685	0.728
Harkin-Jura	A	47.619	58.823
	B	1.7142	1.8823
	R^2	0.840	0.812
Frenkel–Halsey–Hill	1/n	0.544	0.428
	K	0.7231	1.1577
	R^2	0.943	0.996

In the present investigation, the equilibrium data were analyzed using the Langmuir, Freundlich, Temkin, Dubinin-Radushkevich, Harkin-Jura and Frenkel-Halsey-Hill isotherm models. To optimize the design of an adsorption system, it is important to establish the most appropriate isotherm model. The mono-component equilibrium characteristics of adsorption of Cu (II) and Ni (II) ions by TGLRC were described by these six different isotherm models. The experimental equilibrium adsorption data were obtained by varying the concentration of Cu (II) and Ni (II) ions with 200mg/50 mL of TGLRC.

The adsorption data obtained by fitting the different isotherm models with the experimental data are listed in *Table 2*, with the linear regression coefficients, R^2. As seen from *Table 2*, the Langmuir, Freundlich and Frenkel-Halsey-Hill isotherms were generate a satisfactory fit to the experimental data as indicated by correlation coefficients. This shows the heterogeneity of the surface of TGLRC and the multilayer adsorption nature of the Cu (II) and Ni (II) ions on TGLRC.

TGLRC have a homogeneous surface for adsorption of metal ions. The Langmuir isotherm equation is therefore expected to best represent the equilibrium adsorption data. The R^2 values for the Langmuir model are closer to unity than those for the other isotherm models for TGLRC for both Cu (II) ion removal ($R^2 = 0.939$) and for the removal of Ni (II) ($R^2 = 0.979$). Therefore, the equilibrium adsorption of Cu (II) and Ni (II) ions on TGLRC can be represented appropriately by the Langmuir, Freundlich and Frenkel-Halsey-Hill isotherm models in the concentration range studied.

Adsorption kinetics

The kinetics of adsorbate uptake is important for choosing optimum operating conditions for design purposes. In order to investigate the mechanism of adsorption and potential rate controlling steps such as chemical reaction, diffusion control and mass transport process, kinetic models have been used to test experimental data from the adsorption of Cu (II) and Ni (II) ions onto TGLRC. These kinetic models were analyzed using pseudo-first-order, pseudo-second-order and intraparticle diffusion models, which were respectively presented as follows in Eqs. (11) – (14) [39 – 41]:

$$\ln(q_e - q_t) = \ln q_e - k_1 t \qquad \textit{Pseudo first order model} \qquad (11)$$

$$\frac{t}{q_t} = \frac{1}{k_2 q_e^2} + \frac{1}{q_e} t \qquad \textit{Pseudo second order model} \qquad (12)$$

$$q_t = k_{id} t^{1/2} + C \qquad \textit{Intra particle diffusion model} \qquad (13)$$

$$q_t = \frac{1}{\beta \ln(\alpha\beta)} + \frac{1}{\beta \ln t} \qquad \textit{Elovich model} \qquad (14)$$

where t is the contact time of adsorption experiment (min); q_e (mg/g) and q_t (mg/g) are respectively the adsorption capacity at equilibrium and at any time t; k_1 (1/min), k_2 (g/mg min), α (mg/g min), β (g/mg), k_{id} (mg/g min$^{1/2}$) are the rate constants for these models, respectively. The correlation coefficients for all the four kinetic models were calculated and the results are shown in *Table 3.*

Table 3. Comparison of the correlation coefficients of kinetic parameters for the adsorption of Cu (II) and Ni (II) ions onto TGLRC.

Models	**Parameters**	**Cu (II) ion**	**Ni (II) ion**
Pseudo first-order model	k_1 (min^{-1})	0.1658	0.1496
	q_e (mg/g)	173.78	64.71
	R^2	0.677	0.644
Pseudo second-order model	k_2 (g/mg/min)	0.0004	0.0005
	q_e (mg/g)	41.66	38.46
	h	0.7005	0.8613
	R^2	0.9920	0.973
Intra particle diffusion model	k_{dif} (mg/(g.min$^{1/2}$))	3.411	3.510
	C	5.044	4.063
	R^2	0.983	0.989
Elovich model	A_E (mg(g/ min))	0.1452	0.1453
	b (g/ mg)	0.3928	0.6071
	R^2	0.9110	0.9530

The adsorption process of Cu (II) and Ni (II) ions can be well fitted by use of the pseudo-second order rate constant for TGLRC. The linear regression coefficient value $R^2 = 0.992$ for Cu (II) and $R^2 = 0.973$ for Ni (II) obtained for pseudo-second-order kinetics was closer to unity than the R^2 value (0.677 = Cu (II) ions and 0.644 = Ni (II) ions) for first-order kinetics. This indicates that adsorption of Cu (II) and Ni (II) ions by TGLRC follows pseudo-second-order kinetics.

In the intra particle diffusion model, the values of q_t were found to be linearly correlated with the values of $t^{1/2}$. The linear regression coefficient value $R^2 = 0.983$ for Cu (II) and $R^2 = 0.989$ for Ni (II) obtained for Intra particle diffusion model was closer to unity. The k_{dif} values were calculated by use of correlation analysis. $k_{dif} = 3.411$ for the removal of Cu (II) ions and k_{dif} = 3.510 for the removal of Ni (II) ions. The data indicates that the adsorption kinetics follows the pseudo-second-order rate with intraparticle diffusion as one of the rate determining steps.

Influence of other metal ions on the adsorption of Cu (II) and Ni (II) ions.

Effect of Ni (II) ions and Cr(III) ions on adsorption of Cu (II) and Ni (II) ions (binary system)

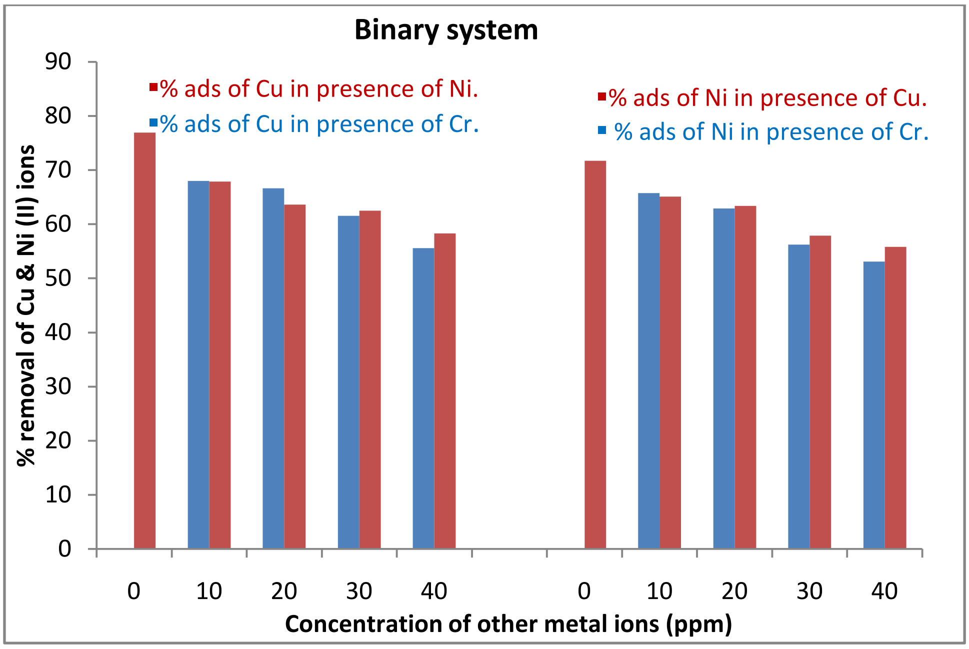

Figure. 8. Effect of other metal ions in binary system on the adsorption of Cu (II) and Ni (II) ions onto TGLRC.

The concentration of the Cu (II) ion solution was kept as 100 ppm. The concentration of Ni (II) ion was varied as 10, 20, 30, and 40 ppm. Each solution was placed in a bottle with TGLRC and the pH was adjusted to 7.04. After shaking for 60 min percentage adsorption was calculated. Percentage adsorption decreased from 76.92 to 55.56 % as the concentration of Ni (II) solution was increased. This showed competitive adsorption was, to some extent, taking place between the Cu (II) ions and the Ni (II) ions. The same procedure was repeated for Cu (II) ions in presence of Cr(III) ions. The percentage adsorption of Cu (II) ions decreased to 76.92–58.33% in the presence of Cr(III) ions. This is clearly shown in Fig. 8 for TGLRC. When the same procedure was repeated for the adsorption of Ni (II) ions onto TGLRC at pH 7.12, adsorption decreased to 71.73–53.13 % in the presence of Cu (II) ions and to 71.73–55.81% in presence of Cr(III) ions. This is clearly shown in Fig. 8.

Effect of Cu (II), Ni (II) and Cr(III) ions on the adsorption of Cu (II) and Ni (II) ions (tertiary system)

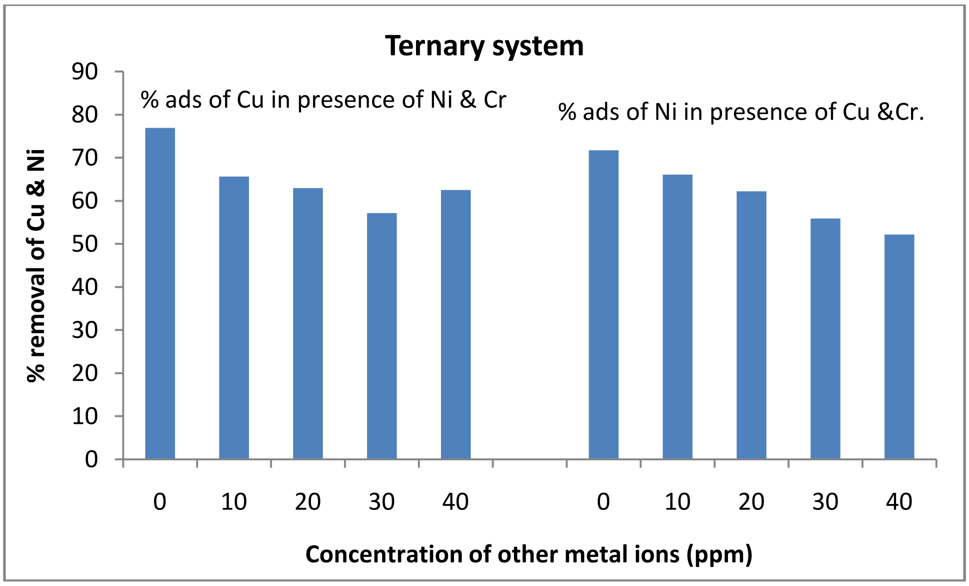

Figure. 9. Effect of other metal ions in tertiary system on the adsorption of Cu (II) and Ni (II) ions onto TGLRC.

The concentration of Cu (II) ion solution was kept as 100 ppm. The concentrations of Ni (II) and Cr(III) ion solutions were varied as 10, 20, 30, and 40 ppm. Solutions of both Ni (II) ions and Cr(II) ions were added to Cu (II) solution in a bottle with TGLRC and the pH was adjusted to 7.12. After shaking 1 h percentage adsorption was calculated. Percentage adsorption decreased from 76.92 to 62.5 % as the concentrations of Ni (II) ions and Cr(III) ions were increased. This showed competitive adsorption was, to some extent, taking place between the Ni (II) ions, the Cu (II) ions, and the Cr(III) ions. Percentage adsorption of Cu (II) was reduced in the presence of the other metals, as is clearly shown in *Fig. 9*. The same procedure was repeated for the adsorption Ni (II) ions onto TGLRC at pH 7.12 and percentage adsorption decreased from 71.71-52.17%, as the concentration of Cu (II) and Cr(III) was increased from 10-40 ppm, as illustrated in *Fig. 9*.

A fixed quantity of Cu (II) ions and Ni (II) ions onto TGLRC could only offer a finite number of surface binding sites, some of which would be expected to be saturated by the competiting metal solutions. The decrease in sorption capacity of same activated carbon in target metal solution than that of single metal may be ascribed to the less availability of binding sites. In case of binary and ternary metal solution, the binding site is competitively divided among the various metal ions.

It is generally complicated to find a common rule to identify how metal properties affect the competitive sorption. Among various factors that affect the sorption preferences of a sorbent, binding of metal ions on material largely depends on physicochemical properties of metals.

The HSAB (hard and soft acids and bases) theory developed by Pearson [42] and extended to activated carbons adsorption by Alfarra et al, [43]. Once acids and bases have been classified as hard or soft, a simple rule of the HSAB principle can be given: hard acids prefer to bond to hard bases, and soft acids prefer to bond to soft bases. Generally, the C–O or C=O bonds are more polar and less polarizable, hence harder than the C–C or C=C bonds. In this concept, the oxygen surface groups of TGLRC are the hard sites that fix hard metal ions. According to this theory, Ni (II), Cu (II) and Cr(III) cations are borderline acids [42]. Changing the experimental conditions, metal ions with a borderline hardness can be biosorbed by the hard sites of TGLRC. The cationic exchange between the oxygenated surface groups (hard base) of TGLRC and borderline acids gives ionic bonds which are more easily dissociated. But the competitive process cannot be explained exactly by the hardness of cations because other effective factors and hardness values of Ni (II), Cu (II) and Cr (III) borderline acids are close each other.

Desorption and Reusability

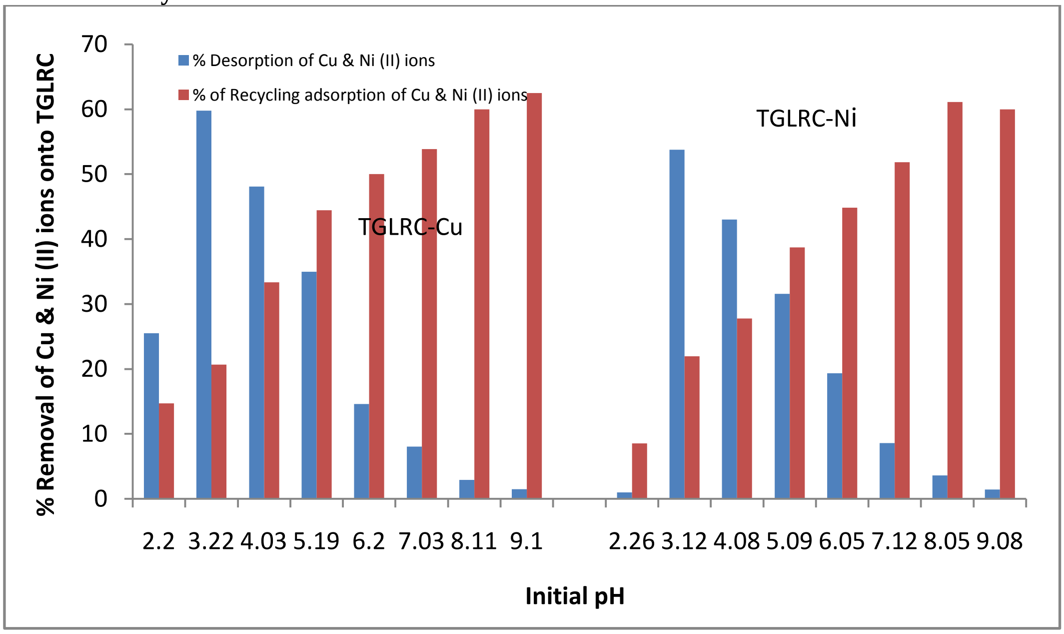

Figure. 10. Effect of pH on the desorption and recycling adsorption of Cu (II) and Ni (II) ions.

To investigate the possibility of repeated use of the adsorbent, desorption experiments were conducted under batch experimental conditions and desorption efficiencies were showed in *Fig. 10*. If the adsorbed Cu (II) ion and Ni (II) ion can be desorbed using neutral pH water, then the attachment of the copper and nickel ion of the adsorbent is by weak bonds. To study the effect of solution pH on Cu (II) and Ni (II) ion desorption, 50 mL of distilled water at different pH values (2 - 9) was agitated with 200 mg of TGLRC in a mechanical orbital shaker at room temperature. The pH was adjusted with 0.1 M NaOH and 0.1 M HCl solutions. We could get maximum removal of 59.77% of adsorbed Cu (II) ion for 3.22 pH water and 53.77% of adsorbed Ni (II) ion for 3.12 pH water onto TGLRC, after 2 h of contact time between the loaded matrix and the desorbing agents.

After desorption, the adsorbents were further used for adsorption of Cu (II) and Ni (II) ions. The percentage removal of Cu (II) ions was found to be 53.85% for TGLRC at pH 7.04 and the removal of Ni (II) ion was found to be 51.85 % for TGLRC at pH 7.12 (Fig.10). The increase in removal of Cu (II) and Ni (II) ions at pH 8 may be because of precipitation of metal ions in alkaline medium rather than adsorption.

IV. CONCLUSION

In this work, Tannin gel derived from Ricinus Communis leaves as a sorbent has been proposed to be an efficient and economical alternative in Cu (II) and Ni (II) ion removal from water. The findings herein made us conclude that:

(1) Batch sorption studies of Cu (II) and Ni (II) ions showed that the TGLRC can be successfully used to remove Cu and Ni (II) ions from aqueous solution.
(2) The adsorption data were well fitted by the Langmuir isotherm model; this is indicative of monolayer adsorption by TGLRC.
(3) By applying the kinetic models to the experimental data, it was found that the kinetics of Cu and Ni (II) ion adsorption onto TGLRC followed by the pseudo-second order rate equation and intra particle diffusion is one of the rate limiting step. Results of kinetic studies demonstrated that the Cu and Ni (II) ion adsorption was rapid and efficient.
(4) Percentage adsorption of Cu (II) and Ni (II) ions on TGLRC was higher in the single-ion systems than in binary and ternary systems, which is indicative of competitive adsorption among the metal ions.
(5) Adsorbed Cu (II) and Ni (II)ions can be desorbed from both the adsorbents by use of double distilled water — 59.7 % of adsorbed Cu (II) ions were recovered from TGLRC and 53.7 % of adsorbed Ni (II) ions were recovered from TGLRC at pH 3.22 and pH 3.12, respectively.
(6) The experimental studies showed that Tannin gel prepared from leaves of *Ricinus Communis* could be used as an alternative, inexpensive and effective material to remove high amount of Cu (II) and Ni (II) ions from aqueous solutions.

REFERENCES

[1] F. Rozada, M. Otero, A. Moran, and A.I. Garcia, Adsorption of heavy metals onto sewage sludge-derived materials, *Bioresource Technology,* 99, 2008, 6332–6338.
[2] K.K. Krishnani, X. Meng, C. Christodoulatos, and V.M. Boddu, Biosorption mechanism of nine different heavy metals onto biomatrix from rice husk," *Journal of Hazardous Materials,* 153, 2008, 222–1234.
[3] S. Liang, XY. Guo, N.C. Feng, and QH. Tian, Application of orange peel xanthate for the adsorption of Pb^{2+} from aqueous solutions, *Journal of Hazardous Materials,* 170, 2009, 425.
[4] R.P. Dhakal, K.N. Ghimiere, K. Inoue, Adsorptive separation of heavy metals from an aquatic environment using orange waste, *Hydrometallurgy.* 79, 2005, 182.
[5] U. Kumar, M. Bandyopadhyay, Sorption of cadmium from aqueous solution using pretreated rice husk, *Bioresource Technology,* 97, 2006, 104.
[6] K.K. Singh, M. Talat, S.H. Hasan, Removal of lead from aqueous solutions by agriculture waste maize bran, *Bioresource Technology,* 97, 2006, 2124.
[7] W. Zhang, QG. Chang, WD. Liu, BJ. Li, WX. Jiang, LJ. Fu, Selecting activated carbon for water and wastewater treatability studies, *Environ Prog.* 26, 2007, 289.
[8] D. Prahas, Y. Kartika, N. Indraswati, and S. Ismadji, Activated carbon from jackfruit peel waste by H_3PO_4 chemical activation: pore structure and surface charac-terization, *Chemical Engineering Journal*, 140, 2007, 32.
[9] S. Altenor, B. Carene, E. Emmanuel, J. Lambert, J.J. Ehrhardt, and S. Gaspard, Adsorption studies of methylene blue and phenol onto Vetiver roots activated carbon prepared by chemicalactivation, *Journal of Hazardous Materials,* 165(1–3), 2009, 1029–1039.
[10] A. Demirbas, A. Heavy metal adsorption onto agro-based waste materials: a review, *Journal of Hazardous Materials*, 157(2–3), 2008, 220–229.
[11] F.A. Pavan, A.C. Mazzocato, Y. Gushikem, Removal of methylene blue dye from aqueous solutions by adsorption using yellow passion fruit peel as adsorbent," *Bioresou. Technol.* 99(8), 2008, 3162–3165.
[12] P. Schofield, D.M. Mbugua, and A.N. Pell, Analysis of condensed tannins: a review, *Animal Feed Science and Technology.* 91(1), 2001, 21–40.
[13] A. Pizzi, Advanced Wood Adhesives Technology, Marcel Dekker, New York. 1994.
[14] N.E. Meikleham, A. Pizzi, Acid- and alkali-catalyzed tannin-based rigid foams," *J. of App. Poly. Sci.* 53(11), 1994, 1547–1556.
[15] G. Tondi, W. Zhao, A. Pizzi, G, Du, V. Fierro, and A. Celzard, Tannin-based rigid foams: a survey of chemical and physical properties, *Bioresource Technology,* 100(21), 2009a, 5162–5169.
[16] W. Zhao, V. Fierro, A. Pizzi, G. Du, A. Celzard, Effect of composition and processing parameters on the characteristics of tannin-based rigid foams, *Part II: Physical properties, Materials Chemistry and Physics*. 123(1), 2010, 210–217.
[17] Y. Nakano, K. Takeshita, T. Tsutsumi, Adsorption mechanism of hexavalent chromium by redox within condensed-tannin gel, *Water Research*.35(2), 2001, 496–500.
[18] Y.H. Kim, Y. Nakano, Adsorption mechanism of palladium by redox within condensed-tannin gel, *Water Research.* 39(7), 2005, 1324–1330.
[19] G. Tondi, C.W. Oo, A. Pizzi, M.F. Thevenon, Metal absorption of tannin-based rigid foams, *Ind. Crops. Prod,* 29(2–3), 2009b, 336–340.
[20] W. Shirato, Y. Kamei, Insoluble tannin preparation process, waste treatment process and adsorption process using tannin, *US patent.* 5, 158, 1992, 711.
[21] G. Vázquez, G. Antorrena, J. González, M.D. Doval, Adsorption of heavy metal ions by chemically modified Pinus pinaster bark, *Bioresource Technology,* 48(3), 1994, 251–255.
[22] G. Vázquez, J. González-Álvarez, S. Freire, M. López-Lorenzo, and G. Antorrena, Removal of cadmium and mercury ions from aqueous solution by sorption on treated Pinus pinaster bark: kinetics and isotherms, *Bioresource Technology,* 82(3), 2002, 247–251.
[23] A. Pizzi, Tannins: major sources, properties, applications, in Monomers, *Polymers and Composites from Renewable Resources(*eds M.N. Belgacem and Gandini), Elsevier, Amsterdam, Ch 8. 2008.

[24] M. Makeswari, T. Santhi, Optimization of Preparation of Activated Carbon from Ricinus communis Leaves by Microwave-Assisted Zinc Chloride Chemical Activation: Competitive Adsorption of Ni^{2+} Ions from Aqueous Solution, *Journal of Chemistry,* Article ID 314790, 12 pages, doi:10.1155/2013/314790. 2013a.
[25] M. Makeswari, and T. Santhi, Use of Ricinus communis leaves as a low cost adsorbent for removal of Cu (II) ions from aqueous solution, *Research on chemical intermediates,* 39(2), 2013b.
[26] M. Yurtsever, I.A. Sengil, Biosorption of Pb(II) ions by modified quebracho tannin resin, *Journal of Hazardous Materials,* 163(1), 2009, 58–64.
[27] A. Kumar, B. Prasad, and I.M. Mishra, Adsorptive removal of acryloinitrile by commercial grade activated carbon: kinetics, equilibrium and thermodynamics, *Journal of Hazardous Materials,* 152, 2008, 589-600.
[28] P. Janos, H. Buchtova, and M. Ryznarova, Sorption of dye from aqueous solution onto fly ash, *Water Research.* 37, 2003, 4938-4944.
[29] K. Nakanishi, Infrared Absorption Spectroscopy-Practical, Holden-Day, San Francisco, CA,17-57, 1962.
[30] J. Chang, R. Law, and C. Chang, Biosorption of lead copper and cadmium by biomass of Pseudomonas aeruginosa, *Water Research,* 31, 1997, 1651.
[31] Z. Elouear, R. Ben Amor, J. Bouzid, N. Boujelben, Use of phosphate rock for the removal of Ni^{2+} from aqueous solutions: kinetic and thermodynamics studies, *Journal of Environmental Engineering,* 135, 2009, 259**.**
[32] I.D. Mall, V.C. Srivastava, N.K. Agarwal, and I.M. Mishra, Removal of congo red from aqueous solution by bagasse fly ash and activated carbon: Kinetic study and equilibrium isotherm analyses, *Chemosphere,* 61, 2005, 492–501.
[33] I. Langmuir, The adsorption of gases on plane surface of glass, mica and platinum, *Journal of American chemical society*, 40, 1918, 1361 – 1403.
[34] H. Freundlich, Uber die adsorption in losungen (Adsorption in solution). Z. Phys. Chem, 57, 1906, 384 - 470.
[35] I.A.W. Tan, B.H. Hameed, A.L. Ahmad, Equilibrium and kinetic studies on basic dye adsorption by oil palm fibre activated carbon, *Chemical Engineering Journal,* 127, 2007, 111–119.
[36] M.M. Dubinin, E.D. Zaverina, L.V. Radushkevich, Sorption and structure of activated carbons, I. Adsorption of organic vapours, *Zh. Fiz. Khim.* 21, 1947, 1351–1362.
[37] C.A. Basker, Applicability of the various adsorption models of three dyes adsorption onto activated carbon prepared from waste apricot, *Journal of Hazardous Materials,* 135B: 2006, 232-241.
[38] J. Halsey, Physical adsorption on Non-uniform surfaces, *Chem. Phys.* 16: 1948, 931.
[39] Y.S. Ho, G. Mckay, G. Sorption of dye from aqueous solution by peat, *Chemical Engineering Journal,* 70, 1998a, 115–124.
[40] Y.S. Ho, G. Mckay, Kinetic models for the sorption of dye from aqueous solution by wood, *Journal of Environmental Science Health Part B: Process Saf. Environ. Prot,* 76(B), 1998b, 184–185.
[41] W.J. Weber Jr, J.C. Morris, Kinetics of adsorption on carbon from solution, *Journal of Sanitary Engineering Division,* 89(2), 1963, 31–60.
[42] R.G. Pearson, Hard and soft acids and bases, *American journal of Chemical Society,*85, 1963, 3533-3539.
[43] A. Alfarra, E. Frackowiak, and F. Beguin, The HSAB concept as a means to interpret the adsorption of metal ions onto activated carbons, *Applied Surface Science,*228, 2004, 84-92.

Optimization of Surface Impedance for Reducing Surface Waves between Antennas

Jean-François D. Essiben[1], Eric R. Hedin[2], and Yong S. Joe[2]

[1]Department of Electrical Engineering, Advanced Teachers' Training College for Technical Education University of Douala, B. P. 1872, Douala, Cameroon

[2]Center for Computational Nanoscience, Department of Physics and Astronomy Ball State University, Muncie, IN 47306, USA

ABSTRACT: *Electromagnetic coupling between two aperture antennas in the shape of the open ends of parallel-plate waveguides located on the same metal surface has been analyzed. The design optimization of the surface impedance model is used to solve this problem. The required level of antenna decoupling is obtained taking into account the initial metal surface, which is a natural decoupling structure. The search method is applied to determine a minimum value of the antenna-coupling coefficient. The method of moments (MoM) technique has been used to solve the integral equations. Numerical solutions for optimized surface impedance distributions and antenna decouplings are presented.*

Keywords: *Aperture Antennas, Coupling, Method of Moments, Surface Impedance.*

I. INTRODUCTION

Nonplanar antennas with radiating apertures find frequent use in radio electronics. These antennas have several advantages compared to traditional antennas with plane apertures. One of these advantages is the possibility of placing such antennas directly on surfaces with a complex shape. Another important advantage is the fact that antennas with nonplanar apertures allow the realization of a wider class of geometries than antennas with planar apertures.

High saturation of modern systems of radio electronics necessitates creating the placement of antennas of different usage in direct proximity relative to other antennas. As a result, these antennas can produce interference with each other. With the aim of reducing this harmful form of mutual influence, various measures are used to increase the decoupling between the antennas. One of the most effective measures, as shown in Refs. [1-3] for the case of surface plane location of antennas, is the use of corrugated structures. The corresponding electrodynamic model has been considered [1, 2, 4], where the problem of coupling of two antennas located on a plane in the presence of an intervening corrugated structure is solved explicitly. The results obtained from this model can be used as an initial proposition or approximation [4].

The main purpose of this paper is the optimization problem of surface impedance for decreasing antenna-coupling coefficients, in the case where the antennas have a common location. The history of this problem is addressed in Refs. [5-7], where the antenna coupling coefficients are defined for different dispositions of antennas on a mobile board. Although the problem of the definition of a minimum value of the antenna-coupling coefficient is not mentioned in these papers, the problem of minimization of the antenna-coupling coefficients for the radio board and electronic systems has been solved using the search method [8]. The minimum value of the antenna-coupling coefficient is defined with the help of the Gauss-Zeidel optimization method [9, 10].

In Section II of this paper, a solution to the problem of the reduction in coupling between two waveguide antennas located on a surface impedance is given. A solution to the design optimization problem of the surface impedance for reducing coupling between antennas is obtained in section III. In section IV, the numerical simulation results are presented. Finally, conclusions are drawn in Section IV.

II. ANALYTICAL FORMULATION

We consider the problem of coupling between two waveguide antennas as shown in Figure 1a. The two aperture antennas in the shape of the open ends of parallel-plate waveguides (transmitting and receiving) with opening sizes of a and b are located on the $y=0$ plane, separated by a distance L. On the surface S, the impedance boundary conditions of Shukin-Leontovich are fulfilled:

$$\vec{n}\times\vec{E} = -Z\vec{n}\times(\vec{n}\times\vec{H}), \tag{1}$$

where $\vec{n}$ is the normal unit to the $y=0$ plane, Z is the surface impedance, and $\vec{E}$ and $\vec{H}$ are the electric and magnetic fields, respectively.

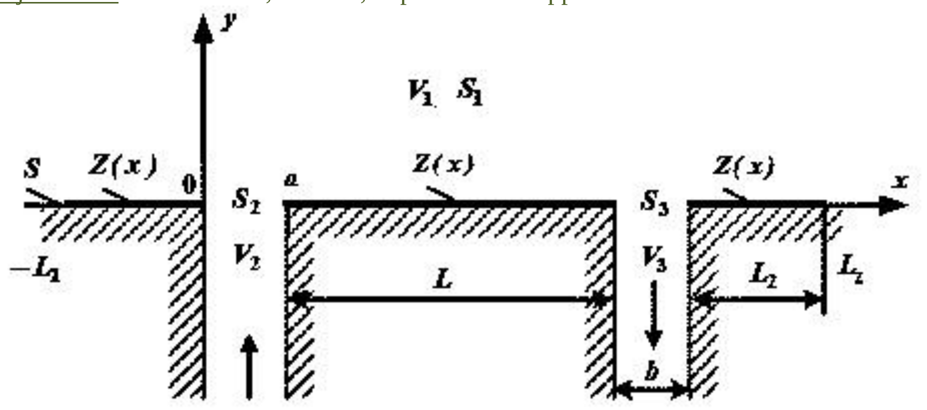

(a)

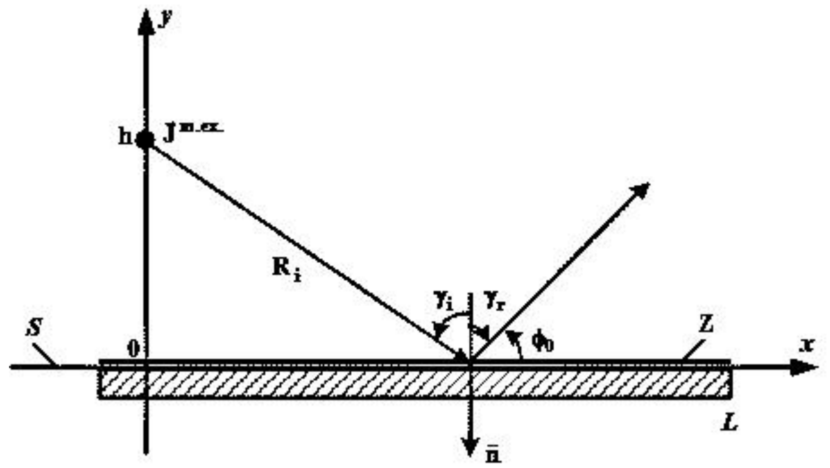

(b)

Figure 1. (a) Geometry of the problem. (b) Geometry of the design problem. The magnetic current $\vec{J}^{m.ex.}$ is located at the height h.

It is necessary to determine the electromagnetic field (EMF) in the following regions: the upper half-space ($y \geq 0$, region V_1), the radiating waveguide ($y = 0$ and $0 \leq x \leq a$, region V_2), and the receiving waveguide ($y = 0$ and $a + L \leq x \leq a + L + b$, region V_3). The minimum level of coupling between the two antennas can then be determined using the surface impedance plane synthesized below. Notice that the required EMF should satisfy boundary conditions on the flange, namely the requirement of infinite tangential components in the openings, and the standard conditions of Maxwell's equations for radiation.

For the solution of the general structure studied in our calculations and sketched schematically in Figure 1a, we use the Lorentz lemma in the integral form and obtain integral correlations for each of the regions, V_1, V_2 and V_3, respectively [1, 2]. We consider the boundary conditions on the surfaces of the impedance flanges, and the equality of the tangential field components in the openings of the waveguides ($H_{z1} = H_{z2}, E_{x1} = E_{x2}$ in $x \in [0, a]$; $H_{z1} = H_{z3}, E_{x1} = E_{x3}$ in $x \in [a + L, a + L + b]$), where the subscript numbers refer to the regions V_1, V_2 and V_3. With regards to the specifics of the electric field at the edges, $x = 0,\ a, a + L,\ a + L + b$, the solution will consist in solving the system of integral equations, subject to the boundary conditions, for the unknown tangential component of the electric field on the surface S ($x \in [-L_1, a + L + b + L_2]$ and $y = 0$) as shown in detail in Refs. [1, 2]. The solution of this equation is conveniently solved with the use of the Krylov–Bogolyubov method [11], which gives an iterative approximation for the required value. After obtaining the system of integral equations relative to the electric field $E_x(x)$ on the $y = 0$ plane, we propose the use of the periodic structure designed below in order to solve the given problem of coupling between the antennas.

III. DESIGN OPTIMIZATION OF THE SURFACE IMPEDANCE PLANE

In this section, we consider a solution to the two-dimensional design problem for the arrangement shown in Figure 1b. Above the plane S $(y = 0)$, there is an infinite thread of in-phase magnetic current $\vec{J}^{m.ex.}$ located at height h. On the surface S, the boundary impedance conditions of Shukin-Leontovich are fulfilled by Eq. (1). It is necessary to determine the dependence of the passive impedance $Z(x)$ $(\mathrm{Re}(Z) \geq 0)$ on the surface S. Once $Z(x)$ is obtained, the complete field in the upper space is found, and then the degree of decoupling between antennas can be obtained.

It is well known that surface impedance, comprising a mathematical model of a corrugated structure, can be used systematically to control the radiation, scattering and propagation characteristics of the waves and, thereby, can be used to design better antennas. Furthermore, the effective solution to the problem of reducing the coupling of airborne antennas requires the solution of the structural design problem. The design of such a two-dimensional structure is obtained in Ref. [12], which investigates the design problem of the impedance surface when an infinite thread of in-phase magnetic current is located above the plane at a certain height. The designed impedance structure has the following form:

$$Z = -iW\cos\gamma_r \tan\frac{\chi}{2} , \qquad (2)$$

where i is the imaginary unit, $W = 120\pi$ (ohms) is the characteristic resistance of a free space and γ_r is the angle of reflection. $\chi = k(R_i - x\cos\phi_0)$ is a dimensionless quantity, $k = 2\pi/\lambda$ is the wave number, $R_i = \sqrt{h^2 + x^2}$, h is the height, and the coordinate x gives the position of the subsidiary source. The derived impedance variation can be used as an independent solution of the problem of providing electromagnetic compatibility, as well as the first step in further optimization of the structure with the help of non-linear programming methods.

IV. NUMERICAL RESULTS

The solution for the designed impedance distribution is given as

$$Z(x) = -i\tan\left(k\left(\sqrt{h^2 + x^2} - x\cos\phi_0\right)\right), \qquad (3)$$

in which the two free parameters h and ϕ_0 are included [12]. These parameters can be used for an optimization of the impedance, $Z(x)$, yielding a minimal coefficient of coupling (maximum decoupling) between the antennas.

In Figure 2, we show a graph of the variation of the impedance distribution, which provides the best decoupling for the parameters, $h = 0.5\lambda$ and $\phi_0 = 54^\circ$. The optimized impedance also gives a nearly hyperbolic reactance. The vertical solid lines represent the geometry of the problem.

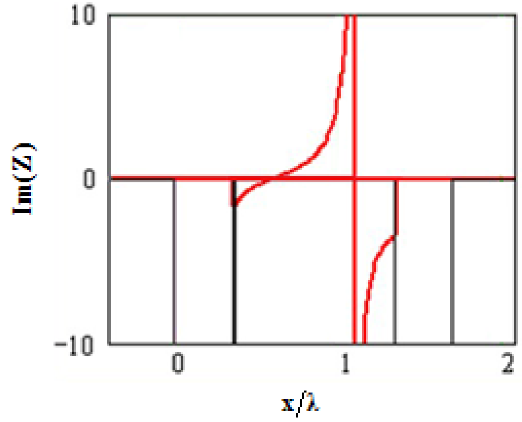

Figure 2. Variation of the optimized surface impedance for the parameters: $h = 0.5\lambda$ and $\phi_0 = 54^\circ$. The vertical solid lines represent the geometry of the problem.

Figure 3 shows the dependence (red solid curve) of the decoupling coefficient K on the parameter ϕ_0 for the fixed value $h = 0.5\lambda$, for a structure with length $L = \lambda$ and $a = b = 0.34\lambda$. The blue dashed curve corresponds to the ideal conducting structure. As seen, the optimum in this case occurs for the angle of 54°. It can be stated that decoupling of antennas does not depend sensitively on the angle ϕ_0. This parameter alters K by not more than 10 dB.

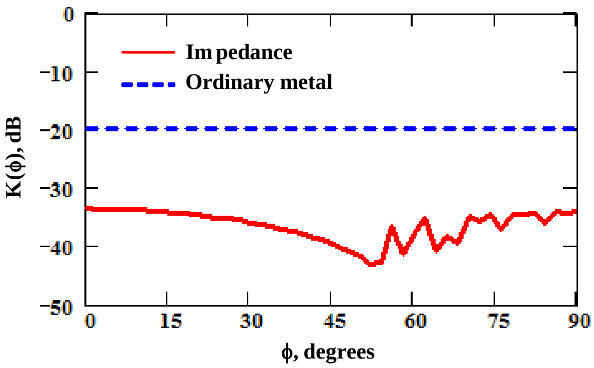

Figure 3. Dependence of the decoupling coefficient K on the parameter ϕ_0 for the fixed value $h = 0.5\lambda$. The optimal decoupling in this case is when the angle equal to 54°. $L = \lambda$ and $a = b = 0.34\lambda$.

In Figure 4, the dependence of the decoupling coefficient K on the parameter h for the fixed angle $\phi_0 = 54^\circ$ is shown for the same structure (red solid curve). As in the previous graph, the blue dashed curve corresponds to the ideal conducting structure. As shown here, the best decoupling of $K \approx -40$ dB is obtained for the parameter $h = 0.5\lambda \sim 0.6\lambda$. Further numerical research shows that alteration of the height h leads to a shift of the maximum reactance from the opening of one antenna to the other. This, in turn, leads to periodic alteration of the decoupling coefficient between antennas. Increasing the length of the structure leads to the appearance of an additional maximum in the variation of the impedance distribution.

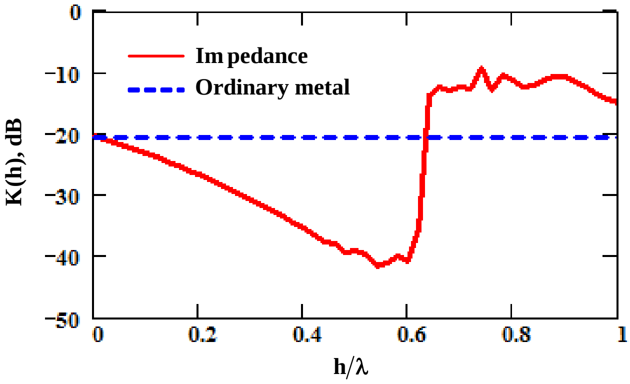

Figure 4. Dependence of the decoupling coefficient K on the parameter h for the fixed angle $\phi_0 = 54^\circ$. The best decoupling is obtained for the parameter $h = 0.5\lambda \sim 0.6\lambda$. The parameters for our calculation are the same as in the previous case.

Figure 5 shows the dependence (red solid curve) of the decoupling coefficient K for the fixed angle $\phi_0 = 45^\circ$, for a structure with the parameters, $L = 2\lambda$ and $a = b = 0.34\lambda$. The impedance distributions for $h = 0.5\lambda$ and $h = 1.8\lambda$, which give the maximum values of decoupling, are also presented in Figures 6 (a) and 6 (b), respectively. Here, it is also possible (with $L = 2\lambda$) to consider the parameter $h = 0.5\lambda$ as optimum. Compared to the reactance of Figure 6 (a), the reactance of Figure 6 (b) shows a shift of $x = 0.5\lambda$ in the values of the sharp transitions. Additionally, the reactance of the Figure 6 (a) shows a half parabola between the points $x = \lambda$ and $x = 2.3\lambda$.

The impedance distributions considered above have a reactance following the functional form of tangent or cotangent over the region x= $0 \sim \lambda$:

$$Z(x) = iZ_0 \tan(qkx) \text{ or } Z(x) = -iZ_0 \cot(qkx). \quad (4)$$

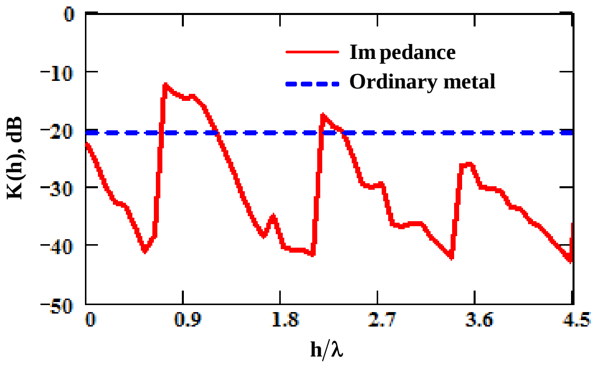

Figure 5. Dependence of the decoupling coefficient K on the parameter h over a wide range for a fixed angle $\phi_0 = 45^\circ$. Parameters used are $a = b = 0.34\lambda$ and $L = 2\lambda$.

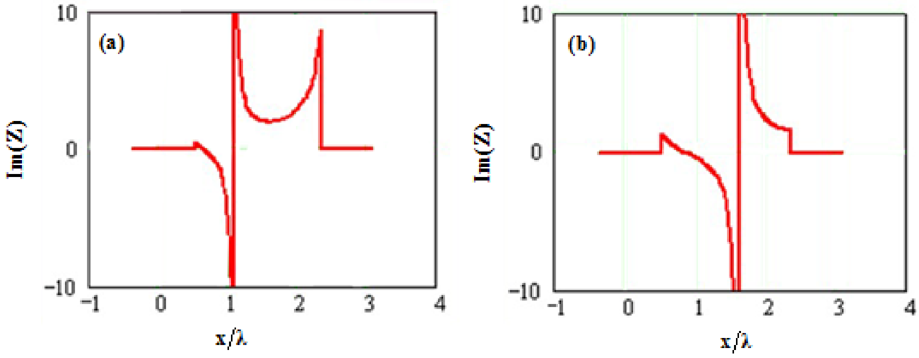

Figure 6. Variations of impedance distribution for (a) $h = 0.5\lambda$ and (b) $h = 1.8\lambda$. In both cases, the parameters used are $a = b = 0.34\lambda$, $\phi_0 = 45^\circ$, and $L = 2\lambda$.

Figure 7 (a) shows (red solid curve) the dependence of the decoupling coefficient of the two antennas $a = b = 0.34\lambda$, separated by the impedance structure with length $L = \lambda$, using the form of the impedance $Z = i\tan(qkx)$ with the dimensionless parameter q. Analogous results (red solid curve) are shown in Figure 7(b) for the structure with the impedance $Z = -i\cot(qkx)$. The reactance with the functional form of the tangent gives larger local minima, reaching -43 dB. The reactance with the functional form of the cotangent gives smaller local minima but has a smoother dependence on the parameter q. As shown, the decoupling coefficient for the cotangent case becomes $K = -30 \sim -40$ dB, reached when $q = 0.4 \sim 2$. This means that if such a structure is calculated with a coefficient $q = 0.4$ on the lower frequency of the range, it will give a decoupling of $K = -30 \sim -40$ dB over the frequency range of interest. From the viewpoint of frequency properties, such a structure is preferable. We observe that in Figures 5, 7(a) and 7(b), the blue dashed curve also corresponds to the decoupling level for the case of an ideal conducting structure.

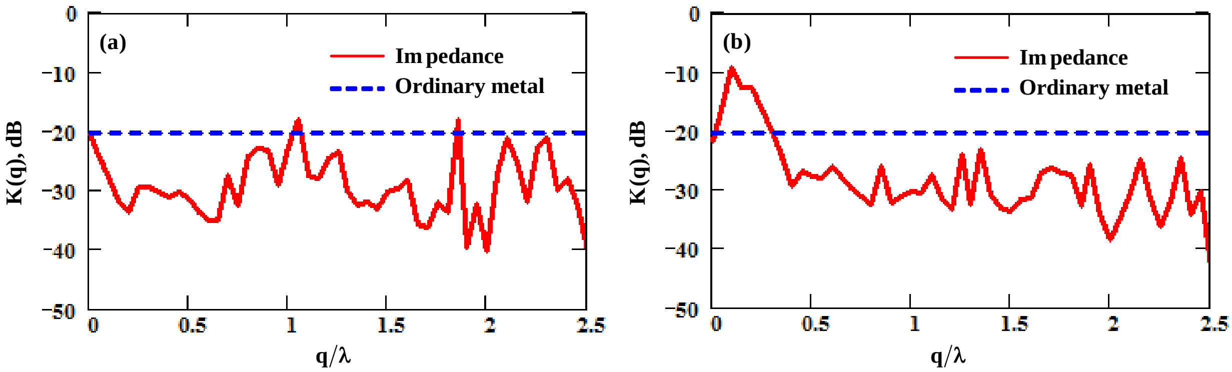

Figure 7. Dependence of the decoupling coefficient K on the parameter q for the impedances (a) $Z = i\tan(qkx)$ and (b) $Z = -i\cot(qkx)$. Parameters used are $a = b = 0.34\lambda$ and $L = \lambda$.

IV. CONCLUSION

We have solved the optimization problem of the surface impedance for reducing surface waves between antennas located on a common plane surface. The optimized surface impedance is an inhomogeneous impedance plane designed by a fixed reflected field. In the optimization results, we have obtained a reactance close to the functional form of tangent or cotangent, which can provide significant decoupling over a large range of frequencies.

REFERENCES

[1] J.-F. D. Essiben, E. R. Hedin, Y. D. Kim, and Y. S. Joe, "Electromagnetic Compatibility of Aperture Antennas Using Electromagnetic Band Gap Structure," *IET Microwaves, Antennas & Propagation, Vol. 6*, pp. 2012, 982-989.
[2] Y. S. Joe, J.-F. D. Essiben and E. M. Cooney, "Radiation Characteristics of Waveguide Antennas Located on the Same Impedance Plane," *Journal of Physics D.: Applied Physics, Vol. 41*, 2008, 125503 (11pp).
[3] R. B. Hwang and S. T. Peng, "Surface-Wave Suppression of Resonance-Type Periodic Structures," *IEEE Transactions on Antennas and Propagation, vol. 51, No. 6*, 2003, pp. 221-229.
[4] Y. S. Joe, J.-F. D. Essiben, E. R. Hedin, J. T. N. Bisse, and J. Matanga, "Optimization of impedance plane reducing coupling between antennas", *Wireless Engineering and Technology journal, Vol. 2*, 2010, pp.1–8.
[5] M. D. Siegel, "Aircraft antenna-coupled interference analysis," *in Proc. Nat. Aerospace Electronic Conf.*, Dayton, OH, 1969, pp.535-540.
[6] E. A. Ibatoulline, "Mathematical modeling of EMC conditions of aircraft electronics systems interference analysis," *in Reception and Processing of Information in Complex Information Systems. Kazan, Russia: Kazan Univ. Press*, 1984, pp. 63-70.
[7] E. A. Ibatoulline, *EMC and Immunity of Information System.* Russia: *Kazan Univ. Press*, 1989.
[8] E. A. Ibatoulline, "Minimization of antenna coupling coefficients of board radio-engineering systems," *in Abstr. 4th Russian Conf. EMC of Technical Devices*, St. Petersburg, Russia, 1996, pp. 262-264.
[9] E. A. Ibatoulline, "Optimum antenna placement on a mobile board with registration of EMC," *in Proc. On EMC' 96 ROMA Int. Sym. EMC, vol. II*, Rome, Italy, 1996, pp. 423-426.
[10] E. A. Ibatoulline, "Electromagnetic compatibility of antennas on a mobile board," *in 3rd OMA Int. Sym. EMC*, St. Petersburg, Russia, 1997, pp. 79-83.
[11] O. N. Tereshin, V. M. Sedov, and A. F. Chaplin, *Synthesis of Antennas on Decelerating Structures*, Communication Press, Moscow, 1980.
[12] Y. S. Joe, J.-F. D. Essiben, J. Cho, and E. R. Hedin, "Design and Modeling of Electromagnetic Impedance Surfaces to Reduce Coupling between Antennas," *Wireless Engineering and Technology Journal, Vol. 3*, 2012, pp.152-159.

International Journal of Modern Engineering Research (IJMER)
www.ijmer.com Vol. 3, Issue. 5, Sep - Oct. 2013 pp-3272-3280 ISSN: 2249-6645

Detection of Duplicate Address in Mobile Adhoc Networks for On Demand Routing Protocols

P. Nagesh[1], G. Ramesh[2], P.V.Gopikrishnarao[3] V.S.Sivakumar[4]
1. NETWORK ENGINEERR AILWIREICT P V T L T D BANGALORE,
2. Assistant PROFESSES O R Dept. Of EIE, RG MCET, NANDYAL, A. P, India
3. Associate PROFESS OR Dept. Of EIE, RG MCET, NANDYAL, A. P, India
4. ASSISTANT PROFESS OR Dept. Of EIE, RG MCET, NANDYAL, A. P, India

ABSTRACT: *MANET is a wireless network in which all nomadic nodes can communicate with each other without relying on a fixed infrastructure. By using the intermediate nodes we will achieve the forwarding and routing of the packet. The necessity of developing the IP addresses auto configuration schemes is because of to send and receive the packets between two nodes with the same IP (unique addresses). In order to assign the unique IP addresses to each node, when one node from one partition moves in to another partition the chance of duplication of IP addresses. For implementing, since IP is also used in MANETS. The addresses detection schemes have been developed to remove the over head manual configuration. This project mainly focuses on passive DAD schemes over on- demand ad hoc routing protocols. The ultimate goal of this project is to improve accuracy of detecting address conflicts and improve detection success ratio.*

Key words: *Mobile Adhoc Networks (MANETS), on demand routing protocols, Duplicate Address Detection*

I. INTRODUCTION

Recently, research interest in MANETs (Mobile Ad Hoc Networks) has increased because of the proliferation of small, inexpensive, portable, mobile personal computing devices. A MANET is a group of mobile, wireless nodes which cooperatively and spontaneously form a network independent of any fixed infrastructure or centralized administration. Since packet forwarding and routing are achieved via intermediate nodes, the MANET working group of IETF has standardized AODV (Ad hoc On- Demand Distance Vector Routing), DSR (Dynamic Source Routing) and OLSR (Optimized Link State Routing) as its reactive and proactive routing protocols, respectively. Nowadays, DYMO and OLSRv2 have been standardized as working group drafts. In proactive protocols, routing information to all possible destinations in the network is maintained by each node so that a packet can be transmitted over an already- existing routing path. In reactive protocols, a routing path is acquired on-demand when a source desires to send packets to a destination. In addition, a hybrid routing protocol like ZRP (Zone Routing Protocol) has been proposed in order to support a large-scale MANET.

In Mobile Ad hoc Networks, routing is needed to find the path between source and the destination and to forward the packets appropriately. In routing, the responsibilities of a routing protocol include exchanging the route information, finding a feasible path to a destination based on the criteria such as hop length, and utilizing minimum bandwidth. Routing in mobile ad hoc network remains a problem given the limited wireless bandwidth and user mobility and insufficient scalability. Routing protocols are divided into two types, they are Proactive routing (Table-Driven), Reactive routing (On Demand). In proactive routing protocols, routing information to reach all the other nodes in a network is always maintained in the format of the routing table at every node.

Reactive routing protocol discovers a route only when actual data transmission takes place. When a node wants to send information to another node in a network, a source node initiates a route discovery process. Once a route is discovered, it is maintained in the temporary cache at a source node unless it expires or some event occurs (e.g., a link failure) that requires another route discovery to start over again. Reactive protocols require less routing information at each node compared to proactive protocols, as there is no need to obtain and maintain the routing info.

In a MANET, node mobility can cause the network to be partitioned into several sub-networks. In partitioned networks, new joining nodes have their unique addresses independent of other partitioned networks. In other words, same addresses can exist between partitioned networks. Therefore, when several partitioned networks or independent networks merge into one network, potential address conflicts must be resolved. Since the address has to be unique, address conflicts need to be detected through a DAD (Duplicate Address Detection) procedure.

II. RELATED WORK AND MOTIVATION

Three previously proposed PDAD (called PACMAN) schemes that operate over on-demand routing protocols are de- scribed in this section: PDAD-RREP-Without-RREQ (RwR), PDAD-RREQ-Never-Sent (RNS), and PDAD-2RREPs-on- RREQ (2RoR).

2.1 RWR scheme

During route discovery, the source node floods an RREQ packet to discover a route towards a destination node, and it then receives an RREP packet from the destination node. However, if the source node receives an RREP packet destined to itself (although it has never sent an RREQ packet), this means that the same address that the source node uses definitely exists in the network (see Figure 1a). Therefore, the source node will invoke an address conflict resolution process.

2.2 RNS scheme

If a node has never sent an RREQ packet, but it receives an RREQ whose source address is the same address that it is using, this indicates an address Both RWR and RNS schemes can be applied to on-demand routing protocols such as AODV and DYMO protocols. How- ever, they still have to resolve a situation in which multiple nodes with the same address want to obtain paths towards their destination nodes and will flood their RREQ packets simultaneously. In addition, to detect address conflicts, each node should store RREQ packets (which was sent from itself) and compare the received RREQ whenever receiving new RREQ packets from other nodes. In particular, the 2RoR scheme has a serious drawback. Since an RREQ packet is flooded into the network, the destination node will receive multiple RREQ packets each of which traverses different intermediate nodes, i.e. different paths. When the destination node receives the first RREQ packet from a source node, it will reply to the source node with an RREP packet. Meanwhile, if an RREQ packet which traversed a better route is received, the node will send a new RREP packet back to the source node. The criteria to determine better routes are based on power saving, route- stability, and others (this is beyond the scope of our paper). Therefore, the destination node can reply with multiple RREP packets back to the source.

III. OUR PROPOS ED SCHEMES

Our schemes have three main goals: (a) improving the accuracy of detecting address conflicts, (b) improving the detection success ratio, and (c) reducing the time taken to detect these conflicts. To detect address conflicts of source nodes, we propose: (a) Location-S scheme and (b) Neighbor- S scheme. To detect address conflicts of destination nodes, we propose: (a) Sequence-D scheme, (b) Location-D scheme, and (c) Neighbor-D scheme. These schemes will be elaborated below.

3.1 Schemes to detect address conflicts of source nodes

We propose two schemes that can detect address conflicts when receiving RREQ packets from multiple nodes using the same address. In our schemes, an RREQ packet contains location or neighbor information that can be used to detect address conflict of source nodes.

3 . 1 . 1 Using location information-PDAD of Source Node with Location Information (Location-S) s c h e m e

In order to differentiate between RREQ packets which contain the same source address but are issued from different nodes, Location-S scheme includes location information (*longitude, latitude, altitude*) into RREQ packets. The location obtained when a node configures its IP address is recorded and utilized to detect address conflicts. Thereafter, when an RREQ packet is flooded from a source node, the source node includes its recorded location in the RREQ packet. When a source node receives an RREQ packet with the same source IP address but with different location information from its own recorded location, this means that an address conflict exists see figure.1

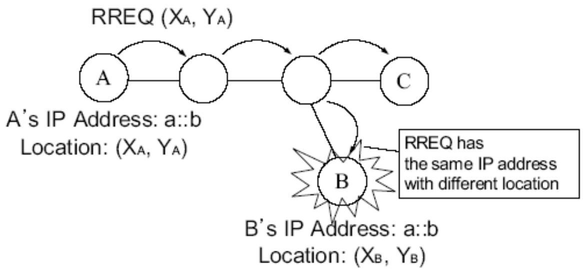

Figure1: Example of Location-S scheme

To obtain the location information of a node, various existing wireless localization schemes can be employed, such as GPS, TOA, TDOA, etc. However, they all have some location errors due to inaccuracy of their localization schemes. Hence, nodes within an error tolerance range may obtain information on the time when nodes acquire their addresses is included into RREQ packets, in addition to location.

3.1.2. Using neighbor information PDAD of Source Node with Neighbor Knowledge (Neighbor-S) scheme

In Neighbor- S scheme, instead of using location information, a list of neighbor nodes is used. A list of neighboring nodes is noted and recorded when the node's IP address is configured. Since nodes with many neighbors produce a large-sized packet, a subset of neighboring nodes (neighbor_list) is utilized to detect the address duplication. To choose the k number of nodes among neighboring nodes, various algorithms can be used: random selection, a sorting of the address list and a selection of the first *k* addresses. As the *k* value increases, the protocol overhead (i.e. the size of RREQ/RREP packets) also increases. However, this overhead can be reduced by taking advantage of packet compression techniques. When an RREQ packet is transmitted, the neighbor subset is included in the RREQ packet. When a source node recognizes the difference between the information of neighbor nodes in the received RREQ packet and its recorded list, it can therefore detect the address conflict.

However, consider an example shown in Figure 2. If nodes S_A and S_B, which have the same address, flood their RREQ packets toward node D using N_A and N_B as their neighboring nodes, duplicate addresses cannot be detected at D. In this case, one possible approach is using "hello" exchange. N_A and N_B will therefore detect the usage of duplicate addresses and invoke an address conflict resolution in case that S_A and S_B are using different MAC addresses. However, we cannot tell whether MAC address is unique in the network due to several reasons Some manufacturers sell network adapters with non-registered MAC addresses; MAC addresses may get corrupted during the manufacturing process, or most network adapters allow users to change the MAC address to an arbitrary value.

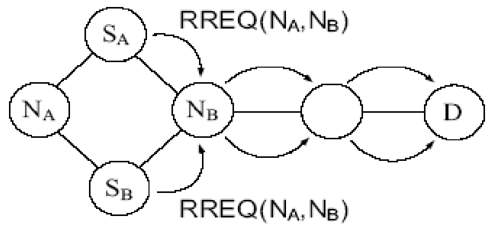

Figure2: Neighbor-S Scheme.

3.2 Schemes to detect address conflicts of destination

In this section, we propose three schemes to detect ad- dress conflicts of destination nodes more accurately. They are: (a) Sequence-D scheme, (b) Location-D scheme, and (c) Neighbor-D scheme. These schemes can address the following Two scenarios: (a) a single destination node sent multiple RREP packets to the source node, and (b) multiple nodes using the same address sending their RREP packets to the Source node.

3.2.1 Using sequence number - PDAD of Destination Node with SEQ (Sequence-D) scheme

Sequence-D scheme requires an incremental sequence number to be included in each PREP packet transmitted by a destination node Sequence number is denoted by DAD-sequence to differentiate between it and the sequence number used by routing protocols such as AODV and DYMO in order to perform route discovery or maintenance. The latter is denoted by Routing-Sequence in this paper.) An additional new DAD-sequence field is needed to perform the DAD functionality in our scheme. Whenever the destination node replies with a new RREP packet because it has received an RREQ packet which traversed a better route, the DAD-sequence number increases and is put into the RREP packet. Therefore, when a source node receives more than one RREP packet with the same DAD-sequence number and the same destination address, the source node can detect the presence of address conflict. Since an RREQ packet contains an Routing-sequence number generated by a source node, the sequence number of RREP packets is reset when a new RREQ Packet with higher Routing-sequence number arrives at the destination. From Figure 4, a source node S can discover that destination nodes D_A and D_B are using the same IP address through The DAD-sequence number included in RREP packets (see sequence numbers in parenthesis in the figure). Node S floods

An RREQ packet with an Routing-sequence number into the Network in order to find a path towards its destination. Nodes D_A and D_B reply with RREP (1, 2, 3) and RREP (1, 2) packets. This is because each destination has received different RREQ packets which traversed better route than the previous RREQ packets. Thus, whenever D_A and D_B reply with a new RREP packet, an incremental DAD-sequence number is put into the RREP packets (i.e. from RREP(1) to RREP(3)). Hence, when the node S receives RREP packets with the same DAD sequence number, it can detect an address conflict.

In addition, consider the occurrence of packet losses. In a case where RREP only is lost, Sequence-D scheme can detect the address conflict successfully by receiving both RREP (1) and RREP packets from each destination node,D_A and D_B . In the other case where RREP (1) of D_A reach node S successfully, node S will fail to detect the address conflict. In Sequence-D scheme, such simultaneous packet losses can cause the source node to miss detecting the address conflict. However, this problem can be resolved by our other DAD schemes, such as Location-D and Sequence-D schemes.

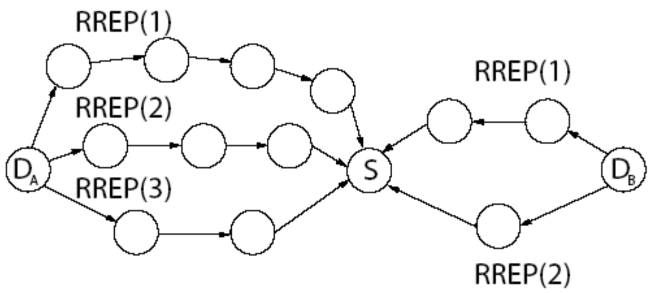

Figure3: Example of Sequence-D scheme.

3.2.2 Using location information - PDAD of Destination Node with Location Information (Location-D) scheme

Similar to the Location-S scheme, in order to differentiate between RREP packets (which contain the same source address , but are issued from other nodes), Location D scheme includes Location information (*longitude*, *latitude*, *altitude*) into RREP packets. The location obtained when a node configures its IP address is recorded and utilized to detect address conflicts (see Figure 4). When sending an RREP packet, a destination node includes its recorded location. When a source node receives more than one RREP packet with different location, it will conclude the existence of duplicate addresses for destination nodes.

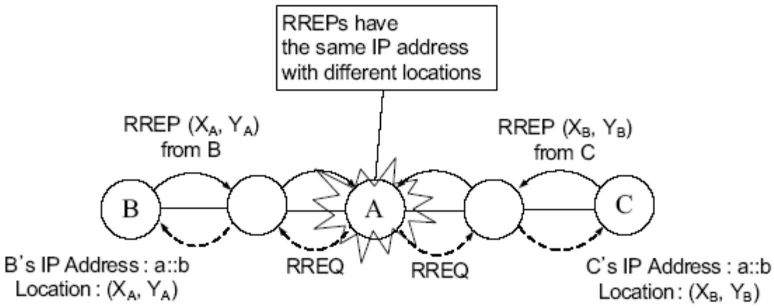

Figure4: Example of Location-D scheme.

3.2.3 Using neighbor information - PDAD of Destination Node with Neighbor Knowledge (Neighbor-D) scheme

Similar to the Neighbor-S scheme, the subset of neighbor nodes (neighbor_list) obtained when a node configures its IP ad- dress is captured and recorded. Then, it is utilized to detect the address duplication. When a destination node replies with an RREP packet, a subset of neighbor nodes of the destination node (neighbor_ list) is included in the RREP packet. When a source node receives more than one RREP packet with different neighbor lists, it will determine the existence of duplicate addresses for destination nodes. addresses due to the same reason mentioned in Section III-A2. Such a collision might occur only if nodes with the same IP address have chosen the same subset of neighbor list (albeit low). If they are one-hop reachable, the collision can be easily addressed by the Neighbor Discovery (ND) protocol. For example, if nodes D_A and D_B are one- hop reachable, after assigning IP address to nodes D_A , it can detect address conflict using existing ND protocols which exchange Neighbor Request and Reply. Otherwise, using a combination of passive DAD scheme is recommended, such as Location-S and Neighbor-S, Sequence-D and Neighbor-D. In our Location-S/D and Neighbor-S/D schemes, we use extra control information (location and/or neighbor list) to achieve 100% detection accuracy. These extra bytes of control information did not incur large overhead. 16 bytes are needed in length. Hence 16 byte location information is needed, also the compression techniques can be used where there are more neighbours.

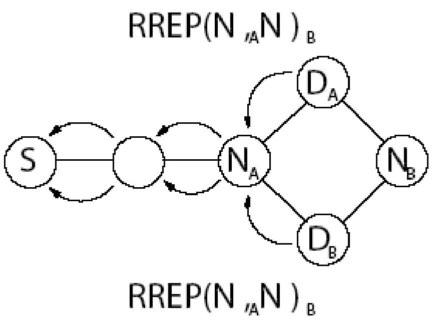

Figure5: The same neighbor list in the Neighbor- D scheme.

3.3 Participation of intermediate nodes

To detect address conflicts, Location-S, Location-D and Neighbor-S, Neighbor-D schemes need some delay with more than one RTT (Round Trip Time) between source and destination nodes. This is because source and destination nodes only can detect address conflicts after exchanging RREQ and RREP packets. This delay, however, can be reduced through the participation of intermediate nodes. When source and destination nodes send RREQ and RREP packets respectively, their recorded location (*longitude*, *latitude*, *altitude*) or their captured neighboring nodes' addresses (*neighbor__list*) will be put into the RREQ and RREP packets. Each intermediate node receiving the RREQ or RREP packets will create a table entry with source_node, the_location or source_node, neighbor_list. Also, the table entry will be deleted after a timeout (i.e. soft-state scheme). Therefore, when an intermediate node receives RREQ or RREP packets from a source or a destination node using the same address, the location or neighbors in the RREQ or RREP packets will be compared with those in the table entry. If a difference is detected, then an address conflict has occurred Multiple intermediate nodes can detect an address conflict for a source or destination address at almost the same time. Hence, they will try to notify all nodes in the network of the address conflict. Consider a case where duplicate addresses exist in the network. Since a routing protocol cannot find any appropriate path towards nodes with duplicate addresses, any communication trial with these nodes will fail. To prevent these problems, a node which detects any address conflict should announce the detection to all nodes in the network, by utilizing an efficient flooding technique. Reducing the overhead of flooding is an important and challenging issue [11] [12]. Since this paper focuses primarily on the detection of address conflicts, conflict resolution is beyond the scope of our paper.

3.4. Consideration of Accuracy and Resolution

As mentioned before in Section III-A1 and Section III-B2, Location-S and Location-D schemes utilize location information using wireless localization schemes such as GPS, DOA and TDOA. However, these localization schemes have location errors due to their inaccuracy. In particular, these errors cause different nodes to obtain the same location information. Nodes with different IP addresses do not create any problems in the network, even if they have the same location information. However, nodes with the same IP address and the same location information can cause a problem which cannot be detected by our DAD schemes.

To address this inaccuracy problem in localization schemes, we additionally utilize the time information and the Neighbor Discovery (ND) protocol [14] with a positioning service. Since the basic Location-S and Location-D schemes utilize (longitude, latitude, altitude), the basic schemes can be extended to include the information on the time when each node was configured with its address (in addition to the location information), so that (longitude, latitude, altitude, configured time) is recorded and utilized to execute a DAD. From the difference of the time information, our scheme can detect address conflicts even if nodes have the same IP address and the same location information. If different nodes are configured with the same IP address at the same location and at the same time, they can detect the address conflict with the ND protocol.

Other information such as a random number might be considered as a means of DAD. For example, techniques using random number generation or hash functions might be applied to our DAD schemes for the secondary identifier such as location and neighbor information. However, these functions still have a probability of collisions even if it is very low. In addition, a similar protocol overhead to ours can occur because including the information into RREQ/RREP packets is required. Moreover, since the hash and the random functions cannot guarantee the uniqueness, it is undesirable to use them for passive DAD schemes

IV. PE R F O R M AN C E EVA L UAT I O N

4.1 Simulation Environment

To evaluate performance, we implemented our passive DAD schemes and an existing scheme (called PACMAN) in ns-2 simulator. The DYMO protocol was used as our underlying routing protocol because the IETF MANET working group has been trying to standardize it. Moreover, DYMO supports the “Generalized MANET Packet/Message Format” (called pack- etBB) [15], so that additional information (location, neighbor list, etc) can be easily added into the packet header through its TLV (type, length, value) block. We extended the DYMO protocol to support our passive DAD schemes. Detailed sim- ulation parameters are described in Table I.

Initially, *n*% (from 5% to 20%) of network nodes are assigned duplicate addresses which are randomly selected among addresses which have been already assigned to the other nodes. Passive DAD schemes can detect address conflicts in the network only when nodes with duplicate addresses receive an RREQ or RREP packet. Hence, we scheduled each node in the network to execute a route discovery during the simulation time to all nodes except itself. This makes each node send RREQ packets from 1 to 5 times every second. All simulation results were plotted with an average of 20 runs.

Parameter Types	Value
Routing protocol	DYMO protocol
Number of nodes	50, 75, 100, 125, 150
Mobility model	Random waypoint
Node Mobility	maximum speed = 1m/s, 5m/s, 10m/s (pause time = 0)
Percentage of Duplicate Addresses	5%, 10%, 20%
Simulation area	1500 m x 1500 m
Simulation duration	100 seconds
MAC protocol	IEEE 802.11b
Transmission Range	250 meters
Topologies	Random

Table 1: Simulation parameters

Our proposed PDAD schemes are performed by source node, destination node, or intermediate nodes. Although each of them can be performed independently, better detection success ratio can be expected by combining these schemes. In our simulations, location based schemes (e.g., Location- S, Location-D, intermediate DAD with location information schemes) were tested, because they have lower routing pro- tocol overhead and less limitations to be applied than other schemes using neighbor or sequence information. The schemes using neighbor list require RREQ/RREP packets to carry the list of neighbor nodes, which needs bigger packet size. In addition, the sequence based schemes can be applied to the detection of address conflicts for destination nodes only. Hence, we investigated performance through two kind of combinations: (a) LOC-SD (Location-S and Location-D without participation of intermediate nodes) and (b) LOC-SD-INT (Location- S and Location-D with intermediate nodes’ participation). Both location and neighbor information based schemes exhibit almost similar performance. The only difference lies in the information type, i.e. location versus neighbors’ list. Hence, we only performed simulations on the location based schemes.

4.2 Evaluation of proposed passive DAD schemes

Important metrics related to passive DAD schemes include: (a) protocol overhead and complexity, (b)detection success ratio, and (c)detection delay. The detection success ratio and detection delay are defined as the ratio of the number of detected nodes to the number of nodes with duplicate addresses, and the time taken to detect address conflicts, respectively. We evaluated the performance with respect to three factors: the number of total nodes in the network (from 50 to 150 nodes), node mobility (from 1m/s to 10m/s) and participation of intermediate node.

4.2.1 Protocol Overhead and Complexity

Compared with ac- tive DAD schemes in terms of overhead, active DAD schemes require a large amount of address allocation time and control overhead For example, RADA and MANET conf which are representative active DAD schemes, need several seconds to complete assigning a unique address to a joining node because control messages for DAD procedures should be flooded into the network. Whenever new nodes come and network merges occur, explicit DAD procedures should be per- formed. This produces much control overhead for exchanging control messages. On the other hand, passive DAD schemes do not re- quire such an explicit DAD procedure while assigning IP addresses to nodes. Hence, the delay and control overhead can be reduced. However, passive DAD schemes have their computational and storage overheads while performing route maintenance procedure, unlike active DAD schemes

In addition, our proposed PDAD schemes require localization and time synchronization schemes. If MANET nodes are equipped with a localization device such as GPS, the location and synchronization capability can be easily provided without any protocol overhead. Alternatively, our schemes can employ various localization schemes such as DOA and TDOA which do not need a special device for localization and are widely used in MANET protocols. As for the time synchronization issue, since the IEEE 802.11 standard [19] provides a time synchronization mechanism for ad hoc mode operation, our proposed scheme can also utilize such synchronization service without additional overhead.

4.2.2 Detection Success Ratio

Figure 7 shows the detection success ratio versus the number of nodes. Initially, 5% of network nodes were assigned duplicate addresses. As the number of nodes increases, better detection success ratio is achieved. This is because a larger number of nodes results in better connectivity with other nodes. Especially, we observe a significant improvement in detection success ratio (Figure 7) when the number of nodes was increased from 50 to 125. The average detection success ratio of LOC-SD and LOC- SD-INT increases from 25% to 92% and from 51% to 93%, respectively. When the number of node is more than 125 nodes, both schemes achieve over 90% of detection success ratio, regardless of node mobility. With the same number of nodes and with mobility, higher mobility yields higher detection success ratio. For LOC-SD-INT, when node mobility is increased from 1m/s to 10m/s, the detection success ratio increases by 9% on the average. For the case of 50 nodes, the detection success ratio increases by 31% on the average. This is because higher mobility creates more opportunities to successfully exchange RREQ/RREP packets with other nodes. When comparing LOC-SD with LOC-SD-INT, LOC-SD-INT performs better than LOC-SD under the same simulation parameters, such as the number of node and node mobility. In case of LOC-SD, the DAD can occur only when the source and destination exchange the RREQ/RREP packets. However, in LOC-SD-INT, an address conflict can be detected via intermediate nodes.

4.2.3 Detection Delay

Figure 8 shows the detection delay under varying number of nodes. The detection delay depends on the RTT (Round Trip Time) between source and desti- nation nodes. From Figure 8, when the number of nodes in the network increases, the detection delay also increases. As the number of node increases (from 50 to 150 nodes), the average detection delays of LOC-SD and LOC-SD-INT increase steadily from 47 ms to 93 ms, and from 36 ms to 81ms, respectively. In other words, LOC-SD-INT achieves 19% shorter delay than LOC-SD, on average. This is because a larger number of nodes create a longer hop path, and hence the RTT is also increased. However, for LOC-SD-INT, since an address conflict can be detected by intermediate nodes, LOC- SD-INT has better detection delay than LOC-SD.

4.2.4 Contribution of DAD

Next, we investigated the extent of each passive DAD scheme's contribution to detecting address conflicts. Table II shows the simulation results for 125 nodes. Location-S and Location-D schemes contribute to
95.4% and 4.6% of the detection, respectively Location-D does not contribute to the detection remarkably due to the characteristics inherent from most on-demand routing protocols such as AODV and DYMO. Consider the case where multiple destination nodes with the same addresses replied with their RREP packets to an RREQ packet. While intermediate nodes are forwarding the RREP packets, some RREP packets may be discarded due to the following reasons: networks (e.g., from 50 to 100 nodes) with 1 m/s mobility, we observe a low detection success ratio, as compared to other cases. In sparse networks, we achieve 54% of detection success ratio on average. However, in other cases, 91% of detection success ratio is observed. This is because a sparse network causes network partitions or route disconnections between the source and destination nodes to occur frequently. Hence, some duplicated addresses can not be detected since packet transmissions between conflicting nodes may not be performed successfully. For LOC-SD-INT, duplicate address can be detected by intermediate nodes. This explains why LOC-SD-INT has 12% higher detection success ratio than others in sparse networks,

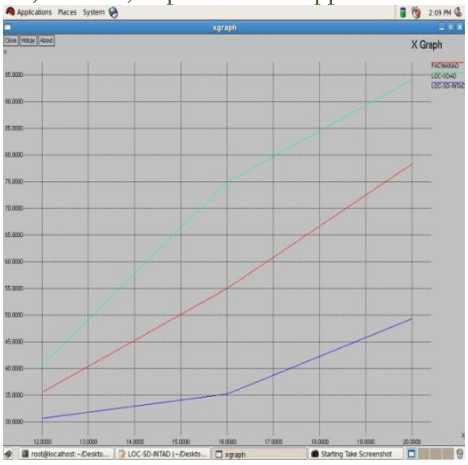

Figure6: average detection delay

In a case where intermediate nodes receive a new RREP packet with the same destination address after they already forwarded an RREP packet, if a Routing-sequence number included in the new RREP packet is less than the Routing-sequence number included in the previously forwarded RREP packet, intermediate nodes discard the new RREP packet according to the DYMO protocol. Thus, the contribution of Location-D is not so high. This is also applied to Neighbor-D. Although Location-D scheme has a relatively low contribution to the detection of duplicated address, it is still needed to improve detection success ratio without any missed detections.

Our scheme using Location-S/Location-D with the par- ticipation of intermediate nodes shows the most significant contribution of 76.7% (see Table II-b). However, the contri- butions of source and destination nodes are 21.7% and 1.7%, respectively (23% in total). This clearly shows the significance of using intermediate nodes for DAD.

4.3 Comparison with an existing passive DAD scheme

We evaluated the performance using three metrics: (a) de- tection success ratio, (b) detection delay and (c) the detection accuracy. From Figure 8 we investigate detection success ra- tio according to node mobility (from 1 to 10m/s). As mobility increases, better detection success ratio is achieved, because more opportunities exist for nodes to exchange RREQ/RREP packets with other nodes. Both LOC-SD and PACMAN can detect address conflicts when the source or destination node receives an RREQ or RREP packet successfully. As a result, they show fairly similar detection success ratio. LOC-SD aims at improving the detection accuracy, not the detection success ratio. Rather than improving the ratio, LOC-SD achieves better detection accuracy, as compared to the PACMAN scheme. nodes' DAD service, it can improve the performance of both the detection success ratio and the detection delay. Figure 8 show the detection success ratio at 1m/s node mobility with various percentage of duplicate addresses (from 5% to 20%). For all the percentages of duplicate addresses, similar results are observed. Hence, the percentage of duplicate addresses does not affect the performance of detection ratio.

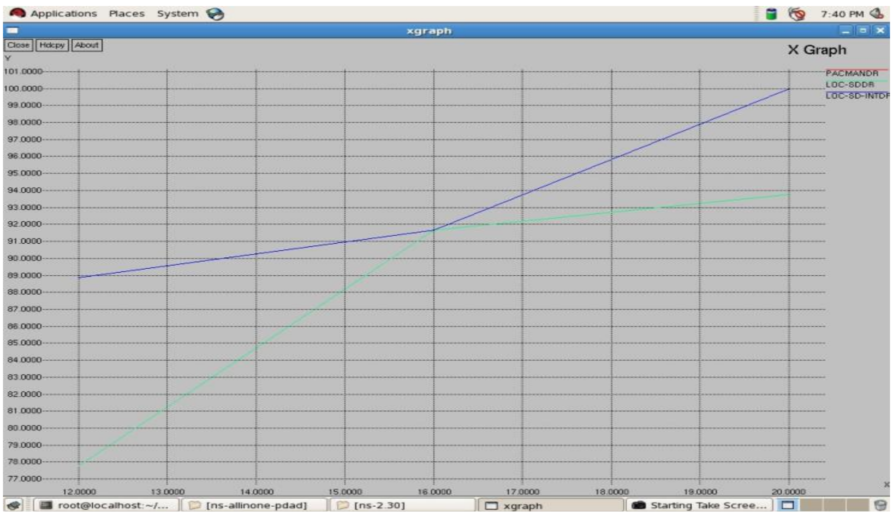

Figure 7 detection success ratio

4.3.1 Comparison of the Detection Delay

The detection delay was measured according to the number of total nodes, node mobility (1m/s, 5m/s and 10m/s) and percentage of duplicate addresses (5%, 10% and 20%). Regardless of node mobility, as the number of nodes increases, the detection delay become no longer. As shown in Figure 8, when increasing the number of nodes, we observe that the detection delay also increases from 52ms to 104ms in PACMAN and increases from 52ms to 100ms in LOC-SD. However, the intervention of intermediate nodes enables the DAD to be completed before the RTT elapses. As node

mobility increases, the overall detection delay decreases. This is because nodes moving at higher speeds tend to create longer hop paths among nodes. As shown in Figures 10a to 10c, when node mobility increases from 1m/s to 10m/s, the average detection delay of LOC-SD-INT decreases from 60ms to 52ms
Figures 10c show simulation results with 10m/s node mobility and various percentages of duplicate addresses (from 5% to 20%). As the percentage of duplicated addresses increases, detection delay decreases, especially when the number of nodes in the network increases.

4.3.2 Comparison of the Detection Accuracy

In the PAC-MAN scheme, a duplicate address can be misdirected. As mentioned in Section II, when multiple nodes invoke route discovery simultaneously, senders of a route request cannot detect the address conflict using RNS, because they can detect the conflict when receiving an RREQ without sending any RREQ. In addition, when a destination node replies with multiple RREPs, 2RoR can misdetect the address conflict. They are called RNS-false and 2RoR-false, respectively in this paper.

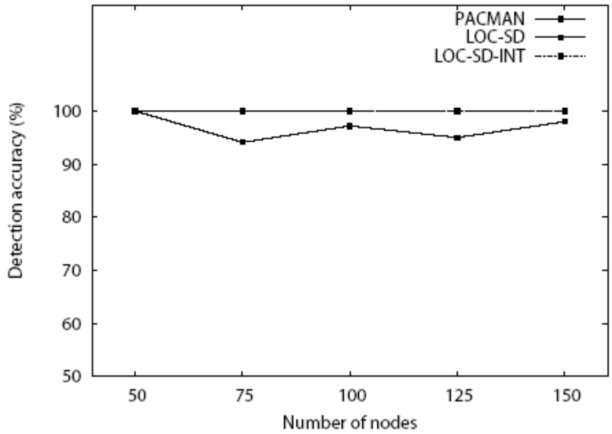

Figure 8: Detection of accuracy of various schemes

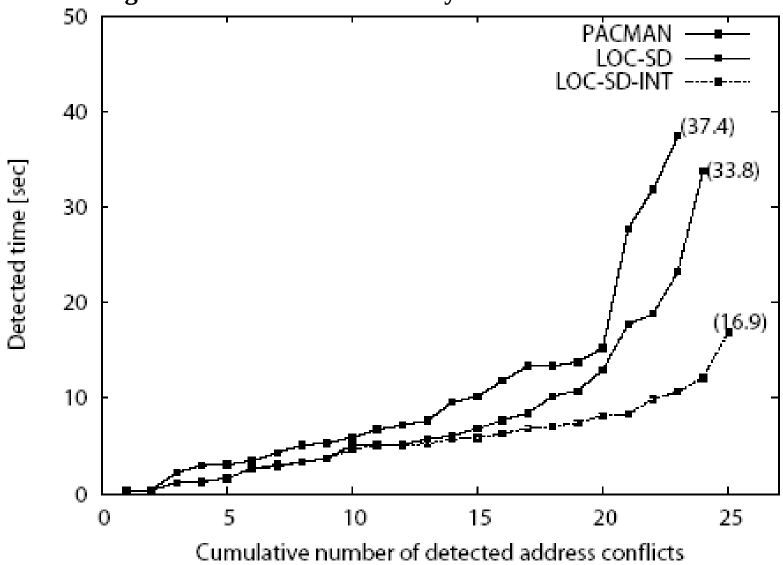

Figure 9: Tracing the DAD execution time of various schemes

We investigated the detection accuracy by measuring the frequency of mis-detections with 10% of duplicate addresses and 5 m/s mobility. Here, the detection accuracy represents the ratio of the number of actual duplicate addresses de- tected to the number of false detections (i.e. RNS-false and 2RoR-false). From Figure 11, we observe that the PACMAN scheme has lower detection accuracy than our schemes (i.e. maximum difference of 7%). There exists none of such RNS- false and 2RoR-false cases through Location-S and Location- D. In addition, our scheme using Sequence-D, Neighbor-S, and Neighbor-D can avoid the occurrence of RNS-false and 2RoR-false successfully. As a result, the PACMAN scheme suffers from poor network resources efficiency caused by these misdetections.

4.3.3 Tracing the DAD Execution Time

We traced the DAD execution time of each duplicate address over simulation time (100 seconds) with 125 nodes and 5 m/s mobility(see Figure 12). Initially, 25 nodes were assigned duplicate addresses. From Figure 12, LOC-SD-INT detects the occurrences of address duplication most quickly and completes all detections at 17s. LOC-SD and PACMAN finish their detections at 34s and 37s, respectively. LOC-SD-INT progresses steadily while detecting all duplicated addresses. PACMAN takes about 15s to detect 20 duplicate addresses. After 15s, PACMAN spends about 20s in detecting three more duplicate addresses. This is because the passive DAD schemes can accomplish the DAD while performing route discovery and maintenance. Thus, if a DAD fails after the exchange of RREQ and RREP packets, the address conflict cannot be detected until a new route discovery from the node is invoked. In this simulation, PACMAN misses several chances to detect address conflicts between 0s and 15s, and it fails to detect five duplicate addresses. In real networks, this is a serious problem that allows duplicate addresses to remain undetected longer and can disrupt data traffic between nodes.

V. CONCLUSIONS

In this paper, In this dissertation, several passive DAD (Duplicate Address Detection) schemes used to quickly and accurately detect address conflicts during route discovery and maintenance over MANET on-demand routing protocols. The main goals which are improved in this project: The accuracy of detecting addresses conflicts, The detection success ratio, and Reduced the time taken to detect these conflicts. By using the simulations (extensive) the ns-2 simulator, PDAD schemes can achieve 100% accurate detection of duplicate addresses with higher detection success ratio when compared to the PACMAN scheme. PDAD schemes utilize sequence number, location of nodes, or a list of neighboring nodes. These information is included into routing control packets (such as RREQ and RREP packets) in order to help detect the duplicate address of source and destination nodes. In addition, the detection success ratio is improved and reduced the detection delay by allowing intermediate nodes to participate in detecting address conflicts.

REFERENCES

[1] Internet Engineering Task Force, “MANET working group charter,”

[2] Dongkyun Kim, Hong-Jong Jeong, C. K. Toh and Sutaek Oh, “Passive Duplicate Address Detection Schemes for on demand Routing Protocols”, IEEE Transaction on vehicular technology,2009

[3] D. Johnson, Y. Hu and D. Maltz, “The Dynamic Source Routing Protocol (DSR) for Mobile Ad Hoc Networks for IPv4,” RFC 4728

[4] I. Chakeres and C. Perkins, “Dynamic MANET On-demand (DYMO) Routing,” IETF Internet-Draft, draft-ietf-manet-dymo-16.txt, December2008.

[5] T. Clausen and P. Jacquet, “The Optimized Link-State Routing Protocol (OLSR),” RFC 3626, IETF, October 2003.

[6] Z. Haas, “A New Routing Protocol for the Reconfigurable Wireless Networks” IEEE International Conference on Universal Personal Communications,

[7] Internet Engineering Task Force, “AUTOCONF working group charter,”

[8] S. Mesargi and R. Prakash, “MANETconf: Configuration of Hosts ina Mobile Ad Hoc Network, in Proc. of IEEE INFOCOM 2002, NewYork, USA, June 2002.

[9] N.H. Vaidya, “Weak Duplicate Address Detection in Mobile Ad Hoc Networks,” in Proc. of MOBIHOC 2002, Lausanne, Switzerlan, June2002.

[10] K. Weniger, “PACMAN: Passive Auto configuration for Mobile Ad Hoc Networks,” IEEE Journal of Selected Areas in Communications Vol.23, No.3, March 2005.

[11] J. Wu and F. Dai, “Efficient Broadcasting with Guaranteed Coverage in Mobile Ad Hoc Networks,” IEEE Transactions on Mobile Computing, Vol.4, No.3, May/June 2005.

[12] M. Heissenbuettel, T. Braun, M. Waelchli and T. Bernoulli, “Optimized Stateless Broadcasting in Wireless Multi-hop Networks,” n Proc. ofINFOCOM 2006, Barcelona, Spain, April 2006.

[13] A. El-Rabbany, “Introduction to GPS: The Global PositioningSystem, Second Edition,” Artech House Publishers.

[14] T. Narten, E. Nordmark and W. Simpson, “Neighbor Discovery for IPVersion 6 (IPv6),” RFC 2461, IETF, December 1998.

[15] T. Clausen, C. Dearlove, J. Dean and C. Adjih, “Generalized MobileAd Hoc Network (MANET) Packet/Message Format,” RF 5444, IETF,February 2009.

International Journal of Modern Engineering Research (IJMER)
www.ijmer.com Vol. 3, Issue. 5, Sep - Oct. 2013 pp-3281-3284 ISSN: 2249-6645

Determination of Some Mechanical And Hydraulic Properties Of Biu Clayey Soils, Nigeria

B.G. Umara*, J.M. Dibal* and I. U. Izuchukwu*

*Department Agricultural and Environmental Resources Engineering, Faculty of Engineering, University of Maiduguri, P.M.B. 1069, Maiduguri. Borno State Nigeria.

ABSTRACT: *The analysis of particle size (PS), Atterberg limit (AL), Maximum Water Holding Capacity (MWHC), and Shear Strength (SS) of Clay Loam and Sandy Clay soils of Biu, Biu Local Government Area were conducted in a laboratory. The soils had varying AL 46.9% and 56.5% liquid limit respectively, 23.5% and 22.7% plastic limits respectively, 23.4% and 33.8% plasticity index respectively for the two soils. For maximum water holding capacity, Sandy clay and Clay loam soils indicated 39% and 41% moisture contents respectively. Sandy clay soil had higher shear strength than Clay loam soil, but Clay loam had higher hydraulic properties. Both soils could be put to agricultural and structural uses but sandy clay would be more preferred for structural uses and clay loam for agricultural. Output of the study could be useful in predicting irrigation scheduling and for determining the sustainability of the soils for structural purposes in the study area.*

Keywords: *Mechanical properties, Hydraulic properties, Clayey soils, Biu area, Semi arid region*

I. INTRODUCTION

The soils in Biu area are clayey-dominated, and are cultivated for agricultural crop production on one hand, and are used civil engineering works either as a construction material or structural support. Agriculture is, however, the major economy of the area. The soils therefore misbehave with hydraulic variation. Problems of structural failure, such as road disruption, settling and cracking of buildings, drainage failure, are not uncommon in the area. This has been one of the sources of socio-economic dilemma confronting the inhabitants of the area. Another factor contributing to the economic insecurity of the area is droughts that usually occur in the first quarters of the rainy seasons. The clayey soils crack when dry, crops dry up correspondingly, and irrigation becomes indispensable for sustainable crop production. Farmers normally replant, but mostly with little or no success. Water holding capacity is the amount of water that is held in a soil after gravitational water loss has ceased and substantive implications on soil and water conservation [1]. It is a measure of the amount of water held in the soil at between field capacity and permanent wilting point of a soil. Shear strength of a soil mass is the internal resistance per unit area that a soil mass can offer against failure and/or sliding along any plane [2]. It is a measure of the soil resistance to deformation by continuous displacement of its individual soil particles that gives the strength of a soil to resist shearing. Shearing displacement has been recognized as important in traction mechanics [2], as the role of displacement in shearing strength measurements is largely dependent on the state of compactness of the soil. Shearing strength characteristics are also influenced by moisture content [3]. Shear strength in soils depends primarily on the interactions between soil particles. The shear resistance of a soil seeks to describe the mechanical properties of a soil mass by indicating its abilities to withstand impact on its cross-sectional area, while water holding capacity symbolize the hydraulic properties of the soil at different water conditions as it relates to water retention within the soil mass. Both the properties are indirectly mutually related and are readily affected by the physical properties of the soil [4]

Up to date data on soil the water holding capacity is an indispensable tool in irrigation scheduling [4], which in turn is necessary for successful design and profitable operation and management of irrigation.

All soils are compressible and could undergo deformation when subjected to stress. Foundation settlements also represent the great problems occurring in building constructions, also many buildings have become distressed due to settlement. This problem, which is often caused by weak or improperly consolidated soils, and affect most buildings which are built on soft but compactable leading to high risk for structural failure. Soils, however, differ significantly in response to varying stress and/moisture contents [5]. This study was therefore initiated to examine the variation in water holding capacity and shear strength of the two major Biu soils with different moisture contents and loads.

II. MATERIALS AND METHODS

Study Area

Biu is a town and a Local Government Area (LGA) is located in the southern Brno State of Nigeria located at Longitude 10.6111°N and Latitude 12.195°E, it lies on the Biu Plateaus at an average elevation of 626 meters above mean sea level. The climate is semi-arid region in the Northern Guinea Savannah (NGA) Agroecological zone with a small portion in the North East lying in the dryer Sudan Savannah Zone.

Sample Collection and Preparation

Soil samples were collected from five randomly selected locations within the Biu Local Government Area. Simple auger was employed in soil sample collection at 15 cm incremental depth from the soil surface to 90 cm depth. The sample collected was then poured in a polythene bag to minimize alteration of the soil properties during conveyance to laboratory. For soil test involving the determination of shear strength, cylindrical moulds (10 mm in diameter and 13 mm in height) were used for sample collection to avoid disturbing the soil.

Sample analysis

The particle sizes of the soils were analyzed applying the Stoke's settling velocity principle as detailed by Day [6]. Approximately 50 grams of air-dried soil passing a 2 mm sieve was weighed and quantitatively poured into dispersing cup and was used for the determination of Particle Size Distribution of the soils. The Atterberg Limits (Liquid limit (LL), Plastic Limit (PL), and Plasticity index (PI) were also determined following the methods adopted [2].

The soil sample was air-dried to reduce the moisture content to 3.72% and 5.53 for sandy clay and clay loam respectively. 500 grams of each of the samples was stirred and fully saturated with 194 ml of water and used for the determination of the maximum water holding capacity of the soil. The Triaxial Machine was used to determine the shear strength of the soils adopting the methods of Dayakar *et al*. [7].

III. RESULTS AND DISCUSSION

Particle Size Distribution

The results of the particle size distribution of the soils are presented in Table 1.

Table 1: Computed Values for Particle Size Analysis

Sample number	Hydrometer reading (H_1)	Hydrometer reading (H_2)	Temp. (T_1)^oC	Temp. (T_2)^oC	% Sand	% Clay	% Silt	Soil Class
1	30.9	21.4	24	25	51.6	40.8	7.6	Sandy clay
2	33.2	18.4	24	25	36.0	34.8	29.2	Sandy clay

The Table above demonstrated the significantly large percentage of clay in the samples following the sand fractions. On the other hand, Clay loam results obtained shows that there was almost equal size distribution between the three particles when analyzed.

Atterberg Limits

The values of liquid and plastic limits of Sandy clay and Clay loam were significantly influenced by affected variation in moisture content. Using the data on Figure 1, the plastic index (I_p) for Biu Sandy clay and Clay Loam soils at 25 blows was computed to be 23.4 % and 33.8 % respectively.

Water Holding Capacity.

Table 2 presents the water holding capacities of the tested soils demonstrating water holding capacity of 195.3 and 202.6 g of water for every meter of the soil at field capacity for Sandy clay and Clay loam soil respectively. This implies 195.3 grams and 202.6grams of water will be required to raise the moisture content of Sandy clay and Clay loam soils respectively to field capacity These figures represent 39 % moisture content for sandy clay and 41% moisture content for clay loam.

Table 2: Computed Values for Water Holding Capacities

Sandy clay Soil							
Sample No	Volume of dry soil used (g)	Volume of water added (g)	Volume of water collected (g)	Time taken for water to drain (g)	Volume of water retained (g)	Droplets	Water holding capacity per meter of soil
1	500	340	145.0	09:56-10:23	195	Max:64d Min:Od	(at 0.39 MC) 195.3g of Water/m of soil at field capacity
2	500	390	195.0	07:25-08:50	195	Max:63d Min:ld	
3	500	390	194.0	09:04-09:44	196	Max:65d Min:ld	

Sandy clay Soil							
Sample No	Volume of dry soil used (g)	Volume of water added (g)	Volume of water collected (g)	Time taken for water to drain (g)	Volume of water retained (g)	Droplets	Water holding capacity per meter of soil
1	500	394	190.0	07:45-09:00	204	Max:60d Min:Od	(at 0.41 MC) 202.6g of water/m of soil at field capacity
2	500	353	152.0	09:23-10:15	201	Max:60d Min:ld	
3	500	394	191.0	08:55-09:32	203	Max:60d Min:ld	

Shear Strength

The results obtained from the shear strength test were computed and polynomial graphs used to represent these values to further buttress the varying shear strength values for the soils tested under different stress conditions as shown in Figures 1 and 2. Similar *intermediate failure* modes (a failure in which soil particles tend slide over another diagonally with a very slight rupture were exhibited by both the soils) when subjected to an axial compressive loads. Sandy clay soil exhibited greater shear strength as compared to clay loam within the limit of experimental errors. While the overall conclusion drawn from the soil tests conducted on disturbed soil sample depicts that for the different number of hammer blows (10, 15 and 20) to which the soil samples were subjected, clay loam exhibited greater shear strength as compared to sandy clay soil. The optimum moisture content was a determining factor that greatly affected the cohesion and densities exhibited by the soil samples used in conducting the test.

For both the soils, shear strength relates to moisture content quadratically with R^2 values near or equal to unity as depicted in Figures 1 and 2.

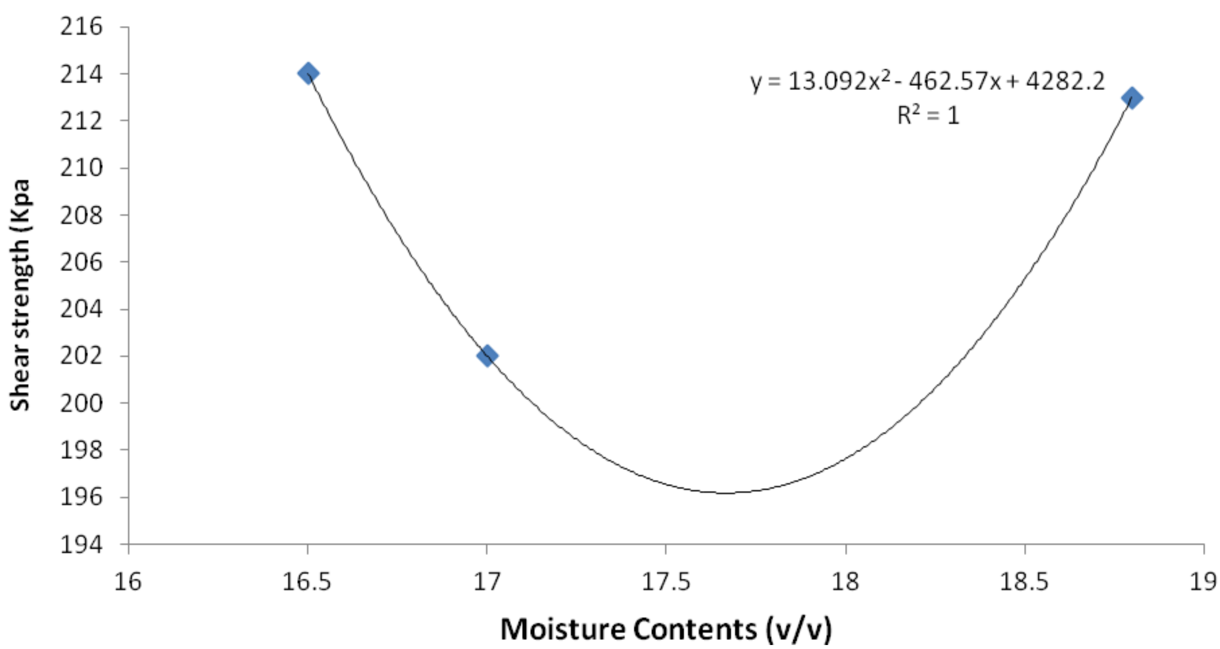

Figure 1: Graph of shear strength for disturbed sandy clay soil at 20 hammer blows

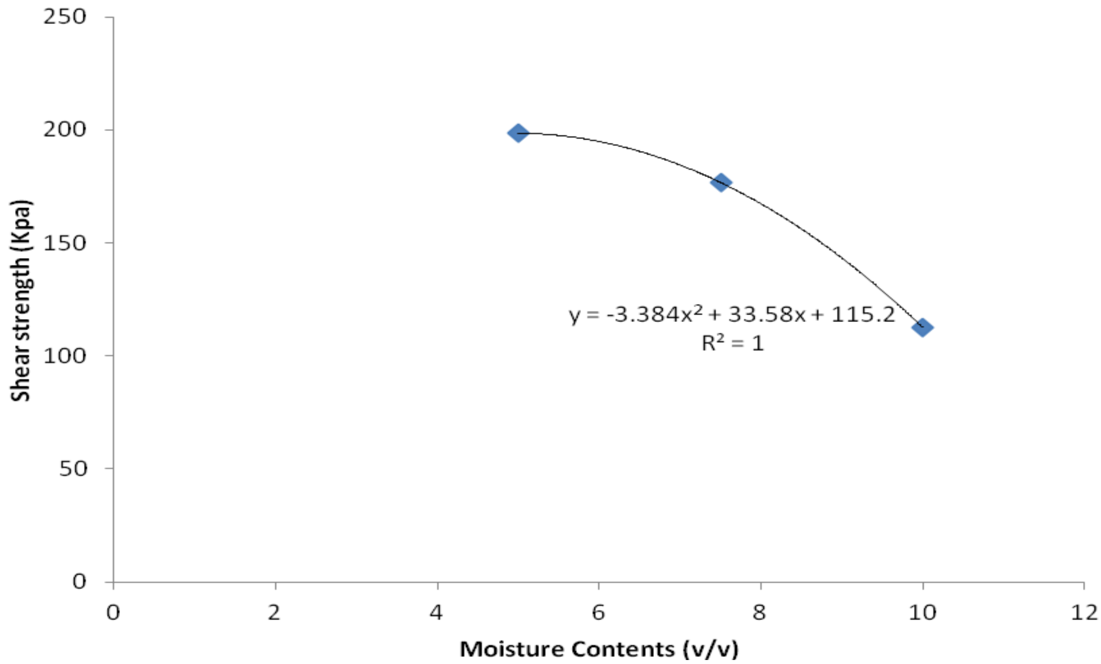

Figure 2: Graph of shear strength for disturbed Clay loam soil at 20 hammer blows

IV. CONCLUSION

From the results, it was observed that clay loam has more proportionate distribution of its particles compared to sandy loam and it had higher moisture characteristics (Atterberg limits and water holding capacities). But Sandy clay proved to have comparatively greater shear strength than the clay loam. Thus in practice, sandy clay would fit in for structural purposes more than clay loam and for agricultural purposes reverse would be the case. The study therefore recommends the consideration adequate modifications of the Clay loam soil when it is to be applied in structural and foundation purposes and suitable the adaptable crop and cropping practice must be employed when the sandy clay must support agriculture.

REFERENCECES

[1.] Junge, B., Dejib, O., Robert, A., Chikoye, D. and Stahr, K. Soil Conservation in Nigeria: Past and present on-station and on-farm initiatives. Soil and Water Conservation Society Ankeny, Iowa. 34p. 2008

[2.] Sridharan, A., Nagaraj, H. B. Plastic limit and compaction characteristics of fine-grained soils. Ground Improv. 9, 17–22, 2005

[3.] Owen, R.C. Soil strength and microclimate in the distribution of shallow landslides. Jl Hydrol (NZ) v 20 (1), 17-26, 1981

[4.] Ellis-Jones, J. and Tengberg, A the impact of indigenous soil and water conservation practices on soil productivity: examples from Kenya, Tanzania and Uganda. Land degradation & Dev. 11:19-36. 2000

[5.] McRae, J. L. Index of compaction characteristics. In: Symposium on application of soil testing in highway design and construction. ASTM Special Technical Publication 239, 119–127. 1958

[6.] Day, Robert W. Soil Testing Manual: Procedures, Classification Data, and Sampling Practices. New York: McGraw Hill, Inc. 293–312. 2001

[7.] Dayakar, P., Rongda, Z. Triaxial compression behavior of sand and gravel using artificial neural networks (ANN). *Comput Geotech*. 24, 207–230. 1999

Quality of Groundwater around Rewa-Gurh Region, Rewa District Madhya Pradesh India

[1]A.K. Singh, [2]P.K. Tiwari, [3]A.K. Tripathi and [4]U.K.Mishra*
[1]Department of Geology Govt. P.G. College Rewa 486001, Madhya Pradesh, India
[2] Geologist, Sharda Energy & Minerals Ltd.Raipur, 462051, CG, India
[3] Principal, Shriyut College Gangeo Rewa – 486111, Madhya Pradesh, India

ABSTRACT: *This paper provides a brief account of the quality of ground water around the Rewa-Gurh region. The principal geological formation of the study area is Ganurgarh shale, Bhander limestone and Upper Rewa sandstone belonging to Vindhyan Super group. A large area of Rewa city is occupied by Bhander limestone. The ground water of this region is affected by Carbonate (CO_3), and Bicarbonate (HCO_3), this is called temporary hardness. Somewhere 1 mm to 5 cm thick layer of gypsum ($CaSO_4.2H_2O$) is found which is not suitable for ground water. In study area this is big problem wherever the well are dug in shale. The Rewa-Gurh areas are also presently facing acute storage of water supply to fulfill the demand of people. So the area around Rewa-Gurh region has been selected for study pertaining to the nature of the ground water resources by carrying out sampling for assessment of its quality and the possible reasons for deterioration.*

Key words*: Quality, Groundwater Gurh, Rewa Madhya Pradesh*

I. INTRODUCTION:

The present investigation is to study the nature of ground water of the Rewa-Gurh area, which is located in Rewa district Madhya Pradesh. The study area located within the geographic co-ordinate of latitude 24^0 30' to 24^0 35' and longitude 81^0 20' to 81^0 30' falling in the Survey of India Toposheet No 63 H/6. Gurh situated on the south east part of the Rewa district. It is 23 km. from Rewa, the area reachable by bus and taxi. The principal villages of the study area are Lohi, Badagaon, Ramnai, Gurh, Raipur and Barahadi. The main road passing through the area is Varanasi-Kanyakumari National highway No 7 and Gwalior Ranchi National highway No 75. The Bichiya River is the main drainage of the study area, which is seasonal river. Except it there is no prominent river or drainage pattern. Upper Vindhyan rocks mainly cover the area they consist of mainly limestone, sandstone and shale(Singh Yamuna 1987).

II. HYDROLOGY

Water is next to air for the existence of life. Being vital, it figures in all phases of man's activity. Ground water one of the most precious and abundant natural resource, which controls the development of civilization on the globe. The water is indispensable for substance of life and also determines its quality. The demand of water for various uses such as drinking, irrigation, domestic and industrial purposes is increasing with time due to the increase of human population. According to (Chow 1964) the total quantity of fresh water is estimated at about $4.1x10^{16}$ m^3 (Piper A.M. 1953). Availability of safe water plays a vital role in national development. The quality of ground water is of equal importance as its quantity in ground water management (Todd 1980,Mishra et al 2013,Tiwari et al 2009).

The ground water quality data provide important clue to the geological history of rocks and indication of ground water recharge, discharge, movement and storage knowledge of water, quality is also essential for rational management of water and land resources (Karanth 1989,1994, Tiwari et al. 2010, Hem J.D. 1975, Singh Yamuna 1987, Singh et al 2002). The quality of ground water depends on physical and chemical composition of soil or rocks through which it passes.

III. MATERIAL AND METHOD

The representative water samples were collected from open dug well located in the area. The water samples were collected in polythene bottles and properly labeled. The necessary care has been taken for protection of sample and to bring them to laboratory at the earliest with a view to avoid the possible contamination.

The Physico-chemical parameters have been determined in selected ground water samples(Mishra et al 2013, Tiwari et al 2011). The determination of ionic concentration and various parameters have been employed for the estimation of quality of ground water. The physical parameters include temperature, pH, Specific conductance and Total dissolved solids, and the chemical parameters include Alkalinity, Hardness, Calcium, Magnesium Sodium, Chloride, and radiological degradation oh ground water samples of the study area, only physical and chemical parameter are evaluated(Raghunath H.M. 1987, Walton W.C. 1970). In the present work 15 water samples has been collected from the existing dug wells in and around Rewa-Gurh area. Hence, these samples subjected to chemical analysis with a view to delineate the quality of ground water and to assess its usage. The values of chemical and physical parameter are given in table no 1. Carbonate, Bicarbonates, Ammonia, Sulphates and Nitrate. Since there are no biological

IV. RESULT AND DISCUSSION

The analysis include the determination of the physical properties such as pH range from 6.90 to 8.44 with an average of7.65 which indicate that it is natural to alkaline in nature. Electrical conductivity of the collected water samples varies from 1050 to 2325 micro mho/cm with an average of 1741.6 micro mho/cm. In the study area the total dissolve solids vary from 700 mg/liter to 978 mg/liter. Higher values of the total dissolve solids affect biomass and the same is the case with industrial use. Low value of total dissolve solids indicates good surface drainage as it facilitates continuous leaching of salts.

The total alkalinity of the investigated area varies from 155 mg/liter to 290 mg/liter, with an average of 227.1 mg/liter. In the study area total hardness varies from 175 mg/liter to 325 mg/liter. The concentration of Calcium in ground water samples of investigated area varies from 62 mg/liter to 88 mg/liter with an average of 74.6 mg/liter. The range of Calcium content in ground water largely depends on the solubility of Calcium carbonates, Sulphide and very rarely Chloride. Magnesium is also one of the alkaline earth metals and Magnesium also occurs in all kind of water with Calcium. The concentration of Magnesium in water samples of the study area varies from 22mg/liter to 35mg/liter with an average of 27.9mg/liter.

Table 1.1 Physical and chemical parameters of ground water of Rewa-Gurh region

Well No.	Location	Sodium	Magnesium	Potassium	Calcium	Chloride	Carbonate	Bi-carbonate	Sulphate
1	**2**	**3**	**4**	**5**	**6**	**7**	**8**	**9**	**10**
1	Lohi	0.52	1.8	0.30	3.39	0.26	0.33	4.18	0.24
2	Khamha	0.60	2.3	0.41	3.94	0.25	0.39	4.36	0.31
3	Khajuhakala	0.56	2.79	0.38	3.79	0.21	0.33	4.62	0.20
4	Badagaon	0.47	2.46	0.46	4.39	0.15	0.39	5.57	0.201
5	Bhiti	0.53	2.63	0.41	25.99	0.09	0.53	4.01	0.15
6	Gurh	0.58	2.22	0.31	3.69	0.27	0.93	4.19	0.17
7	Chandehri	0.61	1.97	0.43	3.09	0.16	0.37	3.69	0.09
8	Barahadi	0.65	1.64	0.41	3.19	0.19	0.91	4.01	0.27
9	Barehi	0.50	2.79	0.66	3.34	0.22	0.71	4.38	0.20
10	Raipur	0.49	2.13	0.71	3.24	0.32	0.57	3.90	0.16
11	Khajuha khurd	0.57	2.22	0.43	3.89	0.25	0.30	3.77	0.18
12	Ramnai	0.69	1.89	0.56	3.74	0.27	0.63	3.93	0.20
13	Naurhiya	0.53	2.30	0.46	4.84	0.22	0.43	4.67	0.20
14	Ratahara	0.57	2.38	0.69	4.39	0.24	0.50	5.247	0.23
15	Sonaura	0.62	2.87	0.38	3.94	0.25	0.56	5.11	0.25

Table 1.2 Common anions and cations content of ground water of Rewa-Gurh region
(Value in epm)

Well No.	Location	Temp.	pH	EC (µ S/cm)	TDS (ppm)	Total alkalinity (ppm)	Total hardness (ppm)
1	**2**	**3**	**4**	**5**	**6**	**7**	**8**
1	Lohi	28	7.45	1065	700	220	190
2	Khamha	30	7.86	1050	890	212	212
3	Khajuhakala	31.3	7.71	1235	875	175	277
4	Badagaon	29.5	8.20	1345	923	182	325
5	Bhiti	29.8	6.90	1800	900	200	240
6	Gurh	29	7.50	2100	850	155	190
7	Chandehri	31.5	8.44	2025	863	225	232
8	Barahadi	32	8.05	2325	925	252	247
9	Barehi	31.3	7.56	1775	876	242	175
10	Raipur	29.8	7.05	1925	935	276	255
11	Khajuha khurd	31	7.09	1655	804	238	195
12	Ramnai	32.3	8.05	1845	925	235	272
13	Naurhiya	30.5	7.70	1936	900	245	300
14	Ratahara	29.3	7.80	2005	978	290	246
15	Sonaura	28.5	7.5	2035	850	260	270

In the study area content of Sodium in samples varies from 11mg/liter to 14.4 mg/liter with an average of 13.26 mg/liter. According to National Academy of Sciences (1977), the higher concentration of Sodium can be related to *Cardiovascular diseases*, and to *Toxemia* associated with pregnancy in women. The concentration of Potassium in ground water samples of the study area varies from 12 mg/liter to 28 mg/liter with an average of 18.3 mg/liter.

In the ground water of the Rewa-Gurh area the concentration range of the Carbonate is 10 mg/liter to 28 mg/liter, with an average of 18.3 mg/liter and Carbonate concentration range from 225 mg/liter to 340 mg/liter, with an average of 267.06 mg/liter. The concentration of Sulphate in water samples of the study area ranges from 9.7 mg/liter to 15 mg/liter, with an average of 10.2 mg/liter. Chloride concentration of the water samples range from 3.2 mg/liter to 11.5 mg/liter with an average of 8.02 mg/lit. Water is required for drinking purposes, must be tasteless and odourless. The ISI has laid down its national standards. The permissible limits of various minerals for domestic purposes are given below in table No. 1.3.

Table 1.3 Indian Drinking Water Quality Standard {Source: ISI (1983)}

Parameter	Highest desirable limit, mg/l	Maximum permissible limit, mg/l	Undesirable effect outside the desirable limit	Average value of the analysed water samples
PH	6.5-8.5	9.2	Effect of mucous membrane	7.65
TDS	500	800	Gastro intestinal disorder	879.6
Hardness	300	600	Encrustation effect domestic use	241.13
Calcium	75	200	Encrustation effect domestic use	74.6
Magnesium	30	100	Encrustation effect domestic use	27.9
Chloride	250	1000	Taste,corrosion, Palatability decrease	8.02
Sulphate	150	400	Gastro intestinal irritation	10.02
Nitrates	45	No relax	Methnamoglobinemia	--------
Fluoride	0.6	1.2	Flourosis	--------

When these water standards are not fully ensured, the water may not be 100% fit for drinking and may be termed as contaminated. It may some times causes numerous waterborne diseases such as typhoid fever, dysentery, gastroenteritis, infectious hepatitis, and jaundice etc. depending upon the type and extent of contamination.

Piper's tri linear diagram is used for the chemical analysis of the data. This method forms a base for the classification scheme of natural water for drinking purposes. With the help of diagram the quality of ground water is easily comparable. From the piper diagram the study area shows three type of ground water hardness, namely

(a) $Ca\text{-}Mg\text{-}HCO_3$
(b) $Na\text{-}HCO_3$
(c) $Ca\text{-}Mg\ (Na)\text{-}SO_4$

In the area under investigation, the water has both types of hardness temporary and permanent hardness, it can be used after boiling and some chemical treatment.

Table 1.4 Ion ratio considered in judging the quality of ground water

Well No	S.A.R.	Na %	Na/(Na+Ca) in epm	$Cl/(Cl+HCO^3)$ in epm
1	0.48	17.31	0.18	0.36
2	0.64	19.78	0.22	0.32
3	0.52	16.90	0.20	0.32
4	0.63	19.24	0.21	0.25
5	0.59	20.03	0.25	0.33
6	0.53	17.10	0.19	0.30
7	0.76	24.59	0.28	0.40
8	0.41	17.99	0.16	0.39
9	0.57	21.33	0.2	0.34
10	0.63	24.64	0.24	0.38
11	0.64	20.38	0.22	0.36
12	0.51	20.27	0.18	0.34
13	0.64	19.02	0.20	0.33
14	0.49	19.13	0.17	0.34
15	0.68	19.43	0.24	0.33

Table1.5 Common anions content of ground water of Rewa-Gurh region

WellNo	Sodium			Magnesium			Potassium			Calcium		
	ppm	epm	%epm	ppm	epm	%epm	ppm	epm	%epm	ppm	Epm	%epm
1	12	0.52	8.65	22	1.8	28.75	12	0.30	4.87	68	3.39	53.92
2	14	0.60	8.38	28	2.3	29.58	16	0.41	5.25	79	3.94	50.63
3	13	0.56	7.50	34	2.79	35.27	15	0.38	4.84	76	3.79	47.82
4	11	0.47	6.13	30	2.46	29.05	18	0.46	5.42	88	4.39	51.69
5	12.4	0.53	8.20	32	2.63	37.41	16	0.41	5.81	60	25.99	42.55
6	13.5	0.58	8.62	27	2.22	31.13	12	0.31	4.30	74	3.69	51.76
7	14.2	0.61	10.09	24	1.97	29.37	17	0.43	6.47	62	3.09	46.03
8	15	0.65	11.05	20	1.64	27.88	16	0.41	6.93	64	3.19	54.12
9	11.6	0.50	6.90	34	2.79	35.83	26	0.66	8.52	67	3.34	42.83
10	11.4	0.49	7.52	26	2.13	29.94	28	0.71	10.02	65	3.24	45.41
11	13.3	0.57	8.11	27	2.22	28.92	17	0.43	5.66	78	3.89	50.68
12	16	0.69	10.0	23	1.89	26.77	22	0.56	7.96	75	3.74	52.95
13	12.4	0.53	6.62	28	2.30	26.1	18	0.46	5.21	97	4.84	54.86
14	13.3	0.57	7.19	29	2.38	28.46	27	0.69	8.23	88	4.39	52.39
15	14.4	0.62	7.99	35	2.87	34.00	15	0.38	4.53	79	3.94	46.56

Table 1.6Common anions content of ground water of Rewa-Gurh region

WellNo	Chloride			Carbonate			Bi-carbonate			Sulphate		
	ppm	epm	%epm	ppm	epm	%epm	ppm	epm	%epm	ppm	Epm	%epm
1	9.5	0.26	5.32	10	0.33	3.98	255	4.18	58.36	12	0.24	3.48
2	8.9	0.25	4.71	12	0.39	4.76	266	4.36	60.41	15	0.31	4.32
3	7.5	0.21	3.93	10	0.33	3.75	282	4.62	62.28	10	0.20	2.80
4	5.4	0.15	2.40	12	0.39	4.38	340	5.57	68.85	9.7	0.201	2.49
5	3.2	0.09	1.88	16	0.53	6.40	245	4.01	59.64	12	0.15	2.25
6	9.6	0.27	4.85	28	0.93	10.51	256	4.19	58.78	15	0.17	2.45
7	5.9	0.16	3.85	11	0.37	4.40	225	3.69	55.58	10	0.09	1.47
8	6.9	0.19	3.54	30	0.91	10.70	245	4.01	50.89	9.7	0.27	3.53
9	7.8	0.22	3.92	24	0.71	8.83	267	4.38	57.30	12	0.20	2.67
10	11.5	0.32	6.54	17	0.57	6.81	238	3.90	55.06	15	0.16	2.29
11	8.9	0.25	5.45	12	0.30	5.02	230	3.77	57.50	10	0.18	2.82
12	9.6	0.27	5.37	19	0.63	6.10	240	3.93	57.59	9.7	0.20	2.98
13	7.8	0.22	3.97	13	0.43	4.64	285	4.67	60.58	12	0.20	2.70
14	8.7	0.24	3.94	15	0.50	4.55	320	5.247	60.17	15	0.23	2.69
15	9.1	0.25	4.14	17	0.56	4.92	312	5.11	60.13	10	0.25	3.01

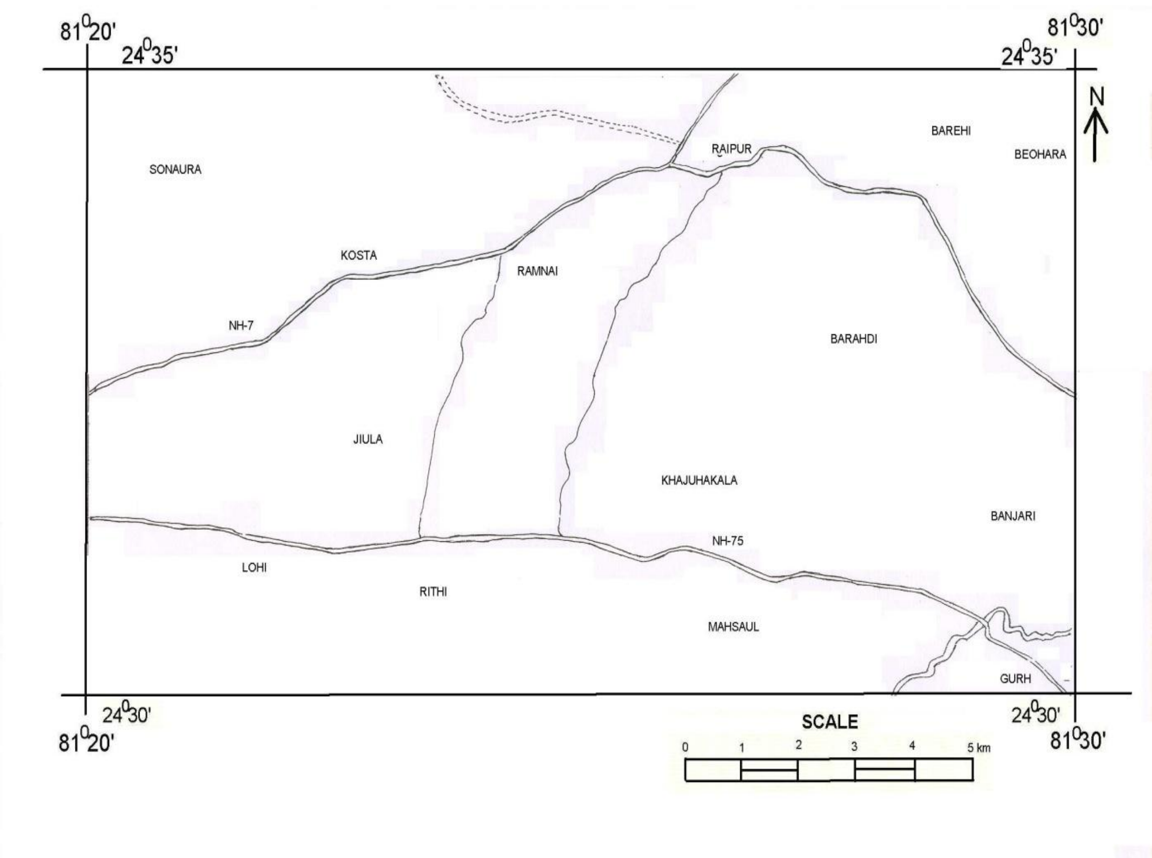

Fig. 1 Location map of the study area

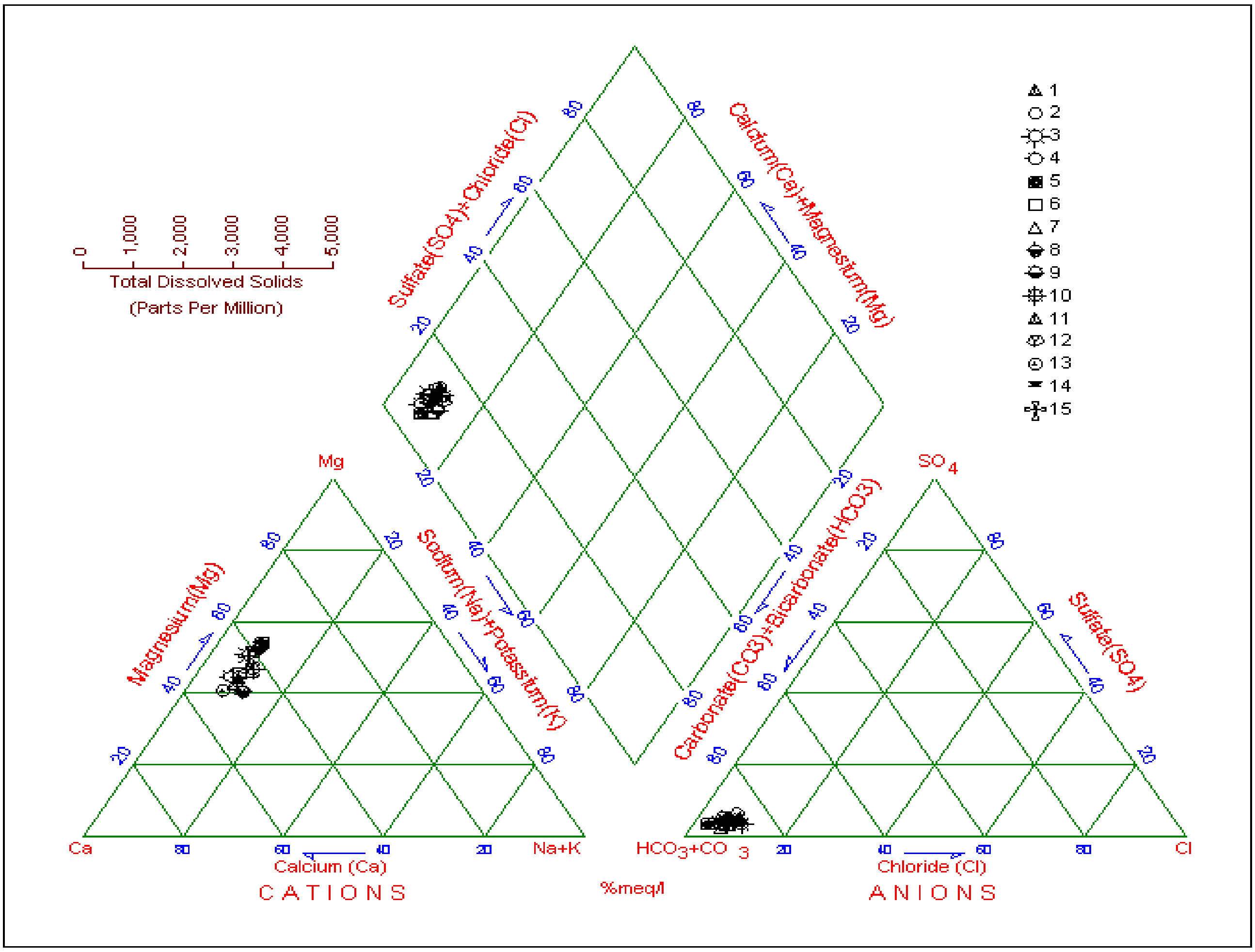

Fig. 2 Trilinear Piper diagram

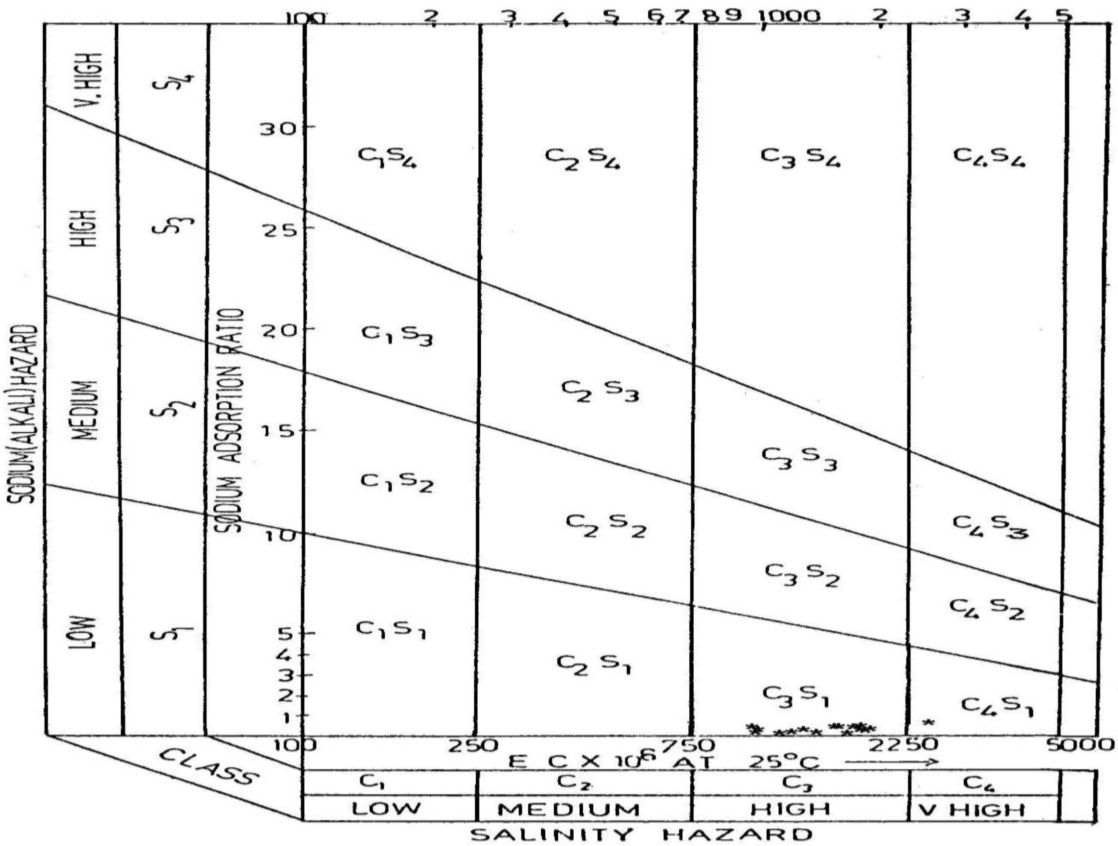

Fig. 3 Data plotted in the U.S. salinity diagram (Richards, 1954)

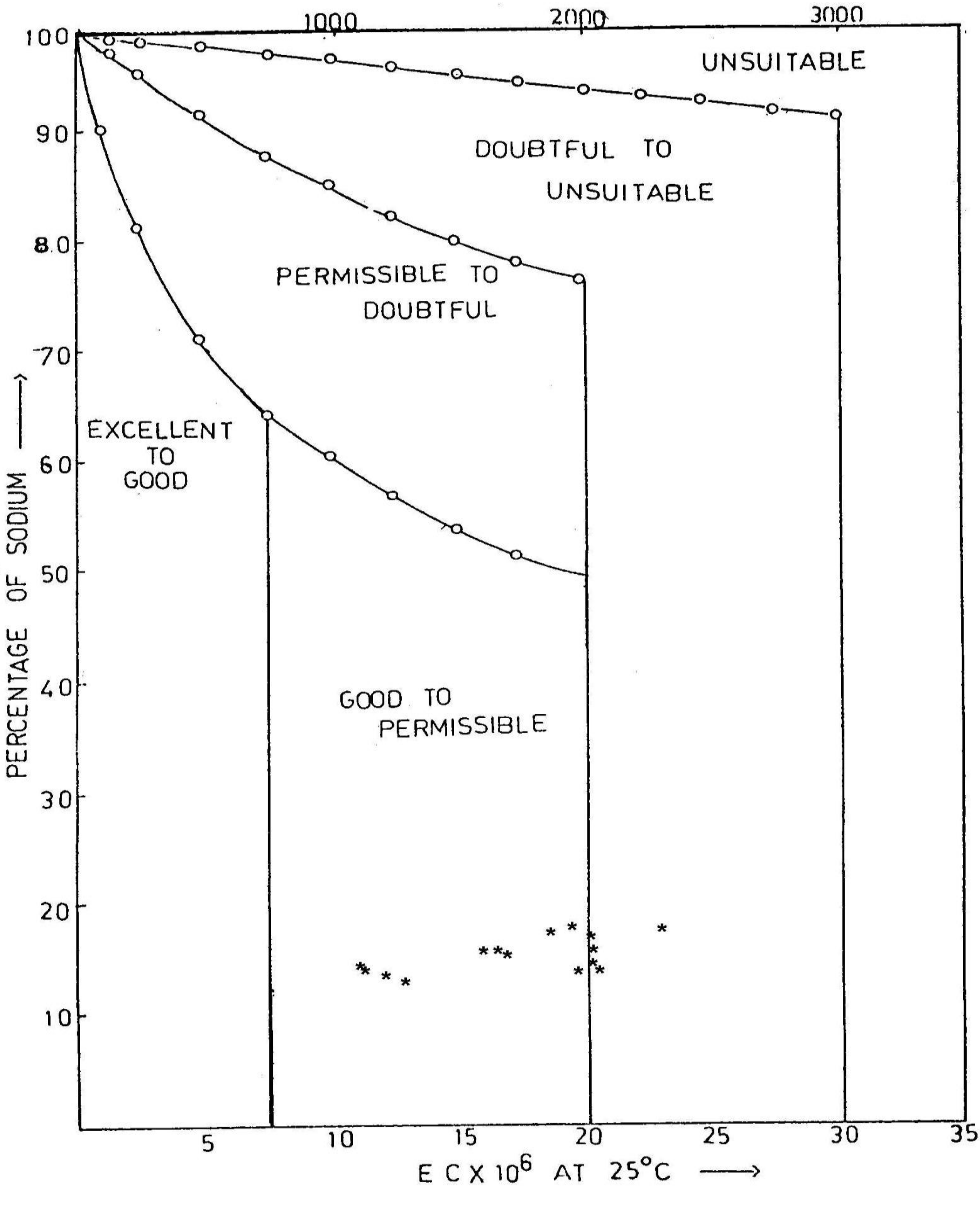

Fig. 4 Data plotted on the diagram (Wilcox, 1955) of Na % against EC values.

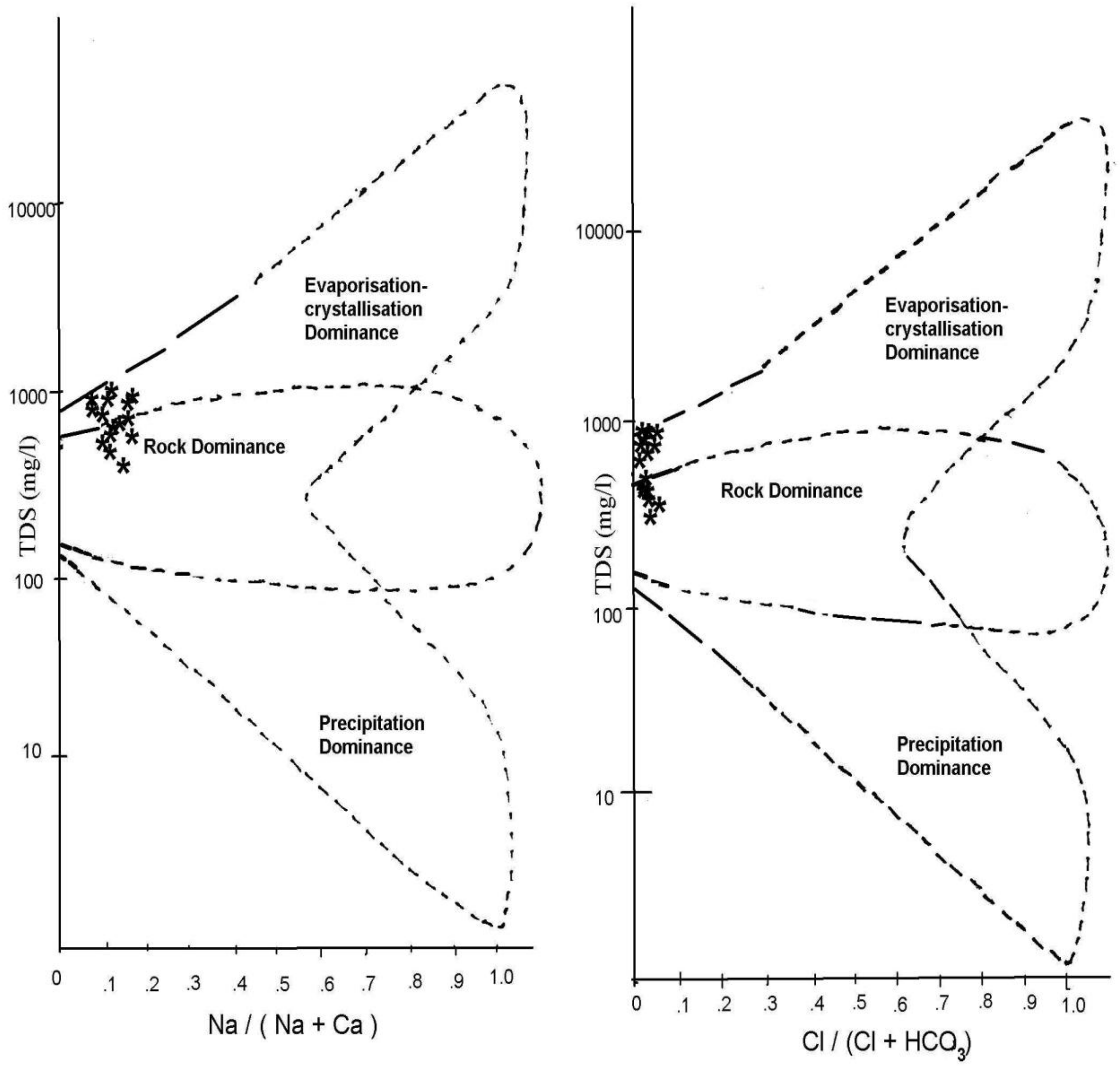

Fig.5 Plotting of chemical data in Gibbs (1950) diagram

REFERENCES

[1.] A.P.H.A. (1985). Standard methods for the examination of water and waste water (14th edn.) Washington D.C., American Public Health Association. pp.06-187.
[2.] Garg, Santosh Kumar: Water Resources and Hydrology, 3rd Edn., pp. 426-441.
[3.] Gibbs, R.J. (1970). Mechanics controlling world's water chemistry, Science,v.170, pp.10-1910.
[4.] Ghandour, E. F. M., Kalidas, J. B. and Atta S. A. (1985): Distribution of CO3 HCO3, and pH, value in ground water , pp35-41.
[5.] Hem. J. D. (1975). Study and interpretation of chemical characteristics of natural water, 3rd
[6.] Edn. U.S. G. S., Water supply paper, pp. 364. S. I. (Indian statistical institute) (1983). Indian standard specification for drinking water.
[7.] Karanth K.R. (1989). Groundwater assessment development and management. Tata Mc- Graw Hill. Pub. House Allahabad.
[8.] Mishra S.K., Mishra U.K.,Tripathi A.K.,Singh A.K. and Mishra A.K.(2013). Hydrogeochemical study in Groundwater quality in and around Sajjanpur area, Satna District M.P.(IJSER)v.8 No.2pp.1-10.
[9.] Mishra U.K.,Tripathi A.K., Mishra Ajay, Mishra S.K. and Dwivedi Rashmi(2013). Assessment of physico-chmical parameterd of Limestone mineral water near J.P. cement plant Rewa District M.P. (IJESI) v.2 No.7 pp58-68.
[10.] Mishra, U.K. (2010). Hydrogeological Studies of Sirmour area, Rewa District, Madhya Pradesh.Unpubl. Ph.D. Thesis, A.P.S. Univ. Rewa, M.P., 173p.
[11.] Piper, A.M. (1953). A graphic procedure in the Geochemical Interpretation of Water Analysis. U.S.G.S. Ground Water. Note 12.
[12.] Radhakrishnan, T.S. (1971). Groundwater investigation for rural water supply in selected
[13.] Villages of Satna and Rewa districts, M.P. Unpublished report G.S.I.
[14.] Raghunath, H.M. (1987). Ground water Wiley Eastern Ltd. New Delhi, *pp.59.*

[15.] Schumm,S.A. (1963). Sinuosity of alluvial river on the Grent plains, Bull. Geol. Soc. Amer., v.74,pp. 1089-1100.
[16.] Singh, Yamuna (1987). Geology and Ground water resources of the south-western region of Rewa district, M.P. Unpublished Ph. D. thesis, Nagpur University
[17.] Singh, Y., Dubey, D.P. and Saxena, V.K. (2002). Assessment of drinking and industrial utility of groundwater of the Rewa region, Central India. Proc. Industrial Conf. Hydrology and Watershed Management, Vol. I, Hyderabad, A.P., India. pp. 629-637.
[18.] Tiwari, R.N. and Dubey, D.P. (2007). Petrography, diagenesis and depositional environments of Govindgarh Sandstone of Rewa Group, Vindhyan Supergroup, Madhya Pradesh. Gond. Geol. Magz. v.22 (2) pp. 11-16.
[19.] Tiwari, R.N., Dubey, D.P. and Bharti, S.L. (2009). Hydrogeochemistry and groundwater quality in Beehar River Basin, Rewa district, Madhya Pradesh, India. Inter. Jour. Earth Eng. Sci., v.2 (4), pp. 324-330.
[20.] Tiwari, R.N., Bharti, S.L., Mishra, Umesh (2010). Hydrogeochemical Studies of Groundwater from Odda River Basin, Rewa District, Madhya Pradesh, Gondwana Geological Magazine, Special v. No. 12, pp.85-93.
[21.] Tiwari, R.N. (2011). Morphometric Analysis of Sirmour Area, Rewa District, Madhya Pradesh using Remote Sensing and GIS. Intnational Jour of eart Sciences and Engineering v.4 N.3 pp.512-521.
[22.] Tiwari, R.N. (2011). Assessment of groundwater quality and pollution potential of Jawa BlockRewa District, Madhya Pradesh, India Proceedings of the International Academy of Ecology and Environmental Sciences, 2011, 1(3-4):202-212
[23.] U.S. Salinity Laboratory Staff (1954). Diagnosis and Improvement of Saline and Alkali Soils. U.S. Deptt. Agriculture, Handbook, 160 p.
[24.] Walton,W.C. (1970). Groundwater resources evaluation. Mc-Graw Hill Book Company, New York, 664p.
[25.] WHO (1984). Guidelines to Drinking water quality. World Organisation Geneva, 186p.
[26.] Wilcox, L.V. (1955). Classification and use of irrigation waters, U.S. Deptt. of Agriculture cire. 969, Washington, D.C., pp.19.

International Journal of Modern Engineering Research (IJMER)
www.ijmer.com Vol. 3, Issue. 5, Sep - Oct. 2013 pp-3293-3295 ISSN: 2249-6645

An Eavesdropping Model for Securing Communications over Wireless Broadcast Networks

G. Vidya Sagar[1], Syed Gulam Gouse[2]
[1]M.Tech, Nimra College of Engineering & Technology, Vijayawada, A.P, India.
[2]Professor, Dept.of CSE, Nimra College of Engineering & Technology, Vijayawada, A.P., India.

ABSTRACT: *Wireless broadcast networks constitute one class of basic and important wireless networks, in which a source node simultaneously transmits a number of information messages to different destinations. However, broadcast communications make use of the open nature of the wireless medium, which presents a great challenge to achieve the secure communication for individual users. This is because information for all users is contained in one transmitted signal, and hence information destined for one user may be obtained by non- intended users unless special coding is used. In this paper, we study a broadcast network, in which a source node transmits confidential message flows to the user nodes, and each message flow is intended to be decoded accurately by one node while being kept secret from all other nodes. Nodes are thus considered to be eavesdroppers with regard to all other messages but their own. Here we consider two eavesdropping models. The first model is referred to as a collaborative eavesdropping model, in which the eavesdroppers can exchange their outputs to interpret the message. The second model is referred to as a non- collaborative eavesdropping model, in which eavesdroppers do not exchange their outputs.*

Keywords: *Broadcasting, Eavesdropping, Wireless network.*

I. INTRODUCTION

Network-wide broadcasting is a fundamental operation in wireless networks. The goal of broadcasting is to transmit a message from a source to all the other nodes in the network. Several network protocols rely on broadcasting, for example, information dissemination, service/resource discovery, or routing in multihop wireless networks. Given that key applications of multihop wireless networks include disaster relief and rescue operations, military communication, and prompt object detection using sensors, the design of low-latency broadcasting scheme is essential to meeting stringent end-to-end delay requirements for higher-level applications. Interference is a fundamental limiting factor in wireless networks. When two or more nodes transmit a message to a common neighbor at the same time, the common node will not receive any of these messages. In such a case, we say that collision has occurred at the common node. Any communication protocol for wireless networks should contend with the issue of interference in the wireless medium.

One of the earliest broadcast mechanisms proposed in the literature is flooding [1] [2], where every node in the network transmits a message to its neighbors after receiving it. Although flooding is extremely simple and easy to implement,

Ni et al. [3] show that flooding can be very costly and can lead to serious redundancy, bandwidth contention, and collision: a situation known as broadcast storm. Since then, a large amount of research has been directed towards designing broadcast protocols which are collision-free and which reduce redundancy by reducing the number of transmissions.

II. RELATED WORK

Wireless broadcast networks constitute one class of basic and important wireless networks, in which a source node simultaneously transmits a number of information communications make use of the open nature of the wireless medium, which presents a great challenge to achieve secure communication for individual users. This is because information for all users is contained in one transmitted signal, and hence information destined for one user may be obtained by no intended users unless special coding is used. Physical layer security, which uses randomness of a physical communication channel to provide security for messages transmitted through the channel, opens a promising new direction toward solving wireless networking security problems. This approach was pioneered by Wyner in [4] and by Csiszár and Körner in [5], and more recently has been extensively explored in the literature[6].

Physical layer security adopts a precise quantitative measure of security level, i.e., the equivocation rate defined by Shannon [7], which equals the entropy rate of the source message conditioned on the channel output at the eavesdropper. This measure of the secrecy level allows security to be considered under the general Shannon framework of information theory [8], and hence provides an analytical basis with which to characterize the fundamental limits on communication rates given the security level constraints. This measure of security level also makes a unified security design across networking layers possible. The goal of such a design is to maximize network utility (i.e., to maximize overall users' satisfaction of the service rate in a certain fair manner among users) under security, reliability, and stability constraints. This motivates a joint design of rate control at the transport layer, rate scheduling at the medium access control layer, and power control and secure coding at the physical layer.

To achieve reliable and secure communication for users, we adopt the physical layer security approach [4], [5] to employ a stochastic encoder at the source node. The source node allocates its power not only among message flows (i.e., among users) but also dynamically according to the channel state information to improve secrecy communication rates. Hence the source power control operates over the symbol time scale, and determines the service rate allocation among users at the packet time level. At the packet time level, to maintain the stability of all queues, the source node implements a rate schedule scheme that adapts its service rate allocation dynamically among users based on the queue lengths. Furthermore, rate control is performed also at the packet time level to maximize the network utility function. Our goal is to study how to jointly design rate control and rate scheduling at the packet time scale and power control and secure coding at the symbol time scale to achieve network utility maximization under reliability, security and stability constraints.

III. COLLABORATIVE EAVESDROPPING MODEL

For the collaborative eaves dropping model, we first obtain the secrecy capacity region, within which each rate vector can be achieved by a time-division scheme, i.e., at each channel state, the source transmits only to the user whose channel gain is better than the sum of the channel gains of all other users. It is clear that this user must have the best channel gain at this state. The power control among the channel states thus determines the rate allocation among users, i.e., rate allocation among components of a rate vector. We further show that all arrival rate vectors contained in this region can be stabilized by a throughput optimal queue-length-based scheduling scheme at the packet time level, where queue length determines the service rate allocation among users, and hence determines the corresponding power control to achieve this service rate vector at the symbol time level [9]. Finally, we obtain a distributed rate control policy that Maximizes the overall network utility maximization given that reliability, secrecy, and stability are achieved. This maximization is achieved by joint design of rate control, rate scheduling, power control, and secure coding.

For a given channel state h=(h1,h2,……hk), let p(h) denote the source power allocation for state h. We use p to denote the set that includes all power allocation functions (i.e., power control policies) that satisfy the power constraints, i.e.,

$$\mathcal{P} = \{p(\underline{h}) : E[p(\underline{h})] \leq P\}.$$

Now let Ai be the set of all channel states for which the channel gain of user is larger than the sum of the channel gains of all other users, i.e.,

$$\mathcal{A}_i = \left\{ \underline{h} : |h_i|^2 \geq \sum_{j \neq i, 1 \leq j \leq K} |h_j|^2 \right\}$$

For the collaborative eavesdropping model, the secrecy capacity region of the fading broadcast network is given by

$$\mathcal{C}_s = \bigcup_{p(\underline{h}) \in \mathcal{P}} \left\{ \begin{array}{l} (R_1, \ldots, R_K) : \\ R_i \leq E_{\underline{h} \in A_i} \Big[\log(1 + p(\underline{h})|h_i|^2) \\ \qquad\qquad - \log\Big(1 + p(\underline{h}) \sum_{j \neq i, 1 \leq j \leq K} |h_j|^2\Big)\Big] \\ \text{for } 1 \leq i \leq K \end{array} \right\}$$

The secrecy capacity region given in above includes all achievable secrecy rate vectors with each component representing the service rate for one user. It still remains to determine a rate scheduling algorithm to choose a service rate vector at each packet time slot to stabilize all queues and correspondingly to determine a power control policy over the symbol time slots to achieve this service rate vector.

IV. NON- COLLABORATIVE EAVESDROPPING MODEL

For the non collaborative eavesdropping model, we study a time-division scheme, in which the source transmits to one user in each channel state. The secrecy rate region based on this scheme is derived. Although the time-division scheme is suboptimal, it is simple and important from a practical point of view. We also provide and discuss improved secure coding schemes based on non-time-division schemes. Based on a simple achievable secrecy rate region, a queue-length-based rate scheduling algorithm is derived that stabilizes the arrival rate vectors contained in this rate region.
For a given channel allocation scheme A(h), we consider the set of states for transmitting to user , i.e.,

$$\{\underline{h} : A(\underline{h}) = i\}.$$

The channel states in this set may not necessarily satisfy the condition that user i has the best channel state among all users.
The channel corresponding to these states can be viewed as parallel channels to every user with each subchannel corresponding to one state realization h.

Applying this scheme, an achievable rate for user can be obtained and is given by

$$R_i = \min_{j \neq i} E_{\underline{h}:A(\underline{h})=i} \left[\log\left(1 + p(\underline{h})|h_i|^2\right) - \log\left(1 + p(\underline{h})|h_j|^2\right) \right]^+$$

we can obtain the achievable secrecy rates for other users, and hence these rates constitute a rate vector achieved for a given power control scheme and a channel allocation scheme p(h) . An achievable secrecy rate region for the broadcast channel includes achievable secrecy rates obtained for any power control scheme and any possible state allocation scheme A(h).

For the noncollaborative eavesdropping model, an achievable secrecy rate region for the fading broadcast channel is given by

$$\mathcal{R}_s = \bigcup_{p(\underline{h}) \in \mathcal{P}, A(\underline{h}) \in \mathcal{A}} \left\{ \begin{array}{l} (R_1, \ldots, R_K) : \\ R_i = \min_{j \neq i} E_{\underline{h}:D(\underline{h})=i} \left[\log\left(1 + p(\underline{h})|h_i|^2\right) \right. \\ \qquad \left. - \log\left(1 + p(\underline{h})|h_j|^2\right) \right]^+ \\ \text{for } 1 \leq i \leq K \end{array} \right\}$$

where the random vector h=(h1,h2,….hk) has the same distribution as the marginal distribution of the random process {hn} at one symbol time instant.

V. CONCLUSION

Wireless telecommunications is the transfer of information between two or more points that are not physically connected. Distances can be short, such as a few meters for television remote control, or as far as thousands or even millions of kilometers for deep-space radio communications. For a collaborative eavesdropping model, in which the eavesdroppers exchange their outputs, the secrecy capacity region is obtained, within which each rate vector is achieved by using a time-division scheme and a source power control policy over channel states. A throughput optimal queue-length-based rate scheduling algorithm is further derived that stabilizes all arrival rate vectors contained in the secrecy capacity region. For a non collaborative eavesdropping model, in which eavesdroppers do not exchange their outputs, an achievable secrecy rate region is derived based on a time-division scheme, and the queue-length-based rate scheduling algorithm and the corresponding power control policy are obtained that stabilize all arrival rate vectors in this region.

REFERENCES

[1] C. Ho, K. Obraczka, G. Tsudik, and K. Viswanath, "Flooding for reliable multicast in multi-hop ad hoc networks," in Proc. of the Int. Work. On Disc. Alg. and Meth. for Mobile Comp. and Comm., 1999, pp. 64–71.
[2] J. Jetcheva, Y. Hu, D. Maltz, and D. Johnson, "A simple protocol for multicast and broadcast in mobile ad hoc networks," July 2001.
[3] S.-Y. Ni, Y.-C. Tseng, Y.-S. Chen, and J.-P. Sheu, "The broadcast storm problem in a mobile ad hoc network," in Proc. of the 5th Ann. ACM/IEEE Int. Conf. on Mobile Comp. and Net., 1999, pp. 151–162.
[4] M. Neely, E. Modiano, and C. Li, "Fairness and optimal stochastic control for heterogeneous networks," in Proc. IEEE INFOCOM, Miami, FL, Mar. 2005, vol. 3, pp. 1723–1734.
[5] A. Stolyar, "Maximizing queueing network utility subject to stability: Greedy primal-dual algorithm," Queueing Syst., vol. 50, no. 4, pp. 401–457, Aug. 2005.
[6] A. Eryilmaz and R. Srikant, "Joint congestion control, routing and MAC for stability and fairness in wireless networks," IEEE J. Sel. Areas Commun., vol. 24, no. 8, pp. 1514–1524, Aug. 2006.
[7] M. Bloch, J. Barros, M. R. D. Rodrigues, and S. W. McLaughlin, "Wireless information-theoretic security," IEEE Trans. Inf. Theory, vol. 54, no. 6, pp. 2515–2534, Jun. 2008.
[8] E. Ekrem and S. Ulukus, "Degraded compound multi-receiver wiretap channels," IEEE Trans. Inf. Theory, 2009, submitted for publication.
[9] P. Gopala, L. Lai, and H. E. Gamal, "On the secrecy capacity of fading channels," IEEE Trans. Inf. Theory, vol. 54, no. 10, pp. 4687–4698, Oct. 2008.

International Journal of Modern Engineering Research (IJMER)
www.ijmer.com Vol. 3, Issue. 5, Sep - Oct. 2013 pp-3296-3299 ISSN: 2249-6645

Review paper on "Various aspects of Weeders for Economical Cultivation"

Mr.Vivek D. Raut[1], Prof.B.D.Deshmukh[2], Prof. Dinesh Dekate[3]
[1, 3](Department of Mechanical Engineering, DMIETR Sawangi (M), Wardha RTMNU, Nagpur, India)
[2] (Department of Mechanical Engineering, YCCE Nagpur, RTMNU, Nagpur India)

ABSTRACT : *In Indian agriculture, it's a very difficult task to weed out unwanted plants manually as well as using bullock operated equipments which may further lead to damage of main crops. More than 33 percent of the cost incurred in cultivation is diverted to weeding operations there by reducing the profit share of farmers. This review paper is a small work towards analyzing weeding-cum-earthingup equipment aspects for economical cultivation which will help to minimize the working fatigue and to reduce labour cost.*

Keywords*: Cultivation, drafts, weeders, weeding aspects, weeding methods and materials.*

I. INTRODUCTION

The 33 percent cost of cultivation is spent on weeding alone when carried out with the manual labor. The complicated operation of weeding is usually performed manually with the use of traditional hand tools in upright bending posture, inducing back pain for majority of laborers.

In India, farmers mainly follow the hand weeding though chemical weeding is slowly becoming popular, in spite of it being costly. Use of herbicides will have residual affect and change in the quality of soil. Flaming produces intensive heat and more expensive equipment is needed. Hand weeding requires more labor, consumes more time leading to higher cost of weeding. An estimate of 400-600 man hours per hectare is the normal man-hour requirement of hand weeding which amounts to Rs.2200 per hectare, which also depends upon weed infestation. Availability of labor is also a main issue. Among all the weeders, the animal drawn blade hoe recorded maximum values of average actual field capacity and minimum number of man-hrs requirement while the maximum value of weeding index and man-hrs requirement were observed for weeding operation by hand khurpi.

II. CHALLENGES IN WEEDING OPERATIONS

Weeds are mostly removed from the field in a manual process as they are seen more as a negative factor for crop growth. The various aspects of weeding equipments consists of ergonomical considerations, it's easy working and easy handling by unskilled farmers, less damaging nature to crops, the distance between two crop rows, maximum efficiency, its important components like blades, critical design areas and the most important from all above is its cost of purchase. Every equipment which is used for weeding like hand khurpi, animal drawn blade hoe, power weeder, single-multiple row weeders etc are certainly possessing some inherent drawbacks which results in unnecessary time consumption, extra labour cost, more power requirement (manually as well as mechanically). Weeding was considered a major constraint in crop production. Most farmers experienced a serious labour bottleneck at weeding time. Extension workers considered that competition from weeds led to major losses and they estimated the yield reduction was over 10%.

Some issues which were identified in weeding operations/weeders are:
1. Should have some arrangement to avoid mud stucking in between the teeth/blades, tyres, wheels,
2. Needs to have built-in adjustability to change the width of working,
3. Need of safeguarding the operator,
4. Should be simple in design so that it can be easily built with less weight
5. Should be made all weather-proof and durable, and
6. sold at cheapest price

III. DISCUSSIONS

To ensure a high-quality equipment or easy weeding operations, we need to give more stress on working posture of labour (different ergonomical constraints for male and female labour), A motorized version should be developed to lessen fatigue/workload on the operator, more concentration should be on vibration constraint when we implement engine to the equipment because it leads to reducing stability. Petrol engine is having more vibration problem as compared to diesel engine, Lack of proper understanding among farmers on the intricacies of weed management, some research studies have amply demonstrated that there is positive correlation between weeder use and crop yields.

In the experiments conducted during 2001 – 2002, Senthilkumar (2003) compared the use of rotary weeder (five times with ten days interval from 20 days after transplanting till booting stage) with the conventional hand weeding (three times) for wet season and chemical weeding and two times hand weeding for dry season. Animal-drawn weeders work between crop rows; weeds left within the rows may be removed manually. The straight blades of traditional hoes can remove weeds within the working width of the blades, but straight blades tend to become clogged with soil and weed debris, which reduces their efficiency. There is therefore a need to develop and use improved blades. Triangular shaped blades, sweep

www.ijmer.com Vol. 3, Issue. 5, Sep - Oct. 2013 pp-3296-3299 ISSN: 2249-6645
blades, straight blades can be used according to their efficient working in different conditions. A best combination would be sweep blades and triangular blades which help in maximum removal of weeds from soil. From discussions with farmers and extension workers it became obvious that weeding tools and implements to be promoted should not only be effective in weed control, but also fairly cheap, durable, locally repairable and easy to use. The technology related to the use of the implements should be in line with farmers' Knowledge levels and aspirations.

IV. MATERIALS & METHODS

Various types of materials and methods used for weeding are as follows:

1. Manual weeding or Hand weeding
2. Chemical weeding
3. Flame weeding
4. Mechanical weeding
5. Animal drawn blade hoe weeders
6. Tractor drawn weeders
7. Power weeders
8. Khurpi
9. Push type weeders etc.

Above discussed materials and methods comparison with each other depends upon different constraints such as efficiency, time consumption, damage prone areas, ergonomically standard specifications, economically acceptable, adaptable nature in every situation, simple and easy maintenance.

V. AVAILABILITY OF WEEDERS

Fig.1 Slim and long sweep blades

Fig.2 Hand Khurpi

Figure 1, 2, 3, 4, and 5 shows the availability of weeders commonly. They are:

- Slim and long sweep blades (fig.1), Hand khurpi (Fig.2), TNAU made power weeder (Fig.3),
- Animal drawn weeder (Fig.4), Hoes (Fig.5).

Fig. 3 TNAU made power weeder

Fig. 4 Animal drawn weeder

Fig. 5 Hoes

VI. WEED CONTROL PRACTICES

It includes various types of weeders such as animal drawn blade hoe weeders, power weeders, khurpi (made up of handle of wood and a steel blade which is curved in shape), push type and pull type weeders having roller with pegs, handle and blade. Methods include hand weeding, chemical weeding, flame weeding, mechanical weeding etc. Although these material and methods are being used as weed removal techniques, they possess some drawbacks. Hand weeding needs more cost, labour, causes fatigue and stress. Chemical weeding is slowly becoming popular but costly and health problems may occur if proper care is not taken. Flame weeding causes extreme heat in surrounding and safeguards needed. Mechanical weeding has its different problems like it can be expensive, difficult to operate, maintenance, weight, its components, difficult for farmers to understand its working, may be not suitable for various types of soils e.g. Vidarbha region has black soil having completely different properties when compared with Marathwada region as the soil contents are different. So it is not possible that equipment used for cultivation in Vidarbha region should be as same as equipments used in Marathwada region.

VII. TRANSFER OF WEEDING TECHNOLOGY

To take weeding technology to a new dimension, we need to concentrate on previous technologies some areas of interest. These areas are:

1. Work capacity
2. Crop yield
3. Energy consumption
4. Cost of operation etc.

Work capacity is the total time needed to complete the desired task; crop yield indicates the crop growth in various techniques; energy consumption shows fuel requirement for the equipment; and cost of operation means the total cost incurred to farmer for one acre or hectare of weeding operation.

VIII. CONCLUSION

The main aim of this review paper is to have a proper understanding of different aspects or constraints of weeders as well as different weeding techniques to reduce the efforts which were put in by farmers in terms of money, labour, time, physical efforts for economical cultivation. Above discussed parameters definitely provides the basic ideas associated with weeding. Sincere efforts must be made to design a suitable weeding equipment or method, in order to provide more profit, stability in terms of economical considerations. There are certain limitations for engine operated equipment. Like vibration. Vibration cannot be eliminated completely as it is needed to provide thrust (positive or negative) to take out unwanted weed. If we completely eliminate the problem of vibration, then it is not possible for equipment to perform the desired task of weeding. Adjustable blades, rotary blades can definitely influence the performance of weeder. Design consideration of equipment also has a greater impact over the performance of weeder.

ACKNOWLEDGEMENTS

We wish to express our gratitude to Prof. Vishwas D. Deshmukh and Prof. G. S. Patange, Farm Machinery Testing and Training center, Mahatma Phule Krushi Vidyapith (MPKV), Rahuri, Ahmadnagar, for valuable discussions and guidelines concerning the manuscript.

REFERENCES

Journal Papers:

[1] H S Biswas , D S Rajput and R S Devnani , Animal power for weed control. Animal-drawn weeders for weed control in India. A resource book of the Animal Traction Network for Eastern and Southern Africa (ATNESA). ISBN 92-9081-136-6.
[2] F. Fogelberg, G. Kritz ,"Intra-row weeding with brushes on vertical axes factors influencing in-row soil height", Soil & Tillage Research 50 (1999) 149-157.
[3] Saeed Firouzi1 and Mohammadreza Alizadeh, "Evaluation of different weeding methods for groundnut in northern Iran", African Journal of Agricultural Research Vol. 7(8), pp. 1307-1311, 26 February, 2012.

[4] Mohammad Reza Alizadeh, "Field performance evaluation of mechanical weeders in the paddy field", Scientific Research and Essays, Vol. 6(25), pp. 5427-5434, 30 October, 2011.
[5] Zoltan Gobor ,Mechatronic "System for Mechanical Weed Control of the Intra-row Area in Row Crops" Springer-Verlag Berlin Heidelberg 2013 DOI 10.1007/s13218-013-0265-0.
[6] M. VEERANGOUDA, ER. SUSHILENDRA AND M. ANANTACHAR, "Performance evaluation of weeders in cotton" Karnataka J. Agric. Sci.,23 (5) : (732-736) 2010.
[7] Md. Aqib Naque, Akhtar Ali Rizvi, Prof. A. B. Tupkar, "Design, Development and Fabrication of Soil Tiller and Weeder" IJET ISSN 2319-1058, VOL2, ISSU APRIL 2013.
[8] K. Duerinckx; A.M. Mouazen; J. Anthonis; H. Ramon, "Effects of Spring-tine Settings and Operational Conditions on the Mechanical Performance of a Weed Harrow Tine" Bio systems Engineering (2005) 91 (1), 21–34.
[9] Dirk A.G. Kurstjens, "Precise tillage systems for enhanced non-chemical weed management" 2006 Elsevier doi:10.1016/j.still.2006.06.011.

Books:

[10] Dr.Normon Uphoff "System of Rice Intensification" A reference compendium pp-1-28.

Theses:

[11] Bin Ahmad, Mohd Taufik, "Development of an Automated Mechanical Intra-Row Weeder for Vegetable Crops" (2012). Graduate Theses and Dissertations. Paper 12278.

Development of a Thermoelectric Micro generation based on Seebeck Effect

Oswaldo Hideo Ando Junior[1-2], Jesiel da Luz Ferro[1], Cleber Lourenço Izidoro[1-2], Everlise Maestrelli[2], Lírio Schaeffer[2]

[1]*Scientific Research Group of Electrical Engineering, Faculty SATC, Brazil*
[2]*Mechanical Transformation Laboratory, UFRGS, Brazil*

ABSTRACT: *This paper presents a study of the national electric power, showing the Brazil consumes electricity in a year and how much you could save if thermoelectric modules were used in some industries and new cars and planes to capture and transformation of residual thermal energy into electrical energy. The conclusion appears really attractive economically, given the fact that many processes generate residual thermal energy and also energy cogeneration using thermoelectric modules is totally clean, which prevents the emission of greenhouse gases to the environment.*

Keywords: *Cogeneration, Economics, Energy Harvesting and Thermoelectric Modules.*

I. INTRODUCTION

With technological development and concern about global warming, the quest for power generation through alternative sources is increasing [1]. Today, electricity is a pretty basic for the development of the population, which improves the quality of life by providing social and economic growth.

Currently we live in an energy crisis that has been evidenced by the limits of energy supply required for the demand of the development, which is based primarily on non-renewable sources [2]. Along with the great dependence of these types of sources, has also the environmental impact, mainly due to the pollution that is a result of production activities that use these types of energy resources.

In view of this, the energy issue has become vital for all countries of the world, are extremely important to reduce dependence on fossil fuels, which today is the most widely used form of generation, finding sustainable solutions to help energy matrix of all countries and minimize the overall environmental impacts, prioritizing the need to replace this by other renewable energy source [3].

For Brazil, the stakes are high for the energetic exploitation of natural resources, as they are scattered unevenly in various regions of the country. Often, the Brazilian potential for generating energy through renewable resources is touted as one of the largest in the world [4].

With the increasing need for clean energy sources, renewable energy from the thermoelectric phenomenon has emerged as an alternative among the possibilities. This is due to the fact the thermoelectric modules present certain advantages, such as high durability, high accuracy and low volume, besides being a way of generating totally clean.

Thus, this paper presents the advantages and applications of thermoelectric modules in the domestic market, using the residual energy harvesting for power cogeneration. Thus, the analysis of their impact on the electricity sector and improving the overall energy efficiency of electrical systems will be shown, proving environmental and economic benefits of the use of thermoelectric modules.

II. THERMOELECTRIC MODULE

A thermoelectric module converts thermal energy into electrical energy and vice versa consisting of a matrix formed by multiple bimetallic junctions connected in series to increase output voltage, and in parallel to increase output current [5, 6].

These are able to operate as generators temperature gradient or as generators of electricity in direct current [5, 6]. Each bimetallic junction element is constituted by a p-type semiconductor and n-type; they are connected in series and grouped in pairs surrounded by a sheath ceramics. The ceramic plates have copper bus way that allows linking semiconductors electrically in series and thermally in parallel [1].

Currently, we use many joints to maximize the power delivered by the module. In Figure 1 presents a series of junctions grouped in matrix form, forming a set, known thermoelectric module.

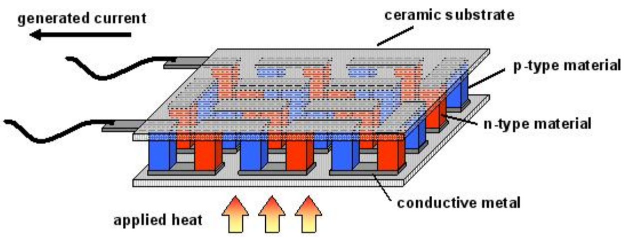

Fig. 1 - Statement of junctions Thermoelectric Module.

III. THERMOELECTRIC GENERATION

The thermoelectric power generation is based on the Seebeck effect. When heat is applied to the junction of two different conductors, a voltage is generated. The temperature difference between the hot side and the cold face is directly proportional to the voltage generated. When heat is applied to a surface of the thermoelectric generator, electrons from the n - type semiconductor and the gaps of the p-type semiconductor will move away from the heat source. This movement of electrons and holes gives rise to an electric current. The current direction is opposite to the movement of electrons, so in the same sense that the movement of the gaps. [3]

The performance of a system for generating electrical power using thermoelectric modules depends not only on the characteristics of the thermoelectric modules used, but a number of factors directly influence , like for example the temperature gradient , the converter used and charge on which to feed. [7]

The temperatures at which the system is exposed to influence the overall yield of the system because the greater the temperature difference, the greater is the voltage output of the modules. In addition, they generate oscillations in the output voltage of the thermoelectric modules, which will be mitigated by the converter responsible for decrease or increase the output voltage. This converter, in turn, also has certain income that affects the system.

The charge also influences the yield, since the maximum energy transfer is obtained when the electric resistance inside of the module is equal to the electrical resistance of the load.

IV. EXPERIMENTAL PROCEDURE

The purpose of the experimental procedure was to prove that it is possible to feed a load with the voltage generated by the thermoelectric modules. For this, followed the methodology developed for designing a thermoelectric generator. In this it is clear that to begin development of a thermoelectric generator is needed some data, such as:

- Load power;
- Supply Voltage;
- Temperature of the hot wall;
- Temperature of the cold wall;
- Number of hours that the system is connected;
- Performance Curve;
- Choose the thermoelectric module.

The load chosen was a lamp with 6 LEDs of 1W power each, totaling an output of 6W, with a supply voltage equal to 17V. It is known that the generation of a thermoelectric system has its voltage as a function of the temperature difference, and that varies continuously in thermal systems. Based on this information, it was possible to maintain the noting that 17V is needed to apply the DC-DC converter. A DC-DC converter may have its input voltage ranging that it will convert this voltage to a value of the output voltage always constant.

The DC-DC converter chosen was a Buck - Boost, where its output voltage can be higher or lower than its input voltage. This had the following characteristics:

- Input Voltage - 3.5 to 30V
- Output voltage - 4 to 30V

The following variables were to find the temperature of the hot side and cold. To simulate a hot wall was used a hot plate, whose even reached a temperature of 300°C. As for the temperature on the cold side, is mounted a system for circulating water. In this system, a pump is sucking water from a tank, causing it to flow through a piece of aluminum. The material chosen is aluminum due to its high thermal conductivity and to have better prices than other similar materials.

In the designed system, the stove is underneath and cooling block sits on top, and they are placed between the thermoelectric modules. Since the heat exchange between the hot part and the cold part, both by conduction and by radiation is too large, rock wool was placed between the stove and refrigerator block to reduce this heat exchange.

With all the data found, choose the left thermoelectric modules. For this step we analyzed the datasheets of some models. The model chosen was the module 1261G - 7L31 - 24CX1 of Custom Thermoelectric. This can resist a maximum temperature of 300°C in a hot face.

Acquired 6 thermoelectric modules of the above model, the temperature of the stove was placed to 250°C, to avoid the risk of damaging the thermoelectric module. Analyzing the graph of the voltage curve with respect to temperature difference, it was found that 250°C at the hot face of the module at 30°C and cold side can achieve a voltage of 3.2 V at the output of each module. Then, with six modules resultant voltage is equal to 19.2 V. Figure 2 shows the graph of the voltage curve present in the datasheet of the selected module.

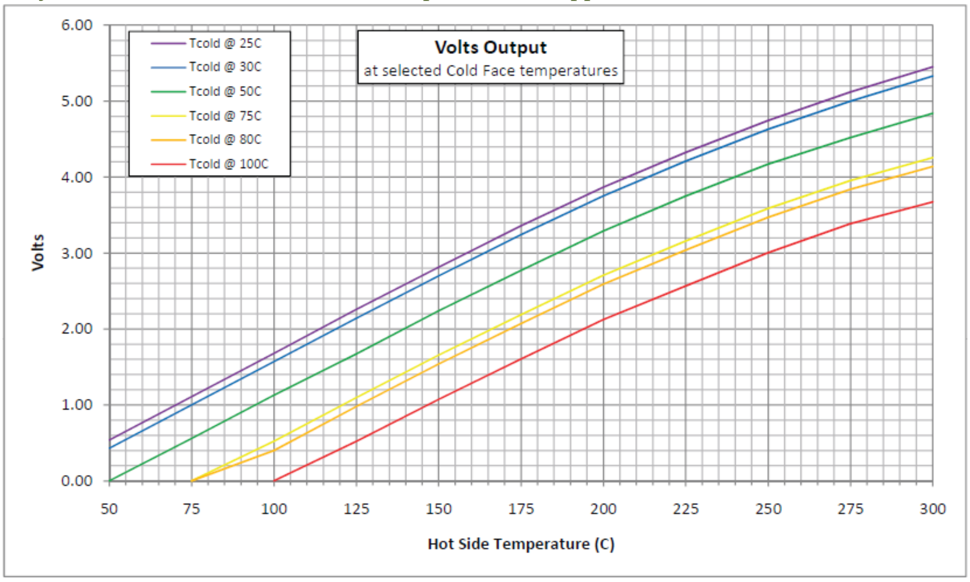

Fig. 2 - Voltage curve as a function of temperature for the thermoelectric module 1261G-7L31-24CX1

The charge, as has already filed a power of 6W. Thus, the current will circulate through it is equal to 350mA because its voltage is 17V. This current is found which will pass through the converter output, but the maximum current is obtained when the input voltage is low, namely equal to 3.5 V. Therefore, knowing that the output power is equal to the power input, the input current is that current which will circulate in the thermoelectric modules is equivalent to approximately 1.7 A. Analyzing the graph of the current applied thermoelectric module, note that with the same temperatures for the maximum current voltage module will bear is greater than 2A, the necessity of supplying easily load.

Getting all the material necessary to perform the experiment began mounting system. First, the hotplate was turned over and the same was placed a sheet of iron to achieve a greater area of application. On this plate were placed 6 parts aluminum, available as a 3 x 2 matrix, with holes for inserting the thermocouple. This process step can be seen in Figure 3.

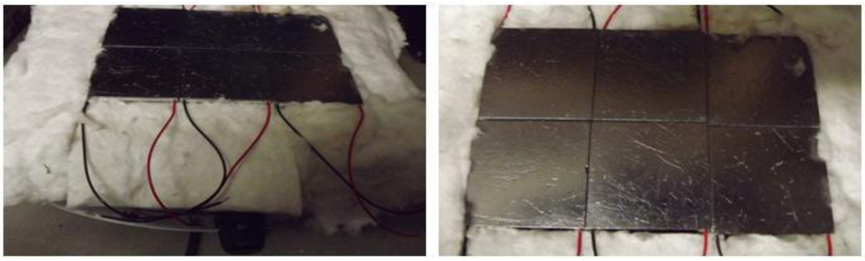

Fig. 3 - Providing aluminum plates on the stove

At the time the temperature reached values close to 230°C it has stabilized. With this, the 6 thermoelectric modules that were already connected in series were placed on each piece of aluminum.

Then, the aluminum block cooled by ice water was drawn from a tank with the aid of a pump, was applied on the cold face of the thermoelectric modules. Instantly, the temperature of the hot side is decreased and stabilized at around 170 ° C due to heat exchange. Figure 4 shows the curve of this temperature fall when the cooling block entered into the system, and the red curve correspond to warm temperature, the curve of the blue and green cold side the difference between these temperatures.

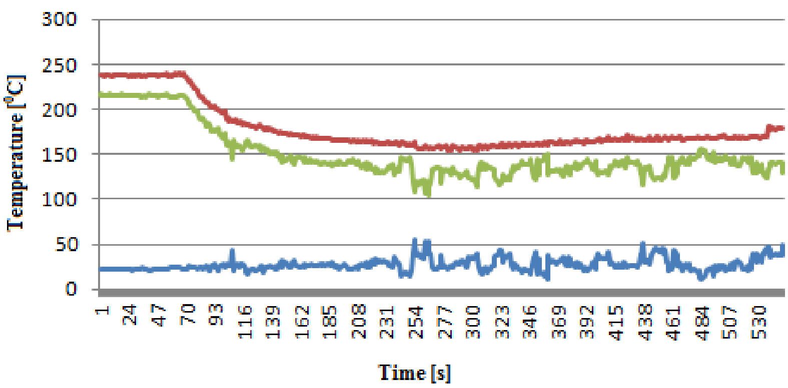

Fig. 4 - Figure temperature when the cooling block is added to the system

In the figure 4, note also that the cold end temperature was stabilized with values close to 30ºC. It is argued then that the equilibrium temperatures of the system were 170ºC and 30ºC. In Figure 5 we can see the picture of the process in thermal equilibrium.

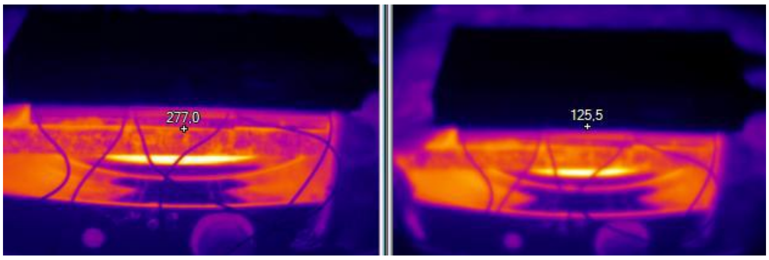

Fig. 5 - Photo thermal experiment

Anyway, the thermoelectric modules with the whole system began to generate electricity, but the results were not expected. The output voltage total module was only 5V, but it still was possible to feed the DC-DC converter. Measuring the 17V outlet in your lamp was connected to the system. The lamp was ignited and turned on during the whole process, and even when thermal equilibrium has entered the lamp still kept on, as expected. In Figure 6 displays the photo with lighted lamp fed by the converter.

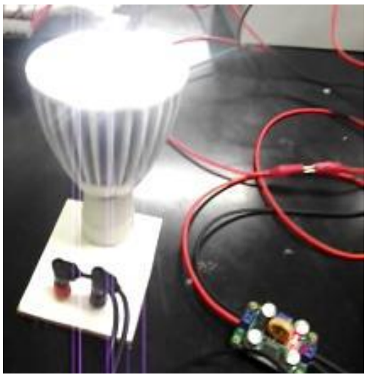

Fig. 6 - Photo of the validation experiment

As already shown the temperature of the system take some time to stabilize. At first, the temperature gradient is greater, therefore the voltage was also higher (5V). This, in turn, has been gradually decreasing as the temperature difference was reduced. When the measured voltage was close to 4V load (lamp) entered the system. Instantly the voltage was reduced to values around 2.8V, making current to be high.

In the graph (Fig. 7) for the voltage variation, is displayed as the value of the voltage is decreasing as the temperature difference diminished by validating the information that voltage generated by a thermoelectric module is directly linked to the temperature gradient. In the same graph perceives a variation of about 1V voltage when the lamp is lit, and after stabilization of the system, as previously mentioned.

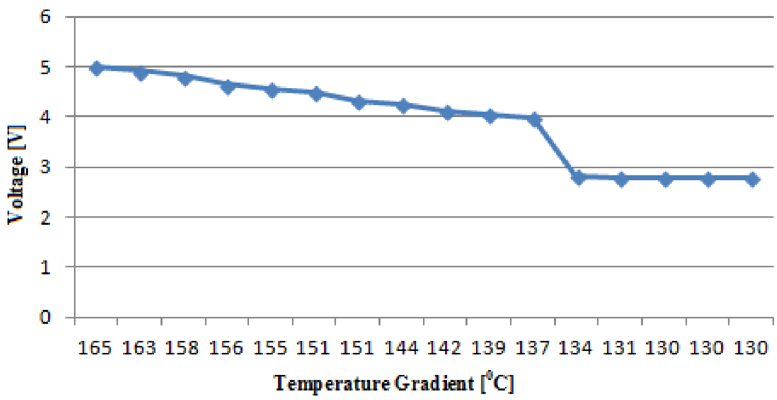

Fig. 7 - Figure referring to the voltage variation due to the temperature gradient

In the graph of the current, present in Figure 8, is seen the opposite of what happened with the tension. In this, we see an increase in current at the time the load is connected. This increase is proportional to the decrease in voltage, since the output power of the converter is equal to the input power then with a lower potential difference in the input current will be larger. Upon entry of the load also is noted that the current remains constant with system heat balance.

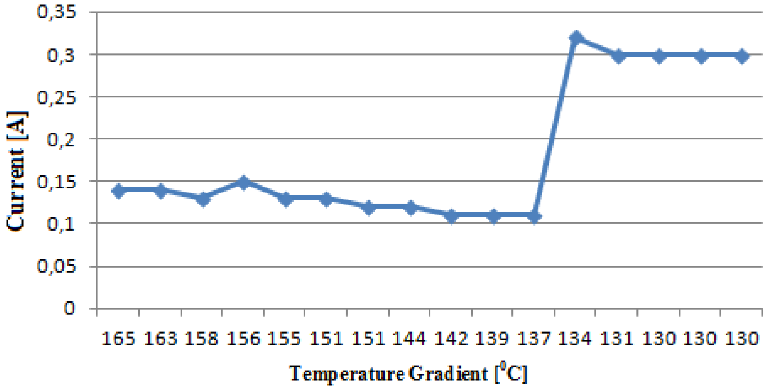

Fig. 8 - Figure respect to the variation of current as a function of the temperature gradient

After the voltage, current and power the system was operating for about 30 minutes, and the lamp went on. It is worth to stress that in real systems changes in temperature are constant, so did the use of a DC-DC converter.

Test to validate the application of cogeneration system, some difficulties were encountered. First, the temperature gradient was not as high as possible, and when the temperatures have stabilized the difference between the hot side and the cold side was at 140°C. Even so, with this temperature difference related to stress response system done, was much lower than expected, since with the temperature read each module would have to generate a little more than 2V, as presented in the manufacturer's datasheet, which together would result in a voltage exceeding 12V.

V. CONCLUSIONS

Based on the research and information exposed, it is clear that cogeneration power using thermoelectric modules is a promising source and presents results feasibly economical with their use, especially if implemented on a wide scale. The results were very significant, considering that only a few systems have been analyzed in this model can be applied cogeneration.

It is also considered that studies and researches are made constantly to improve their efficiency and the requirements for reducing emissions of gases that cause global warming, as well as the need to use renewable sources are increasing, making the applications of thermoelectric modules become increasingly interesting and most sought after because arouses the interest of the government and industries to utilize this technology.

Ends up emphasizing that there are other industries with great potential to capture energy waste to energy cogeneration . Among these are the power plants (8.5% of the national power generation) processes, foundries and potteries , and especially the fleet of buses and trucks .

REFERENCES

[1] S.A. M. Bastos, *Pulseira para Geração de Energia*. Dissertação (Mestrado). Universidade Do Minho. Braga, 2010.

[2] L.P. Santos, *Análise de Desempenho de um Gerador Termoelétrico Baseado no Efeito Seebeck.* Dissertação (Mestrado). Universidade De Taubaté. Taubaté, 2010.

[3] J.A.A. Antunes, *Reaproveitamento de Calor para Geração de Energia Eléctrica no Automóvel*. Dissertação (Mestrado). Universidade Do Minho. Braga, 2011.

[4] A.L.P.F. Landim L.P. Azevedo, O Aproveitamento Energético do Biogás em Aterros Sanitários: Unindo O Inútil Ao Sustentável. *BNDES Setorial*, Rio de Janeiro, p.59-100, mar. 2008.

[5] P.P. Alves, *A Experiência de Joule Revisitada.* Dissertação (Mestrado). Universidade Nova de Lisboa. Lisboa, 2008.

[6] A.V. Rosa. *Fundamentals of renewable energy processes*. 3.ed. Amsterdam; Boston: Elsevier Academic Press, 2013. 689 p.

[7] D.M. Rowe. *CRC Handbook of thermoelectrics.* New York: CRC Press, 1995.